MOBILE COMMUNICATIONS

HANDBOOK

Third Edition

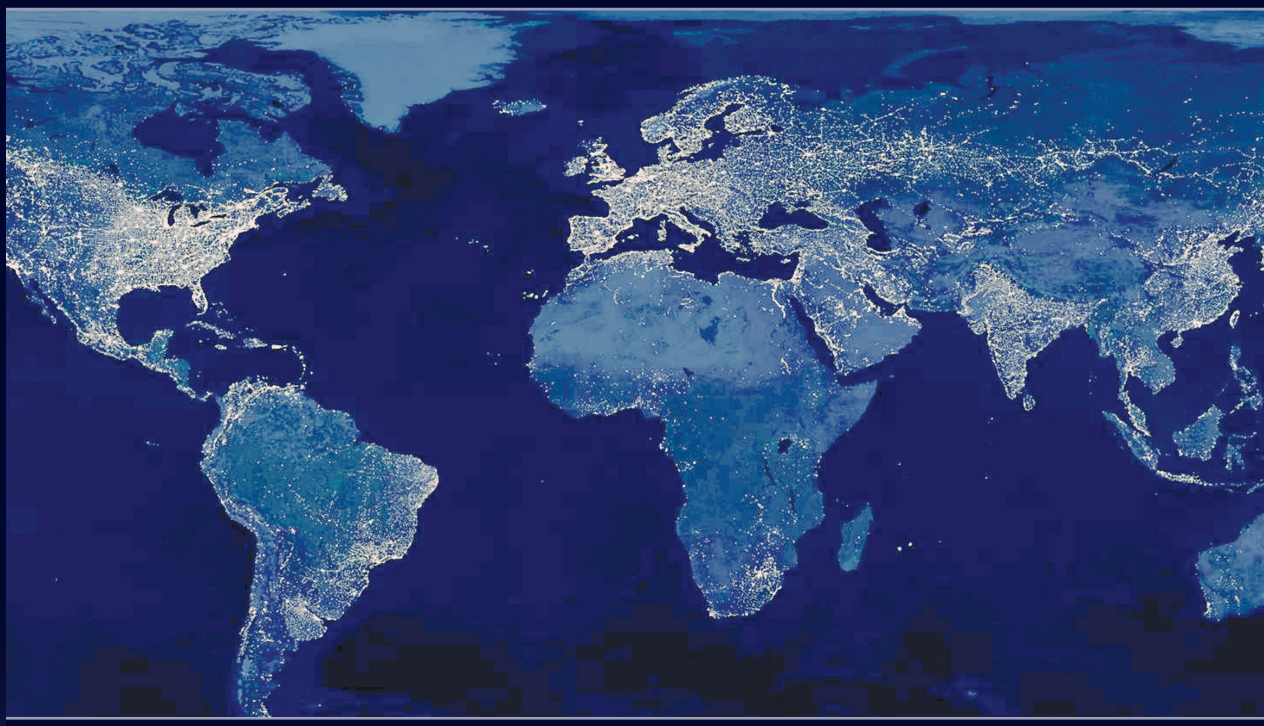

Editor-in-Chief
JERRY D. GIBSON

CRC Press
Taylor & Francis Group

MOBILE COMMUNICATIONS

HANDBOOK

Third Edition

The Electrical Engineering Handbook Series

Series Editor

Richard C. Dorf
University of California, Davis

Titles Included in the Series

The Avionics Handbook, Second Edition, Cary R. Spitzer
The Biomedical Engineering Handbook, Third Edition, Joseph D. Bronzino
The Circuits and Filters Handbook, Third Edition, Wai-Kai Chen
The Communications Handbook, Second Edition, Jerry Gibson
The Computer Engineering Handbook, Vojin G. Oklobdzija
The Control Handbook, Second Edition, William S. Levine
CRC Handbook of Engineering Tables, Richard C. Dorf
Digital Avionics Handbook, Second Edition, Cary R. Spitzer
The Digital Signal Processing Handbook, Vijay K. Madisetti and Douglas Williams
The Electric Power Engineering Handbook, Second Edition, Leonard L. Grigsby
The Electrical Engineering Handbook, Third Edition, Richard C. Dorf
The Electronics Handbook, Second Edition, Jerry C. Whitaker
The Engineering Handbook, Third Edition, Richard C. Dorf
The Handbook of Ad Hoc Wireless Networks, Mohammad Ilyas
The Handbook of Formulas and Tables for Signal Processing, Alexander D. Poularikas
Handbook of Nanoscience, Engineering, and Technology, Second Edition, William A. Goddard, III, Donald W. Brenner, Sergey E. Lyshevski, and Gerald J. Iafrate
The Handbook of Optical Communication Networks, Mohammad Ilyas and Hussein T. Mouftah
The Industrial Electronics Handbook, Second Edition, Bogdan M. Wilamowski and J. David Irwin
The Measurement, Instrumentation, and Sensors Handbook, John G. Webster
The Mechanical Systems Design Handbook, Osita D.I. Nwokah and Yidirim Hurmuzlu
The Mechatronics Handbook, Second Edition, Robert H. Bishop
Mobile Communications Handbook, Third Edition, Jerry D. Gibson
The Ocean Engineering Handbook, Ferial El-Hawary
The RF and Microwave Handbook, Second Edition, Mike Golio
The Technology Management Handbook, Richard C. Dorf
Transforms and Applications Handbook, Third Edition, Alexander D. Poularikas
The VLSI Handbook, Second Edition, Wai-Kai Chen

MOBILE COMMUNICATIONS

HANDBOOK

Third Edition

Editor-in-Chief
JERRY D. GIBSON


CRC Press
Taylor & Francis Group
Boca Raton London New York

CRC Press is an imprint of the
Taylor & Francis Group, an **informa** business

CRC Press
Taylor & Francis Group
6000 Broken Sound Parkway NW, Suite 300
Boca Raton, FL 33487-2742

Version Date: 20120608

International Standard Book Number-13: 978-1-4398-1724-7 (eBook - PDF)

Contents

SECTION IV Wireless Networks

SECTION V Emerging Applications

Preface

This third edition of the *Mobile Communications Handbook* reflects the extraordinary evolution of wireless communications and networks over the last 15 years, with 5 extensively revised chapters and 26 entirely new chapters out of a total of 39 chapters. We use the term *mobile communications* to include technologies ranging from digital cellular mobile radio and evolving personal communication systems to wireless data and wireless networks. This range of topics is presented in 39 concise chapters authored by experts from industry and academia. The chapters are written to provide a succinct overview of each topic, quickly bringing the reader up to date, but with sufficient detail and references to enable deeper investigations. The chapters are more than a "just the facts" presentation, with the authors using their experience in the field to provide insights into how each topic has emerged and to point toward forthcoming developments in mobile communications.

This book is divided into five sections: Basic Principles, Wireless Standards, Source Compression and Quality Assessment, Wireless Networks, and Emerging Applications. The chapters in the Basic Principles section provide the essential underpinnings for the wide-ranging mobile communication technologies currently in use throughout the world. The section on Wireless Standards contains technical details of the standards we use every day, and the chapters give insights into the development of the several standards. The third section covers the compression techniques used to represent voice and video for transmission over mobile communications systems as well as how the delivered voice and video quality are assessed. The Wireless Networks section examines the wide range of current and developing wireless networks and wireless methodologies all the way through the newly developed areas of vehicular communications and 60 GHz wireless communications.

The Basic Principles chapters readily allow the reader to jump right to the mobile communications topic of interest, with the option of efficiently filling in any gaps in one's background by referring back to the Basic Principles section as needed, without flipping through a textbook or searching the Internet.

Although there is an ordering to the chapters, the sequence does not have to be read from the beginning to the end. Each chapter was written to be an independent contribution with intentional overlap between some chapters to show how the many topics interconnect. Interestingly, as the reader will discover, this overlap often admits alternative views of difficult issues.

It has been a great pleasure to work with the authors to publish this third edition. The authors come from all parts of the world and constitute a literal who's who of workers in digital and mobile communications. Certainly, each article is an extraordinary contribution to the communications and networking fields, and the collection, I believe, is the most comprehensive treatment of the mobile communication field available in one volume today.

I appreciate the patience, support, and guidance of the staff at CRC Press/Taylor & Francis, particularly Nora Konopka, and the energetic and responsive assistance of Ashley Gasque during all stages of developing and producing this handbook.

Jerry D. Gibson
Santa Barbara, California

Editor

Jerry D. Gibson is a professor and the department chair of electrical and computer engineering at the University of California, Santa Barbara. He is the coauthor of the books *Digital Compression for Multimedia* (Morgan-Kaufmann, 1998) and *Introduction to Nonparametric Detection with Applications* (Academic Press, 1975 and IEEE Press, 1995) and author of the textbook *Principles of Digital and Analog Communications* (Prentice-Hall, 2nd ed., 1993). He is editor-in-chief of the *Mobile Communications Handbook* (CRC Press, 2nd ed., 1999), editor-in-chief of *The Communications Handbook* (CRC Press, 2nd ed., 2002), and editor of the book *Multimedia Communications: Directions and Innovations* (Academic Press, 2000).

Dr. Gibson was associate editor for speech processing for the *IEEE Transactions on Communications* from 1981 to 1985 and an associate editor for communications for the *IEEE Transactions on Information Theory* from 1988 to 1991. He was president of the IEEE Information Theory Society in 1996 and served on the Board of Governors of the IT Society for 10 years. He was a member of the Speech Technical Committee of the IEEE Signal Processing Society from 1992 to 1994. Dr. Gibson served as technical program chair and founder of the *1999 IEEE Wireless Communications and Networking Conference*, technical program chair of the *1997 Asilomar Conference on Signals, Systems, and Computers*, and general co-chair of the *1993 IEEE International Symposium on Information Theory*. He was an elected Member-at-Large on the Communications Society Board of Governors from 2005 to 2007. Currently, he serves on the Steering Committee for the Wireless Communications and Networking Conference. He was an IEEE Communications Society Distinguished Lecturer for 2007–2008, and he is a member of the IEEE Awards Committee and the IEEE Medal of Honor Committee.

In 1990, Dr. Gibson received the Fredrick Emmons Terman Award from the American Society for Engineering Education, and in 1992, he was elected Fellow of the IEEE "for contributions to the theory and practice of adaptive prediction and speech waveform coding." He was recipient of the 1993 IEEE Signal Processing Society Senior Paper Award for the Speech Processing area. Dr. Gibson received the IEEE Technical Committee on Wireless Communications Recognition Award in 2009 for contributions in the area of Wireless Communications Systems and Networks, and he and his students received the *IEEE Transactions on Multimedia* Best Paper Award in 2010.

His research interests include data, speech, image, and video compression, multimedia over networks, wireless communications, information theory, and digital signal processing.

Contributors

Behnaam Aazhang
Department of Electrical and Computer Engineering
Rice University
Houston, Texas

Emmanuel Abbe
Communication and Computer Sciences School
École polytechnique fédérale de Lausanne
Lausanne, Switzerland

Sassan Ahmadi
Senior Wireless Systems Architect and Cellular Standards Expert
Cupertino, California

Lava N. Al-Doski
Department of Systems Engineering
University of Arkansas
Little Rock, Arkansas

Alireza Babaei
Department of Electrical and Computer Engineering
Auburn University
Auburn, Alabama

Melbourne Barton
Telcordia Technologies
Red Bank, New Jersey

Paolo Bucciol
Politecnico di Torino
Torino, Italy

Madhukar Budagavi
Texas Instruments Inc.
Dallas, Texas

Wai-Yip Chan
Department of Electrical and Computer Engineering
Queen's University
Kingston, Ontario, Canada

Kwang-Cheng Chen
Department of Electrical Engineering
National Taiwan University
Taipei, Taiwan

Giovanni Cherubini
Storage Technologies Department
IBM Reseach
Zurich, Switzerland

Marco Chiani
Department of Electronics, Computer Sciences and Systems
University of Bologna
Bologna, Italy

Sayantan Choudhury
Nokia Research Center
Berkeley, California

Leon W. Couch II
Department of Electrical and Computer Engineering
University of Florida
Gainesville, Florida

Donald C. Cox
Department of Electrical Engineering
Stanford University
Stanford, California

Zhi Ding
Department of Electrical and Computer Engineering
University of California, Davis
Davis, California

Tiago H. Falk
Centre Énergie Matériaux Télécommunications
Montréal, Québec, Canada

Thomas E. Fuja
Department of Electrical Engineering
University of Notre Dame
Notre Dame, Indiana

Costas N. Georghiades
Department of Electrical and Computer Engineering
Texas A&M University
College Station, Texas

Rabindra Ghimire
Department of Applied Science
University of Arkansas
Little Rock, Arkansas

Jerry D. Gibson
Department of Electrical and Computer Engineering
University of California, Santa Barbara
Santa Barbara, California

Tor Helleseth
Department of Infomatics
University of Bergen
Bergen, Norway

Michael L. Honig
Department of Electrical Engineering and Computer Science
Northwestern University
Evanston, Illinois

Bijan Jabbari
Department of Electrical and Computer Engineering
George Mason University
Fairfax, Virginia

Woo-Shik Kim
Texas Instruments Inc.
Dallas, Texas

P. Vijay Kumar
Department of Electrical Engineering-Systems
University of Southern California
Los Angeles, California

Do-Kyoung Kwon
Texas Instruments Inc.
Dallas, Texas

Hyunok Lee
AT&T Labs, Inc.
San Ramon, California

Allen H. Levesque
Department of Electrical and Computer Engineering
Worcester Polytechnic Institute
Worcester, Massachusetts

Upamanyu Madhow
Department of Electrical and Computer Engineering
University of California, Santa Barbara
Santa Barbara, California

Giridhar D. Mandyam
QualComm Inc.
San Diego, California

Juan Carlos De Martin
Politecnico di Torino
Torino, Italy

Gareth Middleton
Department of Electrical and Computer Engineering
Rice University
Houston, Texas

Seshadri Mohan
Department of Systems Engineering
University of Arkansas
Little Rock, Arkansas

Renato Mariz de Moraes
Department of Electrical Engineering
University of Brasília (UnB)
Campus Universitário Darcy Ribeiro
Brasília, Brazil

Matthew Nokleby
Department of Electrical and Computer Engineering
Rice University
Houston, Texas

Geoffrey C. Orsak
Department of Electrical Engineering
Southern Methodist University
Dallas, Texas

Kaveh Pahlavan
Department of Electrical and Computer Engineering
Worcester Polytechnic Institute
Worcester, Massachusetts

John G. Proakis
Department of Electrical and Computer Engineering
Northeastern University
Boston, Massachusetts

Dinesh Rajan
Department of Electrical Engineering
Southern Methodist University
Dallas, Texas

Bixio Rimoldi
Communication Theory Laboratory
École polytechnique fédérale de Lausanne
Lausanne, Switzerland

Hamid R. Sadjadpour
Department of Electrical Engineering
University of California, Santa Cruz
Santa Cruz, California

Jong-Soo Seo
Yonsei University
Seoul, South Korea

Erchin Serpedin
Department of Electrical Engineering
Texas A&M University
College Station, Texas

Antonio Servetti
Politecnico di Torino
Torino, Italy

Sumit Singh
Moseley Wireless Solutions Group
Santa Barbara, California

Bernard Sklar
Communications Engineering Services
Tarzana, California

Gordon L. Stüber
School of Electrical and Computer Engineering
Georgia Institute of Technology
Atlanta, Georgia

Carl-Erik W. Sundberg
SundComm
Sunnyvale, California

Vivienne Sze
Texas Instruments Inc.
Dallas, Texas

Rüdiger Urbanke
Communication Theory Laboratory
École polytechnique fédérale de Lausanne
Lausanne, Switzerland

Bryan Usevitch
Department of Electrical and Computer Engineering
University of Texas, El Paso
El Paso, Texas

Michel Daoud Yacoub
School of Electrical and Computer Engineering
State University of Campinas
São Paulo, Brazil

Rodger E. Ziemer
Department of Electrical and Computer Engineering
University of Colorado, Colorado Springs
Colorado Springs, Colorado

I

Basic Principles

1

The Discrete Fourier Transform

Bryan Usevitch

1.1 Introduction

The discrete Fourier transform (DFT) is a method that represents the frequency content of a finite length time sequence, or sequence of samples. Specifically, it takes N input samples $x(n)$ and converts them into N frequency coefficients $X(k)$

$$X(k) = \sum_{n=0}^{N-1} x(n) W_N^{kn}, \quad k = 0,1,\ldots,N-1, \tag{1.1}$$

where

$$W_N \triangleq e^{-j\frac{2\pi}{N}}.$$

Conversely, given the N frequency coefficients $X(k)$ of a DFT, the time sequence $x(n)$ can be recovered using the inverse formula

$$x(n) = \frac{1}{N} \sum_{k=0}^{N-1} X(k) W_N^{-kn}, \quad n = 0,1,\ldots,N-1. \tag{1.2}$$

An important characteristic of the DFT is that the frequency response is represented with a finite set of values $X(k)$. This is in contrast to the related discrete time Fourier transform (DTFT), which represents the frequency content of a discrete time sequence as a function of a continuous-valued frequency argument. This allows the DFT to be conveniently computed, manipulated, and stored on a general-purpose

computer or digital processor. Furthermore, the discovery of fast methods for computing the DFT, called fast Fourier transforms (FFTs), has led to the widespread use of the DFT and has established digital signal processing as a major research and application area.

The DFT is very closely related to the discrete Fourier series (DFS). In fact, the two transforms share the same formulas (1.1) and (1.2), but differ in their interpretations. The DFS represents a periodic discrete time sequence as a linear combination of complex exponentials. The weights of this linear combination are $X(k)/N$ as shown in Equation 1.2. Since the coefficients $X(k)$ are the sinusoid weights, they represent the frequency content of the time signal $x(n)$. The DFS differs from the continuous time Fourier series (FS) since it requires at most N complex sinusoids to represent a signal, whereas the FS may require an infinite number. This is because the dual constraints of sampling and periodicity with period N limit the total number of possible sinusoids to be N.

In contrast to the DFS, the DFT can be interpreted as a linear transformation from one finite length sequence to another. In this viewpoint the forward and inverse equations can be represented using $N \times N$ matrices, and concepts from linear algebra can be used in analysis. Alternatively, the DFT can be viewed as a frequency-sampled version of the DTFT. The sampling causes both the time signal $x(n)$ and the frequency signal $X(k)$ to be discrete and periodic with period N. These signals are formed by periodically repeating the original time or frequency sequences defined over the original length N intervals. Both interpretations of the DFT are discussed below and both interpretations find use depending on the specific application.

The next section of this chapter discusses how the DFT relates to other Fourier transforms (FTs), and its interpretation from a sampled DTFT as well as a linear algebraic standpoint. The following section derives the main properties of the DFT. The subsequent section gives an overview of FFT algorithms, which are fast computational versions of the DFT.

1.2 DFT Theory

1.2.1 Fourier Transform Review

Much insight into the nature and properties of the DFT can be gained by relating the DFT to other FTs. In particular, the DFT is very closely related to the DTFT. Thus, as a preface to discussing the DFT, we review the commonly used FTs shown in Figure 1.1. The first transform shown is the continuous-time FT, which computes the frequency spectrum of a continuous-time signal. The forward and inverse transform equations of the FT are given by

$$X(\Omega) = \int_{-\infty}^{\infty} x(t)\mathrm{e}^{-\mathrm{j}\Omega t}\,\mathrm{d}t$$

$$x(t) = \frac{1}{2\pi}\int_{-\infty}^{\infty} X(\Omega)\mathrm{e}^{\mathrm{j}\Omega t}\,\mathrm{d}\Omega.$$

When the time signal is continuous and periodic, the frequency spectrum is determined by the FS. The following formulas give the forward and inverse equations for the FS:

$$a(k) = \frac{1}{T_0}\int_{T_0} x(t)\mathrm{e}^{-\mathrm{j}k\Omega_0 t}\,\mathrm{d}t \tag{1.3}$$

$$x(t) = \sum_{k=-\infty}^{\infty} a(k)\mathrm{e}^{\mathrm{j}k\Omega_0 t}, \tag{1.4}$$

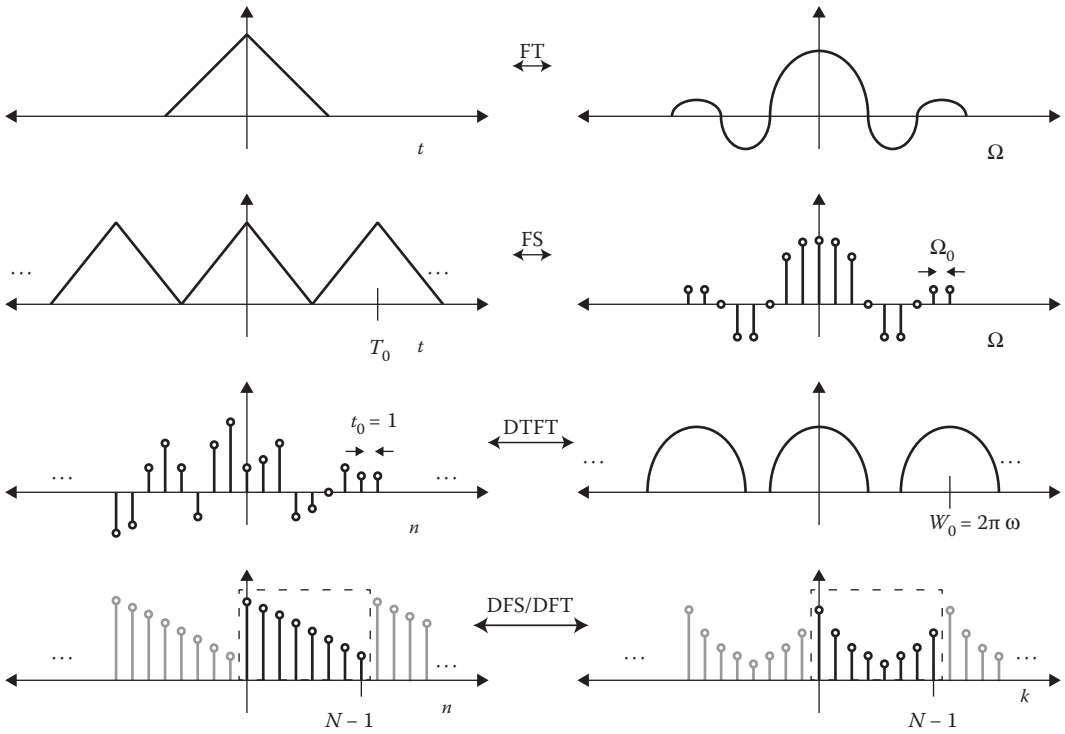

FIGURE 1.1 Figure shows commonly used Fourier transforms including, from the top, the continuous time Fourier transform (FT), the continuous time Fourier series (FS), the discrete time Fourier transform (DTFT), the discrete Fourier series (DFS), and discrete Fourier transform (DFT). (See L. Ludeman. *Fundamentals of Digital Signal Processing*. New York: Harper & Row, 1986.)

where T_0 is the fundamental period of the time function, Ω_0 is the fundamental frequency, and these are related by $\Omega_0 = (2\pi/T_0)$. Observe in particular that continuous-time periodic signals result in a discrete, or sampled, frequency spectrum, and the frequencies are all integer multiples of the fundamental frequency Ω_0.

While the FS results in samples in the frequency domain, what is often needed in signal processing is a transform that operates on sampled time values. This is the case handled by the DTFT which determines the frequency spectrum of sampled time signals. By using the sampling theorem, or equivalently the FS and duality, it can be shown that the resulting frequency spectrum of the DTFT is continuous valued and periodic. The exact mathematical form of the DTFT can be derived by applying the FS in the frequency domain. The formula of this frequency domain FS comes from Equations 1.3 and 1.4 by reversing all frequency and time variables, and also reversing the signs of the exponentials. This results in

$$b(k) = \frac{1}{W_0}\int_{W_0} G(\omega)e^{jkt_0\omega}\,d\omega$$

$$G(\omega) = \sum_{k=-\infty}^{\infty} b(k)e^{-jkt_0\omega}$$

where W_0 is the period of the periodic frequency domain signal, t_0 is the spacing of the samples in the time domain, and $t_0 = (2\pi/W_0)$.

The DTFT is normalized to have sample times fixed on the integers resulting in $t_0 = 1$ and $W_0 = 2\pi$. The resulting DTFT computation formulas are thus

$$X(\omega) = \sum_{n=-\infty}^{\infty} x(n)e^{-j\omega n}$$
$$x(n) = \frac{1}{2\pi}\int_{-\pi}^{\pi} X(\omega)e^{j\omega n}\,dw.$$

The normalization of the DTFT results in $x(n)$ being measured in time units of samples, and ω being measured in units of radian/sample. This explains the use of different frequency variables for the FT/FS (Ω–radians/second) and the DTFT (ω–radians/sample).

1.2.2 The DFT as a Sampled DTFT

We now investigate the effect of sampling the DTFT. Assume that we have a sequence $x(n)$ with DTFT represented by $X(\omega)$. We sample $X(\omega)$ uniformly to obtain the frequency sequence $Y(k)$

$$Y(k) = X\left(\frac{2\pi}{N}k\right), \quad k = 0,1,\ldots,N-1.$$

The question we now want to answer is how does $y(n)$, the time sequence of $Y(k)$, relate to the original signal $x(n)$? This will demonstrate the net result of sampling the DTFT. Since $X(\omega)$ is periodic, $Y(k)$ is discrete periodic. Thus, we can find the time sequence $y(n)$ using the inverse DFS formula of Equation 1.2

$$y(n) = \frac{1}{N}\sum_{k=0}^{N-1} Y(k)W_N^{-kn}, \quad n = 0,1,\ldots,N-1. \tag{1.5}$$

Since $Y(k)$ comes from the sampled DTFT, we can represent it as

$$Y(k) = X(\omega)\big|_{\omega=\frac{2\pi}{N}k} = \sum_{m=-\infty}^{\infty} x(m)e^{-j\frac{2\pi}{N}km}. \tag{1.6}$$

Substituting Equation 1.6 into Equation 1.5 gives

$$\begin{aligned} y(n) &= \frac{1}{N}\sum_{k=0}^{N-1}\left(\sum_{m=-\infty}^{\infty} x(m)e^{-j\frac{2\pi}{N}km}\right)e^{j\frac{2\pi}{N}kn} \\ &= \sum_{m=-\infty}^{\infty} x(m)\frac{1}{N}\sum_{k=0}^{N-1} e^{j\frac{2\pi}{N}k(n-m)}. \end{aligned} \tag{1.7}$$

Equation 1.7 can be simplified using the following identity:

$$\frac{1}{N}\sum_{k=0}^{N-1} e^{j\frac{2\pi}{N}kn} = \begin{cases} 1 & n = lN \\ 0 & \text{otherwise} \end{cases}.$$

Rewriting this identity as

$$\frac{1}{N}\sum_{k=0}^{N-1} e^{j\frac{2\pi}{N}kn} = \sum_{l=-\infty}^{\infty} \delta(n - lN) \triangleq p(n), \tag{1.8}$$

Equation 1.7 can be expressed as a convolution

$$y(n) = \sum_{m=-\infty}^{\infty} x(m)p(n - m) = x(n) * p(n).$$

Carrying out the convolution results in

$$y(n) = \sum_{l=-\infty}^{\infty} x(n - lN) \triangleq x_N^{\mathrm{p}}(n). \tag{1.9}$$

where $x_N^{\mathrm{p}}(n)$ is the periodic extension of $x(n)$ with period N.

This result shows that frequency sampling has the dual effect of time sampling. Namely, it causes a periodic repetition of the time-domain sequence. In order to recover the original $X(\omega)$ from its samples, and thus for the DFT to be a valid transform, requires one more constraint. This constraint is that the signal $x(n)$ be limited to the range $0 \le n \le L - 1$ and the number of samples in the DFT satisfy $N \ge L$. In this case $x(n)$ can be recovered from extracting one period of $x_N^{\mathrm{p}}(n)$, and $X(\omega)$ can be recovered through the DTFT of $x(n)$. This proves that $X(\omega)$ can be recovered from its samples. However, if $N < L$ then $x_N^{\mathrm{p}}(n)$ consists of time-aliased replicas of $x(n)$ and $X(\omega)$ cannot be recovered from the samples $X(\frac{2\pi}{N}k)$.

Example 1.1

In this example we use the DTFT sampling method to compute the DFT of a finite length, complex sinusoid

$$x(n) = e^{j\omega_0 n} p_N(n), \tag{1.10}$$

where

$$p_N(n) = \begin{cases} 1 & 0 \le n \le N-1 \\ 0 & \text{otherwise} \end{cases}.$$

We start by computing the DTFT of the windowing pulse $p_N(n)$

$$\begin{aligned} P_N(\omega) &= \sum_{n=-\infty}^{\infty} p_N(n)e^{-j\omega n} = \sum_{n=0}^{N-1} e^{-j\omega n} = \frac{1 - e^{-j\omega N}}{1 - e^{-j\omega}} \\ &= \frac{\sin\left(\frac{N}{2}\omega\right)}{\sin\left(\frac{1}{2}\omega\right)} e^{-j\frac{N-1}{2}\omega}. \end{aligned} \tag{1.11}$$

The final DTFT of Equation 1.10 results from using the frequency shift property on Equation 1.11

$$X(\omega) = \frac{\sin\left(\frac{N}{2}(\omega - \omega_0)\right)}{\sin\left(\frac{1}{2}(\omega - \omega_0)\right)} e^{-j\frac{N-1}{2}(\omega-\omega_0)}.$$

To get the desired DFT coefficients, we substitute $\omega = (2\pi/N)k$ into the above equation

$$X(k) = \frac{\sin\left(\frac{N}{2}\left(\frac{2\pi}{N}k - \omega_0\right)\right)}{\sin\left(\frac{1}{2}\left(\frac{2\pi}{N}k - \omega_0\right)\right)} e^{-j\frac{N-1}{2}\left(\frac{2\pi}{N}k-\omega_0\right)}. \tag{1.12}$$

Now consider two separate cases of frequencies for the input sinusoid. The first case is for frequencies that have an integer number of cycles in the N sample window: $\omega_0 = (2\pi/N)k_0$. For this case the DFT coefficients of Equation 1.12 simplify to

$$X(k) = \frac{\sin(\pi(k - k_0))}{\sin\left(\frac{\pi}{N}(k - k_0)\right)} e^{-j\frac{N-1}{N}\pi(k-k_0)}.$$

Note that the quotient of sines in the equation above is a digital sinc function. This results in all values of the DFT being zero, except at the index $k = k_0$, which corresponds to the index of the input frequency. A plot of both the DFT coefficients and underlying DTFT for the case of $N = 8$ and $k_0 = 3$ is shown in Figure 1.2.

Now consider the second case where the input frequency does not have an integer number of cycles in the N sample time input. Using Equation 1.12 for the case of $N = 8$ and $\omega_0 = 0.7\pi$ gives the result shown in Figure 1.2. Note in particular that the samples occur at nonzero values of the underlying DTFT frequency response. It may seem counterintuitive that the DFT of a sinusoid results in the spectrum on the right-hand side of Figure 1.2. However, note that the input is only a sinusoid in the initial N sample input window. Frequency sampling causes this window to be periodically repeated as shown by Equation 1.9. Since the input does not have an integer number of frequency cycles in the input window, this results in discontinuities at the repeated window boundaries. The overall periodic input is thus not a clean sinusoid, and the spectrum on the right of Figure 1.2 results.

1.2.3 The DFT as a Change of Basis

A second way of viewing the DFT is as a linear transform from one finite sequence to another. In this case we represent the input $x(n)$ and DFT coefficients $X(k)$ as vectors

$$\mathbf{x} = \begin{bmatrix} x(0) \\ x(1) \\ \vdots \\ x(N-1) \end{bmatrix}, \quad \mathbf{X} = \begin{bmatrix} X(0) \\ X(1) \\ \vdots \\ X(N-1) \end{bmatrix}.$$

As shown below, the transformation from $\mathbf{x}$ to $\mathbf{X}$ is accomplished using an $N \times N$ DFT matrix.

From the linear algebra viewpoint, the DFT becomes a way of representing a vector on an alternative basis

$$\mathbf{x} = \sum_{i=0}^{N-1} \alpha_i \mathbf{b}_i, \tag{1.13}$$

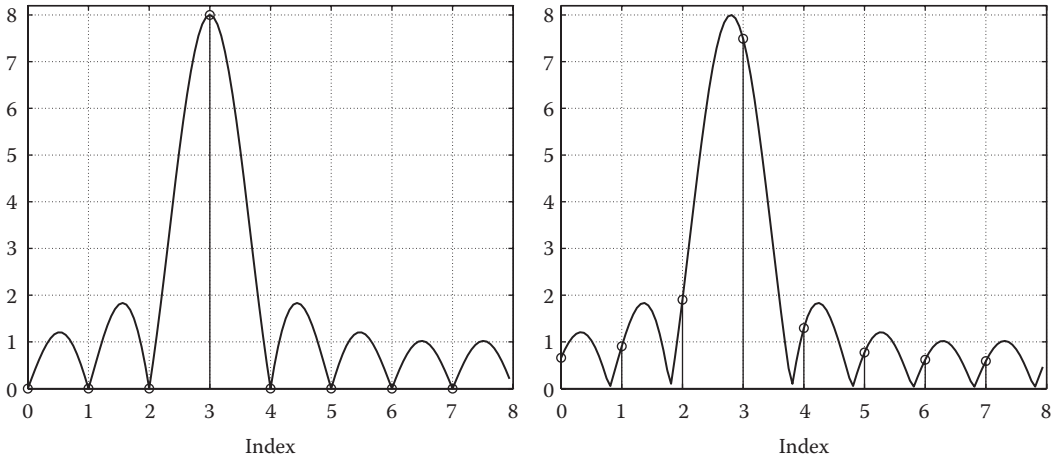

FIGURE 1.2 The left plot shows the magnitude of the DTFT (solid) and 8-point DFT (samples) of a complex sinusoid having an integer number of cycles in the N sample time window $(\omega_0 = \frac{2\pi}{8} \cdot 3 = 0.75\pi)$. For this case the zeros of the DTFT align with the samples of the DFT. The right plot repeats this example except that the sinusoid no longer has an integer number of cycles in the N sample time window ($\omega_0 = 0.7\pi$). As a result, the samples of the DFT no longer align with the zeros of the DTFT.

where $\mathbf{b}_i$ are the basis vectors and the α_i are the scalar weights needed to reconstruct the signal $\mathbf{x}$ using this basis. Specifically, for the DFT, the basis vectors are complex sinusoids at uniformly spaced frequencies, where each basis vector has an integer number of cycles in the N sample window

$$\mathbf{b}_i = \begin{bmatrix} | \\ e^{j\frac{2\pi}{N}in} \\ | \end{bmatrix} = \begin{bmatrix} 1 \\ W_N^{-i} \\ W_N^{-2i} \\ \vdots \\ W_N^{-(N-1)i} \end{bmatrix}.$$

Given these specific basis vectors, the problem becomes one of finding the weights α_i that represent $\mathbf{x}$. This problem can be solved in a straightforward manner by expressing Equation 1.13 in matrix form

$$\mathbf{x} = \mathbf{W}\alpha$$

where

$$\mathbf{W} = \begin{bmatrix} | & | & & | \\ \mathbf{b}_0 & \mathbf{b}_1 & \cdots & \mathbf{b}_{N-1} \\ | & | & & | \end{bmatrix} = \begin{bmatrix} 1 & 1 & 1 & \cdots & 1 \\ 1 & W_N^{-1} & W_N^{-2} & \cdots & W_N^{-(N-1)} \\ 1 & W_N^{-2} & W_N^{-4} & \cdots & W_N^{-2(N-1)} \\ \vdots & \vdots & \vdots & \ddots & \\ 1 & W_N^{-(N-1)} & W_N^{-2(N-1)} & \cdots & W_N^{-(N-1)(N-1)} \end{bmatrix}.$$

Since the basis vectors are orthogonal, the columns of $\mathbf{W}$ are orthogonal (and only differ from orthonormal vectors by a common constant). The inverse of the matrix $\mathbf{W}$ can thus be formed by taking its Hermitian transpose

$$\mathbf{I} = \frac{1}{N}\mathbf{W}^{\mathrm{H}}\mathbf{W} = \frac{1}{N}\mathbf{W}\mathbf{W}^{\mathrm{H}}.$$

The matrix $\mathbf{D} = \mathbf{W}^{\mathrm{H}}$ is called the DFT matrix and is written as

$$\mathbf{D} = \begin{bmatrix} -- & \mathbf{b}_0^{\mathrm{H}} & -- \\ -- & \mathbf{b}_2^{\mathrm{H}} & -- \\ & \vdots & \\ -- & \mathbf{b}_{N-1}^{\mathrm{H}} & -- \end{bmatrix} = \begin{bmatrix} 1 & 1 & 1 & \cdots & 1 \\ 1 & W_N & W_N^2 & \cdots & W_N^{N-1} \\ 1 & W_N^2 & W_N^4 & \cdots & W_N^{2(N-1)} \\ \vdots & \vdots & \vdots & \ddots & \vdots \\ 1 & W_N^{N-1} & W_N^{2(N-1)} & \cdots & W_N^{(N-1)(N-1)} \end{bmatrix}. \tag{1.14}$$

The reason **D** is called the DFT matrix is that it can be readily verified from Equations 1.1 and 1.14 that multiplying a vector by **D** results in computing its DFT: $\mathbf{X} = \mathbf{D}\mathbf{x}$. Returning to the basis representation problem, we have that

$$\mathbf{x} = \mathbf{I}\mathbf{x} = \frac{1}{N}\mathbf{W}\mathbf{D}\mathbf{x} = \frac{1}{N}\mathbf{W}\mathbf{X} = \frac{1}{N}\sum_{k=0}^{N-1} X(k)\mathbf{b}_k. \tag{1.15}$$

We can see from Equation 1.15 that when we represent a vector **x** using the DFT basis vectors, the DFT coefficients divided by N are the scalar weights in the linear combination needed to reconstruct the vector **x**. Since each of the basis vectors represents a separate frequency, the DFT coefficients tabulate the frequency content of the original vector.

1.3 Properties of the DFT

In this section, we enumerate some of the properties of the DFT transform. Many of these properties are similar to those of the continuous time FT and DTFT, which is to be expected since all these transforms decompose signals onto a set of complex sinusoids. However, the DFT has some idiosyncrasies due to it being a transform for finite length (or equivalently periodic) sequences. Properties of the DFT are summarized in Table 1.1.

1.3.1 Periodicity

The sequences $x(n)$ and $X(k)$ are periodic with period N

$$x(n) = x(n+N), \quad X(k) = X(k+N), \quad \text{for all } n \text{ and } k.$$

This property can be proved directly from Equations 1.1 and 1.2. For example, the proof for the time sequence $x(n)$ is

$$\begin{aligned} x(n+N) &= \frac{1}{N}\sum_{k=0}^{N-1} X(k)e^{j\frac{2\pi}{N}k(n+N)} = \frac{1}{N}\sum_{k=0}^{N-1} X(k)e^{j\frac{2\pi}{N}kn}(e^{j2\pi})^k \\ &= \frac{1}{N}\sum_{k=0}^{N-1} X(k)e^{j\frac{2\pi}{N}kn} = x(n). \end{aligned}$$

TABLE 1.1 DFT Properties

Property	Time Domain	Frequency Domain
Signals	$x(n)$, $y(n)$	$X(k)$, $Y(k)$
Linearity	$ax(n) + by(n)$	$aX(k) + bY(k)$
Time reversal	$x((N-n))_N$	$X((N-k))_N$
Time shift	$x((n-n_0))_N$	$X(k)e^{-j\frac{2\pi}{N}kn_0}$
Frequency shift	$x(n)e^{j\frac{2\pi}{N}k_0n}$	$X((k-k_0))_N$
Time convolution	$\sum_{l=0}^{N-1} x(l)y((n-l))_N$	$X(k)Y(k)$
Frequency convolution	$x(n)y(n)$	$\frac{1}{N}\sum_{m=0}^{N-1} X(m)Y((k-m))_N$
Duality	$\frac{1}{N}X(n)$	$x((N-k))_N$
Complex conjugate	$X^*(n)$	$X^*((N-k))_N$
Parseval's theorem	$\sum_{n=0}^{N-1} \lvert x(n)\rvert^2 = \frac{1}{N}\sum_{k=0}^{N-1} \lvert X(k)\rvert^2$	

1.3.2 Circular Shift

Standard time shifting in the DFT presents a problem for a finite length sequence since coefficients can be shifted out of the original N sample time window, $0 \le n \le N-1$. However, this problem is solved by considering the underlying periodic signal corresponding to the finite sequence. Time shifting in the DFT corresponds to linearly shifting this periodic signal and retaining only the values that fall into the original N sample window (see Figure 1.3). Alternatively, the periodic shift can be viewed as circularly shifting the samples in the original N sample window as also shown in Figure 1.3. The locations of circularly shifted samples can be computed using modulo arithmetic. If we represent the circularly shifted $x(n)$ by $x_s(n)$, then $x_s(n)$ can be written in terms of the original sequence $x(n)$ for $0 \le n \le N-1$ as

$$x_s(n) = x_N^p(n-n_0) = x((n-n_0))_N$$

where $((\cdot))_N$ represents the modulo remainder. For positive n, the modulo remainder is computed by writing n as $n = qN + r$, from which the remainder is read directly as $((n))_N = r$. For negative n, multiples of N are added until $kN + n$ is positive and the modulo operator is applied on this positive value. In particular, the time reversal of $x(n)$ can be written $x(-n) = x(N-n)$.

The previous definition of shifting results in a DFT property which parallels those of the FT and DTFT. Namely, the result of shifting a time sequence is to multiply its DFT by a complex exponential

$$x((n-n_0))_N \xleftrightarrow{\text{DFT}} X(k)e^{-j\frac{2\pi}{N}kn_0}.$$

This property is proved for shifts in the range $0 \le n_0 \le N-1$ only, since any shift n_1 outside this range can be written as $n_1 = n_0 + lN$, l an integer, and

$$x((n-n_1))_N = x((n-(n_0+lN)))_N = x((n-n_0))_N$$

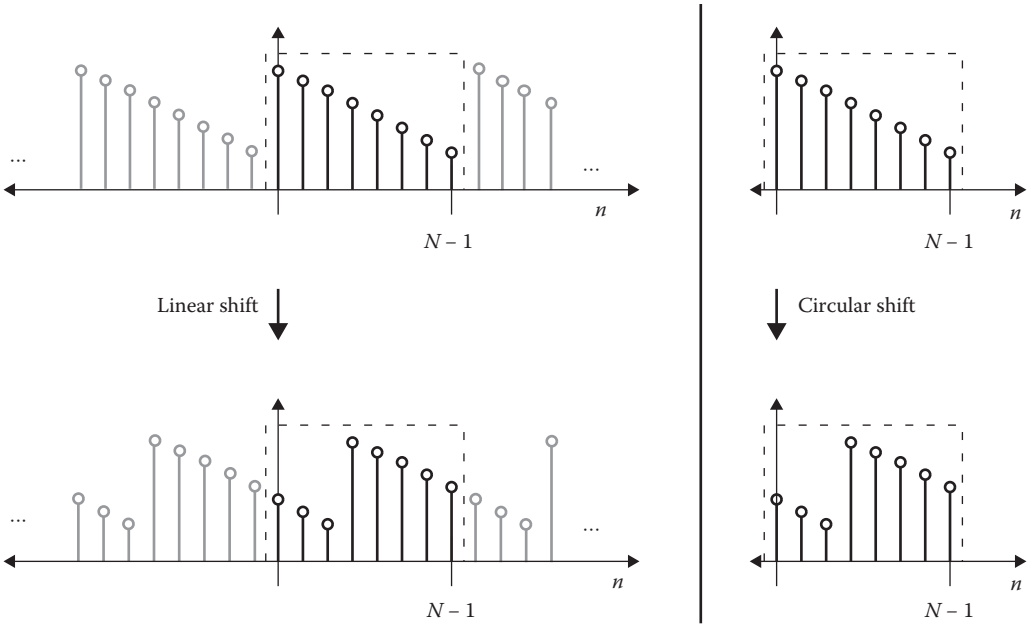

FIGURE 1.3 The left figure shows the linear shift of a periodic, length N sequence, and the right figure shows the circular shift of a finite length N sequence, demonstrating that the two operations are equivalent.

This shows that all shifts can be mapped into this range. We start from the DFT definition

$$x((n-n_0))_N \overset{\text{DFT}}{\longleftrightarrow} \sum_{n=0}^{N-1} x((n-n_0))_N e^{-j\frac{2\pi}{N}kn}.$$

Splitting the sum into positive and negative time indices, and recognizing that for negative indices $((n-n_0))_N = (N+n-n_0)$ gives

$$x((n-n_0))_N \overset{\text{DFT}}{\longleftrightarrow} \sum_{n=0}^{n_0-1} x(N+n-n_0)e^{-j\frac{2\pi}{N}kn} + \sum_{n=n_0}^{N-1} x(n-n_0)e^{-j\frac{2\pi}{N}kn}$$

Using the substitutions $m = N+n-n_0$ and $m = n-n_0$ for the two sums and combining results in

$$x((n-n_0))_N \overset{\text{DFT}}{\longleftrightarrow} \sum_{m=N-n_0}^{N-1} x(m)e^{-j\frac{2\pi}{N}k(m+n_0)} + \sum_{m=0}^{N-n_0-1} x(m)e^{-j\frac{2\pi}{N}k(m+n_0)}$$
$$= \sum_{m=0}^{N-1} x(m)e^{-j\frac{2\pi}{N}km}e^{-j\frac{2\pi}{N}kn_0} = X(k)e^{-j\frac{2\pi}{N}kn_0}$$

which proves the property. A main point to take away from the previous discussion is that because of the underlying periodic nature of the DFT, all time and frequency shifts for sequences are circular shifts. As a result, many texts eliminate the modulo notation for shifts except when explicitly discussing shift operations.

1.3.3 Circular Convolution

Since convolution uses time shifts, the convolution defined for the DFT is circular convolution

$$y(n) = \sum_{l=0}^{N-1} x(l)h((n-l))_N = x(n) \textcircled{N} h(n), \tag{1.16}$$

where $\textcircled{N}$ denotes circular convolution of length N. Like other FTs, circular convolution results in multiplication of the DFT transforms

$$x(n) \textcircled{N} h(n) \xleftrightarrow{\text{DFT}} X(k)H(k). \tag{1.17}$$

This property can be proved by substituting the inverse transform definitions from Equation 1.2 into the circular convolution formula (1.16) and using the time shift property of the DFT

$$\begin{aligned}\sum_{l=0}^{N-1} x(l)h((n-l))_N &= \sum_{l=0}^{N-1}\left(\frac{1}{N}\sum_{k=0}^{N-1} X(k)e^{j\frac{2\pi}{N}kl}\right)\left(\frac{1}{N}\sum_{m=0}^{N-1} H(m)e^{j\frac{2\pi}{N}m(n-l)}\right)\\ &= \frac{1}{N}\sum_{k=0}^{N-1}\sum_{m=0}^{N-1} X(k)H(m)e^{j\frac{2\pi}{N}mn}\left[\frac{1}{N}\sum_{l=0}^{N-1} e^{j\frac{2\pi}{N}kl}e^{-j\frac{2\pi}{N}ml}\right].\end{aligned}$$

Using the identity of Equation 1.8 for the bracketed term, this expression simplifies to

$$\sum_{l=0}^{N-1} x(l)h((n-l))_N = \frac{1}{N}\sum_{k=0}^{N-1} X(k)H(k)e^{j\frac{2\pi}{N}kn}$$

Recognizing that the right-hand side of this equation is the inverse DFT of the product $X(k)H(k)$ proves the DFT transform pair of Equation 1.17.

The dual to the convolution multiplication property can also be proved in a similar manner. This property states that multiplication in the time domain is equivalent to convolution in the frequency domain

$$v(n)x(n) \xleftrightarrow{\text{DFT}} \frac{1}{N}V(k) \textcircled{N} X(k). \tag{1.18}$$

Example 1.2

In this example we compute the four-point circular convolution of the following sequences:

$$x(n) = \{\underset{\downarrow}{5},2,1,3\}, \quad h(n) = \{\underset{\downarrow}{1},2,3,4\} \tag{1.19}$$

Equation 1.16 shows that each output $y(n)$ is computed from an inner product of $x(n)$ and a time reversed and shifted $h(n)$. Thus, for example, $y(0)$ is computed as

$$y(0) = \sum_{k=0}^{3} x(k)h(-k) = 5\cdot 1 + 2\cdot 4 + 1\cdot 3 + 3\cdot 2 = 22.$$

Figure 1.4 shows the circular convolution process and the resulting convolution output.

Index	0	1	2	3	
$x(k)$	5	2	1	3	$y(n)$
$h(-k)$	1	4	3	2	22
$h(1-k)$	2	1	4	3	25
$h(2-k)$	3	2	1	4	32
$h(3-k)$	4	3	2	1	31
$y(n)$	22	25	32	31	

FIGURE 1.4 This figure tabulates the circular convolution of two length 4 time sequences given in Equation 1.19. To compute the output $y(n)$, take the inner (dot) product of the row labeled $x(k)$ with a time-reversed and shifted impulse response row $h(n-k)$. The output of each inner product is shown to the right of the corresponding $h(n-k)$, and also repeated (to give the correct time index values) on the bottom row.

1.3.4 Duality

As can be seen from Equations 1.1 and 1.2, the forward and inverse DFT differ by only a sign in the exponent and a scaling factor. This similarity leads to the duality property which states that if the DFT of $x(n)$ is $X(k)$, then

$$\frac{1}{N}X(n) \xleftrightarrow{\text{DFT}} x(-k).$$

The proof of this property is

$$\frac{1}{N}X(n) \xleftrightarrow{\text{DFT}} \sum_{n=0}^{N-1}\frac{1}{N}X(n)e^{-j\frac{2\pi}{N}kn} = \frac{1}{N}\sum_{n=0}^{N-1}X(n)e^{j\frac{2\pi}{N}(-k)n} = x(-k).$$

This property has theoretic usefulness in that any forward DFT property can be changed into an inverse property, and vice versa. It also has a practical application. Memory-limited computer systems only need to store a forward DFT routine. The inverse DFT, according to the duality property, can then be computed from the forward DFT by the three-step process of: (1) scaling by $1/N$, (2) forward DFT, and (3) time reversal.

1.3.5 Conjugate Property

This property is useful for determining symmetries and also for proving Parseval's theorem. Given a DFT pair, $x(n)$ and $X(k)$, the DFT of the conjugate is

$$x^*(n) \xleftrightarrow{\text{DFT}} X^*(N-k). \tag{1.20}$$

This property is proved as follows:

$$\sum_{n=0}^{N-1}x^*(n)e^{-j\frac{2\pi}{N}kn} = \sum_{n=0}^{N-1}\left(x(n)e^{j\frac{2\pi}{N}kn}\right)^* = \left(\sum_{n=0}^{N-1}(x(n)e^{-j\frac{2\pi}{N}(-k)n}\right)^* = X^*(-k) = X^*(N-k).$$

1.3.6 Symmetries

Signals which are symmetric about the origin, and thus equal their time reversal, are said to be even. An even DFT time sequence thus satisfies

$$x_e(n) = x_e(-n) = x_e(N-n).$$

Sequences which are antisymmetric about the origin are called odd and satisfy

$$x_o(n) = -x_o(-n) = -x_o(N-n).$$

Using these definitions, we now examine the symmetry properties of DFT transforms of real sequences. Real sequences are equal to their conjugates, $x(n) = x^*(n)$. Using the conjugate property (1.20) and noting that the DFT coefficients are unique result in

$$X(k) = X^*(N-k). \tag{1.21}$$

Signals that satisfy Equation 1.21 are called conjugate symmetric. Thus, conjugate symmetric sequences equal the conjugate of their time reversal. Writing Equation 1.21 in terms of real and imaginary parts results in

$$X_R(k) + jX_I(k) = X_R(N-k) - jX_I(N-k),$$

from which we derive the following equalities:

$$\begin{aligned} X_R(k) &= X_R(N-k) \\ X_I(k) &= -X_I(N-k). \end{aligned} \tag{1.22}$$

This shows that for real input sequences the real part of the DFT is even, and the imaginary part is odd.

If we further restrict the real function to be even, we get

$$\begin{aligned} \sum_{n=0}^{N-1} x_e(n) e^{-j\frac{2\pi}{N}kn} &= \sum_{n=0}^{N-1} x_e(n)\cos\left(\frac{2\pi}{N}kn\right) - j\sum_{n=0}^{N-1} x_e(n)\sin\left(\frac{2\pi}{N}kn\right) \\ &= \sum_{n=0}^{N-1} x_e(n)\cos\left(\frac{2\pi}{N}kn\right) = X_R(k). \end{aligned} \tag{1.23}$$

The imaginary term in the equation above is zero since the product $x_e(n)\sin(2\pi nk/N)$ is odd, and the sum over one period of an odd periodic function is zero. Thus, the DFT transform coefficients of an even real sequence are both real (by 1.23) and even (by 1.22). In a similar manner it can be shown that the DFT of an odd real sequence $x_o(n)$ results in a sequence that is both imaginary and odd.

1.3.7 Parseval's Theorem

Parseval's theorem is not a transform pair, but rather an equality. The theorem states that the energy in the time sequence coefficients equals the energy in the DFT transform coefficients:

$$\sum_{n=0}^{N-1} |x(n)|^2 = \frac{1}{N}\sum_{k=0}^{N-1} |X(k)|^2. \tag{1.24}$$

Proof of this theorem starts with the two sequences $x(n)$ and $y^*(n)$. Using the multiplication property (1.18) and conjugate property (1.20) gives the following DFT pair:

$$x(n)y^*(n) \xleftrightarrow{\text{DFT}} \frac{1}{N} X(k) \circledast Y^*(N-k).$$

Writing this pair as an equality gives

$$\sum_{n=0}^{N-1} x(n)y^*(n)e^{-j\frac{2\pi}{N}kn} = \frac{1}{N}\sum_{l=0}^{N-1} X(l)Y^*((l-k))_N.$$

Setting $k = 0$ results in the general form of Parseval's theorem

$$\sum_{n=0}^{N-1} x(n)y^*(n) = \frac{1}{N}\sum_{l=0}^{N-1} X(l)Y^*(l). \tag{1.25}$$

The energy equality form of Parseval's theorem (1.24) follows from Equation 1.25 by setting $x(n) = y(n)$.

1.3.8 Zero Padding and Linear Convolution

In most practical situations it is linear convolution that is needed and not the circular convolution provided by the DFT. Using a straightforward technique called zero padding allows the DFT to compute linear convolution using circular convolution. Zero padding is the lengthening of a sequence through the addition of zeros so that it can be used in a larger-sized DFT. The effect of zero padding can be seen from the viewpoint of the DFT as a sampled DTFT. Recall that for a time sequence of length L, the DFT must have a length of at least $N = L$ to avoid time aliasing, which corresponds to N DTFT frequency samples (see Section 1.2.2). Using a DFT length of $N > L$ also avoids time aliasing and results in an invertible DFT. For this case of $N > L$, the input time vector needs additional values for the indices $L \le n \le N-1$, and these are provided by zero padding. The effect of zero padding on the DFT can be seen by noting that the original length L sequence and the zero-padded length N sequence both have exactly the same DTFT. Thus, increasing the DFT length only serves to sample the DTFT frequency response more densely. This effect is demonstrated in Figure 1.5.

Using zero padding allows circular convolution to compute linear convolution. The key point to note is that when convolving a length L sequence with a length M sequence, the result is a length $L + M - 1$ sequence. Using a DFT length of $N \ge L + M - 1$ avoids the "aliasing" wrap around from circular convolution, and results in linear convolution. This is demonstrated in Figure 1.6 where the convolution of Example 1.2 is repeated with zero padding.

1.4 Fast Fourier Transforms

The Fast Fourier transform (FFT) refers to algorithms that reduce the number of computations required to compute the DFT. The savings achieved by the FFT can be dramatic, usually reducing the computational load by orders of magnitude versus the DFT. In fact, the computational savings in computing the DFT provided by the FFT was a major factor in digital signal processing becoming a major research and application area. It should be noted that the DFT and FFT both give the same results, and differ only in implementation. For example, the popular computing package MATLAB® does not have a "DFT" routine but only an "FFT" routine.

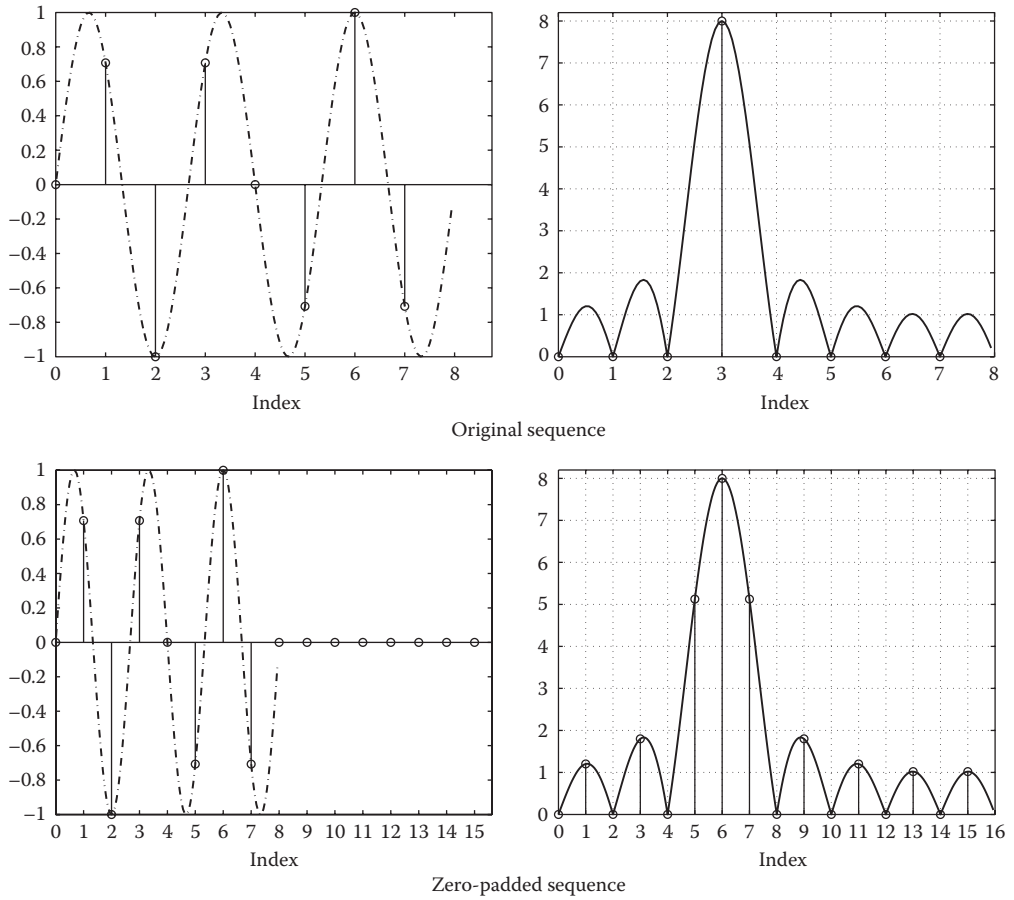

FIGURE 1.5 These plots illustrate the effect of zero padding the DFT. The top left shows the (real) samples of a complex sinusoid of length 8. The top right shows the magnitude of both the DTFT (solid line) and DFT (samples). The bottom figures show what happens when the identical input is zero padded to length 16. Note that the DTFT remains unchanged. However, since the length of the DFT has doubled, the DFT sampling density of the DTFT is twice that of the original length 8 DFT.

Index	0	1	2	3	4	5	6	
$x(k)$	5	2	1	3	0	0	0	$y(n)$
$h(-k)$	1	0	0	0	4	3	2	5
$h(1-k)$	2	1	0	0	0	4	3	12
$h(2-k)$	3	2	1	0	0	0	4	20
$h(3-k)$	4	3	2	1	0	0	0	31
$h(4-k)$	0	4	3	2	1	0	0	17
$h(5-k)$	0	0	4	3	2	1	0	13
$h(6-k)$	0	0	0	4	3	2	1	12
$y(n)$	5	12	20	31	17	13	12	

FIGURE 1.6 This figure repeats the convolution example of Figure 1.4 except that the sequences have been zero padded to guarantee that the resulting convolution is linear. Note, for example, that the values of $h(-k)$ that wrap around due to circular shifting now are multiplied by zero values of $x(k)$. Thus zero padding eliminates "collisions" due to the wrap around of circular shifting.

To understand the computational savings of the FFT, we first examine the computational requirements of the DFT. Referring to the DFT definition (1.1) or the matrix form of Equation 1.14, we see that the computation of each DFT frequency coefficient requires an N point inner product. We assume throughout our the discussion that the time sequence $x(n)$ is complex valued. Thus, to compute each value $X(k)$ requires N complex multiplies, resulting in a total of N^2 complex multiplies to compute the entire DFT. The most commonly used FFT algorithms can compute the DFT using only $\mathcal{O}(N\log_2 N)$ complex multiplies. Specifically, for the power of 2 FFT shown below, only $(N/2)\log_2 N$ multiplies are required.

To appreciate the savings offered by the FFT, consider the ratio of $N^2/((N/2)\log_2 N)$. For $N = 1024$ the ratio is 204.8. Using a time analogy where time is proportional to multiplies, 1 min to compute the FFT would require nearly 3.5 h for the DFT. For length $2^{15} = 32k$, the ratio is 4369 and 1 min for the FFT stretches out to over 3 days for the DFT to compute the same result.

In the following we derive the FFT for the most common case of N being a power of 2 ($N = 2^l$, l an integer). We start with the equation for the forward DFT (1.1) and divide it into sums over even- and odd-indexed coefficients

$$X(k) = \sum_{n,\text{even}} x(n)W_N^{kn} + \sum_{n,\text{odd}} x(n)W_N^{kn}.$$

Representing the even and odd indices with $n = 2m$ and $n = 2m + 1$, respectively, gives

$$X(k) = \sum_{m=0}^{\frac{N}{2}-1} x(2m)W_N^{2km} + W_N^k \sum_{m=0}^{\frac{N}{2}-1} x(2m+1)W_N^{2km}.$$

Observing that

$$W_N^{2km} = e^{-j\frac{2\pi}{N}2km} = e^{-j\frac{2\pi}{N/2}km} = W_{\frac{N}{2}}^{km},$$

the previous equation simplifies to

$$X(k) = \sum_{m=0}^{\frac{N}{2}-1} x(2m)W_{\frac{N}{2}}^{km} + W_N^k \sum_{m=0}^{\frac{N}{2}-1} x(2m+1)W_{\frac{N}{2}}^{km}.$$

We recognize the first term in the previous equation as the $N/2$ point DFT of the even-indexed inputs, and the second term as W_N^k times the $N/2$ point DFT of the odd-indexed inputs. Denoting these DFTs as $A(k)$ and $B(k)$, respectively, and noting the fact that these DFTs are periodic with period $N/2$, we can write this equation as

$$X(k) = A(k) + W_N^k B(k), \quad k = 0,1,\ldots,\frac{N}{2}-1$$
$$X\left(k+\frac{N}{2}\right) = A(k) + W_N^{\left(k+\frac{N}{2}\right)}B(k), \quad k = 0,1,\ldots,\frac{N}{2}-1.$$

An additional savings in multiplies results from noting that

$$W_N^{k+\frac{N}{2}} = e^{-j\frac{2\pi}{N}k}e^{-j\frac{2\pi}{N}\left(\frac{N}{2}\right)} = e^{-j\frac{2\pi}{N}k}e^{-j\pi} = -W_N^k,$$

which allows the results to be written

$$X(k) = A(k) + W_N^k B(k), \quad k = 0,1,\ldots,\frac{N}{2} - 1$$
$$X\left(k + \frac{N}{2}\right) = A(k) - W_N^k B(k), \quad k = 0,1,\ldots,\frac{N}{2} - 1.$$

The previous shows that computation of an N point DFT can be done by computing two $N/2$ point DFTs, weighting the coefficients of one DFT by W_N^k, and adding or subtracting from these results. This is shown in Figure 1.7 for a length 8 DFT using flow graph notation. Significant computational savings results since no additional multiplies are required to compute the last $N/2$ coefficients. All these products were already computed when determining the first $N/2$ coefficients.

The simplification process continues by dividing each $N/2$ DFT into two $N/4$ DFTs, and then into four $N/8$ DFTs, and so on, until all DFTs are length 2. The resulting structure is called a decimation in time (DIT) FFT, and an example DIT FFT for $N = 8$ is shown in Figure 1.8. The total number of multiplies needed to compute the FFT can be determined by noting that each stage of the FFT requires $N/2$ multiplies by the factors W_α^k. Since a length N FFT requires $\log_2 N$ stages, the total number of complex multiplies required is $\frac{N}{2}\log_2 N$. As mentioned previously, this is a significant savings over the N^2 complex multiplies required by direct computation of the DFT. Although this discussion only derived the power of two FFT, similar methods yield FFTs for arbitrary DFT lengths.

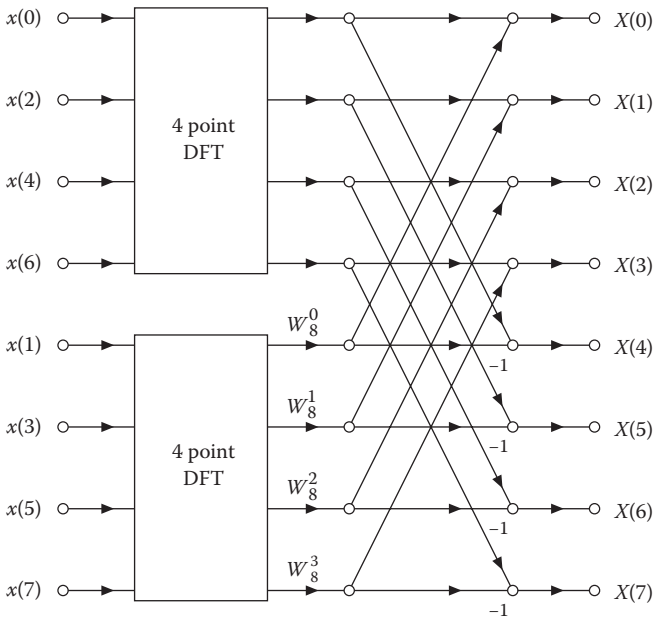

FIGURE 1.7 This figure shows how a DFT of length 8 can be computed by combining the outputs of two length 4 DFTs of the even- and odd-indexed inputs.

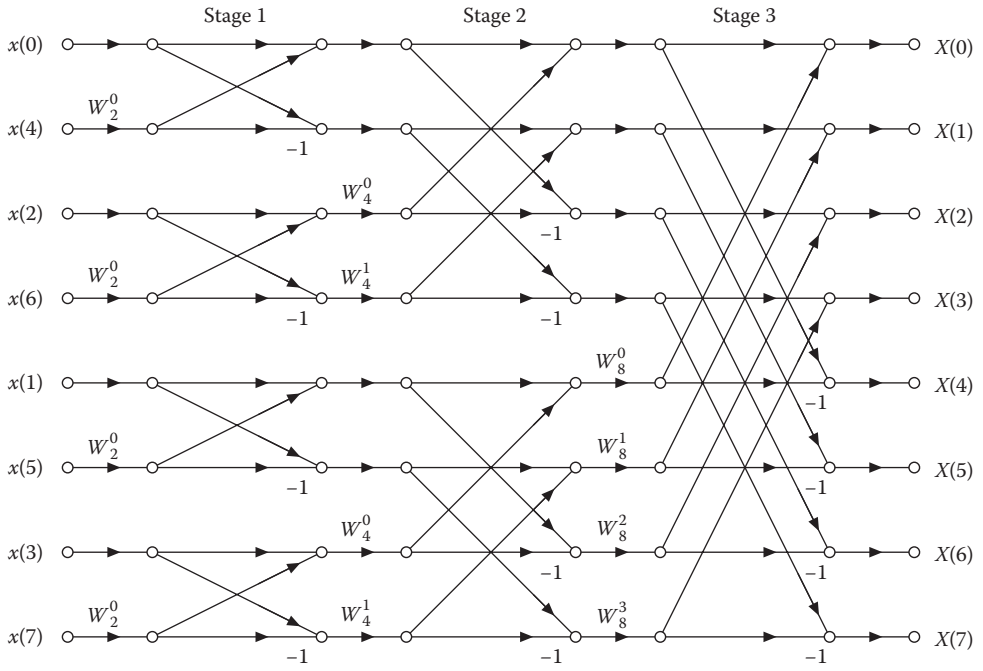

FIGURE 1.8 This figure shows the signal flow diagram of a full decimation in time FFT for $N = 8$. Observe that the output indices are in numerical order, whereas the input indices are in bit-reversed order.

Bibliography

1. L. Ludeman. *Fundamentals of Digital Signal Processing*. New York: Harper & Row, 1986.
2. S. Mitra. *Digital Signal Processing*. New York: McGraw-Hill, 2006.
3. A. Oppenheim and R. Schafer. *Discrete-Time Signal Processing*. NJ: Prentice-Hall, 1989.
4. J. Proakis and D. Manolakis. *Digital Signal Processing*. NJ: Prentice-Hall, 2007.

2

Pulse Code Modulation*

Leon W. Couch II

2.1 Introduction

Pulse code modulation (PCM) is analog-to-digital conversion of a special type where the information contained in the instantaneous samples of an analog signal is represented by digital words in a serial bit stream.

If we assume that each of the digital words has n binary digits, there are $M = 2^n$ unique code words that are possible, each code word corresponding to a certain amplitude level. Each sample value from the analog signal, however, can be any one of an infinite number of levels, so that the digital word that represents the amplitude closest to the actual sampled value is used. This is called quantizing. That is, instead of using the exact sample value of the analog waveform, the sample is replaced by the closest allowed value, where there are M allowed values, and each allowed value corresponds to one of the code words.

PCM is very popular because of the many advantages it offers. Some of these advantages are as follows:

- Relatively inexpensive digital circuitry may be used extensively in the system.
- PCM signals derived from all types of analog sources (audio, video, etc.) may be time-division multiplexed with data signals (e.g., from digital computers) and transmitted over a common high-speed digital communication system.
- In long-distance digital telephone systems requiring repeaters, a *clean* PCM waveform can be regenerated at the output of each repeater, where the input consists of a noisy PCM waveform. The noise at the input, however, may cause bit errors in the regenerated PCM output signal.
- The noise performance of a digital system can be superior to that of an analog system. In addition, the probability of error for the system output can be reduced even further by the use of appropriate coding techniques.

These advantages usually outweigh the main disadvantage of PCM: a much wider bandwidth than that of the corresponding analog signal.

2.2 Generation of PCM

The PCM signal is generated by carrying out three basic operations: sampling, quantizing, and encoding (see Figure 2.1). The sampling operation generates an instantaneously sampled flat-top pulse-amplitude modulated (PAM) signal.

The quantizing operation is illustrated in Figure 2.2 for the $M = 8$ level case. This quantizer is said to be *uniform* since all the steps are of equal size. Since we are approximating the analog sample values by using a finite number of levels ($M = 8$ in this illustration), *error* is introduced into the recovered output analog signal because of the quantizing effect. The error waveform is illustrated in Figure 2.2c. The quantizing error consists of the difference between the analog signal at the sampler input and the output of the quantizer. Note that the peak value of the error (±1) is one-half of the quantizer step size (2). If we sample at the Nyquist rate ($2B$, where B is the absolute bandwidth, in hertz, of the input analog signal) or faster and there is negligible channel noise, there will still be noise, called *quantizing noise*, on the recovered analog waveform due to this error. The quantizing noise can also be thought of as a round-off error. The quantizer output is a *quantized* (i.e., only M possible amplitude values) PAM signal.

The PCM signal is obtained from the quantized PAM signal by encoding each quantized sample value into a digital word. It is up to the system designer to specify the exact code word that will represent a particular quantized level. If a Gray code of Table 2.1 is used, the resulting PCM signal is shown in Figure 2.2d where the PCM word for each quantized sample is strobed and put off the encoder by the next clock pulse. The Gray code was chosen because it has only 1-b change for each step change in the quantized level. Consequently, single errors in the received PCM code word will cause minimum errors in the recovered analog level, provided that the sign bit is not in error.

Here we have described PCM systems that represent the quantized analog sample values by *binary* code words. Of course, it is possible to represent the quantized analog samples by digital words using other than base 2. That is, for base q, the number of quantized levels allowed is $M = q^n$, where n is the number of q base digits in the code word. We will not pursue this topic since binary ($q = 2$) digital circuits are most commonly used.

2.3 Percent Quantizing Noise

The quantizer at the PCM encoder produces an error signal at the PCM decoder output as illustrated in Figure 2.2c. The peak value of this error signal may be expressed as a percentage of the maximum possible analog signal amplitude. Referring to Figure 2.2c, a peak error of 1 V occurs for a maximum analog signal amplitude of $M = 8$ V as shown in Figure 2.1c. Thus, in general,

$$\frac{2P}{100} = \frac{1}{M} = \frac{1}{2^n}$$

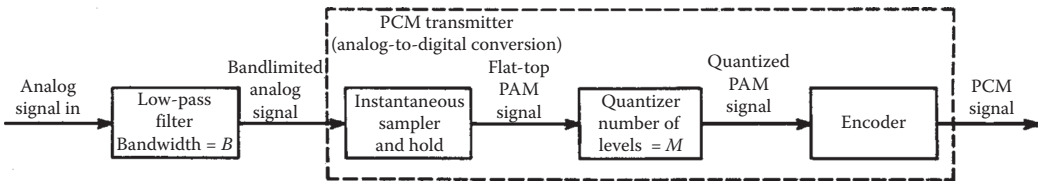

FIGURE 2.1 A PCM transmitter. (From Couch, L.W. II., *Digital and Analog Communication Systems*, 5th ed. Upper Saddle River, NJ: Prentice-Hall, p. 138, 1997. With permission.)

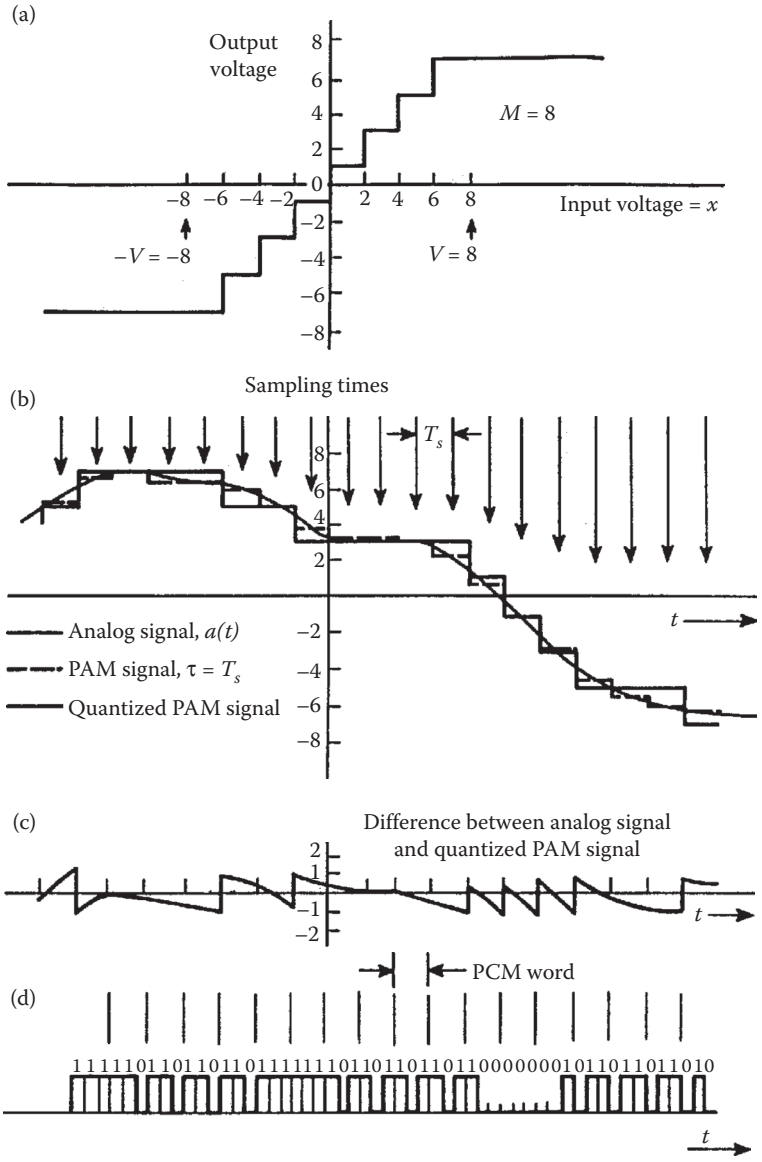

FIGURE 2.2 Illustration of waveforms in a PCM system. (a) Quantizer output–input characteristics. (b) Analog signal, flat-top PAM signal, and quantized PAM signal. (c) Error signal. (d) PCM signal. (From Couch, L.W. II., *Digital and Analog Communication Systems*, 7th ed. Copyright 2007, p. 140. Used by permission of Pearson Education, Inc. Upper Saddle River, NJ.)

or

$$2^n = \frac{50}{P} \tag{2.1}$$

where P is the peak percentage error for a PCM system that uses n bit code words. The design value of n needed in order to have less than P percent error is obtained by taking the base 2 logarithm

TABLE 2.1 3-b Gray Code for $M = 8$ Levels

Quantized Sample Voltage	Gray Code Word (PCM Output)	
+7	110	
+5	111	
+3	101	
+1	100	
−1	000	Mirror image except for sign bit
−3	001	
−5	011	
−7	010	

Source: From Couch, L.W., II., *Digital and Analog Communication Systems*, 7th ed. Copyright 2007, p. 141. Reprinted with permission of Pearson Education, Inc., Upper Saddle River, NJ.

of both sides of Equation 2.1, where it is realized that $\log_2(x) = [\log_{10}(x)]/\log_{10}(2) = 3.32 \log_{10}(x)$. That is,

$$n \geq 3.32 \log_{10}\left(\frac{50}{P}\right) \tag{2.2}$$

where n is the number of bits needed in the PCM word in order to obtain less than P percent error in the recovered analog signal (i.e., decoded PCM signal).

2.4 Practical PCM Circuits

Six techniques are used to implement the analog-to-digital converter (ADC) encoding operation: the *counting or ramp, serial or successive approximation, direct conversion or flash, delta-encoded, pipeline, sigma–delta* encoders. For a description of the encoding methods, see http://en/wikipedia.org. These techniques will be discussed in the following paragraphs.

In the counting encoder, at the same time that the sample is taken, a ramp generator is energized and a binary counter is started. The output of the ramp generator is continuously compared to the sample value; when the value of the ramp becomes equal to the sample value, the binary value of the counter is read. This count is taken to be the PCM word. The binary counter and the ramp generator are then reset to zero and are ready to be reenergized at the next sampling time. This technique requires only a few components, but the speed of this type of ADC is usually limited by the speed of the counter. The Maxim ICL7126 CMOS ADC integrated circuit uses this technique.

The serial encoder compares the value of the sample with trial quantized values. Successive trials depend on whether the past comparator outputs are positive or negative. The trial values are chosen first in large steps and then in small steps so that the process will converge rapidly. The trial voltages are generated by a series of voltage dividers that are configured by (on–off) switches. These switches are controlled by digital logic. After the process converges, the value of the switch settings is read out as the PCM word. This technique requires more precision components (for the voltage dividers) than the ramp technique. The speed of the feedback ADC technique is determined by the speed of the switches. The analog devices AD7923 12-bit ADC uses serial encoding.

The direct conversion or flash encoder uses a set of parallel comparators with reference levels that are the permitted quantized values. The sample value is fed into all of the parallel comparators simultaneously. The high or low level of the comparator outputs determines the binary PCM word with the aid of some digital logic. This is a fast ADC technique, but requires more hardware than the other two methods. The Maxim MAX104 8-bit ADC integrated circuit is an example of this technique.

Some ADCs have parallel output (such as the MAX104). In this case, for the generation of PCM, the parallel output (digital word) needs to be converted to serial form for transmission over a two-wire channel. This conversion is accomplished by using a parallel-to-serial converter integrated circuit, which is also known as a serial-input–output (SIO) chip. The SIO chip includes a shift register that is set to contain the parallel data (usually, from 8 or 16 input lines). Then the data are shifted out of the last stage of the shift register bit by bit onto a single output line to produce the serial format. Furthermore, the SIO chips are usually full duplex, that is, they have two sets of shift registers, one that functions for data flowing in each direction. One shift register converts parallel input data to serial output data for transmission over the channel, and, simultaneously, the other shift register converts received serial data from another input to parallel data that are available at another output. Three types of SIO chips are available: the *universal asynchronous receiver/transmitter* (UART), the *universal synchronous receiver/transmitter* (USRT), and the *universal synchronous/asynchronous receiver transmitter* (USART). The UART transmits and receives asynchronous serial data, the USRT transmits and receives synchronous serial data, and the USART combines both a UART and a USRT on one chip.

At the receiving end, the PCM signal is decoded back into an analog signal by using a digital-to-analog converter (DAC) chip. If the DAC chip has a parallel data input, the received serial PCM data are first converted to a parallel form using an SIO chip as described in the preceding paragraph. The parallel data are then converted to an approximation of the analog sample value by the DAC chip. This conversion is usually accomplished by using the parallel digital word to set the configuration of electronic switches on a resistive current (or voltage) divider network so that the analog output is produced. This is called a *multiplying* DAC since the analog output voltage is directly proportional to the divider reference voltage multiplied by the value of the digital word. The National Semiconductor DAC0808 8-b DAC chips is an example of this technique. The DAC chip outputs samples of the quantized analog signal that approximates the analog sample values. This may be smoothed by a low-pass reconstruction filter to produce the analog output.

Semiconductor companies manufacture several hundred types of ADC and DAC circuits. Data sheets for these ICs can be found on the Web pages of these manufacturers. Many of the ICs are designed for specific applications. For example, the AD1861 from Analog Devices is a PCM audio DAC that generates analog audio from the PCM data on compact disks. The Texas Instruments TP3056B is a PCM codec for encoding and decoding PCM data signals for telephone analog audio applications.

The Communications Handbook [1, pp. 107–117] and *The Electrical Engineering Handbook* [2, pp. 771–782] give more details on ADC, DAC, and PCM circuits.

2.5 Bandwidth of PCM

A good question to ask is: What is the spectrum of a PCM signal? In the case of PAM signaling, the spectrum of the PAM signal could be obtained as a function of the spectrum of the input analog signal because the PAM signal is a linear function of the analog signal. This is not the case for PCM. As shown in Figures 2.1 and 2.2, the PCM signal is a nonlinear function of the input signal. Consequently, the spectrum of the PCM signal is not directly related to the spectrum of the input analog signal. It can be shown that the spectrum of the PCM signal depends on the bit rate, the correlation of the PCM data, and on the PCM waveform pulse shape (usually rectangular) used to describe the bits [3,4]. From Figure 2.2, the bit rate is

$$R = nf_s \tag{2.3}$$

where n is the number of bits in the PCM word ($M = 2^n$) and f_s is the sampling rate. For no aliasing we require $f_s \geq 2B$ where B is the bandwidth of the analog signal (i.e., to be converted to the PCM

signal). The dimensionality theorem [3,4] shows that the bandwidth of the PCM waveform is bounded by

$$B_{\text{PCM}} \geq \frac{1}{2}R = \frac{1}{2}nf_s \tag{2.4}$$

where equality is obtained if a $(\sin x)/x$ type of pulse shape is used to generate the PCM waveform. The exact spectrum for the PCM waveform will depend on the pulse shape that is used as well as on the type of line encoding. For example, if one uses a rectangular pulse shape with polar nonreturn to zero (NRZ) line coding, the first null bandwidth is simply

$$B_{\text{PCM}} = R = nf_s \text{ Hz} \tag{2.5}$$

Table 2.2 presents a tabulation of this result for the case of the minimum sampling rate, $f_s = 2B$. Note that Equation 2.4 demonstrates that the bandwidth of the PCM signal has a lower bound given by

$$B_{\text{PCM}} \geq nB \tag{2.6}$$

where $f_s > 2B$ and B is the bandwidth of the corresponding analog signal. Thus, for reasonable values of n, the bandwidth of the PCM signal will be significantly larger than the bandwidth of the corresponding analog signal that it represents. For the example shown in Figure 2.2 where $n = 3$, the PCM signal bandwidth will be at least three times wider than that of the corresponding analog signal. Furthermore, if the bandwidth of the PCM signal is reduced by improper filtering or by passing the PCM signal through a system that has a poor frequency response, the filtered pulses will be elongated (stretched in width) so that pulses corresponding to any one bit will smear into adjacent bit slots. If this condition becomes too serious, it will cause errors in the detected bits. This pulse smearing effect is called *intersymbol interference* (*ISI*).

TABLE 2.2 Performance of a PCM System with Uniform Quantizing and No-Channel Noise

Number of Quantizer Levels Used (M)	Length of the PCM Word, n (bits)	Bandwidth of PCM Signal (First Null Bandwidth)[a]	Recovered Analog Signal Power-to-Quantizing Noise Power Ratios (dB) $(S/N)_{\text{out}}$
2	1	$2B$	6.0
4	2	$4B$	12.0
8	3	$6B$	18.1
16	4	$8B$	24.1
32	5	$10B$	30.1
64	6	$12B$	36.1
128	7	$14B$	42.1
256	8	$16B$	48.2
512	9	$18B$	54.2
1024	10	$20B$	60.2
2048	11	$22B$	66.2
4096	12	$24B$	72.2
8192	13	$26B$	78.3
16,384	14	$28B$	84.3
32,768	15	$30B$	90.3
65,536	16	$32B$	96.3

Source: Couch, L.W. II., *Digital and Analog Communication Systems*, 7th ed. Copyright 2007, p. 144. Reprinted with permission of Pearson Education, Inc., Upper Saddle River, NJ.

[a] B is the absolute bandwidth of the input analog signal.

2.6 Effects of Noise

The analog signal that is recovered at the PCM system output is corrupted by noise. Two main effects produce this noise or distortion: (1) quantizing noise that is caused by the M-step quantizer at the PCM transmitter and (2) bit errors in the recovered PCM signal. The bit errors are caused by *channel noise* as well as improper channel filtering, which causes ISI. In addition, if the input analog signal is not strictly band limited, there will be some aliasing noise on the recovered analog signal [5]. Under certain assumptions, it can be shown that the recovered analog *average* signal power to the average noise power [3] is

$$\left(\frac{S}{N}\right)_{\text{out}} = \frac{M^2}{1 + 4(M^2 - 1)P_e} \tag{2.7}$$

where M is the number of uniformly spaced quantizer levels used in the PCM transmitter and P_e is the probability of bit error in the recovered binary PCM signal at the receiver DAC before it is converted back into an analog signal. Most practical systems are designed so that P_e is negligible. Consequently, if we assume that there are no bit errors due to channel noise (i.e., $P_e = 0$), the S/N due only to quantizing errors is

$$\left(\frac{S}{N}\right)_{\text{out}} = M^2 \tag{2.8}$$

Numerical values for these S/N ratios are given in Table 2.2.

To realize these S/N ratios, one critical assumption is that the peak-to-peak level of the analog waveform at the input to the PCM encoder is set to the design level of the quantizer. For example, referring to Figure 2.2, this corresponds to the input traversing the range $-V$ to $+V$ volts where $V = 8$ V is the design level of the quantizer. Equation 2.7 was derived for waveforms with equally likely values, such as a triangle waveshape, that have a peak-to-peak value of 2 V and an rms value of $V/\sqrt{3}$, where V is the design peak level of the quantizer.

From a practical viewpoint, the quantizing noise at the output of the PCM decoder can be categorized into four types depending on the operating conditions. The four types are overload noise, random noise, granular noise, and hunting noise. As discussed earlier, the level of the analog waveform at the input of the PCM encoder needs to be set so that its peak level does not exceed the design peak of V volts. If the peak input does exceed V, the recovered analog waveform at the output of the PCM system will have flat tops near the peak values. This produces *overload noise*. The flat tops are easily seen on an oscilloscope, and the recovered analog waveform sounds distorted since the flat topping produces unwanted harmonic components. For example, this type of distortion can be heard on PCM telephone systems when there are high levels such as dial tones, busy signals, or off-hook warning signals.

The second type of noise, *random noise*, is produced by the random quantization errors in the PCM system under normal operating conditions when the input level is properly set. This type of condition is assumed in Equation 2.8. Random noise has a white hissing sound. If the input level is not sufficiently large, the S/N will deteriorate from that given by Equation 2.8; the quantizing noise will still remain more or less random.

If the input level is reduced further to a relatively small value with respect to the design level, the error values are not equally likely from sample to sample, and the noise has a harsh sound resembling gravel being poured into a barrel. This is called *granular noise*. This type of noise can be randomized (noise power decreased) by increasing the number of quantization levels and, consequently, increasing the PCM bit rate. Alternatively, granular noise can be reduced by using a nonuniform quantizer, such as the μ-law or A-law quantizers that are described in Section 2.7.

The fourth type of quantizing noise that may occur at the output of a PCM system is *hunting noise*. It can occur when the input analog waveform is nearly constant, including when there is no signal

(i.e., zero level). For these conditions the sample values at the quantizer output (see Figure 2.2) can oscillate between two adjacent quantization levels, causing an undesired sinusoidal-type tone of frequency $1/2f_s$ at the output of the PCM system. Hunting noise can be reduced by filtering out the tone or by designing the quantizer so that there is no vertical step at the constant value of the inputs, such as at 0-V input for the no-signal case. For the no-signal case, the hunting noise is also called *idle channel noise*. Idle channel noise can be reduced by using a horizontal step at the origin of the quantizer output–input characteristic instead of a vertical step as shown in Figure 2.2.

Recalling that $M = 2^n$, we may express Equation 2.8 in decibels by taking $10 \log_{10}(\cdot)$ of both sides of the equation

$$\left(\frac{S}{N}\right)_{\text{dB}} = 6.02n + \alpha \tag{2.9}$$

where n is the number of bits in the PCM word and $\alpha = 0$. This equation—called the 6-dB rule—points out the significant performance characteristic for PCM: an additional 6-dB improvement in S/N is obtained for each bit added to the PCM word. This is illustrated in Table 2.2. Equation 2.9 is valid for a wide variety of assumptions (such as various types of input waveshapes and quantification characteristics), although the value of α will depend on these assumptions [6]. Of course, it is assumed that there are no bit errors and that the input signal level is large enough to range over a significant number of quantizing levels.

One may use Table 2.2 to examine the design requirements in a proposed PCM system. For example, high-fidelity enthusiasts are turning to digital audio recording techniques. Here PCM signals are recorded instead of the analog audio signal to produce superb sound reproduction. For a dynamic range of 90 dB, it is seen that at least 15-b PCM words would be required. Furthermore, if the analog signal had a bandwidth of 20 kHz, the first null bandwidth for rectangular bit-shape PCM would be $2 \times 20 \text{ kHz} \times 15 = 600$ kHz. Consequently, video-type tape recorders are needed to record and reproduce high-quality digital audio signals. Although this type of recording technique might seem ridiculous at first, it is realized that expensive high-quality analog recording devices are hard pressed to reproduce a dynamic range of 70 dB. Thus, digital audio is one way to achieve improved performance. This is being proven in the marketplace with the popularity of the digital compact disk (CD). The CD uses a 16-b PCM word and a sampling rate of 44.1 kHz on each stereo channel [7,8]. Reed–Solomon coding with interleaving is used to correct burst errors that occur as a result of scratches and fingerprints on the compact disk.

2.7 Nonuniform Quantizing: μ-Law and *A*-Law Companding

Voice analog signals are more likely to have amplitude values near zero than at the extreme peak values allowed. For example, when digitizing voice signals, if the peak value allowed is 1 V, weak passages may have voltage levels of the order of 0.1 V (20 dB down). For signals such as these with nonuniform amplitude distribution, the granular quantizing noise will be a serious problem if the step size is not reduced for amplitude values near zero and increased for extremely large values. This is called nonuniform quantizing since a variable step size is used. An example of a nonuniform quantizing characteristic is shown in Figure 2.3.

The effect of nonuniform quantizing can be obtained by first passing the analog signal through a compression (nonlinear) amplifier and then into the PCM circuit that uses a uniform quantizer. In the United States, a μ-law type of compression characteristic is used. It is defined [9] by

$$|w_2(t)| = \frac{\ln\left(1 + \mu |w_1(t)|\right)}{\ln(1 + \mu)} \tag{2.10}$$

where the allowed peak values of $w_1(t)$ are ±1 (i.e., $|w_1(t)| \leq 1$), μ is a positive constant that is a parameter. This compression characteristic is shown in Figure 2.3b for several values of μ, and it is noted that

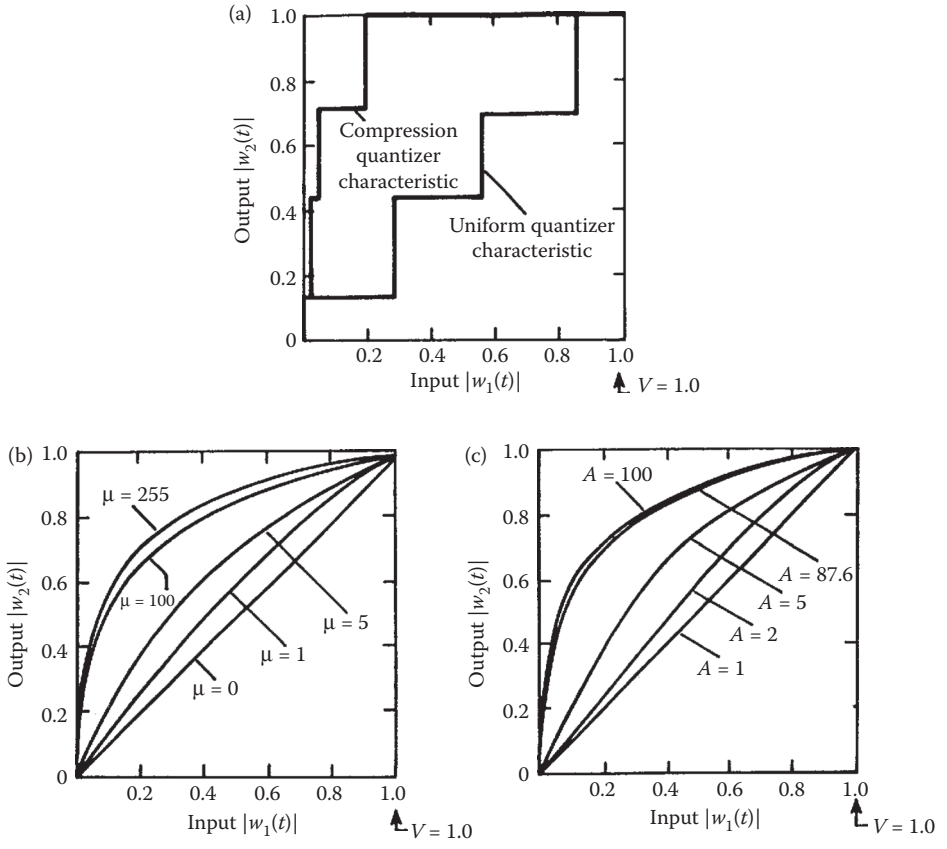

FIGURE 2.3 Compression characteristics (first quadrant shown). (a) $M = 8$ Quantizer characteristic. (b) μ-Law characteristic. (c) A-Law characteristic. (From Couch, L.W. II., *Digital and Analog Communication Systems*, 7th ed. Copyright 2007, p. 148. Reprinted with permission of Pearson Education, Inc., Upper Saddle River, NJ.)

$\mu \to 0$ corresponds to linear amplification (uniform quantization overall). In the United States, Canada, and Japan, the telephone companies use a $\mu = 255$ compression characteristic in their PCM systems [10].

Another compression law, used mainly in Europe, is the A-law characteristic. It is defined [9] by

$$|w_2(t)| = \begin{cases} \dfrac{A|w_1(t)|}{1 + \ln A}, & 0 \le |w_1(t)| \le \dfrac{1}{A} \\ \dfrac{1 + \ln\left(A|w_1(t)|\right)}{1 + \ln A}, & \dfrac{1}{A} \le |w_1(t)| \le 1 \end{cases} \tag{2.11}$$

where $|w_1(t)| < 1$ and A is a positive constant. The A-law compression characteristic is shown in Figure 2.3c. The typical value for A is 87.6 [11].

When compression is used at the transmitter, *expansion* (i.e., decompression) must be used at the receiver output to restore signal levels to their correct relative values. The *expandor* characteristic is the inverse of the compression characteristic, and the combination of a compressor and an expandor is called a *compandor*.

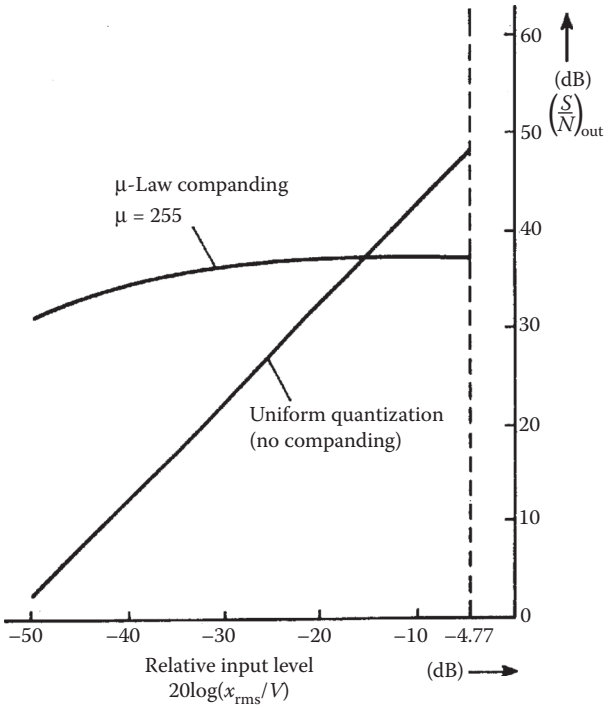

FIGURE 2.4 Output *S*/*N* of 8-b PCM systems with and without companding. (From Couch, L.W. II., *Digital and Analog Communication Systems*, 7th ed. Copyright 2007, p. 151. Reprinted with permission of Pearson Education, Inc., Upper Saddle River, NJ.)

Once again, it can be shown that the output *S*/*N* follows the 6-dB law [3]

$$\left(\frac{S}{N}\right)_{dB} = 6.02 + \alpha \tag{2.12}$$

where for uniform quantizing

$$\alpha = 4.77 - 20\log(V/x_{rms}) \tag{2.13}$$

and for sufficiently large input levels* for μ-law companding

$$\alpha \approx 4.77 - 20\log[\ln(1 + \mu)] \tag{2.14}$$

and for *A*-law companding [6]

$$\alpha \approx 4.77 - 20\log[1 + \ln A] \tag{2.15}$$

n is the number of bits used in the PCM word, *V* is the peak design level of the quantizer, and x_{rms} is the rms value of the input analog signal. Note that the output *S*/*N* is a function of the input level for the uniform quantizing (no companding) case but is relatively insensitive to input level for μ-law and *A*-law companding, as shown in Figure 2.4. The ratio V/x_{rms} is called the *loading factor*. The input level is often

* See Lathi, 1998 for a more complicated expression that is valid for any input level.

set for a loading factor of 4 (12 dB) to ensure that the overload quantizing noise will be negligible. In practice this gives $\alpha = -7.3$ for the case of uniform encoding as compared to $\alpha = 0$, which was obtained for the ideal conditions associated with Equation 2.8.

2.8 Example: Design of a PCM System

Assume that an analog voice-frequency signal, which occupies a band from 300 to 3400 Hz, is to be transmitted over a binary PCM system. The minimum sampling frequency would be $2 \times 3.4 = 6.8$ kHz. In practice the signal is oversampled, and in the United States a sampling frequency of 8 kHz is the standard used for voice-frequency signals in telephone communication systems. Assume that each sample value is represented by 8 b; then the bit rate of the PCM signal is

$$\begin{aligned} R &= (f_s \text{ samples/}s)(n \text{ b/}s) \\ &= (8k \text{ samples/}s)(8 \text{ b/}s) = 64 \text{ kb/}s \end{aligned} \tag{2.16}$$

Referring to the dimensionality theorem (Equation 2.4), we realize that the theoretically minimum absolute bandwidth of the PCM signal is

$$B_{\min} = \frac{1}{2} D = 32 \text{ kHz} \tag{2.17}$$

and this is realized if the PCM waveform consists of $(\sin x)/x$ pulse shapes. If rectangular pulse shaping is used, the absolute bandwidth is infinity, and the first null bandwidth (Equation 2.5) is

$$B_{\text{null}} = R = \frac{1}{T_b} = 64 \text{ kHz} \tag{2.18}$$

That is, we require a bandwidth of 64 kHz to transmit this digital voice PCM signal where the bandwidth of the original analog voice signal was, at most, 4 kHz. Using $n = 8$ in Equation 2.1, the error on the recovered analog signal is ±0.2%. Using Equations 2.12 and 2.13 for the case of uniform quantizing with a loading factor, V/x_{rms}, of 10 (20 dB), we get for uniform quantizing

$$\left(\frac{S}{N}\right)_{\text{dB}} = 32.9 \text{ dB} \tag{2.19}$$

Using Equations 2.12 and 2.14 for the case of $\mu = 255$ companding, we get

$$\left(\frac{S}{N}\right) = 38.05 \text{ dB} \tag{2.20}$$

These results are illustrated in Figure 2.4.

References

1. Gibson, J.D., *The Communications Handbook*. Boca Raton, FL: CRC Press, Inc., 1997.
2. Dorf, R.C., *The Electrical Engineering Handbook*. Boca Raton, FL: CRC Press, Inc., 1993.
3. Couch, L.W., *Digital and Analog Communication Systems*, 7th ed. Upper Saddle River, NJ: Pearson Prentice-Hall, 2007.

4. Couch, L.W., *Modern Communication Systems: Principles and Applications*. New York, NY: Macmillan Publishing, 1995.
5. Spilker, J.J., *Digital Communications by Satellite*. Englewood Cliffs, NJ: Prentice-Hall, 1977.
6. Jayant, N.S. and Noll, P., *Digital Coding of Waveforms*. Englewood Cliffs, NJ: Prentice-Hall, 1984.
7. Miyaoka, S., Digital audio is compact and rugged. *IEEE Spectrum*, 21(3), 35–39, 1984.
8. Peek, J.B.H., Communication aspects of the compact disk digital audio system. *IEEE Communications Magazine*, 23(2), 7–15, 1985.
9. Smith, B., Instantaneous companding of quantized signals. *B. S. T. J.*, 36(5), 653–709, 1957.
10. Dammann, C.L., McDaniel, L.D., and Maddox, C.L., D2 Channel bank—Multiplexing and coding. *B. S. T. J.*, 12(10), 1675–1700, 1972.
11. Cattermole, K.W., *Principles of Pulse-Code Modulation*. New York, NY: American Elsevier, 1969.
12. Lathi, B.P., *Modern Digital and Analog Communication Systems*, 3rd ed. New York, NY: Oxford University Press, 1998.
13. Couch, L.W., II., *Digital and Analog Communication Systems*, 5th ed. Upper Saddle River, NJ: Prentice-Hall, 1997.

Further Reading

Many practical design situations and applications of PCM transmission via twisted-pair T-1 telephone lines, fiber optic cable, microwave relay, and satellite systems are given in [3] and [4]. In computer systems a PCM type of data set called a WAV file is often saved and used to reconstruct analog audio signals. See http://en.wilkipedia.org for more details.

3

Baseband Signaling and Pulse Shaping

Michael L. Honig

Melbourne Barton

Many physical communication channels, such as radio channels, accept a continuous-time waveform as input. Consequently, a sequence of source bits, representing data or a digitized analog signal, must be converted to a continuous-time waveform at the transmitter. In general, each successive group of bits taken from this sequence is mapped to a particular continuous-time pulse. In this chapter, we discuss the basic principles involved in selecting such a pulse for channels that can be characterized as linear and time invariant with finite bandwidth.

3.1 Communication System Model

Figure 3.1a shows a simple block diagram of a communication system. The sequence of source bits $\{b_i\}$ are grouped into sequential blocks (vectors) of m bits $\{\boldsymbol{b}_i\}$, and each binary vector $\boldsymbol{b}_i$ is mapped to one of 2^m pulses, $p(\boldsymbol{b}_i; t)$, which is transmitted over the channel.

The transmitted signal as a function of time can be written as

$$s(t) = \sum_i p(\boldsymbol{b}_i; t - iT) \tag{3.1}$$

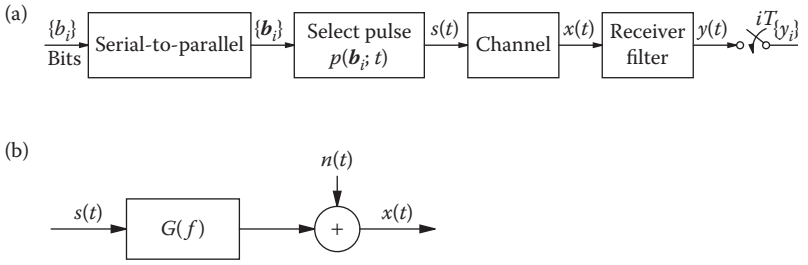

FIGURE 3.1 (a) Communication system model. The source bits are grouped into binary vectors, which are mapped to a sequence of pulse shapes. (b) Channel model consisting of a linear, time-invariant system (transfer function) followed by additive noise.

where $1/T$ is the rate at which each group of m bits, or pulses, is introduced to the channel. The information (bit) rate is therefore m/T.

The channel in Figure 3.1a can be a radio link, which may distort the input signal $s(t)$ in a variety of ways. For example, it may introduce pulse dispersion (due to finite bandwidth) and multipath, as well as additive background noise. The output of the channel is denoted as $x(t)$, which is processed by the receiver to determine estimates of the source bits. The receiver can be quite complicated; however, for the purpose of this discussion, it is sufficient to assume only that it contains a front-end filter and a sampler, as shown in Figure 3.1a. This assumption is valid for a wide variety of detection strategies. The purpose of the receiver filter is to remove noise outside of the transmitted frequency band and to compensate for the channel frequency response.

A commonly used channel model is shown in Figure 3.1b and consists of a linear, time-invariant filter, denoted as $G(f)$, followed by additive noise $n(t)$. The channel output is, therefore,

$$x(t) = [g(t) * s(t)] + n(t) \tag{3.2}$$

where $g(t)$ is the channel impulse response associated with $G(f)$, and the asterisk denotes convolution,

$$g(t) * s(t) = \int_{-\infty}^{\infty} g(t - \tau)s(\tau)\,d\tau$$

This channel model accounts for all linear, time-invariant channel impairments, such as finite bandwidth and time-invariant multipath. It does not account for time-varying impairments, such as rapid fading due to time-varying multipath. Nevertheless, this model can be considered valid over short time periods during which the multipath parameters remain constant.

In Figures 3.1a, and 3.1b, it is assumed that all signals are *baseband signals*, which means that the frequency content is centered around $f = 0$ (DC). The channel passband, therefore, partially coincides with the transmitted spectrum. In general, this condition requires that the transmitted signal be modulated by an appropriate carrier frequency and demodulated at the receiver. In that case, the model in Figures 3.1a, and 3.1b still applies; however, *baseband-equivalent* signals must be derived from their modulated (passband) counterparts. *Baseband signaling* and *pulse shaping* refers to the way in which a group of source bits is mapped to a baseband transmitted pulse.

As a simple example of baseband signaling, we can take $m = 1$ (map each source bit to a pulse), assign a 0 bit to a pulse $p(t)$, and a 1 bit to the pulse $-p(t)$. Perhaps the simplest example of a baseband pulse is the *rectangular* pulse given by $p(t) = 1$, $0 < t \leq T$, and $p(t) = 0$ elsewhere. In this case, we can write the transmitted signal as

$$s(t) = \sum_i A_i p(t - iT) \tag{3.3}$$

where each symbol A_i takes on a value of +1 or –1, depending on the value of the ith bit, and $1/T$ is the *symbol rate*, namely, the rate at which the symbols A_i are introduced to the channel.

The preceding example is called *binary pulse amplitude modulation (PAM)*, since the data symbols A_i are binary valued, and they amplitude modulate the transmitted pulse $p(t)$. The information rate (bits per second) in this case is the same as the symbol rate $1/T$. As a simple extension of this signaling technique, we can increase m and choose A_i from one of $M = 2^m$ values to transmit at bit rate m/T. This is known as M-ary PAM. For example, letting $m = 2$, each pair of bits can be mapped to a pulse in the set $\{p(t), -p(t), 3p(t), -3p(t)\}$.

In general, the transmitted symbols $\{A_i\}$, the baseband pulse $p(t)$, and channel impulse response $g(t)$ can be *complex valued*. For example, each successive pair of bits might select a symbol from the set $\{1, -1, j, -j\}$, where $j = \sqrt{-1}$. This is a consequence of considering the baseband equivalent of passband modulation. (That is, generating a transmitted spectrum which is centered around a carrier frequency f_c.) Here we are not concerned with the relation between the passband and baseband equivalent models and simply point out that the discussion and results in this chapter apply to complex-valued symbols and pulse shapes.

As an example of a signaling technique which is not PAM, let $m = 1$ and

$$\begin{aligned} p(0;t) &= \begin{cases} \sqrt{2}\sin(2\pi f_1 t) & 0 < t < T \\ 0 & \text{elsewhere} \end{cases} \\ p(1;t) &= \begin{cases} \sqrt{2}\sin(2\pi f_2 t) & 0 < t < T \\ 0 & \text{elsewhere} \end{cases} \end{aligned} \tag{3.4}$$

where f_1 and $f_2 \neq f_1$ are fixed frequencies selected so that f_1T and f_2T (number of cycles for each bit) are multiples of 1/2. These pulses are *orthogonal*, namely,

$$\int_0^T p(1;t)p(0;t)\,dt = 0$$

This choice of pulse shapes is called binary *frequency-shift keying (FSK)*.

Another example of a set of orthogonal pulse shapes for $m = 2$ bits/T is shown in Figure 3.2. As these pulses may have as many as three transitions within a symbol period, the transmitted spectrum occupies

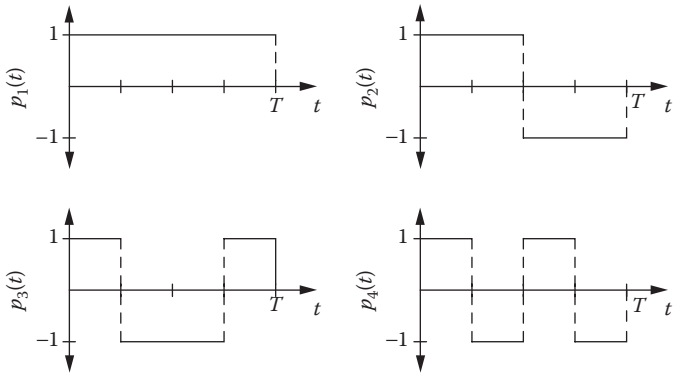

FIGURE 3.2 Four orthogonal spread-spectrum pulse shapes.

roughly four times the transmitted spectrum of binary PAM with a rectangular pulse shape. The spectrum is, therefore, spread across a much larger band than the smallest required for reliable transmission, assuming a data rate of $2/T$. This type of signaling is referred to as *spread-spectrum*. Spread-spectrum signals are more robust with respect to interference from other transmitted signals than are narrowband signals.*

3.2 Intersymbol Interference and the Nyquist Criterion

Consider the transmission of a PAM signal illustrated in Figure 3.3. The source bits $\{b_i\}$ are mapped to a sequence of levels $\{A_i\}$, which modulate the transmitter pulse $p(t)$. The channel input is, therefore, given by Equation 3.3 where $p(t)$ is the impulse response of the transmitter *pulse-shaping filter* $P(f)$ shown in Figure 3.3. The input to the transmitter filter $P(f)$ is the modulated sequence of delta functions $\sum_i A_i\delta(t-iT)$. The channel is represented by the transfer function $G(f)$ (plus noise), which has impulse response $g(t)$, and the receiver filter has transfer function $R(f)$ with associated impulse response $r(t)$.

Let $h(t)$ be the overall impulse response of the combined transmitter, channel, and receiver, which has transfer function $H(f) = P(f)G(f)R(f)$. We can write $h(t) = p(t)^*g(t)^*r(t)$. The output of the receiver filter is then

$$y(t) = \sum_i A_i h(t - iT) + \tilde{n}(t) \tag{3.5}$$

where $\tilde{n}(t) = r(t)^*n(t)$ is the output of the filter $R(f)$ with input $n(t)$. Assuming that samples are collected at the output of the filter $R(f)$ at the symbol rate $1/T$, we can write the kth sample of $y(t)$ as

$$\begin{aligned} y(kT) &= \sum_i A_i h(kT - iT) + \tilde{n}(kT) \\ &= A_k h(0) + \sum_{i \neq k} A_i h(kT - iT) + \tilde{n}(kT) \end{aligned} \tag{3.6}$$

The first term on the right-hand side of Equation 3.6 is the kth transmitted symbol scaled by the system impulse response at $t = 0$. If this were the only term on the right side of Equation 3.6, we could obtain the source bits without error by scaling the received samples by $1/h(0)$. The second term on the right-hand side of Equation 3.6 is called *intersymbol interference*, which reflects the view that neighboring symbols interfere with the detection of each desired symbol.

One possible criterion for choosing the transmitter and receiver filters is to minimize intersymbol interference. Specifically, if we choose $p(t)$ and $r(t)$ so that

$$h(kT) = \begin{cases} 1 & k = 0 \\ 0 & k \neq 0 \end{cases} \tag{3.7}$$

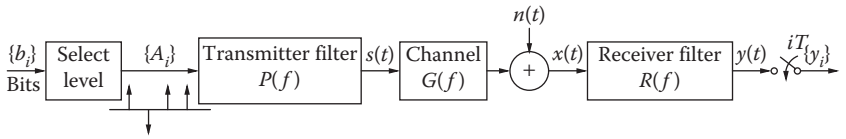

FIGURE 3.3 Baseband model of a pulse amplitude modulation system.

* This example can also be viewed as coded binary PAM. Namely, each pair of two source bits are mapped to 4 coded bits, which are transmitted via binary PAM with a rectangular pulse.

then the kth received sample is

$$y(kT) = A_k + \tilde{n}(kT) \tag{3.8}$$

In this case, the intersymbol interference has been eliminated. This choice of $p(t)$ and $r(t)$ is called a *zero-forcing* solution, since it forces the intersymbol interference to zero. Depending on the type of detection scheme used, a zero-forcing solution may not be desirable. This is because the probability of error also depends on the noise intensity, which generally increases when intersymbol interference is suppressed. It is instructive, however, to examine the properties of the zero-forcing solution.

We now view Equation 3.7 in the frequency domain. Since $h(t)$ has Fourier transform

$$H(f) = P(f)G(f)R(f) \tag{3.9}$$

where $P(f)$ is the Fourier transform of $p(t)$, the bandwidth of $H(f)$ is limited by the bandwidth of the channel $G(f)$. We will assume that $G(f) = 0$, $|f| > W$. The sampled impulse response $h(kT)$ can, therefore, be written as the inverse Fourier transform

$$h(kT) = \int_{-W}^{W} H(f)e^{j2\pi fkT}\,df$$

Through a series of manipulations, this integral can be rewritten as an inverse discrete Fourier transform,

$$h(kT) = T\int_{-1/(2T)}^{1/(2T)} H_{eq}(e^{j2\pi fT})\,e^{j2\pi fkT}\,df \tag{3.10a}$$

where

$$\begin{aligned} H_{eq}(e^{j2\pi fT}) &= \frac{1}{T}\sum_k H\left(f + \frac{k}{T}\right) \\ &= \frac{1}{T}\sum_k P\left(f + \frac{k}{T}\right)G\left(f + \frac{k}{T}\right)R\left(f + \frac{k}{T}\right) \end{aligned} \tag{3.10b}$$

This relation states that $H_{eq}(z)$, $z = e^{j2\pi fT}$, is the discrete Fourier transform of the sequence $\{h_k\}$, where $h_k = h(kT)$. Sampling the impulse response $h(t)$ therefore changes the transfer function $H(f)$ to the *aliased* frequency response $H_{eq}(e^{j2\pi fT})$. From Equations 3.10 and 3.6 we conclude that $H_{eq}(z)$ is the transfer function that relates the sequence of input data symbols $\{A_i\}$ to the sequence of received samples $\{y_i\}$, where $y_i = y(iT)$, in the absence of noise. This is illustrated in Figure 3.4. For this reason, $H_{eq}(z)$ is called the *equivalent discrete-time transfer function* for the overall system transfer function $H(f)$.

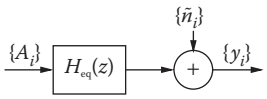

FIGURE 3.4 Equivalent discrete-time channel for the PAM system shown in Figure 3.3 [$y_i = y(iT)$, $\tilde{n}_i = \tilde{n}(iT)$].

Since $H_{eq}(e^{j2\pi fT})$ is the discrete Fourier transform of the sequence $\{h_k\}$, the time-domain, or sequence condition (3.7) is equivalent to the frequency-domain condition

$$H_{eq}(e^{j2\pi fT}) = 1 \tag{3.11}$$

This relation is called the *Nyquist criterion*. From Equations 3.10b and 3.11 we make the following observations.

1. To satisfy the Nyquist criterion, the channel bandwidth W must be at least $1/(2T)$. Otherwise, $G(f + n/T) = 0$ for f in some interval of positive length for all n, which implies that $H_{eq}(e^{j2\pi fT}) = 0$ for f in the same interval.
2. For the minimum bandwidth $W = 1/(2T)$, Equations 3.10b and 3.11 imply that $H(f) = T$ for $|f| < 1/(2T)$ and $H(f) = 0$ elsewhere. This implies that the system impulse response is given by

$$h(t) = \frac{\sin(\pi t/T)}{\pi t/T} \tag{3.12}$$

(Since $\int_{-\infty}^{\infty} h^2(t)\,dt = T$, the transmitted signal $S(t) = \sum_i A_i h(t - iT)$ has power equal to the symbol variance $E[|A_i|^2]$.) The impulse response in Equation 3.12 is called a *minimum bandwidth* or Nyquist pulse. The frequency band $[-1/(2T), 1/(2T)]$ [that is, the passband of $H(f)$] is called the *Nyquist band*.

3. Suppose that the channel is bandlimited to twice the Nyquist bandwidth. That is, $G(f) = 0$ for $|f| > 1/T$. The condition (3.11) then becomes

$$H(f) + H\left(f - \frac{1}{T}\right) + H\left(f + \frac{1}{T}\right) = T \tag{3.13}$$

Assume for the moment that $H(f)$ and $h(t)$ are both real valued, so that $H(f)$ is an even function of f [$H(f) = H(-f)$]. This is the case when the receiver filter is the matched filter (see Section 3.3). We can then rewrite Equation 3.13 as

$$H(f) + H\left(\frac{1}{T} - f\right) = T, \quad 0 < f < \frac{1}{2T} \tag{3.14}$$

which states that $H(f)$ must have odd symmetry about $f = 1/(2T)$. This is illustrated in Figure 3.5, which shows two different transfer functions $H(f)$ that satisfy the Nyquist criterion.

4. The pulse shape $p(t)$ enters into Equation 3.11 only through the product $P(f)R(f)$. Consequently, either $P(f)$ or $R(f)$ can be fixed, and the other filter can be adjusted or adapted to the particular channel. Typically, the pulse shape $p(t)$ is fixed, and the receiver filter is adapted to the (possibly time-varying) channel.

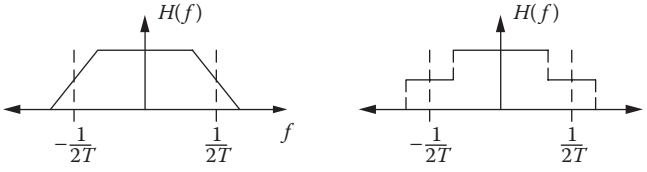

FIGURE 3.5 Two examples of frequency responses that satisfy the Nyquist criterion.

3.2.1 Raised Cosine Pulse

Suppose that the channel is ideal with transfer function

$$G(f) = \begin{cases} 1, & |f| < W \\ 0, & |f| > W \end{cases} \tag{3.15}$$

To maximize bandwidth efficiency, Nyquist pulses given by Equation 3.12 should be used where $W = 1/(2T)$. This type of signaling, however, has two major drawbacks. First, Nyquist pulses are noncausal and of infinite duration. They can be approximated in practice by introducing an appropriate delay, and truncating the pulse. The pulse, however, decays very slowly, namely, as $1/t$, so that the truncation window must be wide. This is equivalent to observing that the ideal bandlimited frequency response given by Equation 3.15 is difficult to approximate closely. The second drawback, which is more important, is the fact that this type of signaling is not robust with respect to sampling jitter. Namely, a small sampling offset ε produces the output sample

$$y(kT + \varepsilon) = \sum_i A_i \frac{\sin[\pi(k - i + \varepsilon/T)]}{\pi(k - i + \varepsilon/T)} \tag{3.16}$$

Since the Nyquist pulse decays as $1/t$, this sum is not guaranteed to converge. A particular choice of symbols $\{A_i\}$ can, therefore, lead to very large intersymbol interference, no matter how small the offset. Minimum bandwidth signaling is therefore impractical.

The preceding problem is generally solved in one of two ways in practice:

1. The pulse bandwidth is increased to provide a faster pulse decay than $1/t$.
2. A *controlled* amount of intersymbol interference is introduced at the transmitter, which can be subtracted out at the receiver.

The former approach sacrifices bandwidth efficiency, whereas the latter approach sacrifices power efficiency. We will examine the latter approach in Section 3.5. The most common example of a pulse, which illustrates the first technique, is the *raised cosine pulse*, given by

$$h(t) = \left[\frac{\sin(\pi t/T)}{\pi t/T}\right]\left[\frac{\cos(\alpha\pi t/T)}{1 - (2\alpha t/T)^2}\right] \tag{3.17}$$

which has Fourier transform

$$H(f) = \begin{cases} T & 0 \le |f| \le \dfrac{1-\alpha}{2T} \\ \dfrac{T}{2}\left\{1 + \cos\left[\dfrac{\pi T}{\alpha}\left(|f| - \dfrac{1-\alpha}{2T}\right)\right]\right\} & \dfrac{1-\alpha}{2T} \le |f| \le \dfrac{1+\alpha}{2T} \\ 0 & |f| > \dfrac{1+\alpha}{2T} \end{cases} \tag{3.18}$$

where $0 \le \alpha \le 1$.

Plots of $p(t)$ and $P(f)$ are shown in Figures 3.6a and 3.6b for different values of α. It is easily verified that $h(t)$ satisfies the Nyquist criterion (3.7) and, consequently, $H(f)$ satisfies Equation 3.11. When $\alpha = 0$, $H(f)$ is the Nyquist pulse with minimum bandwidth $1/(2T)$, and when $\alpha > 0$, $H(f)$ has bandwidth

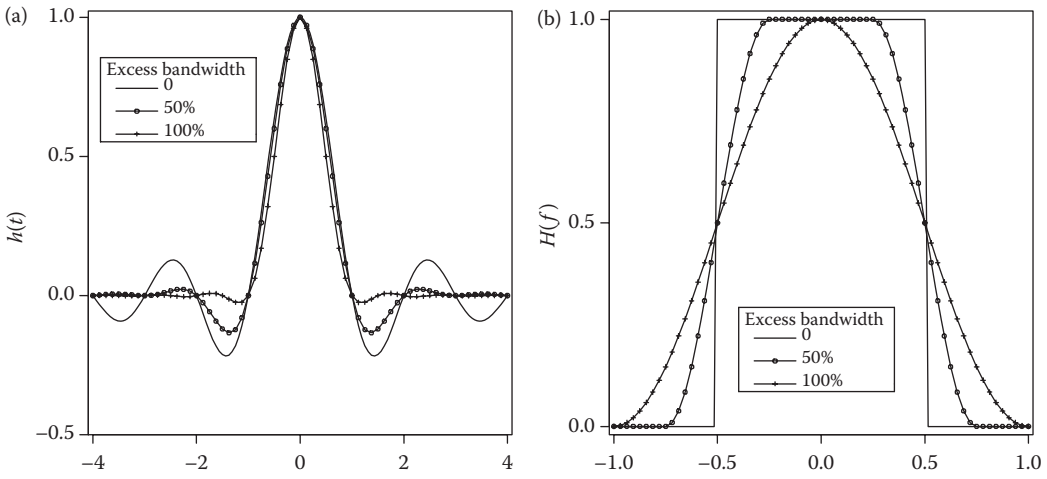

FIGURE 3.6 (a) Raised cosine pulse. (b) Raised cosine spectrum.

$(1 + \alpha)/(2T)$ with a raised cosine rolloff. The parameter α, therefore, represents the additional, or *excess bandwidth* as a fraction of the minimum bandwidth $1/(2T)$. For example, when $\alpha = 1$, we say that the pulse is a raised cosine pulse with 100% excess bandwidth. This is because the pulse bandwidth $1/T$ is twice the minimum bandwidth. As the raised cosine pulse decays as $1/t^3$, performance is robust with respect to sampling offsets.

The raised cosine frequency response (3.18) applies to the combination of transmitter, channel, and receiver. If the transmitted pulse shape $p(t)$ is a raised cosine pulse, then $h(t)$ is a raised cosine pulse only if the combined receiver and channel frequency response is constant. Even with an ideal (transparent) channel, however, the optimum (matched) receiver filter response is generally not constant in the presence of additive Gaussian noise. An alternative is to transmit the *square-root raised cosine* pulse shape, which has frequency response $P(f)$ given by the square-root of the raised cosine frequency response in Equation 3.18. Assuming an ideal channel, setting the receiver frequency response $R(f) = P(f)$ then results in an overall raised cosine system response $H(f)$.

3.3 Nyquist Criterion with Matched Filtering

Consider the transmission of an isolated pulse $A_0\delta(t)$. In this case the input to the receiver in Figure 3.3 is

$$x(t) = A_0\tilde{g}(t) + n(t) \tag{3.19}$$

where $\tilde{g}(t)$ is the inverse Fourier transform of the combined transmitter-channel transfer function $\tilde{G}(f) = P(f)G(f)$. We will assume that the noise $n(t)$ is white with spectrum $N_0/2$. The output of the receiver filter is then

$$y(t) = r(t) * x(t) = A_0[r(t) * \tilde{g}(t)] + [r(t) * n(t)] \tag{3.20}$$

The first term on the right-hand side is the desired signal, and the second term is noise. Assuming that $y(t)$ is sampled at $t = 0$, the ratio of signal energy to noise energy, or *signal-to-noise ratio* (*SNR*) at the sampling instant, is

$$SNR = \frac{E\left[|A_0|^2\right]\left|\int_{-\infty}^{\infty} r(-t)\tilde{g}(t)\,dt\right|^2}{\frac{N_0}{2}\int_{-\infty}^{\infty}|r(t)|^2\,dt} \tag{3.21}$$

The receiver impulse response that maximizes this expression is $r(t) = \tilde{g}^*(-t)$ [complex conjugate of $\tilde{g}(-t)$], which is known as the *matched filter* impulse response. The associated transfer function is $R(f) = \tilde{G}^*(f)$.

Choosing the receiver filter to be the matched filter is optimal in more general situations, such as when detecting a sequence of channel symbols with intersymbol interference (assuming the additive noise is Gaussian). We, therefore, reconsider the Nyquist criterion when the receiver filter is the matched filter. In this case, the baseband model is shown in Figure 3.7, and the output of the receiver filter is given by

$$y(t) = \sum_i A_i h(t - iT) + \tilde{n}(t) \tag{3.22}$$

where the baseband pulse $h(t)$ is now the impulse response of the filter with transfer function $|\tilde{G}(f)|^2 = |P(f)G(f)|^2$. This impulse response is the *autocorrelation* of the impulse response of the combined transmitter-channel filter $\tilde{G}(f)$,

$$h(t) = \int_{-\infty}^{\infty} \tilde{g}^*(s)\tilde{g}(s + t)\,ds \tag{3.23}$$

With a matched filter at the receiver, the equivalent discrete-time transfer function is

$$\begin{aligned} H_{eq}(e^{j2\pi fT}) &= \frac{1}{T}\sum_k \left|\tilde{G}\left(f - \frac{k}{T}\right)\right|^2 \\ &= \frac{1}{T}\sum_k \left|P\left(f - \frac{k}{T}\right)G\left(f - \frac{k}{T}\right)\right|^2 \end{aligned} \tag{3.24}$$

which relates the sequence of transmitted symbols $\{A_k\}$ to the sequence of received samples $\{y_k\}$ in the absence of noise. Note that $H_{eq}(e^{j2\pi fT})$ is positive, real valued, and an even function of f. If the channel is bandlimited to twice the Nyquist bandwidth, then $H(f) = 0$ for $|f| > 1/T$, and the Nyquist condition is given by Equation 3.14 where $H(f) = |G(f)P(f)|^2$. The aliasing sum in Equation 3.10b can therefore be described as a folding operation in which the channel response $|H(f)|^2$ is folded around the Nyquist frequency $1/(2T)$. For this reason, $H_{eq}(e^{j2\pi fT})$ with a matched receiver filter is often referred to as the folded channel spectrum.

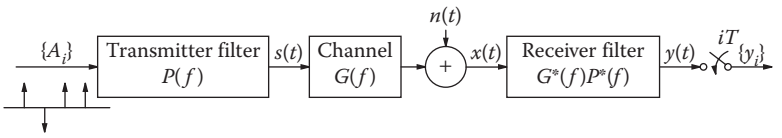

FIGURE 3.7 Baseband PAM model with a matched filter at the receiver.

3.4 Eye Diagrams

One way to assess the severity of distortion due to intersymbol interference in a digital communications system is to examine the *eye diagram*. The eye diagram is illustrated in Figures 3.8a and 3.8b, for a raised cosine pulse shape with 25% excess bandwidth and an ideal bandlimited channel. Figure 3.8a shows the data signal at the receiver

$$y(t) = \sum_i A_i h(t - iT) + \tilde{n}(t) \tag{3.25}$$

where $h(t)$ is given by Equation 3.17, $\alpha = 1/4$, each symbol A_i is independently chosen from the set $\{\pm 1, \pm 3\}$, where each symbol is equally likely, and $\tilde{n}(t)$ is bandlimited white Gaussian noise. (The received *SNR* is 30 dB.) The eye diagram is constructed from the time-domain data signal $y(t)$ as follows (assuming nominal sampling times at kT, $k = 0, 1, 2, \ldots$):

1. Partition the waveform $y(t)$ into successive segments of length T starting from $t = T/2$.
2. Translate each of these waveform segments $[y(t), (k + 1/2)T \le t \le (k + 3/2)T, k = 0, 1, 2, \ldots]$ to the interval $[-T/2, T/2]$, and superimpose.

The resulting picture is shown in Figure 3.8b for the $y(t)$ shown in Figure 3.8a. (Partitioning $y(t)$ into successive segments of length iT, $i > 1$, is also possible. This would result in i successive eye diagrams.) The number of eye openings is one less than the number of transmitted signal levels. In practice, the eye diagram is easily viewed on an oscilloscope by applying the received waveform $y(t)$ to the vertical deflection plates of the oscilloscope and applying a sawtooth waveform at the symbol rate $1/T$ to the horizontal deflection plates. This causes successive symbol intervals to be translated into one interval on the oscilloscope display.

Each waveform segment $y(t)$, $(k + 1/2)T \le t \le (k + 3/2)T$, depends on the particular sequence of channel symbols surrounding A_k. The number of channel symbols that affects a particular waveform segment depends on the extent of the intersymbol interference, shown in Equation 3.6. This, in turn, depends on the duration of the impulse response $h(t)$. For example, if $h(t)$ has most of its energy in the interval $0 < t < mT$, then each waveform segment depends on approximately m symbols. Assuming

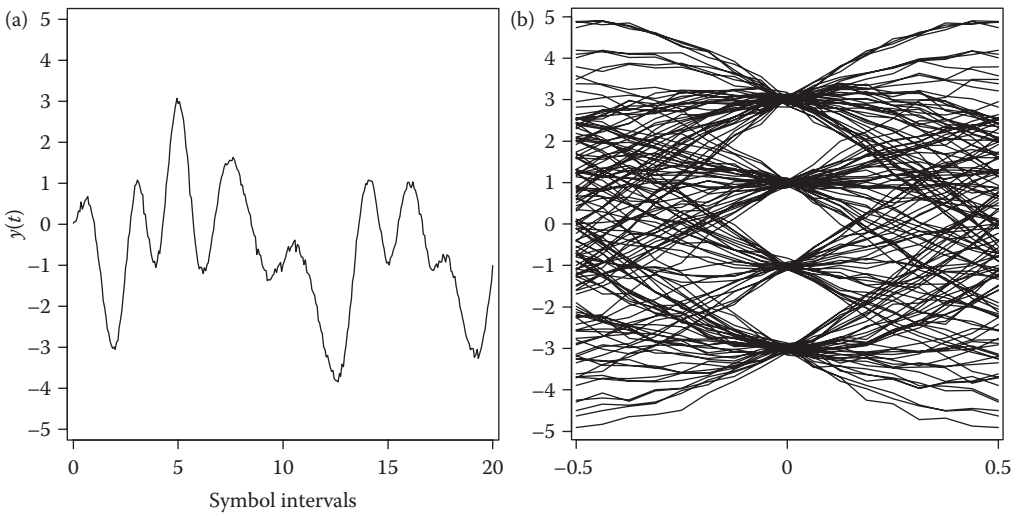

FIGURE 3.8 (a) Received signal $y(t)$. (b) Eye diagram for received signal shown in Figure 3.8a.

binary transmission, this implies that there are a total of 2^m waveform segments that can be superimposed in the eye diagram. (It is possible that only one sequence of channel symbols causes significant intersymbol interference, and this sequence occurs with very low probability.) In current digital wireless applications the impulse response typically spans only a few symbols.

The eye diagram has the following important features which measure the performance of a digital communications system.

3.4.1 Vertical Eye Opening

The vertical openings at any time t_0, $-T/2 \le t_0 \le T/2$, represent the separation between signal levels with worst-case intersymbol interference, assuming that $y(t)$ is sampled at times $t = kT + t_0$, $k = 0, 1, 2, \ldots$. It is possible for the intersymbol interference to be large enough so that this vertical opening between some, or all, signal levels disappears altogether. In that case, the eye is said to be closed. Otherwise, the eye is said to be open. A closed eye implies that if the estimated bits are obtained by thresholding the samples $y(kT)$, then the decisions will depend primarily on the intersymbol interference rather than on the desired symbol. The probability of error will, therefore, be close to 1/2. Conversely, wide vertical spacings between signal levels imply a large degree of immunity to additive noise. In general, $y(t)$ should be sampled at the times $kT + t_0$, $k = 0, 1, 2, \ldots$, where t_0 is chosen to maximize the vertical eye opening.

3.4.2 Horizontal Eye Opening

The width of each opening indicates the sensitivity to timing offset. Specifically, a very narrow eye opening indicates that a small timing offset will result in sampling where the eye is closed. Conversely, a wide horizontal opening indicates that a large timing offset can be tolerated, although the error probability will depend on the vertical opening.

3.4.3 Slope of the Inner Eye

The slope of the inner eye indicates sensitivity to timing jitter or variance in the timing offset. Specifically, a very steep slope means that the eye closes rapidly as the timing offset increases. In this case, a significant amount of jitter in the sampling times significantly increases the probability of error.

The shape of the eye diagram is determined by the pulse shape. In general, the faster the baseband pulse decays, the wider the eye opening. For example, a rectangular pulse produces a box-shaped eye diagram (assuming binary signaling). The minimum bandwidth pulse shape Equation 3.12 produces an eye diagram which is closed for all t except for $t = 0$. This is because, as shown earlier, an arbitrarily small timing offset can lead to an intersymbol interference term that is arbitrarily large, depending on the data sequence.

3.5 Partial-Response Signaling

To avoid the problems associated with Nyquist signaling over an ideal bandlimited channel, bandwidth and/or power efficiency must be compromised. Raised cosine pulses compromise bandwidth efficiency to gain robustness with respect to timing errors. Another possibility is to introduce a controlled amount of intersymbol interference at the transmitter, which can be removed at the receiver. This approach is called *partial-response (PR) signaling*. The terminology reflects the fact that the sampled system impulse response does not have the full response given by the Nyquist condition Equation 3.7.

To illustrate PR signaling, suppose that the Nyquist condition Equation 3.7 is replaced by the condition

$$h_k = \begin{cases} 1 & k = 0, 1 \\ 0 & \text{all other } k \end{cases} \tag{3.26}$$

The kth received sample is then

$$y_k = A_k + A_{k-1} + \tilde{n}_k \tag{3.27}$$

so that there is intersymbol interference from one neighboring transmitted symbol. For now we focus on the spectral characteristics of PR signaling and defer discussion of how to detect the transmitted sequence $\{A_k\}$ in the presence of intersymbol interference. The equivalent discrete-time transfer function in this case is the discrete Fourier transform of the sequence in Equation 3.26,

$$\begin{aligned} H_{\text{eq}}(e^{j2\pi fT}) &= \frac{1}{T}\sum_k H\left(f + \frac{k}{T}\right) \\ &= 1 + e^{-j2\pi fT} = 2e^{-j\pi fT}\cos(\pi fT) \end{aligned} \tag{3.28}$$

As in the full-response case, for Equation 3.28 to be satisfied, the *minimum* bandwidth of the channel $G(f)$ and transmitter filter $P(f)$ is $W = 1/(2T)$. Assuming $P(f)$ has this minimum bandwidth implies

$$H(f) = \begin{cases} 2Te^{-j\pi fT}\cos(\pi fT) & |f| < 1/(2T) \\ 0 & |f| > 1/(2T) \end{cases} \tag{3.29a}$$

and

$$h(t) = T\{\text{sinc}\,(t/T) + \text{sinc}\,[(t-T)/T]\} \tag{3.29b}$$

where $\text{sinc}\, x = (\sin \pi x)/(\pi x)$. This pulse is called a *duobinary* pulse and is shown along with the associated $H(f)$ in Figure 3.9. [Notice that $h(t)$ satisfies Equation 3.26.] Unlike the ideal bandlimited frequency response, the transfer function $H(f)$ in Equation 3.29a is continuous and is, therefore, easily approximated by a physically realizable filter. Duobinary PR was first proposed by Lender, [1], and later generalized by Kretzmer, [2].

The main advantage of the duobinary pulse Equation 3.29b, relative to the minimum bandwidth pulse Equation 3.12, is that signaling at the Nyquist symbol rate is feasible with zero excess bandwidth.

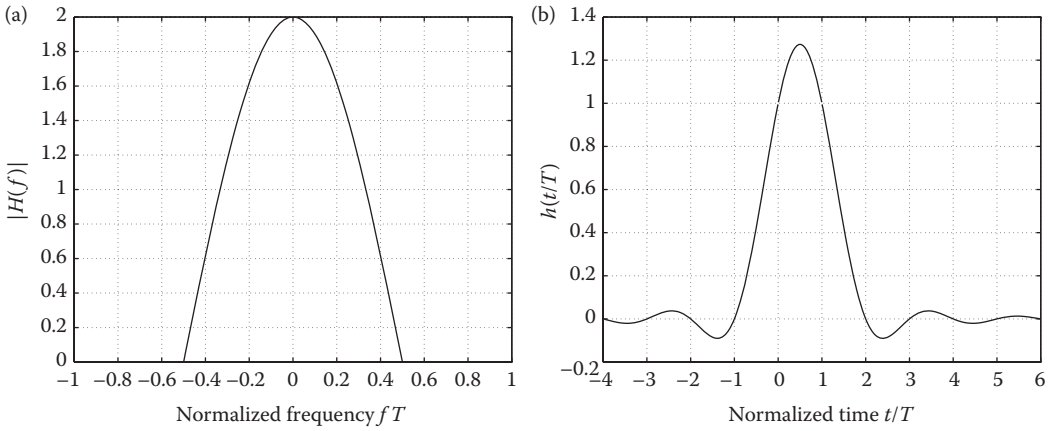

FIGURE 3.9 Duobinary frequency response and minimum bandwidth pulse.

As the pulse decays much more rapidly than a Nyquist pulse, it is robust with respect to timing errors. Selecting the transmitter and receiver filters so that the overall system response is duobinary is appropriate in situations where the channel frequency response $G(f)$ is near zero or has a rapid rolloff at the Nyquist band edge $f = 1/(2T)$.

As another example of PR signaling, consider the *modified* duobinary partial response

$$h_k = \begin{cases} 1 & k = -1 \\ -1 & k = 1 \\ 0 & \text{all other } k \end{cases} \tag{3.30}$$

which has an equivalent discrete-time transfer function

$$\begin{aligned} H_{\text{eq}}(e^{j2\pi fT}) &= e^{j2\pi fT} - e^{-j2\pi fT} \\ &= j2\sin(2\pi fT) \end{aligned} \tag{3.31}$$

With zero excess bandwidth, the overall system response is

$$H(f) = \begin{cases} j2T\sin(2\pi fT) & |f| < 1/(2T) \\ 0 & |f| > 1/(2T) \end{cases} \tag{3.32a}$$

and

$$h(t) = T\{\text{sinc}\,[(t+T)/T] - \text{sinc}\,[(t-T)/T]\} \tag{3.32b}$$

These functions are plotted in Figure 3.10. This pulse shape is appropriate when the channel response $G(f)$ is near zero at both DC ($f = 0$) and at the Nyquist band edge. This is often the case for wire (twisted-pair) channels where the transmitted signal is coupled to the channel through a transformer. Like duobinary PR, modified duobinary allows minimum bandwidth signaling at the Nyquist rate.

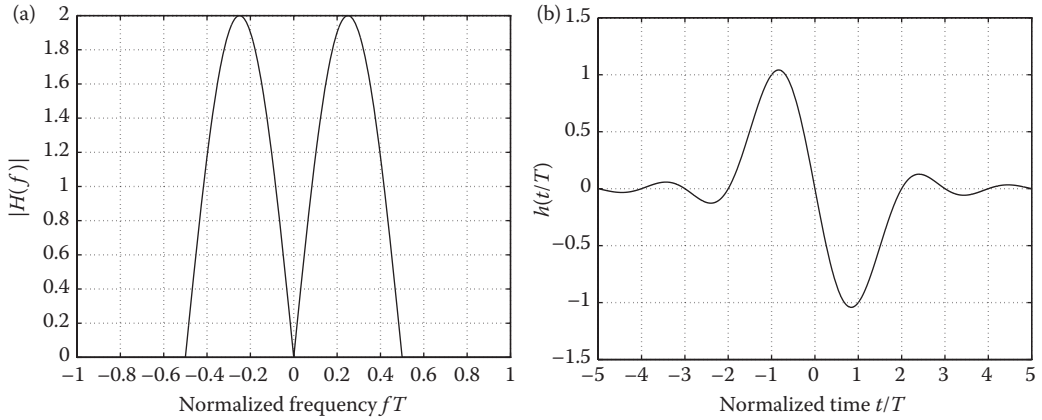

FIGURE 3.10 Modified duobinary frequency response and minimum bandwidth pulse.

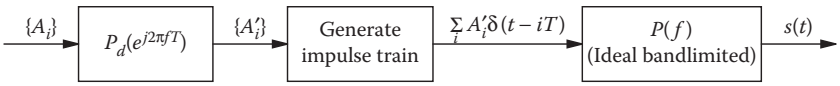

FIGURE 3.11 Generation of PR signal.

A particular partial response is often identified by the polynomial

$$\sum_{k=0}^{K} h_k D^k$$

where D (for delay) takes the place of the usual z^{-1} in the z transform of the sequence $\{h_k\}$. For example, duobinary is also referred to as $1 + D$ partial response.

In general, more complicated system responses than those shown in Figures 3.9 and 3.10 can be generated by choosing more nonzero coefficients in the sequence $\{h_k\}$. This complicates detection, however, because of the additional intersymbol interference that is generated.

Rather than modulating a PR pulse $h(t)$, a PR signal can also be generated by filtering the sequence of transmitted levels $\{A_i\}$. This is shown in Figure 3.11. Namely, the transmitted levels are first passed through a discrete-time (digital) filter with transfer function $P_d(e^{j2\pi fT})$ (where the subscript d indicates discrete). [Note that $P_d(e^{j2\pi fT})$ can be selected to be $H_{eq}(e^{j2\pi fT})$.] The outputs of this filter form the PAM signal, where the pulse shaping filter $P(f) = 1$, $|f| < 1/(2T)$ and is zero elsewhere. If the transmitted levels $\{A_k\}$ are selected independently and are identically distributed, then the transmitted spectrum is $\sigma_A^2 \, |P_d(e^{j2\pi fT})|^2$ for $|f| < 1/(2T)$ and is zero for $|f| > 1/(2T)$, where $\sigma_A^2 = E[|A_k|^2]$.

Shaping the transmitted spectrum to have nulls coincident with nulls in the channel response potentially offers significant performance advantages. By introducing intersymbol interference, however, PR signaling increases the number of received signal levels, which increases the complexity of the detector and may reduce immunity to noise. For example, the set of received signal levels for duobinary signaling is $\{0, \pm 2\}$ from which the transmitted levels $\{\pm 1\}$ must be estimated. The performance of a particular PR scheme depends on the channel characteristics, as well as the type of detector used at the receiver. We now describe a simple suboptimal detection strategy.

3.5.1 Precoding

Consider the received signal sample Equation 3.27 with duobinary signaling. If the receiver has correctly decoded the symbol A_{k-1}, then in the absence of noise A_k can be decoded by subtracting A_{k-1} from the received sample y_k. If an error occurs, however, then subtracting the preceding symbol estimate from the received sample will cause the error to propagate to successive detected symbols. To avoid this problem, the transmitted levels can be *precoded* in such a way as to compensate for the intersymbol interference introduced by the overall partial response.

We first illustrate precoding for duobinary PR. The sequence of operations is illustrated in Figure 3.12. Let $\{b_k\}$ denote the sequence of source bits where $b_k \in \{0, 1\}$. This sequence is transformed to the sequence $\{b'_k\}$ by the operation

$$b'_k = b_k \oplus b'_{k-1} \tag{3.33}$$

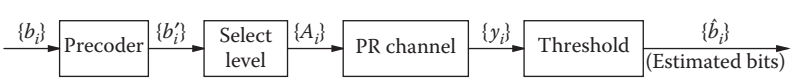

FIGURE 3.12 Precoding for a PR channel.

where $\oplus$ denotes modulo 2 addition (exclusive OR). The sequence $\{b'_k\}$ is mapped to the sequence of binary transmitted signal levels $\{A_k\}$ according to

$$A_k = 2b'_k - 1 \tag{3.34}$$

That is, $b'_k = 0$ ($b'_k = 1$) is mapped to the transmitted level $A_k = -1$ ($A_k = 1$). In the absence of noise, the received symbol is then

$$y_k = A_k + A_{k-1} = 2(b'_k + b'_{k-1} - 1) \tag{3.35}$$

and combining Equations 3.33 and 3.35 gives

$$b_k = \left(\frac{1}{2}y_k + 1\right) \mod 2 \tag{3.36}$$

That is, if $y_k = \pm 2$, then $b_k = 0$, and if $y_k = 0$, then $b_k = 1$. Precoding, therefore, enables the detector to make *symbol-by-symbol* decisions that do not depend on previous decisions. Table 3.1 shows a sequence of transmitted bits $\{b_i\}$, precoded bits $\{b'_i\}$, transmitted signal levels $\{A_i\}$, and received samples $\{y_i\}$.

The preceding precoding technique can be extended to multilevel PAM and to other PR channels. Suppose that the PR is specified by

$$H_{\text{eq}}(D) = \sum_{k=0}^{K} h_k D^k$$

where the coefficients are integers and that the source symbols $\{b_k\}$ are selected from the set $\{0, 1, \ldots, M-1\}$. These symbols are transformed to the sequence $\{b'_k\}$ via the precoding operation

$$b'_k = \left(b_k - \sum_{i=1}^{K} h_i b'_{k-i}\right) \mod M \tag{3.37}$$

Because of the modulo operation, each symbol b'_k is also in the set $\{0, 1, \ldots, M-1\}$. The kth transmitted signal level is given by

$$A_k = 2b'_k - (M-1) \tag{3.38}$$

so that the set of transmitted levels is $\{-(M-1), \ldots, (M-1)\}$ (i.e., a shifted version of the set of values assumed by b_k). In the absence of noise the received sample is

$$y_k = \sum_{i=0}^{K} h_i A_{k-i} \tag{3.39}$$

TABLE 3.1 Example of Precoding for Duobinary PR

$\{b_i\}$:		1	0	0	1	1	1	0	0	1	0
$\{b'_i\}$:	0	1	1	1	0	1	0	0	0	1	1
$\{A_i\}$:	−1	1	1	1	−1	1	−1	−1	−1	1	1
$\{y_i\}$:		0	2	2	0	0	0	−2	−2	0	2

and it can be shown that the kth source symbol is given by

$$b_k = \frac{1}{2}(y_k + (M-1)\cdot H_{\text{eq}}(1)) \bmod M \tag{3.40}$$

Precoding the symbols $\{b_k\}$ in this manner, therefore, enables symbol-by-symbol decisions at the receiver. In the presence of noise, more sophisticated detection schemes (e.g., maximum likelihood) can be used with PR signaling to obtain improvements in performance.

3.6 Additional Considerations

In many applications, bandwidth and intersymbol interference are not the only important considerations for selecting baseband pulses. Here we give a brief discussion on additional practical constraints that may influence this selection.

3.6.1 Average Transmitted Power and Spectral Constraints

The constraint on average transmitted power varies according to the application. For example, low-average power is highly desirable for mobile wireless applications that use battery-powered transmitters. In many applications (e.g., digital subscriber loops, as well as digital radio), constraints are imposed to limit the amount of interference, or crosstalk, radiated into neighboring receivers and communications systems. Because this type of interference is frequency dependent, the constraint may take the form of a spectral mask that specifies the maximum allowable transmitted power as a function of frequency. For example, crosstalk in wireline channels is generally caused by capacitive coupling and increases as a function of frequency. Consequently, to reduce the amount of crosstalk generated at a particular transmitter, the pulse shaping filter generally attenuates high frequencies more than low frequencies.

In radio applications where signals are assigned different frequency bands, constraints on the transmitted spectrum are imposed to limit *adjacent-channel interference*. This interference is generated by transmitters assigned to adjacent frequency bands. Therefore, a constraint is needed to limit the amount of *out-of-band power* generated by each transmitter, in addition to an overall average power constraint. To meet this constraint, the transmitter filter in Figure 3.3 must have a sufficiently steep rolloff at the edges of the assigned frequency band. (Conversely, if the transmitted signals are time multiplexed, then the duration of the system impulse response must be contained within the assigned time slot.)

3.6.2 Peak-to-Average Power

In addition to a constraint on average transmitted power, a *peak-power* constraint is often imposed as well. This constraint is important in practice for the following reasons:

1. The dynamic range of the transmitter is limited. In particular, saturation of the output amplifier will "clip" the transmitted waveform.
2. Rapid fades can severely distort signals with high peak-to-average power.
3. The transmitted signal may be subjected to nonlinearities. Saturation of the output amplifier is one example. Another example that pertains to wireline applications is the companding process in the voice telephone network [3]. Namely, the compander used to reduce quantization noise for pulse-code modulated voice signals introduces amplitude-dependent distortion in data signals.

The preceding impairments or constraints indicate that the transmitted waveform should have a low *peak-to-average power ratio* (*PAR*). For a transmitted waveform $x(t)$, the PAR is defined as

$$\text{PAR} = \frac{\max|x(t)|^2}{E\left\{|x(t)|^2\right\}}$$

where $E(\cdot)$ denotes expectation. Using binary signaling with rectangular pulse shapes minimizes the PAR. However, this compromises bandwidth efficiency. In applications where PAR should be low, binary signaling with rounded pulses is often used. Operating RF power amplifiers with power back-off can also reduce PAR, but leads to inefficient amplification.

For an *orthogonal frequency division multiplexing (OFDM)* system, it is well known that the transmitted signal can exhibit a very high PAR compared to an equivalent single-carrier system. Hence more sophisticated approaches to PAR reduction are required for OFDM. Some proposed approaches are described in Reference 4 and references therein. These include altering the set of transmitted symbols and setting aside certain OFDM tones specifically to minimize PAR.

3.6.3 Channel and Receiver Characteristics

The type of channel impairments encountered and the type of detection scheme used at the receiver can also influence the choice of a transmitted pulse shape. For example, a constant amplitude pulse is appropriate for a fast fading environment with noncoherent detection. The ability to track channel characteristics, such as phase, may allow more bandwidth efficient pulse shapes in addition to multilevel signaling.

High-speed data communications over time-varying channels requires that the transmitter and/or receiver adapt to the changing channel characteristics. Adapting the transmitter to compensate for a time-varying channel requires a feedback channel through which the receiver can notify the transmitter of changes in channel characteristics. Because of this extra complication, adapting the receiver is often preferred to adapting the transmitter pulse shape. However, the following examples are notable exceptions.

1. Mobile cellular systems may dynamically adapt the transmitter power for each link (in both directions) to control the amount of interference generated and to compensate for channel conditions. This can be viewed as a simple form of adaptive transmitter pulse shaping in which a single parameter associated with the pulse shape is varied.
2. Multitone modulation divides the channel bandwidth into small subbands, and the transmitted power and source bits are distributed among these subbands to maximize the information rate. The received signal-to-noise ratio for each subband must be transmitted back to the transmitter to guide the allocation of transmitted bits and power [5].

In addition to multitone modulation, *adaptive precoding* (also known as Tomlinson–Harashima precoding [6,7]) is another way in which the transmitter can adapt to the channel frequency response. Adaptive precoding is an extension of the technique described earlier for partial-response channels. Namely, the equivalent discrete-time channel impulse response is measured at the receiver and sent back to the transmitter, where it is used in a precoder. The precoder compensates for the intersymbol interference introduced by the channel, allowing the receiver to detect the data by a simple threshhold operation. Both multitone modulation and precoding have been used with wireline channels (voiceband modems and digital subscriber loops).

3.6.4 Complexity

Generation of a bandwidth-efficient signal requires a filter with a sharp cutoff. In addition, bandwidth-efficient pulse shapes can complicate other system functions, such as timing and carrier recovery.

If sufficient bandwidth is available, the cost can be reduced by using a rectangular pulse shape with a simple detection strategy (low-pass filter and threshold).

3.6.5 Tolerance to Interference

Interference is one of the primary channel impairments associated with digital radio. In addition to adjacent-channel interference described earlier, *cochannel interference* may be generated by other transmitters assigned to the same frequency band as the desired signal. Cochannel interference can be controlled through frequency (and perhaps time slot) assignments and by pulse shaping. For example, assuming fixed average power, increasing the bandwidth occupied by the signal lowers the power spectral density and decreases the amount of interference into a narrowband system that occupies part of the available bandwidth. Sufficient bandwidth spreading, therefore, enables wideband signals to be overlaid on top of narrowband signals without disrupting either service.

3.6.6 Privacy and Security

The broadcast nature of wireless channels generally makes eavesdropping easier than for wired channels. A requirement for most commercial, as well as military applications, is to guarantee the privacy of user conversations (low probability of intercept). An additional requirement, in some applications, is that determining whether or not communications is taking place must be difficult (low probability of detection). Spread-spectrum waveforms are attractive in these applications since spreading the pulse energy over a wide frequency band decreases the power spectral density, and hence makes the signal less visible. Power-efficient modulation combined with coding enables a further reduction in transmitted power for a target error rate.

3.7 Examples

We conclude this chapter with a brief description of baseband pulse shapes used in existing standards for digital mobile cellular systems.

3.7.1 Wideband Code Division Multiple Access (W-CDMA)

W-CDMA refers to the radio transmission part of *Universal Mobile Telecommunications System (UMTS)*, which is an evolution from the European GSM standard developed by the *Third Generation Partnership Project (3GPP)* [8]. It operates in both *frequency-division duplex (FDD)* and *time-division duplex (TDD)* modes as part of *UMTS Terrestrial Radio Access (UTRA)*. The transmit pulse-shaping filter for W-CDMA is a square-root raised cosine pulse with roll-off factor $\alpha = 0.22$. The chip impulse response is given by

$$p(t) = \frac{\sin\left(\pi \frac{t}{T_C}(1-\alpha)\right) + 4\alpha \frac{t}{T_C}\cos\left(\pi \frac{t}{T_C}(1+\alpha)\right)}{\pi \frac{t}{T_C}\left(1 - \left(4\alpha \frac{t}{T_C}\right)^2\right)}$$

where the chip duration T_c = (1/chiprate) = 0.24414 μs.

3.7.2 CDMA2000

CDMA2000 is an evolution from the *North American Interim Standard-95 (IS-95)* developed by the *Third Generation Partnership Project 2 (3GPP2)*. The 3GPP2 standard has defined baseband filters for

CDMA2000 for the In-phase (I-channel) and Quadrature-phase (Q-channel) signals prior to modulation [9]. These baseband filters have a normalized frequency response given by

$$S(f) = \begin{cases} \pm\delta_1, & \text{in the passband } 0 \ll f \ll f_p \\ -\delta_2, & \text{in the shopband } f \gg f_s \end{cases}$$

where $\delta_1 = 1.5$ dB, $\delta_2 = 40$ dB, $f_p = 590$ kHz, and $f_s = 740$ kHz. The impulse response $s(t)$ of the baseband filter is given by a scaled and delayed version of the coefficients $h(k)$ in Table 2.1.3.1.13.1-1 in Reference 9. Specifically, a scale factor κ and delay τ are selected to minimize the mean squared error

$$MSE = \sum_{k=0}^{\infty} [\kappa s(kT_s - \tau) - h(k)]^2$$

where $T_s = 203.451$ ns is one quarter of the duration of the CDMA2000 chip.

3.7.3 Wireless Local Area Networks (WLAN)

The IEEE 802.11 working group has developed requirements for the spectral mask for WLANs in Sections 17.3.9.2 and 17.3.9.6 of Reference 10.* Any combination of time-domain windowing and frequency-domain filtering methods may be used to achieve those objectives. IEEE 802.11 has provided informative parameters for a time-domain windowing method that may be used to filter the I- and Q-channel signals prior to modulation. The time-windowing function is given by [10]:

$$w_T(t) = \begin{cases} \sin^2\left(\frac{\pi}{2}(0.5T + t/T_{TR})\right), \text{for } -T_{TR}/2 < t < T_{TR}/2 \\ 1, \text{for } T_{TR}/2 \le t < T - T_{TR}/2 \\ \sin^2\left(\frac{\pi}{2}(0.5T - (t-T)/T_{TR})\right), \text{for } T - T_{TR}/2 \le t < T + T_{TR}/2 \end{cases}$$

where T_{TR} (approximately 100 ns) is selected to smooth transitions between consecutive OFDM symbols. This creates a small overlap between the consecutive symbols. Smoothing this transition reduces the spectral sidelobes of the transmitted waveform. In the case of vanishing T_{TR}, the windowing function degenerates to a rectangular pulse of duration T.

3.7.4 Worldwide Interoperability for Microwave Access (WiMAX)

WiMAX is a broadband wireless access technology, and refers to the IEEE 802.16 standard [11]. The 802.16 air interface is based on OFDM, and has specified a square-root raised cosine filter with excess bandwidth factor $\alpha = 0.25$ for the I- and Q-channels prior to modulation. The filter transfer function is therefore the square root of $H(f)$ in Equation 3.18, where T is the OFDM symbol period.

---

* Reference 10 was created by merging 802.11a, b, d, e, g, h, i, and j amendments with the base 802.11 standard and renamed to the current base standard IEEE 802.11-2007. (The high-throughput amendment 802.11n also references this windowing function.)

3.7.5 Long-Term Evolution (LTE)

LTE is an evolution of UMTS, defined in the 3GPP Release 8 specification. *Evolved UTRA (E-UTRA)* is the air interface for LTE, which operates in both FDD and TDD modes, as well as half-duplex FDD with the same radio access technology. LTE uses *Orthogonal Frequency Division Multiple Access (OFDMA)* radio-access for the downlink and *Single-Carrier Frequency Division Multiple Access (SC-FDMA)* on the uplink. Unlike UTRA, which uses a square-root raised cosine pulse shaping filter, E-UTRA uses a rectangular transmit pulse shaping filter [12].

References

1. Lender, A., The duobinary technique for high-speed data Transmission. *AIEE Trans. on Comm. Electronics*, 82 (March), 214–218, 1963.
2. Kretzmer, E. R., Generalization of a technique for binary data communication. *IEEE Trans. Comm. Tech.*, COM-14(Feb.), 67, 68, 1966.
3. Kalet, I. and Saltzberg, B. R., QAM transmission through a companding channel—Signal constellations and detection. *IEEE Trans. on Comm.*, 42(2–4), 417–429, 1994.
4. Muller, S. H. and Huber, J. B., OFDM with reduced peak-to-average power ratio by optimum combination of partial transmit sequences, *Electronic Letters*, 33(5), 368-369, 2002.
5. Bingham, J. A. C., Multicarrier modulation for data transmission: An idea whose time has come. *IEEE Commun. Mag.*, 28(May), 5–14, 1990.
6. Harashima, H. and Miyakawa, H., Matched-transmission technique for channels with intersymbol interference. *IEEE Trans. on Commun.*, COM-20(Aug.), 774–780, 1972.
7. Tomlinson, M., New automatic equalizer employing modulo arithmetic. *Electron. Lett.*, 7(March), 138, 139, 1971.
8. 3GPP TS 25.101 V9.5.0 and 25.102 V9.2.0 (2010-09), 3rd Generation Partnership Project; Technical Specification Group Radio Access Network; User Equipment (UE) radio transmission and reception (FDD and TDD) (Release 9), September 2010.
9. Telecommunication Industry Association. Physical Layer Standard for cdma2000 Standards for Spread Spectrum Systems. TIA/EIA/IS-2000.2-A, March 2000.
10. IEEE Standard 802.11™-2007, Local and metropolitan area networks, Part 11: Wireless LAN Medium Access Control (MAC) and Physical Layer (PHY) Specifications, June, 2007.
11. IEEE Standard 802.16™, Local and metropolitan area networks, Part 16: Air Interface for Broadband Wireless Access Systems, May, 2009.
12. 3GPP TS 36.101 V9.5.0 (2010-10), 3rd Generation Partnership Project; Technical Specification Group Radio Access Network; Universal Terrestrial Radio Access (E-UTRA); User Equipment (UE) radio transmission and reception (Release 9), October 2010.

Further Reading

Baseband signaling and pulse shaping is fundamental to the design of any digital communications system and is, therefore, covered in numerous texts on digital communications. For more advanced treatments see J. Barry, E. A. Lee and D. G. Messerschmitt, *Digital Communication*, Kluwer 2004, and J. G. Proakis and M. Salehi, *Digital Communications*, McGraw-Hill 2008.

4

Complex Envelope Representations for Modulated Signals*

Leon W. Couch II

4.1 Introduction

What is a general representation for bandpass digital and analog signals? How do we represent a modulated signal? How do we evaluate the spectrum and the power of these signals? These are some of the questions answered in this chapter.

A *baseband* waveform has a spectral magnitude that is nonzero for frequencies in the vicinity of the origin (i.e., $f = 0$) and negligible elsewhere. A *bandpass* waveform has a spectral magnitude that is nonzero for frequencies in some band concentrated about a frequency $f = \pm f_c$ (where $f_c \gg 0$), and the spectral magnitude is negligible elsewhere. f_c is called the *carrier frequency*. The value of f_c may be arbitrarily assigned for mathematical convenience in some problems. In others, namely, modulation problems, f_c is the frequency of an oscillatory signal in the transmitter circuit and is the assigned frequency of the transmitter, such as 850 kHz for an AM broadcasting station.

In communication problems, the information source signal is usually a baseband signal—for example, a transistor–transistor logic (TTL) waveform from a digital circuit or an audio (analog) signal from a microphone. The communication engineer has the job of building a system that will transfer the information from this source signal to the desired destination. As shown in Figure 4.1, this usually requires the use of a bandpass signal, $s(t)$, which has a bandpass spectrum that is concentrated at $\pm f_c$ where f_c is selected so that $s(t)$ will propagate across the communication channel (either a wire or a wireless channel).

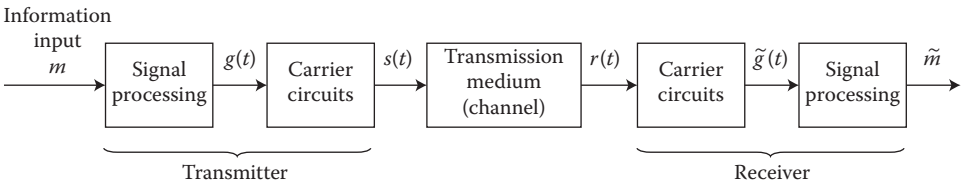

FIGURE 4.1 Bandpass communication system. (From Couch, L. W., II., *Digital and Analog Communication Systems*, 7th ed. Copyright 2007, p. 231. Reprinted with permission of Pearson Education, Inc., Upper Saddle River, NJ.)

Modulation is the process of imparting the source information onto a bandpass signal with a carrier frequency f_c by the introduction of amplitude and/or phase perturbations. This bandpass signal is called the *modulated* signal $s(t)$, and the baseband source signal is called the *modulating* signal $m(t)$. Examples of exactly how modulation is accomplished are given later in this chapter. This definition indicates that modulation may be visualized as a mapping operation that maps the source information onto the bandpass signal $s(t)$ that will be transmitted over the channel.

As the modulated signal passes through the channel, noise corrupts it. The result is a bandpass signal-plus-noise waveform that is available at the receiver input, $r(t)$, as illustrated in Figure 4.1. The receiver has the job of trying to recover the information that was sent from the source; $\tilde{m}$ denotes the corrupted version of m.

4.2 Complex Envelope Representation

All bandpass waveforms, whether they arise from modulated signals, interfering signals, or noise, may be represented in a convenient form given by the following theorem. $\upsilon(t)$ will be used to denote the bandpass waveform canonically. That is, $\upsilon(t)$ can represent the signal when $s(t) \equiv \upsilon(t)$, the noise when $n(t) \equiv \upsilon(t)$, the filtered signal plus noise at the channel output when $r(t) \equiv \upsilon(t)$, or any other type of bandpass waveform.*

Theorem 4.1: Any physical bandpass waveform can be represented by

$$\upsilon(t) = \mathrm{Re}\left\{g(t)e^{j\omega_c t}\right\} \tag{4.1a}$$

Re{·} denotes the real part of {·}. $g(t)$ is called the complex envelope of $\upsilon(t)$, and f_c is the associated carrier frequency (hertz) where $\omega_c = 2\pi f_c$. Furthermore, two other equivalent representations are

$$\upsilon(t) = R(t)\cos[\omega_c t + \theta(t)] \tag{4.1b}$$

and

$$\upsilon(t) = x(t)\cos\omega_c t - y(t)\sin\omega_c t \tag{4.1c}$$

where

$$g(t) = x(t) + jy(t) = \left|g(t)\right|e^{j\angle g(t)} \equiv R(t)e^{j\theta(t)} \tag{4.2}$$

$$x(t) = \mathrm{Re}\{g(t)\} \equiv R(t)\cos\theta(t) \tag{4.3a}$$

* The symbol ≡ denotes an equivalence and the symbol ≜ denotes a definition.

$$y(t) = \text{Im}\{g(t)\} \equiv R(t)\sin\theta(t) \tag{4.3b}$$

$$R(t) \triangleq \left|g(t)\right| \equiv \sqrt{x^2(t) + y^2(t)} \tag{4.4a}$$

$$\theta(t) \triangleq \angle g(t) = \tan^{-1}\left(\frac{y(t)}{x(t)}\right) \tag{4.4b}$$

The waveforms $g(t)$, $x(t)$, $y(t)$, $R(t)$, and $\theta(t)$ are all baseband waveforms, and, except for $g(t)$, they are all real waveforms. $R(t)$ is a nonnegative real waveform. Equations 4.1a through 4.1c is a low-pass-to-bandpass transformation. The $e^{j\omega_c t}$ factor in Equation 4.1a shifts (i.e., translates) the spectrum of the baseband signal $g(t)$ from baseband up to the carrier frequency f_c. In communications terminology the frequencies in the baseband signal $g(t)$ are said to be *heterodyned* up to f_c. The complex envelope, $g(t)$, is usually a complex function of time and it is the generalization of the phasor concept. That is, if $g(t)$ happens to be a complex constant, then $\upsilon(t)$ is a pure sine wave of frequency f_c and this complex constant is the phasor representing the sine wave. If $g(t)$ is not a constant, then $\upsilon(t)$ is not a pure sine wave because the amplitude and phase of $\upsilon(t)$ varies with time, caused by the variations of $g(t)$.

Representing the complex envelope in terms of two real functions in Cartesian coordinates, we have

$$g(x) \equiv x(t) + jy(t) \tag{4.5}$$

where $x(t) = \text{Re}\{g(t)\}$ and $y(t) = \text{Im}\{g(t)\} \cdot x(t)$ is said to be the *in-phase modulation* associated with $\upsilon(t)$, and $y(t)$ is said to be the *quadrature modulation* associated with $\upsilon(t)$. Alternatively, the polar form of $g(t)$, represented by $R(t)$ and $\theta(t)$, is given by Equation 4.2, where the identities between Cartesian and polar coordinates are given by Equations 4.3a, 4.3b and 4.4a, 4.4b. $R(t)$ and $\theta(t)$ are real waveforms and, in addition, $R(t)$ is always nonnegative. $R(t)$ is said to be the *amplitude modulation* (AM) on $\upsilon(t)$, and $\theta(t)$ is said to be the *phase modulation* (PM) on $\upsilon(t)$.

The usefulness of the complex envelope representation for bandpass waveforms cannot be overemphasized. In modern communication systems, the bandpass signal is often partitioned into two channels, one for $x(t)$ called the I (in-phase) channel and one for $y(t)$ called the Q (quadrature-phase) channel. In digital computer simulations of bandpass signals, the sampling rate used in the simulation can be minimized by working with complex envelope, $g(t)$, instead of working with the bandpass signal, $\upsilon(t)$, because $g(t)$ is the baseband equivalent of the bandpass signal [1].

4.3 Representation of Modulated Signals

Modulation is the process of encoding the source information $m(t)$ (modulating signal) into a bandpass signal $s(t)$ (modulated signal). Consequently, the modulated signal is just a special application of the bandpass representation. The *modulated signal* is given by

$$s(t) = \text{Re}\left\{g(t)e^{j\omega_c t}\right\} \tag{4.6}$$

where $\omega_c = 2\pi f_c \cdot f_c$ is the carrier frequency. The complex envelope $g(t)$ is a function of the modulating signal $m(t)$. That is,

$$g(t) = g[m(t)] \tag{4.7}$$

Thus, $g[\cdot]$ performs a mapping operation on $m(t)$. This is shown in Figure 4.1.

Table 4.1 gives an overview of the *big picture* for the modulation problem. Examples of the mapping function $g[m]$ are given for AM, double-sideband suppressed carrier (DSB–SC), PM, frequency modulation

TABLE 4.1 Complex Envelope Functions for Various Types of Modulation[a]

		Corresponding Quadrature Modulation	
Type of Modulation	Mapping Function $g(m)$	$x(t)$	$y(t)$
AM	$A_c[1 + m(t)]$	$A_c[1 + m(t)]$	0
DSB–SC	$A_c m(t)$	$A_c m(t)$	0
PM	$A_c e^{jD_p m(t)}$	$A_c \cos[D_p m(t)]$	$A_c \sin[D_p m(t)]$
FM	$A_c e^{jD_f \int_{-\infty}^{t} m(\sigma)\,d\sigma}$	$A_c \cos\left[D_f \int_{-\infty}^{t} m(\sigma)\,d\sigma\right]$	$A_c \sin\left[D_f \int_{-\infty}^{t} m(\sigma)\,d\sigma\right]$
SSB–AM–SC[b]	$A_c[m(t) \pm j\hat{m}(t)]$	$A_c m(t)$	$\pm A_c \hat{m}(t)$
SSB–PM[b]	$A_c e^{jD_p[m(t) \pm j\hat{m}(t)]}$	$A_c e^{\mp D_p \hat{m}(t)} \cos[D_p m(t)]$	$A_c e^{\mp D_p \hat{m}(t)} \sin[D_p m(t)]$
SSB–FM[b]	$A_c e^{jD_f \int_{-\infty}^{t} [m(\sigma) \pm j\hat{m}(\sigma)]\,d\sigma}$	$A_c e^{\mp D_f \int_{-\infty}^{t} \hat{m}(\sigma)\,d\sigma} \cos\left[D_f \int_{-\infty}^{t} m(\sigma)d\sigma\right]$	$A_c e^{\mp D_f \int_{-\infty}^{t} \hat{m}(\sigma)\,d\sigma} \sin\left[D_f \int_{-\infty}^{t} m(\sigma)d\sigma\right]$
SSB–EV[b]	$A_c e^{\{\ln[1+m(t)] \pm j\widehat{\ln}[1+m(t)]\}}$	$A_c[1 + m(t)] \cos\{\widehat{\ln}[1 + m(t)]\}$	$\pm A_c[1 + m(t)] \sin\{\widehat{\ln}[1 + m(t)]\}$
SSB–SQ[b]	$A_c e^{(1/2)\{\ln[1+m(t)] \pm j\widehat{\ln}[1+m(t)]\}}$	$A_c \sqrt{1 + m(t)} \cos\left\{\frac{1}{2} \widehat{\ln}\,[1 + m(t)]\right\}$	$\pm A_c \sqrt{1 + m(t)} \sin\left\{\frac{1}{2} \widehat{\ln}\,[1 + m(t)]\right\}$
QM	$A_c[m_1(t) + jm_2(t)]$	$A_c m_1(t)$	$A_c m_2(t)$

Type of Modulation	Corresponding Amplitude and Phase Modulation		Linearity	Remarks
	$R(t)$	$\theta(t)$		
AM	$A_c\lvert 1+m(t)\rvert$	$\begin{cases} 0, & m(t)>-1 \\ 180°, & m(t)<-1 \end{cases}$	L[c]	$m(t)>-1$ required for envelope detection
DSB–SC	$A_c\lvert m(t)\rvert$	$\begin{cases} 0, & m(t)>0 \\ 180°, & m(t)<0 \end{cases}$	L	Coherent detection required
PM	A_c	$D_p m(t)$	NL	D_p is the phase deviation constant (rad/volt)
FM	A_c	$D_f\int_{-\infty}^{t} m(\sigma)d\sigma$	NL	D_f is the frequency deviation constant (rad/volt)
SSB–AM–SC[b]	$A_c\sqrt{[m(t)]^2+[\hat{m}(t)]^2}$	$\tan^{-1}[\pm\hat{m}(t)/m(t)]$	L	Coherent detection required
SSB–PM[b]	$A_c e^{\pm D_p\hat{m}(t)}$	$D_p m(t)$	NL	
SSB–FM[b]	$A_c e^{\pm D_f\int_{-\infty}^{t}\hat{m}(\sigma)d\sigma}$	$D_f\int_{-\infty}^{t} m(\sigma)d\sigma$	NL	
SSB–EV[b]	$A_c\lvert 1+m(t)\rvert$	$\pm\widehat{\ln}[1+m(t)]$	NL	$m(t)>-1$ is required so that the $\ln(\cdot)$ will have a real value
SSB–SQ[b]	$A_c\sqrt{1+m(t)}$	$\pm\frac{1}{2}\widehat{\ln}[1+m(t)]$	NL	$m(t)>-1$ is required so that the $\ln(\cdot)$ will have a real value
QM	$A_c\sqrt{m_1^2(t)+m_2^2(t)}$	$\tan^{-1}[m_2(t)/m_1(t)]$	L	Used in NTSC color television: requires coherent detection

Source: From Couch, L.W., II., *Digital and Analog Communication Systems*, 7th ed. Copyright 2007, p. 235, 236. Reprinted with permission of Pearson Education, Inc., Upper Saddle River, NJ.

[a] $A_c>0$ is a constant that sets the power level of the signal as evaluated by use of (4.11): L, linear; NL, nonlinear: and $[\cdot]$ is the Hilbert transform (a –90° phase-shifted version of $[\cdot]$). For example, $\hat{m}(t)=m(t)*\frac{1}{\pi t}=\frac{1}{\pi}\int_{-\infty}^{\infty}\frac{m(\lambda)}{t-\lambda}d\lambda$.

[b] Use upper signs for upper sideband signals and lower signals for lower sideband signals.

[c] In the strict sense, AM signals are not linear because the carrier term does not satisfy the linearity (superposition) condition.

(FM), single-sideband AM suppressed carrier (SSB–AM–SC), single-sideband PM (SSB–PM), single-sideband FM (SSB–FM), single-sideband envelope detectable (SSB–EV), single-sideband square-law detectable (SSB–SQ), and quadrature modulation (QM). For each $g[m]$, Table 4.1 also shows the corresponding $x(t)$ and $y(t)$ quadrature modulation components, and the corresponding $R(t)$ and $\theta(t)$ amplitude and phase modulation components. Digitally modulated bandpass signals are obtained when $m(t)$ is a digital baseband signal—for example, the output of a TTL circuit.

Obviously, it is possible to use other $g[m]$ functions that are not listed in Table 4.1. The question is: Are they useful? $g[m]$ functions are desired that are easy to implement and that will give desirable spectral properties. Furthermore, in the receiver the inverse function $m[g]$ is required. The inverse should be single valued over the range used and should be easily implemented. The inverse mapping should suppress as much noise as possible so that $m(t)$ can be recovered with little corruption.

4.4 Generalized Transmitters and Receivers

A more detailed description of transmitters and receivers as first shown in Figure 4.1 will now be illustrated.

There are two canonical forms for the generalized transmitter, as indicated by Equations 4.1b and 4.1c. Equation 4.1b describes an AM–PM-type circuit as shown in Figure 4.2. The baseband signal processing circuit generates $R(t)$ and $\theta(t)$ from $m(t)$. The R and θ are functions of the modulating signal $m(t)$, as given in Table 4.1, for the particular modulation type desired. The signal processing may be implemented either by using nonlinear analog circuits or a digital computer that incorporates the R and θ algorithms under software program control. In the implementation using a digital computer, one analog-to-digital converter (ADC) will be needed at the input of the baseband signal processor and two digital-to-analog converters (DACs) will be needed at the output. The remainder of the AM–PM canonical form requires radio frequency (RF) circuits, as indicated in the figure.

Figure 4.3 illustrates the second canonical form for the generalized transmitter. This uses in-phase and quadrature-phase (IQ) processing. Similarly, the formulas relating $x(t)$ and $y(t)$ to $m(t)$ are shown in Table 4.1, and the baseband signal processing may be implemented by using either analog hardware or digital hardware with software. The remainder of the canonical form uses RF circuits as indicated.

Analogous to the transmitter realizations, there are two canonical forms of receiver. Each one consists of RF carrier circuits followed by baseband signal processing as illustrated in Figure 4.1. Typically, the carrier circuits are of the superheterodyne-receiver type which consist of an RF amplifier, a down-converter (mixer plus local oscillator) to some intermediate frequency (IF), an IF amplifier, and then detector circuits [1]. In the first canonical form of the receiver, the carrier circuits have amplitude and

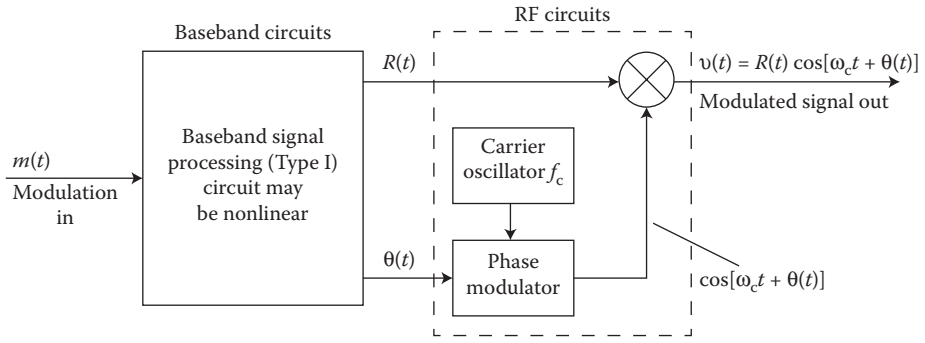

FIGURE 4.2 Generalized transmitter using the AM–PM generation technique. (From Couch, L. W., II., *Digital and Analog Communication Systems*, 7th ed. Copyright 2007, p. 282. Reprinted with permission of Pearson Education, Inc., Upper Saddle River, NJ, p. 278. With permission.)

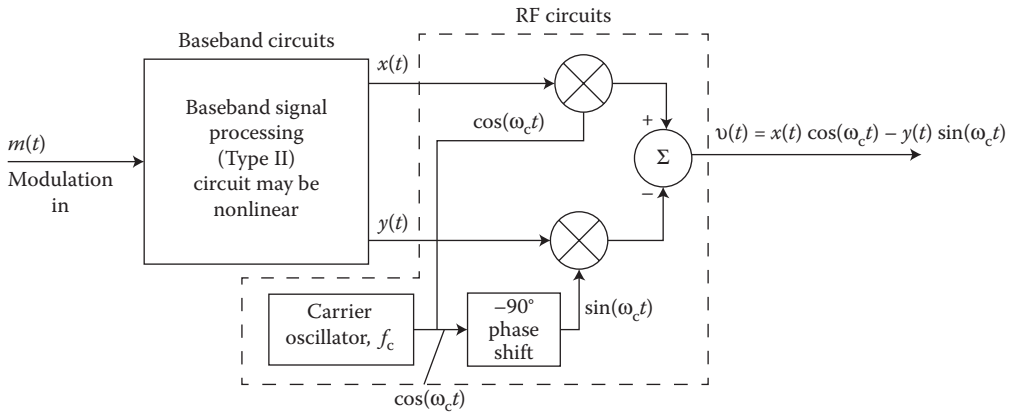

FIGURE 4.3 Generalized transmitter using the quadrature generation technique. (From Couch, L. W., II., *Digital and Analog Communication Systems*, 7th ed. Copyright 2007. Reprinted with permission of Pearson Education, Inc., Upper Saddle River, NJ, p. 283.)

phase detectors that output $\tilde{R}(t)$ and $\tilde{\theta}(t)$, respectively. This pair, $\tilde{R}(t)$ and $\tilde{\theta}(t)$, describe the polar form of the received complex envelope, $\tilde{g}(t) \cdot \tilde{R}(t)$ and $\tilde{\theta}(t)$ are then fed into the signal processor which uses the inverse functions of Table 4.1 to generate the recovered modulation, $\tilde{m}(t)$. The second canonical form of the receiver uses quadrature product detectors in the carrier circuits to produce the Cartesian form of the received complex envelope, $\tilde{x}(t)$ and $\tilde{y}(t)\tilde{x}(t)$ and $\tilde{y}(t)$ are then inputted to the signal processor which generates $\tilde{m}(t)$ at its output.

Once again, it is stressed that any type of signal modulation (see Table 4.1) may be generated (transmitted) or detected (received) by using either of these two canonical forms. Both of these forms conveniently separate baseband processing from RF processing. Digital techniques are especially useful to realize the baseband processing portion. Furthermore, if digital computing circuits are used, any desired modulation type can be realized by selecting the appropriate software algorithm.

4.5 Spectrum and Power of Bandpass Signals

The spectrum of the bandpass signal is the translation of the spectrum of its complex envelope. Taking the Fourier transform of Equation 4.1a, the spectrum of the bandpass waveform is [1]

$$V(f) = \frac{1}{2}[G(f - f_c) + G^*(-f - f_c)] \tag{4.8}$$

where $G(f)$ is the Fourier transform of $g(t)$,

$$G(f) = \int_{-\infty}^{\infty} g(t)e^{-j2\pi ft}\,dt$$

and the asterisk superscript denotes the complex conjugate operation. The power spectra density (PSD) of the bandpass waveform is [1]

$$\mathcal{P}_v(f) = \frac{1}{4}[\mathcal{P}_g(f - f_c) + \mathcal{P}_g(-f - f_c)] \tag{4.9}$$

where $\mathcal{P}_g(f)$ is the PSD of $g(t)$.

The average power dissipated in a resistive load is V_{rms}^2/R_L or $I_{rms}^2 R_L$ where V_{rms} is the rms value of the voltage waveform across the load and is I_{rms} the rms value of the current through the load. For bandpass waveforms, Equations 4.1a through 4.1c may represent either the voltage or the current. Furthermore, the rms values of $V(t)$ and $g(t)$ are related by [1]

$$V_{rms}^2 = \langle v^2(t) \rangle = \frac{1}{2}\langle |g(t)|^2 \rangle = \frac{1}{2} g_{rms}^2 \tag{4.10}$$

where $\langle\rangle$ denotes the time average and is given by

$$\langle [] \rangle = \lim_{t \to \infty} \frac{1}{T} \int_{-T/2}^{T/2} [] \, dt$$

Thus, if $v(t)$ of Equations 4.1a through 4.1c represents the bandpass voltage waveform across a resistive load, the average power dissipated in the load is

$$P_L = \frac{V_{rms}^2}{R_L} = \frac{\langle v^2(t) \rangle}{R_L} = \frac{\langle |g(t)|^2 \rangle}{2R_L} = \frac{g_{rms}^2}{2R_L} \tag{4.11}$$

where g_{rms} is the rms value of the complex envelope and R_L is the resistance of the load.

4.6 Amplitude Modulation

Amplitude modulation (AM) will now be examined in more detail. From Table 4.1 the complex envelope of an AM signal is

$$g(t) = A_c[1 + m(t)] \tag{4.12}$$

so that the spectrum of the complex envelope is

$$G(f) = A_c \delta(f) + A_c M(f) \tag{4.13}$$

Using Equation 4.6, we obtain the AM signal waveform

$$s(t) = A_c[1 + m(t)] \cos \omega_c t \tag{4.14}$$

and, using Equation 4.8, the AM spectrum

$$S(f) = \frac{1}{2} A_c[\delta(f - f_c) + M(f - f_c) + \delta(f + f_c) + M(f + f_c)] \tag{4.15}$$

where $\delta(f) = \delta(-f)$ and, because $m(t)$ is real, $M^*(f) = M(-f)$. Suppose that the magnitude spectrum of the modulation happens to be a triangular function, as shown in Figure 4.4a. This spectrum might arise from an analog audio source where the bass frequencies are emphasized. The resulting AM spectrum, using Equation 4.15, is shown in Figure 4.4b. Note that because $G(f - f_c)$ and $G^*(-f - f_c)$ do not overlap, the magnitude spectrum is

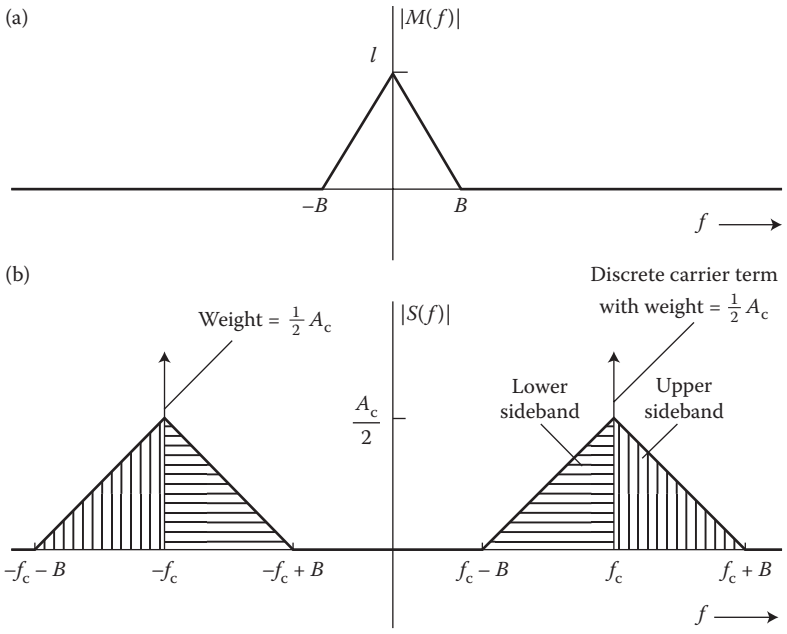

FIGURE 4.4 Spectrum of an AM signal. (a) Magnitude spectrum of modulation. (b) Magnitude spectrum of AM signal. (From Couch, L. W., II., 1997. *Digital and Analog Communication Systems*, 5th ed. Prentice-Hall, Upper Saddle River, NJ, p. 235. With permission.)

$$|S(f)| = \begin{cases} \frac{1}{2}A_c\delta(f - f_c) + \frac{1}{2}A_c|M(f - f_c)|, & f > 0 \\ \frac{1}{2}A_c\delta(f + f)_c + \frac{1}{2}A_c|M(-f - f)_c|, & f < 0 \end{cases}. \tag{4.16}$$

The 1 in

$$g(t) = A_c[1 + m(t)]$$

causes delta functions to occur in the spectrum at $f = \pm f_c$, where f_c is the assigned carrier frequency. Also, from Figure 4.4 and Equation 4.16, it is realized that the bandwidth of the AM signal is 2B. That is, the bandwidth of the AM signal is twice the bandwidth of the baseband modulating signal.

The average power dissipated into a resistive load is found by using Equation 4.11.

$$P_L = \frac{A_c^2}{2R_L}\left\langle |1 + m(t)|^2 \right\rangle = \frac{A_c^2}{2R_L}\left[1 + 2\langle m(t)\rangle + \left\langle m^2(t)\right\rangle\right]$$

If we assume that the *dc* value of the modulation is zero, $\langle m(t)\rangle = 0$, then the average power dissipated into the load is

$$P_L = \frac{A_c^2}{2R_L}\left\langle 1 + m_{rms}^2 \right\rangle \tag{4.17}$$

where m_{rms} is the rms value of the modulation, $m(t)$. Thus, the average power of an AM signal changes if the rms value of the modulating signal changes. For example, if $m(t)$ is a sine wave test tone with a peak value of 1.0 for 100% modulation,

$$m_{rms} = 1/\sqrt{2}$$

Assume that $A_c = 1000$ V and $R_L = 50\ \Omega$, which are typical values used in AM broadcasting. Then the average power dissipated into the 50 Ω load for this AM signal is

$$P_L = \frac{(1000)^2}{2(50)}\left[1 + \frac{1}{2}\right] = 15{,}000 \text{ W} \tag{4.18}$$

The Federal Communications Commission (FCC) rated carrier power is obtained when $m(t) = 0$. In this case, (4.17) becomes $P_L = (1000)^2/100 = 10{,}000$ W and the FCC would rate this as a 10,000 W AM station. The sideband power for 100% sine wave modulation is 5000 W.

Now let the modulation on the AM signal be a binary digital signal such that $m(t) = \pm 1$ where +1 is used for a binary one and −1 is used for a binary 0. Referring to Equation 4.14, this AM signal becomes an *on–off keyed* (OOK) digital signal where the signal is on when a binary one is transmitted and off when a binary zero is transmitted. For $A_c = 1000$ and $R_L = 50\ \Omega$, the average power dissipated would be 20,000 W since $m_{rms} = 1$ for $m(t) = \pm 1$.

4.7 Phase and Frequency Modulation

Phase modulation (PM) and *frequency modulation* (FM) are special cases of angle-modulated signaling. In angle-modulated signaling the complex envelope is

$$g(t) = A_c e^{j\theta(t)} \tag{4.19}$$

Using Equation 4.6, the resulting *angle-modulated* signal is

$$s(t) = A_c \cos[\omega_c + \theta(t)] \tag{4.20}$$

For PM the phase is directly proportional to the modulating signal:

$$\theta(t) = D_p m(t) \tag{4.21}$$

where the proportionality constant D_p is the phase sensitivity of the phase modulator, having units of radians per volt [assuming that $m(t)$ is a voltage waveform]. For FM the phase is proportional to the integral of $m(t)$:

$$\theta(t) = D_f \int_{-\infty}^{t} m(\sigma)\, d\sigma \tag{4.22}$$

where the frequency deviation constant D_f has units of radians/volt-s. These concepts are summarized by the PM and FM entries in Table 4.1.

By comparing the last two equations, it is seen that if we have a PM signal modulated by $m_p(t)$, there is *also* FM on the signal corresponding to a *different* modulating waveshape that is given by

$$m_f(t) = \frac{D_p}{D_f}\left[\frac{dm_p(t)}{dt}\right] \tag{4.23}$$

where the subscripts *f* and *p* denote frequency and phase, respectively. Similarly, if we have an FM signal modulated by $m_f(t)$, the corresponding PM on this signal is

$$m_p(t) = \frac{D_f}{D_p}\int_{-\infty}^{t} m_f(\sigma)d\sigma \tag{4.24}$$

By using Equation 4.24, a PM circuit may be used to synthesize an FM circuit by inserting an integrator in cascade with the phase modulator input.

Other properties of PM and FM are that the real envelope, $R(t) = |g(t)| = A_c$, is a constant, as seen from Equation 4.19. Also, $g(t)$ is a nonlinear function of the modulation. However, from Equations 4.21 and 4.22, $\theta(t)$ is a linear function of the modulation, $m(t)$. Using Equation 4.11, the average power dissipated by a PM or FM signal is the constant

$$P_L = \frac{A_c^2}{2R_L}. \tag{4.25}$$

That is, the average power of a PM or FM signal does not depend on the modulating waveform, $m(t)$.

The *instantaneous frequency deviation* for an FM signal from its carrier frequency is given by the derivative of its phase $\theta(t)$. Taking the derivative of Equation 4.22, the *peak frequency deviation* is

$$\Delta F = \frac{1}{2\pi} D_f M_p \text{ Hz} \tag{4.26}$$

where $M_p = \max[m(t)]$ is the peak value of the modulation waveform and the derivative has been divided by 2π to convert from rad/s to Hz units.

For FM and PM signals, Carson's rule estimates the transmission bandwidth containing approximately 98% of the total power. This FM or PM signal bandwidth is

$$B_T = 2(\beta + 1)B \tag{4.27}$$

where B is bandwidth (highest frequency) of the modulation. The modulation index β, is $\beta = \Delta F/B$ for FM and $\beta = \max[D_p m(t)] = D_p M_p$ for PM.

The popular General Mobile Radio Service (GMRS) handi-talkie portable phones use FM signaling. A peak deviation of 5 kHz is specified with a modulation bandwidth of 3 kHz. From Equation 4.27, this gives a bandwidth of 16 kHz for the GMRS signal and allows a channel spacing of 25 kHz to be used.

The Group Special Mobile (GSM) digital cellular phones use FM with *minimum frequency-shift-keying* (MSK) where the peak frequency deviation is selected to produce orthogonal waveforms for binary one and binary zero data. (Digital phones use a speech codec to convert the analog voice source to a digital data source for transmission over the system.) Orthogonality occurs when $\Delta F = 1/4R$ where R is the bit rate (bits/s) [1]. Actually, GSM uses Gaussian-shaped MSK (GMSK). That is, the digital data waveform (with rectangular binary one and binary zero pulses) is first filtered by a low-pass filter having

a Gaussian-shaped frequency response (to attenuate the higher frequencies). This Gaussian-filtered data waveform is then fed into the frequency modulator to generate the GMSK signal. This produces a digitally modulated FM signal with a relatively small bandwidth.

Other digital cellular standards use QPSK signaling as discussed in the next section.

4.8 QPSK Signaling

Quadrature phase-shift-keying (QPSK) is a special case of quadrature modulation as shown in Table 4.1 where $m_1(t) = \pm 1$ and $m_2(t) = \pm 1$ are two binary bit streams. The complex envelope for QPSK is

$$g(t) = x(t) + jy(t) = A_c[m_1(t) + jm_2(t)]$$

where $x(t) = \pm A_c$ and $y(t) = \pm A_c$. The permitted values for the complex envelope are illustrated by the QPSK signal constellation shown in Figure 4.5a. The *signal constellation* is a plot of the permitted values for the complex envelope, $g(t)$. QPSK may be generated by using the quadrature generation technique seen in Figure 4.3, where the baseband signal processor is a serial-to-parallel converter that reads in two bits of data at a time from the serial binary input stream, $m(t)$ and outputs the first of the two bits to $x(t)$ and the second bit to $y(t)$. If the two input bits are both binary ones, (11), then $m_1(t) = +A_c$ and $m_2(t) = +A_c$. This is represented by the top right-hand dot for $g(t)$ in the signal constellation for QPSK signaling in Figure 4.5a. Likewise, the three other possible two-bit words, (10), (01), and (00), are also shown. The QPSK signal is also equivalent to a four-phase phase-shift-keyed signal (4PSK) since all the points in the signal constellation fall on a circle where the permitted phases are $\theta(t) = 45°$, 135°, 225°, and 315°. There is no AM on the QPSK signal since the distances from the origin to all the signal points on the signal constellation are equal.

For QPSK, the spectrum of $g(t)$ is of the sin x/x type since $x(t)$ and $y(t)$ consists of rectangular data pulses of value $\pm A_c$. Moreover, it can be shown that for equally likely independent binary one and binary zero data, the power spectral density of $g(t)$ for digitally modulated signals with M point signal constellations is [1]

$$\mathcal{P}_g(f) = K\left(\frac{\sin \pi f \ell T_b}{\pi f \ell T_b}\right)^2 \tag{4.28}$$

where K is a constant, $R = 1/T_b$ is the data rate (bits/s) of $m(t)$ and $M = 2^\ell$. M is the number of points in the signal constellation. For QPSK, $M = 4$ and $\ell = 2$. This PSD for the complex envelope, $\mathcal{P}_g(f)$, is plotted in Figure 4.6. The PSD for the QPSK signal ($\ell = 2$) is given by translating $\mathcal{P}_g(f)$ up to the carrier frequency as indicated by Equation 4.9.

Referring to Figure 4.6 or using Equation 4.28, the first-null bandwidth of $g(t)$ is R/ℓ Hz. Consequently, the null-to-null bandwidth of the modulated RF signal is

$$B_{null} = \frac{2R}{\ell} \text{Hz} \tag{4.29}$$

For example, if the data rate of the baseband information source is 9600 bits/s, then the null-to-null bandwidth of the QPSK signal would be 9.6 Hz since $\ell = 2$.

Referring to Figure 4.6, it is seen that the sidelobes of the spectrum are relatively large so, in practice, the sidelobes of the spectrum are filtered off to prevent interference to the adjacent channels. This filtering rounds off the edges of the rectangular data pulses and this causes some AM on the QPSK signal. That is, the points in the signal constellation for the filtered QPSK signal would be fuzzy since the

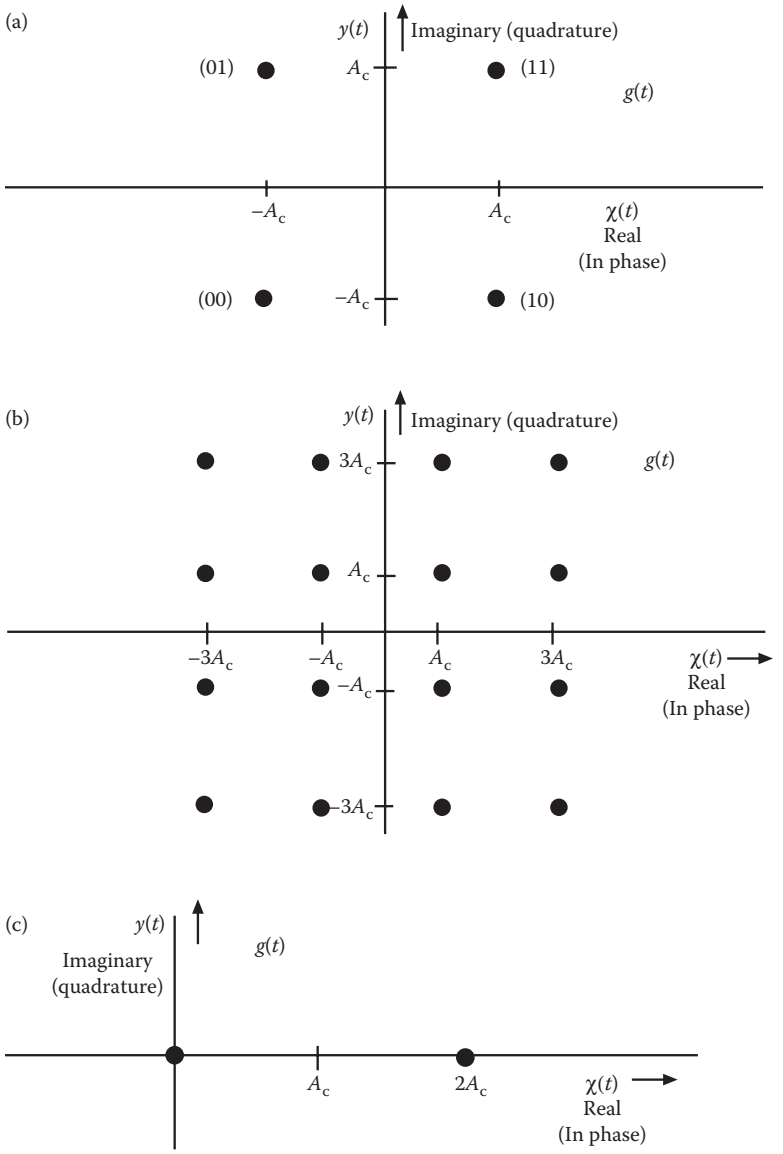

FIGURE 4.5 Signal constellations (permitted values of the complex envelope). (a) QPSK signal constellation. (b) 16 QAM signal constellation. (c) OOK signal constellation.

transition from one constellation point to another point is not instantaneous because the filtered data pulses are not rectangular. QPSK is the modulation used for digital cellular phones with the IS-95 Code Division Multiple Access (CDMA) standard.

Equation 4.28 and Figure 4.6 also represent the spectrum for *quadrature modulation amplitude modulation* (QAM) signaling. QAM signaling allows more than two values for $x(t)$ and $y(t)$. For example, QAM where $M = 16$ has 16 points in the signal constellation with 4 values for $x(t)$ and 4 values for $y(t)$ such as, for example, $x(t) = +A_c,\ -A_c, +3A_c, -3A_c$ and $y(t) = +A_c, -A_c, +3A_c, -3A_c$. This is shown in Figure 4.5b. Each point in the $M = 16$ QAM signal constellation would represent a unique four-bit data word, as compared with the $M = 4$ QPSK signal constellation shown in Figure 4.5a where each point

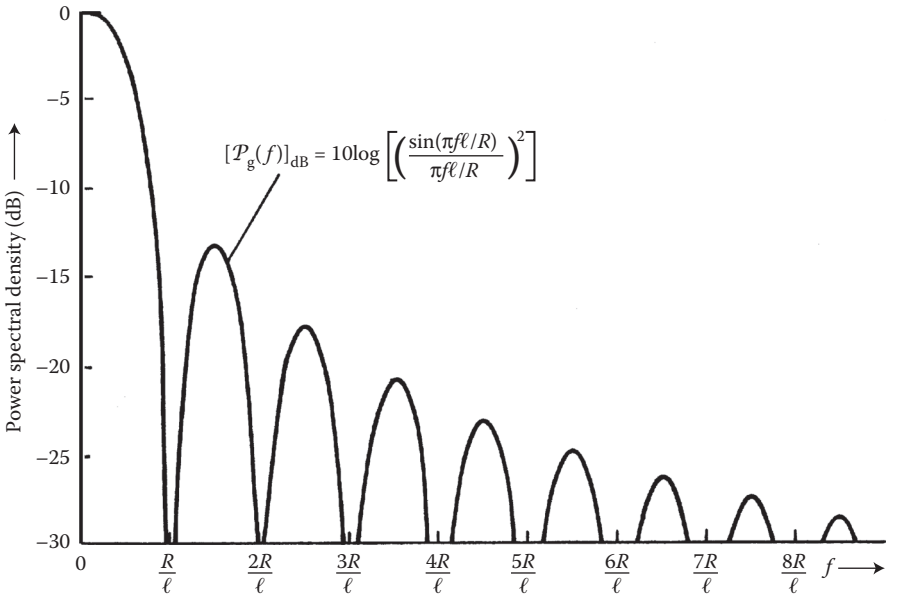

FIGURE 4.6 PSD for the complex envelope of MPSK and QAM where $M = 2^{\ell}$ and R is bit rate (positive frequencies shown). (From Couch, L. W., II., *Digital and Analog Communication Systems*, 7th ed. Copyright 2007, p. 360. Upper Saddle River, NJ. Reprinted with permission of Pearson Education Inc.)

represents a unique two-bit data word. For an $R = 9600$ bits/s information source data rate, a $M = 16$ QAM signal would have a null-to-null bandwidth of 4.8 kHz since $\ell = 4$.

For OOK signaling as described at the end of Section 4.6, the signal constellation would consist of M = 2 points along the x axis where $x = 0$, $2A_c$ and $y = 0$. This is illustrated in Figure 4.5c. For an $R = 9600$ bit/s information source data rate, an OOK signal would have a null-to-null bandwidth of 19.2 kHz since $\ell = 1$.

4.9 OFDM Signaling

Orthogonal frequency division multiplexing (OFDM) is a technique for transmitting data in parallel by using a large number of modulated carriers with sufficient frequency spacing so that the carriers are orthogonal. As we shall see, OFDM provides resistance to data errors caused by multipath channels.

Over a T-s interval, the complex envelope for the OFDM signal is

$$g(t) = A_c \sum_{n=0}^{N-1} w_n \varphi_n(t), \quad 0 > t > T \tag{4.30}$$

where A_c is the carrier amplitude, w_n is the element of the N-element parallel data vector $w = [w_0, w_1, \ldots, w_{N-1}]$ and the orthogonal carriers are

$$\varphi_n(t) = e^{j2\pi f_n t} \quad \text{where } f_n = \frac{1}{T}\left(n - \frac{N-1}{2}\right) \tag{4.31}$$

A key advantage of OFDM is that it can be generated relatively easily by using *fast Fourier transform* (FFT) digital signal processing techniques [1]. From a utilization standpoint, the advantage of OFDM

over single-carrier schemes is the ability of OFDM signaling to provide good data recovery over wireline channels, such as twisted pair line that has severe attenuation at higher frequencies. For wireless channels, OFDM tolerates narrow-band interference and frequency-selective fading due to multipath. OFDM is used in *digital subscriber line* (DSL) wireline signaling, and in wireless Wi-Fi, Wi-Max, and 4G cellular systems.

For more information about OFDM, see http://en.wilkipedia.org.

Reference

1. Couch, L. W., II., *Digital and Analog Communication Systems*, 7th ed. Upper Saddle River, NJ: Pearson Prentice-Hall, 2007.

Further Reading

1. Bedrosian, E., The analytic signal representation of modulated waveforms. *Proc. IRE*, 50(October), 2071–2076, 1962.
2. Dugundji, J., Envelopes and pre-envelopes of real waveforms. *IRE Trans. Information Theory*, IT-4(March), 53–57, 1958.
3. Voelcker, H.B., Toward the unified theory of modulation—Part I: Phase-envelope relationships. *Proc. IRE*, 54(March), 340–353, 1966.
4. Voelcker, H.B., Toward the unified theory of modulation—Part II: Zero manipulation. *Proc. IRE*, 54(May), 735–755, 1966.
5. Ziemer, R.E. and Tranter, W.H., *Principles of Communications*, 4th ed. New York: John Wiley and Sons, 1995.
6. Weinstein, S.B., The history of orthogonal frequency-division multiplexing. *IEEE Communications Magazine*, 47(November), 26–35, 2009.

5

Modulation Methods

Gordon L. Stüber

5.1 Introduction

Modulation is the process whereby message information is embedded into a radio frequency carrier. Message information can be transmitted in the amplitude, frequency, or phase of the carrier, or a combination thereof, in either analog or digital format. Analog modulation schemes include amplitude modulation (AM) and frequency modulation (FM). Analog modulation schemes are still used today for broadcasting AM/FM radio, but all other communication and broadcast systems now use digital modulation. Digital modulation schemes transmit information using a finite set of waveforms and have a number of advantages over their analog counterparts. Digital modulation is a natural choice for digital sources, for example, computer communications. Source encoding or data compression techniques can reduce the required transmission bandwidth with a controlled amount of signal distortion. Digitally modulated waveforms are also more robust to channel impairments such as delay and Doppler spread, and cochannel and adjacent channel interference. Finally, encryption and multiplexing is easier with digital modulation schemes.

Modulation schemes can be designed to provide power and/or bandwidth efficient communication. In an information theoretic sense, we want to operate close to the Shannon capacity limit of a channel. This generally requires the use of error control coding along with a jointly designed encoder and modulator. However, in this chapter we only consider the modulation schemes by themselves. The bandwidth efficiency of a modulation scheme indicates how much information is transmitted per channel use and is measured in units of bits per second per Hertz of bandwidth (bits/s/Hz). The power efficiency can be measured by the received signal-to-interference-plus-noise ratio (SINR) that is required to achieve reliable communication with specified bandwidth efficiency in the presence of channel impairments such

as delay spread and Doppler spread. In general, modulation techniques for spectrally efficient communication systems should have the following properties:

- *Compact power density spectrum:* To minimize the effect of adjacent channel interference, the power radiated into the adjacent band is often limited to be 60–80 dB below that in the desired band. This requires modulation techniques having a power spectrum characterized by a narrow main lobe and fast roll-off of side-lobes.
- *Robust communication:* Reliable communication must be achieved in the presence of delay and Doppler spread, adjacent and cochannel interference, and thermal noise. Modulation schemes that promote good power efficiency in the presence of channel impairments are desirable.
- *Envelope properties:* Portable and mobile devices often employ power-efficient nonlinear (Class-C) power amplifiers to minimize battery drain. However, amplifier nonlinearities will degrade the performance of modulation schemes that transmit information in the amplitude of the carrier and/or have a nonconstant envelope. To obtain suitable performance, such modulation schemes require a less power-efficient linear or linearized power amplifier. Also, spectral shaping is usually performed prior to upconversion and nonlinear amplification. To prevent the regrowth of spectral side lobes during nonlinear amplification, modulation schemes having a relatively constant envelope are desirable.

5.2 Basic Description of Modulated Signals

With any modulation technique, the bandpass signal can be expressed in the form

$$s(t) = \Re\left\{\tilde{s}(t)e^{j2\pi f_c t}\right\} \tag{5.1}$$

where $\tilde{s}(t) = \tilde{s}_I(t) + j\tilde{s}_Q(t)$ is the complex envelope, f_c is the carrier frequency, and $\Re\{z\}$ denotes the real part of z. For any digital modulation scheme, the complex envelope can be written in the standard form [1]

$$\tilde{s}(t) = A\sum_n b(t - nT, \mathbf{x}_n) \tag{5.2}$$

$$\mathbf{x}_n = (x_n, x_{n-1}, \ldots, x_{n-K}), \tag{5.3}$$

where A is the amplitude and $\{x_n\}$ is the sequence of complex data symbols that are chosen from a finite alphabet, and K is the modulator memory order which may be finite or infinite. One data symbol is transmitted every T seconds, so that the baud rate is $R = 1/T$ symbols/s. The function $b(t,\mathbf{x}_i)$ is a generalized shaping function whose exact form, along with the modulator memory order, depends on the type of modulation that is employed. Several examples are provided in this chapter where information is transmitted in the amplitude, phase, or frequency of the bandpass signal.

The power spectral density of the bandpass signal, $S_{ss}(f)$, is related to the power spectral density of the complex envelope, $S_{\tilde{s}\tilde{s}}(f)$, by

$$S_{ss}(f) = \frac{1}{2}\left[S_{\tilde{s}\tilde{s}}(-f - f_c) + S_{\tilde{s}\tilde{s}}(f + f_c)\right]. \tag{5.4}$$

The power density spectrum of the complex envelope for a digital modulation scheme has the general form

$$S_{\tilde{s}\tilde{s}}(f) = \frac{A^2}{T}\sum_{m} S_{\mathrm{b,m}}(f)\mathrm{e}^{-\mathrm{j}2\pi fmT}, \tag{5.5}$$

where

$$S_{\mathrm{b,m}}(f) = \frac{1}{2}\mathrm{E}\left[B(f,\mathbf{x}_{\mathrm{m}})B^{*}(f,\mathbf{x}_{0})\right], \tag{5.6}$$

$B(f,\mathbf{x}_{\mathrm{m}})$ is the Fourier transform of $b(t,\mathbf{x}_{\mathrm{m}})$, and E $[\cdot]$ denotes the expectation operator. Usually symmetric signal sets are chosen so that the complex envelope has zero mean, that is, E $[b(t,\mathbf{x}_0)] = 0$. This implies that the power density spectrum has no discrete components. If in addition $\mathbf{x}_{\mathrm{m}}$ and $\mathbf{x}_0$ are independent for $|m| > K$, then

$$S_{\tilde{s}\tilde{s}}(f) = \frac{A^2}{T}\sum_{|m|<K} S_{\mathrm{b,m}}(f)\mathrm{e}^{-\mathrm{j}2\pi fmT}. \tag{5.7}$$

Another important case arises with uncorrelated zero-mean data, where $S_{\mathrm{b},K}(f) = 0$, $K = 1$. In this case, only the term $S_{\mathrm{b},0}(f)$ remains and

$$S_{\tilde{s}\tilde{s}}(f) = \frac{A^2}{T}S_{\mathrm{b},0}(f), \tag{5.8}$$

where

$$S_{\mathrm{b},0}(f) = \frac{1}{2}\mathrm{E}\left[|\, B(f,\mathbf{x}_0)\,|^2\right]. \tag{5.9}$$

5.3 Quadrature Amplitude Modulation

Quadrature amplitude modulation (QAM) is a bandwidth-efficient modulation scheme that is used in numerous wireless standards. With QAM, the complex envelope of the transmitted waveform is

$$\tilde{s}(t) = A\sum_{n} b(t - nT, \mathbf{x}_n) \tag{5.10}$$

where

$$b(t,\mathbf{x}_n) = x_n h_{\mathrm{a}}(t) \tag{5.11}$$

$h_{\mathrm{a}}(t)$ is the amplitude shaping pulse, and $x_n = x_{\mathrm{I},n} + \mathrm{j}x_{\mathrm{Q},n}$ is the complex-valued data symbol that is transmitted at epoch n. Each symbol x_{k} is mapped onto $\log_2 M$ source bits. It is apparent that both the amplitude and the excess phase of a QAM waveform depend on the complex data symbols. QAM has the advantage of high bandwidth efficiency, but amplifier nonlinearities will degrade its performance due to its nonconstant envelope.

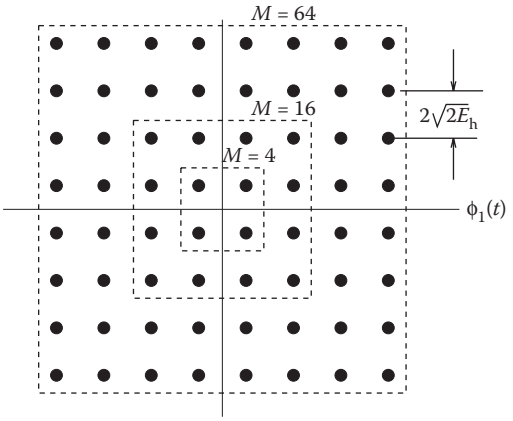

FIGURE 5.1 Complex signal-space diagram for square QAM constellations.

5.3.1 QAM Signal Constellations

A variety of QAM signal constellations may be constructed. Square QAM constellations can be constructed when M is an even power of 2 by choosing $x_{I,m}, x_{Q,m} \in \{\pm 1, \pm 3, \ldots, \pm(N-1)\}$ and $N = \sqrt{M}$. The complex signal-space diagram for the square 4-, 16-, and 64-QAM constellations is shown in Figure 5.1. Note that the minimum Euclidean distance between any two signal vectors is $2\sqrt{2E_h}$, where

$$E_h = \frac{A^2}{2}\int_{-\infty}^{\infty} h_a^2(t)\,dt \tag{5.12}$$

is the energy in the bandpass pulse $Ah_a(t)\cos 2\pi f_c t$ under the condition $f_c T \gg 1$.

When M is an odd power of 2, the signal constellation is not square. Usually, the constellation is given the shape of a cross to minimize the average energy in the constellation for a given minimum Euclidean distance between signal vectors. Examples of the QAM "cross constellations" are shown in Figure 5.2.

5.3.2 Root Raised Cosine Pulse Shaping

The amplitude shaping pulse is very often chosen to be a square root raised cosine pulse, where the Fourier transform of $h_a(t)$ is

$$H_a(f) = \begin{cases} \sqrt{T} & 0 \le |f| \le (1-\beta)/2T \\ \sqrt{\dfrac{T}{2}\left[1 - \sin\dfrac{\pi T}{\beta}\left(f - \dfrac{1}{2T}\right)\right]} & (1-\beta)/2T \le |f| \le (1+\beta)/2T. \end{cases} \tag{5.13}$$

The receiver implements the matched filter $h_a(-t)$ so that the overall pulse produced by the cascade of the transmitter and receiver matched filters is $p(t) = h_a(t)^* h_a(-t)$. It follows that the Fourier transform of $p(t)$ is $P(f) = H_a(f)H_a^*(f) = |H_a(f)|^2$ which is a raised cosine pulse. Taking the inverse Fourier transform of $H_a(f)$ gives the root raised cosine pulse

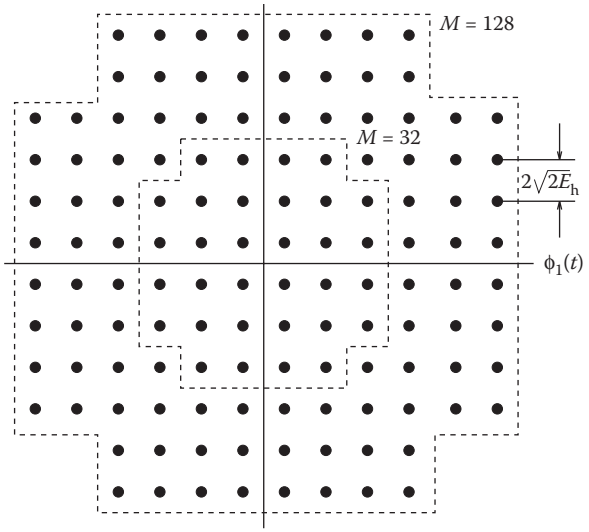

FIGURE 5.2 Complex signal-space diagram for cross QAM constellations.

$$h_a(t) = \begin{cases} 1 - \beta + 4\beta/\pi, & t = 0 \\ (\beta/\sqrt{2})\left[(1 + 2/\pi)\sin(\pi/4\beta) + (1 - 2/\pi)\cos(\pi/4\beta)\right], & t = \pm T/4\beta. \\ \dfrac{4\beta(t/T)\cos[(1+\beta)\pi t/T] + \sin[(1-\beta)\pi t/T]}{\pi(t/T)[1 - (4\beta t/T)^2]}, & \text{elsewhere} \end{cases} \tag{5.14}$$

The overall pulse $p(t)$ is the raised cosine pulse

$$p(t) = \frac{\sin \pi t/T}{\pi t/T} \frac{\cos \beta \pi t/T}{1 - (2\beta t/T)^2}. \tag{5.15}$$

The roll-off factor β usually lies between 0 and 1 and defines the excess bandwidth $100\beta\%$. For $\beta = 0$, the root raised cosine pulse reduces to the sinc pulse $h_a(t) = \text{sinc}(t/T)$. Using a smaller β results in a more compact power density spectrum, but the link performance becomes more sensitive to errors in the symbol timing. The raised cosine and root raised cosine pulses corresponding to $\beta = 0.5$ are shown in Figure 5.3. Strictly speaking, the root raised cosine pulse in Equation 5.14 is noncausal. Therefore, in practice, a truncated and time-shifted approximation of the pulse must be used. For example, in Figure 5.3 the pulse is truncated to length $6T$ and right time-shifted by $3T$ to yield a causal pulse. The time-shifting makes the pulse have a linear phase response, while the pulse truncation will result in a pulse that is no longer strictly bandlimited. Finally, we note that the raised cosine pulse is a Nyquist pulse having equally spaced zero crossings at the baud period T, while the root raised cosine pulse by itself is not a Nyquist pulse.

5.3.3 Power Spectrum of QAM

The power density spectrum of the QAM complex envelope is

$$S_{\tilde{s}\tilde{s}}(f) = \frac{A^2}{T}\sigma_x^2 \left|H_a(f)\right|^2, \tag{5.16}$$

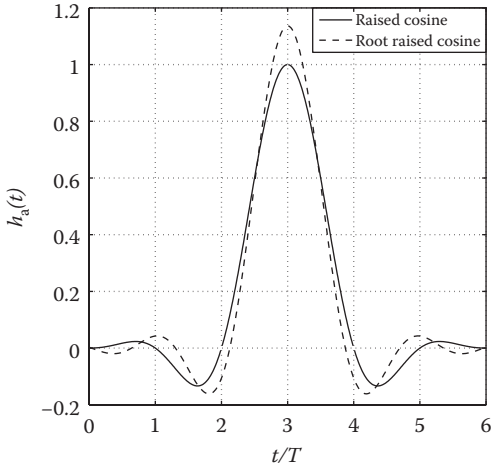

FIGURE 5.3 Raised cosine and root raised cosine pulses with roll-off factor $\beta = 0.5$. The pulses are truncated to length $6T$ and time shifted by $3T$ to yield causal pulses.

where $\sigma_x^2 = 1/2\mathrm{E}[|x_k|^2]$. With root raised cosine pulse shaping, $|H_a(f)|^2 = P(f)$ has the form defined in Equation 5.13 with $h_a(t)$ in Equation 5.14. The root raised cosine pulse is noncausal. When the pulse is implemented as a digital FIR filter, it must be truncated to a finite length $\tau = LT$. This truncation produces the new pulse $\tilde{h}_a(t) = h_a(t)\mathrm{rect}(t/LT)$. The Fourier transform of the truncated pulse $\tilde{h}_a(t)$ is $\tilde{H}_a(f) = H_a(f) * LT\mathrm{sinc}(\pi fLT)$, where* denotes the operation of convolution taken over the frequency variable f. The PSD of QAM with the pulse $\tilde{h}_a(t)$ can again be obtained from Equation 5.16 by simply replacing $H_a(f)$ with $\tilde{H}_a(f)$. As shown in Figure 5.4, pulse truncation can lead to significant side lobe regeneration. Finally, to fairly compare bandwidth efficiencies with different modulation alphabet sizes M, the frequency variable should be normalized by the bit interval T_b such that $T = T_b \log_2 M$.

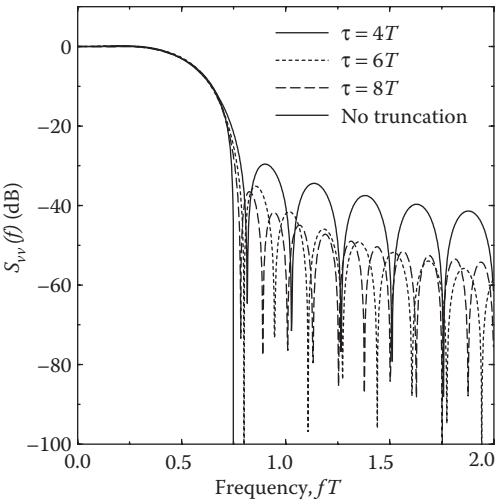

FIGURE 5.4 PSD of QAM with a truncated square root raised cosine amplitude shaping pulse with various truncation lengths; $\beta = 0.5$. Truncation of the amplitude shaping pulse leads to side-lobe regeneration.

5.4 Phase Shift Keying and π/4-QDPSK

With phase shift keying, the complex envelope has the form

$$\tilde{s}(t) = A\sum_{n} b(t - nT, \mathbf{x}_n), \tag{5.17}$$

where

$$b(t, \mathbf{x}_n) = h_{\mathrm{a}}(t)\mathrm{e}^{\mathrm{j}\theta_n}, \tag{5.18}$$

$h_{\mathrm{a}}(t)$ is the amplitude shaping pulse, and the excess phase takes on the values

$$\theta_n = \frac{2\pi}{M}x_n, \tag{5.19}$$

where $x_n \in \{0,1,\ldots, M-1\}$ and M is the size of the modulation alphabet. Each symbol x_k is mapped onto $\log_2 M$ source bits. A quadrature phase shift-keyed (QPSK) signal is obtained by using $M = 4$ resulting in a transmission rate of 2 bits/symbol.

Unlike conventional QPSK that has four possible transmitted phases, π/4 phase-shifted quadrature differential phase shift keying (π/4-QDPSK) has eight possible transmitted phases. Let θ_n be the absolute excess phase for the nth data symbol, and let $\Delta\theta_n = \theta_n - \theta_{n-1}$ be the differential excess phase. With π/4-DQPSK, the differential excess phase is related to the quaternary data sequence $\{x_n\}$, $x_n \in \{\pm 1, \pm 3\}$ through the mapping

$$\Delta\theta_n = x_n\frac{\pi}{4}. \tag{5.20}$$

Note that the excess phase differences are $\pm\pi/4$ and $\pm 3\pi/4$.

The complex envelope of the π/4-DQPSK signal is

$$\tilde{s}(t) = A\sum_{n} b(t - nT, \mathbf{x}_{\mathrm{n}}), \tag{5.21}$$

where

$$\begin{aligned} b(t, \mathbf{x}_n) &= h_{\mathrm{a}}(t)\exp\left\{\mathrm{j}\left(\theta_{n-1} + x_n\frac{\pi}{4}\right)\right\} \\ &= h_{\mathrm{a}}(t)\exp\left\{\mathrm{j}\frac{\pi}{4}\left(\sum_{k=-\infty}^{n-1} x_k + x_n\right)\right\}. \end{aligned} \tag{5.22}$$

The summation in the exponent of Equation 5.22 represents the accumulated excess phase, while the last term is the excess phase increment due to the nth data symbol. The absolute excess phase during the even and odd baud intervals belongs to the sets $\{0,\pi/2,\pi,3\pi/2\}$ and $\{\pi/4,3\pi/4,5\pi/4,7\pi/4\}$, respectively, or vice versa. With π/4-DQPSK the amplitude shaping pulse $h_{\mathrm{a}}(t)$ is often chosen to be the root raised cosine pulse in Equation 5.14.

The signal-space diagrams for QPSK and π/4-DQPSK are shown in Figure 5.5, where E_{h} is the symbol energy. The dotted lines in Figure 5.5 show the allowable phase transitions. The phaser diagram for

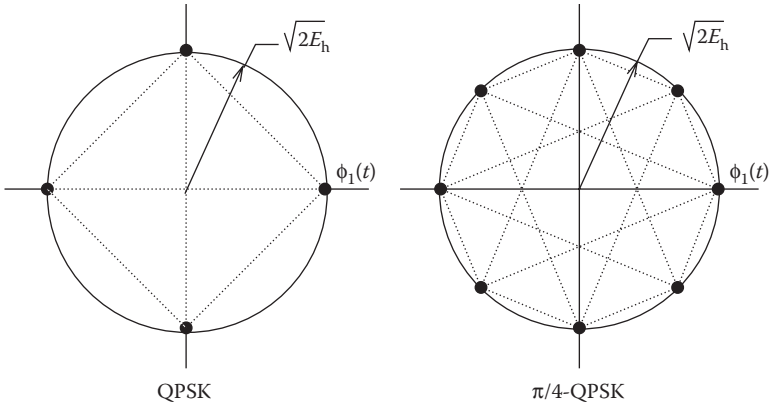

FIGURE 5.5 Complex signal-space diagram QPSK and π/4-DQPSK signals.

π/4-DQPSK with root raised cosine amplitude pulse shaping is shown in Figure 5.6. Note that the phase trajectories do not pass through the origin. Like OQPSK, this property reduces the peak-to-average power ratio (PAPR) of the complex envelope, making the π/4-DQPSK waveform less sensitive to power amplifier nonlinearities. Finally, we observe that the excess phase of π/4-DQPSK changes by ±π/4 or ±3π/4 radians during *every* baud interval. This property makes symbol synchronization easier with π/4-DQPSK as compared with QPSK.

The power density spectrum of QPSK and π/4-QPSK is given by

$$S_{\tilde{s}\tilde{s}}(f) = \frac{A^2}{2T}\left|H_a(f)\right|^2. \tag{5.23}$$

Note that π/4-DQPSK has the same power spectrum as QPSK. Of course π/4-DQPSK has a lower PAPR than QPSK.

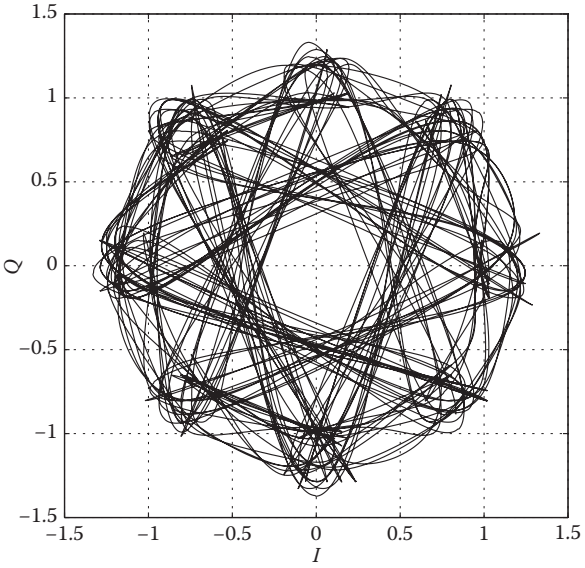

FIGURE 5.6 Phaser diagram for π/4-DQPSK with root raised cosine amplitude pulse shaping; β = 0.5.

5.5 Continuous Phase Modulation, Minimum Shift Keying, and GMSK

Continuous phase modulation (CPM) refers to a broad class of FM techniques where the carrier phase varies in a continuous manner. A comprehensive treatment of CPM is provided in Reference 2. CPM schemes are attractive because they have constant envelope and excellent spectral characteristics. The complex envelope of a CPM waveform has the general form

$$\tilde{s}(t) = Ae^{j(\phi(t)+\theta_0)}, \tag{5.24}$$

where A is the amplitude, θ_0 is initial carrier phase at $t = 0$, and

$$\phi(t) = 2\pi h \int_0^t \sum_{k=0}^{\infty} x_k h_f(\tau - kT)\,d\tau \tag{5.25}$$

is the excess phase, h is the modulation index, $\{x_k\}$ is the data symbol sequence, $h_f(t)$ is the frequency shaping pulse, and T is the baud period. The CPM waveform can be written in the standard form

$$\tilde{s}(t) = A\sum_n b(t - nT, \mathbf{x}_n) \tag{5.26}$$

where

$$b(t, \mathbf{x}_n) = e^{j2\pi h \int_0^t \sum_{k=0}^{\infty} x_k h_f(\tau - kT)d\tau} u_T(t) \tag{5.27}$$

$\mathbf{x}_n = (x_n, x_n–1, \ldots, x_0)$, and we have assumed an initial phase $\theta_0 = 0$. CPM waveforms have the following properties:

- The data symbols are chosen from the alphabet $\{\pm1, \pm3, \ldots, \pm(M-1)\}$, where M is the modulation alphabet size and M is even.
- h is the modulation index and is directly proportional to the peak and/or average frequency deviation from the carrier. The instantaneous frequency deviation from the carrier is

$$f_{dev}(t) = \frac{1}{2\pi}\frac{d\phi(t)}{dt} = h\sum_{k=0}^{\infty} x_k h_f(t - kT). \tag{5.28}$$

- $h_f(t)$ is the frequency shaping function, which is zero for $t < 0$ and $t > LT$, and normalized to have an area equal to 1/2. Full response CPM has $L = 1$, while partial response CPM has $L > 1$.

5.5.1 Minimum Shift Keying

Minimum shift keying (MSK) is a special form of binary CPM ($x_k \in \{–1, +1\}$) that uses a rectangular frequency shaping pulse $h_f(t) = (1/2T)u_T(t)$, and a modulation index $h = 1/2$. In this case,

$$b(t, \mathbf{x}_n) = e^{j\left(\frac{\pi}{2}\sum_{k=0}^{n-1} x_k + \frac{\pi}{2}x_n\frac{t}{T}\right)} u_T(t). \tag{5.29}$$

where $u_T(t) = u(t) \boxtimes u(t \boxtimes T)$ and $u(t)$ is the unit step function.

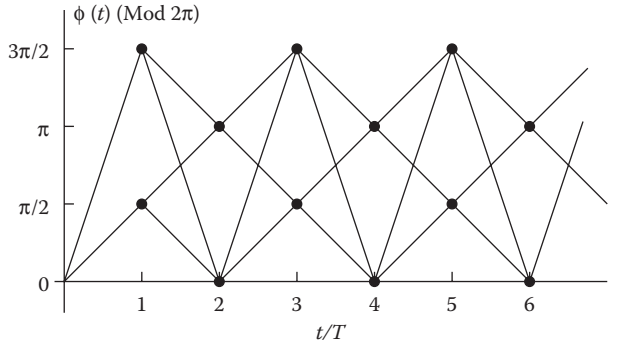

FIGURE 5.7 Phase-trellis for MSK.

The MSK waveform can be described by the phase trellis diagram shown in Figure 5.7 which plots the time behavior of the excess phase

$$\phi(t) = \frac{\pi}{2}\sum_{k=0}^{n-1} x_k + \frac{\pi}{2}x_n\frac{t-nT}{T}. \tag{5.30}$$

At the end of each symbol interval the excess phase $\phi(t)$ takes on values that are integer multiples of $\pi/2$. Since excess phases that differ by integer multiples of 2π are indistinguishable, the values taken by $\phi(t)$ at the end of each symbol interval belong to the finite set $\{0, \pi/2, \pi, 3\pi/2\}$.

An interesting property of MSK can be observed from the MSK bandpass waveform. The bandpass waveform on the interval $[nT,(n+1)T]$ can be obtained from Equation 5.29 as

$$\begin{aligned} s(t) &= A\cos\left(2\pi f_c t + \frac{\pi}{2}\sum_{k=0}^{n-1} x_k + \frac{\pi}{2}x_n\frac{t-nT}{T}\right) \\ &= A\cos\left(2\pi\left(f_c + \frac{x_n}{4T}\right)t + \frac{\pi}{2}\sum_{k=0}^{n-1} x_k - \frac{\pi n}{2}x_n\right). \end{aligned} \tag{5.31}$$

Observe that the MSK bandpass waveform has one of two possible frequencies in each baud interval

$$f_L = f_c - \frac{1}{4T} \quad \text{and} \quad f_U = f_c + \frac{1}{4T} \tag{5.32}$$

depending on the data symbol x_n. The difference between these two frequencies is $f_U - f_L = 1/(2T)$. This is the minimum frequency separation to ensure orthogonality between two cophased sinusoids of duration T and, hence, the name *minimum* shift keying.

Another interesting representation for MSK waveforms can be obtained by using Laurent's decomposition [3] to express the MSK complex envelope in the quadrature form

$$\tilde{s}(t) = A\sum_n b(t-2nT, \mathbf{x}_n), \tag{5.33}$$

where

$$b(t, \mathbf{x}_n) = \hat{x}_{2n+1}h_a(t-T) + j\hat{x}_{2n}h_a(t) \tag{5.34}$$

and where $\mathbf{x}_n = (\hat{x}_{2n+1}, \hat{x}_{2n})$,

$$\hat{x}_{2n} = \hat{x}_{2n-1}\, x_{2n} \tag{5.35}$$

$$\hat{x}_{2n+1} = -\hat{x}_{2n}\, x_{2n+1} \tag{5.36}$$

$$\hat{x}_{-1} = 1 \tag{5.37}$$

and

$$h_{\mathrm{a}}(t) = \sin\left(\frac{\pi t}{2T}\right) u_{2T}(t). \tag{5.38}$$

The sequences, $\{\hat{x}_{2n}\}$ and $\{\hat{x}_{2n+1}\}$, are independent binary symbol sequences taking on values from the set $\{-1, +1\}$. The symbols $\hat{x}_{2n}$ and $\hat{x}_{2n+1}$ are transmitted on the quadrature branches with a half-sinusoid (HS) amplitude shaping pulse of duration $2T$ s and an offset of Ts. Hence, MSK is equivalent to offset quadrature amplitude shift keying (OQASK) with HS amplitude pulse shaping. This linear representation of MSK is useful in practice for linear detection of MSK waveforms.

To obtain the power density spectrum of MSK, we observe from Equation 5.34 that the MSK baseband signal has the quadrature form

$$\tilde{s}(t) = A \sum_n b(t - 2nT, \mathbf{x}_n), \tag{5.39}$$

where

$$b(t, \mathbf{x}_n) = \hat{x}_{2n+1}\, h_{\mathrm{a}}(t - T) + \mathrm{j}\hat{x}_{2n}\, h_{\mathrm{a}}(t) \tag{5.40}$$

$$h_{\mathrm{a}}(t) = \sin\left(\frac{\pi t}{2T}\right) u_{2T}(t), \tag{5.41}$$

$\mathbf{x}_n = (\hat{x}_{2n+1}, \hat{x}_{2n})$ is a sequence of odd–even pairs assuming values from the set $\{\pm 1, \pm 1\}$, and T is the bit period. The Fourier transform of Equation 5.40 is

$$B(f, \mathbf{x}_n) = \left(\hat{x}_{2n+1}\, \mathrm{e}^{-\mathrm{j}2\pi fT} + \mathrm{j}\hat{x}_{2n}\right) H_{\mathrm{a}}(f). \tag{5.42}$$

Since the data sequence is zero-mean and uncorrelated, the MSK psd is

$$\begin{aligned} S_{b,0}(f) &= \frac{1}{2}\mathrm{E}\left[\left|B(f, \mathbf{x}_0)\right|^2\right] \\ &= \frac{1}{2}\mathrm{E}\left[\hat{x}_1^2 + \hat{x}_0^2\right]\left|H_{\mathrm{a}}(f)\right|^2 \\ &= \left|H_a(f)\right|^2. \end{aligned} \tag{5.43}$$

The Fourier transform of the HS pulse in Equation 5.38 is

$$H_{\mathrm{a}}(f) = \frac{2T}{\pi(1 - (4fT)^2)}\left(1 + \mathrm{e}^{-\mathrm{j}4\pi fT}\right). \tag{5.44}$$

Hence, the power spectrum becomes

$$S_{\tilde{s}\tilde{s}}(f) = \frac{A^2}{T}|H_a(f)|^2 = \frac{16A^2T}{\pi^2}\left[\frac{\cos^2(2\pi fT)}{1-(4fT)^2}\right]^2. \tag{5.45}$$

The PSD of MSK is plotted in Figure 5.10. Observe that an MSK signal has fairly large sidelobes compared to π/4-QPSK with a truncated square root raised cosine pulse (cf. Figure 5.4).

5.5.2 Gaussian Minimum Shift Keying

The MSK power spectrum has a relatively broad main lobe and slow roll-off of side lobes. A more compact power spectrum can be achieved by low-pass filtering the MSK modulating signal

$$x(t) = \sum_{n=-\infty}^{\infty} x_n h_f(t-nT) = \frac{1}{2T}\sum_{n=-\infty}^{\infty} x_n u_T(t-nT) \tag{5.46}$$

prior to FM as shown in Figure 5.8. Such filtering suppresses the higher-frequency components in $x(t)$ thus yielding a more compact power spectrum. GMSK is a special type of partial response CPM that uses a low-pass premodulation filter having the transfer function [4]

$$H(f) = \exp\left\{-\left(\frac{f}{B}\right)^2\frac{\ln 2}{2}\right\}, \tag{5.47}$$

where B is the 3 dB bandwidth of the filter. It is apparent that $H(f)$ is shaped like a Gaussian probability density function with mean $f=0$ and, hence, the name "Gaussian" MSK. Convolving the rectangular pulse

$$\frac{1}{2T}\text{rect}(t/T) = \frac{1}{2T}u_T(t+T/2)$$

with the corresponding filter impulse response $h(t)$ yields the frequency shaping pulse

$$\begin{aligned} h_f(t) &= \frac{1}{2T}\sqrt{\frac{2\pi}{\ln 2}}(BT)\int_{t/T-1/2}^{t/T+1/2}\exp\left\{-\frac{2\pi^2(BT)^2x^2}{\ln 2}\right\}dx \\ &= \frac{1}{2T}\left[Q\left(\frac{t/T-1/2}{\sigma}\right)-Q\left(\frac{t/T+1/2}{\sigma}\right)\right], \end{aligned} \tag{5.48}$$

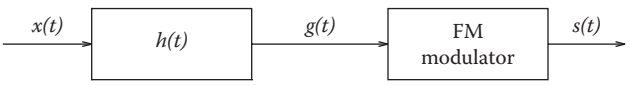

FIGURE 5.8 Premodulation filtered MSK. The MSK modulating signal is low-pass filtered to remove the high-frequency components prior to FM.

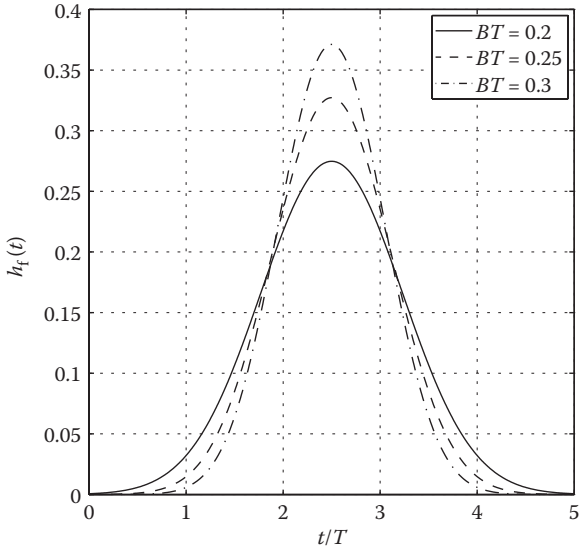

FIGURE 5.9 GMSK frequency shaping pulse for various normalized premodulation filter bandwidths BT.

where

$$Q(\alpha) = \int_{\alpha}^{\infty} \frac{1}{\sqrt{2\pi}} e^{-x^2}\, dx \tag{5.49}$$

$$\sigma^2 = \frac{\ln 2}{4\pi^2 (BT)^2}. \tag{5.50}$$

Figure 5.9 plots the GMSK frequency shaping pulse (truncated to $5T$ and time shifted by $2.5T$ to yield a causal pulse) for various normalized premodulation filter bandwidths BT. The popular GSM cellular standard uses GMSK with $BT = 0.3$.

The power density spectrum of GMSK is quite difficult to obtain, but can be computed by using published methods [5]. Figure 5.10 plots the power density spectrum for $BT = 0.2$, 0.25, and 0.3, obtained from K. Wesolowski (private comm., 1994). Observe that the spectral sidelobes are greatly reduced by the Gaussian low-pass filter.

5.6 Orthogonal Frequency Division Multiplexing

Orthogonal frequency division multiplexing (OFDM) is a block modulation scheme where data symbols are transmitted in parallel on orthogonal subcarriers. A block of N data symbols, each of duration T_s, is converted into a block of N parallel data symbols, each of duration $T = NT_s$. The N parallel data symbols modulate N subcarriers that are spaced in frequency $1/T$ Hz apart. The OFDM complex envelope is given by

$$\tilde{s}(t) = A \sum_{n} b(t - nT, \mathbf{x}_n), \tag{5.51}$$

where

$$b(t, \mathbf{x}_n) = u_T(t) \sum_{k=0}^{N-1} x_{n_k} e^{j\frac{2\pi kt}{T}} \tag{5.52}$$

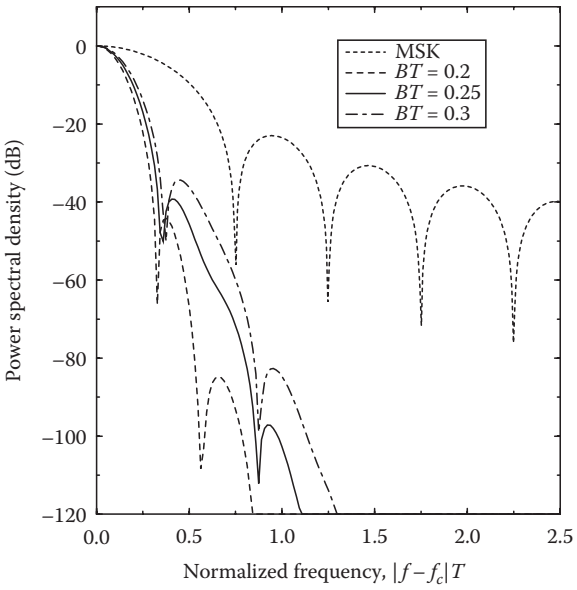

FIGURE 5.10 Power density spectrum of MSK and GMSK.

n is the block index, k is the subcarrier index, N is the number of subcarriers, and $x_n = \{x_{n_0}, x_{n_1}, \ldots, x_{n_{N-1}}\}$ is the data symbol block at epoch n. The data symbols x_{n_k} are usually chosen from a QAM or PSK signal constellation, although any 2-D signal constellation can be used. The $1/T$ Hz frequency separation of the subcarriers ensures that the corresponding subchannels are mutually orthogonal regardless of the random phases that are imparted by the data modulation.

A cyclic extension (or guard interval) is usually added to the OFDM waveform in Equations 5.51 and 5.52 to combat delay spread. The cyclic extension can be in the form of either a cyclic prefix or a cyclic suffix. With a cyclic suffix, the OFDM complex envelope becomes

$$\tilde{s}_g(t) = \begin{cases} \tilde{s}(t), & 0 \le t \le T \\ \tilde{s}(t-T), & T \le t \le (1+\alpha_g)T, \end{cases} \tag{5.53}$$

where $\alpha_g T$ is the length of the guard interval and $\tilde{s}(t)$ is defined in Equations 5.51 and 5.52. The OFDM waveform with cyclic suffix can be rewritten in the standard form

$$\tilde{s}_g(t) = A \sum_n b(t - nT_g, \mathbf{x}_n), \tag{5.54}$$

where

$$b(t, \mathbf{x}_n) = u_T(t) \sum_{k=0}^{N-1} x_{n_k} e^{j\frac{2\pi k t}{T}} + u_{\alpha_g T}(t-T) \sum_{k=0}^{N-1} x_{n_k} e^{j\frac{2\pi k (t-T)}{T}}, \tag{5.55}$$

and $T_g = (1 + \alpha_g)T$ is the OFDM symbol period with the addition of the guard interval. Likewise, with a cyclic prefix, the OFDM complex envelope becomes

$$\tilde{s}_g(t) = \begin{cases} \tilde{s}(t+T), & -\alpha_g T \le t \le 0 \\ \tilde{s}(t), & 0 \le t \le T \end{cases}, \tag{5.56}$$

and

$$b(t, \mathbf{x}_n) = u_{\alpha_g T}(t + \alpha_g T) \sum_{k=0}^{N-1} x_{n_k} e^{j\frac{2\pi k(t+T)}{T}} + u_T(t) \sum_{k=0}^{N-1} x_{n_k} e^{j\frac{2\pi kt}{T}}. \tag{5.57}$$

5.6.1 FFT Implementation of OFDM

A key advantage of using OFDM is that the baseband modulator can be implemented by using an inverse discrete-time Fourier transform (IDFT). In practice, an inverse fast Fourier transform (IFFT) algorithm is used to implement the IDFT. Consider the OFDM complex defined by Equations 5.51 and 5.52. During the interval $nT \le t \le (n+1)T$, the complex envelope has the form

$$\begin{aligned} \tilde{s}(t) &= A u_T(t - nT) \sum_{k=0}^{N-1} x_{n_k} e^{\frac{j2\pi k(t-nT)}{T}} \\ &= A u_T(t - nT) \sum_{k=0}^{N-1} x_{n_k} e^{\frac{j2\pi kt}{NT_s}}, \quad nT \le t \le (n+1)T. \end{aligned} \tag{5.58}$$

Now suppose that the complex envelope in Equation 5.58 is sampled at synchronized T_s second intervals to yield the sample sequence

$$X_{n_m} = \tilde{s}(mT_s) = A \sum_{k=0}^{N-1} x_{n_k} e^{\frac{j2\pi km}{N}}, \quad m = 0,1,\ldots,N-1. \tag{5.59}$$

Observe that the vector $\mathbf{X}_n = \{X_{n_m}\}_{m=0}^{N-1}$ is the IDFT of the vector $A\mathbf{x}_n = A\{x_{n_k}\}_{k=0}^{N-1}$. In contrast to conventional notation, the lower-case vector $A\mathbf{x}_n$ is used to represent the coefficients in the frequency domain, while the upper-case vector $\mathbf{X}_n$ is used to represent the coefficients in the time domain.

As mentioned earlier, a cyclic extension (or guard interval) is usually added to the OFDM waveform as described in Equations 5.54 and 5.55 to combat delay spread. When a cyclic suffix is used, the corresponding sample sequence is

$$X_{n_m}^g = X_{n_{(m)_N}} \tag{5.60}$$

$$= A \sum_{k=0}^{N-1} x_{n_k} e^{\frac{j2\pi km}{N}}, \quad m = 0,1,\ldots,N+G-1, \tag{5.61}$$

where G is the length of the guard interval in samples, and $(m)_N$ is the residue of m modulo N. This gives the vector $\mathbf{X}_n^g = \{X_{n_m}^g\}_{m=0}^{N+G-1}$, where the values in the first and last G coordinates of the vector $\mathbf{X}_n^g$ are the same. Likewise, when a cyclic prefix is used, the corresponding sample sequence is

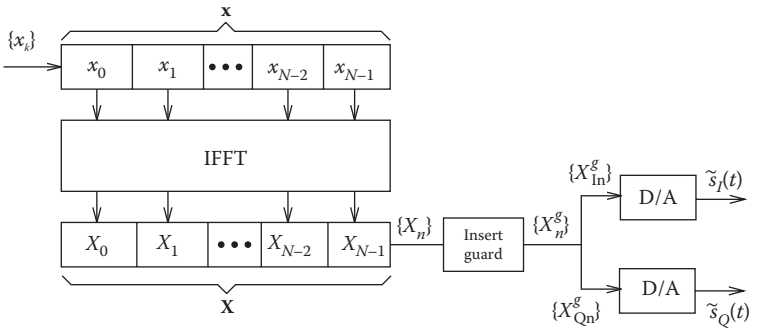

FIGURE 5.11 Block diagram of IDFT-based baseband OFDM modulator with guard interval insertion and digital-to-analog conversion.

$$X^{\mathrm{g}}_{n_m} = X_{n_{(m)_N}} \tag{5.62}$$

$$= A\sum_{k=0}^{N-1} x_{n_k} \mathrm{e}^{\frac{\mathrm{j}2\pi km}{N}}, \quad m = -G, \ldots, -1, 0, 1, \ldots, N-1. \tag{5.63}$$

This yields the vector $\mathbf{X}^{\mathrm{g}}_n = \{X^{\mathrm{g}}_{n_m}\}^{N-1}_{m=-G}$, where again the first and last G coordinates of the vector $\mathbf{X}^{\mathrm{g}}_n$ are the same. The sample duration after insertion of the guard interval, $T^{\mathrm{g}}_{\mathrm{s}}$, is compressed in time such that $(N+G)T^{\mathrm{g}}_{\mathrm{s}} = NT_{\mathrm{s}}$.

The OFDM complex envelope can be generated by splitting the complex-valued output vector $\mathbf{X}_m$ into its real and imaginary parts, $\Re(\mathbf{X}_n)$ and $\Im(\mathbf{X}_n)$, respectively. The sequences $\{\Re(X_{n_m})\}$ and $\{\Im(X_{n_m})\}$ are then input to a pair of balanced digital-to-analog converters (DACs) to generate the real and imaginary components $\tilde{s}_I(t)$ and $\tilde{s}_Q(t)$, respectively, of the complex envelope $\tilde{s}(t)$, during the time interval $nT \le t \le (n+1)T$. As shown in Figure 5.11, the OFDM baseband modulator consists of an IFFT operation, followed by guard interval insertion and digital-to-analog conversion.

It is instructive to realize that the waveform generated by using the IDFT OFDM baseband modulator is *not* exactly the same as the waveform generated from the analog waveform definition of OFDM. Consider for example, the OFDM waveform without a cyclic guard in Equations 5.51 and 5.52. The analog waveform definition uses the rectangular amplitude shaping pulse $u_T(t)$ that is strictly time limited to T seconds. Hence, the corresponding power spectrum will have infinite bandwidth, and any finite sampling rate of the complex envelope will necessarily lead to aliasing and imperfect reconstruction.

5.6.2 Power Spectrum of OFDM

To compute the power spectrum of OFDM, recall that the OFDM waveform with guard interval is given by Equations 5.54 and 5.55. The data symbols x_{n_k}, $k = 0, \ldots, N-1$ that modulate the N subcarriers are assumed to have zero mean, variance $\sigma^2_x = 1/2\,\mathrm{E}[|x_{k,n}|^2]$, and they are mutually uncorrelated. In this case, the psd of the OFDM waveform is

$$S_{\tilde{s}\tilde{s}}(f) = \frac{A^2}{T_g} S_{b,0}(f), \tag{5.64}$$

where

$$S_{b,0}(f) = \frac{1}{2}\mathrm{E}\left[\left|B(f,\mathbf{x}_0)\right|^2\right], \tag{5.65}$$

and

$$B(f,\mathbf{x}_0) = \sum_{k=0}^{N-1} x_{0_k} T\mathrm{sinc}(fT-k) + \sum_{k=0}^{N-1} x_{0_k}\alpha_g T\mathrm{sinc}(\alpha_g(fT-k))\mathrm{e}^{j2\pi fT}. \tag{5.66}$$

Substituting Equation 5.66 into Equation 5.65 along with $T = NT_s$ yields the result

$$S_{\tilde{s}\tilde{s}}(f) = \sigma_x^2 A^2 T\left(\frac{1}{1+\alpha_g}\sum_{k=0}^{N-1}\mathrm{sinc}^2(NfT_s-k) + \frac{\alpha_g^2}{1+\alpha_g}\sum_{k=0}^{N-1}\mathrm{sinc}^2(\alpha_g(NfT_s-k))\right.$$
$$\left. + \frac{2\alpha_g}{1+\alpha_g}\cos(2\pi NfT_s)\sum_{k=0}^{N-1}\mathrm{sinc}(NfT_s-k)\mathrm{sinc}(\alpha_g(NfT_s-k))\right). \tag{5.67}$$

The OFDM PSD is plotted in Figure 5.12 for $N = 16$, $\alpha_g = 0.25$.

It is interesting to examine the OFDM power spectrum, when the OFDM complex envelope is generated by using an IDFT baseband modulator followed by a balanced pair DACs as shown in Figure 5.11. The output of the IDFT baseband modulator is given by $\{\mathbf{X}^g\} = \{X^g_{m,n}\}$, where m is the block index and

$$X^g_{m,n} = X_{m,(n)_N} \tag{5.68}$$

$$= A\sum_{k=0}^{N-1} x_{m,k}\mathrm{e}^{\frac{\mathrm{j}2\pi kn}{N}}, \quad n = 0,1,\ldots,N+G-1. \tag{5.69}$$

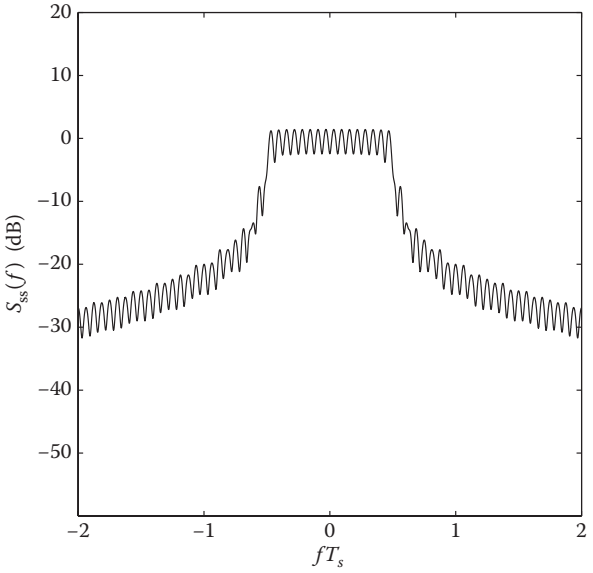

FIGURE 5.12 PSD of OFDM with $N = 16$, $\alpha_g = 0.25$.

The power spectrum of the sequence $\{\mathbf{X}^{g}\}$ can be calculated by first determining the discrete-time autocorrelation function of the time-domain sequence $\{\mathbf{X}^{g}\}$ and then taking a discrete-time Fourier transform of the discrete-time autocorrelation function. The PSD of the OFDM complex envelope with ideal DACs can be obtained by applying the resulting power spectrum to an ideal low-pass filter with a cutoff frequency of $1/(2T_s^g)$ Hz.

The discrete-time autocorrelation function of the sequence $\{\mathbf{X}^{g}\}$ is

$$\phi_{X^gX^g}(\ell) = \begin{cases} A\sigma_X^2 & \ell = 0 \\ \dfrac{G}{N+G} A\sigma_X^2 & \ell = -N, N. \\ 0 & \text{otherwise} \end{cases} \tag{5.70}$$

Taking the discrete-time Fourier transform of the discrete-time autocorrelation function in Equation 5.70 gives

$$\begin{aligned} S_{X^gX^g}(f) &= A\sigma_x^2 \left(1 + \frac{G}{N+G} e^{-j2\pi fNT_s^g} + \frac{G}{N+G} e^{j2\pi fNT_s^g}\right) \\ &= A\sigma_x^2 \left(1 + \frac{2G}{N+G} \cos(2\pi fNT_s^g)\right). \end{aligned} \tag{5.71}$$

Finally, we assume that the sequence $\{\mathbf{X}^{g}\} = \{X_{m,n}^{g}\}$ is passed through a pair of ideal DACs. The ideal DAC is a low-pass filter with cutoff frequency $1/(2T_s^g)$. Therefore, the OFDM complex envelope has the PSD

$$S_{\tilde{s}\tilde{s}}(f) = A\sigma_x^2 \left(1 + \frac{2G}{N+G} \cos(2\pi fNT_s^g)\right) \text{rect}\left(fT_s^g\right). \tag{5.72}$$

Figure 5.13 plots the PSD for $N = 16$ and $G = 4$.

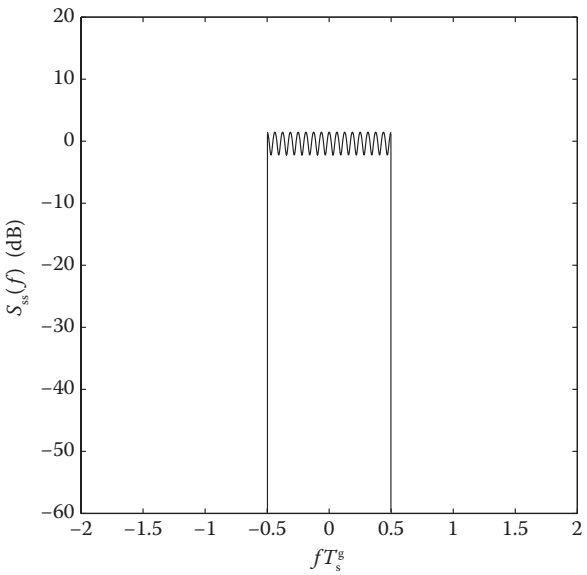

FIGURE 5.13 PSD of IDFT-based OFDM with $N = 16$, $G = 4$.

Finally, we note that the PSD plotted in Figure 5.13 assumes an ideal DAC. A practical DAC with a finite-length reconstruction filter will introduce sidelobes into the spectrum. We note that sidelobes are an inherent feature of the continuous-time OFDM waveform in Equations 5.54 and 5.55 due to the use of rectangular amplitude pulse shaping on the subcarriers. However, sidelobes are introduced into the waveform generated with the IDFT implementation by the nonideal (practical) DAC.

5.7 Summary and Conclusions

A variety of modulation schemes are employed in digital communication systems. Wireless modulation schemes in particular must have a compact power density spectrum, while at the same time providing a good bit error rate performance in the presence of channel impairments such as cochannel interference and fading. This chapter has presented a variety of modulation schemes along with their power spectra.

References

1. G. L. Stüber, *Principles of Mobile Communication*, 3rd edn, Springer Science + Business Media, 2011.
2. J. B. Anderson, T. Aulin, and C. E. Sundberg, *Digital Phase Modulation*. New York, NY: Plenum, 1986.
3. P. A. Laurent, Exact and approximate construction of digital phase modulations by superposition of amplitude modulated pulses (AMP). *IEEE Trans. Commun.*, 34, 150–160, 1986.
4. K. Murota and K. Hirade, GMSK modulation for digital mobile radio telephony. *IEEE Trans. Commun.*, 29(July), 1044–1050, 1981.
5. G. J. Garrison, A power spectral density analysis for digital FM. *IEEE Trans. Commun.*, 23(November), 1228–1243, 1975.

Further Reading

A good discussion on modulation techniques can be found in *Digital Communications*, 5th edn., J. G. Proakis and M. Salehi, McGraw-Hill, 2008. Also *Principles of Mobile Communication*, 3rd edn., G. L. Stüber, Springer Science + Business Media, 2011.

Proceedings of various IEEE conferences such as the *Vehicular Technology Conference, International Conference on Communications*, and *Global Telecommunications Conference*, document the latest developments in the field of wireless communications each year.

Journals such as the *IEEE Transactions on Communications*, *IEEE Transactions on Wireless Communications*, *IEEE Transactions on Vehicular Technology* report advances in wireless modulation.

6

Error Control Coding

Thomas E. Fuja

6.1 Introduction

Error control coding is a branch of communication engineering that addresses the problem of how to make digital transmission more *reliable*—how to recover uncorrupted data at the receiver even in the presence of significant corruption of the transmitted signal.

The modern genesis of error control coding has its roots in the post–World War II work of Claude Shannon (who proved the *existence* of "good codes" but did not indicate how to find them [1]) and Marcel Golay and Richard Hamming (who published the first explicit descriptions of "error correcting codes" based on parity checks [2,3]).

Error control codes make digital transmission more reliable by the careful introduction of *redundancy* into the transmitted signal. The simplest example of such a scheme might be one in which every data bit to be conveyed to the receiver is transmitted three times—that is, a logical "1" would be transmitted as "111" and a logical "0" as "000." The redundancy introduced by repeating each bit can be exploited at the receiver to make errors in the estimated data less likely—by, for instance, making a decision on each of the three bits individually and then taking a "vote" of the three decisions to arrive at an estimate of the associated data bit. In such a scheme, as long as not more than one bit is corrupted out of every three-bit "codeword," the receiver will correctly decode the data; thus, this is a (very simple) *one-error correcting code*.

Error control schemes can be broadly classified into two categories:

- Forward error control (FEC) codes, in which sufficient redundancy is incorporated into the "forward" (transmitter-to-receiver) transmission to enable the receiver to recover the data well enough to meet the requirements of the application.
- Automatic repeat request (ARQ), in which enough redundancy is incorporated into the forward transmission to enable the receiver to *detect* the presence of corruption—but not enough to reliably estimate the data from the (corrupted) received signal. ARQ schemes employ a retransmission

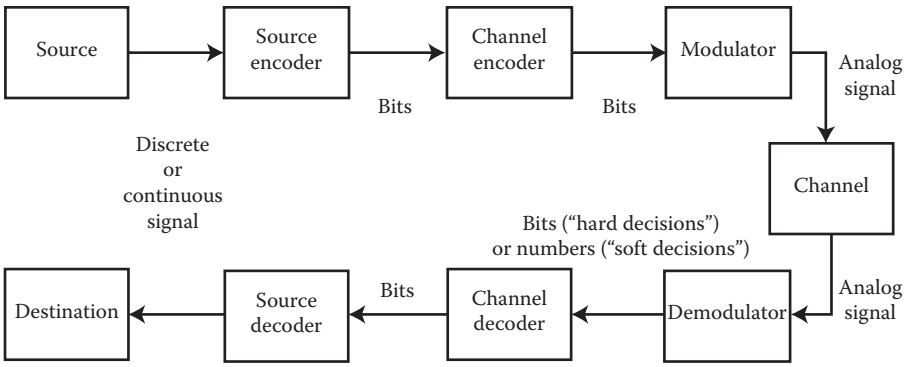

FIGURE 6.1 The communication theorist's "coat of arms," wherein the error control (or "channel") encoder introduces redundancy that is then exploited by the channel decoder to enhance data integrity in the presence of channel noise.

strategy in which the receiver alerts the transmitter (via an "ACK/NACK" protocol on a feedback channel) of the need to retransmit the corrupted data.

A classic depiction of a digital communication system employing FEC is shown in Figure 6.1. Data generated by the source is first compressed by a source encoder—tasked with *removing* redundancy to produce an efficient binary representation of the data—and then passed through the error control (or "channel") encoder, which *adds* redundancy to enable robust recovery by the error control (or "channel") decoder at the receiver. These seemingly conflicting operations—removing redundancy only to then add redundancy—are required because the "natural" redundancy that occurs in (for instance) speech or video signals is not sufficiently structured that it can be exploited at the receiver as effectively as the well-structured redundancy introduced by the error control encoder.

Figure 6.1 suggests that error control is carried out solely at the physical layer, which is not the case. Most notably, when ARQ is employed, the retransmission function is part of the processing at the (data) link layer.

The rest of this chapter discusses a multitude of error control techniques that have been implemented in mobile communication systems. While there are many different approaches, all error control schemes have this in common: They add structure to the transmitted signal in a way that *limits* what can be transmitted, compared with uncoded transmission. In a coded system, there are only certain signals that are *valid* and can thus be transmitted; since the receiver knows what those valid signals are, it can use that knowledge to select the valid sequence that is "most like" what it observes. From another perspective, coding exaggerates the differences between distinct data sequences in their transmitted form, making it easier to discern one from the other at the receiver.

6.2 Block Codes

Classic error control codes can be split into *block codes* and *convolutional codes*. In this section, we explain block codes.

6.2.1 The Fundamentals of Binary Block Codes

The very simple code described in the introduction—in which "1" is transmitted as "111" and "0" as "000"—is called a *block code*. It is given this name because a block of data—in this case, one bit—is represented with another (longer) block of transmitted bits—in this case, three bits. The two valid 3-bit sequences—"000" and "111"—are called the *codewords* of this code, and its *blocklength* is $n = 3$. We refer to this as a rate-1/3 code because there is one data bit for every three encoded (or transmitted) bits.

Generalizing, an (n, k) binary block code is one in which k data bits are represented with an n-bit codeword; thus, there are 2^k different codewords, each n bits long, where $n > k$. The *rate* of the resulting code is $R = k/n$ data bits per encoded bit.

As noted above, error control codes make it easier to differentiate between different "valid" transmitted signals. With regard to block codes, this property is captured (to first order) by the code's *minimum distance*, which is defined as the fewest number of coordinates in which two codewords differ. (So the trivial code in the introduction is a (3,1) code with a minimum distance of $d_{\min} = 3$, because every pair of codewords—and there are only two codewords—differ in at least three coordinates.) The *Hamming distance* between any two n-tuples is defined as the number of coordinates in which they differ, and the *Hamming weight* of a particular vector is the number of its nonzero components.

As a slightly less simple example, consider the $(n = 7, k = 4)$ Hamming code below.

0000 → 0000000	0100 → 0100101	1000 → 1000110	1100 → 1100011
0001 → 0001111	0101 → 0101010	1001 → 1001001	1101 → 1101100
0010 → 0010011	0110 → 0110110	1010 → 1010101	1110 → 1110000
0011 → 0011100	0111 → 0111001	1011 → 1011010	1111 → 1111111

Here, "0010 → 0010011" (for instance) means that the data 4-tuple "0010" is represented with the 7-bit codeword "0010011." There are $2^4 = 16$ codewords, each of length $n = 7$, and the rate of this code is $R = 4/7$ data bits per encoded bit. Moreover, careful inspection reveals that every pair of codeword differs in at least $d_{\min} = 3$ places, so this is a code with a minimum distance of three.

The significance of a block code's minimum distance is most clear if we think in terms of the decoder. Suppose that a codeword is transmitted and that each bit has independent probability p of being "flipped"—that is, of being sufficiently corrupted that a transmitted "1" is misinterpreted by the receiver as a "0" or vice versa. Then, assuming that $p < 1/2$, *most* bits should be received correctly, and so the most likely transmitted codeword is the one that disagrees with the received signal in the fewest coordinates—that is, the "closest" codeword in terms of Hamming distance. A decoder that estimates data based on this principle is called a *minimum distance*—or *maximum-likelihood* (ML)—decoder. ML decoding is optimal, assuming that the data are a sequence of independent, identically distributed bits, each equally likely to be a "1" or a "0."

As an example, suppose that the codeword $\mathbf{c} = [1011010]$ is transmitted but $\mathbf{y} = [1010010]$ is received, with a single error in the fourth coordinate. If you compare $\mathbf{y}$ to every codeword, you find that the codeword closest to $\mathbf{y}$ is, in fact, $\mathbf{c} = [1011010]$; thus, the ML decoder's estimate of the transmitted codeword (and the associated data) is, in fact, correct. In contrast, if $\mathbf{c} = [1011010]$ is transmitted but $\mathbf{y}' = [1011001]$ is received—the last two bits are "flipped"—then the closest codeword to $\mathbf{y}'$ is $\mathbf{c}' = [1001001]$, which means that the ML decoder will assume that $\mathbf{c}'$ was transmitted and will estimate the associated data to be (the incorrect) "1001" rather than (the correct) "1011"—that is, there will be a *decoding error.*

A *t-error correcting binary block code* is one for which minimum distance decoding will yield a correct estimate of the transmitted codeword provided no more than t errors have occurred; thus, a t-error correcting code must have the property that, if you "flip" any set of t or fewer bits in any codeword $\mathbf{c}$, the resulting vector is still "closer" to $\mathbf{c}$—that is, disagrees in fewer places—than to any other codeword. This leads to the relationship: A t-error correcting code must have a minimum distance $d_{\min}$ that satisfies

$$d_{\min} \geq 2t + 1.$$

Equivalently, a code with minimum distance $d_{\min}$ can correct up to $t = \lfloor (d_{\min} - 1)/2 \rfloor$ errors, where "$\lfloor . \rfloor$" indicates the floor function.

A close examination of the 16 codewords in the above (7,4) Hamming code reveals at least two more properties worth noting:

- If you add any two codewords together—here, "add" means component-wise XOR—then you get another codeword. In the language of mathematics, the code forms a *linear vector space* over the binary field {0,1}, and so we say this is a *linear code*. One consequence of linearity is that the code's minimum distance is equal to its minimum nonzero codeword weight.
- The first $k = 4$ bits of every codeword are identical to the associated k data bits. In the language of coding, the encoder is *systematic* on the first k positions.

Linear codes are useful because their algebraic structure enables simpler decoding and simpler analysis. Moreover, there are matrices associated with a linear block code that facilitate the encoding and decoding procedures. The *generator matrix* for an (n, k) binary block code is a $k \times n$ matrix G with binary entries such that its rows form a *basis* for the code—that is, the code is equal to the set of all sums (or "linear combinations") of the rows of G. This is expressed mathematically as $C = \{\mathbf{c}: \mathbf{c} = \mathbf{x}G \text{ for some } \mathbf{x} \in \{0,1\}^k\}$. A generator for the above (7,4) code is given by

$$G = \begin{bmatrix} 1 & 0 & 0 & 0 & 1 & 1 & 0 \\ 0 & 1 & 0 & 0 & 1 & 0 & 1 \\ 0 & 0 & 1 & 0 & 0 & 1 & 1 \\ 0 & 0 & 0 & 1 & 1 & 1 & 1 \end{bmatrix}.$$

Similarly, a parity check matrix for an (n,k) binary code is an $(n - k) \times n$ binary matrix whose rows form a basis for the *null space* of the code—that is, H is a parity check matrix for a code C if and only if $C = \{\mathbf{c}: \mathbf{c} \in \{0,1\}^n, \mathbf{c}H^T = \mathbf{0}\}$, where $\mathbf{0}$ is the $(n - k)$-tuple with all zero entries. The parity check matrix for the (7,4) code above is given by

$$H = \begin{bmatrix} 1 & 1 & 0 & 1 & 1 & 0 & 0 \\ 1 & 0 & 1 & 1 & 0 & 1 & 0 \\ 0 & 1 & 1 & 1 & 0 & 0 & 1 \end{bmatrix}.$$

Note that the rows of the parity check matrix describe the parity constraints that must be satisfied by every codeword. For example, the first row of H above indicates that the first, second, fourth, and fifth bits in every codeword must have even parity—that is, must contain an even number of 1's; the other two rows of H indicate two other parity constraints that must be satisfied by every codeword. More generally, the $(n - k)$ rows of a parity check matrix describe $(n - k)$ parity constraints that characterize the code.

The generator and parity check matrices are used in the encoding and decoding operations, respectively. With regard to encoding, the data vector $\mathbf{x} \in \{0,1\}^k$ is mapped onto the associated codeword $\mathbf{c} = \mathbf{x}G$. With regard to decoding, let $\mathbf{y} \in \{0,1\}^n$ denote a (possibly corrupted) received binary n-tuple—that is, assume that codeword $\mathbf{c}$ was transmitted but $\mathbf{y} = \mathbf{x} + \mathbf{e}$ was received, where $\mathbf{e} \in \{0,1\}^n$ is the a noise vector. Then, a typical "first step" in the decoding process is to compute the *syndrome* $\mathbf{s}$ associated with the received vector:

$$\mathbf{s} = \mathbf{y}H^T = (\mathbf{c} + \mathbf{e})H^T = \mathbf{c}H^T + \mathbf{e}H^T = \mathbf{e}H^T.$$

The syndrome $\mathbf{s}$ is computed from the received vector $\mathbf{y}$ but depends only on the error $\mathbf{e}$—not on the transmitted codeword. The syndrome for a binary code is a binary $(n - k)$-tuple—that is, $\mathbf{s} \in \{0,1\}^{n-k}$—and in *syndrome decoding* the syndrome $\mathbf{s}$ is first computed, and from $\mathbf{s}$ an estimate of the error vector $\mathbf{e}$

is formed. (Of course, once the error vector is estimated it is trivial to estimate the transmitted codeword by subtracting the error estimate from the received vector.)

There is a one-to-one relationship between correctable error patterns and syndromes; for every syndrome $\mathbf{s}$, there are many possible choices of $\mathbf{e}$ satisfying $\mathbf{s} = \mathbf{e}H^T$, but the decoder is capable of correcting exactly one of them. This observation—coupled with the observation that a t-error correcting code can correct (at least) every error pattern affecting t or fewer bits—leads to the following bound, called the *Hamming bound*:

$$1 + \binom{n}{1} + \binom{n}{2} + \cdots + \binom{n}{t} \leq 2^{n-k}.$$

Any binary (n,k) t-error correcting linear code must have parameters that satisfy the Hamming bound; codes that satisfy the Hamming bound with equality are called *perfect codes*. Similarly, the *Singleton bound* states that any (n,k) code with minimum distance $d_{\min}$ must have parameters that satisfy

$$d_{\min} \leq n - k + 1.$$

Codes that satisfy the Singleton bound with equality are called *maximum distance separable codes*.

The advantage of syndrome decoding lies in how it reduces the dimensionality of the decoding problem. The job of the decoder is to find the codeword $\mathbf{c}$ that is closest to the received vector $\mathbf{y}$; without using the code's structure, this could be done (in theory, if not in practice) with a table containing 2^n entries: the received vector $\mathbf{y}$ is used as an index into the table, and the associated entry contains the codeword closest to $\mathbf{y}$. However, if we first compute $\mathbf{s} = \mathbf{y}H^T$ we can now use $\mathbf{s}$ as an index into a table containing the 2^{n-k} correctable error patterns. For a (63,57) Hamming code, this reduces the required table from one containing $2^{63} = 9.22 \times 10^{18}$ entries to one containing only $2^6 = 64$ entries. Of course, for many practical codes this reduction in dimensionality still leaves a formidable problem: A (1023,923) 10-error correcting code produces a 100-bit syndrome, still far too large for a brute-force approach.

The (7,4) code used throughout this section is a *Hamming code*—one of a class of codes presented by Richard Hamming in 1950. More generally, a Hamming code is an $(n = 2^r - 1,\ k = 2^r - 1 - r)$ binary linear block code for any choice of $r = 2,3,4, \ldots$. Hamming codes are single-error correcting codes with minimum distance $d_{\min} = 3$. The Hamming code with blocklength $n = 2^r - 1$ is constructed using a parity check matrix with columns that are the $2^r - 1$ distinct non-all-zero binary r-tuples.

It is possible to *extend* a Hamming code by adding one additional redundant bit to every codeword to guarantee that every codeword has even parity—that is, an even number of ones. This converts the $(2^r - 1,\ 2^r - 1 - \mathrm{r})$ code into a $(2^r,\ 2^r - 1 - r)$ extended code—for example, the (7,4) Hamming code becomes the (8,4) extended Hamming code. Extending the code in this way increases the minimum distance of the code from $d_{\text{free}} = 3$ to $d_{\text{free}} = 4$. This additional minimum distance can be exploited to add a new capability—to not only correct any single error but also simultaneously detect (without miscorrecting) any double error. More generally, a block code is capable of correcting t errors and simultaneously detecting $e \geq t$ errors provided its minimum distance satisfies $d_{\min} \geq t + e + 1$.

6.2.2 Reed–Solomon Codes

The single-error correcting Hamming codes used to illustrate coding basics in the last section were the first practical "error correcting codes." The development of a general technique for constructing t-error correcting codes for $t > 1$ took another decade—until the unveiling of *BCH codes* [4,5] and *Reed–Solomon codes* [6] in 1959 and 1960. Reed–Solomon codes continue to be used today in a wide array of wireless (and other) applications, so we briefly describe their structure.

A Reed–Solomon code is a *nonbinary code*, meaning that each codeword from a Reed–Solomon code with blocklength n consists of n nonbinary symbols. An (n,k) Reed–Solomon code with minimum distance $d_{\min}$ protects k data symbols by adding $n-k$ redundant symbols such that every pair of codewords differs in at least $d_{\min}$ symbols. Moreover, the symbols are drawn from a nonbinary *field*, briefly explained below.

A "field" is a set with two operations—addition and multiplication—that satisfy the "usual" commutative, associative, and distributive properties and also contain additive and multiplicative identities as well as additive inverses and (for nonzero elements) multiplicative inverses. (The set of real numbers form a field under the usual notions of addition and multiplication, as do the set of complex numbers; the set of all integers do not because there are no multiplicative inverses.) A *finite field* (or Galois field) is a field with a finite number of elements; for instance, the binary field—containing just the elements {0,1}, with addition and multiplication performed modulo two—is a finite field.

Let GF(q) denote a field with q elements; then it is possible to construct the field GF(p^m) for any prime number p and any positive integer m, and it is *impossible* to construct a field with q elements if q is *not* a power of a prime. To construct the field GF(p) for prime p, the field consists of the integers {0,1,2, …, $p-1$} and both addition and multiplication are performed modulo p. To construct the field GF(p^m) for $m>1$ requires more subtlety; the field elements of GF(p^m) are the polynomials of degree at most $m-1$, with coefficients drawn from GF(p). There are p^m such polynomials, and if addition and multiplication are defined appropriately, then the resulting structure is a field. Here, "appropriately" means that addition is performed in the "usual" polynomial fashion, component-wise modulo p, while multiplication is performed in polynomial fashion, but the result is reduced modulo $\pi(x)$, where $\pi(x)$ is an *irreducible* polynomial with coefficients in GF(p) of degree exactly m. An irreducible polynomial is one that cannot be factored; it is analogous among polynomials to a prime number among integers.

For details on the construction of finite fields, the reader is referred to any textbook on error control coding or modern algebra. What is important to understand now is that each field element of GF(p^m) can be represented as a symbol made up of m digits drawn from {0,1,2,…, $p-1$}—that is, the m coefficients of the field element polynomial.

In practice, Reed–Solomon codes are designed over GF(2^m), so each symbol in a Reed–Solomon codeword can take one of 2^m values and is represented as an m-bit symbol. Of particular interest are Reed–Solomon codes over GF(256), because $256=2^8$ and therefore each codeword from an (n,k) Reed–Solomon code over GF(256) is n bytes long—with k data bytes and $n-k$ redundant bytes and each byte consisting of eight bits. Such a code has 256^k codewords, and the rate is $R=k/n$ data bytes per encoded byte.

An (n,k) Reed–Solomon code over GF(q) has blocklength $n=q-1$ and minimum distance $d_{\min}=n-k+1$. (So Reed–Solomon codes are *maximum distance separable* codes as defined in Section 6.3.) Such a code is specified by its parity check matrix:

$$H=\begin{bmatrix} 1 & \alpha^{j} & \alpha^{2j} & \alpha^{3j} & \cdots & \alpha^{(n-1)j} \\ 1 & \alpha^{j+1} & \alpha^{2(j+1)} & \alpha^{3(j+1)} & \cdots & \alpha^{(n-1)(j+1)} \\ \vdots & \vdots & \vdots & \vdots & \ddots & \vdots \\ 1 & \alpha^{j+r-1} & \alpha^{2(j+r-1)} & \alpha^{3(j+r-1)} & \cdots & \alpha^{(n-1)(j+r-1)} \end{bmatrix}.$$

Here, α is a *primitive element* of the field GF(q). That means that all of the nonzero elements of GF(q) can be written as powers of α—that is, GF(q) = {0, $\alpha^0=1$, α^1, α^2, α^3, …, α^{q-2}}. As with binary linear codes, the parity check matrix for an (n,k) Reed–Solomon code is an $(n-k)\times n$ array, so in H above, we have $r=n-k$.

The integer j in the above description of H is often (but not always) set to $j=1$. If we think of the components of a codeword $\mathbf{c}=[c_0, c_1, c_2, \ldots, c_{n-1}]$ as representing the coefficients of a polynomial $c(x)=c_0+c_1x+c_2x^2+\cdots+c_{n-1}x^{n-1}$, then the relationship $cH^{\mathrm{T}}=0$ is equivalent to the relationship $c(\alpha^j)=c(\alpha^{j+1})=c(\alpha^{j+2})=\cdots=c(\alpha^{j+r-1})=0$. This suggests an equivalent definition for Reed–Solomon codes: For a fixed integer j and a fixed redundancy $r=n-k$, an $(n=q-1,\ k=n-r)$ Reed–Solomon code over GF(q) consists of all

polynomials over GF(q) of degree $n-1$ or less that have r consecutive powers of a primitive element α as roots: $\alpha^j, \alpha^{j+1}, \alpha^{j+2}, \ldots, \alpha^{j+r-1}$. Such a code has a minimum distance $d_{\min} = r+1$ and so is capable of correcting all error patterns affecting not more than $\lfloor r/2 \rfloor$ symbols.

A few observations complete our discussion on Reed–Solomon codes:

- While, strictly speaking, a Reed–Solomon code over GF(q) has a blocklength $n = q-1$, it is possible to *shorten* a Reed–Solomon code—or any other code, for that matter—by arbitrarily setting some (say s) of the k information symbols to zero and then simply not transmitting them; as a result, an (n,k) code with minimum distance $d_{\min}$ is transformed into an ($n-s$, $k-s$) code with minimum distance *at most* $d_{\min}$. (For Reed–Solomon codes, the minimum distance of the shortened code is unchanged.) For example, the advanced television systems committee (ATSC) standard for terrestrial digital television broadcast employs a (207,187) shortened Reed–Solomon code over GF(256). It is obtained by shortening the (255,235) Reed–Solomon code; the resulting code adds $r = 20$ bytes of redundancy to $k = 187$ bytes of data in a way that guarantees the correction of up to $t = 10$ byte errors in any codeword.
- Because Reed–Solomon codes are organized on a symbol (rather than bit) basis, they are well suited to correcting *bursty errors*—that is, errors highly correlated in time. To illustrate: A burst of (say) 15 corrupted bits can affect no more than three 8-bit symbols and so can be corrected with a relatively modest 3-error correcting Reed–Solomon code over GF(256). This effectiveness with regard to bursty noise can be enhanced through the use of *interleaving*—that is, by interspersing the symbols from different codewords among each other, thereby spreading out the effect of the error burst over multiple codewords. (Example: If a code over GF(256) is interleaved to depth three, then that same 15-bit error burst would affect at most one symbol in each of three different codewords, and therefore it would be ameliorated by an even simpler 1-error correcting code.)

6.2.3 Coding Gain, Hard Decisions, and Soft Decisions

The benefits of channel coding are typically expressed in terms of a *coding gain*—an indication of how much the transmitted power can be reduced in a coded system without a loss in performance, relative to an uncoded system. Coding gain depends not only on the code that is used but also on whether *hard-decision decoding* or *soft-decision decoding* is employed.

In hard-decision decoding, the demodulator makes a "hard decision" about each transmitted bit; those decisions are then conveyed to the FEC decoder which corrects any errors made by the demodulator. In soft-decision decoding, the FEC decoder is provided not with hard decisions it must accept or correct, but rather with "soft" information that reflects the "confidence" with which the demodulator would make such a decision.

As an example, consider binary phase shift keying (BPSK) modulation in the presence of additive white Gaussian noise (AWGN). For each transmitted bit, the receiver observes a matched filter output Y of the form $Y = \pm\sqrt{E} + Z$, where the sign of $\sqrt{E}$ indicates whether the transmitted bit is a "0" or "1," E is the energy of the transmitted pulse, and Z is a 0-mean Gaussian random variable with variance $N_0/2$. In a hard-decision system, the demodulator estimates the transmitted bit based on whether Y is positive or negative, and it then passes that estimate to the decoder. When *soft-decision decoding* is employed, the FEC decoder gets direct access to the "soft information" contained in the unquantized (or very finely quantized) Y. More generally, in soft-decision decoding, the channel decoder is given access to the demodulator's matched filter outputs—typically quantized to several bits of precision.

To compare coded and uncoded transmission, the signal-to-noise ratio is typically expressed as E_b/N_0, where E_b is the *average energy per data bit*. If the (average) energy of each transmitted pulse is E, and each pulse conveys (on average) R data bits, then $E_b = E/R$. Displaying performance as a function of E_b/N_0 facilitates a fair(er) comparison because it includes the energy penalty that FEC codes pay to trans-

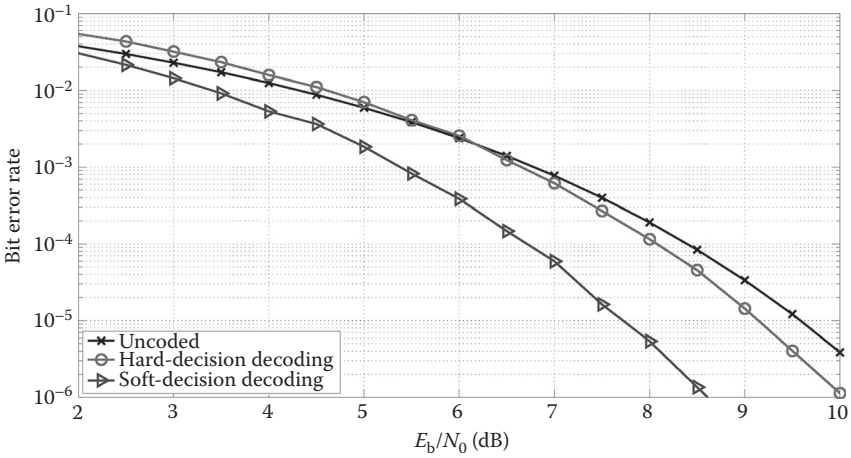

FIGURE 6.2 The bit error rate of a (7,4) Hamming code—with hard-decision and soft-decision decoding—compared with uncoded transmission for a BPSK-modulated AWGN channel.

mit their redundancy. However, these comparisons are not *wholly* fair because they do not address the bandwidth penalty that FEC can incur for a fixed modulation scheme; for instance, in transmitting data over a BPSK-modulated channel, using a (7,4) Hamming code requires 75% more bandwidth than uncoded transmission, because the transmitted bits (including redundancy) must be sent 75% faster after encoding if the data are to be delivered just as fast as in the uncoded case. The question of how to design codes without bandwidth expansion is addressed in Section 6.6.

Figure 6.2 shows the performance of the simple (7,4) Hamming code assuming BPSK modulation and an AWGN channel. It includes the performance with both hard-decision and soft-decision decoding, and uncoded transmission is included for comparison. Observe that hard-decision decoding of the Hamming code provides approximately 0.45 dB of coding gain over uncoded transmission at a bit error rate of 10^{-5}, while soft-decision decoding offers an *additional* 1.4 dB of gain. These coding gains mean that coded transmission requires only 90% (resp., 65%) of the transmitted power required for uncoded transmission to obtain a bit error rate (BER) of 10^{-5} when hard-decision (resp., soft-decision) decoding is used.

As a rule of thumb, at high signal-to-noise ratio (SNR), there is approximately a 2 dB gain associated with soft-decision decoding, compared to hard-decision decoding [7]. However, soft-decision decoding of algebraically constructed block codes is computationally complex; indeed, it was shown in Reference 8 that *optimal* (ML) soft-decision decoding of Reed–Solomon codes is NP-hard, although suboptimal algorithms that exploit soft information remain a subject of considerable research interest [9]. (ML soft-decision decoding selects as its estimate of the transmitted codeword the one that minimizes the Euclidean distance between the received signal and the modulated codeword.)

The formidable challenge of exploiting soft information in the decoding of block codes is one reason why other FEC techniques have evolved—techniques that are more accommodating to soft-decision decoding. One of the most fundamental of those other techniques is convolutional coding.

6.3 Convolutional Codes

Convolutional codes first appeared in a 1955 paper by Peter Elias [10]. Their popularity in practical digital communication systems came about largely because of the discovery in 1968 of a well-suited soft-decision decoding algorithm—the Viterbi algorithm.

6.3.1 The Fundamentals of Convolutional Codes

While an (n,k) binary block code assigns a discrete n-bit codeword to every discrete k-bit data block, an (n,k) binary *convolutional code* is one in which a "sliding block encoder" is used to generate n encoded sequences based on k data sequences. As a simple, illustrative example, consider the convolutional encoder in Figure 6.3. Here, the binary data sequence $\{x_1, x_2, x_3, \ldots\}$ is used to generate the encoded sequences $\{y_1^{(0)}, y_2^{(0)}, y_3^{(0)}, \ldots\}$ and $\{y_1^{(1)}, y_2^{(1)}, y_3^{(1)}, \ldots\}$ according to these rules:

$$y_k^{(0)} = x_k + x_{k-2} \quad \text{and} \quad y_k^{(1)} = x_k + x_{k-1} + x_{k-2}.$$

(As before, " + " indicates the binary XOR operation.) Thus, this is a (2,1) convolutional encoder because it accepts $k = 1$ binary sequence as an input and produces $n = 2$ binary-encoded sequences. More generally, an (n,k) *convolutional encoder* is a k-input, n-output, time-invariant, linear, causal, finite-state binary sequential circuit.

Just as linear block codes have generator and parity check matrices, so do convolutional codes. These representations employ the *D-transform* of a binary sequence: The D-transform of the binary sequence $\{b_0, b_1, b_2, \ldots\}$ is given by $B(D) = b_0 + b_1D + b_2D^2 + \ldots$. Then, a convolutional encoder takes k data sequences—represented by $\mathbf{x} = [x_1(D), x_2(D), \ldots, x_k(D)]$, where $x_i(D)$ is the D-transform of the ith data sequence—and produces n encoded sequences, represented by $\mathbf{y} = [y_1(D), y_2(D), \ldots, y_n(D)]$; the generator matrix G for such an encoder is a $k \times n$ matrix with entries that are rational functions in D such that $\mathbf{y} = \mathbf{x}$G. For example, the generator of the convolutional encoder shown in Figure 6.3 is given by $G = [1 + D^2\ 1 + D + D^2]$.

Convolutional encoders are *finite-state machines*. At any point in time, a convolutional encoder is in a particular "state" determined by its memory values; the encoder then accepts k input bits (one from each of the k data sequences) and produces an n-bit output while transitioning to a new state. This behavior is captured by a *state diagram;* the state diagram associated with the encoder in Figure 6.3 is shown in Figure 6.4a. The state of this particular encoder is determined by the previous two input bits—that is, when the encoder accepts input bit x_i, it is in the state determined by x_{i-1} and x_{i-2}, because there are $\nu = 2$ memory elements in the encoder; thus, this is a 4-state encoder. In general, a convolutional encoder with ν bits of memory has 2^ν states, and ν is referred to as the code's *constraint length*, an indicator of the code's complexity. In Figure 6.4a, each of the four states is represented by a node in a directed graph; the branches between the nodes indicate the possible transitions, and the label "$x/y^{(1)}\ y^{(2)}$" denotes the input (x) that causes the transition along with the two-bit output ($y^{(1)}\ y^{(2)}$) that results.

An alternative representation of a convolutional encoder is the trellis diagram—a graph that includes the same state and transition information as the state diagram but also includes a time dimension. The trellis diagram for the (2,1) convolutional encoder under consideration is shown in Figure 6.4b; it shows, for instance, that when the encoder is in state 1 (corresponding to $x_{i-1} = 1$, $x_{i-2} = 0$) then an input of "0" (resp., "1") will cause a transition to state 2 (resp., 3) and produce an output of "01" (resp., "10").

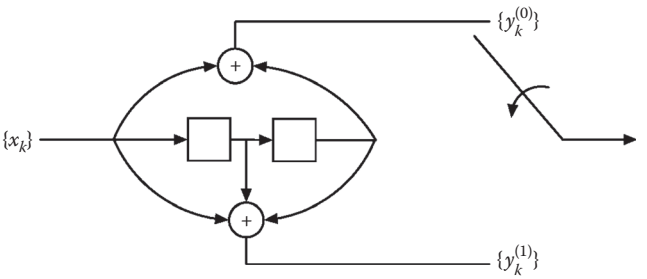

FIGURE 6.3 An encoder for a (2,1) convolutional code; the generator is $G = [1 + D^2\ 1 + D + D^2]$.

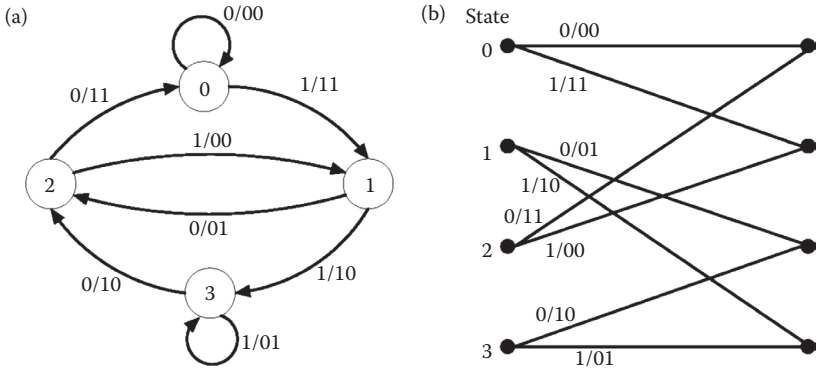

FIGURE 6.4 (a) The state diagram and (b) trellis diagram of the convolutional encoder from Figure 6.2.

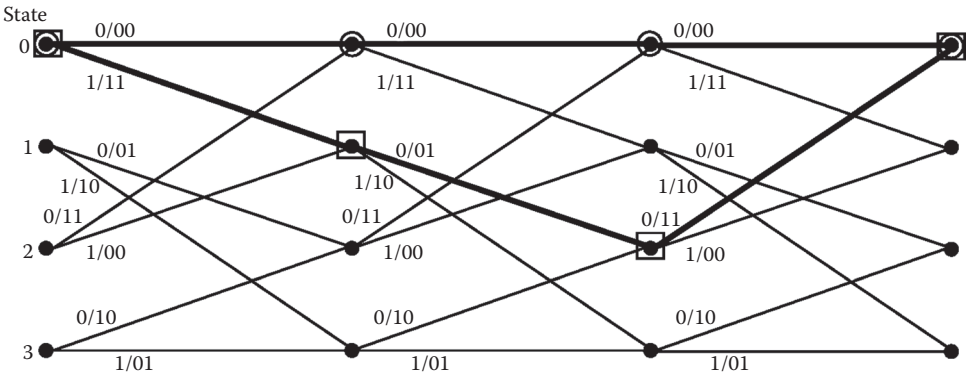

FIGURE 6.5 Two paths through the trellis illustrating that the free distance of the code is $d_{\text{free}} = 5$.

The *free distance* of a convolutional code is the minimum Hamming distance between any two valid encoded sequences; like the minimum distance of a block code, the free distance of a convolutional code indicates how "far apart" two distinct encoded sequences are guaranteed to be. Moreover, because of the assumed linearity of convolutional codes, the free distance of a code is equal to the minimum Hamming weight of any sequence that diverges from the all-zero sequence and then remerges. This is seen in Figure 6.5, where it is shown that the convolutional code with generator $G = [1 + D^2\ 1 + D + D^2]$ has a minimum distance of $d_{\text{free}} = 5$.

6.3.2 The Viterbi Algorithm

In 1967, Dr. Andrew Viterbi published a paper [11] in which he presented an "asymptotically optimum decoding algorithm" for convolutional codes—an algorithm that transformed how digital communication systems were designed.

The Viterbi algorithm as applied to the decoding of convolutional codes is best understood as finding the "best path" through the code trellis. Referring to Figures 6.4b and 6.5, every branch in the trellis corresponds to the encoding of k data bits and the transmission of n channel bits; thus, there are 2^{kL} paths of length L through the trellis—that is, 2^{kL} paths made up of L branches—that start in a particular state at a particular point in time. Finding the "best path" through a brute force approach would quickly

become unwieldy for even moderate values of L, since it would require comparing an observed signal of length L with 2^{kL} candidate paths.

The key insight of the Viterbi algorithm is this: The relevant metrics—that is, the relevant measures of what constitutes the "best path"—are additive over the length of the received sequence, and so when two paths "merge" into the same state, only one path—the best one entering that state—can remain a candidate for the title of "best path." So, instead of keeping track of 2^{kL} candidate paths of length L, we need to retain only 2^{ν}—one for each of the 2^{ν} states, because only the best path entering each state is a "survivor."

The ML metric is the log-likelihood function; if $\mathbf{x}$ is transmitted and $\mathbf{y}$ is received, then $\log[p(\mathbf{y}|\mathbf{x})]$ reflects how likely $\mathbf{y}$ is to have been produced by $\mathbf{x}$. Note that if the channel is "memoryless"—that is, each successive transmission is affected independently by the channel noise—then $p(\mathbf{y}|\mathbf{x}) = \Pi\ p(y_i|x_i)$ and the metric $\log[p(\mathbf{y}|\mathbf{x})] = \Sigma \log[p(y_i|x_i)]$ is indeed additive. For additive Gaussian noise, maximizing this metric is equivalent to *minimizing* the cumulative squared Euclidean distance between $\mathbf{x}$ and $\mathbf{y}$.

6.4 Turbo Codes

At the 1993 International Conference on Communications in Geneva, Switzerland, a groundbreaking new approach to error control coding was unveiled [12]. In a paper titled "Near Shannon Limit Error Correcting Coding and Decoding: Turbo Codes" by Berrou, Glavieux, and Thitimajshima, the authors demonstrated good performance—a bit error rate of 10^{-5}—with a rate-1/2 code at an E_b/N_0 value of only 0.7 dB on the BPSK-modulated AWGN channel. That is only 0.5 dB away from the E_b/N_0 limit mandated by Shannon's capacity result for BPSK-modulated signaling.

The approach taken in Reference 12 (and in the follow-up journal paper [13]) was to use parallel concatenated convolutional encoders with an iterative decoder structure—an approach widely referred to as *turbo (de-)coding.*

The now-classic structure of a turbo encoder is shown in Figure 6.6. Two encoders—both recursive systematic convolutional encoders—are placed in parallel. The same input data are applied to both encoders—to the first encoder in unaltered form and to the second encoder after it has passed through an *interleaver* π. The "job" of the interleaver is to change the order in which the bits are encoded in a pseudo-random—that is, random-looking but deterministic—fashion.

The encoder unveiled in the 1993 paper is shown in Figure 6.7; it uses two rate-1/2 convolutional encoders, each with generator $G = [1(1 + D^4)/(1 + D + D^2 + D^3 + D^4)]$. The encoder thus produces three bitstreams—one consisting of the systematic data bits and two parity streams, one formed by the original data, and the other formed by the interleaved data. As such, this is a rate-1/3 code; however, in References 11 and 12, half of the parity bits are "punctured" (i.e., not transmitted)—alternately from the first parity stream and then the second—to bring the rate of the code up to $R = 1/2$.

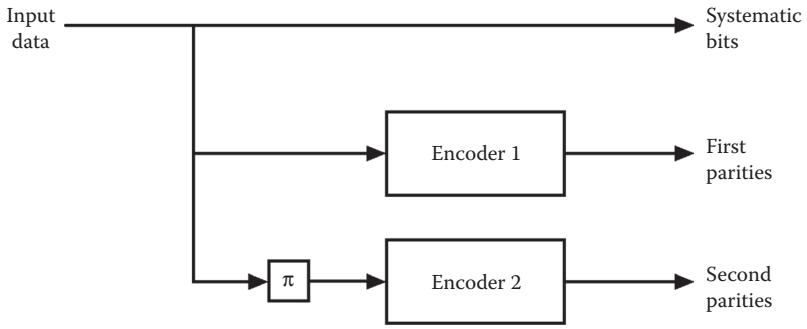

FIGURE 6.6 The structure of a turbo encoder.

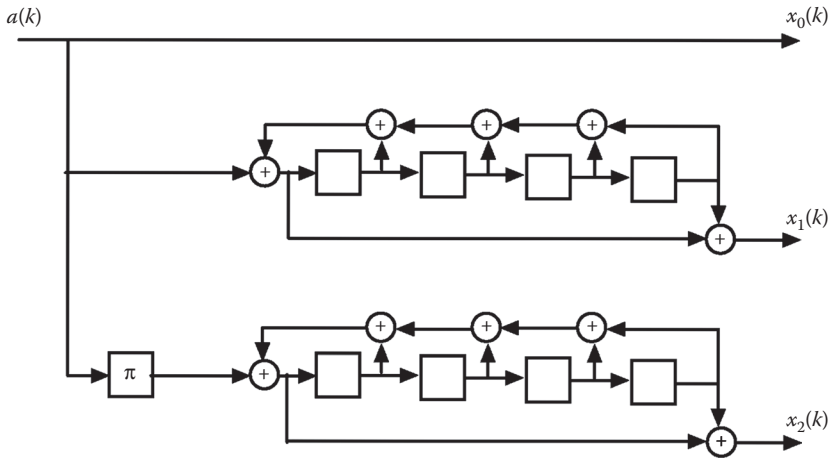

FIGURE 6.7 The turbo encoder from the 1993 ICC paper [10].

A decoder for such a turbo code is shown in Figure 6.8. The two constituent decoders correspond to the two constituent encoders, and they are used iteratively. Each decoder has three inputs—(1) the received channel values corresponding to the systematic (data) bits; (2) the received channel values corresponding to the parity (redundant) bits; and (3) *a priori* values for the systematic bits. The *a priori* values represent the initial probabilities assigned to the systematic bits by the decoder, and they are provided in the iterative framework by the *other* decoder. Heuristically, each decoder is provided with the channel values it needs plus a "first estimate" of the data—that is, for each systematic bit, a probability that that bit is "1." The decoder then produces its own estimate of the data probabilities and passes them on to the other decoder—which uses them as *its* "first estimate." In this way, the two decoders (ideally) make increasingly better estimates of the data.

The algorithm used by each decoder is the Bahl-Cocke-Jelinek-Raviv (BCJR) algorithm [14], a *maximum a posteriori* (MAP) decoding algorithm for convolutional codes. Unlike ML decoding, in which noisy values **y** are observed and the estimate of the data **x** is the value maximizing $p(\mathbf{y}|\mathbf{x})$, a MAP decoder observes **y** and chooses as its estimate of **x** the value maximizing $p(\mathbf{x}|\mathbf{y})$; such a decoder requires not only a probabilistic description of the channel (which is all that is required for an ML decoder) but also the *a priori* probabilities on **x**—something that, in a turbo decoder, is provided by the partner decoder.

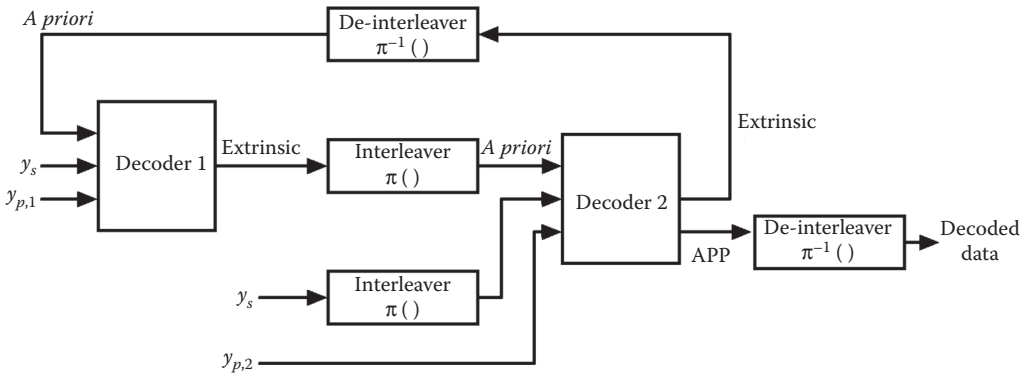

FIGURE 6.8 The structure of a turbo decoder. Here, y_s indicates the received systematic values while $y_{p,1}$ and $y_{p,2}$ represent the received values corresponding to the first and second parity sequences, respectively.

Regarding the "first estimates" that each BCJR decoder produces (and that are used by the *other* decoder as *a priori* probabilities): These are labeled "Extrinsic" in Figure 6.8, and they must be computed in a way that removes (to the extent possible) the transfer of information to a decoder *that is already using that information*. As noted above, each decoder uses three inputs: systematic values, parity values, and *a priori* values. However, the other decoder already has access to two of those—the systematic values and the *a priori* values (which were produced by the other decoder as extrinsic information). Therefore, the effect of the systematic values and the *a priori* values must be removed from each decoder's "first estimate" before it is passed as extrinsic information to the other decoder. (For details on how this is accomplished, see, for example, [15] or [16].)

The algorithm stops either after a maximum number of iterations or when some "stopping condition" indicates to the decoder that the data have been correctly decoded. At that point, Decoder 2 produces its estimate of the data—and it does so without removing the effects of the systematic and *a priori* information as it does when passing extrinsic information. That is, Decoder 2 bases its final decisions on the *a posteriori probabilities* (APP) it computes for each systematic bit.

The performance of the 1993 ICC turbo code is shown in Figure 6.9. The improvement in performance as the number of iterations increases is vast; after only 18 iterations, a BER of 10^{-5} is obtained at a signal-to-noise ratio of only 0.7 dB—just a half dB above the limit implied by the capacity theorem for BPSK-modulated AWGN channels. Also notable is the "error floor"—the sharp reduction in the slope of the BER curve at BER values below 10^{-5}. This phenomenon had not been observed with conventional, "pre-turbo" codes and was not initially understood by early turbo researchers. Subsequent research showed that the impressive "waterfall" performance of turbo codes is due to "spectral thinning"—that is, a reduction in the *multiplicity* of low-weight turbo codewords—while the error floor is due to the (relatively small) minimum distance of turbo codes.

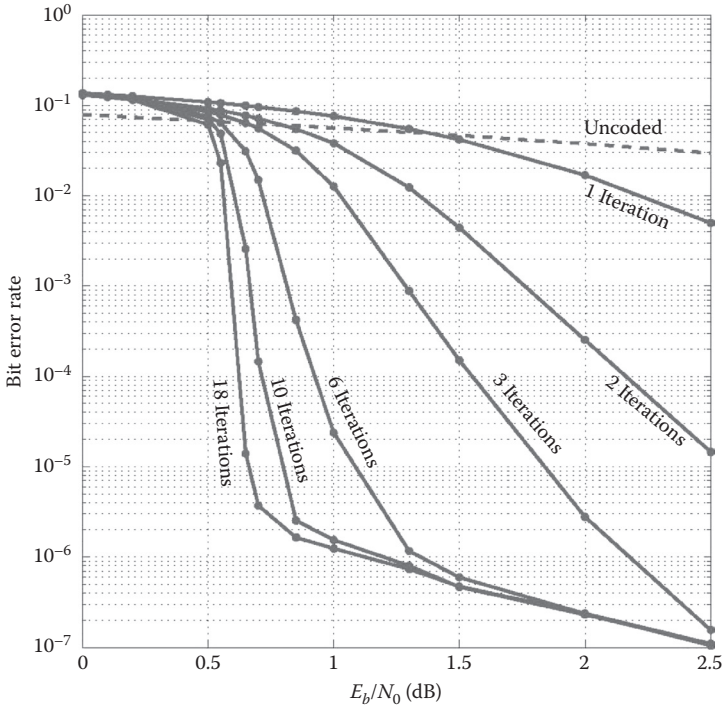

FIGURE 6.9 Performance of the rate-1/2 turbo code from Figure 6.6 assuming BPSK and additive white Gaussian noise.

Turbo codes represented a breakthrough in channel coding. Their startling performance demonstrated that the lessons of Shannon—that good codes should have long blocklengths and appear "random"—are still valid, but it also provided a new insight: That very long codes could be made practical by employing suboptimal iterative decoding techniques. All these lessons were present in the next coding "breakthrough"—low-density parity check (LDPC) codes.

6.5 Low-Density Parity Check Codes

LDPC codes were originally proposed by Dr. Robert Gallagher in the early 1960s [17], but it took more than 30 years—and the maturation of high-speed digital processing technology—for them to be recognized as a practical and powerful solution for many channel coding applications. Indeed, it was only in the aftermath of the discovery of turbo codes that the key elements of LDPC codes—long, random-like codewords made practical by an iterative decoding algorithm—were "rediscovered" and fully appreciated [18].

LDPC codes are block codes with a parity check matrix with a "low density" of ones—that is, relatively few ones. While there is no precise definition of what constitutes "low density"—typically, we take it to mean that the fractions of nonzero components in each row and each column are very small—the decoder complexity increases with the number of ones in the parity check matrix, so keeping the density of ones low is what makes LDPC codes practical.

As a simple example, consider the parity check matrix given by

$$H = \begin{bmatrix} 1 & 1 & 1 & 1 & 0 & 0 & 0 & 0 & 0 & 0 \\ 1 & 0 & 0 & 0 & 1 & 1 & 1 & 0 & 0 & 0 \\ 0 & 1 & 0 & 0 & 1 & 0 & 0 & 1 & 1 & 0 \\ 0 & 0 & 1 & 0 & 0 & 1 & 0 & 1 & 0 & 1 \\ 0 & 0 & 0 & 1 & 0 & 0 & 1 & 0 & 1 & 1 \end{bmatrix}.$$

(This matrix actually contains a relatively *high* density of ones, but it suffices to introduce the necessary terminology and concepts.)

The above parity check matrix illustrates a particular kind of LDPC code, called a *regular* LDPC code, because every row of the matrix and every column of the matrix contains the same number of ones. An (w_c, w_r) regular LDPC code is one for which the associated parity check matrix has w_c ones in every column and w_r ones in every row; thus, each code bit is involved in w_c parity constraints and each parity constraint involves w_r bits. It is easy to show that the rate R of an (w_c, w_r) LDPC code satisfies $R \leq 1 - (w_c/w_r)$, where the quantity $R' = 1 - (w_c/w_r)$ is called the *design rate* of an (w_c, w_r) LDPC code.

Associated with an LDPC code is a *Tanner graph* with two classes of nodes—check nodes and bit nodes; if the parity check matrix is m rows by n columns, then there are m check nodes (one for each parity check) and n bit nodes (one for each codeword bit) in the graph. An edge connects a check node with a bit node if and only if the bit participates in the associated parity check. The Tanner graph for the (2,4) regular LDPC code with parity check matrix H above is shown in Figure 6.10.

The significance of the Tanner graph is that it provides a "map" to the decoding algorithm that is typically used with LDPC codes—an algorithm called *belief propagation* or *message passing*. The details of the belief propagation algorithm can be found in any textbook on coding theory (e.g., [15,19]), but what follows is a brief overview.

- The decoding algorithm is iterative, with each iteration consisting of two phases: In the first phase of an iteration, every bit node sends a "message" to every check node connected to the bit node via the Tanner graph; in the second phase, every check node similarly sends a message to each of the bit nodes to which *it* (the check node) is connected.

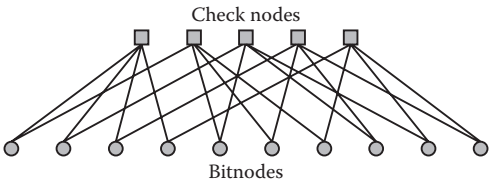

FIGURE 6.10 The bipartite graph for the (2,4)-regular LDPC code with parity check matrix given by H.

- The messages passed from bit nodes to check nodes and from check nodes to bit nodes are called *extrinsic* information—"extrinsic" meaning that we do not pass to a node information that recently originated at that node.
- Let q_{ij} denote a message passed from bit node i to check node j in a given round. Then, q_{ij} is the probability that the transmitted bit value associated with node i is "1," given the received channel value and given all of the extrinsic information that was passed to bit node i in the previous iteration, with the exception of the extrinsic information that was passed to bit node i from check node j.
- Let r_{ji} denote a message passed from check node j to bit node i. Then, r_{ji} is the probability that the parity check constraint described by check node j is satisfied, given that the transmitted bit value associated with node i is "1" and given all the extrinsic information passed to check node j from the other bit nodes (*except* for bit node i) in the previous round.
- At the end of each iteration, the APP distribution for each bit node can be computed based on the associated channel output value as well as the messages passed to the node during that iteration. An estimate for each bit can be made at that point based on the APP value—that is, an estimate of "1" if that is the more likely value, an estimate of "0" otherwise.
- The algorithm continues until either a fixed number of iterations have been completed or some "stopping condition" has been met—for example, if the hard estimates produced by the APP distributions at the end of an iteration satisfy all the parity constraints required by the code.

Figure 6.11 shows the dependencies of messages flowing into and out of a check node f_0; in keeping with the notion that only "extrinsic" information is passed to a node, the message that f_0 sends to X_0 depends on the messages f_0 received from X_1, X_2, and X_3 but *not* X_0—and similarly for the other messages passed by f_0. Similarly, Figure 6.12 shows the dependencies of messages flowing into and out of bit node X_0; here, Y_0 corresponds to the matched-filter channel output corresponding to the value of X_0.

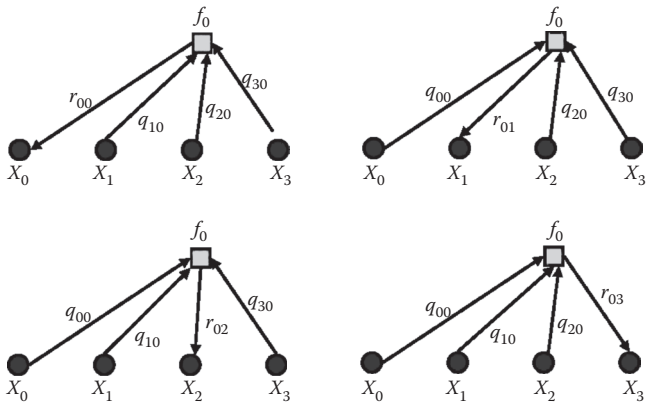

FIGURE 6.11 The dependencies of messages passed to and from check node f_0 in message-passing decoding of LDPC codes.

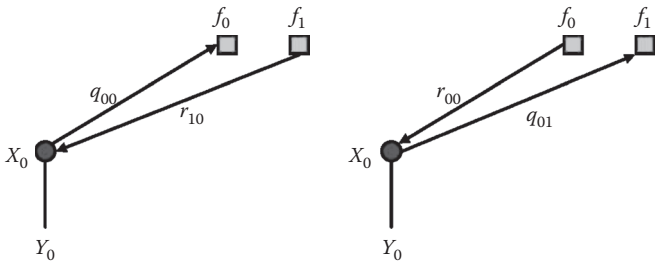

FIGURE 6.12 The dependencies of messages passed to and from a bit node X_0 in message-passing decoding of LDPC codes.

The algorithm as outlined above involves the passing of messages that represent probabilities, or likelihood values; in practice, it is common to carry out the algorithm in the log domain, so the messages become log-likelihood ratios (LLRs) that are either positive or negative—that is, the sign of the LLR indicates whether the associated random variable is more likely to be "1" or "0," and the magnitude of the LLR reflects the confidence of that assertion. Executing the algorithm in the log domain has the advantage of turning costly multiplications into less costly additions and also enhancing numerical stability.

Figure 6.13 demonstrates the performance of three different (6,3)-regular LDPC codes (each of design rate 0.5) over a BPSK-modulated AWGN channel. The advantage of increasing the code's blocklength is

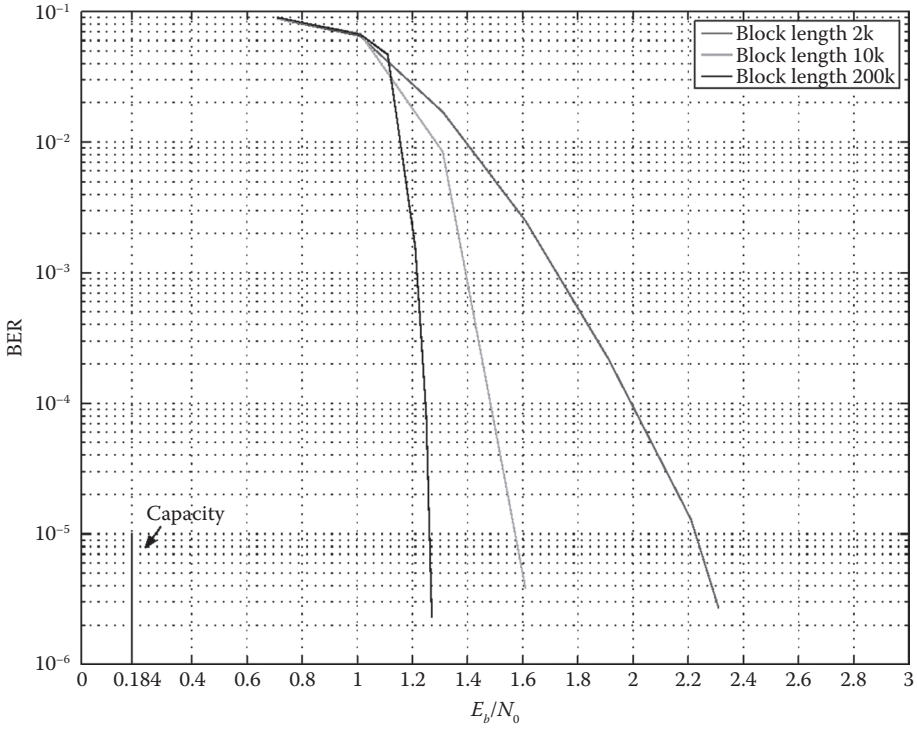

FIGURE 6.13 The performance of a (3,6) regular randomly designed LDPC code over a BPSK-modulated additive white Gaussian channel for blocklengths of $n = 2000$, 10,000, and 200,000 bits.

apparent; for a bit error rate of 10^{-5}, increasing the blocklength from $n = 2000$ to $n = 200{,}000$ provides almost a full decibel of coding gain.

The results in Figure 6.13 show LDPC performance that is still significantly worse than what is promised by Shannon and information theory; the capacity of the BPSK-modulated AWGN channel tells us that there exists a rate-1/2 code that can perform arbitrarily well at $E_b/N_0 = 0.184$ dB—more than a full dB less than the SNR required for the $n = 200{,}000$ LDPC code to attain a bit error rate of 10^{-5}. To get good performance at lower SNR values requires the use of *irregular* LDPC codes—that is, codes with parity check matrices with a nonconstant number of ones in every row and column; indeed, by optimizing the *degree profiles* that characterize the densities of ones in the matrix's rows and columns, it is possible to get good performance within a few hundredths of a dB from the limit imposed by capacity [20].

6.6 Coding and Bandwidth-Efficient Modulation

The bandwidth of a communication channel imposes limits on how rapidly one can signal over the channel. Specifically, the results of Nyquist dictate that it is impossible to transmit more than W two-dimensional symbols per second over a W Hz bandpass channel without incurring intersymbol interference (ISI) at the receiver.

While Nyquist tells us we cannot send more than W symbols per second, it is still possible to improve the data rate over a W Hz channel by conveying more information with each symbol—that is, by using *bandwidth-efficient modulation*. In uncoded transmission, a symbol constellation with $M = 2^b$ symbols conveys b bits with every symbol; Figure 6.14 shows symbol constellations with $M = 4$, 8, and 16 symbols, corresponding to $b = 2$, 3, and 4 bits per symbol; these constellations are called quaternary phase-shift keying (QPSK), octal phase-shift keying (8-PSK), and 16-ary quadrature amplitude modulation (16-QAM).

A brief explanation of what these constellations represent: Each symbol has an associated b-bit label; therefore, the transmission of each symbol is equivalent to the transmission of b bits. But what does it mean to "transmit" a symbol? Think of the constellations in Figure 6.14 as lying in the complex plane, so the "x-coordinate" of each symbol represents its real part and the "y-coordinate" its imaginary part. Then, to transmit the sequence of symbols $[s_0, s_1, s_2, \ldots]$ means to transmit the signal $c(t)$, where

$$c(t) = \sum_i \mathrm{Re}[s_i]p(t - iT_s)\cos(2\pi f_0 t) - \mathrm{Im}[s_i]p(t - iT_s)\sin(2\pi f_0 t).$$

The orthogonality of the two sinusoids creates, in essence, two channels; the *in-phase channel* that carries the real part of each transmitted symbol and the *quadrature channel* that carries the imaginary part. The pulse $p(t)$ is used to shape the spectrum of the transmitted signal, and these pulses are transmitted every T_s seconds, each pulse weighted by the appropriate symbol coordinate. *Raised cosine pulses* are often used in this context; a raised cosine pulse with rolloff parameter α ($0 \le \alpha \le 1$) results in a transmitted signal with a bandwidth of $(1 + \alpha)/T_s$ Hz. Thus, uncoded M-ary transmission provides a bandwidth efficiency of $\gamma = \log_2(M)/(1 + \alpha)$ bits/s/Hz.

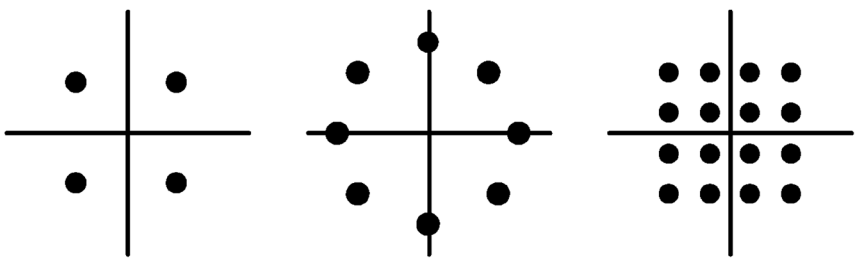

FIGURE 6.14 Three constellations for bandwidth-efficient modulation: QPSK, 8-PSK, and 16-QAM.

While channel coding for power-limited applications (e.g., space communications) yielded useful results as early as the mid-1960s, the application of channel coding to bandlimited environments (such as the telephone channel) came much later. The reason: the straightforward application of binary codes to larger, "denser" symbol constellations—that is, by designing good binary codes and then mapping them via Gray mapping* to the larger constellation—yielded relatively poor results.

With hindsight, the reason for the disappointing performance is obvious. The performance of a digital communication system is, to first order, determined by how "far apart" two different, valid transmitted symbol sequences are required to be; the more "unlike" two sequences are from one another, the less likely the receiver is to mistake one for the other. Here, the "distance" of one sequence from another is given by the square root of the cumulative squared Euclidean distance between the symbols—that is, the distance between the sequence of symbols $[s_0, s_1, s_2, \ldots]$ and the sequence $[r_0, r_1, r_2, \ldots]$ is $\sqrt{\sum_i |s_i - r_i|^2}$. However, encoding data with good binary codes and then "throwing the encoded bits over a wall" to be modulated does not result in a system with good Euclidean distance properties.

In the late 1970s, Gottfried Ungerboeck [21] of IBM unveiled *trellis coded modulation* (TCM), a technique for jointly designing the coding and modulation functions to enhance Euclidean distance properties; TCM is still employed in wireline and wireless systems today. Another approach to bandwidth-efficient coding, *bit-interleaved coded modulation* (BICM), was originally developed to improve performance over fading (mobile) communication channels [22] but has since, with the advent of capacity-approaching codes such as turbo and LDPC codes, been shown to be useful in a variety of applications. The next two subsections describe TCM and BICM.

6.6.1 Trellis-Coded Modulation

TCM is best explained via a (now classic) example. Suppose one wishes to convey two information bits per transmitted symbol—a goal that is realizable with uncoded transmission using QPSK modulation. TCM teaches that, to apply coding to such a system, one doubles the constellation size—to 8-PSK—and then uses the structure of a convolutional encoder to ensure that only certain sequences are valid and can thus be transmitted.

This approach is illustrated in Figure 6.15. Two information bits are passed through a rate-2/3 convolutional encoder to produce the three bits $[y_2 y_1 y_0]$. This convolutional encoder is not "good" in the sense that it has a large free distance; indeed, its free distance is trivially one. Rather, the output of the encoder is interpreted as the label of the transmitted symbol, and the combination of the encoder with the "natural" (rather than Gray) mapping produces an encoder-plus-modulator with better Euclidean distance properties than uncoded QPSK. Specifically, this scheme provides an asymptotic (high-SNR) coding gain of approximately 3 dB in AWGN compared to uncoded QPSK, meaning that the coded system need transmit only half as much power as the uncoded system and still have the same performance.

To understand the TCM encoder in Figure 6.15, it is informative to look at the state transition diagram. Because the encoder has $\nu = 2$ memory elements, this is a four-state encoder. Moreover, because only one of the two input bits is passed through the encoder—the other is *uncoded*—there are parallel transitions between states. For example, if the encoder is in state "00" then an input of either "01" or "11" will cause a transition to state "10"; because the first bit is uncoded, it has no effect on the state transition. Finally, observe that the two transmitted symbols corresponding to these two parallel transitions—symbols S_2 and S_6—are maximally far apart.

These observations lead to an illuminating interpretation of the encoder in Figure 6.15: The encoded bits $[y_1 y_0]$ select a sequence of *subsets* of the symbol constellation—in this example, there are four such subsets: $\{s_0, s_4\}$, $\{s_1, s_5\}$, $\{s_2, s_6\}$, and $\{s_3, s_7\}$—and then the uncoded bit is used to select one of the symbols from the subset. Thereby, the sequence of two-bit inputs selects a sequence of 8-PSK symbols that are transmitted.

* In Gray mapping, labels are assigned to two-dimensional symbols so that adjacent symbols have labels that differ in a single bit. In this way, the most common symbol detection errors result in a single bit error.

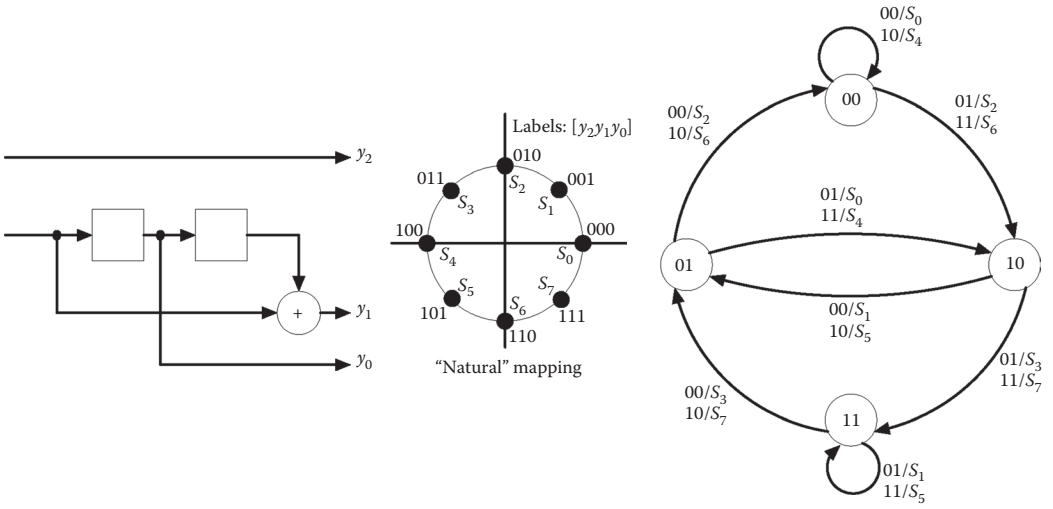

FIGURE 6.15 A trellis-coded modulation (TCM) scheme employing 8-PSK to convey two information bits per symbol.

This approach is generalized in Figure 6.16 to describe a system in which k information bits are conveyed with every transmission of a symbol from a constellation with 2^{k+1} elements—i.e., the constellation size is *doubled* over what is required for uncoded transmission. In this figure, k data bits enter the encoder during each symbol period; m of them are coded while $k–m$ of them are uncoded. The m coded bits are passed through a rate-$m/(m + 1)$ convolutional encoder to produce $m + 1$ bits that form *part* of the label of the transmitted codeword; the $k–m$ uncoded bits form the rest of the $k + 1$-bit label. In this way, the output of the convolutional encoder selects a sequence of constellation subsets—there are 2^{m+1} such subsets, and they each contain $k–m$ symbols—while the uncoded bits select the transmitted symbol from each subset thus selected. (Applying this notation to the example in Figure 6.15, we have $k = 2$ and $m = 1$.)

The 2^{m+1} subsets (each with $2^{k–m}$ symbols) should be designed to be as "sparse" as possible; the minimum Euclidean distance between symbols in each subset should be maximized. This is because two information sequences that differ in a single uncoded bit will be encoded to symbol sequences that are at least $d_{\text{min,uncoded}}$ apart, where $d_{\text{min,uncoded}}$ is the minimum Euclidean distance within a (sparse) subset. On the other hand, two information sequences that differ in *coded* bit(s) will benefit from the structure of the convolutional encoder; the convolutional encoder guarantees that the sequence of (partial) labels it produces will yield a sequence of subsets that are sufficiently different to guarantee a cumulative Euclidean distance of $d_{\text{min,coded}}$. Thus, the overall scheme produces a guaranteed minimum Euclidean

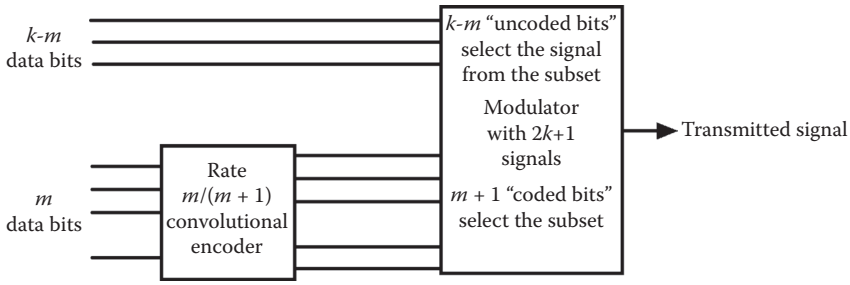

FIGURE 6.16 A block diagram of a generic TCM encoder.

difference of $d_{\min} = \min\{d_{\min,\text{coded}}, d_{\min,\text{uncoded}}\}$ in the two sequences of transmitted symbols associated with two different information sequences.

TCM has been widely extended beyond the simple approach outlined here [15,16]. Examples of those extensions include:

- The design of *multidimensional* trellis codes, in which the symbol constellation is not two-dimensional but rather $2M$-dimensional for some integer $M > 1$. The $2M$-dimensional space is obtained by concatenating M successive two-dimensional spaces created by the in-phase/quadrature representation of M symbol intervals. The advantage of higher-dimensional codes comes from the fact that it is possible to more efficiently "pack" symbols in higher dimensions.
- The design of *rotationally invariant trellis* codes, which enable the receiver to recover the transmitted data even when the symbol constellation is rotated—a phenomenon that occurs when the receiver loses carrier synchronization and is unable to acquire an absolute phase reference.

6.6.2 Bit-Interleaved Coded Modulation

While TCM employs an integrated approach to coding and modulation, BICM takes a partitioned approach—but with the addition of a bit-interleaver between the encoder and the modulator.

In an early paper by Zehavi [22], BICM was motivated by the fading present in mobile communication channels. In the *fully interleaved Rayleigh fading channel*, it is assumed that each transmitted symbol is affected independently by Raleigh fading; this is quite different from the *block Rayleigh fading channel* in which the fading is assumed to be (approximately) constant over some specified blocklength, typically determined by vehicle speed and carrier frequency.* The performance of a coded digital communication system over the fully interleaved Rayleigh fading channel is affected most strongly by its *diversity order*—that is, by the minimum number of distinct modulation symbols between two valid transmitted sequences; this is quite different from the cumulative squared Euclidean distance metric that determines performance over a nonfading AWGN channel—and which motivated TCM. Zehavi's approach, illustrated in Figure 6.17 with a rate-2/3 convolutional code, was to carry out "bit-interleaving" between the encoder and the decoder to "spread out" the bits so that every bit-difference in the convolutional encoder's output produced exactly one corresponding symbol-difference in the transmitted sequence; this leads to a diversity order equal to the minimum Hamming distance of the convolutional encoder—the optimal value.

Subsequent research on BICM [23] indicated that very little capacity is lost (for both fading and AWGN channels) by restricting the encoder to one of the type from [22]—that is, by using bit interleaving to create independent, binary-input equivalent channels and then applying capacity-approaching codes to those channels. This realization, coupled with the concurrent development of capacity-approaching

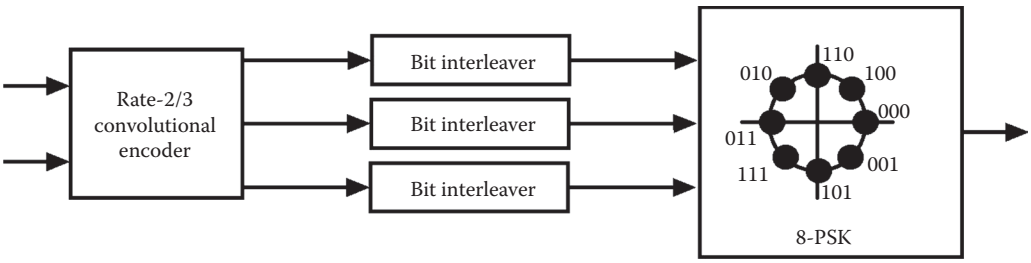

FIGURE 6.17 Block diagram of the rate-2/3 8-PSK BICM encoder. (From Zehavi, E., *IEEE Transactions on Communications*, 40(5), 873–884, 1992.)

* The fully interleaved Rayleigh fading channel can be realized by symbol-interleaving a block-wise (or correlated) fading channel to sufficient depth that the fades from one symbol to the next appear independent.

binary codes such as LDPC and turbo codes, has led to the widespread adoption of the BICM architecture—a binary encoder followed by a bit interleaver followed by a dense Gray-mapped symbol constellation—for bandwidth-efficient communication.

6.7 Automatic Repeat Request

All the approaches to error control described in this chapter up to this point have been examples of FEC. This means that the redundancy incorporated into the transmitted signal is designed to provide enough robustness against channel noise that the information-bearing sequence can be recovered at the receiver well enough to meet the application's requirements without any retransmissions.

For some applications, it is wasteful to provide such a high level of robustness because the channel conditions are usually so benign that the redundancy is unneeded. For such applications, when a "reverse channel"—a channel from the receiver to the transmitter—is available, an ARQ approach is appropriate.

In an ARQ protocol, the receiver does not attempt to recover the encoded data in the presence of corruption; rather, it simply *detects* the corruption and, when upon finding it, requests that the data be retransmitted. Thus, an ARQ protocol requires two elements: a means for *error detection* and a *retransmission strategy*.

Error detection is typically carried out using an error-detecting code. A class of codes commonly used for this purpose is the *cyclic redundancy check* (CRC) codes. CRC codes are (n,k) block codes—that is, codes with k data bits and n-k redundant bits—wherein the redundancy is used to only *detect* the presence of errors rather than *correct* them, as described in Section 6.2. For instance, CRC-12 is a code that adds 12 bits of redundancy to a data packet to create an n-bit codeword, where $n \leq 2047$; these 12 bits of redundancy guarantee that 12 different parity constraints are satisfied across the codeword. This code has a minimum distance of $d_{\min} = 4$, so, provided no more than three bit errors occur in the codeword, the resulting syndrome (see Section 6.2) will be nonzero, flagging a corrupted packet.

A wide variety of CRC codes are used in mobile communication standards. For example, the 3GPP cellular standard alone employs four different CRC codes—codes with three bits of redundancy, six bits of redundancy, eight bits, and fourteen bits—in its various modes.

Retransmission strategies require that the receiver informs the transmitter whether or not it has reliably received a particular packet or frame*; this is done by transmitting an "ACK" (a positive acknowledgment for an apparently uncorrupted frame) or a "NACK" (a negative acknowledgement for a corrupt frame). The transmitted frames typically include a header that contains a packet identification number; these ID numbers allow the receiver to indicate which frames have (and have not) been reliably received. Moreover, frames that have been neither ACKed nor NACKed within a specified "timeout" duration are treated as if they were negatively acknowledged.

Retransmission strategies come in at least three different flavors, corresponding to different trade-offs between complexity and efficiency.

Stop-and-Wait is the simplest retransmission strategy. It requires that a transmitter, upon sending a frame, wait until that frame is acknowledged before it sends (or resends) another. Thus, the protocol proceeds in a "ping pong" fashion with the transmitter and receiver alternately sending frames and acknowledgments (see Figure 6.18). Stop-and-Wait thus does not require a full-duplex channel—that is, it does not require simultaneous transmission in each direction—and, compared with more sophisticated approaches, it requires minimal storage and processing at both the transmitter and the receiver. However, this simplicity comes at a cost in throughput; because most channels are in fact full-duplex and Stop-and-Wait does not exploit this capability, the transmitter is sitting idle, waiting for acknowledgments, when it could be formatting and transmitting additional frames.

* In this chapter, we use the terms "packet" and "frame" interchangeably. Both terms refer to a data unit that typically includes user-supplied "payload" data as well as CRC redundancy and an identification number.

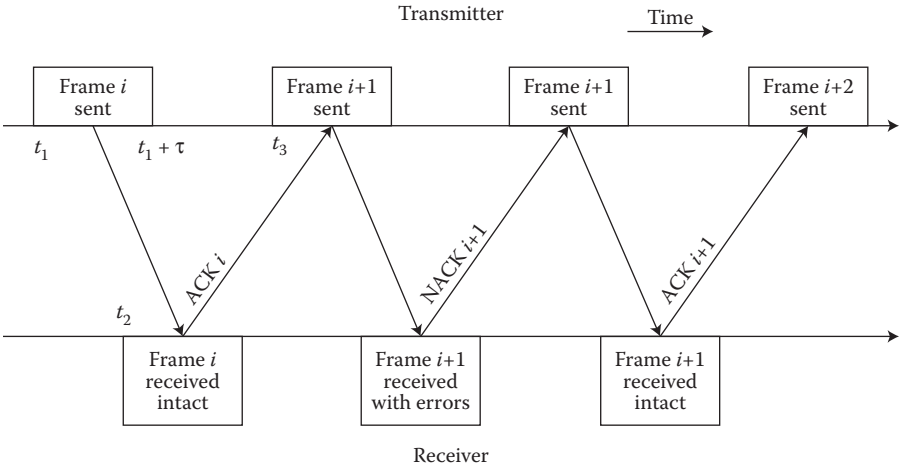

FIGURE 6.18 Timeline for a Stop-and-Wait ARQ protocol.

Go-Back-N is a retransmission strategy designed to address the inefficiency of Stop-and-Wait. In a communication link implementing the Go-Back-N strategy, the transmitter does not have to wait for a request before sending another packet. Rather, the transmitter is permitted to send all of the packets in a "window" maintained at the transmitter. When the first (earliest) packet in the window is ACKed, the transmitter "slides" the window one position, dropping the acknowledged packet and adding a new one which it then transmits; conversely, if a NAK is received for that first packet in the window, the transmitter "backs up" and resends all the packets in the window, beginning with the corrupt packet.

More specifically, suppose that the transmitter has received an ACK for Packet i. Then, under the Go-Back-N protocol, the transmitter may send Packets $i + 1$ through $i + N$ without receiving another ACK; however, the transmitter *must* receive an ACK for Packet $i + 1$ before transmitting Packet $i + N + 1$ (see Figure 6.19).

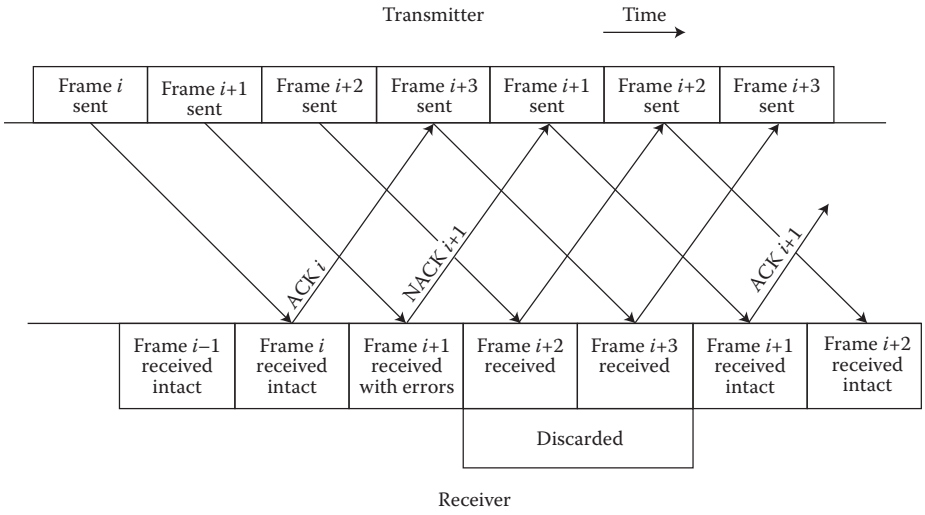

FIGURE 6.19 Timeline for a Go-Back-N ARQ protocol. This timeline assumes $N \geq 3$.

Go-Back-N is often referred to as a *sliding window* protocol because the transmitter maintains a sliding window of "active" frames—that is, up to N frames that have been transmitted but have not yet been acknowledged. It should be clear that the Stop-and-Wait strategy is simply a Go-Back-1 strategy.

Finally, the Go-Back-N protocol is clearly still not as efficient as it could be; when a frame is corrupted under the Go-Back-N protocol, all the frames that were transmitted *after* the bad frame was sent and *before* it was negatively acknowledged must be retransmitted as well—as many as $N-1$ frames in addition to the corrupt frame. These discarded frames may have, in fact, been received error-free; they are discarded only because they followed too closely on the heels of a corrupt frame.

Selective-Repeat ARQ overcomes this inefficiency. In the Select-Repeat protocol, the transmitter does *not* retransmit the contents of the entire window when an NAK is received; rather, the transmitter resends only the frame "selected" as corrupt by the receiver. Selective-Repeat is typically implemented as a sliding window protocol, just like Go-Back-N. This means that, when Frame i is ACKed, Frames $i+1$ through $i+N$ (but *not* Frame $i+N+1$) may be transmitted before Frame $i+1$ is positively acknowledged. Once Frame $i+1$ is ACKed, all the "oldest" frames in the window that have been positively acknowledged are considered complete and are shifted out of the window; the same number of new frames are shifted into the window and are transmitted.

This process is illustrated in Figure 6.20. Here, Frame i is received intact and Frame $i+1$ is corrupt; however, in the Selective-Repeat strategy, Frames $i+2$ and $i+3$—the two frames sent *after* Frame $i+1$ was sent but *before* it was negatively acknowledged—are *not* discarded at the receiver (and resent by the transmitter) but instead are accepted, assuming they are not corrupt.

Finally, it should be noted that *hybrid ARQ* (HARQ) schemes [24,25]—containing elements of both FEC and ARQ—have also found applications in mobile communication systems. Hybrid ARQ schemes employ FEC codes to make a "first attempt" to decode a frame; if that attempt is unsuccessful, then some kind of retransmission is employed. Hybrid ARQ schemes are typically classified into one of two approaches:

- In a type-I hybrid ARQ system, a conventional FEC code (of the type described in Sections 6.2–6.6) is used in each frame. If the decoder can successfully recover the frame, then it does so. If the decoder cannot successfully recover the frame—something typically ascertained by using an "outer" error detection code that checks the results of the "inner" FEC code—then the receiver requests a retransmission of that same frame.
- In a type-II hybrid system, what is retransmitted is not a copy of the same (encoded) frame that failed to decode on the first attempt, but rather *additional* redundant parity check bits for the same data. In this way, the receiver can observe a single (noisy) codeword from a longer, more powerful code spread out over two frames.

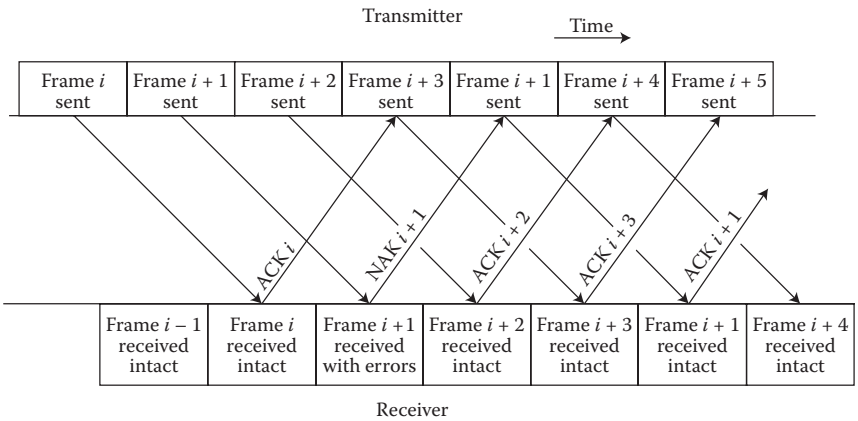

FIGURE 6.20 Timeline for a Selective-Repeat ARQ protocol.

References

1. C. E. Shannon, A mathematical theory of communication, *Bell System Technical Journal*, July–October, 1948, pp. 379–423, 623–565.
2. M. J. E. Golay, Notes on digital coding, *Proceedings of the IRE*, 37, 657, 1949.
3. R. W. Hamming, Error detecting and error correcting codes, *Bell System Technical Journal*, 29, 147–160, 1950.
4. A. Hocquenghem, Codes correcteurs d'Erreurs, *Chiffres*, 2, 147–156, 1959.
5. R. C. Bose and D. K. Ray-Chaudhuri, On a class of error correcting binary group codes, *Information and Control*, 3, 68–79, 1960.
6. I. S. Reed and G. Solomon, Polynomial codes over certain finite fields, *Journal of the Society for Industrial and Applied Mathematics*, 8, 300–304, 1960.
7. John G. Proakis, *Digital Communications*, 4th edition, McGraw-Hill, New York, NY, 2001.
8. V. Guruswami and A. Vardy, Maximum likelihood decoding of Reed-Solomon codes is NP-hard, *IEEE Transactions on Information Theory*, 51(7), 2249–2256, 2005.
9. J. Jing and K. Narayanan, Algebraic soft-decision decoding of Reed-Solomon codes using bit-level soft information, *IEEE Transactions on Information Theory*, 54(9), 3907–3928, 2008.
10. P. Elias, Coding for noisy channels, *IRE Convention Record*, 3, part 4, 37–46, 1955.
11. A. Viterbi, Error bounds for convolutional codes and an asymptotically optimum decoding algorithm, *IEEE Transactions on Information Theory*, IT-13, 260–269, 1967.
12. C. Berrou, A. Glavieux, and P. Thitimajshima, Near Shannon limit error-correcting coding and decoding: Turbo codes, *Proceedings of the 1993 International Conference on Communications*, Geneva, Switzerland, pp. 1064–1070.
13. C. Berrou and A. Glavieux, Near optimum error correcting coding and decoding: Turbo codes, *IEEE Transactions on Communications*, 44(10), 1261–1271, 1996.
14. L. Bahl, J. Cocke, F. Jelinek, and J. Raviv, Optimal decoding of linear codes for minimizing symbol error rate, *IEEE Transactions on Information Theory*, IT-20(2), 284–287, 1974.
15. S. Lin and D. J. Costello, Jr., *Error Control Coding*, 2nd edition, Pearson Prentice-Hall, Upper Saddle River, NJ, 2004.
16. T. Moon, *Error Correction Coding*, Wiley-Interscience, Hoboken, NJ, 2005.
17. Robert G. Gallager, *Low-Density Parity-Check Codes*, MIT Press, Cambridge, MA, 1963.
18. D. J. C. MacKay and R. M. Neal, Near shannon limit performance of low density parity check codes, *Electronic Letters*, 32(18), 457–458, 1996.
19. T. Richardson and R. Urbanke, *Modern Coding Theory*, Cambridge University Press, New York, NY, 2008.
20. S.-Y. Chung, G. D. Forney, T. Richardson, and R. Urbanke, On the design of low-density parity check codes within 0.0045 dB of the Shannon limit, *IEEE Communications Letters*, 5(2), 58–60, 2001.
21. G. Ungerboeck, Channel coding with multilevel/phase signals, *IEEE Transactions on Information Theory*, 28(1), 55–67, 1982.
22. E. Zehavi, 8-PSK Trellis' codes for a Rayleigh channel, *IEEE Transactions on Communications*, 40(5), 873–884, 1992.
23. G. Caire, G. Taricco, and E. Biglieri, Bit-interleaved coded modulation, *IEEE Transactions on Information Theory*, 44(3), 927–946, 1998.
24. S. Lin, D. Costello, Jr., and M. Miller, Automatic repeat request error control schemes, *IEEE Communications Magazine*, December, 5–16, 1984.
25. L. Rasmussen and S. Wicker, The performance of type-I Trellis coded hybrid-ARQ protocols over AWGN and slowly fading channels, *IEEE Transactions on Information Theory*, March, 418–428, 1994.

7

Information Theory

Emmanuel Abbe

Bixio Rimoldi

Rüdiger Urbanke

7.1 Introduction

The field of information theory has its origin in Claude Shannon's 1948 paper, "A Mathematical Theory of Communication." Shannon's motivation was to study "[The problem] of reproducing at one point either exactly or approximately a message selected at another point." In this chapter, we will be concerned only with Shannon's original problem. One should keep in mind that information theory is a growing field of research whose profound impact has reached various areas such as statistical physics, computer science, statistical inference, and probability theory. For an excellent treatment of information theory that extends beyond the area of communication, we recommend Cover and Thomas (1991). For the reader who is strictly interested in communication problems, we also recommend Gallager (1968), Blahut (1987), and McEliece (1977).

7.2 The Communication Problem

A rather general diagram for a (point-to-point) communication system is shown in Figure 7.1.

The source might be digital (e.g., a data file) or analog (e.g., a video signal). Since an analog source can be sampled without loss of information and without loss of generality, we consider only discrete-time sources and model them as discrete-time stochastic processes.

The channel could be a pair of wires, an optical fiber, a radio link, and so on. The channel model specifies the set of possible channel inputs and, for each input, specifies the output process. Most real-world channels are waveform channels, meaning that the input and output sets are sets of waveforms. It is often the case that the communication engineer is given a waveform channel with a modulator and a demodulator. In a satellite communication system, the modulator might be a phase-shift keying modulator whose input alphabet $\mathcal{V}$ is the set {0, 1}; the channel might be modeled by the additive white Gaussian noise channel, and the demodulator attempts to output a guess (perhaps incorrect) of the

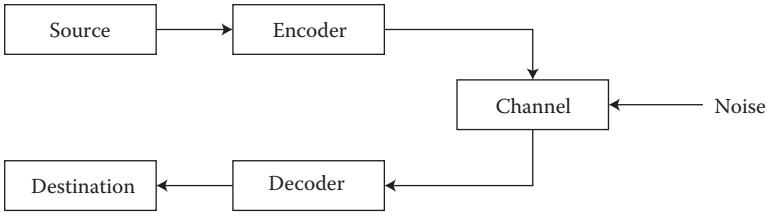

FIGURE 7.1 Block diagram of a communication system.

modulator input. In this case, the modulator output alphabet $\mathcal{W}$ equals $\mathcal{V}$. In more sophisticated cases, where $|\mathcal{W}| > |\mathcal{V}|$ and $|\cdot|$ denotes the number of elements in the enclosed set, the digital data demodulator can also furnish information about the reliability of the decision. Either way, one would consider the modulator and the demodulator as part of the channel. If the statistics of the channel output at a given time depend only on the value of the corresponding position of the input sequence, the channel is a discrete memoryless channel (DMC). This is an important class of channel models that will receive particular attention in this chapter. Even if the modulator and the demodulator are not given, assuming that the bandwidth of the waveform channel is limited, one can always use the sampling theorem to convert a waveform channel into a channel with discrete-time input and output.

The destination is merely a place holder to remind us that the user has some expectation concerning the quality of the reproduced signal. If the source output symbols are elements of a finite set, the destination may specify a maximum value for the probability of error. Otherwise, it may specify a maximum distortion computed according to some specified criterion (e.g., mean square error).

It is generally assumed that the source, the channel, and the destination are given and fixed. On the other hand, the communication engineer usually is completely free to design the encoder and the decoder to meet the desired performance specifications.

An important result of information theory is that, without loss of optimality, the encoder in Figure 7.1 can be decomposed into two parts: a source encoder that produces a sequence of binary data and a channel encoder, as shown in Figure 7.2. Similarly, the decoder may be split into a channel decoder and a source decoder.

The objective of the source encoder is to compress the source, that is, to minimize the average number of bits necessary to represent a source symbol. The most important questions concerning the source encoder are the following: What is the minimum number of bits required (on average) to represent a source output symbol? How do we design a source encoder that achieves this minimum? These questions will be considered here. It turns out that the output of an ideal source encoder is a sequence of independent and uniformly distributed binary symbols. The purpose of the channel encoder/decoder pair is to create a reliable bit pipe for the binary sequence produced by the source encoder. Here, the most important question is whether or not it is possible to design such an encoder/decoder pair. This question will also be considered in some detail. The fact that we can split the encoder into two parts as described is important. First, it allows us to study the source and the channel separately and to assume that they are connected by a binary interface. Second, it tells us that for a given channel, we may design

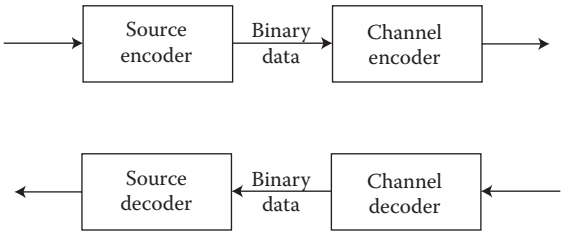

FIGURE 7.2 Block diagram of an encoder and a decoder, each split into two parts.

the channel encoder and the channel decoder to maximize the rate of the resulting (virtually error-free) bit pipe without having to know the nature of the source that will use it.

7.3 Source Coding for Discrete-Alphabet Sources

We start by considering the simplest possible source, namely, a discrete-time discrete-alphabet memoryless information source modeled by a random variable X taking values on a finite alphabet χ. A (binary source) *code* C for X is a mapping from χ into the set of finite length binary sequences called codewords. Such a code can be represented by a binary tree, as shown in the following example.

Example 7.1

Let X take on values in {1, 2, 3, 4, 5, 6, 7}. A possible binary code for X is given by the (ordered) set of binary sequences {1, 010, 011, 0000, 0001, 0010, 0011}. The corresponding tree is shown in Figure 7.3. Note that the codeword corresponding to a given source output symbol is the label sequence from the root to the node corresponding to that symbol.

In Example 7.1, source output symbols correspond to leaves in the tree. Such a code is called *prefix free* since no codeword is the prefix of another codeword. Given a concatenation of codewords of a prefix-free code, we can parse it in a unique way into codewords. Codes with this property are called *uniquely decodable*. Although there are uniquely decodable codes which are *not* prefix free, we will restrict our attention to prefix-free codes, as it can be shown that the performance of general uniquely decodable codes is no better than that of prefix-free codes (see Cover and Thomas (1991)).

For each i in χ, let $C(i)$ be the codeword associated with the symbol i, let l_i be its length, $L \equiv \max_i l_i$, and let p_i be the probability that $X = i$. A complete binary tree of depth L has 2^L leaves. To each leaf at depth l, $l \le L$, of the binary code tree (which is not necessarily complete), there corresponds 2^{L-l} leaves at depth L of the corresponding complete tree (obtained by extending the binary code tree). Further, any two distinct leaves in the code tree have distinct associated leaves at depth L in the complete binary tree. Hence, summing up over all leaves of the code tree (all codewords), we get

$$2^L \ge \sum_i 2^{L-l_i} \Leftrightarrow \sum_i 2^{-l_i} \le 1$$

The right-hand side is called the *Kraft inequality* and is a necessary condition on the codeword lengths of any prefix-free code. Conversely, for any set of codeword lengths satisfying the displayed inequality, we can construct a prefix-free code having codeword lengths l_i (start with a complete binary tree of sufficient length; to each l_i associate a node in this tree at level l_i and make this node a leaf by deleting all of its descendants). The problem of finding the best source code

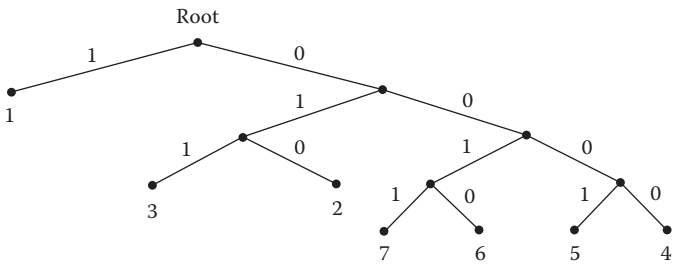

FIGURE 7.3 Example of a code tree.

then reduces to that of finding a set of lengths that satisfies the Kraft inequality and minimizes the average codeword lengths $L^* = \sum_i l_i p_i$. Such a code is called *optimal*.

To any source X with probabilities p_i, we associate the quantity $H(X)$, which we call *entropy* and which is defined as

$$H(X) = -\sum_i p_i \log p_i$$

Usually, we take the base of the logarithm to be 2, in which case the units of entropy are called *bits*.

It is straightforward to show by means of Lagrange multipliers that if we neglect the integer constraint on l_i, the minimization of L^* subject to the Kraft inequality yields $l_i^* = \lceil -\log p_i \rceil$. This noninteger choice of codeword lengths yields

$$L^* = \sum_i p_i l_i^* = -\sum_i p_i \log p_i = H(X)$$

On the other hand, the (not necessarily optimal) integer choice $l_i^* = \lceil -\log p_i \rceil$ satisfies the Kraft inequality and yields an expected codeword length

$$L(C) = \sum_i p_i \lceil -\log p_i \rceil \le -\sum_i p_i \log p_i + \sum_i p_i = H(X) + 1$$

Hence, we have the following theorem.

Theorem 7.1

The average length L^* of the optimal prefix-free code for the random variable X satisfies $H(X) \le L^* \le H(X) + 1$.

Example 7.2

Let X be a random variable that takes on the values 1 and 0 with probabilities θ ($0 \le \theta \le 1$) and $1 - \theta$, respectively. Then, $H(X) = h(\theta)$, where $h(\theta) = -\theta \log \theta - (1 - \theta) \log (1 - \theta)$. The function $h(\theta)$ is called the *binary entropy function*. In particular, it can be shown that $h(\theta) \le 1$ with equality if and only if $q = (1/2)$. More generally, if X takes on $|\chi|$ values, $H(X) \le \log |\chi|$ with equality if and only if X is uniformly distributed.

A simple algorithm that generates optimal prefix-free codes is the Huffman algorithm, which can be described as follows:

Step 1. Reindex to arrange the probabilities in decreasing order, $p_1 \ge p_2 \ge \cdots \ge p_m$.

Step 2. Form a subtree by combining the last two probabilities p_{m-1} and p_m into a single node of weight $p'_m = p_{m-1} + p_m$.

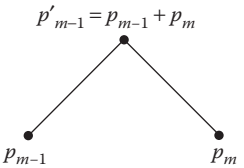

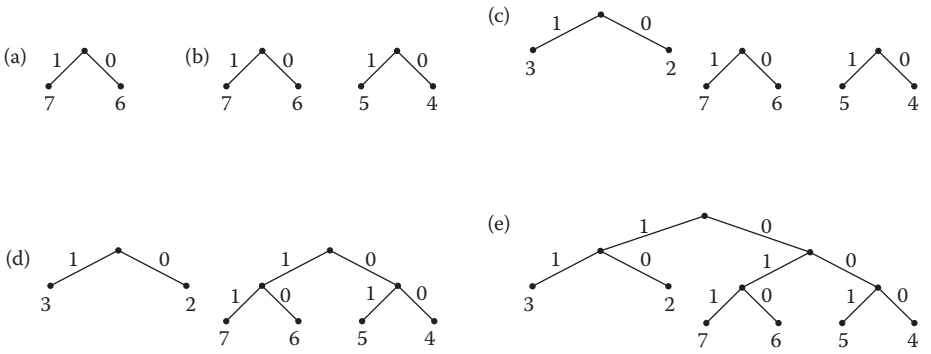

FIGURE 7.4 (a)–(e) Corresponds to the steps in the construction of a Huffman code for X as explained in Example 7.3.

Step 3. Recursively execute steps 1 and 2, decreasing the number of nodes each time, until a single node is obtained.

Stpe 4. Use the tree constructed above to assign codewords.

Example 7.3

As in Example 7.1, let X take on the values {1, 2, 3, 4, 5, 6, 7}. Assume their corresponding probabilities are {0.4, 0.1, 0.1, 0.1, 0.1, 0.1, 0.1}. Figure 7.4 shows the steps in the construction of the *Huffman code*. For simplicity, probabilities are not shown. The final tree is given in Example 7.1.

Given a block of n random variables $X_1, \ldots, X_n$, with joint distribution $p(X_1, \ldots, X_n)$, their entropy as

$$H(X_1, \ldots, X_n) = -\sum_{x_1} \sum_{x_2} \cdots \sum_{x_n} p(x_1, \ldots, x_n) \log p(x_1, \ldots, x_n)$$

Note that for the special case of n independent random variables, we have $H(X_1, \ldots, X_n) = nH(X)$. This agrees with the intuitive notion that if it takes $H(X)$ bits to encode one source output symbol, it should take $nH(X)$ bits to encode n independent output symbols. For a sequence of random variables $X_1, X_2, \ldots, X_n$, we define $H_n = (1/n)H(X_1, \ldots, X_n)$. If $X_1, X_2, \ldots, X_n$ is a stationary random process, as n goes to infinity, H_n converges to a limit H_∞ called the *entropy rate* of the process.

Applying Theorem 7.1 to blocks of random variables, we obtain

$$H_n \leq \frac{L^*}{n} < H_n + \frac{1}{n}$$

In the special case that the process $X_1, X_2, \ldots, X_n$ is stationary, the left and the right side will both tend to H_∞ as $n \to \infty$. This shows that by encoding a sufficiently large number of source output symbols at a time, one can get arbitrarily close to the fundamental limit of H_∞ bits per symbol.

7.4 Universal Source Coding

The Huffman algorithm produces optimal codes, but it requires knowing the statistics of the source. It is a surprising fact that there are source coding algorithms that are asymptotically optimal without requiring prior knowledge of the source statistics. Such algorithms are called *universal* source coding

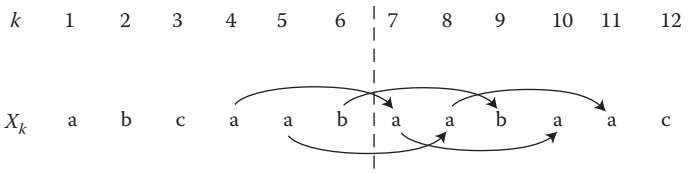

FIGURE 7.5 Encoding procedure of the Lempel–Ziv algorithm.

algorithms. The best-known universal source coding algorithm is the *Lempel–Ziv* algorithm, which has been implemented in various forms on computers (as PKZIP command for Windows- and Linux-based systems). There are two versions of the Lempel–Ziv algorithm: the LZ77, see Ziv and Lempel (1977), and the LZ78, see Ziv and Lempel (1978). We will describe the basic idea of the LZ77.

Consider the sequence $X_1, X_2, \ldots, X_k$ taking values in $\{a, b, c\}$, shown in Figure 7.5, and assume that the first w letters ($w = 6$ in our example) are passed to the decoder with no attempt at compression. At this point the encoder identifies the longest string $X_{w+1}, X_{w+2}, \ldots, X_{w+L}$ such that a copy, $X_{w-p+1}, \ldots, X_{w-p+L}$, begins (but not necessarily ends) in the portion of data already available to the decoder. In our example, this string is *aabaa*, $L = 5$, and $p = 3$; see Figure 7.5. Next, the encoder transmits a binary representation of the pair (L, p) as this is sufficient for the decoder to reconstruct $X_{w+1}, \ldots, X_{w+L}$. At this point, the procedure can be repeated with w replaced by $w + L$. There are two exceptions: the first occurs when X_{w+l} is a new letter that does not appear in $X_1, \ldots, X_w$; the second exception occurs when it is more efficient to encode $X_{w+1}, \ldots, X_{w+L}$ directly than to encode (L, p). In order to handle such special cases, the algorithm has the option of encoding a substring directly, without attempt at compression. It is surprising that the Lempel–Ziv algorithm is asymptotically optimal for all finite alphabet stationary ergodic sources. This has been shown in Wyner and Ziv (1994).

7.5 Rate Distortion Theory

So far we have assumed that X is a discrete alphabet and that the decoder must be able to perfectly reconstruct the source output. Now we drop both assumptions.

Let $X_1, X_2, \ldots$ be a sequence of independent identically distributed random variables. Let χ denote the source alphabet and Υ be a suitably chosen representation alphabet (where Υ is not necessarily equal to χ). A *distortion measure* is a function $d: \chi \times \Upsilon \to \mathrm{R}^+$. The most common distortion measures are the *Hamming distortion* d_H and the *squared error* distortion d_E defined as follows:

$$d_H(x, y) = \begin{cases} 0 & \text{if } x = y \\ 1 & \text{if } x \neq y \end{cases}$$
$$d_E(x, y) = (x - y)^2$$

Such a single-letter distortion measure can be extended to a distortion measure on n-tuples by defining

$$d(x^n, y^n) = \frac{1}{n} \sum_{i=1}^{n} d(x_i, y_i)$$

The *encoder* maps an n-length source output X^n to an index $U \in \{1, 2, \ldots, 2^{\lfloor nR \rfloor}\}$, where R denotes the number of bits per source symbol that we are allowed or willing to use. The *decoder* maps U into an n-tuple Y^n, called the representation of X^n. We will call U together with the associated encoding and decoding function a *rate distortion code*. Let f be the function that maps X^n to its representation Y^n, that

is, f is the mapping describing the concatenation of the encoding and the decoding function. The expected distortion D is then given by

$$D = \sum_{x^n} p(x^n) d(x^n, f(x^n))$$

The objective is to minimize the average number of bits per symbol, denoted by R, for a given average distortion D. What is the minimum R?

Definition 7.1

The rate distortion pair (R, D) is said to be *achievable* if there exists a rate distortion code of rate R with expected distortion D. The *rate distortion function* $R(D)$ is the infimum of rates R such that (R, D) is achievable for a given D.

Entropy played a key role in describing the limits of lossless coding. When distortion is allowed, a similar role is played by a quantity called mutual information.

Definition 7.2

Given the random variables X and Y with their respective distributions $p(x)$, $p(y)$, and $p(x, y)$, the *mutual information* $I(X; Y)$ between X and Y is defined as

$$I(X;Y) = \sum_{x \in X} \sum_{y \in Y} p(x,y) \log \frac{p(x,y)}{p(x)p(y)}$$

This definition can be extended to blocks of random variables X^n and Y^n by replacing $p(x)$, $p(y)$, and $p(x, y)$ with their higher-dimensional counterparts. We can now state the fundamental theorem of rate distortion theory. For its proof, see Cover and Thomas (1991).

Theorem 7.2

The rate distortion function for an independent identically distributed source X with distribution p(x) and distortion function d(x, y) is

$$R(D) = \min_{p(y|x): \sum_{x,y} p(x)p(y|x)d(x,y) \le D} I(X;Y)$$

The rate distortion functions for a *binary source* that outputs 1 with probability θ and Hamming distortion and for a *Gaussian source* of variance σ^2 and squared error distortion are as follows:

$$R_B(D) = \begin{cases} h(\theta) - h(D), & 0 \le D \le \min\{\theta, 1-\theta\} \\ 0, & D > \min\{\theta, 1-\theta\} \end{cases}$$

$$R_G(D) = \begin{cases} \frac{1}{2} \log \frac{\sigma^2}{D}, & 0 \le D \le \sigma^2 \\ 0, & D > \sigma^2 \end{cases}$$

These two functions are plotted in Figure 7.6.

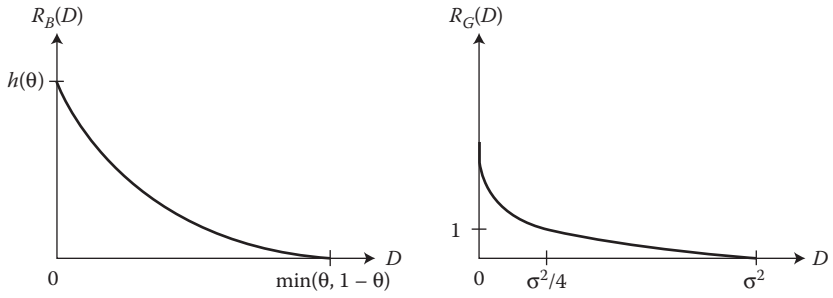

FIGURE 7.6 Examples of rate distortion functions.

Some insight can be gained by considering the extreme values of both $R_B(D)$ and $R_G(D)$. Assume that $X_1, X_2, \ldots$ is a sequence of independent and identically distributed binary random variables and let θ be the probability that $X_i = 1$. Without loss of generality, we may assume that $\theta \geq 1 - \theta$. If we let $Y^n = (0,\ldots,0)$ regardless of X^n, the expected Hamming distortion equals θ. Hence, it must be true that $R_B(D) = 0$ for $D \geq \theta$. On the other hand, $D = 0$ means that the reproduction Y_n must be a perfect copy of X^n. From Theorem 7.1 and Example 7.2 we know that this means $R_B(0) = H(X) = h(q)$. Similar considerations hold for $R_G(D)$. It is interesting to observe that $R_G(D)$ tells us that if we are allowed to use R bits per symbol to describe a sequence of independent Gaussian random variables with variance σ^2, then we need to accept a mean squared error of $\sigma^2 2^{-2R}$.

7.6 Channel Coding

Now, we consider the fundamental limit for the amount of information that can be transmitted through a noisy channel and discuss practical methods to approach it. For simplicity, we assume that the channel can be modeled as a DMC, defined as follows:

A DMC is a system consisting of an input alphabet χ, an output alphabet Υ, and a collection of probability mass functions $p(y|x)$, one for each $x \in \chi$. A specific DMC will be denoted by $(\chi, p(y|x), \Upsilon)$.

An (M, n) channel code for the DMC $(X, p(y|x), Y)$ consists of the following:

1. An index set $\{1, 2, \ldots, M\}$
2. An encoding function X^n: $\{1, 2, \ldots, M\} \rightarrow X^n$, yielding codewords $X^n(1), X^n(2),\ldots, X^n(M)$ (the set of codewords is called the *code book*)
3. A decoding function g: $Y^n \rightarrow \{1,2, \ldots, M\}$, which is a deterministic rule that assigns a guess to each possible received vector.

The most important figures of merit for a channel code for a DMC are the *maximal probability of error*, defined by

$$\lambda^{(n)} \equiv \max_{i \in \{1,2,\ldots,M\}} pr\{g(Y^n) \neq i | X^n = X^n(i)\}$$

and the *transmission rate*

$$R = \frac{\log M}{n} \text{ bits/channel use}$$

It makes sense to define the rate in this way since the M codewords can be labeled with $\log M$ bits. Hence, each time we transmit a codeword, we actually transmit $\log M$ bits of information. Since it takes

n uses of the channel to transmit one codeword, the resulting information rate is $(\log M)/n$ bits per channel use.

For a given DMC, a rate R is said to be *achievable* if, for any desired probability of error P_e and sufficiently large block length n, there exists a $\left(\lceil 2^{nR} \rceil, n\right)$ code for that DMC with maximal probability of error $\lambda^{(n)} \leq P_e$.

The *operational capacity* of a DMC is the supremum of all achievable rates. One would expect that determining the operational capacity would be a formidable task. One of the most remarkable results of information theory is a relatively easy-to-compute way to determine the operational capacity.

We define the *information channel capacity* of a DMC $(\chi, p(y|x), \Upsilon)$ as

$$C \equiv \max_{p(x)} I(X;Y)$$

where the maximum is taken over all possible input distributions $p(x)$. As we will show in the next example, it is straightforward to compute the information channel capacity for many DMCs of interest. Shannon's channel coding theorem establishes that the information channel capacity equals the operational channel capacity.

7.6.1 Theorem (Shannon's Channel Coding Theorem)

For a DMC, the *information* channel capacity equals the operational channel capacity, that is, for every rate $R < C$, there exists a sequence of $\left(\lceil 2^{nR} \rceil, n\right)$ codes for the DMC with maximum probability of error $\lambda^{(n)} \to 0$. Conversely, for any sequence of $\left(\lceil 2^{nR} \rceil, n\right)$ for codes, this DMC with the property that $\lambda^{(n)} \to 0$, the rate R must satisfy $R \leq C$.

This is perhaps the most important result of information theory. In order to shed some light on the interpretation of mutual information and to provide an efficient way to determine C, it is convenient to rewrite $I(X; Y)$ in terms of conditional entropy. Given two random variables X and Y with joint probability mass function $p(x, y)$, marginal probability mass function $p(x) = \sum_y p(x, y)$, and conditional probability mass function $p(x|y) = p(x, y)/p(y)$, we define the conditional entropy of X given that $Y = y$ as

$$H(X|Y = y) = -\sum_x p(x|y) \log p(x|y)$$

Its average is the conditional entropy of X given Y, denoted by $H(X|Y)$ and defined as

$$\begin{aligned} H(X|Y) &= \sum_y p(y) H(X|Y = y) = -\sum_{x,y} p(x, y) \log p(x|y) \\ &= E[-\log p(X|Y)] \end{aligned}$$

Recall that for the discrete variable X with probability mass function $p(x)$, $H(X)$ is the average number of binary symbols necessary to describe X. Now, let X be the random variable at the input of a DMC and let Y be the output. The knowledge that $Y = y$ changes the probability mass function of the channel input from $p(x)$ to $p(x|y)$ and its entropy from $H(X)$ to $H(X|Y = y)$. According to our previous result, $H(X|Y = y)$ is the average number of bits necessary to describe X after the observation that $Y = y$. Since $H(X)$ is the average number of bits needed to describe X (without knowledge of Y), $H(X) - H(X|Y = y)$ is the average amount of information about X acquired by the observation that $Y = y$, and

$$H(X) - H(X|Y)$$

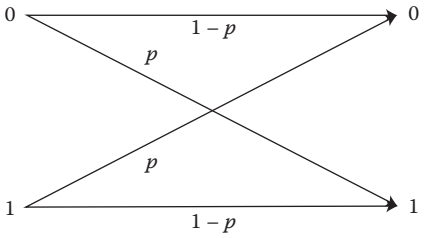

FIGURE 7.7 Discrete memoryless channel with crossover probability p.

is the average amount of information about X acquired by the observation of Y. One can easily verify that the latter expression is another way to write $I(X; Y)$. Moreover,

$$I(X;Y) = H(X) - H(X|Y) = H(Y) - H(Y|X) = I(Y;X)$$

Hence, the amount of information that Y gives about X is the same as the amount of information that X gives about Y. For this reason, $I(X; Y)$ is called the mutual information between X and Y.

7.6.2 Example (Binary Symmetric Channel)

Let $X = \{0, 1\}$, $Y = \{0, 1\}$, and $p(y|x) = p$ when $x \neq y$ and $1 - p$ otherwise. This DMC can be conveniently depicted as in Figure 7.7. For obvious reasons it is called the *binary symmetric channel* (BSC).

For the BSC, we bound the mutual information by

$$\begin{aligned} I(X;Y) &= H(Y) - H(Y|X) = H(Y) - \sum_x p(x)H(Y|X = x) \\ &= H(Y) - h(p) \leq 1 - h(p) \end{aligned}$$

where the last inequality follows because Y is a binary random variable (see Example 7.2). Equality is achieved when the input distribution is uniform since in this case the output distribution is also uniform. Hence, the information capacity of a BSC with parameter p is

$$C = 1 - h(p) \text{ [bits/channel use]}$$

This function is plotted in Figure 7.8.

7.7 Simple Binary Codes

Shannon's channel coding theorem promises the existence of block codes that allow us to transmit reliably through an unreliable channel at any rate below the channel capacity. Unfortunately, the codes constructed in all known proofs of this fundamental result are impractical in that they do not exhibit any structure which can be employed for an efficient implementation of the encoder and the decoder. This is an important issue, as good codes must have long block lengths and, hence, a large number of codewords. For these codes, simple table lookup encoding and decoding procedures are not feasible. The search for good and practical codes has led to the development of coding theory. Although powerful block codes are, in general, described by sophisticated techniques, the main idea is simple. We collect a

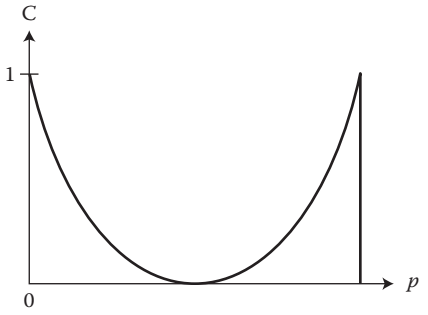

FIGURE 7.8 Capacity of the BSC as a function of p.

number k of information symbols which we wish to transmit, we append r check symbols, and transmit the entire block of $n = k + r$ channel symbols. Assuming that the channel changes a sufficiently small number of symbols within an n-length block, the r check symbols may provide the receiver with sufficient information to detect and/or correct the errors.

Traditionally, good codes have been constructed by sophisticated algebraic schemes. More recent code construction techniques are inspired by Shannon's original work. The idea is to construct the code by making random choices on a suitably defined structure. A key property of the structure is that it leads to codes that may be decoded using powerful iterative techniques. We will demonstrate these two quite distinct concepts by simple examples.

7.7.1 Hamming Codes

For any positive integer m, there is a Hamming code with parameters $k = 2^m - m - 1$ and $n = 2^m - 1$. To illustrate, we consider the k, $n = 7$ Hamming code. All operations will be done modulo 2. Consider the set of all nonzero binary vectors of length $m = 3$. Arrange them in columns to form the matrix

$$H = \begin{pmatrix} 1 & 0 & 1 & 0 & 1 & 0 & 1 \\ 0 & 1 & 1 & 0 & 0 & 1 & 1 \\ 0 & 0 & 0 & 1 & 1 & 1 & 1 \end{pmatrix}$$

The row space of H is a vector space of binary 7-tuples of dimension $m = 3$. The $k = 4$, $n = 7$ Hamming code is the null space of H, that is, the vector space of dimension $n - m = 4$ consisting of all binary 7-tuples c such that $cH^T = 0$. Hence, it contains the $M = 2^k = 16$ codewords shown in Table 7.1 and its rate is $R = (\log M)/n = 4/7$. If c is transmitted and u is received, the error is the unique binary n-tuple e such that $u = c + e$, where addition is component-wise modulo 2. The decoder performs the operation

$$uH^T = (c + e)H^T = cH^T + eH^T = eH^T$$

If there is a single error at position i, that is, if e is zero except for the ith component (which is one), uH^T is the ith row of H^T. This tells us the error location. If e contains 2 ones (channel errors), uH^T is the sum of two rows of H^T. Since this cannot be zero, two channel errors are detectable. They are not correctable, however, since, as one can easily verify when two channel errors occur, there is always a codeword that agrees with the received word in $n - 1$ positions. This is the codeword that would be selected by the decoder if it were forced to make a decision since the transmitted codeword agrees with the

TABLE 7.1 Codewords of the (7, 4) Hamming Code

0	0	0	0	0	0	0		1	0	0	0	1	0	1
0	0	0	1	0	1	1		1	0	0	1	1	1	0
0	0	1	0	1	1	0		1	0	1	0	0	1	1
0	0	1	1	1	0	1		1	0	1	1	0	0	0
0	1	0	0	1	1	1		1	1	0	0	0	1	0
0	1	0	1	1	0	0		1	1	0	1	0	0	1
0	1	1	0	0	0	1		1	1	1	0	1	0	0
0	1	1	1	0	1	0		1	1	1	1	1	1	1

received word in only $n-2$ positions. A simple encoding procedure can be specified as follows: let G be a $k \times n$ matrix whose rows span the null space of H. Such a matrix is

$$G = \begin{pmatrix} 1 & 0 & 0 & 0 & 1 & 1 & 0 \\ 0 & 1 & 0 & 0 & 1 & 0 & 1 \\ 0 & 0 & 1 & 0 & 0 & 1 & 1 \\ 0 & 0 & 0 & 1 & 1 & 1 & 1 \end{pmatrix}$$

Then an information k-tuple a can be mapped into a codeword $c = aG$ by a simple matrix multiplication.

7.7.2 Low-Density Parity-Check Codes

Low-density parity-check (LDPC) codes constitute a family of a new breed of coding techniques variably described as "codes on graphs" or "iterative coding techniques." They were originally introduced by Gallager in his thesis in 1962 (see Gallager (1963)), then long forgotten, and later revived in the wake of the discovery of turbo codes by Berrou et al. (see Berrou et al. 1993, MacKay 1999).

LDPC codes are codes which possess a sparse parity-check matrix. Because of this sparseness, they can be decoded very efficiently in an iterative manner. Although this iterative decoding procedure is, in general, suboptimal, it is sufficiently strong to allow transmission seemingly arbitrarily close to channel capacity.

Example 7.4

Consider the code represented by the following parity-check matrix:

$$H = \begin{pmatrix} 1 & 1 & 1 & 0 & 1 & 1 & 1 & 0 & 0 & 0 \\ 0 & 0 & 1 & 1 & 1 & 1 & 1 & 1 & 0 & 0 \\ 0 & 1 & 1 & 0 & 1 & 0 & 0 & 1 & 1 & 1 \\ 1 & 0 & 0 & 1 & 0 & 1 & 0 & 1 & 1 & 1 \\ 1 & 1 & 0 & 1 & 0 & 0 & 1 & 0 & 1 & 1 \end{pmatrix}$$

Note that each row contains exactly 6 ones and that each column contains exactly 3 ones. Such a code is referred to as a (3, 6)-regular LDPC code. A convenient graphical representation of this code is given by means of the bipartite graph shown in Figure 7.9a. This graph is usually referred to as Tanner graph. In this graph, each left node (variable node) corresponds to one column of the parity-check matrix and each right node (check node) corresponds to one row

of H. A left node is connected to a right node if and only if the corresponding position in the parity-check matrix contains a 1.

Let $(x = x_0, \ldots, x_9)$ be the codeword (0101001010). Assume that we transmit x over a binary erasure channel (BEC) and that the received word is $y = (??01001?10)$ where ? indicates an erasure. Rather than employing a maximum likelihood decoder, we will use the iterative decoding algorithm described in Figures 7.9a–e. The received word y is written on the left (y_0 on the bottom and y_a on the top). We start by passing all known values from the left to the right along the corresponding edges. We next accumulate at each check the partial sum (mod 2) of all known values and delete all edges along which messages have already been passed. The result is shown in Figure 7.9b, where a black box indicates a partial sum equal to 1. Now note that check node one (the second from the bottom) has received already all values except for the one from the erased bit seven. Since, by the code constraints, the sum of all values must be equal to zero, we see that we can deduce the value of variable node seven to be equal to zero. This value can now again be propagated to the right and all involved edges be deleted. The result is shown in Figure 7.9d. After one more iteration all erased values are known (Figure 7.9e).

As we can see, in the above example the given iterative decoding strategy successfully recovered the erased bits. This might seem like a lucky coincidence. Nevertheless, it has been shown that long and suitably defined LDPC codes can achieve capacity on the BEC under iterative decoding (see Luby et al. 1997).

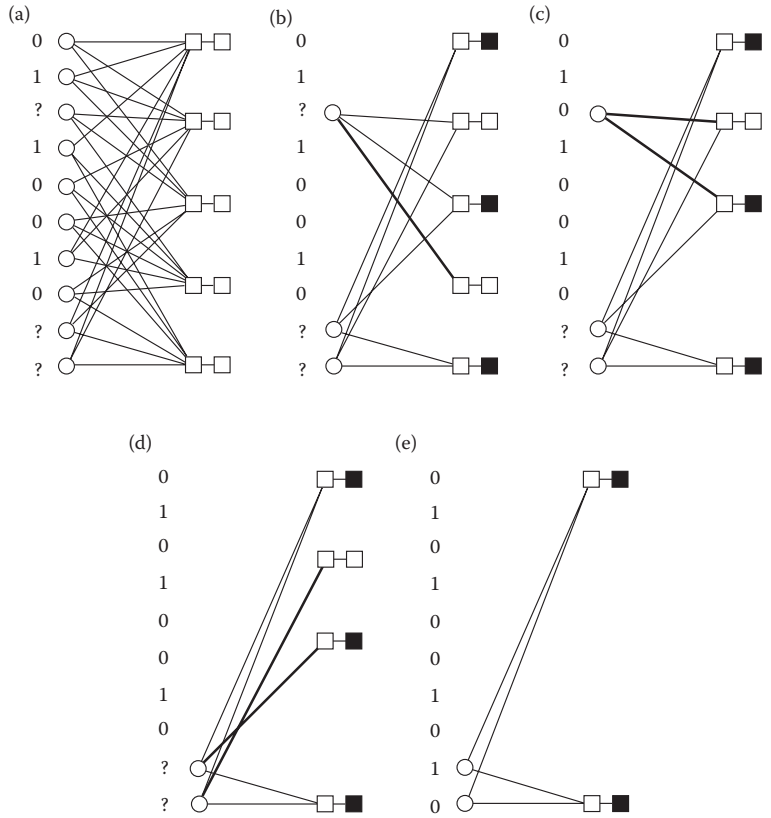

FIGURE 7.9 (a)–(e) Shows the iterations of the decoding algorithm for the code in Example 7.4 and transmission over a BEC.

Even more, the above iterative decoding strategy, suitably extended, can be used to transmit reliably close to capacity over a wide array of channels (see Richardson et al. 2001).

7.7.3 Polar Codes

Invented in 2008 by Erdal Arikan (see Arikan 2009), polar codes constitute a new family of linear codes. The original construction of polar codes relies on a different intuition than the construction of LDPC codes. Rather than focusing on the parity-check matrix, a probabilistic phenomenon called "channel polarization" is used to guide the code construction. We next explain this phenomenon in the source setting, which is also called the "source polarization."

Let X_1 and X_2 be two i.i.d. Bernoulli(p) random variables, that is, binary random variables which take value 1 with probability p. The total entropy of (X_1, X_2) is $2h(p)$. Consider now taking a linear transformation of (X_1, X_2) over the binary field, to obtain

$$(Y_1, Y_2) = (X_1, X_2)\begin{pmatrix} 1 & 0 \\ 1 & 1 \end{pmatrix}.$$

This transformation is illustrated in Figure 7.10a. Since the matrix above is invertible, the total entropy of (Y_1, Y_2) equals that of (X_1, X_2), namely $2h(p)$. However, the entropy of (Y_1, Y_2) is now given by $H(Y_1) + H(Y_2|Y_1)$, since Y_1 and Y_2 are not independent (this is the chain rule formula).

Hence, $2h(p) = H(Y_1) + H(Y_2|Y_1)$. Note that $H(Y_1) \geq h(p)$, since Y_1 is obtained by processing X_1, which has entropy $h(p)$. As a consequence, $H(Y_2|Y_1) \leq h(p)$. This means that Y_1 is now more entropic than X_1, and if Y_1 is observed, Y_2 is less entropic than X_2 (in average over the distribution of Y_1). In other words, out of two equally random variables, we have created one random variable which has more entropy and one random variable which has less entropy upon observing the other variable. The idea behind polarization is to then repeatedly iterate this procedure to create events which become eventually all very entropic or very deterministic. The iterated scheme is illustrated in Figure 7.10b.

Mathematically, if n is a power of two, X^n is an i.i.d. Bernoulli(p) sequence, and if Y^n is given by $Y^n = X^n G_n$, where

$$G_n = \begin{pmatrix} 1 & 0 \\ 1 & 1 \end{pmatrix}^{\otimes \log_2(n)},$$

and where $\otimes$ denotes the Kronecker product, the chain rule yields $nh(p) = H(X^n) = \sum_{i=1}^{n} H(Y_i|Y^{i-1})$ and most of the terms $H(Y_i|Y^{i-1})$ become close to either 0 or 1. Formally, the result is stated as follows.

Theorem 7.3

For any $\varepsilon > 0$, $|\{i = 1, \ldots, n: \varepsilon \leq H(Y_i|Y^{i-1}) \leq 1 - \varepsilon\}| = o(n)$.

Figure 7.11 illustrates this result for a fixed dimension, showing that the conditional entropies concentrate around 0 and 1 except for a small fraction of indices.

This result suggests a simple source compression scheme: store only the components with high conditional entropy. Therefore, only about $nh(p)$ components need to be stored, reaching the lowest possible compression rate prescribed by Shannon. One more argument is needed to establish such a result rigorously. Since the decoding is done sequentially in the components, one needs to ensure that the

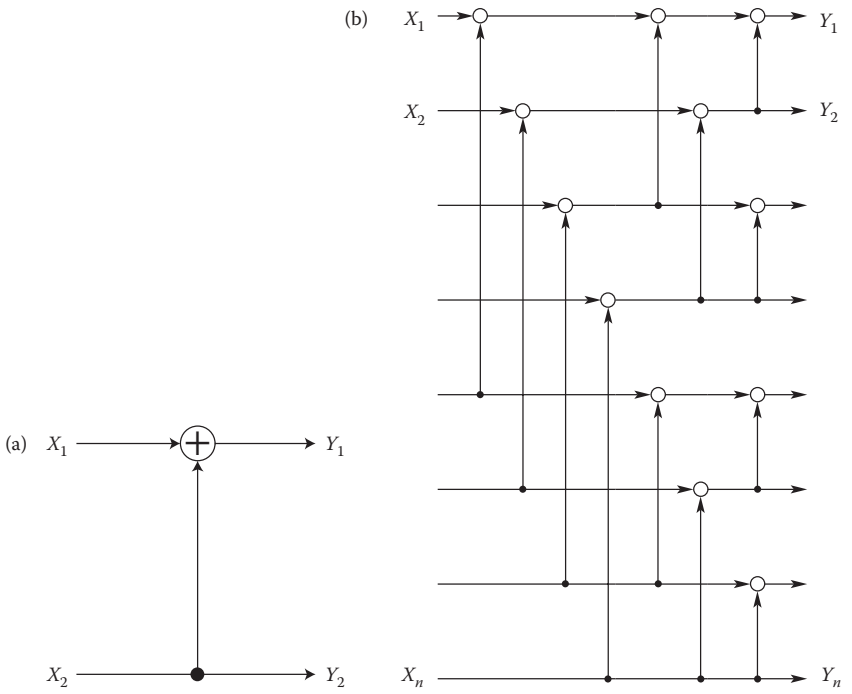

FIGURE 7.10 (a) Circuit for G_2. (b) Circuit for G_n.

probability of error in decoding a component is small compared to n (to prevent error propagation). It turns out that this is loosely achieved, as the error probability can be shown to be roughly exponential in the square root of n (see Arikan and Telatar 2009). Finally, one of the key properties of this compression scheme is that the decoding complexity is only $O(n\log(n))$. This follows from the Kronecker structure of G_n, which allows the use of a divide-and-conquer algorithm for the decoding.

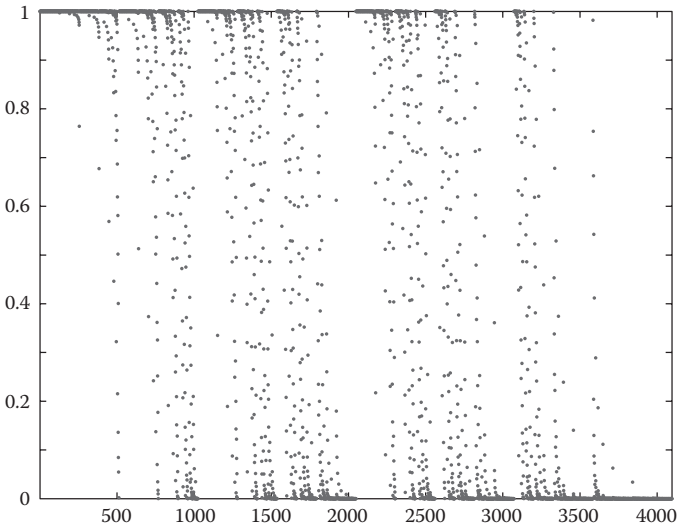

FIGURE 7.11 Plots of $H(Y_i|Y^{i-1})$ for $i = 1, \ldots, n = 4096$, when $H(p) = 1/2$.

A similar phenomenon holds in the channel setting. We provide next a simple derivation for the BSC channel. For a BSC channel, the output Y^n equals the input x^n plus a random sequence Z^n which is i.i.d. Bernoulli(p) (and does not depend on x^n).

By applying G_n to Y^n, one obtains $G_n\ Y^n = G_n\ x^n + G_n\ Z^n$. Note that $\mathcal{W}^n = G_n\ Z^n$ is precisely the transformed sequence studied previously in the source polarization and the components of $\mathcal{W}^n$ can be decomposed into two sets: the high and low conditional entropy components. By arranging $G_n\ x^n$ to have a fixed value known to the decoder, say zero, on the components where $\mathcal{W}^n$ has nonnegligible conditional entropy, one can learn these components and hence decode the entire vector $\mathcal{W}^n$ (as in the source polarization). This allows recovering Z^n, hence the codeword x^n. Note that the number of components which are not fixed in x^n is roughly $n(1 - h(p))$, that is, this scheme achieves the capacity of the BSC channel.

This coding scheme has the following properties:

- It achieves the capacity of the BSC channel (provably).
- The encoding and decoding complexity is $O(n\log(n))$.
- Its construction is explicit.
- Its error probability is $O(2^{-n^\beta})$, for any $\beta < 1/2$.

Indeed, this is the first coding scheme that has such remarkable asymptotic properties over the BSC channel. The generalization of the method to arbitrary binary input memoryless channels is provided in Arikan (2009).

References

Arikan, E. 2009. Channel polarization: A method for constructing capacity-achieving codes for symmetric binary-input memoryless channels, *IEEE Trans. Inform. Theory*, 55:3051–3073.

Arikan, E. and Telatar, E. 2009. On the rate of channel polarization. In *Proceeding of the 2009 IEEE International Symposium on Information Theory*, Seoul, Korea, pp. 1493–1495.

Berrou, C., Glavieux, A., and Thitimajshima, P. 1993. Near Shannon limit error-correcting coding and decoding. In *Proceedings of ICC'93*, Geneva, Switzerland, pp. 1064–1070.

Blahut, R. 1987. *Principles and Practice of Information Theory*, Addison–Wesley, Reading, MA.

Cover, T.M. and Thomas, J.A. 1991. *Elements of Information Theory*, Wiley, New York.

Csiszár, I. and Körner, J. 1981. *Information Theory: Coding Theorems for Discrete Memoryless Systems*, Academic Press, New York.

Gallager, R.G. 1963. *Low-Density Parity-Check Codes*, Monograph, M.I.T. Press, Cambridge, MA.

Gallager, R.G. 1968. *Information Theory and Reliable Communication*, Wiley, New York.

Luby, M., Mitzenmacher, M., Shokrollahi, A., Spielman, D., and Stemann, V. 1997. Practical loss-resilient codes. In *Proceedings of the 29th Annual ACM Symposium on the Theory of Computing*, pp. 150–159.

MacKay, D. 1999. Good error correcting codes based on very sparse matrices, *IEEE Trans. Inf. Theory*, 45:399–431.

McEliece, R.J. 1977. *The Theory of Information and Coding*, Addison–Wesley, Reading, MA.

Richardson, T., Shokrollahi, A., and Urbanke, R. 2001. Design of probably good low-density parity check codes, *IEEE Trans. Inf. Theory*, 47:619–637.

Wyner, A.D. and Ziv, J. 1994. The sliding-window Lempel–Ziv algorithm is asymptotically optimal. In *Communications and Cryptography*, Blahut, R.E., Costello, D.J., Jr., Maurer, V., and Mittclholzer, T. (Eds.), Kluwer Academic Publishers, Boston, MA.

Ziv, J. and Lempel, A. 1977. A universal algorithm for sequential data compression. *IEEE Trans. Inf. Theory*, IT-23(May):337–343.

Ziv, J. and Lempel, A. 1978. Compression of individual sequences by variable rate coding. *IEEE Trans. Inf. Theory*, IT-24 (Sept.):530–536.

Further Reading

For a lucid and up-to-date treatment of information theory extending beyond the area of communication, a most recommended reading is Cover and Thomas (1991). For readers interested in continuous-time channels and sources, we recommend Gallager (1968). For mathematically inclined readers who do not require much physical motivation, strong results for discrete memoryless channels and sources may be found in Csiszár and Körner (1981). Other excellent readings are Blahut (1987) and McEliece (1977). Most results in information theory are published in *IEEE Transactions on Information Theory*.

8

Rayleigh Fading Channels*

* A version of this chapter has appeared as two papers in the *IEEE Communications Magazine*, September 1997, under the titles "Rayleigh Fading Channels in Mobile Digital Communication Systems, Part I: Characterization" and "Part II: Mitigation." A version of this chapter also appears in the book *Digital Communications Fundamentals and Applications*, 2nd edition, Chapter 15, by Bernard Sklar, Prentice-Hall 2001.

Bernard Sklar

8.1 Introduction

When the mechanisms of fading channels were first modeled in the 1950s and 1960s, the ideas were primarily applied to over-the-horizon communications covering a wide range of frequency bands. The 3–30 MHz high-frequency (HF) band is used for ionospheric communications, and the 300 MHz–3 GHz ultra-high-frequency (UHF) and 3–30 GHz super-high-frequency (SHF) bands are used for tropospheric scatter. Although the fading effects in a mobile radio system are somewhat different from those in ionospheric and tropospheric channels, the early models are still quite useful to help characterize fading effects in mobile digital communication systems. This chapter addresses Rayleigh fading, primarily in the UHF band, which affects mobile systems such as cellular and personal communication systems (PCS). The chapter itemizes the fundamental fading manifestations, types of degradation, and methods to mitigate the degradation. Two particular mitigation techniques are examined: the Viterbi equalizer implemented in the Global System for Mobile Communication (GSM), and the Rake receiver used in CDMA systems built to meet Interim Standard-95 (IS-95).

8.2 The Challenge of a Fading Channel

In the study of communication systems, the classical (ideal) additive-white-Gaussian-noise (AWGN) channel, with statistically independent Gaussian noise samples corrupting data samples free of intersymbol interference (ISI), is the usual starting point for understanding basic performance relationships. The primary source of performance degradation is thermal noise generated in the receiver. Often, external interference received by the antenna is more significant than the thermal noise. This external interference can sometimes be characterized as having a broadband spectrum and quantified by a parameter called antenna temperature [1]. The thermal noise usually has a flat power spectral density over the signal band and a zero-mean Gaussian voltage probability density function (pdf). When modeling practical systems, the next step is the introduction of bandlimiting filters. The filter in the transmitter usually serves to satisfy some regulatory requirement on spectral containment. The filter in the receiver often serves the purpose of a classical "matched filter" [2] to the signal bandwidth. Due to the bandlimiting and phase-distortion properties of filters, special signal design and equalization techniques may be required to mitigate the filter-induced ISI.

If a radio channel's propagating characteristics are not specified, one usually infers that the signal attenuation versus distance behaves as if propagation takes place over ideal free space. The model of free space treats the region between the transmit and receive antennas as being free of all objects that might absorb or reflect radio frequency (RF) energy. It also assumes that, within this region, the atmosphere behaves as a perfectly uniform and nonabsorbing medium. Furthermore, the earth is treated as being infinitely far away from the propagating signal (or, equivalently, as having a reflection coefficient that is negligible). Basically, in this idealized free-space model, the attenuation of RF energy between the transmitter and receiver behaves according to an inverse-square law. The received power expressed in terms of transmitted power is attenuated by a factor, $L_s(d)$, where this factor is called *path loss* or *free space loss*. When the receiving antenna is isotropic, this factor is expressed as [1]

$$L_s(d) = \left(\frac{4\pi d}{\lambda}\right)^2 \tag{8.1}$$

In Equation 8.1, d is the distance between the transmitter and the receiver, and λ is the wavelength of the propagating signal. For this case of idealized propagation, received signal power is very predictable.

For most practical channels, where signal propagation takes place in the atmosphere and near the ground, the free-space propagation model is inadequate to describe the channel and predict system performance. In a wireless mobile communication system, a signal can travel from transmitter to receiver over multiple reflective paths; this phenomenon is referred to as *multipath propagation*. The effect can cause fluctuations in the received signal's amplitude, phase, and angle of arrival, giving rise to the terminology *multipath fading*. Another name, *scintillation*, having originated in radio astronomy, is used to describe the multipath fading caused by physical changes in the propagating medium, such as variations in the density of ions in the ionospheric layers that reflect high-frequency (HF) radio signals. Both names, fading and scintillation, refer to a signal's random fluctuations or fading due to multipath propagation. The main difference is that scintillation involves mechanisms (e.g., ions) that are much smaller than a wavelength. The end-to-end modeling and design of systems that mitigate the effects of fading are usually more challenging than those whose sole source of performance degradation is AWGN.

8.3 Mobile Radio Propagation: Large-Scale Fading and Small-Scale Fading

Figure 8.1 represents an overview of fading channel manifestations. It starts with two types of fading effects that characterize mobile communications: large-scale fading and small-scale fading. Large-scale fading represents the average signal power attenuation or the path loss due to motion over large areas. In Figure 8.1, the large-scale fading manifestation is shown in blocks 1, 2, and 3. This phenomenon is affected by prominent terrain contours (e.g., hills, forests, billboards, and clumps of buildings) between the transmitter and receiver. The receiver is often represented as being "shadowed" by such prominences. The statistics of large-scale fading provide a way of computing an estimate of path loss as a function of distance. This is described in terms of a mean path loss (nth-power law) and a log-normally

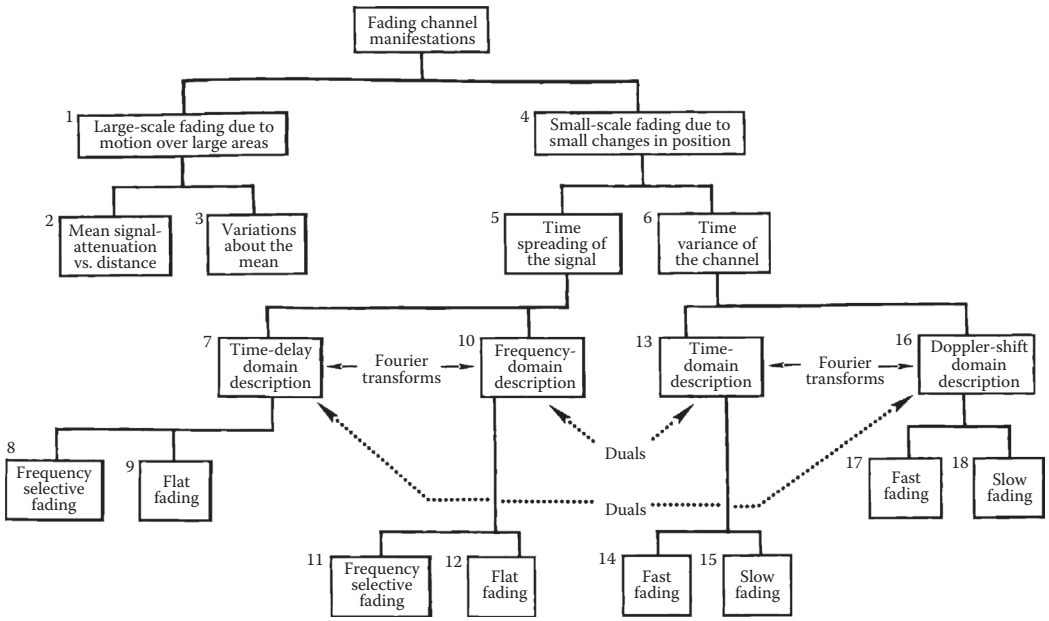

FIGURE 8.1 Fading channel manifestations.

distributed variation about the mean. Small-scale fading refers to the dramatic changes in signal amplitude and phase that can be experienced as a result of small changes (as small as a half-wavelength) in the spatial separation between a receiver and transmitter. As indicated in Figure 8.1, blocks 4, 5, and 6, small-scale fading manifests itself in two mechanisms, namely, time-spreading of the signal (or signal dispersion) and time-variant behavior of the channel. For mobile radio applications, the channel is time-variant because motion between the transmitter and receiver results in propagation path changes. The rate of change of these propagation conditions accounts for the fading rapidity (rate of change of the fading impairments). Small-scale fading is also called Rayleigh fading because if the multiple reflective paths are large in number and there is no line-of-sight signal component, the envelope of the received signal is statistically described by a Rayleigh pdf. When there is a dominant nonfading signal component present, such as a line-of-sight propagation path, the small-scale fading envelope is described by a Rician pdf [3]. A mobile radio roaming over a large area must process signals that experience both types of fading: small-scale fading superimposed on large-scale fading.

There are three basic mechanisms that impact on signal propagation in a mobile communication system. They are reflection, diffraction, and scattering [3].

- Reflection occurs when a propagating electromagnetic wave impinges upon a smooth surface with very large dimensions compared to the RF signal wavelength (λ).
- Diffraction occurs when the radio path between the transmitter and receiver is obstructed by a dense body with large dimensions compared to λ, causing secondary waves to be formed behind the obstructing body. Diffraction is a phenomenon that accounts for RF energy traveling from transmitter to receiver without a line-of-sight path between the two. It is often termed *shadowing* because the diffracted field can reach the receiver even when shadowed by an impenetrable obstruction.
- Scattering occurs when a radio wave impinges on either a large rough surface or any surface whose dimensions are on the order of λ or less, causing the reflected energy to spread out (scatter) in all directions. In an urban environment, typical signal obstructions that yield scattering are lampposts, street signs, and foliage.

Figure 8.1 may serve as a table of contents for the sections that follow. We will examine the two manifestations of small-scale fading: signal time-spreading (signal dispersion) and the time-variant nature of the channel. These examinations will take place in two domains: time and frequency, as indicated in Figure 8.1, blocks 7, 10, 13, and 16. For signal dispersion, we categorize the fading degradation types as being frequency-selective or frequency-nonselective (flat), as listed in blocks 8, 9, 11, and 12. For the time-variant manifestation, we categorize the fading degradation types as fast-fading or slow-fading, as listed in blocks 14, 15, 17, and 18. The labels indicating Fourier transforms and duals will be explained later.

Figure 8.2 illustrates the various contributions that must be considered when estimating path loss for a link budget analysis in a cellular application [4]. These contributions are

- Mean path loss as a function of distance, due to large-scale fading
- Near-worst-case variations about the mean path loss (typically 6–10 dB) or large-scale fading margin
- Near-worst-case Rayleigh or small-scale fading margin (typically 20–30 dB)

In Figure 8.2, the annotations "≈ 1–2%" indicate a suggested area (probability) under the tail of each pdf as a design goal. Hence, the amount of margin indicated is intended to provide adequate received signal power for approximately 98–99% of each type of fading variation (large and small scale).

A received signal is generally described in terms of a transmitted signal $s(t)$ convolved with the impulse response of the channel $h_c(t)$. Neglecting the degradation due to noise, we write

$$r(t) = s(t) * h_c(t) \tag{8.2}$$

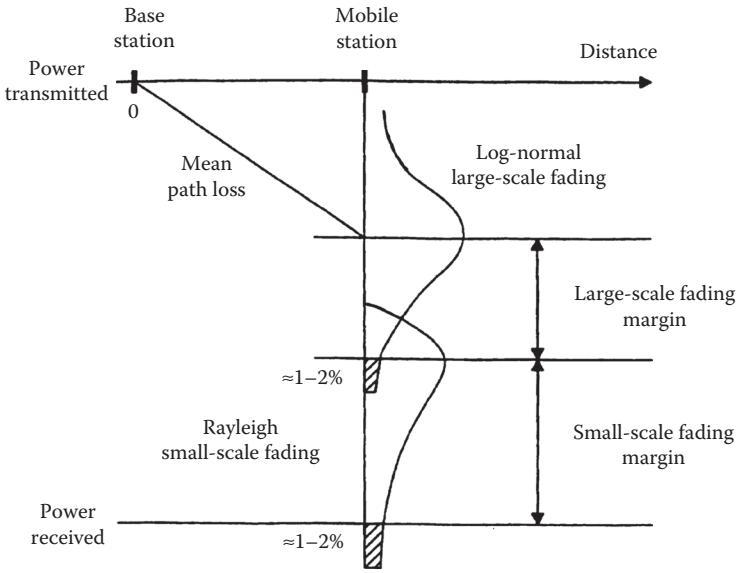

FIGURE 8.2 Link budget considerations for a fading channel.

where ⊠ denotes convolution. In the case of mobile radios, $r(t)$ can be partitioned in terms of two component random variables, as follows [5]:

$$r(t) = m(t) \times r_0(t) \tag{8.3}$$

where $m(t)$ is called the large-scale-fading component and $r_0(t)$ is called the small-scale-fading component. $m(t)$ is sometimes referred to as the *local mean* or *log-normal fading* because the magnitude of $m(t)$ is described by a log-normal pdf (or, equivalently, the magnitude measured in decibels has a Gaussian pdf). $r_0(t)$ is sometimes referred to as multipath or Rayleigh fading. Figure 8.3 illustrates the relationship between large-scale and small-scale fading. In Figure 8.3a, received signal power $r(t)$ versus antenna displacement (typically in units of wavelength) is plotted for the case of a mobile radio. Small-scale fading superimposed on large-scale fading can be readily identified. The typical antenna displacement between the small-scale signal nulls is approximately half wavelength. In Figure 8.3b, the large-scale fading or local mean, $m(t)$, has been removed in order to view the small-scale fading, $r_0(t)$, about some average constant power.

In the sections that follow, we enumerate some of the details regarding the statistics and mechanisms of large-scale and small-scale fading.

8.3.1 Large-Scale Fading: Path-Loss Mean and Standard Deviation

For the mobile radio application, Okumura [6] made some of the earlier comprehensive path-loss measurements for a wide range of antenna heights and coverage distances. Hata [7] transformed Okumura's data into parametric formulas. For the mobile radio application, the mean path loss, $\overline{L_p}(d)$, as a function of distance, d, between the transmitter and receiver is proportional to an nth-power of d relative to a reference distance d_0 [3].

$$\overline{L_p}(d) \propto \left(\frac{d}{d_0}\right)^n \tag{8.4}$$

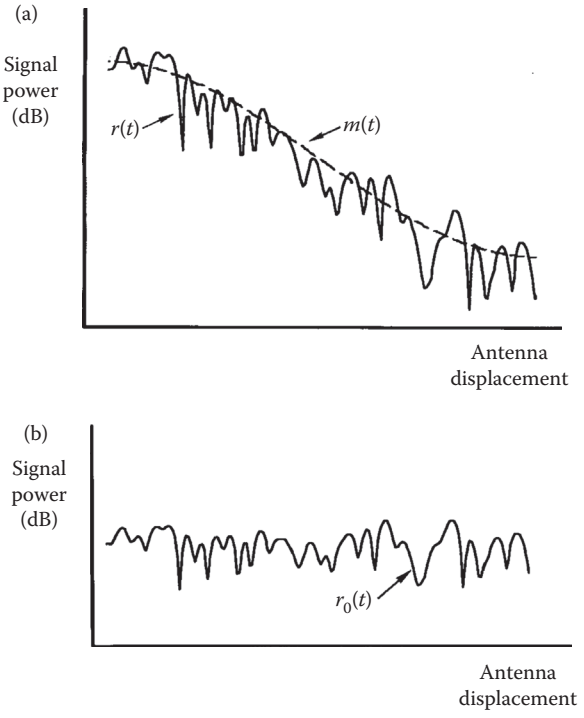

FIGURE 8.3 Large-scale fading and small-scale fading.

$\overline{L_p}(d)$ is often stated in decibels, as shown below.

$$\overline{L_p}(d)(\text{dB}) = L_s(d_0)(\text{dB}) + 10n \log\left(\frac{d}{d_0}\right) \tag{8.5}$$

The reference distance d_0 corresponds to a point located in the far field of the antenna. Typically, the value of d_0 is taken to be 1 km for large cells, 100 m for microcells, and 1 m for indoor channels. $\overline{L_p}(d)$ is the average path loss (over a multitude of different sites) for a given value of d. Linear regression for a minimum mean-squared estimate (MMSE) fit of $\overline{L_p}(d)$ versus d on a log–log scale (for distances greater than d_0) yields a straight line with a slope equal to 10 n dB/decade. The value of the exponent n depends on the frequency, antenna heights, and propagation environment. In free space, $n = 2$, as seen in Equation 8.1. In the presence of a very strong guided wave phenomenon (like urban streets), n can be lower than 2. When obstructions are present, n is larger. The path loss $L_s(d_0)$ to the reference point at a distance d_0 from the transmitter is typically found through field measurements or is calculated using the free-space path loss given by Equation 8.1. Figure 8.4 shows a scatter plot of path loss versus distance for measurements made in several German cities [8]. Here, the path loss has been measured relative to the free-space reference measurement at $d_0 = 100$ m. Also shown are straightline fits to various exponent values.

The path loss versus distance expressed in Equation 8.5 is an average, and therefore not adequate to describe any particular setting or signal path. It is necessary to provide for variations about the mean since the environment of different sites may be quite different for similar transmitter–receiver separations. Figure 8.4 illustrates that path-loss variations can be quite large. Measurements have shown that for any value of d, the path loss $L_p(d)$ is a random variable having a log-normal distribution about

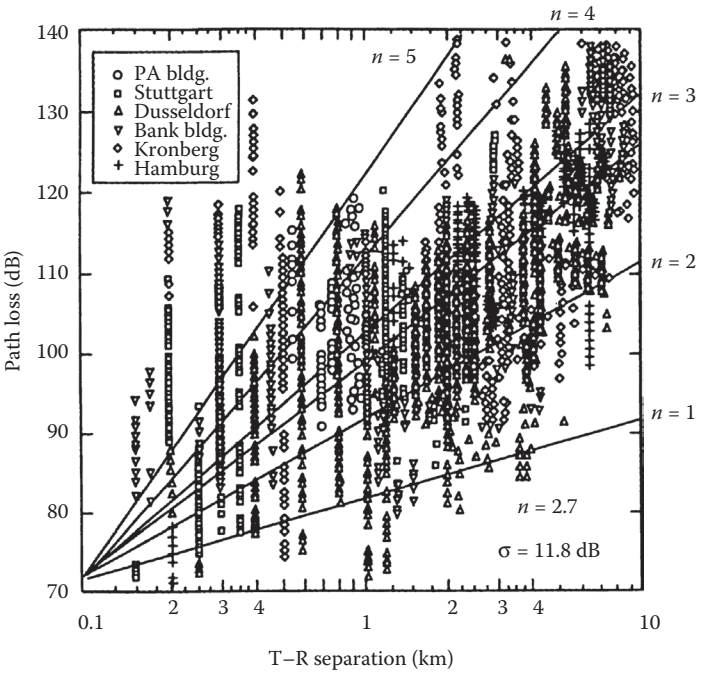

FIGURE 8.4 Path loss versus distance measured in several German cities.

the mean distant-dependent value $\overline{L_p}(d)$ [9]. Thus, path loss $L_p(d)$ can be expressed in terms of $\overline{L_p}(d)$ plus a random variable X_σ, as follows [3]:

$$L_p(d)\ (\text{dB}) = L_s(d_0)\ (\text{dB}) + 10n\ \log_{10}\left(\frac{d}{d_0}\right) + X_\sigma(\text{dB}) \tag{8.6}$$

where X_σ denotes a zero-mean, Gaussian random variable (in decibels) with standard deviation σ (also in decibels). X_σ is site and distance dependent. The choice of a value for X_σ is often based on measurements; it is not unusual for X_σ to take on values as high as 6–10 dB or greater. Thus, the parameters needed to statistically describe path loss due to large-scale fading for an arbitrary location with a specific transmitter–receiver separation are

- The reference distance d_0
- The path-loss exponent n
- The standard deviation σ of X_σ

There are several good references dealing with the measurement and estimation of propagation path loss for many different applications and configurations [3,7–11].

8.3.2 Small-Scale Fading: Statistics and Mechanisms

When the received signal is made up of multiple reflective rays plus a significant line-of-sight (nonfaded) component, the envelope amplitude due to small-scale fading has a Rician pdf, and is referred to as *Rician fading* [3]. The nonfaded component is called the *specular component*. As the amplitude of the specular component approaches zero, the Rician pdf approaches a Rayleigh pdf, expressed as

$$p(r) = \begin{cases} \dfrac{r}{\sigma^2} \exp\left[-\dfrac{r^2}{2\sigma^2}\right] & \text{for } r \geq 0 \\ 0 & \text{otherwise} \end{cases} \tag{8.7}$$

where r is the envelope amplitude of the received signal, and $2\sigma^2$ is the predetection mean power of the multipath signal. The Rayleigh-faded component is sometimes called the *random*, *scatter*, or *diffuse component*. The Rayleigh pdf results from having no specular component of the signal; thus, for a single link, it represents the pdf associated with the worst case of fading per mean received signal power. For the rest of this chapter, it is assumed that loss of signal-to-noise ratio (SNR) due to fading follows the Rayleigh model described. It will also be assumed that the propagating signal is in the UHF band, encompassing present-day cellular and PCS frequency allocations—nominally 1 and 2 GHz, respectively.

As indicated in Figure 8.1, blocks 4, 5, and 6, small-scale fading manifests itself in two mechanisms:

- Time-spreading of the underlying digital pulses within the signal
- A time-variant behavior of the channel due to motion (e.g., a receive antenna on a moving platform)

Figure 8.5 illustrates the consequences of both manifestations by showing the response of a multipath channel to a narrow pulse versus delay, as a function of antenna position (or time, assuming a constant velocity of motion). In Figure 8.5, we distinguish between two different time references—delay time τ and transmission or observation time t. Delay time refers to the time-spreading manifestation which results from the fading channel's nonoptimum impulse response. The transmission time, however, is related to the antenna's motion or spatial changes, accounting for propagation path changes that are perceived as the channel's time-variant behavior. Note that, for constant velocity, as is assumed in Figure 8.5, either antenna position or transmission time can be used to illustrate this time-variant behavior. Figure 8.5a–c shows the sequence of received pulse-power profiles as the antenna moves through a

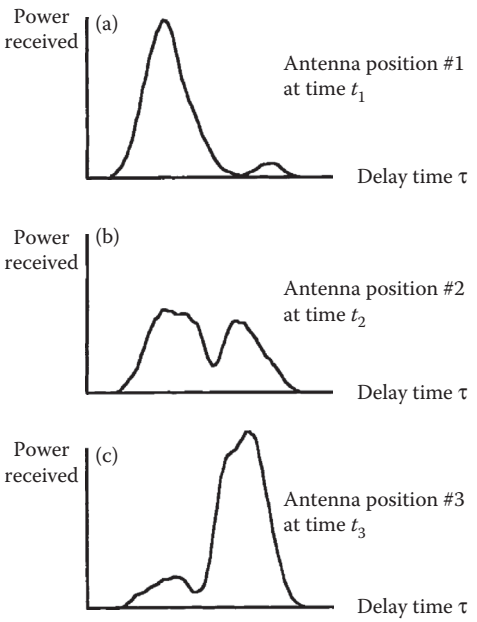

FIGURE 8.5 Response of a multipath channel to a narrow pulse versus delay as a function of antenna position.

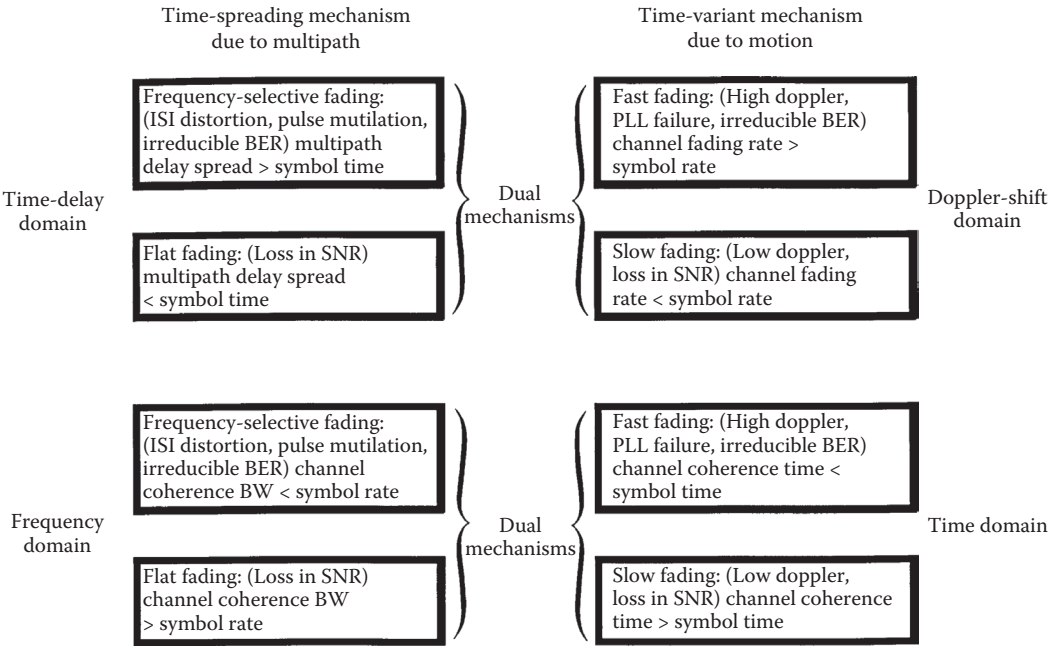

FIGURE 8.6 Small-scale fading: mechanisms, degradation categories, and effects.

succession of equally spaced positions. Here, the interval between antenna positions is 0.4 λ, where λ is the wavelength of the carrier frequency. For each of the three cases shown, the response pattern differs significantly in the delay time of the largest signal component, the number of signal copies, their magnitudes, and the total received power (area) in the received power profile. Figure 8.6 summarizes these two small-scale fading mechanisms, the two domains (time or time-delay and frequency or Doppler shift) for viewing each mechanism and the degradation categories each mechanism can exhibit. Note that any mechanism characterized in the time domain can be characterized equally well in the frequency domain. Hence, as outlined in Figure 8.6, the time-spreading mechanism will be characterized in the time-delay domain as a multipath delay spread and in the frequency domain as a channel coherence bandwidth. Similarly, the time-variant mechanism will be characterized in the time domain as a channel coherence time and in the Doppler-shift (frequency) domain as a channel fading rate or Doppler spread. These mechanisms and their associated degradation categories will be examined in greater detail in the sections that follow.

8.4 Signal Time-Spreading Viewed in the Time-Delay Domain: Figure 8.1, Block 7—The Multipath Intensity Profile

A simple way to model the fading phenomenon was introduced by Bello [13] in 1963; he proposed the notion of wide-sense stationary uncorrelated scattering (WSSUS). The model treats signal variations arriving with different delays as uncorrelated. It can be shown [4,13] that such a channel is effectively WSS in both the time and frequency domains. With such a model of a fading channel, Bello was able to define functions that apply for all time and all frequencies. For the mobile channel, Figure 8.7 contains four functions that make up this model [4,13–16]. We will examine these functions, starting with Figure 8.7a and proceeding counterclockwise toward Figure 8.7d.

In Figure 8.7a, a *multipath-intensity profile*, $S(\tau)$ versus time delay τ is plotted. Knowledge of $S(\tau)$ helps answer the question, "For a transmitted impulse, how does the received power vary as a function of time

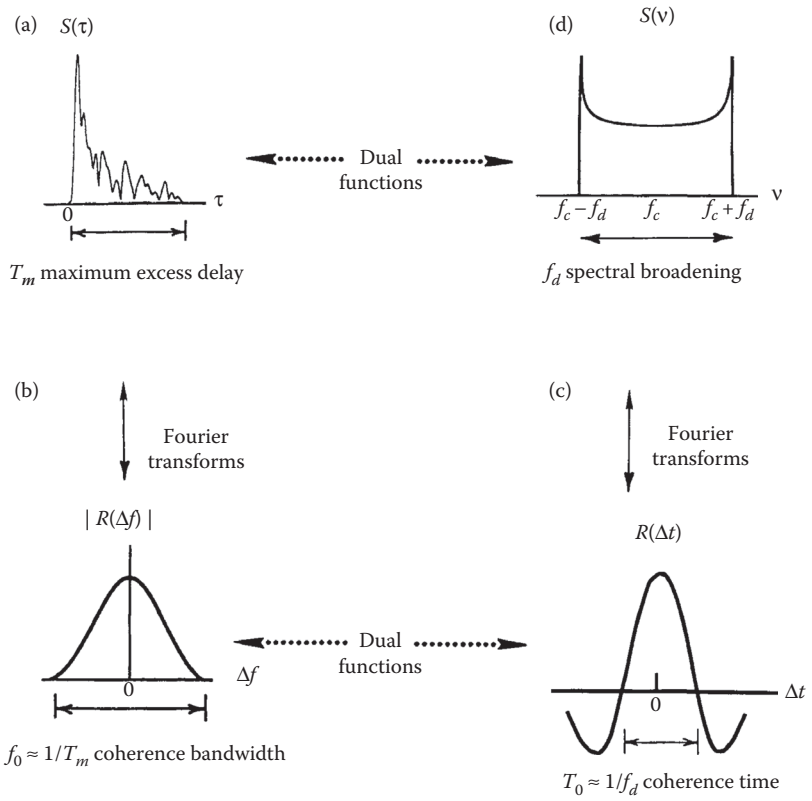

FIGURE 8.7 Relationship between the channel correlation functions and power density functions. (a) Multipath intensity profile, (b) spaced-frequency correlation function, (c) spaced-time correlation function, and (d) doppler power spectum.

delay, τ?" Here, the term "time delay" is used to refer to the excess delay. It represents the signal's propagation delay that exceeds the delay of the first signal arrival at the receiver; thus, the first component of the received signal arrives at $\tau = 0$. For a typical wireless radio channel, the received signal usually consists of several discrete multipath components, sometimes referred to as fingers. For some channels, such as the tropospheric scatter channel, received signals are often seen as a continuum of multipath components [14,16]. For making measurements of the multipath intensity profile, wideband signals (impulses or spread spectrum) need to be used [16]. For a single transmitted impulse, the time, T_m, between the first and last received component represents the *maximum excess delay* of the channel, during which the multipath signal power falls to some threshold level below that of the strongest component. The threshold level might typically be chosen at 10 or 20 dB below the level of the strongest component. Note, that for an ideal system (zero excess delay), the function $S(\tau)$ would consist of an ideal impulse with weight equal to the total average received signal power.

8.4.1 Degradation Categories due to Signal Time-Spreading Viewed in the Time-Delay Domain

In a fading channel, the relationship between maximum excess delay time, T_m, and symbol time, T_s, can be viewed in terms of two different degradation categories, *frequency-selective fading* and *frequency-nonselective* or *flat fading*, as indicated in Figure 8.1, blocks 8 and 9, and Figure 8.6. A channel is said to exhibit frequency-selective fading if $T_m > T_s$. This condition occurs whenever the received multipath

components of a symbol extend beyond the symbol's time duration. Such multipath dispersion of the signal yields the same kind of ISI distortion that is caused by an electronic filter. In fact, another name for this category of fading degradation is *channel-induced ISI*. In the case of frequency-selective fading, mitigating the distortion is possible because many of the multipath components are resolvable by the receiver. Later, several such mitigation techniques are described.

A channel is said to exhibit frequency-nonselective or flat fading if $T_m < T_s$. In this case, all the received multipath components of a symbol arrive within the symbol time duration; hence, the components are not resolvable. Here, there is no channel-induced ISI distortion, since the signal time spreading does not result in significant overlap among neighboring received symbols. There is still performance degradation since the unresolvable phasor components can add up destructively to yield a substantial reduction in SNR. Also, signals that are classified as exhibiting flat fading can *sometimes* experience frequency-selective distortion. This will be explained later when viewing degradation in the frequency domain, where the phenomenon is more easily described. For loss in SNR due to flat fading, the mitigation technique called for is to improve the received SNR (or reduce the required SNR). For digital systems, introducing some form of signal diversity and using error-correction coding is the most efficient way to accomplish this.

8.5 Signal Time-Spreading Viewed in the Frequency Domain: Figure 8.1, Block 10—The Spaced-Frequency Correlation Function

A completely analogous characterization of signal dispersion can begin in the frequency domain. In Figure 8.7b, the function $|R(\Delta f)|$ is seen, designated a *spaced-frequency correlation function*; it is the Fourier transform of $S(\tau)$. $R(\Delta f)$ represents the correlation between the channel's response to two signals as a function of the frequency difference between the two signals. It can be thought of as the channel's frequency transfer function. Therefore, the time-spreading manifestation can be viewed as if it were the result of a filtering process. Knowledge of $R(\Delta f)$ helps answer the question, "What is the correlation between received signals that are spaced in frequency $\Delta f = f_1 - f_2$?" $R(\Delta f)$ can be measured by transmitting a pair of sinusoids separated in frequency by Δf, cross-correlating the two separately received signals, and repeating the process many times with ever-larger separation Δf. Therefore, the measurement of $R(\Delta f)$ can be made with a sinusoid that is swept in frequency across the band of interest (a wideband signal, called a *chirp*). The *coherence bandwidth*, f_0 of the channel, is a statistical measure of the range of frequencies over which the channel passes all spectral components with approximately equal gain and linear phase. Thus, the coherence bandwidth represents a frequency range over which frequency components have a strong potential for amplitude correlation. That is, a signal's spectral components in that range are affected by the channel in a similar manner, as for example, exhibiting fading or no fading. Note that f_0 and T_m are reciprocally related (within a multiplicative constant). As an approximation, it is possible to say that

$$f_0 \oplus \frac{1}{T_m} \tag{8.8}$$

The maximum excess delay, T_m, is not necessarily the best indicator of how any given system will perform on a channel because different channels with the same value of T_m can exhibit very different profiles of signal intensity over the delay span. A more useful measurement of delay spread is most often characterized in terms of the root mean squared (rms) delay spread, σ_τ, where

$$\sigma_\tau = \sqrt{\overline{\tau^2} - (\overline{\tau})^2} \tag{8.9}$$

$\overline{\tau}$ is the mean excess delay, $(\overline{\tau})^2$ is the mean squared, $\overline{\tau^2}$ is the second moment, and σ_τ is the square root of the second central moment of $S(\tau)$ [3].

An exact relationship between coherence bandwidth and delay spread does not exist, and must be derived from signal analysis (usually using Fourier techniques) of actual signal dispersion measurements in particular channels. Several approximate relationships have been described. If coherence bandwidth is defined as the frequency interval over which the channel's complex frequency transfer function has a correlation of at least 0.9, the coherence bandwidth is approximately [17]

$$f_0 \approx \frac{1}{50\sigma_\tau} \tag{8.10}$$

For the case of a mobile radio, an array of radially uniformly spaced scatterers, all with equal-magnitude reflection coefficients but independent, randomly occurring reflection phase angles [18,19] is generally accepted as a useful model for urban surroundings. This model is referred to as the *dense-scatterer channel model*. With the use of such a model, coherence bandwidth has similarly been defined [18] for a bandwidth interval over which the channel's complex frequency transfer function has a correlation of at least 0.5 to be

$$f_0 = \frac{0.276}{\sigma_\tau} \tag{8.11}$$

The ionospheric-effects community employs the following definition

$$f_0 = \frac{1}{2\pi\sigma_\tau} \tag{8.12}$$

A more popular approximation of f_0 corresponding to a bandwidth interval having a correlation of at least 0.5 is [3]

$$f_0 \approx \frac{1}{5\sigma_\tau} \tag{8.13}$$

8.5.1 Degradation Categories due to Signal Time-Spreading Viewed in the Frequency Domain

A channel is referred to as frequency-selective if $f_0 < 1/T_s \approx W$, where the symbol rate $1/T_s$ is nominally taken to be equal to the signal bandwidth W. In practice, W may differ from $1/T_s$ due to system filtering or data modulation type (quaternary phase shift keying (QPSK), minimum shift keying (MSK), etc.) [21]. Frequency-selective fading distortion occurs whenever a signal's spectral components are not all affected equally by the channel. Some of the signal's spectral components, falling outside the coherence bandwidth, will be affected differently (independently) compared to those components contained within the coherence bandwidth. This occurs whenever $f_0 < W$ and is illustrated in Figure 8.8a.

Frequency-nonselective or flat-fading degradation occurs whenever $f_0 > W$. Hence, all of the signal's spectral components will be affected by the channel in a similar manner (e.g., fading or no fading); this is illustrated in (Figure 8.8b). Flat fading does not introduce channel-induced ISI distortion, but performance degradation can still be expected due to the loss in SNR whenever the signal is fading. In

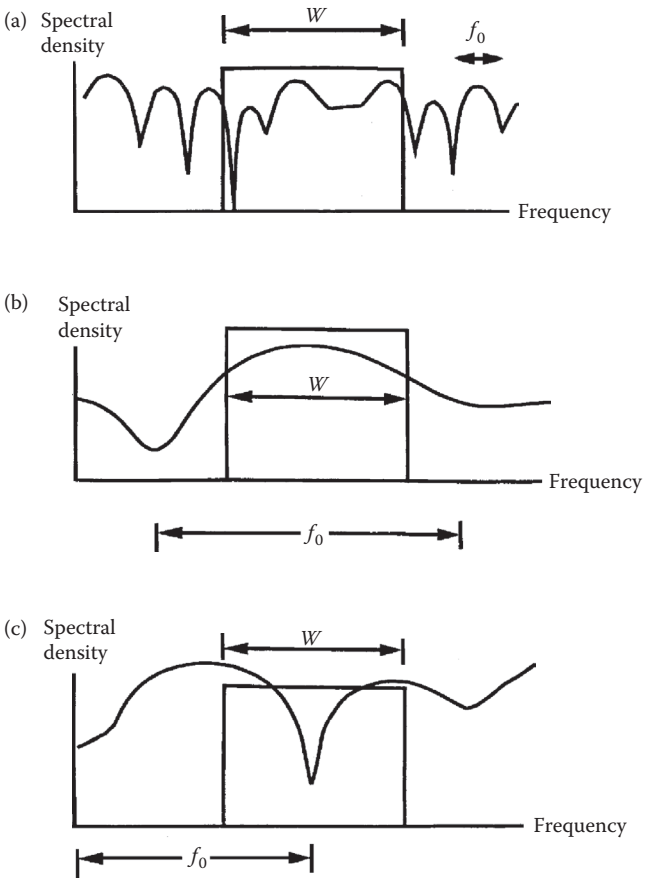

FIGURE 8.8 Relationships between the channel frequency transfer function and a signal with bandwidth W. (a) Typical frequency-selective fading case ($f_0 < W$), (b) typical flat-fading case ($f_0 > W$), and (c) null of channel frequency-transfer function occurs at signal band center ($f_0 > W$).

order to avoid channel-induced ISI distortion, the channel is required to exhibit flat fading by ensuring that

$$f_0 > W \approx \frac{1}{T_s} \tag{8.14}$$

Hence, the channel coherence bandwidth f_0 sets an upper limit on the transmission rate that can be used without incorporating an equalizer into the receiver.

For the flat-fading case, where $f_0 > W$ (or $T_m < T_s$), Figure 8.8b shows the usual flat fading pictorial representation. However, as a mobile radio changes its position, there will be times when the received signal experiences frequency-selective distortion even though $f_0 > W$. This is seen in Figure 8.8c, where the null of the channel's frequency transfer function occurs at the center of the signal band. Whenever this occurs, the baseband pulse will be especially mutilated by deprivation of its DC component. One consequence of the loss of DC (zero mean value) is the absence of a reliable pulse peak on which to establish the timing synchronization, or from which to sample the carrier phase carried by the pulse [18]. Thus, even though a channel is categorized as flat fading (based on rms relationships), it can still manifest frequency-selective fading on occasions. It is fair to say that a mobile radio channel, classified as having

flat fading degradation, cannot exhibit flat fading all the time. As f_0 becomes much larger than W (or T_m becomes much smaller than T_s), less time will be spent in conditions approximating Figure 8.8c. By comparison, it should be clear that in Figure 8.8a, the fading is independent of the position of the signal band, and frequency-selective fading occurs all the time, not just occasionally.

8.6 Typical Examples of Flat Fading and Frequency-Selective Fading Manifestations

Figure 8.9 shows some examples of flat fading and frequency-selective fading for a direct-sequence spread-spectrum (DS/SS) system [20,22]. In Figure 8.9, there are three plots of the output of a pseudonoise (PN) code correlator versus delay as a function of time (transmission or observation time). Each amplitude versus delay plot is akin to $S(\tau)$ versus τ shown in Figure 8.7a. The key difference is that the amplitudes shown in Figure 8.9 represent the output of a correlator; hence, the waveshapes are a function not only of the impulse response of the channel but also of the impulse response of the correlator. The delay time is

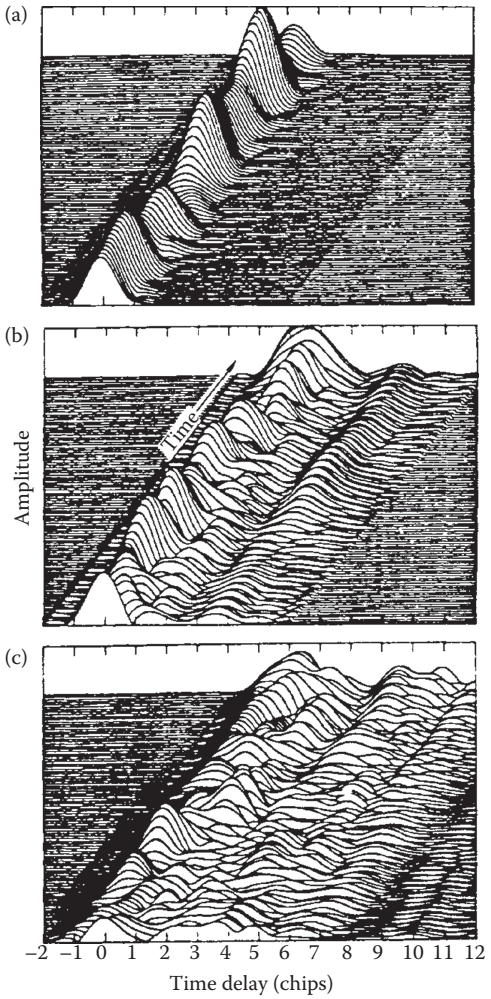

FIGURE 8.9 DS/SS matched-filter output time-history examples for three levels of channel conditions, where T_{ch} is the time duration of a chip. (a) $f_0T_{ch} \approx 1$, (b) $f_0T_{ch} = 0.25$, and (c) $f_0T_{ch} \approx 0.1$.

expressed in units of chip durations (chips), where the chip is defined as the spread-spectrum minimal-duration keying element. For each plot, the observation time is shown on an axis perpendicular to the amplitude versus time-delay plane. Figure 8.9 is drawn from a satellite-to-ground communications link exhibiting scintillation because of atmospheric disturbances. However, Figure 8.9 is still a useful illustration of three different channel conditions that might apply to a mobile radio situation. A mobile radio that moves along the observation-time axis is affected by changing multipath profiles along the route, as seen in the figure. The scale along the observation-time axis is also in units of chips. In Figure 8.9a, the signal dispersion (one "finger" of return) is on the order of a chip time duration, T_{ch}. In a typical DS/SS system, the spread-spectrum signal bandwidth is approximately equal to $1/T_{ch}$; hence, the normalized coherence bandwidth f_0T_{ch} of approximately unity in Figure 8.9a implies that the coherence bandwidth is about equal to the spread-spectrum bandwidth. This describes a channel that can be called frequency-nonselective or slightly frequency-selective. In Figure 8.9b, where $f_0T_{ch} = 0.25$, the signal dispersion is more pronounced. There is definite interchip interference, and the coherence bandwidth is approximately equal to 25% of the spread-spectrum bandwidth. In Figure 8.9c, where $f_0T_{ch} = 0.1$, the signal dispersion is even more pronounced, with greater interchip-interference effects, and the coherence bandwidth is approximately equal to 10% of the spread-spectrum bandwidth. The channels of Figure 8.9b,c can be categorized as moderately and highly frequency-selective, respectively, with respect to the basic signaling element, the chip. Later, we show that a DS/SS system operating over a frequency-selective channel at the chip level does not necessarily experience frequency-selective distortion at the symbol level.

8.7 Time Variance Viewed in the Time Domain: Figure 8.1, Block 13—The Spaced-Time Correlation Function

Until now, we have described signal dispersion and coherence bandwidth, parameters that describe the channel's time-spreading properties in a local area. However, they do not offer information about the time-varying nature of the channel caused by relative motion between a transmitter and receiver, or by movement of objects within the channel. For mobile radio applications, the channel is time variant because motion between the transmitter and the receiver results in propagation-path changes. Thus, for a transmitted continuous wave (CW) signal, as a result of such motion, the radio receiver sees variations in the signal's amplitude and phase. Assuming that all scatterers making up the channel are stationary, then whenever motion ceases, the amplitude and phase of the received signal remain constant; that is, the channel appears to be time invariant. Whenever motion begins again, the channel appears time variant. Since the channel characteristics are dependent on the positions of the transmitter and receiver, time variance in this case is equivalent to spatial variance.

Figure 8.7c shows the function $R(\Delta t)$, designated the *spaced-time correlation function*; it is the autocorrelation function of the channel's response to a sinusoid. This function specifies the extent to which there is correlation between the channel's response to a sinusoid sent at time t_1 and the response to a similar sinusoid sent at time t_2, where $\Delta t = t_2 - t_1$. The *coherence time*, T_0, is a measure of the expected time duration over which the channel's response is essentially invariant. Earlier, we made measurements of signal dispersion and coherence bandwidth by using wideband signals. Now, to measure the time-variant nature of the channel, we use a narrowband signal. To measure $R(\Delta t)$, we can transmit a single sinusoid ($\Delta f = 0$) and determine the autocorrelation function of the received signal. The function $R(\Delta t)$ and the parameter T_0 provide us with knowledge about the fading rapidity of the channel. Note that for an ideal *time-invariant channel* (e.g., a mobile radio exhibiting no motion at all), the channel's response would be highly correlated for all values of Δt, and $R(\Delta t)$ would be a constant function. When using the dense-scatterer channel model described earlier, with constant velocity of motion, and an unmodulated CW signal, the normalized $R(\Delta t)$ is described as

$$R(\Delta t) = J_0(kV\Delta t) \tag{8.15}$$

where $J_0(\cdot)$ is the zero-order Bessel function of the first kind, V is velocity, $V\Delta t$ is distance traversed, and $k = 2\pi/\lambda$ is the free-space phase constant (transforming distance to radians of phase). Coherence time can be measured in terms of either time or distance traversed (assuming some fixed velocity of motion). Amoroso described such a measurement using a CW signal and a dense-scatterer channel model [18]. He measured the statistical correlation between the combination of received magnitude and phase sampled at a particular antenna location x_0, and the corresponding combination sampled at some displaced location $x_0 + \zeta$, with displacement measured in units of wavelength λ. For a displacement ζ of 0.38 λ between two antenna locations, the combined magnitudes and phases of the received CW are statistically uncorrelated. In other words, the state of the signal at x_0 says nothing about the state of the signal at $x_0 + \zeta$. For a given velocity of motion, this displacement is readily transformed into units of time (coherence time).

8.7.1 The Concept of Duality

Two operators (functions, elements, or systems) are dual when the behavior of one with reference to a time-related domain (time or time-delay) is identical to the behavior of the other with reference to the corresponding frequency-related domain (frequency or Doppler shift).

In Figure 8.7, we can identify functions that exhibit similar behavior across domains. For understanding the fading channel model, it is useful to refer to such functions as *duals*. For example, $S(\tau)$ in Figure 8.7a characterizes the channel's effect on signal-time dispersion, T_m. Its dual is seen in Figure 8.7d, where $S(\nu)$ characterizes the channel's effect on signal-spectral dispersion, f_d. Similarly, $R(\Delta f)$ in Figure 8.7b characterizes the channel's coherence bandwidth, f_0 (frequency range over which a signal's spectral components have a strong potential for being correlated). Its dual is seen in Figure 8.7c, where $R(\Delta t)$ characterizes the channel's coherence time, T_0 (time range over which a signal's time components have a strong potential for being correlated). These dualities are also denoted in Figure 8.1, where $S(\tau)$ and its dual $S(\nu)$ are represented by blocks 7 and 16. Similarly, $R(\Delta f)$ and its dual $R(\Delta t)$ are represented by blocks 10 and 13.

8.7.2 Degradation Categories due to Time Variance Viewed in the Time Domain

The time-variant nature of the channel or fading rapidity mechanism can be viewed in terms of two degradation categories as listed in Figure 8.6: *fast fading* and *slow fading*. The terminology "fast fading" is used for describing channels in which $T_0 < T_s$, where T_0 is the channel coherence time and T_s is the time duration of a transmission symbol. Fast fading describes a condition where the time duration in which the channel behaves in a correlated manner is short compared to the time duration of a symbol. Therefore, it can be expected that the fading character of the channel will change several times during the time that a symbol is propagating, leading to distortion of the baseband pulse shape. Analogous to the distortion previously described as channel-induced ISI, here distortion takes place because the received signal's components are not all highly correlated throughout time. Hence, fast fading can cause the baseband pulse to be distorted, resulting in a loss of SNR that often yields an irreducible error rate. Such distorted pulses cause synchronization problems (failure of phase-locked-loop receivers), in addition to difficulties in adequately defining a matched filter.

A channel is generally referred to as introducing slow fading if $T_0 > T_s$. Here, the time duration that the channel behaves in a correlated manner is long compared to the time duration of a transmission symbol. Thus, one can expect the channel state to virtually remain unchanged during the time in which a symbol is transmitted. The propagating symbols will likely not suffer from the pulse distortion described above. The primary degradation in a slow-fading channel, as with flat fading, is loss in SNR.

8.8 Time Variance Viewed in the Doppler-Shift Domain: Figure 8.1, Block 16—The Doppler Power Spectrum

A completely analogous characterization of the time-variant nature of the channel can begin in the Doppler-shift (frequency) domain. Figure 8.7d shows a *Doppler power spectral density*, $S(\nu)$, plotted as a function of Doppler frequency shift, ν. For the case of the dense-scatterer model, a vertical receive antenna with constant azimuthal gain, a uniform distribution of signals arriving at all arrival angles throughout the range $(0, 2\pi)$, and an unmodulated CW signal, the signal spectrum at the antenna terminals is [19]

$$S(\nu) = \frac{1}{\pi f_d \sqrt{1 - \left(\nu - f_c / f_d\right)^2}} \tag{8.16}$$

The equality holds for frequency shifts of ν that are in the range $\pm f_d$ about the carrier frequency f_c and would be zero outside that range. The shape of the RF Doppler spectrum described by Equation 8.16 is classically bowl shaped, as seen in Figure 8.7d. Note that the spectral shape is a result of the dense-scatterer channel model. Equation 8.16 has been shown to match experimental data gathered for mobile radio channels [23]; however, different applications yield different spectral shapes. For example, the dense-scatterer model does not hold for the indoor radio channel; the channel model for an indoor area assumes $S(\nu)$ to be a flat spectrum [24].

In Figure 8.7d, the sharpness and steepness of the boundaries of the Doppler spectrum are due to the sharp upper limit on the Doppler shift produced by a vehicular antenna traveling among the stationary scatterers of the dense scatterer model. The largest magnitude (infinite) of $S(\nu)$ occurs when the scatterer is directly ahead of the moving antenna platform or directly behind it. In that case, the magnitude of the frequency shift is given by

$$f_d = \frac{V}{\lambda} \tag{8.17}$$

where V is relative velocity and λ is the signal wavelength. f_d is positive when the transmitter and receiver move toward each other and negative when moving away from each other. For scatterers directly broadside of the moving platform, the magnitude of the frequency shift is zero. The fact that Doppler components arriving at exactly 0° and 180° have an infinite power spectral density is not a problem, since the angle of arrival is continuously distributed and the probability of components arriving at exactly these angles is zero [3,19].

$S(\nu)$ is the Fourier transform of $R(\Delta t)$. We know that the Fourier transform of the autocorrelation function of a time series is the magnitude squared of the Fourier transform of the original time series. Therefore, measurements can be made by simply transmitting a sinusoid (narrowband signal) and using Fourier analysis to generate the power spectrum of the received amplitude [16]. This Doppler power spectrum of the channel yields knowledge about the spectral spreading of a transmitted sinusoid (impulse in frequency) in the Doppler-shift domain. As indicated in Figure 8.7, $S(\nu)$ can be regarded as the dual of the multipath intensity profile, $S(\tau)$, since the latter yields knowledge about the time spreading of a transmitted impulse in the time-delay domain. This is also noted in Figure 8.1 as the duality between blocks 7 and 16, and in Figure 8.6 as the duality between the time-spreading mechanism in the time-delay domain and the time-variant mechanism in the Doppler-shift domain.

Knowledge of $S(\nu)$ allows us to glean how much spectral broadening is imposed on the signal as a function of the rate of change in the channel state. The width of the Doppler power spectrum is referred to as the *spectral broadening* or *Doppler spread*, denoted by f_d, and sometimes called the *fading bandwidth*

of the channel. Equation 8.16 describes the Doppler frequency shift. In a typical multipath environment, the received signal arrives from several reflected paths with different path distances and different angles of arrival, and the Doppler shift of each arriving path is generally different from that of another path. The effect on the received signal is seen as a Doppler spreading or spectral broadening of the transmitted signal frequency, rather than a shift. Note that the Doppler spread, f_d, and the coherence time, T_0, are reciprocally related (within a multiplicative constant). Therefore, we show the approximate relationship between the two parameters as

$$T_0 \oplus \frac{1}{f_d} \tag{8.18}$$

Hence, the Doppler spread f_d or $1/T_0$ is regarded as the typical *fading rate* of the channel. Earlier, T_0 was described as the expected time duration over which the channel's response to a sinusoid is essentially invariant. When T_0 is defined more precisely as the time duration over which the channel's response to a sinusoid has a correlation of at least 0.5, the relationship between T_0 and f_d is approximately [4]

$$T_0 \approx \frac{9}{16\pi f_d} \tag{8.19}$$

A popular "rule of thumb" is to define T_0 as the geometric mean of Equations 8.18 and 8.19. This yields

$$T_0 = \sqrt{\frac{9}{16\pi f_d^2}} = \frac{0.423}{f_d} \tag{8.20}$$

For the case of a 900 MHz mobile radio, Figure 8.10 illustrates the typical effect of Rayleigh fading on a signal's envelope amplitude versus time [3]. The figure shows that the distance traveled by the mobile in the time interval corresponding to two adjacent nulls (small-scale fades) is on the order of a half-wavelength (λ/2) [3]. Thus, from Figure 8.10 and Equation 8.17, the time (approximately, the coherence time) required to traverse a distance λ/2 when traveling at a constant velocity, V, is

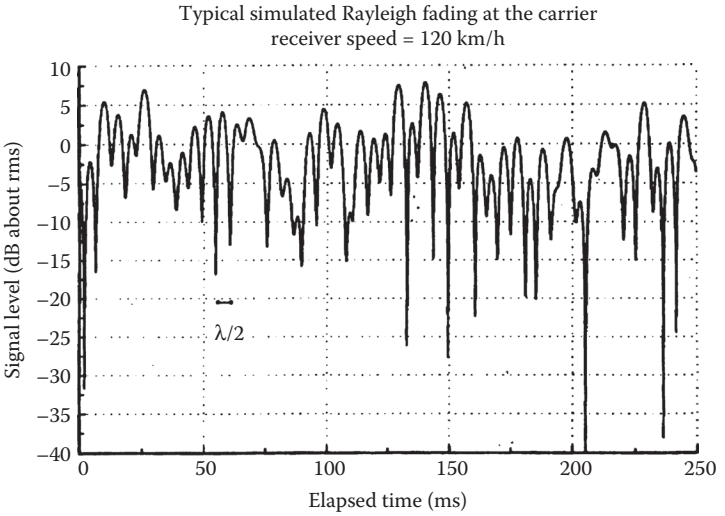

FIGURE 8.10 A typical Rayleigh fading envelope at 900 MHz.

$$T_0 \approx \frac{\lambda/2}{V} = \frac{0.5}{f_d} \tag{8.21}$$

Thus, when the interval between fades is taken to be $\lambda/2$, as in Figure 8.10, the resulting expression for T_0 in Equation 8.21 is quite close to the rule of thumb shown in Equation 8.20. Using Equation 8.21, with the parameters shown in Figure 8.10 (velocity = 120 km/h, and carrier frequency = 900 MHz), it is straightforward to compute that the coherence time is approximately 5 ms and the Doppler spread (channel fading rate) is approximately 100 Hz. Therefore, if this example represents a voice-grade channel with a typical transmission rate of 10^4 symbols/s, the fading rate is considerably less than the symbol rate. Under such conditions, the channel would manifest slow-fading effects. Note that if the abscissa of Figure 8.10 were labeled in units of wavelength instead of time, the figure would look the same for any radio frequency and any antenna speed.

8.9 Analogy between Spectral Broadening in Fading Channels and Spectral Broadening in Digital Signal Keying

Help is often needed in understanding why spectral broadening of the signal is a function of fading rate of the channel. Figure 8.11 uses the keying of a digital signal (such as amplitude-shift-keying or frequency-shift-keying) to illustrate an analogous case. Figure 8.11a shows that a single tone, $\cos 2\pi f_c t$ $(-\infty < t < \infty)$ that exists for all time is characterized in the frequency domain in terms of impulses (at $\pm f_c$). This frequency-domain representation is ideal (i.e., zero bandwidth), since the tone is pure and neverending. In practical applications, digital signaling involves switching (keying) signals on and off at a required rate. The keying operation can be viewed as multiplying the infinite-duration tone in Figure 8.11a by an ideal rectangular (switching) function of duration T in Figure 8.11b. The frequency-domain description of the ideal rectangular function is of the form $(\sin \pi fT)/\pi f$. In Figure 8.11c, the result of the multiplication yields a tone, $\cos 2\pi f_c t$, that is time-duration limited in the interval $-T/2 < t < T/2$. The resulting spectrum is obtained by convolving the spectral impulses in part (a) with the $(\sin \pi fT)/\pi f$ function in part (b), yielding the broadened spectrum in part (c). It is further seen that, if the signaling occurs at a faster rate characterized by the rectangle of shorter duration as seen in part (d), the resulting spectrum of the signal in part (e) exhibits greater spectral broadening. The changing state of a fading

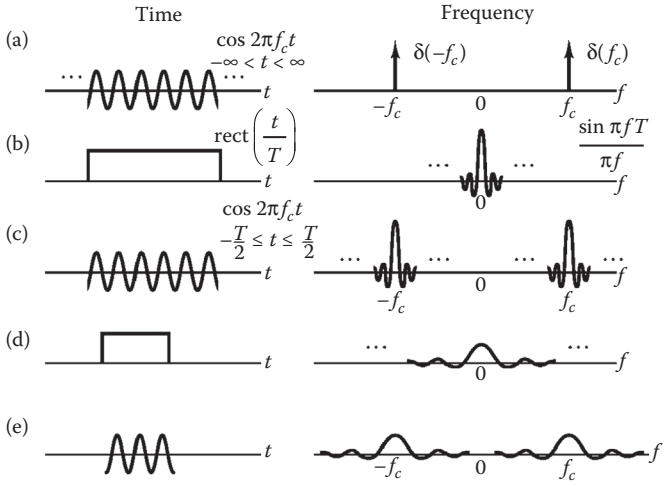

FIGURE 8.11 Analogy between spectral broadening in fading and spectral broadening in keying a digital signal. (a) Sinusoid, (b) keying, (c) digital signal, (d) faster keying, and (e) digital signal.

channel is somewhat analogous to the keying on and off of digital signals. The channel behaves like a switch, turning the signal "on" and "off." The greater the rapidity of the change in the channel state (smaller T), the greater the spectral broadening of the received signals. The analogy is not exact because the on and off switching of signals may result in phase discontinuities, but the typical multipath-scatterer environment induces phase-continuous effects.

8.10 Degradation Categories due to Time Variance, Viewed in the Doppler-Shift Domain

A channel is referred to as fast fading if the symbol rate, $1/T_s$ (approximately equal to the signaling rate or bandwidth W), is less than the fading rate, $1/T_0$ (approximately equal to f_d); that is, fast fading is characterized by

$$W < f_d \tag{8.22a}$$

or

$$T_s > T_0 \tag{8.22b}$$

Conversely, a channel is referred to as slow fading if the signaling rate is greater than the fading rate. Thus, in order to avoid signal distortion caused by fast fading, the channel must be made to exhibit slow fading by insuring that the signaling rate must exceed the channel fading rate. That is

$$W > f_d \tag{8.23a}$$

or

$$T_s < T_0 \tag{8.23b}$$

In Equation 8.14, it was shown that due to signal dispersion, the coherence bandwidth, f_0, sets an upper limit on the signaling rate that can be used without suffering frequency-selective distortion. Similarly, Equation 8.23 shows that due to Doppler spreading, the channel fading rate, f_d, sets a lower limit on the signaling rate that can be used without suffering fast-fading distortion. For HF communicating systems, when teletype or Morse-coded messages were transmitted at a low data rate, the channels were often fast fading. However, most present-day terrestrial mobile radio channels can generally be characterized as slow fading.

Equation 8.23 does not go far enough in describing what we desire of the channel. A better way to state the requirement for mitigating the effects of fast fading would be that we desire $W \gg f_d$ (or $T_s \ll T_0$). If this condition is not satisfied, the random frequency modulation (FM) due to varying Doppler shifts will limit the system performance significantly. The Doppler effect yields an irreducible error rate that cannot be overcome by simply increasing E_b/N_0 [25]. This irreducible error rate is most pronounced for any modulation that involves switching the carrier phase. A single specular Doppler path, without scatterers, registers an instantaneous frequency shift, classically calculated as $f_d = V/\lambda$. However, a combination of specular and multipath components yields a rather complex time dependence of instantaneous frequency which can cause much larger frequency swings than $\pm V/\lambda$ when detected by an instantaneous frequency detector (a nonlinear device) [26]. Ideally, coherent demodulators that lock onto and track the information signal should suppress the effect of this FM noise and thus cancel the impact of Doppler shift. However, for large values of f_d, carrier recovery becomes a problem because very wideband (relative

to the data rate) phase-lock loops (PLLs) need to be designed. For voice-grade applications with bit-error rates of 10^{-3} to 10^{-4}, a large value of Doppler shift is considered to be on the order of $0.01 \times W$. Therefore, to avoid fast-fading distortion and the Doppler-induced irreducible error rate, the signaling rate should exceed the fading rate by a factor of 100 to 200 [27]. The exact factor depends on the signal modulation, receiver design, and required error rate [3,26–29]. Davarian [29] showed that a frequency-tracking loop can help lower, but not completely remove, the irreducible error rate in a mobile system when using differential minimum-shift keyed (DMSK) modulation.

8.11 Mitigation Methods

Figure 8.12 highlights three major performance categories in terms of bit-error probability, P_B, versus E_b/N_0. The leftmost exponentially shaped curve represents the performance that can be expected when using any nominal modulation type in AWGN. Observe that with a reasonable amount of E_b/N_0, good performance results. The middle curve, referred to as the *Rayleigh limit*, shows the performance degradation resulting from a loss in SNR that is characteristic of flat fading or slow fading when there is no line-of-sight signal component present. The curve is a function of the reciprocal of E_b/N_0 (an inverse-linear function), so for reasonable values of SNR, performance will generally be "bad." In the case of Rayleigh fading, parameters with overbars are often introduced to indicate that a mean is being taken over the "ups" and "downs" of the fading experience. Therefore, one often sees such bit-error probability plots with mean parameters denoted by $\overline{P_B}$ and $\overline{E_b}/N_0$. The curve that reaches an irreducible level, sometimes called an *error floor*, represents "awful" performance, where the bit-error probability can approach the value of 0.5. This shows the severe distorting effects of frequency-selective fading or fast fading.

If the channel introduces signal distortion as a result of fading, the system performance can exhibit an irreducible error rate. If such an error floor is larger than the desired error rate, no amount of E_b/N_0 will help achieve the desired level of performance. In such cases, the general approach for improving performance is to use some form of mitigation to remove or reduce the distortion. The mitigation

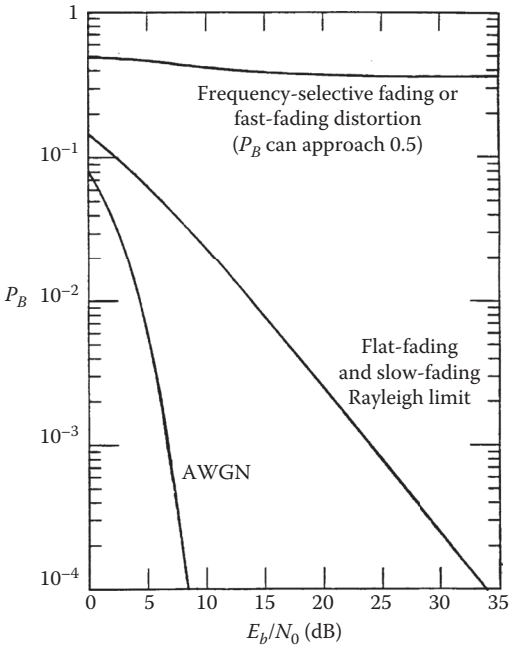

FIGURE 8.12 Error performance: the good, the bad, and the awful.

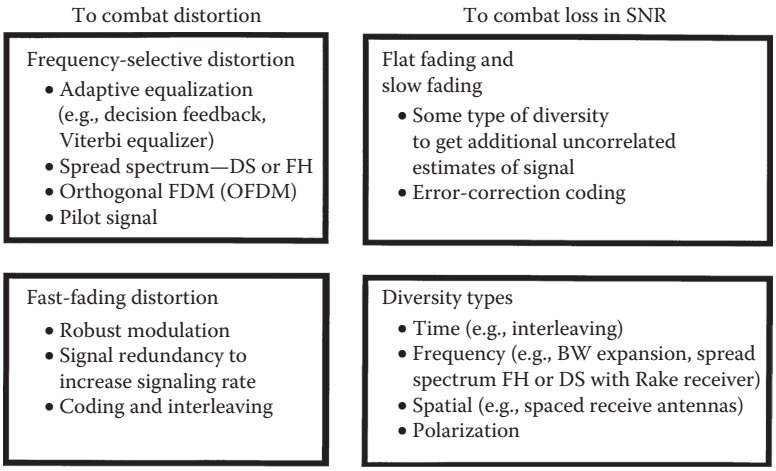

FIGURE 8.13 Basic mitigation types.

method depends on whether the distortion is caused by frequency-selective fading or fast fading. Once the distortion has been mitigated, the P_B versus E_b/N_0 performance should have transitioned from the "awful" bottoming-out curve to the merely "bad" Rayleigh limit curve. Next, we can further ameliorate the effects of fading and strive to approach AWGN performance by using some form of diversity to provide the receiver with a collection of uncorrelated samples of the signal, and by using a powerful error-correction code.

In Figure 8.13, several mitigation techniques for combating the effects of both signal distortion and loss in SNR are listed. Just as Figures 8.1 and 8.6 serve as a guide for characterizing fading phenomena and their effects, Figure 8.13 can similarly serve to describe mitigation methods that can be used to ameliorate the effects of fading. The mitigation approach to be used should follow two basic steps: first, provide distortion mitigation and second, provide diversity.

8.11.1 Mitigation to Combat Frequency-Selective Distortion

- Equalization can compensate for the channel-induced ISI that is seen in frequency-selective fading. That is, it can help move the operating point from the error-performance curve that is "awful" in Figure 8.12 to the one that is "bad." The process of equalizing the ISI involves some method of gathering the dispersed symbol energy back together into its original time interval. In effect, equalization involves insertion of a filter to make the combination of channel and filter yield a flat response with linear phase. The phase linearity is achieved by making the equalizer filter the complex conjugate of the time reverse of the dispersed pulse [30]. Because in a mobile system the channel response varies with time, the equalizer filter must also change or adapt to the time-varying channel. Such equalizer filters are, therefore, called adaptive equalizers. An equalizer accomplishes more than distortion mitigation; it also provides diversity. Since distortion mitigation is achieved by gathering the dispersed symbol's energy back into the symbol's original time interval so that it does not hamper the detection of other symbols, the equalizer is simultaneously providing each received symbol with energy that would otherwise be lost.
- The decision feedback equalizer (DFE) has a feedforward section that is a linear transversal filter [30] whose length and tap weights are selected to coherently combine virtually all of the current symbol's energy. The DFE also has a feedback section which removes energy that remains from previously detected symbols [14,30–32]. The basic idea behind the DFE is that once an informa-

tion symbol has been detected, the ISI that it induces on future symbols can be estimated and subtracted before the detection of subsequent symbols.

- The maximum-likelihood sequence estimation (MLSE) equalizer tests all possible data sequences (rather than decoding each received symbol by itself) and chooses the data sequence that is the most probable of the candidates. The MLSE equalizer was first proposed by Forney [33] when he implemented the equalizer using the Viterbi decoding algorithm (VDA) [34]. The MLSE is optimal in the sense that it minimizes the probability of a sequence error. Because the VDA is the way in which the MLSE equalizer is typically implemented, the equalizer is often referred to as the *Viterbi equalizer*. Later in this chapter, we illustrate the adaptive equalization performed in the GSM using the Viterbi equalizer.
- Spread-spectrum techniques can be used to mitigate frequency-selective ISI distortion because the hallmark of any spread-spectrum system is its capability to reject interference, and ISI is a type of interference. Consider a direct-sequence spread-spectrum (DS/SS) binary phase shift keying (PSK) communication channel comprising one direct path and one reflected path. Assume that the propagation from transmitter to receiver results in a multipath wave that is delayed by τ_k compared to the direct wave. If the receiver is synchronized to the waveform arriving via the direct path, the received signal, $r(t)$, neglecting noise, can be expressed as

$$r(t) = Ax(t)g(t)\cos(2\pi f_c t) + \alpha Ax(t - \tau_k)\cos(2\pi f_c t + \Theta) \tag{8.24}$$

where $x(t)$ is the data signal, $g(t)$ is the PN spreading code, and τ_k is the differential time delay between the two paths. The angle Θ is a random phase, assumed to be uniformly distributed in the range $(0, 2\pi)$, and α is the attenuation of the multipath signal relative to the direct path signal. The receiver multiplies the incoming $r(t)$ by the code $g(t)$. If the receiver is synchronized to the direct path signal, multiplication by the code signal yields

$$Ax(t)g^2(t)\cos(2\pi f_c t) + \alpha Ax(t - \tau_k)g(t)g(t - \tau_k)\cos(2\pi f_c t + \Theta) \tag{8.25}$$

where $g^2(t) = 1$, and if τ_k is greater than the chip duration, then

$$\left|\int g^*(t)g(t - \tau_k)\, dt\right| \ll \int g^*(t)g(t)\, dt \tag{8.26}$$

over some appropriate interval of integration (correlation), where * indicates complex conjugate, and τ_k is equal to or larger than the PN chip duration. Thus, the spread-spectrum system effectively eliminates the multipath interference by virtue of its code-correlation receiver. Even though channel-induced ISI is typically transparent to DS/SS systems, such systems suffer from the loss in energy contained in all the multipath components not seen by the receiver. The need to gather up this lost energy belonging to the received chip was the motivation for developing the Rake receiver [35–37]. The Rake receiver dedicates a separate correlator to each multipath component (finger). It is able to coherently add the energy from each finger by selectively delaying them (the earliest component gets the longest delay) so that they can all be coherently combined.

- Earlier, we described a channel that could be classified as flat fading, but occasionally exhibits frequency-selective distortion when the null of the channel's frequency transfer function occurs at the center of the signal band. The use of DS/SS is a good way to mitigate such distortion because the wideband SS signal would span many lobes of the selectively faded frequency response. Hence, a great deal of pulse energy would then be passed by the scatterer medium, in contrast to the nulling effect on a relatively narrowband signal (see Figure 8.8c) [18].

- Frequency-hopping spread-spectrum (FH/SS) can be used to mitigate the distortion due to frequency-selective fading, provided the hopping rate is at least equal to the symbol rate. Compared to DS/SS, mitigation takes place through a different mechanism. FH receivers avoid multipath losses by rapid changes in the transmitter frequency band, thus avoiding the interference by changing the receiver band position before the arrival of the multipath signal.
- Orthogonal frequency-division multiplexing (OFDM) can be used in frequency-selective fading channels to avoid the use of an equalizer (or by altering the equalization task, so that it becomes a simple scaling in the frequency domain). The signal band is partitioned into multiple subbands, each one exhibiting a lower symbol rate than the original band; thus, the symbol duration is lengthened. The subbands are then transmitted on multiple orthogonal carriers. The goal is to reduce the symbol rate (signaling rate), $W \approx 1/T_s$, on each carrier to be less than the channel's coherence bandwidth f_0. OFDM was originally referred to as Kineplex. The technique has been implemented in the United States in mobile radio systems [38], and has been chosen by the European community under the name Coded OFDM (COFDM), for high-definition television (HDTV) broadcasting [39].
- Pilot signal is the name given to a signal intended to facilitate the coherent detection of waveforms. Pilot signals can be implemented in the frequency domain as an in-band tone [40], or in the time domain as a pilot sequence, which can also provide information about the channel state and thus improve performance in fading [41].

8.11.2 Mitigation to Combat Fast-Fading Distortion

- For fast-fading distortion, use a robust modulation (noncoherent or differentially coherent) that does not require phase tracking, and reduces the detector integration time [20].
- Increase the symbol rate, $W \approx 1/T_s$, to be greater than the fading rate, $f_d \approx 1/T_0$, by adding signal redundancy.
- Error-correction coding and interleaving can provide mitigation; it does so by reducing the required E_b/N_0. For a given E_b/N_0, with coding present, the error probability and error floor will be lowered compared to the uncoded case.
- An interesting filtering technique can provide mitigation in the event of fast-fading distortion and frequency-selective distortion occurring simultaneously. The frequency-selective distortion can be mitigated by the use of an OFDM signal set. Fast fading, however, will typically degrade conventional OFDM because the Doppler spreading corrupts the orthogonality of the OFDM subcarriers. A polyphase filtering technique [42] is used to provide time-domain shaping and duration extension to reduce the spectral sidelobes of the signal set and thus help preserve its orthogonality. The process introduces known ISI and adjacent channel interference (ACI) which are then removed by a postprocessing equalizer and canceling filter [43].

8.11.3 Mitigation to Combat Loss in SNR

After implementing some form of mitigation to combat the possible distortion (frequency selective or fast fading), the next step is to use some form of diversity to move the operating point from the error-performance curve labeled as "bad" in Figure 8.12 to a curve that approaches AWGN performance. The term "diversity" is used to denote the various methods available for providing the receiver with uncorrelated renditions of the signal. Uncorrelated is the important feature here, since it would not help the receiver to have additional copies of the signal if the copies were all equally poor. Listed below are some of the ways in which diversity can be implemented.

- Time diversity—Transmit the signal on L different time slots with time separation of at least T_0. Interleaving, often used with error-correction coding, is a form of time diversity.
- Frequency diversity—Transmit the signal on L different carriers with frequency separation of at least f_0. Bandwidth expansion is a form of frequency diversity. The signal bandwidth, W, is

expanded to be greater than f_0, thus providing the receiver with several independently fading signal replicas. This achieves frequency diversity of the order $L = W/f_0$. Whenever W is made larger than f_0, there is the potential for frequency-selective distortion unless we further provide some mitigation such as equalization. Thus, an expanded bandwidth can improve system performance (via diversity) only if the frequency-selective distortion the diversity may have introduced is mitigated.

- Spread spectrum is a form of bandwidth expansion that excels at rejecting interfering signals. In the case of direct-sequence spread-spectrum (DS/SS), it was shown earlier that multipath components are rejected if they are delayed by more than one chip duration. However, in order to approach AWGN performance, it is necessary to compensate for the loss in energy contained in those rejected components. The Rake receiver makes it possible to coherently combine the energy from each of the multipath components arriving along different paths. Thus, used with a Rake receiver, DS/SS modulation can be said to achieve path diversity. The Rake receiver is needed in phase-coherent reception, but in differentially coherent bit detection, a simple delay line (one bit long) with complex conjugation will do the trick [44].
- Frequency-hopping spread-spectrum (FH/SS) is sometimes used as a diversity mechanism. The GSM system uses slow FH (217 hops/s) to compensate for those cases where the mobile user is moving very slowly (or not at all) and happens to be in a spectral null.
- Spatial diversity is usually accomplished through the use of multiple receive antennas, separated by a distance of at least 10 wavelengths for a base station (much less for a mobile station). Signal processing must be employed to choose the best antenna output or to coherently combine all the outputs. Systems have also been implemented with multiple spaced transmitters; an example is the global positioning system (GPS).
- Polarization diversity [45] is yet another way to achieve additional uncorrelated samples of the signal.
- Any diversity scheme may be viewed as a trivial form of repetition coding in space or time. However, there exist techniques for improving the loss in SNR in a fading channel that are more efficient and more powerful than repetition coding. Error-correction coding represents a unique mitigation technique, because instead of providing more signal energy it reduces the required E_b/N_0 in order to accomplish the desired error performance. Error-correction coding coupled with interleaving [20,46–51] is probably the most prevalent of the mitigation schemes used to provide improved performance in a fading environment.

8.12 Summary of the Key Parameters Characterizing Fading Channels

We summarize the conditions that must be met so that the channel does not introduce frequency-selective distortion and fast-fading distortion. Combining the inequalities of Equations 8.14 and 8.23, we obtain

$$f_0 > W > f_d \tag{8.27a}$$

or

$$T_m < T_s < T_0 \tag{8.27b}$$

In other words, we want the channel coherence bandwidth to exceed our signaling rate, which in turn should exceed the fading rate of the channel. Recall that without distortion mitigation, f_0 sets an upper limit on signaling rate, and f_d sets a lower limit on it.

8.12.1 Fast-Fading Distortion: Example 1

If the inequalities of Equation 8.27 are not met and distortion mitigation is not provided, distortion will result. Consider the fast-fading case where the signaling rate is less than the channel fading rate, that is

$$f_0 > W < f_d \tag{8.28}$$

Mitigation consists of using one or more of the following methods. (See Figure 8.13.)

- Choose a modulation/demodulation technique that is most robust under fast-fading conditions. That means, for example, avoiding carrier recovery with PLLs since the fast fading could keep a PLL from achieving lock conditions.
- Incorporate sufficient redundancy so that the transmission symbol rate exceeds the channel fading rate. As long as the transmission symbol rate does not exceed the coherence bandwidth, the channel can be classified as flat fading. However, even flat fading channels will experience frequency-selective distortion whenever a channel null appears at the band center.

Since this happens only occasionally, mitigation might be accomplished by adequate error-correction coding and interleaving.

- The above two mitigation approaches should result in the demodulator operating at the Rayleigh limit [20] (see Figure 8.12). However, there may be an irreducible floor in the error-performance versus E_b/N_0 curve due to the FM noise that results from the random Doppler spreading. The use of an in-band pilot tone and a frequency-control loop can lower this irreducible performance level.
- To avoid this error floor caused by random Doppler spreading, increase the signaling rate above the fading rate still further (100–200 × fading rate) [27]. This is one architectural motive behind time-division multiple access (TDMA) mobile systems.
- Incorporate error-correction coding and interleaving to lower the floor and approach AWGN performance.

8.12.2 Frequency-Selective Fading Distortion: Example 2

Consider the frequency-selective case where the coherence bandwidth is less than the symbol rate, that is

$$f_0 < W > f_d \tag{8.29}$$

Mitigation consists of using one or more of the following methods. (See Figure 8.13.)

- Since the transmission symbol rate exceeds the channel-fading rate, there is no fast-fading distortion. Mitigation of frequency-selective effects is necessary. One or more of the following techniques may be considered:
- Adaptive equalization, spread spectrum (DS or FH), OFDM, pilot signal. The European GSM system uses a midamble training sequence in each transmission time slot so that the receiver can learn the impulse response of the channel. It then uses a Viterbi equalizer (explained later) for mitigating the frequency-selective distortion.
- Once the distortion effects have been reduced, introduce some form of diversity and error-correction coding and interleaving in order to approach AWGN performance. For direct-sequence spread-spectrum (DS/SS) signaling, the use of a Rake receiver (explained later) may be used for providing diversity by coherently combining multipath components that would otherwise be lost.

8.12.3 Fast-Fading and Frequency-Selective Fading Distortion: Example 3

Consider the case where the coherence bandwidth is less than the signaling rate, which in turn is less than the fading rate. The channel exhibits both fast-fading and frequency-selective fading which is expressed as

$$f_0 < W < f_d \tag{8.30a}$$

or

$$f_0 < f_d \tag{8.30b}$$

Recall from Equation 8.27 that f_0 sets an upper limit on signaling rate and f_d sets a lower limit on it. Thus, the situation expressed in Equation 8.30 is a difficult design problem because, unless distortion mitigation is provided, the maximum allowable signaling rate is (in the strict terms of the above discussion) less than the minimum allowable signaling rate. Mitigation in this case proceeds as follows. Note that, the initial steps are similar to those outlined in Example 1.

- Choose a modulation/demodulation technique that is most robust under fast-fading conditions.
- Use transmission redundancy in order to increase the transmitted symbol rate.
- Provide some form of frequency-selective mitigation in a manner similar to that outlined in Example 2.
- Once the distortion effects have been reduced, introduce some form of diversity and error-correction coding and interleaving in order to approach AWGN performance.

8.13 The Viterbi Equalizer as Applied to GSM

Figure 8.14 shows the GSM TDMA frame, having a duration of 4.615 ms and comprising eight slots, one assigned to each active mobile user. A normal transmission burst occupying one slot of time contains 57 message bits on each side of a 26-bit midamble called a *training* or *sounding sequence*. The slot-time

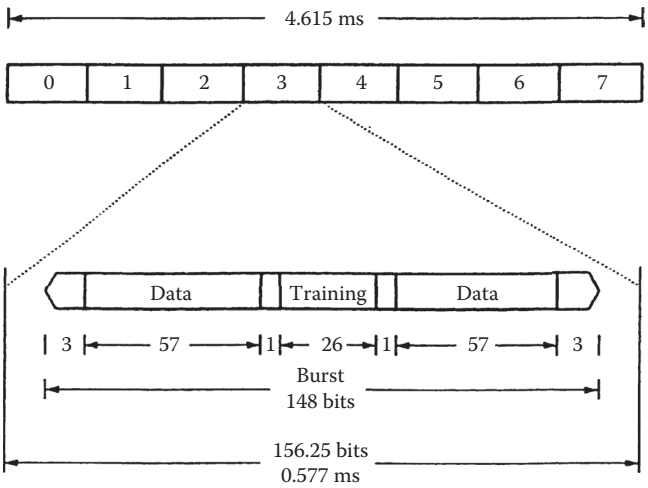

FIGURE 8.14 The GSM TDMA frame and time slot containing a normal burst.

duration is 0.577 ms (or the slot rate is 1733 slots/s). The purpose of the midamble is to assist the receiver in estimating the impulse response of the channel in an adaptive way (during the time duration of each 0.577 ms slot). In order for the technique to be effective, the fading behavior of the channel should not change appreciably during the time interval of one slot. In other words, there should not be any fast-fading degradation during a slot time when the receiver is using knowledge from the midamble to compensate for the channel's fading behavior. Consider the example of a GSM receiver used aboard a high-speed train, traveling at a constant velocity of 200 km/h (55.56 m/s). Assume the carrier frequency to be 900 MHz (the wavelength is $\lambda = 0.33$ m). From Equation 8.21, we can calculate that a half-wavelength is traversed in approximately the time (coherence time)

$$T_0 \approx \frac{\lambda/2}{V} \approx 3 \text{ ms} \tag{8.31}$$

Therefore, the channel coherence time is over five times greater than the slot time of 0.577 ms. The time needed for a significant change in fading behavior is relatively long compared to the time duration of one slot. Note that the choices made in the design of the GSM TDMA slot time and midamble were undoubtedly influenced by the need to preclude fast fading with respect to a slot-time duration, as in this example.

The GSM symbol rate (or bit rate, since the modulation is binary) is 271 kilosymbols/s and the bandwidth is $W = 200$ kHz. If we consider that the typical rms delay spread in an urban environment is of the order of $\sigma_\tau = 2$ μs, then using Equation 8.13 the resulting coherence bandwidth is $f_0 \approx 100$ kHz. It should therefore be apparent that since, in this case, $f_0 < W$, the GSM receiver must utilize some form of mitigation to combat frequency-selective distortion. To accomplish this goal, the Viterbi equalizer is typically implemented.

Figure 8.15 illustrates the basic functional blocks used in a GSM receiver for estimating the channel impulse response, which is then used to provide the detector with channel-corrected reference waveforms [52]. In the final step, the Viterbi algorithm is used to compute the MLSE of the message. As stated in Equation 8.2, a received signal, in the absence of noise, can be described in terms of the transmitted signal convolved with the impulse response of the channel, $h_c(t)$. We show this below, using the notation of a received training sequence, $r_{tr}(t)$, and the transmitted training sequence, $s_{tr}(t)$, as follows:

$$r_{tr}(t) = s_{tr}(t) * h_c(t) \tag{8.32}$$

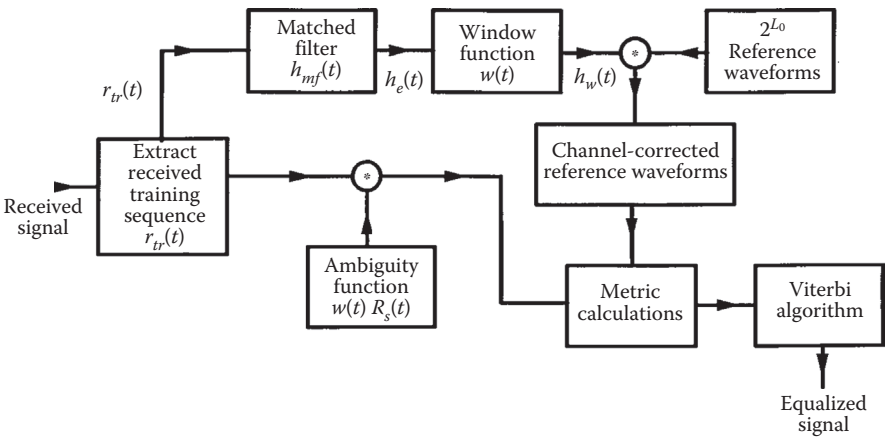

FIGURE 8.15 The Viterbi equalizer as applied to GSM.

where ⊠ denotes convolution, and noise has been neglected. At the receiver, $r_{tr}(t)$ is extracted from the normal burst and sent to a filter having impulse response, $h_{mf}(t)$, that is matched to $s_{tr}(t)$. This matched filter yields at its output an estimate of $h_c(t)$, denoted $h_e(t)$, developed from Equation 8.32 as follows:

$$\begin{aligned} h_e(t) &= r_{tr}(t) * h_{mf}(t) \\ &= s_{tr}(t) * h_c(t) * h_{mf}(t) \\ &= R_s(t) * h_c(t) \end{aligned} \tag{8.33}$$

where $R_s(t)$ is the autocorrelation function of $s_{tr}(t)$. If $R_s(t)$ is a highly peaked (impulse-like) function, then $h_e(t) \approx h_c(t)$.

Next, using a windowing function, $w(t)$, we truncate $h_e(t)$ to form a computationally affordable function, $h_w(t)$. The window length must be large enough to compensate for the effect of typical channel-induced ISI. The required observation interval L_0 for the window can be expressed as the sum of two contributions. The interval of length L_{CISI} is due to the controlled ISI caused by Gaussian filtering of the baseband pulses, which are then MSK modulated. The interval of length L_C is due to the channel-induced ISI caused by multipath propagation; therefore, L_0 can be written as

$$L_0 = L_{CISI} + L_C \tag{8.34}$$

The GSM system is required to provide mitigation for distortion due to signal dispersions of approximately 15–20 μs. The bit duration is 3.69 μs. Thus, the Viterbi equalizer used in GSM has a memory of 4–6 bit intervals. For each L_0-bit interval in the message, the function of the Viterbi equalizer is to find the most likely L_0-bit sequence out of the 2^{L_0} possible sequences that might have been transmitted. Determining the most likely L_0-bit sequence requires that 2^{L_0} meaningful reference waveforms be created by modifying (or disturbing) the 2^{L_0} ideal waveforms in the same way that the channel has disturbed the transmitted message. Therefore, the 2^{L_0} reference waveforms are convolved with the windowed estimate of the channel impulse response, $h_w(t)$ in order to derive the disturbed or channel-corrected reference waveforms. Next, the channel-corrected reference waveforms are compared against the received data waveforms to yield metric calculations. However, before the comparison takes place, the received data waveforms are convolved with the known windowed autocorrelation function $w(t)$ $R_s(t)$, transforming them in a manner comparable to that applied to the reference waveforms. This filtered message signal is compared to all possible 2^{L_0} channel-corrected reference signals, and metrics are computed as required by the VDA. The VDA yields the maximum-likelihood estimate of the transmitted sequence [34].

8.14 The Rake Receiver Applied to Direct-Sequence Spread-Spectrum (DS/SS) Systems

Interim Specification 95 (IS-95) describes a DS/SS cellular system that uses a Rake receiver [35–37] to provide path diversity. In Figure 8.16, five instances of chip transmissions corresponding to the code sequence 1 0 1 1 1 are shown, with the transmission or observation times labeled t_{-4} for the earliest transmission and t_0 for the latest. Each abscissa shows three "fingers" of a signal that arrive at the receiver with delay times τ_1, τ_2, and τ_3. Note that such baseband pulses are typically bipolar $\in(+1,-1)$. But for simplicity, they are all shown with positive polarity. Assume that the intervals between the t_i transmission times and the intervals between the τ_i delay times are each one chip long. From this, one can conclude that the finger arriving at the receiver at time t_{-4}, with delay τ_3, is time coincident with two other fingers, namely the fingers arriving at times t_{-3} and t_{-2} with delays τ_2 and τ_1, respectively. Since, in this example, the delayed components are separated by exactly one chip time, they are just resolvable. At the

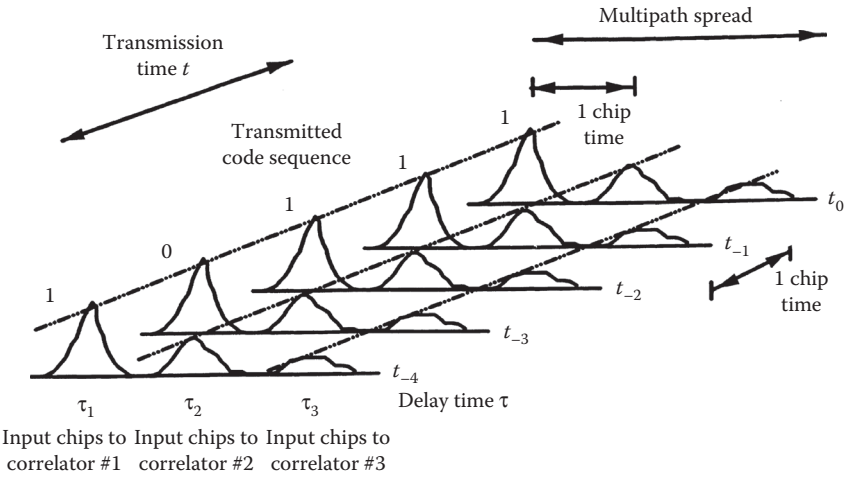

FIGURE 8.16 Example of received chip seen by a three-finger Rake receiver.

receiver, there must be a sounding device that is dedicated to estimating the τ_i delay times. Note that for a terrestrial mobile radio system, the fading rate is relatively slow (milliseconds) or the channel coherence time large compared to the chip time ($T_0 > T_{ch}$). Hence, the changes in τ_i occur slowly enough so that the receiver can readily adapt to them.

Once the τ_i delays are estimated, a separate correlator is dedicated to processing each finger. In this example, there would be three such dedicated correlators, each one processing a delayed version of the same chip sequence 1 0 1 1 1. In Figure 8.16, each correlator receives chips with power profiles represented by the sequence of fingers shown along a diagonal line. Each correlator attempts to match these arriving chips with the same PN code, similarly delayed in time. At the end of a symbol interval (typically there may be hundreds or thousands of chips per symbol), the outputs of the correlators are coherently combined, and symbol detection is made. At the chip level, the Rake receiver resembles an equalizer, but its real function is to provide diversity.

The interference-suppression nature of DS/SS systems stems from the fact that a code sequence arriving at the receiver merely one chip time late, will be approximately orthogonal to the particular PN code with which the sequence is correlated. Therefore, any code chips that are delayed by one or more chip times will be suppressed by the correlator. The delayed chips only contribute to raising the noise floor (correlation sidelobes). The mitigation provided by the Rake receiver can be termed path diversity, since it allows the energy of a chip that arrives via multiple paths to be combined coherently. Without the Rake receiver, this energy would be transparent and therefore lost to the DS/SS system. In Figure 8.16, looking vertically above point τ_3, it is clear that there is interchip interference due to different fingers arriving simultaneously. The spread-spectrum processing gain allows the system to endure such interference at the chip level. No other equalization is deemed necessary in IS-95.

8.15 Example of a DS/SS System Using a Rake Receiver

Figure 8.17a shows the Barker [1] sequence 1 0 1 1 1 (repeated three times), represented with pulses $\in (+1, -1)$. This sequence serves as the spreading code for a DS/SS example. Similarly Figure 8.17b shows the data sequence 1 0 1, similarly represented with pulses $\in (+1, -1)$. Assume that the three data bits 1 0 1 are being sent over a multipath channel via a DS/SS transmission system. Also assume that the channel manifests three returns or fingers for each transmitted chip (one with zero excess delay, plus two delayed echos). Thus, the Rake receiver as described in Section 8.14 requires three correlators (plus an additional

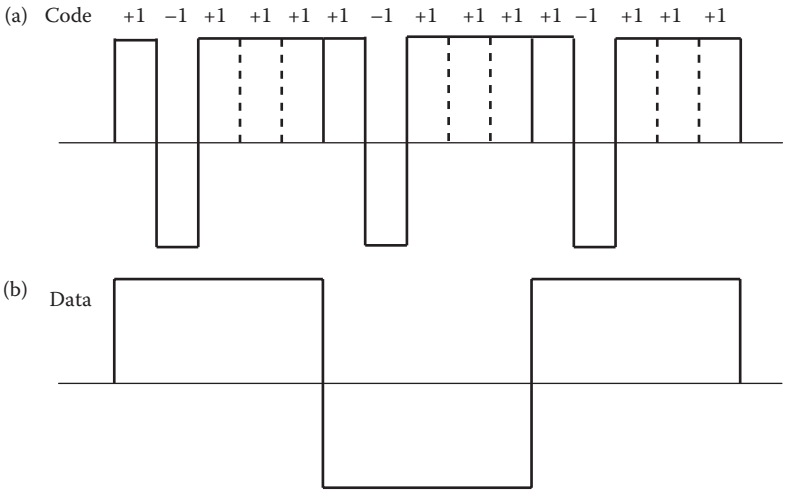

FIGURE 8.17 Example of DS/SS signaling. (a) Barker sequence 1 0 1 1 1 (repeated 3 times) represented with bipolar pulses and (b) data sequence 1 0 1 represented with bipolar pulses.

sounding device to learn the delay times of the arriving fingers). For convenience, assume that the three fingers are each separated by one chip time (corresponding to Figure 8.16).

Figure 8.18a shows the pulse sequence (at the transmitter) which results from the multiplication of data and code. Figure 8.18b shows delayed pulse values (neglecting noise) received due to the multipath channel. To appreciate the motivation that drove Paul Green and Bob Price [35] to invent the Rake receiver, consider the three delayed sequences in Figure 8.18b. They each carry a portion of the overall energy intended for the receiver. However, *without* the Rake methodology, the receiver could only be locked on to one of the three sequences, and the other two would be invisible (lost energy). The Rake receiver invention provides a way of capturing that lost energy.

At the receiver, there are as many correlators implemented as there are finger returns that need to be accounted for (in this example, we are assuming three correlators, plus a sounder device). In Figure 8.18b,

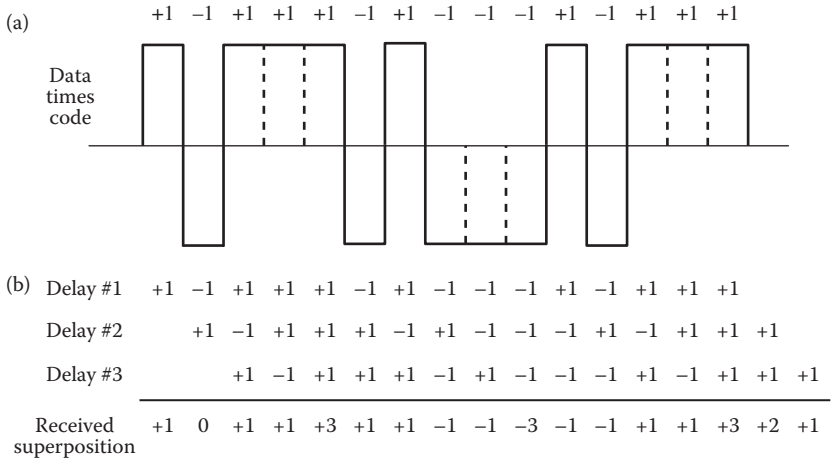

FIGURE 8.18 DS/SS chips received over a multipath channel. (a) Multiplication of data with the code (at the transmitter) and (b) received superposition signal (neglecting noise) is seen by each correlator.

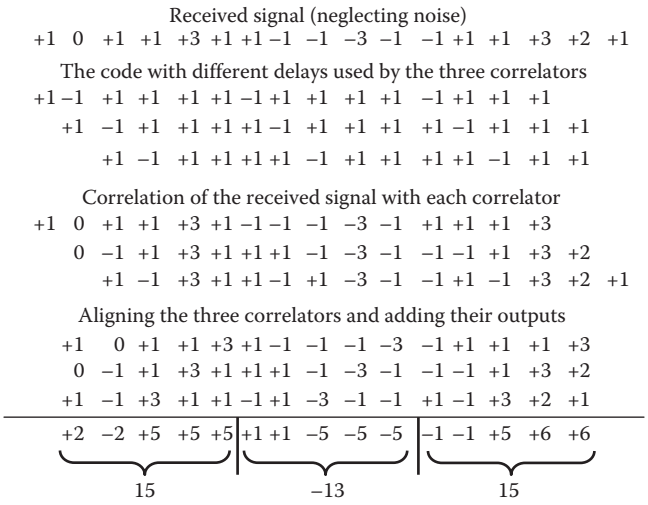

FIGURE 8.19 Detection of DS/SS chips using a three-finger Rake receiver.

the bottom pulse sequence represents the superposition of all three sequences that is seen by each correlator.

In Figure 8.19, the received sequence from Figure 8.18b is repeated. Detection of the DS/SS chips can then be described as follows. In this figure, we see the three delayed versions of the spreading code (one used by each correlator). Next, we see the correlation (multiplication) of the received signal with each correlator's delayed code, followed by the alignment of the three correlator outputs. The next step, of adding the correlator outputs, accomplishes the coherent combining of the correlator outputs. The very last bit-detection step is one of integration (summing the combined chip values over a bit time). In this example, the final integrated values 15, –13, 15 from this detection yields the correctly detected data sequence 1 0 1.

8.16 Conclusion

In this chapter, the major elements that contribute to fading in a communication channel have been characterized. Figure 8.1 was presented as a guide for the characterization of fading phenomena. Two types of fading, large scale and small scale, were described. Two manifestations of small-scale fading (signal dispersion and fading rapidity) were examined, and the examination involved two views, time and frequency. Two degradation categories were defined for dispersion: frequency-selective fading and flat fading. Two degradation categories were defined for fading rapidity: fast and slow. The small-scale fading degradation categories are summarized in Figure 8.6. A mathematical model using correlation and power density functions is presented in Figure 8.7. This model yields a nice symmetry, a kind of "poetry" to help us view the Fourier transform and duality relationships that describe the fading phenomena. Further, mitigation techniques for ameliorating the effects of each degradation category were treated, and these techniques are summarized in Figure 8.13. Finally, mitigation methods that have been implemented in two system types, GSM and CDMA systems meeting IS-95, were described.

References

1. Sklar, B., *Digital Communications: Fundamentals and Applications*, 2nd Edition, Prentice-Hall, Upper Saddle River, NJ, 2001.
2. Van Trees, H. L., *Detection, Estimation, and Modulation Theory, Part I*, John Wiley & Sons, New York, Ch. 4, 1968.

3. Rappaport, T. S., *Wireless Communications*, Prentice-Hall, Upper Saddle River, NJ, Chs. 3 and 4, 1996.
4. Greenwood, D. and Hanzo, L., Characterisation of mobile radio channels, In: *Mobile Radio Communications*, Steele, R., Ed., Pentech Press, London, Ch. 2, 1994.
5. Lee, W. C. Y., Elements of cellular mobile radio systems, *IEEE Trans. Vehicular Technol.*, 35(2), 48–56, 1986.
6. Okumura, Y. et al., Field strength and its variability in VHF and UHF land mobile radio service, *Rev. Elec. Comm. Lab.*, 16(9–10), 825–873, 1968.
7. Hata, M., Empirical formulae for propagation loss in land mobile radio services, *IEEE Trans. Vehicular Technol.*, VT-29(3), 317–325, 1980.
8. Seidel, S. Y. et al., Path loss, scattering and multipath delay statistics in four European cities for digital cellular and microcellular radiotelephone, *IEEE Trans. Vehicular Technol.*, 40(4), 721–730, 1991.
9. Cox, D. C., Murray, R., and Norris, A., 800 MHz Attenuation measured in and around suburban houses, *AT&T Bell Lab. Tech. J.*, 673(6), 921–954, 1984.
10. Schilling, D. L. et al., Broadband CDMA for personal communications systems, *IEEE Commun. Mag.*, 29(11), 86–93, 1991.
11. Andersen, J. B., Rappaport, T. S., and Yoshida, S., Propagation measurements and models for wireless communications channels, *IEEE Commun. Mag.*, 33(1), 42–49, 1995.
12. Amoroso, F., Investigation of signal variance, bit error rates and pulse dispersion for DSPN signalling in a mobile dense scatterer ray tracing model, *Int. J. Satellite Commun.*, 12, 579–588, 1994.
13. Bello, P. A., Characterization of randomly time-variant linear channels, *IEEE Trans. Commun. Syst.*, 360–393, 1963.
14. Proakis, J. G., *Digital Communications*, McGraw-Hill, New York, Ch. 7, 1983.
15. Green, P. E., Jr., Radar astronomy measurement techniques, *MIT Lincoln Laboratory*, Lexington, MA, Tech. Report No. 282, Dec. 1962.
16. Pahlavan, K. and Levesque, A. H., *Wireless Information Networks*, John Wiley & Sons, New York, Chs. 3 and 4, 1995.
17. Lee, W. Y. C., *Mobile Cellular Communications*, McGraw-Hill, New York, 1989.
18. Amoroso, F., Use of DS/SS signalling to mitigate Rayleigh fading in a dense scatterer environment, *IEEE Personal Commun.*, 3(2), 52–61, 1996.
19. Clarke, R. H., A statistical theory of mobile radio reception, *Bell Syst. Tech. J.*, 47(6), 957–1000, 1968.
20. Bogusch, R. L., *Digital Communications in Fading Channels: Modulation and Coding*, Mission Research Corp., Santa Barbara, California, Report No. MRC-R-1043, March 11, 1987.
21. Amoroso, F., The bandwidth of digital data signals, *IEEE Commun. Mag.*, 18(6), 13–24, 1980.
22. Bogusch, R. L. et al., Frequency selective propagation effects on spread-spectrum receiver tracking, *Proc. IEEE*, 69(7), 787–796, 1981.
23. Jakes, W. C., Ed., *Microwave Mobile Communications*, John Wiley & Sons, New York, 1974.
24. *Joint Technical Committee of Committee T1 R1P1.4 and TIA TR46.3.3/TR45.4.4 on Wireless Access*, Draft Final Report on RF Channel Characterization, Paper No. JTC(AIR)/94.01.17–238R4, January 17, 1994.
25. Bello, P. A. and Nelin, B. D., The influence of fading spectrum on the binary error probabilities of incoherent and differentially coherent matched filter receivers, *IRE Trans. Commun. Syst.*, CS-10, 160–168, 1962.
26. Amoroso, F., Instantaneous frequency effects in a Doppler scattering environment, *IEEE International Conference on Communications*, 1458–1466, June 7–10, 1987.
27. Bateman, A. J. and McGeehan, J. P., Data transmission over UHF fading mobile radio channels, *IEEE Proc., 131*, Pt. F(4), 364–374, 1984.
28. Feher, K., *Wireless Digital Communications*, Prentice-Hall, Upper Saddle River, NJ, 1995.
29. Davarian, F., Simon, M., and Sumida, J., DMSK: A practical 2400-bps receiver for the mobile satellite service, Jet Propulsion Laboratory Publication 85–51 (MSAT-X Report No. 111), June 15, 1985.

30. Rappaport, T. S., *Wireless Communications*, Prentice-Hall, Upper Saddle River, NJ, Ch. 6, 1996.
31. Bogusch, R. L., Guigliano, F. W., and Knepp, D. L., Frequency-selective scintillation effects and decision feedback equalization in high data-rate satellite links, *Proc. IEEE*, 71(6), 754–767, 1983.
32. Qureshi, S. U. H., Adaptive equalization, *Proc. IEEE*, 73(9), 1340–1387, 1985.
33. Forney, G. D., The Viterbi algorithm, *Proc. IEEE*, 61(3), 268–278, 1978.
34. Sklar, B., Digital *Communications: Fundamentals and Applications*, 2nd Edition, Prentice-Hall, Upper Saddle River, NJ, Ch. 7, 1988.
35. Price, R. and Green, P. E., Jr., A communication technique for multipath channels, *Proc. IRE*, 555–570, 1958.
36. Turin, G. L., Introduction to spread-spectrum antimultipath techniques and their application to urban digital radio, *Proc. IEEE*, 68(3), 328–353, 1980.
37. Simon, M. K., Omura, J. K., Scholtz, R. A., and Levitt, B. K., *Spread Spectrum Communications Handbook*, McGraw-Hill, New York, 1994.
38. Birchler, M. A. and Jasper, S. C., A 64 kbps Digital Land Mobile Radio System Employing M-16QAM, *Proceedings of the 1992 IEEE Int. Conference on Selected Topics in Wireless Communications*, Vancouver, British Columbia, 158–162, June 25–26, 1992.
39. Sari, H., Karam, G., and Jeanclaude, I., Transmission techniques for digital terrestrial TV broadcasting, *IEEE Commun. Mag.*, 33(2), 100–109, 1995.
40. Cavers, J. K., The performance of phase locked transparent tone-in-band with symmetric phase detection, *IEEE Trans. Commun.*, 39(9), 1389–1399, 1991.
41. Moher, M. L. and Lodge, J. H., TCMP—A modulation and coding strategy for Rician fading channel, *IEEE J. Selected Areas Commun.*, 7(9), 1347–1355, 1989.
42. Harris, F., On the relationship between multirate polyphase FIR filters and windowed, over-lapped FFT processing, *Proceedings of the Twenty Third Annual Asilomar Conference on Signals, Systems, and Computers*, Pacific Grove, California, 485–488, October 30 to November 1, 1989.
43. Lowdermilk, R. W. and Harris, F., Design and performance of fading insensitive orthogonal frequency division multiplexing (OFDM) using polyphase filtering techniques, *Proceedings of the Thirtieth Annual Asilomar Conference on Signals, Systems, and Computers*, Pacific Grove, California, November 3–6, 1996.
44. Kavehrad, M. and Bodeep, G. E., Design and experimental results for a direct-sequence spread-spectrum radio using differential phase-shift keying modulation for indoor wireless communications, *IEEE JSAC*, SAC-5(5), 815–823, 1987.
45. Hess, G. C., *Land-Mobile Radio System Engineering*, Artech House, Boston, 1993.
46. Hagenauer, J. and Lutz, E., Forward error correction coding for fading compensation in mobile satellite channels, *IEEE JSAC*, SAC-5(2), 215–225, 1987.
47. McLane, P. I. et al., PSK and DPSK trellis codes for fast fading, shadowed mobile satellite communication channels, *IEEE Trans. Commun.*, 36(11), 1242–1246, 1988.
48. Schlegel, C. and Costello, D. J., Jr., Bandwidth efficient coding for fading channels: Code construction and performance analysis, *IEEE JSAC*, 7(9), 1356–1368, 1989.
49. Edbauer, F., Performance of interleaved trellis-coded differential 8–PSK modulation over fading channels, *IEEE J. Selected Areas Commun.*, 7(9), 1340–1346, 1989.
50. Soliman, S. and Mokrani, K., Performance of coded systems over fading dispersive channels, *IEEE Trans. Commun.*, 40(1), 51–59, 1992.
51. Divsalar, D. and Pollara, F., Turbo codes for PCS applications, *Proc. ICC'95*, Seattle, Washington, 54–59, June 18–22, 1995.
52. Hanzo, L. and Stefanov, J., The Pan-European digital cellular mobile radio system—known as GSM, In: *Mobile Radio Communications.* Steele, R., Ed., Pentech Press, London, Ch. 8, 1992.

9

Channel Equalization

John G. Proakis

9.1 Characterization of Channel Distortion

Many communication channels, including telephone channels and some radio channels, may be generally characterized as band-limited linear filters. Consequently, such channels are described by their frequency response $C(f)$, which may be expressed as

$$C(f) = A(f)e^{j\theta(f)} \tag{9.1}$$

where $A(f)$ is called the *amplitude response* and $\theta(f)$ is called the *phase response*. Another characteristic that is sometimes used in place of the phase response is the *envelope delay* or *group delay*, which is defined as

$$\tau(f) = -\frac{1}{2\pi}\frac{d\theta(f)}{df} \tag{9.2}$$

A channel is said to be nondistorting or ideal if, within the bandwidth W occupied by the transmitted signal, $A(f) = \text{const}$ and $\theta(f)$ is a linear function of frequency [or the envelope delay $\tau(f) = \text{const}$]. On the other hand, if $A(f)$ and $\tau(f)$ are not constant within the bandwidth occupied by the transmitted signal, the channel distorts the signal. If $A(f)$ is not constant, the distortion is called *amplitude distortion* and if $\tau(f)$ is not constant, the distortion on the transmitted signal is called *delay distortion*.

As a result of the amplitude and delay distortion caused by the nonideal channel frequency response characteristic $C(f)$, a succession of pulses transmitted through the channel at rates comparable to the bandwidth W are smeared to the point that they are no longer distinguishable as well-defined pulses at the receiving terminal. Instead, they overlap and, thus, we have *intersymbol interference* (ISI). As an example of the effect of delay distortion on a transmitted pulse, Figure 9.1a illustrates a band-limited

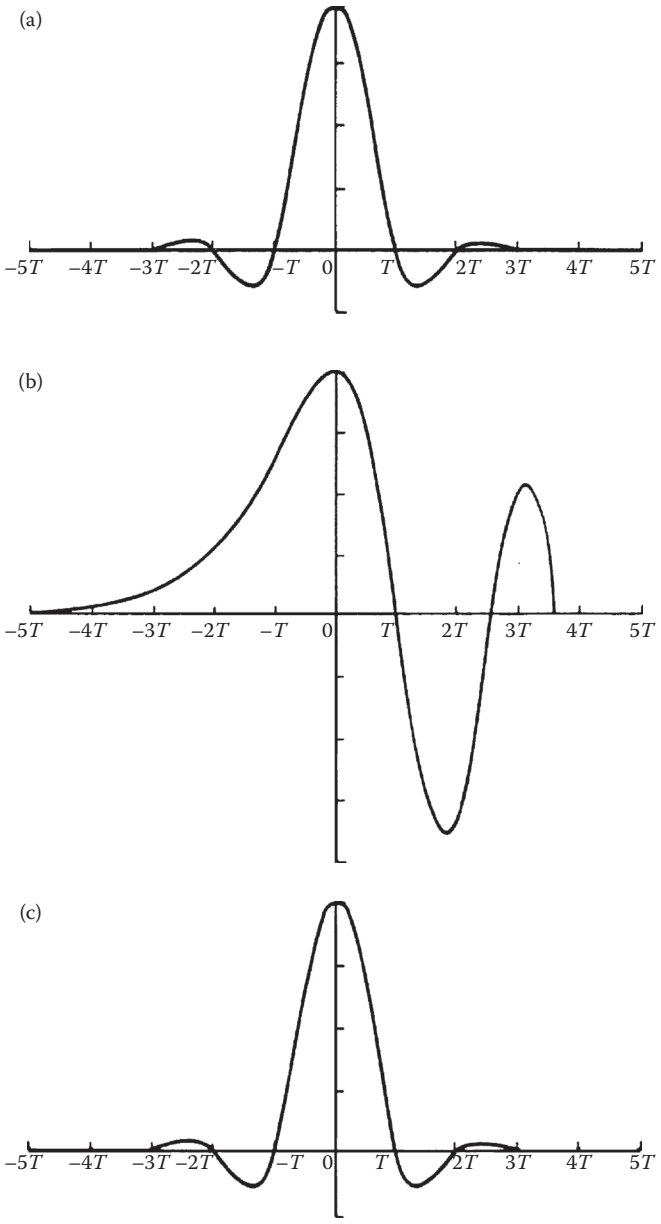

FIGURE 9.1 Effect of channel distortion: (a) channel input, (b) channel output, and (c) equalizer output.

pulse having zeros periodically spaced in time at points labeled $\pm T$, $\pm 2T$, and so on. If information is conveyed by the pulse amplitude, as in pulse amplitude modulation (PAM), for example, then one can transmit a sequence of pulses, each of which has a peak at the periodic zeros of the other pulses. Transmission of the pulse through a channel modeled as having a linear envelope delay characteristic $\tau(f)$ [quadratic phase $\theta(f)$], however, results in the received pulse shown in Figure 9.1b having zero crossings that are no longer periodically spaced. Consequently, a sequence of successive pulses would be smeared into one another, and the peaks of the pulses would no longer be distinguishable. Thus, the channel delay distortion results in intersymbol interference. As is discussed in this chapter, it is possible to compensate for the nonideal frequency response characteristic of the channel by use of a filter or

equalizer at the demodulator. Figure 9.1c illustrates the output of a linear equalizer that compensates for the linear distortion in the channel.

The extent of the intersymbol interference on a telephone channel can be appreciated by observing a frequency response characteristic of the channel. Figure 9.2 illustrates the measured average amplitude and delay as a function of frequency for a medium-range (180–725 mi) telephone channel of the switched telecommunications network as given by Duffy and Tratcher, 1971. We observe that the usable band of the channel extends from about 300 to about 3000 Hz. The corresponding impulse response of the average channel is shown in Figure 9.3. Its duration is about 10 ms. In comparison, the transmitted symbol rates on such a channel may be of the order of 2500 pulses or symbols per second. Hence, intersymbol interference might extend over 20–30 symbols.

Besides telephone channels, there are other physical channels that exhibit some form of time dispersion and, thus, introduce intersymbol interference. Radio channels, such as short-wave ionospheric propagation (HF), tropospheric scatter, and mobile cellular radio are three examples of time-dispersive wireless channels. In these channels, time dispersion and, hence, intersymbol interference is the result of multiple propagation paths with different path delays. The number of paths and the relative time delays among the paths vary with time and, for this reason, these radio channels are usually called time-variant multipath channels. The time-variant multipath conditions give rise to a wide variety of frequency

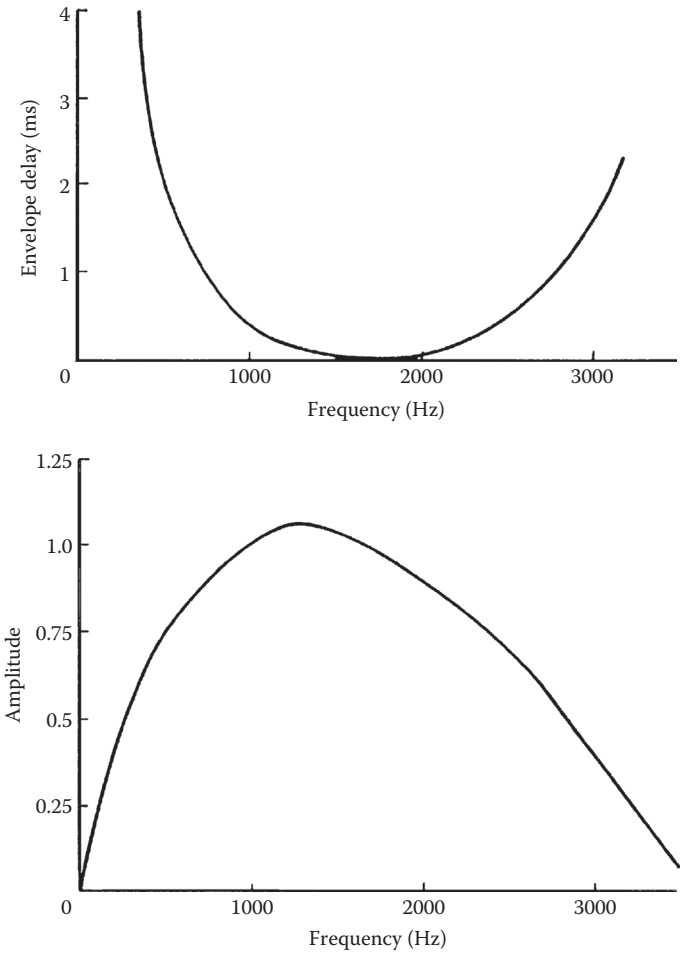

FIGURE 9.2 Average amplitude and delay characteristics of medium-range telephone channel.

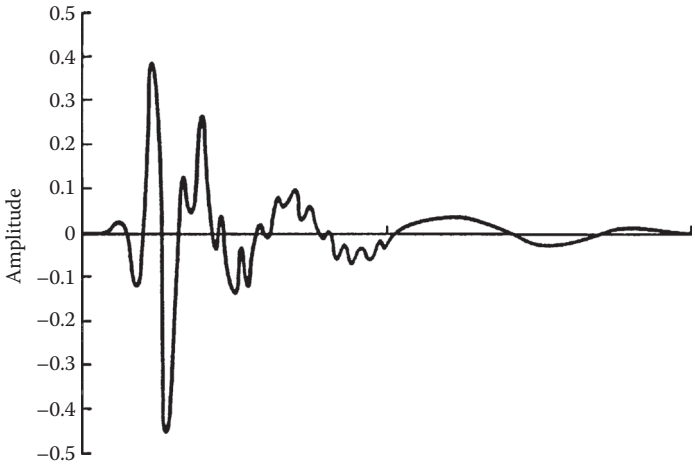

FIGURE 9.3 Impulse response of average channel with amplitude and delay shown in Figure 9.2.

response characteristics. Consequently, the frequency response characterization that is used for telephone channels is inappropriate for time-variant multipath channels. Instead, these radio channels are characterized statistically in terms of the scattering function, which, in brief, is a two-dimensional representation of the average received signal power as a function of relative time delay and Doppler frequency (see Proakis [4]).

For illustrative purposes, a scattering function measured on a medium-range (150 mi) tropospheric scatter channel is shown in Figure 9.4. The total time duration (multipath spread) of the channel response is approximately 0.7 μs on the average, and the spread between half-power points in Doppler

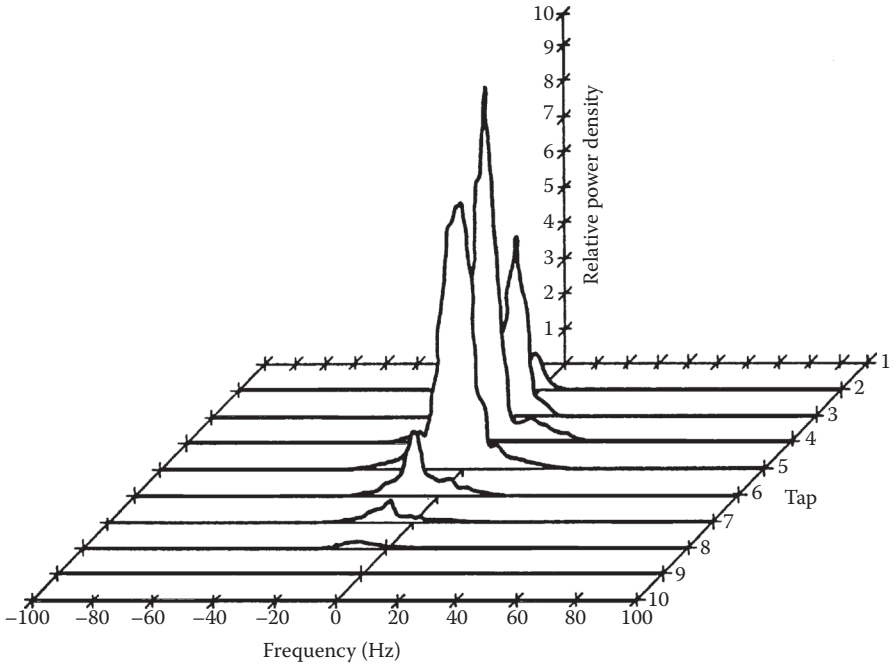

FIGURE 9.4 Scattering function of a medium-range tropospheric scatter channel.

frequency is a little less than 1 Hz on the strongest path and somewhat larger on the other paths. Typically, if one is transmitting at a rate of 10^7 symbols/s over such a channel, the multipath spread of 0.7 μs will result in intersymbol interference that spans about seven symbols.

9.2 Characterization of Intersymbol Interference

In a digital communication system, channel distortion causes intersymbol interference, as illustrated in the preceding section. In this section, we shall present a model that characterizes the ISI. The digital modulation methods to which this treatment applies are PAM, phase-shift keying (PSK), and quadrature amplitude modulation (QAM). The transmitted signal for these three types of modulation may be expressed as

$$\begin{aligned} s(t) &= \upsilon_c(t)\cos 2\pi f_c t - \upsilon_s(t)\sin 2\pi f_c t \\ &= \mathrm{Re}[\upsilon(t)e^{j2\pi f_c t}] \end{aligned} \tag{9.3}$$

where $\upsilon(t) = \upsilon_c(t) + j\upsilon_s(t)$ is called the *equivalent low-pass signal*, f_c is the carrier frequency, and Re[ ] denotes the real part of the quantity in brackets.

In general, the equivalent low-pass signal is expressed as

$$\upsilon(t) = \sum_{n=0}^{\infty} I_n g_T(t - nT) \tag{9.4}$$

where $g_T(t)$ is the basic pulse shape that is selected to control the spectral characteristics of the transmitted signal, $\{I_n\}$ the sequence of transmitted information symbols selected from a signal constellation consisting of M points, and T the signal interval ($1/T$ is the symbol rate). For PAM, PSK, and QAM, the values of I_n are points from M-ary signal constellations. Figure 9.5 illustrates the signal constellations for the case of $M = 8$ signal points. Note that for PAM, the signal constellation is one dimensional. Hence, the equivalent low-pass signal $\upsilon(t)$ is real valued, that is, $\upsilon_s(t) = 0$ and $\upsilon_c(t) = \upsilon(t)$. For M-ary ($M > 2$) PSK and QAM, the signal constellations are two dimensional and, hence, $\upsilon(t)$ is complex valued.

The signal $s(t)$ is transmitted over a bandpass channel that may be characterized by an equivalent low-pass frequency response $C(f)$. Consequently, the equivalent low-pass received signal can be represented as

$$r(t) = \sum_{n=0}^{\infty} I_n h(t - nT) + w(t) \tag{9.5}$$

where $h(t) = g_T(t)^* c(t)$, and $c(t)$ is the impulse response of the equivalent low-pass channel, the asterisk denotes convolution, and $w(t)$ represents the additive noise in the channel.

To characterize the ISI, suppose that the received signal is passed through a receiving filter and then sampled at the rate of $1/T$ samples/s. In general, the optimum filter at the receiver is matched to the received signal pulse $h(t)$. Hence, the frequency response of this filter is $H^*(f)$. We denote its output as

$$y(t) = \sum_{n=0}^{\infty} I_n x(t - nT) + \nu(t) \tag{9.6}$$

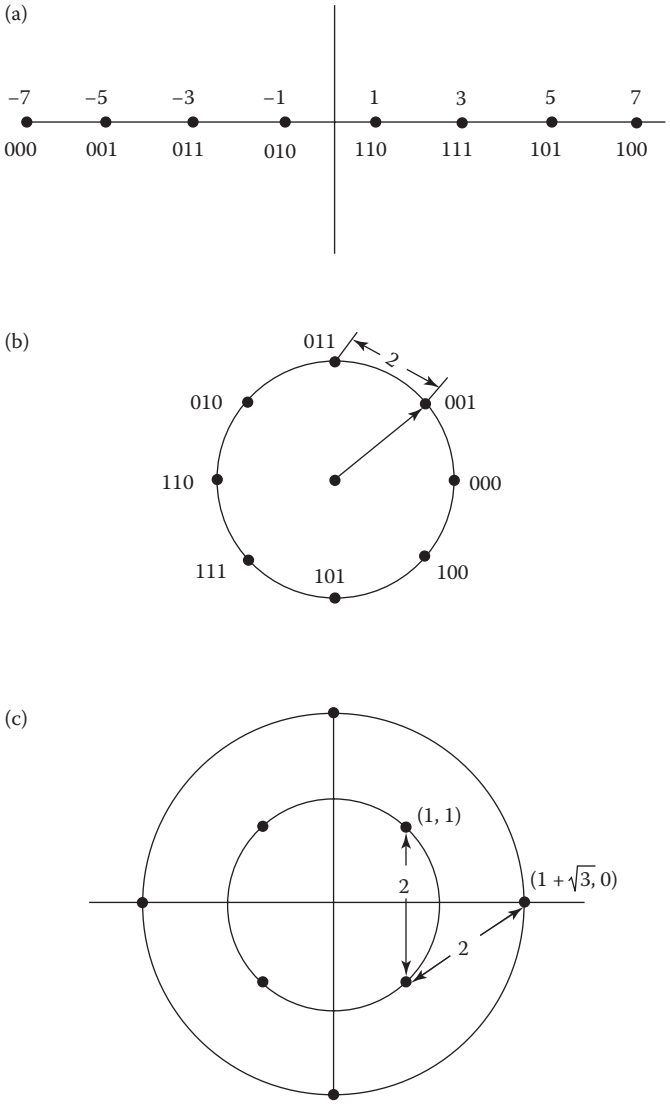

FIGURE 9.5 $M = 8$ signal constellations for (a) PAM, (b) PSK, and (c) QAM.

where $x(t)$ is the signal pulse response of the receiving filter, that is, $X(f) = H(f)H^*(f) = |H(f)|^2$, and $\nu(t)$ is the response of the receiving filter to the noise $w(t)$. Now, if $y(t)$ is sampled at times $t = kT$, $k = 0, 1, 2, \ldots$, we have

$$y(kT) \equiv y_k = \sum_{n=0}^{\infty} I_n x(kT - nT) + \nu(kT)$$
$$= \sum_{n=0}^{\infty} I_n x_{k-n} + \nu_k, \quad k = 0,1,\ldots \tag{9.7}$$

The sample values $\{y_k\}$ can be expressed as

$$y_k = x_0\left(I_k + \frac{1}{x_0}\sum_{\substack{n=0\\n\neq k}}^{\infty} I_n x_{k-n}\right) + \nu_k, \quad k = 0,1,\ldots \tag{9.8}$$

The term x_0 is an arbitrary scale factor, which we arbitrarily set equal to unity for convenience. Then

$$y_k = I_k + \sum_{\substack{n=0\\n\neq k}}^{\infty} I_n x_{k-n} + \nu_k \tag{9.9}$$

The term I_k represents the desired information symbol at the kth sampling instant, the term

$$\sum_{\substack{n=0\\n\neq k}}^{\infty} I_n x_{k-n} \tag{9.10}$$

represents the ISI, and ν_k is the additive noise variable at the kth sampling instant.

The amount of ISI, and noise in a digital communication system can be viewed on an oscilloscope. For PAM signals, we can display the received signal $y(t)$ on the vertical input with the horizontal sweep rate set at $1/T$. The resulting oscilloscope display is called an *eye pattern* because of its resemblance to the human eye. For example, Figure 9.6 illustrates the eye patterns for binary and four-level PAM modulation. The effect of ISI is to cause the eye to close, thereby reducing the margin for additive noise to cause errors. Figure 9.7 graphically illustrates the effect of ISI in reducing the opening of a binary eye. Note that intersymbol interference distorts the position of the zero crossings and causes a reduction in the eye opening. Thus, it causes the system to be more sensitive to a synchronization error.

For PSK and QAM, it is customary to display the eye pattern as a two-dimensional scatter diagram illustrating the sampled values $\{y_k\}$ that represent the decision variables at the sampling instants. Figure 9.8 illustrates such an eye pattern for an 8-PSK signal. In the absence of intersymbol interference and noise, the superimposed signals at the sampling instants would result in eight distinct points corresponding to the eight transmitted signal phases. Intersymbol interference and noise result in a deviation of the received

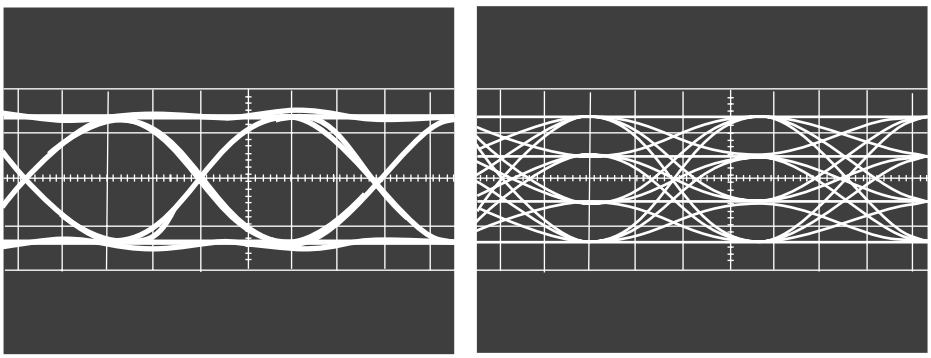

FIGURE 9.6 Examples of eye patterns for binary and quaternary amplitude shift keying (or PAM).

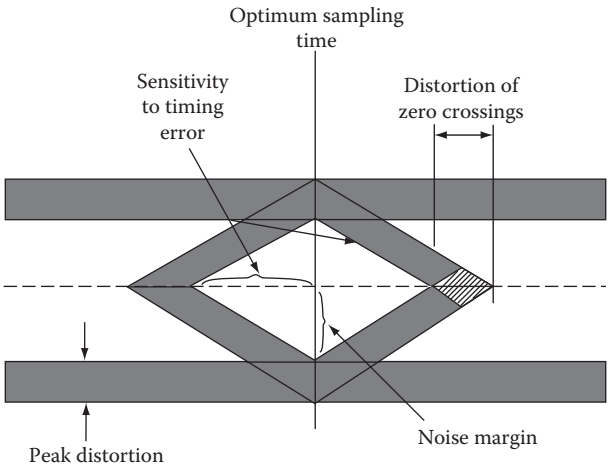

FIGURE 9.7 Effect of intersymbol interference on eye opening.

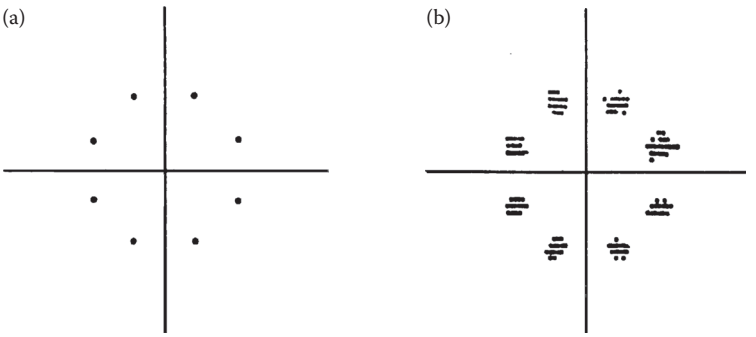

FIGURE 9.8 Two-dimensional digital eye patterns. (a) Transmitted eight-phase signal and (b) received signal samples at the output of demodulation.

samples $\{y_k\}$ from the desired 8-PSK signal. The larger the intersymbol interference and noise, the larger the scattering of the received signal samples relative to the transmitted signal points.

In practice, the transmitter and receiver filters are designed for zero ISI at the desired sampling times $t = kT$. Thus, if $G_T(f)$ is the frequency response of the transmitter filter and $G_R(f)$ is the frequency response of the receiver filter, then the product $G_T(f)\, G_R(f)$ is designed to yield zero ISI.

For example, the product $G_T(f)\, G_R(f)$ may be selected as

$$G_T(f)G_R(f) = X_{rc}(f) \tag{9.11}$$

where $X_{rc}(f)$ is the raised-cosine frequency response characteristic, defined as

$$X_{rc}(f) = \begin{cases} T, & 0 \le |f| \le \dfrac{(1-\alpha)}{2T} \\ \dfrac{T}{2}\left[1 + \cos\dfrac{\pi T}{\alpha}\left(|f| - \dfrac{1-\alpha}{2T}\right)\right], & \dfrac{1-\alpha}{2T} \le |f| \le \dfrac{1+\alpha}{2T} \\ 0, & |f| > \dfrac{1+\alpha}{2T} \end{cases} \tag{9.12}$$

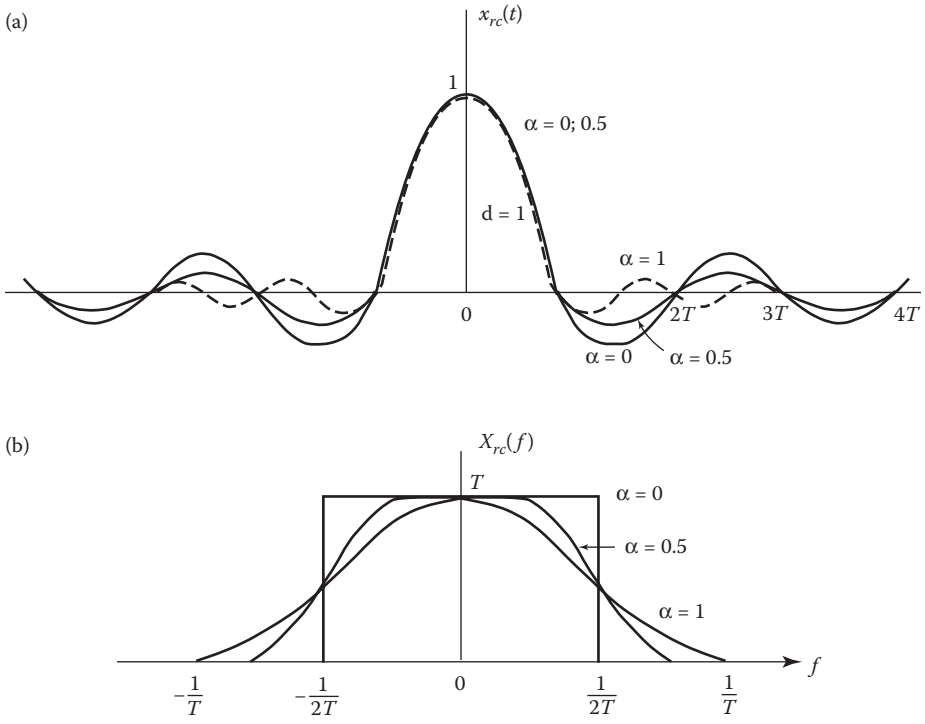

FIGURE 9.9 Pulses having a raised cosine spectrum. (a) Time response, (b) frequency response.

where α is called the *rolloff* factor, which takes values in the range $0 \le \alpha \le 1$, and $1/T$ is the symbol rate. The time response and frequency response are illustrated in Figure 9.9 for $\alpha = 0$, 1/2, and 1. Note that when $\alpha = 0$, $X_{rc}(f)$ reduces to an ideal brick wall physically nonrealizable frequency response with bandwidth occupancy $1/2T$. The frequency $1/2T$ is called the *Nyquist frequency*. For $\alpha > 0$, the bandwidth occupied by the desired signal $X_{rc}(f)$ beyond the Nyquist frequency $1/2T$ is called the *excess bandwidth*, and is usually expressed as a percentage of the Nyquist frequency. For example, when $\alpha = 1/2$, the excess bandwidth is 50% and when $\alpha = 1$, the excess bandwidth is 100%. The signal pulse $x_{rc}(t)$ having the raised-cosine spectrum is

$$x_{rc}(t) = \frac{\sin \pi t/T}{\pi t/T} \quad \frac{\cos(\pi \alpha t/T)}{1 - 4\alpha^2 t^2/T^2} \tag{9.13}$$

Figure 9.9b illustrates $x_{rc}(t)$ for $\alpha = 0$, 1/2, and 1. Note that $x_{rc}(t) = 1$ at $t = 0$ and $x_{rc}(t) = 0$ at $t = kT$, $k = \pm 1, \pm 2, \ldots$. Consequently, at the sampling instants $t = kT$, $k \neq 0$, there is no ISI from adjacent symbols when there is no channel distortion. In the presence of channel distortion, however, the ISI given by Equation 9.10 is no longer zero, and a *channel equalizer* is needed to minimize its effect on system performance.

9.3 Linear Equalizers

The most common type of channel equalizer used in practice to reduce SI is a linear transversal filter with adjustable coefficients $\{c_i\}$, as shown in Figure 9.10.

On channels whose frequency response characteristics are unknown, but time invariant, we may measure the channel characteristics and adjust the parameters of the equalizer; once adjusted, the

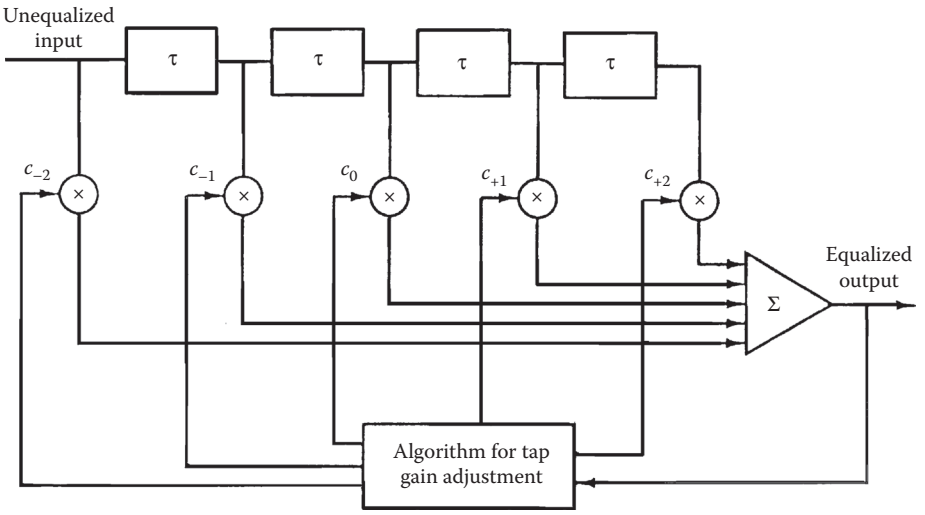

FIGURE 9.10 Linear transversal filter.

parameters remain fixed during the transmission of data. Such equalizers are called *preset equalizers*. On the other hand, *adaptive equalizers* update their parameters on a periodic basis during the transmission of data and, thus, they are capable of tracking a slowly time-varying channel response.

First, let us consider the design characteristics for a linear equalizer from a frequency domain viewpoint. Figure 9.11 shows a block diagram of a system that employs a linear filter as a *channel equalizer.*

The demodulator consists of a receiver filter with frequency response $G_R(f)$ in cascade with a channel equalizing filter that has a frequency response $G_E(f)$. As indicated in the preceding section, the receiver filter response $G_R(f)$ is matched to the transmitter response, that is, $G_R(f) = G_T^*(f)$, and the product $G_R(f)G_T(f)$ is usually designed so that there is zero ISI at the sampling instants as, for example, when $G_R(t)G_T(f) = X_{rc}(f)$.

For the system shown in Figure 9.11, in which the channel frequency response is not ideal, the desired condition for zero ISI is

$$G_T(f)C(f)G_R(f)G_E(f) = X_{rc}(f) \tag{9.14}$$

where $X_{rc}(f)$ is the desired raised-cosine spectral characteristic. Since $G_T(f)G_R(f) = X_{rc}(f)$ by design, the frequency response of the equalizer that compensates for the channel distortion is

$$G_E(f) = \frac{1}{C(f)} = \frac{1}{|C(f)|}e^{-j\theta_c(f)} \tag{9.15}$$

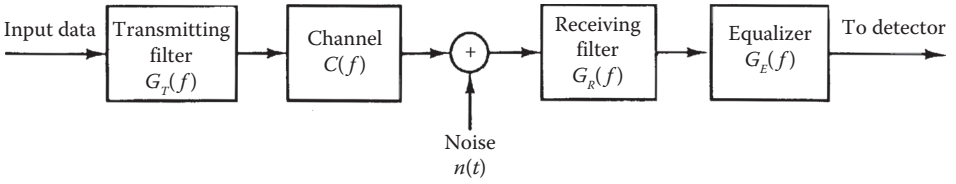

FIGURE 9.11 Block diagram of a system with an equalizer.

Thus, the amplitude response of the equalizer is $|G_E(f)| = 1/|C(f)|$ and its phase response is $\theta_E(f) = -\theta_c(f)$. In this case, the equalizer is said to be the *inverse channel filter* to the channel response.

We note that the inverse channel filter completely eliminates ISI caused by the channel. Since it forces the ISI to be zero at the sampling instants $t = kT$, $k = 0, 1, \ldots$, the equalizer is called a *zero-forcing equalizer*. Hence, the input to the detector is simply

$$z_k = I_k + \eta_k, \quad k = 0,1,\ldots \tag{9.16}$$

where η_k represents the additive noise and I_k is the desired symbol.

In practice, the ISI caused by channel distortion is usually limited to a finite number of symbols on either side of the desired symbol. Hence, the number of terms that constitute the ISI in the summation given by Equation 9.10 is finite. As a consequence, in practice the channel equalizer is implemented as a finite duration impulse response (FIR) filter, or transversal filter, with adjustable tap coefficients $\{c_n\}$, as illustrated in Figure 9.10. The time delay τ between adjacent taps may be selected as large as T, the symbol interval, in which case the FIR equalizer is called a *symbol-spaced equalizer*. In this case, the input to the equalizer is the sampled sequence given by Equation 9.7. We note that when the symbol rate $1/T < 2W$, however, frequencies in the received signal above the folding frequency $1/T$ are aliased into frequencies below $1/T$. In this case, the equalizer compensates for the aliased channel-distorted signal.

On the other hand, when the time delay τ between adjacent taps is selected such that $1/\tau \geq 2W > 1/T$, no aliasing occurs and, hence, the inverse channel equalizer compensates for the true channel distortion. Since $\tau < T$, the channel equalizer is said to *have fractionally spaced taps* and it is called a *fractionally spaced equalizer*. In practice, τ is often selected as $\tau = T/2$. Note that, in this case, the sampling rate at the output of the filter $G_R(f)$ is $2/T$.

The impulse response of the FIR equalizer is

$$g_E(t) = \sum_{n=-N}^{N} c_n \delta(t - n\tau) \tag{9.17}$$

and the corresponding frequency response is

$$G_E(f) = \sum_{n=-N}^{N} c_n e^{-j2\pi fn\tau} \tag{9.18}$$

where $\{c_n\}$ are the $(2N + 1)$ equalizer coefficients and N is chosen sufficiently large so that the equalizer spans the length of the ISI, that is, $2N + 1 \geq L$, where L is the number of signal samples spanned by the ISI. Since $X(f) = G_T(f)C(f)G_R(f)$ and $x(t)$ is the signal pulse corresponding to $X(f)$, then the equalized output signal pulse is

$$q(t) = \sum_{n=-N}^{N} c_n x(t - n\tau) \tag{9.19}$$

The zero-forcing condition can now be applied to the samples *of* $q(t)$ taken at times $t = mT$. These samples are

$$q(mT) = \sum_{n=-N}^{N} c_n x(mT - n\tau), \quad m = 0, \pm 1, \ldots, \pm N \tag{9.20}$$

Since there are $2N + 1$ equalizer coefficients, we can control only $2N + 1$ sampled values of $q(t)$. Specifically, we may force the conditions

$$q(mT) = \sum_{n=-N}^{N} c_n x(mT - n\tau) = \begin{cases} 1, & m = 0 \\ 0, & m = \pm 1, \pm 2, \ldots, \pm N \end{cases} \tag{9.21}$$

which may be expressed in matrix form as $\boldsymbol{Xc} = \boldsymbol{q}$, where $\boldsymbol{X}$ is a $(2N + 1) \times (2N + 1)$ matrix with elements $\{x(mT - n\tau)\}$, $\boldsymbol{c}$ is the $(2N + 1)$ coefficient vector, and $\boldsymbol{q}$ is the $(2N + 1)$ column vector with one nonzero element. Thus, we obtain a set of $2N + 1$ linear equations for the coefficients of the zero-forcing equalizer.

We should emphasize that the FIR zero-forcing equalizer does not completely eliminate ISI because it has a finite length. As N is increased, however, the residual ISI can be reduced, and in the limit as $N \to \infty$, the ISI is completely eliminated.

Example 9.1

Consider a channel distorted pulse $x(t)$, at the input to the equalizer, given by the expression

$$x(t) = \frac{1}{1 + \left(\frac{2t}{T}\right)^2}$$

where $1/T$ is the symbol rate. The pulse is sampled at the rate $2/T$ and equalized by a zero-forcing equalizer. Determine the coefficients of a five-tap zero-forcing equalizer.

SOLUTION

According to Equation 9.21, the zero-forcing equalizer must satisfy the equations

$$q(mT) = \sum_{n=-2}^{N} c_n x(mT - nT/2) = \begin{cases} 1, & m = 0 \\ 0, & m = \pm 1, \pm 2 \end{cases}$$

The matrix $\boldsymbol{X}$ with elements $x(mT - nT/2)$ is given as

$$\boldsymbol{X} = \begin{bmatrix} \frac{1}{5} & \frac{1}{10} & \frac{1}{17} & \frac{1}{26} & \frac{1}{37} \\ 1 & \frac{1}{2} & \frac{1}{5} & \frac{1}{10} & \frac{1}{17} \\ \frac{1}{5} & \frac{1}{2} & 1 & \frac{1}{2} & \frac{1}{5} \\ \frac{1}{17} & \frac{1}{10} & \frac{1}{5} & \frac{1}{2} & 1 \\ \frac{1}{37} & \frac{1}{26} & \frac{1}{17} & \frac{1}{10} & \frac{1}{5} \end{bmatrix} \tag{9.22}$$

The coefficient vector $\boldsymbol{c}$ and the vector $\boldsymbol{q}$ are given as

$$\boldsymbol{c} = \begin{bmatrix} c_{-2} \\ c_{-1} \\ c_0 \\ c_1 \\ c_2 \end{bmatrix} \qquad \boldsymbol{q} = \begin{bmatrix} 0 \\ 0 \\ 1 \\ 0 \\ 0 \end{bmatrix} \tag{9.23}$$

Then, the linear equations $\boldsymbol{Xc} = \boldsymbol{q}$ can be solved by inverting the matrix $\boldsymbol{X}$. Thus, we obtain

$$\boldsymbol{c}_{\text{opt}} = \boldsymbol{X}^{-1}\boldsymbol{q} = \begin{bmatrix} -2.2 \\ 4.9 \\ -3 \\ 4.9 \\ -2.2 \end{bmatrix} \tag{9.24}$$

One drawback to the zero-forcing equalizer is that it ignores the presence of additive noise. As a consequence, its use may result in significant noise enhancement. This is easily seen by noting that in a frequency range where $C(f)$ is small, the channel equalizer $G_E(f) = 1/C(f)$ compensates by placing a large gain in that frequency range. Consequently, the noise in that frequency range is greatly enhanced. An alternative is to relax the zero ISI condition and select the channel equalizer characteristic such that the combined power in the residual ISI and the additive noise at the output of the equalizer is minimized. A channel equalizer that is optimized based on the minimum mean square error (MMSE) criterion accomplishes the desired goal.

To elaborate, let us consider the noise-corrupted output of the FIR equalizer, which is

$$z(t) = \sum_{n=-N}^{N} c_n y(t - n\tau) \tag{9.25}$$

where $y(t)$ is the input to the equalizer, given by Equation 9.6. The equalizer output is sampled at times $t = mT$. Thus, we obtain

$$z(mT) = \sum_{n=-N}^{N} c_n y(mT - n\tau) \tag{9.26}$$

The desired response at the output of the equalizer at $t = mT$ is the transmitted symbol I_m. The error is defined as the difference between I_m and $z(mT)$. Then, the mean square error (MSE) between the actual output sample $z(mT)$ and the desired values I_m is

$$\begin{aligned} \text{MSE} &= E\left|z(mT) - I_m\right|^2 = E\left[\left|\sum_{n=-N}^{N} c_n y(mT - n\tau) - I_m\right|^2\right] \\ &= \sum_{n=-N}^{N}\sum_{k=-N}^{N} c_n c_k R_Y(n-k) - 2\sum_{k=-N}^{N} c_k R_{IY}(k) + E\left(\left|I_m\right|^2\right) \end{aligned} \tag{9.27}$$

where the correlations are defined as

$$R_Y(n-k) = E\left[y^*(mT - m\tau)y(mT - k\tau)\right]$$
$$R_{IY}(k) = E\left[y(mT - k\tau)I_m^*\right] \tag{9.28}$$

and the expectation is taken with respect to the random information sequence $\{I_m\}$ and the additive noise.

The minimum MSE solution is obtained by differentiating Equation 9.27 with respect to the equalizer coefficients $\{c_n\}$. Thus, we obtain the necessary conditions for the minimum MSE as

$$\sum_{n=-N}^{N} c_n R_Y(n-k) = R_{IY}(k), \quad k = 0, \pm 1, 2, \ldots, \pm N \tag{9.29}$$

These are the $(2N + 1)$ linear equations for the equalizer coefficients. In contrast to the zero-forcing solution already described, these equations depend on the statistical properties (the autocorrelation) of the noise as well as the ISI through the autocorrelation $R_Y(n)$.

In practice, the autocorrelation matrix $R_Y(n)$ and the cross-correlation vector $R_{IY}(n)$ are unknown *a priori*. These correlation sequences can be estimated, however, by transmitting a test signal over the channel and using the time-average estimates

$$\hat{R}_Y(n) = \frac{1}{K}\sum_{k=1}^{K} y^*(kT - m\tau)y(kT)$$
$$\hat{R}_{IY}(n) = \frac{1}{K}\sum_{k=1}^{K} y(kT - m\tau)I_k^* \tag{9.30}$$

in place of the ensemble averages to solve for the equalizer coefficients given by Equation 9.29.

9.3.1 Adaptive Linear Equalizers

We have shown that the tap coefficients of a linear equalizer can be determined by solving a set of linear equations. In the zero-forcing optimization criterion, the linear equations are given by Equation 9.21. On the other hand, if the optimization criterion is based on minimizing the MSE, the optimum equalizer coefficients are determined by solving the set of linear equations given by Equation 9.29.

In both cases, we may express the set of linear equations in the general matrix form

$$\boldsymbol{Bc} = \boldsymbol{d} \tag{9.31}$$

where $\boldsymbol{B}$ is a $(2N + 1) \times (2N + 1)$ matrix, $\boldsymbol{c}$ is a column vector representing the $2N + 1$ equalizer coefficients, and $\boldsymbol{d}$ is a $(2N + 1)$-dimensional column vector. The solution of Equation 9.31 yields

$$\boldsymbol{c}_{\text{opt}} = \boldsymbol{B}^{-1}\boldsymbol{d} \tag{9.32}$$

In practical implementations of equalizers, the solution of Equation 9.31 for the optimum coefficient vector is usually obtained by an iterative procedure that avoids the explicit computation of the inverse of the matrix $\boldsymbol{B}$. The simplest iterative procedure is the method of steepest descent, in which one begins by

choosing arbitrarily the coefficient vector $\boldsymbol{c}$, say $\boldsymbol{c}_0$. This initial choice of coefficients corresponds to a point on the criterion function that is being optimized. For example, in the case of the MSE criterion, the initial guess $\boldsymbol{c}_0$ corresponds to a point on the quadratic MSE surface in the $(2N + 1)$-dimensional space of coefficients. The gradient vector, defined as $\boldsymbol{g}_0$, which is the derivative of the MSE with respect to the $2N + 1$ filter coefficients, is then computed at this point on the criterion surface, and each tap coefficient is changed in the direction opposite to its corresponding gradient component. The change in the jth tap coefficient is proportional to the size of the jth gradient component.

For example, the gradient vector denoted as $\boldsymbol{g}_k$, for the MSE criterion, found by taking the derivatives of the MSE with respect to each of the $2N + 1$ coefficients, is

$$\boldsymbol{g}_k = \boldsymbol{B}\boldsymbol{c}_k - \boldsymbol{d}, \quad k = 0,1,2,\ldots \tag{9.33}$$

Then the coefficient vector $\boldsymbol{c}_k$ is updated according to the relation

$$\boldsymbol{c}_{k+1} = \boldsymbol{c}_k - \Delta\boldsymbol{g}_k \tag{9.34}$$

where Δ is the *step-size parameter* for the iterative procedure. To ensure convergence of the iterative procedure, Δ is chosen to be a small positive number. In such a case, the gradient vector $\boldsymbol{g}_k$ converges toward zero, that is, $\boldsymbol{g}_k \to \boldsymbol{0}$ as $k \to \infty$, and the coefficient vector $\boldsymbol{c}_k \to \boldsymbol{c}_{\text{opt}}$ as illustrated in Figure 9.12 based on two-dimensional optimization. In general, convergence of the equalizer tap coefficients to $\boldsymbol{c}_{\text{opt}}$ cannot be attained in a finite number of iterations with the steepest-descent method. The optimum solution $\boldsymbol{c}_{\text{opt}}$, however, can be approached as closely as desired in a few hundred iterations. In digital communication systems that employ channel equalizers, each iteration corresponds to a time interval for sending one symbol and, hence, a few hundred iterations to achieve convergence to $\boldsymbol{c}_{\text{opt}}$ corresponds to a fraction of a second.

Adaptive channel equalization is required for channels whose characteristics change with time. In such a case, the ISI varies with time. The channel equalizer must track such time variations in the channel response and adapt its coefficients to reduce the ISI. In the context of the preceding discussion, the optimum coefficient vector $\boldsymbol{c}_{\text{opt}}$ varies with time due to time variations in the matrix $\boldsymbol{B}$ and, for the case of the MSE criterion, time variations in the vector $\boldsymbol{d}$. Under these conditions, the iterative method described can be modified to use estimates of the gradient components. Thus, the algorithm for adjusting the equalizer tap coefficients may be expressed as

$$\hat{\boldsymbol{c}}_{k+1} = \hat{\boldsymbol{c}}_k - \Delta\hat{\boldsymbol{g}}_k \tag{9.35}$$

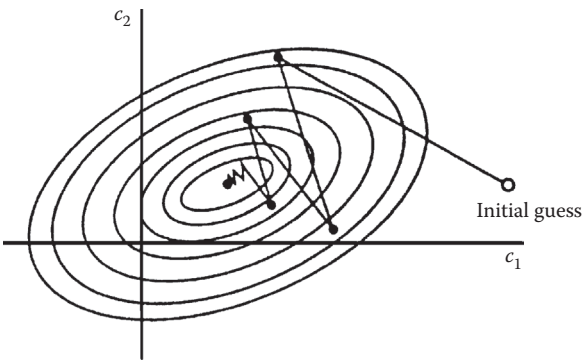

FIGURE 9.12 Examples of convergence characteristics of a gradient algorithm.

where $\hat{\boldsymbol{g}}_k$ denotes an estimate of the gradient vector $\boldsymbol{g}_k$ and $\hat{\boldsymbol{c}}_k$ denotes the estimate of the tap coefficient vector.

In the case of the MSE criterion, the gradient vector $\boldsymbol{g}_k$ given by Equation 9.33 may also be expressed as

$$\boldsymbol{g}_k = -\boldsymbol{E}(e_k y_k^*)$$

An estimate $\hat{\boldsymbol{g}}_k$ of the gradient vector at the kth iteration is computed as

$$\hat{\boldsymbol{g}}_k = -e_k \boldsymbol{y}_k^* \tag{9.36}$$

where e_k denotes the difference between the desired output from the equalizer at the kth time instant and the actual output $z(kT)$, and $\boldsymbol{y}_k$ denotes the column vector of $2N + 1$ received signal values contained in the equalizer at time instant k. The *error signal* e_k is expressed as

$$e_k = \boldsymbol{I}_k - z_k \tag{9.37}$$

where $z_k = z(kT)$ is the equalizer output given by Equation 9.26 and $\boldsymbol{I}_k$ is the desired symbol. Hence, by substituting Equation 9.36 into Equation 9.35, we obtain the adaptive algorithm for optimizing the tap coefficients (based on the MSE criterion) as

$$\hat{\boldsymbol{c}}_{k+1} = \hat{\boldsymbol{c}}_k + \Delta e_k \boldsymbol{y}_k^* \tag{9.38}$$

Since an estimate of the gradient vector is used in Equation 9.38, the algorithm is called a *stochastic gradient algorithm*; it is also known as the *LMS algorithm*.

A block diagram of an adaptive equalizer that adapts its tap coefficients according to Equation 9.38 is illustrated in Figure 9.13. Note that the difference between the desired output $\boldsymbol{I}_k$ and the actual output z_k from the equalizer is used to form the error signal e_k. This error is scaled by the step-size parameter Δ, and the scaled error signal Δe_k multiplies the received signal values $\{y(kT - n\tau)\}$ at the $2N + 1$ taps. The products $\Delta e_k\, y^*(kT - n\tau)$ at the $(2N + 1)$ taps are then added to the previous values of the tap coefficients to obtain the updated tap coefficients, according to Equation 9.38. This computation is repeated as each new symbol is received. Thus, the equalizer coefficients are updated at the symbol rate.

Initially, the adaptive equalizer is trained by the transmission of a known pseudo-random sequence $\{I_m\}$ over the channel. At the demodulator, the equalizer employs the known sequence to adjust its coefficients. Upon initial adjustment, the adaptive equalizer switches from a *training mode* to a *decision-directed mode*, in which case the decisions at the output of the detector are sufficiently reliable so that the error signal is formed by computing the difference between the detector output and the equalizer output, that is,

$$e_k = \tilde{\boldsymbol{I}}_k - z_k \tag{9.39}$$

where $\tilde{\boldsymbol{I}}_k$ is the output of the detector. In general, decision errors at the output of the detector occur infrequently and, consequently, such errors have little effect on the performance of the tracking algorithm given by Equation 9.38.

A rule of thumb for selecting the step-size parameter so as to ensure convergence and good tracking capabilities in slowly varying channels is

$$\Delta = \frac{1}{5(2N + 1)P_R} \tag{9.40}$$

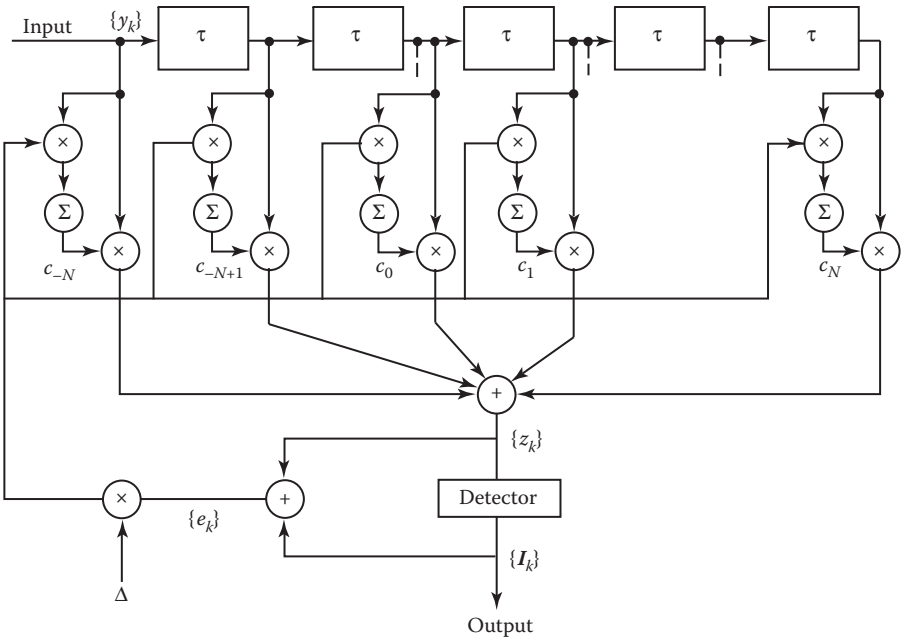

FIGURE 9.13 Linear adaptive equalizer based on the MSE criterion.

where P_R denotes the received signal-plus-noise power, which can be estimated from the received signal (see Reference 4).

The convergence characteristic of the stochastic gradient algorithm in Equation 9.38 is illustrated in Figure 9.14. These graphs were obtained from a computer simulation of an 11-tap adaptive equalizer operating on a channel with a rather modest amount of ISI. The input signal-plus-noise power P_R was normalized to unity. The rule of thumb given in Equation 9.40 for selecting the step size gives $\Delta = 0.018$. The effect of making Δ too large is illustrated by the large jumps in MSE as shown for $\Delta = 0.115$. As Δ is decreased, the convergence is slowed somewhat, but a lower MSE is achieved, indicating that the estimated coefficients are closer to c_{opt}.

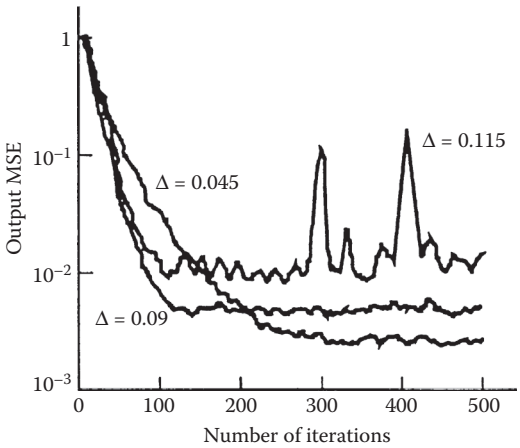

FIGURE 9.14 Initial convergence characteristics of the LMS algorithm with different step sizes.

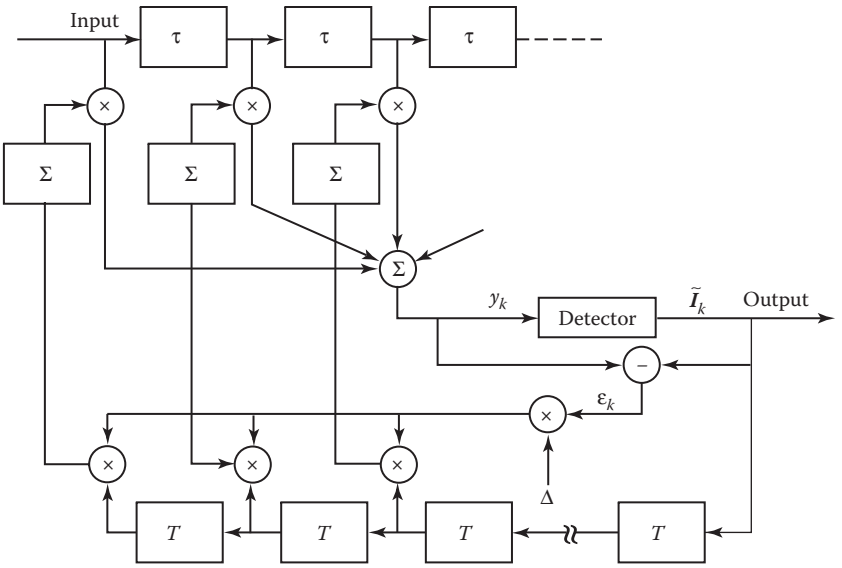

FIGURE 9.15 An adaptive zero-forcing equalizer.

Although we have described in some detail the operation of an adaptive equalizer that is optimized on the basis of the MSE criterion, the operation of an adaptive equalizer based on the zero-forcing method is very similar. The major difference lies in the method for estimating the gradient vectors g_k at each iteration. A block diagram of an adaptive zero-forcing equalizer is shown in Figure 9.15.

For more details on the tap coefficient update method for a zero-forcing equalizer, the reader is referred to the papers by Lucky [2,3], and the text by Proakis [4].

9.4 Decision-Feedback Equalizer

The linear filter equalizers described in the preceding section are very effective on channels, such as wire line telephone channels, where the ISI is not severe. The severity of the ISI is directly related to the spectral characteristics and not necessarily to the time span of the ISI. For example, consider the ISI resulting from the two channels that are illustrated in Figure 9.16. The time span for the ISI in channel A is five symbol intervals on each side of the desired signal component, which has a value of 0.72. On the other hand, the time span for the ISI in channel B is one symbol interval on each side of the desired signal component, which has a value of 0.815. The energy of the total response is normalized to unity for both channels.

In spite of the shorter ISI span, channel B results in more severe ISI. This is evidenced in the frequency response characteristics of these channels, which are shown in Figure 9.17. We observe that channel B has a spectral null [the frequency response $C(f) = 0$ for some frequencies in the band $|f| \leq W$] at $f = 1/2T$, whereas this does not occur in the case of channel A. Consequently, a linear equalizer will introduce a large gain in its frequency response to compensate for the channel null. Thus, the noise in channel B will be enhanced much more than in channel A. This implies that the performance of the linear equalizer for channel B will be sufficiently poorer than that for channel A. This fact is borne out by the computer simulation results for the performance of the two linear equalizers shown in Figure 9.18. Hence, the basic limitation of a linear equalizer is that it performs poorly on channels having spectral nulls. Such channels are often encountered in radio communications, such as ionospheric transmission at frequencies below 30 MHz and mobile radio channels, such as those used for cellular radio communications.

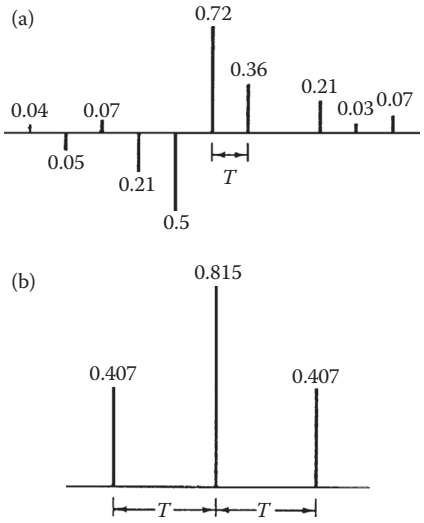

FIGURE 9.16 Two channels with ISI. (a) Channel A, (b) channel B.

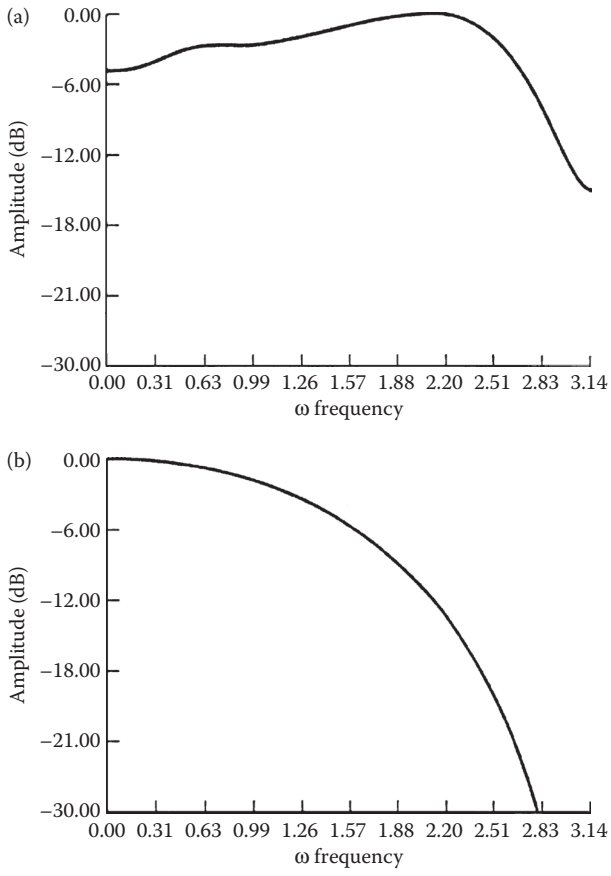

FIGURE 9.17 Amplitude spectra for (a) channel A shown in Figure 9.16a and (b) channel B shown in Figure 9.16b.

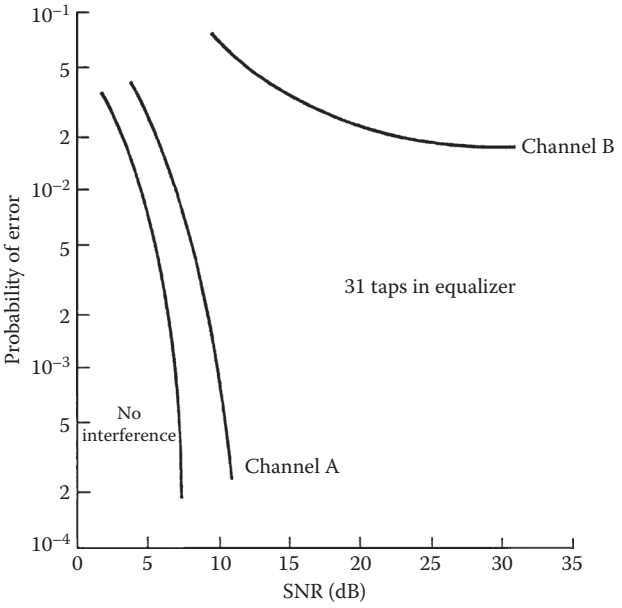

FIGURE 9.18 Error-rate performance of linear MSE equalizer.

A *decision-feedback equalizer* (DFE) is a nonlinear equalizer that employs previous decisions to eliminate the ISI caused by previously detected symbols on the current symbol to be detected. A simple block diagram for a DFE is shown in Figure 9.19. The DFE consists of two filters. The first filter is called *a feedforward filter* and it is generally a fractionally spaced FIR filter with adjustable tap coefficients. This filter is identical in form to the linear equalizer already described. Its input is the received filtered signal $y(t)$ sampled at some rate that is a multiple of the symbol rate, for example, at rate $2/T$. The second filter is a *feedback filter*. It is implemented as an FIR filter with symbol-spaced taps having adjustable coefficients. Its input is the set of previously detected symbols. The output of the feedback filter is subtracted from the output of the feedforward filter to form the input to the detector. Thus, we have

$$z_m = \sum_{n=-N_1}^{0} c_n y(mT - n\tau) - \sum_{n=1}^{N_2} b_n \tilde{\boldsymbol{I}}_{m-n} \tag{9.41}$$

where $\{c_n\}$ and $\{b_n\}$ are the adjustable coefficients of the feedforward and feedback filters, respectively, $\tilde{\boldsymbol{I}}_{m-n}$, $n = 1, 2, \ldots, N_2$ are the previously detected symbols, $N_1 + 1$ is the length of the feedforward filter, and N_2 is the length of the feedback filter. Based on the input z_m, the detector determines which of the possible transmitted symbols is closest in distance to the input signal $\boldsymbol{I}_m$. Thus, it makes its decision and outputs $\tilde{\boldsymbol{I}}_m$.

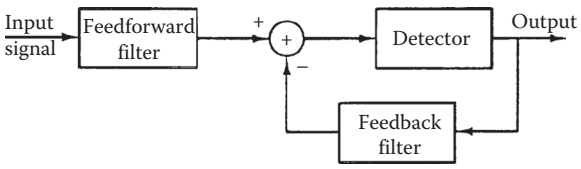

FIGURE 9.19 Block diagram of DFE.

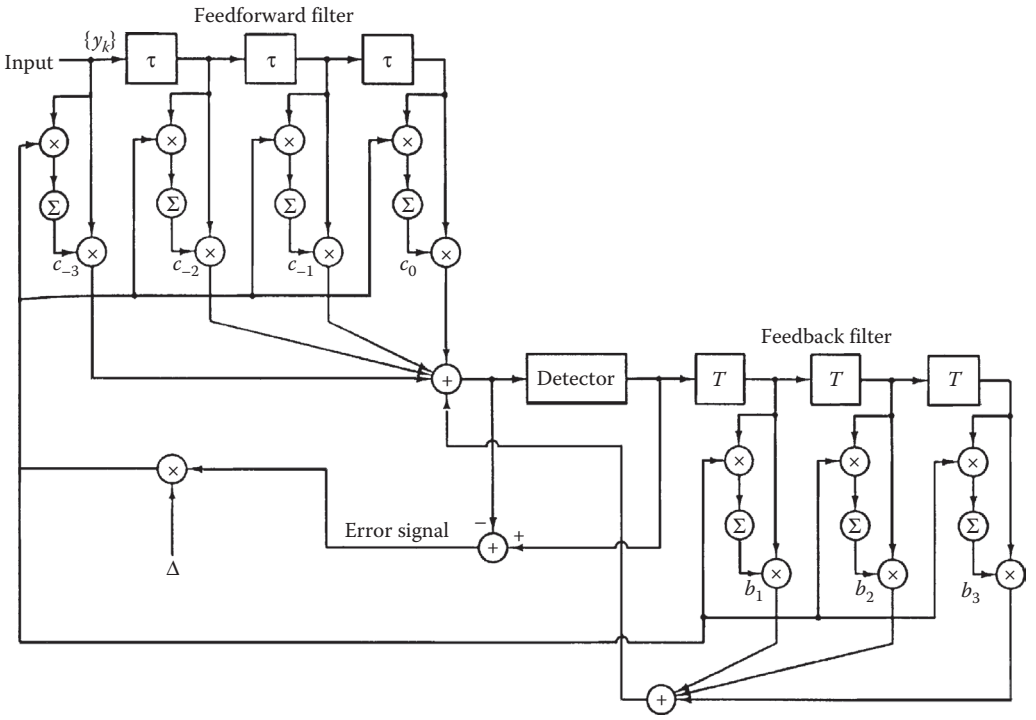

FIGURE 9.20 Adaptive DFE.

What makes the DFE nonlinear is the nonlinear characteristic of the detector that provides the input to the feedback filter.

The tap coefficients of the feedforward and feedback filters are selected to optimize some desired performance measure. For mathematical simplicity, the MSE criterion is usually applied, and a stochastic gradient algorithm is commonly used to implement an adaptive DFE. Figure 9.20 illustrates the block diagram of an adaptive DFE whose tap coefficients are adjusted by means of the LMS stochastic gradient algorithm. Figure 9.21 illustrates the probability of error performance of the DFE, obtained by computer simulation, for binary PAM transmission over channel B. The gain in performance relative to that of a linear equalizer is clearly evident.

We should mention that decision errors from the detector that are fed to the feedback filter have a small effect on the performance of the DFE. In general, a small loss in performance of one to two decibels is possible at error rates below 10^{-2}, as illustrated in Figure 9.21, but the decision errors in the feedback filters are not catastrophic.

9.5 Maximum-Likelihood Sequence Detection

Although the DFE outperforms a linear equalizer, it is not the optimum equalizer from the viewpoint of minimizing the probability of error in the detection of the information sequence $\{I_k\}$ from the received signal samples $\{y_k\}$ given in Equation 9.5. In a digital communication system that transmits information over a channel that causes ISI, the optimum detector is a maximum-likelihood symbol sequence detector which produces at its output the most probable symbol sequence $\{\tilde{\boldsymbol{I}}_k\}$ for the given received sampled sequence $\{y_k\}$. That is, the detector finds the sequence $\{\tilde{\boldsymbol{I}}_k\}$ that maximizes the *likelihood function*

$$\Lambda(\{I_k\}) = \ln p(\{y_k\}) \mid \{I_k\}) \tag{9.42}$$

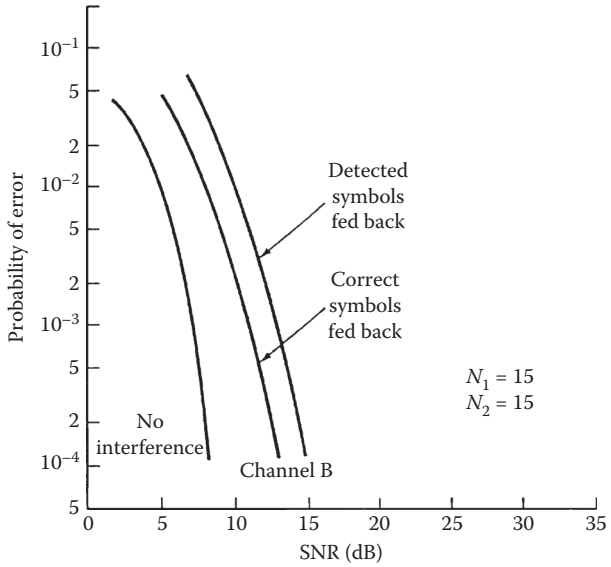

FIGURE 9.21 Performance of DFE with and without error propagation.

where $p(\{y_k\} \mid \{I_k\})$ is the joint probability of the received sequence $\{y_k\}$ conditioned on $\{I_k\}$. The sequence of symbols $\{\tilde{\boldsymbol{I}}_k\}$ that maximizes this joint conditional probability is called the *maximum-likelihood sequence detector.*

An algorithm that implements maximum-likelihood sequence detection (MLSD) is the Viterbi algorithm, which was originally devised for decoding convolutional codes. For a description of this algorithm in the context of sequence detection in the presence of ISI, the reader is referred to the paper by Forney [1] and the text by Proakis [4].

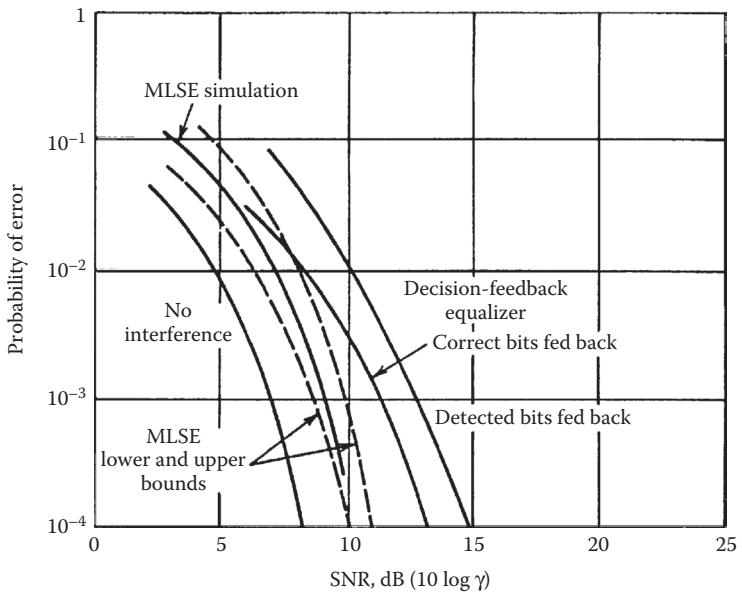

FIGURE 9.22 Comparison of performance between MLSE and decision-feedback equalization for channel B of Figure 9.16.

The major drawback of MLSD for channels with ISI is the exponential behavior in computational complexity as a function of the span of the ISI. Consequently, MLSD is practical only for channels where the ISI spans only a few symbols and the ISI is severe, in the sense that it causes a severe degradation in the performance of a linear equalizer or a DFE. For example, Figure 9.22 illustrates the error probability performance of the Viterbi algorithm for a binary PAM signal transmitted through channel B (see Figure 9.16). For purposes of comparison, we also illustrate the probability of error for a DFE. Both results were obtained by computer simulation. We observe that the performance of the maximum-likelihood sequence detector is about 4.5 dB better than that of the DFE at an error probability of 10^{-4}. Hence, this is one example where the ML sequence detector provides a significant performance gain on a channel with a relatively short ISI span.

9.6 Conclusions

Channel equalizers are widely used in digital communication systems to mitigate the effects of ISI caused by channel distortion. Linear equalizers are widely used for high-speed modems that transmit data over telephone channels. For wireless (radio) transmission, such as in mobile cellular communications and interoffice communications, the multipath propagation of the transmitted signal results in severe ISI. Such channels require more powerful equalizers to combat the severe ISI. The DFE and the MLSD are two nonlinear channel equalizers that are suitable for radio channels with severe ISI.

References

1. Forney, G. D., Jr., Maximum-likelihood sequence estimation of digital sequences in the presence of intersymbol interference. *IEEE Trans. Inform. Theory*, IT-18, 363–378, 1972.
2. Lucky, R. W., Automatic equalization for digital communications. *Bell Syst. Tech. J.*, 44, 547–588, 1965.
3. Lucky, R. W., Techniques for adaptive equalization of digital communication. *Bell Syst. Tech. J.*, 45, 255–286, 1966.
4. Proakis, J. G., *Digital Communications*, 4th ed., McGraw-Hill, New York, 2001.

Further Reading

For a comprehensive treatment of adaptive equalization techniques and their performance characteristics, the reader may refer to the book by Proakis [4]. The two papers by Lucky [2,3] provide a treatment on linear equalizers based on the zero-forcing criterion. Additional information on decision-feedback equalizers may be found in the journal papers "An Adaptive Decision-Feedback Equalizer" by D.A. George, R.R. Bowen, and J.R. Storey, *IEEE Transactions on Communications Technology*, Vol. COM-19, pp. 281–293, June 1971, and "Feedback Equalization for Fading Dispersive Channels" by P. Monsen, *IEEE Transactions on Information Theory*, Vol. IT-17, pp. 56–64, January 1971. A thorough treatment of channel equalization based on maximum-likelihood sequence detection is given in the paper by Forney [1].

10

Echo Cancellation

Giovanni Cherubini

10.1 Introduction

Full-duplex data transmission over a single twisted-pair cable permits the simultaneous flow of information in two directions when the same frequency band is used. Examples of applications of this technique are found in digital communications systems that operate over the telephone network. In a digital subscriber loop, at each end of the full-duplex link, a circuit, known as hybrid, separates the two directions of transmission. To avoid signal reflections at the near- and far-end hybrid, a precise knowledge of the line impedance would be required. Since the line impedance depends on line parameters that, in general, are not exactly known, an attenuated and distorted replica of the transmit signal leaks to the receiver input as an echo signal. Data-driven adaptive echo cancellation mitigates the effects of impedance mismatch.

A similar problem is caused by crosstalk in transmission systems over voice-grade unshielded twisted-pair cables for local-area network applications, where multipair cables are used to physically separate the two directions of transmission. Crosstalk is a statistical phenomenon due to randomly varying differential capacitive and inductive coupling between adjacent two-wire transmission lines. At the rates of several megabits per second that are usually considered for local-area network applications, near-end crosstalk (NEXT) represents the predominant disturbance; hence, adaptive NEXT cancellation must be performed to ensure reliable communications.

In voiceband data modems, the model for the echo channel differs considerably from the echo model adopted in baseband transmission. The transmitted signal is a passband signal obtained by quadrature amplitude modulation (QAM), and the far-end echo may exhibit significant carrier-phase jitter and carrier-frequency shift, which are caused by signal processing at intermediate points in the telephone network. Therefore, a digital adaptive echo canceller for voiceband modems needs to embody algorithms that account for the presence of such additional impairments.

In this chapter, we describe the echo channel models and adaptive echo canceller structures that are obtained for various digital communications systems, which are classified according to the modulation techniques employed. We also address the trade-offs between complexity, speed of adaptation, and accuracy of cancellation in adaptive echo cancellers.

10.2 Echo Cancellation for Pulse–Amplitude Modulation Systems

The model of a full-duplex baseband data transmission system employing pulse–amplitude modulation (PAM) and adaptive echo cancellation is shown in Figure 10.1. To describe system operations, we consider one end of the full-duplex link. The configuration of an echo canceller for a PAM transmission system is shown in Figure 10.2. The transmitted data consist of a sequence $\{a_n\}$ of independent and identically distributed (i.i.d.) real-valued symbols from the M-ary alphabet $\mathcal{A} = \{\pm 1, \pm 3, \ldots, \pm(M-1)\}$. The sequence $\{a_n\}$ is converted into an analog signal by a digital-to-analog (D/A) converter. The conversion to a staircase signal by a zero-order hold D/A converter is described by the frequency response $H_{\mathrm{D/A}}(f) = T \sin(\pi fT)/(\pi fT)$, where T is the modulation interval. The D/A converter output is filtered by the analog transmit filter and is input to the channel through the hybrid.

The signal $x(t)$ at the output of the low-pass analog receive filter has three components, namely, the signal from the far-end transmitter $r(t)$, the echo $u(t)$, and additive Gaussian noise $w(t)$. The signal $x(t)$ is given by

$$\begin{aligned} x(t) &= r(t) + u(t) + w(t) \\ &= \sum_{n=-\infty}^{\infty} a_n^R h(t - nT) + \sum_{n=-\infty}^{\infty} a_n h_E(t - nT) + w(t), \end{aligned} \tag{10.1}$$

where $\{a_n^R\}$ is the sequence of symbols from the remote transmitter, and $h(t)$ and $h_E(t) = \{h_{\mathrm{D/A}} \otimes g_E\}(t)$ are the impulse responses of the overall channel and the echo channel, respectively. In the expression of

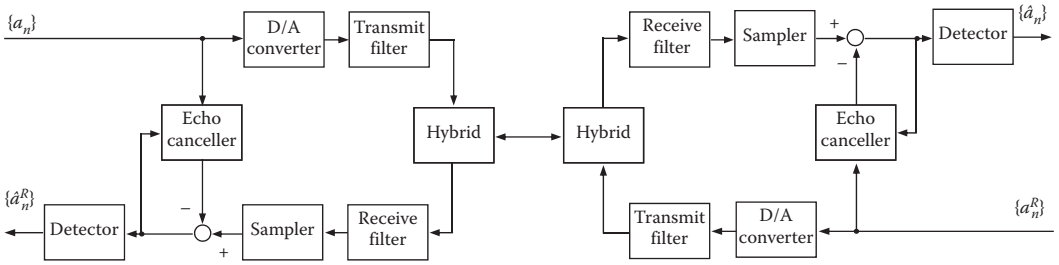

FIGURE 10.1 Model of a full-duplex PAM transmission system.

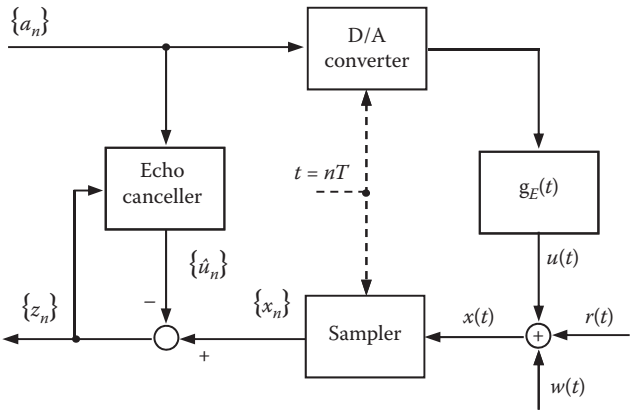

FIGURE 10.2 Configuration of an echo canceller for a PAM transmission system.

$h_E(t)$, the function $h_{D/A}(t)$ is the inverse Fourier transform of $H_{D/A}(f)$, and the operator $\otimes$ denotes convolution. The signal obtained after echo cancellation is processed by a detector that outputs the sequence of estimated symbols $\{\hat{a}_n^R\}$. In the case of full-duplex PAM data transmission over multipair cables for local-area network applications, where NEXT represents the main disturbance, the configuration of a digital NEXT canceller is obtained from Figure 10.2, with the echo channel replaced by the crosstalk channel. For these applications, however, instead of *mono-duplex* transmission, where one pair is used to transmit only in one direction and the other pair to transmit only in the reverse direction, *dual-duplex* transmission may be adopted. Bidirectional transmission at rate ρ over two pairs is then accomplished by full-duplex transmission of data streams at rate ρ/2 over each of the two pairs. The lower modulation rate and/or spectral efficiency required per pair for achieving an aggregate rate equal to ρ represents an advantage of dual-duplex over mono-duplex transmission. Dual-duplex transmission requires two transmitters and two receivers at each end of a link, as well as separation of the simultaneously transmitted and received signals on each pair, as illustrated in Figure 10.3. In dual-duplex transceivers, it is therefore necessary to suppress echoes returning from the hybrids and impedance discontinuities in the cable, as well as self NEXT, by adaptive digital echo and NEXT cancellation [2]. Although a dual-duplex scheme might appear to require higher implementation complexity than a mono-duplex scheme, it turns out that the two schemes are equivalent in terms of the number of multiply-and-add operations per second needed to perform the various filtering operations.

One of the transceivers in a full-duplex link will usually employ an externally provided reference clock for its transmit and receive operations. The other transceiver will extract timing from the received signal, and use this timing for its transmitter operations. This is known as *loop timing*, also illustrated in Figure 10.3. If signals were transmitted in opposite directions with independent clocks, signals received from the remote transmitter would generally shift in phase relative to the also-received echo signals. To cope with this effect, some form of interpolation would be required that can significantly increase the transceiver complexity [4].

In general, we consider baseband signaling techniques such that the signal at the output of the overall channel has nonnegligible excess bandwidth, that is, nonnegligible spectral components at frequencies larger than half of the modulation rate, $|f| \geq 1/2T$. Therefore, to avoid aliasing, the signal $x(t)$ is sampled at twice the modulation rate or at a higher sampling rate. Assuming a sampling rate equal to m/T, $m > 1$, the ith sample during the nth modulation interval is given by

$$\begin{aligned} x\left[(nm+i)\frac{T}{m}\right] = x_{nm+i} &= r_{nm+i} + u_{nm+i} + w_{nm+i}, \quad i = 0,\ldots,m-1 \\ &= \sum_{k=-\infty}^{\infty} h_{km+i} a_{n-k}^R + \sum_{k=-\infty}^{\infty} h_{E,km+i} a_{n-k} + w_{nm+i}, \end{aligned} \tag{10.2}$$

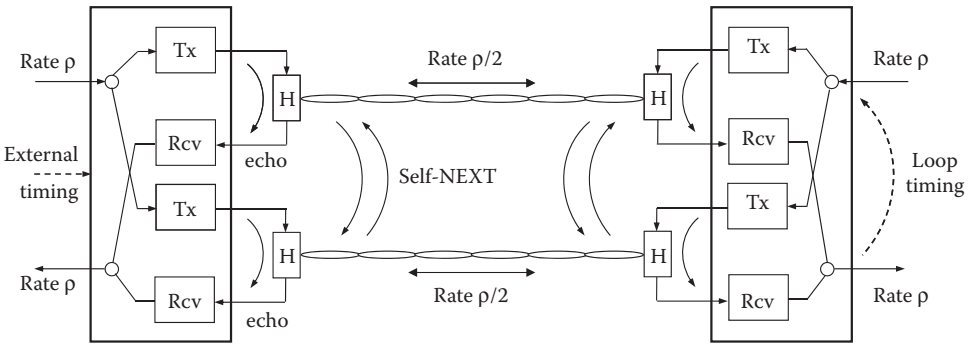

FIGURE 10.3 Model of a dual-duplex transmission system.

where $\{h_{nm+i}, i = 0, \ldots, m-1\}$ and $\{h_{E,nm+i}, i = 0, \ldots, m-1\}$ are the discrete-time impulse responses of the overall channel and the echo channel, respectively, and $\{w_{nm+i}, i = 0, \ldots, m-1\}$ is a sequence of Gaussian noise samples with zero mean and variance σ_w^2. Equation 10.2 suggests that the sequence of samples $\{x_{nm+i}, i = 0, \ldots, m-1\}$ be regarded as a set of m interleaved sequences, each with a sampling rate equal to the modulation rate. Similarly, the sequence of echo samples $\{u_{nm+i}, i = 0, \ldots, m-1\}$ can be regarded as a set of m interleaved sequences that are output by m independent echo channels with discrete-time impulse responses $\{h_{E,nm+i}\}$, $i = 0, \ldots, m-1$, and an identical sequence $\{a_n\}$ of input symbols [8]. Hence, echo cancellation can be performed by m interleaved echo cancellers, as shown in Figure 10.4. Since the performance of each canceller is independent of the other $m-1$ units, we will consider the operations of a single echo canceller in the remaining part of this section.

The echo canceller generates an estimate $\hat{u}_n$ of the echo signal. If we consider a transversal filter realization, $\hat{u}_n$ is obtained as the inner product of the vector of filter coefficients at time $t = nT$, $\boldsymbol{c}_n = (c_{n,0}, \ldots, c_{n,N-1})'$, and the vector of signals stored in the echo canceller delay line at the same instant, $\boldsymbol{a}_n = (a_n, \ldots, a_{n-N+1})'$ expressed by

$$\hat{u}_n = \boldsymbol{c}_n' \boldsymbol{a}_n = \sum_{k=0}^{N-1} c_{n,k} a_{n-k}, \tag{10.3}$$

where $\boldsymbol{c}_n'$ denotes the transpose of the vector $\boldsymbol{c}_n$. The estimate of the echo is subtracted from the received signal. The result is defined as the cancellation error signal

$$z_n = x_n - \hat{u}_n = x_n - \boldsymbol{c}_n' \boldsymbol{a}_n. \tag{10.4}$$

The echo attenuation that must be provided by the echo canceller to achieve proper system operation depends on the application. For example, for the integrated services digital network (ISDN) U-Interface

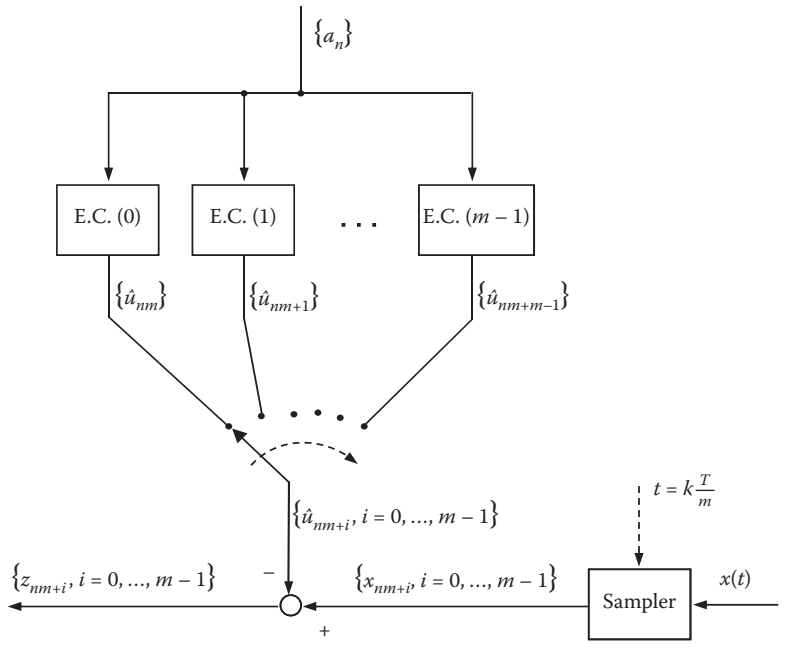

FIGURE 10.4 A set of m interleaved echo cancellers.

transceiver, the echo attenuation must be larger than 55 dB [11]. It is then required that the echo signals outside of the time span of the echo canceller delay line be negligible, that is, $h_{E,n} \approx 0$ for $n < 0$ and $n > N - 1$. As a measure of system performance, we consider the mean square error ε_n^2 at the output of the echo canceller at time $t = nT$, defined by

$$\varepsilon_n^2 = E\{z_n^2\}, \tag{10.5}$$

where $\{z_n\}$ is the error sequence and $E\{\cdot\}$ denotes the expectation operator. For a particular coefficient vector $\boldsymbol{c}_n$, substitution of Equation 10.4 into Equation 10.5 yields

$$\varepsilon_n^2 = E\{x_n^2\} - 2\boldsymbol{c}_n'\boldsymbol{q} + \boldsymbol{c}_n'\boldsymbol{R}\boldsymbol{c}_n, \tag{10.6}$$

where $\boldsymbol{q} = E\{x_n \boldsymbol{a}_n\}$ and $\boldsymbol{R} = E\{\boldsymbol{a}_n\boldsymbol{a}_n'\}$. With the assumption of i.i.d. transmitted symbols, the correlation matrix $\boldsymbol{R}$ is diagonal. The elements on the diagonal are equal to the variance of the transmitted symbols, $\sigma_a^2 = (M^2 - 1)/3$. The minimum mean square error is given by

$$\varepsilon_{\min}^2 = E\{x_n^2\} - \boldsymbol{c}_{\text{opt}}'\boldsymbol{R}\boldsymbol{c}_{\text{opt}}, \tag{10.7}$$

where the optimum coefficient vector is $\boldsymbol{c}_{\text{opt}} = \boldsymbol{R}^{-1}\boldsymbol{q}$. We note that proper system operation is achieved only if the transmitted symbols are uncorrelated with the symbols from the remote transmitter. If this condition is satisfied, the optimum filter coefficients are given by the values of the discrete-time echo channel impulse response, that is, $c_{\text{opt},k} = h_{E,k}$, $k = 0, \ldots, N - 1$.

By the decision-directed stochastic gradient algorithm, also known as the least mean square (LMS) algorithm, the coefficients of the echo canceller converge in the mean to $\boldsymbol{c}_{\text{opt}}$. The LMS algorithm for an N-tap adaptive linear transversal filter is formulated as follows:

$$\boldsymbol{c}_{n+1} = \boldsymbol{c}_n - \frac{1}{2}\alpha\nabla_{\boldsymbol{c}}\{z_n^2\} = \boldsymbol{c}_n + \alpha z_n \boldsymbol{a}_n, \tag{10.8}$$

where α is the adaptation gain and

$$\nabla_{\boldsymbol{c}}\{z_n^2\} = \left(\frac{\partial z_n^2}{\partial c_{n,0}}, \ldots, \frac{\partial z_n^2}{\partial c_{n,N-1}}\right)' = -2z_n\boldsymbol{a}_n,$$

is the gradient of the squared error with respect to the vector of coefficients. The block diagram of an adaptive transversal filter echo canceller is shown in Figure 10.5.

If we define the vector $\boldsymbol{p}_n = \boldsymbol{c}_{\text{opt}} - \boldsymbol{c}_n$, the mean square error can be expressed as

$$\varepsilon_n^2 = \varepsilon_{\min}^2 + \boldsymbol{p}_n'\boldsymbol{R}\boldsymbol{p}_n, \tag{10.9}$$

where the term $\boldsymbol{p}_n'\boldsymbol{R}\boldsymbol{p}_n$ represents an "excess mean square distortion" due to the misadjustment of the filter settings. The analysis of the convergence behavior of the excess mean square distortion was first proposed for adaptive equalizers [14] and later extended to adaptive echo cancellers [10]. Under the assumption that the vectors $\boldsymbol{p}_n$ and $\boldsymbol{a}_n$ are statistically independent, the dynamics of the mean square error are given by

$$E\{\varepsilon_n^2\} = \varepsilon_0^2[1 - \alpha\sigma_a^2(2 - \alpha N\sigma_a^2)]^n + \frac{2\varepsilon_{\min}^2}{2 - \alpha N\sigma_a^2}, \tag{10.10}$$

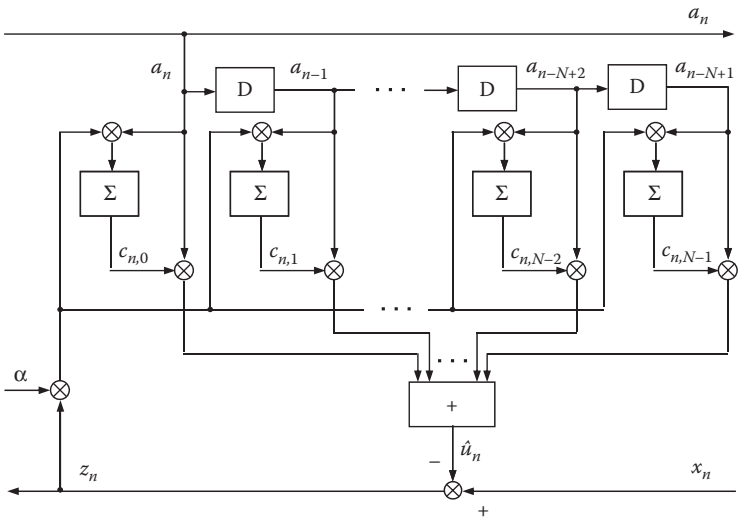

FIGURE 10.5 Block diagram of an adaptive transversal filter echo canceller.

where ε_0^2 is determined by the initial conditions. The mean square error converges to a finite steady-state value ε_∞^2 if the stability condition $0 < \alpha < 2/(N\sigma_a^2)$ is satisfied. The optimum adaptation gain that yields fastest convergence at the beginning of the adaptation process is $\alpha_{opt} = 1/(N\sigma_a^2)$. The corresponding time constant and asymptotic mean square error are $\tau_{opt} = N$ and $\varepsilon_\infty^2 = 2\varepsilon_{min}^2$, respectively.

We note that a fixed adaptation gain equal to α_{opt} could not be adopted in practice, since after echo cancellation the signal from the remote transmitter would be embedded in a residual echo having approximately the same power. If the time constant of the convergence mode is not a critical system parameter, an adaptation gain smaller than α_{opt} will be adopted to achieve an asymptotic mean square error close to ε_{min}^2. On the other hand, if fast convergence is required, a variable gain will be chosen.

Several techniques have been proposed to increase the speed of convergence of the LMS algorithm. In particular, for echo cancellation in data transmission, the speed of adaptation is reduced by the presence of the signal from the remote transmitter in the cancellation error. To mitigate this problem, the data signal can be adaptively removed from the cancellation error by a decision-directed algorithm [6].

Modified versions of the LMS algorithm have also been proposed to reduce system complexity. For example, the sign algorithm suggests that only the sign of the error signal be used to compute an approximation of the stochastic gradient [5]. An alternative means to reduce the implementation complexity of an adaptive echo canceller consists in the choice of a filter structure with a lower computational complexity than the transversal filter.

At high data rates, very-large-scale integration (VLSI) technology is needed for the implementation of transceivers for full-duplex data transmission. High-speed echo cancellers and NEXT cancellers that do not require multiplications represent an attractive solution because of their low complexity. As an example of architecture suitable for VLSI implementation, we consider echo cancellation by a distributed-arithmetic filter, where multiplications are replaced by table lookup and shift-and-add operations [13]. By segmenting the echo canceller into filter sections of shorter lengths, various trade-offs concerning the number of operations per modulation interval and the number of memory locations needed to store the lookup tables are possible. Adaptivity is achieved by updating the values stored in the lookup tables by the LMS algorithm.

To describe the principles of operations of a distributed-arithmetic echo canceller, we assume that the number of elements in the alphabet of input symbols is a power of two, $M = 2^W$. Therefore, each symbol is represented by the vector $(a_n^{(0)}, \ldots, a_n^{(W-1)})$ where $a_n^{(i)}$, $i = 0, \ldots, W-1$ are independent binary random variables, that is,

$$a_n = \sum_{w=0}^{W-1} \left(2a_n^{(w)} - 1\right) 2^w = \sum_{w=0}^{W-1} b_n^{(w)} 2^w, \tag{10.11}$$

where $b_n^{(w)} = \left(2a_n^{(w)} - 1\right) \in \{-1, +1\}$. By substituting Equation 10.11 into Equation 10.1 and segmenting the delay line of the echo canceller into L sections with $K = N/L$ delay elements each, we obtain

$$\hat{u}_n = \sum_{\ell=0}^{L-1} \sum_{w=0}^{W-1} 2^w \left[\sum_{k=0}^{K-1} b_{n-\ell K-k}^{(w)} c_{n,\ell K+k} \right]. \tag{10.12}$$

Equation 10.12 suggests that the filter output can be computed using a set of $L2^K$ values that are stored in L tables with 2^K memory locations each. The binary vectors $\boldsymbol{a}_{n,\ell}^{(w)} = \left(a_{n-(\ell+1)K+1}^{(w)}, \ldots, a_{n-\ell K}^{(w)}\right)$, $w = 0, \ldots, W-1$, $\ell = 0, \ldots, L-1$, determine the addresses of the memory locations where the values needed to compute the filter output are stored. The filter output is obtained by WL table lookup and shift-and-add operations.

We observe that $\boldsymbol{a}_{n,\ell}^{(w)}$ and its binary complement $\overline{\boldsymbol{a}}_{n,\ell}^{(w)}$ select two values that differ only in their sign. This symmetry is exploited to halve the number of values to be stored. To determine the output of a distributed-arithmetic filter with reduced memory size, we reformulate Equation. 10.12 as

$$\hat{u}_n = \sum_{\ell=0}^{L-1} \sum_{w=0}^{W-1} 2^w b_{n-\ell K-k_0}^{(w)} \left[c_{n,\ell K+k_0} + b_{n-\ell K-k_0}^{(w)} \sum_{\substack{k=0 \\ k \neq k_0}}^{K-1} b_{n-\ell K-k}^{(w)} c_{n,\ell K+k} \right], \tag{10.13}$$

where k_0 can be any element of the set $\{0, \ldots, K-1\}$. In the following, we take $k_0 = 0$. Then the binary symbol $b_{n-\ell K}^{(w)}$ determines whether a selected value is to be added or subtracted. Each table has now 2^{K-1} memory locations, and the filter output is given by

$$\hat{u}_n = \sum_{\ell=0}^{L-1} \sum_{w=0}^{W-1} 2^w b_{n-\ell K}^{(w)} d_n(i_{n,\ell}^{(w)}, \ell), \tag{10.14}$$

where $d_n(k, \ell)$, $k = 0, \ldots, 2^{K-1}-1$, $\ell = 0, \ldots, L-1$ are the lookup values, and $i_{n,\ell}^{(w)}, w = 0, \ldots, W-1$, $\ell = 0, \ldots, L-1$, are the lookup indices computed as follows:

$$i_{n,\ell}^{(w)} = \begin{cases} \displaystyle\sum_{k=1}^{K-1} a_{n-\ell K-k}^{(w)} 2^{k-1} & \text{if } a_{n-\ell K}^{(w)} = 1 \\ \displaystyle\sum_{k=1}^{K-1} \overline{a}_{n-\ell K-k}^{(w)} 2^{k-1} & \text{if } a_{n-\ell K}^{(w)} = 0. \end{cases} \tag{10.15}$$

We note that, as long as Equations 10.12 and 10.13 hold for some coefficient vector $(c_{n,0},\ldots, c_{n,N-1})$, the distributed-arithmetic filter emulates the operation of a linear transversal filter. For arbitrary values $d_n(k, \ell)$, however, a nonlinear filtering operation results.

The expression of the LMS algorithm to update the values of a distributed-arithmetic echo canceller takes the form

$$\boldsymbol{d}_{n+1} = \boldsymbol{d}_n - \frac{1}{2}\alpha\nabla_{\boldsymbol{d}}\{z_n^2\} = \boldsymbol{d}_n + \alpha z_n \boldsymbol{y}_n, \tag{10.16}$$

where $\boldsymbol{d}'_n = \left[\boldsymbol{d}'_0(0), \ldots, \boldsymbol{d}'_n(L-1)\right]$, with $\boldsymbol{d}'_n(\ell) = \left[d_n(0,\ell), \ldots, d_n\left(2^{K-1}-1, \ell\right)\right]$, and $\boldsymbol{y}'_n = \left[\boldsymbol{y}'_0(0), \ldots, \boldsymbol{y}'_n(L-1)\right]$, with

$$\boldsymbol{y}'_n(\ell) = \sum_{w=0}^{W-1} 2^w b_{n-\ell K}^{(w)} \left(\delta_{0,i_{n,\ell}^{(w)}}, \ldots, \delta_{2^{K-1}-1,i_{n,\ell}^{(w)}}\right),$$

are $L2^{K-1} \times 1$ vectors and where $\delta_{i,j}$ is the Kronecker delta. We note that in each iteration only those values are updated that are selected to generate the filter output. The block diagram of an adaptive distributed-arithmetic echo canceller with input symbols from a quaternary alphabet is shown in Figure 10.6.

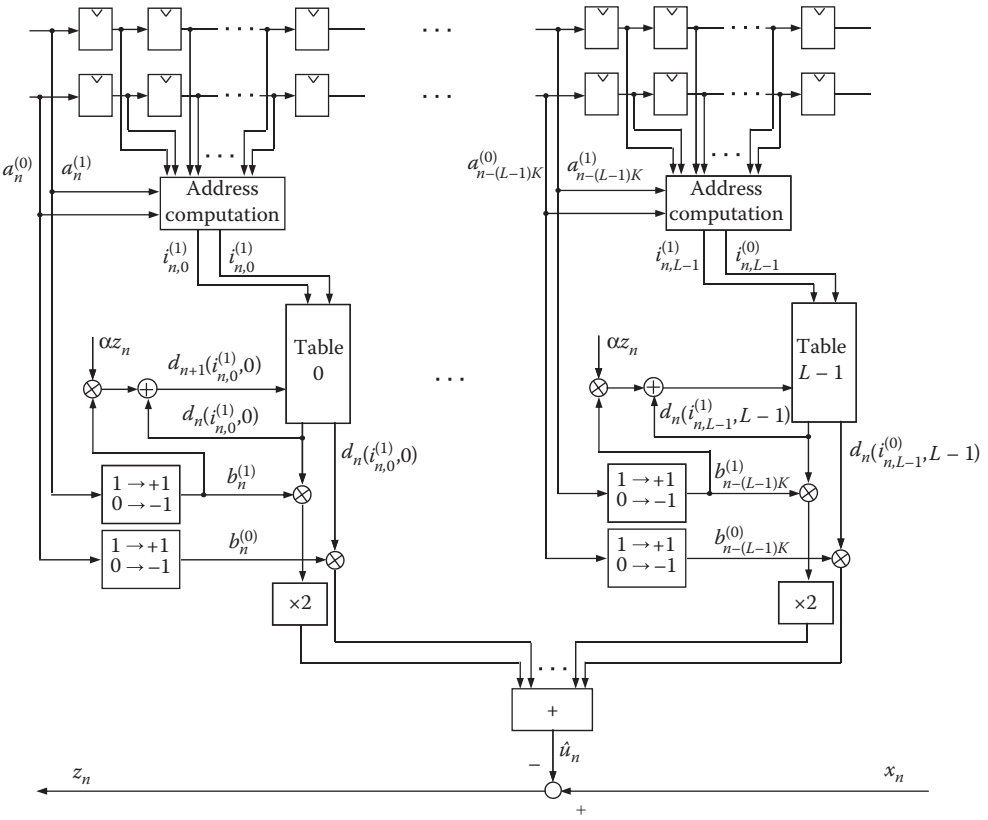

FIGURE 10.6 Block diagram of an adaptive distributed-arithmetic echo canceller.

The analyses of the mean square error convergence behavior and steady-state performance have been extended to adaptive distributed-arithmetic echo cancellers [1]. In this case, the dynamics of the mean square error are given by

$$E\{\varepsilon_n^2\} = \varepsilon_0^2\left[1 - \frac{\alpha\sigma_a^2}{2^{K-1}}(2 - \alpha L\sigma_a^2)\right]^n + \frac{2\varepsilon_{\min}^2}{2 - \alpha L\sigma_a^2}. \tag{10.17}$$

The stability condition for the echo canceller is $0 < \alpha < 2/(L\sigma_a^2)$. For a given adaptation gain, the stability of the echo canceller depends on the number of tables and on the variance of the transmitted symbols. Therefore, the time span of the echo canceller can be increased without affecting system stability, provided that the number L of tables is kept constant. In that case, however, mean square error convergence will be slower. From Equation 10.17, we find that the optimum adaptation gain that permits the fastest mean square error convergence at the beginning of the adaptation process is $\alpha_{\text{opt}} = 1/(L\sigma_a{}^2)$. The time constant of the convergence mode is $\tau_{\text{opt}} = L2^{K-1}$. The smallest achievable time constant is proportional to the total number of values. The realization of a distributed-arithmetic echo canceller can be further simplified by updating at each iteration only the values that are addressed by the most significant bits of the symbols stored in the delay line. The complexity required for adaptation can thus be reduced at the price of a slower rate of convergence.

10.3 Echo Cancellation for Quadrature Amplitude Modulation Systems

Although most of the concepts presented in the preceding sections can be readily extended to echo cancellation for communications systems employing QAM, the case of full-duplex transmission over a voiceband data channel requires a specific discussion. We consider the system model shown in Figure 10.7. The transmitter generates a sequence $\{a_n\}$ of i.i.d. complex-valued symbols from a two-dimensional constellation $\mathcal{A}$, which are modulated by the carrier $e^{j2\pi f_c nT}$, where T and f_c denote the modulation interval and the carrier frequency, respectively. The discrete-time signal at the output of the transmit Hilbert filter may be regarded as an analytic signal, which is generated at the rate of m/T samples/s, $m > 1$. The real part of the analytic signal is converted into an analog signal by a D/A converter and input to the channel. We note that by transmitting the real part of a complex-valued signal positive- and negative-frequency components become folded. The image band attenuation of the transmit Hilbert filter thus determines the

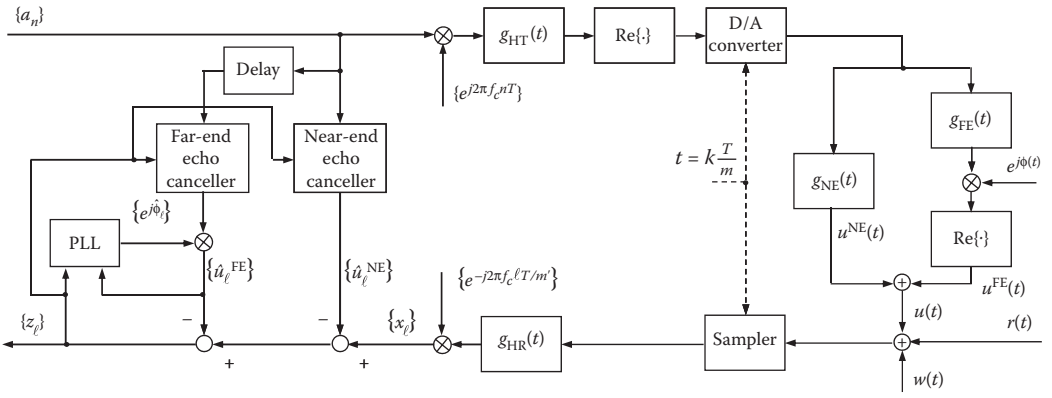

FIGURE 10.7 Configuration of an echo canceller for a QAM transmission system.

achievable echo suppression. In fact, the receiver cannot extract aliasing image-band components from desired passband frequency components, and the echo canceller is able to suppress only echo arising from transmitted passband components.

The output of the echo channel is represented as the sum of two contributions. The near-end echo $u^{\mathrm{NE}}(t)$ arises from the impedance mismatch between the hybrid and the transmission line, as in the case of baseband transmission. The far-end echo $u^{\mathrm{FE}}(t)$ represents the contribution due to echos that are generated at intermediate points in the telephone network. These echos are characterized by additional impairments, such as jitter and frequency shift, which are accounted for by introducing a carrier-phase rotation of an angle $\phi(t)$ in the model of the far-end echo.

At the receiver, samples of the signal at the channel output are obtained synchronously with the transmitter timing, at the sampling rate of m/T samples/s. The discrete-time received signal is converted to a complex-valued baseband signal $\{x_{nm'+i},\ i = 0, \ldots, m' - 1\}$, at the rate of m'/T samples/s, $1 < m' < m$, through filtering by the receive Hilbert filter, decimation, and demodulation. From delayed transmit symbols, estimates of the near- and far-end echo signals after demodulation, $\left\{\hat{u}^{\mathrm{NE}}_{nm'+i},\ i = 0, ..., m' - 1\right\}$ and $\left\{\hat{u}^{\mathrm{FE}}_{nm'+i},\ i = 0, ..., m' - 1\right\}$, respectively, are generated using m' interleaved near- and far-end echo cancellers. The cancellation error is given by

$$z_\ell = x_\ell - \hat{u}^{\mathrm{NE}}_\ell - \hat{u}^{\mathrm{FE}}_\ell. \tag{10.18}$$

A different model is obtained if echo cancellation is accomplished before demodulation. In this case, two equivalent configurations for the echo canceller may be considered. In one configuration, the modulated symbols are input to the transversal filter, which approximates the passband echo response. Alternatively, the modulator can be placed after the transversal filter, which is then called a baseband transversal filter [15].

In the realization considered, the estimates of the echo signals after demodulation are given by

$$\hat{u}^{\mathrm{NE}}_{nm'+i} = \sum_{k=0}^{N_{\mathrm{NE}}-1} c^{\mathrm{NE}}_{n,km'+i} a_{n-k}, \quad i = 0, ..., m' - 1, \tag{10.19}$$

and

$$\hat{u}^{\mathrm{FE}}_{nm'+i} = \left[\sum_{k=0}^{N_{\mathrm{FE}}-1} c^{\mathrm{FE}}_{n,km'+i} a_{n-k-D_{\mathrm{FE}}}\right] e^{j\hat{\phi}_{nm'+i}}, \quad i = 0, ..., m' - 1, \tag{10.20}$$

where $\left(c^{\mathrm{NE}}_{n,0}, \ldots, c^{\mathrm{NE}}_{n,m'N_{\mathrm{NE}}-1}\right)$ and $\left(c^{\mathrm{FE}}_{n,0}, \ldots, c^{\mathrm{FE}}_{n,m'N_{\mathrm{FE}}-1}\right)$ are the coefficients of the m' interleaved near- and far-end echo cancellers, respectively, $\{\hat{\phi}_{nm'+i}, i = 0, \ldots, m' - 1\}$ is the sequence of far-end echo phase estimates, and D_{FE} denotes the bulk delay accounting for the round-trip delay from the transmitter to the point of echo generation. To prevent overlap of the time span of the near-end echo canceller with the time span of the far-end echo canceller, the condition $D_{\mathrm{FE}} > N_{\mathrm{NE}}$ must be satisfied. We also note that, because of the different nature of near- and far-end echo generation, the time span of the far-end echo canceller needs to be larger than the time span of the near-end echo canceller, that is, $N_{\mathrm{FE}} > N_{\mathrm{NE}}$.

Adaptation of the filter coefficients in the near- and far-end echo cancellers by the LMS algorithm leads to

$$c^{\mathrm{NE}}_{n+1,km'+i} = c^{\mathrm{NE}}_{n,km'+i} + \alpha z_{nm'+i}(a_{n-k})^*, \quad k = 0, \ldots, N_{\mathrm{NE}} - 1, i = 0, \ldots, m' - 1 \tag{10.21}$$

and

$$c_{n+1,km'+i}^{\mathrm{FE}} = c_{n,km'+i}^{\mathrm{FE}} + \alpha z_{nm'+i}(a_{n-k-D_{\mathrm{FE}}})^*, e^{-j\hat{\phi}_{nm'+i}} \quad k = 0, \ldots, N_{\mathrm{FE}} - 1, \quad i = 0, \ldots, m' - 1, \tag{10.22}$$

respectively, where the asterisk denotes complex conjugation.

The far-end echo phase estimate is computed by a second-order phase-lock loop algorithm, where the following stochastic gradient approach is adopted:

$$\begin{cases} \hat{\phi}_{\ell+1} = \hat{\phi}_\ell - \dfrac{1}{2}\gamma_{\mathrm{FE}}\nabla_{\hat{\phi}}|z_\ell|^2 + \Delta\phi_\ell \pmod{2\pi} \\ \Delta\phi_{\ell+1} = \Delta\phi_\ell - \dfrac{1}{2}\zeta_{\mathrm{FE}}\nabla_{\hat{\phi}}|z_\ell|^2, \end{cases} \tag{10.23}$$

where $\ell = nm' + i$, $i = 0, \ldots, m' - 1$, γ_{FE} and ζ_{FE} are step-size parameters, and

$$\nabla_{\hat{\phi}}|z_\ell|^2 = \frac{\partial|z_\ell|^2}{\partial\hat{\phi}_\ell} = -2\,\mathrm{Im}\left\{z_\ell(\hat{u}_\ell^{\mathrm{FE}})^*\right\}. \tag{10.24}$$

We note that algorithm (10.23) requires m' iterations per modulation interval, that is, we cannot resort to interleaving to reduce the complexity of the computation of the far-end echo phase estimate.

10.4 Echo Cancellation for Orthogonal Frequency Division Multiplexing Systems

Orthogonal frequency division multiplexing (OFDM) is a modulation technique whereby blocks of M symbols are transmitted in parallel over M subchannels by employing M orthogonal subcarriers. We consider a real-valued discrete-time channel impulse response $\{h_i, i = 0, \ldots, L\}$ having length $L + 1 \ll M$. To illustrate the basic principles of OFDM systems, let us consider a noiseless ideal channel with impulse response given by $\{h_i\} = \{\delta_i\}$, where $\{\delta_i\}$ is defined as the discrete-time delta function. Modulation of the complex-valued input symbols at the n-th modulation interval, denoted by the vector $\boldsymbol{A}_n = \{A_n(i), i = 0, \ldots, M - 1\}$, is performed by an inverse discrete Fourier transform (IDFT), as shown in Figure 10.8. We assume that M is even, and that each block of symbols satisfies the Hermitian symmetry conditions, that is, $A_n(0)$ and $A_n(M/2)$ are real valued, and $A_n(i) = A_n^*(M - i)$, $i = 1, \ldots, M/2 - 1$. Then the signals $\boldsymbol{a}_n = \{a_n(i), i = 0, \ldots, M - 1\}$ obtained at the output of the IDFT are real valued. After parallel-to-serial conversion, the M signals are sent over the channel at the given transmission rate M/T, where T denotes the modulation interval. At the output of the channel, the noiseless signals are received without distortion. Serial-to-parallel conversion yields blocks of M elements, with boundaries placed such that each block obtained at the modulator output is also presented at the demodulator input. Then demodulation

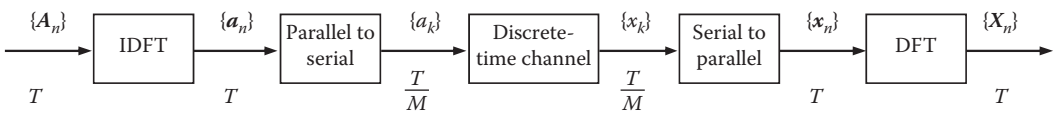

FIGURE 10.8 Block diagram of an OFDM system.

performed by a discrete Fourier transform (DFT) will reproduce the blocks of M input symbols. The overall input–output relationship is therefore equivalent to that of a bank of M parallel, independent subchannels.

In the general case of a noisy channel with impulse response having length greater than one, M independent subchannels are obtained by a variant of OFDM that is also known as discrete multitone modulation (DMT) [12]. In a DMT system, modulation by the IDFT is performed at the rate $1/T' = M/[(M + L)T] < 1/T$. After modulation, each block of M signals is cyclically extended by copying the last L signals in front of the block, and converted from parallel to serial. The resulting $L + M$ signals are sent over the channel. At the receiver, blocks of samples with length $L + M$ are taken. Block boundaries are placed such that the last M samples depend only on the elements of one cyclically extended block of signals. The first L samples are discarded, and the vector $\boldsymbol{x}_n$ of the last M samples of the block received at the n-th modulation interval can be expressed as

$$\boldsymbol{x}_n = \boldsymbol{\Gamma}_n \boldsymbol{h} + \boldsymbol{w}_n, \tag{10.25}$$

where $\boldsymbol{h}$ is the vector of the impulse response extended with $M - L - 1$ zeros, $\boldsymbol{w}_n$ is a vector of additive white Gaussian noise samples, and $\boldsymbol{\Gamma}_n$ is an $M \times M$ circulant matrix given by

$$\boldsymbol{\Gamma}_n = \begin{bmatrix} a_n(0) & a_n(M-1) & \dots & a_n(1) \\ a_n(1) & a_n(0) & \dots & a_n(2) \\ \vdots & \vdots & & \vdots \\ a_n(M-1) & a_n(M-2) & \dots & a_n(0) \end{bmatrix}. \tag{10.26}$$

Recalling that $\mathcal{F}_M \boldsymbol{\Gamma}_n \mathcal{F}_M^{-1} = \text{diag}(\boldsymbol{A}_n)$, where $\mathcal{F}_M$ is the $M \times M$ DFT matrix defined as $\mathcal{F}_M = \left[(e^{-j2\pi/M})^{km}\right]$, $k, m = 0, \dots, M-1$, and $\text{diag}(\boldsymbol{A}_n)$ denotes the diagonal matrix with elements on the diagonal given by $\boldsymbol{A}_n$, we find that the output of the demodulator is given by

$$\boldsymbol{X}_n = \text{diag}(\boldsymbol{A}_n)\boldsymbol{H} + \boldsymbol{W}_n, \tag{10.27}$$

where $\boldsymbol{H}$ denotes the DFT of the vector $\boldsymbol{h}$, and $\boldsymbol{W}_n$ is a vector of independent Gaussian random variables. Equation 10.27 indicates that the sequence of transmitted symbol vectors can be detected by assuming a bank of M independent subchannels, at the price of a decrease in the data rate by a factor $(M + L)/M$. Note that in practice the computationally more efficient inverse fast Fourier transform and fast Fourier transform are used instead of IDFT and DFT.

We discuss echo cancellation for OFDM with reference to a DMT system [7,16], as shown in Figure 10.9. The real-valued discrete-time echo impulse response is $\{h_{E,i},\ i = 0, \dots, N-1\}$, having length $N < M$. We initially assume $N \le L + 1$. Furthermore, we assume that the boundaries of the received blocks are placed such that the last M samples of the n-th received block are expressed by the vector

$$\boldsymbol{x}_n = \boldsymbol{\Gamma}_n^R \boldsymbol{h} + \boldsymbol{\Gamma}_n \boldsymbol{h}_E + \boldsymbol{w}_n, \tag{10.28}$$

where $\boldsymbol{\Gamma}_n^R$ is the circulant matrix with elements given by the signals from the remote transmitter, and $\boldsymbol{h}_E$ is the vector of the echo impulse response extended with $M - N$ zeros. In the frequency domain, the echo is expressed as $\boldsymbol{U}_n = \text{diag}(\boldsymbol{A}_n)\boldsymbol{H}_E$, where $\boldsymbol{H}_E$ denotes the DFT of the vector $\boldsymbol{h}_E$. In this case, the echo canceller provides an echo estimate that is given by $\hat{U}_n = \text{diag}(\boldsymbol{A}_n)\boldsymbol{C}_n$, where $\boldsymbol{C}_n$ denotes the DFT of the vector $\boldsymbol{c}_n$ of the N coefficients of the echo canceller filter extended with $M - N$ zeros.

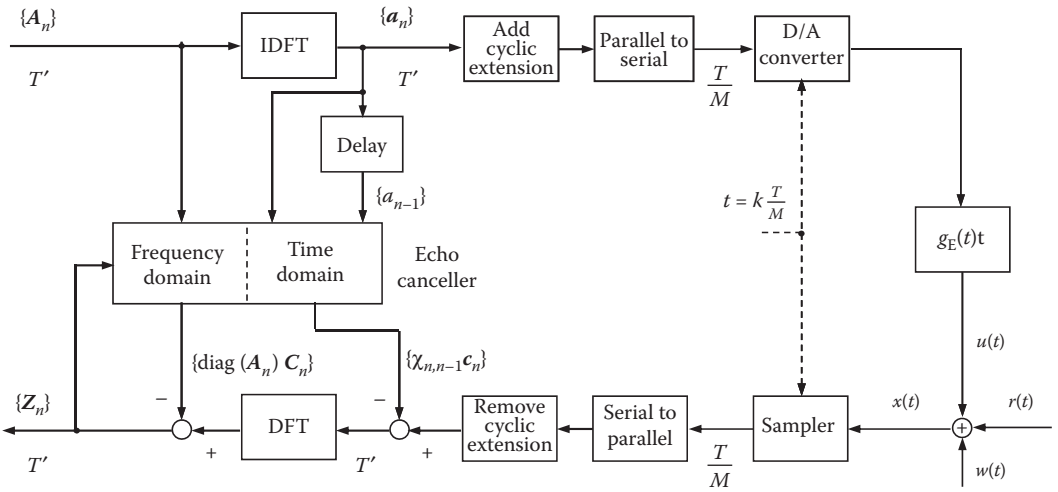

FIGURE 10.9 Configuration of an echo canceller for a DMT transmission system.

In practice, however, we need to consider the case $N > L + 1$. The expression of the cancellation error is then given by

$$\boldsymbol{z}_n = \boldsymbol{x}_n - \boldsymbol{\Psi}_{n,n-1}\boldsymbol{c}_n, \tag{10.29}$$

where the vector of the last M elements of the n-th received block is now $\boldsymbol{x}_n = \boldsymbol{\Gamma}_n^R\boldsymbol{h} + \boldsymbol{\Psi}_{n,n-1}\boldsymbol{h}_E + \boldsymbol{w}_n$, and $\boldsymbol{\Psi}_{n,n-1}$ is an $M \times M$ Toeplitz matrix given by

$$\boldsymbol{\Psi}_{n,n-1} = \begin{bmatrix} a_n(0) & a_n(M-1) & \dots & a_n(M-L) & a_{n-1}(M-1) & \dots & a_{n-1}(L+1) \\ a_n(1) & a_n(0) & \dots & a_n(M-L+1) & a_n(M-L) & & a_{n-1}(L+2) \\ \vdots & & & \ddots & & & \vdots \\ a_n(M-1) & a_n(M-2) & \dots & a_n(M-L-1) & a_n(M-L-2) & \dots & a_n(0) \end{bmatrix}. \tag{10.30}$$

In the frequency domain, the cancellation error can be expressed as

$$\boldsymbol{Z}_n = \mathcal{F}_M(\boldsymbol{x}_n - \chi_{n,n-1}\boldsymbol{c}_n) - \text{diag}(\boldsymbol{A}_n)\boldsymbol{C}_n, \tag{10.31}$$

where $\chi_{n,n-1} = \boldsymbol{\Psi}_{n,n-1} - \boldsymbol{\Gamma}_n$ is an $M \times M$ upper triangular Toeplitz matrix. Equation 10.31 suggests a computationally efficient, two-part echo cancellation technique. First, in the time domain, a short convolution is performed and the result subtracted from the received signals to compensate for the insufficient length of the cyclic extension. Second, in the frequency domain, cancellation of the residual echo is performed over a set of M independent echo subchannels. Observing that Equation 10.31 is equivalent to $\boldsymbol{Z}_n = \boldsymbol{X}_n - \tilde{\boldsymbol{\Psi}}_{n,n-1}\boldsymbol{C}_n$, where $\tilde{\boldsymbol{\Psi}}_{n,n-1} = \mathcal{F}_M\boldsymbol{\Psi}_{n,n-1}\mathcal{F}_M^{-1}$, the echo canceller adaptation by the LMS algorithm in the frequency domain takes the form

$$\boldsymbol{C}_{n+1} = \boldsymbol{C}_n + \alpha\tilde{\boldsymbol{\Psi}}_{n,n-1}^*\boldsymbol{Z}_n, \tag{10.32}$$

where α is the adaptation gain, and $\tilde{\boldsymbol{\Psi}}^{*}_{n,n-1}$ denotes the transpose conjugate of $\tilde{\boldsymbol{\Psi}}_{n,n-1}$. We note that, alternatively, echo canceller adaptation may also be performed by the algorithm $\boldsymbol{C}_{n+1} = \boldsymbol{C}_n + \alpha\,\mathrm{diag}(\boldsymbol{A}^{*}_n)\boldsymbol{Z}_n$, which entails a substantially lower computational complexity than the LMS algorithm, at the price of a slower rate of convergence.

In DMT systems, it is essential that the length of the channel impulse response be much less than the number of subchannels, so that the reduction in data rate due to the cyclic extension may be considered negligible. Therefore, equalization is adopted in practice to shorten the length of the channel impulse response. From Equation 10.31, however, we observe that transceiver complexity depends on the relative lengths of the echo and of the channel impulse responses. To reduce the length of the cyclic extension as well as the computational complexity of the echo canceller, various methods have been proposed to shorten both the channel and the echo impulse responses jointly [9].

Recently, multitone modulation techniques based on filter banks have been proposed in which the *M*-branch filters yield very high spectral containment of individual subchannel signals [3]. The filters are a frequency-shifted version of a prototype filter designed to reduce the interchannel interference to a level that is negligible compared with that of other noise signals. In this case, echo cancellation can be performed by taking into account, for each subchannel, only the echo generated by transmission in the opposite direction on the same subchannel. The implementation of per-subchannel echo cancellation then requires *M* adaptive echo cancellers.

10.5 Summary and Conclusions

Digital signal processing techniques for echo cancellation provide large echo attenuation, and eliminate the need for additional line interfaces and digital-to-analog and analog-to-digital converters that are required by echo cancellation in the analog signal domain. In voiceband modems for data transmission over the telephone network, digital techniques for echo cancellation allow a precise tracking of the carrier phase and frequency shift of far-end echos.

The realization of digital echo cancellers in transceivers for high-speed full-duplex data transmission today is possible at a low cost, thanks to the advances in VLSI technology. Digital techniques for echo cancellation are appropriate for NEXT cancellation in transceivers for transmission over cables at rates of several gigabits per second for local-area network applications.

References

1. Cherubini, G., Analysis of the convergence behavior of adaptive distributed-arithmetic echo cancellers. *IEEE Trans. Commun*., 41(11), 1703–1714, 1993.
2. Cherubini, G., Creigh, J., Ölçer, S., Rao, S.K., and Ungerboeck, G., 100BASE-T2: A new standard for 100 Mb/s Ethernet transmission over voice-grade cables. *IEEE Commun. Mag*., 35(11), 115–122, 1997.
3. Cherubini, G., Eleftheriou, E., and Ölçer, S., Filtered multitone modulation for very high-speed digital subscriber lines. *IEEE J. Sel. Areas Commun.*, 20(5), 1016–1028, 2002.
4. Cherubini, G., Ölçer, S., and Ungerboeck, G., A quaternary partial-response class-IV transceiver for 125 Mbit/s data transmission over unshielded twisted-pair cables: Principles of operation and VLSI realization. *IEEE J. Sel. Areas Commun*., 13(9), 1656–1669, 1995.
5. Duttweiler, D.L., Adaptive filter performance with nonlinearities in the correlation multiplier. *IEEE Trans. Acoust., Speech, Signal Processing*, 30(8), 578–586, 1982.
6. Falconer, D.D., Adaptive reference echo-cancellation. *IEEE Trans. Commun*., 30(9), 2083–2094, 1982.
7. Ho, M., Cioffi, J.M., and Bingham, J.A.C., Discrete multitone echo cancellation. *IEEE Trans. Commun*., 44(7), 817–825, 1996.
8. Lee, E.A. and Messerschmitt, D.G., *Digital Communication*, 2nd ed., Kluwer Academic Publishers, Boston, MA, 1994.

9. Melsa, P.J.W., Younce, R.C., and Rohrs, C.E., Impulse response shortening for discrete multitone transceivers. *IEEE Trans. Commun.*, 44(12), 1662–1672, 1996.
10. Messerschmitt, D.G., Echo cancellation in speech and data transmission. *IEEE J. Sel. Areas Commun.*, 2(2), 283–297, 1984.
11. Messerschmitt, D.G., Design issues for the ISDN U-Interface transceiver. *IEEE J. Sel. Areas Commun.*, 4(8), 1281–1293, 1986.
12. Ruiz, A., Cioffi, J.M., and Kasturia, S., Discrete multiple tone modulation with coset coding for the spectrally shaped channel. *IEEE Trans. Commun.*, 40(6), 1012–1029, 1992.
13. Smith, M.J., Cowan, C.F.N., and Adams, P.F., Nonlinear echo cancellers based on transpose distributed arithmetic. *IEEE Trans. Circuits Systems*, 35(1), 6–18, 1988.
14. Ungerboeck, G., Theory on the speed of convergence in adaptive equalizers for digital communication. *IBM J. Res. Develop.*, 16(6), 546–555, 1972.
15. Weinstein, S.B., A passband data-driven echo-canceller for full-duplex transmission on two-wire circuits. *IEEE Trans. Commun.*, 25(7), 654–666, 1977.
16. Ysebaert, G., Pisoni, F., Bonaventura, M., Hug, R., and Moonen, M., Echo cancellation in DMT-receivers: Circulant decomposition canceler. *IEEE Trans. Signal Processing*, 52(9), 2612–2624, 2004.

Further Reading

For further information on adaptive transversal filters with application to echo cancellation, see *Adaptive Filters: Structures, Algorithms, and Applications*, M.L. Honig and D.G. Messerschmitt, Kluwer, 1984.

11

Synchronization of Communication Receivers

Costas N. Georghiades

Erchin Serpedin

11.1 Introduction

Etymologically, the word synchronization refers to the process of making two or more events occur at the same time, or, by duality, at the same frequency. In a digital communication context, various levels of synchronization must be established before data decoding can take place, including *carrier synchronization*, *symbol synchronization*, and *frame synchronization*.

In radio frequency communications, carrier synchronization refers to the process of generating a sinusoidal signal that closely tracks the *phase* and *frequency* of a received noisy carrier, transmitted by a possibly distant transmitter. Thus, carrier synchronization in general refers to both frequency and phase acquisition and tracking. Of the two, in many cases the more difficult problem is extracting the carrier phase, which is often a much faster-varying process compared to frequency offset. This is especially so since the advent of highly stable crystal oscillators operating in the UHF or lower-frequency bands, although the problem is still prevalent at the higher, microwave, frequencies where crystal oscillators are not available. Frequency acquisition is also a problem in mobile radio applications where due to the Doppler effect, there is an offset in the frequency of the received carrier.

Communication systems that have available, or somehow extract and make use of good (theoretically perfect) carrier frequency and phase information are known as *coherent* systems, in contrast to *incoherent* systems that neglect the carrier phase. Systems that attempt to acquire phase information, but do not do a perfect job, are known as *partially coherent* systems. Coherent systems are known to perform better than incoherent ones, at the price, however, of more complexity required

for carrier synchronization. In this chapter we discuss some of the classical techniques for carrier acquisition, as well as some of the modern techniques, which often involve operating on sampled instead of analog data.

Symbol synchronization is the process of deriving at the receiver timing signals that indicate where in time the transmitted symbols are located. The decision part of the receiver subsequently uses this information in order to decide what the symbols are. As with carrier synchronization, the data available to the receiver for making timing estimates is noisy. Thus, perfect timing information cannot be obtained in practice, although practical systems come close.

Once symbol synchronization is achieved, the next highest synchronization level is frame synchronization. Frame synchronization is necessary in systems for which the unit of information is not a symbol, but rather a sequence of symbols. Such systems are, for example, coded systems where the unit of information is a codeword which consists of a number of symbols. In this case, it is clear that knowing where the symbols are is not enough, and further knowledge of where the codewords are is needed. It is easily seen that the existence of frame synchronization automatically implies symbol synchronization, but the converse is not true. Thus, one might be tempted to attempt frame synchronization before symbol synchronization is achieved, thus achieving both at once. Such an approach, although in theory resulting in better performance, has the disadvantage of requiring more complex processing than the approach of first achieving lower-level synchronization before higher ones are attempted. In practice, almost invariably the latter approach is followed. A rather standard approach to achieving frame synchronization is for the transmitter to insert at the start of every frame a special synchronization pattern, whose detection at the receiver locates frame boundaries. We will look at the optimal frame synchronization processing, as well as some of the desirable characteristics of synchronization sequences later.

There are two general methodologies for achieving the various synchronization levels needed by the receiver. One way is to provide at the receiver side an unmodulated carrier, or a carrier modulated by a known sequence, which can be used solely for the purpose of synchronization. This approach has the advantage of decoupling the problem of data detection and synchronization, and makes the synchronization system design easier. On the other hand, the overall communication efficiency suffers since signal energy and time are used but no information is sent. A second approach, which is often preferred, is to derive synchronization from the data-modulated carrier, the same signal used for symbol decisions. In this way, no efficiency is sacrificed, but the processing becomes somewhat more involved. In the sequel, we will only consider algorithms that use a modulated received signal to derive synchronization. We first start with a look at carrier synchronization algorithms. Excellent general treatments of this and the other synchronization problems studied later can be found in the classic texts of Stiffler [1] and Lindsey and Simon [2], and more recently by Meyr [3,4], and Mengali and D'Andrea [5].

11.2 Carrier Synchronization

11.2.1 Carrier Frequency Synchronization

The objective of a carrier frequency synchronization system consists of estimating and compensating the carrier frequency offset that may be induced at the receiver by oscillator instabilities and/or Doppler shifts. According to the degree of knowledge of the transmitted symbols, carrier frequency synchronizers are classified into three main categories: Data-Aided (DA), Decision-Directed (DD), and Non-Data-Aided (NDA), or blind methods. DA methods assume perfect knowledge of the transmitted symbols, while NDA methods do not require such knowledge. Being more spectrally efficient, the NDA methods are well suited for burst applications. As an intermediate category between the DA and NDA methods, the DD methods rely on knowledge of the symbols obtained at the output of a symbol-by-symbol

decoder. According to the magnitude of the carrier frequency offset that they can cope with, carrier frequency synchronizers may be classified into two classes:

1. Carrier frequency synchronizers that can compensate frequency offsets much smaller than the symbol rate ($1/T$), in general less than 10% of the symbol rate
2. Carrier frequency synchronizers that can compensate for large frequency offsets of the order of the symbol rate ($1/T$)

During initial carrier frequency acquisition, the second class of carrier synchronizers are used in order to reduce large carrier frequency offsets to a small percentage of the symbol rate and to facilitate other carrier or symbol synchronization operations. Compensation of large frequency offsets with magnitudes in the range of 100% of the symbol rate can be performed using either closed-loop (feedback) or open-loop (feedforward) frequency synchronizers. Within the class of closed-loop frequency synchronizers, the most used carrier recovery systems are the approximate maximum likelihood (ML) frequency error detectors [6,7], quadricorrelators [8–11] and dual-filter detectors [12,10], which were shown to be equivalent in Reference 13. Open-loop frequency recovery schemes [14,15], also referred to as delay-and-multiply methods, present shorter acquisition time and are simpler to implement than the closed-loop frequency recovery methods. They also exhibit comparable performance as the approximate ML frequency error detectors [6,7]. Due to these features, open-loop carrier recovery schemes are used in spontaneous packet transmissions, where the frequency synchronization must be performed within a fixed time interval.

Once that the compensation of the large carrier frequency offsets has been accomplished and the receiver operates under steady-state conditions, carrier frequency recovery systems that can track and compensate carrier frequency offsets of magnitude much less than the symbol rate are usually employed. Compensation of frequency offsets with magnitudes in the range of 10% of the symbol rate can be performed by employing DA methods, such as those proposed by Fitz [16,17], Luise and Reggiannini [18], and the approximate ML estimator [5,p.91],[15]. These methods appear to be the best methods available in the literature in terms of implementation complexity and performance. All these methods practically achieve the Cramer–Rao bound at a signal-to-noise ratio (SNR) of zero dB. For burst mode applications, open-loop NDA frequency recovery schemes have been proposed for arbitrary QAM and M-ary PSK input symbol constellations [19–21]. Open-loop NDA frequency recovery schemes estimate the frequency offset based on certain higher-order statistics computed from the received samples, and present limited performance due to the self-noise that is induced by computing the associated higher-order statistics. Due to this reason, second-order cyclostationary statistics-based methods were proposed for NDA carrier frequency offset estimation in both flat-fading and frequency-selective channels (see, e.g. [22–25]).

11.3 Carrier Phase Synchronization

In this section we will formulate the carrier synchronization problem in mathematical terms as an estimation problem and then see how the optimal equations derived can be practically implemented through appropriate approximations. Our optimality criterion is in the sense of ML, under which estimates maximize with respect to the parameter to be estimated the conditional probability density of the data given the parameter (see, e.g., [26]). As pointed out in the Introduction, carrier synchronization may be achieved rather easily by tracking the phase of an unmodulated carrier that is frequency multiplexed with the modulated carrier. In this case, we need not worry about the noise (uncertainty) introduced by the random modulation. On the other hand, the resulting system is inefficient since part of the transmitter power carries no information and is used solely for carrier phase estimation. Although we will look at such synchronizers, our emphasis will be on the more efficient carrier synchronizers that derive their carrier phase estimates from suppressed carrier signals.

11.3.1 Unmodulated Carrier

The received unmodulated signal $r(t)$ is

$$r(t) = s(t;\phi) + n(t), \quad t \in T_0 \tag{11.1}$$

where $s(t, \phi) = A\cos(2\pi f_c t - \phi)$ is the transmitted (unmodulated) signal, ϕ is the carrier phase, and $n(t)$ is a zero-mean, white Gaussian noise process with spectral density $N_0/2$. The ML estimate of the received noisy carrier is the value of ϕ that maximizes the likelihood function, given by (see, e.g., [26])

$$L(\phi) = \exp\left[\frac{2}{N_0}\int_{T_0} r(t)s(t;\phi)\mathrm{d}t - \frac{1}{N_0}\int_{T_0} s^2(t;\phi)\mathrm{d}t\right]. \tag{11.2}$$

Since the second integral above is not a function of ϕ, it can be dropped. Taking the logarithm of the resulting expression, we can equivalently maximize the simplified log-likelihood function given by

$$\ell(\phi) = \frac{2}{N_0}\int_{T_0} r(t)s(t;\phi)\mathrm{d}t. \tag{11.3}$$

Differentiating with respect to ϕ and setting to zero we obtain the following necessary condition for the ML estimate $\hat{\phi}$

$$\int_{T_0} r(t)\sin(2\pi f_c t - \hat{\phi})\mathrm{d}t = 0. \tag{11.4}$$

Solving for $\hat{\phi}$ we obtain

$$\hat{\phi} = \tan^{-1}\left[\frac{\int_{T_0} r(t)\sin(2\pi f_c t)\mathrm{d}t}{\int_{T_0} r(t)\cos(2\pi f_c t)\mathrm{d}t}\right].$$

Figure 11.1 shows how the above estimator can be implemented in block-diagram form in what is referred to as an *open-loop* realization.

A *closed-loop* or tracking synchronizer that uses the optimality condition in Equation 11.4 in a tracking loop referred to as a *phase-locked loop* (PLL) is shown in Figure 11.2. In this figure, VCO stands for voltage controlled oscillator and is a device that produces a sinusoid at the carrier frequency f_c and having an instantaneous frequency which is proportional to its input (or equivalently a phase that is the integral of its input). The integrator in Figure 11.2 over the interval T_0 is a linear filter that in general can be modeled by an impulse response $g(t)$ or a transfer function $G(s)$ and is referred to as the *loop filter*.

Let us now investigate the performance of the PLL synchronizer. We have the following equation describing the PLL in Figure 11.2:

$$\frac{\mathrm{d}\hat{\phi}(t)}{\mathrm{d}t} = \left\{r(t)\sin\left[2\pi f_c t + \hat{\phi}(t)\right]\right\} * g(t) \tag{11.5}$$

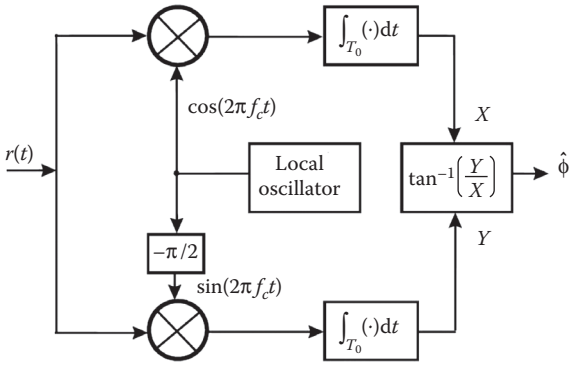

FIGURE 11.1 ML synchronizer: Open-loop.

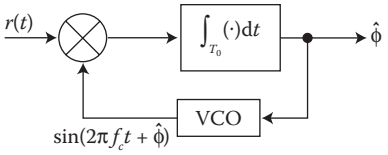

FIGURE 11.2 Phase-locked loop estimator.

where * represents convolution. Substituting for $r(t)$ from Equation 11.1 the product term becomes

$$r(t)\sin\left[2\pi f_c t + \hat{\phi}(t)\right] = \frac{A}{2}\left\{\sin\left[4\pi f_c t + \hat{\phi}(t) + \phi\right] + \sin\left[\hat{\phi}(t) - \phi\right]\right\} + n'(t) \tag{11.6}$$

where $n'(t)$ can be argued to be white and Gaussian with zero mean and spectral density $N_0/4$. Dropping the double-frequency term in Equation 11.6, since it will be filtered out by the much lower bandwidth of the loop, we obtain the following model for the PLL:

$$\frac{d\hat{\phi}(t)}{dt} = \left[\frac{A}{2}\sin\left[\hat{\phi}(t) - \phi\right] + n'(t)\right] * g(t). \tag{11.7}$$

Equation 11.7 is a nonlinear stochastic differential equation that describes the evolution of the phase estimate and is modeled in Figure 11.3. If we let $e(t) = [\hat{\phi}(t) - \phi]$ be the phase error, then it is easily seen (since ϕ is not a function of time) that the phase-error is described by

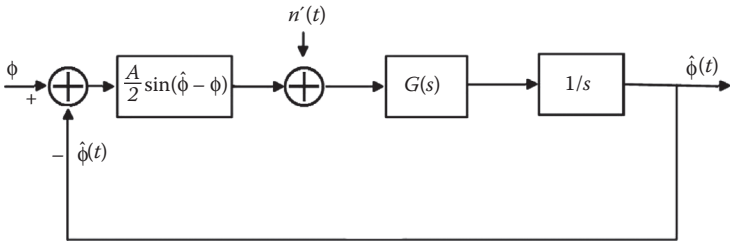

FIGURE 11.3 Equivalent PLL model for performance analysis.

$$\frac{de(t)}{dt} = \left[\frac{A}{2}\sin\left[e(t)\right] + n'(t)\right] * g(t). \tag{11.8}$$

An analytical solution for the density of the error $e(t)$ in steady state has been derived (see Viterbi [27]) for the special case when $G(s) = 1$ and is given by the *Tichonov density function*

$$p(e) = \frac{\exp\left[\alpha\ \cos(e)\right]}{2\pi\ I_0(\alpha)}, \quad -\pi \le e \le \pi. \tag{11.9}$$

where $\alpha = 4A/N_0$ and $I_0(\cdot)$ is the zero-order modified Bessel function. For large α, that is, large signal-to-noise ratios (SNRs), the variance of the phase-error computed from Equation 11.9 can be approximated by $\sigma_e^2 \cong 1/\alpha$. Further, for large SNRs, the error will be small on the average, and so in Equation 11.8 $\sin(e) \cong e$. Under this approximation, Equation 11.8 (and consequently Equation 11.7) become linear. Figure 11.4 shows the linearized model for a PLL.

For the linear model in Figure 11.4, an expression for the variance of the estimation error in steady state can be derived easily by computing the variance of the output $\hat{\phi}$ when the input is just the noise $n'(t)$. The following expression for the variance of the estimation error can be derived (which is a good approximation to the actual variance at high SNRs when the linearized model is valid)

$$\sigma_e^2 = \frac{2N_0B_L}{A^2}, \tag{11.10}$$

where the parameter B_L is known as the (one sided) *loop noise equivalent bandwidth* and is given by

$$B_L = \frac{1}{\max\ \left|H(f)\right|^2}\int_0^\infty \left|H(f)\right|^2 df. \tag{11.11}$$

In Equation 11.11, $H(s)$ is the closed-loop transfer function of the (linearized) loop and is given by

$$H(s) = \frac{AG(s)}{2s + AG(s)}. \tag{11.12}$$

A simple computation of the variance given by Equation 11.9 for the special case when $G(s) = 1$ yields $1/\alpha$, as expected. The advantage of Equation 11.10 is that it can be used for a general function $G(s)$, provided the signal-to-noise ratio is large enough for the linear approximation to hold. Note also that the estimation error becomes smaller with decreasing bandwidth B_L. Thus, one might be tempted to reduce B_L to zero. The

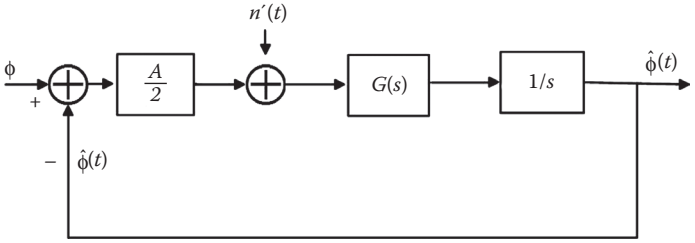

FIGURE 11.4 Linearized PLL model for performance computation.

problem in this case is that the transient performance of the loop degrades to the extent that it may take a longer period of time to achieve a small error. Also, in practice the input phase ϕ is time varying, in which case the loop bandwidth should be large enough so that the loop can track the changes in the input. We now turn our attention to finding the performance of the ML carrier synchronizer in Figure 11.1.

We make use of the Cramer–Rao lower bound [26] that states that under some conditions, the variance of the estimation error for *any* unbiased estimate of a parameter ϕ is lower bounded by

$$\sigma_e^2 = \frac{-1}{E\left[\dfrac{\partial^2 \ln p(r|\phi)}{\partial \phi^2}\right]}, \tag{11.13}$$

where $\ln p(r|\phi)$ is the log-likelihood function, given by Equation 11.3 for the phase estimation problem. Using Equation 11.13, we obtain

$$\sigma_e^2 \geq \left\{\frac{2A}{N_0}\int_{T_0} E\left[r(t)\right]\cos(2\pi f_c t + \phi)\mathrm{d}t\right\} = \frac{2N_0}{A^2}\frac{1}{2T_0}. \tag{11.14}$$

Simple calculations show that $1/T_0$ corresponds to the equivalent noise bandwidth of the integrator. Thus, if the equivalent noise bandwidths in Equations 11.10 and 11.14 are the same, the performances of the ML and the PLL synchronizers are the same (assuming that the bound in Equation 11.14 is achieved closely). Next, we address carrier extraction from a modulated carrier, which as pointed out earlier, is in practice the preferred approach for efficiency reasons.

11.3.2 Synchronization from a Modulated Carrier

A suboptimal approach, often used in practice, to extract carrier synchronization from a modulated signal is to first nonlinearly pre-process the signal to "wipe off" the modulation, and then follow that by, for example, a PLL, as described above. For M-ary phase-shift keying (PSK), the nonlinear pre-processing involves taking the M-th power of the signal. This has the effect of multiplying the carrier phase by M, and thus a subsequent division by M is needed to match the original carrier phase. For PSK signaling, a side effect of the power-law nonlinearity is to introduce a phase ambiguity, which must be resolved either by using pilot symbols or (which is the case in practice) through the use of *differential encoding* of the data (information is conveyed by the change in the phase relative to the previous baud interval, rather than absolute phase).

Besides the suboptimal power-law technique, ML estimation can be used to suggest the optimal processing and possible approximations, which we study next. Let the modulated data be

$$r(t) = s(t;d,\phi) + n(t) \tag{11.15}$$

where d is a sequence of N modulation symbols. For simplicity we will assume binary antipodal signals in which case each component, d_k, of d is either 1 or -1. If we let the baud rate be $1/T$ symbols/s, then the signal part in Equation 11.15 can be expressed as

$$s(t;d,\phi) = A\sum_{k=0}^{N-1} d_k \cos(2\pi f_c t + \phi)\, p(t - kT), \tag{11.16}$$

where $p(t)$ is a baseband pulse which determines to a large extent the spectral content of the transmitted signal. In addition, we are assuming a data window of length N. For simplicity, we will assume a unit

height rectangular pulse next, but the results can be generalized to any arbitrary pulse shape. Assuming for the moment that the modulation sequence d is known, we have the following conditional likelihood function

$$L(\phi) = \exp\left[\frac{2}{N_0}\int_0^{NT} r(t)s(t;d,\phi)\mathrm{d}t\right] = \exp\left[\frac{2A}{N_0}\sum_{k=0}^{N-1} d_k \int_{kT}^{(k+1)T} r(t)\cos(2\pi f_c t + \phi)\,\mathrm{d}t\right]. \tag{11.17}$$

All we need to do now is take the expectation of the conditional likelihood function in Equation 11.17 with respect to the random modulation sequence. Assuming that each binary symbol occurs with probability 1/2 and that symbols are independent, we obtain the following log-likelihood function after dropping terms that are not functions of ϕ and taking the logarithm of the resulting expression

$$\Lambda(\phi) = \sum_{k=0}^{N-1} \ln\cosh\left[\frac{2A}{N_0}\int_{kT}^{(k+1)T} r(t)\cos(2\pi f_c t + \phi)\,\mathrm{d}t\right]. \tag{11.18}$$

A ML estimator maximizes the above expression with respect to the phase ϕ. To reduce the implementation complexity, the following approximations $\ln\cosh(x) \propto x^2$ and $\ln\cosh(x) \propto |x|$, are used at small and large signal-to-noise ratios, respectively. In the case of small SNRs, the log-likelihood simplifies to

$$\ell(\phi) = \sum\left[\int_{kT}^{(k+1)T} r(t)\cos(2\pi f_c t + \phi)\,\mathrm{d}t\right]^2. \tag{11.19}$$

Taking the derivative of Equation 11.19 with respect to ϕ, the following necessary condition for the ML estimate $\hat{\phi}$ of ϕ is obtained

$$\sum_{k=0}^{N-1}\int_{kT}^{(k+1)T} r(t)\cos(2\pi f_c t + \hat{\phi})\mathrm{d}t \times \int_{kT}^{(k+1)T} r(t)\sin(2\pi f_c t + \hat{\phi})\mathrm{d}t = 0. \tag{11.20}$$

A tracking loop that dynamically forces the condition in Equation 11.20 is shown in Figure 11.5. Note that the product of the two integrals effectively removes the modulation. In practice, the summation operator may be replaced by a digital filter that applies different weights to the past and present data in order to improve response.

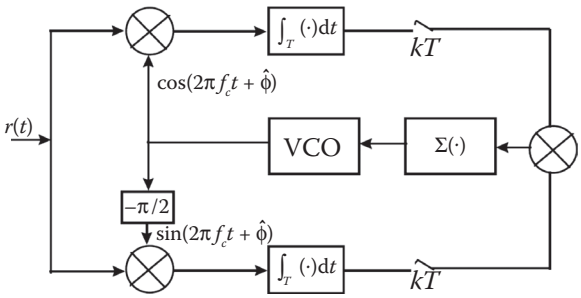

FIGURE 11.5 Carrier synchronization from modulated data.

11.4 Carrier Acquisition for QAM Constellations

The need for high throughputs required by several high-speed applications (such as digital TV, satellite communications, broadcasting networks) has pushed system designers toward more throughput-efficient modulation schemes. Because of their relatively good performance, large QAM constellations are being used in many of these applications. One of the problems associated with their use is that of carrier acquisition, which for reasons of efficiency must often be done without the use of a preamble. The problem is further complicated for cross QAM constellations, for which the high-SNR corner points used by some simple carrier phase estimators are not available. Clearly, due to the phase symmetry of QAM constellations, only phase offsets modulo $\pi/2$ are detectable and differential encoding is used to resolve the ambiguity.

The phase synchronization problem is invariably divided into an acquisition and a tracking part. In many practical systems, tracking is done simply and efficiently in a DD mode after acquisition has been established, and it is the acquisition problem that is the most problematic, especially in applications where no preamble is allowed. For square QAM constellations a simple technique for phase acquisition is based on detecting the signals at the four corners and using them to produce an estimate of the phase-offset which can be averaged in time to converge to a reliable estimate. The problem is more complicated for cross constellations which do not have the corner points.

We first look at the ML carrier phase estimator. Let

$$r_k = d_k e^{j\theta} + n_k$$

be the baud-rate samples of the output of a matched filter, where d_k is a complex number denoting the transmitted QAM symbol at time kT ($1/T$ is the signaling rate), and θ denotes the unknown phase-offset to be estimated. The effect of noise is modeled in terms of the variables n_k, which are complex, independent, identically distributed (i.i.d.), zero-mean Gaussian random variables with independent real and imaginary parts of variance σ^2. Without loss of generality, we assume that $E\left[d_k^2\right] = 1$ (i.e., a unit average energy constellation), in which case the signal-to-noise ratio per symbol is $\mathrm{SNR} = 1/2\sigma^2$. Then the ML phase estimate of θ from data over a window of length N is easily obtained as the value of ϕ that maximizes the log-likelihood function

$$L(\phi) = \sum_{k=1}^{N} \ln\left[\sum_{d} \exp\left(-\frac{1}{2\sigma^2}\left|r_k - d \cdot e^{\phi\theta}\right|^2\right)\right],$$

where the inner summation is performed with respect to the data d present in the constellation. The complexity of the ML algorithm is due in part to this inner summation, which even for small constellations will require more computations than possible, especially for high-speed systems. Another complication in implementing the ML estimator is the need to solve a nonlinear maximization problem in order to find the ML estimate of ϕ. Some simplifications of the ML estimator can be obtained for square constellations, but they are not sufficient to bring the ML estimator into a practical form.

For square constellations, a simple algorithm can be used to extract carrier phase by detecting the presence of one of the four corner points in the constellation. These points can be detected by setting an amplitude threshold between the peak amplitude of the corner points and the second-largest amplitude. The angles of these four points can be expressed as

$$\phi^i = \frac{\pi}{4} + i \cdot \frac{\pi}{2}, \quad i = 0,1,2,3.$$

Thus,

$$\phi^i = \frac{\pi}{4} \mod\left(\frac{\pi}{2}\right).$$

Since only phase rotations modulo π/2 are required, a simple estimator looks at the angle of the received sample r_k modulo π/2 and subtracts it from π/4. The result is the required estimate, which can be refined in time as more data are observed.

Another often used algorithm, which has been shown in Reference 28 to be asymptotically the ML estimator in the limit of small SNRs, is the M-th power-law estimator, where $M = 4$ for QAM constellations, and it equals the size of the constellation for PSK signaling. For QAM signaling, the 4-the power estimator extracts a phase estimate according to

$$\hat{\varphi} = \frac{1}{4}\arg\left[E[d^{*4}] \cdot \sum_{k=1}^{N} r_k^4\right].$$

The approximate mean-square error performance of the above estimator was also obtained in Reference 28. Another algorithm that seems to work well for both square and cross constellations was reported in Reference 29. The algorithm referred to as the histogram algorithm (HA) assumes the following steps: (1) For each received sample r_k it finds the set of signals whose magnitude is closest to $|r_k|$. (2) Compute the angle of the subset of signals from Step 1 belonging to the first quadrant. (3) Subtract each of the angles computed at Step 2 from the angle of r_k. (4) Uniformly quantize the angle interval from 0° to 90° into L bins, and associate a counter with each; increment the counters corresponding to the quantization intervals where the angles computed at Step 3 fall in. (5) Repeat this process for new data r_k as they arrive. (6) When enough data is received, find the bin that has the largest counter value. The angle corresponding to this bin is produced as the phase estimate.

Figure 11.6 compares the performance of the ML and HA algorithms obtained through simulation to the Cramer–Rao bound for the 128-QAM (cross) constellation. Results for the 4-th power estimator are

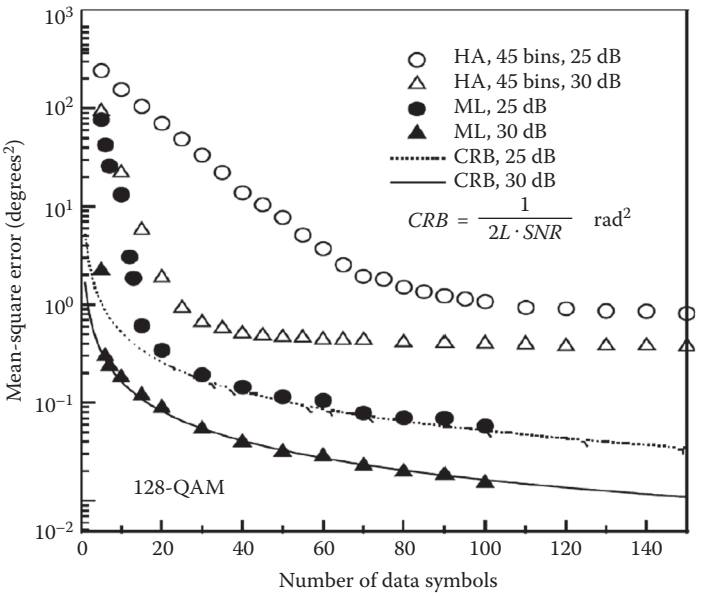

FIGURE 11.6 Mean square error for the various algorithms and 128-QAM.

shown separately in Figure 11.7 since the performance of this estimator is about two orders of magnitude worse than the ML and HA algorithms. The reason behind the poor performance of the 4-th power estimator is the existence of large self-noise, partly due to the absence of the corner points. These results indicate that the 4-th power estimator is not an option for cross constellations, at least not for sizes greater than or equal to 128.

Figure 11.8 compares the HA and the 4-th power estimators for the 256-QAM (square) constellation. As can be seen, the 4-th power estimator performs much better with square constellations, and in fact it outperforms the HA for a range of data sequence lengths at 25 dB SNR. As the SNR increases, however, the self-noise dominates and the performance of the 4-th power estimator degrades.

In closing this section, we mention that an algorithm for joint estimation of carrier phase and frequency for 16-QAM input constellations was proposed in Reference 30 and shown to achieve the Cramer–Rao bound for SNR's greater than 15 dB. A comprehensive performance analysis of the NDA

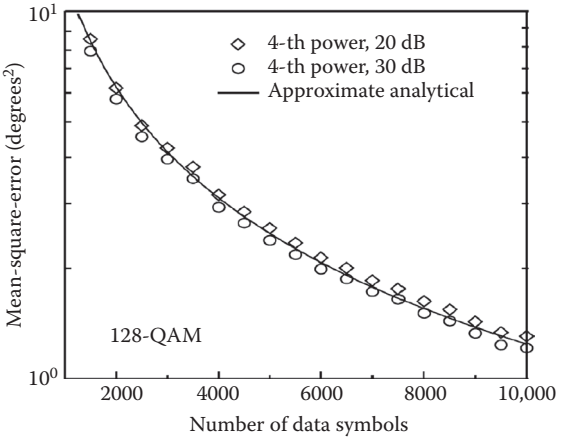

FIGURE 11.7 The performance of the 4-th power estimator for 128-QAM.

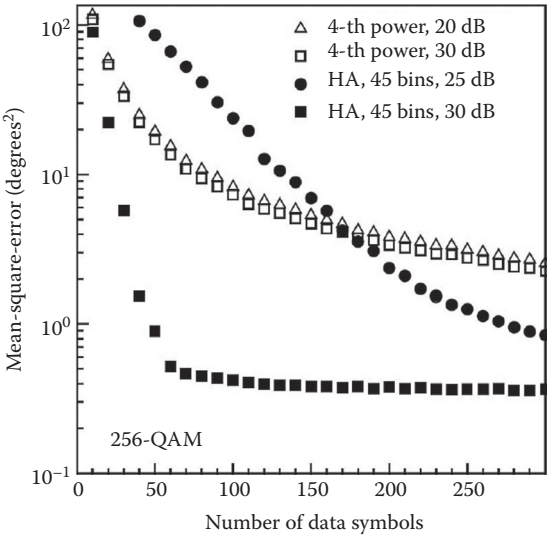

FIGURE 11.8 The HA versus the 4-th power algorithms for 256-QAM.

carrier phase estimators that have been proposed for large QAM modulations and assessment of their relative merits was reported in Reference 31.

11.5 Symbol Synchronization

We first investigate symbol synchronizers that are optimal in a ML sense. The ML symbol synchronizer can be used to suggest suboptimal but more easily implementable algorithms, and provides a benchmark against which the performance of other synchronizers can be compared. Let T be the symbol duration and $r(t)$ be the received data. A channel model of the following form is assumed:

$$r(t) = s(t;d,\tau) + n(t), \tag{11.21}$$

where $n(t)$ is zero-mean white Gaussian noise having spectral density $N_0/2$, d denotes the sequence of modulation symbols d_k, $k = \ldots, -1,0,1, \ldots$, and τ stands for the timing-error. Assuming pulse-amplitude modulation (PAM), the data carrying signal is described explicitly by

$$s(t;d,\tau) = \sum_k d_k p(t - kT - \tau), \tag{11.22}$$

where $p(t)$ stands for the baseband pulse. The timing recovery problem reduces to processing the received signal $r(t)$ in order to obtain an estimate of the timing-error τ. To avoid loss in communication efficiency, we will do this in the presence of modulation symbols. For simplicity, a binary system with antipodal signals (one signal is just the negative of the other), $d_k \in \{1, -1\}$, is assumed.

As previously for carrier phase estimation, ML synchronization requires the probability density function of the data given the timing-error τ. Conditioned on knowing the data sequence d, the likelihood function is given by Equation 11.2 (with the signal part now given by Equation 11.22). Since the quadratic term does not depend on τ, the ML function can be reduced to

$$L(\tau,d) = \exp\left[\frac{2}{N_0}\sum_k d_k \int_{-\infty}^{\infty} r(t)p(t - kT - \tau)\mathrm{d}t\right]. \tag{11.23}$$

All we need to do now is take the expectation of the above conditional likelihood function with respect to the data sequence to obtain the likelihood function. Performing the expectation and assuming independent and equiprobable data, we obtain (after taking the logarithm of the resulting expression) the reduced log-likelihood function

$$\ell(\tau) = \sum \ln\cosh\left[\frac{2q_k(\tau)}{N_0}\right], \tag{11.24}$$

where

$$q_k(\tau) = \int_{-\infty}^{\infty} r(t)p(t - kT - \tau)\mathrm{d}t. \tag{11.25}$$

A ML synchronizer finds the estimate $\hat{\tau}$, which maximizes the log-likelihood function in Equation 11.24 based on the received data. Several problems arise as we try to implement this optimal synchronizer: (a) obtaining an ML estimate requires maximizing in real-time (11.24), an impossible task in most

practical cases; (b) implementation of Equation 11.24 requires knowledge of the signal-to-noise ratio, which is not readily available and must be estimated; (c) there is no simple way to exploit Equation 11.24 to extract timing estimates in real time. The problem associated with (a) above can be partly alleviated by approximating the ln cosh (·) function for large and small SNRs as was done before, which results in

$$\begin{aligned} \ell(\tau) &\cong \sum_k q_k^2(\tau), \quad \text{low SNR,} \\ \ell(\tau) &\cong \sum_k |q_k(\tau)|, \quad \text{high SNR.} \end{aligned} \tag{11.26}$$

In addition to simplifying the log-likelihood function, the approximations above also obviate the need for knowing the SNR. The need, however, to maximize a nonlinear function in real time still exists.

As for the carrier synchronization problem, a number of open-loop realizations of the ML timing estimator exist. Perhaps the more interesting algorithms from a practical viewpoint are the closed-loop algorithms, two of which we motivate next. Taking the derivative of Equation 11.24 with respect to τ and equating to zero results in an equation whose solution yields the ML timing estimate:

$$\begin{aligned} \left.\frac{\partial \ell(\tau)}{\partial \tau}\right|_{\tau=\hat{\tau}} &= \sum_k \left[\frac{2}{N_0}\int_{-\infty}^{\infty} r(t)\frac{\partial p(t-kT-\tau)}{\partial \tau}\mathrm{d}t\right] \\ &\quad \times \tanh\left[\frac{2}{N_0}\int_{-\infty}^{\infty} r(t)p(t-kT-\tau)\mathrm{d}t\right] = 0, \end{aligned} \tag{11.27}$$

where we have assumed that $p(-\infty) = p(\infty) = 0$. Note that if the timing τ is other than the ML estimate $\hat{\tau}$ that makes the left-hand side of Equation 11.27 equal to zero, the above derivative will be either positive or negative depending on the sign of the error $(\tau - \hat{\tau})$. Thus, the derivative can be used in a tracking loop to provide a correcting signal in a system that dynamically produces the ML timing estimate. Such a system is shown in Figure 11.9, where the timing pulse generator adjusts the phase of the timing depending on the output of the accumulator once every T seconds. In practice, the accumulator may be replaced by a digital filter whose response is such that it puts more emphasis on recent data and less on past data. Clearly, when the timing-jitter is fast changing, better results may be obtained by employing a short memory filter. On the other hand, if the timing-jitter is slowly varying, a filter with a long memory (low bandwidth) will yield better results.

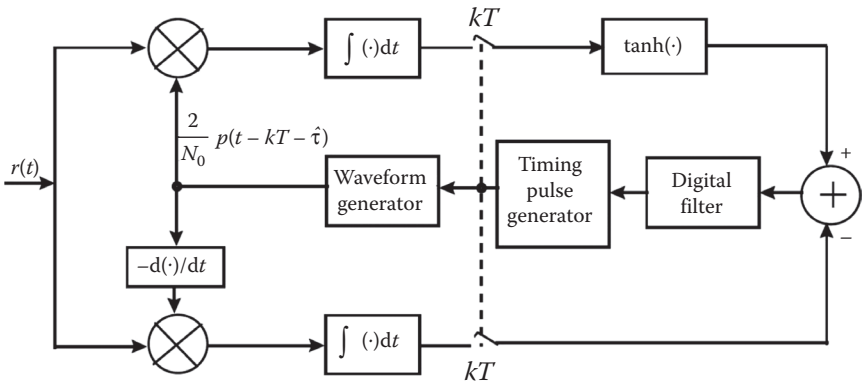

FIGURE 11.9 Closed-loop timing synchronizer.

Further simplifications to the above tracking synchronizer can be made under the assumptions of low or high signal-to-noise ratios, in which case Equation 11.26 instead of Equation 11.24 may be used. If the derivative of the likelihood function with respect to τ is approximated by the difference

$$\frac{\partial \ell(\tau)}{\partial \tau} \cong \frac{\ell(\tau + \delta/2) - \ell(\tau - \delta/2)}{\delta}, \tag{11.28}$$

then under the high-SNR approximation, Equation 11.27 can be replaced by

$$\frac{\partial \ell(\tau)}{\partial \tau} \cong \sum_k \left[\left| \int_{-\infty}^{\infty} r(t) p(t - kT - \tau - \delta/2) \mathrm{d}t \right| - \left| \int_{-\infty}^{\infty} r(t) p(t - kT - \tau + \delta/2) \mathrm{d}t \right| \right]. \tag{11.29}$$

A tracking-loop synchronizer, known as an *early-late gate symbol synchronizer*, implements Equation 11.29 and is shown in Figure 11.10. A similar synchronizer using a low-SNR approximation can be developed. The intuitive explanation of how early-late gate symbol synchronizers work is simple and can be easily illustrated for the case of nonreturn to zero (NRZ) pulses whose pulse shape $p(t)$ and autocorrelation function $a(t)$ are shown in Figure 11.11.

In the absence of timing-error, the receiver samples the output of the matched filter at the times corresponding to the peak of the autocorrelation function of the NRZ pulse (which results in the largest SNR). When a timing error exists, the samples occur at either side of the peak depending on whether the error is positive or negative. In either case, because of the symmetry of the autocorrelation function, the samples are of the same value (on the average). In an early–late gate synchronizer, two samples are taken, separated by δ seconds and centered around the current timing estimate. Depending on whether the

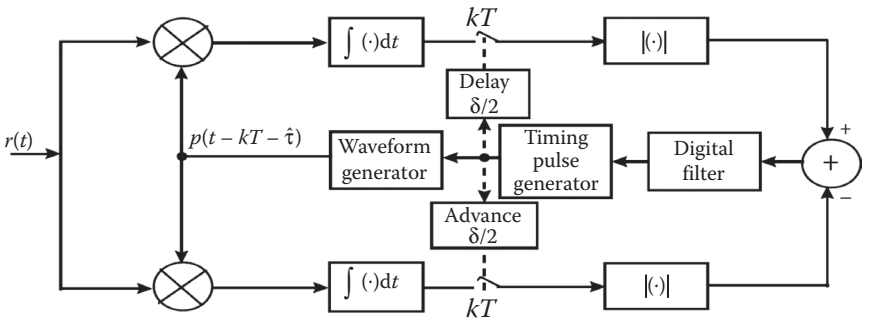

FIGURE 11.10 The early–late gate synchronizer.

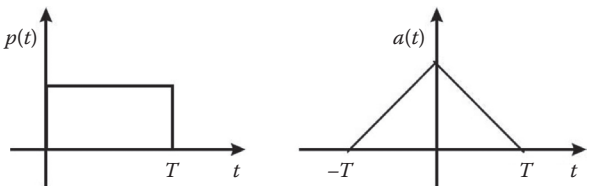

FIGURE 11.11 Example for NRZ pulses.

error is positive or negative, the difference between the absolute values of these samples will be positive or negative, thus providing a control signal to increase or decrease $\hat{\tau}$ in the desired direction to reduce the error. Note that on the average, due to the even symmetry of the autocorrelation function, the difference between the absolute values of the two samples is zero at the actual symbol timing phase, that is, when the timing error is zero. Thus, at least intuitively, the system in Figure 11.10 is a stable loop for tracking the symbol timing phase. We end this section by noting that a number of practical implementations based on some further simplification of the synchronizers discussed above are used in practice [3–5,32].

11.6 To Browse Further

In modern receivers, more and more of the processing is done in the discrete domain, which allows for more complicated algorithms to be accurately implemented compared to analog implementations. For timing recovery, the preferred technique is to process samples taken at the output of a matched (or other suitable) filter at rates as low as the baud rate to a few samples per baud. The advantage of baud-rate sampling is that it uses the same samples that the detector uses to make symbol decisions, and it is the lowest rate possible, making the sampler less costly, and processing of samples faster. The disadvantage is that baud-rate sampling is below the Nyquist rate and thus acquisition performance tends to suffer somewhat. For bandlimited signaling, two or more samples per baud are at or above the Nyquist rate, and thus all information contained in the original analog signal is preserved by the sampling process. This means that the sampler can be free-running without the need to adjust its sampling phase since that can be done in the discrete domain through interpolation.

Perhaps the most known paper on timing-recovery from baud-rate samples is that by Mueller and Muller [33]. The timing algorithms studied in [33] are decision-directed (make use of tentative symbol decisions) and use the baud-rate samples in order to estimate the timing error. The timing error information is then used to adjust the phase of the sampler toward reducing the timing error. Other works that consider two or more samples per baud have been reported in References 34 through 36.

11.7 Frame Synchronization

As noted in the introduction, frame synchronization is obtained in practice by locating at the receiver the position of a frame synchronization pattern (referred to also as a *marker*), periodically inserted in the data stream by the transmitter. In most systems, partly for simplicity and partly because the periodicity of the marker insertion makes it easily identifiable when enough frames are processed, the marker is not prevented from appearing in the random data stream. This means that it should be long enough compared to the frame length to make the probability of it appearing in the data small. If we let the synchronization pattern be of length L and the frame size (including the marker) be of length N, then the efficiency of such a system, measured by the number of data symbols per total frame length is

$$e = 1 - \frac{L}{N}. \tag{11.30}$$

The efficiency can be made arbitrarily close to one by increasing N for a fixed L, or by decreasing L for a fixed N. In both cases, however, the probability of correctly detecting the position of the marker is reduced. In practice, good first pass acquisition probabilities can be achieved with efficiencies of about 97%. Figure 11.12 shows the contents of a frame.

As for the symbol synchronization case, we will first introduce the optimum (ML) frame synchronizer and then investigate some sub-optimum synchronizers. For simplicity, we will only look at binary antipodal baseband signaling, although in qualitative terms similar results hold for nonbinary systems.

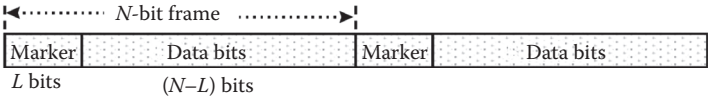

FIGURE 11.12 The composition of a frame.

In the sequel, we assume that perfect symbol synchronization is present. As usual, we assume an additive white Gaussian noise channel, in which case the sufficient statistic (loosely speaking, the simplest function of the data required by the optimum synchronizer to retain its efficiency) is the baud-rate samples of the output of a matched filter. Let $r = (r_1, r_2, \ldots, r_N)$ be the vector of the observed data obtained by sampling the output of a matched filter (matched to the baseband pulse) at the correct symbol rate and phase (no symbol timing-error), but not necessarily at the correct frame phase. Under a Gaussian noise assumption, the discrete matched filter samples can be modeled by

$$r_k = \sqrt{E}d_k + n_k, \tag{11.31}$$

where E is the signal energy, $d_k \in \{1, -1\}$ is the k-th modulation symbol and the n_k's constitute a sequence of independent and identically distributed (i.i.d.) Gaussian random variables with zero mean and variance σ^2.

It is clear that since the frame length is N, there is exactly one frame marker within the observation window. Our problem is to locate the position $m \in (0,1,2,\ldots,N-1)$ of the marker from the observed data r. If m is the actual position of the marker, then the data vector corresponding to the observed vector r is

$$d = (d_1, d_2, \ldots, d_{m-1}, d_m, \ldots, d_{m+L-1}, \ldots, d_N),$$

where the L-symbol sequence starting at position m is the marker. If we denote the marker by S, this means

$$S = (s_1, s_2, \ldots, s_L) = (d_m, d_{m+1}, \ldots, d_{m+L-1}).$$

For ML estimation of m, we need to maximize the following conditional density:

$$p(r|m) = \sum_{d'} p[r|m, d']\Pr(d') \tag{11.32}$$

where d' is the $(N-L)$-symbol data sequence that surrounds the marker. Assuming equiprobable symbols, Massey [37] derived the following log-likelihood function

$$L(m) = \sum_{k=1}^{L} s_k r_{k+m} - \frac{\sigma^2}{\sqrt{E}} \sum \ln\cosh\left(\frac{\sqrt{E}}{\sigma^2} r_{k+m}\right). \tag{11.33}$$

To account for the periodicity of the marker, indices in Equation 11.33 are interpreted modulo N. An optimal frame synchronizer computes the above expression for all values of m and chooses as its best estimate of the marker position the value that maximizes $L(m)$.

A few observations are now in order regarding the above likelihood function. First, we note that $L(m)$ is the sum of two terms: a linear term and a nonlinear term. The first term can be recognized as the

correlation between the received data r and the known marker, while the second term can be interpreted as an energy correction term that accounts for the random data surrounding the marker.

For practical implementation, some approximations of the optimal rule can be obtained easily by approximating ln cosh(·). For high SNRs, by replacing ln cosh(x) by $|x|$, it follows that

$$L(m) \cong \sum_{k=1}^{L} s_k r_{k+m} - \sum_{k=1}^{L} |r_{k+m}|. \tag{11.34}$$

For low SNR's, replacing ln cosh(x) by $x^2/2$, the optimal rule becomes

$$L(m) \cong \sum_{k=1}^{L} s_k r_{k+m} - \frac{\sqrt{E}}{2\sigma^2} \sum_{k=1}^{L} r_{k+m}^2. \tag{11.35}$$

A further approximation that is quite often used is to drop the second nonlinear term altogether. The resulting rule then becomes

$$L(m) \cong \sum_{k=1}^{L} s_k r_{k+m}, \tag{11.36}$$

and is known as the *simple correlation rule* for obvious reasons. The high SNR approximation and the simple correlation rule have the added advantage that no knowledge of the SNR is needed for implementation, compared to the optimum and the low-SNR approximation rules.

Practical frame synchronizers use the periodicity of the marker in order to improve performance in time, and usually include algorithms for detecting loss of synchronization in which reacquisition is initiated. The above algorithms can be used as the basis for these practical synchronizers in estimating the marker position from a frame's-worth of data. Their performance in correctly identifying the marker position significantly affects the overall performance of the frame synchronizer, as measured not only by the probability of correct acquisition, but also the time it takes for the algorithm to acquire.

Other techniques for marker acquisition (besides those based on the ML principle) can be used as well. For example, in some practical implementations of the simple correlation rule, often sequential detection of the marker is implemented: the correlation of the marker with the data is computed sequentially for each frame position and the result is compared to some threshold. When for some value of m the computed correlation exceeds the threshold, the frame synchronizer declares a marker presence. Otherwise the search continues. The value of the threshold is critical for performance and it is usually chosen to minimize the time to marker acquisition.

Another important aspect of frame synchronization design is the design of good marker sequences. Although the above algorithms work with any chosen sequence, the resulting performance of the synchronizer depends critically on the sequence used. In general, sequences that have good autocorrelation properties perform well as frame markers. These sequences have the property that their autocorrelation function is uniformly small for all shifts other than the zero shift. Examples of such sequences include the *Barker sequences* [38] and the *Neuman–Hofman sequences* [39]. Barker sequences are binary sequences whose largest side-lobe (nonzero shift correlation) is at most 1. Unfortunately, the largest known Barker sequence is of length 13, and there is proof that no Barker sequences of length between 14 and 6084 exist. In many cases, however, there is a need for larger sequences to improve performance. Neuman–Hofman sequences were specifically designed to maximize performance when a simple correlation rule is used. Thus, these sequences perform somewhat better than Barker sequences when a

correlation rule is used. What is more important though is that Neuman–Hofman sequences of large length exist. Examples of Barker and Neuman–Hofman sequences of length 7 and 13 are

(1, −1, 1, 1, −1, −1, −1), Barker, $L = 7$,
(1, 1, 1, 1, 1, −1, −1, 1, 1, −1, 1, 1, 1), Barker, $L = 13$,
(−1, −1, −1, −1, −1, −1, 1, 1, −1, −1, 1, −1, 1), Neuman–Hofman, $L = 13$.

11.7.1 Performance

We address briefly next the performance of the ML and two suboptimal synchronizers given above, as measured by the probability of erroneous synchronization. First, we look at the question of how well *any* frame synchronizer can perform, as a function of the frame length N, marker length L, and SNR. Clearly, in the limit of infinite SNR we obtain the best performance (smallest probability of erroneous marker detection). In this case, an error can be made when the marker appears randomly in one or more positions in the random data part. For *bifix-free* sequences (i.e., sequences for which no prefix is also a suffix) Nielsen [40] has obtained the following expression for the probability of erroneous synchronization:

$$P_{LB} = \sum_{k=1}^{R} \frac{(-1)^{k+1}}{k+1} \cdot \binom{N - L - k(L-1)}{k} \cdot M^{-kL}, \tag{11.37}$$

where

$$R = \left\lfloor \frac{N-L}{L} \right\rfloor, \tag{11.38}$$

and M is the size of the modulation ($M = 2$ for binary signaling). The bifix-free condition guarantees that no partial overlap of the marker with itself results in a perfect match for the overlapped parts. Figure 11.10 shows simulation results for the performance of the ML, high-SNR approximation, and simple-correlation rules of Equations 11.33, 11.34, and 11.36, respectively. Shown also is the lower bound in Equation 11.37, which is achieved by the ML rule and its high SNR approximation. On the other hand, the simple-correlation rule performs significantly worse (Figure 11.13).

11.8 Synchronization of MIMO Systems

11.8.1 General Considerations

Deployment of multiple transmit and receive antennas over multiple-input multiple-output (MIMO) wireless fading channels has been considered an efficient means to increase channel capacity and overcome channel fading via diversity. However, to take advantage of the capacity and diversity gains, carrier and timing synchronization is required at the multiple-antenna-based receiver to perform optimum demodulation.

In general, achieving synchronization in a MIMO communication system is much more complex and difficult than in a single-input single-output (SISO) system. This is due to the fact that synchronization of a MIMO system assumes acquisition of an increased number of parameters (e.g., different carrier frequency offsets/Doppler shifts between different transmit (Tx)—receive (Rx) antennas, and different timing delays in the data streams collected by the Rx antennas) relative to a SISO system. In addition, the data streams sent in parallel by different Tx antennas get superposed at each Rx antenna. Therefore, the output of each Rx antenna represents a combination of different signals with possibly different frequency offsets and timing delays, which makes the synchronization problem difficult.

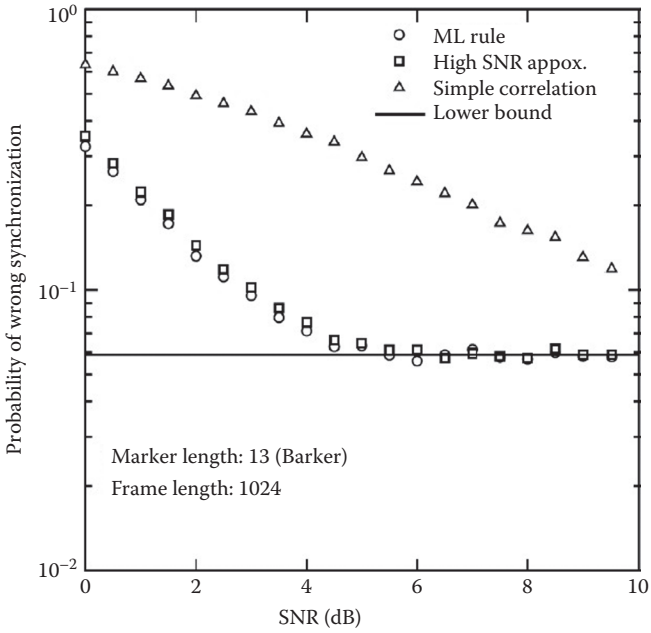

FIGURE 11.13 The performance of the ML and other rules.

Fortunately, for many applications the Tx and Rx antennas are placed in close proximity of one another, and different collocated antennas use the same oscillator or different oscillators with a prior known and correctable difference. Therefore, a quite general modeling framework is to suppose that all Tx/Rx antenna pairs are subject to the same carrier frequency offset (Doppler shift) and timing delay. Under such a modeling framework, we will see that the synchronization of MIMO systems greatly simplifies and resembles to the synchronization in parallel of multiple SISO systems. In fact, we will see that some of the standard carrier and timing acquisition schemes (e.g., the ML-based schemes) proposed for SISO systems find their equivalent extensions in the context of MIMO systems.

11.8.2 Timing Recovery in MIMO Systems

To illustrate the effects of spatial diversity on timing acquisition and the special design considerations, next we examine the problem of time synchronization in a MIMO system which assumes no carrier frequency offset. The channel modeling framework is depicted in Figure 11.14, where a generic $N_T \times N_R$ MIMO system, consisting of N_T transmit antennas and N_R receive antennas, is shown.

The MIMO propagation channel will be represented by the $N_R \times N_T$ channel matrix $\mathbf{H}$, and it is assumed frequency flat and quasi-static. The (i,j)th entry h_{ij} of $\mathbf{H}^T$ represents the channel coefficient between the ith Tx antenna and the jth Rx antenna. The complex envelope of the received signal at the jth receive antenna takes the expression:

$$r_j(t) = \sqrt{\frac{E_s}{N_T T}} \sum_{i=1}^{N_T} h_{ij} \sum_k d_i(k) p(t - nT - \tau_o T) + n_j(t), \quad j = 1,\ldots,N_R \tag{11.39}$$

where E_s/N_T stands for the Tx symbol energy, $d_i(k)$ denotes the data symbol transmitted by the ith Tx antenna at time k, $p(t)$ represents the transmit pulse (e.g., a square-root raised cosine pulse), T denotes the symbol period and the unknown time phase offset is represented by the variable $\tau_o \in (0,1)$. The term

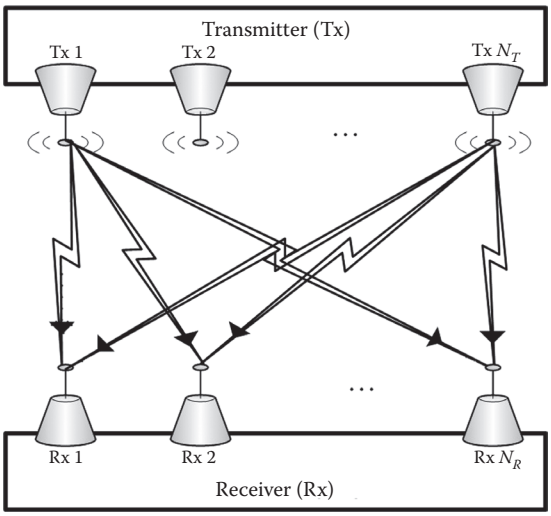

FIGURE 11.14 An $N_T \times N_R$ MIMO system.

$n_j(t)$ in Equation 11.39 represents the complex circularly distributed Gaussian noise at receive antenna j and it assumes the power density N_o. The outputs of Rx antennas are sampled at the rate $f_s = 1/T_s$, where $T_s = T/Q$ and $Q \geq 1$ denotes the oversampling factor. The length of observation data (measured in symbol periods) is equal to K. Furthermore, stacking together into the vector $\mathbf{r}_j$ the KQ consecutive samples collected at the output of the jth receive antenna: $\mathbf{r}_j = \left[r_j(0)\ \ r_j(T_s)\ \ldots\ r_j((KQ-1)T_s)\right]^T$, from Equation 11.39 it follows that:

$$\mathbf{r}_j = \alpha \mathbf{P}_{\tau_o} \mathbf{D} \mathbf{H}^T_{j,:} + \mathbf{n}_j \tag{11.40}$$

where $\alpha = \sqrt{E_s/N_T T}$, $\mathbf{H}_{j,:}$ denotes the jth column of $\mathbf{H}$, and

$$\begin{aligned}
\mathbf{P}_\tau &= \left[\mathbf{p}_{-K_p}(\tau)\ \ \mathbf{p}_{-K_p+1}(\tau)\ \ \ldots\ \ \mathbf{p}_{K+K_p-1}(\tau)\right] \\
\mathbf{P}_i(\tau) &= \left[\mathbf{p}(-iT-\tau T)\ \ \mathbf{p}(T_s - iT - \tau T)\ \ \ldots\ \ \mathbf{p}((KQ-1)T_s - iT - \tau T)\right]^T \\
\mathbf{D} &= \left[\mathbf{d}_1\ \ \mathbf{d}_2\ \ \ldots\ \ \mathbf{d}_{N_T}\right] \\
\mathbf{d}_i &= \left[d_i(-K_p)\ \ d_i(-K_p+1)\ \ \ldots\ \ d_i(K+K_p-1)\right]^T \\
\mathbf{n}_j &= \left[n_j(0)\ \ n_j(T_s)\ \ \ldots\ \ n_j((KQ-1)T_s)\right]^T
\end{aligned}$$

The variable K_p stands for the number of symbols affected by the intersymbol interference (ISI) generated by one side of pulse $p(t)$, whose support is $-K_pT \leq t \leq K_pT$. Therefore, the observation interval $0 \leq t \leq KT$ contains contributions from the symbols $d(-K_p)$, …, $d(0)$, …, $d(K+K_p-1)$. Stacking together all the vectors $\mathbf{r}_j$, $j = 1,\ldots,N_R$, into the column vector $\mathbf{r} = \left[\mathbf{r}_1^T\ \ \mathbf{r}_2^T\ \ \ldots\ \mathbf{r}_{N_R}^T\right]^T$ yields the modeling equation:

$$\mathbf{r} = \alpha(\mathbf{I}_{N_R} \otimes \mathbf{P}_{\tau_o}) vec(\mathbf{D}\mathbf{H}^T) + \mathbf{n}, \tag{11.41}$$

where $\mathbf{n} = \left[\mathbf{n}_1^T \;\; \mathbf{n}_2^T \;\; \ldots \;\; \mathbf{n}_{N_R}^T\right]^T$, notations $\otimes$ and *vec* stand for Kronecker product and vectorization of a matrix (i.e., stacking all the matrix columns one on top of another), respectively, and $\mathbf{I}_{N_R}$ denotes the $N_R \times N_R$ unit matrix. Equation 11.41 will prove pivotal in the development of the ML estimator of timing delay τ_o. We will derive the ML timing delay estimator under two general frameworks: the DA ML setup which assumes knowledge of training data (pilot symbols, training sequences), and NDA or blind ML setup in which the transmit data symbols are supposed unknown.

11.8.2.1 Data-Aided Symbol Training Recovery

Using formula $vec(\mathbf{ABC}) = (\mathbf{C}^T \otimes \mathbf{A})vec(\mathbf{B})$, the contributions of matrix data $\mathbf{D}$ and channel matrix $\mathbf{H}$ can be separated in Equation 11.41. It turns out that Equation 11.41 can be recast as

$$\mathbf{r} = \alpha(\mathbf{I}_{N_R} \otimes \mathbf{P}_{\tau_o}\mathbf{D})vec(\mathbf{H}^T) + \mathbf{n}. \tag{11.42}$$

Because $\mathbf{n}$ assumes a Gaussian distribution, the joint ML estimator of unknown timing delay τ_o and propagation channel $\mathbf{h} = vec(\mathbf{H}^T)$ is obtained by minimizing the reduced negative log-likelihood function:

$$L_{DA}(\mathbf{r} \mid \tau, \mathbf{h}) = (\mathbf{r} - \overline{\mathbf{P}}_\tau \mathbf{h})^H (\mathbf{r} - \overline{\mathbf{P}}_\tau \mathbf{h}), \tag{11.43}$$

where $\overline{\mathbf{P}}_\tau = \alpha(\mathbf{I}_{N_R} \otimes \mathbf{P}_\tau \mathbf{D})$, and τ, $\mathbf{h}$ denote trial values for τ_o and $vec(\mathbf{H}^T)$, respectively. Equating to zero the gradient of $L(\mathbf{r}|\ \tau, \mathbf{h})$ with respect to $\mathbf{h}$, it follows that the ML estimate of channel vector $\hat{\mathbf{h}}$ can be expressed in terms of unknown timing delay as follows:

$$\hat{\mathbf{h}} = (\overline{\mathbf{P}}_\tau{}^H \overline{\mathbf{P}}_\tau)^{-1} \overline{\mathbf{P}}_\tau{}^H \mathbf{r}. \tag{11.44}$$

Plugging Equation 11.49 into Equation 11.48 and simplifying, it follows that the ML timing delay estimate must minimize the function:

$$L_{DA}(\tau) = \mathbf{r}^H \overline{\mathbf{P}}_\tau (\overline{\mathbf{P}}_\tau{}^H \overline{\mathbf{P}}_\tau)^{-1} \overline{\mathbf{P}}_\tau{}^H \mathbf{r}, \tag{11.45}$$

which can be further expanded as

$$L_{DA}(\tau) = \sum_{j=1}^{N_R} \mathbf{r}_j^H \mathbf{P}_\tau \mathbf{D}(\mathbf{D}^H \mathbf{P}_\tau{}^H \mathbf{P}_\tau \mathbf{D})^{-1} \mathbf{D}^H \mathbf{P}_\tau{}^H \mathbf{r}_j^H. \tag{11.46}$$

Therefore, the DA ML timing delay estimator can be expressed as

$$\hat{\tau}_{ML} = \arg\max_\tau L_{DA}(\tau), \tag{11.47}$$

with $L_{DA}(\tau)$ expressed in Equation 11.46 as a sum of N_R terms that depend nonlinearly with respect to τ. Therefore, finding $\hat{\tau}_{ML}$ requires solving a nonlinear optimization problem and no closed-form expression for DA ML estimator is possible. Determination of the global maximum of Equation 11.47 could be performed via a two-step approach. First, a grid-based search might be performed to localize approximately the location of global maxim, which might then be followed by a gradient descent or interpolation-based approach to refine the location of global maximum.

Assuming that the training sequences sent by different Tx antennas are orthonormal, $p(t)$ is a square-root raised cosine pulse and the observation interval K is sufficiently large, then the DA reduced log-likelihood function (11.46) simplifies further to [41]

$$L_{DA}(\tau) = \sum_{j=1}^{N_R} \sum_{i=1}^{N_T} \left| \mathbf{d}_i^H \mathbf{P}_\tau{}^H \mathbf{r}_j \right|^2, \tag{11.48}$$

where $\mathbf{P}_\tau{}^H \mathbf{r}_j$ represents the matched filtering output of the jth Rx antenna with one sample per symbol. Equations 11.46 and 11.48 show that the reduced log-likelihood function for timing recovery in a MIMO system reduces to a sum of N_R reduced log-likelihood functions corresponding to the N_R Rx antennas. This suggests that the tracking and timing estimation techniques from SISO systems could be extended *mutatis-mutandis* to the MIMO setup.

The performance of the resulting ML timing estimator can be assessed by comparing its mean-square-error (MSE) with performance bounds such as the conditional Cramer–Rao bound (CCRB) [42] and modified Cramer–Rao bound (MCRB) [43]. CCRB represents the Cramer–Rao bound derived under the assumption that the nuisance parameters are treated as deterministic and estimated jointly with the unknown time delay. Proposed as a computational efficient alternative to CCRB, MCRB represents a lower bound to any unbiased estimator, in which the unwanted parameters are averaged out from the log-likelihood function. For a given delay τ_o, CCRB assumes the expression [42]:

$$\mathrm{CCRB}(\tau_o) = \frac{N_o Q}{2T\, tr(\overline{\mathbf{B}}_{\tau_o}^H \mathbf{S}_{\overline{P}}^{\perp} \overline{\mathbf{B}}_{\tau_o} \mathbf{C}_h)}, \tag{11.49}$$

where $tr(\cdot)$ denotes the trace operator, $\mathbf{B}_\tau = d\mathbf{P}_\tau/d\tau$, $\overline{\mathbf{B}}_\tau = d\overline{\mathbf{P}}_\tau/d\tau$, $\mathbf{S}_{\overline{P}}^{\perp}$ represents the orthogonal projector onto the null space of $\overline{\mathbf{P}}_{\tau_o}$ and $\mathbf{C}_h = \mathrm{E}(\mathbf{h}\mathbf{h}^H) = \mathbf{I}_{N_T N_R}$. Similarly, the MCRB for a given time delay τ_o can be expressed as [21]:

$$\mathrm{MCRB}(\tau_o) = \frac{N_o Q}{2T\, tr(\overline{\mathbf{B}}_{\tau_o}^{\mathrm{H}} \overline{\mathbf{B}}_{\tau_o} \mathbf{C}_h)}. \tag{11.50}$$

Numerical evaluation of Equations 11.49 and 11.50 show that $\mathrm{CCRB}(\tau_o)$ and $\mathrm{MCRB}(\tau_o)$ depend inversely proportional with respect to the number of Rx antennas (N_R) [44]. Therefore, the spatial diversity manifests not only through the averaging of N_R SISO log-likelihood functions as in Equation 11.46 but also through the inverse proportional dependence on N_R in *CCRB* and *MCRB*. Thus, every increase in the number of Rx antennas (N_R) translates through a proportional reduction in CCRB and MCRB, and, as the computer simulations illustrate in Figures 11.15 and 11.16, in a proportional reduction of the MSE of DA ML estimator. Assuming orthonormal training sequences sent by Tx antennas, Figures 11.15 and 11.16 depict the MSE performance of ML estimator and CCRB for different numbers of Tx and Rx antennas. It turns out that the MSE of DA ML estimator improves when the number of Rx antennas increases, and remains invariant to changes in the number of Tx antennas. The MSE simulation plots also illustrate that DA ML estimator is efficient because it approaches the CCRB. Although not plotted explicitly, numerical evaluations show that in the DA-estimation setup MCRB coincides with CCRB. For the DA synchronization setup, the simulation results shown in Figures 11.15 and 11.16 assumed that the length of training data was 40 ($K = 32$, $K_g = 4$), oversampling factor $Q = 2$, and a square-root raised cosine pulse with roll-off factor 0.3. The timing delay τ_o was uniformly distributed in the interval [0,1), and 10^4 Monte-Carlo simulations were conducted for each value of τ_o.

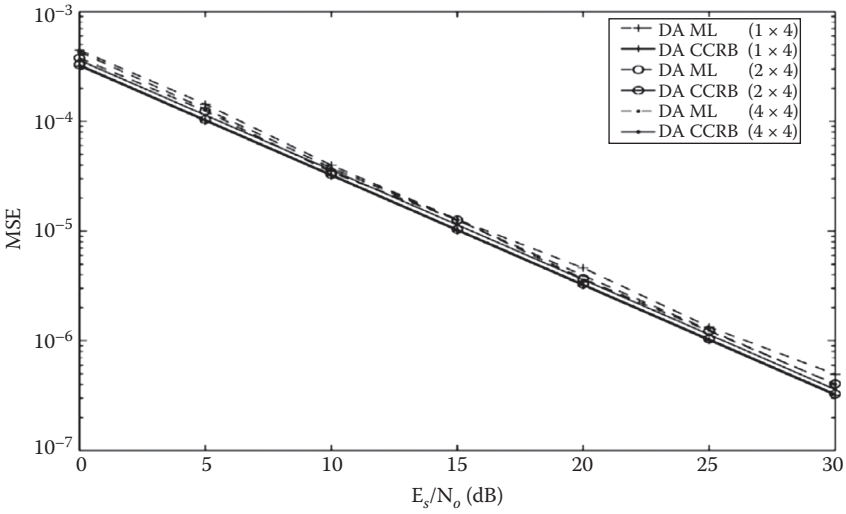

FIGURE 11.15 MSE performance of DA ML estimator versus CCRB for different number of Tx antennas.

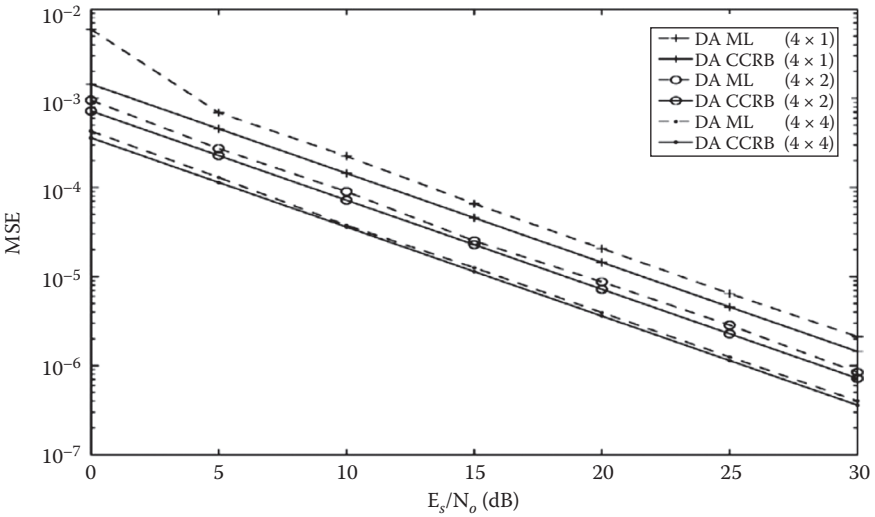

FIGURE 11.16 MSE performances of DA ML and CCRB for different number of Rx antennas.

11.8.2.2 Non-Data-Aided Symbol Timing Recovery

Determination of non-data-aided (NDA) or blind ML estimator for timing delay follows similar steps to the derivation of DA ML estimator. Examining Equation 11.41, it follows that the unknown data matrix $\mathbf{D}$ and channel matrix $\mathbf{H}$ could be merged together into the unknown vector $\mathbf{z} = vec(\mathbf{D}\mathbf{H}^T)$, and therefore, NDA ML joint estimation of τ and $\mathbf{z}$ reduces to the minimization of function:

$$L_{NDA}(\mathbf{r} \mid \tau, \mathbf{z}) = (\mathbf{r} - \breve{\mathbf{P}}_\tau \mathbf{z})^H (\mathbf{r} - \breve{\mathbf{P}}_\tau \mathbf{z}), \tag{11.51}$$

where $\breve{\mathbf{P}}_\tau = \alpha(\mathbf{I}_{N_R} \otimes \mathbf{P}_\tau)$. Equating to zero the gradient of Equation 11.51 with respect to $\mathbf{z}$, it follows that the ML of $\mathbf{z}$ is given by

$$\hat{\mathbf{z}} = (\breve{\mathbf{P}}_\tau^H \breve{\mathbf{P}}_\tau)^{-1} \breve{\mathbf{P}}_\tau^H \mathbf{r}. \tag{11.52}$$

Finally, plugging Equation 11.52 back into Equation 11.51, it follows that the NDA ML estimate of τ can be expressed as the argument that maximizes the reduced log-likelihood function:

$$L_{NDA}(\tau) = \mathbf{r}^H \breve{\mathbf{P}}_\tau (\breve{\mathbf{P}}_\tau^H \breve{\mathbf{P}}_\tau)^{-1} \breve{\mathbf{P}}_\tau^H \mathbf{r}, \tag{11.53}$$

which can be further reduced to

$$L_{NDA}(\tau) = \sum_{j=1}^{N_R} \mathbf{r}_j^H \mathbf{P}_\tau (\mathbf{P}_\tau^H \mathbf{P}_\tau)^{-1} \mathbf{P}_\tau^H \mathbf{r}. \tag{11.54}$$

Hence, the MIMO log-likelihood function in Equation 11.54 is expressed as a sum of N_R SISO log-likelihood functions corresponding to each of the N_R Rx antennas. As in the DA ML estimation case, in the NDA ML estimation framework, spatial diversity manifests through the exploitation of information (averaging of the log-likelihood functions) at all N_R receive antennas. This remark is enforced by the computer simulations, which illustrate that the MSE performance of NDA ML estimator is inversely proportional to the number of Rx antennas (N_R). Also, the CCRB and MCRB are inversely proportional with respect to the number of Rx antennas. Following the calculations in [42,43], the following closed-form expressions for CCRB and MCRB were found [44]:

$$\mathrm{CCRB}(\tau_o) = \frac{N_o Q}{2T\, tr(\breve{\mathbf{B}}_{\tau_o}^H \mathbf{S}_{\breve{P}}^{\perp} \breve{\mathbf{B}}_{\tau_o} \mathbf{C}_z)}, \tag{11.55}$$

$$\mathrm{MCRB}(\tau_o) = \frac{N_o Q}{2T\, tr(\breve{\mathbf{B}}_{\tau_o}^H \breve{\mathbf{B}}_{\tau_o} \mathbf{C}_z)}, \tag{11.56}$$

where $\breve{\mathbf{B}}_\tau = d\breve{\mathbf{P}}_{\tau_o}/d\tau$, $\mathbf{S}_{\breve{P}}^{\perp}$ represents the orthogonal projection onto nullspace of $\breve{\mathbf{P}}_{\tau_o}$ and $\mathbf{C}_z = \mathrm{E}(\mathbf{z}\mathbf{z}^H)$.

Assuming the same simulation conditions as in the previous subsection, and QPSK data symbols, Figures 11.17 and 11.18 illustrate the MSE performance of the NDA ML estimator and the corresponding CCRB for different number of Tx and Rx antennas. Similar to the DA ML estimator, the MSE performance of NDA ML estimator is inversely proportional with respect to the number (N_R) of Rx antennas. In addition, the performance of NDA ML estimator is well predicted by the NDA CCRB.

Finally, in Figure 11.19, we plotted the MSE performances of DA ML and NDA ML estimators and their corresponding CCRBs and MCRBs for a 4×4 MIMO system. Figure 11.19 shows the superior performance of DA ML estimator relative to NDA ML estimator. This is a reasonable fact because DA ML exploits the additional information given by knowledge of Tx data symbols. Furthermore, Figure 11.19 shows that in the NDA estimation framework, there a significant gap between CCRB and MCRB, a fact which might suggest the existence of NDA estimators with improved performance with respect to NDA ML estimator.

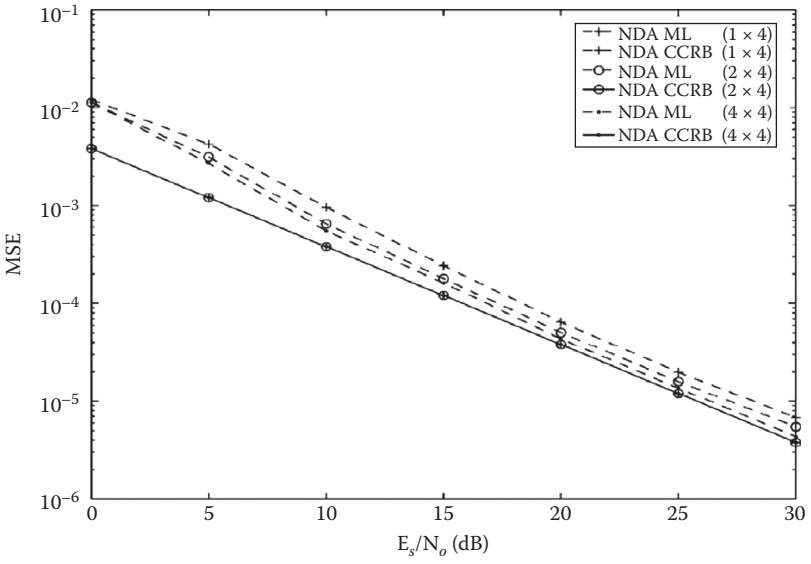

FIGURE 11.17 MSE performance of NDA ML estimator and CCRB for different number of Tx antennas.

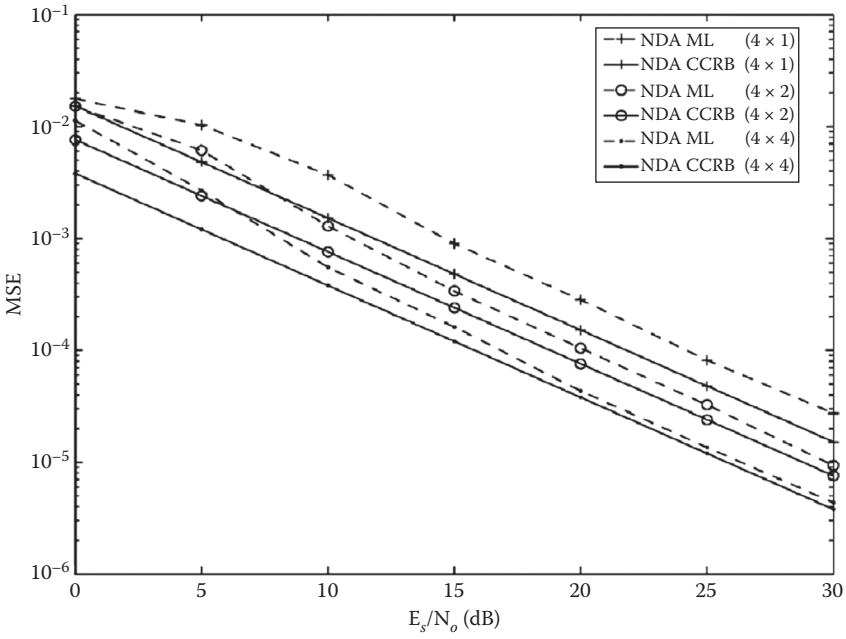

FIGURE 11.18 MSE performance of NDA ML estimator and CCRB for different number of Rx antennas.

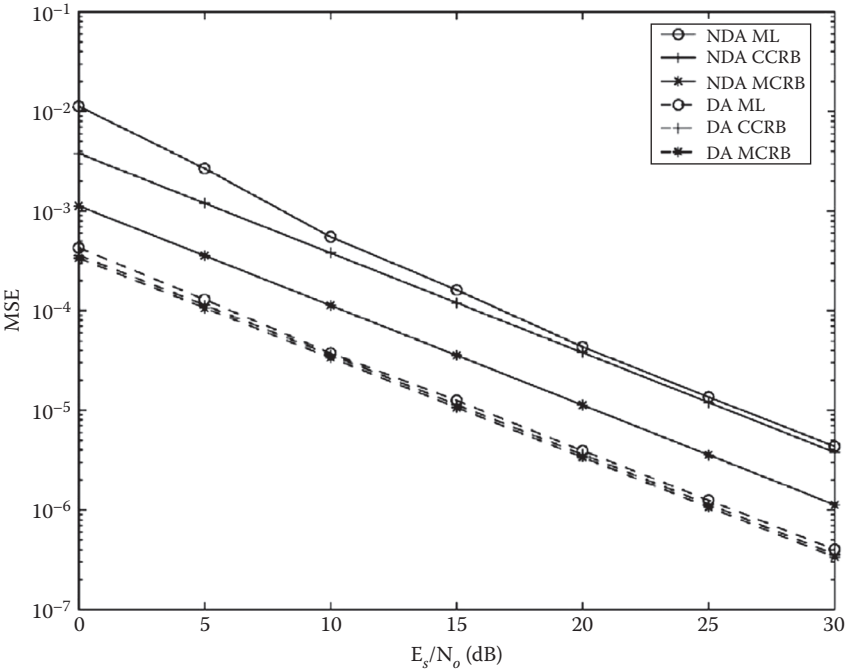

FIGURE 11.19 MSE performance of DA ML and NDA ML estimators and their CCRBs and MCRBs.

11.8.3 Carrier Recovery in MIMO Systems

Herein subsection, we will consider the carrier synchronization problem in an $N_T \times N_R$ MIMO flat-fading channel, where all the Tx/Rx antenna pairs are subject to the same frequency offset F. Assuming perfect timing synchronization (no timing delay $\tau_o = 0$), based on Equation 11.39 the output of the jth Rx antenna is modeled as

$$r_j(t) = \sqrt{\frac{E_s}{N_T T}} e^{j2\pi Ft} \sum_{i=1}^{N_T} h_{ij} \sum_k d_i(k) p(t - kT) + n_j(t). \tag{11.57}$$

Sampling $r_j(t)$ at the symbol period T leads to the discrete-time model for the output of the jth antenna:

$$r_j(k) = \sqrt{\frac{E_s}{N_T T}} e^{j2\pi FTk} \sum_{i=1}^{N_T} h_{ij} d_i(k) + n_j(k),\ k = 0,\ldots,K-1, \tag{11.58}$$

where $r_j(k) = r_j(kT)$ and $n_j(k) = n_j(kT)$. Introducing the vectors: $\mathbf{r}(k) = \left[r_1(k) \ \ldots \ r_{N_R}(k)\right]^T$, $\mathbf{d}(k) = \left[d_1(k) \ \ldots \ d_{N_T}(k)\right]^T$, and $\mathbf{n}(k) = \left[n_1(k) \ \ldots \ n_{N_R}(k)\right]^T$, Equation 11.58 is expressed in the equivalent vector-form equation:

$$r(k) = \alpha \mathbf{H}^T \mathbf{d}(k) e^{j2\pi FTk} + \mathbf{n}(k), \quad k = 0,\ldots,K-1. \tag{11.59}$$

Based on Equation 11.59, the DA ML estimates of carrier frequency offset F and unknown channel matrix $\mathbf{H}$ are obtained by following the same steps as in the SISO case, and it reduces to the minimization of the nonlinear least-squares criterion:

$$L(r \mid \mathbf{H}, F) = \sum_{k=0}^{K-1} \left| \mathbf{r}(k) - \alpha \mathbf{H}^T \mathbf{d}(k) e^{j2\pi FTk} \right|^2. \tag{11.60}$$

Equating to zero the gradient of $L(r|\mathbf{H},F)$ with respect to $\mathbf{H}$ and F, it follows that the DA ML estimates of $\mathbf{H}$ and F are given by [45]:

$$\hat{F} = \arg\max_{F} \mathrm{Re}\left[\sum_{k=0}^{K-1} R(k) e^{-j2\pi \hat{F} Tk} \right], \tag{11.61}$$

$$\hat{\mathbf{H}}^T = \frac{1}{\alpha} \left(\sum_{k=0}^{K-1} \mathbf{r}(k) \mathbf{d}^H(k) e^{-j2\pi \hat{F} Tk} \right) \left(\sum_{k=0}^{K-1} \mathbf{d}(k) \mathbf{d}^H(k) \right)^{-1}, \tag{11.62}$$

where

$$R(k) = \sum_{j=k}^{K-1} \mathbf{r}^H(j-k) \mathbf{r}(j) D(j, j-k)$$

and

$$D(i,j) = \mathbf{d}^H(i) \left(\sum_{k=0}^{K-1} \mathbf{d}_k \mathbf{d}_k^H \right)^{-1} \mathbf{d}(j).$$

Similar to the SISO setup, no closed-form expression exists for the DA ML estimator of carrier frequency offset in the MIMO setup. Because finding the maximum of Equation 11.61 is computationally expensive, in practice, sub-optimal but more computationally efficient carrier frequency offset estimators are preferred. An example of such sub-optimal but computationally efficient carrier offset estimator was recently proposed in Reference 45 by mimicking the frequency estimators proposed for SISO channels in [17,18], which basically resumes to weighting appropriately the phases of correlation terms $R(k)$ and taking advantage of diversity offered by the N_R receive antennas. In closing this subsection, we remark that the ML estimator (11.61) is efficient in the sense that it achieves the CRB at medium and high SNRs [45,46].

11.8.4 Conclusions

The slightly more general problem of DA ML joint estimation of carrier frequency offsets and channel gains in a MIMO flat-fading channel with different frequency offsets between different Tx/Rx antenna pairs was recently addressed in Reference 46. However, the more general problem of designing computationally efficient ML algorithms for joint estimation of carrier frequency offsets, timing delays and propagation channel in a MIMO flat or frequency-selective fading channel is still open. Partial attempts based on the use of EM-algorithm and message passing algorithms in factor graphs were proposed for SISO and MIMO joint carrier synchronization and data demodulation. However, the high computational

complexity and lack of guaranteed convergence results still prohibit the wide spread of these algorithms to practical systems. Another open research problem is the design of optimal training sequences to reduce the implementation complexity of channel estimation and synchronization algorithms and in the same time to improve the estimation accuracy of channel and synchronization parameters. In this context, [46] developed a set of optimal training sequences that minimize the asymptotic Cramer–Rao bound of carrier frequency offsets in a MIMO system and that also reduce the implementation complexity of the ML estimator.

Good functioning of communication receivers requires proper time and carrier frequency and phase synchronization. Despite the huge advances reported during the last few decades, synchronization continues to represent a complex, and very challenging and important task in the design of any communication system. Furthermore, current developments in the field of telecommunications suggest that more complex and diverse communications systems are being built. Therefore, one expects a proportional increase in the complexity and diversity of the synchronization schemes that will have to satisfy the design challenges and requirements of these new communications systems. It is interesting to observe that current research directions in the field of cooperative (virtual MIMO) wireless communications networks and wireless ad-hoc (sensor) networks bring new challenges in terms of synchronizing the nodes of these networks. These trends have also been visible during the recent years due to the huge interest toward developing efficient synchronization schemes for multicarrier OFDM, OFDMA and MIMO–OFDM systems, as well as for ultra-wideband communication systems.

References

1. J.J. Stiffler, *Theory of Synchronous Communications*, Englewood Cliffs, NJ, Prentice-Hall, 1971.
2. W. Lindsey and M. Simon, *Telecommunication Systems Engineering*, Englewood Cliffs, NJ, Prentice-Hall, 1973.
3. H. Meyr and G. Ascheid, *Synchronization in Digital Communications*, New York, Wiley, 1990.
4. H. Meyr, M., Moeneclaey, and S.A. Fechtel, *Digital Communication Receivers*, New York, Wiley, 1998.
5. U. Mengali and A.N. D'Andrea, *Synchronization Techniques for Digital Receivers*, Plenum Press, New York, 1997.
6. F.M. Gardner, *Frequency detectors for digital demodulators via maximum-likelihood derivation*, Final Report: Part II, ESTEC Contract No. 8022/88/NL/DG, ESA, June 4, 1990.
7. A.N. D'Andrea and U. Mengali, Noise performance of two frequency-error detectors derived from maximum likelihood estimation methods, *IEEE Transactions on Communications*, 42, 793–802, 1994.
8. A.N. D'Andrea and U. Mengali, Design of quadricorrelators for automatic frequency control systems, *IEEE Transactions on Communications*, 41, 988–997, 1993.
9. A.N. D'Andrea and U. Mengali, Performance of a quadricorrelator driven by modulated signals, *IEEE Transactions on Communications*, 38, 1952–1957, 1990.
10. F.M. Gardner, Demodulator reference recovery techniques suited for digital implementation, *European Space Agency*, Final Report, ESTEC Contract No. 6847/86/NL/DG, August 1988.
11. F.M. Gardner, Properties of frequency difference detectors, *IEEE Transactions on Communications*, 33, 131–138, 1985.
12. T. Alberty and V. Hespelt, A new pattern jitter free frequency error detector, *IEEE Transactions on Communications*, 37, 159–163, 1989.
13. M. Moeneclaey, Overview of digital algorithms for carrier frequency synchronization, *International ESA Workshop on DSP Techniques Applied to Space Communications*, pp. 1.1–1.7, London, UK, September 26–28, 1994.

14. F. Classen and H. Meyr, Two frequency estimation schemes operating independently of timing information, *Globecom '93 Conference*, pp. 1996–2000, Houston, TX, USA, November 29–December 2, 1993.
15. F. Classen, H. Meyr, and P. Sehier, Maximum likelihood open loop carrier synchronizer for digital radio, *ICC '93*, pp. 493–497, Geneva, Switzerland, 1993.
16. M.P. Fitz, Planar filtered techniques for burst mode carrier synchronization, *Globecom '91*, paper 12.1, Phoenix, AZ, December 1991.
17. M.P. Fitz, Further results in the fast estimation of a single frequency, *IEEE Transactions on Communications*, 42, 862–864, 1994.
18. M. Luise and R. Reggiannini, Carrier frequency recovery in all-digital modems for burst-Mode transmissions, *IEEE Transactions on Communications*, 43, 1169–1178, 1995.
19. J.C.-I. Chuang and N.R. Sollenbeger, Burst coherent demodulation with combined symbol timing, frequency offset estimation, and diversity selection, *IEEE Transactions on Communications*, 39, 1157–1164, 1991.
20. Y. Wang, E., Serpedin, and P. Ciblat, Optimal blind carrier recovery for burst M-PSK transmissions, *IEEE Transactions on Communications*, 51(9), 1571–1581, 2003.
21. Y. Wang, E. Serpedin and P. Ciblat, Optimal blind nonlinear least-squares carrier phase and frequency offset estimation for general QAM modulations, *IEEE Transactions on Wireless Communications*, 2(5), 1040–1054, 2003.
22. E. Serpedin, G.B. Giannakis, A. Chevreuil, and P. Loubaton, Blind joint estimation of carrier frequency offset and channel using non-redundant periodic modulation precoders, *The 9th IEEE Statistical Signal and Array Processing Workshop*, pp. 288–291, Portland, OR, Sept. 1998.
23. P. Ciblat, P. Loubaton, E. Serpedin, and G.B. Giannakis, Performance analysis of blind carrier frequency offset estimators for noncircular transmissions through frequency-selective channels, *IEEE Transactions on Signal Processing*, 50(1), 130–140, 2002.
24. F. Gini and G.B. Giannakis, Frequency offset and symbol timing recovery in flat fading channels: A cyclostationary approach, *IEEE Transactions on Communications*, 46, 400–411, 1998.
25. Y. Wang, E. Serpedin, P. Ciblat, and P. Loubaton, Performance analysis of a class of non-data aided carrier frequency offset and symbol timing delay estimators for flat-fading channels, *IEEE Transactions on Signal Processing*, 50(9), 2295–2305, 2002.
26. H.L. Van Trees, *Detection, Estimation, and Modulation Theory*, New York, Wiley 1968.
27. A. Viterbi, *Principles of Coherent Communication*, New York, McGraw-Hill, 1966.
28. M. Moeneclaey and G. de Jonghe, ML-Oriented NDA carrier synchronization for general rotationally symmetric signal constellations, *IEEE Transactions on Communications*, 42, 2531–2533, 1994.
29. C.N. Georghiades, Blind carrier phase acquisition for QAM constellations, *IEEE Transactions on Communications*, 45, 1477–1486, 1997.
30. M. Morelli, A.N. D'Andrea, and U. Mengali, Feedforward estimation techniques for carrier recovery in 16-QAM modulation, in M. Luise and S. Pupolin (Eds.) *Broadband Wireless Communications*, Springer-Verlag, London, 1998.
31. E. Serpedin, P. Ciblat, G.B. Giannakis, and P. Ciblat, Performance analysis of blind carrier phase estimators for general QAM constellations, *IEEE Transactions on Signal Processing*, 49(8), 1816–1823, 2001.
32. F. M. Gardner, *Phaselock Techniques*, 3rd edition, 2005, John Wiley & Sons.
33. K.H. Mueller and M. Muller, Timing recovery in digital synchronous data receivers, *IEEE Transactions on Communications*, COM-24, 516–531, 1976.
34. O. Agazzi, C.-P.J. Tzeng, D.G. Messerschmitt, and D.A. Hodges, Timing recovery in digital subscriber loops, *IEEE Transactions on Communications*, COM-33, 558–569, 1985.
35. F.M. Gardner, A BPSK/QPSK Timing-error detector for sampled receivers, *IEEE Transactions on Communication*, COM-34, 423–429, 1986.

36. C.N. Georghiades and M. Moeneclaey, Sequence estimation and synchronization from nonsynchronized samples, *IEEE Transactions on Information Theory*, 37, 1649–1657, 1991.
37. J.L. Massey, Optimum frame synchronization, *IEEE Transactions on Communications*, COM-20, 115–119, 1972.
38. R.H. Barker, Group synchronization of binary systems, *Communication Theory*, W. Jackson Editor, London, pp. 273–287, 1953.
39. F. Neuman and L. Hofman, New pulse sequences with desirable correlation properties, *Proceedings of the National Telemetry Conference*, Washington, DC, pp. 272–282, 1971.
40. P.T. Nielsen, On the expected duration of a search for a fixed pattern in random data, *IEEE Transactions on Information Theory*, September, 702–704, 1973.
41. Y.C Wu, S.C. Chan and E. Serpedin, Symbol-timing estimation in space–time coding systems based on orthogonal training sequences, *IEEE Transactions on Wireless Communications*, 4(2), pp. 603–613, 2005.
42. J. Riba, J. Sala, and G. Vazguez, Conditional maximum likelihood timing recovery: Estimators and bounds, *IEEE Transactions on Signal Processing*, 49, 835–850, 2001.
43. A.N. D'Andrea, V. Mengali, and R. Reggiannini, The modified Cramer–Rao bound and its application to synchronization problem, *IEEE Transactions on Communications*, 42, 1391–1399, 1994.
44. Y.C. Wu and E. Serpedin, Symbol timing estimation in MIMO correlated fading channels, *Wireless Communications and Mobile Computing (WCMC) Journal*, Wiley, 4(7), 773–790, 2004.
45. F. Simoens and M. Moeneclaey, Reduced-complexity data-aided and code-aided frequency offset estimation for flat-fading MIMO channels, *IEEE Transactions on Wireless Communications*, 5(6), 1558–1567, 2006.
46. O. Besson and P. Stoica, On parameter estimation of MIMO flat-fading channels with frequency offsets, *IEEE Transactions on Signal Processing*, 51(3), 602–613, 2003.

Further Reading

The *Proceedings of the International Communications Conference* (ICC), *Global Telecommunications Conference* (GLOBECOM), and *International Conference on Acoustics, Speech and Signal Processing* (ICASSP) are good sources of current information on synchronization work. Other sources of archival value are the *IEEE Transactions on Communications*, *IEEE Transactions on Wireless Communications*, and *IEEE Transactions on Signal Processing.*

12

Pseudonoise Sequences

Tor Helleseth

P. Vijay Kumar

12.1 Introduction

Pseudonoise sequences (PN sequences), also referred to as pseudorandom sequences, are sequences that are deterministically generated and yet possess some properties that one would expect to find in randomly generated sequences. Applications of PN sequences include signal synchronization, navigation, radar ranging, random number generation, spread-spectrum communications, multipath resolution, cryptography, and signal identification in multiple-access communication systems. The *correlation* between two sequences $\{x(t)\}$ and $\{y(t)\}$ is the complex inner product of the first sequence with a shifted version of the second sequence. The correlation is called (1) an autocorrelation if the two sequences are the same, (2) a cross-correlation if they are distinct, (3) a periodic correlation if the shift is a cyclic shift, (4) an aperiodic correlation if the shift is not cyclic, and (5) a partial-period correlation if the inner product involves only a partial segment of the two sequences. More precise definitions are given subsequently.

Binary *m* sequences, defined in the next section, are perhaps the best-known family of PN sequences. The balance, run-distribution, and autocorrelation properties of these sequences mimic those of random sequences. It is perhaps the random-like correlation properties of PN sequences that make them most attractive in a communication system, and it is common to refer to any collection of low-correlation sequences as a family of PN sequences.

Section 12.2 begins by discussing *m* sequences. Thereafter, the discussion continues with a description of sequences satisfying various correlation constraints along the lines of the accompanying self-explanatory figure (Figure 12.1).

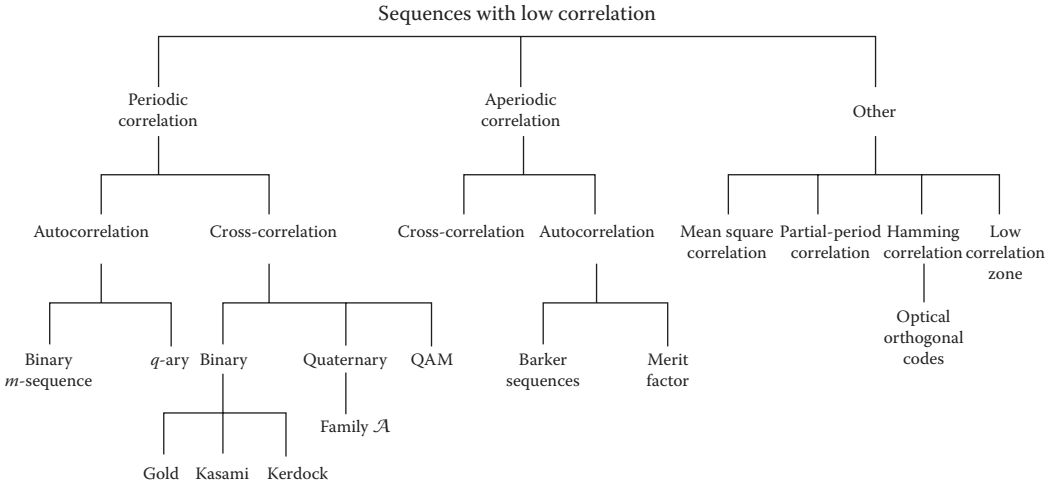

FIGURE 12.1 Overview of pseudonoise sequences.

Expanded tutorial discussions on pseudorandom sequences may be found in [9], [11], [12], [13, Chapter 21], [27], and [28, Chapter 5]. Sequence design related to peak-power control is covered in [19] while some recent advances in the area are covered in [10].

12.2 *m* Sequences

A binary {0,1} shift-register sequence $\{s(t)\}$ is a sequence that satisfies a linear recurrence relation of the form

$$\sum_{i=0}^{r} f_i s(t+i) = 0, \quad \text{for all } t \geq 0 \tag{12.1}$$

where $r \geq 1$ is the *degree* of the recursion; the coefficients f_i belong to the field $GF(2) = \{0,1\}$ where the leading coefficient $f_r = 1$. Thus, both sequences $\{a(t)\}$ and $\{b(t)\}$ appearing in Figure 12.2 are shift-register sequences.

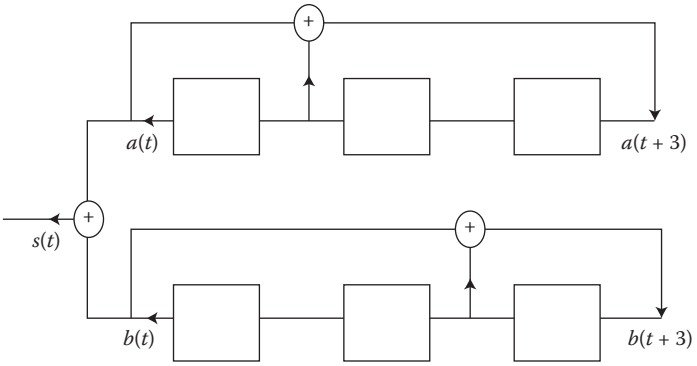

FIGURE 12.2 An example Gold sequence generator. Here, $\{a(t)\}$ and $\{b(t)\}$ are *m* sequences of length 7.

A sequence satisfying a recursion of the form in Equation 12.1 is said to have *characteristic polynomial* $f(x) = \sum_{i=0}^{r} f_i x^i$. Thus, $\{a(t)\}$ and $\{b(t)\}$ have characteristic polynomials given by $f(x) = x^3 + x + 1$ and $f(x) = x^3 + x^2 + 1$, respectively.

Since an r-bit binary shift register can assume a maximum of 2^r different states, it follows that every shift-register sequence $\{s(t)\}$ is eventually periodic with period $n \leq 2^r$, that is,

$$s(t) = s(t + n), \quad \text{for all } t \geq N$$

for some integer N. In fact, the maximum period of a shift-register sequence is $2^r - 1$, since a shift register that enters the all-zero state will remain forever in that state. The upper shift register in Figure 12.2 when initialized with starting state 001 generates the periodic sequence $\{a(t)\}$ given by

$$0010111 \quad 0010111 \quad 0010111 \quad \cdots \tag{12.2}$$

of period $n = 7$. It follows then that this shift register generates sequences of maximal period starting from any nonzero initial state.

An m sequence is simply a binary shift-register sequence having maximal period. For every $r \geq 1$, m sequences are known to exist. The periodic *autocorrelation* function θ_s of a binary {0,1} sequence $\{s(t)\}$ of period n is defined by

$$\theta_s(\tau) = \sum_{t=0}^{n-1} (-1)^{s(t+\tau)-s(t)}, \quad 0 \leq \tau \leq n-1.$$

An m sequence of length $n = 2^r - 1$ has the following attributes: (1) *Balance property*: in each period of the m sequence there are 2^{r-1} ones and $2^{r-1} - 1$ zeros. (2) *Run property:* every nonzero binary s-tuple, $s \leq r$ occurs 2^{r-s} times, the all-zero s-tuple occurs $2^{r-s} - 1$ times. (3) *Two-level autocorrelation function*:

$$\theta_s(\tau) = \begin{cases} n & \text{if } \tau = 0 \\ -1 & \text{if } \tau \neq 0. \end{cases} \tag{12.3}$$

The first two properties follow immediately from the observation that every nonzero r-tuple occurs precisely once in each period of the m sequence. For the third property, consider the difference sequence $\{s(t + \tau) - s(t)\}$ for $\tau \neq 0$. This sequence satisfies the same recursion as the m sequence $\{s(t)\}$ and is clearly not the all-zero sequence. It follows, therefore, that $\{s(t + \tau) - s(t)\} \equiv \{s(t + \tau')\}$ for some τ', $0 \leq \tau' \leq n-1$, that is, a different cyclic shift of the m sequence $\{s(t)\}$. The balance property of the sequence $\{s(t + \tau')\}$ then gives us attribute 3. The m sequence $\{a(t)\}$ in Equation 12.2 can be seen to have the three listed properties.

If $\{s(t)\}$ is any sequence of period n and d is an integer, $1 \leq d \leq n$, then the mapping $\{s(t)\} \rightarrow \{s(dt)\}$ is referred to as a *decimation* of $\{s(t)\}$ by the integer d. If $\{s(t)\}$ is an m sequence of period $n = 2^r - 1$ and d is an integer relatively prime to $2^r - 1$, then the decimated sequence $\{s(dt)\}$ clearly also has period n. Interestingly, it turns out that the sequence $\{s(dt)\}$ is always also an m sequence of the same period. For example, when $\{a(t)\}$ is the sequence in Equation 12.2, then

$$a(3t) = 0011101 \quad 0011101 \quad 0011101 \quad \ldots \tag{12.4}$$

and

$$a(2t) = 0111001 \quad 0111001 \quad 0111001 \quad \ldots . \tag{12.5}$$

The sequence $\{a(3t)\}$ is also an m sequence of period 7, since it satisfies the recursion

$$s(t+3) + s(t+2) + s(t) = 0 \quad \text{for all } t$$

of degree $r = 3$. In fact, $\{a(3t)\}$ is precisely the sequence labeled $\{b(t)\}$ in Figure 12.2. The sequence $\{a(2t)\}$ is simply a cyclically shifted version of $\{a(t)\}$ itself; this property holds in general. If $\{s(t)\}$ is any m sequence of period $2^r - 1$, then $\{s(2t)\}$ will always be a shifted version of the same m sequence. Clearly, the same is true for decimations by any power of 2.

Starting from an m sequence of period $2^r - 1$, it turns out that one can generate all m sequences of the same period through decimations by integers d relatively prime to $2^r - 1$. The set of integers d, $1 \le d \le 2^r - 1$ satisfying $(d, 2^r - 1) = 1$ forms a group under multiplication modulo $2^r - 1$, with the powers $\{2^i | 0 \le i \le r - 1\}$ of 2 forming a subgroup of order r. Since decimation by a power of 2 yields a shifted version of the same m sequence, it follows that the number of distinct m sequences of period $2^r - 1$ is $[\phi(2^r - 1)/r]$, where $\phi(n)$ denotes the number of integers d, $1 \le d \le n$, relatively prime to n. For example, when $r = 3$, there are just two cyclically distinct m sequences of period 7, and these are precisely the sequences $\{a(t)\}$ and $\{b(t)\}$ discussed in the preceding paragraph. The tables provided in [25] can be used to determine the characteristic polynomial of the various m sequences obtainable through the decimation of a single given m sequence. The classical reference on m sequences is [11].

If one obtains a sequence of some large length n by repeatedly tossing an unbiased coin, then such a sequence will very likely satisfy the balance, run, and autocorrelation properties of an m sequence of comparable length. For this reason, it is customary to regard the extent to which a given sequence possesses these properties as a measure of randomness of the sequence. Quite apart from this, in many applications such as signal synchronization and radar ranging, it is desirable to have sequences $\{s(t)\}$ with low autocorrelation sidelobes, that is, $|\theta_s(\tau)|$ is small for $\tau \neq 0$. Whereas m sequences are a prime example, there exist other methods of constructing binary sequences with low out-of-phase autocorrelation.

Sequences $\{s(t)\}$ of period n having an autocorrelation function identical to that of an m sequence, that is, having θ_s satisfying Equation 12.3 correspond to well-studied combinatorial objects known as *cyclic Hadamard difference sets*. Known infinite families of such difference sets fall into three classes: (1) Singer and Gordon, Mills, and Welch (GMW), (2) quadratic residue, and (3) twin-prime difference sets. These correspond, respectively, to sequences of period n of the form $n = 2^r - 1$, $r \ge 1$; n prime; and $n = p(p + 2)$ with both p and $p + 2$ being prime in the last case. For a detailed treatment of cyclic difference sets, see [3].

Some 40 years after the appearance of the GMW construction, new and interesting cyclic Hadamard difference sets with Singer parameters were discovered in the late 1990s by several research groups. In 1998, Maschietti [21] constructed a new family of cyclic Hadamard difference sets that were based on the theory of hyperovals in finite projective geometry. Around the same time, several difference sets were postulated by No et al. in [23] based on the results of a numeric search and these led to a subsequent postulate by Dobbertin [8]. All postulates have now been confirmed to hold. The difference sets postulated by No et al. and Dobbertin were subsequently shown by Dillon [6] and Dillon and Dobbertin [7] to be examples of difference sets constructed by considering the image set, in a finite field with 2^m elements, of one of two mappings

$$x \to (x+1)^d + x^d + 1 \quad \text{for } d = 2^{2k} - 2^k + 1 \quad \text{and} \quad \gcd(m,k) = 1 \quad \text{or}$$
$$x \to (x+1)^d + x^d \quad \text{for } d = 2^{2k} - 2^k + 1 \quad \text{and} \quad 3k \equiv 1 \bmod (m).$$

The status at present is that all binary sequences of period $2^n - 1$ with ideal autocorrelation for $n \le 10$ can now be explained using known constructions.

12.3 The *q*-ary Sequences with Low Autocorrelation

As defined earlier, the autocorrelation of a binary {0,1} sequence $\{s(t)\}$ leads to the computation of the inner product of an {–1, +1} sequence $\{(-1)^{s(t)}\}$ with a cyclically shifted version $\{(-1)^{s(t+\tau)}\}$ of itself. The {–1, +1} sequence is transmitted as a phase shift by either 0° or 180° of a radio-frequency carrier, that is, using binary phase-shift keying (PSK) modulation. If the modulation is q-ary PSK, then one is led to consider sequences $\{s(t)\}$ with symbols in the set $\mathbb{Z}_q$, that is, the set of integers modulo q. The relevant autocorrelation function $\theta_s(\tau)$ is now defined by

$$\theta_s(\tau) = \sum_{t=o}^{n-1} \omega^{s(t+\tau)-s(t)},$$

where n is the period of $\{s(t)\}$ and ω is a complex primitive qth root of unity such as, for example, $\omega = e^{i(2\pi/q)}$. It is possible to construct sequences $\{s(t)\}$ over $\mathbb{Z}_q$ whose autocorrelation function satisfies

$$\theta_s(\tau) = \begin{cases} n & \text{if } \tau = 0 \\ 0 & \text{if } \tau \neq 0. \end{cases}$$

For obvious reasons, such sequences are said to have an *ideal autocorrelation function*.

We provide without proof two sample constructions. The sequences in the first construction are given by

$$s(t) = \begin{cases} t^2/2 & (\mathrm{mod}\, n) \quad \text{when } n \text{ is even} \\ t(t+1)/2 & (\mathrm{mod}\, n) \quad \text{when } n \text{ is odd.} \end{cases}$$

Thus, this construction provides sequences with ideal autocorrelation for any period n. Note that the size q of the sequence symbol alphabet equals n when n is odd and $2n$ when n is even.

The second construction also provides sequences over $\mathbb{Z}_q$ of period n but requires that n be a perfect square. Let $n = r^2$ and let π be an arbitrary permutation of the elements in the subset $\{0,1,2,\ldots,(r-1)\}$ of $\mathbb{Z}_n$: Let g be an arbitrary function defined on the subset $\{0,1,2,\ldots,r-1\}$ of $\mathbb{Z}_n$. Then, any sequence of the form

$$s(t) = rt_1\pi(t_2) + g(t_2) \quad (\mathrm{mod}\, n),$$

where $t = rt_1 + t_2$ with $0 \leq t_1,\ t_2 \leq r-1$ is the base-r decomposition of t, has an ideal autocorrelation function. When the alphabet size q equals or divides the period n of the sequence, ideal autocorrelation sequences also go by the name *generalized bent functions*. For details, see [17]. A different approach to the construction of ideal autocorrelation sequences and based on the Zak transform, is described in [1].

12.4 Families of Sequences with Low Cross-Correlation

Given two sequences $\{s_1(t)\}$ and $\{s_2(t)\}$ over $\mathbb{Z}_q$ of period n, their cross-correlation function $\theta_{1,2}(\tau)$ is defined by

$$\theta_{1,2}(\tau) = \sum_{t=o}^{n-1} \omega^{s_1(t+\tau)-s_2(t)},$$

where ω is as before a primitive qth root of unity. The cross-correlation function is important in code-division multiple-access (CDMA) communication systems. Here, each user is assigned a distinct signature sequence and to minimize interference due to the other users, it is desirable that the signature sequences have pairwise, low values of cross-correlation function. To provide the system in addition with a self-synchronizing capability, it is desirable that the signature sequences have low values of the autocorrelation function as well.

Let $\mathcal{F} = \{\{s_i(t)\} | 1 \le i \le M\}$ be a family of M sequences $\{s_i(t)\}$ over $\mathbb{Z}_q$, each of period n. Let $\theta_{i,j}(\tau)$ denote the cross-correlation between the ith and jth sequence at shift τ, that is,

$$\theta_{i,j}(\tau) = \sum_{t=o}^{n-1} \omega^{s_i(t+\tau)-s_j(t)}, \quad 0 \le \tau \le n-1.$$

The classical goal in sequence design for CDMA systems has been minimization of the parameter

$$\theta_{\max} = \max\{|\, \theta_{i,j}(\tau) \,|\, \text{either } i \ne j \text{ or } \tau \ne 0\}$$

for fixed n and M. It should be noted though that, in practice, because of data modulation the correlations that one runs into are typically of an aperiodic rather than a periodic nature (see Section 12.5). The problem of designing for low aperiodic correlation, however, is a more difficult one. A typical approach, therefore, has been to design based on periodic correlation, and then to analyze the resulting design for its aperiodic correlation properties. Again, in many practical systems, the mean square correlation properties are of greater interest than the worst-case correlation represented by a parameter such as $\theta_{\max}$. The mean square correlation is discussed in Section 12.6.2. Low correlation zone sequences, described in Section 12.6.3, are of interest when the CDMA system possesses approximate, but not perfect synchronism.

Bounds on the minimum possible value of $\theta_{\max}$ for given period n, family size M, and alphabet size q are available that can be used to judge the merits of a particular sequence design. The most efficient bounds are those due to Welch, Sidelnikov, and Levenshtein; see [13]. In CDMA systems, there is greatest interest in designs in which the parameter $\theta_{\max}$ is in the range $\sqrt{n} \le \theta_{\max} \le 2\sqrt{n}$. Accordingly, Table 12.1 uses the Welch, Sidelnikov, and Levenshtein bounds to provide an order-of-magnitude upper bound on the family size M for certain $\theta_{\max}$ in the cited range.

Practical considerations dictate that q be small. The bit-oriented nature of electronic hardware makes it preferable to have q a power of 2. With this in mind, a description of some efficient sequence families having low auto- and cross-correlation values and alphabet sizes $q = 2$ and $q = 4$ are described below. Also included below is a description of a family of low-correlation sequences over the M^2-quadrature amplitude modulation (QAM) alphabet for $M = 2^m$ as this is an alphabet in common use in present-day communication systems. A discussion on the construction of families of *ideal-autocorrelation* q-ary sequences with low values of cross-correlation can be found in [1].

TABLE 12.1 Bounds on Family Size M for Given n, $\theta_{\max}$

$\theta_{\max}$	Upper Bound on M ($q = 2$)	Upper Bound on M ($q > 2$)
$\sqrt{n}$	$n/2$	n
$\sqrt{2n}$	n	$n^2/2$
$2\sqrt{n}$	$3n^2/10$	$n^3/2$

12.4.1 Gold and Kasami Sequences

Given the low autocorrelation sidelobes of an m sequence, it is natural to attempt to construct families of low correlation sequences starting from m sequences. Two of the better known constructions of this type are the families of Gold and Kasami sequences.

Let r be odd and $d = 2^k + 1$, where k, $1 \le k \le r - 1$, is an integer satisfying $(k, r) = 1$. Let $\{s(t)\}$ be a cyclic shift of an m sequence of period $n = 2^r - 1$ that satisfies $s(\mathrm{d}t) \not\equiv 0$ and let $\mathcal{G}$ be the *Gold* family of $2^r + 1$ sequences given by

$$\mathcal{G} = \{s(t)\} \cup \{s(\mathrm{d}t)\} \cup \{\{s(t) + s(d[t + \tau])\} \mid 0 \le \tau \le n - 1\}.$$

Then, each sequence in $\mathcal{G}$ has period $2^r - 1$ and the maximum-correlation parameter $\theta_{\max}$ of $\mathcal{G}$ satisfies

$$\theta_{\max} \le \sqrt{2^{r+1}} + 1.$$

An application of the Sidelnikov bound coupled with the information that $\theta_{\max}$ must be an odd integer yields that for the Family $\mathcal{G}$, $\theta_{\max}$ is as small as it can possibly be. In this sense, Family $\mathcal{G}$ is an optimal family. We remark that these comments remain true even when d is replaced by the integer $d = 2^{2k} - 2^k + 1$ with the conditions on k remaining unchanged. The Gold family remains the best-known family of m sequences having low cross-correlation. Applications include the Navstar Global Positioning System whose signals are based on Gold sequences.

The family of Kasami sequences has a similar description. Let $r = 2v$ and $d = 2^v + 1$. Let $\{s(t)\}$ be a cyclic shift of an m sequence of period $n = 2^r - 1$ that satisfies $s(\mathrm{d}t) \not\equiv 0$, and consider the family of Kasami sequences given by

$$\mathcal{K} = \{s(t)\} \cup \{\{s(t) + s(d[t + \tau])\} \mid 0 \le \tau \le 2^v - 2\}.$$

Then the Kasami family $\mathcal{K}$ contains 2^v sequences of period $2^r - 1$. It can be shown that in this case

$$\theta_{\max} = 1 + 2^v.$$

This time an application of the Welch bound and the fact that $\theta_{\max}$ is an integer shows that the Kasami family is optimal in terms of having the smallest possible value of $\theta_{\max}$ for given n and M.

12.4.2 Quaternary Sequences

The entries in Table 12.1 suggest that nonbinary (i.e., $q > 2$) designs may be used for improved performance. A family of quaternary sequences that outperform the Gold and Kasami sequences is now discussed below.

Let $f(x)$ be the characteristic polynomial of a binary m sequence of length $2^r - 1$ for some integer r. The coefficients of $f(x)$ are either 0 or 1. Now, regard $f(x)$ as a polynomial over $\mathbb{Z}_4$ and form the product $(-1)^r f(x)f(-x)$. This can be seen to be a polynomial in x^2. Define the polynomial $g(x)$ of degree r by setting $g(x^2) = (-1)^r f(x)f(-x)$. Let $g(x) = \sum_{i=0}^{r} g_i x^i$ and consider the set of all quaternary sequences $\{a(t)\}$ satisfying the recursion $\sum_{i=0}^{r} g_i a(t + i) = 0 \pmod 4$ for all t.

It turns out that with the exception of the all-zero sequence, all of the sequences generated in this way have period $2^r - 1$. Thus, the recursion generates a Family A of $2^r + 1$ cyclically distinct quaternary

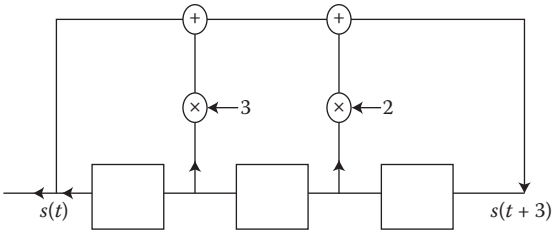

FIGURE 12.3 Shift register that generates family $\mathcal{A}$ quaternary sequences $\{s(t)\}$ of period 7.

sequences. Closer study reveals that the maximum correlation parameter θ_{max} of this family satisfies $\theta_{max} \leq 1 + \sqrt{2^r}$. Thus, in comparison with the family of Gold sequences, the Family $\mathcal{A}$ offers a lower value of θ_{max} (by a factor of $\sqrt{2}$) for the same family size. In comparison with the set of Kasami sequences, it offers a much larger family size for the same bound on θ_{max}. Family $\mathcal{A}$ sequences are discussed in [13] and in the references contained therein.

We illustrate with an example. Let $f(x) = x^3 + x + 1$ be the characteristic polynomial of the m sequence $\{a(t)\}$ in Equation 12.1. Then, over $\mathbb{Z}_4$

$$g(x^2) = (-1)^3 f(x) f(-x) = x^6 + 2x^4 + x^2 + 3$$

so that $g(x) = x^3 + 2x^2 + x + 3$. Thus, the sequences in Family $\mathcal{A}$ are generated by the recursion $s(t + 3) + 2s(t + 2) + s(t + 1) + 3s(t) = 0 \pmod 4$. The corresponding shift register is shown in Figure 12.3.

By varying initial conditions, this shift register can be made to generate nine cyclically distinct sequences, each of length 7. In this case, $\theta_{max} \leq 1 + \sqrt{8}$.

12.4.3 Binary Kerdock Sequences

The Gold and Kasami families of sequences are closely related to binary linear cyclic codes. It is known in coding theory, that there exists nonlinear binary codes the performance of which exceeds that of the best-possible linear code. Surprisingly, some of these examples come from binary codes, which are images of *linear quaternary* ($q = 4$) *codes* under the Gray map: $0 \to 00$, $1 \to 01$, $2 \to 11$, $3 \to 10$. A prime example of this is the Kerdock code, which has been shown to be the Gray image of a quaternary linear code. Thus, it is not surprising that the Kerdock code yields binary sequences, which we term as Kerdock sequences here, which improve upon the performance of the family of Kasami sequences.

The Kerdock sequences may be constructed as follows: let $f(x)$ be the characteristic polynomial of an m sequence of period $2^r - 1$, r odd. As before, regarding $f(x)$ as a polynomial over $\mathbb{Z}_4$ (which happens to have {0, 1} coefficients), let the polynomial $g(x)$ over $\mathbb{Z}_4$ be defined via $g(x^2) = -f(x)f(-x)$. Thus, $g(x)$ is the characteristic polynomial of a Family $\mathcal{A}$ sequence set of period $2^r - 1$. Set $h(x) = -g(-x) = \sum_{i=0}^{r} h_i x^i$, and let S be the set of all $\mathbb{Z}_4$ sequences satisfying the recursion $\sum_{i=0}^{r} h_i s(t + i) = 0$. Then, Family S contains 4^r-distinct sequences corresponding to all possible distinct initializations of the shift register.

Let T denote a subset of S of size 2^r consisting of those sequences corresponding to initializations of the shift register only using the symbols 0 and 2 in $\mathbb{Z}_4$. Then the set $S - T$ of size $4^r - 2^r$ contains a set $\mathcal{U}$ of 2^{r-1} cyclically distinct sequences each of period $2(2^r - 1)$. Given $x = a + 2b \in \mathbb{Z}_4$ with $a,b \in \{0,1\}$, let μ denote the most significant bit (MSB) map $\mu(x) = b$. Let $\mathcal{K}_E$ denote the family of 2^{r-1} binary sequences obtained by applying the map μ to each sequence in $\mathcal{U}$. It turns out that each sequence in $\mathcal{U}$ also has period $2(2^r - 1)$ and that, furthermore, for the Family $\mathcal{K}_E$, $\theta_{max} \leq 2 + \sqrt{2^{r+1}}$. Thus, $\mathcal{K}_E$ is a much larger family than the Kasami family, while having almost exactly the same value of θ_{max}.

For example, taking $r = 3$ and $f(x) = x^3 + x + 1$, we have from the previous Family $\mathcal{A}$ example that $g(x) = x^3 + 2x^2 + x + 3$, so that $h(x) = -g(-x) = x^3 + 2x^2 + x + 1$. Applying the MSB map to the head of the shift register, and discarding initializations of the shift register involving only 0's and 2's yields a family of four cyclically distinct binary sequences of period 14. Kerdock sequences are discussed in [13] and in the references contained therein.

12.4.3.1 QAM Sequences

For M an even integer, the M^2-QAM alphabet is given by

$$\{a + ib \mid -(M-1) \le a,b \le (M-1),\ \ a,b \ \text{ odd}\}.$$

When $M = 2^m$, $m \ge 2$, this alphabet can alternately be represented in the form:

$$\left\{\sqrt{2}i \sum_{k=0}^{m-1} 2^k i^{a_k} \mid a_k \in \mathbb{Z}_4\right\}.$$

The connection with $\mathbb{Z}_4$ suggests the use of quaternary sequences in the construction of low-correlation QAM sequences and an example construction over the 16-QAM alphabet is presented below. Sequences over the QAM alphabet are of interest as QAM is a signaling alphabet that is commonly employed in practice, and additionally, in the context of a CDMA system, a QAM sequence can potentially be made to carry a greater amount of data. Let the 2^r sequences in Family $\mathcal{A}$ of period $N := 2^r - 1$ be partitioned into 2^{r-1} disjoint pairs $\{\{a_i(t), b_i(t)\} \mid 1 \le i \le 2^{r-1}\}$. Then, a Family $\mathbb{CQ}$ (for canonical QAM family) of 16-QAM sequences may be described as follows:

$$\mathbb{CQ} = \{s_i(t) \mid 1 \le i \le 2^{r-1}\},$$

where

$$s_i(t) = \sqrt{2}i(i^{a_i(t)} + 2i^{b_i(t)}).$$

For the Family $\mathbb{CQ}$, it can be shown that the maximum correlation parameter $\theta_{\max}$, after normalization, satisfies

$$\theta_{\max} \le 1.8\sqrt{N}.$$

Normalization is carried out by dividing each correlation value $\theta_{i,j}(\tau)$ by the factor 10 because each sequence $s_i(t)$ has energy

$$\sum_{t=0}^{2^r-2} |s_i(t)|^2 \approx 10N,$$

when one neglects terms of order $\sqrt{N}$, whereas, in comparison, each q-ary sequences of period N has energy N. To convey data, the actual signal transmitted by the user is then given by

$$s_i(t, \kappa) = \sqrt{2}i(i^{a_i(t)+\kappa_a} + 2i^{b_i(t)+\kappa_b}),$$

where κ_a, κ_b lie in $\mathbb{Z}_4$ and represent data, so that one period of the sequence carries 4 bits of data. Further details including improved constructions and generalization to the general 2^{2m}-QAM constellation alphabet can be found in [2], [5], and [10].

12.5 Aperiodic Correlation

Let $\{x(t)\}$ and $\{y(t)\}$ be complex-valued sequences of length (or period) n, not necessarily distinct. Their *aperiodic correlation* values $\{\rho_{x,y}(\tau)| - (n-1) \le \tau \le n-1\}$ are given by

$$\rho_{x,y}(\tau) = \sum_{t=\max\{0,-\tau\}}^{\min\{n-1,n-1-\tau\}} x(t+\tau)y^*(t),$$

where $y^*(t)$ denotes the complex conjugate of $y(t)$. When $x \equiv y$, we will abbreviate and write ρ_x in place of $\rho_{x,y}$. The sequences described next are perhaps the most famous example of sequences with low-aperiodic autocorrelation values.

12.5.1 Barker Sequences

A binary $\{-1, +1\}$ sequence $\{s(t)\}$ of length n is said to be a *Barker sequence* [3] if the aperiodic autocorrelation values $\rho_s(\tau)$ satisfy $|\rho_s(\tau)| \le 1$ for all τ, $-(n-1) \le \tau \le n-1$. The Barker property is preserved under the following transformations:

$$s(t) \to -s(t), \quad s(t) \to (-1)^t s(t) \quad \text{and} \quad s(t) \to s(n-1-t)$$

as well as under compositions of the preceding transformations. Only the following Barker sequences are known:

$n = 2$ + +
$n = 3$ + + −
$n = 4$ + + + −
$n = 5$ + + + − +
$n = 7$ + + + − − + −
$n = 11$ + + + − − − + − − + −
$n = 13$ + + + + + − − + + − + − +,

where + denotes +1 and − denotes −1, apart from sequences that are generated from these via the transformations already discussed. It is known that if any other Barker sequence exists, it must have length $n > 1{,}898{,}884$, that is a multiple of 4.

An upper bound on the maximum out-of-phase aperiodic autocorrelation of an m sequence can be found in [26].

12.5.2 Sequences with High Merit Factor

The *merit factor* F of a $\{-1, +1\}$ sequence $\{s(t)\}$ is defined by

$$F = \frac{n^2}{2\sum_{\tau=1}^{n-1} \rho_s^2(\tau)}.$$

Since $\rho_s(\tau) = \rho_s(-\tau)$ for $1 \le |\tau| \le n-1$ and $\rho_s(0) = n$, the factor F may be regarded as the ratio of the square of the in-phase autocorrelation, to the sum of the squares of the out-of-phase aperiodic

autocorrelation values. Thus, the merit factor is one measure of the aperiodic autocorrelation properties of a binary {–1, +1} sequence. It is also closely connected with the signal to self-generated noise ratio of a communication system in which coded pulses are transmitted and received.

Let F_n denote the largest merit factor of any binary {–1, +1} sequence of length n. For example, at length $n = 13$, the Barker sequence of length 13 has a merit factor $F = F_{13} = 14.08$. Assuming a certain ergodicity postulate it was established by Golay that $\lim_{n\to\infty} F_n = 12.32$. Exhaustive computer searches carried out for $n \le 40$ have revealed the following.

1. For $1 \le n \le 40$, $n \ne 11,13$.
2. $F_{11} = 12.1$, $F_{13} = 14.08$, $3.3 \le F_n \le 9.85$.

The value F_{11} is also achieved by a Barker sequence. From partial searches, for lengths up to 117, the highest known merit factor is between 8 and 9.56; for lengths from 118 to 200, the best-known factor is close to 6. For lengths >200, statistical search methods have failed to yield a sequence having merit factor exceeding 5.

An *offset sequence* is one in which a fraction θ of the elements of a sequence of length n are chopped off at one end and appended to the other end, that is, an offset sequence is a cyclic shift of the original sequence by $n\theta$ symbols. It turns out that the asymptotic merit factor of m sequences is equal to 3 and is independent of the particular offset of the m sequence. There exist offsets of sequences associated with quadratic-residue and twin-prime difference sets that achieve a larger merit factor of 6. Details may be found in [14,15].

In 1999, Kirilusha and Narayanaswamy made the interesting observation that when one started with a sequence from a family with asymptotic merit factor 6 and appended the initial part of the sequence to the sequence, the resultant sequence was found through numerical experiments, to often have a merit factor strictly greater than 6. Following up on this approach, [4] and [16] were able to construct sequence families whose asymptotic merit factor was numerically observed to approach a value greater than 6.34. An analytical proof of the same however, is still lacking. Their constructions were based on cyclic shifts S_r of a Legendre sequence S by a fraction r of the period to which is then appended, a fraction t, $0 < t < 1$, of the initial portion of S_r. There is extensive numerical evidence to indicate that for large n, the merit factor of the new sequence is greater than 6.2 when $r = 0.25$ and $t \approx 0.03$ and further that when $r \approx 0.22$ and $t \approx 0.06$, the merit factor of the new sequence is greater than 6.34. Providing an analytical proof of these properties remains a challenging open problem. There is of course beyond this, the larger open question of determining the largest possible asymptotic merit factor F_n of any binary sequence.

12.5.3 Sequences with Low Aperiodic Cross-Correlation

If $\{u(t)\}$ and $\{v(t)\}$ are sequences of length $2n - 1$ defined by

$$u(t) = \begin{cases} x(t) & \text{if } 0 \le t \le n-1 \\ 0 & \text{if } n \le t \le 2n-2 \end{cases}$$

and

$$\upsilon(t) = \begin{cases} y(t) & \text{if } 0 \le t \le n-1 \\ 0 & \text{if } n \le t \le 2n-2, \end{cases}$$

then

$$\{\rho_{x,y}(\tau) \mid -(n-1) \le \tau \le n-1\} = \{\theta_{u,v}(\tau) \mid 0 \le \tau \le 2n-2\}. \tag{12.6}$$

Given a collection

$$U = \{\{x_i(t)\} \mid 1 \le i \le M\}$$

of sequences of length n over $\mathbb{Z}_q$, let us define

$$\rho_{\max} = \max\left\{\left|\rho_{a,b}(\tau)\right| \ \middle| \ a,b \in U, \text{either } a \ne b \text{ or } \tau \ne 0\right\},$$

It is clear from Equation 12.6 how bounds on the *periodic* correlation parameter $\theta_{\max}$ can be adapted to give bounds on $\rho_{\max}$. Translation of the Welch bound (mentioned earlier in Section 12.4) gives that for every integer $k \ge 1$,

$$\rho_{\max}^{2k} \ge \left(\frac{n^{2k}}{M(2n-1)-1}\right)\left\{\frac{M(2n-1)}{\binom{2n+k-2}{k}} - 1\right\}.$$

Setting $k = 1$ in the preceding bound gives

$$\rho_{\max} \ge n\sqrt{\frac{M-1}{M(2n-1)-1}}. \tag{12.7}$$

Thus, for fixed M and large n, Welch's bound gives

$$\rho_{\max} \ge \mathcal{O}(n^{1/2}).$$

There exist sequence families which asymptotically achieve $\rho_{\max} \approx \mathcal{O}(n^{1/2})$ [22].

12.6 Other Correlation Measures

12.6.1 Partial-Period Correlation

The *partial-period* (*p-p*) *correlation* between the sequences $\{u(t)\}$ and $\{v(t)\}$ is the collection $\{\Delta_{u,v}(l,\tau,t_0) | 1 \le l \le n, 0 \le \tau \le n-1, 0 \le t_0 \le n-1\}$ of inner products

$$\Delta_{u,v}(l,\tau,t_0) = \sum_{t=t_0}^{t_0+l-1} u(t+\tau)v^*(t),$$

where l is the length of the partial period and the sum $t + \tau$ is again computed modulo n. In direct-sequence CDMA systems, the pseudorandom signature sequences used by the various users are often very long for reasons of data security. In such situations, to minimize receiver hardware complexity, correlation over a partial period of the signature sequence is often used to demodulate data as well as to achieve synchronization. For this reason, the *p-p* correlation properties of a sequence are of interest.

Researchers have attempted to determine the moments of the p-p correlation. Here, the main tool is the application of the Pless power-moment identities of coding theory [20]. The identities often allow the first and second *p-p* correlation moments to be completely determined. For example, this is true in the case of *m* sequences (the remaining moments turn out to depend upon the specific characteristic polynomial of the *m* sequence). Further details may be found in [28].

12.6.2 Mean Square Correlation

Frequently in practice, there is a greater interest in the mean-square correlation distribution of a sequence family than in the parameter θ_{max}. Quite often in sequence design, the sequence family is derived from a linear, binary cyclic code of length n by picking a set of cyclically distinct sequences of period n. The families of Gold and Kasami sequences are so constructed. In this case, as pointed out by Massey, the mean square correlation of the family can be shown to be either optimum or close to optimum, under certain easily satisfied conditions, imposed on the minimum distance of the dual code. A similar situation holds even when the sequence family does not come from a linear cyclic code. In this sense, mean square correlation is not a very discriminating measure of the correlation properties of a family of sequences. More details may be found in [13].

12.6.3 Low-Correlation Zone Sequences

For the case when there is approximate, but not perfect synchronism present in a CDMA communication system, there is interest in the design of families of sequences whose auto- and cross-correlations are small for small values of relative time shift [18]. In this context, a low correlation zone (LCZ) sequence family $\{s_i(t)\}_{i=1}^{M}$ is defined as one in which the nontrivial auto- and cross-correlation values are small (typically 0 or −1) for small values of the time-shift parameter τ, that is,

$$|\theta_{i,j}(\tau)| \le \delta \quad \text{for } |\tau| < L, \quad i \ne j, \quad \text{and for } 1 \le |\tau| < L, \quad \text{when } i = j.$$

Four parameters (N,M,L,δ) characterize an LCZ sequence family, namely, the size M of the family, the common period N of each sequence in the family, the time duration L of the low correlation zone, and the upper bound δ on correlation magnitudes within the low correlation zone. The size M of an (N,M,L,δ) LCZ sequence family is upper bounded [29] by

$$ML - 1 \le \frac{N-1}{1-\dfrac{\delta^2}{N}}. \tag{12.8}$$

For more details, the reader is referred to the overview in [10] and to the references cited therein.

12.6.4 Optical Orthogonal Codes

Given a pair of {0,1} sequences $\{s_1(t)\}$ and $\{s_2(t)\}$ each having period n, we define the *Hamming correlation* function $\theta_{12}(\tau)$, $0 \le \tau \le n-1$, by

$$\theta_{12}(\tau) = \sum_{t=0}^{n-1} s_1(t+\tau)s_2(t).$$

Such correlations are of interest, for instance, in optical communication systems where the 1's and 0's in a sequence correspond to the presence or absence of pulses of transmitted light.

An (n,w,λ) optical orthogonal code (OOC) is a Family $\mathcal{F} = \{\{s_i(t)\}|i = 1,2,\ldots,M\}$, of $M\{0,1\}$ sequences of period n, constant Hamming weight w, where w is an integer lying between 1 and $n-1$ satisfying $\theta_{ij}(\tau) \le \lambda$ whenever either $i \ne j$ or $\tau \ne 0$.

Note that the Hamming distance $d_{a,b}$ between a period of the corresponding codewords $\{a(t)\}$, $\{b(t)\}$, $0 \le t \le n-1$ in an (n,w,λ) OOC having Hamming correlation ρ, $0 \le \rho \le \lambda$, is given by $d_{a,b} = 2(w-\rho)$, and, thus, OOCs are closely related to constant-weight error correcting codes. Given an (n,w,λ) OOC, by enlarging the OOC to include every cyclic shift of each sequence in the code, one obtains a constant-weight, minimum-distance $d_{\min} \ge 2(w-\lambda)$ code. Conversely, given a constant-weight cyclic code of length n, weight w, and minimum distance $d_{\min}$, one can derive an (n,w,λ) OOC code with $\lambda \le w - d_{\min}/2$ by partitioning the code into cyclic equivalence classes and then picking precisely one representative from each equivalence class of size n.

By making use of this connection, one can derive bounds on the size of an OOC from known bounds on the size of constant-weight codes. The bound given next follows directly from the Johnson bound for constant weight codes [20]. The number $M(n,w,\lambda)$ of codewords in a (n,w,λ) OOC satisfies

$$M(n,w,\lambda) \le \frac{1}{w}\left\lfloor \frac{n-1}{w-1}\cdots\left\lfloor \frac{n-\lambda+1}{w-\lambda+1}\left\lfloor \frac{n-\lambda}{w-\lambda}\right\rfloor\right\rfloor\cdots\right\rfloor. \tag{12.9}$$

An OOC code that achieves the Johnson bound is said to be optimal. A family $\{\mathcal{F}_n\}$ of OOCs indexed by the parameter n and arising from a common construction is said to be asymptotically optimum if

$$\lim_{n\to\infty} \frac{|\mathcal{F}_n|}{M(n,w,\lambda)} = 1.$$

Constructions for OOCs are available for the cases when $\lambda = 1$ and $\lambda = 2$. For larger values of λ, there exist constructions which are asymptotically optimum. Further details may be found in [13].

2-D OOC: The OOC discussed above correspond to sequences of pulses of a single beam of monochromatic light. The advent of wavelength-division multiplexing has made it possible to design low-correlation optical signals that are spread across both wavelength and time. While such signals are often called wavelength-time hopping codes or multiple-wavelength codes, we will refer to these codes as two-dimensional OOCs (2-D OOCs). A 2-D $(\Lambda \times T,\omega,\kappa)$ OOC C is a family of $\{0,1\}$ $(\Lambda \times T)$ arrays of constant Hamming weight ω. Every pair $\{A,B\}$ of arrays in C is required to satisfy

$$\sum_{\lambda=1}^{\Lambda}\sum_{t=0}^{T-1} A(\lambda,t)B(\lambda,\ t \oplus_T \tau) \le \kappa, \tag{12.10}$$

where either $A \ne B$ or $\tau \ne 0$. We will refer to κ as the maximum collision parameter (MCP) if $\kappa \ge 0$ is the smallest integer for which Equation 12.10 holds. Note that asynchronism is present here only along the time axis. As in the 1-D case, in a 2-D optical CDMA system, each user is assigned a distinct 2-D OOC and when the particular user wishes to send either a 1 or a 0, the user either transmits or else does not transmit the user's code sequence, respectively. Given a parameter set, let $\phi(\Lambda \times T,\omega,\kappa)$ denote the largest possible cardinality of a 2-D OOC having these parameters. The analog of the Johnson bound for 2-D OOC is given by

$$\phi(\Lambda \times T,\omega,k) \le \left\lfloor \frac{\Lambda}{\omega}\left\lfloor \frac{\Lambda T-1}{\omega-1}\cdots\left\lfloor \frac{\Lambda T-\kappa}{\omega-\kappa}\right\rfloor\right\rfloor\right\rfloor. \tag{12.11}$$

The parameters n in the case of a 1-D OOC and the parameter T in the case of a 2-D OOC represent the multiplicative factor by which the pulse rate in the optical communication system has to be raised.

Comparing Equation 12.11 with Equation 12.9, we see that for the same family size ϕ, the value of T in Equation 12.11 is significantly smaller than the value of n in Equation 12.9 and this is an important advantage enjoyed by a 2-D OOC. For details and constructions of 2-D OOC, the reader is referred to [24] and [30].

References

1. An M., Brodzik A.K., and Tolimieri R. *Ideal Sequence Design in Time-Frequency Space: Applications to Radar, Sonar and Communication Systems*, Birkhauser, Boston, 2009.
2. Anand M. and Kumar P.V. Low-correlation sequences over the QAM constellation, *IEEE Transactions on Information Theory*, IT-54, 791–810, 2008.
3. Baumert L.D. *Cyclic Difference Sets*, Lecture Notes in Mathematics, Vol. 182, Springer–Verlag, New York, 1971.
4. Borwein P., Choi K.-K.S., and Jedwab J. Binary sequences with merit factor greater than 6.34, *IEEE Transactions on Information Theory*, IT-50, 3234–3249, 2004.
5. Boztas S. CDMA over QAM and other arbitrary energy constellations, *IEEE International Conference on Communication Systems*, 2, 21.7.1–21.7.5, 1996.
6. Dillon J. Multiplicative difference sets via additive characters, *Designs Codes and Cryptography*, 17, 225–235, 1999.
7. Dillon J. and Dobbertin H. New cyclic difference sets with Singer parameters, *Finite Fields and Their Applications*, 10, 342–389, 2004.
8. Dobbertin H. Kasami power functions, permutation polynomials and cyclic difference sets, In *Difference Sets, Sequences and Their Correlation Properties* (eds.) A. Pott et al. pp. 133–158, The Netherlands, Kluwer Academic Publishers, 1999.
9. Fan P. and Darnell M. *Sequence Design for Communications Applications*, John Wiley & Sons, London, 1996.
10. Garg G., Helleseth T., and Kumar P.V. Recent advances in low-correlation sequences, In *New Directions in Wireless Communications Research* (ed.) V. Tarokh, Springer, Berlin, 2009.
11. Golomb S.W. *Shift Register Sequences*, Aegean Park Press, San Francisco, CA, 1982.
12. Golomb S.W. and Gong G. *Signal Design for Good Correlation: For Wireless Communication, Cryptography, and Radar*, Cambridge University Press, New York, 2005.
13. Helleseth T. and Kumar P.V. Sequences with low correlation. In *Handbook of Coding Theory* (eds.) V.S. Pless and W.C. Huffman, Elsevier Science Publishers, Amsterdam, 1998.
14. Jedwab J. A survey of the merit factor problem for binary sequences, *Proceedings of Sequences and Their Applications*, 3486, 30–55, 2004.
15. Jensen J.M., Jensen H.E., and Høholdt T. The merit factor of binary sequences related to difference sets, *IEEE Transactions on Information Theory*, IT-37, 617–626, 1991.
16. Kristiansen R.A. and Parker M.G. Binary sequences with merit factor >6.3, *IEEE Transactions on Information Theory*, IT-50, 3385–3389, 2004.
17. Kumar P.V., Scholtz R.A., and Welch L.R. Generalized bent functions and their properties, *Journal of Combinatorial Theory Series A*., 40, 90–107, 1985.
18. Long B., Zhang P., and Hu J. A generalized QS-CDMA system and the design of new spreading codes, *IEEE Transactions on Vehicular Technology*, 47, 1268–1275, 1998.
19. Litsyn S. *Peak Power Control in Multicarrier Communications*, Cambridge University Press, New York, 2007.
20. MacWilliams F.J. and Sloane N.J.A. *The Theory of Error-Correcting Codes*, North-Holland, Amsterdam, 1977.
21. Maschietti A. Difference sets and hyperovals, *Designs, Codes and Cryptography*, 14, 89–98, 1998.
22. Mow W.H. On McEliece's open problem on minimax aperiodic correlation, *Proceedings of the IEEE International Symposium on Information Theory*, 75, 1994.

23. No J.-S., Golomb S.W., Gong G., Lee H.-K., and Gaal P. Binary pseudorandom sequences of period $2^n - 1$ with ideal autocorrelation properties, *IEEE Transactions on Information Theory*, IT-44, 814–817, 1998.
24. Omrani R. and Kumar P.V. Improved constructions and bounds for 2-D optical orthogonal codes, *Proceedings of the IEEE International Symposium on Information Theory*, 127–131, 2005.
25. Peterson W.W. and Weldon E.J., Jr. *Error-Correcting Codes*, 2nd ed., MIT Press, Cambridge, MA, 1972.
26. Sarwate D.V. An upper bound on the aperiodic autocorrelation function for a maximal-length sequence. *IEEE Transactions on Information Theory*, IT-30, 685–687, 1984.
27. Sarwate D.V. and Pursley M.B. Crosscorrelation properties of pseudorandom and related sequences, *Proceedings of the IEEE*, 68, 593–619, 1980.
28. Simon M.K., Omura J.K., Scholtz R.A., and Levitt B.K. *Spread Spectrum Communications Handbook*, revised ed., McGraw Hill, New York, 1994.
29. Tang X.H., Fan P.Z., and Matsufuji S. Lower bounds on correlation of spreading sequence set with low or zero correlation zone, *Electronics Letters*, 36, 551–552, 2000.
30. Yang G.C. and Kwong W.C. Two-dimensional spatial signature patterns, *IEEE Transactions on Communications*, 44, 184–191, 1996.

Further Reading

A more in-depth treatment of pseudonoise sequences may be found in [9], [11], [12], [13, Chapter 21], [27], and [28, Chapter 5]. Sequence design related to peak-power control of transmitted signal energy, not covered here, is covered in [19]. Recent advances in low-correlation sequence design, relating to new cyclic difference sets, sequences with high merit factor, sequences over a QAM alphabet, and low-correlation zone sequences appear in [10].

13

Introduction to Spread Spectrum Systems

Dinesh Rajan

13.1 Introduction

Spread spectrum signals typically refer to signals that use a bandwidth that is significantly higher than the minimum bandwidth required to transmit that information sequence. Although bandwidth is a precious commodity, increasing the bandwidth of the signal prior to transmission results in several advantages: (i) The resulting power spectral density (PSD) of the spread signal is lower than the PSD of the signal prior to spreading. (ii) The resulting signal is more resistant to narrow band interference/jamming. (iii) The signal has a low probability of being intercepted. (iv) The spread signal is readily suitable for multiple access. These advantages have resulted in several military and commercial applications for spread spectrum systems.

The early developments in spread spectrum systems were primarily in military applications, where the low probability of intercept and antijam features were especially useful. Subsequently, they found utility in the commercial area. For instance, commercial applications of spread spectrum in the cellular wide area networks are similar to the military predecessors in many aspects. However, a few specific innovations enable them to attain superior performance. For instance, in the cellular application, primary innovations include the use of universal frequency reuse with intelligent adaptive power control and the use of noise-like signal waveforms. Further, wireless personal area networks such as Zigbee [1,2] and Bluetooth networks [3,4] are based on spread spectrum technology.

Consider a simple multiuser spread spectrum system where the received signal is at power P and the interference from $(M-1)$ users equals $(M-1)P$. Given a system bandwidth of W Hz, the received E_b/N_0 can be calculated as $(P/R)/(N+(M-1)P/W)$, where R is the data rate in bits per second and N is the noise power spectral density. Thus, the desired minimum value of E_b/N_0 can be satisfied in the presence of large number of users, if the bandwidth W is appropriately scaled. A similar analysis can be used to demonstrate the advantages of spread spectrum system, if the interference is from an intentional narrow band jammer.

This chapter is organized as follows. In Section 13.2, we discuss direct sequence spread spectrum systems. In Section 13.3, we focus on frequency hopping systems. Applications of spread spectrum are discussed in Section 13.4 followed by some brief concluding remarks in Section 13.5.

13.2 Direct Sequence Spread Spectrum

In a direct sequence (DS) code division multiple access (CDMA) system, the data sequence is multiplied by a pseudo-random signal before transmission. This pseudo-random signal is derived from a spreading code or spreading sequence. Each bit of the spreading sequence is also sometimes referred to as a chip. The time period, T_c, of a chip is usually much smaller than the symbol time period, T_s and the ratio $L = T_s/T_c$ is referred to as the bandwidth expansion factor. In many systems this value L is selected to be an integer. The value L also represents the maximum number of orthogonal users that can be supported without any multiuser interference.

In a multiuser uplink scenario, the signals transmitted by the various users are not synchronous with each other. However, for simplicity of exposition, we first consider a synchronous DS–CDMA system. In a synchronous system, the signals of all the users are perfectly synchronized at the receiver. Such a model is appropriate for a downlink cellular system in which the signals of all the users are transmitted from a single base station. Let there be K users and let the bit sequence of the kth user be denoted by $b_k(n)$. Let $c_k(t)$ denote the spreading signal used to modulate the kth user's signal. Let the channel from the kth user to the central receiver be denoted by A_k. The received signal, $r(t)$, is given by

$$r(t) = \sum_{n,k} A_k b_k(n) c_k(t - nT_s) + z(t), \tag{13.1}$$

where $z(t)$ represents the additive noise at the receiver and is typically modeled as a Gaussian process. The spreading sequence, $c_k(t)$ is usually nonzero only in the interval $0 \le t < T_s$. Thus, there is no inter-symbol interference (ISI) in the system. This code sequence is generated based on the PN spreading sequence and a pulse shaping signal $p(t)$ which is nonzero in the interval $0 \le t < T_c$. An example of the time-domain and frequency domain representation of the DS-CDMA signal is shown in Figure 13.1a and b, respectively.

Depending on the length of the spreading codes, the sequences are also referred to as long codes or short codes. In a short code DS–CDMA system, the same spreading code is used for all symbols of a particular user. In other words, the spreading code length L_c equals L the bandwidth expansion factor. In this case, the spreading signal $c_k(t)$ is given by

$$c_k(t) = \sum_{m=0}^{L-1} d_{k,m} p(t - mT_c) \tag{13.2}$$

In a long code DS–CDMA system, the length of the code L_c is much greater than L the bandwidth expansion factor. In this case, the received signal $r(t)$ is given by

$$r(t) = \sum_{n,k} A_k b_k(n) c_{k,\tilde{n}}(t - nT_s) + z(t) \tag{13.3}$$

where $\tilde{n} = n$ modulo L and the concatenation of the L_c/L segments of the spreading signal is based on the long spreading code. Many practical systems such as IS-95 and CDMA-2000 use a combination of both a short code and long code. Short orthogonal codes are used to separate the signals of the various users in a cell. Long codes are used for synchronization purposes and to differentiate the signals of users in different cells.

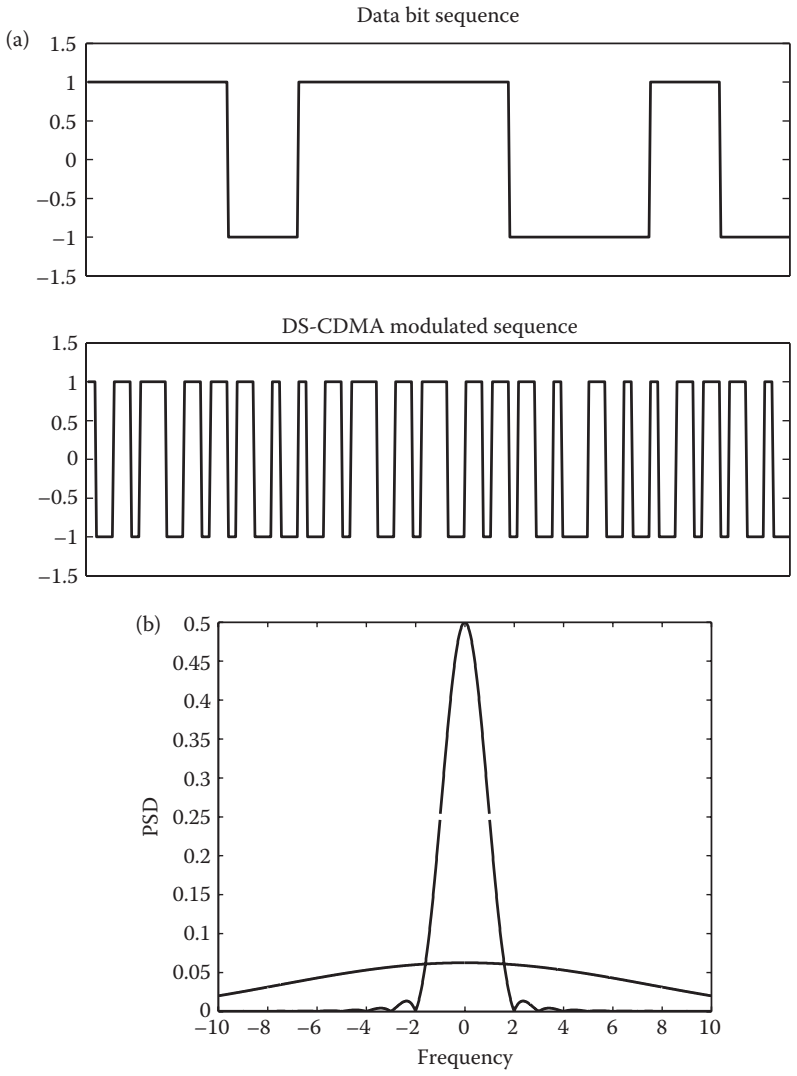

FIGURE 13.1 (a) The time domain representation of a narrow band signal and the equivalent DS-CDMA signal. (b) The frequency domain representation of the same narrow band signal and DS-CDMA signal.

At the receiver, the signal is first typically passed through a set of matched filters (MFs) corresponding to each of the users. The output of the MF corresponding to the nth bit for the kth user is given by

$$y_k(n) = \int_{(n-1)T_s}^{nT_s} \left(\sum_{n,j} A_j b_j(n) c_j(t - nT_s) + z(t) \right) c_k(t)\,\mathrm{d}t \tag{13.4}$$

$$= A_k b_k + \sum_j A_j b_j \rho_{jk} + z_k \tag{13.5}$$

where $\rho_{jk} = \int_{t=0}^{T} c_j(t)c_k(t)\,dt$ represents the cross-correlation between the spreading waveforms of user j and user k.

The outputs $y_k(n)$ from the MFs essentially represent a discrete time equivalent signal for the DS–CDMA signal. The collection of these outputs is succinctly represented in matrix form as follows:

$$y = \mathbf{RA}b + z, \tag{13.6}$$

where **R** and **A** represent, respectively, the code correlation and channel gain of the various users. The vector $b = [b_1\ b_2 \ldots b_K]^T$ represents the information from all users.

In the special case of the cross-correlation between the various spreading waveforms being 0, the multiuser interference in Equation 13.6 is completely eliminated and the channel effectively behaves like K orthogonal single user channels. In general, for nonorthogonal spreading waveforms, the performance of the MF receiver is dependent on the amount of cross correlation and the relative amplitudes of the various users. For instance, the bit error rate (BER) $P_{e,MF}(k)$ of user k using a MF in the synchronous case is bounded as

$$P_{e,MF}(k) \le Q\left(\frac{A_k}{\sigma} - \sum_{m \ne k} \frac{A_m\,|\,\rho_{mk}\,|}{\sigma}\right). \tag{13.7}$$

If the spreading waveforms of the users are not orthogonal, then a multiuser detector is used to improve the performance [5] over that of a simple MF receiver. The optimum receiver that minimizes the probability of error is the maximum likelihood sequence detector. However, the complexity of such a receiver is high since it involves enumeration of a large set of possible sequences. Two alternate receivers with lower complexity are the linear minimum mean squared error (LMMSE) and the decorrelating receiver. In a decorrelating receiver, the signal in Equation 13.6 is multiplied by the inverse $\mathbf{R}^{-1}$ of the cross-correlation matrix **R**. The advantage of such a decorrelating receiver is that it completely eliminates the multiuser interference. However, the decorrelating receiver can result in an increase in the effective noise variance. The LMMSE receiver on the other hand offers an optimal trade-off between reducing the multiuser interference and the effective noise. In the LMMSE receiver, the signal in Equation 13.6 is multiplied by $M = (\mathbf{R} + \sigma^2\mathbf{A}^{-2})^{-1}$ and the resulting output is passed through a sign detector (in the case of antipodal signaling). The exact probability of error of the LMMSE receiver has been calculated in Reference 5, but as in the earlier case, its evaluation requires a computational complexity that is exponential in the number of users. Consequently, low complexity approximations for the error rate have been obtained using a Gaussian approximation for the multiuser interference. One such approximation for the error rate for user k is given by

$$P_{e,\mathrm{LMMSE}}(k) \approx Q\left(\frac{\mu_k}{\sqrt{1 + \mu_k^2 \sum_{j \ne k} \beta_j^2}}\right), \tag{13.8}$$

where $\mu_k = \left(A_k(MR)_{kk}/\sigma\sqrt{(MRM)_{kk}}\right)$.

A plot of the BER of the various multiuser detectors is given in Figure 13.2a as a function of the SNR. In this case, each user is assigned a random binary code. It is clear from the figure that the performance of the MF is poor due to the presence of significant multiuser interference. As expected the LMMSE

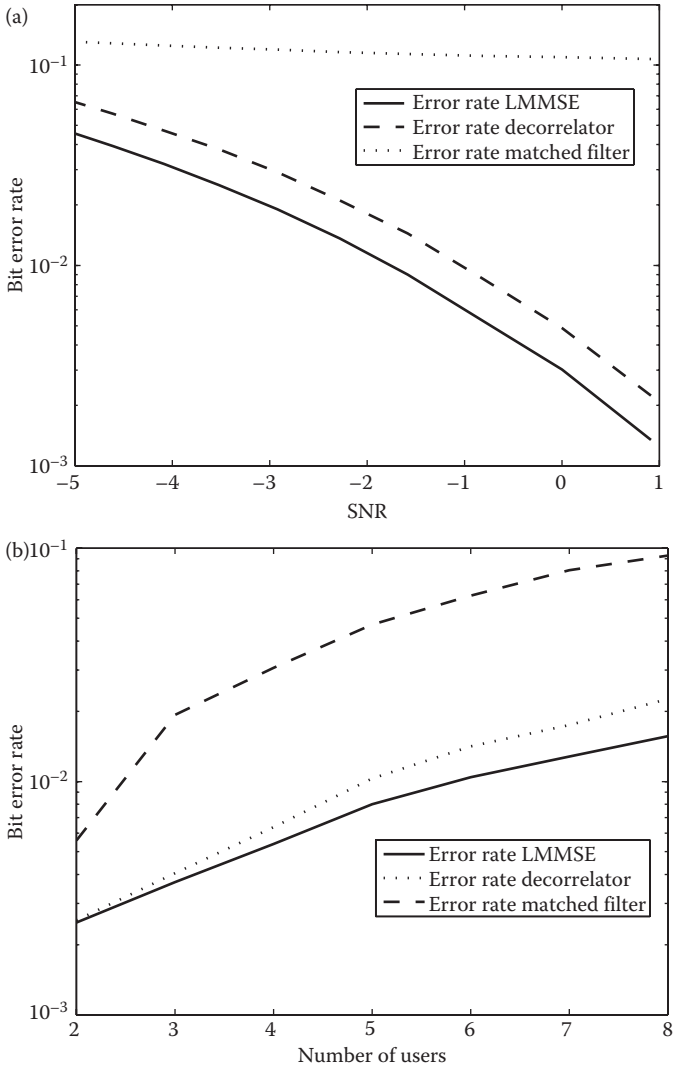

FIGURE 13.2 BER of various multiuser detectors are shown as a function of (a) the SNR and (b) the number of users.

detector performs slightly better than the decorrelating receiver. The variation of the BER with the number of users is given in Figure 13.2b for the various multiuser detectors. Owing to the random nature of the spreading codes used to generate this figure, it can be clearly seen that the BER increases as the number of users increase. In addition to the various multiuser detectors discussed so far, there are several other linear and nonlinear multiuser detectors such as serial or parallel interference cancellation receivers [5].

Another advantage of the DS–CDMA systems when used for voice applications is that the voice users are not active for the entire duration of the call. The typical voice activity factor α is lesser than 50% and ensures that the effective interference is only a fraction α of the total interference. Thus, unlike in fixed TDMA systems, the actual interference experienced in a DS–CDMA system is smaller.

The analysis of an asynchronous CDMA system follows along similar lines with some additional modifications. In this case, the received signal is given by

$$r(t) = \sum_{n,k} A_k b_k(n) c_k(t - nT_s - \tau_k) + z(t) \tag{13.9}$$

The maximum likelihood sequence detector, LMMSE and decorrelating receivers are defined in a manner similar to the synchronous case. The performance evaluation can also be generalized to this case; however, the analysis is more involved since each bit for a particular user may be affected by portions of 2 bits from each of the other users. In other words, each bit sees interference from $2(K - 1)$ other bits.

The power spectral density (PSD) of a DS–CDMA system using a raised cosine transmit pulse is shown in Figure 13.1. For reference the PSD of the data sequence as well as a realization of the data sequence and spread sequence are shown in Figure 13.1. The increased bandwidth of DS–CDMA sequence is clearly evident from this figure.

A DS–CDMA signal has good performance even in the presence of a narrow band interference signal. Clearly, the process of spreading at the transmitter ensures that a narrow band signal is now spread over a wider bandwidth. The narrow band interference now additively interferes with the spread CDMA signal. The process of despreading gathers the energy from the spread signal into a narrow band. On the other hand, the despreading operation results in a *spreading* of the narrow band interference signal over a wider band. Hence, the effective power spectral density of the narrow band interference after despreading is reduced and thus its effect on the CDMA signal is also reduced. If σ_I^2 is the energy of the interfering signal, then the effective SNR of the DS–CDMA signal is given by $(P/\sigma_n^2 + \sigma_I^2/N)$, where N is the length of the spreading code.

It has, however, been shown that the performance of the DS–CDMA signal can be significantly improved by actively suppressing the narrow band interference signal prior to despreading at the receiver [6,7]. These active noise suppression schemes have been widely investigated and can be classified into the following major schemes.

- Time domain estimation and interference subtraction. In these methods, an estimator is used to predict the narrow band signal and then subtract this estimated narrow band signal from the spread signal using a notch filter.
- Frequency domain filtering. A Fourier transform of the spread signal is first created and then the signal is filtered at a few selected frequencies. The resulting signal is passed through an inverse Fourier transform. The frequencies to filter can be calculated in an adaptive manner, for instance, by selecting spectral components that have energy higher than a certain threshold.
- Nonlinear techniques. Unlike the earlier two methods, there are also several nonlinear filtering methods that have been studied in the literature for narrow band interference suppression. One such method uses a decision feedback mechanism to predict the narrow band interference signal and then cancel its effect from the spread signal.

13.3 Frequency Hopping Spread Spectrum

Frequency hopping was first invented during World War II by Hedy Lamarr in a patent titled "Secret Communication System" [8]. In a frequency hopping spread spectrum system, the actual signal transmitted has narrow bandwidth. However, the center frequency of the transmission signal is varied over a wide band. The rate at which the center frequency of the signal is varied determines whether the system is a slow-hopping or fast-hopping system. The variation of the frequency, commonly referred to as hopping pattern, is usually based on a pseudorandom sequence. The advantage of a frequency hopping system is that its performance is not significantly affected by a narrow band interference source, since only the

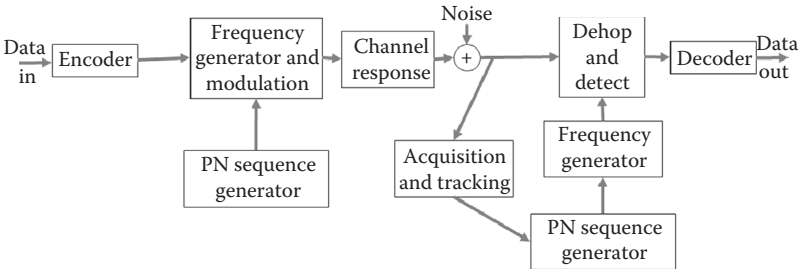

FIGURE 13.3 Block diagram of a frequency hopping system.

packets that are transmitted when the systems hops at the frequencies of the interfering signal are affected. The FH system also enables multiple point-to-point links in a given location if the hopping sequences used by the various links are *effectively* different. Note that the difference in the effective hopping pattern used by the various nodes could result from the use of different phases of the same hopping sequence for the various links. A block diagram of a typical FH spread spectrum signal is shown in Figure 13.3.

The modulation in an FH system is typically selected to be a form of Frequency Shift Keying (FSK) or Phase Shift Keying (PSK). For instance, in a binary FSK–FH system a binary "0" could be represented by a negative frequency deviation f_d from the carrier frequency f_c and a binary "1" could be represented by a positive frequency deviation f_d from f_c. The center frequency f_c is varied based on the PN sequence generated. In a MFSK system the frequency spacing between carriers is carefully selected to ensure optimum performance for a given receiver structure. In a noncoherent energy-based detector for the MFSK signal, it is desirable for the various tones representing the bits to be orthogonal to each other. This orthogonality can be achieved by spacing the carriers at integer multiples of $1/T_s$. A common arrangement for a FH–MFSK system is to consider nonoverlapping blocks of spectrum of width $M \cdot 1/T_s$. Each block of this spectrum is assigned to one hopping pattern of the PN code. Such an arrangement of tones is depicted in Figure 13.4. In Figure 13.4, there are N groups of M tones and each of these groups can be selected based on a PN code of length $\log(N)$.

As another example, consider a FH–PSK system. Using differential PSK in a FH system, the transmitted bandpass signal $s(t)$ can be represented as

$$s(t) = \mathrm{Re}\left\{m(t)e^{j2\pi f_c t}\right\} \tag{13.10}$$

where $m(t)$ is the low-pass signal. This differential PSK signal $m(t)$ can be generated using a pulse shape $p(t)$ as

$$m(t) = \sum_k m_k p(t - kT) \tag{13.11}$$

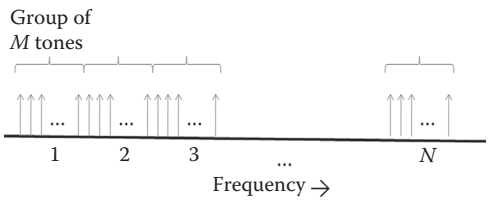

FIGURE 13.4 One possible arrangement of tones in a M-FSK frequency hopping system.

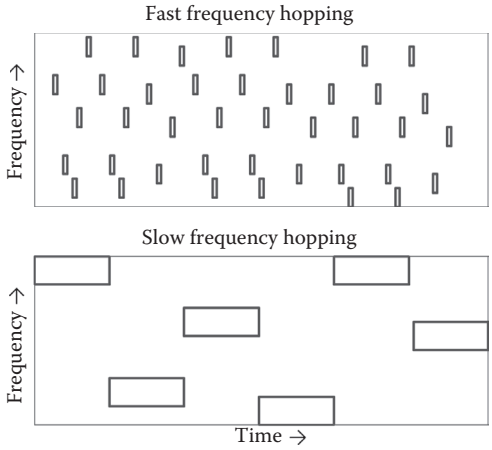

FIGURE 13.5 Depiction of slow and fast frequency hopping systems.

where $m_k = m_{k-1}e^{j\phi_k}$ is the differential PSK signal. For an 8-ary signal, $\phi_k \in \{0, \pi/4, \pi/2, 3\pi/4, \pi, 5\pi/4, 3\pi/2, 7\pi/8\}$. The pulse shape $p(t)$ that is commonly used is the raised cosine pulse [9].

At the receiver, acquisition and tracking of the PN sequence used for frequency hopping is critical for successful decoding of the signal, as discussed in Section 13.4.4. Once the carrier frequency is obtained, the received signal is then converted into baseband in a process that is sometimes called *frequency dehopping*. The differential PSK signal can then be detected using a noncoherent detector.

In a slow frequency hop system multiple symbols are transmitted on each hop. In contrast, in a fast frequency hop system there are one or more hops for each symbol. A graphical representation of the slow and fast hopping FH systems is shown in Figure 13.5.

The BER of a slow FH system with orthogonal FSK can be derived as

$$P_e = \frac{1}{2}e^{-E_b/N_0} \tag{13.12}$$

This expression for the BER is derived for the signal transmission in the presence of AWGN. In a fast FH system with M hops per bit, the signal from each of the M subintervals corresponding to a bit are combined together before detection. In this scenario, it turns out that the probability of error is greater than Equation 13.12 and the difference is known as the noncoherent combining loss [9]. The performance of FH systems in fading channels is studied in Reference 10 and the performance in the presence of an interference signal is discussed in Reference 11.

13.3.1 Time Hopping Spread Spectrum

A time hopping spread spectrum (THSS) system is analogous to a frequency hopping spread spectrum system. In a THSS each time slot of duration T is divided into smaller subintervals of length T_m. The coded information bits of the user are transmitted in a pseudo-randomly selected subintervals. Let the information data be at rate R bits/s and the coded rate equals R/r, where r is the rate of the channel code used. Since this rate needs to be transmitted in an interval of length $T_m < T$, the bandwidth required is increased.

13.4 Applications of Spread Spectrum

In this section, we highlight some of the important applications of spread spectrum signals. We first discuss cellular applications in Section 13.4.1, followed by applications in Bluetooth (Section 13.4.2) and ultrawideband systems (Section 13.4.3). Finally, we discuss synchronization issues in Section 13.4.4.

13.4.1 DS–CDMA-Based Cellular Systems

One of the original applications of DS–CDMA in digital cellular systems is the IS-95 standard. The second-generation cellular technology uses a combination of a Walsh code and a long PN code to spread the data bits. The receiver uses a rake receiver to combine the signal from the various multipaths and boost signal performance. The standard also supports a soft handover process between multiple cells. Subsequently, this standard has been replaced by the CDMA2000 and W-CDMA standards.

13.4.2 Bluetooth

The Bluetooth technology is an excellent example that demonstrates the commercial success of spread spectrum technology in enabling multiple independent peer-to-peer networks to simultaneously operate in the same geographical area. The first version of the Bluetooth standard was released in 1999. It has subsequently been revised multiple times with the latest version being Version 4. Bluetooth is designed as a short range, low energy, and inexpensive means for transferring voice, video and data between two or more devices without any infrastructure support. Bluetooth-based products have appeared in several applications such as hands free calling in cars and mobile phones, wireless game controllers, and wireless computer peripheral devices.

The basic Bluetooth network architecture is a piconet in which upto 8 devices communicate with each other by selecting one of the participating nodes as a master. The remaining nodes in the piconet are labeled as the slave nodes. Bluetooth operates in the 2.4 GHz ISM band and uses 79 channels of 1 MHz bandwidth from 2.402 to 2.48 GHz. Bluetooth is essentially an FH system in which the hopping frequency is determined by the Master node in a piconet from among these 79 frequencies. In addition, Bluetooth also uses an adaptive frequency hopping mechanism [12] to avoid interference from other devices operating in the same frequency band and also to better exploit the frequency-dependent behavior of the wideband channel.

13.4.3 Ultrawideband Systems

Ultrawideband communication systems have a long history with the original transmit signal pulses of very short duration, resulting in very large bandwidths. Subsequently, the need for multiplexing and coexistence of various signals in a given area resulted in the use of narrow band signals of larger time duration. More recent interest in UWB signals is a result of the FCC's decision (followed by similar rules in several other countries) to open up the spectrum from 3.1 to 10.6 GHz for the operation of unlicensed UWB devices.

Ultrawideband systems are loosely defined as systems that transmit information over a bandwidth in excess of the minimum of 500 MHz or using a fractional bandwidth of at least 0.2, that is, the bandwidth exceeds 20% of the center frequency of transmission [13]. These systems include both UWB based radar/imaging systems and short range, high data rate communication systems.

Buoyed by the commercial success of Bluetooth, several companies decided to create a high-speed, ultrawideband personal area communication system to replace wires between the computer and peripherals such as monitors and also between media players and high-definition TVs. The wireless community developed two competing approaches to achieve this goal. The first approach, labeled the multiband

OFDM ultrawideband system, uses a combination of OFDM and frequency hopping [14]. The second approach is based on DS–CDMA signaling [15].

While both approaches have their advantages and disadvantages, the lack of a consensus solution was detrimental to the standardization process and to the development of an ecosystem to support this technology and led to the eventual commercial failure. It is the hope of this author that newer ultrawideband systems based on spread spectrum signaling would become available in the near future.

13.4.4 Synchronization Issues in Spread Spectrum Systems

One of the major challenges in a spread spectrum system is to ensure that the PN sequences at the transmitter and receiver are perfectly synchronized. There are several factors that cause an uncertainty in time and frequency between the PN sequences at the transmitter and receiver. For instance, the propagation delay, the use of different clocks and different phases of the carrier cause a temporal shift. Similarly, the Doppler effect due to the relative motion between the transmitter and receiver cause a frequency error.

A maximum-likelihood estimator of the various user's amplitude, phase and delay is given in Reference 16. In most practical system, the PN synchronization is accomplished as a two-step process. In the first step, called as the acquisition step, a coarse alignment of the sequences is obtained. In the second phase, called the tracking phase, fine synchronization is obtained and continually updated. The acquisition is essentially carried out by correlating the received signal with various shifted versions of a copy of the transmitted signal. The goal is to select the shift that results in the maximum value of this correlation. In practice, the value of the correlation becoming higher than a threshold is used to indicate a potential acquisition of the PN signal. The fine synchronization is obtained using for instance a delay locked loop. In this case, the symmetric property of the autocorrelation is used to establish fine synchronization. The received signal is correlated with two versions of the coarse estimated PN sequence with shifts $+\tau$ and $-\tau$, respectively. The difference in value of the correlation for these two shifts is used in a feedback loop to obtain and maintain fine synchronization.

13.5 Conclusions

This chapter provides a basic introduction to spread spectrum signals. Additional details are available in several texts such as in References 17 through 20. A note of caution is appropriate when discussing the applicability of spread spectrum signals to very large bandwidths. It is well known that for the additive white Gaussian noise (AWGN) channel, as the bandwidth is increased the capacity equals P/N_0, where P is the power constraint and $N_0/2$ is the noise spectral density. It is also known that any orthogonal signaling (over time, frequency, or code space) can achieve this capacity for asymptotically large bandwidths. However, for time-varying channels, under certain conditions, it has been shown that uniformly spreading the signals in time and frequency as in DS–CDMA system does not achieve the asymptotic capacity for large bandwidths [21]. Instead, peaky signaling using for instance a combination of FH and DS–CDMA could be used to achieve capacity [21]. It is this author's expectation that spread spectrum signals will continue to play a vital role in the future wireless networks.

References

1. A. Wheeler, Commercial applications of wireless sensor networks using ZigBee, *IEEE Communications Magazine*, 45(4), 70–77, 2007.
2. C. Park and T. Rappaport, Short-range wireless communications for next-generation networks: UWB, 60 GHz Millimeter-Wave WPAN, and ZigBee, *IEEE Wireless Communications*, 14(4), 70–78, 2007.

3. J. Bray and C. F. Sturman, *Bluetooth 1.1: Connect without Cables*, 2nd ed. Upper Saddle River, NJ: Prentice-Hall, 2001.
4. B. Chatschik, An overview of the Bluetooth wireless technology, *IEEE Communications Magazine*, 39(12), 86–94, 2001.
5. S. Verdu, *Multiuser Detection*. Cambridge, UK: Cambridge University Press, 1998.
6. H. Poor and L. Rusch, A promising multiplexing technology for cellular telecommunications: Narrowband interference suppression in spread spectrum CDMA, *IEEE Personal Communications*, 1(3), 14, 1994.
7. T. H. Stitz and M. Renfors, Filter-bank-based narrowband interference detection and suppression in spread spectrum systems, *EURASIP Journal of Applied Signal Processing*, 2004, 1163–1176, 2004. [Online]. Available: http://dx.doi.org/10.1155/S1110865704312102.
8. H. Lamarr and G. Antheil, Secret communication system, U.S. Patent 2292 387, August, 1942.
9. J. G. Proakis, *Digital Communications*. New York: McGraw-Hill Inc., 2008.
10. O.-S. Shin and K. B. Lee, Performance comparison of FFH and MCFH spread-spectrum systems with optimum diversity combining in frequency-selective Rayleigh fading channels, *IEEE Transactions on Communications*, 49(3), 409–416, 2001.
11. J. Wang and C. Jiang, Analytical study of FFH systems with square-law diversity combining in the presence of multitone interference, *IEEE Transactions on Communications*, 48(7), 1188–1196, 2000.
12. N. Golmie, O. Rebala, and N. Chevrollier, Bluetooth adaptive frequency hopping and scheduling, in *Proceedings of MILCOM*, Boston, MA, October 2003, pp. 1138–1142.
13. F. C. C., Revision of part 15 of the commissions rules regarding ultra-wideband transmission systems, Online at http://hraunfoss.fcc.gov/edocs-public/attachmatch/FCC-02-48A1.pdf, April 2002, eT Docket 98–153.
14. J. Balakrishnan, A. Batra, and A. Dabak, A multi-band OFDM system for UWB communication, in *IEEE Conference on Ultra Wideband Systems and Technologies*, November 2003, pp. 354–358.
15. P. Runkle, J. McCorkle, T. Miller, and M. Welborn, DS–CDMA: The modulation technology of choice for UWB communications, in *IEEE Conference on Ultra Wideband Systems and Technologies*, November 2003, pp. 364–368.
16. S. Bensley and B. Aazhang, Maximum-likelihood synchronization of a single user for code-division multiple-access communication systems, *IEEE Transactions on Communications*, 46(3), 392–399, 1998.
17. C. F. Cook, F. W. Ellersick, L. B. Milstein, and D. L. Schilling, *Spread Spectrum Communications*. New York: IEEE Press, 1983.
18. R. C. Dixon, *Spread Spectrum Systems*. New York: John Wiley and Sons Inc., 1994.
19. M. K. Simon, J. K. Omura, R. A. Scholtz, and B. K. Levitt, *Spread Spectrum Communications Handbook*. New York: McGraw-Hill Inc., 1994.
20. A. J. Viterbi, *CDMA: Principles of Spread Spectrum Communication*. Reading, MA: Addison-Wesley Publishing Company, 1995.
21. M. Medard and R. Gallager, Bandwidth scaling for fading multipath channels, *IEEE Trans. Inf. Thy.*, 48(4), 840–852, 2002.

14

Signal Space

Rodger E. Ziemer

14.1 Introduction

The concept of signal space has its roots in the mathematical theory of inner product spaces known as *Hilbert spaces* (Stakgold, 1967). Many books on linear systems touch on the subject of signal spaces in the context of Fourier series and transforms (Ziemer et al., 1998). The applications of signal space concepts in communication theory find their power in the representation of signal detection and estimation problems in geometrical terms, which provides much insight into signaling techniques and communication system design. The first person to have apparently exploited the power of signal space concept in communication theory was the Russian Kotel'nikov (1968), who presented his doctoral dissertation in January, 1947. Wozencraft and Jacobs (1965) expanded on this approach and their work is still today widely referenced. Arthurs and Dym (1962) made use of signal space concepts in the performance analysis of several digital modulation schemes. A one-chapter summary of the use of signal space methods in signal detection and estimation is provided in Ziemer and Tranter (2009). Another application of signal space concepts is in signal and image compression. Wavelet theory (Rioul and Vetterli, 1991) is currently finding use in these application areas. Finally, the application of signal space concepts to nonlinear filtering is discussed. In the next section, the fundamentals of generalized vector spaces are summarized, followed by an overview of several applications to signal representations.

14.2 Fundamentals

A linear space or *vector space* (signal space) (Stakgold, 1967) is a collection of elements (called vectors) $\mathbf{x}, \mathbf{y}, \mathbf{z}, \ldots$, for which the following axioms are satisfied:

1. To every pair of vectors $\mathbf{x}$ and $\mathbf{y}$ there corresponds a vector $\mathbf{x} + \mathbf{y}$ with the properties:
   a. $\mathbf{x} + \mathbf{y} = \mathbf{y} + \mathbf{x}$
   b. $\mathbf{x} + (\mathbf{y} + \mathbf{z}) = (\mathbf{x} + \mathbf{y}) + \mathbf{z}$

   c. There exists a unique element **0** such that $\mathbf{x} + \mathbf{0} = \mathbf{x}$, for every $\mathbf{x}$
   d. To every $\mathbf{x}$, there exists a unique vector labeled $-\mathbf{x}$ such that $\mathbf{x} + (-\mathbf{x}) = \mathbf{0}$
2. To all vectors, $\mathbf{x}$ and $\mathbf{y}$, and all numbers (scalars), α and β, the following commutative and associative rules hold:
   a. $\alpha(\beta\mathbf{x}) = (\alpha\beta)\mathbf{x}$
   b. $(\alpha + \beta)\mathbf{x} = \alpha\mathbf{x} + \beta\mathbf{x}$
   c. $\alpha(\mathbf{x} + \mathbf{y}) = \alpha\mathbf{x} + \alpha\mathbf{y}$
   d. $1\mathbf{x} = \mathbf{x}$ where 1 is the *identity element*

A vector is said to be a *linear combination* of the vectors $\mathbf{x}_1, \mathbf{x}_2, \ldots, \mathbf{x}_k$ in a vector space if there exist numbers (not all 0) $\alpha_1, \alpha_2, \ldots, \alpha_k$ such that

$$\mathbf{x} = \sum_{i=1}^{k} \alpha_i \mathbf{x}_i \tag{14.1}$$

The vectors $\mathbf{x}_1, \mathbf{x}_2, \ldots, \mathbf{x}_k$ are said to be *linearly dependent* (or form a dependent set) if there exist numbers $\alpha_1, \alpha_2, \ldots, \alpha_k$ not all zero, such that

$$\alpha_1 \mathbf{x}_1 + \alpha_2 \mathbf{x}_2 + \cdots + \alpha_k \mathbf{x}_k = 0 \tag{14.2}$$

If Equation 14.2 can be satisfied only for $\alpha_1 = \alpha_2 = \cdots = \alpha_k = 0$, the vectors are *linearly independent*.

One is tempted to use the infinite-sum version of Equation 14.2 in defining the notion of independence for an infinite set of vectors. This is not true in general; one needs the notion of convergence, which is based on the concept of distance between vectors.

With the idea of linear independence firmly in mind, the concept of *dimension* of a vector space readily follows. A vector space is *n-dimensional* if it possesses a set of *n independent vectors*, but every set of $n + 1$ vectors is a dependent set. If for every positive integer k, a set of k independent vectors in the space can be found, the space is said to be infinite dimensional. A *basis* for a vector space means a finite set of vectors $\boldsymbol{e}_1, \boldsymbol{e}_2, \ldots, \boldsymbol{e}_n$ with the following attributes:

1. They are linearly independent
2. Every vector $\mathbf{x}$ in the space can be written as a linear combination of the basis vectors; that is

$$\mathbf{x} = \sum_{i=1}^{n} \xi_i \mathbf{e}_i \tag{14.3}$$

It can be proved that the representation (14.3) is unique and that if the space is n-dimensional, any set of n independent vectors $\mathbf{e}_1, \mathbf{e}_2, \ldots, \mathbf{e}_n$ forms a basis.

The next concept to be developed is that of a *metric space*. In addition to the addition of vectors and multiplication of vectors by scalars, as is true of ordinary three-dimensional vectors, it is important to have the notions of length and direction of a vector imposed. In other words, a metric structure must be added to the algebraic structure already defined. A collection of elements $\mathbf{x}, \mathbf{y}, \mathbf{z}, \ldots$ in a space will be called a metric space if to each pair of elements $\mathbf{x}, \mathbf{y}$ there corresponds a real number satisfying the properties:

1. $d(\mathbf{x}, \mathbf{y}) = d(\mathbf{y}, \mathbf{x})$
2. $d(\mathbf{x}, \mathbf{y}) \geq 0$ with equality if and only if $\mathbf{x} = \mathbf{y}$
3. $d(\mathbf{x}, \mathbf{z}) \leq d(\mathbf{x}, \mathbf{y}) + d(\mathbf{y}, \mathbf{z})$ (called the *triangle inequality*)

The function $d(\mathbf{x}, \mathbf{y})$ is called a *metric* (or distance function). Note that the definition of $d(\mathbf{x}, \mathbf{y})$ *does not require that the elements be vectors*; there may not be any way of adding elements or multiplying them by scalars as required for a vector space.

With the definition of a metric, one can now discuss the idea of *convergence* of a sequence $\{\mathbf{x}_k\}$ of elements in the space. Note that $d(\mathbf{x}, \mathbf{x}_k)$ is a sequence of real numbers. Therefore, it is sensible to write that

$$\lim_{k\to\infty} \mathbf{x}_k = \mathbf{x} \tag{14.4}$$

if the sequence of numbers $d(\mathbf{x}, \mathbf{x}_k)$ converges to 0 in the ordinary sense of convergence of sequences of real numbers. If

$$\lim_{m,p\to\infty} \mathrm{d}\left(\mathbf{x}_m, \mathbf{x}_p\right) = 0 \tag{14.5}$$

the sequence $\{\mathbf{x}_k\}$ is said to be a *Cauchy sequence*. It can be shown that if a sequence $\{\mathbf{x}_k\}$ converges, it is a Cauchy sequence. The converse is not necessarily true, for the limit may have carelessly been excluded from the space. If the converse is true, then the metric space is said to be *complete*.

The next vector space concept to be defined is that of length or *norm* of a vector. A *normed vector space* (or linear space) is a vector space in which a real-valued function $\|\mathbf{x}\|$ (known as the *norm* of $\mathbf{x}$) is defined, with the properties

1. $\|\mathbf{x}\| \geq 0$ with equality if and only if $\mathbf{x} = 0$.
2. $\|\alpha\, \mathbf{x}\| = |\alpha|\, \|\mathbf{x}\|$.
3. $\|\mathbf{x}_1 + \mathbf{x}_2\| \leq \|\mathbf{x}_1\| + \|\mathbf{x}_2\|$.

A normed vector space is automatically a metric space if the metric is defined as

$$d(\mathbf{x}, \mathbf{y}) = \|\mathbf{x} - \mathbf{y}\| \tag{14.6}$$

which is called the natural metric for the space. A normed vector space may be viewed either as a linear space, a metric space, or both. Its elements may be interpreted as *vectors* or *points*, a case in point being ordinary three-dimensional geometry wherein we can identify points as vectors emanating from the origin to the point in question.

The structure of a normed vector space will now be refined further with the definition of the notion of angle between two vectors. In particular, it will be possible to tell whether two vectors are perpendicular. The notion of angle between two vectors will be obtained by defining the *inner product* (also known as a scalar or dot product). In general, an inner product in a vector space is a complex-valued function of ordered pairs $\mathbf{x}$, $\mathbf{y}$ with the properties

1. $\langle \mathbf{x}, \mathbf{y} \rangle = \langle \mathbf{y}, \mathbf{x} \rangle^*$ (the asterisk denotes complex conjugate)
2. $\langle \alpha\, \mathbf{x}, \mathbf{y} \rangle = \alpha\, \langle \mathbf{x}, \mathbf{y} \rangle$
3. $\langle \mathbf{x}_1 + \mathbf{x}_2, \mathbf{y} \rangle = \langle \mathbf{x}_1, \mathbf{y} \rangle + \langle \mathbf{x}_2, \mathbf{y} \rangle$
4. $\langle \mathbf{x}, \mathbf{x} \rangle \geq 0$ with equality if and only if $\mathbf{x} = \mathbf{0}$

From the first two properties, it follows that

$$\left\langle \mathbf{x}, \alpha\mathbf{y} \right\rangle = \alpha^* \left\langle \mathbf{x}, \mathbf{y} \right\rangle \tag{14.7}$$

Also, *Schwarz's inequality* can be proved and is given by

$$\left|\left\langle \mathbf{x}, \mathbf{y} \right\rangle\right| \leq \left\langle \mathbf{x}, \mathbf{x} \right\rangle^{1/2} \left\langle \mathbf{y}, \mathbf{y} \right\rangle^{1/2} \tag{14.8}$$

with equality if and only if $\mathbf{x} = \alpha\mathbf{y}$ (or $\mathbf{x} = \mathbf{0}$ or $\mathbf{y} = \mathbf{0}$). The real, nonnegative quantity $\langle \mathbf{x}, \mathbf{x} \rangle^{1/2}$ satisfies all the properties of a norm. Therefore, it is adopted as the definition of the norm, and Schwartz's inequality assumes the form

$$\left|\langle \mathbf{x}, \mathbf{y} \rangle\right| \leq \|\mathbf{x}\|\|\mathbf{y}\| \tag{14.9}$$

The natural metric in the space is given by Equation 14.6. An inner product space, which is complete in its natural metric, is called a Hilbert space.

Example 14.1

Consider the space of all complex-valued functions $x(t)$ defined on $a \leq t \leq b$ for which the integral

$$E_x = \int_a^b |x(t)|^2 \, dt \tag{14.10}$$

exists (i.e., the space of all finite-energy signals in the interval $[a,b]$). The inner product may be defined as

$$\langle \mathbf{x}, \mathbf{y} \rangle = \int_a^b x(t) y^*(t) dt \tag{14.11}$$

The natural norm is

$$\|\mathbf{x}\| = \left[\int_a^b |x(t)|^2 \, dt \right]^{1/2} \tag{14.12}$$

and the metric is

$$d(\mathbf{x}, \mathbf{y}) = \|\mathbf{x} - \mathbf{y}\| = \left[\int_a^b |x(t) - y(t)|^2 \, dt \right]^{1/2} \tag{14.13}$$

respectively. Schwarz's inequality becomes

$$\int_a^b x(t) y^*(t) dt \leq \left[\int_a^b |x(t)|^2 dt \right]^{1/2} \left[\int_a^b |y(t)|^2 dt \right]^{1/2} \tag{14.14}$$

It can be shown that this space is complete and, hence, is a Hilbert space.

An additional requirement that can be imposed on a Hilbert space is separability, which, roughly speaking, restricts the number of elements in the space. A Hilbert space H is *separable* if there exists a *countable* (i.e., can be put in one-to-one correspondence with the positive integers) set of elements ($\mathbf{f}_1$, $\mathbf{f}_2$, …, $\mathbf{f}_n$, …) whose finite linear combinations are such that for any element $\mathbf{f}$ in H and $\varepsilon > 0$ there exist an index N and constants $\alpha_1, \alpha_2, \ldots, \alpha_N$ such that

$$\left\| \mathbf{f} - \sum_{k=1}^{N} \alpha_k \mathbf{f}_k \right\| < \varepsilon \tag{14.15}$$

The set ($\mathbf{f}_1, \mathbf{f}_2, \ldots, \mathbf{f}_n, \ldots$) is called a *spanning set*. The discussions from here on are limited to separable Hilbert spaces.

Any finite-dimensional Hilbert space E_n is separable. In fact, there exists a set of n vectors ($\mathbf{f}_1, \mathbf{f}_2, \ldots, \mathbf{f}_n$) such that each vector $\mathbf{x}$ in E_n has the representation

$$\mathbf{x} = \sum_{k=1}^{n} \alpha_k \mathbf{f}_k \tag{14.16}$$

It can be shown that the spaces consisting of square-integrable functions on the intervals $[a, b]$, $(-\infty, b]$, $[a, \infty)$, and $(-\infty, \infty)$ are all separable, where a and b are finite, and spanning sets exist for each of these spaces. For example, a spanning set for the space of square-integrable functions on $[a,b]$ is the set $(1,t,t^2, \ldots)$, which is clearly countable. For such function spaces, convergence is in the sense of convergence in the mean defined as

$$\lim_{k\to\infty} \int \left| x_k(t) - x(t) \right|^2 dt = 0 \tag{14.17}$$

Similarly, the ideas of independence and basis sets apply to Hilbert spaces in infinite-dimensional form.

It is necessary to distinguish between the concepts of a *basis* and a *spanning* set consisting of independent vectors. As ε *is* reduced in Equation 14.15, it is expected that N must be increased, and it may also be necessary to change the previously found coefficients $\alpha_1, \alpha_2, \ldots, \alpha_N$. Hence, there might not exist a fixed sequence of constants $\xi_1, \xi_2, \ldots, \xi_n, \ldots$ with the property

$$\mathbf{x} = \sum_{k=1}^{\infty} \xi_k \mathbf{f}_k \tag{14.18}$$

as would be required if the set $\{\mathbf{f}_k\}$ were a basis. For example, on the space of square-integrable functions on $[-1,1]$, the independent set $\mathbf{f}_0 = 1$, $\mathbf{f}_1 = t$, $\mathbf{f}_2 = t^2, \ldots$ is a spanning set, but not a basis, since there are many square-integrable functions on $[-1,1]$ that cannot be expanded in a series like Equation 14.18 (an example is $|t|$). Odd as it may seem at first, it is possible if the powers of t in this spanning set are regrouped into the set of polynomials known as the Legendre polynomials, $P_k(t)$.

Two vectors $\mathbf{x}$, $\mathbf{y}$ are *orthogonal* or perpendicular if $\langle \mathbf{x}, \mathbf{y} \rangle = 0$. A finite or countably infinite set of vectors $\{\phi_1, \phi_2, \ldots, \phi_k, \ldots\}$ is said to be an *orthogonal set* if $\langle \phi_i, \phi_j \rangle = 0$, $i \neq j$. A *proper orthogonal set* is an orthogonal set none of whose elements is the zero vector. A proper orthogonal set is an independent set. A set is *orthonormal* if

$$\left\langle \phi_i, \phi_j \right\rangle = \begin{cases} 0, & i \neq j \\ 1, & i = j \end{cases} \tag{14.19}$$

An important concept is that of a *linear manifold* in a Hilbert space. A set M is said to be a linear manifold if, for $\mathbf{x}$ and $\mathbf{y}$ belonging to M, so does $\alpha\mathbf{x} + \beta\mathbf{y}$ for arbitrary complex numbers α and β; thus, M is itself a linear space. If a linear manifold is a closed set, it is called a closed linear manifold (i.e., every Cauchy sequence has a limit in the space) and is itself a Hilbert space. In three-dimensional Euclidean space, linear manifolds are simply lines and planes containing the origin. In a finite-dimensional space, every linear manifold is necessarily closed.

Let M be a linear manifold, closed or not. Consider the set $M^{\perp}$ of all vectors which are orthogonal to every vector in M. It is a linear manifold that can be shown to be closed. If M is closed, M and $M^{\perp}$ are

known as *orthogonal complements*. Given a linear manifold M, each vector in the space can be decomposed in a unique manner as a sum $\mathbf{x}_p + \mathbf{z}$, where $\mathbf{x}_p$ is in M and $\mathbf{z}$ is in $M^{\perp}$.

Given an infinite orthonormal set $\{\phi_1, \phi_2, \ldots, \phi_k, \ldots\}$ in the space of all square-integrable functions on the interval $[a,b]$, let $\{a_n\}$ be a sequence of complex numbers. The *Riesz–Fischer theorem* tells us how to represent an element in the space and states:

1. If

$$\sum_{n=1}^{\infty} |a_n|^2 \tag{14.20}$$

   diverges, then

$$\sum_{n=1}^{\infty} a_n \phi_n \tag{14.21}$$

   diverges.
2. If Equation 14.20 converges, then Equation 14.21 also converges to some element $\mathbf{g}$ in the space and

$$a_n = \langle \mathbf{g}, \phi_n \rangle \tag{14.22}$$

The next question that arises is how to construct an orthonormal set from an independent set $\{\mathbf{e}_1, \mathbf{e}_2, \ldots, \mathbf{e}_n\}$. A way of doing this is known as the *Gram–Schmidt procedure*. The construction is as follows:

1. Pick a vector from the set $\{\mathbf{e}_1, \mathbf{e}_2, \ldots, \mathbf{e}_n\}$, say $\mathbf{e}_1$. Let

$$\phi_1 = \frac{\mathbf{e}_1}{\langle \mathbf{e}_1, \mathbf{e}_1 \rangle^{1/2}} \tag{14.23}$$

2. Remove from a second vector in the set, say $\mathbf{e}_2$, its projection on ϕ_1. This yields

$$\mathbf{g}_2 = \mathbf{e}_2 - \langle \mathbf{e}_2, \phi_1 \rangle \phi_1 \tag{14.24}$$

   The vector $\mathbf{g}_2$ is a linear combination of $\boldsymbol{e}_1$ and $\boldsymbol{e}_2$, and is orthogonal to ϕ_1. To normalize it, form

$$\phi_2 = \frac{\mathbf{g}_2}{\langle \mathbf{g}_2, \mathbf{g}_2 \rangle^{1/2}} \tag{14.25}$$

3. Pick another vector from the set, say $\mathbf{e}_3$, and form

$$\mathbf{g}_3 = \mathbf{e}_3 - \langle \mathbf{e}_3, \phi_2 \rangle \phi_2 - \langle \mathbf{e}_3, \phi_1 \rangle \phi_1 \tag{14.26}$$

   Normalize $\boldsymbol{g}_3$ in a manner similar to that used for $\boldsymbol{g}_2$.
4. Continue until all vectors in the set $\{\mathbf{e}_k\}$ have been used.

Note that the sets $\{\mathbf{e}_k\}$, $\{\mathbf{g}_k\}$, and $\{\phi_k\}$ all generate the same linear manifold. (Also, if $\{\mathbf{e}_k\}$ is not an independent set, the construction will result in $\mathbf{0}$ at one or more steps.)

A basis consisting of orthonormal vectors is known as an *orthonormal basis*. If the basis vectors are not normalized, it is simply an *orthogonal basis*.

Example 14.2

Consider the interval [–1, 1] and the independent set $\mathbf{e}_0 = 1$, $\mathbf{e}_1 = t$, …, $\mathbf{e}_k = t^k$, …. The Gram–Schmidt procedure applied to this set without normalization, but with the requirement that all orthogonal functions take on the value 1 at $t = 1$, gives the set of *Lengendre polynomials*, which is

$$\psi_0(t) = 1,\ \psi_1(t) = t,\ \psi_2(t) = \frac{1}{2}(3t^2 - 1),\ \psi_3(t) = \frac{1}{2}(5t^3 - 3t),\ \ldots \tag{14.27}$$

It is next desired to approximate an arbitrary vector $\mathbf{x}$ in a Hilbert space in terms of a linear combination of the independent set $\{\mathbf{e}_1, \mathbf{e}_2, \ldots, \mathbf{e}_k\}$, where $k \leq n$ if the space is an n-dimensional Euclidean space, and k is an arbitrary integer if the space is infinite dimensional. First, the orthonormal set $\{\phi_k\}$ is constructed from $\{\mathbf{e}_k\}$. The unique, best approximation to $\mathbf{x}$ is the *Fourier sum*

$$\sum_{i=1}^{k} \langle \mathbf{x},\ \phi_i \rangle\ \phi_i \tag{14.28}$$

which is geometrically the projection of $\mathbf{x}$ onto the linear manifold generated by $\{\phi_k\}$, or equivalently, the sum of the projections along the individual axes defined by $\phi_1, \phi_2, \ldots, \phi_k$. The square of the distance between $\mathbf{x}$ and its projection is

$$\left\| \mathbf{x} - \sum_{i=1}^{k} \langle \mathbf{x}, \phi_i \rangle\ \phi_i \right\|^2 = \|\mathbf{x}\| - \sum_{i=1}^{k} \left| \langle \mathbf{x}, \phi_i \rangle \right|^2 \tag{14.29}$$

Since the left-hand side is nonnegative, Equation 14.29 gives *Bessel's inequality*, which is

$$\|\mathbf{x}\|^2 \geq \sum_{i=1}^{k} \left| \langle \mathbf{x}, \phi_i \rangle \right|^2 \tag{14.30}$$

A convenient feature of the Fourier sum is as follows: If another vector ϕ_{k+1} is added to the orthonormal approximating set of vectors, the best approximation now becomes

$$\sum_{i=1}^{k+1} \langle \mathbf{x}, \phi_i \rangle\ \phi_i \tag{14.31}$$

Thus, an additional term is added to the series expansion without changing previously computed coefficients, which makes the extension to a countably infinite orthonormal approximating set simple to envision. In the case of an infinite orthonormal approximating set, Bessel's inequality (14.30) now has an infinite limit on the sum. Does the approximating sum (14.31) converge to $\mathbf{x}$? The answer is that convergence can be guaranteed only if the set $\{\phi_k\}$ is extensive enough, that is, if it is a *basis or a complete*

orthonormal set. In such cases, Equation 14.30 becomes an equality. In fact, a number of equivalent criteria can be stated to determine whether an orthonormal set $\{\phi_k\}$ is a basis or not (Stakgold, 1967). These are

1. In finite n-dimensional Euclidean space, $\{\phi_k\}$ has exactly n elements for completeness
2. For every $\mathbf{x}$ in the space of square-integrable functions

$$\mathbf{x} = \sum_i \langle \mathbf{x}, \phi_i \rangle \, \phi_i \tag{14.32}$$

3. For every $\mathbf{x}$ in the space of square-integrable functions

$$\|\mathbf{x}\|^2 = \sum_i \left| \langle \mathbf{x}, \phi_i \rangle \right|^2 \tag{14.33}$$

   (known as Parseval's equality)
4. The only $\mathbf{x}$ in the space of square-integrable functions for which all the Fourier coefficients vanish is the $\mathbf{0}$ function
5. There exists no function $\phi(t)$ in the space of square-integrable functions such that $\{\phi, \phi_1, \phi_2, \ldots, \phi_k, \ldots\}$ is an orthonormal set

Examples of complete orthonormal sets of trigonometric functions over the interval $[0,T]$ are as follows: (1) The complex exponentials with frequencies equal to the harmonics of the fundamental frequency $\omega_0 = 2\pi/T$, or

$$\frac{1}{\sqrt{T}}, \frac{\exp(j\omega_0 t)}{\sqrt{T}}, \frac{\exp(-j\omega_0 t)}{\sqrt{T}}, \frac{\exp(j2\omega_0 t)}{\sqrt{T}}, \frac{\exp(-j2\omega_0 t)}{\sqrt{T}}, \ldots \tag{14.34}$$

The factor $T^{1/2}$ in the denominator is necessary to normalize the functions and is often not included in the definition of the complex exponential Fourier series. (2) The sines and cosines with frequencies equal to harmonics of the fundamental frequency $\omega_0 = 2\,\pi/T$ or

$$\frac{1}{\sqrt{T}}, \frac{\cos(\omega_0 t)}{\sqrt{T/2}}, \frac{\sin(\omega_0 t)}{\sqrt{T/2}}, \frac{\cos(2\omega_0 t)}{\sqrt{T/2}}, \frac{\sin(2\omega_0 t)}{\sqrt{T/2}}, \ldots \tag{14.35}$$

Note that if any function is left out of these sets, the basis is incomplete.

14.3 Application of Signal Space Representation to Signal Detection

The M-ary signal detection problem is as follows: given M signals, $s_1(t)$, $s_2(t)$, …, $s_M(t)$, defined over $0 \le t \le T$. One is chosen at random and sent each T-second interval through a channel that adds white, Gaussian noise of power spectral density $N_0/2$ to it. The challenge is to design a receiver that will decide which signal was sent through the channel during each T-second interval with minimum probability of making an error.

An approach to this problem, as expanded upon in greater detail by Wozencraft and Jacobs (1965, Chapter 4) and Ziemer and Tranter (2009, Chapter 10), is to construct a linear manifold, called the signal space, using the Gram–Schmidt procedure on the M signals. Suppose that this results in the orthonormal

basis set $\{\phi_1, \phi_2, \ldots, \phi_K\}$ where $K \leq M$ (the number of basis functions may be less than the number of signals because the signals are not necessarily linearly independent). The received signal plus noise is represented in this signal space as vectors with coordinates (note that they depend on the signal transmitted)

$$Z_{ij} = A_{ij} + N_j, \quad \begin{matrix} j = 1,2,\ldots,K \\ i = 1,2,\ldots M \end{matrix} \tag{14.36}$$

where

$$A_{ij} = \int_0^T s_i(t)\phi_j(t)\,\mathrm{d}t \tag{14.37}$$

The numbers Z_{ij} are components of vectors referred to as the *signal vectors*, and the space of all signal vectors is called the *observation space*. They may be produced by a bank of matched filters or correlators, with one filter matched to each orthonormal function.

An apparent problem with this approach is that not all possible noise waveforms added to the signal can be represented as vectors in this K-dimensional observation space. The part of the noise that is represented is

$$n_{\parallel}(t) = \sum_{j=1}^{K} N_j \phi_j(t) \tag{14.38}$$

where

$$N_j = \int_0^T n(t)\phi_j(t) \tag{14.39}$$

In terms of Hilbert space terminology, Equation 14.38 is the projection of the noise waveform onto the observation space (i.e., a linear manifold). The unrepresented part of the noise is

$$n_{\perp}(t) = n(t) - n_{\parallel}(t) \tag{14.40}$$

and is the part of the noise that must be represented in the orthogonal complement of the observation space. The question is whether the decision process will be harmed by ignoring this part of the noise. It can be shown that $n_{\perp}(t)$ is uncorrelated with $n_{\parallel}(t)$. Thus, since $n(t)$ is Gaussian they are statistically independent and $n_{\perp}(t)$ has no bearing on the decision process; nothing is lost by ignoring $n_{\perp}(t)$.

The decision process can be shown to reduce to choosing that signal $s_l(t)$ minimizing the distance to the data vector; that is,

$$d(\mathbf{z},\mathbf{s}_l) = \|\mathbf{z} - \mathbf{s}_l\| = \left[\sum (Z_{ij} - A_{ij})^2\right]^{1/2} = \text{minimum}, \quad l = 1,2,\ldots,M \tag{14.41}$$

where

$$z(t) = \sum_{j=1}^{K} Z_{ij}\phi_j(t) \tag{14.42}$$

and

$$s_l(t) = \sum_{j=1}^{K} A_{lj}\phi_j(t) \tag{14.43}$$

Thus, the signal detection problem is reduced to a geometrical one, where the observation space is subdivided into decision regions in order to make a decision. Each decision region is constructed to ensure that each observation point included in it is closer to the chosen signal point than to any other.

14.4 Application of Signal Space Representation to Parameter Estimation

The procedure used in applying signal space concepts to estimation is similar to that used for signal detection. Consider the observed waveform consisting of additive signal and noise of the form

$$y(t) = s(t, A) + n(t), \quad 0 \le t \le T \tag{14.44}$$

where A is a parameter to be estimated and the noise is white as before. Let $\{\phi_1, \phi_2, \ldots, \phi_k, \ldots\}$ be a complete orthonormal basis set. The observed waveform can be represented as

$$y(t) = \sum_{j=1}^{\infty} S_j(A)\phi_j(t) + \sum_{j=1}^{\infty} N_j\phi_j(t) \tag{14.45}$$

where

$$S_j(A) = \langle s, \phi_j \rangle = \int_0^T s(t, A)\phi_j^*(t)\,dt \tag{14.46}$$

and N_j is defined by Equation 14.39. Hence, an estimate can be made on the basis of the set of coefficients

$$Z_j = S_j(A) + N_j \tag{14.47}$$

or on the basis of a vector in the signal space with these coordinates. A reasonable criterion for estimating A is to maximize the likelihood ratio, or a monotonic function thereof. Its logarithm, for $n(t)$ Gaussian, can be shown to reduce to

$$l(A) = \lim_{K\to\infty} L_K(A) = \lim_{K\to\infty}\left[\frac{2}{N_0}\sum_{k=1}^{K} Z_K S_K(A) - \frac{1}{N_0}\sum_{k=1}^{K} S_K^2(A)\right] \tag{14.48}$$

In the limit as $K \to \infty$, this becomes

$$l(A) = \frac{2}{N_0}\int_0^T z(t)s(t, A)\,dt - \frac{1}{N_0}\int_0^T s^2(t, A)\,dt \tag{14.49}$$

A necessary condition for the value of A that maximizes Equation 14.49 is

$$\frac{\partial l(A)}{\partial A} = \frac{2}{N_0}\int_0^T [z(t) - s(t, A)]\frac{\partial s(t,A)}{\partial A}\,\mathrm{d}t\Bigg|_{A=\hat{A}} = 0 \tag{14.50}$$

The value of A that maximizes Equation 14.49, denoted $\hat{A}$, is called the maximum likelihood estimate.

14.5 Miscellaneous Applications

14.5.1 Wavelet Transforms

Wavelet transforms can be continuous time or discrete time. They find applications in speech and image compression, signal and image classification, and pattern recognition.

The continuous-time *wavelet transform* of a signal $x(t)$ takes the form (Rioul and Vetterli, 1991)

$$W_x(\tau, a) = \int_{-\infty}^{\infty} x(t) h^*_{a,\tau}(t)\,\mathrm{d}t \tag{14.51}$$

where

$$h_{a,\tau}(t) = \frac{1}{\sqrt{a}} h\left(\frac{t-\tau}{a}\right) \tag{14.52}$$

are basis functions called *wavelets*. Thus, the wavelets defined in Equation 14.52 are scaled and translated versions of the basic wavelet prototype $h(t)$ (also known as the *mother wavelet*), and the wavelet transform is seen to be a convolution of the conjugate of a wavelet with the signal $x(t)$. Substitution of Equation 14.52 to 14.51 yields

$$W_x(\tau, a) = \frac{1}{\sqrt{a}}\int_{-\infty}^{\infty} x(t) h^*\left(\frac{t-\tau}{a}\right)\mathrm{d}t \tag{14.53}$$

Note that $h(t/a)$ is contracted if $a < 1$ and expanded if $a > 1$. Thus, an interpretation of Equation 14.53 is that as a increases, the function $h(t/a)$ becomes spread out over time and takes the long-term behavior of $x(t)$ into account; as a decreases the short-time behavior of $x(t)$ is taken into account. A change of variables in Equation 14.53 gives

$$W_x(\tau, a) = \sqrt{a}\int_{-\infty}^{\infty} x(at) h^*\left(t - \frac{\tau}{a}\right)\mathrm{d}t \tag{14.54}$$

Now the interpretation of Equation 14.54 is as the scale increases ($a < 1$), an increasingly contracted version of the signal is seen through a constant-length sifting function, $h(t)$. This is only the barest of introductions to wavelets, and the reader is urged to consult the references to learn more about wavelets and their applications, particularly their discrete-time implementation.

14.5.2 Mean-Square Estimation: The Orthogonality Principle

Given n random variables, $X_1, X_2, \ldots, X_n$ it is desired to find n constants $a_1, a_2, \ldots, a_n$ such that when another random variable S is estimated by the sum

$$\hat{S} = \sum_{i=1}^{n} a_i X_i \tag{14.55}$$

then the mean-square error (MSE)

$$\text{MSE} = E\left\{\left|S - \sum_{i=1}^{n} a_i X_i\right|^2\right\} \tag{14.56}$$

is a minimum, where $E\{\ \}$ denotes expectation or statistical average. It is shown in (Papoulis and Pillai, 2001) that the MSE is minimized when the error is orthogonal to the data, or when

$$E\left\{\left[S - \sum_{i=1}^{n} a_i X_i\right] X_j^*\right\} = 0, \quad j = 1,2,\ldots,n \tag{14.57}$$

This is known as the orthogonality principle or projection theorem and can be interpreted as stating that the MSE is minimized when the error vector is orthogonal to the subspace (linear manifold) spanned by the vectors $X_1, X_2, \ldots, X_n$. The projection theorem has many applications including filtering of noisy signals, known as Wiener filtering.

14.5.3 Volterra Adaptive Lattice Filtering

Volterra filters are nonlinear filters which, in discrete time, can be characterized by input–output relationships of the form (Mathews, 1991)

$$\begin{aligned} y[n] = &\sum_{m_1=0}^{N-1} h_1[m_1]\,x[n-m_1] + \sum_{m_2=0}^{N-1}\sum_{m_1=0}^{N-1} h_2[m_1,m_2]\,x[n-m_1]\,x[n-m_2] \\ &+ \cdots + \sum_{m_p=0}^{N-1}\cdots\sum_{m_1=0}^{N-1} h_p[m_1,m_2,\ldots,m_p]\,x[n-m_1]\ldots x[n-m_p] \end{aligned} \tag{14.58}$$

where $x[n]$ is the input and $y[n]$ is the output of the system at discrete time instantn. An important area for their application is inverse filtering, or equalization, for nonlinear communications channels (Benedetto and Biglieri, 1983) wherein some type of feedback adjustment algorithm is used to adjust the Volterra kernels (Haykin, 1996), $h_p\ [m_1, m_2, \ldots, m_p]$.

Clearly, Equation 14.58 becomes rapidly complex as the number of terms included is increased. Some simplification is obtained by assuming that $h_p\ [m_1, m_2, \ldots, m_p]$ is symmetrical in its indices. Further simplification may be obtained in many cases if the channels being equalized have odd symmetry, which is often the case. As an example, assume that both of these to be the case and let the series (14.58) be truncated at the third-order sum and let $N = 3$. Then, the Volterra expansion for this case becomes

$$\begin{aligned} y[n] = {} & h_1[0]x[n] + h_1[1]x[n-1] + h_1[2]x[n-2] + h_3[0,0,0]x^3[n] \\ & + h_3[0,0,1]x^2[n]x[n-1] + h_3[0,0,2]x^2[n]x[n-2] \\ & + h_3[0,1,1]x[n]x^2[n-1] + h_3[0,1,2]x[n]x[n-1]x[n-2] \\ & + h_3[0,2,2]x[n]x^2[n-2] + h_3[1,1,1]x^3[n-1] \\ & + h_3[1,1,2]x^2[n-1]x[n-2] + h_3[1,2,2]x[n-1]x^2[n-2] \\ & + h_3[2,2,2]x^3[n-2] \end{aligned} \tag{14.59}$$

The terms can be grouped in the following manner:

$$\begin{bmatrix} x[n] & x[n-1] & x[n-2] \\ x^2[n] & x^2[n-1] & x^2[n-2] \\ x^3[n] & x^3[n-1] & x^3[n-2] \\ & x^2[n]x[n-1] & x^2[n]x[n-2] \\ & x[n]x^2[n-1] & x[n]x^2[n-2] \\ \text{Col. 0} & \text{Col. 1} & \text{Col. 2} \end{bmatrix} \tag{14.60}$$

The basic idea for forming the lattice Volterra filter is to obtain a Gram–Schmidt orthogonal decomposition of the three columns, $\mathbf{x}_0^b[n], \mathbf{x}_1^b[n], \mathbf{x}_2^b[n]$. Let $\mathbf{b}_0[n], \mathbf{b}_1[n], \mathbf{b}_2[n]$ represent the corresponding orthogonal basis set. Then, any linear combination of $\mathbf{x}_0^b[n], \mathbf{x}_1^b[n], \mathbf{x}_2^b[n]$ can be equivalently written as another linear combination of $\mathbf{b}_0[n]$, $\mathbf{b}_1[n]$, $\mathbf{b}_2[n]$. Let $d[n]$ be the desired signal, and let its estimate be

$$\hat{\mathrm{d}}[n] = \left(\mathbf{k}_0^d\right)^T \mathbf{b}_0[n] + \left(\mathbf{k}_1^d\right)^T \mathbf{b}_1[n] + \left(\mathbf{k}_2^d\right)^T \mathbf{b}_2[n] \tag{14.61}$$

A big advantage of the lattice structure is that because of the orthogonality of $\mathbf{b}_0[n]$, $\mathbf{b}_1[n]$, $\mathbf{b}_2[n]$ the coefficient vector $\mathbf{k}_i^d$ can be computed solely from the joint statistics of $d[n]$ and $b_1 n]$.

References

Arthurs, E. and Dym, H. 1962. On the optimum detection of digital signals in the presence of white gaussian noise—A geometric approach and a study of three basic data transmission systems. *IRE Trans. Commun. Syst.*, CS-10(Dec.): 336–372.

Benedetto, S. and Biglieri, E. 1983. Nonlinear equalization of digital satellite channels. *IEEE J. Sel. Areas in Commun.*, SAC-1(Jan.): 57–62.

Haykin, S. 1996. *Adaptive Filter Theory*, 3rd ed. Englewood Cliffs, NJ: Prentice Hall.

Kotel'nikov, V.A. 1968. *The Theory of Optimum Noise Immunity* (trans. R.A. Silverman), Dover, New York.

Mathews, V. 1991. Adaptive polynomial filters. *IEEE Signal Proc. Mag.*, 8(Jul.): 10–26.

Papoulis, A. and Pillai, S. Unnikrishna. 2001. *Probability, Random Variables, and Stochastic Processes*, 3rd ed., New York: McGraw–Hill.

Rioul, O. and Vetterli, M. 1991. Wavelets in signal processing. *IEEE Signal Proc. Mag.*, 8(Oct.):14–38.

Stakgold, I. 1967. *Boundary Value Problems of Mathematical Physics*, Vol. 1, London: Macmillan, Collier–Macmillan Ltd.

Wozencraft, J.M. and Jacobs, I.M. 1965. *Principles of Communication Engineering*, New York: Wiley. (Available from Prospect Heights, IL: Waveland Press.)

Ziemer, R.E., Tranter, W.H., and Fannin, D.R. 1998. *Signals and Systems: Continuous and Discrete*, 4th ed. New York: Macmillan.

Ziemer, R.E. and Tranter, W.H. 2009. *Principles of Communications: Systems, Modulation, and Noise*, 6th ed. Boston, MA: Houghton Mifflin.

Further Reading

Very readable expositions of signal space concepts as applied to signal detection and estimation are found in Chapter 4 of the classic book by Wozencraft and Jacobs. The paper by Arthurs and Dym listed in the references is also worth reading. A treatment of signal space concepts and applications to signal detection and parameter estimation is given in Chapter 10 of the book by Ziemer and Tranter. For the mathematical theory behind signal space concepts, the book by Stakgold is recommended. For those interested in wavelet transforms and their relationship to signal spaces, the April 1992 issue of the *IEEE Signal Processing Magazine* provides a tutorial article on wavelet transforms. A tutorial treatment on adaptive Volterra filters is provided in the paper by Mathews.

15

Optimum Receivers

Geoffrey C. Orsak

15.1 Introduction

Every engineer strives for optimality in design. This is particularly true for communications engineers since in many cases implementing suboptimal receivers and sources can result in dramatic losses in performance. As such, this chapter focuses on design principles leading to the implementation of optimum receivers for the most common communication environments.

The main objective in digital communications is to transmit a sequence of bits to a remote location with the highest degree of accuracy. This is accomplished by first representing bits (or more generally short bit sequences) by distinct waveforms of finite time duration. These time-limited waveforms are then transmitted (broadcasted) to the remote sites in accordance with the data sequence.

Unfortunately, because of the nature of the *communication channel*, the remote location receives a corrupted version of the concatenated signal waveforms. The most widely accepted model for the communication channel is the so-called *additive white Gaussian noise* channel (AWGN channel)*. Mathematical arguments based upon the central limit theorem [7], together with supporting empirical evidence, demonstrate that many common communication channels are accurately modeled by this abstraction. Moreover, from the design perspective, this is quite fortuitous since design and analysis with respect to this channel model is relatively straightforward.

* For those unfamiliar with AWGN, a random process (waveform) is formally said to be white Gaussian noise if all collections of instantaneous observations of the process are jointly Gaussian and mutually independent. An important consequence of this property is that the power spectral density of the process is a constant with respect to frequency variation (spectrally flat). For more on AWGN, see Papoulis [4].

15.2 Preliminaries

To better describe the digital communications process, we shall first elaborate on so-called binary communications. In this case, when the source wishes to transmit a bit value of 0, the transmitter broadcasts a specified waveform $s_0(t)$ over the *bit interval* $t \in [0, T]$. Conversely, if the source seeks to transmit the bit value of 1, the transmitter alternatively broadcasts the signal $s_1(t)$ over the same bit interval. The received waveform $R(t)$ corresponding to the first bit is then appropriately described by the following hypotheses testing problem:

$$\begin{aligned} H_0 &: R(t) = s_0(t) + \eta(t) \quad 0 \le t \le T \\ H_1 &: R(t) = s_1(t) + \eta(t) \end{aligned} \tag{15.1}$$

where, as stated previously, $\eta(t)$ corresponds to AWGN with spectral height nominally given by $N_0/2$. It is the objective of the receiver to determine the bit value, that is, the most accurate hypothesis from the received waveform $R(t)$.

The optimality criterion of choice in digital communication applications is the *total probability of error* normally denoted as P_e. This scalar quantity is expressed as

$$\begin{aligned} P_e = {} & Pr(\text{declaring } 1 | 0 \text{ transmitted})\, Pr(0 \text{ transmitted}) \\ & + Pr(\text{declaring } 0 | 1 \text{ transmitted})\, Pr(1 \text{ transmitted}) \end{aligned} \tag{15.2}$$

The problem of determining the optimal binary receiver with respect to the probability of error is solved by applying stochastic representation theory [10] to detection theory [5,9]. The specific waveform representation of relevance in this application is the *Karhunen–Loève (KL) expansion*.

15.3 Karhunen–Loève Expansion

The Karhunen–Loève expansion is a generalization of the Fourier series designed to represent a random process in terms of deterministic basis functions and uncorrelated random variables derived from the process. Whereas the Fourier series allows one to model or represent deterministic time-limited energy signals in terms of linear combinations of complex exponential waveforms, the Karhunen–Loève expansion allows us to represent a second-order random process in terms of a set of *orthonormal* basis functions scaled by a sequence of random variables. The objective in this representation is to choose the basis of time functions so that the coefficients in the expansion are mutually uncorrelated random variables.

To be more precise, if $R(t)$ is a zero mean second-order random process defined over $[0, T]$ with covariance function $K_R(t, s)$, then so long as the basis of deterministic functions satisfy certain integral constraints [9], one may write $R(t)$ as

$$R(t) = \sum_{i=1}^{\infty} R_i \phi_i(t) \quad 0 \le t \le T \tag{15.3}$$

where

$$R_i = \int_0^T R(t)\phi_i(t)\, dt$$

In this case the R_i will be mutually uncorrelated random variables with the ϕ_i being deterministic basis functions that are complete in the space of square-integrable time functions over $[0, T]$. Importantly, in this case, equality is to be interpreted as *mean-square equivalence*, that is,

$$\lim_{N\to\infty} E\left[\left(R(t) - \sum_{i=1}^{N} R_i\phi_i(t)\right)^2\right] = 0$$

for all $0 \le t \le T$.

FACT 15.1: If $R(t)$ is AWGN, then any basis of the vector space of square-integrable signals over $[0, T]$ results in uncorrelated and therefore independent Gaussian random variables.

The use of Fact 15.1 allows for a conversion of a continuous time detection problem into a finite-dimensional detection problem. Proceeding, to derive the optimal binary receiver, we first construct our set of basis functions as the set of functions defined over $t \in [0, T]$ beginning with the signals of interest $s_0(t)$ and $s_1(t)$. That is,

$$\{s_0(t), s_1(t), \text{plus a countable number of functions which complete the basis}\}.$$

In order to ensure that the basis is *orthonormal*, we must apply the Gramm–Schmidt procedure* [6] to the full set of functions beginning with $s_0(t)$ and $s_1(t)$ to arrive at our final choice of basis $\{\phi_i(t)\}$.

FACT 15.2: Let $\{\phi_i(t)\}$ be the resultant set of basis functions.

Then for all $i > 2$, the $\phi_i(t)$ are orthogonal to $s_0(t)$ and $s_1(t)$. That is,

$$\int_0^T \phi_i(t)s_j(t)\mathrm{d}t = 0$$

for all $i > 2$ and $j = 0,1$.

Using this fact in conjunction with Equation 15.3, one may recognize that only the coefficients R_1 and R_2 are functions of our signals of interest. Moreover, since the R_i are mutually independent, the optimal receiver will, therefore, only be a function of these two values.

Thus, through the application of the KL expansion, we arrive at an equivalent hypothesis testing problem to that given in Equation 15.1,

$$\begin{aligned} H_0 : \boldsymbol{R} &= \begin{bmatrix} \int_0^T \phi_1(t)s_0(t)\,\mathrm{d}t \\ \int_0^T \phi_2(t)s_0(t)\,\mathrm{d}t \end{bmatrix} + \begin{bmatrix} \eta_1 \\ \eta_2 \end{bmatrix} \\ H_1 : \boldsymbol{R} &= \begin{bmatrix} \int_0^T \phi_1(t)s_1(t)\,\mathrm{d}t \\ \int_0^T \phi_2(t)s_1(t)\,\mathrm{d}t \end{bmatrix} + \begin{bmatrix} \eta_1 \\ \eta_2 \end{bmatrix} \end{aligned} \tag{15.4}$$

where it is easily shown that η_1 and η_2 are mutually independent, zero-mean, Gaussian random variables with variance given by $N_0/2$, and where ϕ_1 and ϕ_2 are the first two functions from our *orthonormal* set of basis functions. Thus, the design of the optimal binary receiver reduces to a simple two-dimensional detection problem that is readily solved through the application of detection theory.

* The Gramm–Schmidt procedure is a deterministic algorithm that simply converts an arbitrary set of basis functions (vectors) into an equivalent set of *orthonormal* basis functions (vectors).

15.4 Detection Theory

It is well-known from detection theory [5] that under the minimum P_e criterion, the optimal detector is given by the *maximum a posteriori rule* (*MAP*),

$$\text{choose}_i \text{ largest } p_{H_i|R}(H_i \mid \boldsymbol{R} = \boldsymbol{r}) \tag{15.5}$$

that is, determine the hypothesis that is most likely, given that our observation vector is $\boldsymbol{r}$. By a simple application of Bayes theorem [4], we immediately arrive at the central result in detection theory: the optimal binary detector is given by the likelihood ratio test (LRT),

$$L(\boldsymbol{R}) = \frac{p_{\boldsymbol{R}} \mid H_1(\boldsymbol{R})}{p_{\boldsymbol{R}} \mid H_0(\boldsymbol{R})} \underset{H_0}{\overset{H_1}{\gtrless}} \frac{\pi_0}{\pi_1} \tag{15.6}$$

where the π_i are the *a priori* probabilities of the hypotheses H_i being true. Since in this case we have assumed that the noise is white and Gaussian, the LRT can be written as

$$L(\boldsymbol{R}) = \frac{\prod_1^2 \frac{1}{\sqrt{\pi N_0}} \exp\left\{-\frac{1}{2}\frac{(R_i - s_{1,i})^2}{N_0/2}\right\}}{\prod_1^2 \frac{1}{\sqrt{\pi N_0}} \exp\left\{-\frac{1}{2}\frac{(R_i - s_{0,i})^2}{N_0/2}\right\}} \underset{H_0}{\overset{H_1}{\gtrless}} \frac{\pi_0}{\pi_1} \tag{15.7}$$

where

$$s_{j,i} = \int_0^T \phi_i(t) s_j(t) \mathrm{d}t$$

By taking the logarithm and cancelling common terms, it is easily shown that the optimum binary receiver can be written as

$$\frac{2}{N_0} \sum_1^2 \boldsymbol{R}_i (s_{1,i} - s_{0,i}) - \frac{1}{N_0} \sum_1^2 \left(s_{1,i}^2 - s_{0,i}^2\right) \underset{H_0}{\overset{H_1}{\gtrless}} \ln \frac{\pi_0}{\pi_1} \tag{15.8}$$

This finite-dimensional version of the optimal receiver can be converted back into a continuous time receiver by the direct application of Parseval's theorem [4] where it is easily shown that

$$\begin{aligned} \sum_{i=1}^2 R_i s_{k,i} &= \int_0^T R(t) s_k(t) \mathrm{d}t \\ \sum_{i=1}^2 s_{k,i}^2 &= \int_0^T s_k^2(t) \mathrm{d}t \end{aligned} \tag{15.9}$$

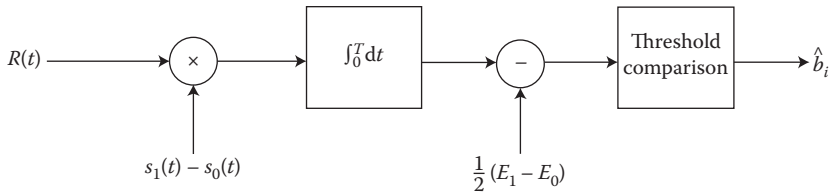

FIGURE 15.1 Optimal correlation receiver structure for binary communications.

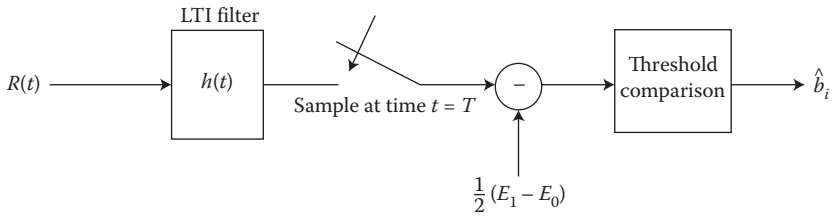

FIGURE 15.2 Optimal matched filter receiver structure for binary communications. In this case $h(t) = s_1(T - t) - s_0(T - t)$.

By applying Equation 15.9 to 15.8 the final receiver structure is then given by

$$\int_0^T R(t)[s_1(t) - s_0(t)]dt - \frac{1}{2}(E_1 - E_0) \underset{H_0}{\overset{H_1}{\gtrless}} \frac{N_0}{2} \ln \frac{\pi_0}{\pi_1} \tag{15.10}$$

where E_1 and E_0 are the energies of signals $s_1(t)$ and $s_0(t)$, respectively. (See Figure 15.1 for a block diagram.) Importantly, if the signals are equally likely ($\pi_0 = \pi_1$), the optimal receiver is independent of the typically unknown spectral height of the background noise.

One can readily observe that the optimal binary communication receiver correlates the received waveform with the difference signal $s_1(t) - s_0(t)$ and then compares the statistic to a threshold. This operation can be interpreted as identifying the signal waveform $s_i(t)$ that best correlates with the received signal $R(t)$. Based on this interpretation, the receiver is often referred to as the *correlation receiver.*

As an alternate means of implementing the correlation receiver, we may reformulate the computation of the left-hand side of Equation 15.10 in terms of standard concepts in filtering. Let $h(t)$ be the impulse response of a linear, time-invariant (LTI) system. By letting $h(t) = s_1(T - t) - s_0(T - t)$, then it is easily verified that the output of $R(t)$ to an LTI system with impulse response given by $h(t)$ and then sampled at time $t = T$ gives the desired result. (See Figure 15.2 for a block diagram.) Since the impulse response is matched to the signal waveforms, this implementation is often referred to as the *matched filter receiver.*

15.5 Performance

On account of the nature of the statistics of the channel and the relative simplicity of the receiver, performance analysis of the optimal binary receiver in AWGN is a straightforward task. Since the

conditional statistics of the log likelihood ratio are Gaussian random variables, the probability of error can be computed directly in terms of Marcum Q functions* as

$$P_e = Q\left(\frac{\| s_0 - s_1 \|}{\sqrt{2N_0}}\right)$$

where the s_i are the two-dimensional signal vectors obtained from Equation 15.4, and where $\|\boldsymbol{x}\|$ denotes the Euclidean length of the vector $\boldsymbol{x}$. Thus, $\|s_0 - s_1\|$ is best interpreted as the distance between the respective signal representations. Since the Q function is monotonically decreasing with an increasing argument, one may recognize that the probability of error for the optimal receiver decreases with an increasing separation between the signal representations, that is, the more dissimilar the signals, the lower the P_e.

15.6 Signal Space

The concept of a *signal space* allows one to view the signal classification problem (receiver design) within a geometrical framework. This offers two primary benefits: first it supplies an often more intuitive perspective on the receiver characteristics (e.g., performance) and second it allows for a straightforward generalization to standard M-ary signaling schemes.

To demonstrate this, in Figure 15.3, we have plotted an arbitrary signal space for the binary signal classification problem. The axes are given in terms of the basis functions $\phi_1(t)$ and $\phi_2(t)$. Thus, every point in the signal space is a time function constructed as a linear combination of the two basis functions. By Fact 15.2, we recall that both signals $s_0(t)$ and $s_1(t)$ can be constructed as a linear combination of $\phi_1(t)$ and $\phi_2(t)$ and as such we may identify these two signals in this figure as two points.

Since the decision statistic given in Equation 15.8 is a linear function of the observed vector $\boldsymbol{R}$ which is also located in the signal space, it is easily shown that the set of vectors under which the receiver declares hypothesis H_i is bounded by a line in the signal space. This so-called *decision boundary* is obtained by solving the equation $\ln[L(\boldsymbol{R})] = 0$. (Here again we have assumed equally likely hypotheses.)

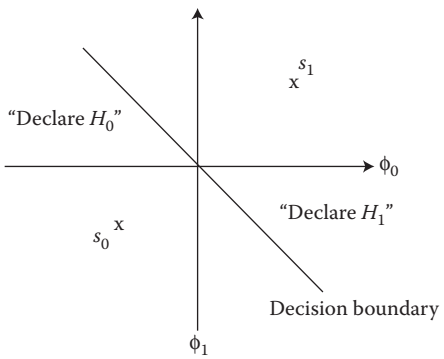

FIGURE 15.3 Signal space and decision boundary for optimal binary receiver.

* The Q function is the probability that a standard normal random variable exceeds a specified constant, that is, $Q(x) = \int_x^\infty 1/\sqrt{2\pi}\exp(-z^2/2)\,dz$.

In the case under current discussion, this decision boundary is simply the hyperplane separating the two signals in signal space. Because of the generality of this formulation, many problems in communication system design are best cast in terms of the signal space, that is, signal locations and decision boundaries.

15.7 Standard Binary Signaling Schemes

The framework just described allows us to readily analyze the most popular signaling schemes in binary communications: amplitude-shift keying (ASK), frequency-shift keying (FSK), and phase-shift keying (PSK). Each of these examples simply constitute a different selection for signals $s_0(t)$ and $s_1(t)$.

In the case of ASK, $s_0(t) = 0$, while $s_1(t) = \sqrt{2E/T}\sin(2\neq f_c t)$, where E denotes the energy of the waveform and f_c denotes the frequency of the carrier wave with $f_c T$ being an integer. Because $s_0(t)$ is the null signal, the signal space is a one-dimensional vector space with $\phi_1(t) = \sqrt{2/T}\sin(2\pi f_c t)$. This, in turn, implies that $\|s_0 - s_1\| = \sqrt{E}$. Thus, the corresponding probability of error for ASK is

$$P_e(\text{ASK}) = Q\left(\sqrt{\frac{E}{2N_0}}\right)$$

For FSK, the signals are given by equal amplitude sinusoids with distinct center frequencies, that is, $s_i(t) = \sqrt{2E/T}\sin(2\pi f_i t)$ with $f_i T$ being two distinct integers. In this case, it is easily verified that the signal space is a two-dimensional vector space with $\phi_i(t) = \sqrt{2/T}\sin(2\pi f_i t)$ resulting in $\|\boldsymbol{s}_0 - \boldsymbol{s}_1\| = \sqrt{2\boldsymbol{E}}$. The corresponding error rate is given to be

$$P_e(\text{FSK}) = Q\left(\sqrt{\frac{E}{N_0}}\right)$$

Finally, with regard to PSK signaling, the most frequently utilized binary PSK signal set is an example of an antipodal signal set. Specifically, the antipodal signal set results in the greatest separation between the signals in the signal space subject to an energy constraint on both signals. This, in turn, translates into the energy constrained signal set with the minimum P_e. In this case, the $s_i(t)$ are typically given by $\sqrt{2E/T}\sin[2\pi f_c t + \theta(i)]$, where $\theta(0) = 0$ and $\theta(1) = \pi$. As in the ASK case, this results in a one-dimensional signal space, however, in this case $\|\boldsymbol{s}_0 - \boldsymbol{s}_1\| = 2\sqrt{\boldsymbol{E}}$ resulting in probability of error given by

$$P_e(\text{PSK}) = Q\left(\sqrt{\frac{2E}{N_0}}\right)$$

In all three of the described cases, one can readily observe that the resulting performance is a function of only the signal-to-noise (SNR) ratio E/N_0. In the more general case, the performance will be a function of the intersignal energy to noise ratio. To gauge the relative difference in performance of the three signaling schemes, in Figure 15.4, we have plotted the P_e as a function of the SNR. Please note the large variation in performance between the three schemes for even moderate values of SNR.

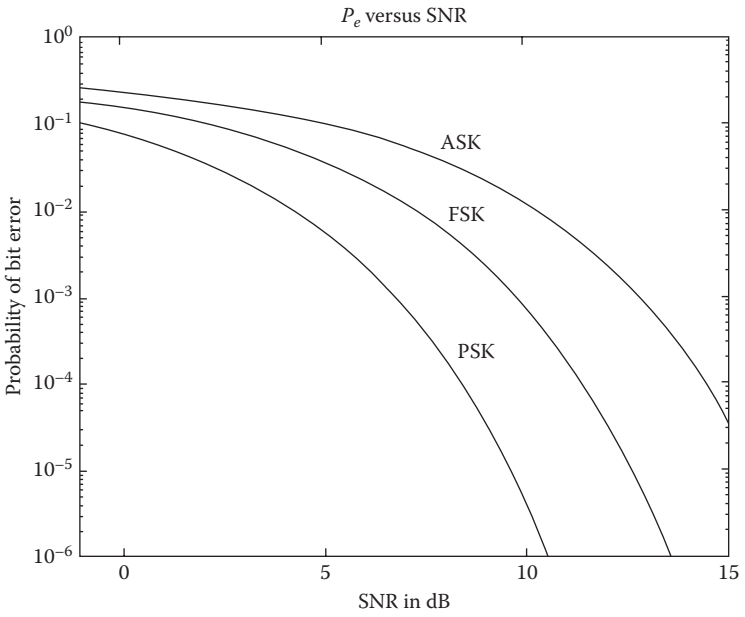

FIGURE 15.4 P_e versus the signal to noise ratio in decibels [dB = 10 log(E/N_0)] for amplitude-shift keying, frequency-shift keying, and phase-shift keying; note that there is a 3 dB difference in performance from ASK to FSK to PSK.

15.8 *M*-ary Optimal Receivers

In binary signaling schemes, one seeks to transmit a single bit over the bit interval [0, T]. This is to be contrasted with M-ary signaling schemes where one transmits multiple bits simultaneously over the so-called symbol interval [0, T]. For example, using a signal set with 16 separate waveforms will allow one to transmit a length four-bit sequence per symbol (waveform). Examples of M-ary waveforms are quadrature phase-shift keying (QPSK) and quadrature amplitude modulation (QAM).

The derivation of the optimum receiver structure for M-ary signaling requires the straightforward application of fundamental results in detection theory. As with binary signaling, the Karhunen–Loève expansion is the mechanism utilized to convert a hypotheses testing problem based on continuous waveforms into a vector classification problem. Depending on the complexity of the M waveforms, the signal space can be as large as an M-dimensional vector space.

By extending results from the binary signaling case, it is easily shown that the optimum M-ary receiver computes

$$\xi_i[R(t)] = \int_0^T s_i(t)R(t)\,dt - \frac{E_i}{2} + \frac{N_0}{2}\ln\pi_i \quad i = 1,\ldots, M$$

where, as before, the $s_i(t)$ constitute the signal set with the π_i being the corresponding *a priori* probabilities. After computing M separate values of ξ_i, the minimum probability of error receiver simply choose the largest amongst this set. Thus, the M-ary receiver is implemented with a bank of correlation or matched filters followed by choose-largest decision logic.

In many cases of practical importance, the signal sets are selected so that the resulting signal space is a two-dimensional vector space irrespective of the number of signals. This simplifies the receiver

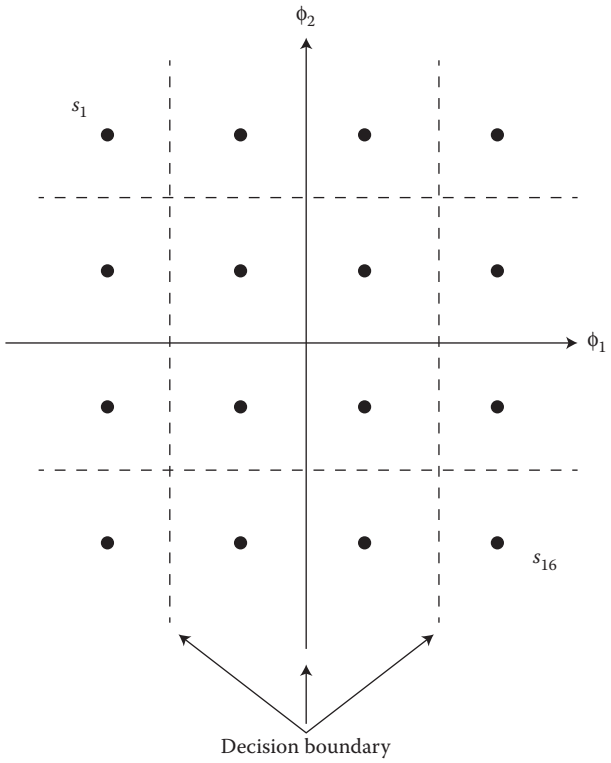

FIGURE 15.5 Signal space representation of 16-QAM signal set. Optimal decision regions for equally likely signals are also noted.

structure in that the sufficient statistics are obtained by implementing only two matched filters. Both QPSK and QAM signal sets fit into this category. As an example, in Figure 15.5, we have depicted the signal locations for standard 16-QAM signaling with the associated decision boundaries. In this case we have assumed an equally likely signal set. As can be seen, the optimal decision rule selects the signal representation that is closest to the received signal representation in this two-dimensional signal space.

15.9 More Realistic Channels

As is unfortunately often the case, many channels of practical interest are not accurately modeled as simply as an AWGN channel. It is often that these channels impose nonlinear effects on the transmitted signals. The best example of this is channels that impose a random phase and random amplitude onto the signal. This typically occurs in applications such as in mobile communications, where one often experiences rapidly changing path lengths from source to receiver.

Fortunately, by the judicious choice of signal waveforms, it can be shown that the selection of the ϕ_i in the Karhunen–Loève transformation is often independent of these unwanted parameters. In these situations, the random amplitude serves only to scale the signals in signal space, whereas the random phase simply imposes a rotation on the signals in signal space.

Since the Karhunen–Loève basis functions typically do not depend on the unknown parameters, we may again convert the continuous time classification problem to a vector channel problem where the received vector $\boldsymbol{R}$ is computed as in Equation 15.3. Since this vector is a function of both the unknown

parameters (i.e., in this case amplitude A and phase ν), to obtain a likelihood ratio test independent of A and ν, we simply apply Bayes theorem to obtain the following form for the LRT:

$$L(\boldsymbol{R}) = \frac{E[p_{\boldsymbol{R}} \mid H_1, A, \nu(\boldsymbol{R} \mid H_1, A, \nu)]}{E[p_{\boldsymbol{R}} \mid H_0, A, \nu(\boldsymbol{R} \mid H_0, A, \nu)]} \begin{matrix} H_1 \\ > \\ < \\ H_0 \end{matrix} \frac{\pi_0}{\pi_1}$$

where the expectations are taken with respect to A and ν, and where $p_R|H_i, A, \nu$ are the conditional probability density functions of the signal representations. Assuming that the background noise is AWGN, it can be shown that the LRT simplifies to choosing the largest amongst

$$\xi_i[R(t)] = \pi_i \int_{\substack{A,\nu \\ i = 1,\ldots, M}} \exp\left\{ \frac{2}{N_0} \int_0^T R(t) s_i(t \mid A, \nu)\, \mathrm{d}t - \frac{E_i(A,\nu)}{N_0} \right\} p_{A,\nu}(A,\nu)\, \mathrm{d}A\, \mathrm{d}\nu \tag{15.11}$$

It should be noted that in the Equation 15.11 we have explicitly shown the dependence of the transmitted signals s_i on the parameters A and ν. The final receiver structures, together with their corresponding performance are, thus, a function of both the choice of signal sets and the probability density functions of the random amplitude and random phase.

15.9.1 Random Phase Channels

If we consider first the special case where the channel simply imposes a uniform random phase on the signal, then it can be easily shown that the so-called in-phase and quadrature statistics obtained from the received signal $R(t)$ (denoted by R_I and R_Q, respectively), are sufficient statistics for the signal classification problem. These quantities are computed as

$$R_I(i) = \int_0^T R(t) \cos[2\pi f_c(i) t]\, \mathrm{d}t$$

and

$$R_Q(i) = \int_0^T R(t) \sin[2\pi f_c(i) t]\, \mathrm{d}t$$

where in this case the index i corresponds to the center frequencies of hypotheses H_i, (e.g., FSK signaling). As in Figure 15.6, the optimum binary receiver selects the largest from amongst

$$\xi_i[R(t)] = \pi_i \exp\left(-\frac{E_i}{N_0} \right) I_0 \left[\frac{2}{N_0} \sqrt{R_I^2(i) + R_Q^2(i)} \right] \qquad i = 1,\ldots, M$$

where I_0 is a zeroth-order, modified Bessel function of the first kind. If the signals have equal energy and are equally likely (e.g., FSK signaling), then the optimum receiver is given by

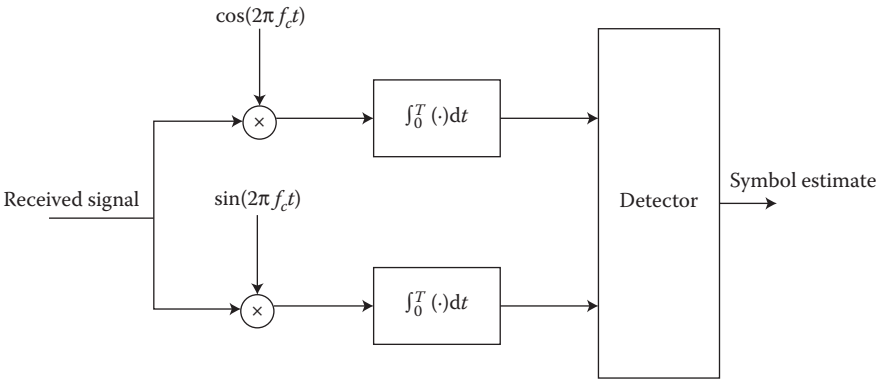

FIGURE 15.6 Optimum receiver structure for noncoherent (random or unknown phase) ASK demodulation.

$$R_I^2(1) + R_Q^2(1) \underset{H_0}{\overset{H_1}{\gtrless}} R_I^2(0) + R_Q^2(0)$$

One may readily observe that the optimum receiver bases its decision on the values of the two envelopes of the received signal $\sqrt{R_I^2(i) + R_Q^2(i)}$ and, as a consequence, is often referred to as an envelope or square-law detector. Moreover, it should be observed that the computation of the envelope is independent of the underlying phase of the signal and is as such known as a noncoherent receiver.

The computation of the error rate for this detector is a relatively straightforward exercise resulting in

$$P_e(\text{noncoherent}) = \frac{1}{2}\exp\left(-\frac{E}{2N_0}\right)$$

As before, note that the error rate for the noncoherent receiver is simply a function of the SNR.

15.9.2 Rayleigh Channel

As an important generalization of the described random phase channel, many communication systems are designed under the assumption that the channel introduces both a random amplitude and a random phase on the signal. Specifically, if the original signal sets are of the form $s_i(t) = m_i(t)\cos(2\pi f_c t)$ where $m_i(t)$ is the baseband version of the message (i.e., what distinguishes one signal from another), then the so-called *Rayleigh channel* introduces random distortion in the received signal of the following form:

$$s_i(t) = Am_i(t)\cos(2\pi f_c t + \nu)$$

where the amplitude A is a Rayleigh random variable* and where the random phase ν is uniformly distributed between zero and 2π.

* The density of a Rayleigh random variable is given by $p_A(a) = a/\sigma^2 \exp(-a^2/2\sigma^2)$ for $a \geq 0$.

To determine the optimal receiver under this distortion, we must first construct an alternate statistical model for $s_i(t)$. To begin, it can be shown from the theory of random variables [4] that if X_I and X_Q are statistically independent, zero mean, Gaussian random variables with variance given by σ^2, then

$$Am_i(t)\cos(2\pi f_c t + \nu) = m_i(t)X_I \cos(2\pi f_c t) + m_i(t)X_Q \sin(2\pi f_c t)$$

Equality here is to be interpreted as implying that both A and ν will be the appropriate random variables. From this, we deduce that the combined uncertainty in the amplitude and phase of the signal is incorporated into the Gaussian random variables X_I and X_Q. The in-phase and quadrature components of the signal $s_i(t)$ are given by $s_{Ii}(t) = m_i(t)\cos(2\pi f_c t)$ and $s_{Qi}(t) = m_i(t)\sin(2\pi f_c t)$, respectively. By appealing to Equation 15.11, it can be shown that the optimum receiver selects the largest from

$$\xi_i[R(t)] = \frac{\pi_i}{1 + \frac{2E_i}{N_0}\sigma^2} \exp\left[\frac{\sigma^2}{\frac{1}{2} + \frac{E_i}{N_0}\sigma^2}\left(\left\langle R(t), s_{Ii}(t)\right\rangle^2 + \left\langle R(t), s_{Qi}(t)\right\rangle^2\right)\right]$$

where the inner product

$$\left\langle R(t), S_i(t)\right\rangle = \int_0^T R(t)s_i(t)\mathrm{d}t$$

Further, if we impose the conditions that the signals be equally likely with equal energy over the symbol interval, then optimum receiver selects the largest amongst

$$\xi_i[R(t)] = \sqrt{\left\langle R(t), s_{I_i}(t)\right\rangle^2 + \left\langle R(t), s_{Q_i}(t)\right\rangle^2}$$

Thus, much like for the random phase channel, the optimum receiver for the Rayleigh channel computes the projection of the received waveform onto the in-phase and quadrature components of the hypothetical signals. From a signal space perspective, this is akin to computing the length of the received vector in the subspace spanned by the hypothetical signal. The optimum receiver then chooses the largest amongst these lengths.

As with the random phase channel, computing the performance is a straightforward task resulting in (for the equally likely, equal energy case)

$$P_e(\text{Rayleigh}) = \frac{\frac{1}{2}}{\left(1 + \frac{E\sigma^2}{N_0}\right)}$$

Interestingly, in this case the performance depends not only on the SNR, but also on the variance (spread) of the Rayleigh amplitude A. Thus, if the amplitude spread is large, we expect to often experience what is known as deep fades in the amplitude of the received waveform and as such expect a commensurate loss in performance.

15.10 Dispersive Channels

The *dispersive channel* model assumes that the channel not only introduces AWGN but also distorts the signal through a filtering process. This model incorporates physical realities such as multipath effects and frequency selective fading. In particular, the standard model adopted is depicted in the block diagram given in Figure 15.7. As can be seen, the receiver observes a filtered version of the signal plus AWGN. If the impulse response of the channel is known, then we arrive at the optimum receiver design by applying the previously presented theory. Unfortunately, the duration of the filtered signal can be a complicating factor. More often than not, the channel will increase the duration of the transmitted signals, hence, leading to the description, dispersive channel.

However, if the designers take this into account by shortening the duration of $s_i(t)$ so that the duration of $s_i^*(t)$ is less than T, then the optimum receiver chooses the largest amongst

$$\xi_i(R(t)) = \frac{N_0}{2}\ln\pi_i + \left\langle R(t), s_i^*(t)\right\rangle - \frac{1}{2}E_i^*$$

If we limit our consideration to equally likely binary signal sets, then the minimum P_e matches the received waveform to the filtered versions of the signal waveforms. The resulting error rate is given by

$$P_e(\text{dispersive}) = Q\left(\frac{\left\|\boldsymbol{s}_0^* - \boldsymbol{s}_0^*\right\|}{\sqrt{2\boldsymbol{N}_0}}\right)$$

Thus, in this case the minimum P_e is a function of the separation of the filtered version of the signals in the signal space.

The problem becomes substantially more complex if we cannot ensure that the filtered signal durations are less than the symbol lengths. In this case we experience what is known as intersymbol *interference* (ISI). That is, observations over one symbol interval contain not only the symbol information of interest but also information from previous symbols. In this case we must appeal to optimum sequence estimation [5] to take full advantage of the information in the waveform. The basis for this procedure is the maximization of the joint likelihood function conditioned on the sequence of symbols. This procedure not only defines the structure of the optimum receiver under ISI but also is critical in the decoding of convolutional codes and coded modulation. Alternate adaptive techniques to solve this problem involve the use of channel equalization.

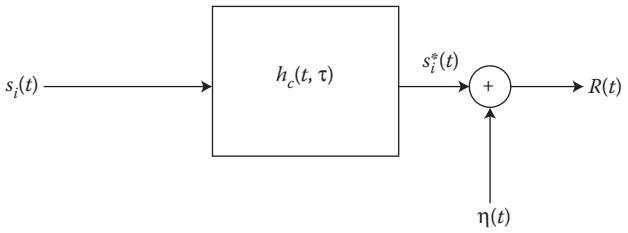

FIGURE 15.7 Standard model for dispersive channel. The time-varying impulse response of the channel is denoted by $h_c(t, \tau)$.

References

1. Gibson, J. D., *Principles of Digital and Analog Communications*, 2nd ed. New York: MacMillan. 1993.
2. Haykin, S., *Communication Systems*, 3rd ed. New York: John Wiley & Sons. 1994.
3. Lee, E. A. and Messerschmitt, D. G., *Digital Communication*. Norwell, MA: Kluwer Academic Publishers. 1988.
4. Papoulis, A., *Probability, Random Variables, and Stochastic Processes*, 3rd ed. New York: McGraw-Hill. 1991.
5. Poor, H. V., *An Introduction to Signal Detection and Estimation*. New York: Springer-Verlag. 1988.
6. Proakis, J. G., *Digital Communications*, 2nd ed. New York: McGraw-Hill. 1989.
7. Shiryayev, A. N., *Probability*. New York: Springer-Verlag. 1984.
8. Sklar, B., *Digital Communications, Fundamentals and Applications*. Englewood Cliffs, NJ: Prentice Hall. 1988.
9. Van Trees, H. L., *Detection, Estimation, and Modulation Theory, Part I*. New York: John Wiley & Sons. 1968.
10. Wong, E. and Hajek, B., *Stochastic Processes in Engineering Systems*. New York: Springer-Verlag. 1985.
11. Wozencraft, J. M. and Jacobs, I., *Principles of Communication Engineering* (Reissue), Prospect Heights, Illinois: Waveland Press. 1990.
12. Ziemer, R. E. and Peterson, R. L., *Introduction to Digital Communication*, New York: Macmillan. 1992.

Further Reading

The fundamentals of receiver design were put in place by Wozencraft and Jacobs in their seminal book. Since that time, there have been many outstanding textbooks in this area. For a sampling see [1,2,3,8,12]. For a complete treatment on the use and application of detection theory in communications see [5,9]. For deeper insights into the Karhunen–Loève expansion and its use in communications and signal processing see [10].

16

MIMO Systems for Diversity and Interference Mitigation

Marco Chiani

16.1 Advantages of Multiple Antennas Systems

Systems with multiple antennas (see Figure 16.1) can exploit, besides the usual time and frequency, the spatial dimension, with large improvements in terms of diversity, interference mitigation, and throughput. For this reason, they are among the key technologies in modern wireless transmission systems [1–7]. Even in wired systems (such as in digital subscriber line (DSL) and in power line communication (PLC) systems), since cables usually contain multiple wires, the channel can be seen as a multiple-input multiple-output (MIMO). In the following, we will focus on MIMO wireless systems, but several of the described techniques can also be applied in wired systems.

The advantages of multiple antennas can be summarized as follows:

- Array gain

This is the increase in the average signal-to-noise ratio (SNR) at the receiver due to coherent combination of signals. It can be obtained for both multiple transmit or multiple receive antennas, requiring channel state information at the transmitter (CSIT) or channel state information at the receiver (CSIR), respectively.

We define the array gain as

$$\frac{\mathbb{E}\left\{\mathrm{SNR}_{\mathrm{out}}\right\}}{\mathbb{E}\left\{\mathrm{SNR}_{SISO}\right\}}$$

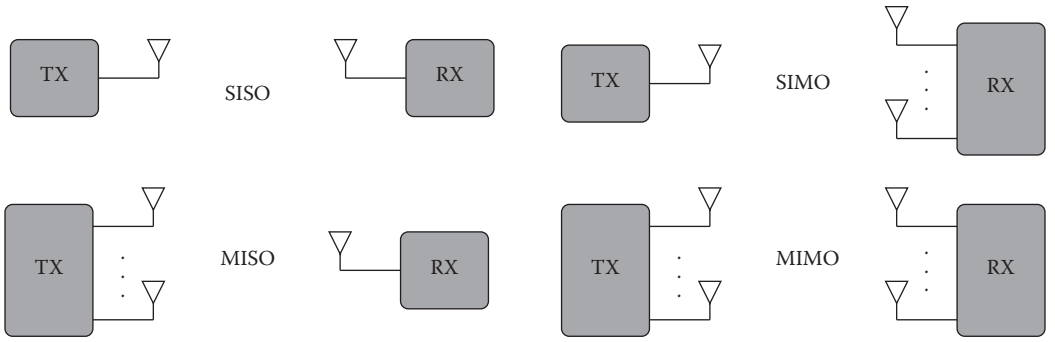

FIGURE 16.1 Multiple antenna systems: single-input single-output (SISO), single-input multiple-output (SIMO), multiple-input single-output (MISO), and multiple-input multiple-output (MIMO).

where $\mathrm{SNR}_{\mathrm{out}}$ and SNR_{SISO} are the output SNR of the multiple antenna system and of the SISO system, respectively, and the average $\mathbb{E}\{\cdot\}$ is taken with respect to fading (see following sections).

- Diversity gain

In the presence of fading, the received power level can present large variations. Diversity is used to reduce the variations of the SNR level due to fading, by sending each information symbol through different channels with independent fading levels, and then combining the outputs. In a $N_T \times N_R$ MIMO channel, there are potentially $N_T \cdot N_R$ links. Spatial diversity can be obtained with multiple receiving antennas with CSIR (receive diversity), and with multiple transmit antennas (transmit diversity). Transmit diversity is possible both with CSIT (beamforming) and even in the absence of CSIT (Alamouti's code, space–time codes).

We can consider, as an indicator of the diversity order, the reduction of SNR variance:

$$\mathrm{var}\left\{\frac{\mathrm{SNR}_{SISO}}{\mathbb{E}\{\mathrm{SNR}_{SISO}\}}\right\} \Big/ \mathrm{var}\left\{\frac{\mathrm{SNR}_{\mathrm{out}}}{\mathbb{E}\{\mathrm{SNR}_{\mathrm{out}}\}}\right\}$$

- Interference mitigation

Multiple antennas can be used as a spatial filter to reduce the power received from cochannel interfering sources. The enhanced robustness to cochannel interference increases the number of served users per unit area in wireless cellular systems.

- Multipath multiplexing (spatial multiplexing) for high-throughput transmission

In MIMO channels with multipath, it is possible to transmit up to $N_{\min} = \min\{N_T, N_R\}$ "parallel" streams over the same band, with an increase of the link throughput. Multipath multiplexing, also called spatial multiplexing, is not possible for SIMO or MISO channels.

In this chapter, we describe systems with multiple antennas for diversity and interference mitigation. High-throughput MIMO systems are described in Chapter 17.

We start with the single-user scenario, and, for the sake of clarity, we focus on frequency-flat fading channels. The extension to wideband channel models is easy by assuming multicarrier transmission techniques, where the channel is frequency-flat for each subcarrier.

Throughout the chapter, vectors and matrices are indicated by bold, det **A** denotes the determinant of the matrix **A**, and $a_{i,j}$ is the (i,j)th element of **A**. The expectation operator is denoted by $\mathbb{E}\{\cdot\}$, the superscript $()^H$ denotes conjugation and transposition, **I** is the identity matrix, and tr{**A**} is the trace of **A**.

16.2 SISO Systems

16.2.1 System Model

Assume slowly varying frequency-flat wireless channels with additive white Gaussian noise (AWGN). For the SISO channel, this means that the discrete-time equivalent lowpass model (Figure 16.2) at time $k \in \mathbb{Z}$ is

$$y(k) = h\,x(k) + n(k) \tag{16.1}$$

where $y(k) \in \mathbb{C}$ are the received samples, $x(k) \in \mathbb{C}$ are the transmitted symbols (e.g., belonging to M-ary quadrature amplitude modulation (M-QAM) or phase shift keying (PSK) constellations), $n(k) \sim \mathcal{CN}(0,\sigma^2)$ are the noise samples, assumed independent, identically distributed (i.i.d.) circularly symmetric complex Gaussian (CSCG) random variables (r.v.s) with* $\mathbb{E}\left\{|\, n(k)\,|^2\right\} = \sigma^2$. The channel gain $h \in \mathbb{C}$ is assumed constant over several symbols. Note that multiplication of the symbols $x(k)$ by a complex gain h means that the constellation is scaled by $|h|$ and rotated of an angle $\varphi = \arg h$.

The SNR conditional to h is†

$$\mathrm{SNR} = \frac{\mathbb{E}\left\{|\, x(k)\,|^2\right\}}{\mathbb{E}\left\{|\, n(k)\,|^2\right\}}\,|\,h\,|^2 = \frac{P_t}{\sigma^2}\,|\,h\,|^2 \tag{16.2}$$

where P_t is the average transmitted power, and the Shannon capacity is

$$C(h) = \log_2\left(1 + \frac{P_t}{\sigma^2}\,|\,h\,|^2\right) \quad [\text{info bits/s/Hz}] \tag{16.3}$$

achieved when the symbols $x(k)$ are i.i.d. CSCG. A different formula would hold when the symbols $x(k)$ are constrained to belong to a specific constellation.

For ease of notation in the following we will drop, when possible, the time index k.

16.2.2 Fading, Ergodic Capacity, Outage Capacity

Assume now a fading channel, where h varies in time. In the so-called block fading channel (BFC) model, the channel h remains constant over a block of several symbols, taking i.i.d. values across different blocks. Thus, the fading process is specified by the block length (characterizing the time-correlation of the fading process) and by the distribution of the fading level within a block (e.g., h is a CSCG r.v. for

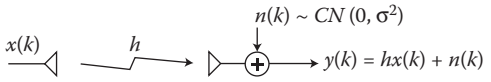

FIGURE 16.2 Discrete-time equivalent lowpass representation of SISO.

* Note that circular symmetry implies zero mean, so $\mathbb{E}\left\{n(k)\right\} = 0$.

† This SNR can be shown to be the ratio between the received energy per symbol and N_0, conditional to a channel gain h, where N_0 is the one-sided noise spectral density.

a Rayleigh fading channel). In the following, we indicate with $h(m)$ the fading level for the mth block.* The discrete-time process $\cdots, h(1), h(2), \cdots$ is ergodic (time averages equal ensemble averages) if the block duration is finite, and nonergodic if a realization is composed of just one block, that is, one fading level, lasting forever (in practice, for the duration of the communication).

In Figure 16.3, we report a realization $|h(m)|^2 P_t/\sigma^2$ for $m = 0, \ldots, 50$ of a Rayleigh BFC (dashed curves). We set $P_t/\sigma^2 = 10$, the channel gain has been normalized to give $\mathbb{E}\{|h(m)|^2\} = 1$, giving the average signal-to-noise ratio $\mathbb{E}\{\mathrm{SNR}(m)\} = P_t/\sigma^2$. We observe that, due to Rayleigh fading, there are large fluctuations of the SNR values with m. The variations normalized to the average of the SNR are reported on the right plot. In the same figure, we show a realization of the SNR at the output of a SIMO system with $N_R = 8$ antennas and maximal ratio combiner (MRC) receive diversity described in Section 16.4.1. We observe two effects of MRC: first, the average SNR is increased by a factor 8; second, the normalized SNR fluctuations are less severe. The first effect is called "array gain" (improvement in the average SNR). The second is called "diversity gain" (reduced variance of the normalized SNR as reported on the right plot).

The variation of the SNR in time produces a variation of the link quality (throughput, error rate, delay, etc.). For example, we show in Figure 16.4 an example of $C(h(m))$ from Equation 16.3 for a realization of the time-discrete process $h(m)$. Hereafter, we refer to Equation 16.3 as mutual information, since the concept of capacity requires some care (below). In the same figure, we report the capacity of the unfaded AWGN channel, $\log_2(1 + \mathrm{SNR})$, and the average $\mathbb{E}\{C(h(m))\}$ where the average is taken with respect to the distribution of $h(m)$. The difference between the unfaded capacity and $\mathbb{E}\{C(h(m))\}$ is relatively small (3.46 and 2.91 [bits/s/Hz], respectively). However, $C(h(m))$ shows large fluctuations around its average.

Recalling that the capacity is the maximum information rate that can be sent reliably across a noisy channel by using forward error correction (FEC) with sufficiently long codewords, we can distinguish two situations: the case where the codeword length is large with respect to a block (that we indicate as fast fading, or system with ideal time interleaving), and the case where the block duration is larger than the codeword length (slow fading, or system with no interleaving).

In this regard, $\mathbb{E}\{C(h)\}$ is called *ergodic capacity* with channel unknown at the transmitter, and represents the information rate that a system with constant transmit power can achieve by using FEC when

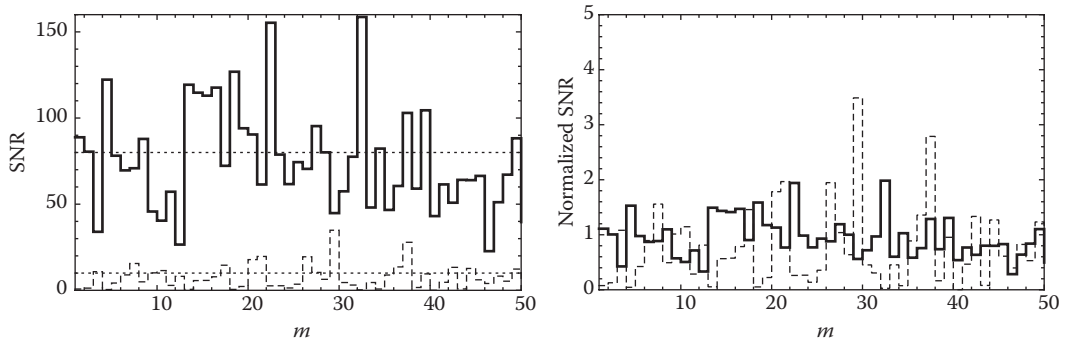

FIGURE 16.3 Example of behavior of the signal-to-noise ratio (left) and of the normalized output SNR defined as $\mathrm{SNR}_{\mathrm{out}}/\mathbb{E}\{\mathrm{SNR}_{\mathrm{out}}\}$ (right) for a system without diversity (dashed curves) and with diversity and array gain (solid curves). Rayleigh BFC model, m is the block index, average SNR per antenna equal to 10. Note that each block can consist of several thousands symbols. Red curve: SISO. Blue curve: SIMO MRC with $N_R = 8$. The dotted curves on the left represent the average SNR. With MRC we have both an array gain (increase in the average SNR from 10 to 80) and diversity gain (a reduced variance of the normalized SNR as reported on the right).

* The block index m should not to be confused with the time index k. The two are coincident only when the block length is one symbol.

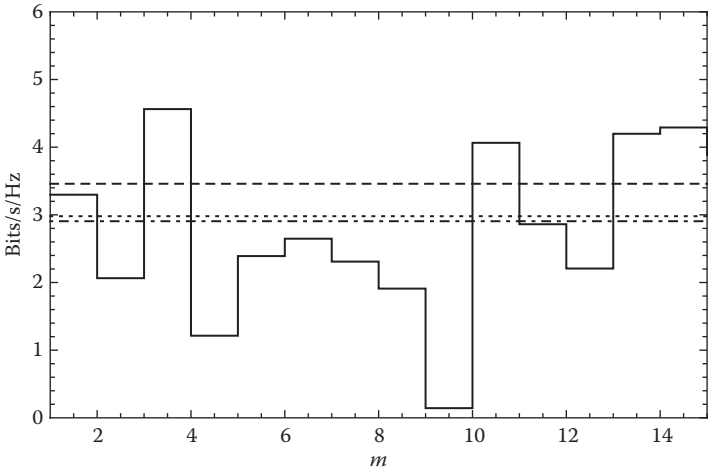

FIGURE 16.4 Example of behavior of $C(h(m))$ for the channel $h(m)$, Rayleigh BFC model, average SNR equal to 10 dB, m is the block index. Note that each block can consist of several thousands symbols. Solid curve (3.46 [bits/s/Hz]): mutual information (16.3). Dashed curve: capacity for the unfaded AWGN. Dot-dashed curve (2.91 [bits/s/Hz]): mean value of Equation 16.3 with respect to the distribution of h (ergodic capacity with channel unknown at the transmitter). Dotted curve (2.98 [bits/s/Hz]): ergodic capacity with channel known at the transmitter, power, and rate time-adaptive system.

each codeword spans many fading blocks, that is, with *ideal time interleaving*. In this case, the fluctuations of the channel are somewhat averaged out by time interleaving.

When the codeword length is of the order of the fading block (slow fading), and assuming the information rate R (information bits/s/Hz) at the channel input is constant, the mutual information (16.3) will be for some blocks smaller than R, and for some larger than R. From information theory we know that the codewords in the former case will not be correctly decoded,* while for the latter the codewords will be successfully decoded, provided a sufficiently powerful FEC coding scheme is adopted. We can therefore define the channel outage probability as follows:

$$P_{\text{out}}(R) = \Pr\{C(h) < R\} \tag{16.4}$$

which represents a lower bound on the codeword error rate for coded systems with information rate R at the input of a slow-fading channel without interleaving. We can also define the *outage capacity* at codeword error rate P_{target} as the value R_{out} to use at the channel input to guarantee a target outage probability P_{target}

$$R_{\text{out}}(P_{\text{target}}) = P_{\text{out}}^{-1}(P_{\text{target}}) \tag{16.5}$$

and the resulting effective rate is $R_{\text{out}}\,(1 - P_{\text{out}}(R_{\text{out}}))$ (correctly received [information bits/s/Hz] over many fading blocks). This is sometimes called *outage rate*.

Assume now that the channel state $h(m)$ is available at the transmitter side, a situation indicated as CSIT. In this case, a possibility, for the slow-fading channel case, is to change the information rate $R(m)$ (information bits/s/Hz) for each block m, adapting its value below $C(h(m))$, so that the received codeword can be successfully decoded. The information rate is adapted by changing the FEC code rate and

* Recall that, for rates above capacity, the error probability goes exponentially to 1.

modulation format. In practice, a predefined set of couples (codes, modulation format) can be used to discretize the information rate. The transmitter then chooses the couple based on $C(h(m))$. Over a large number N of blocks the transferred rate achievable is bounded by $1/N \sum_{m=1}^{N} C(h(m))$ which, for the law of large numbers, converges to $\mathbb{E}\{C(h)\}$. Thus, $\mathbb{E}\{C(h)\}$ is also the achievable rate for a *rate time-adaptive* system.

Still assuming CSIT, if we can also adapt the transmit power on a block-by-block bases, we could spend, for a given time-average power, more energy on the blocks with better SNR, and less on those with lower SNR, according to the water-filling principle. This *power and rate time-adaptive* system has a slightly larger achievable rate than the *rate time-adaptive* system, but with some additional practical issues due to the power variation with time.

For both *rate time-adaptive* and *power and rate time-adaptive* techniques, the information rate (i.e., number of information bits per block) change from block to block. For delay-sensitive applications this can be a problem, and constant rate solutions are preferable. For example, the transmit power can be varied to maintain a constant SNR at the receiver, and consequently a constant rate (like power control in cellular systems, also called channel inversion).

These considerations will be extended to MIMO channels in Chapter 17.

16.3 MIMO Channel Models

We here summarize some characteristics of MIMO channels [7–9]. Assuming a frequency-flat channel, matched filtering, and sampling with proper timing, the discrete-time equivalent lowpass model at time $k \in \mathbb{Z}$ for MIMO channels is

$$\mathbf{y}(k) = \mathbf{H}\mathbf{x}(k) + \mathbf{n}(k) \tag{16.6}$$

where $\mathbf{x}(k) = [x_1(k) \cdots x_{N_T}(k)]^T$, $x_j(k)$ is the symbol transmitted at sample time k from the jth transmit antenna, the vector $\mathbf{y}(k) = [y_1(k) \cdots y_{N_R}(k)]^T$ is the vector of the samples at the output of the N_R antennas, and $\mathbf{n}(k) = [n_1(k) \cdots n_{N_R}(k)]^T$ is a vector of noise samples, assumed i.i.d. CSCG r.v.s. The channel matrix $\mathbf{H} \in \mathbb{C}^{N_T \times N_R}$ has entries $h_{i,j}$ representing the complex gain from the jth transmit antenna to the ith receive antenna.

Important characteristics of the channel model (16.6) are the rank of the channel matrix* $\mathbf{H}$ (for a specific matrix) or the correlation among its elements (for statistical models). We will analyze below some specific situations.

16.3.1 MIMO Line-of-Sight Channel

Let us assume the transmission of a passband signal $\tilde{s}(t) = \Re\{s(t)e^{j2\pi f_0 t}\}$, where f_0 is the carrier frequency and $s(t)$ is the equivalent lowpass of $\tilde{s}(t)$. We assume that the signaling interval is T, which means that the variation rate of $s(t)$ is approximately $1/T$. A delay τ on the passband signal introduces a delay and a phase variation on the equivalent lowpass, since $\tilde{s}(t-\tau) = \Re\{s(t-\tau)e^{-j2\pi f_0 \tau} e^{j2\pi f_0 t}\}$.

The MIMO channel with line-of-sight (LOS) propagation is depicted in Figure 16.5. We indicate as $d_{i,j}$ and $\tau_{i,j}$ the path length and delay associated with the path from the jth transmit antenna to the ith receive antenna, respectively. We also indicate with $h_{i,j} = |h_{i,j}| e^{-j2\pi f_0 \tau_{i,j}}$ the complex channel gain whose modulus is related to the path loss and antenna gains, and whose argument is related to the path delay. The equivalent lowpass of the signal at the output of the ith receive antenna is therefore

* Note that the rank of $\mathbf{H}$ is always limited by the minimum between N_T and N_R.

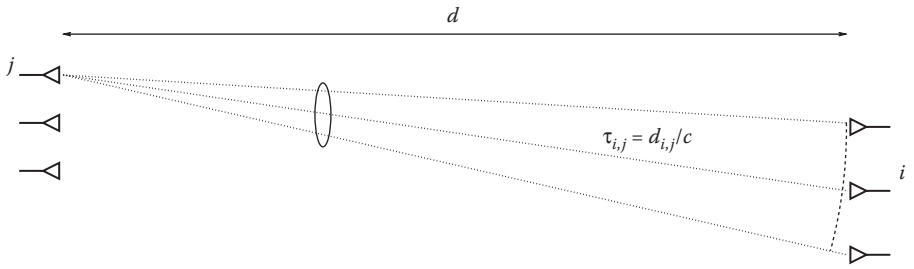

FIGURE 16.5 Geometry for a MIMO line of sight. The delay for the generic path is $\tau_{i,j} = d_{i,j}/c$, where $d_{i,j}$ is the path length and c is the light speed.

$$y_i(t) = \sum_j h_{i,j}\, s_j(t - \tau_{i,j}) + n_i(t) \tag{16.7}$$

where $n_i(t)$ is the thermal noise. Although the path lengths $d_{i,j}$ are, strictly speaking, different, if the distance d between the transmitter and the receiver is much greater than the antenna elements spacing, the difference among them is negligible and we can write $\tau_{i,j} \simeq \tau, |\, h_{i,j}\,| \simeq |\, h\,|$. Therefore, in the above hypotheses, we can write

$$y_i(t) = \sum_j h_{i,j}\, s_j(t - \tau) + n_i(t) \tag{16.8}$$

where the $h_{i,j} \simeq |\, h\,|\, e^{-j2\pi f_0 \tau}$ are all equal. Assuming matched filtering and sampling with proper timing, the discrete-time equivalent lowpass model at time $k \in \mathbb{Z}$ is therefore given by Equation 16.6 where the channel matrix $\mathbf{H} \in \mathbb{C}^{N_T \times N_R}$ has entries $h_{i,j}$ which are practically identical, and has therefore rank 1. Thus, for MIMO LOS channels with link length d large compared to the antenna elements spacing, the channel model is given in Equation 16.6 where the matrix $\mathbf{H}$ can be considered rank 1.

16.3.2 MIMO with a Point Scatterer

Consider now the situation in Figure 16.6, where the emitted radiation is scattered by a single point scatter. We assume that all delay differences are small compared to the signaling interval T. Thus, the channel model is still of the form (16.6) but with a channel matrix $\mathbf{H} = \mathbf{h}_{(S \to RX)} \mathbf{h}^T_{(TX \to S)}$, where $\mathbf{h}_{(TX \to S)}$ is the $N_T \times 1$ propagation vector from the transmitter to the scatterer, and $\mathbf{h}_{(S \to RX)}$ is the $N_R \times 1$ propagation vector from the scatterer to the receiver. These two vectors can be expressed precisely from the geometry depicted in Figure 16.6. From basic algebra, we know that, since $\mathbf{H}$ is the product of two vectors, it is rank 1. Thus, with one point scatterer, the channel matrix $\mathbf{H}$ in Equation 16.6 is rank 1.

16.3.3 MIMO with Multiple Scatterers

Assume now several point scatterers with delay differences which are small compared to the signaling interval T. Then, by the previous argument, the channel model is still of the form (16.6) with a channel matrix

$$\mathbf{H} = \sum_k \mathbf{h}_{(S_k \to RX)} \mathbf{h}^T_{(TX \to S_k)} \tag{16.9}$$

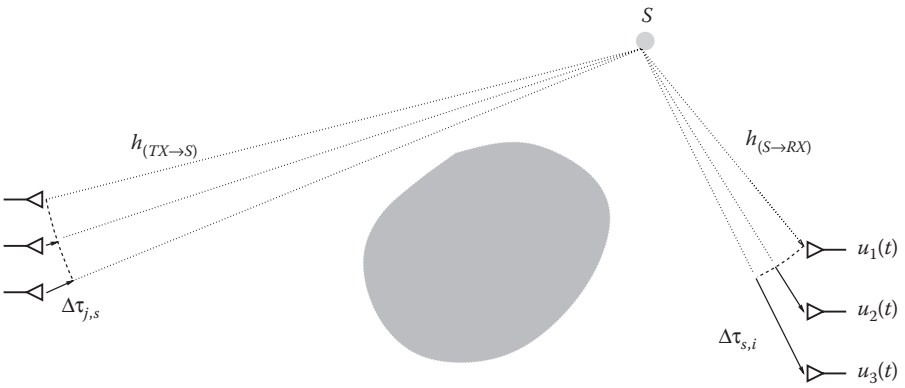

FIGURE 16.6 Geometry for propagation with a single point scatterer.

where $\mathbf{h}_{(TX\to S_k)}$, $\mathbf{h}_{(S_k\to RX)}$ are the $N_T \times 1$ and $N_R \times 1$ propagation vectors for kth scatterer. From basic algebra, we thus obtain that the rank of $\mathbf{H}$ is at most equal to the number of scatterers (scatterers with the same direction of departure or of arrival will not increase the channel matrix rank). For a very large number of scatterers, the sum in Equation 16.9 can be thought of as an integral.

16.3.4 Statistical MIMO Channel Models

Consider now the ensemble of all possible channel matrices $\mathbf{H}$, when the relative positions of the scatterers are subject to small random variations, due, for example, to movement of the transmitter, of the receiver, or of the environment. In this case the evolution of $\mathbf{H}$ with k is described by a discrete-time random process, where the elements of the channel matrix are randomly varying. The rate of variation of $\mathbf{H}$ depends on the rate of variation of the environment, that is, on the mobility of transmitter, receiver, and scatterers. The channel $\mathbf{H}$ at a given time k can be considered a random matrix, that is, a matrix with elements that are random variables, and a realization of it can be interpreted as the channel for a specific snapshot of the varying environment [10].

Let us consider a stationary channel, so that the first-order description of $\mathbf{H}(k)$ does not depend on k. If we assume that the randomly placed scatterers introduce delay differences which are small compared to the signaling interval T, the system model is still given by Equation 16.6, where $\mathbf{H}$ has elements $h_{i,j}$ described as random variables. When the number of independent scatterers is large, from the central limit theorem, the elements $h_{i,j}$ are complex Gaussian r.v.s, and their joint distribution can be given by specifying all mean values, $\mathbb{E}\{\mathbf{H}\}$, and all pairs correlation, that is, the matrix $\mathbb{E}\{\text{vec}(\mathbf{H})\text{vec}(\mathbf{H})^H\}$, where vec($\mathbf{H}$) is the $(N_T \cdot N_R) \times 1$ vector obtained by stacking the columns of $\mathbf{H}$ on top of one another.

Often, the correlation at the transmitter side (i.e., among the elements of a row of $\mathbf{H}$) is the same for all rows, and the correlation at the receiver side (i.e., among the elements of a column of $\mathbf{H}$) is the same for all columns. In this case, the correlation matrix can be factorized as $\mathbb{E}\{\text{vec}(\mathbf{H})\text{vec}(\mathbf{H})^H\} = \mathbf{R}_T \otimes \mathbf{R}_R$, where $\otimes$ denotes Kronecker product, and $\mathbf{R}_T$ and $\mathbf{R}_R$ describe the correlation at the transmitter and receiver side, respectively. This Kronecker model implies that the correlation at the receiver (transmitter) does not affect the spatial properties of the signals at the transmitter (receiver).

The spatial correlation is in general related to the angular distribution of the rays and the antenna elements spacing. Roughly speaking, many scatterers around the receiver (transmitter) give low correlation at the receiver (transmitter) side, while if all paths at one side arrive from a small angle, the correlation on that side is large, implying an overall rank-deficient channel.

For rich scattering environments with no dominant paths, one common model consists in assuming the elements $h_{i,j}$ as CSCG, implying $\mathbb{E}\{\mathbf{H}\} = 0$ (Rayleigh MIMO channels). Generally, if the spread of the

angles of departure and of arrival are large,* the correlation is also small and the $h_{i,j}$ can be considered i.i.d. This is the Rayleigh uncorrelated MIMO channel model.

16.4 Diversity Techniques

16.4.1 Receive Diversity: SIMO with CSIR (MRC)

Consider the SIMO scheme in Figure 16.7. The N_R-dimensional signal at the output of the receiving antennas at time k can be written as

$$\mathbf{y}(k) = \mathbf{h}x(k) + \mathbf{n}(k) \tag{16.10}$$

where $\mathbf{h} \in \mathbb{C}^{N_R}$ is a vector containing the complex gains between the transmit antenna and the N_R receive antenna, $x(k) \in \mathbb{C}$ is the transmitted symbol at time k, $\mathbf{n}(k) \in \mathbb{C}^{N_R}$ is the noise vector at time k with i.i.d. CSCG entries and covariance matrix $\mathbf{R}_n = \mathbb{E}\left\{\mathbf{n}(k)\mathbf{n}^H(k)\right\} = \sigma^2\mathbf{I}$.

Here, conditionally to $\mathbf{h}x(k)$, the vector $\mathbf{y}(k)$ is Gaussian, and the best linear estimate of the transmitted symbol is†

$$\hat{x}(k) = \frac{\mathbf{h}^H\mathbf{y}(k)}{\mathbf{h}^H\mathbf{h}} = \mathbf{w}^H\mathbf{y}(k) \tag{16.11}$$

with weights

$$\mathbf{w} = \frac{\mathbf{h}}{\|\mathbf{h}\|^2} \tag{16.12}$$

Note that Equation 16.12 requires that the channel gains (amplitude and phase) are known at the receiver. So, for each antenna element, we need a channel estimator (e.g., based on pilot symbols periodically embedded in the data symbols). Linear combining of the received signals with weights of the type $\mathbf{w} = K\mathbf{h}$, as in Equation 16.12, with K an arbitrary constant, is called Maximal Ratio Combiner (MRC).‡ The SNR at the combiner output is

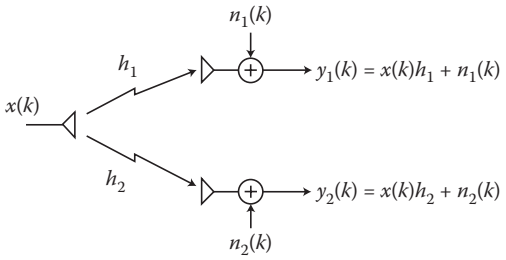

FIGURE 16.7 Discrete-time equivalent lowpass representation of a 1×2 SIMO.

* This condition in some particular cases is not sufficient. An example is the so-called keyhole channel, where, despite scattering, all paths are forced to pass through an intermediate point like in Figure 16.6; thus, as in Section 16.3.2, the overall channel matrix is rank 1 since it can be expressed as the product of two vectors.

† This estimate produces a sufficient statistic for the detection of the transmitted symbol and, as we will see later, is capacity-optimal.

‡ It is easy to show that weights in the form $\mathbf{w} = K\mathbf{h}$ give the maximum SNR after the combiner.

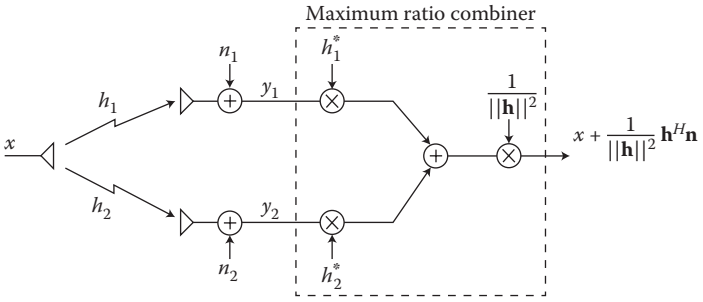

FIGURE 16.8 Implementation of MRC (time is dropped for ease of notation).

$$\mathrm{SNR}_{\mathrm{out}} = \frac{\mathbb{E}\left\{|\, x(k)\,|^2\right\}}{\sigma^2} \,||\, \mathbf{h}\,||^2 = \frac{P_t}{\sigma^2} \,||\, \mathbf{h}\,||^2 \tag{16.13}$$

where P_t is the average transmitted power. It is easy to verify that, when the h_i are i.i.d., the array gain is N_R and the diversity order is also N_R.

The implementation of MRC is sketched in Figure 16.8.

16.4.1.1 Optimality of MRC

For a given **h**, with MRC we have turned the SIMO into a SISO channel with capacity

$$C(\mathbf{h}) = \log_2\left(1 + \frac{P_t}{\sigma^2} \,||\, \mathbf{h}\,||^2\right) \quad [\text{info bits/s/Hz}] \tag{16.14}$$

This is also the capacity of the original SIMO (see Chapter 17); therefore, we can say that MRC is *capacity-optimal for SIMO channels* with perfect CSIR.

16.4.1.2 MRC in Fading Channels

Up to now we assumed a given channel **h**. Let us now assume slowly varying multipath propagation. Then, if for a time window of, let us say, a thousand symbols, there is a given **h**, for another window, due to the different combination of multipaths, there could be a different **h**. In other words, we assume to have a BFC, where the channel is constant for several symbols (a block), and varies from a block to another. So, if we focus on what happens to a block, we need to describe the first-order statistical variations of the channel, and consider **h** as a random vector with a given distribution.

For example, for the Rayleigh channel model, the elements of the vector **h** are CSCG. If the fading levels are uncorrelated from antenna to antenna, these elements are i.i.d., and the random variable $||\,\mathbf{h}\,||^2 = |\,h_1\,|^2 + \cdots + |\,h_{N_R}\,|^2 = h_{1,I}^2 + h_{1,Q}^2 + \cdots + h_{N_R,I}^2 + h_{N_R,Q}^2$ is the sum of the modulus square of $2N_R$ real i.i.d. Gaussian r.v.s.

The distribution of the sum of the squares of N i.i.d. zero-mean real Gaussian r.v.s is called central chi-square with N degrees of freedom and indicated as $\mathcal{X}_N^2$. Therefore, the distribution of $||\mathbf{h}||^2$ is related to $\mathcal{X}_{2N_R}^2$. By using this distribution it results that, for Rayleigh fading channels where the fading is uncorrelated from antenna to antenna, the probability density function (p.d.f.) of the output SNR in Equation 16.13 results as

$$f_{\mathrm{SNR}_{\mathrm{out}}}(\gamma) = \frac{1}{\overline{\mathrm{SNR}}^{N_R}} \frac{1}{(N_R - 1)!} \gamma^{N_R - 1} e^{-\gamma/\overline{\mathrm{SNR}}} \quad \gamma \geq 0 \tag{16.15}$$

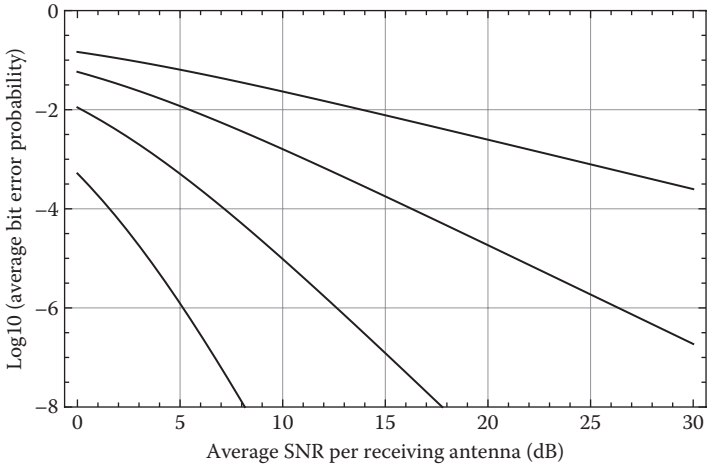

FIGURE 16.9 Performance of $1 \times N_R$ SIMO, MRC (so, with CSIR), Rayleigh fading, $N_R = 1,2,4,8$ antennas, BPSK modulation. The same curves applies to $N_T \times 1$ MISO beamforming (so, with CSIT), with $N_T = 1,2,4,8$, where the abscissa is $\mathbb{E}\left\{| h_i |^2\right\} P_t/\sigma^2$.

where

$$\overline{\text{SNR}} = \frac{P_t}{\sigma^2}\mathbb{E}\left\{| h_i |^2\right\} \tag{16.16}$$

can be interpreted as the average SNR per receiving antenna. This distribution can be used to evaluate the performance of digital modulation and coding schemes. For example, in Figure 16.9, the average bit error probability (BEP) for an uncorrelated Rayleigh fading SIMO channel with MRC, for a system using binary phase shift keying (BPSK) modulation is reported. As can be noticed, over Rayleigh uncorrelated channels, the BEP of uncoded systems with diversity order **div** has, for large SNR, a linear behavior in a log-log plot, with a slope of 10/**div** (dB/decade).

16.4.2 MISO and Diversity with CSIT (Beamforming)

Consider the MISO scheme in Figure 16.10, and assume that the transmitter knows perfectly the channel. The objective is to improve the performance by sending on the transmit antennas a linearly precoded version of the symbol $x(k)$.

The weights α_1, α_2 must be designed to focus the transmitted energy toward the receiver, to produce the maximum SNR at the receive antenna. The power at the ith transmit antenna is $\mathbb{E}\left\{| x(k) |^2\right\} | \alpha_i |^2$,

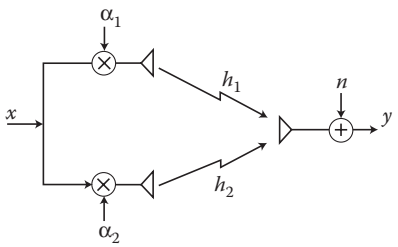

FIGURE 16.10 2×1 MISO beamforming.

and we impose the normalization $\sum_i |\alpha_i|^2 = ||\mathbf{a}||^2 = 1$ to have an average total transmitted power $P_t = \mathbb{E}\{|x(k)|^2\}$ as for the single transmit antenna case.

The received signal is

$$y(k) = (\alpha_1 h_1 + \cdots + \alpha_{N_T} h_{N_T}) x(k) + n(k) \tag{16.17}$$

It is easy to see that the best SNR for $y(k)$ is obtained by choosing $\alpha_i = K h_i^*$, where K is a normalization constant with $|K|^2 \sum_i |h_i|^2 = |K|^2 ||\mathbf{h}||^2 = 1$. Taking $K > 0$ real (the phase of K can be included in the carrier phase), we have

$$y(k) = ||\mathbf{h}|| \, x(k) + n(k) \tag{16.18}$$

The choice $\alpha_i = K h_i^*$ makes the signals at the receive antenna to add coherently, and the resulting SNR at the receiver is

$$\mathrm{SNR}_{bf} = \frac{\mathbb{E}\{|x(k)|^2\}}{\sigma^2} ||\mathbf{h}||^2 = \frac{P_t}{\sigma^2} ||\mathbf{h}||^2 \tag{16.19}$$

which is exactly the same as for the MRC output (16.13).

This scheme can be called beamforming or eigenbeamforming and gives, for MISO with CSIT, exactly the same performance as for a SIMO MRC with CSIR (for the same total power P_t and channel gains h_ℓ). In particular, the array gain is N_T and the diversity order is N_T.

Different from MRC, here *the transmitter* must know the channel (amplitudes and phases for all h_l). The ways to obtain this information are essentially two:

- If the system adopts a time division duplex (TDD) technique, the channel estimated in reception (e.g., by using pilot symbols) can be used, for reciprocity, as an estimate of the channel in transmission (assuming the channel does not vary too fast).
- In closed-loop systems, the receiver estimates the channel and sends the estimates back to the transmitter. This requires a feedback channel, with problems related to delays, quantization, and transmission errors.

16.4.2.1 Optimality of Beamforming for MISO

For a MISO with beamforming, the resulting end-to-end SISO has capacity given again by Equation 16.14, which is also the capacity of the original MISO assuming CSIT. Thus, beamforming is capacity-optimal for MISO with CSIT.

16.4.3 MIMO Beamforming or Eigenbeamforming (Single Beam)

The previous approach can be easily extended to the case when both the TX and the RX are equipped with multiple antenna (Figure 16.11). We call this MIMO beamforming or eigenbeamforming (single beam).

The received vector is

$$\mathbf{y}(k) = \mathbf{H}\mathbf{a}\, x(k) + \mathbf{n}(k) = \tilde{\mathbf{h}} x(k) + \mathbf{n}(k) \tag{16.20}$$

where $\tilde{\mathbf{h}} = \mathbf{H}\mathbf{a}$. Since the last expression looks like Equation 16.10 for SIMO channels, we have that the optimum weights to use in reception are immediately given by the MRC principle as

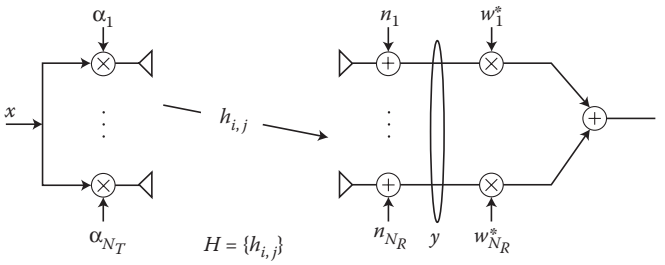

FIGURE 16.11 MIMO beamforming.

$$\mathbf{w} = K\tilde{\mathbf{h}} \tag{16.21}$$

where K is an arbitrary constant and the corresponding SNR is

$$\text{SNR} = \text{SNR}(\alpha) = \frac{\mathbb{E}\left\{|\, x(k)\,|^2\right\}}{\sigma^2} \|\, \tilde{\mathbf{h}}\,\|^2 \tag{16.22}$$

For the weights in transmission, we have to find the vector $\boldsymbol{\alpha}$, with $\|\mathbf{a}\| = 1$, which maximizes Equation 16.22, that is, maximizing $\|\, \tilde{\mathbf{h}}\,\|^2 = \tilde{\mathbf{h}}^H\tilde{\mathbf{h}} = \mathbf{a}^H\mathbf{H}^H\mathbf{H}\mathbf{a}$. Since $\mathbf{H}^H\mathbf{H}$ is Hermitian, we can use the spectral decomposition $\mathbf{H}^H\mathbf{H} = \mathbf{V}\Lambda\mathbf{V}^H$, where the columns of the unitary matrix $\mathbf{V}$ are the eigenvectors of $\mathbf{H}^H\mathbf{H}$, and $\boldsymbol{\Lambda}$ is diagonal with elements on the diagonal that are the eigenvalues of $\mathbf{H}^H\mathbf{H}$. From linear algebra we recall that the vector α maximizing $\boldsymbol{\alpha}^H\mathbf{V}\boldsymbol{\Lambda}\mathbf{V}^H\boldsymbol{\alpha}$ is the eigenvector of $\mathbf{H}^H\mathbf{H}$ corresponding to the largest eigenvalue $\lambda_{\max}$ of $\mathbf{H}^H\mathbf{H}$. In this case, it results as $\boldsymbol{\alpha}^H\mathbf{V}\boldsymbol{\Lambda}\mathbf{V}^H\boldsymbol{\alpha} = \lambda_{\max}$.

Thus, in summary

- The optimum precoding vector $\boldsymbol{\alpha}_{\text{opt}}$ is the eigenvector of $\mathbf{H}^H\mathbf{H}$ corresponding to the largest eigenvalue $\lambda_{\max}$ of $\mathbf{H}^H\mathbf{H}$
- The optimum combining vector is $\mathbf{w} = K\mathbf{H}\boldsymbol{\alpha}_{\text{opt}}$
- The resulting SNR at the output of the MIMO beamforming is

$$\text{SNR}_{\max} = \frac{P_t}{\sigma^2}\lambda_{\max} \tag{16.23}$$

16.4.3.1 Optimality of Beamforming

The capacity of the end-to-end SISO obtained by the original MIMO with beamforming is therefore

$$C(\mathbf{H}) = \log_2\left(1 + \frac{P_t}{\sigma^2}\lambda_{\max}\right) \qquad [\text{info bits/s/Hz}] \tag{16.24}$$

It is interesting to note that, since $\sum_\ell \lambda_\ell = \text{tr}\left\{\mathbf{H}^H\mathbf{H}\right\} = \|\, \mathbf{H}\,\|_F^2$, we have $\lambda_{\max} \le \|\, \mathbf{H}\,\|_F^2$, where the equality is achieved when the channel matrix $\mathbf{H}$ has just one nonzero eigenvalue, that is, when it is rank 1. We will see that, for rank 1 channels, Equation 16.24 is indeed the capacity of the MIMO (see Chapter 17). Therefore, we can say that the scheme in Figure 16.11 is capacity-optimal for MIMO channels with rank 1 and CSIT (and sometimes also in other cases).

16.4.4 MISO and Diversity without CSIT, with CSIR (Alamouti's Scheme, Space–Time Codes)

We have seen that MISO beamforming requires CSIT, but is it possible to have transmit diversity without CSIT? Even looking at the simple 2×1 MISO it is quite clear that, if the TX does not know the channel, it is not possible by using a beamforming-like approach to find weights able to build distinct channels (and thus to provide diversity). However, it has been shown that by using, besides the spatial, the time dimension, it is actually possible to have transmit diversity even without CSIT. We discuss below the Alamouti's scheme for 2×1 MISO.

While in previous schemes we assumed to transmit a symbol $x(k)$ (in a given time symbol T) and our aim was to recover that symbol, the key idea in space–time codes is to use time to build separable channels. So, assume we look at two consecutive symbols, $x(k)$, $x(k+1)$, to be transmitted in two symbol periods. In a first symbol period T, we transmit $x(k)$ on the first antenna and $x(k+1)$ on the second. In the second period, we transmit $x^*(k+1)$ on the first antenna and $-x^*(k)$ on the second, as reported in Figure 16.12. The symbols are "precoded" by a factor $1/\sqrt{2}$ to maintain $P_t = \mathbb{E}\left\{|\, x\,|^2\right\}$.

At the receiver, the two samples received in the two consecutive time instants k, $k+1$ are

$$y(k) = x(k)h_1\frac{1}{\sqrt{2}} + x(k+1)h_2\frac{1}{\sqrt{2}} + n(k)$$
$$y(k+1) = -x^*(k)h_2\frac{1}{\sqrt{2}} + x^*(k+1)h_1\frac{1}{\sqrt{2}} + n(k+1)$$

By conjugating the second equation and defining $\tilde{\mathbf{y}}(k) = (y(k), y^*(k+1))^T$, $\tilde{\mathbf{n}}(k) = (n(k), n^*(k+1))^T$, $\mathbf{x}(k) = (x(k), x(k+1))^T$, we can write

$$\begin{pmatrix} y(k) \\ y^*(k+1) \end{pmatrix} = \frac{1}{\sqrt{2}}\begin{pmatrix} h_1 & h_2 \\ -h_2^* & h_1^* \end{pmatrix}\begin{pmatrix} x(k) \\ x(k+1) \end{pmatrix} + \begin{pmatrix} n(k) \\ n^*(k+1) \end{pmatrix} \tag{16.25}$$

or, in short, $\tilde{\mathbf{y}}(k) = \frac{1}{\sqrt{2}}\mathbf{A}\mathbf{x}(k) + \tilde{\mathbf{n}}(k)$, where

$$\mathbf{A} = \begin{pmatrix} h_1 & h_2 \\ -h_2^* & h_1^* \end{pmatrix} \tag{16.26}$$

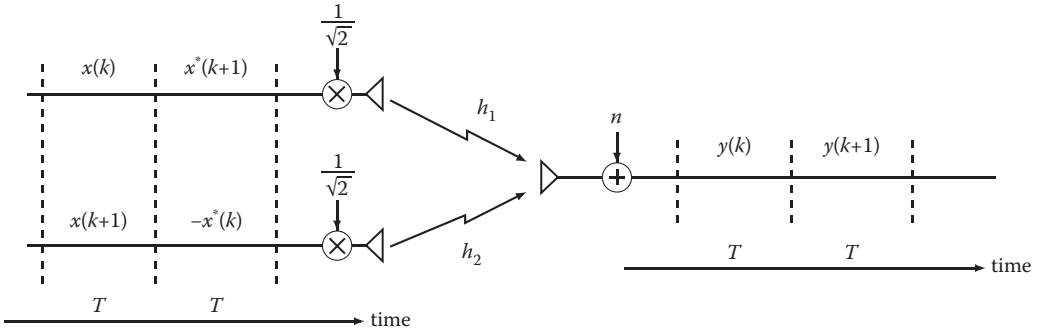

FIGURE 16.12 MISO Alamouti's scheme.

Now, by using time, with this construction we have in Equation 16.25 a virtual 2×2 MIMO. In principle, assuming the receiver knows $\mathbf{h}$ and therefore $\mathbf{A}$ (this means CSIR), the symbols $x(k)$, $x(k+1)$ can be detected by using, for example, maximum likelihood (ML). However, here the situation is even simpler, since we observe that

$$\mathbf{A}^H\mathbf{A} = \begin{pmatrix} h_1^* & -h_2 \\ h_2^* & h_1 \end{pmatrix}\begin{pmatrix} h_1 & h_2 \\ -h_2^* & h_1^* \end{pmatrix} = \| \mathbf{h} \|^2 \, \mathbf{I} \tag{16.27}$$

that is, the matrix $\mathbf{A}$ is proportional to a unitary matrix. Therefore, if we compute $\hat{\mathbf{y}}(k) = 1/\| \mathbf{h} \| \, \mathbf{A}^H\tilde{\mathbf{y}}(k)$, we have

$$\hat{\mathbf{y}}(k) = \frac{1}{\| \mathbf{h} \|}\mathbf{A}^H\tilde{\mathbf{y}}(k) = \frac{\| \mathbf{h} \|}{\sqrt{2}}\mathbf{x}(k) + \hat{\mathbf{n}}(k) \tag{16.28}$$

where it is easy to verify that the Gaussian vector $\hat{\mathbf{n}}(k) = (\hat{n}(k),\hat{n}(k+1))^T = 1/\| \mathbf{h} \| \, \mathbf{A}^H\tilde{\mathbf{n}}(k)$ has $\mathbb{E}\left\{\hat{\mathbf{n}}(k)\right\} = 0$ and $\mathbb{E}\left\{\hat{\mathbf{n}}(k)\hat{\mathbf{n}}^H(k)\right\} = 1/\| \mathbf{h} \|^2 \, \sigma^2\mathbf{A}^H\mathbf{A} = \sigma^2\mathbf{I}$, and is therefore statistically equivalent to the original noise $\mathbf{n}(k) = (n(k),n(k+1))^T$. Therefore, we have the equivalent space–time channel

$$\hat{y}(k) = \frac{\| \mathbf{h} \|}{\sqrt{2}}x(k) + n(k)$$
$$\hat{y}(k+1) = \frac{\| \mathbf{h} \|}{\sqrt{2}}x(k+1) + n(k+1)$$

In other words, with this approach, the 2×1 MISO without CSIT can be interpreted as the SISO in Figure 16.13. In particular, we do not need to rethink to specific modulation and coding, since we can apply here all modulation and coding/decoding techniques for the SISO channel.

The virtual SISO channel obtained by the Alamouti's scheme has output SNR

$$\mathrm{SNR}_{\mathrm{Ala}} = \frac{\mathbb{E}\left\{| x |^2\right\}}{2\sigma^2}\| \mathbf{h} \|^2 = \frac{P_t}{2\sigma^2}\| \mathbf{h} \|^2 \tag{16.29}$$

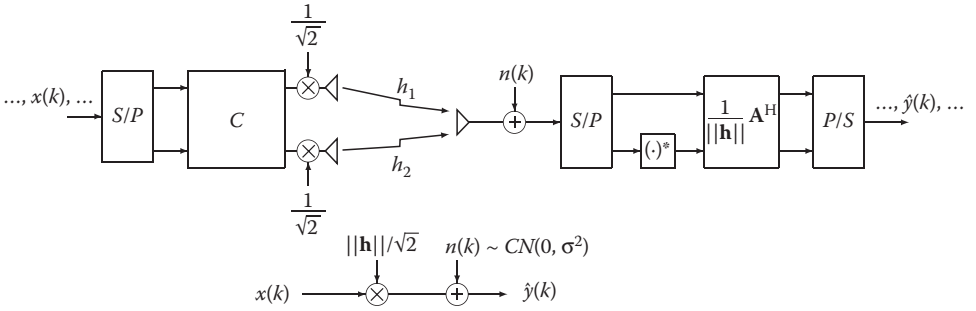

FIGURE 16.13 MISO Alamouti's scheme and its equivalent SISO. In the figure, C is the encoder block, providing the two codewords $C_1 = (x(k), x^*(k+1))$ and $C_2 = (x(k+1), -x^*(k))$ to be transmitted over the first and second antenna, respectively. Note that these codewords are orthogonal for any $x(k)$, $x(k+1)$.

Comparing this expression with Equation 16.19, we see that this 2×1 MISO scheme with no CSIT has the same performance of a 2×1 MISO with perfect CSIT and beamforming, except for a 3 dB loss (factor 2) in SNR. This loss is due to the lack of CSIT which does not allow precoding, like in beamforming, to have the coherent sum of signals at the receive antenna (here the weights in transmission are both equal to $1/\sqrt{2}$, meaning that the energy is transmitted uniformly in all directions).

In fact, the array gain is 1 (no array gain), while the diversity gain is $N_R = 2$.

It is also easy to show that, for a $2 \times N_R$ MIMO Alamouti's scheme with channel matrix $\mathbf{H} \in \mathbb{C}^{2 \times N_R}$, we can replicate the scheme above for each receiving antenna (rows of $\mathbf{H}$) and add the outputs. The SNR at the output of the combiner is the sum of the corresponding SNRs, that is,

$$\mathrm{SNR}_{Ala} = \frac{P_t}{2\sigma^2} \| \mathbf{H} \|_F^2 = \frac{P_t}{2\sigma^2} \sum_{i=1}^{N_R} \sum_{j=1}^{2} | h_{i,j} |^2 \tag{16.30}$$

From this expression, we see that the Alamouti's scheme uses the full $2 \cdot N_R$ diversity available.

This scheme, specifically designed for $N_T = 2$, has the same spectral efficiency of a SISO, in the sense that two symbols are transmitted in two symbol periods. In this regard, the encoder used (see $\mathcal{C}$ in Figure 16.13) is rate 1.

For $N_T > 2$ it has been proved that similar orthogonal codes can be designed, but with rates strictly smaller than 1.

More in general, schemes like that in Figure 16.13, with suitable decoders, lead to the so-called *space–time codes*, where we can have block encoders (space–time block codes (STBC)), or trellis encoders (space–time trellis codes (STTC)). The Alamouti's scheme can be considered an STBC with $N_T = 2$ and orthogonal codewords.

16.4.4.1 Optimality of the Alamouti's Scheme

The end-to-end capacity of the equivalent SISO obtained from the 2×1 MISO with the Alamouti's scheme is

$$C(\mathbf{h}) = \log_2 \left(1 + \frac{P_t}{2\sigma^2} \| \mathbf{h} \|^2 \right) \quad [\text{info bits/s/Hz}] \tag{16.31}$$

which is also the capacity of the original MISO, assuming no CSIT (see Chapter 17). Therefore, the Alamouti's scheme is capacity-optimal for the 2×1 MISO with no CSIT.

For $N_R > 1$, the capacity is

$$C(\mathbf{H}) = \log_2 \left(1 + \frac{P_t}{2\sigma^2} \| \mathbf{H} \|_F^2 \right) \quad [\text{info bits/s/Hz}] \tag{16.32}$$

Similar to beamforming, since Equation 16.32 also represents the capacity for MIMO with rank 1 channels, we have that Alamouti's scheme for a generic $2 \times N_R$ MIMO with no CSIT is capacity-optimal if the channel matrix $\mathbf{H}$ is rank 1.

16.4.5 Performance of Alamouti's Scheme

The Alamouti's scheme can be used with coding and modulation designed for SISO channels, so its performances are those of a SISO system, with the SNR given by Equation 16.30. For example, in Figure 16.14,

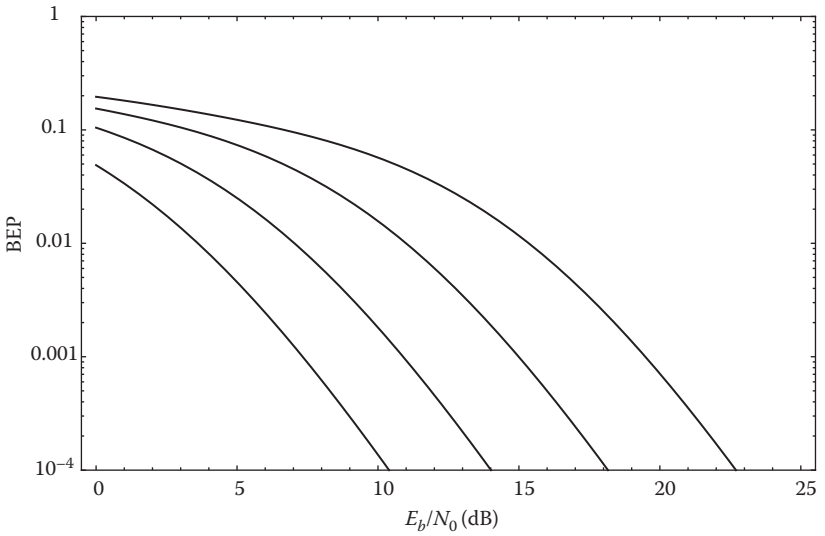

FIGURE 16.14 BEP for uncoded Alamouti's scheme with M-QAM over a (2×2) MIMO Rayleigh uncorrelated fading channel with $\mathbb{E}\left\{|h_{i,j}|^2\right\} = 1$, as a function of E_b/N_0, where E_b is the energy transmitted per bit. From left to right: $M = 4,16,64,256$ corresponding to 2,4,6,8 (bit/s/Hz).

we report the BEP for uncoded Alamouti's scheme with M-QAM over a (2×2) MIMO Rayleigh uncorrelated fading channel with $\mathbb{E}\left\{| h_{i,j} |^2\right\} = 1$, as a function of E_b/N_0 where E_b is the energy transmitted per information bit (see also Chapter 17).

16.5 SIMO with Interference (Optimum Combining, MMSE Receivers)

Multiple antennas have also the important advantage of mitigating cochannel interference. Consider for instance the situation in Figure 16.15, where the transmitted desired symbol x is received in the presence of cochannel interference due to one user transmitting on the same frequency band.

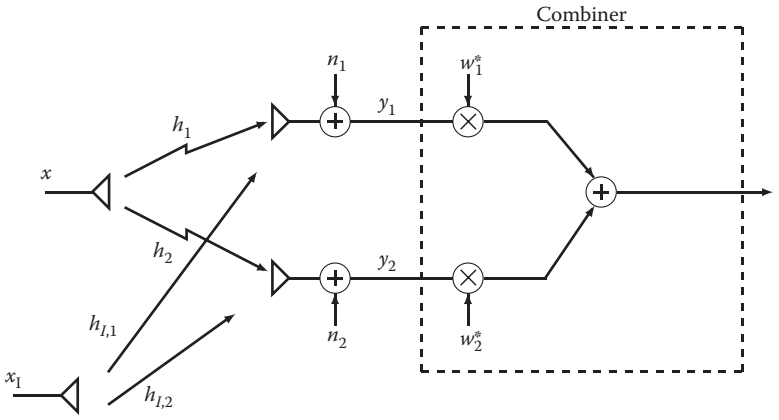

FIGURE 16.15 SIMO with interference.

The received vector is

$$\mathbf{y} = \mathbf{h}x + \mathbf{h}_I x_I + \mathbf{n} = \mathbf{h}x + \tilde{\mathbf{n}} \tag{16.33}$$

where the time index has been omitted for ease of notation and $\mathbf{h}_I$, x_I refers to the channel and symbols of the interferer, respectively. We can apply multiuser detection techniques to decode x, assuming the channels $\mathbf{h}$, $\mathbf{h}_I$ are static and known at the receiver.

For example, we here focus on linear estimation of x, obtained with weights $\mathbf{w}$. The generic linear estimate is thus $\mathbf{w}^H\mathbf{y}$. By defining the overall disturb as $\tilde{\mathbf{n}} = \mathbf{h}_I x_I + \mathbf{n}$, we see that the signal model is similar to that used for the MRC case (16.10), where now the disturb includes both noise and interference, and therefore instead of the SNR we will maximize the signal-to-interference plus noise ratio (SINR)

$$\text{SINR} = \frac{\mathbb{E}\left\{ | \mathbf{w}^H\mathbf{h}x |^2 \right\}}{\mathbb{E}\left\{ | \mathbf{w}^H\tilde{\mathbf{n}} |^2 \right\}} \tag{16.34}$$

The difference is that, while $\mathbf{n}$ is spatially white, in the sense that $\mathbb{E}\left\{\mathbf{n}\mathbf{n}^H\right\} = \sigma^2\mathbf{I}$ due to the fact that the thermal noise is uncorrelated from antenna to antenna, the disturb $\tilde{\mathbf{n}}$ is spatially colored due to the presence of interference. In fact, with the assumption of independence between signals and noise, we readily obtain

$$\mathbf{R} = \mathbb{E}\left\{\tilde{\mathbf{n}}\tilde{\mathbf{n}}^H\right\} = \mathbb{E}\left\{ | x_I |^2 \right\}\mathbf{h}_I\mathbf{h}_I^H + \sigma^2\mathbf{I}$$

where the expectation is taken with respect to noise and symbols. For this reason, we cannot use the MRC principle here. However, we can first whiten the disturb, turning the problem of optimum combining into an equivalent MRC problem. To this aim we first multiply $\mathbf{y}$ by $\mathbf{R}^{-1/2}$, obtaining

$$\hat{\mathbf{y}} = \mathbf{R}^{-1/2}\mathbf{y} = \mathbf{R}^{-1/2}\mathbf{h}x + \mathbf{R}^{-1/2}\tilde{\mathbf{n}} = \hat{\mathbf{h}}x + \hat{\mathbf{n}} \tag{16.35}$$

where now $\mathbb{E}\left\{\hat{\mathbf{n}}\hat{\mathbf{n}}^H\right\} = \mathbb{E}\left\{\mathbf{R}^{-1/2}\tilde{\mathbf{n}}\tilde{\mathbf{n}}^H\mathbf{R}^{-1/2}\right\} = \mathbf{I}$. Thus, applying the MRC principle we suddenly get that the optimal weights (in the sense of maximizing the SINR) to apply to $\hat{\mathbf{y}}$ are $\hat{\mathbf{w}} = K\hat{\mathbf{h}} = K\mathbf{R}^{-1/2}\mathbf{h}$, and the corresponding (maximum) output SNR is $\mathbb{E}\left\{ | x |^2 \right\} || \hat{\mathbf{h}} ||^2$. Returning to our original problem, since $\hat{\mathbf{y}} = \mathbf{R}^{-1/2}\mathbf{y}$ the weights to apply to $\mathbf{y}$ are

$$\mathbf{w} = K\mathbf{R}^{-1}\mathbf{h} \tag{16.36}$$

and the resulting maximum SINR is

$$\text{SINR}_{\max} = \mathbb{E}\left\{ | x |^2 \right\}\mathbf{h}^H\mathbf{R}^{-1}\mathbf{h} \tag{16.37}$$

In the presence of N_I interferers with channels $\mathbf{h}_{I,1}\cdots\mathbf{h}_{I,N_I}$ and transmission powers $\mathbb{E}\left\{ | x_{I,1} |^2 \right\},\ldots,\mathbb{E}\left\{ | x_{I,N_I} |^2 \right\}$, the weights and SINR are still given by Equations 16.36 and 16.37 with

$$\mathbf{R} = \mathbb{E}\left\{\tilde{\mathbf{n}}\tilde{\mathbf{n}}^H\right\} = \sum_{m=1}^{N_I} \mathbb{E}\left\{ | x_{I,m} |^2 \right\}\mathbf{h}_{I,m}\mathbf{h}_{I,m}^H + \sigma^2\mathbf{I} \tag{16.38}$$

The weights (16.36) provide the largest SINR at the combiner output (optimum combining (OC)). It is also easy to show that these weights (apart for the irrelevant constant K) give the minimum mean-square error (MMSE) linear estimate of the symbol x.

Other approaches to mitigate the interference can use a zero forcing (ZF) criterion, or other nonlinear techniques like successive interference cancellation (SIC) or ML joint detection (see also Chapter 17).

Finally, the considerations made in this chapter can be extended to distributed antenna systems, where single antenna nodes cooperate to constitute a virtual multiple antennas system.

Acronyms

AWGN	Additive white Gaussian noise
BEP	Bit error probability
BFC	Block fading channel
BPSK	Binary phase shift keying
CSCG	Circularly symmetric complex Gaussian
CSIR	Channel state information at the receiver
CSIT	Channel state information at the transmitter
DSL	Digital subscriber line
FEC	Forward error correction
i.i.d.	Independent, identically distributed
LOS	Line of sight
MIMO	Multiple-input multiple-output
MISO	Multiple-input single-output
ML	Maximum likelihood
MMSE	Minimum mean-square error
M-QAM	M-ary quadrature amplitude modulation
MRC	Maximal ratio combiner
OC	Optimum combining
p.d.f.	Probability density function
PLC	Power line communication
PSK	Phase shift keying
r.v.	Random variable
SIC	Successive interference cancellation
SIMO	Single-input multiple-output
SINR	Signal-to-interference plus noise ratio
SISO	Single-input single-output
SNR	Signal-to-noise ratio
STBC	Space–time block codes
STTC	Space–time trellis codes
TDD	Time division duplex
ZF	Zero forcing

References

1. J. H. Winters, On the capacity of radio communication systems with diversity in Rayleigh fading environment, *IEEE J. Select. Areas Commun.*, SAC-5(5), 871–878, 1987.
2. G. J. Foschini, Layered space-time architecture for wireless communication a fading environment when using multiple antennas, *Bell Labs Tech. J.*, 1(2), 41–59, 1996.
3. G. J. Foschini and M. J. Gans, On limits of wireless communications in a fading environment when using multiple antennas, *Wireless Personal Commun.*, 6(3), 311–335, 1998.

4. E. Telatar, Capacity of multi-antenna Gaussian channels, *Eur. Trans. Telecomm.*, 10(6), 585–595, 1999.
5. A. Goldsmith, *Wireless Communications*. Cambridge University Press, New York, 2005.
6. D. Tse and P. Viswanath, *Fundamentals of Wireless Communication*. Cambridge University Press, New York, 2006.
7. A. Molisch, *Wireless Communications*. John Wiley & Sons Ltd., England, 2011.
8. D. Gesbert, H. Bolcskei, D. Gore, and A. Paulraj, Outdoor MIMO wireless channels: Models and performance prediction, *IEEE Trans. Commun.*, 50(12), 1926–1934, 2002.
9. P. Almers, E. Bonek, A. Burr, N. Czink, M. Debbah, V. Degli-Esposti, H. Hofstetter, et al. Survey of channel and radio propagation models for wireless MIMO systems, *EURASIP J. Wirel. Commun. Netw.*, 2007, 56–56, 2007.
10. A. Giorgetti, P. J. Smith, M. Shafi, and M. Chiani, MIMO capacity, level crossing rates and fades: The impact of spatial/temporal channel correlation, *KICS/IEEE Int. J. Commun. Netw.*, 5(2), 104–115, 2003 (special issue on Coding and Signal Processing for MIMO systems).

17

High-Throughput MIMO Systems

Marco Chiani

17.1 Introduction

Systems with multiple antennas (Figure 17.1) can exploit, besides the usual time and frequency, the spatial dimension, with large improvements in terms of diversity, interference mitigation and throughput. For this reason, they are among the key technologies in modern wireless transmission systems [1–7]. Even in wired systems (such as in digital subscriber line (DSL) and in power line communication (PLC) systems) since cables usually contain multiple wires, the channel can be seen as a multiple-input multiple-output (MIMO). In the following we will focus on MIMO wireless systems, but several of the described techniques can be applied also in wired systems.

The advantages of multiple antennas can be summarized as follows.

- *Array gain*: This is the increase in the average signal-to-noise ratio (SNR) at the receiver due to coherent combination of signals. It can be obtained for both multiple transmit or multiple receive antennas, requiring channel state information at the transmitter (CSIT) or channel state information at the receiver (CSIR), respectively.
- *Diversity gain*: In the presence of fading, the received power level can present large variations. Diversity is used to reduce the variations of the SNR level due to fading, by sending each information symbol through different channels with independent fading levels, and then combining the outputs. In an $N_T \times N_R$ MIMO channel there are potentially $N_T N_R$ links. Spatial diversity can

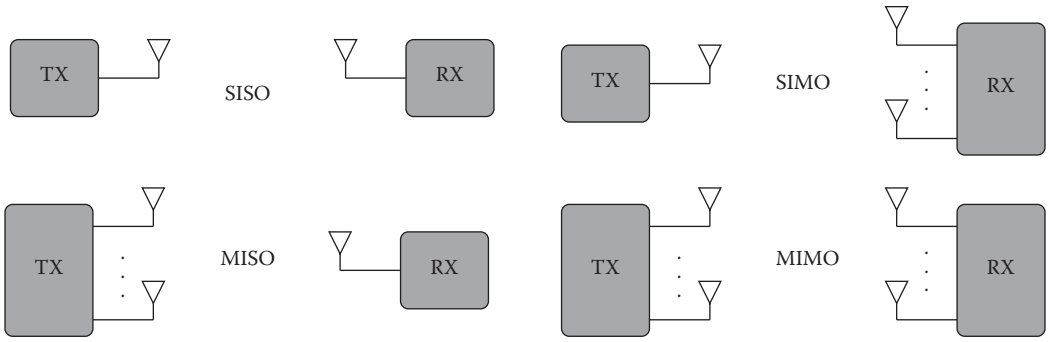

FIGURE 17.1 Multiple antenna systems: single-input single-output (SISO), single-input multiple-output (SIMO), multiple-input single-output (MISO), multiple-input multiple-output (MIMO).

be obtained with multiple receiving antennas with CSIR (receive diversity), and with multiple transmit antennas (transmit diversity). Transmit diversity is possible both with CSIT (beamforming) and even in the absence of CSIT (Alamouti's code, space-time codes).

- *Interference mitigation*: Multiple antennas can be used as a spatial filter to reduce the power received from cochannel interfering sources. The enhanced robustness to cochannel interference increases the number of served users per unit area in wireless cellular systems.
- *Multipath multiplexing (spatial multiplexing) for high-throughput transmission*: In MIMO channels with multipath it is possible to transmit up to $N_{\min} = \min\{N_T, N_R\}$ "parallel" streams over the same band, with an increase of the link throughput. Multipath multiplexing, also called spatial multiplexing, is not possible for SIMO or MISO channels.

In Chapter 16 we described the MIMO channel model, and how systems with multiple antennas can be used for diversity and for interference mitigation.

In this chapter we focus on the Shannon capacity of MIMO channels, and on the design principles for practical high-throughput MIMO systems.

As in Chapter 16 we start with the single-user scenario, and, for the sake of clarity, we focus on frequency-flat fading channels. The extension to wideband channel models is easy by assuming multicarrier transmission techniques, where the channel is frequency-flat for each subcarrier.

Throughout the chapter vectors and matrices are indicated by bold, det **A** denote the determinant of the matrix **A**, and $a_{i,j}$ is the (i,j)th element of **A**. Expectation operator is denoted by $\mathbb{E}\{\cdot\}$, the superscript $()^H$ denotes conjugation and transposition, **I** is the identity matrix, and tr{**A**} is the trace of **A**.

17.2 Capacity of Fixed MIMO Channels

17.2.1 Capacity of Frequency-Flat MIMO Channels

Consider a frequency-flat MIMO channel, whose discrete-time equivalent lowpass model (Figure 17.2) is*

$$\mathbf{y}(k) = \mathbf{H}\,\mathbf{x}(k) + \mathbf{n}(k) \tag{17.1}$$

* See also Chapter 16.

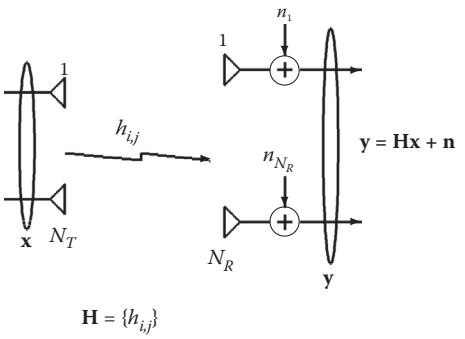

FIGURE 17.2 MIMO.

where k is the time index, $\mathbf{x}(k)$ and $\mathbf{y}(k)$ are the input and output vectors, respectively. The noise vectors $\mathbf{n}(k) \in \mathbb{C}^{N_R}$ are independent, identically distributed (i.i.d.) with circularly symmetric complex Gaussian (CSCG) entries and covariance matrix $\mathbf{R}_n = \mathbb{E}\left\{\mathbf{n}(k)\mathbf{n}^H(k)\right\} = \sigma^2\mathbf{I}$. Assume the channel matrix $\mathbf{H}$ is fixed, and let us assume zero-mean vectors $\mathbb{E}\left\{\mathbf{x}(k)\right\} = 0$ with covariance matrix $\mathbf{R}_x = \mathbb{E}\left\{\mathbf{x}(k)\mathbf{x}^H(k)\right\}$. The average total transmitted power can be written as $\mathbb{E}\left\{|\, x_1(k)\,|^2\right\} + \cdots + \mathbb{E}\left\{|\, x_{N_T}(k)\,|^2\right\} = \mathbb{E}\left\{\mathbf{x}^H(k)\mathbf{x}(k)\right\} = \mathrm{tr}\left\{\mathbf{R}_x\right\}$.

The Shannon capacity for this MIMO channel is the maximum of the mutual information between the input and the output vectors. It is easy to verify that, similar to the usual SISO, this is obtained by using i.i.d. input vectors $\mathbf{x}(k)$ with CSCG distribution. Since for CSCG vectors with covariance $\mathbf{R}$ the differential entropy is $\log_2[(\pi e)^{N_R} \det\mathbf{R}]$, the maximum of the mutual information for the vector channel with the specified constraints is

$$\begin{aligned} C(\mathbf{H},\mathbf{R}_x) &= \log_2\left[(\pi e)^{N_R}\det\mathbf{R}_y\right] - \log_2\left[(\pi e)^{N_R}\det\mathbf{R}_n\right] \\ &= \log_2\det\left(\mathbf{R}_y\mathbf{R}_n^{-1}\right) \\ &= \log_2\det\left(\mathbf{I} + \frac{1}{\sigma^2}\mathbf{H}\mathbf{R}_x\mathbf{H}^H\right) \qquad [\text{info bits/s/Hz}] \end{aligned} \tag{17.2}$$

where $\mathbf{R}_y = \mathbb{E}\left\{\mathbf{y}(k)\mathbf{y}^H(k)\right\} = \mathbf{H}\mathbf{R}_x\mathbf{H}^H + \mathbf{R}_n$.

Assume now that we constrain the total transmitted power $\mathbb{E}\left\{\mathbf{x}^H(k)\mathbf{x}(k)\right\} = \mathrm{tr}\left\{\mathbf{R}_x\right\} \le P_t$. We distinguish here between two cases:

1. Channel perfectly known at the transmitter: finding $\mathbf{R}_x$ by means of SVD and water-filling.
   The conditional MIMO capacity with both CSIT and CSIR is obtained by finding the optimal transmit covariance matrix $\mathbf{R}_x$ which maximizes (17.2) under the power constraint:

$$C(\mathbf{H}) = \max_{\mathrm{tr}\{\mathbf{R}_x\}\le P_t} \log_2\det\left(\mathbf{I} + \frac{1}{\sigma^2}\mathbf{H}\mathbf{R}_x\mathbf{H}^H\right) \ [\text{info bits/s/Hz}] \tag{17.3}$$

   Here is not easy to see what is the best $\mathbf{R}_x$. However, as we will see later, with CSIT we can think to "diagonalize" the channel by means of a singular values decomposition (SVD) of the channel matrix $\mathbf{H}$, which allows to have separated parallel virtual channels. Then, the problem of finding $\mathbf{R}_x$ reduces to the well known water-filling problem.

2. Channel unknown at the transmitter: uniform power allocation among the transmit antenna. When the transmitter has no information about the channel, a reasonable choice is to transmit independent, parallel streams over the transmit antennas, allocating to each the same power P_t/N_T, that is, to use $\mathbf{R}_x = (P_t/N_T)\mathbf{I}$.

   Therefore, from Equation 17.2 the capacity without CSIT is

$$C(\mathbf{H}) = \log_2 \det\left(\mathbf{I} + \frac{P_t}{N_T\sigma^2}\mathbf{H}\mathbf{H}^H\right) \quad [\text{info bits/s/Hz}]$$
$$= \sum_{\ell=1}^{N_{\min}} \log_2\left(1 + \frac{P_t}{N_T\sigma^2}\lambda_\ell\right) \quad [\text{info bits/s/Hz}] \tag{17.4}$$

   where again we indicate with $\lambda_1 \geq \lambda_2 \geq \cdots \geq \lambda_{N_{\min}} \geq 0$ the possibly nonzero eigenvalues of $\mathbf{H}\mathbf{H}^H$ or, equivalently, of $\mathbf{H}^H\mathbf{H}$.

17.2.2 An Equivalent Diagonalized MIMO by SVD or Multiple Beamforming

17.2.2.1 Diagonalization by SVD

By the SVD we can decompose $\mathbf{H} = \mathbf{U}\mathbf{D}\mathbf{V}^H$, where $\mathbf{U} \in \mathbb{C}^{N_R \times N_R}$, $\mathbf{V} \in \mathbb{C}^{N_T \times N_T}$ are unitary matrices, $\mathbf{D} \in \mathbb{C}^{N_R \times N_T}$ is a diagonal matrix with $N_{\min} = \min\{N_T, N_R\}$ diagonal entries $\sqrt{\lambda_1} \geq \sqrt{\lambda_2} \geq \cdots \geq \sqrt{\lambda_{N_{\min}}} \geq 0$, and λ_i are the possibly nonzero eigenvalues of $\mathbf{H}\mathbf{H}^H$. Of these, only the first $r = \text{rank}\{\mathbf{H}\} \leq N_{\min}$ are greater than zero.*

For example, for a 3×4 MIMO channel, we have

$$\mathbf{H} = \mathbf{U}\mathbf{D}\mathbf{V}^H = \mathbf{U}\begin{bmatrix} \sqrt{\lambda_1} & 0 & 0 \\ 0 & \sqrt{\lambda_2} & 0 \\ 0 & 0 & \sqrt{\lambda_3} \\ 0 & 0 & 0 \end{bmatrix}\mathbf{V}^H$$

where λ_ℓ are the possibly non-zero eigenvalues of $\mathbf{H}\mathbf{H}^H$ or of $\mathbf{H}^H\mathbf{H}$.

Thus, if we apply the linear transformation $\mathbf{U}^H$ at the received vector (this requires CSIR) we have

$$\underbrace{\mathbf{U}^H\mathbf{y}}_{\hat{\mathbf{y}}} = \mathbf{D}\underbrace{\mathbf{V}^H\mathbf{x}}_{\hat{\mathbf{x}}} + \underbrace{\mathbf{U}^H\mathbf{n}}_{\hat{\mathbf{n}}}$$

where, since $\mathbf{U}$ is unitary, the noise vector $\hat{\mathbf{n}}$ has the same statistical description of $\mathbf{n}$. Moreover, if we define $\hat{\mathbf{x}} = \mathbf{V}^H\mathbf{x}$ which implies $\mathbf{x} = \mathbf{V}\hat{\mathbf{x}}$ we can write

$$\hat{\mathbf{y}} = \mathbf{D}\hat{\mathbf{x}} + \hat{\mathbf{n}} = \begin{bmatrix} \sqrt{\lambda_1} & 0 & 0 \\ 0 & \sqrt{\lambda_2} & 0 \\ 0 & 0 & \sqrt{\lambda_3} \\ 0 & 0 & 0 \end{bmatrix}\hat{\mathbf{x}} + \hat{\mathbf{n}}$$

* The hermitian matrix $\mathbf{H}\mathbf{H}^H$ is nonnegative definite, and can have at most $N_{\min}$ nonzero eigenvalues, i.e., $r = \text{rank}\{\mathbf{H}\mathbf{H}^H\} = \text{rank}\{\mathbf{H}\} \leq N_{\min}$. Also, $\mathbf{H}\mathbf{H}^H$ and $\mathbf{H}^H\mathbf{H}$ have the same nonzero eigenvalues.

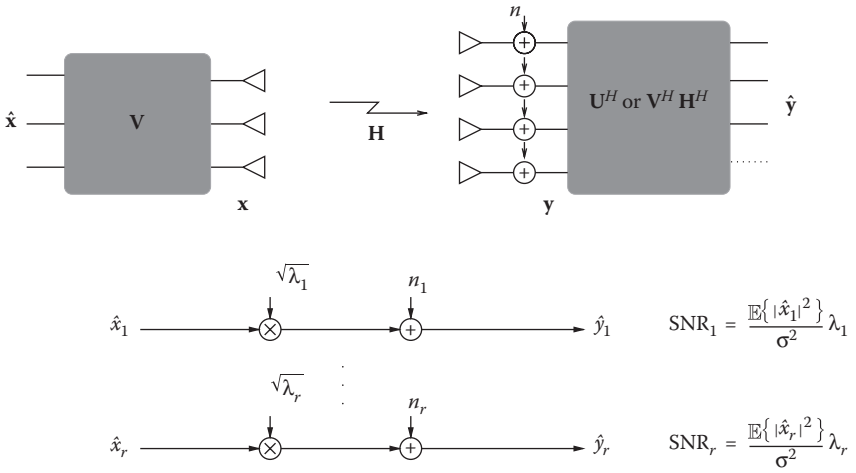

FIGURE 17.3 Diagonalization of a 3 × 4 MIMO. Diagonalization is achieved by using at the receiver $\mathbf{U}^H$ (SVD) or $\mathbf{V}^H\mathbf{H}^H$ (multimode beamforming). Note that r = rank $\{\mathbf{H}\} \le 3$, so there are at most three eigenmodes available.

We have thus obtained another MIMO, whose input is $\hat{\mathbf{x}}$ and output is $\hat{\mathbf{y}}$, as in Figure 17.3. In this scheme, since $\mathbf{D}$ is diagonal

$$\hat{y}_\ell = \sqrt{\lambda_\ell}\,\hat{x}_\ell + \hat{n}_\ell \quad \ell = 1, \ldots, r \tag{17.5}$$

$$\hat{y}_\ell = \hat{n}_\ell \qquad \ell = r+1, \ldots, N_R \tag{17.6}$$

that means, in other words, that we have now "diagonalized" the channel, obtaining r = rank $\{\mathbf{H}\}$ parallel SISO subchannels with SNR $\mathbb{E}\left\{|\hat{x}_\ell|^2\right\}\lambda_\ell/\sigma^2$.

17.2.2.2 Diagonalization by Multiple Beamforming

It is interesting to note that, given the spectral decomposition $\mathbf{H}^H\mathbf{H} = \mathbf{V}\Lambda\mathbf{V}^H$, another way to diagonalize the channel is to use $\mathbf{V}$ at the transmitter side, as for the SVD, and $\mathbf{V}^H\mathbf{H}^H$ in reception (instead of $\mathbf{U}^H$ of the SVD). In fact, when we multiply the received vector by $\mathbf{V}^H\mathbf{H}^H$ we get

$$\hat{\mathbf{y}} = \mathbf{V}^H\mathbf{H}^H\mathbf{y} = \mathbf{V}^H\mathbf{H}^H\mathbf{H}\mathbf{x} + \mathbf{V}^H\mathbf{H}^H\mathbf{n} \tag{17.7}$$

$$= \mathbf{L}\hat{\mathbf{x}} + \tilde{\mathbf{n}} \tag{17.8}$$

where $\mathbb{E}\left\{\tilde{\mathbf{n}}\tilde{\mathbf{n}}^H\right\} = \mathbf{L}$. With this diagonalization the useful (decoupled) subchannels are

$$\tilde{y}_\ell = \lambda_\ell\hat{x}_\ell + \tilde{n}_\ell \quad \ell = 1, \ldots, r$$

where the noise terms have $\mathbb{E}\left\{|\tilde{n}_\ell|^2\right\} = \sigma^2\lambda_\ell$ and therefore the SNR is, as for the SVD, $\mathrm{SNR}_\ell = \lambda_\ell\mathbb{E}\left\{|\hat{x}_\ell|^2\right\}/\sigma^2$. Hence, MIMO SVD is equivalent to MIMO beamforming with multiple eigenmodes.

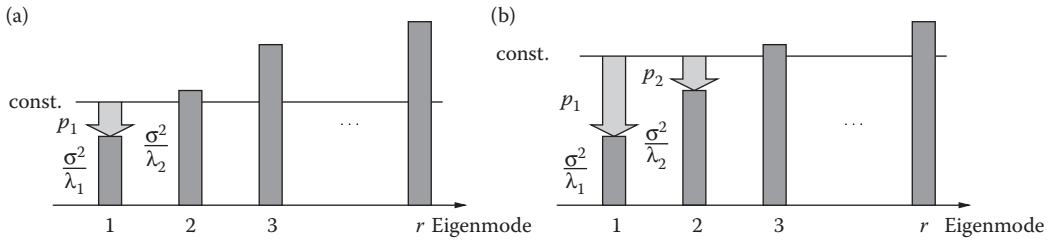

FIGURE 17.4 Examples of power allocation by water-filling. If P_t is small, only the strongest mode is used as in (a), reducing to (single mode) beamforming. By increasing P_t, more modes are activated as in (b).

Also, note that the first subchannel (corresponding to the strongest eigenvalue) is exactly that discussed for the beamforming in Chapter 16. In other words, while with the (single mode) eigenbeamforming in Chapter 16 we use just the strongest subchannel of the MIMO, putting on it all power, with diagonalization we can use up to r subchannels.

17.2.2.3 Capacity for the Diagonalized MIMO

The capacity of the diagonalized MIMO is the same as that of the original MIMO. In particular, the symbols $\hat{x}_\ell$ should be independent CSCG, and the MIMO capacity can be rewritten

$$C(\mathbf{H}) = \max_{\sum_m p_m \le P_t} \sum_{\ell=1}^{N_{\min}} \log\left(1 + \lambda_\ell \frac{p_\ell}{\sigma^2}\right) \tag{17.9}$$

where $p_\ell = \mathbb{E}\left\{|\hat{x}_\ell|^2\right\}$ is the power allocated to the ℓth subchannel. The power levels p_ℓ giving the capacity in Equation 17.9 can therefore be calculated by the water-filling approach, that is, by finding the number of activated subchannels $a \le N_{\min}$ and associated power levels $p_1 \ge p_2 \ge \cdots \ge p_a > 0$ satisfying $p_1 + \cdots + p_a = P_t$ and

$$p_1 + \frac{\sigma^2}{\lambda_1} = p_2 + \frac{\sigma^2}{\lambda_2} = \cdots = p_a + \frac{\sigma^2}{\lambda_a} = \text{const.}$$

The remaining subchannels with index $a+1, \ldots, N_{\min}$ are not used. An example is reported in Figure 17.4.

17.3 Capacity of MIMO Fading Channels

The previous analysis assumed a fixed channel $\mathbf{H}$. In the presence of fading and mobility, the channel varies in time. Let us assume a block fading channel (BFC), where the channel is constant over a block composed of several symbols, and takes i.i.d. values across different blocks. This fading channel is characterized by the discrete-time process …, $\mathbf{H}(1)$, $\mathbf{H}(2)$, … where $\mathbf{H}(m)$ is the channel matrix for the mth block. Thus, $C = C(\mathbf{H}(m))$ of the previous sections is also randomly varying from block to block. The considerations of Chapter 16 are generalized to MIMO channels as follows.

- For MIMO channels without CSIT the ergodic capacity is defined as $\mathbb{E}\left\{C(\mathbf{H})\right\}$ where $C(\mathbf{H})$ is given in Equation 17.4, and the expectation is taken respect to the distribution of the eigenvalues of $\mathbf{H}^H\mathbf{H}$. This ergodic capacity is valid for systems without CSIT with coding and perfect time-interleaving (fast fading). The evaluation of $\mathbb{E}\left\{C(\mathbf{H})\right\}$ is related to the theory of random matrices,

and is in general cumbersome especially for spatially correlated channels [8]–[11]. However, when the channel gains $h_{i,j}$ are zero-mean uncorrelated with $\mathbb{E}\left\{|\, h_{i,j}\,|^2\right\} = 1$, by using Jensen's inequality we get the simple universal bound

$$\mathbb{E}\left\{C(\mathbf{H})\right\} \le \min\left\{N_R, N_T\right\} \log_2\left(1 + \frac{P_t}{\sigma^2}\frac{\max\left\{N_R, N_T\right\}}{N_T}\right) = \begin{cases} N_T \log_2\left(1 + \dfrac{P_t}{\sigma^2}\dfrac{N_R}{N_T}\right) & N_R \ge N_T \\ N_R \log_2\left(1 + \dfrac{P_t}{\sigma^2}\right) & N_R \le N_T \end{cases} \tag{17.10}$$

This bound applies in particular to Rayleigh uncorrelated fading (i.e., when the entries of H are i.i.d. CSCG variables). An example is reported in Figure 17.5. We note that, for the zero-mean uncorrelated scattering MIMO channel, the ergodic capacity bound increases linearly with the minimum between N_T and N_R. More precisely, it is like to have $N_{\min}$ parallel SISO channels, with an additional array gain $\max\{N_R, N_T\}/N_T$. Also, increasing N_T beyond N_R does not change the bound. Thus, for a fixed SNR the ergodic capacity increases linearly with $N_{\min}$. For fixed (N_T, N_R), the ergodic capacity increases logarithmically with the SNR (i.e., in a semi-log graph $\mathbb{E}\left\{C(\mathbf{H})\right\}$ vs. P_t/σ^2 [dB], the behavior is linear for large SNRs). Other examples of the ergodic capacity without CSIT, obtained as described in Reference 8, are reported in Figures 17.6 and 17.7.

- For MIMO channels without CSIT, when the codeword length is of the order of the fading block (slow fading), and assuming a constant information rate R [information bits/s/Hz] at the channel input, we define the channel outage probability as

$$P_{\text{out}}(R) = \Pr\left\{C(\mathbf{H}) < R\right\} \tag{17.11}$$

which represents a lower bound on the codeword error rate for coded systems. We can also define the *outage capacity* at codeword error rate P_{target} as the value R_{out} to use at the channel input to guarantee an outage probability P_{target}

$$R_{\text{out}}(P_{\text{target}}) = P_{\text{out}}^{-1}(P_{\text{target}}) \tag{17.12}$$

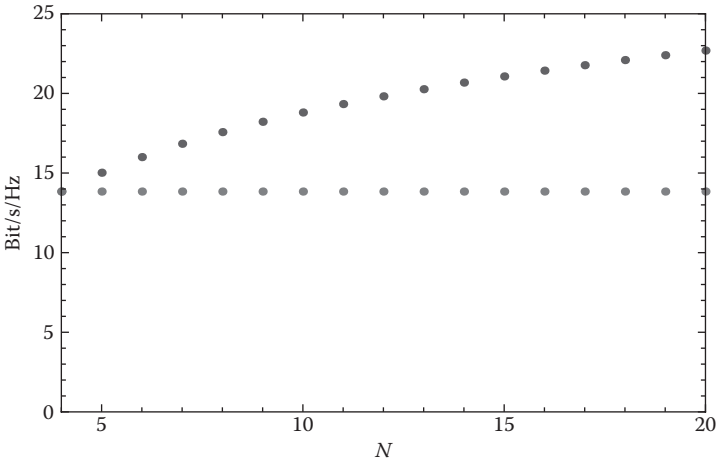

FIGURE 17.5 Ergodic capacity bound (17.10) for zero-mean uncorrelated fading, no CSIT, vs. number of antennas. Comparison between $(4 \times N)$ MIMO (upper points) and $(N \times 4)$ MIMO (lower points). SNR = 10 dB.

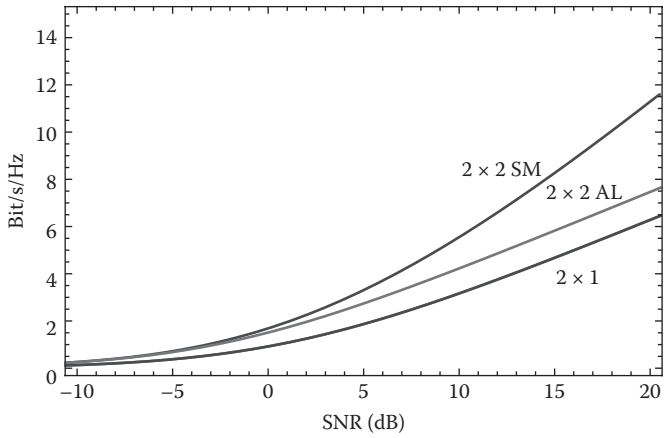

FIGURE 17.6 Ergodic capacity for $(2 \times N_R)$ MIMO, no CSIT, uncorrelated Rayleigh channel, for $N_R = 1,2$ (top and bottom curves). AL: Alamouti's 2×2 scheme. Note that the Alamouti's 2×1 has the same capacity of the 2×1 MIMO (the lower curve).

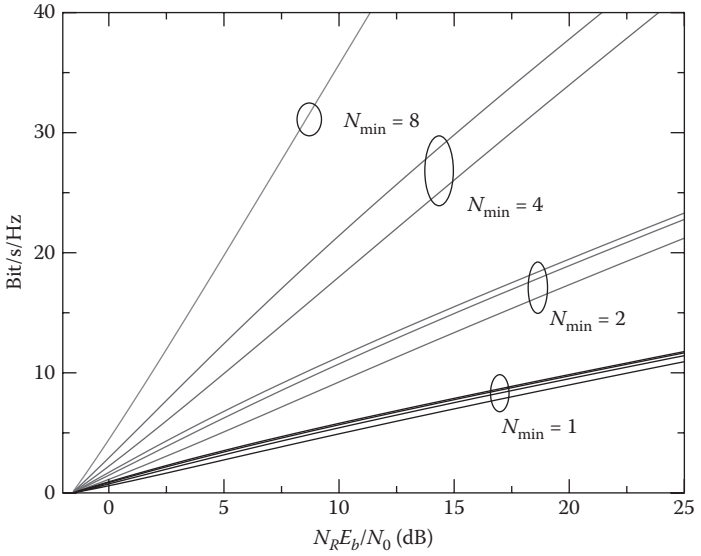

FIGURE 17.7 Ergodic capacity as a function of $N_R E_b/N_0$, no CSIT, $(N_T \times N_R)$ MIMO uncorrelated Rayleigh channel. Note that $N_R E_b$ represents the average energy per information bit received by all antennas. The curves are all pairs with $N_R, N_T = 1,2,4,8$. Note that the curves for $n \times m$ and $m \times n$ are coincident in this graph. The minimum energy per bit-to-noise spectral density ratio is $\ln 2 = -1.6$ dB for all curves (as for the SISO AWGN channel). Note that, from the energy efficiency point of view, MIMO is better than SISO for all spectral efficiencies.

and the resulting effective rate is $R_{out}\,(1 - P_{out}(R_{out}))$ (correctly received [info. bits/s/Hz] over many fading blocks). This is sometimes called *outage rate*. The outage probability versus SNR curves for MIMO uncorrelated Rayleigh channels and with a spectral efficiency $R = 8$ [info. bits/s/Hz] are reported in Figure 17.8. Examples of outage probability vs. R for MIMO uncorrelated Rayleigh channels with SNR = 10 dB, obtained as described in Reference 8, are reported in Figures 17.9 through 17.11.

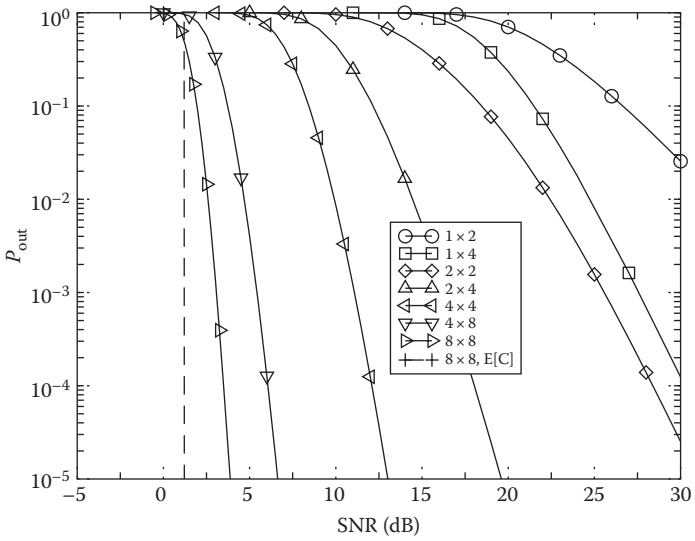

FIGURE 17.8 Example of outage probability for $R = 8$ [info bit/s/Hz], no CSIT, MIMO ($N_T \times N_R$) uncorrelated Rayleigh channel.

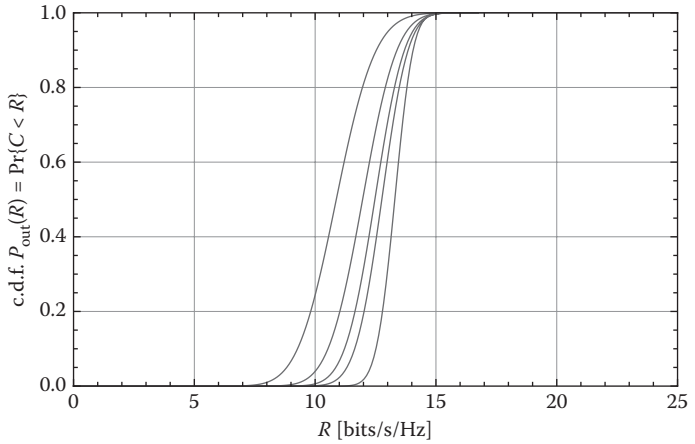

FIGURE 17.9 Outage capacity for ($N_T \times 4$) MIMO uncorrelated Rayleigh channel, no CSIT. From left to right: $N_T = 4,6,8,10,20$, SNR = 10 dB.

- For MIMO slow fading channels with knowledge of $C(\mathbf{H}(m))$ at the transmitter (partial CSIT), assume the information rate $R(m)$ [information bits/s/Hz] for each block m is adapted to stay below $C(\mathbf{H}(m))$, so that the received codewords can be successfully decoded. The information rate is adapted by changing the forward error correction (FEC) coderate and modulation format in the schemes described later (Section 17.4.2). In practice, a predefined set of couples (codes, modulation format) can be used to discretize the information rate, and the transmitter chooses for each block the best couple based on $C(\mathbf{H}(m))$. Over a large number N of blocks the transferred rate achievable is bounded by $1/N \sum_{m=1}^{N} C(\mathbf{H}(m))$ which, for the law of large numbers, converges to $\mathbb{E}\{C(\mathbf{H})\}$. Thus, $\mathbb{E}\{C(\mathbf{H})\}$ is also the achievable rate for a *rate-adaptive* system.
- For MIMO channels with perfect CSIT, and assuming the power P_t is kept constant in time for all blocks, we can apply diagonalization of MIMO, and optimally allocate on a block basis the power

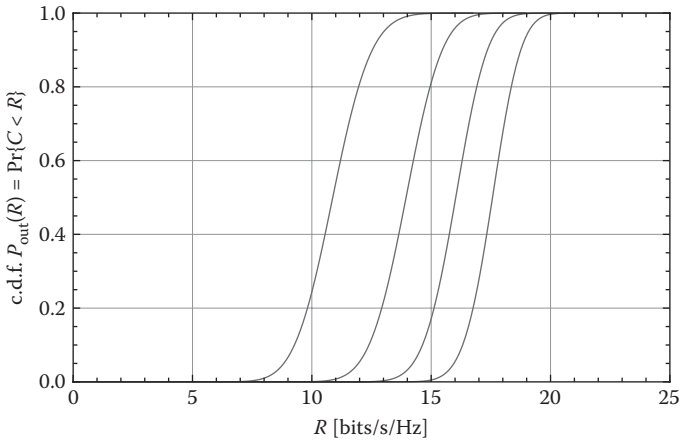

FIGURE 17.10 Outage capacity for $(4 \times N_R)$ MIMO uncorrelated Rayleigh channel, no CSIT. From left to right: $N_R = 4,6,8,10$, SNR = 10 dB.

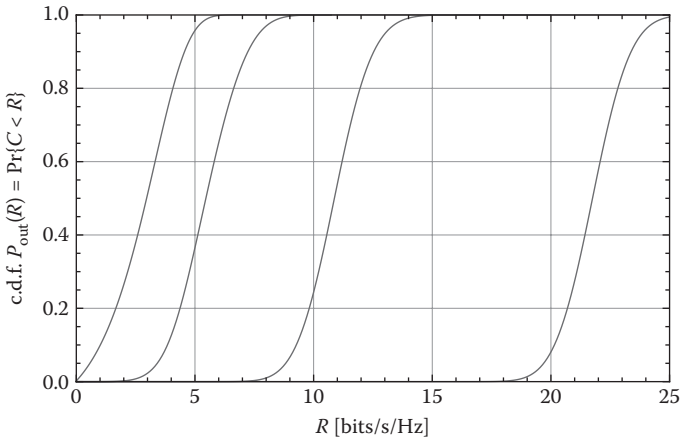

FIGURE 17.11 Outage capacity for $(N \times N)$ MIMO uncorrelated Rayleigh channel, no CSIT. From left to right: $N = 1,2,4,8$, SNR = 10 dB.

on the submodes (more energy on the submodes with better channel gain, and less on those with lower channel gain), according to the water-filling principle. In this case the ergodic capacity is given by $\mathbb{E}\{C(\mathbf{H})\}$ where $C(\mathbf{H})$ is given in Equation 17.9. This *power and rate space-adaptive* system has a slightly larger rate than the *rate time-adaptive* system.

- If the constraint is on the average power over time, we can also optimally allocate the transmit power in both space and time, allocating more energy to channels with high gains, and less to those with low gains, according to the water-filling principle in space and time (ergodic capacity with CSIT and time-average power constraint). This *power and rate space-time-adaptive* system has a slightly larger rate than the *power and rate space-adaptive* system. A comparison between the ergodic capacities without CSIR and with CSIT (power and rate space-time-adaptive) for MIMO uncorrelated Rayleigh channels, obtained as described in References 8 and 12, is reported in Figure 17.12.

For all *rate-adaptive* techniques, the information rate (i.e., number of information bits per codeword) changes from block to block. For delay-sensitive applications this can be a problem, and constant rate

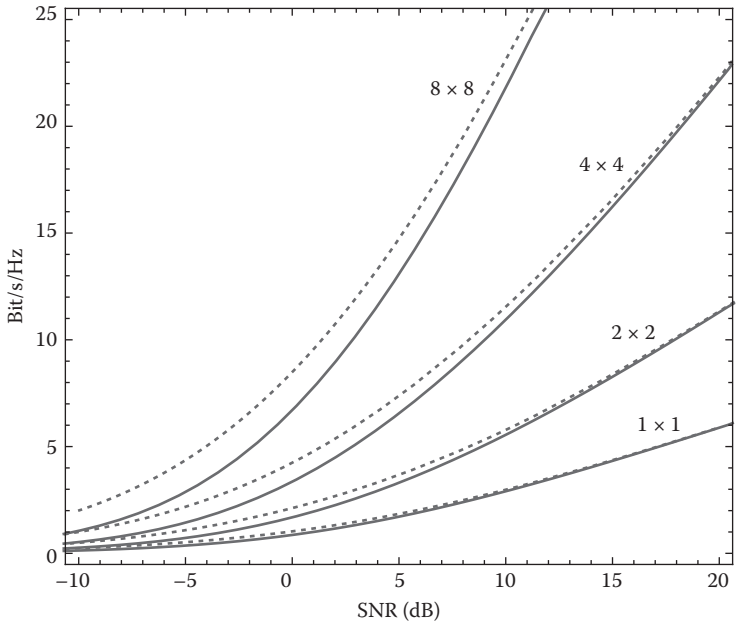

FIGURE 17.12 Ergodic capacity for $(M \times M)$ MIMO uncorrelated Rayleigh channel, for $M = 1,2,4,8$. Dashed curves: capacity with CSIT and space-time water-filling power allocation. Continuous lines: capacity for channel unknown at the transmitter. Power allocation gives a negligible improvement for large SNRs when $N_T = N_R$. It is possible to show that the improvement with CSIT is larger for $N_T > N_R$, where the capacity without CSIT is limited (see Equation 17.10).

solutions are preferable. For example, the transmit power can be varied to maintain a constant SNR at the receiver, and consequently a constant rate (like power control in cellular systems, also called channel inversion).

17.3.1 Signal-to-Noise Power Ratio, Energy per Information Bit, Energy Efficiency

In the following, we report some example of ergodic capacity and outage probability, assuming fading channels with normalized average gains, that is, $\mathbb{E}\left\{|h_{i,j}|^2\right\} = 1 \ \forall i, j$, and independent signals at different transmit antennas. With this normalization, the SNR defined as the ratio of the total transmitted power, P_t, and the noise power per antenna, σ^2

$$\text{SNR} = \frac{P_t}{\sigma^2} \tag{17.13}$$

represents the SNR measurable at each receive antenna element.

However, to have an idea of the efficiency of the system we must determine how many information bits we can transfer per unit energy (Joule) spent. In this regard, if the transmission rate is R [information bit/s/Hz], the energy transmitted per information bit is $E_b = P_t T/R$ where T is the signaling period. We can then define the ratio

$$\frac{E_b}{N_0} = \frac{P_t}{R\sigma^2} = \frac{\text{SNR}}{R} \tag{17.14}$$

where N_0 is the thermal noise single-sided power spectral density (the same for each receive antenna). Note that E_b represents the average energy per bit at each receive antenna, due to the normalization imposed on the channel gains.

For a fair comparison with SISO we can eliminate the array gain by considering the ratio

$$\frac{N_R E_b}{N_0} = \frac{N_R \mathrm{SNR}}{R} \tag{17.15}$$

where $N_R E_b$ represents the average energy received in total by all antennas per information bit. Once the thermal noise is known, this ratio allows determining the total energy the receiver must harvest (on average) from all antennas.

17.4 MIMO Systems for Spatial Multiplexing

17.4.1 High-Throughput MIMO Systems with Channel Known at the Transmitter (Closed-Loop MIMO)

Assuming perfect CSIT and CSIR are available, the simplest way to implement high-throughput MIMO systems is to apply the linear transformations indicated in Section 17.2.2, so to diagonalize the MIMO channel (diagonalization is often indicated as MIMO-SVD). The r decoupled ISO channels have different gains (related to the corresponding channel eigenvalues λ_ℓ). For each subchannel we can use modulation and coding techniques of the usual SISO AWGN channel, for example, M-ary quadrature amplitude modulation (M-QAM) and low-density parity-check (LDPC) codes, with constellation sizes and code rates compatible with the capacity of the eigenmode (resulting also from power allocation).

Note that, if the channel has few strong eigenmodes (i.e., subchannels with large λ_ℓ) or if it is low rank, applying water-filling with small P_t implies to use few subchannels, turning off the eigenmodes with poor gains. In particular, if the difference between the largest eigenvalue and the next is large, and more precisely if

$$\frac{P_t}{\sigma^2} < \frac{1}{\lambda_2} - \frac{1}{\lambda_1}$$

then just one mode is used, resulting in the MIMO single mode beamforming of Chapter 16 (see Figure 17.4).

Here the complications are related to the channel estimation at the RX, to the way to obtain CSIT, and to power allocation [13].

For example, in closed-loop systems where the receiver estimates the channel and sends the channel state information (CSI) at the transmitter, the number of bits needed to quantize the matrix $\mathbf{V}$ with the necessary precision could be large, with a consequent throughput loss in the feedback channel. In this case, the ensemble of possible matrices is suitably quantized to form a small codebook of precoding matrices. Then, the receiver sends to the transmitter just the index (requiring few bits) of the matrix in the codebook which best approximates the estimated $\mathbf{V}$. If the codebook is well designed, the loss in performance due to quantization is justified by the reduction in the number of bits required for the feedback channel.

17.4.2 High-Throughput MIMO Systems with Channel Unknown at the Transmitter (Open-Loop MIMO)

If CSIT are not available the simplest way to have a high-throughput system is to transmit parallel independent (sub)streams over the N_T transmit antennas (like e.g., in vertical-Bell laboratories layered

space-time (V-BLAST)). The substreams are transmitted at the same time in the same frequency band, with an increase in the transmission rate proportional to the number of transmitter antennas.

The received signal is

$$\mathbf{y}(k) = \mathbf{H}\mathbf{x}(k) + \mathbf{n}(k) \tag{17.16}$$

where k is the time index, $\mathbf{x}(k)$ and $\mathbf{y}(k)$ are the input and output vectors, respectively. Also, note that the elements of $\mathbf{x}(k)$ are symbols from some constellation (e.g., M-QAM). The noise vectors $\mathbf{n}(k) \in \mathbb{C}^{N_R}$ are i.i.d. with CSCG entries and covariance matrix $\mathbf{R}_n = \mathbb{E}\left\{\mathbf{n}(k)\mathbf{n}^H(k)\right\} = \sigma^2\mathbf{I}$.

The decoder has to detect the transmitted symbols $x_1(k), \ldots, x_{N_T}(k)$ given the observed $\mathbf{y}(k)$. Assume that $\mathbf{H}$ is known at the receiver (CSIR).

Intuitively, if for a moment we neglect the noise, we see that Equation 17.16 reduces to the linear system $\mathbf{y}(k) = \mathbf{H}\mathbf{x}(k)$, where $\mathbf{y}(k)$, $\mathbf{H}$ are known, and $\mathbf{x}(k)$ is the unknown vector.

If the unknown vector $\mathbf{x}(k)$ is unconstrained (i.e., each symbol $x_\ell(k)$ can assume an arbitrary value in $\mathbb{C}$) then the system can be solved only if $N_R \geq N_T$ and $\mathbf{H}$ is full rank. The presence of the noise $\mathbf{n}(k)$ makes the problem much more difficult, and having a large N_R helps the decoding process. In any case, we see that a necessary condition for having a successful decoding with this scheme is that the channel matrix $\mathbf{H}$ is full rank. Clearly, this depends on several factors like richness of the multipath and antenna spacing. If the multipath is rich and independent from antenna to antenna, the elements of $\mathbf{H}$ take random independent values. In this case, the probability that two rows or columns of $\mathbf{H}$ are linearly dependent is essentially zero. So, for rich uncorrelated multipath we can say that the matrix $\mathbf{H}$ is almost surely full rank.

If the symbols $x_\ell(k)$ are taken in a given constellation (e.g., M-QAM), it is sometimes possible, by using ML decoding, to recover the transmitted vector $\mathbf{x}(k)$ even if $\mathbf{H}$ is not full rank. For example, with one receive antenna and no noise we have $y_1(k) = h_1 x_1(k) + \cdots + h_{N_T} x_{N_T}(k)$ which can be interpreted as a symbol in a constellation of M^{N_T} points corresponding to all possible symbols $x_1(k), \supset, x_{N_T}(k)$. If the h_i are such that these points are all distinct, from the single sample $y_1(k)$ we can recover all transmitted symbols.

17.4.2.1 ML Detection

The optimum detector, assuming the symbols $x_\ell(k)$ are i.i.d. and take values in a constellation $\mathcal{X}$ with cardinality $|\mathcal{X}| = M$ (e.g., M-QAM) with uniform probability, is based on maximum likelihood (ML) that, due to the Gaussian noise $\mathbf{n}$, reduces to the search, among all possible transmitted vectors $\mathbf{x} \in \mathcal{X}^{N_T}$, of the one producing $\mathbf{H}\mathbf{x}$ closer in Euclidean distance to the observed vector $\mathbf{y}(k)$, that is,

$$\hat{\mathbf{x}}(k) = \arg \min_{\mathbf{x} \in \mathcal{X}^{N_T}} \| \mathbf{H}\mathbf{x} - \mathbf{y}(k) \| \tag{17.17}$$

For each received vector $\mathbf{y}(k)$, the ML decoder must therefore test all M^{N_T} possible transmitted vectors $\mathbf{x}$. Thus, the complexity of ML decoding depends on the constellation size used and increases exponentially with the number of parallel streams. For example, for a 2×2 MIMO where two 4-QAM streams are transmitted in parallel, the ML decoder will make $M^{N_T} = 4^2 = 16$ [comparisons/decoded vector]. For a 4×4 MIMO where four 16-QAM streams are transmitted in parallel, the ML decoder will make $M^{N_T} = 16^4 = 65536$ [comparisons/decoded vector]. For this reason, for MIMO with a large number of parallel streams ML becomes too complex, and suboptimal decoders must be employed.

An example of performance (upper bound on the bit error probability (BEP)) for uncoded MIMO with ML decoding, obtained by using the method in Reference 14, is reported in Figure 17.13.

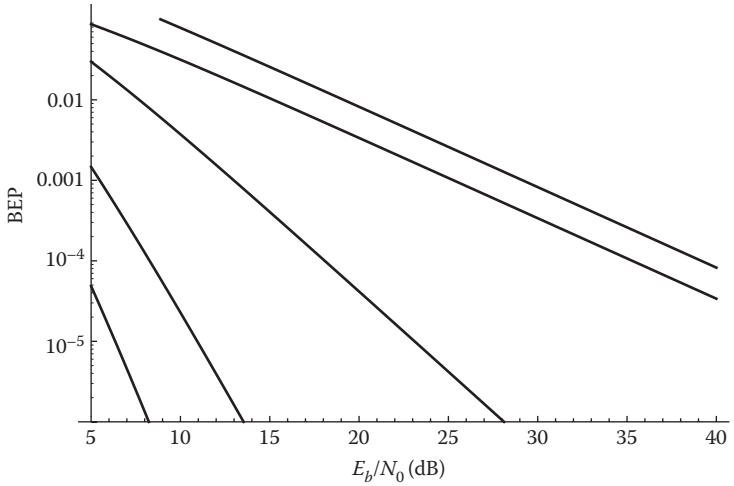

FIGURE 17.13 BEP upper bound versus E_b/N_0, uncoded VBLAST MIMO systems, QPSK, ML decoding, uncorrelated Rayleigh channel. From left to right, MIMO with $N_T \times N_R$ antennas: 6×6, 4×4, 2×2, 1×1, 2×1. The corresponding spectral efficiencies are 12,8,4,2,4 [bits/s/Hz].

17.4.2.2 Linear Detection

Assume we want a linear estimate $\hat{x}_1(k) = \mathbf{w}_1^H \mathbf{y}(k)$ of the symbol $x_1(k)$ transmitted from the first antenna. Then, we can consider this problem as the reception of a signal in the presence of interference, leading to the optimum combining or minimum mean-square error (MMSE) receiver of Chapter 16, where now $x_1(k)$ is the desired symbol, and $x_2(k), \supset, x_{N_T}(k)$ are interfering symbols. Thus, the optimal weights $\mathbf{w}_1$ are obtained by tuning the MMSE combiner to $x_1(k)$, considering $x_2(k), \supset, x_{N_T}(k)$ as interfering symbols. The MMSE weights are thus given by Equation 16.36 in Chapter 16, that is, $\mathbf{w}_1 = K\mathbf{R}_1^{-1}\mathbf{h}_1$ where $\mathbf{h}_1$ is the propagation vector from the first transmit antenna, i.e., the first column of $\mathbf{H}$, and $\mathbf{R}_1 = \sum_{m=2}^{N_T} \mathbb{E}\left\{ \left| x_m(k) \right|^2 \right\} \mathbf{h}_m \mathbf{h}_m^H + \sigma^2 \mathbf{I}$.

This can be done "in parallel" from the received vector $\mathbf{y}(k)$ for all transmit antennas, by considering, for each stream, the other antennas as interferers, that is, with weights:

$$\mathbf{w}_\ell = K\mathbf{R}_\ell^{-1}\mathbf{h}_\ell \tag{17.18}$$

where $\mathbf{h}_\ell$ is the ℓth column of $\mathbf{H}$, and $\mathbf{R}_\ell = \sum_{m=1, m\neq\ell}^{N_T} \mathbb{E}\left\{ \left| x_m(k) \right|^2 \right\} \mathbf{h}_m \mathbf{h}_m^H + \sigma^2 \mathbf{I}$ is the disturb covariance for the ℓth stream. The signal-to-interference-plus-noise ratio (SINR) for the ℓth estimate is $\mathbb{E}\left\{ \left| x_\ell(k) \right|^2 \right\} \mathbf{h}_\ell \mathbf{R}_\ell^{-1} \mathbf{h}_\ell^H$. The linear receiver as a bank of parallel combiners designed to mitigate interference as in Chapter 16 is sketched in Figure 17.14.

If we collect the weights $\mathbf{w}_\ell$ in a matrix $\mathbf{W} = [\mathbf{w}_1 \mid \cdots \mid \mathbf{w}_{N_T}]$, the MMSE linear estimate of the transmitted vector is

$$\hat{\mathbf{x}}(k) = \mathbf{W}^H \mathbf{y}(k) \tag{17.19}$$

It is possible to show that, assuming $\mathbf{R}_x = P_t/N_T \mathbf{I}$, the matrix $\mathbf{W}$ can be also directly derived as

$$\mathbf{W} = K\left(\mathbf{H}\mathbf{H}^H + \sigma^2 N_T/P_t \mathbf{I}\right)^{-1} \mathbf{H} = K\mathbf{H}\left(\mathbf{H}^H\mathbf{H} + \sigma^2 N_T/P_t \mathbf{I}\right)^{-1}.$$

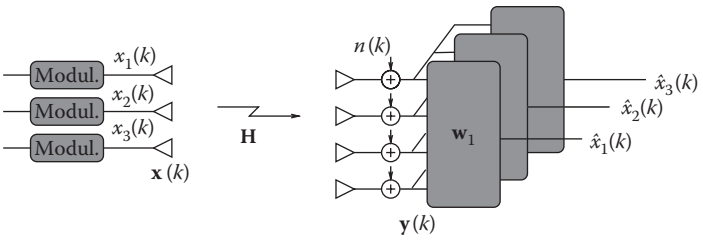

FIGURE 17.14 MMSE linear receiver as a bank of parallel MMSE combiners.

The complexity of linear detection is low: for each received vector we need to compute the matrix-vector product in Equation 17.19. The weights $\mathbf{W}$ are updated at the fading rate, which depends on user's mobility.

Instead of using the MMSE we can use a zero forcing (ZF) criterion, where the weighting vectors $\mathbf{w}_\ell$ are designed to null the interference: by using the matrix $\mathbf{W} = K\mathbf{H}(\mathbf{H}^H\mathbf{H})^{-1}$, which is the pseudo-inverse of $\mathbf{H}$, we obtain from Equations 17.19 and 17.17 $\mathbf{W}^H\mathbf{y}(k) = K\,\mathbf{x}(k) + \mathbf{W}^H\mathbf{n}(k)$, and the mutual interference is canceled. However, the noise can be enhanced with the ZF, and the MMSE detector is generally better.

17.4.2.3 Improving Linear Detection by SIC and Ordering

Observe that the contribution of $x_\ell(k)$ in $\mathbf{y}(k)$ is exactly $x_\ell(k)\mathbf{h}_\ell$. So, calculating $\mathbf{y}(k) - x_\ell(k)\mathbf{h}_\ell$ is like to cancel the ℓth transmit antenna. In successive interference cancellation, the linear estimate $\hat{x}_1(k) \in \mathbb{C}$ of the first stream is decoded producing the hard decision $\tilde{x}_1(k) \in \mathcal{X}$; then, the received vector is updated as $\mathbf{y}^{(1)}(k) = \mathbf{y}(k) - \tilde{x}_1(k)\mathbf{h}_1$. Assuming $\tilde{x}_1(k) = x_1(k)$ (correct decision on the first stream), for the second stream $x_2(k)$ the interferers are only the $N_T - 2$ remaining symbols $x_3(k), \supset, x_{N_T}(k)$. Thus, the weight vector $\mathbf{w}_2$ is calculated considering these as interfering symbols, and the process is iterated. The resulting scheme, reported in Figure 17.15, is denoted as MMSE-successive interference cancellation (SIC) or ZF-SIC depending on the criterion used for the weights.

SIC improves the performance of linear detection because, assuming previous decisions are correct, the ℓth stream will be detected in the presence of $N_T - \ell$ interfering symbols (those still not canceled), instead of the $N_T - 1$ of the linear detector. The most difficult decision is for the first stream, for which all $N_T - 1$ remaining symbols are to be considered as interferers.

Although the scheme suffers for the error propagation phenomenon, its performance is better than that of pure linear detection [15].

A further significant improvement is obtained by decoding first, among the N_T streams, that with the best SINR; then, after cancellation, by choosing, among the remaining $N_T - 1$ streams, that with the best SINR (assuming the first stream has been successfully canceled). The process is repeated until the last

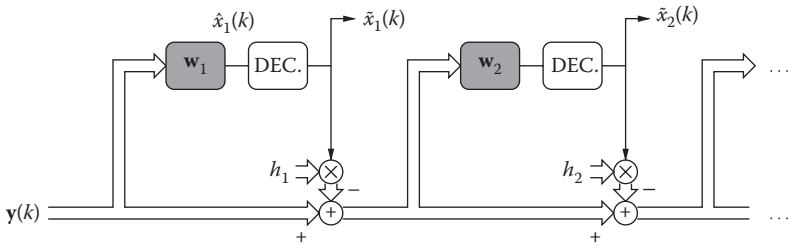

FIGURE 17.15 Linear detection with SIC. In SIC with ordering, the order of detection/cancellation of the streams depends on the channel state.

stream. This is called SIC with *ordering*, and its scheme is like in Figure 17.15, except that the order in which the streams are detected depends on the channel.

The ordering process improves the performance of linear detectors with SIC at the price of increased complexity, which however remains much lower than for ML. Although SIC and ordering improve the performance for low SNR, the diversity for all linear schemes with or without SIC and ordering is limited by $N_R - (N_T - 1)$, while the ML detector has diversity N_R.

In practice, ML detectors can be used in MIMO systems with few antennas, while reduced complexity suboptimal detectors (based e.g. on branch and bound, semidefinite relaxation, or SIC techniques) are suitable for increasingly larger systems [16,17].

In the above-described V-BLAST architecture, since the transmitted symbols are independent from one transmit antenna to another, the maximum diversity is N_R (which is, indeed, achieved by the ML detector). In order to exploit even transmit diversity, there must be some form of coding across the transmit antennas. A way to exploit transmit diversity is to rotate the symbol across the transmit antennas like in the diagonal-Bell laboratories layered space-time (D-BLAST) architecture. The diagonally layered architecture of D-BLAST requires encoding the transmitted symbol information along space-time diagonals. The advantage is that the full $N_T N_R$ diversity is exploited in such a diagonally layered architecture. However, decoding is based on SIC, and suffers from error propagation which may limit the number of transmitted streams. Moreover, with diagonal layering, some space-time resource is wasted at the start and end of a burst, and therefore the rate is reduced.

The big advantage of the described schemes is however that the complexity scales approximately linearly with the number of antennas. Therefore, it has been possible to demonstrate the feasibility of systems with very large numbers of antennas ($N_T > 10$), and spectral efficiencies of more than 25 [bits/s/Hz]. For smaller systems, transmit diversity can also be exploited by using an outer code, together with iterative demodulation and decoding.

17.5 Multiuser MIMO

Consider now a multiuser (MU)-MIMO scenario as in Figure 17.16, where two mobile users are connected to a base station.

17.5.1 Up-Link (Multiple-Access Channel)

Here, for the up-link (from users to base station, also called multiple access channel), since the users terminals are not connected, the situation is like for single user MIMO without CSIT. The users can thus

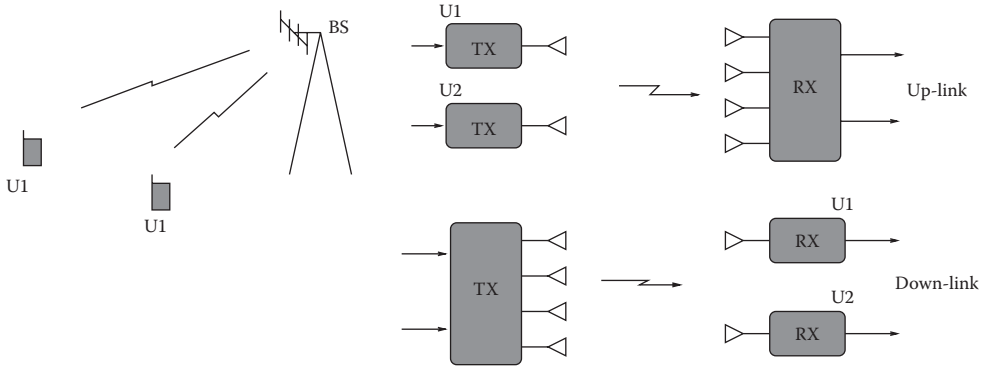

FIGURE 17.16 MU-MIMO scenario with two single-antenna mobile users (U1,U2), and a multiple-antennas base station (BS). MIMO interpretation of the uplink and of the downlink.

directly transmit their data streams, and the streams are jointly detected at the base station, for example, with an MMSE-SIC detector, as in Section 17.4.2. The advantage here is that two users transmit on the same frequency band at the same time. Since the multiple access is made possible by the use of antennas for discriminating the respective signals, this is sometimes called space division multiple access (SDMA). The scheme can be generalized to a number N of single-antenna users, provided that the base station has at least N antennas (see Section 17.4.2). If the number of users is larger, a properly chosen subset is allowed to transmit in each time-slot (*scheduling*). Note that, due to the spatial separation among the mobile users, the virtual MIMO consisting of the users and the multiple antennas at the base station is generally full rank even if the scattering is poor or in line-of-sight (LOS) propagation.

In a more general scenario, also the terminals may have multiple antennas. In this MIMO networks with no CSIT, the more antennas per terminal, the more difficult will be for the base station to perform joint detection (e.g., by MMSE-SIC). The optimum number of antennas per terminal in a MIMO network depends on the user's power levels and number of antennas at the base station [18].

17.5.2 Down-Link (Broadcast Channel)

The situation is more challenging for the down-link (sometimes called broadcast channel), since each user has available just one antenna output (and not all outputs as for the single-user MIMO). We might think of reusing some schemes from single-user MIMO. However, the techniques illustrated for single user-MIMO without CSIT (Section 17.4.2) are clearly not useful when the users' terminals are equipped with a single antenna. Even assuming that the base station has perfect knowledge of the channels (CSIT), schemes like those based on the SVD cannot be applied since each receiver works independently of the others.

The optimal transmit strategy is a techniques based on dirty paper coding, which however is difficult to implement in practical systems. Suboptimal techniques based on a combination of linear (beamforming (BF)) or nonlinear precoding (based e.g., on Tomlinson-Harashima precoding (THP)), together with scheduling strategies, are considered in practice.

With linear precoding (MU-MIMO BF, see Figure 17.17), a linear transformation is applied at the transmitter, so that the signals at the receivers have a given quality. Each user stream is coded independently, multiplied by a beamforming weight vector and transmitted through multiple antennas. The weight vectors are designed to reduce (or cancel) mutual interference among different streams by taking advantage of spatial separation to serve multiple users simultaneously (SDMA). Let us indicate by $x_\ell(k)$, $\ell = 1, \ldots, N_R$ the transmitted symbols at time k, where $x_\ell(k)$ is the symbol transmitted to user ℓ. If $\mathbf{w}_\ell$ is the beamforming weight for user ℓ, the received sample is $y_\ell(k) = \mathbf{h}_\ell \mathbf{w}_\ell x_\ell(k) + \mathbf{h}_\ell \sum_{m \neq \ell}^{N_R} \mathbf{w}_m x_m(k) + n_\ell(k)$, with $n_\ell(k)$ representing the noise sample. Given a set of weight vectors $\mathbf{w}_m$ and powers $\mathbb{E}\left\{ | x_m(k) |^2 \right\}$, the SINR at the ℓth receiver is

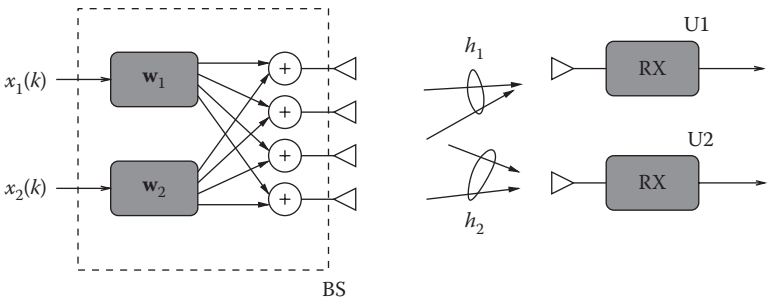

FIGURE 17.17 Linear precoding for the MU-MIMO downlink. Scenario with two single-antenna mobile users (U1,U2), and a four antennas base station (BS). For single-antenna terminals, the number of receive antennas N_R of the equivalent MIMO is equal to the number of users.

$$\mathrm{SINR}_\ell = \frac{\mathbb{E}\left\{|\, x_\ell(k)\,|^2\right\}|\, \mathbf{h}_\ell \mathbf{w}_\ell\,|^2}{\sum_{m\neq\ell}\mathbb{E}\left\{|\, x_m(k)\,|^2\right\}|\, \mathbf{h}_\ell \mathbf{w}_m\,|^2 + \sigma^2} \tag{17.20}$$

and the related sum rate is $R\left(\{\mathbf{w}_m\},\left\{\mathbb{E}\left\{|\, x_m(k)\,|^2\right\}\right\}\right) = \sum_{\ell=1}^{N_R}\log_2\left(1+\mathrm{SINR}_\ell\right)$. The vectors $\mathbf{w}_m$ and the powers $\mathbb{E}\left\{|\, x_m(k)\,|^2\right\}$ are then designed to satisfy some constraints. For example, we could aim to maximize the sum rate, subject to a constraint on the total transmitted power, or to satisfy a set of SINR constraints. Determining the optimal weights and powers is a difficult optimization problem in practice, especially for a large number of users.

A simplified approach is to design the weights to null the mutual interference at each receiver, eventually allocating the power levels. To this aim, let us write compactly all received signals as

$$\mathbf{y}(k) = \mathbf{H}\mathbf{W}\mathbf{x}(k) + \mathbf{n}(k) \tag{17.21}$$

where $\mathbf{h}_\ell$ are the rows of $\mathbf{H}\in\mathbb{C}^{N_R\times N_T}$, and $\mathbf{w}_\ell$ are the columns of the weighting matrix $\mathbf{W}\in\mathbb{C}^{N_T\times N_R}$. If $\mathbf{H}$ is rank N_R (the number of antennas N_T at the base station must be greater than the number of served users N_R), one simple approach could be to choose $\mathbf{W} = K\mathbf{H}^H(\mathbf{H}\mathbf{H}^H)^{-1}$, so that $\mathbf{y}(k) = K\mathbf{x}(k) + \mathbf{n}(k)$ and the signals do not interfere at the receivers. In other words, the weighting matrix for this zero forcing beamforming (ZFBF) approach is proportional to the (right) pseudoinverse of $\mathbf{H}$. We can then also allocate different powers $\mathbb{E}\left\{|\, x_m(k)\,|^2\right\}$ to the users, according to water-filling. The constant K is chosen to control the total transmitted power. This approach is not efficient when the users are not easily separable (i.e., when some of the eigenvalues of $\mathbf{H}\mathbf{H}^H$ are very small). If the number of users is large, the solution could be to choose to serve a subset N_T of users (*scheduling*) with orthogonal (as much as possible) propagation vectors $\mathbf{h}_\ell$, such that the approach previously described works well. Assuming rich scattering, the propagation vectors vary randomly and it is generally possible to find subsets of nearly orthogonal users; among these, the scheduler chooses the subset where the users have the largest SNRs. The possibility to choose among many users gives clear advantages to the whole system, and is called multiuser diversity effect. Due to multiuser diversity, it has been proved that the suboptimal ZFBF scheme approaches the sum rate of the optimal receiver under large number of users.

The design can be extended to the case when the user terminals are equipped with multiple antennas. In any case, resource allocation techniques and scheduling are essential in MU-MIMO [19,20].

17.6 Other Applications of MIMO: Cooperative Communications, Virtual MIMO, Distributed Antenna Systems

The techniques presented can be applied in a plurality of different contexts, where multiple antennas can be effectively co-located and connected to a terminal, or even not co-located if some form of cooperation is allowed, as already discussed in Chapter 16 on MIMO systems [1].

For example, in mobile cellular networks multiple base stations can be seen as a virtual MIMO system, provided that the stations can cooperate, with improvements in terms of diversity and capacity. A similar situation arises in cooperative networks, where the relay stations can be seen as distributed antenna elements. In general, virtual antenna arrays can be realized, for example, to reduce the effects of correlation and spatial limitations.

There are many examples of distributed antenna systems in the recent literature, for which the reader is referred to the bibliography. We describe in the following an original proposal called wireless Remote ANtenna Elements system (WRANE) which is especially suited to overcome, by means of a specific Body Area Network, the space limitation in mobile terminals.

17.6.1 Wireless Remote Antenna Elements Systems (WRANE)

The advantages of using multiple elements antennas are strictly related to the possibility of receiving signals at the various antenna elements experiencing independent, as much as possible, fading levels. In receiver diversity systems the presence of strong correlation removes the benefits of using multiple antennas. The same is true for high-capacity MIMO links [8]. For this reason, the antenna elements must be spaced from few to many wavelengths, depending on the scattering environment, to have low correlation among fading levels over the antenna elements. This is sometimes not possible: for example, a mobile terminal station has dimensions that usually do not allow to place elements spaced more than a wavelength, and therefore spatial antenna diversity is intrinsically limited by the terminal geometric dimensions.

To overcome the spatial limitation on a generic wireless terminal we can devise a WRANE: the key idea is to make use of remote antenna elements that are connected to the main wireless terminal through a dedicated short-range wireless link. With this approach, the wireless antenna elements can be placed far enough from each other and from the main wireless terminal to achieve sufficient uncorrelation. Each antenna element receives the signal from the far transmitter, and sends this signal to the main receiver through a dedicated, short-range link (using, e.g., wideband signals). The same remote antennas can be used as transmitting units, for the reverse link, and to build MIMO systems, with low correlation among the remote antenna elements.

Acronyms

AWGN	Additive White Gaussian Noise
BEP	Bit error probability
BF	Beamforming
BFC	Block fading channel
CSCG	Circularly-symmetric complex Gaussian
CSI	Channel state information
CSIR	Channel state information at the receiver
CSIT	Channel state information at the transmitter
D-BLAST	Diagonal-Bell laboratories layered space-time
DSL	Digital subscriber line
FEC	Forward error correction
i.i.d.	Independent, identically distributed
LDPC	Low-density parity-check
LOS	Line-of-sight
MIMO	Multiple-input multiple-output
MISO	Multiple-input single-output
ML	Maximum likelihood
MMSE	Minimum mean-square error
M-QAM	*M*-ary quadrature amplitude modulation
MU	Multiuser
PLC	Power line communication
SDMA	Space division multiple access
SIC	Successive interference cancellation
SIMO	Single-input multiple-output
SINR	Signal-to-interference plus noise ratio
SISO	Single-input single-output
SNR	Signal-to-noise ratio
SVD	Singular values decomposition
THP	Tomlinson-Harashima precoding

V-BLAST	Vertical-Bell laboratories layered space-time
ZF	Zero forcing
ZFBF	Zero forcing beamforming

References

1. J. H. Winters, On the capacity of radio communication systems with diversity in Rayleigh fading environment, *IEEE J. Select. Areas Commun.*, SAC-5(5), 871–878, 1987.
2. G. J. Foschini, Layered space-time architecture for wireless communication a fading environment when using multiple antennas, *Bell Labs Tech. J.*, 1(2), 41–59, 1996.
3. G. J. Foschini and M. J. Gans, On limits of wireless communications in a fading environment when using multiple antennas, *Wireless Personal Commun.*, 6(3), 311–335, 1998.
4. E. Telatar, Capacity of multi-antenna Gaussian channels, *Europ. Trans. on Telecomm.*, 10(6), 585–595, 1999.
5. A. Goldsmith, *Wireless Communications*. Cambridge University Press, New York, 2005.
6. D. Tse and P. Viswanath, *Fundamentals of Wireless Communication*. Cambridge University Press, New York, 2006.
7. A. Molisch, *Wireless Communications*. Wiley, John Wiley & Sons, England, 2011.
8. M. Chiani, M. Z. Win, and A. Zanella, On the capacity of spatially correlated MIMO Rayleigh fading channels, *IEEE Trans. Inform. Theory*, 49(10), 2363–2371, 2003.
9. P. J. Smith, S. Roy, and M. Shafi, Capacity of MIMO systems with semicorrelated flat fading, *IEEE Trans. Inform. Theory*, 49(10), 2781–2788, 2003.
10. H. Shin, M. Win, J. H. Lee, and M. Chiani, On the capacity of doubly correlated MIMO channels, *IEEE Trans. Wireless Commun.*, 5(8), 2253–2266, 2006.
11. M. McKay and I. Collings, General capacity bounds for spatially correlated Rician MIMO channels, *Information Theory, IEEE Transactions on*, 51(9), 3121–3145, 2005.
12. S. Jayaweera and H. Poor, Capacity of multiple-antenna systems with both receiver and transmitter channel state information, *Information Theory, IEEE Transactions on*, 49(10), 2697–2709, 2003.
13. A. Zanella and M. Chiani, Analytical comparison of power allocation methods in MIMO systems with singular value decomposition, in *Proc. IEEE Global Telecomm. Conf.*, Honolulu, HI, Nov./Dec. 2009, pp. 101–106.
14. M. Chiani, D. Dardari, and M. K. Simon, New exponential bounds and approximations for the computation of error probability in fading channels, *IEEE Trans. Wireless Commun.*, 2(4), 840–845, 2003.
15. A. Zanella, M. Chiani, and M. Z. Win, MMSE reception and successive interference cancellation for MIMO systems with high spectral efficiency, *IEEE Trans. Wireless Commun.*, 4(3), 1244–1253, 2005.
16. M. Damen, H. El Gamal, and G. Caire, On maximum-likelihood detection and the search for the closest lattice point, *IEEE Trans. on Information Theory,* 49(10), 2389–2402, 2003.
17. Z. Luo, W. Ma, A. So, Y. Ye, and S. Zhang, Semidefinite relaxation of quadratic optimization problems, *Signal Process. Mag., IEEE*, 27(3), 20–34, 2010.
18. M. Chiani, M. Z. Win, and H. Shin, MIMO networks: the effects of interference, *IEEE Trans. Inf. Theory*, 56(1), 336–349, 2010.
19. Q. Spencer, C. Peel, A. Swindlehurst, and M. Haardt, An introduction to the multi-user MIMO downlink, *Commun. Mag., IEEE*, 42(10), 60–67, 2004.
20. D. Gesbert, M. Kountouris, R. Heath, C.-B. Chae, and T. Salzer, Shifting the MIMO Paradigm, *Signal Process. Mag., IEEE*, 24(5), 36–46, 2007.

18

Digital Communication System Performance*

Bernard Sklar

18.1 Introduction

In this section, we examine some fundamental trade-offs among bandwidth, power, and error performance of digital communication systems. The criteria for choosing modulation and coding schemes, based on whether a system is bandwidth limited or power limited, are reviewed for several system examples. Emphasis is placed on the subtle, but straightforward, relationships we encounter when transforming from data bits to channel bits to symbols to chips.

The design or definition of any digital communication system begins with a description of the communication link. The *link* is the name given to the communication transmission path from the modulator and transmitter, through the channel, and up to and including the receiver and demodulator. The *channel*

* A version of this chapter has appeared in the *IEEE Communications Magazine*, November 1993, under the title "Defining, Designing, and Evaluating Digital Communication Systems." A version of this chapter also appears in the book *Digital Communications Fundamentals and Applications*, 2nd edition, Chapter 9, by Bernard Sklar, Prentice-Hall 2001.

is the name given to the propagating medium between the transmitter and receiver. A link description quantifies the average signal power that is received, the available bandwidth, the noise statistics, and other impairments, such as fading. Also needed to define the system are basic requirements, such as the data rate to be supported and the error performance.

18.1.1 The Channel

For radio communications, the concept of *free space* assumes a channel region free of all objects that might affect radio frequency (RF) propagation by absorption, reflection, or refraction. It further assumes that the atmosphere in the channel is perfectly uniform and nonabsorbing, and that the earth is infinitely far away or its reflection coefficient is negligible. The RF energy arriving at the receiver is assumed to be a function of distance from the transmitter (simply following the inverse-square law of optics). In practice, of course, propagation in the atmosphere and near the ground results in refraction, reflection, and absorption, which modify the free space transmission.

18.1.2 The Link

A radio transmitter is characterized by its average output signal power P_t and the gain of its transmitting antenna G_t. The name given to the product P_tG_t, with reference to an isotropic antenna is *effective radiated power* (EIRP) in watts (or dBW). The predetection average signal power S arriving at the output of the receiver antenna can be described as a function of the EIRP, the gain of the receiving antenna G_r, the path loss (or space loss) L_s, and other losses L_o as follows [14,15]:

$$S = \frac{\text{EIRP}\, G_r}{L_s L_o} \tag{18.1}$$

The path loss L_s can be written as follows [15]:

$$L_s = \left(\frac{4\pi d}{\lambda}\right)^2 \tag{18.2}$$

where d is the distance between the transmitter and receiver and λ is the wavelength.

We restrict our discussion to those links corrupted by the mechanism of additive white Gaussian noise (AWGN) only. Such a noise assumption is a very useful model for a large class of communication systems. A valid approximation for average received noise power N that this model introduces is written as follows [5,9]:

$$N \cong kT^\circ W \tag{18.3}$$

where k is Boltzmann's constant (1.38×10^{-23} J/K), T° is effective temperature in kelvin, and W is bandwidth in hertz. Dividing Equation 18.3 by bandwidth enables us to write the received noise-power spectral density N_0 as follows:

$$N_0 = \frac{N}{W} = kT^\circ \tag{18.4}$$

Dividing Equation 18.1 by N_0 yields the received average signal-power to noise-power spectral density S/N_0 as

$$\frac{S}{N_0} = \frac{\text{EIRP}\ G_r/T^\circ}{k\,L_s\,L_o} \tag{18.5}$$

where G_r/T° is often referred to as the receiver figure of merit. A link budget analysis is a compilation of the power gains and losses throughout the link; it is generally computed in decibels, and thus takes on the bookkeeping appearance of a business enterprise, highlighting the assets and liabilities of the link. Once the value of S/N_0 is specified or calculated from the link parameters, we then shift our attention to optimizing the choice of signaling types for meeting system bandwidth and error performance requirements.

Given the received S/N_0, we can write the received bit-energy to noise-power spectral density E_b/N_0, for any desired data rate R, as follows:

$$\frac{E_b}{N_0} = \frac{ST_b}{N_0} = \frac{S}{N_0}\left(\frac{1}{R}\right) \tag{18.6}$$

Equation 18.6 follows from the basic definitions that received bit energy is equal to received average signal power times the bit duration and that bit rate is the reciprocal of bit duration. Received E_b/N_0 is a key parameter in defining a digital communication system. Its value indicates the apportionment of the received waveform energy among the bits that the waveform represents. At first glance, one might think that a system specification should entail the symbol-energy to noise-power spectral density E_s/N_0 associated with the arriving waveforms. We will show, however, that for a given S/N_0 the value of E_s/N_0 is a function of the modulation and coding. The reason for defining systems in terms of E_b/N_0 stems from the fact that E_b/N_0 depends only on S/N_0 and R and is unaffected by any system design choices, such as modulation and coding.

18.2 Bandwidth and Power Considerations

Two primary communications resources are the received power and the available transmission bandwidth. In many communication systems, one of these resources may be more precious than the other and, hence, most systems can be classified as either bandwidth limited or power limited. In bandwidth-limited systems, spectrally efficient modulation techniques can be used to save bandwidth at the expense of power; in power-limited systems, power-efficient modulation techniques can be used to save power at the expense of bandwidth. In both bandwidth- and power-limited systems, error-correction coding (often called channel coding) can be used to save power or to improve error performance at the expense of bandwidth. Trellis-coded modulation (TCM) schemes can be used to improve the error performance of bandwidth-limited channels without any increase in bandwidth [17], but these methods are beyond the scope of this chapter.

18.2.1 The Bandwidth Efficiency Plane

Figure 18.1 shows the abscissa as the ratio of bit-energy to noise-power spectral density E_b/N_0 (in decibels) and the ordinate as the ratio of throughput, R (in bits per second), which can be transmitted per hertz in a given bandwidth W. The ratio R/W is called bandwidth efficiency, since it reflects how efficiently the bandwidth resource is utilized. The plot stems from the Shannon–Hartley capacity theorem [12,13,15], which can be stated as

$$C = W\log_2\left(1 + \frac{S}{N}\right) \tag{18.7}$$

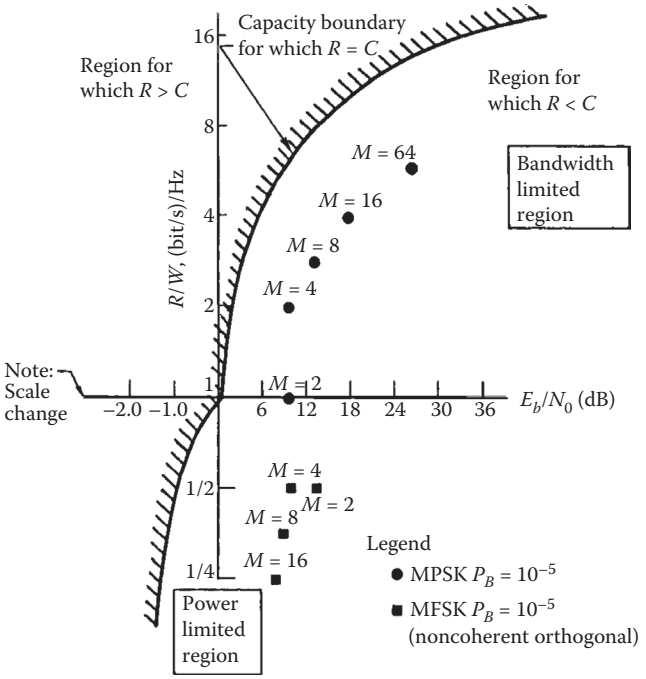

FIGURE 18.1 Bandwidth-efficiency plane.

where S/N is the ratio of received average signal power to noise power. When the logarithm is taken to the base 2, the capacity C, is given in bits per second. The capacity of a channel defines the maximum number of bits that can be reliably sent per second over the channel. For the case where the data (information) rate R is equal to C, the curve separates a region of practical communication systems from a region where such communication systems cannot operate reliably [12,15].

18.2.2 *M*-ary Signaling

Each symbol in an M-ary alphabet can be related to a unique sequence of m bits, expressed as

$$M = 2^m \quad \text{or} \quad m = \log_2 M \tag{18.8}$$

where M is the size of the alphabet. In the case of digital transmission, the term "symbol" refers to the member of the M-ary alphabet that is transmitted during each symbol duration T_s. To transmit the symbol, it must be mapped onto an electrical voltage or current waveform. Because the waveform represents the symbol, the terms symbol and waveform are sometimes used interchangeably. Since one of M symbols or waveforms is transmitted during each symbol duration T_s, the data rate R in bits per second can be expressed as

$$R = \frac{m}{T_s} = \frac{\log_2 M}{T_s} \tag{18.9}$$

Data-bit-time duration is the reciprocal of data rate. Similarly, symbol-time duration is the reciprocal of symbol rate. Therefore, from Equation 18.9, we write that the effective time duration T_b of each bit in terms of the symbol duration T_s or the symbol rate R_s is

$$T_b = \frac{1}{R} = \frac{T_s}{m} = \frac{1}{mR_s} \tag{18.10}$$

Then, using Equations 18.8 and 18.10, we can express the symbol rate R_s in terms of the bit rate R as follows:

$$R_s = \frac{R}{\log_2 M} \tag{18.11}$$

From Equations 18.9 and 18.10, any digital scheme that transmits $m = \log_2 M$ bits in T_s seconds, using a bandwidth of W hertz, operates at a bandwidth efficiency of

$$\frac{R}{W} = \frac{\log_2 M}{WT_s} = \frac{1}{WT_b} \quad \text{(b/s)/Hz} \tag{18.12}$$

where T_b is the effective time duration of each data bit.

18.2.3 Bandwidth-Limited Systems

From Equation 18.12, the smaller the WT_b product, the more bandwidth efficient will be any digital communication system. Thus, signals with small WT_b products are often used with bandwidth-limited systems. For example, the European digital mobile telephone system known as Global System for Mobile Communications (GSM) uses Gaussian minimum shift keying (GMSK) modulation having a WT_b product equal to 0.3 Hz/(b/s), where W is the 3 dB bandwidth of a Gaussian filter [4].

For uncoded bandwidth-limited systems, the objective is to maximize the transmitted information rate within the allowable bandwidth, at the expense of E_b/N_0 (while maintaining a specified value of bit-error probability P_B). The operating points for coherent M-ary phase-shift keying (MPSK) at $P_B = 10^{-5}$ are plotted on the bandwidth-efficiency plane of Figure 18.1. We assume Nyquist (ideal rectangular) filtering at baseband [10]. Thus, for MPSK, the required double-sideband (DSB) bandwidth at an intermediate frequency (IF) is related to the symbol rate as follows:

$$W = \frac{1}{T_s} = R_s \tag{18.13}$$

where T_s is the symbol duration and R_s is the symbol rate. The use of Nyquist filtering results in the minimum required transmission bandwidth that yields zero intersymbol interference; such ideal filtering gives rise to the name Nyquist minimum bandwidth.

From Equations 18.12 and 18.13, the bandwidth efficiency of MPSK-modulated signals using Nyquist filtering can be expressed as

$$R/W = \log_2 M \,(\text{b/s})/\text{Hz} \tag{18.14}$$

The MPSK points in Figure 18.1 confirm the relationship shown in Equation 18.14. Note that MPSK modulation is a bandwidth-efficient scheme. As M increases in value, R/W also increases. MPSK modulation can be used for realizing an improvement in bandwidth efficiency at the cost of increased E_b/N_0. Although beyond the scope of this chapter, many highly bandwidth-efficient modulation schemes have been investigated [1].

18.2.4 Power-Limited Systems

Operating points for noncoherent orthogonal M-ary frequency shift keying (FSK) (MFSK) modulation at $P_B = 10^{-5}$ are also plotted on Figure 18.1. For MFSK, the IF minimum bandwidth is as follows [15]:

$$W = \frac{M}{T_s} = MR_s \tag{18.15}$$

where T_s is the symbol duration and R_s is the symbol rate. With MFSK, the required transmission bandwidth is expanded M-fold over binary FSK since there are M different orthogonal waveforms, each requiring a bandwidth of $1/T_s$. Thus, from Equations 18.12 and 18.15, the bandwidth efficiency of noncoherent orthogonal MFSK signals can be expressed as

$$\frac{R}{W} = \frac{\log_2 M}{M} \text{ (b/s)/Hz} \tag{18.16}$$

The MFSK points plotted in Figure 18.1 confirm the relationship shown in Equation 18.16. Note that MFSK modulation is a bandwidth-expansive scheme. As M increases, R/W decreases. MFSK modulation can be used for realizing a reduction in required E_b/N_0 at the cost of increased bandwidth.

In Equations 18.13 and 18.14 for MPSK, and Equations 18.15 and 18.16 for MFSK, and for all the points plotted in Figure 18.1, ideal filtering has been assumed. Such filters are not realizable! For realistic channels and waveforms, the required transmission bandwidth must be increased in order to account for realizable filters.

In the examples that follow, we will consider radio channels that are disturbed only by AWGN and have no other impairments, and for simplicity, we will limit the modulation choice to constant-envelope types, that is, either MPSK or noncoherent orthogonal MFSK. For an uncoded system, MPSK is selected if the channel is bandwidth limited, and MFSK is selected if the channel is power limited. When error-correction coding is considered, modulation selection is not as simple because coding techniques can provide power-bandwidth trade-offs more effectively than would be possible through the use of any M-ary modulation scheme considered in this chapter [3].

In the most general sense, M-ary signaling can be regarded as a waveform-coding procedure, that is, when we select an M-ary modulation technique instead of a binary one, we in effect have replaced the binary waveforms with better waveforms—either better for bandwidth performance (MPSK) or better for power performance (MFSK). Even though orthogonal MFSK signaling can be thought of as being a coded system, that is, a first-order Reed–Muller code [8], we restrict our use of the term "coded system" to those traditional error-correction codes using redundant bits, for example, block codes or convolutional codes.

18.2.5 Minimum Bandwidth Requirements for MPSK and MFSK Signaling

The basic relationship between the symbol (or waveform) transmission rate R_s and the data rate R was shown in Equation 18.11. Using this relationship together with Equations 18.13 through 18.16 and $R = 9600$ b/s, a summary of symbol rate, minimum bandwidth, and bandwidth efficiency for MPSK and noncoherent orthogonal MFSK was compiled for $M = 2$, 4, 8, 16, and 32 (Table 18.1). Values of E_b/N_0 required to achieve a bit-error probability of 10^{-5} for MPSK and MFSK are also given for each value of M. These entries (which were computed using relationships that are presented later in this chapter) corroborate the trade-offs shown in Figure 18.1. As M increases, MPSK signaling provides more bandwidth efficiency at the cost of increased $E_b/N_{0,}$ whereas MFSK signaling allows for a reduction in E_b/N_0 at the cost of increased bandwidth.

TABLE 18.1 Symbol Rate, Minimum Bandwidth, Bandwidth Efficiency, and Required E_b/N_0 for MPSK and Noncoherent Orthogonal MFSK Signaling at 9600 bit/s

M	m	R (b/s)	R_s (symbol/s)	MPSK Minimum Bandwidth (Hz)	MPSK R/W	MPSK E_b/N_0 (dB) $P_B = 10^{-5}$	Noncoherent Orthogonal MFSK Minimum Bandwidth (Hz)	MFSK R/W	MFSK E_b/N_0 (dB) $P_B = 10^{-5}$
2	1	9600	9600	9600	1	9.6	19,200	1/2	13.4
4	2	9600	4800	4800	2	9.6	19,200	1/2	10.6
8	3	9600	3200	3200	3	13.0	25,600	3/8	9.1
16	4	9600	2400	2400	4	17.5	38,400	1/4	8.1
32	5	9600	1920	1920	5	22.4	61,440	5/32	7.4

18.3 Example 1: Bandwidth-Limited Uncoded System

Suppose we are given a bandwidth-limited AWGN radio channel with an available bandwidth of $W = 4000$ Hz. Also, suppose that the link constraints (transmitter power, antenna gains, path loss, etc.) result in the ratio of received average signal-power to noise-power spectral density S/N_0 being equal to 53 dB-Hz. Let the required data rate R be equal to 9600 b/s, and let the required bit-error performance P_B be at most 10^{-5}. The goal is to choose a modulation scheme that meets the required performance. In general, an error-correction coding scheme may be needed if none of the allowable modulation schemes can meet the requirements. In this example, however, we shall find that the use of error-correction coding is not necessary.

18.3.1 Solution to Example 1

For any digital communication system, the relationship between received S/N_0 and received bit-energy to noise-power spectral density E_b/N_0 was given in Equation 18.6 and is briefly rewritten as

$$\frac{S}{N_0} = \frac{E_b}{N_0} R \tag{18.17}$$

Solving for E_b/N_0 in decibels, we obtain

$$\begin{aligned} \frac{E_b}{N_0}(\text{dB}) &= \frac{S}{N_0}(\text{dB-Hz}) - R\,(\text{dB-b/s}) \\ &= 53\ \text{dB-Hz} - (10 \times \log_{10} 9600)\ \text{dB-b/s} \\ &= 13.2\ \text{dB (or 20.89)} \end{aligned} \tag{18.18}$$

Since the required data rate of 9600 b/s is much larger than the available bandwidth of 4000 Hz, the channel is bandwidth limited. We therefore select MPSK as our modulation scheme. We have confined the possible modulation choices to be constant-envelope types; without such a restriction, we would be able to select a modulation type with greater bandwidth efficiency. To conserve power, we compute *smallest possible* value of M such that the MPSK minimum bandwidth does not exceed the available bandwidth of 4000 Hz. Table 18.1 shows that the smallest value of M meeting this requirement is $M = 8$. Next, we determine whether the required bit-error performance of $P_B \leq 10^{-5}$ can be met by using 8-PSK

modulation alone or whether it is necessary to use an error-correction coding scheme. Table 18.1 shows that 8-PSK alone will meet the requirements, since the required E_b/N_0 listed for 8-PSK is less than the received E_b/N_0 derived in Equation 18.18. Let us imagine that we do not have Table 18.1, however, and evaluate whether or not error-correction coding is necessary.

Figure 18.2 shows the basic modulator/demodulator (MODEM) block diagram summarizing the functional details of this design. At the modulator, the transformation from data bits to symbols yields an output symbol rate R_s, that is, a factor $\log_2 M$ smaller than the input data-bit rate R, as is seen in Equation 18.11. Similarly, at the input to the demodulator, the symbol-energy to noise-power spectral density E_s/N_0 is a factor $\log_2 M$ larger than E_b/N_0, since each symbol is made up of $\log_2 M$ bits. Because E_s/N_0 is larger than E_b/N_0 by the same factor that R_s is smaller than R, we can expand Equation 18.17 as follows:

$$\frac{S}{N_0} = \frac{E_b}{N_0} R = \frac{E_s}{N_0} R_s \tag{18.19}$$

The demodulator receives a waveform (in this example, one of $M = 8$ possible phase shifts) during each time interval T_s. The probability that the demodulator makes a symbol error $P_E(M)$ is well approximated by the following equation for $M > 2$ [6]:

$$P_E(M) \cong 2Q\left[\sqrt{\frac{2E_s}{N_0}} \sin\left(\frac{\pi}{M}\right)\right] \tag{18.20}$$

where $Q(x)$, sometimes called the complementary error function, represents the probability under the tail of a zero-mean unit-variance Gaussian density function. It is defined as follows [18]:

$$Q(x) = \frac{1}{\sqrt{2\pi}} \int_x^\infty \exp\left(-\frac{u^2}{2}\right) du \tag{18.21}$$

A good approximation for $Q(x)$, valid for $x > 3$, is given by the following equation [2]:

$$Q(x) \cong \frac{1}{x\sqrt{2\pi}} \exp\left(-\frac{x^2}{2}\right) \tag{18.22}$$

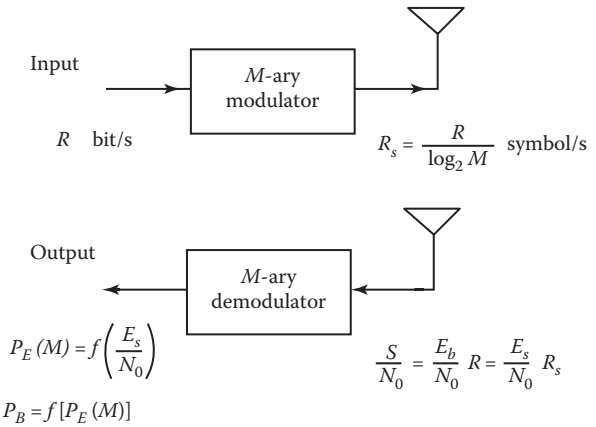

FIGURE 18.2 Basic modulator/demodulator (MODEM) without channel coding.

In Figure 18.2 and all of the figures that follow, rather than show explicit probability relationships, the generalized notation $f(x)$ has been used to indicate some functional dependence on x.

A traditional way of characterizing communication efficiency in digital systems is in terms of the received E_b/N_0 in decibels. This E_b/N_0 description has become standard practice, but recall that there are no bits at the input to the demodulator; there are only waveforms that have been assigned bit meanings. The received E_b/N_0 represents a bit-apportionment of the arriving waveform energy.

To solve for $P_E(M)$ in Equation 18.20, we first need to compute the ratio of received symbol-energy to noise-power spectral density E_s/N_0. Since from Equation 18.18

$$\frac{E_b}{N_0} = 13.2\,\text{dB}\,(\text{or}\,20.89)$$

and because each symbol is made up of $\log_2 M$ bits, we compute the following using $M = 8$:

$$\frac{E_s}{N_0} = (\log_2 M)\frac{E_b}{N_0} = 3 \times 20.89 = 62.67 \tag{18.23}$$

Using the results of Equation 18.23 in Equation 18.20, yields the symbol-error probability $P_E = 2.2 \times 10^{-5}$. To transform this to bit-error probability, we use the relationship between bit-error probability P_B and symbol-error probability P_E, for multiple-phase signaling [8] for $P_E \ll 1$ as follows:

$$P_B \cong \frac{P_E}{\log_2 M} = \frac{P_E}{m} \tag{18.24}$$

which is a good approximation when Gray coding is used for the bit-to-symbol assignment [6]. This last computation yields $P_B = 7.3 \times 10^{-6}$, which meets the required bit-error performance. No error-correction coding is necessary, and 8-PSK modulation represents the design choice to meet the requirements of the bandwidth-limited channel, which we had predicted by examining the required E_b/N_0 values in Table 18.1.

18.4 Example 2: Power-Limited Uncoded System

Now, suppose that we have exactly the same data rate and bit-error probability requirements as in Example 1, but let the available bandwidth W be equal to 45 kHz, and the available S/N_0 be equal to 48 dB-Hz. The goal is to choose a modulation or modulation/coding scheme that yields the required performance. We shall again find that error-correction coding is not required.

18.4.1 Solution to Example 2

The channel is clearly not bandwidth limited since the available bandwidth of 45 kHz is more than adequate for supporting the required data rate of 9600 bit/s. We find the received E_b/N_0 from Equation 18.18 as follows:

$$\frac{E_b}{N_0}(\text{dB}) = 48\,\text{dB-Hz} - (10 \times \log_{10} 9600)\,\text{dB-b/s} = 8.2\,\text{dB}\,(\text{or}\,6.61) \tag{18.25}$$

Since there is abundant bandwidth but a relatively small E_b/N_0 for the required bit-error probability, we consider that this channel is power limited and choose MFSK as the modulation scheme. To conserve

power, we search for the *largest possible M* such that the MFSK minimum bandwidth is not expanded beyond our available bandwidth of 45 kHz. A search results in the choice of $M = 16$ (Table 18.1). Next, we determine whether the required error performance of $P_B \leq 10^{-5}$ can be met by using 16-FSK alone, that is, without error-correction coding. Table 18.1 shows that 16-FSK alone meets the requirements, since the required E_b/N_0 listed for 16-FSK is less than the received E_b/N_0 derived in Equation 18.25. Let us imagine again that we do not have Table 18.1, and evaluate whether or not error-correction coding is necessary.

The block diagram in Figure 18.2 summarizes the relationships between symbol rate R_s and bit rate R, and between E_s/N_0 and E_b/N_0, which is identical to each of the respective relationships in Example 1. The 16-FSK demodulator receives a waveform (one of 16 possible frequencies) during each symbol time interval T_s. For noncoherent orthogonal MFSK, the probability that the demodulator makes a symbol error $P_E(M)$ is approximated by the following upper bound [19]:

$$P_E(M) \leq \frac{M-1}{2}\exp\left(-\frac{E_s}{2N_0}\right) \tag{18.26}$$

To solve for $P_E(M)$ in Equation 18.26, we compute E_s/N_0 as in Example 1. Using the results of Equation 18.25 in Equation 18.23, with $M = 16$, we get

$$\frac{E_s}{N_0} = (\log_2 M)\frac{E_b}{N_0} = 4 \times 6.61 = 26.44 \tag{18.27}$$

Next, using the results of Equation 18.27 in Equation 18.26 yields the symbol-error probability $P_E = 1.4 \times 10^{-5}$. To transform this to bit-error probability, P_B, we use the relationship between P_B and P_E for orthogonal signaling [19], given by

$$P_B = \frac{2^{m-1}}{(2^m - 1)}P_E \tag{18.28}$$

This last computation yields $P_B = 7.3 \times 10^{-6}$, which meets the required bit-error performance. Thus, we can meet the given specifications for this power-limited channel by using 16-FSK modulation, without any need for error-correction coding, as we had predicted by examining the required E_b/N_0 values in Table 18.1.

18.5 Example 3: Bandwidth-Limited and Power-Limited Coded System

We start with the same channel parameters as in Example 1 ($W = 4000$ Hz, $S/N_0 = 53$ dB-Hz, and $R = 9600$ b/s), with one exception.

In this example, we specify that P_B must be at most 10^{-9}. Table 18.1 shows that the system is both bandwidth limited and power limited, based on the available bandwidth of 4000 Hz and the available E_b/N_0 of 13.2 dB, from Equation 18.18; 8-PSK is the only possible choice to meet the bandwidth constraint; however, the available E_b/N_0 of 13.2 dB is certainly insufficient to meet the required P_B of 10^{-9}. For this small value of P_B, we need to consider the performance improvement that error-correction coding can provide within the available bandwidth. In general, one can use convolutional codes or block codes.

The Bose–Chaudhuri–Hocquenghem (BCH) codes form a large class of powerful error-correcting cyclic (block) codes [7]. To simplify the explanation, we shall choose a block code from the BCH family. Table 18.2 presents a partial catalog of the available BCH codes in terms of n, k, and t, where k represents

TABLE 18.2 BCH Codes (Partial Catalog)

n	k	t
7	4	1
15	11	1
	7	2
	5	3
31	26	1
	21	2
	16	3
	11	5
63	57	1
	51	2
	45	3
	39	4
	36	5
	30	6
127	120	1
	113	2
	106	3
	99	4
	92	5
	85	6
	78	7
	71	9
	64	10

the number of information (or data) bits that the code transforms into a longer block of n coded bits (or channel bits), and t represents the largest number of incorrect channel bits that the code can correct within each n-sized block. The rate of a code is defined as the ratio k/n; its inverse represents a measure of the code's redundancy [7].

18.5.1 Solution to Example 3

Since this example has the same bandwidth-limited parameters given in Example 1, we start with the same 8-PSK modulation used to meet the stated bandwidth constraint. We now employ error-correction coding, however, so that the bit-error probability can be lowered to $P_B \leq 10^{-9}$.

To make the optimum code selection from Table 18.2, we are guided by the following goals:

1. The output bit-error probability of the combined modulation/coding system must meet the system error requirement.
2. The rate of the code must not expand the required transmission bandwidth beyond the available channel bandwidth.
3. The code should be as simple as possible. Generally, the shorter the code, the simpler will be its implementation.

The uncoded 8-PSK minimum bandwidth requirement is 3200 Hz (Table 18.1) and the allowable channel bandwidth is 4000 Hz, and so the uncoded signal bandwidth can be increased by no more than a factor of 1.25 (i.e., an expansion of 25%). The very first step in this (simplified) code selection example is to eliminate the candidates in Table 18.2 that would expand the bandwidth by more than 25%. The remaining entries form a much reduced set of bandwidth-compatible codes (Table 18.3).

TABLE 18.3 Bandwidth-Compatible BCH Codes

n	k	t	Coding Gain, G (dB) MPSK, $P_B = 10^{-9}$
31	26	1	2.0
63	57	1	2.2
	51	2	3.1
127	120	1	2.2
	113	2	3.3
	106	3	3.9

In Table 18.3, a column designated Coding Gain G (for MPSK at $P_B = 10^{-9}$) has been added. Coding gain in decibels is defined as follows:

$$G = \left(\frac{E_b}{N_0}\right)_{\text{uncoded}} - \left(\frac{E_b}{N_0}\right)_{\text{coded}} \tag{18.29}$$

G can be described as the reduction in the required E_b/N_0 (in decibels) that is needed due to the error-performance properties of the channel coding. G is a function of the modulation type and bit-error probability, and it has been computed for MPSK at $P_B = 10^{-9}$ (Table 18.3). For MPSK modulation, G is relatively independent of the value of M. Thus, for a particular bit-error probability, a given code will provide about the same coding gain when used with any of the MPSK modulation schemes. Coding gains were calculated using a procedure outlined in Section 18.5.2.

A block diagram summarizes this system, which contains both modulation and coding (Figure 18.3). The introduction of encoder/decoder blocks brings about additional transformations. The relationships that exist when transforming from R b/s to R_c channel-b/s to R_s symbol/s are shown at the encoder/modulator. Regarding the channel-bit rate R_c, some authors prefer to use the units of channel-symbol/s (or code-symbol/s). The benefit is that error-correction coding is often described more efficiently with nonbinary digits. We reserve the term "symbol" for that group of bits mapped onto an electrical waveform for transmission, and we designate the units of R_c to be channel-b/s (or coded-b/s).

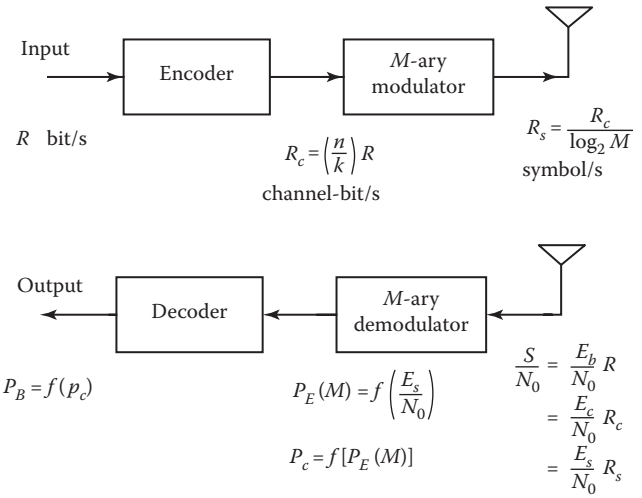

FIGURE 18.3 MODEM with channel coding.

We assume that our system is a real-time communication system, which denotes that it cannot tolerate any message delay, so that the channel-bit rate R_c must exceed the data-bit rate R by the factor n/k. Further, each symbol is made up of $\log_2 M$ channel bits, and so the symbol rate R_s is less than R_c by the factor $\log_2 M$. For a system containing both modulation and coding, we summarize the rate transformations as follows:

$$R_c = \left(\frac{n}{k}\right) R \tag{18.30}$$

$$R_s = \frac{R_c}{\log_2 M} \tag{18.31}$$

At the demodulator/decoder in Figure18.3, the transformations among data-bit energy, channel-bit energy, and symbol energy are related (in a reciprocal fashion) by the same factors as shown among the rate transformations in Equations 18.30 and 18.31. Since the encoding transformation has replaced k data bits with n channel bits, the ratio of channel-bit energy to noise-power spectral density E_c/N_0 is computed by decrementing the value of E_b/N_0 by the factor k/n. Also, since each transmission symbol is made up of $\log_2 M$ channel bits, E_s/N_0, which is needed in Equation 18.20 to solve for P_E, is computed by incrementing E_c/N_0 by the factor $\log_2 M$. For a real-time communication system, we summarize the energy to noise-power spectral density transformations as follows:

$$\frac{E_c}{N_0} = \left(\frac{k}{n}\right) \frac{E_b}{N_0} \tag{18.32}$$

$$\frac{E_s}{N_0} = (\log_2 M) \frac{E_c}{N_0} \tag{18.33}$$

Using Equations 18.30 and 18.31, we can now expand the expression for S/N_0 in Equation 18.19 as follows (Appendix A):

$$\frac{S}{N_0} = \frac{E_b}{N_0} R = \frac{E_c}{N_0} R_c = \frac{E_s}{N_0} R_s \tag{18.34}$$

As before, a standard way of describing the link is in terms of the received E_b/N_0 in decibels. However, there are no data bits at the input to the demodulator, and there are no channel bits; there are only waveforms that have bit meanings and, thus, the waveforms can be described in terms of bit-energy apportionments.

Since S/N_0 and R were given as 53 dB-Hz and 9600 b/s, respectively, we find as before, from Equation 18.18, that the received $E_b/N_0 = 13.2$ dB. The received E_b/N_0 is fixed and independent of n, k, and t (Appendix A). As we search in Table 18.3 for the ideal code to meet the specifications, we can iteratively repeat the computations suggested in Figure 18.3. It might be useful to program on a personal computer (or calculator) the following four steps as a function of n, k, and t. Step 1 starts by combining Equations 18.32 and 18.33 as follows:

Step 1:

$$\frac{E_s}{N_0} = (\log_2 M) \frac{E_c}{N_0} = (\log_2 M) \left(\frac{k}{n}\right) \frac{E_b}{N_0} \tag{18.35}$$

Step 2:

$$P_E(M) \cong 2Q\left[\sqrt{\frac{2E_s}{N_0}}\sin\left(\frac{\pi}{M}\right)\right] \tag{18.36}$$

which is the approximation for symbol-error probability P_E rewritten from Equation 18.20. At each symbol-time interval, the demodulator makes a symbol decision, but it delivers a channel-bit sequence representing that symbol to the decoder. When the channel-bit output of the demodulator is quantized to two levels, 1 and 0, the demodulator is said to make hard decisions. When the output is quantized to more than two levels, the demodulator is said to make soft decisions [15]. Throughout this chapter, we shall assume hard-decision demodulation.

Now that we have a decoder block in the system, we designate the channel-bit-error probability out of the demodulator and into the decoder as p_c, and we reserve the notation P_B for the bit-error probability out of the decoder. We rewrite Equation 18.24 in terms of p_c for $P_E \ll 1$ as follows:

Step 3:

$$P_c \cong \frac{P_E}{\log_2 M} = \frac{P_E}{m} \tag{18.37}$$

relating the channel-bit-error probability to the symbol-error probability out of the demodulator, assuming Gray coding, as referenced in Equation 18.24.

For traditional channel-coding schemes and a given value of received S/N_0, the value of E_s/N_0 with coding will always be less than the value of E_s/N_0 without coding. Since the demodulator with coding receives less E_s/N_0, it makes more errors! When coding is used, however, the system error-performance does not only depend on the performance of the demodulator, it also depends on the performance of the decoder. For error-performance improvement due to coding, the decoder must provide enough error correction to more than compensate for the poor performance of the demodulator.

The final output decoded bit-error probability P_B depends on the particular code, the decoder, and the channel-bit-error probability p_c. It can be expressed by the following approximation [11]:

Step 4:

$$P_B \cong \frac{1}{n}\sum_{j=t+1}^{n} j\binom{n}{j} p_c^j(1-p_c)^{n-j} \tag{18.38}$$

where t is the largest number of channel bits that the code can correct within each block of n bits. Using Equations 18.35 through 18.38 in the four steps, we can compute the decoded bit-error probability P_B as a function of n, k, and t for each of the codes listed in Table 18.3. The entry that meets the stated error requirement with the largest possible code rate and the smallest value of n is the double-error correcting (63, 51) code. The computations are as follows:

Step 1:

$$\frac{E_s}{N_0} = 3\left(\frac{51}{63}\right)20.89 = 50.73$$

where $M = 8$, and the received $E_b/N_0 = 13.2$ dB (or 20.89).

Step 2:

$$P_E \cong 2Q\left[\sqrt{101.5} \times \sin\left(\frac{\pi}{8}\right)\right] = 2Q(3.86) = 1.2 \times 10^{-4}$$

Step 3:

$$p_c \cong \frac{1.2 \times 10^{-4}}{3} = 4 \times 10^{-5}$$

Step 4:

$$\begin{aligned} P_B &\cong \frac{3}{63}\binom{63}{3}(4 \times 10^{-5})^3(1 - 4 \times 10^{-5})^{60} \\ &\quad + \frac{4}{63}\binom{63}{4}(4 \times 10^{-5})^4(1 - 4 \times 10^{-5})^{59} + \cdots \\ &= 1.2 \times 10^{-10} \end{aligned}$$

where the bit-error-correcting capability of the code is $t = 2$. For the computation of P_B in step 4, we need only consider the first two terms in the summation of Equation 18.38 since the other terms have a vanishingly small effect on the result. Now that we have selected the (63, 51) code, we can compute the values of channel-bit rate R_c and symbol rate R_s using Equations 18.30 and 18.31, with $M = 8$

$$\begin{aligned} R_c &= \left(\frac{n}{k}\right)R = \left(\frac{63}{51}\right)9600 \approx 11{,}859 \text{ channel-b/s} \\ R_s &= \frac{R_c}{\log_2 M} = \frac{11859}{3} = 3953 \text{ symbol/s} \end{aligned}$$

18.5.2 Calculating Coding Gain

Perhaps a more direct way of finding the simplest code that meets the specified error performance is to first compute how much coding gain G is required in order to yield $P_B = 10^{-9}$ when using 8-PSK modulation alone; then, from Table 18.3, we can simply choose the code that provides this performance improvement. First, we find the uncoded E_s/N_0 that yields an error probability of $P_B = 10^{-9}$, by writing from Equations 18.24 and 18.36, the following:

$$P_B \cong \frac{P_E}{\log_2 M} \cong \frac{2Q\left[\sqrt{\frac{2E_s}{N_0}}\sin\left(\frac{\pi}{M}\right)\right]}{\log_2 M} = 10^{-9} \tag{18.39}$$

At this low value of bit-error probability, it is valid to use Equation 18.22 to approximate $Q(x)$ in Equation 18.39. By trial and error, or by using the MATLAB® program Qinv.m (Appendix B), we find the argument of $Q(x)$ to be $x = 5.123$, and thus the uncoded $E_s/N_0 = 120.67 = 20.8$ dB, and since each symbol is made up of $\log_2 8 = 3$ bits, the required $(E_b/N_0)_{\text{uncoded}} = 120.67/3 = 40.22 = 16$ dB. From the

given parameters and Equation 18.18, we know that the received $(E_b/N_0)_{\text{coded}} = 13.2$ dB. Using Equation 18.29, the required coding gain to meet the bit-error performance of $P_B = 10^{-9}$ in decibels is

$$G = \left(\frac{E_b}{N_0}\right)_{\text{uncoded}} - \left(\frac{E_b}{N_0}\right)_{\text{coded}} = 16 - 13.2 = 2.8$$

To be precise, each of the E_b/N_0 values in the preceding computation must correspond to exactly the same value of bit-error probability (which they do not). They correspond to $P_B = 10^{-9}$ and $P_B = 1.2 \times 10^{-10}$, respectively. At these low probability values, however, even with such a discrepancy, this computation still provides a good approximation of the required coding gain. In searching Table 18.3 for the simplest code that will yield a coding gain of at least 2.8 dB, we see that the choice is the (63, 51) code, which corresponds to the same code choice that we made earlier.

18.6 Example 4: Direct-Sequence Spread-Spectrum Coded System

Spread-spectrum systems are not usually classified as being bandwidth or power limited. They are generally perceived to be power-limited systems, however, because the bandwidth occupancy of the information is much larger than the bandwidth that is intrinsically needed for the information transmission. In a direct-sequence spread-spectrum (DS/SS) system, spreading the signal bandwidth by some factor permits lowering the signal-power spectral density by the same factor (the total average signal power is the same as before spreading). The bandwidth spreading is typically accomplished by multiplying a relatively narrowband data signal by a wideband spreading signal. The spreading signal or spreading code is often referred to as a pseudorandom code or PN code.

18.6.1 Processing Gain

A typical DS/SS radio system is often described as a two-step binary phase shift keying (BPSK) modulation process. In the first step, the carrier wave is modulated by a bipolar data waveform having a value +1 or −1 during each data-bit duration; in the second step, the output of the first step is multiplied (modulated) by a bipolar PN-code waveform having a value +1 or −1 during each PN-code-bit duration. In reality, DS/SS systems are usually implemented by first multiplying the data by the PN-code (performed with gates when the signals are represented as logic levels) and then making a single pass through a BPSK modulator. For this example, however, it is useful to characterize the modulation process in two separate steps—the outer modulator/demodulator for the data and the inner modulator/demodulator for the PN code (Figure 18.4).

A spread-spectrum system is characterized by a processing gain G_p that is defined in terms of the spread-spectrum bandwidth W_{ss} and the data rate R as follows [20]:

$$G_p = \frac{W_{ss}}{R} \tag{18.40}$$

For a DS/SS system, the PN-code bit has been given the name chip, and the spread-spectrum signal bandwidth can be shown to be about equal to the chip rate R_{ch}. Thus, Equation 18.40 can be written as follows:

$$G_p = \frac{R_{ch}}{R} \tag{18.41}$$

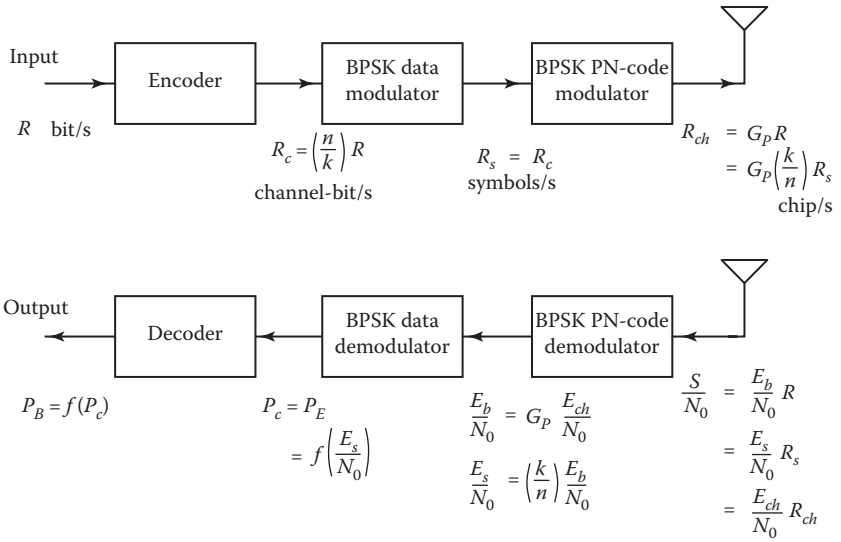

FIGURE 18.4 Direct-sequence spread-spectrum MODEM with channel coding.

Some authors define processing gain to be the ratio of the spread-spectrum bandwidth to the symbol rate. This definition separates the system performance that is due to bandwidth spreading from the performance that is due to error-correction coding. Since we ultimately want to relate all of the coding mechanisms relative to the information source, we shall conform to the most usually accepted definition for processing gain, as expressed in Equations 18.40 and 18.41.

A spread-spectrum system can be used for interference rejection and for multiple access (allowing multiple users to access a communication resource simultaneously). The benefits of DS/SS signals are best achieved when the processing gain is very large; in other words, the chip rate of the spreading (or PN) code is much larger than the data rate. In such systems, the large value of G_p allows the signaling chips to be transmitted at a power level well below that of the thermal noise plus other interferers. We will use a value of $G_p = 1000$. At the receiver, the despreading operation correlates the incoming signal with a synchronized copy of the PN code and, thus, accumulates the energy from multiple (G_p) chips to yield the energy per data bit. The value of G_p has a major influence on the performance of the spread-spectrum system application. We shall see, however, that the value of G_p has no effect on the received E_b/N_0. In other words, spread-spectrum techniques offer no error-performance advantage over thermal noise. For DS/SS systems, there is no disadvantage either! Sometimes such spread-spectrum radio systems are employed only to enable the transmission of very small power-spectral densities and thus avoid the need for Federal Communications Commission (FCC) licensing [16].

18.6.2 Channel Parameters for Example 4

Consider a DS/SS radio system that uses the same (63, 51) code as in the previous example. Instead of using MPSK for the data modulation, we shall use BPSK. Also, we shall use BPSK for modulating the PN-code chips. Let the received $S/N_0 = 48$ dB-Hz, the data rate $R = 9600$ b/s, and the required $P_B \leq 10^{-6}$. For simplicity, assume that there are no bandwidth constraints. Our task is simply to determine whether or not the required error performance can be achieved using the given system architecture and design parameters. In evaluating the system, we will use the same type of transformations used in the previous examples.

18.6.3 Solution to Example 4

A typical DS/SS system can be implemented more simply than the one shown in Figure 18.4. The data and the PN code would be combined at baseband, followed by a single pass through a BPSK modulator. We will, however, assume the existence of the individual blocks in Figure 18.4 because they enhance our understanding of the transformation process. The relationships in transforming from data bits, to channel bits, to symbols, and to chips (Figure 18.4) have the same pattern of subtle but straightforward transformations in rates and energies as previous relationships (Figures 18.2 and 18.3). The values of R_c, R_s, and R_{ch} can now be calculated immediately since the (63, 51) BCH code has already been selected. From Equation 18.30, we write

$$R_c = \left(\frac{n}{k}\right) R = \left(\frac{63}{51}\right) 9600 \approx 11{,}859 \text{ channel-b/s}$$

Since the data modulation considered here is BPSK, then from Equation 18.31, we write

$$R_s = R_c \approx 11{,}859 \text{ symbol/s}$$

and from Equation 18.41, with an assumed value of $G_p = 1000$

$$R_{ch} = G_p R = 1000 \times 9600 = 9.6 \times 10^6 \text{ chip/s}$$

Since we have been given the same S/N_0 and the same data rate as in Example 2, we find the value of received E_b/N_0 from Equation 18.25 to be 8.2 dB (or 6.61). At the demodulator, we can now expand the expression for S/N_0 in Equation 18.34 and Appendix A as follows:

$$\frac{S}{N_0} = \frac{E_b}{N_0} R = \frac{E_c}{N_0} R_c = \frac{E_s}{N_0} R_s = \frac{E_{ch}}{N_0} R_{ch} \tag{18.42}$$

Corresponding to each transformed entity (data bit, channel bit, symbol, or chip), there is a change in rate and, similarly, a reciprocal change in energy-to-noise spectral density for that received entity. Equation 18.42 is valid for any such transformation when the rate and energy are modified in a reciprocal way. There is a kind of *conservation of power* (or energy) phenomenon that exists in the transformations. The total received average power (or total received energy per symbol duration) is fixed regardless of how it is computed, on the basis of data bits, channel bits, symbols, or chips.

The ratio E_{ch}/N_0 is much lower in value than E_b/N_0. This can be seen from Equations 18.42 and 18.41 as follows:

$$\frac{E_{ch}}{N_0} = \frac{S}{N_0}\left(\frac{1}{R_{ch}}\right) = \frac{S}{N_0}\left(\frac{1}{G_p R}\right) = \left(\frac{1}{G_p}\right)\frac{E_b}{N_0} \tag{18.43}$$

But, even so, the despreading function (when properly synchronized) accumulates the energy contained in a quantity G_p of the chips, yielding the same value $E_b/N_0 = 8.2$ dB, as was computed earlier from Equation 18.25. Thus, the DS spreading transformation has no effect on the error performance of an AWGN channel [15], and the value of G_p has no bearing on the value of P_B in this example.

From Equation 18.43, we can compute, in decibels

$$\begin{aligned}\frac{E_{ch}}{N_0} &= \frac{E_b}{N_0} - G_p \\ &= 8.2 - (10 \times \log_{10} 1000) \\ &= -21.8\end{aligned} \tag{18.44}$$

The chosen value of processing gain ($G_p = 1000$) enables the DS/SS system to operate at a value of chip energy well below the thermal noise, with the same error performance as without spreading.

Since BPSK is the data modulation selected in this example, each message symbol therefore corresponds to a single channel bit, and we can write

$$\frac{E_s}{N_0} = \frac{E_c}{N_0} = \left(\frac{k}{n}\right)\frac{E_b}{N_0} = \left(\frac{51}{63}\right) \times 6.61 = 5.35 \tag{18.45}$$

where the received $E_b/N_0 = 8.2$ dB (or 6.61). Out of the BPSK data demodulator, the symbol-error probability P_E (and the channel-bit error probability p_c) is computed as follows [15]:

$$p_c = P_E = Q\left(\sqrt{\frac{2E_c}{N_0}}\right) \tag{18.46}$$

Using the results of Equation 18.45 in Equation 18.46 yields

$$p_c = Q(3.27) = 5.8 \times 10^{-4}$$

Finally, using this value of p_c in Equation 18.38 for the (63, 51) double-error correcting code yields the output bit-error probability of $P_B = 3.6 \times 10^{-7}$. We can, therefore, verify that for the given architecture and design parameters of this example the system does, in fact, achieve the required error performance.

18.7 Conclusion

The goal of this chapter was to review fundamental relationships used in evaluating the performance of digital communication systems. First, we described the concept of a link and a channel and examined a radio system from its transmitting segment up through the output of the receiving antenna. We then examined the concept of bandwidth-limited and power-limited systems and how such conditions influence the system design when the choices are confined to MPSK and MFSK modulation. Most important, we focused on the definitions and computations involved in transforming from data bits to channel bits to symbols to chips. In general, most digital communication systems share these concepts; thus, understanding them should enable one to evaluate other such systems in a similar way.

Appendix A: Received E_b/N_0 Is Independent of the Code Parameters

Starting with the basic concept that the received average signal power S is equal to the received symbol or waveform energy, E_s, divided by the symbol-time duration, T_s (or multiplied by the symbol rate, R_s), we write

$$\frac{S}{N_0} = \frac{E_s/T_s}{N_0} = \frac{E_s}{N_0}R_s \tag{A18.1}$$

where N_0 is noise-power spectral density.

Using Equations 18.27 and 18.25, rewritten as

$$\frac{E_s}{N_0} = (\log_2 M)\frac{E_c}{N_0} \quad \text{and} \quad R_s = \frac{R_c}{\log_2 M}$$

let us make substitutions into Equation A18.1, which yields

$$\frac{S}{N_0} = \frac{E_c}{N_0} R_c \tag{A18.2}$$

Next, using Equations 18.26 and 18.24, rewritten as

$$\frac{E_c}{N_0} = \left(\frac{k}{n}\right)\frac{E_b}{N_0} \quad \text{and} \quad R_c = \left(\frac{n}{k}\right) R$$

let us now make substitutions into Equation A18.2, which yields the relationship expressed in Equation 18.11

$$\frac{S}{N_0} = \frac{E_b}{N_0} R \tag{A18.3}$$

Hence, the received E_b/N_0 is only a function of the received S/N_0 and the data rate R. It is independent of the code parameters n, k, and t. These results are summarized in Figure 18.3.

Appendix B: MATLAB® Program Qinv.m for Calculating $Q^{-1}(x)$

```
function[y]=Qinv(x);
x=2*x;
y=sqrt(2)erfcinv(x);
```

References

1. Anderson, J.B. and Sundberg, C.-E.W., Advances in constant envelope coded modulation, *IEEE Commun., Mag.*, 29(12), 36–45, 1991.
2. Borjesson, P.O. and Sundberg, C.E., Simple approximations of the error function $Q(x)$ for communications applications, *IEEE Trans. Comm.*, COM-27, 639–642, 1979.
3. Clark Jr., G.C. and Cain, J.B., *Error-Correction Coding for Digital Communications*, Plenum Press, New York, 1981.
4. Hodges, M.R.L., The GSM radio interface, *British Telecom Technol. J.*, 8(1), 31–43, 1990.
5. Johnson, J.B., Thermal agitation of electricity in conductors, *Phys. Rev.*, 32, 97–109, 1928.
6. Korn, I., *Digital Communications*, Van Nostrand Reinhold Co., New York, 1985.
7. Lin, S. and Costello Jr., D.J., *Error Control Coding: Fundamentals and Applications*, Prentice-Hall, Englewood Cliffs, NJ, 1983.
8. Lindsey, W.C. and Simon, M.K., *Telecommunication Systems Engineering*, Prentice-Hall, Englewood Cliffs, NJ, 1973.
9. Nyquist, H., Thermal agitation of electric charge in conductors, *Phys. Rev.*, 32, 110–113, 1928.
10. Nyquist, H., Certain topics on telegraph transmission theory, *Trans. AIEE*, 47, 617–644, 1928.
11. Odenwalder, J.P., *Error Control Coding Handbook*, Linkabit Corp., San Diego, CA, July 15, 1976.

12. Shannon, C.E., A mathematical theory of communication, *BSTJ*., 27, 379–423, 623–657, 1948.
13. Shannon, C.E., Communication in the presence of noise, *Proc. IRE*., 37(1), 10–21, 1949.
14. Sklar, B., What the system link budget tells the system engineer or how I learned to count in decibels, *Proc. Int. Telemetering Conf.*, San Diego, CA, November 1979.
15. Sklar, B., *Digital Communications: Fundamentals and Applications*, 2nd Edition, Prentice-Hall, Upper Saddle River, NJ, 2001.
16. Title 47, *Code of Federal Regulations*, Part 15 Radio Frequency Devices.
17. Ungerboeck, G., Trellis-coded modulation with redundant signal sets, Pt. I and II, *IEEE Comm. Mag.*, 25, 5–21. 1987.
18. Van Trees, H.L., *Detection, Estimation, and Modulation Theory*, Pt. I, John Wiley & Sons, New York, 1968.
19. Viterbi, A.J., *Principles of Coherent Communication*, McGraw-Hill, New York, 1966.
20. Viterbi, A.J., Spread spectrum communications—Myths and realities, *IEEE Comm. Mag.*, 11–18, 1979.

Further Reading

A useful compilation of selected papers can be found in *Cellular Radio and Personal Communications—A Book of Selected Readings*, edited by Theodore S. Rappaport, Institute of Electrical and Electronics Engineers, Inc., Piscataway, New Jersey, 1995. Fundamental design issues, such as propagation, modulation, channel coding, speech coding, multiple-accessing, and networking, are well represented in this volume.

Another useful sourcebook that covers the fundamentals of mobile communications in great detail is *Mobile Radio Communications*, edited by Raymond Steele, Pentech Press, London 1992. This volume is also available through the Institute of Electrical and Electronics Engineers, Inc., Piscataway, New Jersey.

For spread-spectrum systems, an excellent reference is *Spread Spectrum Communications Handbook*, by Marvin K. Simon, Jim K. Omura, Robert A. Scholtz, and Barry K. Levitt, McGraw-Hill Inc., New York, 1994.

For coverage of digital communication fundamentals that emphasizes system subtleties, some of which were explored in this chapter, see the book *Digital Communications Fundamentals and Applications*, 2nd edition, by Bernard Sklar, Prentice-Hall 2001.

19

Fundamental Limitations on Increasing Data Rate in Wireless Systems

Donald C. Cox

19.1 Introduction

There is a continuing quest for increasing the data transmission rate in wireless systems. However, because of the complexity of these systems, it appears that fundamental physical relationships among transmission rate, transmitter power, and range over which transmission is possible are frequently overlooked. This can result in overly optimistic expectations for new wireless data systems or comparisons between systems that are not on an equal basis.

Cellular mobile radio systems have advanced from second generation digital technologies with limited data capability to third generation systems with data transmission rates on the order of a few megabits per second and on to fourth generation systems with even higher data rates. Wireless local area networks (WLANs) based on various versions of IEEE 802.11 standards and known collectively as WiFi, have evolved from having data transmission rates of several megabits per second to hundreds of megabits per second.

While increasing the capability of the protocols to handle ever increasing data rates, the parameters of wireless systems have, if anything, changed to increase the overall wireless link loss that must be

overcome at a specific range. Increased link loss reduces the data rate at the specific range. Note that increasing the data rate is easily within the capability of the semiconductor devices used in the wireless data systems. The issue is the reduction in range that results with increased data rate when other system parameters remain unchanged.

As examples of parameter changes, cellular mobile system base stations have been deployed with lower antenna heights, and cellular system frequencies have been increased from 800 MHz to 1.9 GHz for some systems and even higher for others. WLAN frequencies have increased from 900 MHz to 2.4 GHz and to over 5 GHz in some systems. As antenna heights decrease and as transmission frequencies increase, wireless link loss increases. While the frequency band in which a system operates and the antenna heights are factors in range that are discussed in Section 19.5, the emphasis in the earlier part of this chapter is on the fundamental relationship between data transmission rate, transmitter power, and range. Increasing data rate in other ways than increasing transmission bandwidth are discussed in later sections.

Both WLANs and cellular mobile radio systems have implemented options of higher-level modulation (up to 64 level quadrature amplitude modulation, 64-QAM). Higher-level modulations permit higher data rates in a specified bandwidth, but they incur higher signal-to-noise ratio penalties compared to lower level modulations, for example, binary or 4-QAM, for the increased data transmission rates. Other ways of increasing data transmission rates in CDMA and TDMA systems are considered in later sections.

One system innovation that overcomes somewhat more wireless link loss is the incorporation of multiple antennas that implement multiple input multiple output (MIMO) signal processing. MIMO may provide some increase in effective sensitivity or an increase in data rate from signal processing and wireless link multipath characteristics. However, with the limited space available on small handsets and computer cards, the number of antennas is usually limited to 2×3, resulting at most in an upper bound in data rate increase of $\times 6$. However, this upper bound is seldom realized in actual systems where increases are usually significantly less.

It should be noted that some cellular systems use transmit power control to reduce the transmitted power when power lower than the maximum possible is needed. However, in order to provide maximum data transmission rate at maximum range, the maximum possible transmitter power is required. Therefore, the only value of transmitter power considered herein is the maximum possible from a transmitter.

Table 19.1 compares the radio link data transmission rate (bit rate) of current popular wireless data systems with typical usable range between transmitting and receiving locations for these systems in urban and suburban environments. The relationships between range, transmitter power, and transmission rate depend on several factors, some of which are discussed herein. Because of different factors, often unspecified, the range and transmission rate for different systems have uncertainty in their values as noted in the table.

Other factors that affect data transmission rate are interference, either from other users in the same system or from transmissions from other wireless systems, multipath fading, and spread in time delays (frequency selective fading). These other factors are not considered in this chapter; however, their effect often is to further reduce the data transmission rate below the fundamental limit due to signal-to-noise ratio (SNR) considered in this article.

TABLE 19.1 Radio Link Transmission Rate and Typical Usable Range in Urban and Suburban Environments for Current Popular Wireless Data Systems

	Link Rate	Range	Frequency
Cellular	A few Mb/s	A few km	0.8 and 1.9 GHz
WiFi	<100 Mb/s	<100 m	2.4 and 5 × GHz

19.2 Increasing Data Rate by Increasing Bandwidth

A straight forward way to increase wireless data transmission rate is to increase the bandwidth occupied. However, an often forgotten issue when increasing data transmission rate by increasing bandwidth is that receiver bandwidth must be increased proportional to the data rate if all other system characteristics remain the same (e.g., the modulation level, coding, and number of antennas, etc.). This increased bandwidth requires an increase in total received signal power for a specified bit error rate (BER). The increase in required signal power is linear with the increase in bandwidth and thus with the increase in data rate. This increase in required received signal power is referred to as a decrease in the sensitivity of the receiver. Thus, the sensitivity of a receiver decreases linearly with an increase in data rate, assuming all other receiver parameters remain the same, for example, noise figure, filter shapes, demodulator efficiencies, and so on. If modulation levels are increased, the bandwidth may remain the same, but the required received signal power increases even more, resulting in a decrease in sensitivity that will be even greater as the data rate increases. Other ways of increasing data transmission rate while holding bandwidth constant incur equivalent reductions in range and are discussed in later sections.

19.2.1 Signal, Noise, Transmitter Power, Range, and Data Rate Relationships

Two key limitations establish the fundamental relationship between date transmission rate and range for digital wireless systems. The received signal power, S, for a transmitter power, P_t, as a function of the distance, d, between a transmitting antenna and a receiving antenna in a wireless system can be represented as

$$S = P_t k_s / d^m, \tag{19.1}$$

where the system constant k_s includes factors for antenna gains, antenna heights, frequency, and other factors related to the environment, the system configuration, and the statistics of the coverage [1–4,11]. The exponent m depends on the environment in which the system operates and the system configuration.

The other fundamental limitation relates the transmission bit rate, r_b, to the noise power, N, of the receiver referred to the input as

$$N = n_o B_n = k_n r_b, \tag{19.2}$$

where n_o is the noise power spectral density, B_n is the receiver effective noise bandwidth, r_b is the bit rate, and k_n is a system constant that includes factors for modulation, type of detection, coding, receiver noise figure, antenna temperature, and so on [5,11].

A relationship between transmission range, d, and bit rate, r_b, can be established from two somewhat different, but similar, starting points.

DERIVATION 1

This derivation starts by noting that for wireless digital systems the probability of a bit error, P_e, is a function, $fn(\ )$ of signal-to-noise ratio, S/N, [5]; that is,

$$P_e = fn\left(S/N\right) \tag{19.3}$$

A useful way to look at the fundamental relationship between range and bit rate is to compare two systems with different bit rates but for which all other system factors are the same, for example, the same transmitter powers, receiver noise figures, antennas, frequencies, modulations, detection schemes, coding, and so on. This removes the complexities that result from attempting to compare systems with different system factors. Of course, the receiver bandwidth must be scaled linearly with bit rate.

In order to ensure a fair comparison, two systems, *A* and *B*, must be compared at the same probability of bit error and in the same environment. Then, from Equation 19.3, the *S*/*N* of the two systems must be the same; that is,

$$\frac{S_A}{N_A} = \frac{S_B}{N_B},$$

and substituting Equations 19.1 and 19.2 for *S* and *N* yields

$$d_A = \left(\frac{r_{bB}}{r_{bA}}\right)^{1/m} \cdot d_B. \tag{19.4}$$

DERIVATION 2

This derivation starts from the highly idealized Shannon theoretical channel capacity equation

$$C = B\log_2\left(1 + \frac{S}{N}\right), \tag{19.5}$$

where *C* is the maximum bit rate that can be transmitted without making any errors over a channel with bandwidth *B* in additive white Gaussian noise (AWGN) having noise power *N* and signal power *S* [5]. The capacity normalized to bandwidth, *C*/*B*, will be the same for systems having the same modulation, detection schemes, coding, filter shapes, and so on. Therefore, to make a fair comparison between two systems, *A* and *B*, having all system factors the same except bit rate and range, the ratios of *C*/*B* must be equal. Then, from Equation 19.5,

$$\log_2\left(1 + \frac{S_A}{N_A}\right) = \log_2\left(1 + \frac{S_B}{N_B}\right),$$

and substituting Equations 19.1 and 19.2 again yields Equation 19.4.

19.2.2 Data Rate versus Range Examples

Different wireless environments have different propagation exponents, *m*, representing the decrease of signal power with distance, *d*. For example, in free space, $m = 2$. However, for environments cluttered with buildings, trees, and terrain irregularities, *m* is determined empirically and can vary from 2 to perhaps 5 or 6. Typical values for *m* are between 3 and 4 [1–4,11].

The fundamental relationship between data transmission rate, r_b, and range (distance *d*) in Equation 19.4 can be illustrated by starting with a data rate and range for a typical system and plotting the relationship 19.4. Digital cellular systems have bit rates from 8 kb/s to perhaps 14 kb/s for voice

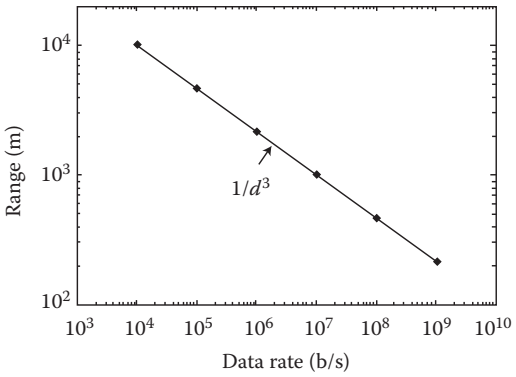

FIGURE 19.1 Transmission rate versus range for comparing systems in an environment with a propagation exponent $m = 3$ for a reference system having a bit rate of 10 kb/s and a range of 10 km.

transmission [4]. In some typical environments cluttered with buildings, digital voice cellular systems operating around 800 MHz can cover users up to a range of 10 km with a probability of perhaps 90%. Thus, a bit rate of 10 kb/s and a range of 10 km are useful for exploring the range/bit rate relationship of systems having different bit rates but otherwise the same system factors. Note that these digital cellular voice systems use (1) heavy forward error correction (on the order of 1/2 to 1/3), (2) receivers with state-of-the-art sensitivities, (3) handset transmitter power as large as is permissible considering transmitting time from small batteries and user safety, (4) antennas as efficient as possible in small handsets, and (5) base station antennas with heights and gains that will provide the 10 km range in typical environments. Thus, new digital wireless systems will not have significantly better system performance except perhaps for use of multiple antennas.

Using the typical values of 10 kb/s and 10 km range for system *B*, the relationship between bit rate and range from Equation 19.4 for a comparative system *A* with the same system factors is plotted in Figure 19.1 for a propagation exponent of $m = 3$. The relationship in Figure 19.1 is fundamental. Any change in system factors will only shift the lines horizontally. Changes in system factors will not change the slope of the relationship. The slope is determined solely by the propagation exponent, m, and the propagation exponent is determined by the environment.

19.2.3 Changing the Percentage of Area Covered

The reference range of 10 km used for Figure 19.1 was based on covering 90% of the areas at that distance between a base station and a user located in an environment cluttered with buildings, trees, and terrain irregularities. However, the statistics of received signal power at any given fixed range can usually be represented by a log normal distribution with standard deviation, σ, typically varying in different environments between $\sigma = 6$ dB and 12 dB [1–4,11]. Thus, with 90% of areas covered and typical values of σ, perhaps 50% (half) of the areas could have 10 dB higher received signal power. This 10 dB would be reflected in a factor of 10 increase in the reference bit rate, r_b in Equation 19.4. Thus, the typical digital cellular voice system could support 100 kb/s over 50% of the areas at 10 km range. This reference of 100 kb/s at 10 km for covering 50% of the areas is plotted in Figure 19.2 for $m = 3$ along with the reference of 10 kb/s at 10 km for covering 90% of the areas. The slope from Equation 19.4 is unchanged; the lines merely shift to the right by a factor of 10. That is, as the system bit rate is increased, the range decreases with slope determined by the propagation exponent m.

The argument above can be further extended to consider covering only 10% of the areas at 10 km range. This would result in 1 Mb/s being possible at 10 km range, but only for 10% of the areas. An issue that always arises is what percentage of an area should be covered at a coverage range claimed for a

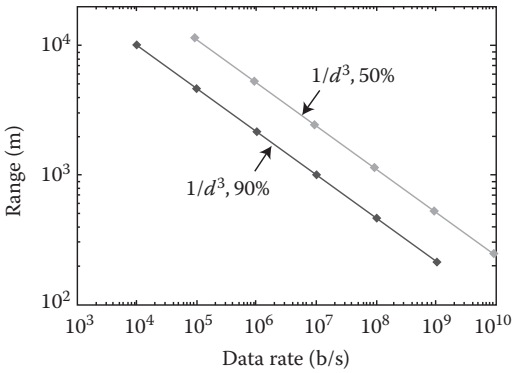

FIGURE 19.2 Transmission rate versus range for comparing systems with 50% coverage compared to a reference system of 10 kb/s, 10 km, $m = 3$, and 90% coverage.

wireless data system. This range is always a statistical factor in environments cluttered with buildings, trees, and terrain features (small hills and valleys). Unless the conditions are specified, a range claim for a wireless system is meaningless. This is one reason the values specified in Table 19.1 are not precise. (The spread in values for digital cellular in Table 19.1 are consistent with the differences between the 90% and 50% lines in Figure 19.2 and uncertainty in the propagation exponent, m, and standard deviation, σ, used to estimate range also contribute to the spread. Other factors discussed later in this article also contribute to the imprecision of values in Table 19.1.)

19.3 Changing Modulation Levels

The previous data rate-versus-range comparisons were made for wireless data systems with the same system factors. However, in the quest for higher data rates within the limited available bandwidths, evolving wireless data systems have made use of higher-level modulation than the two-level (binary) or four-level modulation used in earlier digital voice systems. Examples include four-level quadrature amplitude modulation (4-QAM) sometimes called four-level phase shift keying (4-PSK), used in the IS-54/IS-136 North American time division multiple access (NATDMA) [sometimes referred to as digital advanced mobile phone service (D-AMPS) or North American digital cellular (NADC)] or the two level amplitude shift keying (ASK), sometimes called phase shift keying (PSK), used in IS-95 CDMA, and two level frequency shift keying (FSK), that is, Gaussian minimum shift keying (GMSK), used in GSM [4]. While higher-level modulations, for example, 16-level quadrature amplitude modulation (16-QAM) and 64-QAM, permit higher transmission bit rates within a given bandwidth, they require a higher SNR for any particular probability of bit error, P_e [5]. Thus, to compare transmission rate and range for systems A and B having different level modulation but having all other system factors the same requires

$$\frac{S_B}{N_B} = k_\Delta \frac{S_A}{N_A},$$

where k_Δ accounts for the different S/N required for the different level digital modulations. Then by either Derivation 1 or 2, Equation 19.4 becomes

$$d_A = \left(k'_\Delta \frac{r_{bB}}{r_{bA}} \right)^{1/m} \cdot d_B, \tag{19.6}$$

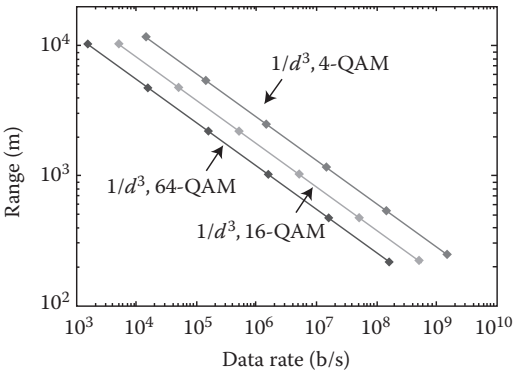

FIGURE 19.3 Transmission rate versus range for comparing systems with different modulation levels compared to a reference system of 10 kb/s, 10 km, $m = 3$, 90% coverage, and 4-QAM.

where k_Δ and k'_Δ may be different because of different relationships for P_e for the different modulations, and the effect of k'_Δ again is only to offset the lines; the factor does not affect the slope. Equation 19.6 is plotted for $m = 3$ and 90% coverage in Figure 19.3 to compare 16-QAM and 64-QAM with the basic 4-QAM where the reference 10 kb/s and 10 km were for 4-QAM. All relationships in Figure 19.3 are for 90% coverage.

Higher-level modulation is used for the higher-data-rate options in the enhanced data rates for GSM evolution (EDGE) cellular data standard, in the 802.11a, g, and n wireless LAN standards, in WiMax, and in Long Term Evolution (LTE). In these systems, in areas of low *S*/*N*, low-level modulation is used with the resulting lower data transmission rate within the fixed system bandwidth. However, in locations with higher signal level and resulting higher *S*/*N*, the modulation level is increased adaptively to increase the data rate. Thus, these systems can provide higher data rates, but mostly at much shorter ranges consistent with the relationships in Figures 19.1 through 19.3. Since these systems use fixed bandwidths, they will not follow the curves in the figures that result from optimizing bandwidth for a given bit rate as incorporated in Equation 19.2 and therefore also in Equations 19.4 and 19.6. Instead, constant-bandwidth adaptive-bit rate systems will follow a series of vertical lines in steps in Figure 19.3 transitioning at ranges where the signal level will be high enough to support a higher bit rate. Such a relationship is not fundamental but is a result of system implementation with a fixed bandwidth and adaptive modulation (and coding).

19.4 Multiple-Input, Multiple-Output

Sometimes claims are made that using multiple antennas in transmitting and receiving in multiple-input, multiple-output (MIMO) systems will solve the bit rate limitation problem in wireless data systems. MIMO may help increase the bit rate at a given *S*/*N*, or increase the *S*/*N* at a given range, but it does not overcome the range versus bit rate limitations. (MIMO may also provide considerable mitigation of co-channel interference from other users, but this is a different issue than the *S*/*N* limited fundamental range limitation that is the subject of this section.) Also, it should be noted that room for multiple antennas is very limited on a small handset and even on a small laptop card. It seems unlikely that more than two or three antennas will be useful on such small user terminals.

Relationships among numbers of antennas, capacity (bit rate), *S*/*N*, and environmental factors for MIMO are complex and tend to obscure the fundamental dependency between range and bit rate. There are at least two approaches that can be used to ascertain the relationship between range and bit rate for systems using multiple transmit and receive antennas.

The first approach considers the use of the antennas for increasing the *S*/*N* at a given range by transmitting the same signal, pre-coded if the channel is known at the transmitter, across all M_T transmit

antennas and properly combining the received signal from M_R receive antennas at the receiver. With some assumptions on the matrix representing transmission among the antennas, **H**, and other idealizations, the average S/N gain from using MIMO in such a scenario is upper-bounded by [6]:

$$\left(S/N\right)_{MIMO} \leq M_T M_R \left(S/N\right)_{SISO}. \tag{19.7}$$

A possible usable MIMO wireless system configuration could be two transmit antennas and three receive antennas, that is, a 2×3 MIMO system. Then, according to Equation 19.7, this could yield up to a factor of six increase in $(S/N)_{MIMO}$, over an otherwise equal single-input, single-output (SISO) system. However, it should be noted that because of several nonidealities and perhaps different definitions of equality of systems, this upper bound will seldom be achieved and factors of 3 or even 2 may be more likely for 2×3 MIMO systems. With a propagation parameter $m = 3$, a factor of 6 in (S/N) would be reflected in a factor of $(6)^{1/3}$ in range. The range versus bit rate for the upper bound for a 2×3 MIMO system is plotted on Figure 19.4 by applying the factor of $(6)^{1/3}$ in range to the $m = 3$, 90% coverage, and 4-QAM SISO system. The reference SISO digital cellular voice system used in the previous figures which provides 10 kb/s at 10 km over 90% of the areas is included for comparison. Thus, as stated earlier and noted in the figure, MIMO can provide increased bit rate at a given range with other system factors being equal in some sense, but it does not overcome the fundamental range versus bit rate relationship for a given set of system factors.

Another way to approach the MIMO versus SISO comparison is to considers a highly idealized theoretical capacity equation [6–8], which is a MIMO equivalent of the SISO capacity Equation 19.5. However, the complexity of the equation obscures the relationships among bit rate, range, S/N, and so on. The equation can be simplified to

$$C = B \cdot fn\left(M_T, M_R, \mathbf{H}, T_S, \frac{S'}{N'}\right), \tag{19.8}$$

where M_T, M_R, **H**, B, and C are as earlier defined, T_s is a characteristic of the transmitted signal(s), S'/N' is a measure of SNR that may or may not be the same as the S/N for an equivalent SISO system, and $fn(\,)$ is a functional relationship. While determining equivalence may be an issue, it is clear that Equation 19.8 also depends on a measure of signal power S' and noise power N', where S' will depend on distance as in Equation 19.1 and N' will depend on bit rate as in Equation 19.2. Thus, Equations 19.8, 19.1, and 19.2 will also yield a relationship like Equation 19.6 with some k'_Δ determined by M_T, M_R, **H**, T_s, and other

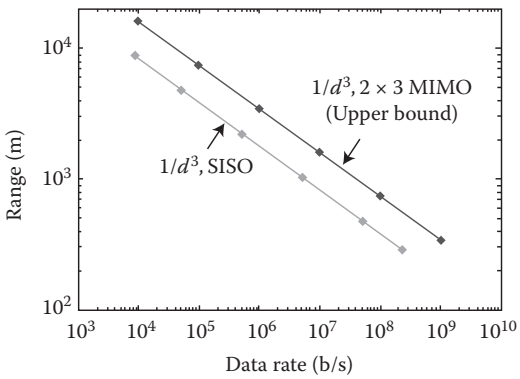

FIGURE 19.4 Transmission rate versus range (upper bound) for comparing systems with 2×3 MIMO configuration compared to a reference system of 10 kb/s, 10 km, $m = 3$, 90% coverage, 4-QAM, and 1×1 SISO configuration.

system factors, for example, modulation, type of detection, and so on. Thus, for a 2×3 MIMO system, Equation 19.8 will result in a line somewhere between the SISO line and the upper bound 2×3 MIMO line in Figure 19.4. The slope will still be determined by the propagation parameter, m, and the offset will be determined by the $fn(\ )$ and parameters in Equation 19.8 that depend on $\mathbf{H}$, T_s, and other system factors. Thus, bit rate and range for MIMO and SISO systems can be compared using Equation 19.6 with appropriate values for k'_{Δ}, and an example of one comparison is shown in Figure 19.4.

An experimental demonstration of the variation of signal power and MIMO capacity as a function of distance inside a laboratory building is found in Reference 8. While the distances in this indoor experiment are less than those for outdoor wireless data systems, the decrease in capacity (data rate) due to the decrease of signal power with distance in this indoor environment is consistent with the relationship in Figure 19.4.

19.5 Changing Carrier Frequency Band and Base Station Antenna Height

At any specified range, the received signal power, S, decreases with frequency from the 800 MHz cellular band to the 1.9 GHz frequency band and decreases further to the 2.4 GHz ISM band used for 802.11 g and in wireless fidelity (WiFi) systems. Some measurements [9] suggest a decrease of about 8 dB between 800 MHz and 1.9 GHz and perhaps 10 dB between 800 MHz and 2.4 GHz. This is approximately a variation of f^2. Thus, at these higher frequency bands, the reference bit rate would be a factor of about six less at 1.9 GHz than the 10 kb/s 800 MHz reference used in Figures 19.1 through 19.4 and a factor of 10 less at 2.4 GHz. Different operating frequencies also contribute to imprecision in values in Table 19.1.

Digital cellular systems for covering distances of 10 km in cluttered environments usually have base station antenna heights on the order of 30 m. Base stations for covering shorter ranges often have shorter antenna heights, sometimes on the order of 10 m or less, and outdoor WiFi systems often have access point (base station) antenna heights even less than 10 m. Received signal power, S, decreases with antenna height, h, at a rate on the order of h^{-2}, [1,2,4,10,11]. Different base station antenna heights are another reason that values specified in Table 19.1 are not precise.

WiFi systems usually use 64 QAM modulation for 54 Mb/s transmission rates. From Figure 19.3, this would result in a range of about 300 m for the d^{-3} variation from the reference 10 kb/s and 10 km digital cellular voice coverage. However, WiFi operates at 2.4 GHz, not the 800 MHz of the reference cellular systems, and WiFi usually has access point (base station) antennas less than 10 m high compared to the 30 m height of the reference digital cellular antennas. These two factors—frequency and antenna height—then would reduce the 300 m range by factors of $[(10)]^{1/3}$ for frequency and at least $[(3)^2]^{1/3}$ for antenna height for an overall reduction of a factor of approximately 4.5. This reduces the WiFi range estimate to less than 100 m at a 54 Mb/s rate consistent with the value in Table 19.1.

A further reduction in range for WiFi will result from replacing the cellular base station antenna with a gain on the order of 15 dB with a small access point antenna with a gain of less than 5 dB and, of course, MIMO can be implemented as in 802.11n to increase the bit rate.

19.6 Other Ways to Increase Data Transmission Rate

Data transmission rate can be increased in other ways besides increasing bandwidth or modulation levels or incorporating MIMO as discussed in the preceding sections. However, as considered in the following sections, other ways incur a penalty in range equivalent to that from increasing bandwidth.

19.6.1 Increasing Data Rate by Decreasing Spreading Gain in CDMA

A definition of spreading gain or spreading factor in CDMA systems is the chip rate of the CDMA chip sequence, r_c divided by the bit rate of the transmitted data r_b, that is, r_c/r_b.

The bandwidth occupied by a CDMA system is proportional to the chip rate and for most systems the bandwidth is fixed at one or at least a few values. The data transmission rate, proportional to the bit rate, can be varied by varying the spreading gain while holding the chip rate and thus the occupied bandwidth fixed. This is one of the techniques used in the UMTS/WCDMA third-generation cellular systems to increase data transmission rate.

The CDMA signal is spread with the chip sequence to the occupied bandwidth for transmitting and then de-spread at the receiver back to the bandwidth occupied by the transmitted data bit rate. The noise spectral density in the receiver is not affected by the dispreading process and remains at n_o as in Equation 19.2. Thus, the noise at the de-spreader output is again the N in Equation 19.2. Equation 19.1 still holds for the received signal power, S. Thus, Derivation 1 and 2 in Section 19.2.1 are still applicable and the data rate versus range examples in section 19.2.2 are still valid. Thus there is no difference between the affect of decreasing spreading gain in a CDMA system and increasing the bandwidth in a system as discussed earlier since the effect of decreasing spreading gain is to increase the post de-spread bandwidth in the same way.

19.6.2 Increasing Data Rate by Increasing Number of CDMA Code

Another way to increase the transmitted data rate in a CDMA system is to keep the chip rate and spreading gain fixed but to add additional different spreading sequences (spreading codes) to spread different segments of the transmitted data stream. The transmitted bit-rate is then quantized by the number of spreading codes used to spread the data. This is another technique used in the UMTS/WCDMA third generation cellular systems to increase data transmission rate.

In this case, the noise out of each de-spreader remains nearly constant with increased bit rate. However, one must consider the transmitter power and resulting received signal power per spreading code, that is, the received power per spreading sequence. For an equal comparison between two systems, they must be compared based on equal total transmitted power P_t in Equation 19.1. Thus, the power allocated to each spreading code decreases linearly with the increase in number of spreading codes, m_c, and thus with the quantized increase in transmitted bit rate. For each different code, the received signal power per code, S_c, is given by Equation 19.1 with the

$$P_{tc} = P_t \text{ total}/m_c.$$

Note, some CDMA systems can allocate different transmitter power to different codes. However, in order to transmit the maximum data rate at a maximum range, the maximum transmitter power per code is needed. Therefore, herein the transmitter power considered is the maximum possible and that power is considered to be distributed uniformly to the different codes in order to have the error performance uniform across the different codes.

Substituting the relationships above into the derivations in Section 19.2.1 yields the same relationships between data rate and range as in Section 19.2.2, that is, Equation 19.4, and the data rate versus range relationship is the same for increasing the number of spreading codes as for increasing the data rate by increasing the bandwidth.

An additional issue not included in the idealized discussion above is the fact that as the number of spreading codes is increased, the peak-to-average ratio of the transmitted signal increases. This occurs because of the increased number of levels needed to accommodate the increased number of spreading codes. The efficiency of transmitter amplifiers generally decreases as the peak-to-average ratio of the signal increases. Thus, as the data transmission rate increases for a CDMA system that increases data rate by increasing the number of spreading codes, the range will decrease even faster than indicated in the figures in Section 9.2.2 because the transmitter power will have to decrease to accommodate the increased peak-to-average power ratio required for the increasing number of spreading codes.

Also, the discussion above considers the noise out of a de-spreader to be independent of the number of codes. This may not be true depending on the correlation among codes, and so on. That is, the self-noise out of a de-spreader may increase with the number of codes. This would again cause the range to decrease even faster than indicated in the figures in Section 19.2.2.

19.6.3 Increasing Data Rate by Increasing Number of TDMA Time Slots

In some TDMA systems, for example, GPRS and EDGE derived from GSM, the transmission data rate is increased by increasing the number of TDMA time slots used and transmitting different segments of the transmitted data stream over different time slots. The transmitted bit-rate is then quantized by the number of time slots used.

19.6.3.1 Holding Total Transmitted Power Constant

In this case, the noise over each time slot remains constant. However, one must consider the transmitter power and resulting received signal power per time slot. For an equal comparison between two systems, they must be compared based on equal total transmitted power P_t in Equation 19.1. Thus, the power allocated to each time slot decreases linearly with the increase in number of time slots, m_s, and thus with the quantized increase in transmitted bit rate. For each different time slot, the received signal power per slot, s_s, is given by Equation 19.1 with the

$$P_{ts} = P_t \text{ total}/m_s.$$

To transmit the maximum data rate at a maximum range, the maximum transmitter power per time slot is needed. Therefore, herein the transmitter power considered is the maximum possible and that power is considered to be distributed uniformly over the different time slots in order to have the error performance uniform across the different slots.

Substituting the relationships above into the derivations in Section 19.2.1 yields the same relationship between data rate and range as in Section 19.2.2, that is, Equation 19.4, and the data rate versus range relationship is the same for increasing the number of time slots as for increasing the data rate by increasing the bandwidth.

19.6.3.2 Holding Power per Time Slot Constant

This case is trivial. Holding the transmitted power per time slot constant yields the same signal-to-noise ratio regardless of the number of time slots used. Thus, in this case, the range remains the same even as the transmission data rate increases. However, "you can't get something for nothing" in systems constrained by physics, that is, "there is no free lunch"! Obviously, as the number of time slots m_s increases, the total transmitted power increases by m_s. The total transmitter power is a dominant consumer of dc power in a handset so the dc power consumed increases as the transmission data rate increases. The result is a decrease in battery usage time, that is, in transmitting time. This is accompanied by an increase in handset temperature as more power is dissipated in transmitter circuit inefficiencies. As was observed in some early GPRS data handsets, the handset can become so hot that it is not comfortable to hold. This case can occur in TDMA systems because transmitter amplifiers are usually peak power limited. Thus, they can transmit the same amount of power in each time slot as long as they do not overheat on the increased total power transmitted.

19.7 Line-of-Sight Wireless Link Considerations

The data rate versus range relationships in the previous sections were derived for wireless transmission in environments cluttered with buildings, trees, and other obstacles. In these environments the wireless

signals experience greater transmission loss than in free space and the signal power decreases with distance faster than the $1/d^2$ of free space as indicated in Equation 19.1. This can result in much greater range for a given data rate over an unobstructed line-of-sight path than can be achieved in a cluttered environment. Examples of data transmission over line-of-sight paths are discussed below.

19.7.1 Terrestrial Line-of-Sight

In cluttered environments the excess transmission loss of the median of the log normal variation can range from perhaps 25 to 55 dB greater than free space values [1–4,11]. Wireless systems designed to provide coverage in such environments, for example, cellular systems, must have enough margin to overcome the excess loss at a given distance. Thus, if these systems were used on line-of-sight transmission paths, they could provide either much greater transmission bit rates at a particular distance, or a much greater range for a particular transmission bit rate.

The main reason cellular systems are able to operate successfully in severely cluttered environments is that they are designed to have large margins over what would be required to operate over line-of-sight paths. While a small part of the margin, only a few dB, is provided by forward error correcting codes in digital systems and perhaps signal processing in MIMO, by far the largest part of the margin is provided by the transmitter power, the receiver sensitivity, and the gain of base station antennas.

As an example, consider a middle value of excess loss of 40 dB below free space for the median of a lognormal large-scale variation at 10 km range. The 100 kb/s transmission possible for the median from Figure 19.2 in the cluttered environments would become 1 Gb/s possible for the same system over a free space (line-of-sight) path (40 dB is ×10,000 which multiplied by 100 kb/s yields 1 Gb/s). This transmission rate and distance are consistent with free space calculations (Friis equation) using typical cellular wireless system parameters.

Greater range than the 10 km could be provided by trading transmission bit rate for range with the free space attenuation increasing with $1/d^2$. For example, if the 1 Gb/s were reduced to 1 Mb/s, the receiver sensitivity would increase by a factor of 1000 or 30 dB (see Section 19.2). With free space attenuation increasing as $1/d^2$, the increase in range would be $\sqrt{1000}$ or a factor of about × 31. The 10 km range would increase to about 310 km for 1 Mb/s.

From the comments in Section 19.5 regarding reduced transmission link capabilities of WiFi compared to cellular systems, one would expect WiFi to have somewhat less range than the 310 km indicated above unless additional gain were provided in the radio link. On fixed wireless links, higher gain antennas are sometimes used to provide additional link gain.

A demonstration was run between mountain tops in 2005 by some radio amateurs [12]. They used WiFi transmitters with 30 mw output power and succeeded in transmitting at 1 Mb/s over a 34 mile path (~56 km) using 26 dB gain antennas on both ends of the path. The error control protocols were not capable of coping with the large delay, so even though the transmission rate was 1 Mb/s, the throughput was much lower because of repeated transmissions. The same group used different WiFi cards with changed retry time parameters to transmit between mountains separated by 56 miles (~93 km). The transmission bit rate over the 56 mile path is not reported but the authors state the data was transferred with "great data transfer rates." While the descriptions of these demonstrations do not include all the details, for example, received signal power is not reported, they do show that low-power WiFi can transmit a M b/s over many km over line-of-sight paths, and thus are consistent with the range and bit rate discussion above for line-of-sight wireless transmission.

19.7.2 Satellite Line-of-Sight

Mobile satellite systems, for example, Iridium and Globalstar, generally only support low data rate transmissions in line-of-sight conditions. Because of the very large ranges (many thousands of km) and

limited power on satellites to use for transmitters, these systems do not provide enough wireless link margin to work in cluttered environments, for example, within buildings, in city streets or canyons when line-of-sight does not exist, or under trees. While there is some gain from the satellite antennas, the user terminal antennas have essentially no gain. For these satellite mobile systems, the receiving antenna temperatures are essentially "room temperature," for example, 293°K so receiver sensitivity is ultimately limited by antenna temperature, regardless of how low the noise figure of the receiver amplifiers are.

In contrast, fixed satellite systems usually have high gain antennas at the earth terminals that aid in overcoming the large link loss associated with the long line-of-sight transmission paths. These high gain antennas have narrow beams that point at "cold sky." Thus, the satellite receiving antennas have low noise temperatures and the receivers benefit considerably from low noise receiving amplifiers. These two factors in fixed satellite systems, high antenna gain (and narrow beams) and high receiver sensitivity (from low noise temperature), contribute to wireless links that can support much higher data transmission rates than can be supported by mobile satellite systems.

19.8 Discussion

This chapter has considered the fundamental relationships between data transmission rate (bit rate), transmitter power and distance between transmitters and receivers (range) for wireless data systems. Other factors that offset the fundamental bit rate versus range curves were also noted, for example, percent of area covered, modulation level, use of MIMO, carrier frequency, and antenna height. It has been noted several times that the slope of the bit-rate-versus-range relationship was determined by the propagation environment and that this was a fundamental physical relationship. However, sometimes it is pointed out that the loss in glass optical fibers has been reduced significantly over time from the 1970s and that this permitted significant increases in the range of fiber systems and also increases in their bit rates. The implication is that wireless system attenuation too should be able to be reduced by advances in technology. The fallacy in this reasoning occurs from ignoring the fundamental difference between propagation in a one-dimensional (1-D) bounded medium, that is, glass optical fiber, and propagation in multi-dimensional unbounded media, that is, wireless propagation between antennas in open areas.

In ideal 1-D propagation, the signal power is confined to within the "pipe," that is, the fiber. The only loss mechanisms in nonideal 1-D propagation are leakage through the walls of the pipe and ohmic loss, that is, heating due to resistance in the walls and/or the medium within the pipe (for example, loss in the glass in the case of optical fiber). These losses result in a decrease in signal power along the pipe as $e^{-\alpha d}$, where α is an attenuation factor and d is distance along the pipe. This loss can also be expressed as decibels per unit distance, for example, dB/m or dB/ft. With this loss mechanism, the attenuation of signal power in the pipe can be reduced by reducing the wall leakage and/or the ohmic loss in the propagating medium. The reduction of these loss mechanisms in the glass in optical fibers was what permitted the large increases in range for glass optical fibers over the years. Improvements in technology also contributed to large increases in transmission rates in optical fibers.

However, the propagation mechanism for wireless signals transmitted between antennas in open areas is much different. Even in free space where there is no ohmic loss, at sufficient distance between the antennas the signal power from a transmitting antenna continues to expand (i.e., spread) to fill the increasing space. This results in the power density decreasing as $1/d^2$. Antennas with gain confine the angle within which the power spreads, but the power still spreads over a surface proportional to d^2 as distance increases. This so called spreading loss is fundamental to propagation in space that is not completely enclosed by walls, that is, unbounded. The presence of a ground reflection, reflections from objects, and shadowing by buildings and objects cause the propagation in cluttered environments to follow exponents, m, greater than 2, that is, to propagate as $1/d^m$. If this propagation in an unbounded region is in a medium with ohmic loss, an additional $e^{-\alpha d}$ factor is superimposed on the $1/d^m$ factor.

Thus, even in lossless media where $\alpha = 0$, wireless signals follow a fundamental $1/d^m$ relationship, and this results in the fundamental bit rate versus distance relationships plotted in the figures in this section. The wireless signal power received at some reference distance can be changed by changing antenna gains and other system factors, but a fundamental bit rate versus distance relationship still applies as discussed in this chapter. Wireless propagation cannot be improved in the same manner as propagation in glass optical fiber was improved.

Acknowledgments

The author acknowledges the partial support from Ericsson Inc. for preparing the original articles [13,14] on which this chapter is based. The author also benefited from discussions with Hyunok Lee, coauthor of Reference 13, and with Meriam Rezk.

References

1. W.C. Jakes, *Microwave Mobile Communications*. New York: Wiley, 1974; reissued by IEEE Press, 1994.
2. D.C. Cox, Universal digital portable radio communications, *Proc. IEEE*, 75(4), 436–477, 1987.
3. D.C. Cox, R.R. Murray, and A.W. Norris, 800 MHz attenuation measured in and around suburban houses, *Bell Labs Tech. J.*, 63(6), 921–954, 1984.
4. T.S. Rappaport, *Wireless Communications: Principles and Practice*, 2nd ed. New York: Prentice-Hall, 2002.
5. A.B. Carlson, P.B. Crilly, and J. Rutledge, *Communication Systems*, 4th ed. New York: McGraw-Hill, 2002.
6. A. Paulraj, R. Nabar, and D. Gore, *Introduction to Space-Time Wireless Communications*. London: Cambridge University Press, 2003.
7. E. Telatar, Capacity of multi-antenna Gaussian channels, *Eur. Trans. Telecomm.*, 10(6), 585–595, 1999.
8. P. Kyritsi, *Multiple Element Antenna Systems in an Indoor Environment*, PhD thesis, Stanford University, Stanford, CA, Nov. 2001.
9. D.M. Devasirvatham, R.R. Murray, H.W. Arnold, and D.C. Cox, Four-frequency CW measurements in residential environments for personal communications, in *Proc. IEEE Int. Symp. Personal, Indoor and Mobile Communications (PIMRC)*, Yokohama, Japan, Sept. 1993, pp. 201–205.
10. D.C. Cox, R.R. Murray, and A.W. Norris, Antenna height dependence of 800 MHz attenuation measured in houses, *IEEE Trans.Veh. Tech.*, 34(2), 108–115, 1985.
11. D.C. Cox, *Introduction to Wireless Communications*, course reader for EE276, Available from Stanford University Bookstore, Stanford, CA 94305.
12. D.R. Fordham, IEEE 802.11 experiments in Virginia's Shenandoah Valley, *QST*, 89(7), 35–41, 2005.
13. Donald C. Cox and Hyunok Lee, Physical relationships, *IEEE Microwave Magazine*, pp. 89–94, August 2008.
14. Donald C. Cox, Fundamental limitations on increasing data rate in wireless systems, *Technology Leaders Forum*, *IEEE Communications Magazine*, pp. 16–17, December 2008.

20

Interference and Its Impact on System Capacity

Bijan Jabbari

Alireza Babaei

20.1 Introduction

Wireless networks are fundamentally limited by two main factors: interference and fading. While fading results in random variation in the desired signal level, interference hinders the wireless users to decode their data successfully. The major reason for fading is known to be multipath propagation and its mathematical modeling using random processes is a well-studied subject [1]. Interference, however, is affected by many uncertainties present in the wireless networks whose precise modeling requires a holistic and multilayered approach.

The geometry of wireless networks, that is, the spatial distribution of wireless nodes which determines the internodal distances and thereby the path loss that the interfering signals undergo, as well as the shadowing and fading effects are two important factors which impact on the interference. Moreover, the choices of wireless protocols also impact on the characteristics of interference. For example, the MAC protocols and the scheduling algorithms used in the network determine the simultaneous wireless transmitters and thereby the set of interfering nodes. The routing algorithms used in a multihop wireless network also determine the interpath and intrapath interference experienced by wireless users [2].

Traditionally, wireless networks have used the spatial reuse to multiply the use of spectrum by considering a minimum separation between concurrent wireless transmitters on the same channel. This has brought about the cellular design for wireless networks [3]. The cellular design along with the reservation-based multiple access techniques (FDMA/TDMA/CDMA) used to be the main design principles for voice-centric wireless networks until recently. Inspired by the ever-increasing demand for wireless Internet and due to the intermittent and dynamic nature of Internet traffic, random access techniques (e.g., ALOHA, CSMA, etc.), which are more efficient for the sporadic Internet type of data, have become more popular in the wireless networks. Moreover, due to the recent requirements for emergency disaster recovery, wireless sensor networks, wireless mesh structures, and so on infrastructure-less wireless networks have recently become very important. Such wireless networks are highly decentralized and may

not benefit from a centralized agent to coordinate their transmissions. Interference characterization in such uncoordinated environments becomes an even more involved task.

20.2 Interference in Wireless Networks

Co-channel interference has been a major limiting factor ever since wireless communication evolved from the merely point-to-point or broadcast (i.e., one to many) communication scenarios to networks of wireless users. In a wireless network, many users share a common wireless medium, that is, a chunk of radio spectrum, to transmit information to their intended destinations. The transmitter–receiver pairs which use the same frequencies for communication will interfere and as a result neither may be successful in their communications. The medium access regulations and the interference management are therefore very important to share the wireless resources efficiently and maximize the network capacity.

Interference mitigation has been quite efficient in centralized wireless networks. These are infrastructure-based networks which utilize base stations (BS) or access points (AP) to facilitate the access of wireless users to a wired backbone. The network coverage area is usually partitioned into a number of cells and the users within these cells communicate directly to their associated BS. To avoid interference among users that transmit information on the same frequency (i.e., co-channel users), a natural solution is to take advantage of attenuation of wireless signals with distance and let the co-channel users transmit simultaneously only if their spatial separation is large enough to avoid interference. The cellular concept is a generalization of the spatial reuse approach. The idea is to allocate a portion of radio spectrum to each cell while keeping a minimum distance between co-channel cells. This results in frequency reuse as the same frequencies can be reused many times throughout the network [3]. Multiple access techniques have been implemented in the cellular networks under broad classification of narrowband and wideband systems [4].

There is a class of emerging wireless networks, like ad hoc, sensor, mesh and cognitive networks, where centralized control is not generally feasible and resource allocation is considered to be distributed. In such scenarios, the network self-interference is subject to considerable uncertainty and is not tightly controllable. Interference is the main limiting factor in these networks and its characterization is therefore critical. The locations of interfering nodes play the most important role in determining the characteristics of interference. The field of interferers is a function of underlying nodes distribution and the medium access technique used in the network. In order to model the interference behavior, mathematical models are required for the spatial locations of the interferers [5].

20.3 Interference Modeling

Sharing the space and the radio spectrum, wireless users transmit information to their intended destinations which results in multiuser interference (MUI). Interference impacts on key performance metrics in the network including outage, capacity, coverage, and connectivity. Knowledge of the statistical models for interference is of considerable importance for modeling and performance evaluation of wireless networks. To find the statistics of interference, it is important to have mathematical models which characterize the *geometry* of wireless networks. The geometry of a network determines the relative positions of the interfering nodes with respect to a given receiver. The propagation loss inflicted on the interference signals depend on the distances between the interferers and the receiver as well as the shadowing/fading effects which may be location dependent [1]. To investigate the effect of interference on successful communications, some of the models used in the literature are either pairwise, which means that they consider the effect of only one interfering signal at a time, or consider the cumulative effects of interference signals but assume that the network geometry is deterministic and channel gains are known. On the other hand, stochastic geometry and particularly, Theory of point processes have proven to be very useful disciplines for stochastic modeling of wireless networks and interference [6,7]. In the following, we consider some of the deterministic as well as random interference models that have been adopted in the literature.

20.3.1 Deterministic Interference Models

Deterministic interference models are based on the assumptions that the network geometry is not random and the channel gains between any two nodes are known. Let us denote the channel gain between two nodes X and Y in the network as $G_{X,Y}$. In the following, we discuss some of the deterministic models which have been commonly used in the literature.

Additive Interference and SINR Threshold [8]: This model is based on additive interference (i.e., considers the interference aggregation) and a signal-to-interference-plus-noise ratio (SINR) threshold for successful communications. The SINR threshold depends on the physical layer technique and the decoding strategy used. For a certain acceptable BER (bit error rate), the SINR needs to exceed an appropriate threshold. Let us denote the set of concurrently active links in the network as Λ. For a given link $m \in \Lambda$, m_o and m_d denote the transmitter node and the receiver node of link m respectively. The SINR perceived by m_d (denoted by γ_m) can be written as

$$\gamma_m = \frac{G_{m_o,m_d} P_m}{N + \sum_{l \in \Lambda \setminus \{m\}} G_{l_o,m_d} P_l}$$

where N denotes the noise power. Assuming that the SINR threshold for link m is β_m, communication on link m is successful if $\gamma_m \geq \beta_m$.

Capture Threshold Model: This is the model which is used in network simulator NS-2 [9]. This model makes use of thresholds: RxThreshold and CpThreshold which denote the receive and capture thresholds, respectively. Packet reception on link m is successful, provided that during the transmission time of packet

$$P_m G_{m_o,m_d} \geq \text{RxThreshold}$$

$$\frac{P_m G_{m_o,m_d}}{P_l G_{l_o,m_d}} \geq \text{CpThreshold} \quad \forall\, l \in \Lambda \setminus \{m\}$$

This model does not take into account the interference aggregation and interference is accounted only for one interfering signal at a time.

Protocol Model [8]: Based on the Protocol model, a packet transmission on link m is successful, provided that for each link $l \in \Lambda \setminus \{m\}$, we have

$$|l_o - m_d| \geq (1 + \Delta)|m_o - m_d| \quad \text{and} \quad |m_o - m_d| \leq R_C$$

where Δ is a positive parameter and R_C is the communication range.

Interference Range Model [10]: This model assumes fixed range for communication and interference. According to this model, a packet reception on link m is successful, provided that for each link $l \in \Lambda \setminus \{m\}$, we have

$$|l_o - m_d| \geq R_I \quad \text{and} \quad |m_o - m_d| \leq R_C,$$

where R_I is the interference range and R_C is the communication range. In the interference range model, the interferer–receiver separation is required to be larger than a fixed quantity. Protocol model, on the other hand, requires that this separation be larger than a quantity which is proportional to the transmitter–receiver separation.

In Reference 11, it is shown that some of these interference models are essentially equivalent. For example, the capture threshold model is shown to be equivalent to the protocol model under the power-law

path loss model ($G_{X,Y} = k|X - Y|^{-\alpha}$, where α is the path loss exponent and k is a constant) and when all nodes use the same modulation and coding schemes. As mentioned earlier, deterministic interference models are simple, however not always realistic mainly for following reasons: (i) interference aggregation is not considered in these models (except for the additive interference model), and (ii) the channel gains or distances between nodes are assumed to be known for any two nodes in the network.

20.3.2 Statistical Modeling of Aggregate Interference

Now, we consider the scenario that the wireless nodes are randomly distributed in space. This is a more realistic scenario as the locations of nodes at a given time instant is more likely to be random due to mobility. We focus on a Poisson network which is a well-adopted model in the literature. The Poisson assumption is valid when the nodes move in an uncorrelated fashion in a mobile wireless network which avoids the clustering of nodes. In a fixed wireless network, like wireless sensor networks, the Poisson assumption is also valid when the nodes are deployed randomly in the measurement field of sensors.

20.3.2.1 Mathematical Preliminaries

Point Processes: Point processes are random collection of points that are localized in space or time. Renewal processes are well-known one-dimensional examples of point processes in the time domain. These processes are stochastic models for events that occur randomly in time [12]. On the other hand, spatial point processes are defined in $\Re^d$, $d \geq 2$. These processes have found applications in disciplines like Seismology, Ecology, and Forestry [13–15]. Point processes are also considered for modeling the spatial distribution of nodes in wireless networks [6].

Poisson Point Processes: Poisson point process (PPP) is a valid and widely accepted model when the distribution of nodes in a random network lack correlation and the nodes do not form clusters. This is particularly useful to model the distribution of nodes in a mobile network when the mobile nodes move independently. Let us consider a Poisson point process defined in the Euclidean space: $\Re^d$, $d \leq 3$ with density $\lambda > 0$ and define a counting variable $N(A)$ for every $A \subset \Re^d$ as the number of points falling in A. In order to qualify as a Poisson point process, the point process defined over $S \subset \Re^d$ must have following properties:

Property 1: If $A \subseteq S$ is a bounded closed set, $N(A)$ is a Poisson random variable with mean $\lambda\mu(A)$ where $\mu(A)$ is the length, area or volume of A depending on the dimension of the space.

Property 2: Given that $A_1, \ldots, A_m$ are disjoint subsets of S, $N(A_1), \ldots, N(A_m)$ are independent random variables.

It is also noteworthy that a Poisson point process remains Poisson under probabilistic thinning. According to this property, if the points of a PPP with density λ are retained randomly with some retention probability p, the resulting point process will remain a PPP but with a smaller density of λp. Figure 20.1 shows a Poisson point process with density 0.01 defined in the two dimensional Euclidean space along with a thinned version with retention probability 0.1.

Random Sums: Let us consider a Poisson point process Π and a real valued function $f(x)$ which is defined for $x \in \Pi$, that is, for the points of point process. The sum

$$F = \sum_{x \in \Pi} f(x), \tag{20.1}$$

is a random variable. For any point process defined in the region R, it is known that the mean of F reduces to an integral over the region R as

$$E\{F\} = E\left\{\sum_{x \in \Pi} f(x)\right\} = \int_R f(x)\lambda(x)\mathrm{d}x.$$

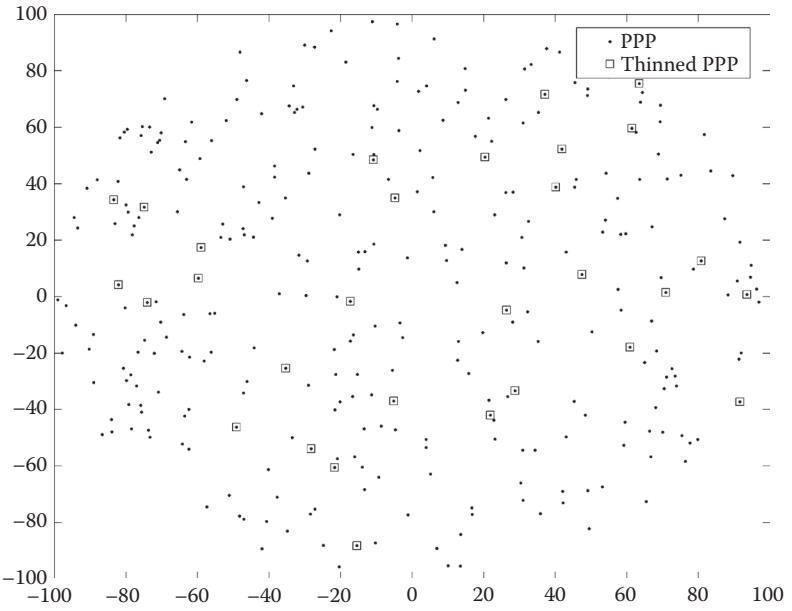

FIGURE 20.1 Sample PPP with $\lambda = 0.01$ in a disk with radius 100 and its thinned version with $p = 0.1$.

where $\lambda(x)$ is the density at point x (the point process can also be nonhomogeneous). Closed-form results for higher moments are not generally known for an arbitrary point process. For Poisson point processes, on the other hand, characteristic function of the random sum is known in closed from. Higher-order statistics of F can be obtained from the characteristic function [16]. Random sums have many applications in physics, signal processing, and communication problems.

Campbell's Theorem: The characteristic function of F defined in Equation 20.1 is [17]

$$\psi_F(\omega) = E\left\{e^{j\omega F}\right\} = \exp\left(\int_R \left(\exp\left(j\omega f(x)\right) - 1\right)\lambda(x)\,dx\right).$$

The nth cumulant of F can be found from the characteristics function:

$$\kappa_n = \frac{1}{j^n}\left[\frac{\partial^n \ln \psi_F(\omega)}{\partial \omega^n}\right]_{\omega=0} = \int_R f^n(x)\lambda(x)\,dx.$$

The cumulants and moments can be determined uniquely from one another.

20.3.2.2 Statistics of Interference from a Poisson Field of Interferers

Let us consider an infinite homogeneous Poisson point process with density λ defined on the two-dimensional Euclidean plane (i.e., $\Re^2$) and denote it by Π'. Assume that the points of Π' represent the locations of the interferers. The receiver can be assumed to be located at the origin without loss of generality. Our goal is to obtain the statistics of interference perceived at the receiver.

The propagation model is considered to be a combination of a deterministic path loss component as well as random fading. The propagation loss incurred on the received signal of a transmitter with

distance d apart from the receiver is assumed to be $Xg(d)$ where X denotes the random fading variable and $g(d)$ denotes the deterministic amplitude loss component. For example, for a power-law path loss model [18], we have $g(d) = d^{-\alpha/2}$, where α is the path loss exponent (note that the power loss is $d^{-\alpha}$). The random fading component is assumed to be independent and identically distributed (i.i.d) across different interferers and the probability distribution function (PDF) of X is denoted as $f_X(x)$.

Note that the power-law path loss model is not valid for distances less than 1 as it leads to amplification of transmitted power level and has a singularity at $d = 0$. To circumvent this problem, we make the assumption that no interferer can be physically located at the distances less than 1.

The ith nearest interferer to the receiver is denoted by node i and the distance from node i to the origin (i.e., the receiver) is denoted as R_i (see Figure 20.2). Using the above definitions, we obtain statistics of interference power and amplitude.

Statistics of Interference Power: Assuming that all the interferers use the same power level which is normalized to 1 and denoting $Y_i = X_i^2$, the aggregate interference power at the receiver can be shown as

$$I = \sum_i Y_i R_i^{-\alpha}. \tag{20.2}$$

One can see that aggregate interference is a random sum over the Poisson point process that models the locations of the interferers and has the same form as Equation 20.1. The effect of fading on each of the signals can be interpreted as a mark associated with the underlying Poisson point process [6,17]. We define the marked Poisson point process Π as

$$\Pi = \{(S,Y) | S \in \Pi'\}.$$

Since each point of Π' is marked independently, using the *marking Theorem* (see Reference 17), Π is a Poisson point process with density $\lambda f_Y(y)$ over $\Re^2 \setminus b(o,1) \times \Re^+$ where $\setminus$ and $b(o,1)$ denote the set exclusion operator and unit disk centered at the origin. Applying the Campbell's Theorem, the characteristic function of I can be found as

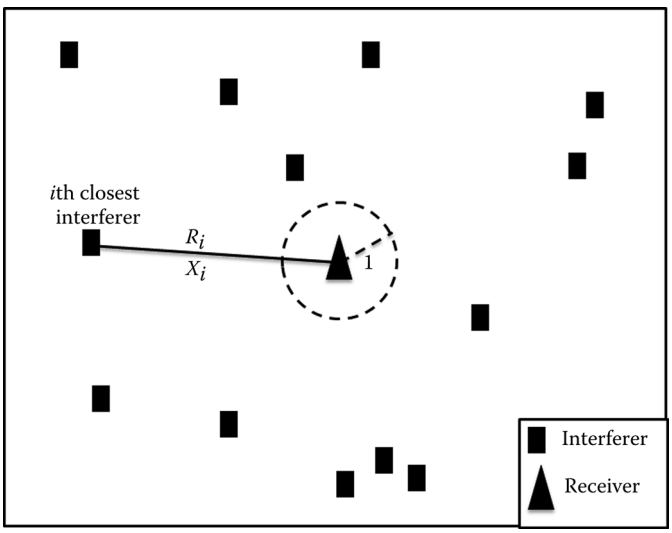

FIGURE 20.2 Poisson field of interferers.

$$\psi_I(\omega) = E\left\{e^{j\omega I}\right\} = \exp\left\{2\pi \int_Y \int_1^\infty \left[\exp\left(j\omega x r^{-\alpha}\right) - 1\right] r \, dr \lambda f_Y(y) dy\right\}.$$

The nth cumulant of I can be found as

$$\kappa_n = \frac{1}{j^n}\left[\frac{\partial^n \ln \psi_F(\omega)}{\partial \omega^n}\right]_{\omega=0}.$$

After simplification, and provided that $\alpha > 2$, we have

$$\begin{aligned}\kappa_n(I) &= 2\pi\lambda \int_0^\infty \int_1^\infty y^n r^{1-n\alpha} f_Y(y) dr \, dy \\ &= \frac{2\pi\lambda E\{Y^n\}}{n\alpha - 2}.\end{aligned} \tag{20.3}$$

Note that except for the free space path loss model for which we have $\alpha = 2$, the $\alpha > 2$ condition is always satisfied.

Statistics of Interference Amplitude: Now, let us consider the statistics of aggregate interference *amplitude* after the correlation detection at the receiver. These statistics are important for outage and capacity analysis. Denoting that the transmitted information symbol by node i as b_i with $E\{b_i^2\} = 1$ (note that b_i is also the transmitted baseband signal assuming amplitude modulation and transmit power normalized to 1), the received signal from node i in baseband will be $b_i X_i e^{-j\varphi_i} R_i^{-\alpha/2}$, where the φ_i factor is due random propagation delay which impacts on the phase of the received signal. Assuming that the arrival time of the interference signal is uniformly distributed between two sampling instants, the PDF of φ_i can be assumed uniform in $[0,2\pi]$. To simplify the analysis, we assume that only real-valued symbols are used by the interferers and therefore the in-phase component of interference is important for detection. The in-phase component of the aggregate interference amplitude, denoted by $\hat{I}$ can be written as

$$\hat{I} = \sum_i b_i X_i \cos(\varphi_i) R_i^{-\alpha/2}. \tag{20.4}$$

Denoting $U_i = \cos(\varphi_i)$, we have $\hat{I} = \sum_i b_i X_i U_i R_i^{-\alpha/2}$.

The statistics of $\hat{I}$ can also be found using Campbell's Theorem. The characteristic function of $\hat{I}$ can be found as

$$\psi_{\hat{I}}(\omega) = E\left\{e^{j\omega\hat{I}}\right\} = \exp\left\{2\pi \sum_i p(b_i) \int_X \int_U \int_1^\infty \left[\exp\left(j\omega b_i x u r^{-\alpha/2}\right) - 1\right] \lambda f_X(x) r \, dr \, du \, dx\right\},$$

where $p(b_i)$ is the probability of symbol b_i. The nth cumulant $\hat{I}$ can also be found as

$$\begin{aligned}\kappa_n(\hat{I}) &= \frac{1}{j^n}\left[\frac{\partial^n \ln \psi_F(\omega)}{\partial \omega^n}\right]_{\omega=0} \\ &= 2\pi\lambda E\{b_i^n\}\mu_n E\{X^n\} \int_1^\infty r^{1-n\alpha/2} dr.\end{aligned} \tag{20.5}$$

where $\mu_n = E\{U_i^n\}$. Note that for $n = 1$, we will see later that $\mu_1 = 0$ and consequently $\kappa_1 = 0$. For $n \geq 2$ and for $\alpha > 2$ the integral in the above equation converges and we have

$$\kappa_n(\hat{I}) = \frac{2\pi\lambda E\{b_i^n\}\mu_n E\{X^n\}}{(n\alpha/2) - 2}. \tag{20.6}$$

With the uniform pdf assumption for φ_i and using the transformation rule for random variables, we have

$$f_{U_i}(u) = \frac{1}{\pi\sqrt{1-u^2}}, \quad -1 < u < 1,$$

and

$$\mu_n = E\left\{U_i^n\right\} = \frac{\left((-1)^n + 1\right)\Gamma\left(\frac{n+1}{2}\right)}{\sqrt{\pi}n\Gamma\left(\frac{n}{2}\right)}. \tag{20.7}$$

Assuming Rayleigh fading with $E\{X^2\} = 1$, we have $E\{X^n\} = \Gamma(1 + n/2)$ and $E\{Y^n\} = n!$ Also with a BPSK assumption for transmitted symbols, we have

$$E\left\{b_i^n\right\} = \begin{cases} 1 & \text{even } n \\ 0 & \text{odd } n \end{cases}.$$

In Figure 20.3, assuming a Poisson field of interferers, with density $\lambda = 0.01$, analytical results for variance of interference power (i.e., $\kappa_2(I)$ using Equation 20.3) along with simulation results are provided.

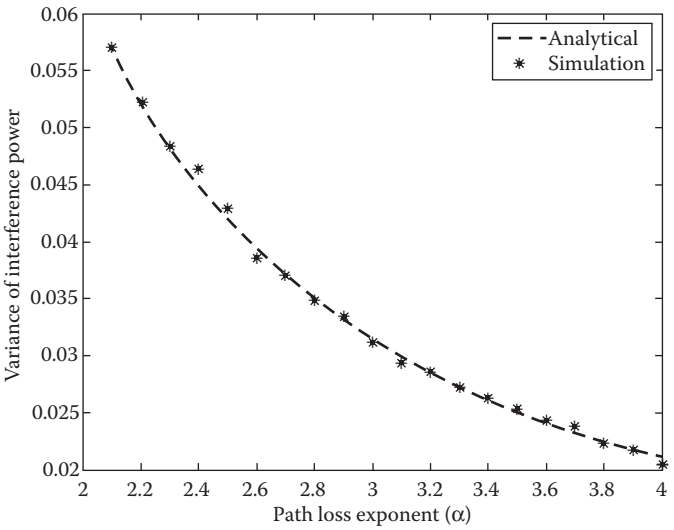

FIGURE 20.3 Variance of interference power versus path loss exponent ($\lambda = 0.01$).

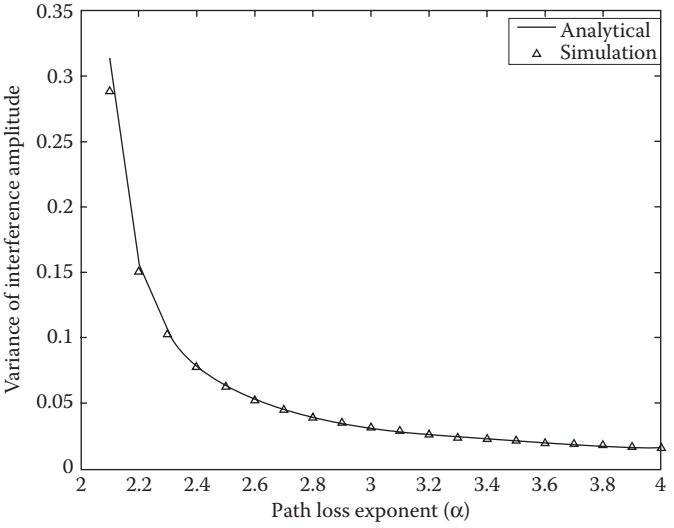

FIGURE 20.4 Variance of interference amplitude versus path loss exponent ($\lambda = 0.01$).

Analytical results for variance of interference amplitude (i.e., $\kappa_2(\hat{I})$ using Equation 20.6) along with simulation values are also shown in Figure 20.4.

20.3.2.3 Interference from a Thinned Poisson Network

20.3.2.3.1 Thinning due to Medium Access Regulations

Medium access regulations influence on the field of interferers by filtering the point process corresponding to a wireless network and determining the set of simultaneous transmitters or the interferers. In the following, we consider two well-adopted medium-access techniques and discuss their effect on the field of interferers and through that on the statistics of interference.

20.3.2.3.1.1 ALOHA Networks Using the ALOHA protocol, the field of simultaneous transmitters is the result of a probabilistic thinning of the original point process that models the network. For a Poisson network, the field of interferers will remain Poisson but with a smaller density. For example, assuming a Poisson network with density λ and ALOHA medium access with transmission attempt probability of p, the field of simultaneous transmitters will be a Poisson point process with density λp. If we consider the desired transmitter to be isolated from this process, the field of interferers is a PPP and the obtained results in the previous section can be applied to find the interference statistics.

20.3.2.3.1.2 CSMA Networks In a CSMA network, the distance between concurrent transmitters are kept above a minimum level, which implies that the numbers of points in disjoint areas are no longer independent. The Poisson point process, therefore, cannot be used to be model these networks. The point processes used to model these networks are known to be Matérn hard-core processes of types I and II [19]. Both of these processes are based on a parent PPP of intensity λ_p. In the type I process, all nodes with a neighbor within the hard-core distance δ are silenced, whereas in the type II process, each node has a random associated mark, and a node is silenced only if there is another node within distance δ with a smaller mark [20]. In Reference 20, it is shown that the type II Matérn hard-core process generates a level of interference which is comparable to the one of a Poisson point process. On the other hand, the type I process generates an excess interference (relative to the Poisson case) which grows exponentially in the hard-core distance.

20.3.2.3.2 Interference from Randomly Punctured Poisson Networks

Consider a random wireless network, where the field of simultaneous transmitters is a Poisson point process, denoted by Π. Assume that the receiver is interested in the signals transmitted by kth nearest transmitter for $k \in T$ and T represents the set of desired transmitters. In a random wireless network, the locations of the desired transmitter(s) are random. By excluding the desired transmitter(s), the field of interferers will be a randomly punctured version of Π. Examples for the above communications scenario include: cooperative communications where multiple users cooperate to transmit their information and the receiver requires the signals from all of these users to perform signal processing and detect their signals; or multiuser detection where the receiver wishes to detect signals from multiple users.

Most of the works for interference modeling in wireless networks assume that the interferers are distributed according to a PPP and isolate the desired transmitter from this point process. The desired transmitter is assumed to have a deterministic fixed distance to the receiver and to be separate from the PPP (e.g., [21–23]). The aggregate interference originated from a Poisson field of interferers can be modeled as a random sum over the PPP (see Section 20.3.2.2). In a more realistic scenario, the desired transmitter (or transmitters) also belongs to the point process that models the field of concurrent transmitters. By excluding the desired transmitter(s), the interference is coming from a randomly punctured PPP.

In Reference 24, an approximation approach is followed to obtain the statistics of interference from a randomly punctured Poisson field of interferers. The model adopted in Reference 24 considers carving out annular regions with inner and outer radii of R_{k-1} and R_{k+1} from the Euclidean plane for any $k \in T$. The resulting region, denoted by S, contains all the interferers. With equal transmission power levels from the interferers, the normalized interference power perceived at the receiver is

$$I = \sum_{i \in S} X_i R_i^{-\alpha}$$

As the inner and outer radii of annular regions are random variables, S has random boundaries. Depending on the indices of the desired transmitters, the annular regions may overlap. For example, for $T = \{4,5\}$, the regions: $\{R_3 \le r \le R_5\}$ and $\{R_4 \le r \le R_6\}$ overlap and the excluded region, which is the union of these annuli, is $\{R_3 \le r \le R_6\}$. Considering the overlap, the excluded region consists of M disjoint annului where M is less than or equal to the number of desired transmitters. Denoting the inner and outer radii of kth such annulus are denoted as $R_{k,l}$ and $R_{k,u}$, the boundaries of region S are $B = \bigcup_{k=1}^{M} \{R_{k,l}, R_{k,u}\}$. For example, for $T = \{4,5\}$, we have $M = 1$ and $B = \{R_3, R_6\}$ and for $T = \{4,7\}$, we have $M = 2$ and $B = \{R_3, R_5, R_6, R_8\}$.

To find statistics of interference power, we assume that the punctured point process keeps its Poisson property and therefore Campbell's Theorem can be used to find the statistics of interference. Conditioning on the random boundaries (i.e., the elements of B), the conditional cumulants of interference is found in Reference 24 and law of total cumulance is used to find the cumulants. Defining $Y_n = 1 - \sum_{i=1}^{M} (R_{i,u}^{2-n\alpha} - R_{i,l}^{2-n\alpha})$, the conditional cumulants of interference power are

$$\kappa_n\left(I \mid B\right) = \frac{2\pi\lambda E\{X^n\}}{n\alpha - 2} Y_n.$$

The mean of interference is therefore

$$E\{I\} = E\{\kappa_1(I \mid B)\} = \frac{2\pi\lambda E\{X\}}{\alpha - 2} E\{Y_1\}$$

where $E\{Y_1\} = 1 - \sum_{i=1}^{M}\left(E\{R_{i,u}^{2-\alpha}\} - E\{R_{i,l}^{2-\alpha}\}\right)$. For variance, the law of total cumulance degenerates to the law of total variance and we have

$$\begin{aligned}\text{var}\{I\} &= E\left\{\text{var}\left\{I \mid B\right\}\right\} + \text{var}\left\{E\left\{I \mid B\right\}\right\} \\ &= \frac{2\pi\lambda E\{X^2\}}{2\alpha - 2} E\{Y_2\} + \left(\frac{2\pi\lambda E\{X\}}{\alpha - 2}\right)\text{var}\{Y_1\},\end{aligned}$$

where

$$E\{Y_2\} = \frac{2\pi\lambda E\{X^2\}}{2\alpha - 2}\left(1 + \sum_{i=1}^{M}\left(E\left\{R_{i,u}^{2-2\alpha}\right\} - E\left\{R_{i,l}^{2-2\alpha}\right\}\right)\right),$$

and

$$\text{var}\{Y_1\} = \left(\frac{2\pi\lambda E\{X\}}{\alpha - 2}\right)^2 \text{var}\left\{\sum_{i=1}^{M}\left(R_{i,l}^{2-\alpha} - R_{i,u}^{2-\alpha}\right)\right\}.$$

To find the variance of interference, as can be seen from the above equation, the joint statistics of R_i and R_j, $i \neq j$, are required. The joint statistics are also required to find higher cumulants of interference. In Reference 24, it is found that for β a real number and for any set of indices $\{l_1, l_2, \ldots, l_n\}$ where $l_1 < l_2 < \cdots < l_n$, the joint moments can be found using

$$E\left\{R_{l_1}^{\beta} R_{l_2}^{\beta} \ldots R_{l_n}^{\beta}\right\} = \frac{1}{(\lambda\pi)^{n\beta/2}} \prod_{k=1}^{n} \frac{\Gamma(l_k + k\beta/2)}{\Gamma(l_k + (k-1)\beta/2)}.$$

Assuming the field of simultaneous transmitters is a two-dimensional Poisson point process with density $\lambda = 0.5$ and the desired transmitter is node k(i.e., kth nearest transmitter to the receiver), the analytical and simulation results for mean and variance of interference are shown in Figure 20.5. Rayleigh fading with $E\{X^2\} = 1$ and path loss exponent α equals 4 is assumed to obtain these results. As shown in these figures, the obtained analytical results and simulation values for interference statistics match.

20.4 Interference Statistics and Capacity

When it comes to the capacity of multiuser wireless networks, interference is conventionally assumed to have the characteristics of additive white Gaussian noise (AWGN). With this assumption, the well-known results for capacity of additive Gaussian noise channels can be used for capacity analysis. This assumption, however, is the most pessimistic one. This can be seen from Shannon's capacity bound for general additive channels [25]:

$$W \log_2\left(1 + \frac{P_r}{N_1}\right) \leq C \leq W \log_2\left(\frac{N}{N_1} + \frac{P_r}{N_1}\right), \tag{20.8}$$

where P_r is the received power, N_1 is the entropy power of interference and N is the interference power. To find the entropy power, complete statistics of interference is required. For a given N, it is always true that

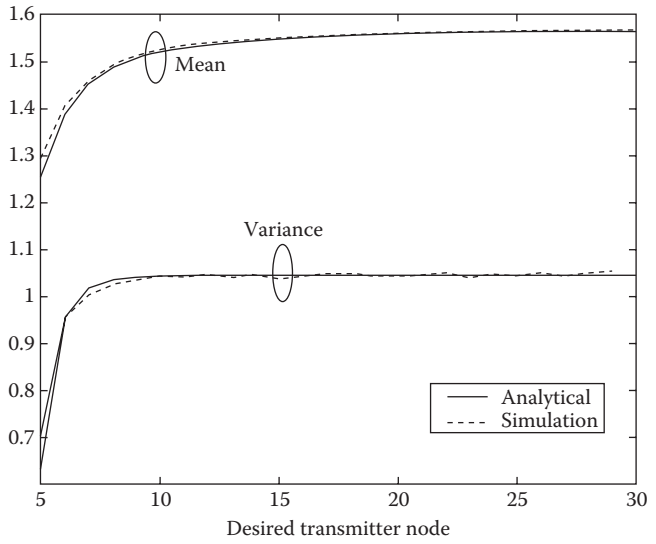

FIGURE 20.5 Mean and variance of interference versus desired transmitter index.

$N_1 \leq N$ for a general probability distribution of interference and the equality holds for the Gaussian-distributed interference. This is due to the *maximum entropy property* of Gaussian distribution. On the other hand, both upper and lower bounds of capacity decrease with entropy power. For the case of Gaussian-distributed interference, capacity is minimum and the bound degenerates to equality ($N = N_1$ and $C = \log_2(1 + (P/N))$). As can be observed from the above equation, to maximize the upper and lower bounds of capacity it is desirable to minimize the entropy power of interference for a given interference power. In Reference 26, it is shown that using the Gram–Charlier series expansion for the distribution of interference, we have

$$N_1 = \frac{N}{\exp\left(\dfrac{\text{kurt}^2(\hat{I})}{24}\right)}.$$

We can observe that to minimize the entropy power of interference for a given interference power (variance), its kurtosis needs to be maximized. Kurtosis, on the other hand, is one of the measures used for non-Gaussianity of random variables. The smaller the kurtosis is, the closer the distribution is to Gaussian.

20.4.1 Capacity Improvement through Interference Statistics Shaping

Now that we have demonstrated the effect of higher-order statistics of interference on the capacity, in this section we seek to answer this question: is it possible to shape the statistics of interference and thereby improve the capacity? To answer this question, we first consider the interference zones in a Poisson network.

Interference Zones: In Reference 27, interference power from a Poisson wireless network is shown to be comprised of a non-Gaussian component, mainly from the interfering nodes close to the receiver, and a Gaussian component, from the rest of interfering nodes. These components are shown to be statistically independent. The Euclidean plane is divided into the regions: $\{1 \leq r < R_b\}$ and $\{r \geq R_b\}$, where R_b

is the border of Gaussian and non-Gaussian zones. The interference from non-Gaussian and Gaussian regions are denoted as $\hat{I}_1$ and $\hat{I}_2$ respectively.

We consider two cases when the interfering nodes employ power control and the nodes inside the two interference regions employ different power levels P_1 and P_2, respectively, and the case that there is no power control and nodes inside the two regions employ the same power level. It will be shown that through power control, it is possible to control the higher-order statistics of interference and particularly the kurtosis of interference.

Interference Statistic with Power Control: The aggregate interference at the primary receiver will be $\hat{I} = \hat{I}_1 + \hat{I}_2$. By defining

$$S_1 = \left\{\mathrm{i} : 1 \le R_i < R_b\right\},$$
$$S_2 = \left\{\mathrm{i} : R_i \ge R_b\right\},$$

and assuming nodes in these regions use the power levels P_1 and P_2 respectively, we have

$$\hat{I}_j = \sum_{i \in S_j} \sqrt{P_i} b_i X_i U_i R_i^{-\alpha/2}, \quad j = 1, 2.$$

With the above definitions, $\kappa_n(\hat{I}_1)$ can be found by modifying Equation 20.5 as

$$\kappa_n(\hat{I}_1) = 2\pi\lambda P_1^{n/2} E\{b_i^n\} E\{U_i^n\} E\{X^n\} \int_1^{R_b} r^{1-n\alpha/2}\, \mathrm{d}r = A_n P_1^{n/2}$$

where

$$A_n = \frac{2\pi\lambda E\{b_i^n\} E\{U_i^n\} E\{X^n\} (1 - R_b^{2-n\alpha/2})}{n\alpha/2 - 1}.$$

Similarly, $\kappa_n(\hat{I}_2)$ can be found from as

$$\kappa_n(\hat{I}_2) = 2\pi\lambda P_2^{n/2} E\{b_i^n\} E\{U_i^n\} E\{X^n\} \int_{R_b}^{\infty} r^{1-n\alpha/2}\, \mathrm{d}r = B_n P_2^{n/2}$$

where

$$B_n = \frac{2\pi\lambda E\{b_i^n\} E\{U_i^n\} E\{X^n\} R_b^{2-n\alpha/2}}{n\alpha/2 - 1}.$$

Using the independence of $\hat{I}_1$ and $\hat{I}_2$, we have $\kappa_n(\hat{I}) = \kappa_n(\hat{I}_1) + \kappa_n(\hat{I}_2)$. Note that the interference will be zero mean as $\kappa_1(\hat{I}) = \kappa_1(\hat{I}_1) + \kappa_1(\hat{I}_2) = 0$. The kurtosis of interference will be

$$\mathrm{Kurtosis}(\hat{I}) = \frac{\kappa_4(\hat{I})}{\kappa_2^2(\hat{I})} = \frac{A_4 P_1^2 + B_4 P_2^2}{(A_2 P_1 + B_2 P_2)^2}.$$

When there is no power control and the same power level is used in the interference zones (i.e., $P_1 = P_2$), the kurtosis is a fixed value:

$$\text{Kurtosis}(\hat{I}) = \frac{A_4 + B_4}{(A_2 + B_2)^2},$$

and independent of the choice of power level.

Capacity Maximization Problem: As shown in Equation 20.8, to maximize the capacity, it is desirable to maximize the entropy power N_1. By choosing the appropriate levels of P_1 and P_2, capacity can be increased. Generally, following optimization problem can be solved to maximize the entropy power:

$$\text{Maximize } N_1 = \frac{N}{\exp\left(\frac{\text{kurt}^2(\hat{I})}{24}\right)}$$

$$\text{where kurtosis}(\hat{I}) = \frac{A_4P_1^2 + B_4P_2^2}{\left(A_2P_1 + B_2P_2\right)^2} \quad \text{and} \quad N = \kappa_2(\hat{I}) = A_2P_1 + B_2P_2.$$

$$\text{subject to} \quad P_{\min} \le P_1, \quad P_2 \le P_{\max}$$

where $P_{\min}$ and $P_{\max}$ are the minimum and maximum acceptable power levels and are system-defined parameters.

20.5 Applications in Cognitive Radio Networks

Cognitive radios (CR) are the enabling technology for dynamic spectrum access (DSA). In this access paradigm, an existing network which has an exclusive access right to a certain spectrum band and commonly known as *Primary Network* coexists and shares the spectrum with an unlicensed *Secondary Network*. The secondary network can coexist with the primary provided that the interference from the secondary users is below a certain threshold and does not cause any problem in detection of the primary data [28]. In other words, the presence of the secondary network should go unnoticed by the primary users. In this section, we discuss some of the previous results for interference modeling in the context of cognitive radio networks.

To avoid interference, a secondary unlicensed device has to fulfill node-level as well as network-level obligations. At the node level, it is only allowed to transmit if it does not detect data reception from its nearby primary neighbors. This is typically satisfied by secondary nodes performing spectrum sensing. Two well-known spectrum sensing approaches are in-band and out-of-band sensing [29,30]. In in-band sensing, a secondary device periodically (say every τ seconds) ceases its transmission on the primary network's spectrum band, senses the channel and quits transmission if it detects primary activity. The choice of τ depends on the sensitivity of a primary receiver to the secondary interference. The more sensitive the primary user is the smaller the τ must be. In out-of band sensing, a primary receiver makes its presence known to the secondary users by transmitting a beacon signal on a control out-of-band channel. Upon detecting this beacon, a secondary device knows that a primary receiver is in its range and therefore avoids transmission. In the following, we assume out-of band spectrum sensing in our analysis. We also assume that there is full correlation between the control channel and the primary data channel. This can be justified when the frequency separation of two channels is less than the coherence bandwidth of channel.

Denoting the amplitude of aggregate secondary interference by I_S, the interference constraint is shown as

$$\Pr\{I_S^2 > \beta\} < \varepsilon. \tag{20.9}$$

where β and ε are system-defined parameters.

System Model: We focus on a primary base station (BS) coexisting with an infinite secondary network with nodes randomly distributed according to a Poisson point process with density λ. The primary BS is assumed to be located at the origin. Similar to Section 20.3.2, we assume that no secondary node can be physically located at distances smaller than 1 to the BS. This will circumvent the invalidity of power-law path loss model for distances smaller than 1. We denote the ith closest secondary neighbor to the primary BS as node i and its distance as $R_{S,i}$. Secondary nodes are assumed to transmit at the same power level equal to P_S.

Spectrum Sensing Model: an out-of-band spectrum sensing where a primary receiver indicates its reception activity by transmitting a beacon on a control out-of-band channel is considered. The secondary nodes that detect this beacon signal avoid transmission. Assume that the power of beacon signal is P_b and the channel power gain from node i to the primary receiver is $X_i^2/R_{S,i}^{\alpha}$, where $\{X_i\}$ are i.i.d. Rayleigh random variables with $E\{X_i^2\} = 1$. Node i will therefore interfere with the primary receiver if the SNR of bean is less than a system-defined threshold. This happens if $P_b X_i^2/NR_{S,i}^{\alpha} < \gamma_0$, where N is the noise power, α is the path loss exponent and γ_0 is the threshold SNR for detection of the beacon.

Aggregate Interference Model: The aggregate interference amplitude has the same form as Equation 20.4 with necessary modification to include the spectrum sensing factor:

$$\hat{I} = \sum_i \sqrt{P_S} b_i X_i U_i R_{S,i}^{-\alpha/2} \mathbf{1}\left(\frac{P_b X_i^2}{NR_{S,i}^{\alpha}} < \gamma_0\right).$$

The received interference signal from node i will be $\left(\sqrt{P_S} a_i X_i / R_{S,i}^{\alpha/2}\right)\cos(\omega_0 t + \varphi_i)\mathbf{1}((P_b X_i^2/NR_{S,i}^{\alpha}) < \gamma_0)$ where $\mathbf{1}(.)$ is an indicator function which takes the value 1 if node i cannot sense the beacon and therefore contribute to the aggregate interference. Note that node i will sense the primary activity and avoid transmission only if $(X_i^2/R_{S,i}^{\alpha}) < (\gamma_0 N/P_b)$ or $R_{S,i} > (P_b X_i^2/\gamma_0 N)^{1/\alpha}$ where $(P_b X_i^2/\gamma_0 N)^{1/\alpha}$ can be interpreted as the sensing range for a given level of fading X_i.

Statistics of interference from secondary networks: Using Campbell's Theorem,

$$\begin{aligned}\kappa_n(I_S) &= 2\pi\lambda P^{n/2} E\{b_i^n\} \int_{-1}^{1}\int_{0}^{\infty}\int_{[1,\infty]\cap(h(x),\infty)} (xur^{-\alpha/2})^n r\,\mathrm{d}r f_X(x)\mathrm{d}x f_U(u)\mathrm{d}u \\ &= 2\pi\lambda P^{n/2} E\{b_i^n\}\mu_n \int_{0}^{\infty}\int_{[1,\infty]\cap(h(x),\infty)} r^{1-n\alpha/2}\,\mathrm{d}r x^n f_X(x)\mathrm{d}x \end{aligned} \tag{20.10}$$

where $h(x) = (P_b x^2/\gamma_0 N)^{1/\alpha}$ is the sensing range and μ_n is found in Equation 20.7. It is possible to further simplify $\kappa_n(I_S)$ by splitting the integral in Equation 20.10 into two parts as follows:

$$\kappa_n(I_S) = 2\pi\lambda P_S^{n/2} E\{b_i^n\}\mu_n \left\{\int_0^{x_1}\int_1^{\infty} r^{1-n\alpha/2} dr x^n f_X(x)\mathrm{d}x + \int_{x_1}^{\infty}\int_{h(x)}^{\infty} r^{1-n\alpha/2}\,\mathrm{d}r x^n f_X(x)\mathrm{d}x\right\},$$

where $x_1 = \sqrt{(\gamma_0 N/P_b)}$ is the fading value which results in sensing range equal to 1. After simplification,

$$\kappa_n(I_S) = \frac{2\pi\lambda P_S^{n/2} E\{b_i^n\}\mu_n}{2 - n\alpha/2}\left\{\int_0^{x_1} x^n f_X(x)\mathrm{d}x - \left(\frac{P_b}{\gamma_0 N}\right)^{\frac{4-n\alpha}{2\alpha}} \int_{x_1}^{\infty} x^{4/\alpha} f_X(x)\mathrm{d}x\right\}. \tag{20.11}$$

When X has Rayleigh distribution with $E\{X^2\} = 1$, the pdf of X is $f_X(x) = 2xe^{-x^2}, x \geq 0$ and for A, B, and C real numbers, we have

$$\int_0^A x^C f_X(x)\,dx = \Gamma_l(1 + C/2, A^2),$$

$$\int_A^\infty x^C f_X(x)\,dx = \Gamma_u(1 + C/2, A^2),$$

where $\Gamma_l(.)$ and $\Gamma_u(.)$ are the lower and upper incomplete gamma functions respectively [31]. These results can be used to find $\kappa_n(I_S)$ in Equation 20.11.

Considering a Poisson field of secondary interference with density $\lambda = 0.01$ and assuming $P_b = 10$ μW, $N = 1$ μW, and $\gamma_0 = -30$ dB, the second cumulant of interference (i.e., $\kappa_2(I_S)$) for the cases that nodes are equipped or are not equipped with spectrum sensing are shown in Figure 20.6. Analytical results are shown along with the simulation values for each case. Note that the case of no spectrum sensing is equivalent to assuming $\gamma_0 = \infty$. These results indicate that spectrum sensing significantly decreases the power of secondary interference perceived at the primary receiver.

Interference avoidance in cognitive radio networks: Now that statistical models for secondary interference are found, question arises as to how the interference power constraint can be satisfied by tuning the parameters of the secondary network's interference statistics. The secondary network can adjust the statistical parameters of interference either by controlling the density of interfering secondary nodes (e.g., through media access (MAC) regulation techniques) or by controlling the power level(s) chosen by secondary nodes. In the following, the power control for secondary network as a means for satisfying the interference constraint is discussed.

Using the interference constraint given in Equation 20.9, a probability distribution function for interference needs to be specified. Interference has been approximated using different probability distribution functions, including Gaussian distribution [32] (which requires up to second-order statistics), generalized Gaussian distribution [33] (which requires up to fourth-order statistics), Gaussian mixture distribution [34], and so on.

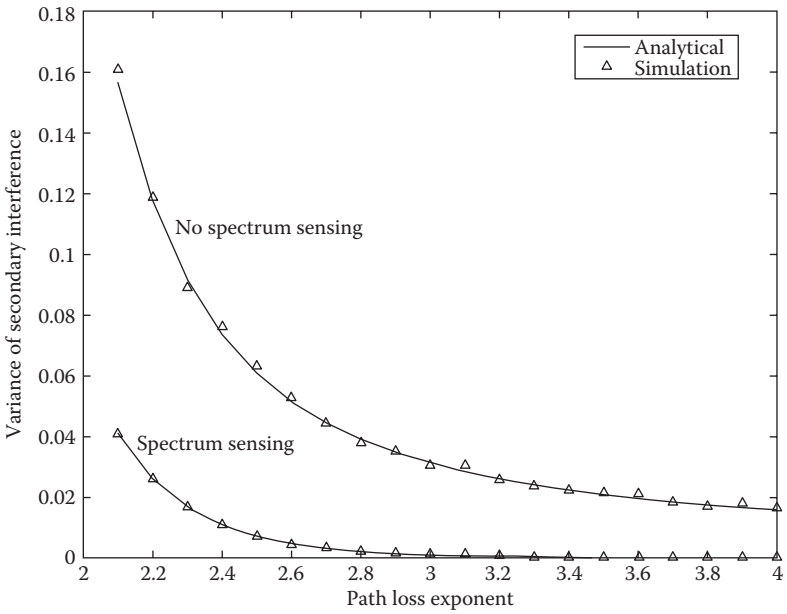

FIGURE 20.6 Variance of secondary interference with and without spectrum sensing.

Assuming a Gaussian distribution for interference statistics and using the interference constraint given in Equation 20.9, we must have

$$2Q\left(\frac{\sqrt{\beta}}{\sqrt{\text{var}\{I\}}}\right) < \varepsilon,$$

or equivalently, P_S must be chosen such that

$$\text{var}\{I_S\} = \kappa_2(I_S) < \frac{\beta}{\left[Q^{-1}\left(\frac{\varepsilon}{2}\right)\right]^2}.$$

With a generalized Gaussian assumption for interference, interference statistics up to fourth order need to be considered. The PDF of a zero-mean generalized Gaussian interference can be written as

$$f_{I_S}(x) = \frac{\theta}{2\rho\Gamma(1/\theta)}\exp\left(-\left(\frac{|x|}{\rho}\right)^{\theta}\right)$$

where $\theta > 0$ is the shape parameter and $\rho > 0$ is the scale parameter. The variance and the kurtosis of a generalized Gaussian distribution are given by

$$\text{variance} = \frac{\rho^2\Gamma(3/\theta)}{\Gamma(1/\theta)},$$

$$\text{kurtosis} = \frac{\Gamma(5/\theta)\Gamma(1/\theta)}{\Gamma^2(3/\theta)} - 3,$$

where ρ and θ are the shape and scale parameters, respectively, and the kurtosis equals $(\kappa_4(I_S)/\kappa_2^2(I_S))$. The shape and scale parameters can be uniquely determined by solving the above equations for a given variance and kurtosis of interference.

For a generalized gamma distributed I_S, we have [35]

$$\Pr\left\{I_S^2 > \beta\right\} = 1 - \frac{\Gamma_l\left(\frac{1}{\theta}, \left(\frac{\beta}{\rho^2}\right)^{\theta/2}\right)}{\Gamma(1/\theta)}.$$

The choice of P_S influences on the variance and kurtosis and through them on the shape and scale parameters of interference and consequently, on $\Pr\{I_S^2 > \beta\}$. The power level can therefore be adjusted so that $\Pr\{I_S^2 > \beta\} < \varepsilon$ and interference constraint is satisfied.

20.6 Conclusions

Emerging wireless networks tend to favor distributed resource allocation and local interference management. The effect of aggregate interference may be significant in a large wireless network. Interference,

on the other hand, limits the networks performance in terms of capacity, outage and connectivity. Statistical modeling of interference is important for performance evaluation and design of wireless networks. In this chapter, we consider modeling of interference assuming deterministic and random network geometries. The effect of interference statistics on capacity and capacity enhancement by shaping higher-order statistics of interference is discussed. Some applications of the obtained results in cognitive radio networks are also examined.

References

1. W. C. Jakes, *Microwave Mobile Communications*, Wiley-IEEE Press, Piscataway, NJ, 1994.
2. A. P. Subramanian, M. M. Buddhikot, and S. Miller, Interference aware routing in multi-radio wireless mesh networks, in *Proceedings of IEEE WiMesh 2006*, Reston, Virginia, Sept. 2006.
3. V. H. MacDonald, Advanced mobile phone service the cellular concept, *Bell System Technical Journal*, 58(1), 15–41, 1979.
4. D. Tse and P. Wisvanath, *Fundamentals of Wireless Communications*, Cambridge University Press, New York, 2005.
5. J. G. Andrews, M. Haenggi, N. Jindal, and S. Weber, A primer on spatial modeling and analysis in wireless networks, *IEEE Communications Magazine*, Nov. 2–9, 2010.
6. F. Baccelli and B. Blaszczyszyn, *Stochastic Geometry and Wireless Networks*, Foundation and Trends in Wireless Networking, NOW Publishers, Paris, France, 2009.
7. M. Haenggi, J. G. Andrews, F. Baccelli, O. Dousse, and M. Franceschetti, Stochastic geometry and random graphs for the analysis and design of wireless networks, *IEEE Journal of Selected Areas in Communications*, 27(7), 1029–1046, 2009.
8. P. Gupta and P. R. Kumar, The capacity of wireless networks, *IEEE Transactions on Information Theory*, 46(2), 388–404, 2000.
9. The NS2 Network Simulator, available online at www.isi.edu/nsnam/ns/
10. T. Nandagopal, T. E. kim, X. Gao, and V. Bharghavan, Achieving MAC layer fairness in wireless packet networks, in *Proceedings of IEEE/ACM Mobicom 2000*, Boston, Massachusetts, Aug. 2000.
11. A. Iyer, C. Rosenberg, and A. Karnik, What is the right model for wireless channel interference, *IEEE Transactions on Wireless Communications*, 8(5), 2662–2671, 2009.
12. David Cox, *Renewal Theory*, Methuen, London, UK, 1970.
13. P. J. Diggle, *Statistical Analysis of Spatial Point Patterns*, 2nd Edition, Arnold, London, UK, 2003.
14. J. A. Ludwig and J. F. Reynolds, *Statistical Ecology:* A *Primer on Methods and Computing*, John Wiley & Sons, New York, 1988.
15. J. Ohser and F. Mucklich, *Statistical Analysis of Microstructures in Materials Science*, John Wiley & Sons, Chichester, 2000.
16. N. Campbell, The study of discontinuous phenomena, *Mathematica Proceedings of the Cambridge Philosophy Society*, 15, 117–136, 1909.
17. J. Kingman, *Poisson Processes*, Oxford University Press, New York, 1993.
18. M. Schwartz, *Mobile Wireless Communications*, Cambridge University Press, New York, 2005.
19. B. Matérn, *Spatial Variation*, Springer Lecture Notes in Statistics, New York, 2nd edition, 1986.
20. M. Haenggi, Mean interference in hard-core wireless networks, *IEEE Communications Letters*, 15(8), 2011.
21. E. S. Sousa and J. A. Silvester, Optimum transmission ranges in a direct-sequence spread-spectrum multihop packet radio network, *IEEE Journal of Selected Areas in Communications*, 8(5), 762–771, 1990.
22. J. Ilow and D. Hatzinakos, Analytical alpha-stable noise modeling in a poisson field of interferers or scatterers, *IEEE Trans. Signal Process.,* 46(6), 1601–1611, 1998.
23. K. Gulati, B. L. Evans, J. G. Andrews, and K. R. Tinsley, Statistics of co-channel interference in a field of poisson and poisson-poisson clustered interferers, *IEEE Trans. Signal Process.*, 58(12), 2010.

24. A. Babaei, M. Haenggi, P. Agrawal, and B. Jabbari, Interference statistics of a poisson field of interferers with random puncturing, in *Proceedings of IEEE Military communications Conference 2011*, Baltimore, Maryland, Nov. 2011.
25. S. Ihara, On the capacity of channels with additive non-gaussian noise, *Information and Control*, 37, 34–39, 1978.
26. A. Babaei, P. Agrawal, and B. Jabbari, Capacity bounds in random wireless networks, *Journal of Communications and Networks*, 14(1), 2012.
27. A. Babaei and B. Jabbari, Interference modeling and avoidance in spectrum underlay cognitive wireless networks, In *Proceedings of ICC 2010*, Cape Town, South Africa, May 2010, pp. 1–5.
28. S. Haykin, Cognitive radio: brain-empowered wireless communications, *IEEE Journal on Selected Areas in Communications*, 32(2), 201–220, 2005.
29. D. Cabric, S. M. Mishra, and R. W. Brodersen, Implementation issues in spectrum sensing for cognitive radios, in *Proceedings of Asilomar Conference on Signals, Systems, and Computers*, Monterey, California, Nov. 2004, pp. 772–776.
30. A. P. Hulbert, Spectrum sharing through beacons, In *Proc. IEEE Int. Symp. Personal, Indoor and Mobile Radio Communications (PIMRC'05)*, Berlin, Germany, Sept. 2005, pp. 989–993.
31. M. Abramowitz, Milton, and I. A., *Handbook of Mathematical*, New York: Dover Publications, 1972.
32. A. Babaei and B. Jabbari, Internodal distance distribution and power control for coexisting radio networks, in *Proceedings of Globecom 2008*, Dec. 2008, pp. 1–5.
33. A. Babaei, P. Agrawal, and B. Jabbari, Cooperative spectrum sharing for a primary network with capacity constraint, In *Proceedings of IEEE VTC-Spring 2011,* Budapest, Hungary, 2011.
34. D. Middleton, Statistical-physical models of electromagnetic interference, U.S. department of commerce, office of telecommunications, *Tech. Rep.*, Apr. 1976.
35. A. Papoulis and S. U. Pillai, *Probability, Random Variables and Stochastic Processes*, 4th Edition, McGraw-Hill, New York, 2002.

21

Cell Design Principles

Michel Daoud Yacoub

21.1 Introduction

Designing a cellular network is a challenging task that invites engineers to exercise all their knowledge in telecommunications. Although it may not be necessary to work as an expert in all of the fields, the interrelationship among the areas involved impels the designer to naturally search for a deeper understanding of the main phenomenon. In other words, the time for segregation, when radio engineers and traffic engineers would not talk to each other, at least through a common vocabulary, is probably gone.

A great many aspects must be considered in a cellular network planning. The main ones include the following.

Radio Propagation: Here the topography and the morphology of the terrain, the urbanization factor and the clutter factor of the city, and some other aspects of the target geographical region under investigation will constitute the input data for the radio coverage design.

Frequency Regulation and Planning: In most countries there is a centralized organization, usually performed by a government entity, regulating the assignment and use of the radio spectrum. The frequency planning within the assigned spectrum should then be made so that interferences are minimized and the traffic demand is satisfied.

Modulation: As far as analog systems are concerned, the narrowband FM is widely used due to its remarkable performance in the presence of fading. The North American Digital Cellular Standard IS-54 proposes the $\pi/4$ differential quadrature phase-shift keying ($\pi/4$ DQPSK) modulation, whereas the Global Standard for Mobile Communications (GSM) establishes the use of the Gaussian minimum-shift keying (GMSK).

Antenna Design: To cover large areas and for low-traffic applications omnidirectional antennas are recommended. Some systems at their inception may have these characteristics, and the utilization of omnidirectional antennas certainly keeps the initial investment low. As the

traffic demand increases, the use of some sort of capacity enhancement technique to meet the demand, such as replacing the omnidirectional by directional antennas, is mandatory.

Transmission Planning: The structure of the channels, both for signaling and for voice, is one of the aspects to be considered in this topic. Other aspects include the performance of the transmission components (power capacity, noise, bandwidth, stability, etc.) and the design or specification of transmitters and receivers.

Switching Exchange: In most cases this consists of adapting the existing switching network for mobile radio communication purposes.

Teletraffic: For a given grade of service and number of channels available, how many subscribers can be accommodated into the system? What is the proportion of voice and signaling channels?

Software Design: With the use of microprocessors throughout the system there are software applications in the mobile unit, in the base station, and in the switching exchange.

Other aspects, such as human factors, economics, and so on, will also influence the design.

This chapter outlines the aspects involving the basic design steps in cellular network planning. Topics, such as traffic engineering, cell coverage, and interference, will be covered, and application examples will be given throughout the section so as to illustrate the main ideas. We start by recalling the basic concepts including *cellular principles, performance measures and system requirements*, and *system expansion techniques.*

21.2 Cellular Principles

The basic idea of the cellular concept is *frequency reuse* in which the same set of channels can be reused in different geographical locations sufficiently apart from each other so that *co-channel interference* is within tolerable limits. The set of channels available in the system is assigned to a group of *cells* constituting the *cluster.* Cells are assumed to have a *regular hexagonal* shape and the number of cells per cluster determines the *repeat pattern*. Because of the hexagonal geometry only certain repeat patterns can tessellate. The number N of cells per cluster is given by

$$N = i^2 + ij + j^2 \tag{21.1}$$

where i and j are integers. From Equation 21.1 we note that the clusters can accommodate only certain numbers of cells such as 1, 3, 4, 7, 9, 12, 13, 16, 19, 21 most common being 4 and 7. The number of cells per cluster is intuitively related with system capacity as well as with transmission quality. The fewer cells per cluster, the larger the number of channels per cell (higher traffic carrying capacity) and the closer the co-cells (potentially more co-channel interference). An important parameter of a cellular layout relating these entities is the D/R ratio, where D is the distance between co-cells and R is the cell radius. In a hexagonal geometry it is found that

$$D/R = \sqrt{3N} \tag{21.2}$$

21.3 Performance Measures and System Requirements

Two parameters are intimately related with the grade of service of the cellular systems: carrier-to-co-channel interference ratio and blocking probability.

A high carrier-to-co-channel interference ratio in connection with a low-blocking probability is the desirable situation. This can be accomplished, for instance, in a large cluster with a low-traffic condition. In such a case the required grade of service can be achieved, although the resources may not be efficiently

utilized. Therefore, a measure of efficiency is of interest. The spectrum efficiency η_s expressed in erlang per square meter per hertz, yields a measure of how efficiently space, frequency, and time are used, and it is given by

$$\eta_s = \frac{\text{number of reuses}}{\text{coverage area}} \times \frac{\text{number of channels}}{\text{bandwidth available}} \times \frac{\text{time the channel is busy}}{\text{total time of the channel}}$$

Another measure of interest is the trunking efficiency in which the number of subscribers per channel is obtained as a function of the number of channels per cell for different values of blocking probability. As an example, assume that a cell operates with 40 channels and that the mean blocking probability is required to be 5%. Using the erlang-B formula (refer to the Traffic Engineering section of this chapter), the traffic offered is calculated as 34.6 erlang. If the traffic per subscriber is assumed to be 0.02 erl, a total of $34.6/0.02 = 1730$ subscribers in the cell is found. In other words, the trunking efficiency is $1730/40 = 43.25$ subscribers per channel in a 40-channel cell. Simple calculations show that the trunking efficiency decreases rapidly when the number of channels per cell falls below 20.

The basic specifications require cellular services to be offered with a fixed telephone network quality. Blocking probability should be kept below 2%. As for the transmission aspect, the aim is to provide good-quality service for 90% of the time. Transmission quality concerns the following parameters:

- Signal-to-co-channel interference (S/I_c) ratio
- Carrier-to-co-channel interference ratio (C/I_c)
- Signal plus noise plus distortion-to-noise plus distortion (*SINAD*) ratio
- Signal-to-noise (*S/N*) ratio
- Adjacent channel interference selectivity (*ACS*)

The S/I_c is a subjective measure, usually taken to be around 17 dB. The corresponding C/I_c depends on the modulation scheme. For instance, this is around 8 dB for 25-kHz FM, 12 dB for 12.5-kHz FM, and 7 dB for GMSK, but the requirements may vary from system to system. A common figure for *SINAD* is 12 dB for 25-kHz FM. The minimum *S/N* requirement is 18 dB, whereas *ACS* is specified to be no less than 70 dB.

21.4 System Expansion Techniques

The obvious and most common way of permitting more subscribers into the network is by allowing system performance degradation but within acceptable levels. The question is how to objectively define what is acceptable. In general, the subscribers are more likely to tolerate a poor-quality service rather than not having the service at all. Some alternative expansion techniques, however, do exist that can be applied to increase the system capacity. The most widely known are as follows.

Adding New Channels: In general, when the system is set up not all the channels need to be used, and growth and expansion can be planned in an orderly manner by utilizing the channels that are still available.

Frequency Borrowing: If some cells become more overloaded than others, it may be possible to reallocate channels by transferring frequencies so that the traffic demand can be accommodated.

Change of Cell Pattern: Smaller clusters can be used to allow more channels to attend a bigger traffic demand at the expense of a degradation of the transmission quality.

Cell Splitting: By reducing the size of the cells, more cells per area, and consequently more channels per area, are used with a consequent increase in traffic capacity. A radius reduction by a factor of *f* reduces the coverage area and increases the number of base stations by a

factor of f^2 Cell splitting usually takes place at the midpoint of the congested areas and is so planned in order that the old base stations are kept.

Sectorization: A cell is divided into a number of sectors, three and six being the most common arrangements, each of which is served by a different set of channels and illuminated by a directional antenna. The sector, therefore, can be considered as a new cell. The base stations can be located either at the center or at the corner of the cell. The cells in the first case are referred to as center-excited cells and in the second as corner-excited cells. Directional antennas cut down the co-channel interference, allowing the co-cells to be more closely spaced. Closer cell spacing implies smaller D/R ratio, corresponding to smaller clusters, that is, higher capacity.

Channel Allocation Algorithms: The efficient use of channels determines the good performance of the system and can be obtained by different channel assignment techniques. The most widely used algorithm is based on fixed allocation. Dynamic allocation strategies may give better performance but are very dependent on the traffic profile and are usually difficult to implement.

21.5 Basic Design Steps

Engineering a cellular system to meet the required objectives is not a straightforward task. It demands a great deal of information, such as market demographics, area to be served, traffic offered, and other data not usually available in the earlier stages of system design. As the network evolves, additional statistics will help the system performance assessment and replanning. The main steps in a cellular system design are as follows.

Definition of the Service Area: In general, the responsibility for this step of the project lies on the operating companies and constitutes a tricky task, because it depends on the market demographics and, consequently, on how much the company is willing to invest.

Definition of the Traffic Profile: As before, this step depends on the market demographics and is estimated by taking into account the number of potential subscribers within the service area.

Choice of Reuse Pattern: Given the traffic distribution and the interference requirements a choice of the reuse pattern is carried out.

Location of the Base Stations: The location of the first base station constitutes an important step. A significant parameter to be taken into account in this is the relevance of the region to be served. The base station location is chosen so as to be at the center of or as close as possible to the target region. Data, such as available infrastructure and land, as well as local regulations are taken into consideration in this step. The cell radius is defined as a function of the traffic distribution. In urban areas, where the traffic is more heavily concentrated, smaller cells are chosen so as to attend the demand with the available channels. In suburban and in rural areas, the radius is chosen to be large because the traffic demand tends to be small. Once the placement of the first base station has been defined, the others will be accommodated in accordance with the repeat pattern chosen.

Radio Coverage Prediction: Given the topography and the morphology of the terrain, a radio prediction algorithm, implemented in the computer, can be used to predict the signal strength in the geographic region. An alternative to this relies on field measurements with the use of appropriate equipment. The first option is usually less costly and is widely used.

Design Checkup: At this point it is necessary to check whether or not the parameters with which the system has been designed satisfy the requirements. For instance, it may be necessary to re-evaluate the base station location, the antenna height, and so on, so that better performance can be attained.

Field Measurements: For a better tuning of the parameters involved, field measurements (radio survey) should be included in the design. This can be carried out with transmitters and towers provisionally set up at the locations initially defined for the base station.

The cost assessment may require that a redesign of the system should be carried out.

21.6 Traffic Engineering

The starting point for engineering the traffic is the knowledge of the required grade of service. This is usually specified to be around 2% during the busy hour. The question lies on defining the busy hour. There are usually three possible definitions: (1) busy hour at the busiest cell, (2) system busy hour, and (3) system average over all hours.

The estimate of the subscriber usage rate is usually made on a demographic basis from which the traffic distribution can be worked out and the cell areas identified. Given the repeat pattern (cluster size), the cluster with the highest traffic is chosen for the initial design. The traffic A in each cell is estimated and, with the desired blocking probability $E(A, M)$, the erlang-B formula as given by Equation 21.3 is used to determine the number of channels per cell, M

$$E(M, A) = \frac{A^M/M!}{\sum_{i=0}^{M} A^i/i!} \tag{21.3}$$

In case the total number of available channels is not large enough to provide the required grade of service, the area covered by the cluster should be reduced in order to reduce the traffic per cell. In such a case, a new study on the interference problems must be carried out. The other clusters can reuse the same channels according to the reuse pattern. Not all channels need to be provided by the base stations of those cells where the traffic is supposedly smaller than that of the heaviest loaded cluster. They will eventually be used as the system grows.

The traffic distribution varies in time and space, but it is commonly bell shaped. High concentrations are found in the city center during the rush hour, decreasing toward the outskirts. After the busy hour and toward the end of the day, this concentration changes as the users move from the town center to their homes. Note that because of the mobility of the users handoffs and roaming are always occurring, reducing the channel holding times in the cell where the calls are generated and increasing the traffic in the cell where the mobiles travel. Accordingly, the erlang-B formula is, in fact, a rough approximation used to model the traffic process in this ever-changing environment. A full investigation of the traffic performance in such a dynamic system requires all the phenomena to be taken into account, making any traffic model intricate. Software simulation packages can be used so as to facilitate the understanding of the main phenomena as well as to help system planning. This is a useful alternative to the complex modeling, typically present in the analysis of cellular networks, where closed-form solutions are not usually available.

On the other hand, conventional traffic theory, in particular, the erlang-B formula, is a handy tool widely used in cellular planning. At the inception of the system the calculations are carried out based on the best available traffic estimates, and the system capacity is obtained by grossly exaggerating the calculated figures. With the system in operation some adjustments must be made so that the requirements are met.

The approach just mentioned assumes the simplest channel assignment algorithm: the fixed allocation. It has the maximum spatial efficiency in channel reuse, since the channels are always assigned at the minimum reuse distance. Moreover, because each cell has a fixed set of channels, the channel assignment control for the calls can be distributed among the base stations.

The main problem of fixed allocation is its inability to deal with the alteration of the traffic pattern. Because of the mobility of the subscribers, some cells may experience a sudden growth in the traffic offered, with a consequent deterioration of the grade of service, whereas other cells may have free channels that cannot be used by the congested cells.

A possible solution for this is the use of dynamic channel allocation algorithms in which the channels are allocated on a demand basis. There is an infinitude of strategies using the dynamic assignment principles, but they are usually complex to implement. An interim solution can be exercised if the

change of the traffic pattern is predictable. For instance, if a region is likely to have an increase of the traffic on a given day (say, a football stadium on a match day), a mobile base station can be moved toward such a region in order to alleviate the local base.

Another specific solution uses the traffic available at the boundary between cells that may well communicate with more than one base station. In this case, a call that is blocked in its own cell can be directed to the neighboring cell to be served by its base station. This strategy, called *directed retry*, is known to substantially improve the traffic capacity. On the other hand, because channels with marginally acceptable transmission quality may be used, an increase in the interference levels, both for adjacent channel and for co-channel, can be expected. Moreover, subscribers with radio access only to their own base will experience an increase in blocking probability.

21.7 Cell Coverage

The propagation of energy in a mobile radio environment is strongly influenced by several factors, including the natural and artificial relief, propagation frequency, antenna heights, and others. A precise characterization of the signal variability in this environment constitutes a hard task. Deterministic methods, such as those described by *the free space, plane earth*, and *knife-edge diffraction* propagation models, are restricted to very simple situations. They are useful, however, in providing the basic mechanisms of propagation. Empirical methods, such as those proposed by many researchers (e.g., [1,4,5,8]; and others), use curves and/or formulas based on field measurements, some of them including deterministic solutions with various correction factors to account for the propagation frequency, antenna height, polarization, type of terrain, and so on. Because of the random characteristics of the mobile radio signal, however, a single deterministic treatment of this signal will certainly lead the problem to a simplistic solution. Therefore, we may treat the signal on a statistical basis and interpret the results as random events occurring with a given probability. The cell coverage area is then determined as the proportion of locations where the received signal is greater than a certain threshold considered to be satisfactory.

Suppose that at a specified distance from the base station the *mean signal strength* is considered to be known. Given this we want to determine the cell radius such that the mobiles experience a received signal above a certain threshold with a stipulated probability. The mean signal strength can be determined either by any of the prediction models or by field measurements. As for the statistics of the mobile radio signal, five distributions are widely accepted today: lognormal, Rayleigh, Suzuki [11], Rice, and Nakagami. The lognormal distribution describes the variation of the mean signal level (large-scale variations) for points having the same transmitter–receiver antennas separation, whereas the other distributions characterize the instantaneous variations (small-scale variations) of the signal. In the calculations that follow we assume a lognormal environment. The other environments can be analyzed in a like manner; although this may not be of interest if some sort of diversity is implemented, because then the effects of the small-scale variations are minimized.

21.7.1 Propagation Model

Define m_w and k as the mean powers at distances x and x_0, respectively, such that

$$m_w = k\left(\frac{x}{x_0}\right)^{-\alpha} \tag{21.4}$$

where α is the path loss coefficient. Expressed in decibels, $M_w = 10 \log m_w$, $K = 10 \log k$ and

$$m_w = k - 10\alpha \log\left(\frac{x}{x_0}\right) \tag{21.5}$$

Define the received power as $w = \upsilon^2/2$, where υ is the received envelope. Let $p(W)$ be the probability density function of the received power W, where $W = 10 \log w$. In a lognormal environment, v has a lognormal distribution and

$$p(W) = \frac{1}{\sqrt{2\pi}\sigma_w} \exp\left(-\frac{(W - M_w)^2}{2\sigma_w^2} \right) \tag{21.6}$$

where M_w is the mean and σ_w is the standard deviation, all given in decibels. Define w_T and $W_T = 10 \log w_T$ as the threshold above which the received signal is considered to be satisfactory. The probability that the received signal is below this threshold is its *probability distribution function* $P(W_t)$, such that

$$P(W_T) = \int_{-\infty}^{w_T} p(W) \mathrm{d}W = \frac{1}{2} + \frac{1}{2} \mathrm{erf}\left[\frac{(W_T - M_W)^2}{2\sigma_w^2} \right] \tag{21.7}$$

Where erf() is the error function defined as

$$\mathrm{erf}(y) = \frac{2}{\sqrt{\pi}} \int_0^y \exp(-t^2)\, \mathrm{d}t \tag{21.8}$$

21.7.2 Base Station Coverage

The problem of estimating the cell area can be approached in two different ways. In the first approach, we may wish to determine the proportion β of locations at x_0 where the received signal power w is above the threshold power w_T. In the second approach, we may estimate the proportion μ of the circular area defined by x_0 where the signal is above this threshold. In the first case, this proportion is averaged over the perimeter of the circumference (cell border); whereas in the second approach, the average is over the circular area (cell area).

The proportion β equals the probability that the signal at x_0 is greater than this threshold. Hence,

$$\beta = \mathrm{prob}(W \geq W_T) = 1 - P(W_T) \tag{21.9}$$

Using Equations 21.5 and 21.7 in Equation 21.9 we obtain

$$\beta = \frac{1}{2} - \frac{1}{2} \mathrm{erf}\left[\frac{w_T - K + 10\alpha \log(x/x_0)}{\sqrt{2\sigma_w}} \right] \tag{21.10}$$

This probability is plotted in Figure 21.1, for $x = x_0$ (cell border).

Let prob($W \geq W_T$) be the probability of the received power W_T being above the threshold WT within an infinitesimal area dS. Accordingly, the proportion μ of locations within the circular area S experiencing such a condition is

$$\mu = \frac{1}{S} \int_S [1 - P\ (W_T)]\ \mathrm{d}S \tag{21.11}$$

where $S = \pi r^2$ and $\mathrm{d}S = x\, \mathrm{d}x\mathrm{d}\theta$. Note that $0 \leq x \leq x_0$ and $0 \leq \theta \leq 2\pi$. Therefore, solving for dθ, we obtain

$$\mu = 2 \int_0^1 u\beta\ \mathrm{d}u \tag{21.12}$$

where $u = x/x_0$ is the normalized distance.

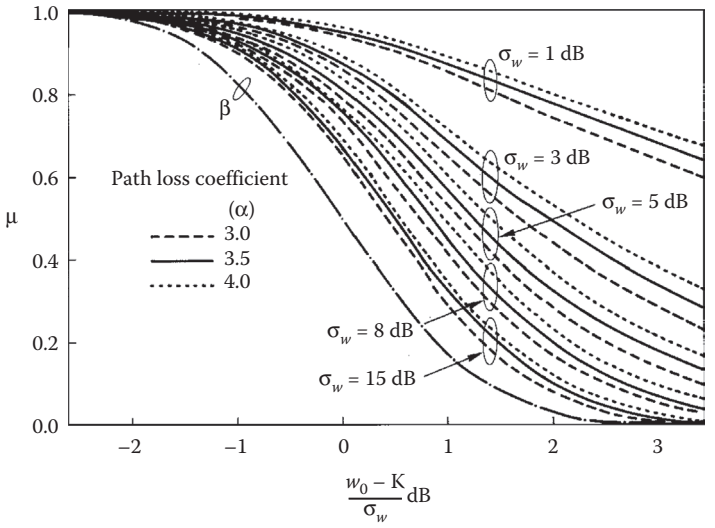

FIGURE 21.1 Proportion of locations where the received signal is above a given threshold; the dashdot line corresponds to the ⊠ approach and the other lines to the μ approach.

Inserting Equation 21.10 into Equation 21.12 results in

$$\mu = 0.5\left\{1 + \text{erf}(a) + \exp\left(\frac{2ab+1}{b^2}\right)\left[1 - \text{erf}\left(\frac{ab+1}{b}\right)\right]\right\} \tag{21.13}$$

where $a = (K - W_T)/\sqrt{2\sigma_w}$ and $b = 10\alpha \log(e)/\sqrt{2\sigma_w}$.

These probabilities are plotted in Figure 21.1 for different values of standard deviation and path loss coefficients.

21.7.3 Application Examples

From the theory that has been developed it can be seen that the parameters affecting the probabilities β and μ for cell coverage are the path loss coefficient α, the standard deviation σ_w, the required threshold W_T, and a certain power level K, measured or estimated at a given distance from the base station.

The applications that follow are illustrated for two different standard deviations: $\sigma_w = 5$ dB and $\sigma_w = 8$ dB. We assume the path loss coefficient to be $\alpha = 4$ (40 dB/decade), the mobile station receiver sensitivity to be –116 dB (1 mW), and the power level estimated at a given distance from the base station as being that at the cell border, $K = -102$ dB (1 mW). The receiver is considered to operate with a *SINAD* of 12 dB for the specified sensitivity. Assuming that co-channel interference levels are negligible and given that a signal-to-noise ratio *S/N* of 18 dB is required, the threshold W_t will be –116 dB (1 mW) + (18–12) dB (1 mW) = –110 dB (1 mW).

Three cases will be explored as follows.

Case 1: We want to estimate the probabilities β and μ that the received signal exceeds the given threshold (1) at the border of the cell, probability β and (2) within the area delimited by the cell radius, probability μ.

Case 2: It may be interesting to estimate the cell radius x_0 such that the received signal be above the given threshold with a given probability (say 90%) (1) at the perimeter of the cell and

(2) within the cell area. This problem implies the calculation of the mean signal strength K at the distance x_0 (the new cell border) of the base station. Given K and given that at a distance x_0 (the former cell radius) the mean signal strength M_w is known [note that in this case $M_w = -102$ dB (1 mW)], the ratio x_0/x can be estimated.

Case 3: To fulfill the coverage requirement, rather than calculating the new cell radius, as in Case 2, a signal strength at a given distance can be estimated such that a proportion of the locations at this distance, proportion β, or within the area delimited by this distance, proportion μ, will experience a received signal above the required threshold. This corresponds to calculating the value of the parameter K already carried out in Case 2 for the various situations.

The calculation procedures are now detailed for $\sigma_w = 5$ dB. Results are also shown for $\sigma_w = 8$ dB.

Case 1: Using the given parameters we obtain $(W_t - K)/\sigma_w = -1.6$. With this value in Figure 21.1, we obtain the probability that the received signal exceeds –116 dB (1 mW) for $S/N = 18$ dB given that at the cell border the mean signal power is –102 dB (1 mW) given in Table 21.1.

Note, from Table 21.1, that the signal at the cell border exceeds the receiver sensitivity with 97% probability for $\sigma_w = 5$ dB and with 84% probability for $\sigma_w = 8$ dB. If, on the other hand, we are interested in the area coverage rather than in the border coverage, then these figures change to 100% and 95%, respectively.

Case 2: From Figure 21.1, with $\beta = 90\%$ we find $(W_T - K)/\sigma_w = -1.26$. Therefore, $K = -103.7$ dB (1 mW). Because $M_w - K = -10\alpha \log(x/x_0)$, then $x_0/x = 1.10$. Again, from Figure 21.1, with $\mu = 90\%$ we find $(W_T - K)/\sigma_w = -0.48$, yielding $K = -107.6$ dB(1 mW). Because $M_w - K = -10\alpha \log(x/x_0)$, then $x_0/x = 1.38$. These results are summarized in Table 21.2, which shows the normalized radius of a cell where the received signal power is above –116 dB (1 mW) with 90% probability for S/N = 18 dB, given that at a reference distance from the base station (the cell border) the received mean signal power is –102 dB (1 mW).

Note, from Table 21.2, that in order to satisfy the 90% requirement at the cell border the cell radius can be increased by 10% for $\sigma_w = 5$ dB. If, on the other hand, for the same standard deviation the 90% requirement is to be satisfied within the cell area, rather than at the cell border, a substantial gain in power is achieved. In this case, the cell radius can be increased by a factor of 1.38. For $\sigma_w = 8$ dB and 90% coverage at the cell border, the cell radius should be reduced to 88% of the original radius. For area coverage, an increase of 27% of the cell radius is still possible.

Case 3: The values of the mean signal power K are taken from Case 2 and shown in Table 21.3, which shows the signal power at the cell border such that 90% of the locations will experience a received signal above –116 dB for $S/N = 18$ dB.

TABLE 21.1 Case 1 Coverage Probability

Standard Deviation, dB	β Approach (Border Coverage), %	μ Approach (Area Coverage), %
5	97	100
8	84	95

TABLE 21.2 Case 2 Normalized Radius

Standard Deviation, dB	β Approach (Border Coverage)	μ Approach (Area Coverage)
5	1.10	1.38
8	0.88	1.27

TABLE 21.3 Case 3 Signal Power

Standard Deviation dB	β Approach (Border Coverage), dB (1 mW)	μ Approach (Area Coverage), dB (1 mW)
5	–103.7	–107.6
8	–99.8	–106.2

21.8 Interference

Radio-frequency interference is one of the most important issues to be addressed in the design, operation, and maintenance of mobile communication systems. Although both intermodulation and intersymbol interferences also constitute problems to account for in system planning, a mobile radio system designer is mainly concerned about adjacent-channel and co-channel interferences.

21.8.1 Adjacent Channel Interference

Adjacent-channel interference occurs due to equipment limitations, such as frequency instability, receiver bandwidth, filtering, and so on. Moreover, because channels are kept very close to each other for maximum spectrum efficiency, the random fluctuation of the signal, due to fading and near-far effect, aggravates this problem.

Some simple, but efficient, strategies are used to alleviate the effects of adjacent channel interference. In narrowband systems, the total frequency spectrum is split into two halves so that the reverse channels, composing the uplink (mobile to base station) and the forward channels, composing the downlink (base station to mobile), can be separated by half of the spectrum. If other services can be inserted between the two halves, then a greater frequency separation, with a consequent improvement in the interference levels, is accomplished. Adjacent channel interference can also be minimized by avoiding the use of adjacent channels within the same cell. In the same way, by preventing the use of adjacent channels in adjacent cells a better performance is achieved. This strategy, however, is dependent on the cellular pattern. For instance, if a seven-cell cluster is chosen, adjacent channels are inevitably assigned to adjacent cells.

21.8.2 Co-Channel Interference

Undoubtedly, the most critical of all interferences that can be engineered by the designer in cellular planning is co-channel interference. It arises in mobile radio systems using cellular architecture because of the frequency reuse philosophy.

A parameter of interest to assess the system performance in this case is the carrier-to-co-channel interference ratio C/I_c. The ultimate objective of estimating this ratio is to determine the reuse distance and, consequently, the repeat pattern. The C/I_c ratio is a random variable, affected by random phenomena such as (1) location of the mobile, (2) fading, (3) cell site location, (4) traffic distribution, and others. In this subsection we shall investigate the outage probability, that is, the probability of failing to achieve adequate reception of the signal due to co-channel interference. This parameter will be indicated by $p(CI)$. As can be inferred, this is intrinsically related to the repeat pattern.

Co-channel interference will occur whenever the wanted signal does not simultaneously exceed the minimum required signal level s_0 and the n interfering signals, $i_1, i_2, \ldots, i_n$, by some protection ratio r. Consequently, the conditional outage probability, given n interferers, is

$$p(CI \mid n) = 1 - \int_{S_0}^{\infty} p(s) \int_{0}^{s/r} p(i_1) \int_{0}^{(s/r)-i_1} p(i_2) \ldots \times \int_{0}^{(s/r)-i_1-\cdots-i_{n-1}} p(i_n)\, di_n \cdots di_2 di_1 ds \tag{21.14}$$

The total outage probability can then be evaluated by

$$p(CI) = \sum_{n} p(CI \mid n)p(n) \tag{21.15}$$

where $p(n)$ is the distribution of the number of active interferers.

In the calculations that follow we shall assume an interference-only environment, that is, $s_0 = 0$, and the signals to be Rayleigh faded. In such a fading environment the probability density function of the signal-to-noise ratio x is given by

$$p(x) = \frac{1}{x_m}\exp\left(-\frac{x}{x_m}\right) \tag{21.16}$$

where x_m is the mean signal-to-noise ratio. Note that $x = s$ and $x_m = s_m$ for the wanted signal, and $x = i_j$ and $x_m = i_{mj}$ for the interfering signal j, with s_m and i_{mj} being the mean of s and i_j, respectively.

By using the density of Equation 21.16 in Equation 21.14 we obtain

$$p\,(CI \mid n) = \sum_{i=1}^{n}\prod_{k=1}^{j}\frac{Z_k}{1+Z_k} \tag{21.17}$$

where $z_k = rs_m/i_{mk}$

If the interferers are assumed to be equal, that is, $z_k = z$ for $k = 1,2, \ldots, n$, then

$$p(CI \mid n) = 1 - \left(\frac{z}{1+z}\right)^n \tag{21.18}$$

Define $Z = 10 \log z$, $S_m = 10 \log s_m$, $I_m = 10 \log i_m$, and $R_r = 10 \log r$. Then, $Z = S_m - (I_m + R_r)$. Equation 21.18 is plotted in Figure 21.2 as a function of Z for $n = 1$ and $n = 6$, for the situation in which the interferers are equal.

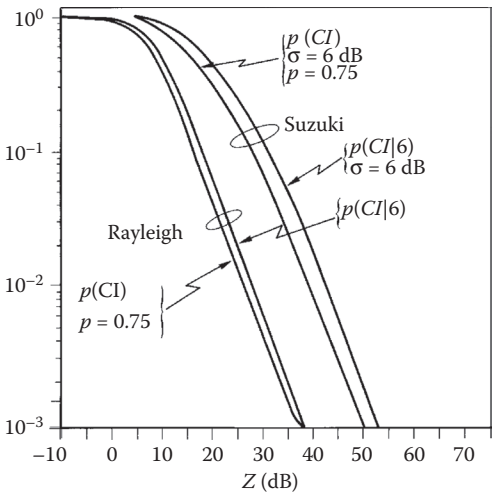

FIGURE 21.2 Conditional and unconditional outage probability for $n = 6$ interferes in a Rayleigh environment and in a Suzuki environment with $\sigma = 6$ dB.

If the probability of finding an interferer active is p, the distribution of active interferers is given by the binomial distribution. Considering the closest surrounding co-channels to be the most relevant interferers we then have six interferers. Thus,

$$p(n) = \binom{6}{n} p^n (1-p)^{6-n} \tag{21.19}$$

For equal capacity cells and an evenly traffic distribution system, the probability p is approximately given by

$$p = \sqrt[M]{B} \tag{21.20}$$

where B is the blocking probability and M is the number of channels in the cell.

Now Equations 21.18, 21.19, and 21.20 can be combined into Equation 21.15 and the outage probability is estimated as a function of the parameter Z and the channel occupancy p. This is shown in Figure 21.2 for $p = 75\%$ and $p = 100\%$.

A similar, but much more intricate, analysis can be carried out for the other fading environments. Note that in our calculations we have considered only the situation in which both the wanted signal and the interfering signals experience Rayleigh fading. For a more complete analysis we may assume the wanted signal to fade differently from the interfering signals, leading to a great number of possible combinations. A case of interest is the investigation of the influence of the standard deviation in the outage probability analysis. This is illustrated in Figure 21.2 for the Suzuki (lognormal plus Rayleigh) environment with $\sigma = 6$ dB.

Note that by definition the parameter z is a function of the carrier-to-co-channel interference ratio, which, in turn, is a function of the reuse distance. Therefore, the outage probability can be obtained as a function of the cluster size, for a given protection ratio.

The ratio between the mean signal power s_m and the mean interfering power i_m equals the ratio between their respective distances d_s and d_i such that

$$\frac{s_m}{i_m} = \left(\frac{d_s}{s_i}\right)^{-\alpha} \tag{21.21}$$

where α is the path loss coefficient. Now, (1) let D be the distance between the wanted and interfering base stations, and (2) let R be the cell radius. The co-channel interference worst case occurs when the mobile is positioned at the boundary of the cell, that is, $d_s = R$ and $di = D - R$. Then,

$$\frac{i_m}{s_m} = \left(\frac{D}{R} - 1\right)^{-\alpha} \tag{21.22a}$$

or, equivalently,

$$S_m - I_m = 10\alpha \log\left(\frac{D}{R} - 1\right) \tag{21.22b}$$

In fact, $S_m - I_m = \mathrm{Z} + R_r$. Therefore,

$$Z + R_r = 10\alpha \log\left(\sqrt{3N} - 1\right) \tag{21.23}$$

TABLE 21.4 Probability of Co-Channel Interference in Different Cell Clusters

		Outage Probability, %			
		Rayleigh		Suzuki σ = 6 dB	
N	*Z* + *R*, dB	*p* = 75%	*p* = 100%	*p* = 75%	*p* = 100%
1	–4.74	100	100	100	100
3	10.54	31	40	70	86
4	13.71	19	26	58	74
7	19.40	4.7	7	29	42
12	24.46	1	2.1	11	24
13	25.19	0.9	1.9	9	22

With Equation 21.23 and the curves of Figure 21.2, we can compare some outage probabilities for different cluster sizes. The results are shown in Table 21.4 where we have assumed a protection ratio $R_r = 0$ dB. The protection ratio depends on the modulation scheme and varies typically from 8 dB (25-kHz FM) to 20 dB [single sideband (SSB) modulation].

Note, from Table 21.4, that the standard deviation has a great influence in the calculations of the outage probability.

21.9 Conclusions

The interrelationship among the areas involved in a cellular network planning is substantial. Vocabularies belonging to topics, such as radio propagation, frequency planning and regulation, modulation schemes, antenna design, transmission, teletraffic, and others, are common to all cellular engineers.

Designing a cellular network to meet system requirements is a challenging task which can only be partially and roughly accomplished at the design desk. Field measurements play an important role in the whole process and constitute an essential step used to tune the parameters involved.

References

1. Egli, J., Radio above 40 Mc over irregular terrain. *Proc. IRE*., 45(10), 1383–1391, 1957.
2. Hata, M., Empirical formula for propagation loss in land-mobile radio services. *IEEE Trans. Vehicular Tech*., VT-29, 317–325, 1980.
3. Ho, M. J. and Stüber, G. L., Co-channel interference of microcellular systems on shadowed Nakagami fading channels. *Proc. IEEE Vehicular Tech. Conf*., 568–571, 1993.
4. Ibrahim, M. F. and Parsons, J. D., Signal strength prediction in built-up areas, Part I: median signal strength. *Proc. IEEE*. Pt. F. (130), 377–384, 1983.
5. Lee, W. C. Y., *Mobile Communications Design Fundamentals*, Howard W. Sams, Indianapolis, IN, 1986.
6. Leonardo, E. J. and Yacoub, M. D., A statistical approach for cell coverage area in land mobile radio systems. *Proceedings of the 7th IEE. Conf. on Mobile and Personal Comm*., Brighton, UK, 16–20, Dec. 1993a.
7. Leonardo, E. J. and Yacoub, M. D., (Micro) Cell coverage area using statistical methods. *Proceedings of the IEEE Global Telecom. Conf. GLOBECOM'93*, Houston, TX, 1227–1231, Dec. 1993b.
8. Okumura, Y., Ohmori, E., Kawano, T., and Fukuda, K., Field strength and its variability in VHF and UHF land mobile service. *Rev. Elec. Comm. Lab*., 16, 825–873, 1968.
9. Reudink, D. O., Large-scale variations of the average signal. In *Microwave Mobile Communications*, Jakes, W. C. (ed.), pp. 79–131, John Wiley & Sons, New York, 1974.
10. Sowerby, K. W. and Williamson, A. G., Outage probability calculations for multiple cochannel interferers in cellular mobile radio systems. *IEE Proc*., Pt. F. 135(3), 208–215, 1988.
11. Suzuki, H., A statistical model for urban radio propagation. *IEEE Trans. Comm*., 25(7), 673–680, 1977.

Further Reading

The fundamentals of mobile radio engineering in connection with many practical examples and applications as well as an overview of the main topics involved can be found in Yacoub, M. D., *Foundations of Mobile Radio Engineering*, CRC Press, Boca Raton, FL, 1993.

II

Wireless Standards

22

Wireless Data

Allen H. Levesque

Kaveh Pahlavan

22.1 Introduction

The second half of the twentieth century witnessed enormous transformations in electronic communications, including the development of data transmission over legacy telephone networks, the introduction of packet-data networks, development of high-speed local area networks (LANs), and the development of mobile wireless communications networks, most notably cellular networks, paging systems, and even mobile satellite systems [1,2]. By the start of the current century, cellular and paging services had come into widespread use in support of business communications and personal communications as well. The early analog cellular networks were rapidly supplanted by digital networks affording increased traffic capacity and capable of supporting an expanding array of data-enabled services. In the first decade of the new century, we saw rapidly increasing interest in higher-rate forms of wireless data communication, including multimedia transmission to and from portable phones, and wireless access to the Internet from laptop computers.

The worldwide growth of the wireless communications industry has been truly phenomenal. At this writing, it is estimated that the number of cellular telephone users throughout the world is approaching five billion, and the aggregate annual revenue of the wireless industry exceeds the revenues of the wired-telephone service industry. In the mid-1990s, Internet access began expanding from the business

environment to include the home environment, and this soon generated annual revenues comparable to traditional telephone service and wireless service. Currently, the *information exchange industry*, defined to include both wired and wireless phone services as well as Internet access, enjoys annual revenues of several trillion dollars and is by far the largest industry in the world. Underlying this rapid development of all communications services and networks has been the ongoing evolution of digital technology, particularly large-scale integration and microprocessor chip technology. The digital revolution enabled the transformation of the core of traditional telephone network to a digital infrastructure providing greater reliability, increased capacity, and an ever-widening array of services to customers. In the mid-1990s, digital technology began to have a major impact on mobile wireless services and networks, increasing network capacities and capabilities, as well as lowering the cost and increasing the battery life of mobile devices. An interesting and important aspect of the burgeoning worldwide wireless communications industry has been the resurgence of Wireless Local Area Network (WLAN) technology, driven by the steadily increasing popularity of laptop computers, the demand for wireless Internet access, and the expanding deployment of wireless access points on campuses, in office buildings and, increasingly, in public commercial venues served by Wi-Fi hotspots. All of these new and emerging services are built upon an underlying infrastructure of data transport technology.

In recent years, the wireless industry has seen a steady high growth rate in the demand for services enabled by wireless data, spurred in large part by the introduction of *smartphones* and the enormous popularity of services such as social networking and video downloading and streaming. Consequently, the use of mobile wireless networks for simple voice communication is being dwarfed by the volume of data traffic for Internet access and multimedia services. Furthermore, new areas of applications for wireless data are continually opening up, ranging from marketing, sales, and customer support to social networking, and health-care delivery. In response to the steadily growing worldwide demand for data-enabled services, the cellular industry has migrated through successive generations of wireless access technology, a new generation about every 10 years.

While the wireless data industry continues to become increasingly diverse, one can observe that two mainstreams of the industry are dominant. On the one hand there are still-growing demands for data services at ever-higher data rates to serve mobile users over wide geographical areas, enabled principally by cellular telephone networks. On the other hand, there are requirements for wireless access to corporate and campus LANs and to the Internet and World Wide Web. In recent years, with the growing popularity of wireless-enabled laptop computer smart tablets and the widespread deployment of "Wi-Fi hot spots," there is steady convergence of these user requirements, as users expect all forms of connectivity while on the move. In this chapter we focus on data services supported by wide-area networks, often termed as *mobile data services* or *cellular data services*. However, it is useful to briefly review the evolution of Wireless LAN (WLAN) technology and to note several technical developments along the way that have been incorporated into evolving wide-area networking standards.

22.1.1 Evolution of WLAN Technology

WLAN developments began in the late 1970s with need to find an alternative to cabled LANs in manufacturing and office environments. The objective was to find a wireless replacement for cabling that would support the data rates then available, typically rates up to 2 Mb/s. Early WLAN products were developed using several different wireless technologies, and many of those products were based on proprietary designs. However, the WLAN industry gradually shifted its attention to standards-based designs, giving support to the IEEE 802.11 standardization initiative [3]. Since the 1999 release of the original IEEE 802.11 standard, the WLAN industry has converged on the manufacture of interoperable WLAN products based on the evolving 802.11 family of standards [4]. At about the time that the first 802.11 standards were released, six wireless product manufacturers came together to adopt the name Wireless Fidelity (Wi-Fi) for WLAN technology and to form the Wi-Fi Alliance. Their purpose is to

promote the growth of the WLAN industry and, through their certification program, to ensure the conformance and interoperability of products manufactured to IEEE 802.11 standards. By the year 2010, the Alliance comprised over 400 member companies, and for some years now, the name Wi-Fi has become synonymous with 802.11-based WLAN technology.

Today, essentially all WLAN products are based on IEEE 802.11 standards, which have undergone a number of revisions over the last dozen years. All of the 802.11-based WLANs operate in the Industrial, Scientific and Medical (ISM) frequency bands. These are termed as unlicensed bands, since no license is required for operation of a device within these bands, though each new product must be certified for compliance with FCC Part 15 rules regarding signal structure and transmitted power level [3]. The original ISM bands were released in the US by the FCC in 1985, and the availability of unlicensed operation soon became an important stimulus to the early growth of the WLAN industry [2].

As noted earlier, the initial WLAN developments were motivated by the need to replace cabled connections to legacy wired LANS, and thus the technical objectives from the outset included providing data rates comparable to those available on cabled LANs. As WLAN designs advanced, of course, data rates achievable on wired LANs were moving steadily higher, and thus the WLAN industry continued to strive for ever-higher data rates, and this has been reflected in the evolving 802.11 family of standards.

The first standard, issued in mid-1999, was IEEE 802.11b, which operated in the 2.4 GHz ISM band at raw data rates as high as 11 Mbits/s using a modulation scheme called Complementary Code Keying (CCK), as well as Direct-Sequence Spread Spectrum (DSSS) modulation. Almost simultaneously, another standard, 802.11a, was released, using a different modulation technique, Orthogonal Frequency Division Multiplexing (OFDM), operating in the 5 GHz ISM band [5]. While 802.11a provided higher maximum rates, up to 54 Mb/s, its operation in a higher-frequency range resulted in poorer signal coverage and costlier design and manufacture. Thus, 802.11a failed to gain wide adoption in the marketplace, and 802.11b quickly became the dominant Wi-Fi standard. In 2003, in response to growing market demands for higher data rates, the 802.11g standard was released, operating in the 2.4 GHz band, using OFDM modulation and providing raw data rates up to 54 Mbits/s, as in 802.11a. For several years now, 802.11g capability has been included in almost all laptop computers. It is useful to point out that the advantages of the OFDM modulation scheme were recognized at an early point in WLAN technology development, and this modulation format has subsequently been adopted for the two principle designs for fourth-generation cellular systems, discussed later in this chapter.

Along the way in the evolution of the 802.11 family of standards, enhancements were added to the standard, some of which have counterparts in cellular standards, such as handover (in 802.11f), power control (in 802.11h), and authentication and encryption (in 802.11i). Another major step in the 802.11 evolution was the adoption in late 2009 of 802.11n, which can operate at either 2.4 GHz or 5 GHz and offers a wide array of selectable modulation and coding combinations, achieving maximum data rates as high as 600 Mb/s, Table 22.1 summarizes the chief characteristics of the four main generations of 802.11 standards.

Another WLAN standardization activity begun in 1992 is High performance radio LAN (HiperLAN), a European alternative to the IEEE 802.11 standards. The HiperLAN standard was developed by the

TABLE 22.1 802.11 Standards

	802.11a	802.11b	802.11g	802.11n
Approval Date	July 1999	July 1999	June 2003	October 2009
Maximum Data Rate Mb/s	54	11	54	600
Modulation	OFDM	CCK or DSSS	CCK, DSSS, or OFDM	CCK, DSSS, or OFDM
RF Band (GHz)	5	2.4	2.4	2.4 or 5
Channel BW (MHz)	20	20	20	20 or 40

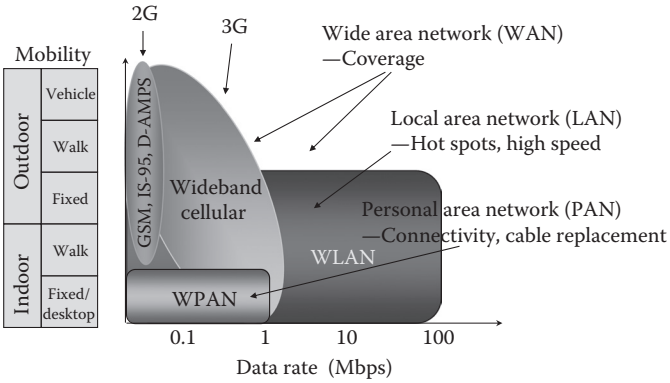

FIGURE 22.1 Mobility and data rates for wireless networks.

European Telecommunications Standards Institute (ETSI) primarily for European markets. Planning for the first version of the standard, HiperLAN/1, began in 1991, when the planning for IEEE 892.11 was already underway, with the goal of providing data rates up to 23 Mb/s, significantly higher than 802.11 rates. The HiperLAN/1 standard was approved in 1996. A subsequent version of the standard, HiperLAN/2, very similar to IEEE 802.11a and providing data rates up to 54 Mb/s with operation in the 5 GHz band, includes capability for rapid connectivity to a variety of other networks, including IP networks. Further details on the HiperLAN standards can be found in [5].

The work of the IEEE 802.11 group has also spawned other standardization initiatives, including Wireless Metropolitan Area Networks (WMAN, discussed in Section 21.9), Wireless Personal Area Network (WPAN) and Wireless Body Area Network (WBAN). More detailed discussions on the IEEE 802.11 standards evolution and related standards initiatives can be found in [2,3,5]. Figure 22.1 illustrates the relative signal coverage and data rate capabilities of 2G and 3G cellular, WLAN, and WPAN technologies.

22.1.2 Evolution of Wide-Area Mobile Data Technology

In contrast to the WLAN industry, which grew out of the need to find wireless replacements for cabled connections to legacy LANs operating at megabit data rates, the mobile data industry had its origins in early paging and messaging systems serving low-data-rate applications for small populations of users. These were followed by specialized packet-data networks serving specific categories of applications, such as service technician support, delivery services and some public safety applications. The development of cellular telephone technology in the early 1980s opened up a new industry perspective: wide-area wireless access to the vast Public Switched Telephone Network (PSTN).

Initial cellular service was of course Plain Old Telephone Service (POTS), but wireless technology had in effect "cut the tether" to the public network, and the telephone industry soon realized that the technology could also facilitate data communication, then being implemented mostly with wireline modems operating over the PSTN. Since the cellular networks had been designed to support voice service, the early forms of cellular data were simply overlays onto cellular voice channels, initially using mobile versions of existing wireline modems. Then, as digital cellular technology emerged, techniques were developed to incorporate data services, either circuit-oriented or packet-formatted, into cellular networks. As the cellular business began to grow, manufacturers and service providers began to categorize wireless communications systems into defined *generations*; the terminology was eventually formalized in the deliberations of international standards bodies, and the terms 1G, 2G, 3G and 4G are now in common use. What is instructive to note is that with the introduction of digital cellular technology in 2G, the chief characteristic identified with each successive generation is the achievable data rates. The 2G cellular

standards included data services with rates comparable to those provided by wireline modems operating in the PSTN. For 3G standards, a major selling point was the promise of data rates approaching those already provided on many cabled LANs, introduced at a time when business travelers were making increasing use of laptop computers while on the move. This has given way to the current rapid growth in use of smartphones and smartpads, in turn spurring the introduction of new data-hungry user applications, largely based on accessing Internet content. The 3G standards are widely deployed in cellular service networks today, and the deployment of some 4G network technology, offering another major step in data rate capability, is underway in the industry. Thus, we see that as user demand for a widening array of features built on underlying data services has grown, the evolving technology has increasingly been defined by the expansion of data transport capability. Thus, the phrase "data is king," is a slogan now used frequently in the wireless industry. The wireless data aspect of these wireless communications developments is the specific focus of this handbook chapter. In the remainder of this chapter, we discuss the characteristics of wireless data networks and then review the principal existing and evolving wireless data networks and the related standards activities currently in progress.

22.2 Characteristics of Wireless Data Networks

From the perspective of the data user, the basic requirement for wireless data service is convenient, reliable access to data services over a geographical area appropriate to the user's pattern of daily business or social activity. In the early days of cellular service, this requirement could be met by low-speed data services, by which we mean data rates comparable to those then provided by standard data modems operating over the Public Switched Telephone Network (PSTN). This form of service could support a wide variety of short-message applications such as notice of electronic mail or voice mail, as well as short file transfers or even facsimile transmissions that were not overly lengthy. The user's requirements and expectations for these types of services were different in several ways from the requirements placed on voice communication over wireless networks. In a wireless voice service, the user usually understands the general characteristics and limitations of radio transmission, and is tolerant of occasional *signal fades*, and brief *dropouts*. An overall level of acceptable voice quality is what the user expects. In a data service, the user is instead concerned with the accuracy of delivered messages and data, the time-delay characteristics of the service network, the ability to maintain service while moving about, and of course the cost of the service. All of these factors are dependent upon the technical characteristics of wireless data networks, which we discuss next. In this discussion we focus on the characteristics of outdoor wireless propagation, which is relevant to wide-area service networks. Detailed treatments of the characteristics of indoor radio propagation can be found in References 2 and 6.

The chief factor affecting the design and performance of outdoor wireless data networks is the nature of radio propagation over wide geographic areas. The most important mobile data services are implemented in various radio bands from roughly 700 MHz to 2 GHz. In these frequency bands, radio transmission is characterized by distance-dependent field strength, as well as the well-known effects of *multipath fading*, signal shadowing, and signal blockage. The signal coverage provided by a radio transmitter, which in turn determines the area over which a mobile data terminal can receive a usable signal, is governed primarily by the *power–distance relationship*, which gives signal power as a function of distance between transmitter and receiver. Broadly stated, for a given transmit power and given transmit and receive antenna gains, the received signal power will vary with an inverse square-law to fourth-law dependence on distance. In general, the power–distance relationship for mobile radio systems is a complicated relationship which depends upon the nature of the terrain between transmitter and receiver [2,6]. The overall inverse relationship of received signal power to distance is very important, and becomes especially important if a service provider contemplates migrating a wireless data service from a higher-frequency band to a lower-frequency band.

When user terminals are used in mobile situations, the received signal is generally characterized by rapid fading of the signal strength, caused by the vector summation of reflected signal components, the

vector summation changing constantly as the mobile terminal moves from one place to another in the service area. Measurements made by many researchers show that when the fast fading is averaged out, the signal strength is described by a Rayleigh distribution having a log-normal mean. In general, the power–distance relationship for mobile radio systems is a more complicated relationship which depends upon the nature of the terrain between transmitter and receiver. Chapter 8 discusses Rayleigh fading channels in detail.

Various propagation models are used in the cellular industry for network planning purposes, and a number of these models are described in [7]. Propagation models for mobile communications networks must take an account of the terrain irregularities existing over the intended service area. Most of the models used in the industry have been developed from measurement data collected over various geographic areas. A very popular model is the *Longley–Rice model* [8,9]. Many wireless networks are concentrated in urban areas. A widely used model for propagation prediction in urban areas is one usually referred to as the *Okumura–Hata Model* [10,11]. Aspects of radio wave propagation are treated in Chapters 8, "Rayleigh Fading Channels," and Chapter 39, "60 GHz Wireless Communication" of this handbook. The reader can also find detailed treatments of radio propagation characteristics for both indoor and outdoor environments, together with discussions of measurement systems and simulation modeling techniques, in References 2 and 6.

By using appropriate propagation prediction models, one can determine the range of signal coverage for a base station of given transmitted power. In a wireless data system, if one knows the level of received signal needed for satisfactory performance, the area of acceptable performance can in turn be determined. Cellular telephone networks utilize base stations that are typically spaced 1–5 mi apart, though in some mid-town areas, microcell separations of half a mile or less are now being used.

An important additional factor which must be considered in planning a wireless data system is the in-building penetration of signals. Many applications for wireless data services involve the use of mobile data terminals inside buildings, for example, for trouble-shooting and servicing computers on customers' premises. Another example is wireless communications into hospital buildings in support of emergency medical services. It is usually estimated that in-building signal penetration losses will be in the range of 15–30 dB [2]. Thus, received signal strengths can be satisfactory in the outside areas around a building but totally unusable inside the building. This becomes an important issue when a service provider intends to support customers using mobile terminals inside buildings.

One important consequence of the rapid fading experienced on mobile channels is that errors tend to occur in bursts, causing the transmission to be very unreliable for short intervals of time. Another problem is signal dropouts which occur, for example, when a data call is handed over from one base station to another, or when the mobile user moves into a location where the signal is severely attenuated. Because of this, mobile data protocols employ various error-correction and error-recovery techniques to ensure accurate and reliable delivery of data messages.

22.3 Circuit-Switched versus Packet-Switched Service

One of the interesting and instructional aspects of the development of wireless data systems is the evolution that has taken place with respect to use of *packet-switched data* transmission versus *circuit-switched data* transmission. The earliest wireless data networks, notably the ARDIS and Mobitex networks (discussed later), were designed specifically to provide wireless data connectivity primarily for applications that required short bursty data interchanges. Spectrum allocated to these services was limited, and thus it had to be used efficiently. Packet-switched transmission, sometimes termed as *packet-mode* transmission can make very efficient use of radio resources, especially when the applications use short, intermittent bursts of data traffic. The early specialized wireless data services were in fact designed to support applications in which most data transfers were interactive and occurred in a bursty fashion, and thus were best served by packet-switched service. Typical data transfers occurred in short bundles, interspersed with longer intervals when there was little or no activity.

Packet-switched transmission enables efficient use of transmission resources by allowing the overall channel capacity to be shared among multiple users. To achieve this, each user's data stream to be transmitted is segmented into packets, and tags are inserted into the packets to provide destination addressing and other information. When one user's packet has been transmitted, the channel is made available for another user's packets. Packets from multiple sources can then be interspersed and transmitted over the channel. As it is unlikely that the data bursts for different users will occur all at the same time, by sharing the overall resource in this manner, the channel can be used far more efficiently than if the channels are used in a dedicated, rather than shared, manner.

As the cellular telephone industry was established and began to grow, the first cellular networks, termed *first generation* or 1G, were designed to support only analog voice service, in effect providing wireless extensions to the legacy PSTN. Thus, cellular voice service was configured as a circuit-*switched* service, in which an end-to-end circuit connection is set up through the network and stays in place for the full duration of the call session. While this form of network service is perfectly suitable for voice service, it is not so for data traffic. Given the bursty nature of typical data transfers, the circuit-switched mode of service does not make the most efficient use of transmission capacity in the network. Thus, in North America, the early analog cellular networks were augmented with Cellular Digital Packet Data (CDPD, described later), which assigned small numbers of frequency channels to carry wireless modem traffic in packet mode.

As the initial *digital cellular* standards, termed *second generation* or 2G, were being developed, they incorporated a variety of circuit-switched data services, as well as circuit-mode services that carried packet-formatted data for interoperation with external packet-switched data networks. In the case of the Pan-European standard, Global System for Mobile Communications (GSM), transitional technologies, GPRS and EDGE, were developed as add-ons to GSM circuit-switched networks. As with other add-ons to developed cellular networks, these packet-mode services anticipated the next generation in wireless network evolution.

In defining the technical objectives for the third-generation networks, designated as 3G, true packet data services were incorporated into the specifications. As the wireless industry begins its deployment of the next-generation systems, 4G, we are seeing an evolution to a network architecture in which not only data services, but all wireless services, will be formatted, transmitted and switched as data packets.

22.4 Early Developments in Wireless Data Services

The initial deployment of cellular mobile phone service networks in the early 1980s marked a major milestone in the evolution of the telecommunications industry. There had already been a decade-long history of development in radio communications technology—transoceanic radio telegraphy services beginning at the end of the nineteenth century, land-mobile radio networks for police cars and taxis beginning the 1920s, military use of *walkie-talkies* in WWII, and AT&T's early *mobile telephone service* introduced just after the war. These early technologies of course were designed strictly for mobile voice communications.

As communications and microprocessor technologies advanced, more extensive forms of mobile communications became available in the marketplace. In the early 1960s, the earliest paging networks were launched, supporting simple tone paging. Tone paging was soon replaced by special paging codes, beginning with numeric codes introduced in North American networks in the 1970s. This was eventually followed by alphanumeric paging and two-way alphanumeric paging. Until the cellular telephone began to dominate the market, pagers filled the role of common personal and mobile communications devices. Today a number of paging service providers are still in place, mainly supporting the "critical messaging" markets. While paging services met the demand for minimal connectivity, growing needs were perceived for more comprehensive data services to support various categories of service and

business people on the move. Notable were two wireless data networks that provided mobile data services to users in a number of major metropolitan areas in the United States and other countries as well, and we discuss these next.

22.4.1 ARDIS and Mobitex

At about the same time when cellular technology was being developed, several low-rate wide-area data packet data systems were developed and deployed in several countries. Most prominent among these were the Advanced Radio Data Information Service (ARDIS) and Mobitex data networks. ARDIS was a two-way wireless data service developed as joint venture between IBM and Motorola and first implemented in 1983. The ARDIS system consisted of a small number of network control centers plus network controllers and base stations deployed in about 400 US cities. The service provided two-way transfer of short data files and was used primarily for computer-aided dispatching, such as used by field service personnel. In mid-1994, IBM sold its interest in ARDIS to Motorola, and in early 1998 ARDIS was acquired by American Mobile Satellite (now TerreStar Corporation). The ARDIS service is no longer deployed.

Mobitex is an open-standard packet-switched wireless data technology developed by Ericsson and Swedish Telecom [12]. The first Mobitex network went into operation in Sweden in 1986. In 1990, Mobitex was introduced in Canada by Rogers Cantel and in 1991 in the US by RAM Mobile Data. In 1995, RAM Mobile Data were sold and renamed as BellSouth Wireless Data and later became Cingular Interactive when BellSouth and SBC Communications formed Cingular Wireless. In 2005, the Mobitex division within Cingular Wireless was sold and became Velocita Wireless. In 2006 Velocita Wireless was purchased by Sprint Nextel and became a Sprint Nextel company. During the mid-1990s, Mobitex gained popularity by providing two-way paging services. It was also the first wireless data transport for Research in Motion's Blackberry and for PDAs such as Palm devices. RIM eventually phased out Mobitex and current Blackberry devices utilize other wireless data services. In the United States, Velocita Wireless still operates Mobitex networks, which primarily serve Machine-to-Machine (M2M) telemetry applications.

Mobitex is now implemented on more than 30 networks on five continents. In Europe in the early 1990s, the introduction of GSM and its array of data bearer services overshadowed Mobitex service. On the European continent today, Mobitex networks operate primarily in the Netherlands, Belgium and Luxemburg. In the United Kingdom, Mobitex was deployed initially by RAM Mobile Data, the UK part of which became Transcomm and was purchased by British Telecom in 2001. Transcomm still operates Mobitex services in the United Kingdom, with emphasis on M2M services such as vehicle recovery.

The Mobitex interface standard is maintained by the Mobitex Association, and all networks implement the same standard-base specification. Currently, Mobitex networks operate at 400–450 MHz in Europe and 900 MHz in the United States. The Mobitex protocol is a packet-switched data-only service transmitting half-duplex at 8000 b/s in 12.5 kHz channels. The multiple-access scheme is Slotted-Aloha, and useful user-data throughput is typically about half the raw transmission rate. The modulation technique is Gaussian Minimum Shift Keying (GMSK) and demodulation is noncoherent. The transmission protocol is best suited for short-burst traffic, using a maximum packet size of 512 bytes and a 24-bit address field. Forward error-correction, as well as retransmission, is used to ensure the quality of delivered data packets.

The early wide-area wireless data systems were eventually displaced by the development of the cellular system concept and the widespread deployment of cellular service networks. A major advantage of cellular was that it provided an efficient integration of radio technology with the ubiquitous Public Switched Telephone Network (PSTN), providing customers with the mobility and convenience of access to at least basic telephone service—*telephony*—over wide geographic areas. Basic cellular voice service was soon augmented with cellular data services, and the evolution to the modern world of data service on the move was underway. The new era of *tetherless access* to public networks had opened up, and the world of communications was changed forever.

22.5 The Four Generations of Cellular Technology Evolution

The wireless industry has adopted a nomenclature of *generations* referring broadly to fundamental changes in transmission technology and supported services. The technology for the first-generation (1G) analog cellular systems was developed at AT&T Bell Laboratories in the 1970s. However, the earliest deployment of these systems occurred in the Nordic countries under the name Nordic Mobile Telephone (NMT) about a year earlier than the deployment of AT&T's Advanced Mobile Phone Service (AMPS) in the US. The first-generation cellular networks, which provided only basic voice service using analog FM transmission with Frequency Division Multiple Access (FDMA), were followed in the early 1990s by second-generation (2G) networks employing digital voice coding and digital transmission. The second-generation networks were first developed in Europe with the formation of the GSM standardization group [13].

The original motivation for the GSM standardization initiative was to address international roaming, which was a serious problem for European operators, since their existing analog networks were not interoperable. The standardization group quickly decided to adopt a new digital Time-Division Multiple Access (TDMA) technology, since it would allow the integration of other services to expand the horizon of wireless applications [14,15]. However, in the US the reason for migrating to digital cellular technology was that the traffic loads on the analog networks in major metropolitan market areas such as New York and Los Angeles were nearing capacity limits in the then-allocated frequency bands. The second-generation networks provided increased traffic-handling capacity and improved voice quality in poor signal environments. They also provided the means for circuit-oriented wireless data transmission and facsimile transmission well as various enhanced features and services that were already being offered in the PSTN.

The cellular telephone service industry grew very rapidly, as network coverage and service quality steadily improved. Costs to consumers declined due to advancements in integrated circuit technology and service prices fell in response to industry competition. Although the Nordic countries, led by Finland, have always had the highest rate of cellular penetration, in the early days of the industry the US cellular market was by far the largest. By 1994, there were 41 million subscribers worldwide, 25 million of them in the United States. In the past decade, the number of wireless subscribers in the United States has tripled to about 300 million. In North America the transition to digital cellular began with the development of the IS-54 and IS-136 standards, using TDMA as in GSM, but with 30 kHz radio frequency channels as then used for AMPS. As in the GSM standard, the IS-54/136 standard provided an array of circuit-oriented data services. As IS-54/136 systems were being deployed, providing a threefold increase in capacity, concern was already growing with respect to looming capacity limitations. The need for even higher capacity motivated the investigation of CDMA, perceived as offering significantly higher capacity than the TDMA systems. As in the IS-54/136 and GSM systems, the CDMA system included circuit-oriented data services, though still at modest data rates.

While the debate between TDMA and CDMA for 2G systems was ongoing in the United States, GSM deployment began in the EU in the early 1990s. At the same time, developing countries started their planning for cellular networks and most of them adopted the GSM digital technology rather than analog technology. Soon, GSM was being deployed in more than 100 countries. An interesting phenomenon in the evolution of the cellular industry was the unexpectedly rapid expansion of the industry in developing countries. In these countries, the build-out of infrastructure for traditional landline service was too slow to meet the demand for new subscriptions, and the new cellular networks could be deployed much more rapidly than the wireline infrastructure could be expanded.

In early stages of the TDMA vs. CDMA race, CDMA networks were being deployed in only a few countries. Testing and early operational experience had shown that the relative capacity advantage for CDMA was not as great as initially projected. In the mid-1990s, when the first CDMA deployments appeared in the United States, most service providers were subsidizing the cost of cellular phones to stay in the race with TDMA and analog capacity improvements such as band-splitting. However, as

experience was gained with CDMA, it quickly became evident that the received voice quality in CDMA systems was superior to that of TDMA systems, and CDMA quickly grew in popularity with users. Meanwhile, given the huge success of digital cellular technology, manufacturers worldwide began working on standards for third-generation (3G) international mobile telephone (IMT-2000) wireless networks.

The motivation for migrating to 3G networks was to develop an international standard that would assimilate and gradually replace 2G networks. At the same time, 3G systems were intended to improve voice quality and network capacity and to provide significantly increased data rates to accommodate the rapidly growing demand for data-enabled services by mobile users. The 3G systems also provided a transition from circuit-oriented data to packet data services at rates up to about 2 Mb/s. Among multiple radio access technologies proposed to the International Telecommunications Union (ITU), the dominant technology for 3G systems was Wideband CDMA (W-CDMA).

The fourth generation (4G) of cellular wireless standards is the successor to the 3G and 2G families of standards. In 2009, the ITU Radio (ITU-R) organization established the International Mobile Telecommunications Advanced (IMT-Advanced) requirements for 4G standards, setting peak speed requirements for 4G service at 100 Mb/s for high mobility communications such as access from moving vehicles and 1 Gbit/s for low-mobility communication such as access by pedestrians and stationary users.

A 4G system is expected to provide a comprehensive and secure all-IP based mobile broadband solution to laptop computer wireless modems, smartphones, and other mobile devices. Facilities such as ultra-broadband Internet access, IP telephony, gaming services, and streamed multimedia may be provided to users. Two radio access technologies have been developed to meet the requirements for 4G: LTE-Advanced and WiMAX2. Because these systems do not yet fully achieve the data rate requirements defined for 4G, they are unofficially referred to as 3.9G systems. Nevertheless, some service providers have been using the 4G designation for these systems, and it is generally agreed that these systems are paving the way for strictly defined 4G technology.

22.6 Wireless Data in 1G Cellular Networks

The first generation of cellular telephone networks, AMPS in the US and about half a dozen analog cellular networks in across Europe, were designed strictly for analog voice service, in effect simply providing wireless connections to the PSTN over wide geographic areas. They had a capability for cell-to-cell handover and in some cases the ability to roam from one cellular service provider's network to another. However, it soon became evident that many users, particularly business travelers, real estate agents, and service technicians, would like to be able to use the cellular networks for data transmission, just as they were becoming accustomed to using the PSTN for data connections with dial-up modems. Thus, manufacturers began to offer portable modems and facsimile devices for use by "road warriors."

22.6.1 Modems over Analog Cellular Channels

In this form of data communication, the user simply accessed a cellular voice channel just as he would in making a traditional voice call over the cellular network. The user then operated the modem or fax device just as he would have done from office to office over the PSTN. In this form of data communication, the cellular network was not providing a data service, but simply an analog RF link over which the mobile data modem or fax device could interoperate with a corresponding data modem or standard fax machine in the office or service center. The call connection from the Mobile Switching Center (MSC) to the PSTN was a standard landline connection, exactly the same as provided for a cellular voice call. Very soon, many mobile devices came into the marketplace, including, eventually, modems and fax devices built into laptop computers, giving rise to the popular term "mobile office" for the traveling business person.

At the same time, law enforcement personnel began making use of this form of wireless data over cellular and radio dispatch networks to gain rapid access to databases for verification of vehicle registrations and drivers' licenses. Mobile devices came into the marketplace able to operate at transmission rates up to 9.6 or 14.4 kb/s. Error correction modem protocols such as MNP-10, V.34, and V.42 were used to provide reliable delivery of data in the error-prone wireless transmission environment.

In another form of data communication over the analog cellular networks, the mobile subscriber used a portable modem or fax device as described above, but now accessed a modem provisioned by the cellular operator as part of a *modem pool* connected to the MSC. Some modem pools provided the subscriber with a choice of several standard modem types. The call connection from the modem pool to the office was a digital connection provided by any one of a number of public packet data networks, such as those providing X.25 service. Here, the cellular operator provided a special service in the form of modem pool access, and this service usually carried a higher tariff than did standard cellular telephone service, due to the operator's added investment in the modem pools. In this form of service, however, the user in the office or service center did not require a modem but instead had a direct digital connection to the packet data network from his desk-top or host computer.

Each of the types of wireless data transmission just described was in effect an appliqué onto an underlying analog cellular service and, therefore, had limitations imposed by the characteristics of the underlying voice-circuit connection. That is, the cellular segment of the call connection was a circuit-mode service, which might have been cost-effective and bandwidth-efficient if the user was transferring large files or long fax transmissions, but not if only short messages were to be transmitted. As is well understood by communications engineers, packet data transmission can make much more efficient use of transmission capacity than does circuit-mode transmission, since segmenting communication into packets allows a communication path to be shared among multiple users. In the operation of cellular networks, where RF bandwidth is a limited and expensive resource, it soon became clear than packet services would provide a more efficient way to use available bandwidth. In the previous section, we described the ARDIS and Mobitex networks, which were designed *ab initio* as packet data networks. Here, we describe a packet data service that was conceived as a service to be integrated with already-deployed 1G analog cellular networks.

22.6.2 Cellular Digital Packet Data

In each generation of evolution of mobile networking technology, there have been one or more developments anticipating the next generation. In North America, the 1G cellular system was AMPS, providing analog voice service over 30 kHz channels in the 800–900 MHz cellular band. As market demand for mobile data services grew, the cellular industry looked for ways to capitalize on their considerable investments in AMPS networks and use those networks to deliver data service. The result was the Cellular Digital Packet Data (CDPD) system, designed to provide packet data service as an overlay onto existing AMPS networks. (It was also possible to overlay CDPD service onto a D-AMPS network, described below.) CDPD was developed by IBM in collaboration with the major cellular carriers [16]. Any cellular carrier owning a license for AMPS service was free to implement CDPD service without need for further licensing.

The basic concept of the CDPD system was to provide packet data service on a noninterfering basis simultaneously with analog cellular voice service using the same set of 30-kHz RF channels. This was accomplished typically by allocating one or a few 30-kHz channels in each cell site to CDPD service. Each CDPD channel supported packet data transmission at rates up to 19.2 kb/s, though degraded radio channel conditions limited useful data throughput to lower levels and introduced additional time delays due to error-detection and retransmission protocols. The CDPD radio link physical layer used GMSK modulation on both forward (base-to-mobile) and reverse (mobile-to-base) links. Transmit pulse-shaping ensured that the average signal power spectrum satisfied the emission requirements for analog cellular systems.

The participating companies issued the first release of the CDPD specification in 1993 and a second release in 1994. Typical applications for CDPD service included: electronic mail, field support service, package-delivery tracking, inventory control, credit card verification, security reporting, vehicle theft recovery, traffic and weather advisory services, and a wide range of information retrieval services. Some CDPD networks provided service for PDAs. While a number of wireless carriers implemented CDPD service, it achieved only limited success in the marketplace, due in part to the availability of lower-cost public data services such as Mobitex, as well as the anticipation of higher-speed services that would be available in 2G digital cellular systems. By 2005, most CDPD networks had been shut down, and higher-speed data services were available as features of 2G and 3G digital cellular systems.

22.7 Wireless Data in 2G Cellular Networks

In the 1980s, as the cellular industry began to develop digital systems to replace the first-generation analog systems, the need for cellular data services was becoming apparent, and the thus the 2G cellular systems were designed to incorporate data services as well as digital voice service. In this section we summarize the evolution of cellular data services in the principal 2G systems as well as the transitional technologies that anticipated the next step in the evolution of cellular systems.

22.7.1 Data Services in Digital AMPS

In the US and Canada, the Electronic Industries Alliance (EIA) and the Telecommunications Industry Association (TIA) together developed the interim standard IS-54, the first of the digital cellular standards in the US. The IS-54 standard was soon followed in early 2000 by IS-54B and IS-136, and this set of three standards came to be known collectively as Digital AMPS (D-AMPS), though the name United States Digital Cellular (USDC) was also used to refer to these standards, as well as the simpler designation IS-54.

The D-AMPS system used the existing 30-kHz AMPS radio channels but replaced the analog AMPS signal with a six-slot TDMA transmission structure, As in the GSM system, the D-AMPS system defined full-rate and half-rate logical channels. The initial systems implemented only full-rate channels, in which two out of the six slots carried each digitally compressed voice signal, thus tripling the number of *full-rate* voice calls that could be carried on a single cell. The six-slot format allowed for later introduction of half-rate vocoders, which would provide a doubling of voice-call capacity. In addition to digital voice service, the D-AMPS system eventually incorporated circuit-switched data services, as well as facsimile service for mobile connectivity with Group-3 fax machines in common use on the PSTN. The data service modes included full-rate and half-rate modes, all circuit-switched. The air interface for the D-AMPS system used $\pi/4$-shift Differential Quaternary Phase Shift Keying ($\pi/4$-shift DQPSK) with a transmission rate of 48.6 kb/s. After accounting for overhead bits in the TDMA frames, a full-rate data mode would carry 13 kb/s, but error-control coding brought the user data rates to lower levels.

As D-AMPS networks were being built out in North America, Qualcomm's CDMA system was being developed and tested, and D-AMPS was ultimately displaced by CDMA and, in some US markets, by GSM. At this writing, there are no longer any D-AMPS networks in operation.

22.7.2 Data Services in GSM

In the early 1980s, a technical group was formed to develop a Pan-European standard for a digital cellular system, called Global System for Mobile Communications (GSM), which would replace six incompatible analog cellular systems then in use throughout Europe. Soon, throughout much of Europe and surrounding regions, spectrum was reallocated so that a completely new system could be developed. The GSM system went into operation in 1992 and rapidly gained adoption throughout Europe and elsewhere in the world, particularly in the Asia-Pacific region. In a GSM system, each RF channel supports

multiple user channels with a TDMA signal format. This radio channel structure, termed FDMA/TDMA, was also adopted for 2G systems in North America and Japan, though many details of the channel structures differed from one system to another.

In GSM each 200-kHz frequency channel has an aggregate bit rate of 270.833 kb/s, carried over the radio interface using *Gaussian Minimum Shift Keying* (GMSK). The 270-kb/s data stream in each frequency channel in divided into eight fixed-assignment TDMA channels termed *logical channels*. The GSM radio interface standard provides a variety of traffic and control channels, defined in a hierarchy built upon the underlying 8-slot TDMA transmission format. The details of the GSM protocol structure can be found in many references including [17]. For our purposes here, where we focus on cellular data services, it suffices to say that the basic building block of the frame hierarchy is a 4.615-ms frame comprising eight 5.77-μs time slots. The next level in the hierarchy is a 120-ms GSM *multiframe*, a multiframe comprising 26 eight-slots. In each multiframe, 24 frames carry user information, while two frames carry control information. This structure allowed for the implementation of *full-rate* and *half-rate* services in GSM networks. The earliest implementation of GSM provided full-rate digital voice service in which all 24 frames in a multiframe were used. Later, as voice coding technology advanced, providing good-quality voice reproduction at lower compressed data rates, half-rate voice service would be implemented by allocating only 12 frames per multiframe to a user channel. The aggregate data rate in a full-rate GSM channel is 22.8 kb/s, and in a half-rate channel 11.4 kb/s, each including coding incorporated for error protection.

The GSM standard eventually specified a number of *bearer services* to support transmission of unspecified data [18]. For use on a full-rate channel, several data rates up to 9.6 kb/s are provided. For use on a half-rate channel, the data rates up to 4.8 kb/s are specified. The stated rates are user data rates, but the aggregate transmission rate in each case is higher, due to the addition of error-control coding. The error-control coding specified in GSM data services is more powerful than the coding used in digital voice service, since data transmissions are less tolerant of errors than are voice transmissions. For each GSM data rate, a different coding method is used, though each employs punctured convolutional coding with interleaving. Detailed examples of channel coding for GSM data channels can be found in Reference 17.

GSM supports both asynchronous and synchronous transmission and a choice of Transparent or Non-Transparent mode. Transparent mode provides forward error correction (FEC), constant bit rate and constant transport delay. Nontransparent mode activates a *Radio Link Protocol*, which uses Automatic Repeat Request (ARQ) with retransmission. In addition to the asynchronous and synchronous circuit-switched services, GSM also provides packet data services. These are either asynchronous access to a *Packet Assembler/Disassembler* (PAD), or direct asynchronous access to a packet data network. It should be noted that while these services supported packet-oriented interfaces to the GSM network, they simply carried packet-formatted data over the air interface in on a circuit-switched channel for the full duration of the call connection. Thus, they did not provide the efficiency of true packet data in use of frequency resources.

GSM also provided for Short Message Service (SMS), which carries short text messages on control channels and is the basis for *texting*, which has become extremely popular with cell phone users. GSM data services are described in considerable detail in Reference 18.

22.7.2.1 High-Speed Circuit Switch Data

While the circuit-switched data services in conventional GSM provided data rates comparable to legacy dial-up modems, much higher rates were already being deployed in fixed networks. Accordingly, in the Phase 2+ stage of GSM development, one of the GSM standardization groups specified *High-Speed Circuit Switch Data* (HSCSD) service [18]. The GSM designation Phase 2+ denotes the fact that these services are built upon the Phase 2 GSM architecture while providing some of the capabilities envisioned for a subsequent third generation (3G) of wireless systems. HSCSD provides higher data rates than the original CSD services, using two innovations. The first innovation is to allow different levels of

error correction coding, which can be chosen in accordance with channel quality. For example, a data call made under very good channel conditions can employ a coding scheme having a small amount of redundancy, thus higher user data rate for the same channel transmission rate. A second innovation in HSCSD is the ability to use multiple time slots simultaneously. Thus, combining four time slots a user could be provided error-protected data at 38.4 kb/s instead of 9.6 kb/s. Of course HSCSD services could not be accessed with conventional GSM mobile terminals, due to the increased complexity required for multislot operation and for the enhanced coding options. Today mobile devices are available in the market place providing data speeds of 38.4–57.6 kb/s, slightly more than what can be achieved with data modems in the PSTN.

22.7.2.2 General Packet Radio Service

Soon after the first GSM networks became operational in the early 1990s and customers gained experience with the GSM data services, it became evident that the circuit-switched bearer services were not particularly well suited for certain types of applications where data traffic was bursty. The circuit-switched data services, while satisfactory for long file transfers, were not cost-effective for the customer using the service for connections to the Internet or corporate networks, applications of growing importance in the business world. Similarly, from the service provider's perspective, the use of circuit-switched connections for carrying bursty traffic did not make efficient use of cellular network capacity. At the same time, customer demand for higher-rate data services was growing steadily as new software applications for mobile users were entering the marketplace. The development of General Packet Radio Service (GPRS), begun in 1994 as part of the GSM Phase 2+ specification, was an important step toward satisfying the evolving needs of mobile customers and cellular service providers as well. The primary GPRS specifications were approved by 1997 [19].

Stated briefly, GPRS overlays true packet data service onto a GSM network in a way that maintains strict separation between radio subsystem and the network system, with the advantage that no modifications to Mobile Switching Centers (MSCs) are required [20]. GPRS provisioning does require some enhancements and modifications to GSM infrastructure and, as with HSCSD, to mobile stations (MSs). In GPRS, the allocation of the eight timeslots on one RF channel is flexible. One to eight time slots in a TDMA frame can be assigned to the service, and uplink and downlink timeslots are allocated separately. The capacity of an RF channel can be shared dynamically between circuit-switched and packet data services. GPRS provides data rates up to 171.2 kb/s, this upper limit achieved by assigning all eight time slots in a GSM radio channel to a single user [21,22].

The GPRS system brings packet-switched data services to the existing GSM system, providing the customer many advantages not provided by the earlier GSM circuit-switched data services. In the GPRS system, mobile users can access public data networks directly using their standard protocol addresses, such as IP or X.25. The resource allocation in the GPRS network is dynamic and dependent on demand and resource availability. Packets can also be sent in idle periods between speech calls. With the GPRS system, it is possible for customers to communicate point-to-point (PTP) or point-to-multipoint (PT2MP), and the system also supports SMS. The theoretical maximum throughput in the GPRS system is 160 kb/s per MS using all eight channels without error-correction coding redundancy [23]. Because GPRS builds upon a 2G network technology while approaching higher data rates envisioned for 3G systems, GPRS is often described as a 2.5G technology, that is, a transitional technology between 2G and 3G. It should be noted here that the terms 2G and 3G are official designations adopted by standardization groups, but the term 2.5G has no official definition and has been used in the industry primarily for marketing purposes.

22.7.2.3 Enhanced Data for Global Evolution

Soon after the year-2000 introduction of GPRS, it was perceived by network operators that GSM-based networks would have to provide even higher data rates. The need for higher rates has grown out of the market demand for an expanding menu of services, such as multimedia transmission. In response to this market demand, the European Technical Standards Institute (ETSI) defined a new family of data

services, built upon the existing structure of GPRS. This new family of data services was initially named Enhanced Data Rates for GSM Evolution, and subsequently renamed Enhanced Data for Global Evolution (EDGE). While the primary motivation for EDGE development was enhancement of data services in GSM/GPRS networks, EDGE can also be introduced into networks built to the D-AMPS standard [24]. In Europe, EDGE is considered a 2.5G standard, providing a transition between 2G and 3G systems. As is the case with GPRS, a GSM network operator requires no new license to implement EDGE services in its network, since the 200-kHz RF channel organization of conventional GSM is reused with a different organization of logical channels within each RF channel. EDGE technology became available in 2001, and was deployed in GSM networks beginning in 2003. Next we describe the implementation of EDGE in GSM/GPRS networks.

EDGE enhances data service performance over GPRS in two ways [21,25]. First, it replaces the GMSK radio link modulation used in GSM with an 8-PSK modulation scheme capable of tripling the data rate on a single radio channel. Second, EDGE provides more reliable transmission of data using a link adaptation technique, which dynamically chooses a modulation and coding scheme (MCS) in accordance with the current transmission conditions on the radio channel. The EDGE link adaptation mechanism is an enhanced version of the link adaptation used in GPRS.

EDGE provides two forms of enhanced data service for GSM networks—Enhanced Circuit-Switched Data (ECSD) for circuit-switched services and Enhanced GPRS (EGPRS) for packet-switched services. In each form of EDGE data service, there are provisions for combining logical channels (time slots) in the GSM transmission format to provide a wide menu of achievable data rates.

The major impact that EDGE has on the GSM/GPRS protocol structure is at the physical layer of the radio interface, and there is only minor impact on MAC and radio link control (RLC) layers [21]. The EDGE RF specification and definition of burst structures are common to EGPRS and ECSD. A major modification in EGPRS, relative to GPRS, is the link quality control (LQC) function, which provides a wider array of link error-control schemes than exist in conventional GSM or in GPRS. The LQC function provides nine different modulation and coding schemes, MCS-1 to MCS-9, as well as related signaling and adaptation procedures for switching between MCSs in response to radio link conditions. Table 22.2 summarizes the nine MCSs used in EGPRS and shows the data throughput provided by each MCS. The EGPRS modulation and coding schemes are organized into three families, A–C, according to their RLC block sizes. For example, in family A, MCS-9 carries 1184 payload bits in two RLC data blocks during one EGPRS radio block of four consecutive bursts (radio blocks). MCS-6 carries 592 payload bits in one RLC frame, and MC-3 carries 296 payload bits within the RLC block. In each family, the numbers of payload bits carried in the lower-rate coding schemes are submultiples of the payloads at higher rates. This feature enables efficient retransmission of negatively acknowledged RLC blocks when this functionality is needed following a sudden change in radio

TABLE 22.2 EGPRS Modulation and Coding Parameters

Modulation and Coding Scheme	Code Rate	Modulation Type	Data Rate per Time Slot (kb/s)	MCS Family
MCS-9	1.00	8-PSK	59.2	A
MCS-8	0.92	8-PSK	54.4	A
MCS-7	0.76	8-PSK	44.8	B
MCS-6	0.49	8-PSK	29.6	A
MCS-5	0.37	8-PSK	22.4	B
MCS-4	1.00	GMSK	17.6	C
MCS-3	0.80	GMSK	14.8	A
MCS-2	0.66	GMSK	11.2	B
MCS-1	0.53	GMSK	8.8	C

TABLE 22.3 ECSD Service Rates in EDGE

Coding Scheme	Code Rate	Modulation Type	Gross Rate (kb/s)	Radio Interface	User Rate (kb/s)
TCH/28.8 (NT/T)	0.419	8-PSK	69.2	29.0	28.8
TCH/32.0 (T)	0.462	8-PSK	69.2	32.0	32.0
TCH/43.2 (NT)	0.629	8-PSK	69.2	43.5	43.2

Note: NT, Non-Transparent Service; T, Transparent Service.

channel conditions. For a detailed discussion on EGPRS link adaptation and analysis of its performance, the reader is referred to [21].

The ECSD service is built upon the high-speed circuit-switched data HSCSD service standardized in the GSM Phase 2+ specification. While the user data rates provided by ECSD (up to 64 kb/s) are not higher than those in HSCSD, the same data rates are achieved in ECSD by using smaller numbers of time slots and simpler implementation in the mobile stations [21]. As was the case with HSCSD, ECSD provides both transparent (T) and nontransparent (NT) services. Table 22.3 shows the data rates provided by ECSD service in EDGE.

A further extension of the GSM standard, termed as Evolved EDGE (E-EDGE) upgrades EDGE further to provide even higher data speeds. Also called EDGE Evolution, it provides downlink data rates up to 600 kb/s. There has been much interest in E-EDGE technology on the part of carriers, some of whom see this technology as an alternative or a step in transition to full 3G networks. At this writing, however, there has been little or no adoption of E-EDGE technology.

22.7.3 Data Services in 2G CDMA Networks

In contrast to the GSM and D-AMPS standardization work carried out by multiple organizations working together, the CDMA initiative was based on a cellular system design developed by Qualcomm, Inc. [26]. Proponents of the CDMA system projected that the system would provide a significantly larger capacity increase (over analog AMPS) than would be achieved with the D-AMPS standard. Subsequently, the TIA established subcommittee TR45.5, which began developing a standard based on the Qualcomm CDMA design.

The resulting air-interface specification IS-95 was released in July 1993. A revised standard, IS-95A, was released in 1995, and first deployed in commercial service soon thereafter. The IS-95A standard provided the basis for many of the first CDMA networks deployed throughout the world. In 1997, Qualcomm's CDMA technology was re-branded as *cdmaOne*, though the earlier designation IS-95 is still used frequently in the industry. In addition to digital voice service, the IS-95A CDMA networks provide circuit-switched data service at rates up to 14.4 kb/s. A subsequent revision of the standard provided for packet-switched data services at rates up to 64 kb/s, termed as *medium data rate* (MDR), in addition to voice service. Due to this increased data rate capability, cdmaOne was referred to as a 2.5G technology.

As the new digital cellular equipment became available, service providers in North America adopted both the TDMA and CDMA standards, some operators implementing one standard in a given market area and the other standard in another market area. However, as the cellular service market grew, subscribers and service providers showed an increasing preference for the CDMA technology; better voice quality was typically cited as the deciding factor. Today IS-95-based CDMA, usually referred to collectively as *cdmaOne*, is the dominant cellular technology in North America and has become a *de facto* worldwide standard as well. Also, cdmaOne was accepted as the basis for one leg of the cellular industry evolution to Third-Generation (3G) systems, as *cdma2000*. A key driver in the evolution toward 3G systems is the requirement for data service rates significantly higher than those offered by 2G systems. An important development proposed to meet this requirement was CDMA-based *High-Data-Rate* (HDR) service, the basis for EV-DO, discussed later.

22.8 Data Services in 3G Networks

In 1998, the ITU called for proposals for a set of globally harmonized standards for third-generation (3G) mobile services and equipment, to be called International Mobile Communications 2000 (IMT-2000). They received many proposals based on TDMA and CDMA access technology. The European Telecommunications Standards Institute (ETSI) and GSM equipment manufacturers backed wideband code division multiple access (W-CDMA), while US manufacturers backed CDMA2000, which had its origins in IS-95 and cdmaOne. Subsequently, two groups of standards bodies formed: 3rd Generation Partnership Project (3GPP), and 3rd Generation Partnership Project 2 (3GPP2). The scope of work in each of these two groups is very comprehensive, encompassing radio access, network architecture, services, and security. However, given the subject of this chapter, we confine our discussions to data services standardized by each of the groups.

22.8.1 Universal Mobile Telecommunications System 3GPP

The set of standards developed by 3GPP is called Universal Mobile Telecommunications System (UMTS), comprising three different air interfaces. The currently most widely implemented air interface is Wideband CDMA (W-CDMA), which uses two 5 MHz channels in frequency division duplex (FDD) operation. The second UMTS air interface specification is a TD-CDMA access scheme that uses 5 MHz channels, but formats the signal in each channel as consecutive frames containing time slots. The time slots are assigned at a fixed percentage for uplink and downlink communication, eliminating the need for separate upstream and downstream frequency channels, thus allowing deployment in tighter frequency bands.

The third air-interface specification, termed as Time Division Synchronous Code Division Multiple Access (TD-SCDMA) uses TDMA combined with an adaptive synchronous CDMA component on 1.6 MHz frequency channels. TD-SCDMA uses Time-Division Duplex (TDD) transmission, in contrast with the FDD scheme used in W-CDMA. By dynamically adjusting the number of timeslots used for downlink and uplink, the system can more easily accommodate asymmetric traffic than can FDD schemes. Since it does not require paired spectrum for downlink and uplink, spectrum allocation flexibility is also increased. Using the same frequency channel for uplink and downlink also means that the channel condition is the same on both directions, and the base station can deduce downlink channel information from uplink channel estimates, which is helpful in the application of beamforming techniques.

With respect to data services, the first release of the UMTS standard in 1999 specified circuit-switched data at 64 kb/s and packet-switched data at 384 kb/s, but later releases introduced High-Speed Packet Access (HSPA), providing significantly higher data rates, followed in 2008 by Evolved HSPA (HSPA+).

22.8.1.1 HSPA and HSPA+

HSPA is combination of two protocols, High-Speed Downlink Packet Access (HSDPA) and High-Speed Uplink Packet Access (HSUPA). High-Speed Downlink Packet Access (HSDPA), specified in Release 5, introduced a high-speed downlink shared channel (HS-DSCH), which is shared among the users. The theoretical peak data rate is of the order of 14 Mb/s. HSDPA provides average data throughput speeds of 550–1100 kb/s to the user. The delay within the network (latency) is also lower than in earlier UMTS data services.

HSUPA, introduced in 3GPP Release 6, uses an uplink enhanced dedicated channel (E-DCH) on which it employs link adaptation methods similar to those employed by HSDPA, namely: shorter Transmission Time Interval enabling faster link adaptation; and hybrid ARQ (HARQ) with incremental redundancy making retransmissions more effective. HSUPA provides uplink data speeds up to 5.76 Mb/s. Subsequent releases of the 3GPP specification provided a series of enhancements to the HSPA suite of packet data services.

22.8.1.2 HSPA+

Evolved High-Speed Packet Access (HSPA+), first defined in 3GPP Release 7, provides data rates up to 84 Mb/s on the downlink and 22 Mb/s on the uplink, through the use of the multiple-antenna technique termed Multiple-Input and Multiple-Output (MIMO) [27] and 64-ary Quadrature Amplitude Modulation (MIMO systems are discussed in Chapter 16 of this handbook.) The 84 Mb/s and 22 Mb/s represent theoretical peak speeds, while user data rates will typically be lower. Chapters 16 and 17 address MIMO techniques in greater detail.

Beginning with Release 8, the 3GPP specifications provide for further evolution of HSPA+ , by means of *carrier aggregation*. UMTS licenses are typical issued as 10 MHz or 15 MHz paired spectrum allocations. However, in deployments where multiple channels are available, multicarrier operation offers advantages of higher data rates and improved queuing efficiency, especially for packet data. Two names are being used to describe carrier aggregation schemes: *dual-cell* and *dual-carrier* operation, depending upon whether the frequency channels to be aggregated are contiguous or non-contiguous, respectively. Carrier aggregation techniques provide cellular carriers with an alternative to MIMO techniques, which entail significant redesign of hardware and antenna systems. HSPA+ also introduces optional all-IP architecture for the network, where base stations are directly connected to IP based backhaul and then to the ISP's edge routers. Thus, the HSPA family of specifications represents a major transitional step from 3G technology to fourth-generation networks, which will be based on an all-IP architecture.

3GPP Release 8, published in early 2009, introduced dual-cell operation on the downlink using adjacent channels, called Dual-Cell HSPDA (DC-HSPDA). Using DC-HSPDA with 64-QAM modulation on two adjacent 5 MHz channels, downlink data rates up to about 42 Mb/s are achievable. Release 8 also introduced Long-Term Evolution (LTE) into the 3GPP standards evolution. LTE is discussed in Section 22.8.3. 3GPP Release 9, completed in early 2010, introduced Dual-Cell HSUPA (DC-HSUPA), which uses carrier aggregation on the uplink. Release 9 allows the paired frequency channels to be in two different frequency bands, and also provides for the simultaneous use of MIMO and DC-HSPA operation. 3GPP Release 10, and Release 11, both in progress at this writing, will specify further enhancements to HSPA, including additional multicarrier and MIMO options and advanced antenna techniques.

22.8.2 CDMA2000 and EV-DO

As stated earlier, the second standardization body formed under the IMT-2000 initiative, 3GPP2, developed the CDMA2000 family of cellular standards, which provide backward compatibility with the widely deployed 2G CDMA networks that evolved from the original IS-95 standard. CDMA2000 allows smooth evolution to 3G capabilities within an operator's existing 2G spectrum allocation. As in the IS-95 cdmaOne networks, CDMA2000 utilizes a duplex pair of 1.25 MHz channels, supporting digital voice and data services. Here we confine our attention to CDMA2000 data services.

22.8.2.1 1 × RTT and EV-DO

Many cdmaOne network operators followed a two-stage migration path to CDMA2000. The first stage was implementation of CDMA2000 Single Carrier Radio Transmission Technology (1 × RTT), which used a 1.25 MHz CDMA channel to support packet-switched data service at a speeds up to 144 kb/s, and also doubled voice traffic capacity relative to cdmaOne networks. The CDMA2000 1 × RTT technology was usually categorized as 2.5G, since the achievable data rate was significantly lower than objectives set by the IMT-2000 program for 3G networks. However, 1 × RTT soon evolved into CDMA2000 Single-Carrier EVolution, Data Optimized (EV-DO), which was adopted by 3GPP2 as part of the CDMA2000 family of standards for 3G, and ratified by the ITU under the designation TIA-856. Subsequently, the TIA-856 standard has gone through several stages of revision. In order to emphasize the data-only aspect of EV-DO, mobile terminals used for data-only applications are referred to as *access terminals* (ATs). Also, the TIA-856 standard refers to base stations as *access networks* (ANs).

While TIA-856 had its origins in the 1 × RTT technology, its channel structure is quite different. The downlink signal format is composed of slots of length 2048 chips, or 1.67 ms at the channel chip rate of 1.2288 Mc/s. Groups of 16 slots are synchronized to system timing on even-second time ticks. The system uses GPS to maintain precise time synchronism. Each time slot is divided into two half-slots, each of which is time division multiplexed into Medium Access Control (MAC, 28 chips), Pilot (96 chips), and Data (800 chips) fields. The Data fields support either a Forward Traffic channel or a Control channel, distinguishable at the mobile terminal by a preamble inserted into the data. Each Pilot channel burst is centered at the midpoint of a half-slot and between a pair of MAC channel bursts. The Pilot channel bursts provide a reference in the AT for coherent demodulation of Traffic and MAC channel signals, and also enable SNR estimation at the AT. All fields in a 2048-chip Active slot are transmitted at the same power level.

The primary characteristic differentiating EV-DO from 1 × RTT, seen in TIA-856 Release 0, is that downlink transmission is time-multiplexed, meaning that a mobile terminal has full use of the downlink traffic channel in a cell sector during a given time slot. With this technique, the mobile terminal is able to select an appropriate modulation for that user's time slot, depending upon signal reception conditions, namely received signal strength, multipath and fading. The mobile tries to select a modulation that will provide a sustainable data rate while maintaining a frame error rate in the range of 1–2%. This is described as a *data rate control scheme*, rather than power control, since the downlink signal is always transmitted at full power. Release 0 provided downlink packet data speeds ranging from 38 kb/s up to 2.4 Mb/s. The transmission is organized into blocks called *physical layer packets*, and a packet may utilize 1–16 time slots, depending upon the data rate. When more than one slot is allocated, consecutive slots are separated by three intervening slots, which are occupied by slots of other physical layer packets transmitted to the same AT or to other ATs. For further details, the reader is referred to the 3GPP2 web site.

The Forward Traffic channel is a packet-based variable-rate channel, in which user data can be transmitted to an AT at data rates ranging from 38.4 kb/s to 2.4576 Mb/s.

In order to receive data, an AT measures SNR on the forward link pilot channel as often as every 1.66… ms, that is, every slot time. Based upon the SNR measurement, the AT requests a data rate by sending a Data Rate Control (DRC) message to the AN. Typically, the AN receives requests from a number of ATs, and determines which ATs are to be served next, based on which terminals have reported the best SNR values. The DRC message indicates not only the data rate but also the modulation, Turbo-coding rate, preamble length and maximum number of time slots needed to transmit a physical layer packet to the AT. Table 22.4 shows the modulation parameters for a selection of HDR data rates on the forward link. The Traffic channel utilizes 1600 chips in every slot, as described earlier; however in the first slot of a physical layer packet, a number of chips are allocated to a preamble of length shown in Table 22.4.

The downlink user data stream is Turbo-encoded, then scrambled with a pseudonoise (PN) sequence unique to each user. The data rate going to each user is adjusted by repetition of the channel-coded bits,

TABLE 22.4 Modulation Parameters for HDR Rates

Data Rate (kb/s)	Packet Length (bytes)	Code Rate	Modulation Type	TDM Chips per Packet	Preamble Chips per Packet
38.4	128	1/4	QPSK	24,576	1024
76.8	128	1/4	QPSK	12,288	512
153.6	128	1/4	QPSK	6144	256
307.2	128	1/4	QPSK	3072	128
614.4	128	1/4	QPSK	1536	64
1228.8	256	1/2	QPSK	1536	64
1843.2	384	1/2	8-PSK	1536	64
2457.6	512	1/2	16-QAM	1536	64

lower rates using higher repetition factors. Code *puncturing* is also used to adjust some of the data rates. The coded data stream is block interleaved then modulated using QPSK, 8-PSK or 16-QAM, depending upon the data rate, as indicated in Table 22.4. The resulting modulated data sequence has a chip rate of 1.2288 Mchips/s, regardless of the data rate. The in-phase and quadrature channels are then time-demultiplexed into 16 separate streams, each running at 76.8 kchips/s, each of which is covered by a 16-chip Walsh Code sequence. The 16 Walsh-coded streams are then summed and spread by quadrature PN sequences, bandlimited and upconverted. The resulting RF signal has the same characteristics as an IS-95 CDMA signal, thus allowing the reuse of all analog and RF circuits developed for IS-95 (or cdmaOne) base stations.

The Control Channel transmits broadcast messages and AT-directed messages at a data rate of 38.4 kb/s or 76.8 kb/s, using the same modulation parameters as given in Table 22.4 for Traffic Channels at those two rates. As noted earlier, Control Channel transmissions are distinguished from Traffic Channel transmissions by a preamble, which in a Control Channel is covered by a special bi-orthogonal cover sequence.

In contrast with the downlink, which always transmits at maximum power, the EV-DO uplink uses power control—both open-loop and closed-loop. In open-loop, the uplink signal power is set based upon the power received on the downlink. In closed loop, the uplink power is adjusted up or down 800 times per second, as indicated by the serving sector at the base station. The uplink data traffic channel can support five data rates ranging in doubling steps from 9.6 to 153.6 kb/s, though the higher data rates are typically not achievable under real-world conditions.

22.8.2.2 TIA-856 Revision A

TIA-856 Revision A made several additions to the standard while maintaining full backward compatibility with Release 0. The changes included the addition of several new downlink data rates increasing the maximum burst data rate from 2.4 Mb/s to 3.1 Mb/s. Revision A also added the capability for more than one mobile to share the same time slot.

In addition to changes in the downlink specification, Revision A also added uplink enhancements to support higher-order modulation schemes, and thus higher data rates, up to a maximum of 1.8 Mb/s, though actual user data rates are more typically two to three times lower than the maximum theoretical rates.

22.8.2.3 TIA-856 Revision B

Revision B of TIA-856, which went into commercial operation early in 2010, enhances Revision A systems by providing higher data rates on each frequency channel and also the capability to bundle multiple channels for even higher rates. With Revision B, single-channel downlink data rates up to 4.9 Mb/s are specified, and bundling of three channels can provide rates up to 14.7 Mb/s.

22.8.3 3GPP Long-Term Evolution

As discussed in Section 22.8.1, the set of mobile networking standards produced by the 3GPP group is called Universal Mobile Telecommunications System. In early 2009, 3GPP Release 8 was frozen, specifying Long-Term Evolution (LTE) as an international standard for mobile communications. Much of Release 8 focuses on migration to 4G technology, including an all-IP flat networking architecture. Work on LTE had been ongoing in 3GPP since 2004, and elements of an all-IP architecture were addressed in earlier releases, beginning with Release 4. The LTE specification provides for peak downlink data rates of at least 100 Mb/s, peak uplink rates of at least 50 Mb/s. and low latency with round trip delays less than 10 ms. Higher data rates will be feasible with the use of MIMO and beamforming techniques. LTE supports scalable channel bandwidths ranging from 1.4–20 MHz. LTE supports both FDD and TDD full-duplex modes, allowing cellular operators flexibility in utilizing their available spectrum. LTE is designed to co-exist with legacy 3G networks by means of multimode mobile devices, and thus can be viewed as an overly onto existing networks. LTE is also designed to support high data rates for high-speed mobile

terminals. LTE systems, on the market since 2009, currently support data services only. Carriers are planning to introduce voice services using Voice over IP (VOIP) technology sometime in 2013.

At the physical layer, the LTE downlink employs Orthogonal Frequency Division Multiplexing (OFDM), a modulation format that provides great flexibility in adjusting data rates for multiple mobile users using dynamic channel allocation and channel-dependent scheduling [28]. On the uplink, LTE uses Single Channel FDMA (SC-FDMA) transmission, which has lower peak-to-average power fluctuation than OFDM and thus lessens power consumption in the mobile terminal.

LTE, while it provides modes of operation at data rates higher than are achievable with widely used 3G services such as HSPA+, does not meet the high data rate requirements set formally for 4G networks—100 Mb/s for high mobility communications and 1 Gbit/s for low mobility and pedestrian communications. Nevertheless, over the last few years, some service providers have been identifying LTE and HSPA+ as well, as 4G technologies. In the meantime, progress has been made on other systems that are candidates for fulfillment of 4G requirements, and they are addressed in the following section.

22.9 Evolution to 4G Networks

In the fall of 2009, technology proposals were submitted to the ITU as candidates for 4G standardization. Essentially all the proposals fell into two categories, (1) LTE-Advanced as already standardized by 3GPP and (2) IEEE 802.16 m as standardized by the IEEE and commonly termed as WiMAX. Initial implementations of LTE-Advanced and WiMAX do not meet the maximum data rate requirements set for 4G; however, their designs are ultimately extendable to meet the requirements, and thus are considered by the wireless industry to be 4G technologies. Here we summarize the primary features of these two standards, which are treated in greater detail in other chapters of this handbook.

22.9.1 LTE Advanced

In September 2009, the 3GPP Partners made a formal submission to the ITU proposing that LTE Release 10 & beyond (LTE-Advanced) be evaluated as a candidate for IMT-Advanced. The submission was made jointly in the name of 3GPP organizational partners representing the North American, European and Asian regions, and it is now adopted as a major enhancement of the LTE standard. LTE Advanced will provide improvements to both LTE radio technology and network architecture, while assuring backward compatibility with LTE. One of the important aspects of LTE Advanced will be the ability to take advantage of new network topologies, such as heterogeneous networks comprising combinations of high-power macrocells with lower-power picocells and femtocells. LTE Advanced will also introduce multicarrier transmission, providing up to 100 MHz of spectrum in support of very high data rates. It is expected that LTE Advanced will provide peak downlink data rates as high as 3.3 Gb/s under ideal conditions. It is expected that 3GPP Release 10, specifying LTE Advanced, will be issued in late 2011. Chapter 24 discusses LTE Advanced in greater detail.

22.9.2 WiMAX

The WiMAX standard had its origins in the IEEE standardization work on Wireless Local Area Networks (WLANs), carried out by the IEEE 802.11 committee, which began its work in the late 1980s. After a slow start in early years, by the late 1990s, the WLAN industry was in a strong growth mode, and support was growing for the idea of a wireless standard for point-to-multipoint outdoor networks, termed as Wireless Metropolitan Area Networks (WMANs). This interest led to the forming of the IEEE 802.16 standardization committee in 1999. The charter of this committee was to define an air interface standard for fixed and mobile broadband wireless systems using a point-to-multipoint and/or mesh technology. The mesh technology portion of the work plan was later moved to the IEEE 802.20 committee working on mobile broadband wireless access as a separate standard [5].

22.9.2.1 Evolution of IEEE 802.16

The first IEEE 802.16 standard for point-to-multipoint WMAN systems was designed for operation in the microwave range 10–66 GHz and was approved in 2001.This standard specified data rates up to 134 Mb/s using QPSK, 16-QAM and 64-QAM modulations to cover ranges of to 1–3 miles under Line-of-Sight (LOS) propagation conditions. This original 802.16 standard, also called Local Multipoint Distribution Service (LMDS), did not prove to be commercially successful. However, it attracted considerable attention from cellular network equipment manufacturers.

Subsequently, in mid-2001, an industry alliance was formed under the name WiMAX Forum (for Wordwide Interoperability for Microwave Access) to improve the 802.16 standard and to promote this technology and certify conformance of equipment to the standard. The WiMAX Forum parallels the Wi-Fi Alliance (for Wireless Fidelity), which serves in an equivalent role with respect to WLAN products based on the IEEE 802.11 family of standards (see Section 22.1.1). This initiative led to a revival of interest in the 802.16 standard. In 2003, 802.16a was ratified as an amended standard to operate in the 2–11 GHz band using OFDM technology and extend signal coverage to non-line-of-sight (NLOS) conditions. Then, 802.16b extended the standard to the 5–6 GHz band and added features to support Quality of Service (QoS). The next amendment, 802.16c, approved in late 2002, provided a more complete specification for deployment at 10–66 GHz.

The next iteration of the standard, 802.16d, also called 802.16–2004, was a revision aligning the standardization project with ETSI's HIPERMAN (for High-Performance Radio Metropolitan Area Network), an outdoor version of the HIPERLAN (for High-Performance Radio Local Area Network) standard and superseding the earlier amendments 802.16 a, b and c. By this time, WiMAX technology was attracting considerable interest in the cellular industry, and in 2005, 802.16e was ratified, adding mobility to the standard and making it more like a cellular networking technology. Important elements of this amendment were scalable OFDM and a more detailed QoS functionality. The IEEE 802.16e standard is sometimes referred to as "Mobile WiMAX," while earlier generations of 02.16 are termed as "Fixed WiMAX."

With the completion of 802.16d and 202.16e, WiMAX provided a comprehensive MAN technology well suited to deployment in areas of low population density and perhaps developing countries lacking sufficient backbone network infrastructure. WiMAX might be described as an intermediate technology between WLANs and cellular networks. WiMAX can provide fixed or mobile Internet access across whole cities or even small countries. In many cases this technology has provided alternative Internet access in markets that typically access only through an incumbent DSL or cable operator. WiMAX is often described as a "last-mile option" for broadband network access. Following the release of 802.16e, there were several further amendments to standard that added refinements to the Mobile WiMAX standard. Then, in March 2011, the IEEE announced the approval of IEEE 802.16 m, providing performance characteristics that will comply with the IMT-Advanced Recommendations for 4G wireless technology, supporting low-to-high-mobility applications, a wide range of data rates in multiple user environments, high-quality multimedia applications, and significant improvements in performance and quality of service. Chapter 25 treats the 802.16 m standard in greater detail.

22.10 Conclusions

Three decades ago, at the introduction of cellular telephone services in the industrial societies of the world, it would have seemed foolhardy to predict the phenomenal rate of growth that the wireless communications industry has actually experienced since that time. In this chapter, we have traced the development of an important segment of this industry, wireless data communications, from its origins in paging services and specialized low-speed packet data networks to modern wide-area networks that support a steadily increasing array of *untethered* services that have become part of our everyday lives. It is notable that the principal driver in the strong market growth has been demand for services that are

enabled by underlying data services. The industry has observed a new generation of technical capabilities occurring about every ten years. Key trends have been steadily increasing data rate capability, migration toward packet-switched services, and IP-based architecture, and a steady movement toward convergence of standards with each new generation. With 4G technology now entering the marketplace, we will see important performance enhancements gained through the use of MIMO and other advanced antenna techniques, as well as further development of heterogeneous networking concepts. At the same time, we expect to see the demand for new data-enabled services continue to grow at a vigorous pace.

References

1. Pahlavan, K. and Levesque, A. H. Wireless data communications, *Proceedings of the IEEE*, 82(9): 1398–1430, 1994.
2. Pahlavan, K. and Levesque, A. H. *Wireless Information Networks*, 2nd ed., J. Wiley & Sons, New York, NY, 2005.
3. Geier, J. *Wireless LANs*, MacMillan Technical Publishing, New York, 1999.
4. IEEE 802.11 Standard Group Document, IEEE 802.11-00/282r2, 2000.
5. Pahlavan, K. and Krishnamurthy, P. *Networking Fundamentals*, J. Wiley & Sons, New York, NY, 2009.
6. Rappaport, T. *Wireless Communications—Principles and Practice*, 2nd ed., Prentice-Hall, Upper Saddle River, NJ, 2002.
7. Bodson, D. McClure, G. F., and McConoughey, S. R. (Eds.). *Land-Mobile Communications Engineering*, Selected Reprint Series, IEEE Press, New York, NY, 1984.
8. Rice, P. L., Longley, A. G., Norton, K. A., and Barsis, A. P. Transmission loss predictions for tropospheric communication circuits, *NBS Technical Note*, 101, 1967.
9. Longley, A. G. and Rice, P. L. Prediction of Tropospheric Radio Transmission Over Irregular Terrain. A. Computer Method—1968, ESSA Technical Report ERL 79-ITS 67, U.S. Government Printing Office, Washington, DC, 1968.
10. Okumura, Y. E. et al. Field Strength and its variability in VHF and UHF land-mobile service, *Review of the Electronic Communication Laboratory*, 16: 825–873, 1968.
11. Hata, M. Empirical formula for propagation loss in land-mobile radio services, *IEEE Transactions on Vehicular Technology*, 29(3): 317–325, 1980.
12. Khan, M. and Kilpatrick, J. Mobitex and mobile data standards, *IEEE Communications Magazine*, 33(3): 96–101, 1995.
13. Mouly, M. and Pautet, M.-B. *The GSM System for Mobile Communications*, Palaiseau, France, 1992.
14. Haug, T. Overview of GSM: Philosophy and results. *International Journal of Wireless Information Networks*, 1, 7–16, 1994.
15. Heine, G. *GSM Networks: Protocols, Terminology, and Implementation*. Artech House, Norwood, MA, 1999.
16. Quick, R. R. Jr., and Balachandran, K. Overview of the Cellular Packet Data (CDPD) System, *Proceedings of the Personal, Indoor and Mobile Radio Conference (PIMRC'93)*, Yokoham, Japan: 338–343, 1993.
17. Redl, S. M., Weber, M. K., and Oliphant, M. W. An *Introduction to GSM*, Artech House, Norwood, MA, 1995.
18. Eberspächer, J., Vogel, H.-J., and Bettstetter, C. *GSM Switching, Services and Protocols, Second Edition*. Chichester, UK: John Wiley & Sons, Ltd., 2001.
19. Bates, R. J. *GPRS—General Packet Radio Service*. New York: McGraw-Hill, 2002.
20. Steele, S., Lee, C.-C., and Gould, P. *GSM, cdmaOne and 3G Systems*. Chichester, UK: John Wiley & Sons, Ltd., 2001.
21. Halonen, T., Romero, J., and Melero, J., (Eds.) *GSM, GPRS and EDGE Performance*. Chichester, UK: John Wiley & Sons, Ltd., 2003.

22. Levesque, A. H. General Packet Radio Service, In Bidgoli, H. (Ed.) *The Handbook of Computer Networks*, Volume 2, Hoboken, NJ: John Wiley & Sons, 658–674, 2008.
23. Hakaste, M., Nikula, E., and Hamiti, S. GSM/EDGE Standards Evolution (up to Rel'4). In Halonen, T., Romero, J. and Melero, J. (Eds.). *GSM, GPRS and EDGE Performance, Second Edition*. Chichester, UK: John Wiley & Sons, Ltd., 2003.
24. Furuskar, A. et al. EDGE: enhanced data rates for GSM and TDMA/136 evolution. *IEEE Personal Communications*, 6, 56–66, 1999.
25. Seurre, E., Savelli, P., and Pietri, P.-J. *EDGE for Mobile Internet*. Artech House, Norwood, MA, 2003.
26. Gilhausen, K. S. et al. On the capacity of a cellular CDMA system, *IEEE Trans. Veh. Technol.*, VT-40, 303–313, 1991.
27. Foschini, G. J. et al. Simplified processing for high spectral efficiency wireless communication employing multi-element arrays, *IEEE J. Sel. Areas Commun.*, SAC-17(11), 1999.
28. Van Nee, R. and Prasad, R. *OFDM for Wireless Multimedia Communications*, Artech House, Norwood, MA, 2000.

Further Reading

Reference 5 provides a comprehensive review of the wireless data field as of 2009, covering major topics in both WLANs and wide-area networks and standards. Up to date information on the progress of leading standards initiatives can be found on the 802.11, 3GPP and 3GPP2 websites. The journals *IEEE Communications Magazine, IEEE Wireless Communications Magazine*, and the *IEEE Transactions on Vehicular Technology* regularly report advances in many areas of mobile communications, including wireless data. For subscription information contact: IEEE Service Center, 445 Hoes Lane, P. O. Box 1331, Piscataway, NJ 08855–1131. Phone: (732) 981–0060. Internet: www.comsoc.org

23

Third-Generation Cellular Communications: An Air Interface Overview

Giridhar D. Mandyam

23.1 Introduction

Cellular communications systems have been developed and commercialized since the advent of the advanced mobile phone system (AMPS) [1], whose initial commercial deployments date back to 1981 but existed in the lab for nearly two decades prior. Since AMPS was intended to provide full terrestrial coverage for mobile users, a distributed network architecture using the cellular paradigm was employed. This meant that a large number of base stations (fixed location transceivers that are networked with each other), each with its own coverage area (or *cell*), to communicate with mobile equipment. The primary service offered was full-duplex voice telephony. AMPS is a primarily analog transmission system, using frequency-division multiple access (FDMA) as its underlying networking solution. These early analog cellular communications systems are also known as "first generation."

Frequency multiplexing as used in AMPS has inherent capacity limitations, as the available bandwidth for a single mobile user is based on channelization of the total transmission spectrum. When one user occupies a channel, then no other user can use it. Therefore new cellular systems were implemented that involved multiplexing in time in addition to frequency, as well as digital transmission. This led to the development of the first digital cellular systems based on time-division multiple accesses (TDMA). Two TDMA systems came about: In the early 1980s (starting in 1982), the Groupe Special Mobile (GSM)

in Europe developed a digital TDMA standard to work within 200 kHz channels. Afterward, the 30 kHz channel TDMA system known as US Digital Cellular (USDC) or Digital AMPS (D-AMPS) was developed in the late 1980s. These TDMA-based digital systems are also known as "second generation." Although the capacity improvements of second generation systems were substantial, inherent limitations remained due to the number of users on any single frequency being limited by the number of available time slots.

Although digital cellular communications was a great advancement, in the 1980s many researchers started to examine code division multiple access (CDMA) as a method to increase capacity given the limited bandwidth available for transmission. Up until this point, CDMA was a technology primarily used for military applications. CDMA is based on spread-spectrum communications, which involves the transformation of a user's narrowband information signal to a much wider bandwidth for transmission. By modulating the information signal with a high-frequency binary code, the transmitted signal can be recovered even if it is steeped in background noise. CDMA is achieved by assigning each user a unique code.

Qualcomm Incorporated in San Diego, California, is generally recognized as having developed the first commercialized CDMA cellular system in the early 1990s. This system is often referred to by its standards designation by the Telecommunications Industry Association (TIA), which is *IS-95*.

23.1.1 Frequency Reuse versus Code Reuse

A cellular network consists of many cells laid out over a geographical area, with the aim of minimizing coverage gaps. In order to avoid interference, a first- or second-generation base station in a given cell will use a different frequency (or frequencies) for communication than the base stations in neighboring cells. The concept of *frequency reuse factor* refers to the minimum number of transmission frequencies needed for a cellular network to ensure that interference within the same frequency (i.e., *cochannel interference*) is below an acceptable level. For illustration purposes, cells are often represented as hexagonal in shape to describe an ideal cellular network. This type of representation often results in a reuse factor of 3 (see Figure 23.1), that is, the minimum number of frequencies needed to ensure that no neighboring base stations have to occupy the same frequency.

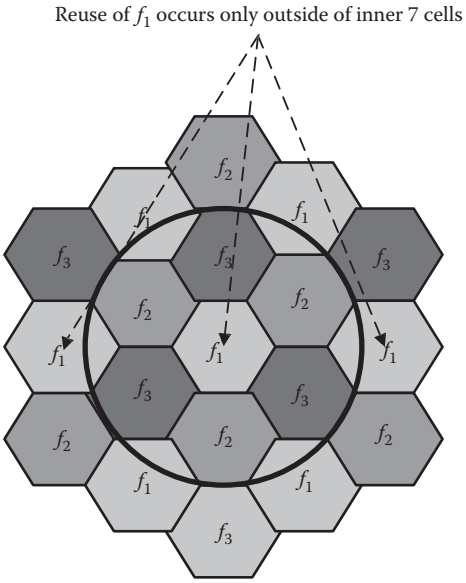

FIGURE 23.1 Frequency reuse for hexagonal cell layout.

The hexagonal representation for cells is idealized. Cell coverage is determined by several factors including site selection, terrain, and radio propagation characteristics based on the area surrounding the base station. CDMA leverages the properties of spreading codes to provide a reuse factor of 1, as all base stations transmit on the same frequency but can be separated based on *cross-correlation* properties of the spreading codes (derived from shift-register generated sequences known as *pseudorandom* codes). In this way, cochannel interference is mitigated, and frequency planning of the cellular network is minimized.

23.1.2 Pseudorandom Sequences

Spreading sequences used in CDMA are known at both the transmitter and receiver, and are used to spread the user information. The most widely used spreading sequences in CDMA are pseudorandom, in that they appear random in nature to an outside observer. They are normally binary to reduce complexity, and are periodic in nature.

Pseudorandom sequences are typically generated through the use of digital logic, using shift registers with feedback. A shift register consists of several memory stages linked consecutively together along with feedback logic. The shift register operates with a master clock, and with each clock cycle a new output from the shift register is generated. A generic N-stage shift register is shown in Figure 23.2.

In Figure 23.2, the coefficients $\{d_i\}$ are also binary and simply act as switches: if the coefficient is "1," then the input is passed through. The content of memory stage i is represented by x_i. If the output of the shift register sequence at clock sample index n is denoted as c_n, then this value can be represented as the modulo-2 sum of a combination of the future output values and the coefficients $\{d_i\}$ as

$$c_n = \sum_{i=1}^{N} d_{N-i+1} c_{n+i} \tag{23.1}$$

This representation leads to shift register usually being described in terms of a polynomial function of a delay variable X. Thus, the generator polynomial that describes the shift register sequence may also be represented as

$$G = \sum_{i=1}^{N} d_i X^i \tag{23.2}$$

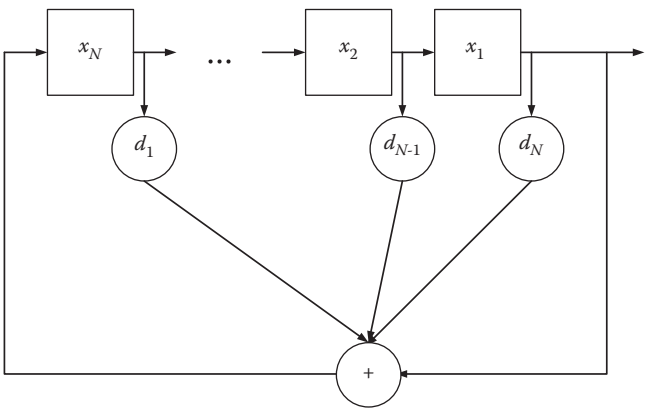

FIGURE 23.2 Shift register with feedback.

where X_i represents a delay of i clock pulses. This polynomial is also known as the *characteristic polynomial* of the shift register sequence. Pseudorandom sequences are also sometimes known as *pseudonoise* (PN) sequences.

An important property of PN sequences is that a time-shifted version of any PN sequence can be generated by forming a modulo-2 addition of the PN sequence with a delayed version of itself, that is, the "delay-and-add" property. The delay-and-add property of PN sequences implies that temporal shifting of the PN sequence can be formed with simple logic operations involving a shift register. This leads to the concept of a PN *mask*. A mask is a binary value with the same number of bits as there are delay elements in the shift register used to generate the PN sequence. The mask is AND'ed bitwise with the contents of each corresponding delay element, and a modulo-2 addition is performed on the results of these AND operations. The resulting sequence is a delayed version of the original PN sequence.

23.1.2.1 Orthogonal Sequences

Optimal PN sequences are limited in number for any given sequence length. In order to accommodate several different users simultaneously in a CDMA system, assigning each user a unique PN spreading code is not possible. Therefore, in order to increase the bandwidth efficiency in CDMA systems, different users are modulated using their own unique codes derived from orthogonal functions combined with PN spreading sequences.

A set of functions $\{f_n\}$ all of length N is mutually orthogonal if the following relationship holds:

$$\sum_{i=1}^{N} f_k(i) f_l(i) = \begin{cases} N, k = l \\ 0, k \neq l \end{cases} = N\delta_{k-l} \tag{23.3}$$

In Equation 23.3, δ_r is known as the *dirac-delta* operator. This operator is 1 when $r = 0$, or zero otherwise. If the summation in Equation 23.3 is simply δ_{k-l} rather than $N\delta_{k-l}$, then the functions are *orthonormal*.

Walsh functions are generally the preferred basis for orthogonal modulation. Walsh functions are derived from the rows of Walsh matrices (also known as Walsh–Hadamard matrices). These matrices are square matrices whose dimensions are 2^r by 2^r, where r is a nonnegative integer. Assume that the N by N Walsh matrix is denoted as $\mathbf{H}_N$. Then the first two Walsh matrices in the series $\{\mathbf{H}_1, \mathbf{H}_2, \mathbf{H}_4, \ldots\}$ are

$$\begin{aligned} \mathbf{H}_1 &= [1] \\ \mathbf{H}_2 &= \begin{bmatrix} 1 & 1 \\ 1 & -1 \end{bmatrix} \end{aligned} \tag{23.4}$$

In fact, each consecutive Walsh matrix in the series can be generated recursively from the previous Walsh matrix in the series, that is,

$$\mathbf{H}_{2N} = \begin{bmatrix} \mathbf{H}_N & \mathbf{H}_N \\ \mathbf{H}_N & -\mathbf{H}_N \end{bmatrix} \tag{23.5}$$

23.1.3 Spreading

Now that the concepts of PN sequences and orthogonal functions have been introduced, these areas may be used to develop the idea of spreading a signal. Recall that in any direct-sequence spread spectrum system, the objective is to transform narrowband information to a wideband signal for transmission. This is achieved by modulating the narrowband signal with a waveform with a higher bandwidth. For a

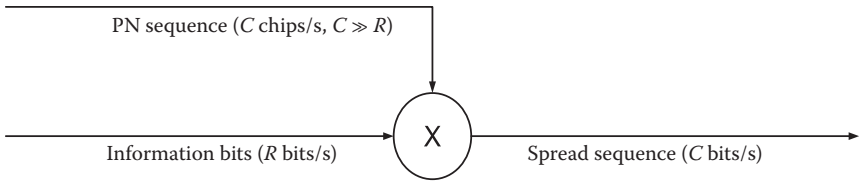

FIGURE 23.3 Spreading operation.

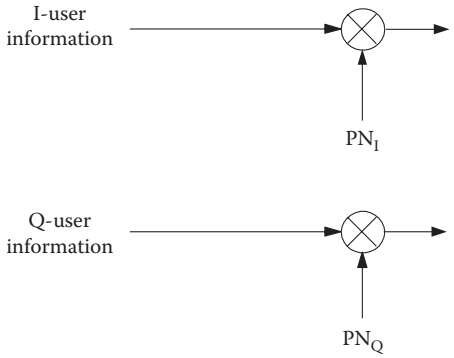

FIGURE 23.4 Quadrature spreading.

spreading sequence in a CDMA system, its bandwidth is a function of the duration of one of its spreading sequence samples. This duration is known as a *chip*.

Recall that PN sequence samples are generated according to a clock signal supplied to the associated shift register. This clock frequency is essentially the *chip rate* (also "chipping rate") of the spreading sequence. If the chipping rate is designated as C and the information bit rate is R, then C must be greater than R for bandwidth expansion to occur.

The basic spreading operation is depicted in Figure 23.3.

The multiplication operation in Figure 23.3 can also be accomplished through the use of an exclusive-NOR gate if the input signals are binary.

23.1.3.1 Quadrature Spreading

CDMA systems usually utilize two spreading sequences to modulate user information. User information in this case is usually split into two information streams, one corresponding to an "in-phase" or "I" component and one corresponding to a "quadrature" or "Q" component. If the two spreading sequences are denoted as PN_I and PN_Q, then the basic *quadrature spreading* operation is as depicted in Figure 23.4.

Another form of quadrature spreading is *hybrid* quadrature spreading, which involves representation of the two PN sequences and I and Q input signals as complex quantities and accomplishes spreading by modulating the input signal with the complex PN sequence. This operation is shown in Figure 23.5.

23.2 The IS-95 Cellular CDMA System [2]

CDMA, like its FDMA and TDMA counterparts, suffers from cochannel interference even with the use of spreading codes. This is due to the fact that several users may be simultaneously communicating with the base station. Each individual user can be seen as interference to every other user, making it difficult for mobile receivers to correctly demodulate a desired user's signal. The problem manifests itself in the *near–far* effect, wherein users far away from the base station could have their signals drowned out from users near the base station if those users are transmitting at unacceptably high power levels.

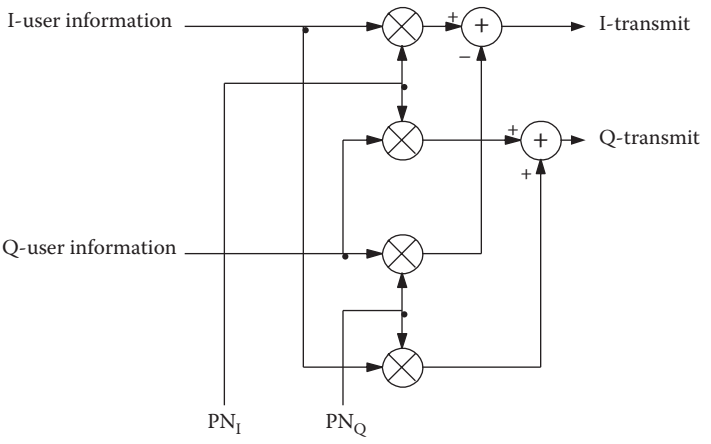

FIGURE 23.5 Hybrid quadrature spreading.

Power control was introduced primarily by the IS-95 standard as a means of combating the near–far effect. In a power-controlled CDMA system, the base station uses power control whereby it commands handsets to increase or decrease their individual radiated power levels depending on the detected levels of the individual users' signals at the base station. This is accomplished by a series of up/down single-bit commands to drive the mobile radiated power to a desired level.

In addition, as a mobile moves from one cell to another, a *handover* between cells must take place. In TDMA and FDMA systems, this is usually a *hard* handover, meaning that the connection between the mobile and base station in the serving cell must be discontinued before initiating communication with the base station in the cell to which the mobile is transitioning (sometimes referred to as *make before break*). Hard handovers sometimes result in communications gaps and even dropped calls. IS-95 however was the first commercialized system to introduce *soft* handover, which involves a mobile station simultaneously communicating with multiple base stations as long as each individual base station's signal was received at an acceptable level.

The IS-95 system is designed to work in a 1.25 MHz bandwidth. The IS-95 system achieved channelization in the forward link (base station to mobile) and reverse link (mobile to base station) using different means. Channelization in the forward link was accomplished through the use of orthogonal Walsh codes, while channelization in the reverse link was achieved using temporal offsets of the spreading sequence.

Different base stations are identified on the downlink based on unique time offsets utilized in the spreading process. Therefore, all base stations must be tightly coupled to a common time reference. In practice, this is accomplished through the use of the *global positioning system* (GPS) satellite broadcast system.

There are two types of PN spreading sequences used in IS-95: the *long* code and the *short* codes. Both the PN sequences are clocked at 1.2288 MHz, which is the chipping rate. Two short code PN sequences are used since IS-95 employs quadrature spreading. These two codes are the in-phase sequence $P_I(x) = x^{15} + x^{13} + x^9 + x^8 + x^7 + x^5 + 1$ and the quadrature sequence $P_Q(x) = x^{15} + x^{12} + x^{11} + x^{10} + x^6 + x^5 + x^4 + x^3 + 1$. These two sequences are generated by length-15 shift register sequences; although they are nominally $2^{15} - 1 = 32767$ chips, a binary "0" is inserted in each sequence after a string of 14 consecutive 0's appears in either sequence to make the final length of the spreading sequence an even 32768 chips.

The long code is given by the polynomial $p(x) = x^{42} + x^{35} + x^{33} + x^{31} + x^{27} + x^{26} + x^{25} + x^{22} + x^{21} + x^{19} + x^{18} + x^{17} + x^{16} + x^{10} + x^7 + x^6 + x^5 + x^3 + x^2 + x^1 + 1$. It is of length $2^{42} - 1$ chips as it is generated by a 42-length shift register. It is primarily used for privacy, as each user of the mobile network may be assigned a unique temporal offset for the long code with reference to system time. The offset is accomplished with the use of a 42-bit long code mask.

23.2.1 IS-95 Forward Link

Channelization by means of code multiplexing is a fundamental feature of IS-95 systems. In particular, channelization is accomplished using length-64 Walsh codes, which are assigned to different channels. The types of channels used can be grouped into *common* channels and *dedicated* channels. Common channels are *broadcast* to all the users in the cell served by the base station. Dedicated channels are meant to be heard by only one user.

23.2.1.1 Common Channels

The three types of common channels used in IS-95 are the Pilot, Sync, and Paging channels. Each has a unique Walsh code associated with it, and serves a particular purpose in the IS-95 forward link.

23.2.1.1.1 Pilot Channel

The mobile uses the pilot channel for the following purposes:

1. Multipath channel amplitude estimation for coherent detection.
2. Timing recovery for synchronization to network time reference (GPS-based).
3. Frequency offset correction for the mobile receiver.
4. Pilot strength measurements for soft and hard handoff decisions.

There are also several other possible uses for the pilot at the mobile receiver, such as interference correction and interfrequency handoff measurements. The pilot channel must be a known sequence to be useful at the mobile station. In this case, the pilot channel is simply all-binary 0's.

The pilot channel undergoes orthogonal modulation with Walsh code 0, which is the first row of the Walsh-64 matrix and is the all binary-0's code. The amount of power dedicated to the pilot channel is directly related to the base station coverage area, as all mobiles must successfully decode the pilot channel to communicate with the base station.

23.2.1.1.2 Sync Channel (FSYN)

The sync channel is primarily used by the mobile to acquire a timing reference. The mobile station, when it acquires the pilot channel, knows the PN timing of that particular base station. However, the mobile does not know how the timing of this base station relates to other base stations in the network. The Sync Channel Message appears on the sync channel to let the mobile know timing parameters such as the PN timing offset of the base station relative to system time. The bit rate of this message is 1.2 kbps. The Sync Channel also has its own unique Walsh code.

23.2.1.1.3 Paging Channel (FPCH)

Up to 7 paging channels, each with their own unique Walsh code, may be used by the IS-95 base station. This channel provides system parameters, voice pages, short message services, and any other broadcast messaging to users in the cell. The paging channel can take two bit rates, 4800 or 9600 bps. The rate is given in the Sync Channel Message.

23.2.1.2 Dedicated Channels

Dedicated channels deliver user traffic and user-specific signaling. There are two types of dedicated channels that are used in IS-95: the forward fundamental channel and the forward supplemental code channel. The forward fundamental channel was simply called the forward traffic channel in IS-95-A, as it was the only channel capable of delivering dedicated traffic. In IS-95-B, the forward supplemental code channel was introduced as a means of improving data rates to individual users. Voice always goes over a fundamental channel and can never go over a supplemental code channel. However, data may travel over both types of channels.

The fundamental channel is variable rate. This is to take advantage of periods of time where the voice activity is low and therefore the voice codec (i.e., *co*der/*dec*oder) rate may be reduced. In IS-95 systems, voice codecs generally take four rates, sometimes denoted as full rate, half-rate, quarter-rate, and eight-rate. The first IS-95 systems used source rates of 9.6, 4.8, 2.4, and 1.2 kbps; this set of data rates is known as *Rate Set 1*. These data rates were necessary for the first 8 kbps IS-95 vocoder (i.e., *vo*ice en*coder*), known as QCELP8. *Rate Set 2* (14.4, 7.2, 3.6, 1.8 kbps) was introduced to accommodate a 13 kbps vocoder known as QCELP13. The supplemental code channel is not variable-rate, yet can take either 9.6 or 14.4 kbps forms. This channel is primarily used for providing higher data rates to individual users through the use of *code channel aggregation*.

23.2.2 IS-95 Reverse Link

The IS-95 reverse link channels may also be grouped into common and dedicated channels. The common channels in the IS-95 reverse link are meant primarily for tasks such as call origination, registration and authentication, page responses, and delivery of short messages. Channelization of users in the reverse link is accomplished by the use of long code masks. Since the mobile must acquire a time reference from the network, each mobile can utilize a unique long code mask. Therefore the mobile transmits with a unique long code mask known only to the base station.

23.2.2.1 Common Channels: Reverse Access Channel

The reverse access channel (R-ACH) is the reverse link common channel in IS-95. The R-ACH messaging is at 4.8 kbps. It is convolutionally encoded, repeated, and interleaved over 576 symbols. Note that the next step is *64-ary orthogonal modulation*. This step entails grouping each set of six consecutive bits output from the interleaver into a row address to a memory that contains the 64 by 64 Walsh matrix. Once a row is selected, all 64 bits that make up the row entry are output at a rate of 307.2 kHz. Since the mobile is not transmitting a pilot signal on the reverse link (unlike the forward link), coherent detection is not possible. As a result, the base station receiver may correlate the received signal with all of the 64 possible Walsh codes and determine a peak correlation to determine which row was sent. After orthogonal modulation, the sequence is spread to 1.2288 MHz by the long code; the long code generator state should be synchronized with the base station long code generator based on the information the mobile has received from the sync channel.

The signal may now be quadrature spread; however, note that there is a 1/2-chip delay in the Q-branch of the quadrature spreader. This results in *offset-QPSK* modulation. Offset-QPSK modulation reduces the *peak-to-average ratio* (PAR) in the signal the mobile must transmit.

23.2.3 CDMA2000 [3–6]

cdma2000 came about as a response to the ITU's IMT-2000 effort for developing global third-generation wireless services. cdma2000 is backward compatible, which ensures that second-generation products could be easily evolved to meet third-generation requirements.

23.2.3.1 Spreading and Modulation Solutions

A complex spreading as shown in Figure 23.6, helps to reduce the peak-to-average power and thus improves power efficiency.

23.2.3.2 Coherent Detection in the Reverse Link

Coherent detection can improve the performance of the reverse link up to 3 dB compared to noncoherent reception used by the second-generation CDMA system. To facilitate coherent detection a pilot signal is required. The actual performance improvement depends on the proportion of the pilot signal power to the data signal power and the fading environment.

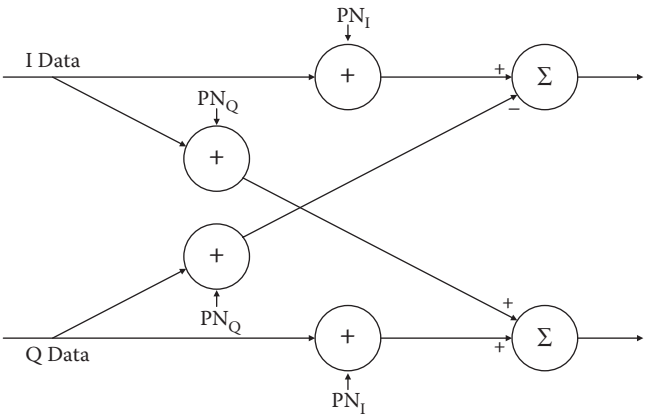

FIGURE 23.6 Complex spreading.

23.2.3.3 Fast Power Control in Forward Link

To improve the forward link performance fast power control is used. The impact of the fast power control in the forward link is twofold. First, it improves the performance in a fading multipath channel. Second, it increases the multiuser interference variance within the cell since orthogonality between users is not perfect due to multipath channel. The net effect, however, is improved performance at low speeds.

23.2.3.4 Soft Handoff

Soft handoff was to remain essentially the same in operation as in IS-95. This was possible due to the fact that cdma2000 is backward compatible, and therefore existing cells did not need to be redeployed. As a result, handoff mechanisms did not need to change either.

23.2.3.5 Transmit Diversity

The forward link performance can be improved in many cases by using transmit diversity. For direct spread CDMA schemes, this can be performed by splitting the data stream and spreading the two streams using orthogonal sequences or switching the entire data stream between two antennas. For multicarrier CDMA, the different carriers can be mapped into different antennas.

23.3 CDMA2000 Physical Layer

The cdma2000 physical layer retains backward compatibility not only to leverage IS-95 equipment development but to also provide a smooth upgrade path for cellular operators. The cdma2000 physical layer classifies different modes of operation into *radio configurations* (RCs) for both the forward and reverse links. For instance, RCs 1 and 2 (RC1 and RC2) are the Rate Set 1 and Rate Set 2 modes of operation respectively in IS-95. However, RCs greater than two define new modes of operation in cdma2000.

In addition, the cdma2000 RCs encompass two modes of operation: 1X and 3X. 1X refers to the mode that is bandwidth-compatible with IS-95, that is, its bandwidth is 1.25 MHz. 3X refers to the *multicarrier* option, which involves the use of 3 1X carriers to increase the data rate to the mobile user on the forward link. The data rates on the reverse link in the multicarrier version increase data rates via direct-spreading up to three times the 1X chip rate of 1.2288 MHz. More recently, modes that involve 3X forward link and 1X reverse link have been adopted to allow for asymmetric high-speed data services. As the 1X option has turned out to be the almost exclusive choice for deployment, this will be the focus for the ensuing subsections.

23.3.1 Forward Link

In the cdma2000, several new code channels are introduced to improve data services. To ensure backward compatibility, the cdma2000 forward link includes pilot, paging, and sync channels which are identical in operation to their IS-95 counterparts. The dedicated channels for RC3 and higher have a different structure.

The basic spreading structure now involves hybrid quadrature spreading with the same baseband filter as in IS-95. This is depicted in Figure 23.7.

The spreading function takes as inputs the appropriate Walsh function, and in-phase and quadrature inputs Y_I and Y_Q respectively. These inputs are derived from a demultiplexing operation (see Figure 23.8). With reference to Figure 23.8, when the input is X, then the output is split into the two streams Y_I and Y_Q by mapping each bit in the input stream to one of the two output streams alternately (starting from Y_I, i.e. a "top-to-bottom" approach). This is a pure QPSK system, as two bits of information are transmitted for each (I,Q) pair of inputs. However, two inputs X_I and X_Q may be mapped directly to Y_I and Y_Q as well. This feature is useful for backward-compatible channels, as will be seen in the next section.

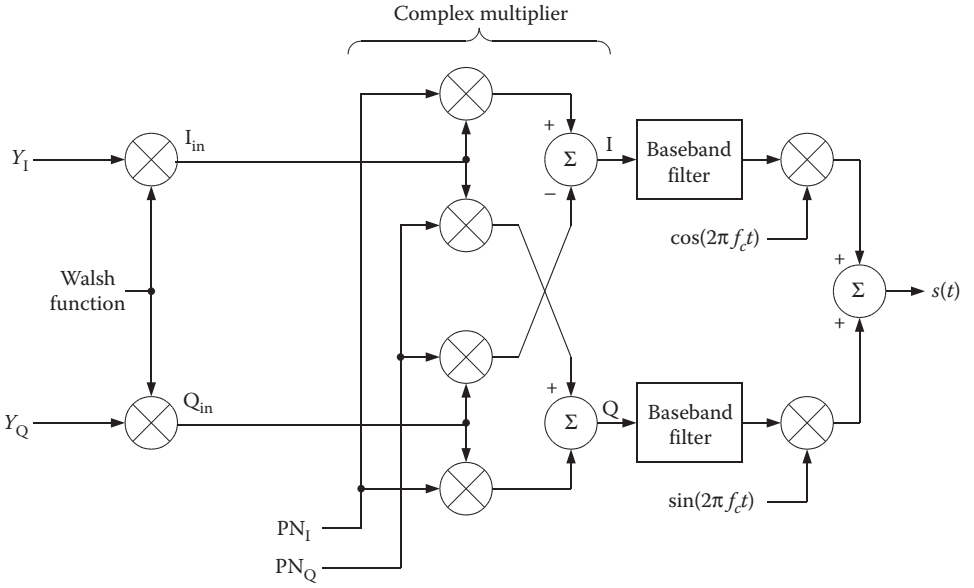

FIGURE 23.7 cdma2000 spreading.

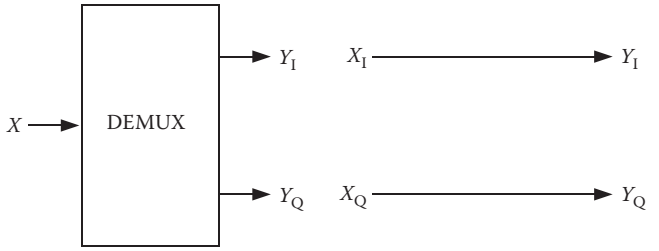

FIGURE 23.8 Demultiplexing operation for 1X.

23.3.1.1 New cdma2000 1X Common Channels

Several new common channels were introduced for cdma2000. The forward common control channel (FCCCH) and forward broadcast control channel (FBCCH) may be used for carrying common signaling much like the paging channel. These channels may be used specifically for cdma2000 mobiles, thus relieving some of the overhead on the paging channel.

The forward quick paging channel (FQPCH) is an on–off keyed (OOK) indicator to the mobile to wake up for a message on the paging channel. This is useful for conserving battery life in the mobile when it is idling.

In addition, for new access modes on the reverse link, a forward common power control channel (FCPCH) exists in which users' power control bits may be slotted in time.

23.3.1.2 New cdma2000 1X Dedicated Channels

cdma2000 1X introduces the forward dedicated common control channel (FDCCH) and forward supplemental channel (FSCH). The FDCCH may be used primarily for signaling and can be used for other high priority (nonvoice) traffic such as retransmissions for data protocols. The FSCH is strictly for data traffic, and can take much higher rates than an IS-95 compatible forward supplemental code channel. The forward fundamental channel (FFCH) is still primarily for voice, although the lowest data rates for Rate Set 1-compatible data rates changed slightly from 1.2 and 2.4 to 1.5 and 2.7 kbps respectively.

RC3 and RC4 in general are Rate Set 1-compatible, while RC5 is Rate Set 2-compatible. Note two notable exceptions regarding framing; now the dedicated channels can carry 5 ms frames for short messages, and the FFCH and FSCH can have longer framing (40 and 80 ms) in addition to 20 ms.

23.3.1.3 Transmit Diversity

A new feature in cdma2000 that was not present in IS-95 was the capability to transmit over two antennas in the forward link, also known as *transmit diversity*. All channels except for pilot channels, forward paging channel (FPCH) and forward sync channel (FSYN) may be transmitted in this fashion.

23.3.2 Reverse Link

The reverse link in cdma2000 was designed to introduce two important concepts that were not available in IS-95, namely coherent reverse link detection and fast forward link power control. As a result, a new physical layer was necessary for cdma2000. The basic spreading structure is depicted in Figure 23.9. Note certain aspects of this spreading method which differ from the IS-95 reverse link:

- Inclusion of a pilot channel for coherent demodulation.
- Use of Walsh code multiplexing for transmission of multiple data channels.
- Long code spreading is slightly different so as to reduce peak-to-average ratio.
- Use of hybrid quadrature spreading rather than offset-QPSK spreading.

Several new code channels exist and will be discussed in the ensuing subsections. Each code channel will result in a modulation symbol indexed by A, B, or C. These indices are with respect to the complex spreading inputs in Figure 23.9.

The main backward-compatible feature that exists in the cdma2000 reverse link for common channels is the R-ACH.

23.3.2.1 New cdma2000 1X Common Channels

The reverse common control channel (RCCCH) and reverse enhanced access channel (REACH) were introduced to provide more reliable access by means of slotting different users before they transmit bursts on the reverse link and to provide a coherence form of reception for the base station access probe receiver. In addition, some burst data service that was not possible over the IS-95 access channel could be accommodated using these features.

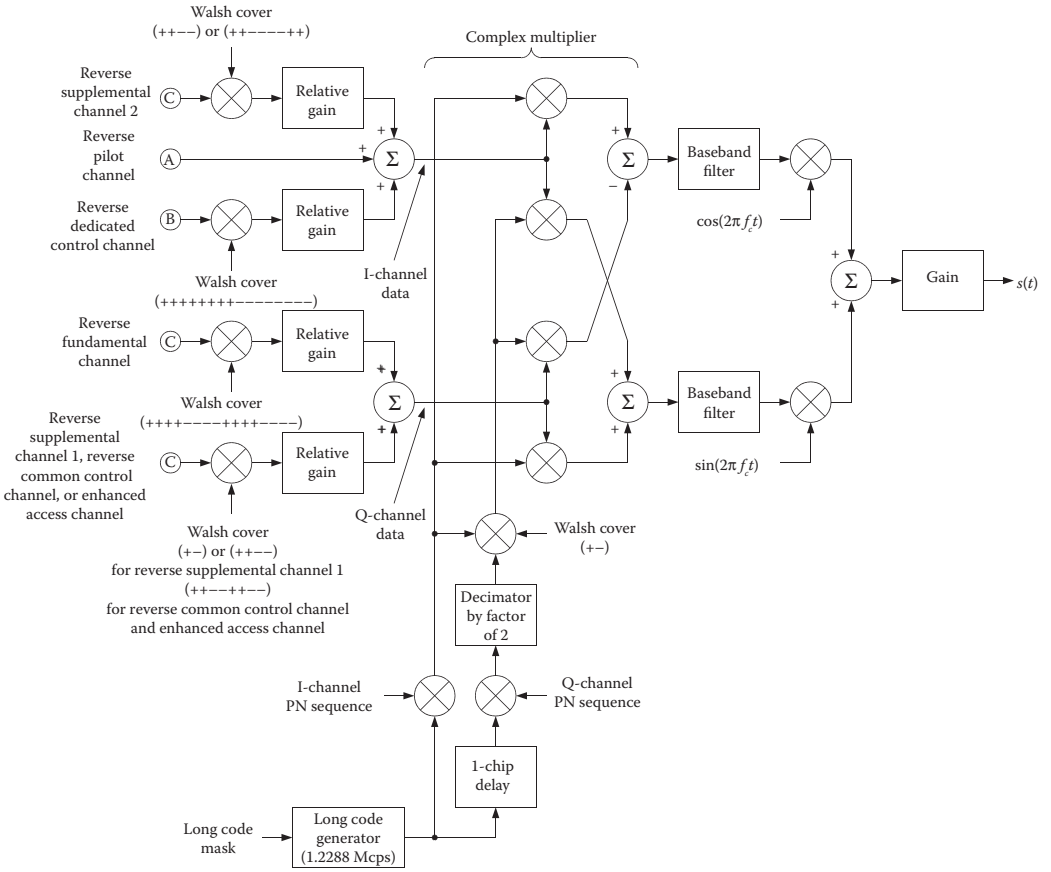

FIGURE 23.9 Reverse link spreading.

23.3.2.2 New cdma2000 1X Dedicated Channels

Several new dedicated control channels exist for the cdma2000 reverse link. Among them are the reverse pilot channel (RPICH), the reverse fundamental channel (RFCH), the reverse supplemental channel (RSCH), and the reverse dedicated common control channel (RDCCH). Except for the RPICH, the types of data associated with each channel are identical to their forward link counterparts. The RPICH has power control commands for fast forward power control multiplexed into the constant stream of all 0's at an 800 Hz rate. Just as with the forward link dedicated channels, the other three reverse link dedicated channels are associated with RCs. In general RC3 corresponds to Rate Set 1-compatible data rates, while RC4 corresponds to Rate Set 2-compatible data rates.

23.4 1X-EV-DO [7,8]

The 1X-EV-DO standard proposed leveraged cdma2000 1X to provide an enhancement of data services over a dedicated 1.25 MHz carrier on the forward link. The name "1X-EV-DO" is in fact a shortened version of 1X Evolution for Data Only. The first version ("Release 0") of the reverse link retains much of the elements of the cdma2000 reverse link, with additional features to provide enhancements for data services on the forward link as well.

One of the main features in 1X-EV systems is the use of *link adaptation*. This is a feature whereby individual users are assigned different physical layer attributes depending on the wireless conditions

each user experiences. For instance, a user near the base station may be assigned a higher data rate than a user further away from the base station. The data rates on the forward link are adjusted by a mechanism known as *adaptive modulation and coding* (AMC). AMC involves the use of different bandwidth-efficient modulation methods (e.g., QPSK, QAM) along with changing the forward error correcting (FEC) code rate. Based on the user's forward link channel quality, there exists a modulation and coding scheme (MCS) that maximizes throughput to the user. This principle can also be applied to the reverse link, which is one of the main features of the Release A version of 1X-EV-DO.

In 1X-EV-DO, the user sends active feedback to the base station to select the best MCS based on wireless channel conditions. The user can select lower data throughput MCS's when channel conditions are poor and higher-throughput MCS's when channel quality conditions improve. Since data services (unlike voice) are bursty, 1X-EV-DO time-multiplexes users over a shared forward link channel. This utilizes radio resources effectively, as the forward link channels are not wasted on users who are not receiving data at the moment. Therefore additional signaling is needed to schedule users on the forward link. In addition, it is very difficult to co-ordinate base stations on the forward link for a true soft handoff scenario. This is because different base stations may have different users, and the times over which they schedule an individual user may differ. As a result, in 1X-EV-DO systems mobile user can only receive data from one base station at a time.

The reverse link has to include new control information to provide data requests for the forward link, signal to the base station a new rate to be used on the reverse link, and provide indications to the network which base station is the best base station to serve the user (since only one base station can deliver traffic to the user).

In addition, a fast automatic repeat reQuest (ARQ) method is implemented in 1X-EV-DO. ARQ involves the redelivery of a frame of information when the previous attempt at transmission has failed. The transmitter knows that the attempt has failed based upon the failure to receive an ACK (acknowledgment) indication from the receiver.

23.4.1 Forward Link

The forward link is one shared pipe over which all users may receive information. Forward link channels are all time-multiplexed, meaning that forward link power control is not applicable—the entire base station transmitter power is allocated to the channel being transmitted at any particular moment in time. The forward link spreading and channelization are depicted in Figure 23.10.

Note the presence of different channels all being time multiplexed over the same modulation sequence. The time multiplexing is based on units of time called *slots*, where a slot is 1.67 ms (slots occur at a 600 Hz rate). The time multiplexing sequence is given in Figure 23.11.

The 1X-EV-DO forward link still takes advantage of the short codes of IS-95/cdma2000 and uses PN offsets to distinguish between different base stations. In addition, the baseband filtering is identical to IS-95/cdma2000.

23.4.1.1 Pilot Channel

The pilot channel serves the same function as the IS-95/cdma2000 pilot channel, except it is time multiplexed and occurs twice per slot. The total number of chips the pilot channel is spread over is 182, based on 96 chips per half-slot.

23.4.1.2 MAC Channel

The MAC channel in 1X-EV-DO provides for scheduling different users onto the forward link and also providing information to the different users about reverse link capabilities of the system. Length-64 Walsh codes are used to transmit different types of information to different users.

In addition to global control information, the MAC channel also indicated reverse activity (RA) to all users and reverse power control (RPC) commands to individual users. RPC information must constantly

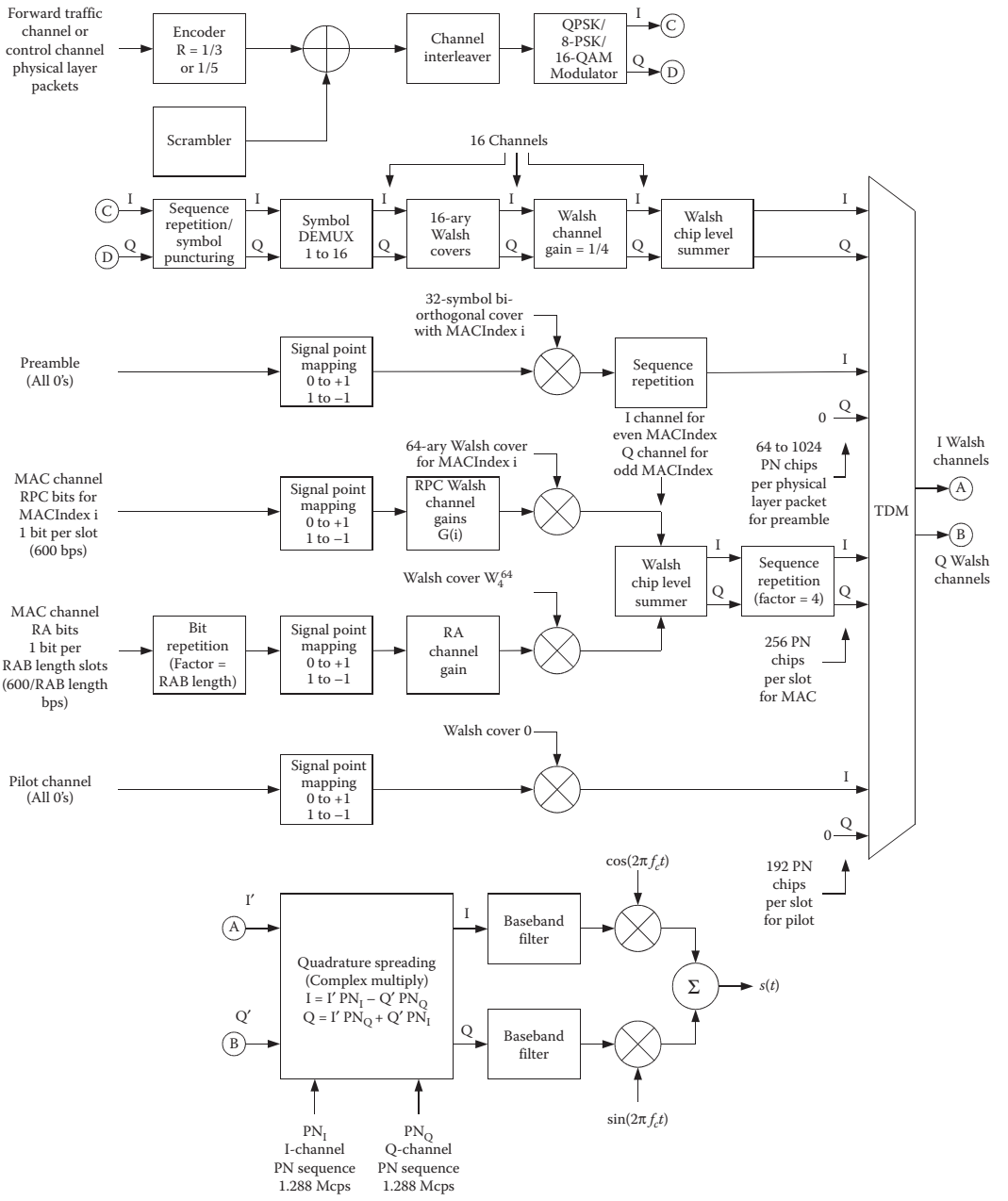

FIGURE 23.10 1X-EV-DO forward link spreading.

be transmitted to users who are actively transmitting data. RA bit (RAB) is more of a broadcast indication to users that their data rates should be reduced (due to unacceptably high load levels on the reverse link) or may be increased.

23.4.1.3 Traffic Channel Preamble

The preamble is important in that it indicates to the mobile what sort of MCS it will be receiving for the ensuing traffic bits. The preamble uses *biorthogonal* modulation. A biorthogonal signal set with M sig-

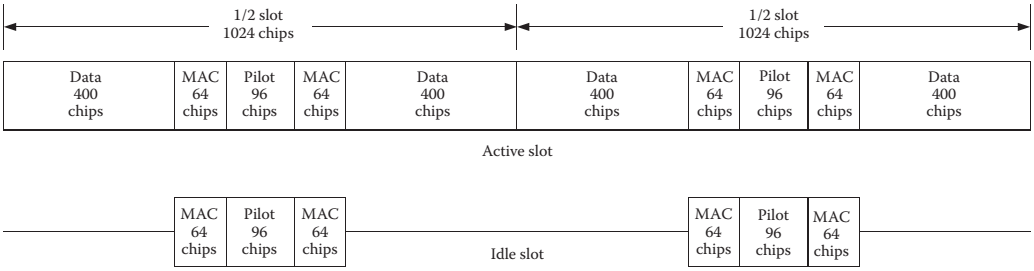

FIGURE 23.11 1X-EV-DO forward link time multiplexing structure.

nals can be constructed from an orthogonal signal set of $M/2$ signals by simply concatenating the negation of those $M/2$ signals. In the case of the 1X-EV-DO preamble, $M = 32$, that is, the Walsh codes of length 32 are used for biorthogonal modulation. Each of the 32-chip codes may be assigned to an individual user or to a control channel for broadcast use.

Based on a predefined repetition sequence for the Walsh code assigned to an individual user, that user may discern the traffic channel data rate assignment.

23.4.1.4 Traffic Channel

The MCS's along with their associated number of slots and total time-multiplexed chips for is given in Table 23.1.

23.4.2 Reverse Link

The 1X-EV-DO reverse link, in addition to providing sufficient feedback for control of the forward link (particularly link adaptation), also provides different reverse traffic data rates.

The 1X-EV-DO reverse link has one common channel, the access channel. The dedicated channel is the reverse traffic channel, which collectively includes the pilot, reverse rate indication (RRI), data rate control (DRC), acknowledgment (ACK), and data channels.

TABLE 23.1 MCS and Slot Assignments

	Number of Values per Physical Layer Packet				
Data Rate (kbps)	Slots	Bits	Code Rate	Modulation Type	Total Chips (Preamble, Pilot, MAC, Data)
38.4	16	1024	1/5	QPSK	1024, 3072, 4096, 24,576
76.8	8	1024	1/5	QPSK	512, 1536, 2048, 12,288
153.6	4	1024	1/5	QPSK	256, 768, 1024, 6144
307.2	2	1024	1/5	QPSK	128, 384, 512, 3072
614.4	1	1024	1/3	QPSK	64, 192, 256, 1536
307.2	4	2048	1/3	QPSK	128, 768, 1024, 6272
614.4	2	2048	1/3	QPSK	64, 384, 512, 3136
1228.8	1	2048	1/3	QPSK	64, 192, 256, 1536
921.6	2	3072	1/3	8-PSK	64, 384, 512, 3136
1843.2	1	3072	1/3	8-PSK	64, 192, 256, 1536
1228.8	2	4096	1/3	16-QAM	64, 384, 512, 3136
2457.6	1	4096	1/3	16-QAM	64, 192, 256, 1536

23.4.3 1X-EV-DO Revisions A and B

The next version of the 1X-EV-DO standard, Revision A, introduced enhancements that allowed for (23.1) the increase of the maximum forward link instantaneous data rate to 3.1 Mbps, (23.2) the increase of reverse link maximum data rates through the use of AMC (up to 1.8 Mbps), and (23.3) multiplexing efficiencies on the forward link through the use of multiuser packets. The ensuing standard version, Revision B, achieved increases in throughput by allowing for the grouping of DO carriers (groups of 2 or 3), therein increasing the maximum data rates provided to any single user.

23.5 Wideband CDMA

23.5.1 Standardization History

In January 1998, the European Telecommunications Standards Institute (ETSI) selected wideband CDMA (WCDMA) as its Universal Mobile Telephony System (UMTS) radio technology. During that same year, ETSI and ARIB (the Japanese counterpart of ETSI) agreed to make a common UMTS standard under the Third Generation Partnership Project (3GPP). The 3GPP has as part of its mission to provide a complete set of specifications defining the 3G-network functionality, procedures, and service aspects.

The first release of the WCDMA standard, Release 99 (3GPP R99), focuses on the backward compatibility and inter-operability with GSM networks. The second release, 3GPP R00, includes two parts (3GPP Release 4 and Release 5). Release 4 contains minor modification to Release 99, and the changes in the UMTS core network circuit-switched data flows and control mechanisms. Release 5 contains items such as high-speed downlink packet access (HSDPA), radio resource management (RRM), uplink synchronous transmission, and IP based transport.

The 3GPP has defined two variants of WCDMA: frequency-division duplex (FDD) and time-division duplex (TDD). FDD uses two different radio frequencies separately for uplink and downlink transmissions [9]. A pair of 60 MHz frequency bands is allocated for uplink and downlink spectrum (paired bands). For TDD mode, uplink and downlink transmissions use the same radio frequency with synchronized time intervals. Two frequency bands of 20 and 15 MHz are allocated for TDD operation (unpaired bands).

23.5.2 WCDMA Parameters and Features

Compared to IS-95/cdma2000's 1.25 MHz carrier bandwidth (1.2288 Mcps spreading rate), WCDMA uses a 5 MHz bandwidth per carrier (3.84 Mcps spreading). Note that the TDD mode also allows 1.28 Mcps spreading as an option. WCDMA uses a 10 ms radio frame, and is subdivided into 15 time slots (0.667 ms per slot). For 3.84 Mcps rate, there are 38,400 chips per frame and 2560 chips per slot.

23.6 WCDMA Channelization [10–14]

23.6.1 Radio Interface Architecture

Like cdma2000, WCDMA is defined with respect to protocol layering. For the over-the-air (radio) interface between the base station (denoted as Node B) and the mobile station (denoted as user equipment, or UE), a three-layer protocol is implemented. These layers are the network layer (Layer 3, or L3), the data link layer (Layer 2, or L2), and the physical layer (Layer 1, or L1).

Layer 3 provides the signaling necessary for radio resource management (RRM) and radio resource control (RRC), mobility management (MM), connection management (CM), and logical link control (LLC). It is divided into the control plane (C-plane) and the user plane (U-plane). The control plane carriers the signaling bearers. The user plane offers frame protocol (FP) for user data transfer through the interface and the underlying transport protocols. Layer 2 provides services and functionality such as medium access control (MAC), radio link control (RLC), packet data convergence protocol (PDCP), and

broadcast/multicast control (BMC). (Note that PDCP and BMC only exist in the U-plane. Layer 1 transports information to and from the MAC and higher layers.

23.6.1.1 Logical, Transport, and Physical Channels

WCDMA system uses also a three-layer channel structure to carry control information and user data between Layer 2 and Layer 1. These three types of channels are logical channels, transport channels, and physical channels. In the following subsections, the functionality and relationship between these different channels will be described. The logical channels provide data transfer service from the MAC layer, and they are categorized into two groups: control channels and traffic channels (see Figure 23.12).

23.6.1.1.1 Control Channels (CCh's)

- *Broadcast control channel (BCCH):* A downlink channel for broadcasting system control information.
- *Paging control channel (PCCH):* A downlink channel used for transferring paging information.
- *Common control channel (CCCH):* Bidirectional channel for transmitting control information between the network and UE's.
- *Dedicated control channel (DCCH):* A point-to-point bidirectional channel that transmits dedicated control information between a single UE and the network.

23.6.1.1.2 Traffic Channels (TrCh's)

- *Dedicated traffic channel (DTCH):* A point-to-point channel that dedicated to one UE service for user information transfer.
- *Common traffic channel (CTCH):* A point-to-multipoint downlink channel to transmit dedicated user information for all or a group of specified UE's.

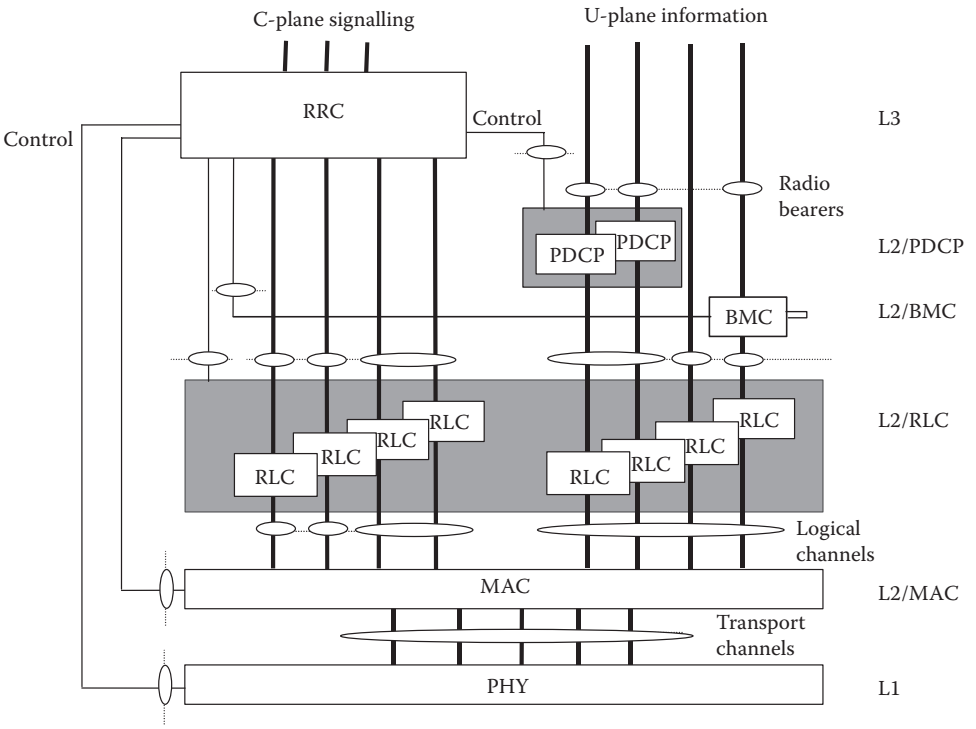

FIGURE 23.12 WCDMA radio interface protocol model.

23.6.1.2 Transport Channels

Transport channels (TrCh's) are responsible for mapping L2 information to L1. All transport channels are unidirectional. Transport channels are classified dedicated or common. The dedicated transport channel is known as the dedicated channel (DCH). It is transmitted over the entire cell and carries all the information intended for the given user from the higher layers, which includes data and signaling. DCH's are assigned to individual users. In contrast, common transport channels are shared among users within the coverage area of a single base station. There are several types of common transport channels:

- *Broadcast channel (BCH):* A downlink channel that carries system and cell specific information, and is transmitted over the entire cell.
- *Forward access channel (FACH):* A downlink channel carries control information to UE's. The FACH can be transmitted over the entire cell or part of a cell.
- *Paging channel (PCH):* A downlink transport channel that is always transmitted over the entire cell. The PCH carries the information relevant to the paging procedure.
- *Random access channel (RACH):* An uplink channel that carries control information from the terminal, such as RRC connection setup request. The RACH is not collision-free, and is received from the entire cell.
- *Common packet channel (CPCH):* An uplink packet-based transport channel. CPCH is associated with a dedicated channel on the downlink that provides power control and CPCH control commands for the uplink CPCH.
- *Downlink shared channel (DSCH):* A downlink channel shared by several UE's. The DSCH carries dedicated user data and/or control information, and is associated with one or several downlink DCH's.

23.6.1.3 Physical Channels

Physical channels are specified by the carrier frequency, codes (channelization code and scrambling code), and phase (0 or $\pi/2$ for uplink). As with transport channels, both uplink and downlink physical channels can be classified as dedicated and common channels.

23.6.1.3.1 Uplink Physical Channels

23.6.1.3.1.1 Dedicated Uplink Physical Channels There are two types of dedicated uplink physical channels:

- *Dedicated physical data channel (DPDCH):* This channel carries the user data and higher layer signaling from the DCH transport channel, and its bit rate can be changed frame-to-frame (i.e., every 10 ms). The spreading factor for the DPDCH ranges from 4 to 256.
- *Dedicated Physical Control Channel (DPCCH):* The DPCCH channel contains control information such as the pilot bits, feedback information (FBI), transmit power control (TPC), and an optional transport format combination indicator (TFCI). In order to maintain accurate channel estimation, for higher data rates the DPCCH transmit power level needs to be relatively higher than that of the lower bit rates. The spreading factor for the DPCCH is always 256 (15 ksps channel symbol rate). The constant bit rate is to ensure reliable detection.

The DPDCH and DPCCH are I/Q multiplexed within each radio frame with complex scrambling.

23.6.1.3.1.2 Common Uplink Physical Channels

- *Physical random access channel (PRACH):* The PRACH carries the RACH information from the transport channel. The UE can start transmission at certain predefined time offsets (access slots). The spreading factor for the data segment ranges from 256 (15 ksps) to 32 (120 ksps). The spreading factor for the control segment is always 256.

- *Physical common packet channel (PCPCH):* The PCPCH carries the transport channel CPCH information. The UE starts transmitting at a defined slot timing that is identical to the RACH. The PCPCH access transmission includes one or several access preambles over 4096 chips, one collision detection preamble, one DPCCH power control preamble, and an ensuing message.

23.6.1.3.2 Downlink Physical Channels

23.6.1.3.2.1 Dedicated Downlink Physical Channels The Layer 2 DCH information is carried by the downlink dedicated physical channels (downlink DPCH's). Similar to the uplink dedicated channel, the downlink DPCH consists of two types of channels—DPDCH and DPCCH. Downlink DPCH's are time multiplexed with Layer 1 related control information (such as pilot bits, UL TPC, and optional TFCI). The DPCH spreading factor can be 512 (7.5 ksps), 256 (15 ksps), down to 4 (960 ksps). The downlink DPCH bit rate can change frame by frame, and lower data rate transmission can be handled by discontinuous transmission (DTX).

23.6.1.3.2.2 Common Downlink Physical Channels

- Common pilot channel (CPICH)

The CPICH is a continuously transmitted pilot channel for downlink channel estimation and for UE intra-frequency measurement of neighboring cells for the soft handovers. Similar to the pilot channels in cdma2000 and 1X-EV-DO, the CPICH typically requires a significant percentage of the total base station transmitted power. The CPICH uses a predefined bit/symbol sequence, transmitted at 15 ksps (30 kbps) with a spreading factor 256. This physical channel can be further divided into two types:

- *Primary common pilot channel (P-CPICH):* The P-CPICH always uses the same channelization code and is scrambled by the primary scrambling code. There is only one P-CPICH per cell
- *Secondary common pilot channel (S-CPICH):* The S-CPICH can use an arbitrary channelization code with a spreading factor equal to 256, and is scrambled by either the primary or a secondary scrambling code. When the S-CPICH is scrambled by secondary scrambling code, it can be used for beam steering in adaptive antenna applications so as to increase system capacity.
- Primary common control physical channel (P-CCPCH).

The P-CCPCH carries the BCH transport channel system and cell information, and is broadcast over the whole cell. It uses a fixed channelization code. For each 2560-chip slot, the first 256 chips are not transmitted in P-CCPCH. This interval is reserved for the primary synchronization channel (SCH) or secondary SCH transmission.

- Secondary common control physical channel (S-CCPCH).

The S-CCPCH carries the FACH and PCH from the transport channel, and these channels can be mapped to the same S-CCPCH or to separate S-CCPCH's. The spreading factor can be 256 down to 4 (15 to 960 ksps). The S-CCPCH is transmitted only if there is data available. It also supports variable rates when the TFCI bits are included.

- Synchronization channel (SCH)

The synchronization channel is used for cell search and slot/frame synchronization. Since the UE's need the SCH information to locate the cell and synchronize before the decoding process, the SCH does not go through the spreading and scrambling process.

The synchronization channel consists of two subchannels—the primary SCH and the secondary SCH.

- *Primary SCH:* It is a 256-chip length code and is transmitted at the beginning of every slot For the UE to be able to lock on to the strongest SCH among different base stations to obtain slot synchronization, the same primary SCH code is used for every cell in the system.

- *Secondary SCH:* The secondary SCH repeatedly transmits a length-15 sequence of codes with 256 chips per code. Similar to the primary SCH, each 256-chip code is transmitted at the beginning of every slot. The sequence of the Secondary SCH allows downlink frame synchronization, and indicates which of the code groups the cell downlink scrambling code belongs.
- *Acquisition indictor channel (AICH):* The AICH carries the Layer 1 acknowledgment information corresponding to the PRACH preambles. It is broadcast over the entire cell. When the UE receives the AI acknowledgment, it will start transmitting the PRACH. The AICH uses a fixed rate (256 spreading factor) and consists of a repeated sequence of 15 consecutive access slots (AS). There are 5120 chips per AS, therefore, the duration of an AICH is 20 ms.
- *Paging indictor channel (PICH):* The paging indicator channel (PICH) is a downlink common channel, which carries the paging indicator for the UE's. The paging channel uses a fixed-rate spreading factor (SF = 256). Therefore one 10 ms PICH radio frame consists of 300 bits. The first 288 bits contains of paging indication information, and the last 12 bits are not transmitted.
- *Physical downlink shared channel (PDSCH):* As mentioned in the common transport channel section, the downlink shared channel (DSCH) is shared by a group of downlink users to effectively utilize channelization codes for packet data services. The radio frame-based PDSCH carries the DSCH in a physical channel, and one PDSCH is allocated to a single UE. Within the same radio frame, several PDSCH's can be allocated for a single UE for multicode transmission. Or, different PDSCH's can be used for different UE's for channel sharing using code multiplexing. The PDSCH is always associated with the DPCH. The TFCI in DPCCH provides the PDSCH information to the UE (such as the transport format parameters and the PDSCH channelization code).

23.7 High-Speed Downlink Packet Access

The 3GPP as part of its Release 5 version of the UMTS standard [15–17], was seeking to enhance the features of the physical downlink shared channel (PDSCH or simply DSCH) so that high-speed data services could be made available to the user without providing circuit-switched connections. The high-speed DSCH (HS-DSCH) takes advantage of adaptive modulation and coding to enhance data rates to data users in a time-multiplexed manner. The basic modulation and coding is depicted in Figure 23.13. Much like 1X-EV-DO, the number of codes allocated to the HS-DSCH varies and is a function of the offered load. In other words, if a large number of voice users are present, then the number of codes available for the HS-DSCH will most likely become less.

An N-channel stop-and-wait fast ARQ method is also one of the key features. In other words, the mobile and base station retain the state of each ARQ "channel," each channel being its own separate ARQ instance. When a retransmission needs to occur, that retransmission's timing will correspond to a

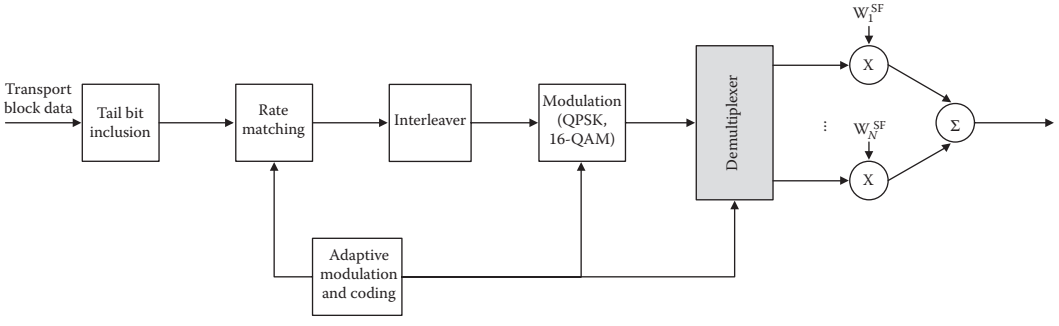

FIGURE 23.13 HSDPA downlink shared channel coding and modulation.

time slot assigned to the ARQ channel of the original transmission. However, while the mobile awaits the retransmission for an ARQ channel, it can still receive data on the additional N-1 ARQ channels.

23.8 High-Speed Uplink Packet Access

High-speed uplink packet access (HSUPA) was introduced in the Release 6 version of UMTS [18,19]. In seeking to provide a similar level of adaptability to HSDPA, the enhanced dedicated channel (E-DCH) was introduced as a new uplink transport channel. Based on a request–grant mechanism, whereby the mobile can request an uplink data rate and the base station can grant it, AMC could now be applied for upstream traffic [20]. The variable data rates are not achieved through higher-order modulation methods such as QPSK or 16-QAM, but through the combined us of multicode transmission along with variable spreading factor. In fact, the spreading factor can be reduced to as little as two to achieve the maximum data rate of 5.76 MBps. N-channel hybrid ARQ is possible, and the configuration is dependent on the transmission time interval selected (2 or 10 ms). Note that the combined offering of HSDPA and HSUPA is sometimes simply referred to as high-speed packet access (HSPA).

23.9 Transition to Fourth Generation

Many operators around the world have selected the "Fourth Generation" version of UMTS system design, long-term evolution (LTE) [21], as the future upgrade path for HSPA. This involves a brand new physical layer based on orthogonal frequency division multiplexing (OFDM), sometimes also known as multicarrier communication. However, leveraging the existing WCDMA design to approach the high data rates achieved by LTE has lead to new features in the Release 7 and Release 8 versions of UMTS. Such enhancements include the use of higher-order modulation (up to 64-QAM), incorporating the use of downlink multiantenna transmission (using multi-input multi-output, that is, *MIMO* transmission methods), and even allowing for the use of multiple HSDPA carriers (bundling them for combined transmission to individual users). This has provided some operators with an alternative to LTE that still leverages their initial UMTS investment.

It should also be noted that UMTS and cdma2000 services still have an important place in cellular communications alongside LTE due to their ability to offer reliable voice communications. This has proven to be beneficial as LTE systems continue to develop and roll out voice-over-LTE (VoLTE) communications services [22], as the availability of UMTS and cdma2000 systems allows for the possibility of *circuit-switched fallback* (CSFB) for providing voice telephony to LTE users. Using CFSB, voice users on LTE are directed back to available second- or third-generation cellular systems such as cdma2000 or UMTS. As a result, even as many operators pursue fourth generation cellular solutions, the existing third-generation solutions will have a place alongside them.

References

1. Mandyam, G. and J. Lai. *Third Generation CDMA Systems for Enhanced Data Services*. San Diego, CA: Elsevier, 2002.
2. The Telecommunications Industry Association. *TIA/EIA IS-95: Mobile Station-Base Station Compatibility Standards for Dual-Mode Wideband Spread Spectrum Cellular Systems.* 1994.
3. 3GPP2 C.S0002-A. *Physical Layer Standard for cdma2000 Spread Spectrum Systems-Release A*. TIA as IS-2000.2-A, Arlington, VA: The Telecommunications Industry Association, 2000.
4. 3GPP2 C.S0004-A. *Link Access Control (LAC) Standard for cdma2000 Spread Spectrum Systems-Release A*. TIA as IS-2000.4-A, Arlington, VA: The Telecommunications Industry Association, 2000.
5. 3GPP2 C.S0005-A. *Upper Layer (Layer 3) Standard for cdma2000 Spread Spectrum Systems-Release A*. TIA as IS-2000.5-A, Arlington, VA: The Telecommunications Industry Association, 2000.

6. 3GPP2 C.S0005-A. *Upper Layer (Layer 3) Standard for cdma2000 Spread Spectrum Systems -Release A*. TIA as IS-2000.5-A, Arlington, VA: The Telecommunications Industry Association, 2000.
7. Bender, P., P. Black, M. Grob, R. Padovani, N. Sindhushayana, and A. Viterbi. CDMA/HDR: A bandwidth efficient high speed wireless data service for Nomadic users. *IEEE Communications Magazine* 38(7), 2000, 70–77.
8. 3GPP2 C.S0024. *cdma2000 High Rate Packet Data Air Interface Specification*. October 27, 2000.
9. Holma, H. and A. Toskala, (eds.) *WCDMA for UMTS: Radio Access for Third Generation Mobile Communications*. West Sussex, United Kingdom: John Wiley & Sons, 2000.
10. Third Generation Partnership Project. TS 25.101 Version 4.1.0. *UE Radio Transmission and Reception (FDD)*. June 2001.
11. Third Generation Partnership Project. TS 25.211 Version 4.0.0. *Physical Channels and Mapping of Transport Channels onto Physical Channels (FDD)*. March 2001.
12. Third Generation Partnership Project. TS 25.212 Version 4.0.0. *Multiplexing and Channel Coding (FDD)*. December 2000.
13. Third Generation Partnership Project. TR 25.944 Version 4.1.0. *Channel Coding and Multiplexing Examples*. June 2001.
14. Third Generation Partnership Project. TS 25.213 Version 4.0.0. *Spreading and Modulation (FDD)*. March 2001.
15. Third Generation Partnership Project. TR 25.848 Version 4.0.0. *Physical Layer Aspects of UTRA High Speed Downlink Packet Access*. March 2001.
16. Third Generation Partnership Project. TR 25.855 Version 5.0.0. *High Speed Downlink Packet Access*. September 2001.
17. Third Generation Partnership Project. TR 25.855 Version 5.0.0. *High Speed Downlink Packet Access; Physial Layer Aspects*. March 2002.
18. Third Generation Partnership Project. TR 25.309 Version 6.6.0. *FDD Enhanced Uplink; Overall Description*. March 2006.
19. Third Generation Partnership Project. TR 25.211 Version 6.7.0. *Physical Channels and Mapping of Transport Channels onto Physical Channels (FDD)*. December 2005.
20. Holma, H. and A. Toskala, (eds.) *HSDPA/HSUPA for UMTS: High Speed Radio Access for Mobile Communications*. West Sussex, United Kingdom: John Wiley & Sons, 2006.
21. Holma, H. and A. Toskala, (eds.) *LTE for UMTS: OFDMA and SC-FDMA Based Radio Access*. West Sussex, United Kingdom: John Wiley & Sons, 2009.
22. Voice over LTE. Ericsson white paper. December 2010. http://www.ericsson.com/res/docs/whitepapers/voice-over-lte.pdf.

24

3GPP LTE/LTE-Advanced Radio Access Technologies

Sassan Ahmadi

24.1 Introduction

The growing demand for mobile Internet and wireless multimedia applications such as Internet browsing, interactive gaming, mobile TV, video and audio streaming has motivated development of broadband wireless access technologies in recent years. The 3rd-Generation Partnership Project (3GPP) initiated the work on the Long-Term Evolution (LTE) as part of 3GPP Release 8 in late 2004 [1]. The Evolved UMTS Terrestrial Radio Access Network (E-UTRAN) substantially improved user throughput, cell capacity, and reduced user-plane and control-plane latencies, bringing significantly improved user experience with full mobility. With the emergence of Internet protocol as the protocol of choice for carrying all types of traffic, the 3GPP LTE provides support for IP-based traffic with end-to-end Quality of Service (QoS). Voice traffic will be supported mainly as voice over IP, enabling better integration with other multimedia services. Initial deployments of 3GPP LTE began in late 2010 and commercial availability on a larger scale is expected in a few years. 3GPP LTE has been further enhanced in 3GPP Release 10 to satisfy the functional and service requirements of ITU-R/IMT-Advanced [2–5].

Unlike its predecessors, which were developed within the framework of Release 99 UMTS architecture, 3GPP specified the Evolved Packet Core (EPC) architecture to support the E-UTRAN through reduction in the number of network elements and simplification of functionality but most importantly allowing for connections and handover to other fixed and wireless access technologies, providing the network operators the ability to deliver seamless mobility. The main objectives of 3GPP LTE were to minimize the

system and User Equipment (UE) complexities, to allow flexible deployments in the existing or new frequency bands, and to enable coexistence with other 3GPP and non-3GPP radio access technologies.

The downlink transmission scheme is based on conventional Orthogonal Frequency Division Multiple Access (OFDMA) to provide robustness against frequency selectivity of the communication channel and multipath effects while allowing for low-complexity receiver implementations at wider bandwidths. The uplink transmission scheme is based on DFT-spread OFDM. The use of DFT-spread OFDM transmission for the uplink was motivated by the lower Peak-to-Average Power Ratio (PAPR) of the transmitted signal compared to conventional OFDMA. This allows for more efficient usage of the power amplifier at the terminal, which translates into an increased coverage and/or reduced terminal power consumption.

The 3GPP LTE/LTE-Advanced supports both FDD and TDD duplex schemes as well as transmission bandwidths in the range of 1.4–100 MHz. The carrier aggregation; that is, the simultaneous transmission of multiple component carries to the same terminal, is used to support contiguous/noncontiguous bandwidths larger than 20 MHz. Component carriers do not have to be contiguous in frequency and can even be located in different frequency bands in order to utilize fragmented spectrum allocations by means of spectrum aggregation. Channel-dependent scheduling in time and frequency domains is supported for both downlink and uplink with the base station scheduler being responsible for dynamic selection of transmission format. Semi-persistent scheduling is supported to allow semi-static resource allocation to a given UE for a longer time period in order to reduce the control signaling overhead.

Multi-antenna transmission scheme is an integral part of 3GPP LTE/LTE-Advanced standards. The multi-antenna precoding with dynamic rank adaptation supports both spatial multiplexing (single-user MIMO) and beam-forming. Spatial multiplexing with up to eight layers in the downlink and four layers in uplink is supported. The multiuser MIMO scheme, where multiple users are assigned to the same time-frequency resources is also supported. The 3GPP LTE/LTE-Advanced further includes transmit diversity based on Space Frequency Block Coding (SFBC) or a combination of SFBC and Frequency Switched Transmit Diversity (FSTD).

Enhanced Inter-cell Interference Coordination (eICIC), where neighbor cells exchange information aiding the scheduling in order to reduce intercell interference, is also supported. The eICIC scheme can be used for homogenous deployments with nonoverlapping cells of similar transmission power, as well as for heterogeneous deployments where a higher-power cell overlays one or several lower-power nodes (e.g., femto-cells). The relay functionality is supported where the relay node appears as a conventional base station (e-Node B or eNB) to terminals but is wirelessly connected to the remaining part of the radio-access network using the 3GPP LTE/LTE-Advanced radio-interface.

This chapter describes the prominent functional features of 3GPP LTE/LTE-Advanced technologies including protocols, control signaling, transmission formats, and physical layer and MAC processing.

24.2 Overall Network Architecture

As shown in Figure 24.1, the evolved UMTS terrestrial radio access network consists of eNBs or equivalently E-UTRA base stations, providing the E-UTRA user-plane and control-plane protocol terminations toward the user equipment (mobile station). As part of the evolution from and enhancement of the legacy UMTS systems, the Radio Network Controller (RNC) functions have been included in the eNB to reduce the architectural complexity and further reduce the latency across the network. As illustrated in Figure 24.1, the eNBs are interconnected with each other through X2 interface [6]. The X2 interface allows eNBs to communicate directly with each other and coordinate their activities. The X2 interface is split into separate control and user planes. The X2 control plane carries X2 Application Protocol (X2AP) messages between eNBs and uses Stream Control Transmission Protocol (SCTP) for reliable delivery of messages. The X2AP is used to manage inter-eNB mobility and handovers, UE context transfers, intercell interference management and various error handling functions. The X2 user plane uses GPRS Tunneling Protocol (GTP-U) to tunnel user traffic between eNBs.

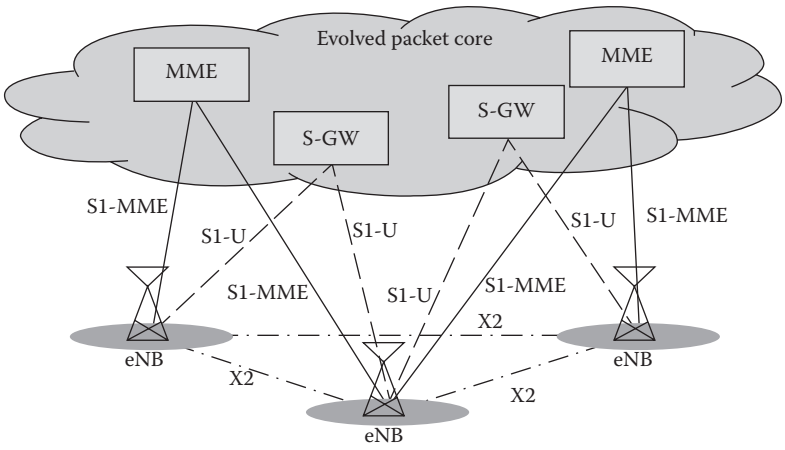

FIGURE 24.1 E-UTRAN architecture. (Adapted from 3GPP TS 36.300, Evolved Universal Terrestrial Radio Access (E-UTRA) and Evolved Universal Terrestrial Radio Access Network (E-UTRAN); Overall Description; Stage 2, December 2010.)

The eNBs are also connected via S1 interface to the EPC or more specifically to the Mobility Management Entity (MME) through the S1-MME reference point and to the Serving Gateway (S-GW) via the S1-U interface. The S1 interface supports a multi-point connection among MMEs/Serving Gateways and eNBs. The S1-MME carries S1 Application Protocol (S1AP) messages, using SCTP over IP to provide guaranteed data delivery. Each SCTP association between an eNB and an MME can support multiple UEs. The S1-MME is responsible for EPC bearer setup and release procedures, handover signaling, paging, and NAS signaling transport. The S1-U consists of GTP-U protocol running on top of User Datagram Protocol (UDP), which provides best-effort data delivery. One GTP tunnel is established for each radio bearer in order to carry user traffic between the eNB and the selected S-GW.

The E-UTRAN overall architecture is described in References 6 and 7. Some general principles taken into consideration in the design of E-UTRAN architecture as well as the E-UTRAN interfaces are as follows [6]:

- Signaling and data transport networks are logically separated.
- E-UTRAN and EPC functions are separated from transport functions. The addressing schemes used in E-UTRAN and EPC are not associated with the addressing schemes of transport functions. Some E-UTRAN or EPC functions reside in the same equipment.
- The mobility for RRC connection is controlled by the E-UTRAN.
- The interfaces are based on the logical model of the entity which is controlled through this interface.
- One physical network element can implement multiple logical nodes.

The eNB typically performs the following functions [6]:

- Radio Resource Management (RRM) including radio bearer control, radio admission control, connection management, dynamic allocation of resources to UEs in both uplink and downlink (i.e., scheduling).
- Header compression and encryption of user payloads.
- Selection of an MME at UE attachment when no routing to an MME can be determined from the information provided by the UE.
- Routing of U-Plane data toward S-GW.
- Scheduling and transmission of paging messages (originated from the MME).
- Scheduling and transmission of broadcast information (originated from the MME).
- Measurement and reporting for support of mobility and scheduling.

The MME is the key control-node for the 3GPP LTE access-network. It is responsible for idle mode UE tracking and paging procedure including retransmissions. The MME functions include Non-Access Stratum (NAS) signaling and NAS signaling security, Inter-core-network signaling for mobility between 3GPP access networks, Idle mode UE accessibility (including control and execution of paging retransmission), Tracking area list management (for UE in idle and active mode), Packet Data Network (PDN) gateway and S-GW selection, MME selection for handovers with MME change, Roaming, Authentication of the users, and Bearer management functions including dedicated bearer establishment [6,7]. The NAS signaling terminates at the MME and it is also responsible for generation and allocation of temporary identities to the UEs. It verifies the authorization of the UE to camp on the service provider's Public Land Mobile Network (PLMN) and enforces UE roaming restrictions.

The S-GW routes and forward user data packets, while also acting as the mobility anchor for the user-plane during inter-eNB handovers and as the anchor for mobility between 3GPP LTE and other 3GPP technologies. The S-GW functions include local mobility anchor point for inter-eNB handover, Mobility anchoring for inter-3GPP mobility, E-UTRAN idle mode downlink packet buffering and initiation of network triggered service request procedure, Lawful interception, Packet routing and forwarding, and Transport-level packet marking in the uplink and the downlink [6,7].

The Packet Data Network Gateway (P-GW) provides connectivity of the UE to external packet data networks by being the point of exit and entry of traffic for the UE. A UE may have simultaneous connectivity with more than one P-GW for accessing multiple packet data networks. The P-GW functions include Per-user packet filtering, Lawful interception, UE IP address allocation, and Transport level packet marking in the downlink [6,7].

24.3 3GPP LTE Protocol Structure

In this section, we describe the functions of different protocol layers and their location in the 3GPP LTE/LTE-Advanced protocol structure. Figure 24.2 shows the functional split between the eNB and EPC. In the control-plane, the NAS functional block is used for network attachment, authentication, setting up bearers, and mobility management. All NAS messages are ciphered and integrity protected by the MME and UE. The Radio Resource Control (RRC) sub-layer in the eNB makes handover decisions based on neighbor cell measurements reported by the UE, performs paging of the users over the air-interface, broadcasts system information, controls UE measurement and reporting functions such as the periodicity of Channel Quality Indicator (CQI) reports and further allocates cell-level temporary identifiers to active users. It also executes transfer of UE context from the serving eNB to the target eNB during handover, and performs integrity protection of RRC messages. The RRC sublayer is responsible for setting up and maintenance of radio bearers. Note that RRC sublayer in 3GPP protocol hierarchy is considered as Layer 3 [6,8].

In the user plane, the Packet Data Convergence Protocol (PDCP) sublayer is responsible for compressing or decompressing the headers of user-plane IP packets using Robust Header Compression (RoHC) to enable efficient use of air interface resources [6,9]. This layer also performs ciphering of both user-plane and control-plane traffic. Because the NAS messages are carried in RRC, they are effectively double ciphered and integrity protected, once at the MME and again at the eNB.

The Radio Link Control (RLC) sublayer is used to format and transport traffic between the UE and the eNB [6,18]. The RLC sublayer provides three different reliability modes for data transport; that is, Acknowledged Mode (AM), Unacknowledged Mode (UM), and Transparent Mode (TM). The unacknowledged mode is suitable for transport of real-time services since such services are delay sensitive and cannot tolerate delay due to retransmissions. The acknowledged mode is appropriate for nonreal-time services such as file transfers. The transparent mode is used when the size of packet data units are known in advance such as for broadcasting system configuration information. The RLC sublayer also provides sequential delivery of service data units to the upper layers and eliminates duplicate packets from being delivered to the upper layers. It may also segment the service data units. Furthermore, there

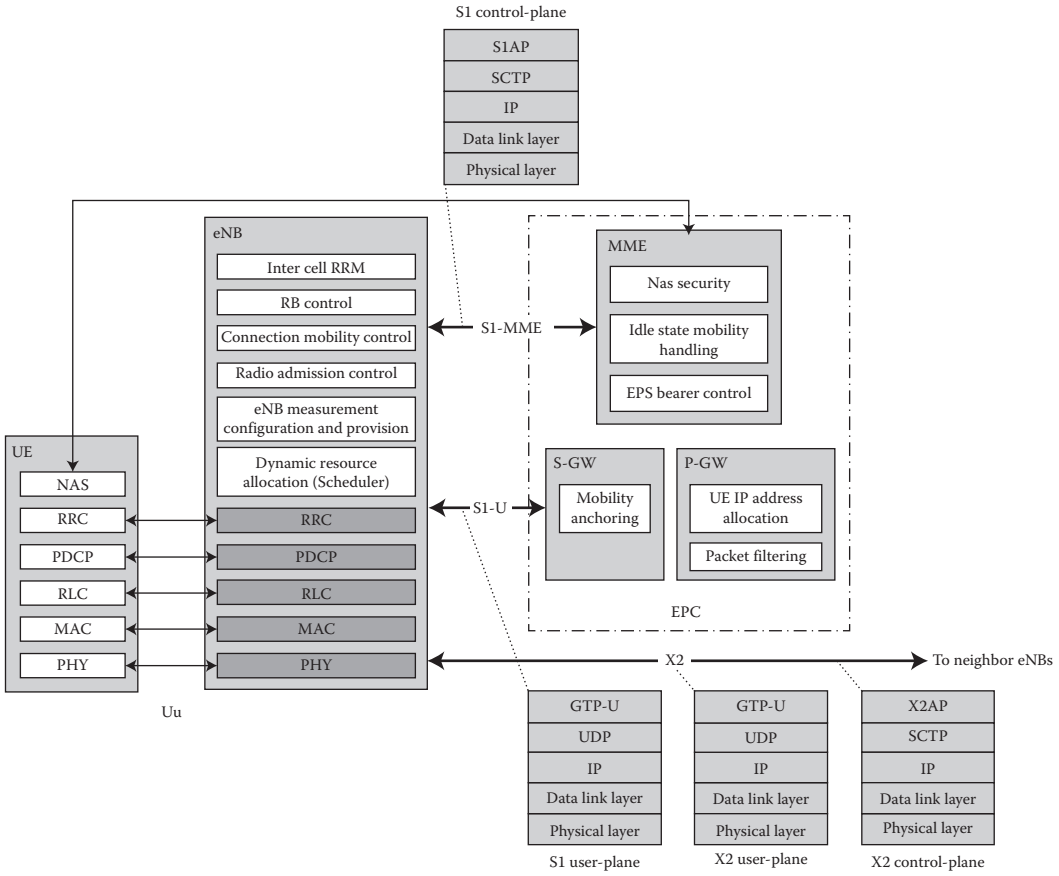

FIGURE 24.2 Protocol layers and function split in UE, eNB, MME, S-GW, and P-GW. (Adapted from 3GPP TS 36.300, Evolved Universal Terrestrial Radio Access (E-UTRA) and Evolved Universal Terrestrial Radio Access Network (E-UTRAN); Overall Description; Stage 2, December 2010.)

are two levels of retransmissions for providing reliability, the Hybrid Automatic Repeat reQuest (HARQ) at the MAC sublayer and ARQ at the RLC sublayer. The ARQ is required to handle residual errors that are not corrected by HARQ. An N-process stop-and-wait HARQ protocol is employed that has asynchronous retransmissions in the downlink and synchronous retransmissions in the uplink. Synchronous HARQ means that the retransmissions of HARQ sub-packets occur at predefined periodic intervals. Hence, no explicit signaling is required to indicate to the receiver the retransmission schedule. Asynchronous HARQ offers the flexibility of scheduling retransmissions based on air interface conditions (i.e., scheduling gain).

24.4 Overview of the 3GPP LTE Physical Layer

The main functional elements of the physical layer processing are described in the following sections [10–13].

24.4.1 Multiple Access Schemes

3GPP LTE/LTE-Advanced uses asymmetric multiple access schemes in the downlink and uplink. The multiple access scheme for the 3GPP LTE/LTE-Advanced physical layer is based on Orthogonal

Frequency Division Multiple Access (OFDMA) with a Cyclic Prefix (CP) in the downlink and Single Carrier Frequency Division Multiple Access (SC-FDMA) with CP in the uplink.

The OFDMA scheme is particularly suited for frequency-selective channels and high data rates. It transforms a wideband frequency selective channel into a set of parallel flat fading narrowband channels. This ideally, allows the receiver to perform a less complex equalization process in frequency domain; that is, single-tap frequency-domain equalization.

24.4.1.1 Downlink Multiple Access

The downlink transmission scheme is based on conventional OFDMA using a cyclic prefix. The 10 ms radio frame is divided into 10 equally sized subframes. Each subframe is further divided into two slots of 0.5 ms length. The basic transmission parameters in the downlink are specified in Table 24.1.

The CP length is chosen to be longer than the maximum delay spread in the radio channel. For 3GPP LTE/LTE-Advanced, the normal CP length has been set to 4.69 μs, enabling the system to tolerate delay variations due to propagation over cells up to 1.4 km. Note that the insertion of longer CP increases the physical-layer overhead, thus reducing the overall throughput.

To provide enhanced multicast and broadcast services, 3GPP LTE/LTE-Advanced has the capability to transmit multicast and broadcast over a Single-Frequency Network (MBSFN), where a time-synchronized common waveform is transmitted from multiple eNBs, allowing macro-diversity combining of multicell transmissions at the UE. The cyclic prefix is utilized to mitigate the difference in the propagation delays, which makes the MBSFN transmission appear to the UE as a transmission from a single large cell. Transmission on a dedicated carrier for MBSFN with the possibility to use a longer CP with a subcarrier bandwidth of 7.5 kHz is supported as well as transmission of MBSFN on a carrier with both MBMS and unicast transmissions using time division multiplexing [6].

24.4.1.2 Uplink Multiple Access

The basic transmission scheme in the uplink is single-carrier transmission (SC-FDMA) with cyclic prefix to achieve uplink interuser orthogonality and to enable efficient frequency-domain equalization at the receiver side. The frequency-domain generation of the SC-FDMA signal, also known as DFT-spread OFDM, is similar to OFDMA and is illustrated in Figure 24.3. This allows for a relatively high degree of commonality with the downlink OFDMA baseband processing using the same parameters; for example, clock frequency, subcarrier spacing, FFT/IFFT size, and so on. The use of SC-FDMA in the uplink is mainly due to relatively inferior PAPR properties of OFDMA that results in worse uplink coverage

TABLE 24.1 3GPP LTE/LTE-Advanced OFDMA Parameters

Parameter	Value					
Channel bandwidth (MHz)	1.4	3	5	10	15	20
Number of resource blocks	6	15	25	50	75	100
Number of occupied subcarriers	72	180	300	600	900	1200
IDFT/FFT size	128	256	512	1024	1536	2048
Subcarrier spacing Δf (kHz)	15 (7.5)					
Sampling rate (MHz)	1.92	3.84	7.68	15.36	23.04	30.72
Samples/slot	960	1920	3840	7680	11,520	15,360
CP size						
Normal CP($\Delta f = 15$ kHz)	5.21 μs (first symbol of the slot) 4.69 μs (other symbols of the slot) 7 symbols/slot					
Extended CP ($\Delta f = 15$ kHz)	16.67 μs (6 symbols/slot)					
Extended CP ($\Delta f = 7.5$ kHz)	33.33 μs (3 symbols/slot)					

Source: Adapted from 3GPP TS 36.101, Evolved Universal Terrestrial Radio Access (E-UTRA); User Equipment (UE) Radio Transmission and Reception, January 2011; E. Dahlman et al., *3G Evolution: HSPA and LTE for Mobile Broadband*, 2nd Edition, Academic Press, October 2008.

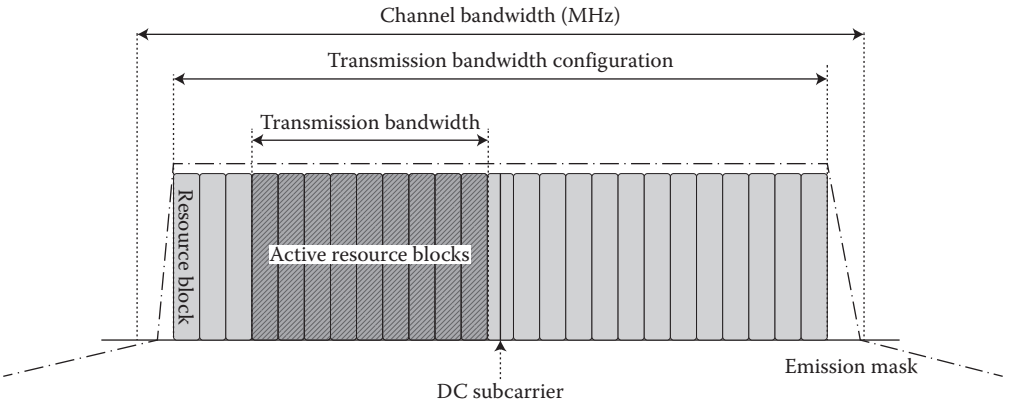

FIGURE 24.3 Transmitter/receiver structure of SC-FDMA. (Adapted from 3GPP TS 36.101, Evolved Universal Terrestrial Radio Access (E-UTRA); User Equipment (UE) Radio Transmission and Reception, January 2011.)

compared to SC-FDMA. The PAPR characteristics are important for cost-effective design of UE power amplifiers.

The subcarrier mapping in Figure 24.3 determines which part of the spectrum is used for transmission by inserting a suitable number of zeros at the upper and/or lower end. Between each DFT output sample L-1 zeros are inserted. A mapping with $L = 1$ corresponds to localized transmissions; that is, transmissions where the DFT outputs are mapped to consecutive subcarriers. There are two subcarrier mapping schemes (localized and distributed) that could be used in the uplink. However, 3GPP LTE only specified localized subcarrier mapping in the uplink.

24.4.2 Operating Frequencies and Bandwidths

The E-UTRA is designed to operate in the frequency bands defined in Table 24.2. The requirements were defined for 1.4, 3, 5, 10, 15, and 20 MHz bandwidth with a specific configuration in terms of number of resource blocks (see Table 24.2). Using carrier aggregation, a number of contiguous and/or noncontiguous frequency bands can be aggregated to create a virtually larger bandwidth.

Figure 24.4 illustrates the relationship between the total channel bandwidth and the transmission bandwidth; that is, the number of resource blocks. The 3GPP LTE/LTE-Advanced channel raster is 100 kHz, which means the center frequency must be a multiple of 100 kHz [14]. To support transmission in paired and unpaired spectrum, two duplexing schemes are supported: Frequency Division Duplex (FDD), allowing both full and half-duplex terminal operation, as well as Time Division Duplex (TDD). Table 24.2 shows the band classes where the 3GPP LTE systems can be deployed.

24.4.3 Frame Structure

Downlink and uplink transmissions are organized in form of radio frames with 10 ms duration. 3GPP LTE/LTE-Advanced supports two radio frame structures, Type 1, applicable to FDD duplex scheme and Type 2, applicable to TDD duplex scheme. In frame structure Type 1, as illustrated in Figure 24.5, each 10 ms radio frame is divided into 10 equally sized subframes. Each subframe consists of two equally sized slots. For FDD, 10 subframes are available for downlink transmission and 10 subframes are available for uplink transmissions in each radio frame. Uplink and downlink transmissions are separated in the frequency domain. The transmission time interval (TTI) of the downlink/uplink is 1 ms [10,6].

Frame structure Type 2 is illustrated in Figure 24.6. Each 10 ms radio frame consists of two 5 ms half-frames. Each half-frame consists of eight slots of 0.5 ms length and three special fields: Downlink Pilot

TABLE 24.2 3GPP LTE/LTE-Advanced Band Classes

Band Class	Uplink Operating Band eNB Receive/ UE Transmit (MHz) F_{UL_low}–F_{UL_high}			Downlink Operating Band eNB Transmit /UE Receive (MHz) F_{DL_low}–F_{DL_high}			Duplex Mode
1	1920	–	1980	2110	–	2170	FDD
2	1850	–	1910	1930	–	1990	FDD
3	1710	–	1785	1805	–	1880	FDD
4	1710	–	1755	2110	–	2155	FDD
5	824	–	849	869	–	894	FDD
6	830	–	840	865	–	875	FDD
7	2500	–	2570	2620	–	2690	FDD
8	880	–	915	925	–	960	FDD
9	1749.9	–	1784.9	1844.9	–	1879.9	FDD
10	1710	–	1770	2110	–	2170	FDD
11	1427.9	–	1447.9	1475.9	–	1495.9	FDD
12	698	–	716	728	–	746	FDD
13	777	–	787	746	–	756	FDD
14	788	–	798	758	–	768	FDD
15		Reserved			Reserved		–
16		Reserved			Reserved		–
17	704	–	716	734	–	746	FDD
18	815	–	830	860	–	875	FDD
19	830	–	845	875	–	890	FDD
20	832	–	862	791	–	821	FDD
21	1447.9	–	1462.9	1495.9	–	1510.9	FDD
22	3410	–	3500	3510	–	3600	FDD
…							
33	1900	–	1920	1900	–	1920	TDD
34	2010	–	2025	2010	–	2025	TDD
35	1850	–	1910	1850	–	1910	TDD
36	1930	–	1990	1930	–	1990	TDD
37	1910	–	1930	1910	–	1930	TDD
38	2570	–	2620	2570	–	2620	TDD
39	1880	–	1920	1880	–	1920	TDD
40	2300	–	2400	2300	–	2400	TDD
41	3400	–	3600	3400	–	3600	TDD

Source: Adapted from 3GPP TS 36.101, Evolved Universal Terrestrial Radio Access (E-UTRA); User Equipment (UE) Radio Transmission and Reception, January 2011.

Time Slot (DwPTS), Guard Period (GP), and Uplink Pilot Time Slot (UpPTS). The length of DwPTS and UpPTS is configurable subject to the total length of DwPTS, GP, and UpPTS being equal to 1 ms (see [10] for more details). Both 5 ms and 10 ms switching-point periodicity are supported. The first subframe in all configurations and the sixth subframe in configuration with 5 ms switching-point periodicity consist of DwPTS, GP, and UpPTS. The sixth subframe in configuration with 10 ms switching-point periodicity consists of DwPTS only. All other subframes consist of two equally sized slots.

For TDD systems, the GP is reserved for downlink to uplink transition. Other subframes/fields are assigned for either downlink or uplink transmission as shown in Table 24.3. Uplink and downlink transmissions are separated in the time domain.

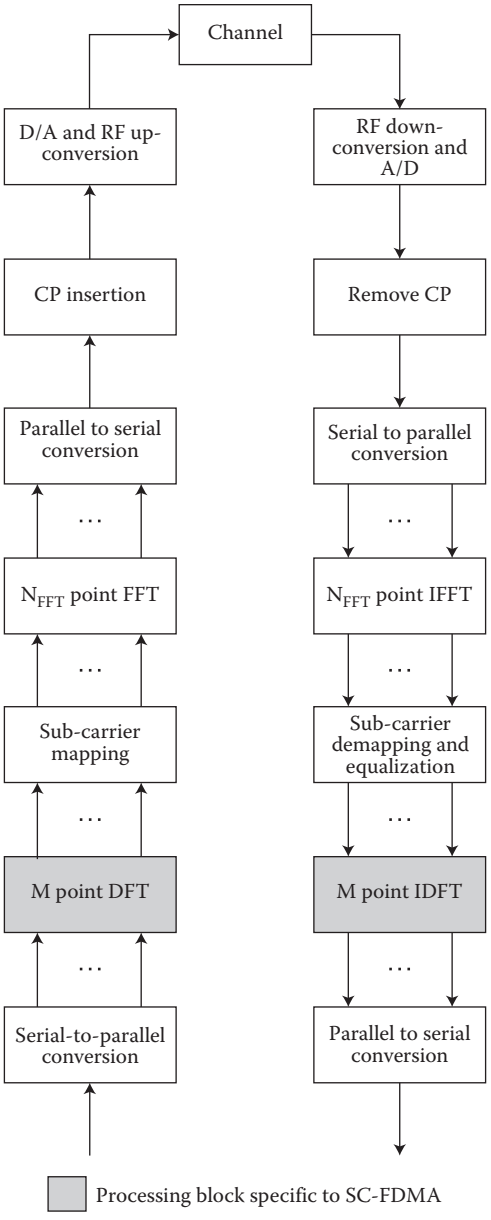

FIGURE 24.4 Illustration of the relationship between channel bandwidth and transmission bandwidth.

24.4.4 Physical Resource Blocks

The smallest time–frequency resource unit used for downlink/uplink transmission is called a resource element, defined as one subcarrier over one symbol [10]. For both TDD and FDD duplex schemes as well as in both downlink and uplink, a group of 12 subcarriers contiguous in frequency over one slot in time form a Resource Block (RB) as shown in Figure 24.7 (corresponding to one slot in the time domain and 180 kHz in the frequency domain). Transmissions are allocated in units of RB. One downlink/uplink slot using the normal CP length contains 7 symbols. There are 6, 15, 25, 50, 75, and 100 RBs corresponding to

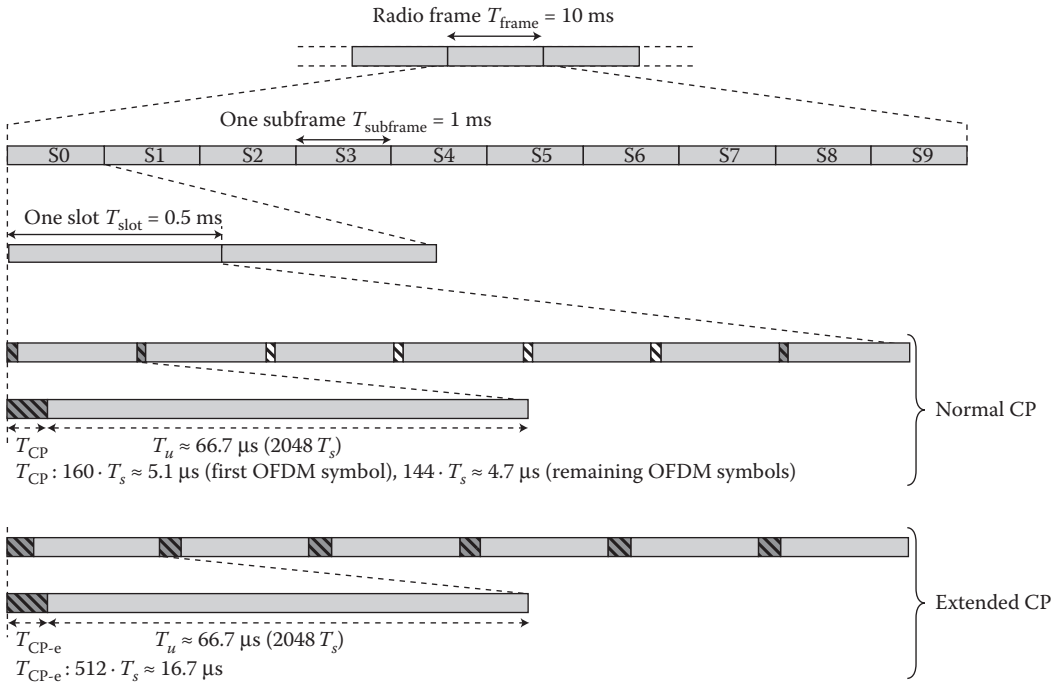

FIGURE 24.5 3GPP LTE/LTE-advanced FDD frame structure.

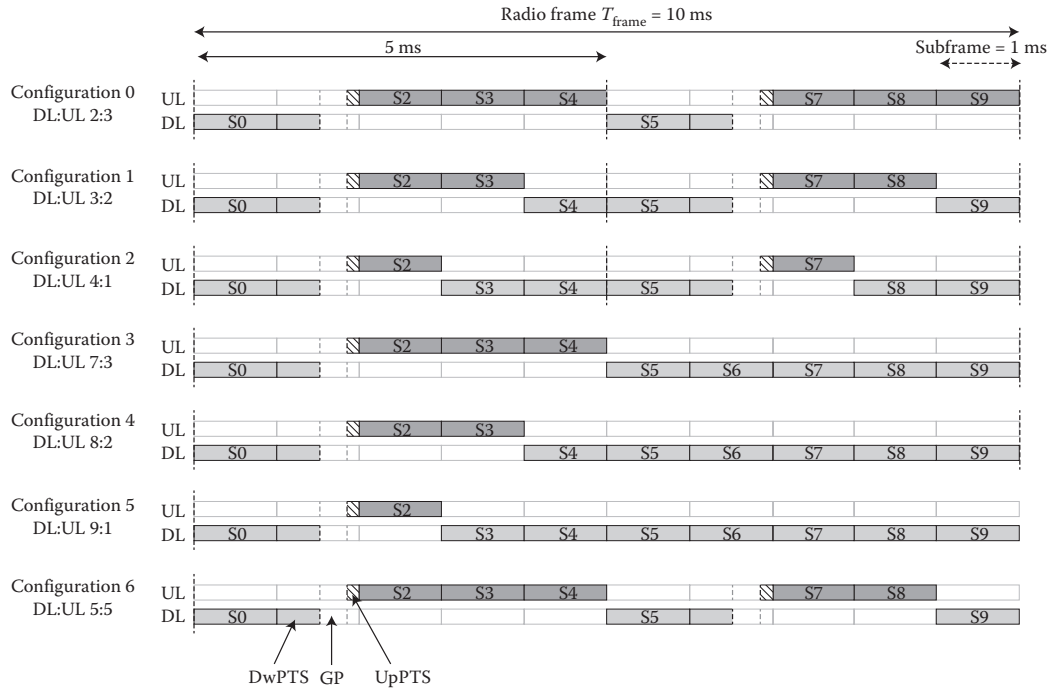

FIGURE 24.6 3GPP LTE/LTE-advanced TDD frame configurations.

TABLE 24.3 Uplink/Downlink Configurations in Frame Structure Type 2 where "S" denotes the Special Subframe

Configuration	Switching Point Periodicity (ms)	Subframe Number									
		0	1	2	3	4	5	6	7	8	9
0	5	DL	S	UL	UL	UL	DL	S	UL	UL	UL
1	5	DL	S	UL	UL	DL	DL	S	UL	UL	DL
2	5	DL	S	UL	DL	DL	DL	S	UL	DL	DL
3	10	DL	S	UL	UL	UL	DL	DL	DL	DL	DL
4	10	DL	S	UL	UL	DL	DL	DL	DL	DL	DL
5	10	DL	S	UL	DL	DL	DL	DL	DL	DL	DL
6	10	DL	S	UL	UL	UL	DL	S	UL	UL	DL

Source: Adapted from 3GPP TS 36.211, Evolved Universal Terrestrial Radio Access (E-UTRA); Physical Channels and Modulation, December 2010.

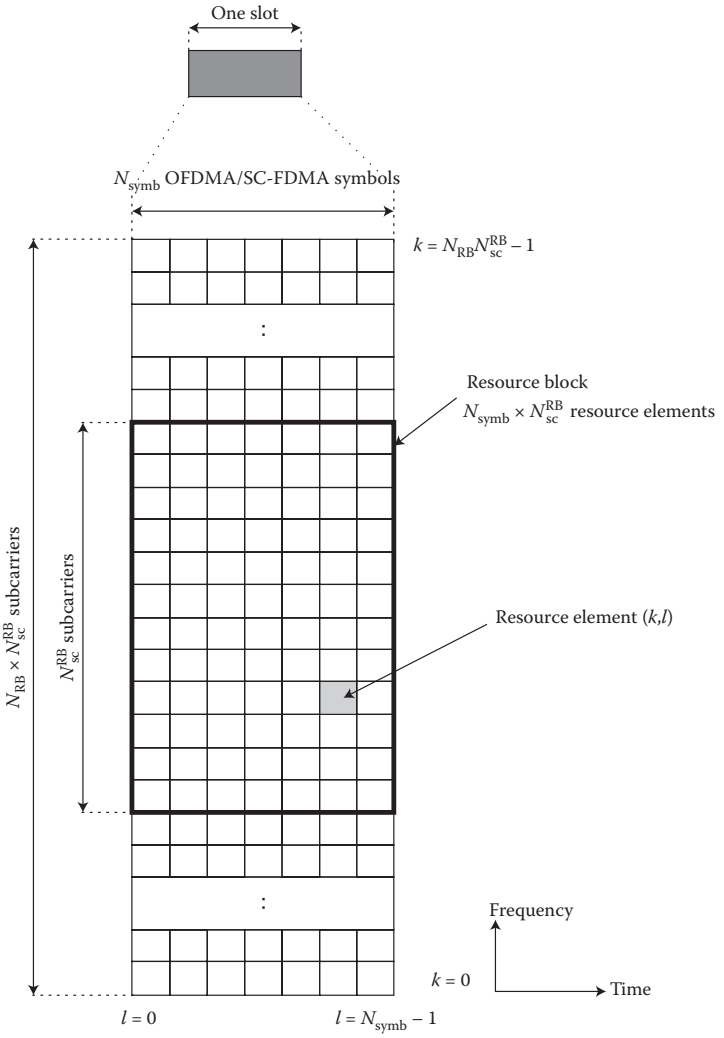

FIGURE 24.7 The structure of 3GPP LTE physical resource block. (Adapted from 3GPP TS 36.211, Evolved Universal Terrestrial Radio Access (E-UTRA); Physical Channels and Modulation, December 2010.)

1.4, 3, 5, 10, 15, 20 MHz channel bandwidths, respectively [10]. Note that the physical resource block size is the same for all bandwidths.

24.4.5 Modulation and Coding

The baseband modulation schemes supported in the downlink and uplink of 3GPP LTE/LTE-Advanced are QPSK, 16QAM and 64QAM. The channel coding scheme for transport blocks in 3GPP LTE is Turbo Coding similar to UTRA, with the minimum coding rate of $R = 1/3$, two 8-state constituent encoders and a contention-free Quadratic Permutation Polynomial (QPP) turbo internal interleaver [11]. Trellis termination is performed by taking the tail bits from the shift register feedback after all information bits are encoded. The tail bits are padded after the encoding of information bits. Before the turbo coding, transport blocks are segmented into octet-aligned segments with a maximum information block size of 6144 bits. Error detection is supported by the use of 24 bit CRC. The coding and modulation schemes for various physical channels in the downlink and uplink of 3GPP LTE are shown in Table 24.4 [15,16].

24.4.6 Physical Channel Processing

Figure 24.7 illustrates different stages of 3GPP LTE physical channel processing in the downlink and uplink. In the downlink, the coded bits in each of the codewords are scrambled for transmission on a physical channel. The scrambled bits are modulated to generate complex-valued modulation symbols that are later mapped to one or several transmission layers. The complex-valued modulation symbols on each layer are precoded for transmission and are further mapped to resource elements for each antenna port. The complex-valued time-domain OFDMA signal for each antenna port is then generated following these stages [10].

In the uplink, the baseband signal is processed by scrambling the input coded bits and then by modulation of scrambled bits to generate complex-valued symbols. The complex-valued modulation symbols are transform-precoded (DFT-based precoding) and are later mapped to resource elements. The complex-valued time-domain SC-FDMA signal for each antenna port is then generated.

24.4.7 Reference Signals

In 3GPP LTE Release 8/9, four types of downlink reference signals are defined, cell-specific reference signals, associated with non-MBSFN transmission, MBSFN reference signals, associated with MBSFN transmission, positioning reference signals, and demodulation or UE-specific reference signals. There is one cell-specific reference signal transmitted per downlink antenna port [10]. Note that antenna port is a logical entity and shall not be confused with the physical transmit antennas, although there is a mapping between the two entities during operation in various transmission modes (see Figure 24.8). The cell-specific downlink reference signals consist of predetermined reference symbols that are inserted in the time-frequency grid over each subframe and are used for downlink channel estimation [10,6] and physical layer identifier (cell identifier) detection. The exact sequence is derived from cell identifiers. The number of downlink antenna ports with cell-specific reference signals equals 1, 2, or 4. The reference signal sequence is derived from a pseudo-random sequence and results in a QPSK type constellation. Cell-specific frequency shifts are applied when mapping the reference signal sequence to the sub-carriers. The two-dimensional reference signal sequence is generated as the symbol-by-symbol product of a two-dimensional orthogonal sequence and a two-dimensional pseudo-random sequence. There are 3 different two-dimensional orthogonal sequences and 168 different two-dimensional pseudo-random sequences. Each cell identity corresponds to a unique combination of one orthogonal sequence and one pseudo-random sequence, thus allowing for 504 unique cell identities (i.e., 168 cell identity groups with 3 cell identities in each group).

TABLE 24.4 Physical Channels and Signals and Their Corresponding Modulation Schemes for the 3GPP LTE Downlink and Uplink

Link	Channel Type	Channel	Transmission Format	Purpose
Downlink	Physical Channels	Physical Broadcast Channel (PBCH)	QPSK	Transmission of system information (master information block)
		Physical Downlink Control Channel (PDCCH)	QPSK	Transmission of downlink scheduling assignments and uplink scheduling grants
		Physical Downlink Shared Channel (PDSCH)	QPSK, 16QAM, 64QAM	Transmission of downlink user data, RRC signaling, paging, and broadcast
		Physical Multicast Channel (PMCH)	QPSK, 16QAM, 64QAM	Transmission of multicast services
		Physical Control Format Indicator Channel (PCFICH)	QPSK	Indication of the size of the control region in number of OFDM symbols
		Physical HARQ Indicator Channel (PHICH)	BPSK modulated on I and Q with the spreading factor 2 or 4 orthogonal codes	Transmission of ACK/NACK associated with uplink transmission
	Physical Signals	Reference Signals (RS)	Complex $I + jQ$ pseudo-random sequence of length 31 Gold sequence derived from cell ID	Channel estimation
		Primary Synchronization signal	One of 3 Zadoff-Chu sequences	Acquisition of slot timing
		Secondary Synchronization Signal	Two 31-bit BPSK M-sequence	Frame timing synchronization
Uplink	Physical Channels	Physical Uplink Shared Channel (PUSCH)	QPSK, 16QAM, 64QAM	Transmission of user data and control in the uplink
		Physical Uplink Control Channel (PUCCH)	BPSK, QPSK	Transmission of ACK/NACK associated with downlink data, scheduling request, and feedback of downlink channel quality and precoding matrix index
		Physical Random Access Channel (PRACH)	uth root Zadoff-Chu sequence	Random access transmission
	Physical Signals	Demodulation Reference Signal (DRS) (narrowband)	Zadoff-Chu	Coherent modulation of uplink data
		Sounding Reference Signal (SRS) (wideband)	Based on Zadoff-Chu	Uplink channel estimation

Source: Adapted from 3GPP TS 36.211, Evolved Universal Terrestrial Radio Access (E-UTRA); Physical Channels and Modulation, December 2010.

The downlink MBSFN reference signals consist of known reference symbols inserted every other subcarrier in the 3rd, 7th, and 11th OFDM symbols of subframe in case of 15 kHz subcarrier spacing and extended cyclic prefix. The MBSFN reference signals are transmitted on antenna port 4.

The UE-specific reference signals are supported for single-antenna-port transmission of PDSCH and transmitted on antenna port 5, 7, or 8. The UE-specific reference signals are also supported for spatial

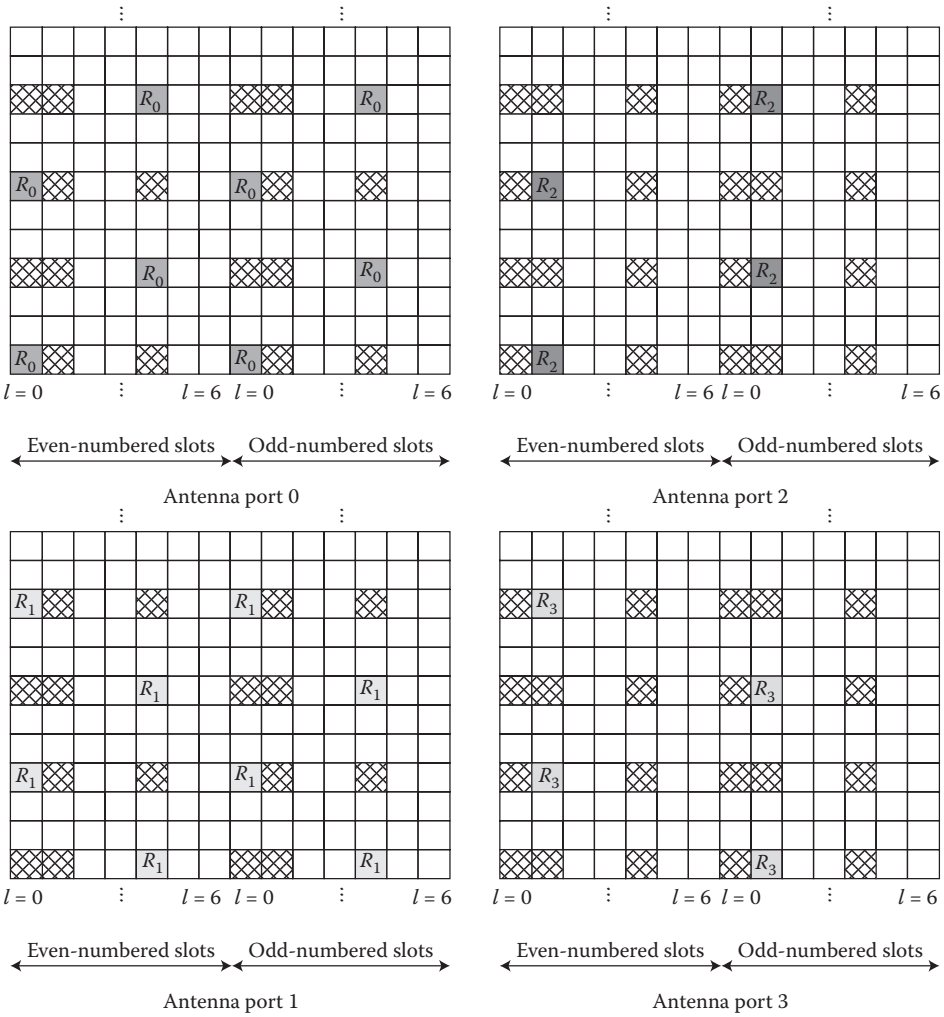

FIGURE 24.8 Downlink cell-specific reference signals for antenna ports 0, 1, 2, and 3. (Adapted from 3GPP TS 36.211, Evolved Universal Terrestrial Radio Access (E-UTRA); Physical Channels and Modulation, December 2010.)

multiplexing on antenna ports 7 and 8. These reference signals are utilized for PDSCH coherent demodulation, if the PDSCH transmission is associated with the corresponding antenna port. They are transmitted only on the resource blocks to which the corresponding PDSCH is mapped. The UE-specific reference signals are not transmitted in resource elements where one of the physical channels or physical signals other than UE-specific reference signal are transmitted using resource elements with the same index pair regardless of their antenna port.

Positioning reference signals are only transmitted in downlink subframes configured for positioning reference signal transmission. If both normal and MBSFN subframes are configured as positioning subframes within a cell, the OFDM symbols in an MBSFN subframe configured for positioning reference signal transmission use the same cyclic prefix as used for the first subframe. Otherwise, if only MBSFN subframes are configured as positioning subframes within a cell, the OFDM symbols configured for positioning reference signals in these subframes use the extended cyclic prefix. The positioning reference signals are transmitted on antenna port 6 and are not mapped to resource elements allocated to physical broadcast, primary and secondary synchronization channels, regardless of their antenna port.

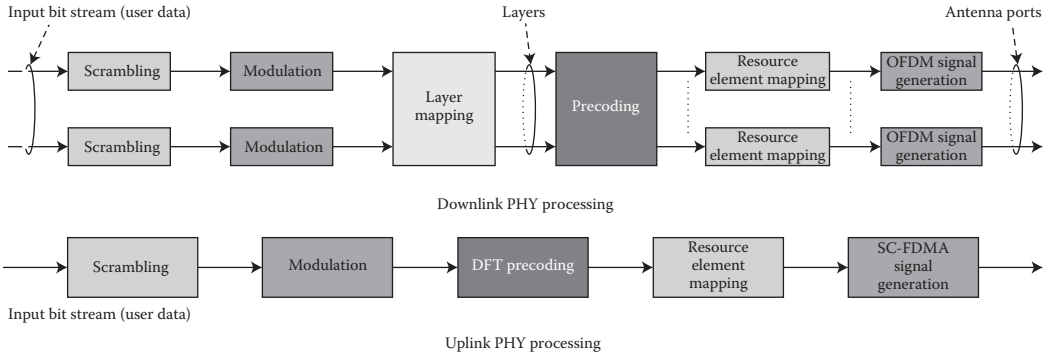

FIGURE 24.9 Overview of downlink/uplink physical channel processing. (Adapted from 3GPP TS 36.211, Evolved Universal Terrestrial Radio Access (E-UTRA); Physical Channels and Modulation, December 2010.)

In 3GPP Release 10, a new set of reference signals called Channel State Information-Reference Signals (CSI-RS) were added which are used to support reporting of channel-state information from the user terminals to the network. The CSI reference signals are sparse in the time and frequency and transmitted at a configurable periodicity. Figure 24.9 shows the cell-specific reference signals corresponding to antenna ports 0 through 3 in the downlink. The physical resources at the locations of the reference signals of another antenna port are not used for data transmission on the other antenna ports.

The uplink reference signals, used for channel estimation for coherent demodulation, are transmitted in the 4th SC-FDMA symbol in each slot assuming normal CP. 3GPP LTE uses UE-specific reference signals in the uplink. The uplink reference signal sequence length equals the size (number of subcarriers) of the assigned resource. The uplink reference signals are based on Zadoff–Chu sequences that are either truncated or cyclically extended to the desired length. There are two types of uplink reference signals (1) the demodulation reference signal is used for channel estimation in the eNB receiver in order to demodulate control and data channels. It is located on the 4th symbol in each slot (for normal cyclic prefix) and spans the same bandwidth as the allocated uplink data, and (2) the sounding reference signal provides uplink channel quality information as a basis for scheduling decisions in the base station (see Figure 24.10). The UE sends a sounding reference signal in different parts of the bandwidths where no uplink data transmission is available. The sounding reference signal is transmitted in the last symbol of the

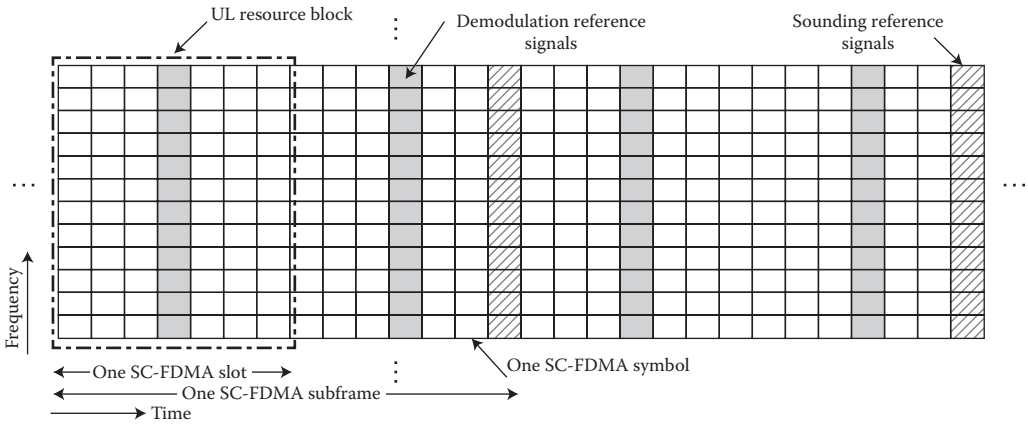

FIGURE 24.10 Uplink physical resource blocks and reference signals.

subframe. The configuration of the sounding signal; for example, bandwidth, duration, and periodicity are configured by higher layers.

24.4.8 Physical Control Channels

The Physical Downlink Control Channel (PDCCH) is primarily used to carry scheduling information to individual UEs; that is, resource assignments for uplink and downlink data and control information. As shown in Figure 24.11, the PDCCH is located in the first few OFDM symbols of a subframe. For frame structure Type 2, PDCCH can also be mapped to the first two OFDM symbols of the DwPTS field. An additional Physical Control Format Indicator Channel (PCFICH), located on specific resource elements in the first OFDM symbol of the subframe, is used to indicate the number of OFDM symbols occupied by the PDCCH (1, 2, 3, or 4 OFDM symbols may be consumed where 4-OFDM-symbol PDCCH is only used when operating in the minimum supported system bandwidth). Depending on the number of users in a cell and the signaling formats conveyed on PDCCH, the size of PDCCH may vary. The information carried in PDCCH is referred to as Downlink Control Information (DCI), where depending on the purpose of the control message, different DCI formats are defined [15,16]. This information enables the UE to identify the location and size of the resources in that subframe, as well as provide the UE with information on the

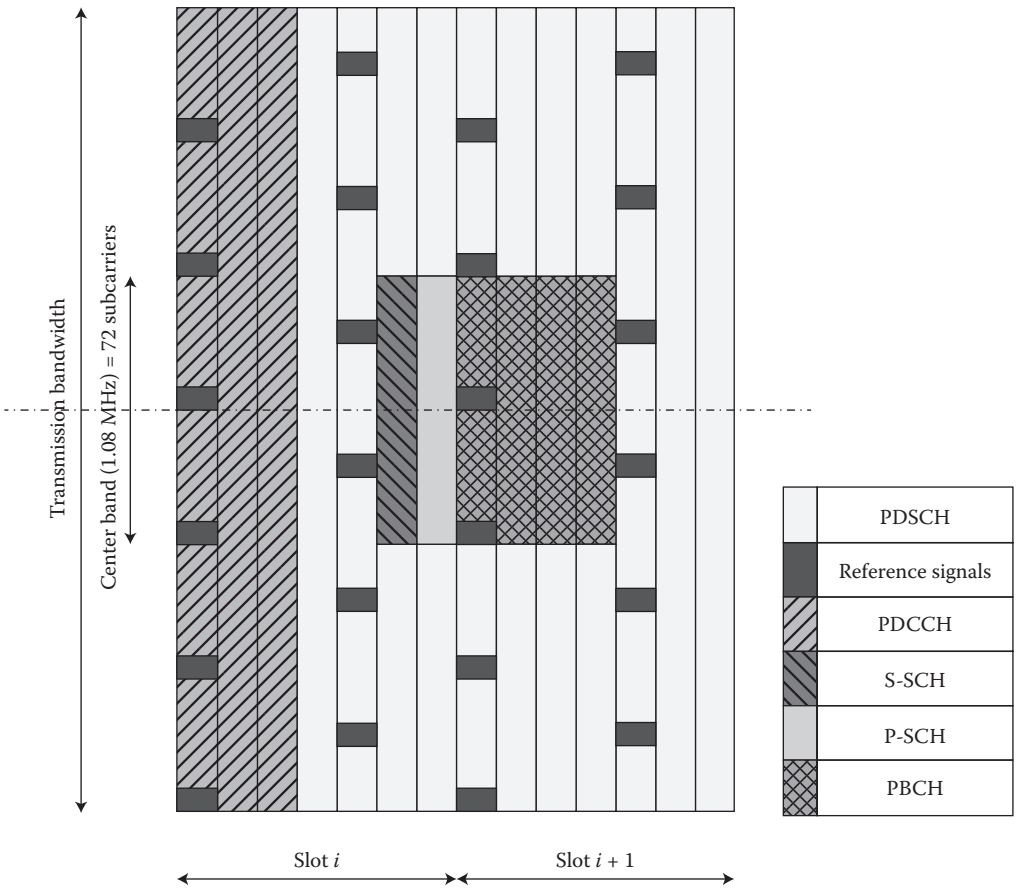

FIGURE 24.11 Structure of physical downlink control channel for frame structure Type 1. (Note that the density of the cell-specific reference signals is to not to scale in this figure.)

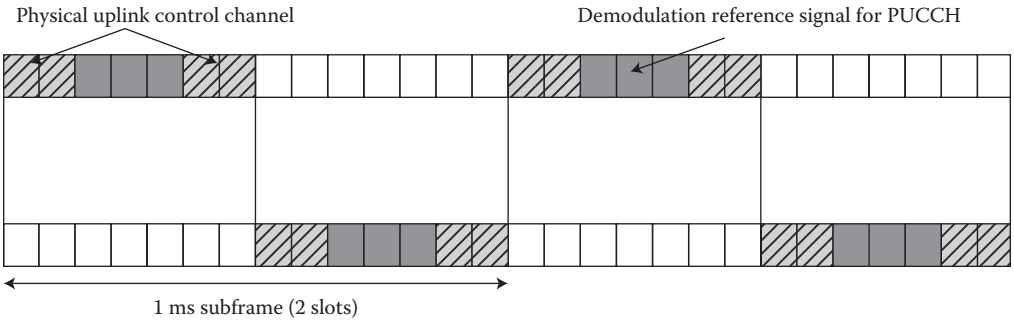

FIGURE 24.12 Structure of physical uplink control channel for frame structure type 1 and PUCCH format 1, 1a, and 1b.

modulation and coding scheme, and HARQ operation. As mentioned earlier, the information fields in the downlink scheduling grant are used to convey the information needed to demodulate the downlink shared channel. They include resource allocation information such as resource block size and duration of assignment, transmission format such as multiantenna mode, modulation scheme, payload size, and HARQ operational parameters such as process number, redundancy version, and new data indicator. Similar information is also included in the uplink scheduling grants.

Control channels are formed by aggregation of Control Channel Elements (CCE), each control channel element consists of a set of resource elements. Different code rates for the control channels are realized by aggregating different numbers of control channel elements. QPSK modulation is used for all control channels. There is an implicit relationship between the uplink resources used for dynamically scheduled data transmission, or the downlink control channel used for assignment, and the downlink ACK/NACK resource used for feedback.

The Physical Uplink Control Channel (PUCCH) is mapped to a control channel resource in the uplink as shown in Figure 24.12. A control channel resource is defined by a code and two resource blocks, consecutive in time, with hopping at the slot boundary. Depending on presence or absence of uplink timing synchronization, the uplink physical control signaling can differ. In the case of time synchronization being present, the out-of-band control signaling consists of CQI, ACK/NACK, and Scheduling Request (SR). Note that a UE only uses PUCCH when it does not have any data to transmit on PUSCH. If a UE has data to transmit on PUSCH, it would multiplex the control information with data on PUSCH.

By use of uplink frequency hopping on PUSCH, frequency diversity effects can be exploited and interference can be averaged. The UE derives the uplink resource allocation as well as frequency hopping information from the uplink scheduling grant. The downlink control information format 0 is used on PDCCH to convey the uplink scheduling grant. 3GPP LTE supports both intrasubframe and intersubframe frequency hopping. The hopping pattern is configured per cell by higher layers. In intrasubframe hopping, the UE hops to another frequency allocation from one slot to another within one subframe. In intersubframe hopping, the frequency resource allocation changes from one subframe to another.

The CQI reports are provided to the scheduler by the UE, measuring the current channel conditions. If MIMO transmission is used, the CQI includes necessary MIMO-related feedback.

The HARQ feedback in response to downlink data transmission consists of a single ACK/NACK bit per HARQ process. The PUCCH resources for SR and CQI reporting are assigned and can be revoked through RRC signaling. An SR is not necessarily assigned to UEs acquiring synchronization through the RACH (i.e., synchronized UEs may or may not have a dedicated SR channel). The PUCCH resources for SR and CQI are lost when the UE is no longer synchronized.

In 3GPP LTE, uplink control signaling includes ACK/NACK, CQI, scheduling request indicator, and MIMO feedback. When users have simultaneous uplink data and control transmission, control signaling is multiplexed with data prior to the DFT to preserve the single-carrier property in uplink

transmission. In the absence of uplink data transmission, this control signaling is transmitted in a reserved frequency region on the band edge as shown in Figure 24.12. Note that additional control regions may be defined as needed. Allocation of control channels with their small occupied bandwidth to band edge resource blocks reduces out-of-band emissions caused by data resource allocations on innerband resource blocks and maximizes the frequency diversity for control channel allocations while preserving the single-carrier property of the uplink waveform.

24.4.9 Physical Random Access Channel

The physical layer random access preamble, illustrated in Figure 24.13 consists of a cyclic prefix of length T_{CP} and a sequence part of length T_{SEQ}. There are five random access preamble formats specified by the standard [10] where the parameter values depend on the frame structure and the random access configuration. The preamble format is configured through higher-layer signaling. Each random access preamble occupies a bandwidth corresponding to 6 consecutive resource blocks for both frame structures. The transmission of a random access preamble, if triggered by the MAC sublayer, is restricted to certain time and frequency resources. These resources are enumerated in increasing order of the subframe number within the radio frame and the physical resource blocks in the frequency domain such that index zero corresponds to the lowest numbered physical resource block and subframe within the radio frame.

The random access preambles are generated from Zadoff–Chu sequences with zero correlation zone. The network configures the set of preamble sequences the UE is allowed to use. There are 64 preambles available in each cell. The set of 64 preamble sequences in a cell is found by including first, in the order of increasing cyclic shift, all the available cyclic shifts of a root Zadoff–Chu sequence with the logical index RACH_ROOT_SEQUENCE, where RACH_ROOT_SEQUENCE is broadcasted as part of the System Information [10,15,16].

The random access procedure in 3GPP LTE consists of 4 steps. In step 1, the preamble is sent by UE. The time/frequency resource where the preamble is sent is associated with a Random Access Radio Network Temporary Identifier (RA-RNTI). In step 2, a random access response is generated by eNB and is sent on the downlink shared channel. It is addressed to the UE using the temporary identifier and contains a timing advance value, an uplink grant, and a temporary identifier. Note that eNB may generate multiple random access responses for different UEs which can be concatenated inside one MAC protocol data unit. The preamble identifier is contained in the MAC subheader of each random access response so that the UE can detect whether a random access response for the used preamble exists. In Step 3, UE will send an RRC CONNECTION REQUEST message on the uplink common control channel, based on the uplink grant received in the previous step. In Step 4, the eNB sends back a MAC PDU containing the uplink CCCH service data unit that was received in Step 3. The message is sent on downlink shared channel and addressed to the UE via the temporary identifier. When the received message matches the one sent in Step 3, the contention resolution is considered successful [13,15,16]; otherwise, the procedure is restarted at Step 1.

Paging is used for setting up network-initiated connection. A power-saving efficient paging procedure should allow the UE to sleep without having to process any information and only to briefly wake up at predefined intervals to monitor paging information (as part of control signaling in the beginning of each subframe) from the network [6,9].

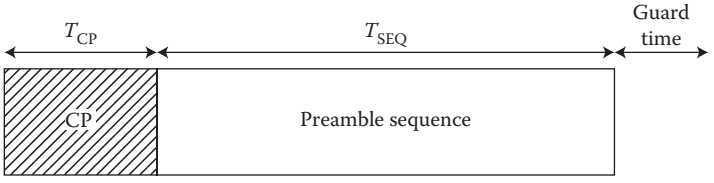

FIGURE 24.13 Random access preamble format.

24.4.10 Cell Selection

Cell search is a procedure performed by a UE to acquire timing and frequency synchronization with a cell and to detect the cell ID of that cell. 3GPP LTE uses a hierarchical cell search scheme similar to WCDMA. As shown in Figure 24.14, the E-UTRA cell search is based on successful acquisition of the following downlink signals: (1) the primary and secondary synchronization signals that are transmitted twice per radio frame, and (2) the downlink reference signals as well as based on the broadcast channel that carries system information such as system bandwidth, number of transmit antennas, and system frame number. The 504 available physical layer cell identities are grouped into 168 physical layer cell identity groups, each group containing 3 unique identities. The secondary synchronization signal carries the physical layer cell identity group, and the primary synchronization signal carries the physical layer identity 0, 1, or 2 [6].

As shown in Figure 24.11, the primary synchronization signal is transmitted on the 6th symbol of slots 0 and 10 of each Type 1 radio frame; it occupies 62 subcarriers, centered on the DC subcarrier. The primary synchronization signal is generated from a frequency-domain Zadoff–Chu sequence. The secondary synchronization signal is transmitted on the 5th symbol of slots 0 and 10 of each radio frame. It occupies 62 subcarriers centered on the DC sub-carrier. The second synchronization signal is an interleaved concatenation of two length-31 M-sequences. The concatenated sequence is scrambled with a scrambling sequence given by the primary synchronization signal [15,16].

As shown in Figure 24.11, PBCH is transmitted on OFDM symbols 0–3 of slot 1 and occupies 72 subcarriers centered on the DC subcarrier. The coded BCH transport block is mapped to 4 subframes within a 40 ms interval. The 40 ms timing is blindly detected; that is, there is no explicit signaling to indicate 40 ms timing [6,15,16]. These channels are contained within the central 1.08 MHz (corresponding to 6 resource blocks or 72 subcarriers) frequency band so that the system operation can be independent of the channel bandwidth.

24.4.11 Link Adaptation

Uplink link adaptation is used in order to improve data throughput in a fading channel. This technique varies the downlink modulation and coding scheme based on the channel conditions of each user. Different types of link adaptation are performed according to the channel conditions, the UE capability (such as the maximum transmission power, maximum transmission bandwidth, etc.), and the required QoS (such as the data rate, latency, and packet error rate, etc.). These link adaptation methods are as follows: (1) adaptive transmission bandwidth, (2) transmission power control, and (3) adaptive modulation and coding [6].

24.4.12 Multi-Antenna Schemes in 3GPP LTE/LTE-Advanced

For the 3GPP LTE Release 8/9 downlink, the 2×2 MIMO configuration is assumed to be the baseline; that is, two transmit antennas at the base station and two receive antennas at the terminal side [10,6,15,16]. Configurations with 4 transmit/receive antennas are also supported in the specification. Different downlink MIMO modes are supported in 3GPP LTE, which can be adapted based on channel condition, traffic requirements, and the UE capability. Those include Transmit diversity, Open-loop spatial multiplexing (no UE feedback), Closed-loop spatial multiplexing (with UE feedback), Multiuser MIMO (more than one UE is assigned to the same resource block), and Closed-loop rank-1 precoding.

In 3GPP LTE spatial multiplexing, up to two codewords can be mapped to different layers. Each codeword represents an output from the channel coder. The number of layers available for transmission is equal to the rank of the channel matrix. Precoding in transmitter side is used to support spatial multiplexing. This is achieved by multiplying the signal with a precoding matrix prior to transmission. The optimum precoding matrix is selected from a predefined codebook which is known to both eNB and UE. The optimum precoding matrix is the one which maximizes the capacity.

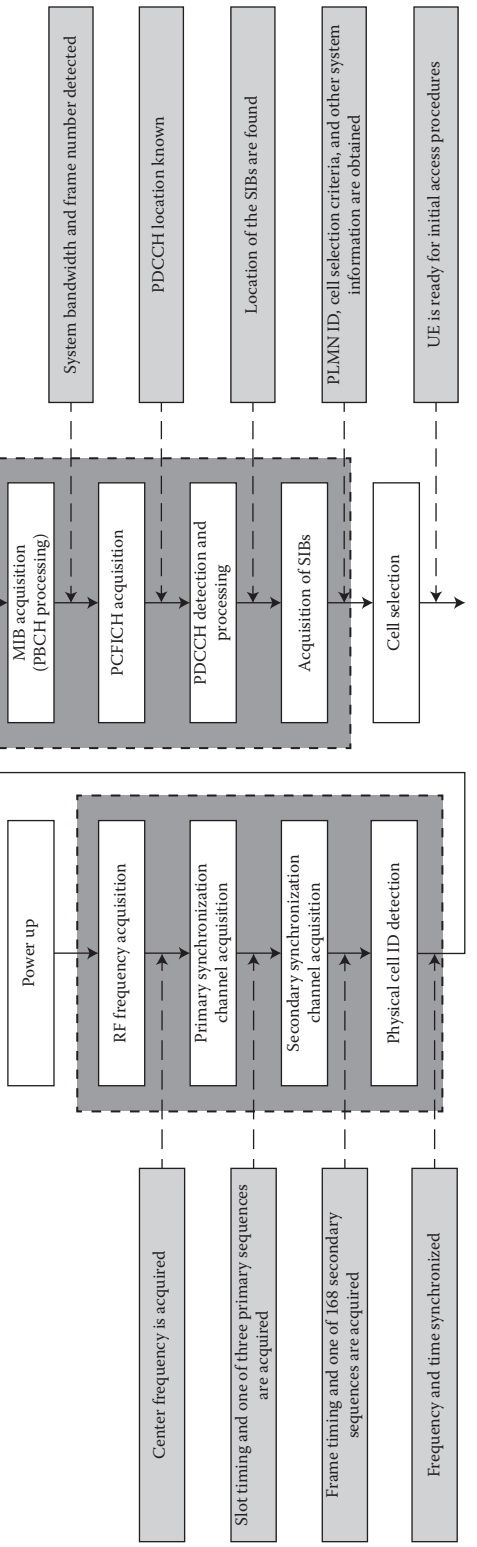

FIGURE 24.14 Cell selection procedure in 3GPP LTE.

The UE estimates the channel and selects the optimum precoding matrix. This feedback is provided to the eNB. Depending on the available bandwidth, this information is made available per resource block or group of resource blocks, since the optimum precoding matrix may vary between resource blocks. The network may configure a subset of the codebook that the UE is able to select from. In the case of UEs with high velocity, the quality of the feedback may deteriorate. Thus, an open-loop spatial multiplexing mode is also supported which is based on predefined settings for spatial multiplexing and precoding. In the case of 4 antenna ports, different precoders are cyclically assigned to the resource elements. The eNB will select the optimum MIMO mode and precoding configuration. The information is conveyed to the UE as part of the downlink control information on PDCCH.

In order for MIMO schemes to work properly, each UE has to report information about the channel to the base station. Several measurement and reporting schemes are available which are selected according to MIMO mode and network preference. The reporting may include wideband or narrowband CQI which is an indication of the downlink radio channel quality as experienced by this UE, Precoding Matrix Index (PMI) which is an indication of the optimum precoding matrix to be used in the base station for a given radio condition, and Rank Indication (RI) which is the number of useful transmission layers when spatial multiplexing is used [10,15,16].

In the case of transmit diversity mode, only one codeword can be transmitted. Each antenna transmits the same information stream, but with different coding. 3GPP LTE employs SFBC as transmit diversity scheme. A special precoding matrix is applied at the transmitter side in the precoding stage in Figure 24.9.

Cyclic Delay Diversity (CDD) is an additional type of diversity which can be used in conjunction with spatial multiplexing in 3GPP LTE. An antenna-specific delay is applied to the signals transmitted from each antenna port. This effectively introduces artificial multipath to the signal as seen by the receiver. As a special method of delay diversity, cyclic delay diversity applies a cyclic shift to the signals transmitted from each antenna port [10].

For the 3GPP LTE Release 8/9 uplink, MU-MIMO can be used. Multiple user terminals may transmit simultaneously on the same resource block. The scheme requires only one transmit antenna at UE side. The UEs sharing the same resource block have to apply mutually orthogonal pilot patterns. To take advantage of two or more transmit antennas, transmit antenna selection can be used. In this case, the UE has two transmit antennas but only one transmission chain. A switch will then choose the antenna that provides the best channel to the eNB [15,16].

3GPP LTE-Advanced extends the MIMO capabilities of 3GPP LTE Release 8/9 by supporting up to 8 downlink transmit-antennas and up to 4 uplink transmit-antennas. In addition to legacy MIMO transmission schemes, transmit diversity is possible in both downlink and uplink directions. In the downlink, using single-user spatial multiplexing scenario of 3GPP LTE-Advanced, up to two transport blocks can be transmitted to a scheduled UE in one subframe per downlink component carrier. Each transport block is assigned its own modulation and coding scheme. For HARQ ACK/NACK feedback on uplink, one bit is used for each transport block [10]. In addition to the spatial multiplexing scheme, the 3GPP LTE-Advanced downlink reference signal structure has been modified to allow an increased number of antennas and PDSCH demodulation as well as channel-state information estimation for the purpose of CQI/PMI/RI reporting when needed.

The reference signals for PDSCH demodulation are UE specific; that is, the PDSCH and the demodulation reference signals intended for a specific UE are subject to the same precoding operation. Therefore, these reference signals are mutually orthogonal between the layers at the eNB.

The design principle for the reference signals targeting PDSCH modulation is an extension of the concept of Release 8 UE-specific reference signals to multiple layers. Reference signals targeting CSI estimation are cell specific, are sparse in the frequency and time domain and are punctured into the data region of normal subframes.

With 3GPP LTE-Advanced, a scheduled UE may transmit up to two transport blocks. Each transport block has its own modulation and coding scheme. Depending on the number of transmission layers, the modulation symbols associated with each of the transport blocks are mapped to one or two layers. The

transmission rank can be dynamically adapted. Different codebooks are defined depending on the number of layers that are used. Furthermore, different precoding is used depending on whether 2 or 4 transmit antennas are available. Also the number of bits used for the codebook index is different depending on the 2 and 4 transmit antenna case, respectively.

For uplink spatial multiplexing with two transmit-antennas, a 3-bit precoding method is defined. In contrast to the Release 8 downlink scheme, where several matrices for full-rank transmission are available, only the identity precoding matrix is supported in 3GPP LTE-Advanced uplink direction. 3GPP LTE-Advanced further supports transmit diversity in the uplink. However, for those UEs with multiple transmit antennas, an uplink single-antenna-port mode is defined. In this mode, the Release 10 UE behavior is the same as the one with a single antenna from eNB's point of view and it is always used before the eNB is aware of the UE antenna configuration. In the transmit diversity scheme, the same modulation symbol from the uplink channel is transmitted from two antenna ports, on two separate orthogonal resources.

24.5 Overview of the 3GPP LTE/LTE-Advanced Layer-2

The Layer-2 functions in 3GPP LTE/LTE-Advanced are classified into MAC, RLC, and PDCP sublayers [6,17,18,9,8]. Figures 24.15 and 24.16 illustrate the structure of Layer-2 in 3GPP LTE/LTE-Advanced downlink and uplink. The Service Access Point (SAP) for peer-to-peer communication is marked with circles at the interface between the sublayers. The SAP between the physical layer and the MAC sublayer provides the transport channels. The SAP between the MAC sublayer and the RLC sublayer provides the logical channels. The multiplexing of several logical channels (i.e., radio bearers) on the same transport channel (i.e., transport block) is performed by the MAC sublayer [6].

In the case of carrier aggregation, the multicarrier nature of the physical layer is only exposed to the MAC sublayer for which one HARQ entity is required per serving cell. In both uplink and downlink, there is one independent HARQ entity per serving cell and one transport block is generated per TTI per serving cell in the absence of spatial multiplexing. Each transport block and the associated HARQ retransmissions are mapped to a single serving cell.

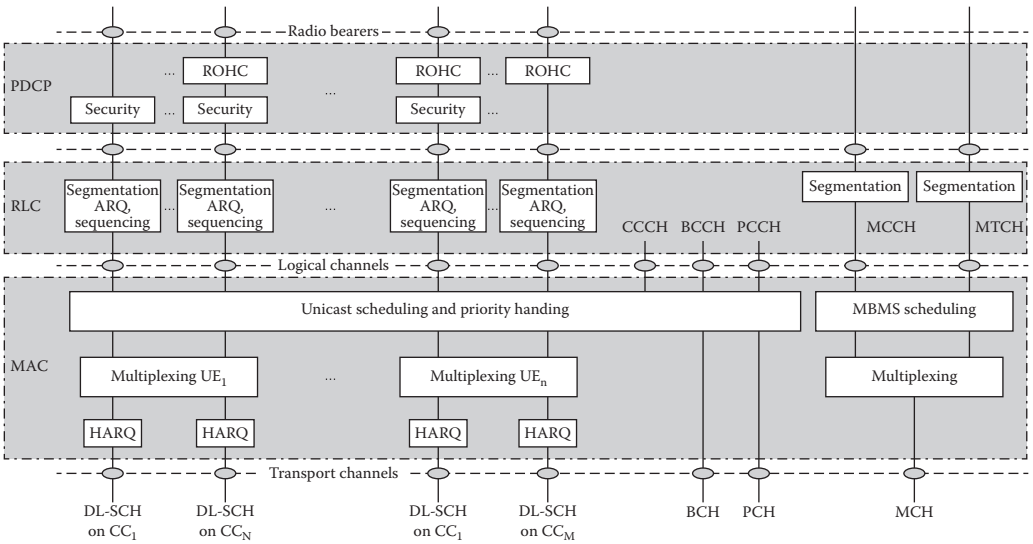

FIGURE 24.15 3GPP LTE/LTE-advanced layer-2 structure in the downlink. (Adapted from 3GPP TS 36.300, Evolved Universal Terrestrial Radio Access (E-UTRA) and Evolved Universal Terrestrial Radio Access Network (E-UTRAN); Overall Description; Stage 2, December 2010.)

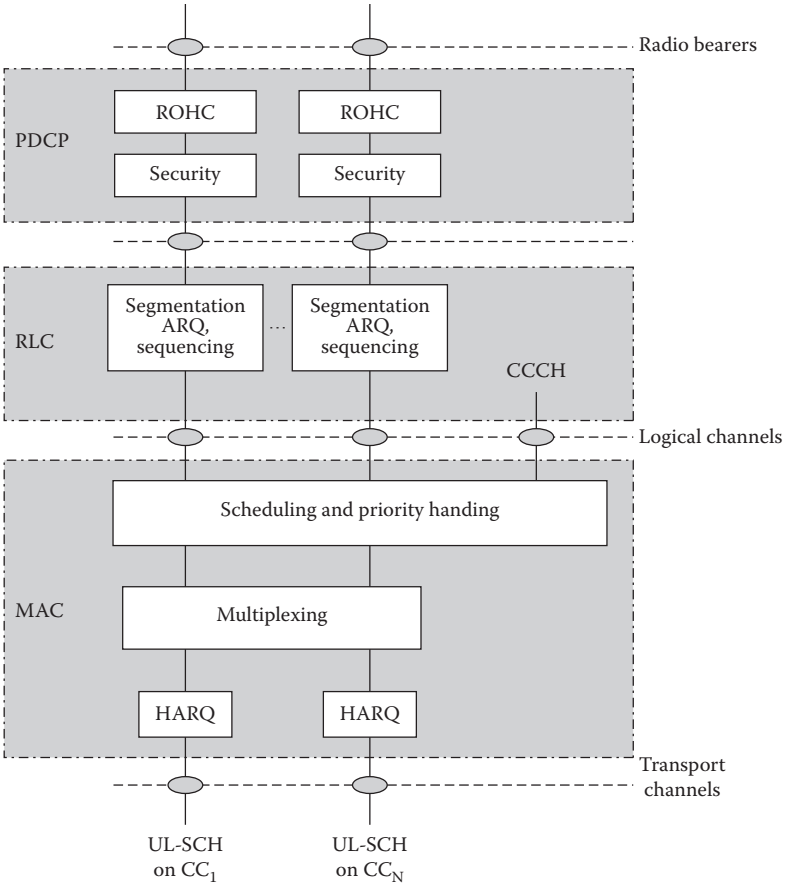

FIGURE 24.16 3GPP LTE/LTE-advanced layer-2 structure in the uplink. (Adapted from 3GPP TS 36.300, Evolved Universal Terrestrial Radio Access (E-UTRA) and Evolved Universal Terrestrial Radio Access Network (E-UTRAN); Overall Description; Stage 2, December 2010.)

The services and functions provided by the MAC sublayer can be summarized as follows:

- Mapping between logical channels and transport channels;
- Multiplexing/de-multiplexing of RLC protocol data units corresponding to one or different radio bearers into/from transport blocks delivered to/from the physical layer on transport channels;
- Traffic volume measurement reporting;
- Error correction through HARQ;
- Priority handling between logical channels of one UE;
- Priority handling between UEs through dynamic scheduling;
- Transport format selection;

24.5.1 Logical and Transport Channels

The logical and transport channels in 3GPP LTE/LTE-Advanced are illustrated in Figures 24.17 and 24.18, respectively. Each logical channel type is defined by what type of information is transferred. The logical channels are generally classified into two groups: (1) Control Channels (for the transfer of control-plane information) and (2) Traffic Channels (for the transfer of user-plane information) as shown in Figure 24.17 [6].

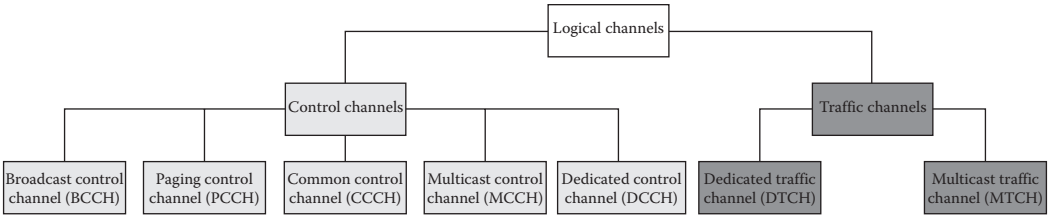

FIGURE 24.17 Classification of 3GPP LTE logical channels. (Adapted from 3GPP TS 36.300, Evolved Universal Terrestrial Radio Access (E-UTRA) and Evolved Universal Terrestrial Radio Access Network (E-UTRAN); Overall Description; Stage 2, December 2010.)

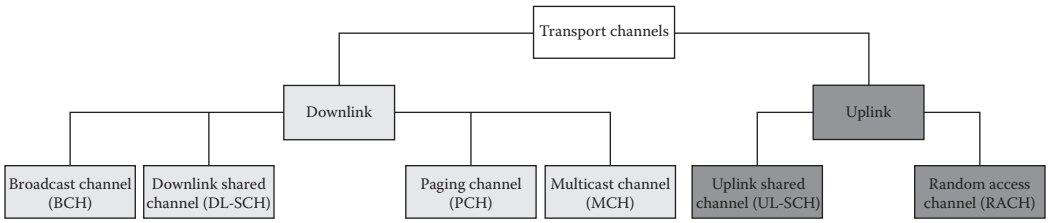

FIGURE 24.18 Classification of 3GPP LTE transport channels. (Adapted from 3GPP TS 36.300, Evolved Universal Terrestrial Radio Access (E-UTRA) and Evolved Universal Terrestrial Radio Access Network (E-UTRAN); Overall Description; Stage 2, December 2010.)

The control channels are exclusively used for transfer of control-plane information. The control channels supported by MAC can be classified as follows (see Figure 24.17):

- Broadcast Control Channel (BCCH): A downlink channel for broadcasting system control information.
- Paging Control Channel (PCCH): A downlink channel that transfers paging information and system information change notifications. This channel is used for paging when the network does not know the location of the UE.
- Common Control Channel (CCCH): Channel for transmitting control information between UEs and eNBs. This channel is used for UEs having no RRC connection with the network.
- Multicast Control Channel (MCCH): A point-to-multipoint downlink channel used for transmitting MBMS control information from the network to the UE, for one or several MTCHs. This channel is only used by UEs that receive MBMS.
- Dedicated Control Channel (DCCH): A point-to-point bidirectional channel that transmits dedicated control information between a UE and the network. It is used by UEs that have an RRC connection.

The traffic channels are exclusively used for the transfer of user-plane information. The traffic channels supported by MAC can be classified as follows (as shown in Figure 24.18):

- Dedicated Traffic Channel (DTCH): A point-to-point bidirectional channel dedicated to a single UE for the transfer of user information.
- Multicast Traffic Channel (MTCH): A point-to-multipoint downlink channel for transmitting traffic data from the network to the UE. This channel is only used by UEs that receive MBMS.

The physical layer provides information transfer services to MAC and higher layers. The physical layer transport services are described by how and with what characteristics data are transferred over the radio interface. This should be clearly separated from the classification of what is transported, which

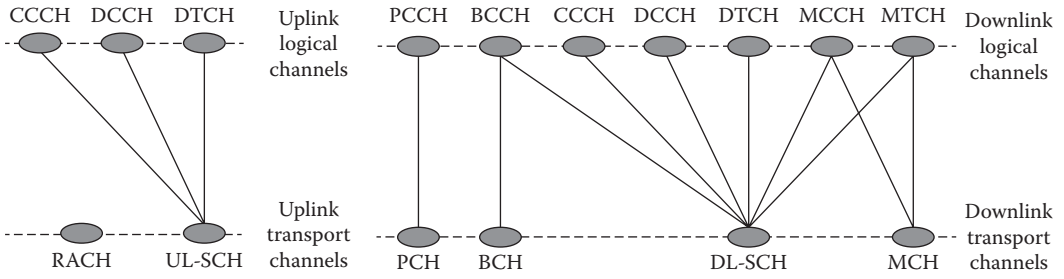

FIGURE 24.19 Mapping of logical to transport channels in the downlink and uplink. (Adapted from 3GPP TS 36.300, Evolved Universal Terrestrial Radio Access (E-UTRA) and Evolved Universal Terrestrial Radio Access Network (E-UTRAN); Overall Description; Stage 2, December 2010.)

relates to the concept of logical channels at MAC sublayer. As shown in Figure 24.18, downlink transport channels can be classified as follows:

- Broadcast Channel (BCH) that is characterized by fixed, predefined transport format and is required to be broadcasted in the entire coverage area of the cell.
- Downlink Shared Channel (DL-SCH) that is characterized by support for HARQ, support for dynamic link adaptation by varying the modulation, coding and transmit power, possibility for broadcast in the entire cell, possibility to use beamforming, support for both dynamic and semi-static resource allocation, support for UE discontinuous reception to enable power saving, and support for MBMS transmission.
- Paging Channel (PCH) that is characterized by support for UE discontinuous reception in order to enable power saving, requirement for broadcast in the entire coverage area of the cell, mapped to physical resources which can be used dynamically also for traffic or other control channels.
- Multicast Channel (MCH) which is characterized by requirement to be broadcast in the entire coverage area of the cell, support for macro-diversity combining of MBMS transmission on multiple cells, support for semi-static resource allocation.

The uplink transport channels are classified as follows (see Figure 24.18):

- Uplink Shared Channel (UL-SCH) which is characterized by possibility to use beamforming, support for dynamic link adaptation by varying the transmit power and modulation and coding schemes, support for HARQ, support for both dynamic and semi-static resource allocation.
- Random Access Channel (RACH) that is characterized by limited control information and collision risk.

The mapping of the logical channels to the transport channels in the downlink and uplink is shown in Figure 24.19.

As shown in Figures 24.15 and 24.16, the main services and functions provided by the RLC sublayer include Transfer of upper layer PDUs supporting AM or UM, TM data transfer, Error correction through ARQ (since CRC check is provided by the physical layer, no CRC is needed at RLC level), Segmentation according to the size of the transport block, Re-segmentation of PDUs that need to be retransmitted, Concatenation of SDUs for the same radio bearer, In-sequence delivery of upper layer PDUs except during handover, Duplicate detection, and Protocol error detection and recovery.

24.5.1.1 ARQ and HARQ in 3GPP LTE/LTE-Advanced

The E-UTRA provides ARQ and HARQ functionalities. The ARQ functionality provides error correction by retransmissions in acknowledged mode at Layer-2. The HARQ functionality ensures delivery between peer entities at Layer-1. The HARQ within the MAC sublayer is characterized by an N-process

stop-and-wait protocol and retransmission of transport blocks upon failure of earlier transmissions. The ACK/NACK transmission in the FDD mode refers to the downlink packet that was received 4 subframes earlier. In TDD mode, the uplink ACK/NACK timing depends on the uplink/downlink configuration. For TDD, the use of a single ACK/NACK response for multiple PDSCH transmissions is possible. A total of 8 HARQ processes are supported [6,15,16].

An asynchronous adaptive HARQ is used in the downlink. The uplink ACK/NACK signaling in response to downlink retransmissions is sent on PUCCH or PUSCH. The PDCCH signals the HARQ process number and whether it is a fresh transmission or retransmission. The retransmissions are always scheduled through PDCCH.

A synchronous HARQ scheme is supported in the uplink. The maximum number of retransmissions can be configured per UE basis as opposed to per radio bearer. The downlink ACK/NACK signaling in response to uplink retransmissions is sent on PHICH.

The ARQ functionality within the RLC sub-layer is responsible for retransmission of RLC PDUs or RLC PDU segments. The ARQ retransmissions are based on RLC status reports and optionally based on HARQ/ARQ interactions. The polling for RLC status report is used when needed by RLC and status reports can be triggered by upper layers [6].

24.5.1.2 Packet Data Convergence Sublayer

Services and functions provided by the PDCP sublayer for the user plane include header compression and decompression, transfer of user data between NAS and RLC sublayer, sequential delivery of upper-layer PDUs at handover for RLC AM, duplicate detection of lower layer SDUs at handover for RLC AM, retransmission of PDCP SDUs at handover for RLC AM, and ciphering.

Services and functions provided by the PDCP for the control-plane include ciphering and integrity protection and transfer of control-plane data where PDCP receives PDCP SDUs from RRC and forward it to the RLC sublayer and vice versa.

24.6 Radio Resource Control Functions

The main services and functions of the RRC sublayer include [6]

- Broadcast of system information
- Paging
- Establishment, maintenance, and release of a RRC connection between the UE and E-UTRAN including allocation of temporary identifiers between UE and E-UTRAN and configuration of signaling radio bearer(s) for RRC connection
- Security functions including key management
- Establishment, configuration, maintenance, and release of point-to-point radio bearers
- Mobility functions including UE measurement reporting and control of the reporting for intercell and inter-RAT mobility, handover, UE cell selection and reselection and control of cell selection and reselection, context transfer at handover.
- Establishment, configuration, maintenance, and release of radio bearers for MBMS services
- QoS management functions
- UE measurement reporting and control of the reporting

The RRC consists of the following states:

- RRC_IDLE is a state where a UE-specific Discontinuous Reception (DRX) may be configured by upper layers. In the idle mode, the UE is saving power and does not inform the network of each cell change. The network knows the location of the UE to the granularity of a few cells, called the Tracking Area (TA). The UE monitors a paging channel to detect incoming traffic, performs neighboring cell measurements and cell selection/reselection, and acquires system information.

TABLE 24.5 Summary of the Differences between MAC and RRC Control

	MAC Control		RRC Control
Control Entity	MAC		RRC
Signaling type	PDCCH	MAC Control PDU	RRC message
Signaling reliability	~10^{-2} (no retransmission)	~10^{-3} (after HARQ)	~10^{-6} (after ARQ)
Control latency	Very short	Short	Longer
Extensibility	None	Limited	High
Security	No integrity protection no ciphering	No integrity protection no ciphering	Integrity protected ciphering

Source: Adapted from 3GPP TS 36.300, Evolved Universal Terrestrial Radio Access (E-UTRA) and Evolved Universal Terrestrial Radio Access Network (E-UTRAN); Overall Description; Stage 2, December 2010.

- RRC_CONNECTED is a state where transfer of unicast data to/from UE is performed and the UE may be configured with a UE specific DRX or Discontinuous Transmission (DTX). The UE monitors control channels associated with the shared data channel to determine if data is scheduled for it, sends channel quality and feedback information, performs neighboring cell measurements and measurement reporting, and acquires system information.

The main difference between MAC and RRC control lies in the signaling reliability. The signaling corresponding to state transitions and radio bearer configurations should be performed by the RRC sublayer due to signaling reliability. The different characteristics of MAC and RRC control are summarized in Table 24.5.

24.7 Mobility Management and Handover in 3GPP LTE/LTE-Advanced

In order to support mobility, a 3GPP LTE-compliant UE may conduct the following measurements (physical layer measurements include Reference Signal Received Power and E-UTRA carrier Received Signal Strength Indicator [6]):

- Intrafrequency E-UTRAN measurements
- Interfrequency E-UTRAN measurements
- Inter-RAT measurements

Measurement commands are used by E-UTRAN to instruct the UE to start measurements, modify measurements or stop measurements. The reporting criteria that are used include event-triggered reporting, periodic reporting, and event-triggered periodic reporting.

In RRC_CONNECTED state, network-controlled UE-assisted handovers are performed and various DRX cycles are supported. In RRC_IDLE state, cell reselections are performed and DRX is supported.

The Intra-E-UTRAN-Access mobility support for UEs in Evolved Packet System (EPS) Connection Management (ECM-CONNECTED) manages all necessary steps for relocation or handover procedures, such as processes that precede the final handover decision on the serving network, preparation of resources on the target network, commanding the UE to the new radio resources, and finally releasing resources on the serving network side. It contains mechanisms to transfer context data between eNBs and to update node relations on control plane and user plane. The UE makes measurements of attributes of the serving and neighbor cells to enable the process [6]. Depending on whether the UE needs transmission/reception gaps to perform the relevant measurements, measurements are classified as gap assisted or nongap assisted. A nongap-assisted measurement is a measurement on a cell that does not require transmission/reception gaps to allow the measurement to be performed. A gap-assisted measurement is a measurement on a cell that does require transmission/reception gaps to allow the measurement to be performed. Gap patterns are configured and activated by the RRC functional block [6].

The handover procedure is performed without EPC involvement; that is, preparation messages are directly exchanged between the eNBs. The release of the resources at the serving eNB (or source eNB) during the handover completion phase is triggered by the eNB. Figure 24.20 illustrates the handover procedure between eNBs within the same MME/S-GW. After the downlink path is switched at the S-GW, downlink packets on the forwarding path and on the new direct path may arrive interchanged at the target eNB (see Figure 24.20). The target eNB should first deliver all forwarded packets to the UE before delivering any of the packets received on the new direct path. Upon handover, the serving eNB forward in an orderly manner all downlink PDCP SDUs that have not been acknowledged by the UE to the target eNB. The serving eNB discards any remaining downlink RLC PDUs. Correspondingly, the source eNB does not forward the downlink RLC context to the target eNB.

The measurements to be performed by a UE for intra/interfrequency mobility can be controlled by E-UTRAN, using broadcast or dedicated control signaling. In RRC_IDLE state, a UE follows the measurement parameters defined for cell reselection. In RRC_CONNECTED state, a UE follows the measurement

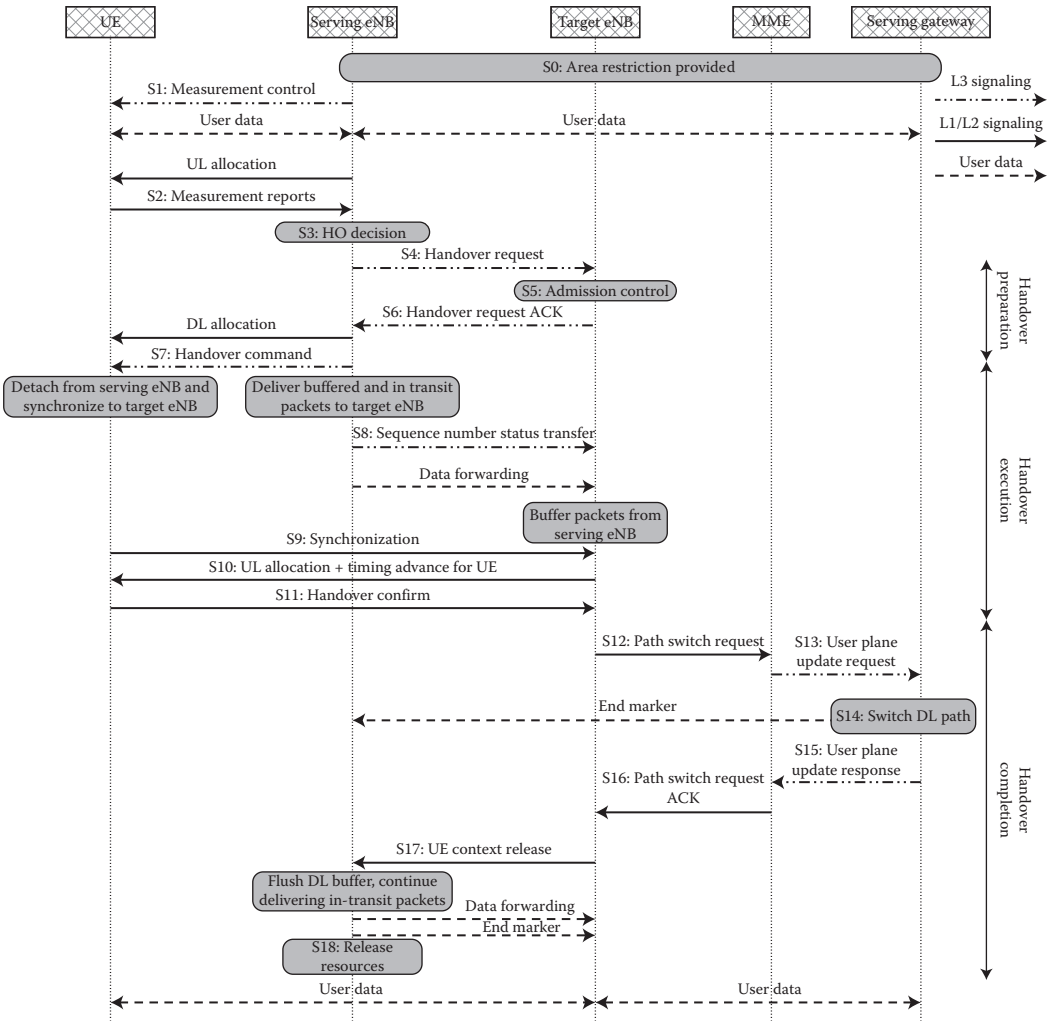

FIGURE 24.20 Intra-MME/S-GW handover procedures. (Adapted from 3GPP TS 36.300, Evolved Universal Terrestrial Radio Access (E-UTRA) and Evolved Universal Terrestrial Radio Access Network (E-UTRAN); Overall Description; Stage 2, December 2010.)

configurations specified by RRC managed by the E-UTRAN. The neighbor cell measurements performed by the UE are intrafrequency measurements when the current and target cell operate on the same carrier frequency. The neighbor cell measurements performed by the UE are interfrequency measurements when the neighbor cell operates on a different carrier frequency compared to the current cell.

24.8 Multicarrier Operation

When carrier aggregation is configured, the UE only has one RRC connection with the network. At RRC connection establishment/reestablishment/handover, one serving cell provides the NAS mobility information, and at RRC connection re-establishment/handover, one serving cell provides the security input. This cell is referred to as the Primary Cell (PCell). In the downlink, the carrier corresponding to the PCell is the downlink primary component carrier, while in the uplink it is the uplink primary component carrier. Depending on UE capabilities, Secondary Cells (SCells) can be configured to form, together with the PCell, a set of serving cells. In the downlink, the carrier corresponding to a SCell is a downlink secondary component carrier, while in the uplink it is an uplink secondary component carrier. The configured set of serving cells for a UE always consist of one PCell and one or more SCells. For each SCell the usage of uplink resources by the UE in addition to the downlink ones is configurable. From the UE point of view, each uplink resource only belongs to one serving cell. The number of serving cells that can be configured depends on the aggregation capability of the UE. The PCell can only be changed with handover procedure (i.e., with security key change and RACH procedure). The PCell is used for transmission of PUCCH and unlike SCells, PCell cannot be deactivated. The reestablishment is triggered only when PCell experiences a radio link failure and not when SCells experience radio link failure. The NAS information is obtained from PCell. The reconfiguration, addition, and removal of SCells can be performed by RRC signaling. In intra-LTE handover, RRC can also add, remove, or reconfigure SCells for usage with the target PCell. When adding a new SCell, dedicated RRC signaling is used for sending all required system information of the SCell; that is, while in connected mode, UEs do not need to acquire broadcasted system information directly from the SCells.

References

1. 3GPP TS 25.913, Requirements for Evolved UTRA (E-UTRA) and Evolved UTRAN (E-UTRAN), March 2006.
2. 3GPP TR 36.913, Requirements for Further Advancements for E-UTRA (LTE-Advanced), June 2008.
3. 3GPP TR 36.814, Further Advancements for E-UTRA Physical Layer Aspects, March 2010.
4. 3GPP TR 36.912, Further Advancements for E-UTRA (LTE-Advanced), June 2010.
5. ITU Global Standard for International Mobile Telecommunications 'IMT-Advanced', http://www.itu.int/ITU-R.
6. 3GPP TS 36.300, Evolved Universal Terrestrial Radio Access (E-UTRA) and Evolved Universal Terrestrial Radio Access Network (E-UTRAN); Overall Description; Stage 2, December 2010.
7. 3GPP TS 36.401, Evolved Universal Terrestrial Radio Access Network (E-UTRAN); Architecture Description, December 2010.
8. 3GPP TS 36.331, Evolved Universal Terrestrial Radio Access (E-UTRA); Radio Resource Control (RRC); Protocol Specification, December 2010.
9. 3GPP TS 36.323, Evolved Universal Terrestrial Radio Access (E-UTRA); Packet Data Convergence Protocol (PDCP) Specification, December 2010.
10. 3GPP TS 36.201, Evolved Universal Terrestrial Radio Access (E-UTRA); Long Term Evolution (LTE) Physical Layer; General description, December 2010.
11. 3GPP TS 36.211, Evolved Universal Terrestrial Radio Access (E-UTRA); Physical Channels and Modulation, December 2010.

12. 3GPP TS 36.212, Evolved Universal Terrestrial Radio Access (E-UTRA); Multiplexing and Channel Coding, December 2010.
13. 3GPP TS 36.213, Evolved Universal Terrestrial Radio Access (E-UTRA); Physical layer Procedures, December 2010.
14. 3GPP TS 36.101, Evolved Universal Terrestrial Radio Access (E-UTRA); User Equipment (UE) Radio Transmission and Reception, January 2011.
15. E. Dahlman et al., *3G Evolution: HSPA and LTE for Mobile Broadband*, 2nd Edition, Academic Press, UK, October 2008.
16. Stefania Sesia, Issam Toufik, Matthew Baker, *LTE, the UMTS Long Term Evolution: From Theory to Practice*, John Wiley & Sons, UK, April 2009.
17. 3GPP TS 36.321, Evolved Universal Terrestrial Radio Access (E-UTRA); Medium Access Control (MAC) Protocol Specification, December 2010.
18. 3GPP TS 36.322, Evolved Universal Terrestrial Radio Access (E-UTRA); Radio Link Control (RLC) Protocol Specification, December 2010.

25

IEEE 802.16m Radio Access Technology

Sassan Ahmadi

25.1 Introduction

The IEEE 802.16 Working Group began the development of a new amendment to the IEEE 802.16 baseline standard in January 2007 as an advanced air interface, in order to materialize the ITU-R vision for the IMT-Advanced systems as laid out in Recommendation ITU-R M.1645 [1]. The requirements for the IEEE 802.16m standard were selected to ensure competitiveness with the emerging 4th-generation radio access technologies, while extending and significantly improving the functionality and efficiency of the legacy system. The areas of improvement and extension included control/signaling mechanisms, overhead reduction, coverage of control and traffic channels at the cell-edge, downlink/uplink link budget, air-link access latency, client power consumption, transmission and detection of control channels, scan latency and network entry/reentry procedures, downlink and uplink subchannelization schemes, MAC management messages, MAC headers, support of the FDD duplex scheme, advanced single-user MIMO (SU-MIMO) and multiuser MIMO (MU-MIMO) techniques, relay, femto-cells, enhanced multicast and broadcast, enhanced location-based services, and self-configuration networks.

The IMT-Advanced requirements defined and approved by ITU-R and published as Report ITU-R M.2134 [2], referred to as target requirements in the IEEE 802.16m system requirement document [3], were evaluated based on the methodology and guidelines specified by Report ITU-R M.2135-1 [4]. The IEEE 802.16m baseline functional and performance requirements were evaluated according to the IEEE 802.16m evaluation methodology document [5]. The IMT-Advanced requirements are a subset of the IEEE 802.16m system requirements, and thus are less stringent than baseline requirements. Since satisfaction of the baseline requirements would imply a minimum-featured system, thus the

minimum-performance implementation of the IEEE 802.16m can meet the IMT-Advanced requirements and can be certified as an IMT-Advanced technology. The candidate proposal submitted by the IEEE to the ITU-R in October 2009 met and exceeded the requirements of IMT-Advanced systems, and subsequently qualified as an IMT-Advanced technology [6].

This chapter describes the prominent functional features of IEEE 802.16m radio access technology including air-interface protocols, control signaling, transmission formats, and physical layer and MAC functional components.

25.2 Mobile WiMAX Network Architecture

The WiMAX Network Architecture Release 1.5 [7] specifies a nonhierarchical end-to-end network reference model (NRM) for mobile WiMAX that can be expanded to further include optional relay entities (specified by IEEE 802.16m standard) for coverage and performance enhancement. It is expected that the future releases of WiMAX network architecture will specify the reference points between the base station (BS) and relay station and between two relay stations in a multihop network.

The NRM is a logical representation of the network architecture. The NRM identifies functional entities and reference points over which interoperability is achieved. Figure 25.1 illustrates the mobile WiMAX network architecture, consisting of the following logical entities: mobile station (MS), access service network (ASN), and connectivity service network (CSN). The interfaces R1–R8 are normative reference points [7]. Each of the MS, ASN, and CSN entities represents a group of functions that can be realized in a single physical entity or may be distributed over multiple physical entities. The reference model is used to ensure interoperability among different implementations of functional entities in the network. Interoperability is verified based on the definition of logical interfaces in order to achieve an end-to-end functionality, for example, security or mobility management. Thus, the functional entities on either side of a reference point represent a collection of control or data-planes end-points. The MS is a communication device providing radio connectivity between a user terminal and a WiMAX BS that

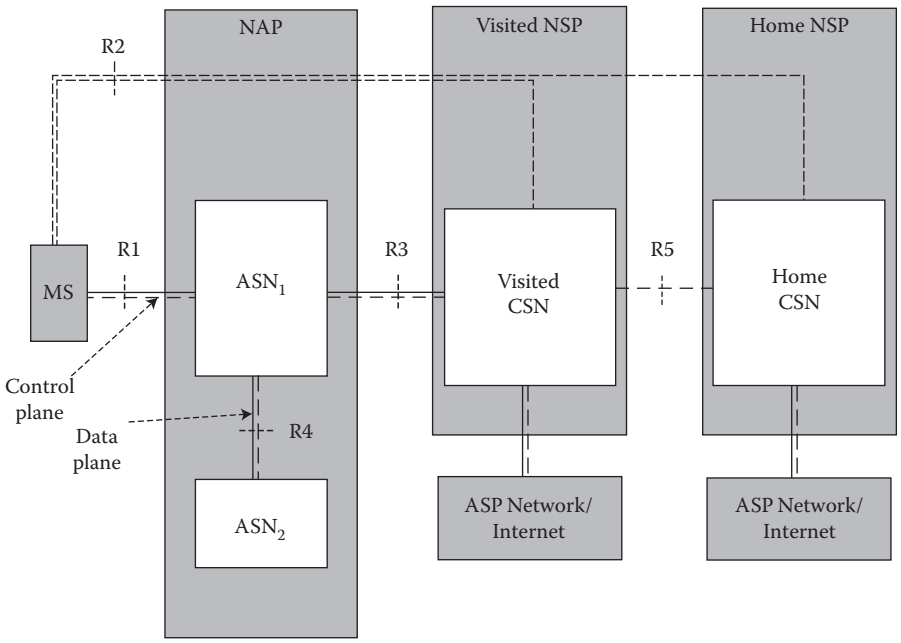

FIGURE 25.1 Mobile WiMAX NRM.

is compliant with WiMAX Forum mobile system profiles [8]. The ASN is defined as a complete set of network functions required to provide radio access to a terminal. The ASN provides the following functions:

- Layer-2 connectivity with the MS.
- Transfer of Authentication, Authorization, and Accounting messages to subscriber's Home network service provider (H-NSP) for authentication, authorization, and session accounting for subscriber sessions.
- Network discovery and selection of the subscriber's preferred NSP.
- Relay functionality for establishing Layer-3 connectivity or IP address assignment to an MS.
- Radio resource management (RRM).

In addition to the above functions and to support mobility, an ASN supports the following functions:

- ASN-anchored mobility
- CSN-anchored mobility
- Paging and Idle State operation
- ASN-CSN tunneling

The ASN comprises network elements such as one or more BSs and one or more ASN Gateways. An ASN may be shared by more than one CSN. The radio resource control functions in the BS would allow RRM within the BS. The CSN is defined as a set of functions that provide IP connectivity to user terminals.

25.3 IEEE 802.16m Protocol Structure

In this section, we further examine the functional elements of each protocol layer and their interactions. The 802.16m MAC common part sublayer functions are classified into radio resource control and management functional group and medium access control functional group. The control-plane functions and data-plane functions are also separately classified. As shown in Figure 25.2, the radio resource control and management functional group comprises several functional blocks including

- RRM block adjusts radio network parameters related to the traffic load, and also includes the functions of load control (load balancing), admission control, and interference control.
- Mobility management block scans neighbor BSs and decides whether MS should perform handover (HO) operation.
- Network-entry management block controls initialization and access procedures and generates management messages during initialization and access procedures.
- Location management block supports Location-Based Service (LBS), generates messages including the LBS information, and manages location update operation during idle mode.
- Idle mode management block controls idle mode operation, and generates the paging advertisement message based on paging message from paging controller in the core network.
- Security management block performs key management for secure communication. Using managed key, traffic encryption/decryption, and authentication are performed.
- System configuration management block manages system configuration parameters, and generates broadcast control messages such as superframe headers.
- Multicast and Broadcast Service (MBS) block controls and generates management messages and data associated with MBS.
- Service flow and connection management block allocates Station Identifier (STID) and Flow Identifiers (FIDs) during access/HO service flow creation procedures.

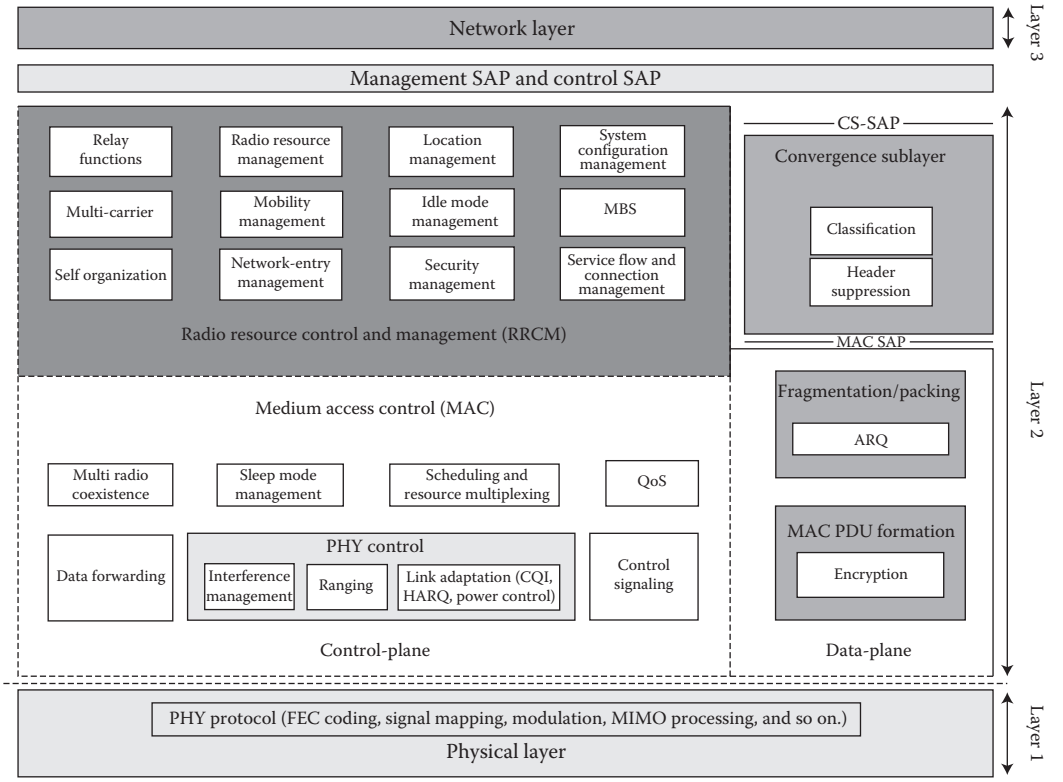

FIGURE 25.2 IEEE 802.16m protocol stack. (Adapted from Sassan Ahmadi, *Mobile WiMAX; A Systems Approach to Understanding IEEE 802.16m Radio Access Technology*, 1st Edition, Academic Press, 2010; IEEE 802.16m-08/0034r4, *IEEE 802.16m System Description Document*, (http://ieee802.org/16/tgm/index.html), December 2010.)

The medium-access control functional group, on the control plane, includes functional blocks which are related to physical layer and link controls such as

- PHY control block performs PHY signaling such as ranging, channel quality measurement/feedback (CQI), and HARQ ACK or NACK signaling
- Control signaling block generates resource allocation messages such as advanced medium access protocol, as well as specific control signaling messages
- Sleep mode management block handles sleep mode operation and generates management messages related to sleep operation, and may communicate with the scheduler block in order to operate properly according to sleep period
- Quality-of-service block performs rate control based on QoS input parameters from connection management function for each connection
- Scheduling and resource multiplexing block schedules and multiplexes packets based on properties of connections

The MAC functional group on the data-plane includes functional blocks such as

- Fragmentation/packing block performs fragmentation or packing of MAC service data units based on input from the scheduling and resource multiplexing block.
- Automatic repeat request (ARQ) block performs MAC ARQ function. For ARQ-enabled connections, a logical ARQ block is generated from fragmented or packed MAC service data units of the same flow and sequentially numbered.

- MAC protocol data unit formation block constructs MAC protocol data units such that BS/MS can transmit user traffic or management messages into PHY channels.

The IEEE 802.16m protocol structure is similar to that of the legacy system with some additional functional blocks in the control-plane for the new features including the following:

- Relay functions enable relay functionalities and packet routing in relay networks.
- Self-organization and self-optimization functions enable home BS or femto-cells and plug and-play form of operation for indoor BS (i.e., femto-cell).
- Multicarrier functions enable control and operation of a number of adjacent or nonadjacent RF carriers (i.e., virtual wideband operation) where the RF carriers can be assigned to unicast and/or MBS s. A single MAC instantiation will be used to control several physical layers. The mobile terminal is not required to support multicarrier operation. However, if it does support multicarrier operation, it may receive control and signaling, broadcast, and synchronization channels through a primary carrier and traffic assignments (or services) via the secondary carriers.
- Multiradio coexistence functions in IEEE 802.16m enable the MS to generate MAC management messages in order to report information on its collocated radio activities, and enable the BS to generate MAC management messages to respond with the appropriate actions to support multiradio coexistence operation. Furthermore, the multiradio coexistence functional block at the BS communicates with the scheduler functional block to assist proper scheduling of the MS according to the reported collocated coexistence activities. The multiradio coexistence function is independent of the sleep mode operation to enable optimal power efficiency with a high level of coexistence support.
- Interference management functions are used to manage the inter-cell/sector interference effects. The procedures include MAC layer functions (e.g., interference measurement/assessment reports sent via MAC signaling and interference mitigation by scheduling and flexible frequency reuse), and PHY functions (e.g., transmit power control, interference randomization, interference cancellation, interference measurement, transmit beamforming/precoding). The inter-BS coordination functions coordinate the operation of multiple BSs by exchanging information, about interference statistics between the BSs via core-network signaling.

The carriers utilized in a multicarrier system, from perspective of a MS can be divided into two categories:

- A primary RF carrier is the carrier that is used by the BS and the MS to exchange traffic and full PHY/MAC control information. The primary carrier delivers control information for proper MS operation, such as network entry. Each MS is assigned only one primary carrier in a cell.
- A secondary RF carrier is an additional carrier which the BS may use for traffic allocations for MSs capable of multicarrier support. The secondary carrier may also include dedicated control signaling to support multicarrier operation.

Based on the primary and/or secondary designation, the carriers of a multicarrier system may be configured differently as follows:

- *Fully configured carrier*: A carrier for which all control channels including synchronization, broadcast, multicast, and unicast control signaling are configured. Furthermore, information and parameters regarding multicarrier operation and the other carriers can also be included in the control channels. A primary carrier is fully configured, while a secondary carrier may be fully or partially configured depending on usage and deployment model.
- *Partially configured carrier*: A carrier with only essential control channel configuration to support traffic exchanges during multicarrier operation.

In the event that the user terminal RF front-end and/or its baseband is not capable of processing more than one RF carrier simultaneously, the user terminal may be allowed, in certain intervals, to monitor

secondary RF carriers and to resume monitoring of the primary carrier prior to transmission of the synchronization, broadcast, and common control channels.

25.4 IEEE 802.16m MS State Diagram

The IEEE 802.16m MS state diagram (i.e., a finite set of states and procedures between which the MS transit when operating in the cellular network to receive and transmit data) is defined consisting of the following states (see Figure 25.3):

- *Initialization State*: a state where an MS without any connection performs cell selection by scanning and synchronizing to a BS preamble and acquires the system configuration information through the superframe header.
- *Access State*: a state where the MS performs network entry to the selected BS. The MS performs the initial ranging process in order to obtain uplink synchronization. Then the MS performs basic capability negotiation with the BS. The MS later performs the authentication and authorization procedure. Next, the MS performs the registration process. The MS receives IEEE 802.16m specific user identification as part of Access State procedures. The IP address assignment may follow using appropriate procedures.

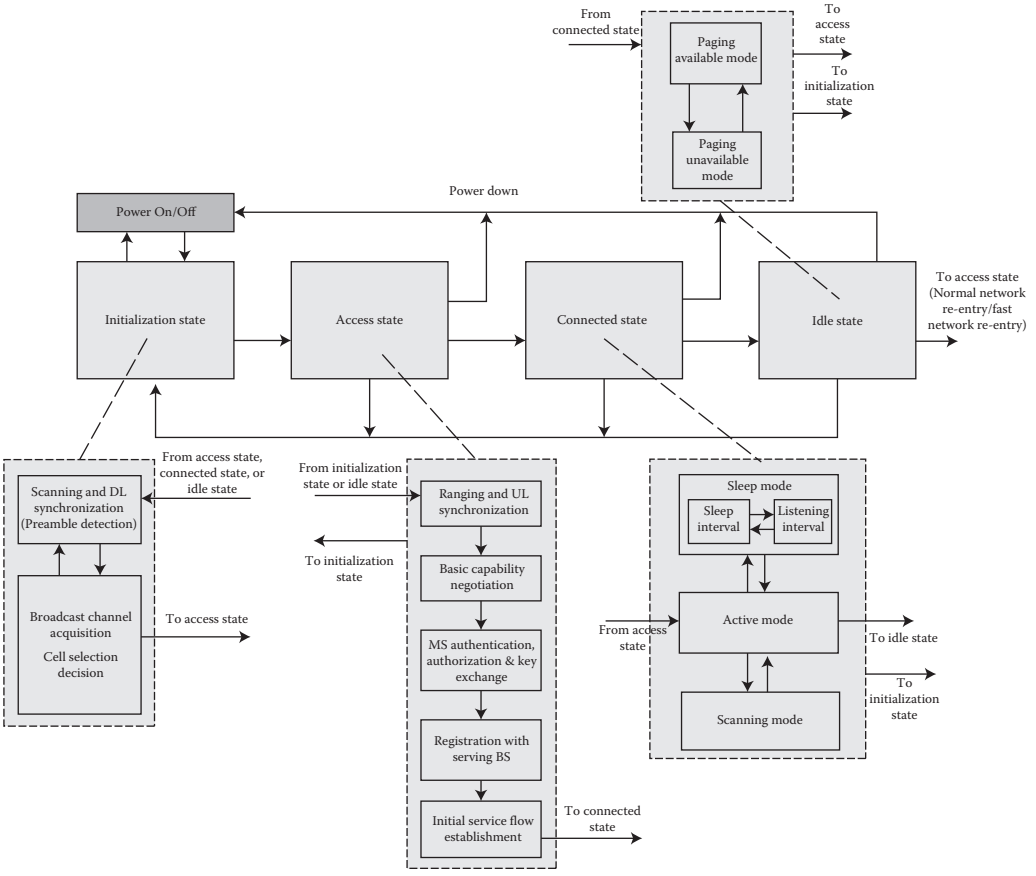

FIGURE 25.3 Mobile station state diagram. (Adapted from Sassan Ahmadi, *Mobile WiMAX; A Systems Approach to Understanding IEEE 802.16m Radio Access Technology*, 1st Edition, Academic Press, 2010; IEEE 802.16m-08/0034r4, *IEEE 802.16m System Description Document*, (http://ieee802.org/16/tgm/index.html), December 2010.)

- *Connected State*: a state consisting of the following modes: Sleep Mode, Active Mode, and Scanning Mode. During Connected State, the MS maintains at least one transport connection and two management connections as established during Access State, while the MS and BS may establish additional transport connections. In order to reduce power consumption of the MS, the MS or BS can request a transition to sleep mode. Also, the MS can scan neighbor BSs to reselect a cell which provides more robust and reliable services.
- *Idle State*: a state comprising two separate modes, paging available mode and paging unavailable mode. During Idle State, the MS may save power by switching between Paging Available mode and Paging Unavailable mode. In the Paging Available mode, the MS may be paged by the BS. If the MS is paged, it transitions to the Access State for its network reentry. The MS performs location update procedure during Idle State.

The MS state diagram for the IEEE 802.16m is similar to that of the legacy system with the exception of the initialization state that has been simplified to reduce the scan latency and to enable fast cell selection or reselection. The location of the essential system configuration information is fixed so that upon successful DL synchronization, the essential system configuration information can be acquired, this would enable the MS to make decision for attachment to the BS without acquiring and decoding MAC management messages and waiting for the acquisition of the system parameters, resulting in power saving in the MS due to shortening and simplification of the initialization procedure. Although both normal and fast network reentry processes are shown as transition from the Idle State to the Access State in Figure 25.3, there are differences that differentiate the two processes. The network reentry is similar to network entry, except that it may be shortened by providing the target BS with MS information through paging controller or other network entity over the backhaul.

25.5 Overview of IEEE 802.16m Physical Layer

25.5.1 Multiple Access Schemes

IEEE 802.16m uses OFDMA as the multiple-access scheme in downlink and uplink. It further supports both TDD and FDD duplex schemes including H-FDD operation of the MSs in the FDD networks. The majority of the frame structure attributes and baseband processing are common for both duplex schemes. The OFDMA parameters are summarized in Table 25.1. Tone dropping at both edges of the frequency band based on 10 and 20 MHz systems can be used to support other bandwidths. In Table 25.1, TTG and RTG acronyms denote transmit/receive and receive/transmit transition gaps in TDD mode of operation, respectively.

25.5.2 Frame Structure

In IEEE 802.16m, a superframe is defined as a collection of consecutive equally sized radio frames whose beginning is marked with a superframe header. The superframe header carries short-term and long-term system configuration information.

In order to decrease the air-link access latency, the radio frames are further divided into a number of subframes where each subframe comprises an integer number of OFDM symbols. The transmission time interval is defined as the transmission latency over the air-link and is equal to an integer multiple of subframe length (default is one subframe). There are four types of subframes: (1) type-1 subframe, which consists of six OFDM symbols, (2) type-2 subframe, which consists of seven OFDM symbols, (3) type-3 subframe which consists of five OFDM symbols, and (4) type-4 subframe, which consists of nine OFDM symbols. In the basic frame structure shown in Figure 25.4, superframe length is 20 ms (comprising four radio frames), radio frame size is 5 ms (comprising eight subframes), and subframe

TABLE 25.1 IEEE 802.16m OFDM Parameters

Nominal channel bandwidth (MHz)			5	7	8.75	10	20
Sampling factor			28/25	8/7	8/7	28/25	28/25
Sampling frequency (MHz)			5.6	8	10	11.2	22.4
FFT size			512	1024	1024	1024	2048
Subcarrier spacing (kHz)			10.94	7.81	9.76	10.94	10.94
Useful symbol time T_u (μs)			91.429	128	102.4	91.429	91.429
CP T_g = 1/8 T_u	Symbol time T_s (μs)		102.857	144	115.2	102.857	102.857
	FDD	Number of OFDM symbols per 5 ms frame	48	34	43	48	48
		Idle time (μs)	62.857	104	46.40	62.857	62.857
	TDD	Number of OFDM symbols per 5 ms frame	47	33	42	47	47
		TTG + RTG (μs)	165.714	248	161.6	165.714	165.714
CP T_g = 1/16 T_u	Symbol time T_s (μs)		97.143	136	108.8	97.143	97.143
	FDD	Number of OFDM symbols per 5 ms frame	51	36	45	51	51
		Idle time (μs)	45.71	104	104	45.71	45.71
	TDD	Number of OFDM symbols per 5 ms frame	50	35	44	50	50
		TTG + RTG (μs)	142.853	240	212.8	142.853	142.853
CP T_g = 1/4 T_u	Symbol time T_s (μs)		114.286	160	128	114.286	114.286
	FDD	Number of OFDM symbols per 5 ms frame	43	31	39	43	43
		Idle time (μs)	85.694	40	8	85.694	85.694
	TDD	Number of OFDM symbols per 5 ms frame	42	30	37	42	42
		TTG + RTG (μs)	199.98	200	264	199.98	199.98

Source: Adapted from Sassan Ahmadi, *Mobile WiMAX; A Systems Approach to Understanding IEEE 802.16m Radio Access Technology*, 1st Edition, Academic Press, 2010; IEEE Std 802.16m-2011, *IEEE Standard for Local and Metropolitan Area Networks—Part 16: Air Interface for Broadband Wireless Access Systems, Amendment 3: Advanced Air Interface*, May 2011.

length is 0.617 ms. The use of subframe concept with the latter parameter set would reduce the one-way air-link access latency to <10 ms.

Separate time–frequency regions are used to support new and legacy MSs that are time-division multiplexed across time domain in the downlink. For the uplink transmissions, both time- and frequency-division multiplexing approaches can be used to support legacy and new terminals. The non-backward compatible features are restricted to the new zones. All backward compatible functions are used in the legacy zones. In the absence of any legacy system, the legacy zones will disappear and the entire frame will be allocated to the new zones.

Coexistence between IEEE 802.16m and 3GPP LTE in TDD mode may be facilitated by inserting either an idle symbol or idle subframes within the IEEE 802.16m frame for certain 3GPP LTE TDD configurations [6]. An operator configurable delay or offset between the beginning of an IEEE 802.16m frame and a 3GPP LTE TDD frame can be applied in some configurations to minimize the waste of radio resources consumed by idle symbols or idle subframes.

In the case where an IEEE 802.16m BS coexists with legacy BSs, the switching points are limited to two in each TDD radio frame. The support for multiple RF carriers can be accommodated with the same frame structure used for single-carrier operation. All RF carriers are time aligned at the frame, subframe, and symbol level. Alternative frame structures for CP = 1/16 and CP = 1/4 are used that incorporate different number of OFDM symbols in certain subframes or different number of subframes per frame [6,10].

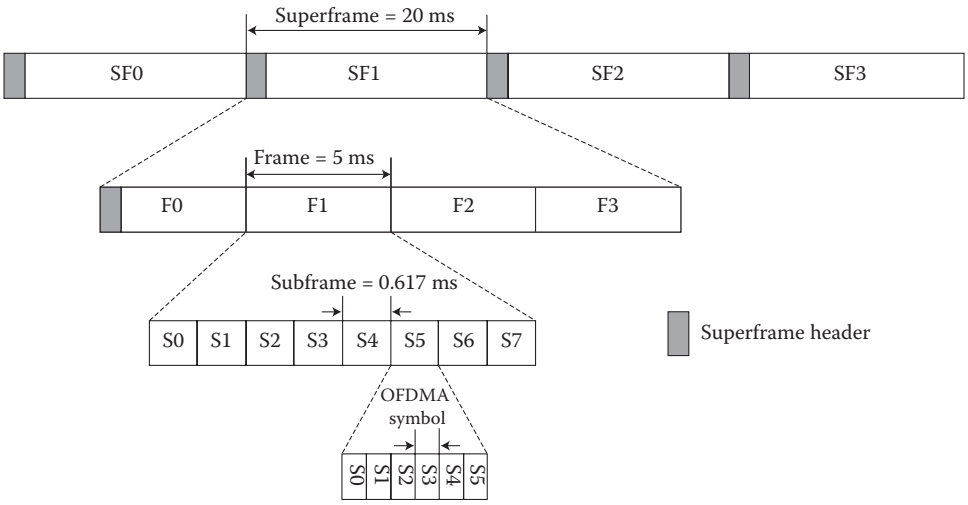

FIGURE 25.4 IEEE basic frame structure. (Adapted from Sassan Ahmadi, *Mobile WiMAX; A Systems Approach to Understanding IEEE 802.16m Radio Access Technology*, 1st Edition, Academic Press, 2010; IEEE Std 802.16m-2011, *IEEE Standard for Local and Metropolitan Area Networks—Part 16: Air Interface for Broadband Wireless Access Systems, Amendment 3: Advanced Air Interface*, May 2011.)

25.5.3 Subchannelization Schemes

The downlink/uplink subframes are divided into a number of frequency partitions, where each partition consists of a set of physical resource units (PRU) over the available number of OFDM symbols in the subframe. Each frequency partition can include localized and/or distributed PRUs. This is different from the legacy system where each zone can only accommodate localized or distributed subchannels. Frequency partitions can be used for different purposes such as fractional frequency reuse (FFR). The downlink/uplink resource partitioning and mapping procedure is illustrated in Figure 25.5.

25.5.3.1 Downlink Resource Structure

A PRU is the basic physical unit for resource allocation that comprises P_{sc} contiguous subcarriers by N_{sym} contiguous OFDM symbols where P_{sc} is 18 subcarriers and N_{sym} is 6, 7, or 5 OFDM symbols for type-1, type-2, or type-3 subframes, respectively. A logical resource unit (LRU) is the basic logical unit for distributed and localized resource allocations. A LRU comprises $P_{sc} \times N_{sym}$ subcarriers.

Distributed resource units (DRU) are used to achieve frequency diversity gain. A DRU contains a group of subcarriers which are spread across a frequency partition. The size of the DRUs is equal to that of PRU. The minimum unit for forming a DRU in the downlink is equal to a pair of subcarriers also known as a tone-pair. Localized or Contiguous resource units (CRU) are used to achieve frequency-selective scheduling gain. A localized resource unit comprises a group of subcarriers which are contiguous across frequency. The size of the localized resource units is equal to that of the PRUs. To form distributed and localized resource units, the subcarriers over the OFDM symbols of a subframe are partitioned into guard and used subcarriers. The DC subcarrier is not used. The used subcarriers are grouped into integer number of PRUs. Each PRU contains pilots and data subcarriers. The number of used pilot and data subcarriers depends on MIMO mode, rank and number of multiplexed MSs over the resource block, as well as the number of OFDM symbols within a subframe.

The PRUs are subsequently divided into subbands and mini-bands where a subband comprises N_1 adjacent PRUs and a mini-band comprises N_2 adjacent PRUs, where $N_1 = 4$ and $N_2 = 1$. The subbands are suitable for frequency-selective allocations as they provide a contiguous allocation of PRUs in frequency. The mini-bands are suitable for frequency diverse allocations and are permuted in frequency. Each

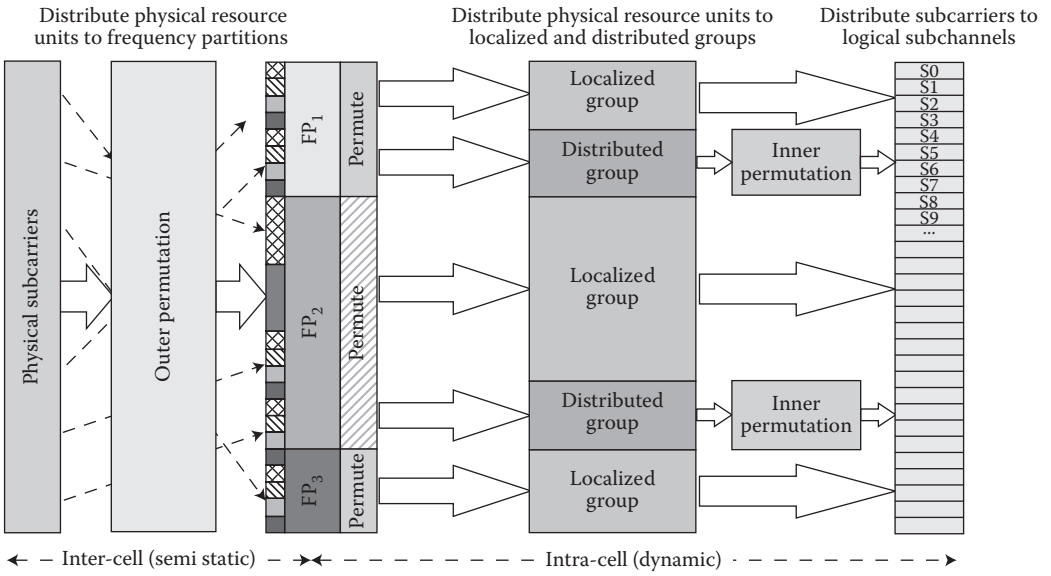

FIGURE 25.5 Illustration of the downlink/uplink subcarrier to resource unit mapping where P_i denotes the ith frequency partition. (Adapted from Sassan Ahmadi, *Mobile WiMAX; A Systems Approach to Understanding IEEE 802.16m Radio Access Technology*, 1st Edition, Academic Press, 2010; IEEE Std 802.16m-2011, *IEEE Standard for Local and Metropolitan Area Networks—Part 16: Air Interface for Broadband Wireless Access Systems, Amendment 3: Advanced Air Interface*, May 2011.)

frequency partition is divided into localized and/or distributed resource allocations. The size of the distributed/localized groups is flexibly configured per sector. Adjacent sectors are not required to have the same configuration for the localized and distributed groups. The localized and DRUs are further mapped into LRUs by direct mapping for CRUs and by subcarrier permutation for DRUs.

The subcarrier permutation defined for the downlink distributed resource allocations spreads the subcarriers of the DRU across all the distributed resource allocations within a frequency partition. After mapping all pilots, the remaining used subcarriers are used to define the DRUs.

25.5.3.2 Uplink Resource Structure

Similar to the downlink subchannelization scheme, a PRU in the uplink is defined as the basic physical unit for resource allocation that comprises P_{sc} consecutive subcarriers by N_{sym} consecutive OFDM symbols. The value of P_{sc} is 18 subcarriers and the possible values of N_{sym} are 6, 7, 5, and 9 OFDM symbols for type-1, type-2, type-3, and type-4 subframes, respectively. An LRU is the basic logical unit for distributed and localized resource allocations whose size is $P_{sc} \times N_{sym}$ subcarriers for data transmission. The subcarriers of an OFDM symbol are partitioned into $N_{g,\text{left}}$ left guard subcarriers, $N_{g,\text{right}}$ right guard subcarriers, and N_{used} used subcarriers. The DC subcarrier is not used. The N_{used} subcarriers are grouped into integer number of PRUs. Each PRU contains pilots and data subcarriers. The number of pilots and data subcarriers depends on MIMO mode, rank and number of MSs multiplexed over the resource block, and the type of resource allocation; that is, distributed or localized resource allocations as well as the type of the subframe.

The uplink distributed units comprise a group of subcarriers which are spread over a frequency partition. The size of distributed unit is equal to logical resource blocks. The minimum unit for constructing a DRU in the uplink is a tile. The uplink tile sizes are six subcarriers by N_{sym} OFDM symbols. The localized resource unit is used to achieve frequency-selective scheduling gain. A localized resource unit contains a group of subcarriers which are contiguous across frequency. The size of the localized resource unit equals the size of the LRUs for localized allocations; that is, 18 subcarriers by N_{sym} OFDM symbols.

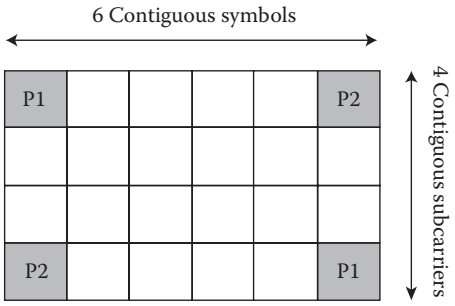

FIGURE 25.6 New uplink PUSC structure for two streams. (Adapted from Sassan Ahmadi, *Mobile WiMAX; A Systems Approach to Understanding IEEE 802.16m Radio Access Technology*, 1st Edition, Academic Press, 2010; IEEE Std 802.16m-2011, *IEEE Standard for Local and Metropolitan Area Networks—Part 16: Air Interface for Broadband Wireless Access Systems, Amendment 3: Advanced Air Interface*, May 2011.)

The PRUs are first subdivided into subbands and mini-bands, where a subband comprises N_1 adjacent PRUs and a mini-band consists of N_2 adjacent PRUs, where $N_1 = 4$ and $N_2 = 1$. The subbands are suitable for frequency-selective allocations whereas the mini-bands are suitable for frequency diverse allocation and are permuted in frequency. An inner permutation is defined for the uplink distributed resource allocations that spreads DRU tiles across the entire distributed resource allocations within a frequency partition. Each DRU in an uplink frequency partition is divided into three tiles of six adjacent subcarriers over N_{sym} symbols. The tiles within a frequency partition are collectively tile-permuted to obtain frequency diversity gain across the allocated resources.

The IEEE 802.16m uplink physical structure supports both frequency- and time-division multiplexing of the new and the legacy systems. A new partial use of subcarriers (PUSC) subchannelization scheme is specified for mixed mode operation with the legacy system. The new PUSC scheme contains six tiles of four subcarriers by six symbols as shown in Figure 25.6.

25.5.4 Modulation and Coding

The performance of adaptive modulation generally suffers from the power inefficiencies of multilevel modulation schemes. This is due to the variations in bit reliabilities caused by the bit-mapping onto the signal constellation. To overcome this issue, a constellation-rearrangement (CoRe) scheme is utilized where signal constellation of QAM signals between retransmissions is rearranged; that is, the mapping of the bits into the complex-valued symbols between successive HARQ retransmissions is changed, resulting in averaging bit reliabilities over several retransmissions and lower packet error rates. The mapping of bits to the constellation point depends on the CoRe type used for HARQ re-transmissions and may also depend on the MIMO scheme. The complex-valued modulated symbols are mapped to the input of the MIMO encoder. Incremental redundancy HARQ (HARQ-IR) is used in by determining the starting position of the bit selection for HARQ retransmissions.

Figure 25.7 shows the channel coding and modulation procedures. A cyclic redundancy check (CRC) is appended to a burst (i.e., a physical layer data unit) prior to partitioning. The 16-bit CRC is calculated over the entire bits in the burst. If the burst size including burst CRC exceeds the maximum block size,

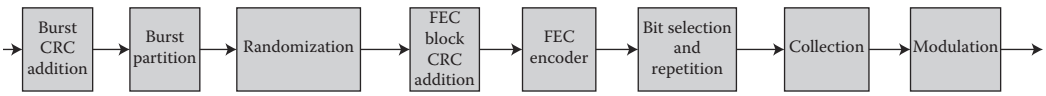

FIGURE 25.7 Coding and modulation procedures.

the burst is partitioned into K_{FB} forward error correction (FEC) blocks, each of which is encoded separately. If a burst is partitioned into more than one FEC blocks, an FEC block CRC is appended to each FEC block before the FEC encoding. The FEC block CRC of an FEC block is calculated based on the entire bits in that FEC block. Each partitioned FEC block including 16-bit FEC block CRC has the same length. The maximum FEC block size is 4800 bits. Concatenation rules are based on the number of information bits and do not depend on the structure of the resource allocation (number of LRUs and their size). The IEEE 802.16m uses the convolutional turbo code (CTC) with code rate of 1/3 as defined in References 10 and 11. The CTC scheme is extended to support additional FEC block sizes. The FEC block sizes which are multiple of seven are removed for the tail-biting encoding structure. The encoder block depicted in Figure 25.7 includes the interleaver.

Bit selection and repetition are used in IEEE 802.16m to achieve rate matching. The bit selection mechanism adapts the number of coded-bits to the size of the resource unit and the subframe type. The total number of subcarriers in the allocated resource unit is divided among the designated FEC blocks. The total number of information and parity bits generated by FEC encoder are considered the maximum size of the circular buffer. The code repetition is performed when the number of transmitted bits is larger than the number of selected bits. The selection of coded bits is conducted cyclically over the buffer. The mother-code bits, the total number of information and parity bits generated by FEC encoder, are considered as the maximum size of circular buffer. If the size of the circular buffer N_{buffer} is smaller than the number of mother-code bits, the first N_{buffer} bits of mother-code bits are considered as the selected bits.

The QPSK, 16QAM, and 64QAM baseband modulation schemes are supported similar to that of the legacy system. The mapping of bits to the constellation points depends on the CoRe version that may be used for HARQ retransmissions depending on the MIMO scheme. The QAM symbols are mapped to the input of the MIMO encoder. The FEC block sizes specified in the standard include the additional CRC; that is, per burst and per FEC block, if applicable. Other sizes may require padding to the next larger burst size. The code rate and modulation order depend on the burst size and the resource allocation.

HARQ-IR scheme is used in IEEE 802.16m by determining the starting position of the bit selection for HARQ retransmissions. Chase Combining HARQ is also supported and considered as a special case of HARQ-IR. The 2-bit subpacket identifier is used to identify the starting position of the subpackets. The CoRe scheme can be expressed by a bit-level interleaver. The resource allocation and transmission formats in each retransmission in the downlink can be configured with control signaling. The resource allocation in each retransmission in the uplink can be fixed or adaptive as configured by control signaling. In HARQ retransmissions, the bits or symbols can be transmitted in a different order to exploit the frequency diversity of the channel. For HARQ retransmission, the mapping of bits or modulated symbols to spatial streams may be applied to exploit spatial diversity with a given mapping pattern, depending on the type of HARQ-IR. In this case, the predefined set of mapping patterns should be known to the transmitter and receiver. In the downlink HARQ, the BS may transmit coded bits exceeding current available soft buffer capacity.

25.5.5 Pilot Structure

25.5.5.1 Downlink Pilot Structure

Transmission of pilot subcarriers in the downlink is necessary to allow channel estimation, channel quality measurement (e.g., CQI), frequency offset estimation, and so on. To optimize the system performance in different propagation environments, IEEE 802.16m supports both common and dedicated pilot structures. The common pilots can be used in distributed allocations by all MSs. The dedicated pilots can be used with both localized and distributed allocations and are associated with a user-specific pilot index. The dedicated pilots are associated with a specific resource allocation and are used by the MSs assigned to specific resource block; therefore, they can be precoded or beam-formed in the same manner as the data subcarriers of the resource block. Pilot subcarriers that can be used only by a group of MSs within an FFR group are a special case of common pilots. The downlink pilot structure is defined for up to

eight streams and the design of common and dedicated pilots is consistent. There is an equal pilot density per spatial stream; nevertheless, there is not necessarily equal pilot density per OFDM symbols. There is the same number of pilots for each PRU allocated to a particular MS. For the subframes consisting of 5 or 7 OFDM symbols, one of OFDM symbols is deleted or repeated. To overcome the effects of pilot interference among the neighboring sectors or BSs, an interlaced pilot structure is used by cyclically shifting the base pilot pattern such that the pilots of neighboring cells do not overlap.

The E-MBS-zone-specific pilots are transmitted for multicell multicast broadcast single-frequency network (SFN) transmissions. An E-MBS zone is a group of BSs involved in the SFN transmission. The E-MBS-zone-specific pilots are common within an E-MBS zone but different between neighboring E-MBS zones. Synchronous transmissions of the same content with common pilot from multiple BSs in an E-MBS zone would result in improved channel estimation. The E-MBS-zone-specific pilot-patterns depend on the maximum number of transmit streams. Pilot structures up to two transmit streams are supported.

25.5.5.2 Uplink Pilot Structure

The uplink pilots are dedicated to localized and DRUs and are precoded in the same manner as the data subcarriers of the resource unit. The uplink pilot structure is defined for up to four streams for SU-MIMO and up to eight streams for Collaborative Spatial Multiplexing. When pilots are power-boosted, each data subcarrier should have the same transmission power across all OFDM symbols in a resource unit. The 18×6 uplink LRUs use the same pilot patterns as the downlink counterpart. The pilot pattern for 6×6 tile structure is different and it is shown in Figure 25.8.

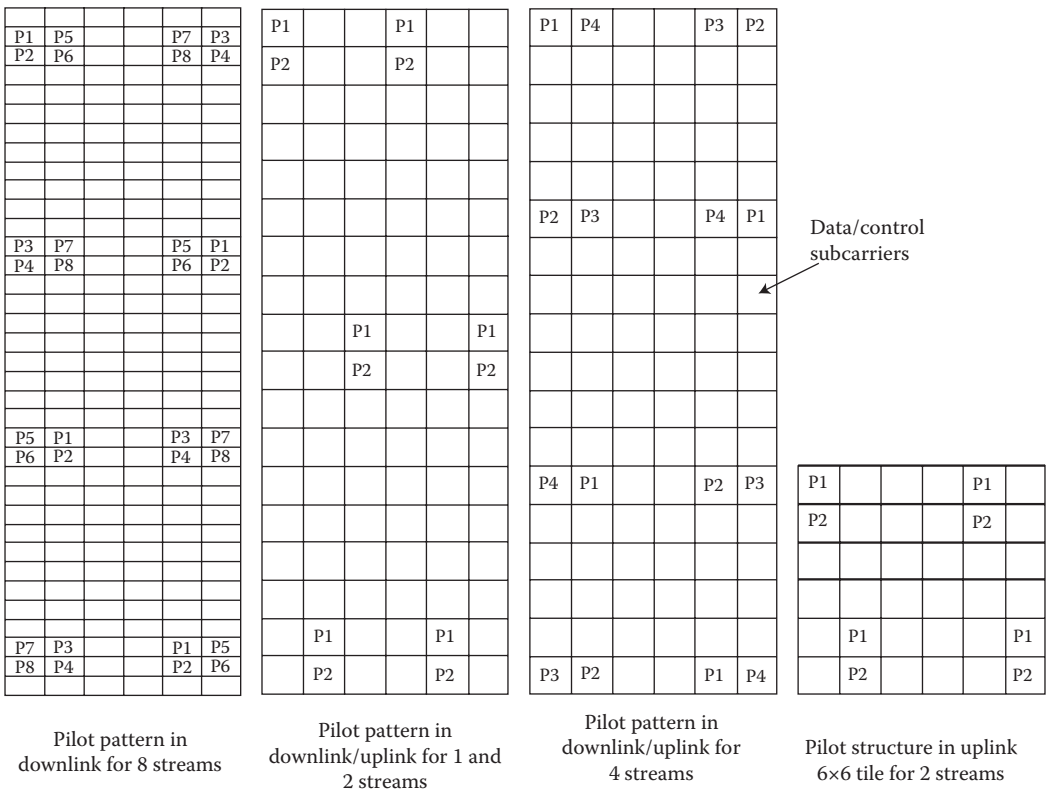

FIGURE 25.8 Downlink/uplink pilot structures for 1, 2, 4, and 8 streams for type-1 subframe.

25.5.6 Control Channels

Downlink control channels carry essential information for system operation. Depending on the type of control signaling, information is transmitted over different time intervals (i.e., from superframe to subframe intervals). The system configuration parameters are transmitted at the superframe intervals, whereas control signaling related to user data allocations is transmitted at the frame/subframe intervals. An IEEE 802.16m-compliant MS can access the network without decoding the legacy frame control header and legacy DL/UL-MAP messages [6,10].

25.5.6.1 Downlink Control Channels

25.5.6.1.1 Superframe Header

The superframe header carries essential system parameters and configuration information. The content of superframe header is divided into two parts referred to as primary and secondary superframe headers. The information transmitted in secondary superframe header is further divided into different subpackets. The primary superframe header is transmitted every superframe, whereas the secondary superframe header is transmitted over one or more superframes. The primary and secondary superframe headers are located in the first subframe within a superframe and are time-division multiplexed with the advanced preamble. The superframe header is confined to 5 MHz of bandwidth. The primary superframe header is transmitted using predetermined modulation and coding scheme. The secondary superframe header is transmitted using predetermined modulation scheme while its code repetition factor is signaled in the primary superframe header. The primary and secondary superframe headers are transmitted using two spatial streams and space–frequency block coding to improve their coverage and reliability. The MS is not required to know the antenna configuration prior to decoding the primary superframe header. The information transmitted in the secondary superframe header is divided into different subpackets. The secondary superframe header Subpacket 1 (SP1) includes information needed for network reentry. The secondary superframe header Subpacket 2 (SP2) contains information for initial network entry. The secondary superframe header Subpacket 3 (SP3) contains remaining system information for maintaining communication with the BS.

25.5.6.1.2 Advanced MAP

The advanced MAP (A-MAP) consists of both user-specific (dedicated control channel) and nonuser-specific (common control channel) control information. The nonuser-specific control information includes information that is not dedicated to a specific user or a specific group of users. It contains information required to decode user-specific control signaling. User-specific control information consists of information intended for one or more users. It includes scheduling assignment, power control, and HARQ ACK/NACK. Resources can be allocated persistently to the MSs. The periodicity of the allocation is configurable. Group control information is used to allocate resources or to configure resources to one or multiple MSs within a user group. Each group is associated with a set of radio resources. Voice over IP (VoIP) is an example of the class of services that can take advantage of group allocation messages. Within a subframe, control and data channels are frequency-division multiplexed. Both control and data channels are transmitted on LRUs that span over all OFDM symbols within a subframe [6,10].

Each downlink subframe contains a control region with both nonuser-specific and user-specific control information. All A-MAPs share a time-frequency region known as A-MAP region. The control regions are located in every subframe. The corresponding uplink allocations occurs L subframes later, where the value of L is determined by A-MAP relevance. The coding rate of the control blocks is known to the MS through group size indication in nonuser-specific control information in order to reduce the complexity of blind detection by the MS.

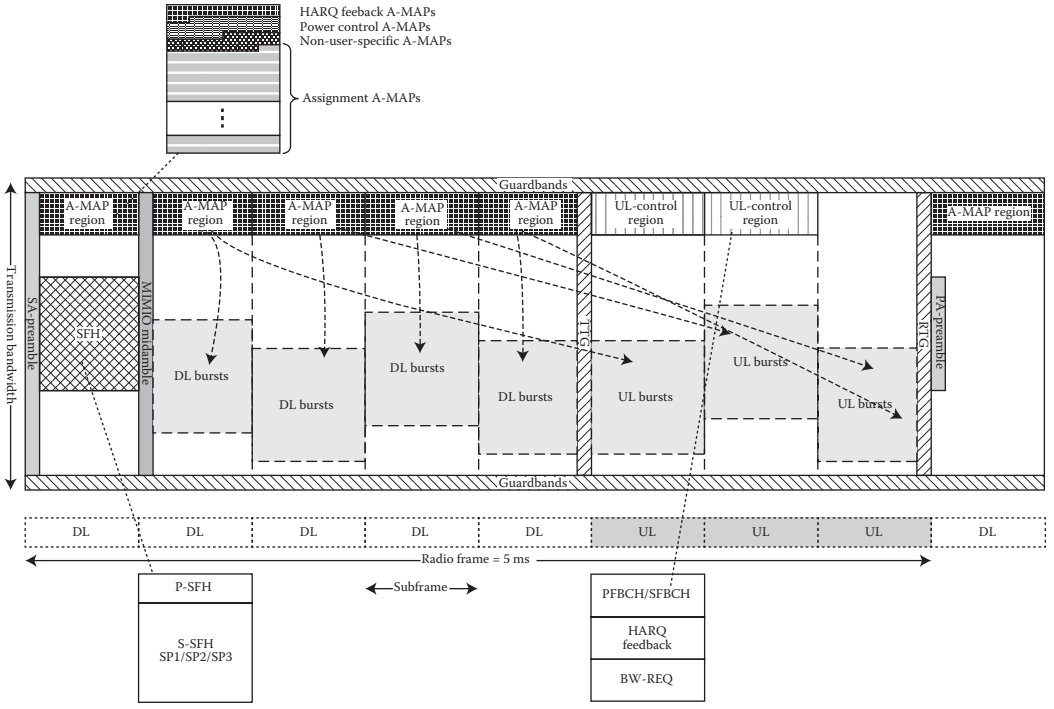

FIGURE 25.9 Structure of IEEE 802.16m overhead channels in the downlink and uplink in TDD mode (example). (Adapted from Sassan Ahmadi, *Mobile WiMAX; A Systems Approach to Understanding IEEE 802.16m Radio Access Technology*, 1st Edition, Academic Press, 2010.)

An A-MAP allocation information element (IE) is defined as the basic element of unicast control signaling. A unicast control IE may be addressed to one user using a unicast identifier or to multiple users via multicast/broadcast identifier. The CRC is masked with the identifier A-MAP allocation IE. It may contain information related to resource allocation, HARQ, MIMO transmission mode, and so on. Each unicast control IE is coded separately. Note that this method is different from the legacy system control mechanism where the IEs of all users are jointly coded. Nonuser-specific control information is encoded separately from the user-specific control information. The transmission format of nonuser-specific control information is predetermined. In the downlink subframes, each frequency partition may contain an A-MAP region. The A-MAP region occupies the first few DRUs in a frequency partition. The structure of an A-MAP region is illustrated in Figure 25.9. The amount of resource occupied by each A-MAP physical channel may vary depending on the system configuration and scheduling parameters. There are different types of A-MAP as follows:

- Assignment A-MAP contains resource assignment information which is categorized into multiple types of assignment A-MAP IEs. Each assignment A-MAP IE is coded separately and carries information for one or a group of users. The minimum unit of logical resources in the assignment A-MAP consists of 56 data subcarriers. Assignment A-MAP IEs with <40 bits are zero-padded to 40 bits. Assignment A-MAP IEs with >40 bits are divided into several segments, each with 40 bits. Segments of an assignment A-MAP IE are separately coded and modulated and occupy a number of logically CRUs. Assignment A-MAP IEs are grouped together based on channel coding rate. Assignment A-MAP IEs in the same group are transmitted in the same frequency partition with the same channel coding rate. Each assignment A-MAP group contains several logically CRUs.

TABLE 25.2 Assignment A-MAP IE Types and Their Usage

Assignment A-MAP IE Type	Usage
DL basic assignment	Allocation information for MS to decode DL bursts using contiguous logical resources
UL basic assignment	Allocation information for MS to transmit UL bursts using contiguous logical resources
DL subband assignment	Allocation information for MS to decode DL bursts using sub-band based resources
UL subband assignment	Allocation information for MS to transmit UL bursts using sub-band based resources
Feedback allocation	Allocation or de-allocation of UL fast feedback control channels to an MS
UL sounding command	Control information for MS to request UL sounding transmission
CDMA allocation	Allocation for MS requesting bandwidth using a ranging or BW-REQ codes
DL persistent allocation	DL persistent resource allocation
UL persistent allocation	UL persistent resource allocation
Group resource allocation	Group scheduling and resource allocation
Feedback polling	Allocation for MS to send MIMO feedback using MAC messages or signaling headers
BR-ACK	Indication of decoding status of BW-REQ opportunities and resource allocation of BW-REQ header
Broadcast	Broadcast burst allocation and other broadcast information

The number of assignment A-MAP IEs in each assignment A-MAP group is signaled through nonuser-specific A-MAP in the same subframe. If two assignment A-MAP groups using two channel coding rates are present in an A-MAP region, assignment A-MAP group using lower channel coding rate is allocated first, followed by assignment A-MAP group using higher channel coding rate. The maximum number of assignment A-MAP IEs in one subframe that the BS may allocate to an MS is 8. This number includes all the assignment A-MAP IEs that are required to be monitored by the MS. For a segmentable assignment A-MAP IE (i.e., an assignment A-MAP IE that occupies >1 minimum LRU using QPSK 1/2), each segment is counted as one assignment A-MAP IE.

- HARQ Feedback A-MAP contains HARQ ACK/NACK information for uplink data transmission.
- Power Control A-MAP carries power control commands to the MSs.

There are different assignment A-MAP IE types that distinguish between DL/UL, persistent/nonpersistent, single-user/group resource allocation, basic/extended IE scenarios. Different types of assignment A-MAPs and their usage are shown in Table 25.2.

25.5.6.2 Uplink Control Channels

25.5.6.2.1 MIMO Feedback

MIMO feedback provides wideband and/or narrowband spatial characteristics of the channel that are required for MIMO operation. The MIMO mode, precoding matrix index (PMI), rank adaptation information, channel covariance matrix elements, and best subband index are examples of MIMO feedback information.

25.5.6.2.2 HARQ Feedback

HARQ feedback (ACK/NACK) is used to acknowledge downlink data transmissions. The uplink HARQ feedback channel starts at a predetermined offset with respect to the corresponding downlink transmission. The HARQ feedback channel is frequency-division multiplexed with other control and data channels (see Figure 25.9). Orthogonal codes are used to multiplex multiple HARQ feedback channels. The HARQ feedback channel comprises three distributed mini-tiles.

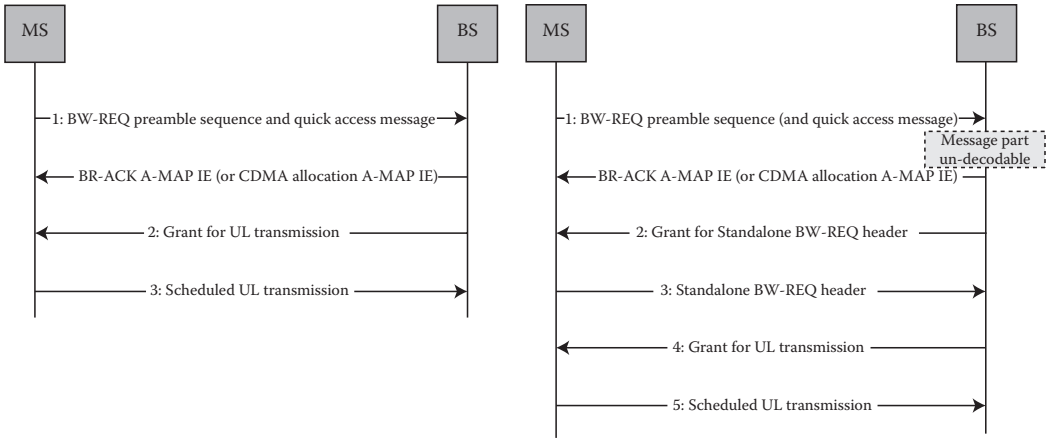

FIGURE 25.10 Bandwidth request procedure. (Adapted from Sassan Ahmadi, *Mobile WiMAX; A Systems Approach to Understanding IEEE 802.16m Radio Access Technology*, 1st Edition, Academic Press, 2010; IEEE Std 802.16m-2011, *IEEE Standard for Local and Metropolitan Area Networks—Part 16: Air Interface for Broadband Wireless Access Systems, Amendment 3: Advanced Air Interface*, May 2011.)

25.5.6.2.3 Bandwidth Request

Bandwidth requests (BW-REQ) are used to indicate the amount of bandwidth required by a user. BW-REQs are transmitted through indicators or messages. A BW-REQ indicator notifies the BS of an uplink grant request by the MS sending the indicator. BW-REQ messages can include information about the status of queued traffic at the MS such as buffer size and quality-of-service parameters. Contention- or noncontention-based random access is used to transmit BW-REQ information on this control channel. The contention-based BW-REQ procedure is illustrated in Figure 25.10. A five-step regular procedure or an optional three-step quick access procedure is used. Steps 2 and 3 can be skipped in a quick access procedure. In step 1, the MS sends a BW-REQ indicator for quick access that may indicate information such as MS addressing and/or request size and/or uplink transmit power report, and/or QoS parameters, and the BS may allocate uplink grant based on certain policy. The MS may piggyback additional BW-REQ information along with user data during uplink transmission (step 5). In steps 2 and 4, the BS acknowledges receipt of the messages as shown in Figure 25.10.

The BW-REQ channel starts at a configurable location with the configuration defined in a downlink broadcast control message. The BW-REQ channel is frequency-division multiplexed with other uplink control and data channels (see Figure 25.9). A BW-REQ tile is defined by six subcarriers over six OFDM symbols. Each BW-REQ channel consists of three distributed BW-REQ tiles. Multiple BW-REQ indicators can be transmitted on the same BW-REQ channel using code-division multiplexing.

25.5.6.2.4 Channel Quality Indicators

Channel quality feedback provides information about channel conditions as seen by the user. This information is used by the BS for link adaptation, resource allocation, power control, and so on. The channel quality measurement includes both narrowband and wideband measurements. The CQI feedback overhead can be reduced through differential feedback or other compression techniques. Examples of CQI include effective carrier-to-interference-plus-noise ratio (CINR), band selection, and so on. The default subframe size for transmission of uplink control information is six OFDM symbols. The fast feedback channel carries channel quality and MIMO feedback. There are two types of uplink fast feedback control channels known as primary and secondary fast feedback channels. The secondary fast feedback control channel carries narrowband CQI and MIMO feedback information. The secondary fast feedback channel can be used to support CQI reporting at higher code rate and thus more CQI information

bits. The fast feedback channel is frequency-division multiplexed with other uplink control and data channels.

The fast feedback channel starts at a predetermined location with the size defined in a downlink broadcast control message. Fast feedback allocations to a MS can be periodic and the allocations are configurable. The specific type of feedback information carried on each fast feedback opportunity can be different. The number of bits carried in the fast feedback channel can be adaptive. For efficient transmission of feedback channels a mini-tile is defined comprising two subcarriers by six OFDM symbols. One LRU consists of nine mini-tiles and can be shared by multiple fast feedback channels [6,10].

25.5.6.2.5 Uplink Sounding Channel

The sounding channel is used by a user terminal to transmit sounding reference signals to enable the BS to measure uplink channel conditions. The sounding channel may occupy either specific uplink subbands or the entire bandwidth over one OFDM symbol. The BS can configure an MS to transmit the uplink sounding signal over predefined subcarriers within specific subbands or the entire bandwidth. The sounding channel is orthogonally multiplexed (in time or frequency) with other control and data channels. Furthermore, the BS can configure multiple user terminals to transmit sounding signals on the corresponding sounding channels using code-, frequency-, or time-division multiplexing. Power control for the sounding channel can be used to adjust the sounding signal quality. The transmit power from each mobile terminal may be separately controlled according to certain CINR target values [6,10].

25.5.6.2.6 Ranging Channel

The ranging channel is used for uplink synchronization. The ranging channel can be further classified into ranging for nonsynchronized and synchronized MSs. A random access procedure, which can be contention or noncontention based, is used for ranging. The contention-based random access is used for initial ranging. The noncontention-based random access is used for periodic ranging and HO. The ranging channel for nonsynchronized MSs starts at a configurable location with the configuration signaled in a downlink broadcast control message. The ranging channel for nonsynchronized MSs is frequency-division multiplexed with other uplink control and data channels.

The ranging channel for nonsynchronized MSs consists of three fields: (1) Ranging cyclic prefix (RCP), (2) Ranging preamble (RP), and (3) Guard time (GT). The length of RCP is longer than the sum of the maximum delay spread and round trip delay of supported cell size. The length of GT is chosen longer than the round trip delay of the supported cell size. The length of RP is chosen equal to or longer than the length of RCP. To support large cell sizes, the ranging channel for nonsynchronized user terminals can span multiple concatenated subframes. Figure 25.11 shows the two ranging channel formats. A single preamble can be used by different nonsynchronized users for increasing ranging opportunities. When the preamble is repeated as a single opportunity, the second RCP can be omitted for coverage extension. A number of guard subcarriers are reserved at the edges of nonsynchronized ranging channel physical resource.

When multiantenna transmission is supported by MS, it can be used to increase the ranging opportunity by using spatial multiplexing. The ranging channel for synchronized MSs is used for periodic ranging. The ranging channel for synchronized user terminals starts at a configurable location with the configuration signaled in a downlink broadcast control message. The ranging channel for synchronized MSs is frequency-division multiplexed with other uplink control and data channels.

25.5.6.2.7 Power Control

Power control mechanism is supported for downlink and uplink. The BS controls the transmit power per subframe and per user. Using downlink power control, user-specific information is received by the terminal with the controlled power level. The downlink A-MAPs are power-controlled based on the terminal uplink channel quality feedback. The uplink power control is supported to compensate for the path loss, shadowing, fast fading, and implementation loss as well as to mitigate intercell and intracell interference. The uplink power control includes open-loop and closed-loop power control

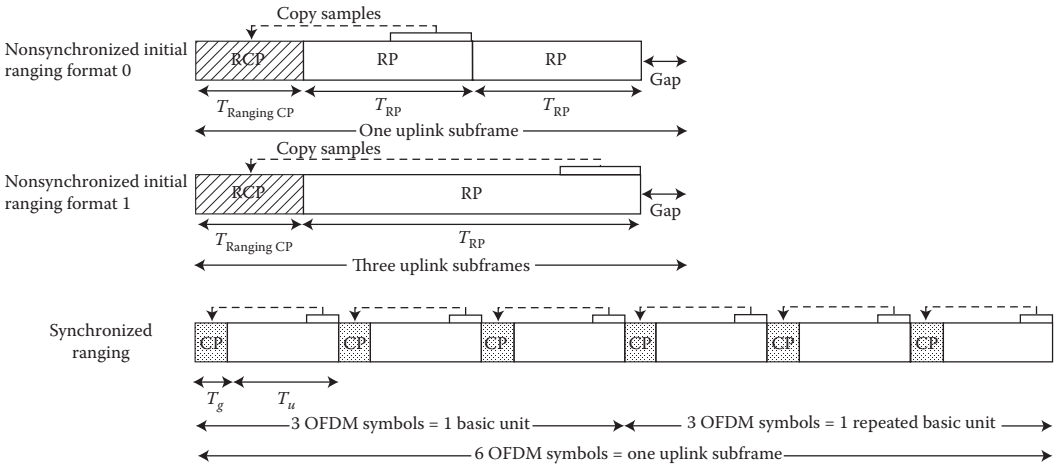

FIGURE 25.11 Ranging channel structure for synchronized and nonsynchronized access. (Adapted from Sassan Ahmadi, *Mobile WiMAX; A Systems Approach to Understanding IEEE 802.16m Radio Access Technology*, 1st Edition, Academic Press, 2010; IEEE Std 802.16m-2011, *IEEE Standard for Local and Metropolitan Area Networks—Part 16: Air Interface for Broadband Wireless Access Systems, Amendment 3: Advanced Air Interface*, May 2011.)

mechanisms. The BS can transmit necessary information through control channel or message to terminals to support uplink power control. The parameters of power control algorithm are optimized on a system-wide basis by the BS and broadcasted periodically or triggered by certain events.

In high-mobility scenarios, power control scheme may not be able to compensate the fast fading channel effect because of the variations of the channel impulse response. As a result, the power control is used to compensate for the distance-dependent path loss, shadowing, and implementation loss only.

The channel variations and implementation loss are compensated via open-loop power control without frequently interacting with the BS. The terminal can determine the transmit power based on the transmission parameters sent by the serving BS, uplink channel transmission quality, downlink channel state information (CSI), and interference knowledge obtained from downlink. Open-loop power control provides a coarse initial power setting of the terminal when an initial connection is established.

The dynamic channel variations are compensated via closed-loop power control with power control commands from the serving BS. The BS measures uplink channel state and interference information using uplink data and/or control channel transmissions and sends power control commands to the terminal. The terminal adjusts its transmission power based on the power control commands from the BS.

25.5.7 Downlink Synchronization Channel (Advanced Preamble)

IEEE 802.16m utilizes a new hierarchical structure for the downlink synchronization where two sets of preambles at superframe and frame intervals are transmitted (Figure 25.12). The first set of preamble sequences mark the beginning of the superframe and are common to a group of sectors or cells. The primary advanced preamble carries information about system bandwidth and carrier configuration. The primary advanced preamble has a fixed bandwidth of 5 MHz and can be used to facilitate location-based services. A frequency reuse of one is applied to the primary advanced preamble in the frequency domain. The second set of advanced preamble sequences (secondary advanced preamble) is repeated every 10 ms and spans the entire system bandwidth and carries the physical cell identifier. A frequency reuse of three is used for this set of sequences to mitigate intercell interference. The secondary advanced preambles carry 768 distinct physical cell identifiers. The set of secondary advanced preamble sequences are partitioned and each partition is dedicated to a specific BS type such as macro-BS, femto-BS, and

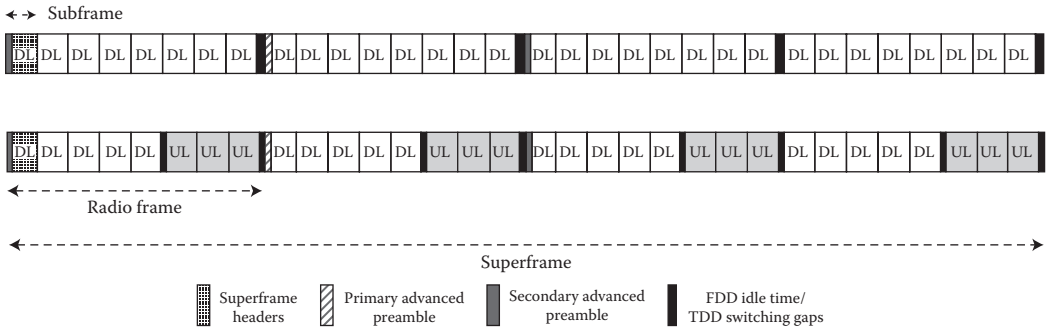

FIGURE 25.12 Structure of the IEEE 802.16m advanced preambles. (Adapted from Sassan Ahmadi, *Mobile WiMAX; A Systems Approach to Understanding IEEE 802.16m Radio Access Technology*, 1st Edition, Academic Press, 2010; IEEE 802.16m-08/0034r4, *IEEE 802.16m System Description Document*, (http://ieee802.org/16/tgm/index.html), December 2010.)

so on. The partition information is broadcasted in the secondary superframe header and system configuration description message.

25.5.8 Multi-Antenna Techniques in IEEE 802.16m

25.5.8.1 Downlink MIMO Structure

IEEE 802.16m supports several advanced multiantenna techniques including single and MU-MIMO (spatial multiplexing and beamforming) as well as a number of transmit diversity schemes. In SU-MIMO scheme only one user can be scheduled over one (time, frequency, spatial) resource unit. In MU-MIMO, on the other hand, multiple users can be scheduled in one resource unit. Vertical encoding (or single codeword) utilizes one encoder block (or layer), whereas horizontal encoding (or multicodeword) uses multiple encoders (or multiple layers) in the transmit chain. A layer is defined as a coding and modulation input path to the MIMO encoder. A stream is defined as the output of the MIMO encoder that is further processed through the beamforming or the precoder block [6]. For spatial multiplexing, the rank is defined as the number of streams to be used for the user. Each SU-MIMO or MU-MIMO open-loop or closed-loop scheme is defined as a MIMO mode.

The DL MIMO transmitter structure is shown in Figure 25.13. The encoder block contains the channel encoder, interleaving, rate-matching, and modulating blocks per layer. The resource mapping block

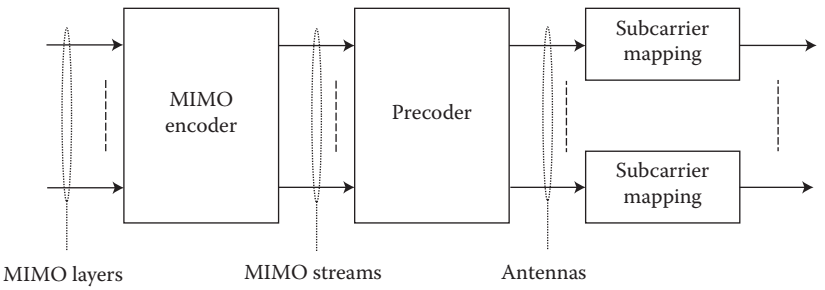

FIGURE 25.13 Illustration of downlink/uplink MIMO structure. (Adapted from Sassan Ahmadi, *Mobile WiMAX; A Systems Approach to Understanding IEEE 802.16m Radio Access Technology*, 1st Edition, Academic Press, 2010; IEEE Std 802.16m-2011, *IEEE Standard for Local and Metropolitan Area Networks—Part 16: Air Interface for Broadband Wireless Access Systems, Amendment 3: Advanced Air Interface*, May 2011.)

TABLE 25.3 Downlink MIMO Modes

Mode Index	Description	MIMO Encoding Format	MIMO Precoding
Mode 0	Open-loop SU-MIMO	SFBC	NonAdaptive
Mode 1	Open-loop SU-MIMO (spatial multiplexing)	Vertical encoding	NonAdaptive
Mode 2	Closed-loop SU-MIMO (spatial multiplexing)	Vertical encoding	Adaptive
Mode 3	Open-loop MU-MIMO (spatial multiplexing)	Horizontal encoding	Nonadaptive
Mode 4	Closed-loop MU-MIMO (spatial multiplexing)	Horizontal encoding	Adaptive
Mode 5	Open-loop SU-MIMO (TX diversity)	Conjugate data repetition	Nonadaptive

Source: Adapted from Sassan Ahmadi, *Mobile WiMAX; A Systems Approach to Understanding IEEE 802.16m Radio Access Technology*, 1st Edition, Academic Press, 2010; IEEE Std 802.16m-2011, *IEEE Standard for Local and Metropolitan Area Networks—Part 16: Air Interface for Broadband Wireless Access Systems, Amendment 3: Advanced Air Interface*, May 2011.

maps the complex-valued modulation symbols to the corresponding time–frequency resources. The MIMO encoder block maps the layers onto the streams, which are further processed through the precoder block. The precoder block maps the streams to antennas by generating the antenna-specific data symbols according to the selected MIMO mode. The OFDM symbol construction block maps antenna-specific data to the OFDM symbols. The feedback block contains feedback information such as CQI or CSI from the MS. Table 25.3 contains more information on various MIMO modes supported by the IEEE 802.16m.

The minimum antenna configuration in the downlink and uplink is 2×2 and 1×2, respectively. For open-loop spatial multiplexing and closed-loop SU-MIMO, the number of streams is constrained to the minimum of number of transmit or receive antennas. For open-loop transmit diversity modes, the number of streams depends on the space-time coding schemes that are used by the MIMO encoder. The MU-MIMO can support up to two streams with two transmit antennas and up to four streams for four transmit antennas and up to eight streams for eight transmit antennas. Table 25.4 summarizes downlink MIMO parameters for various MIMO modes.

For SU-MIMO, vertical encoding is utilized, whereas for MU-MIMO horizontal encoding is employed at the BS. The stream to antenna mapping depends on the MIMO scheme that is used. CQI and rank feedback are transmitted to assist the BS in rank adaptation, mode switching, and rate adaptation. For spatial multiplexing, the rank is defined as the number of streams to be used for each user. In FDD and TDD systems, unitary codebook-based precoding is used for closed-loop SU-MIMO. An MS may feed back some information to the BS in closed-loop SU-MIMO such as rank, subband selection, CQI, PMI, and long-term CSI.

The MU-MIMO transmission with up to two streams per user is supported. The MU-MIMO schemes include two transmit antennas for up to two users, and four and eight transmit antennas for up to four users. Both unitary and nonunitary MU-MIMO schemes are supported. If the columns of the precoding matrix are orthogonal to each other, it is defined as unitary MU-MIMO. Otherwise, it is defined as nonunitary MU-MIMO [6]. Beamforming is enabled with this precoding mechanism. IEEE 802.16m has the capability to adapt between SU-MIMO and MU-MIMO in a predefined and flexible manner. Multi-BS MIMO techniques are also supported for improving sector and cell-edge throughput using multi-BS collaborative precoding, network coordinated beamforming, or intercell interference cancellation.

25.5.8.2 Uplink MIMO

The block diagram of uplink MIMO transmitter is illustrated in Figure 25.13. The BS assigns users to resource blocks and determines the modulation and coding scheme level and MIMO parameters (mode, rank, etc.). The supported antenna configurations include 1, 2, or 4 transmit antennas and >2 receive antennas. In the uplink, the MS measurements of the channel are based on downlink reference signals (e.g., common pilots or a midamble). The uplink MIMO modes and their parameters are contained in Tables 25.5 and 25.6.

TABLE 25.4 Downlink MIMO Parameters

	Number of Transmit Antennas	Rate per Layer	Number of Streams	Number of Subcarriers	Number of Layers
MIMO mode 0	2	1	2	2	1
	4	1	2	2	1
	8	1	2	2	1
MIMO mode 1 and MIMO mode 2	2	1	1	1	1
	2	2	2	1	1
	4	1	1	1	1
	4	2	2	1	1
	4	3	3	1	1
	4	4	4	1	1
	8	1	1	1	1
	8	2	2	1	1
	8	3	3	1	1
	8	4	4	1	1
	8	5	5	1	1
	8	6	6	1	1
	8	7	7	1	1
	8	8	8	1	1
MIMO mode 3 and MIMO mode 4	2	1	2	1	2
	4	1	2	1	2
	4	1	3	1	3
	4	1	4	1	4
	8	1	2	1	2
	8	1	3	1	3
	8	1	4	1	4
MIMO mode 4	4	2 and 1[a]	3	1	2
	4	2 and 1[b]	4	1	3
	4	2	4	1	2
	8	2 and 1[a]	3	1	2
	8	2 and 1[b]	4	1	3
	8	2	4	1	2
	8	1	8	1	8
	8	2 and 1[c]	8	1	7
	8	2 and 1[d]	8	1	6
	8	2 and 1[e]	8	1	5
	8	2	8	1	4
MIMO mode 5	2	1/2	1	2	1
	4	1/2	1	2	1
	7	1/2	1	2	1

Source: Adapted from Sassan Ahmadi, *Mobile WiMAX; A Systems Approach to Understanding IEEE 802.16m Radio Access Technology*, 1st Edition, Academic Press, 2010; IEEE Std 802.16m-2011, *IEEE Standard for Local and Metropolitan Area Networks—Part 16: Air Interface for Broadband Wireless Access Systems, Amendment 3: Advanced Air Interface*, May 2011.

[a] 2 streams to one MS and one stream to another MS each with one layer.

[b] 2 streams to one MS and one stream each to the other two MSs each with one layer.

[c] 2 streams to one MS and one stream each to the other six MSs each with one layer.

[d] 2 streams each to two MS and one stream each to the other four MSs each with one layer.

[e] 2 streams each to three MS and one stream each to the other two MSs each with one layer.

TABLE 25.5 Uplink MIMO Modes

Mode Index	Description	MIMO Encoding Format	MIMO Precoding
Mode 0	Open-loop SU-MIMO (transmit diversity)	SFBC	Nonadaptive
Mode 1	Open-loop SU-MIMO (spatial multiplexing)	Vertical encoding	Nonadaptive
Mode 2	Closed-loop SU-MIMO (spatial multiplexing)	Vertical encoding	Adaptive
Mode 3	Open-loop collaborative spatial multiplexing (MU-MIMO)	Vertical encoding	Nonadaptive
Mode 4	Closed-loop collaborative spatial multiplexing (MU-MIMO)	Vertical encoding	Adaptive

Source: Adapted from Sassan Ahmadi, *Mobile WiMAX; A Systems Approach to Understanding IEEE 802.16m Radio Access Technology*, 1st Edition, Academic Press, 2010; IEEE Std 802.16m-2011, *IEEE Standard for Local and Metropolitan Area Networks—Part 16: Air Interface for Broadband Wireless Access Systems, Amendment 3: Advanced Air Interface*, May 2011.

TABLE 25.6 Uplink MIMO Parameters

	Number of Transmit Antennas	Rate per Layer	Number of Streams	Number of Subcarriers	Number of Layers
MIMO mode 0	2	1	2	2	1
	4	1	2	2	1
MIMO mode 1	1	1	1	1	1
MIMO mode 1 and MIMO mode 2	2	1	1	1	1
	2	2	2	1	1
	4	1	1	1	1
	4	2	2	1	1
	4	3	3	1	1
	4	4	4	1	1
MIMO mode 3 and MIMO mode 4	1	1	1	1	1
	2	1	1	1	1
	2	2	2	1	1
	4	1	1	1	1
	4	2	2	1	1
	4	3	3	1	1
	4	4	4	1	1

Source: Adapted from Sassan Ahmadi, *Mobile WiMAX; A Systems Approach to Understanding IEEE 802.16m Radio Access Technology*, 1st Edition, Academic Press, 2010; IEEE Std 802.16m-2011, *IEEE Standard for Local and Metropolitan Area Networks—Part 16: Air Interface for Broadband Wireless Access Systems, Amendment 3: Advanced Air Interface*, May 2011.

A number of antenna configurations and transmission rates are supported in uplink open-loop SU-MIMO including 2 and 4 transmit antennas with rate 1 (i.e., transmit diversity mode), 2 and 4 transmit antennas with rates 2, 3, and 4 (i.e., spatial multiplexing). The supported uplink transmit diversity modes include 2 and 4 transmit antenna schemes with rate 1 such as space frequency block coding (SFBC) and dual-stream precoder. The multiplexing modes supported for open-loop SU-MIMO include 2 and 4 transmit antenna rate 2 schemes with and without precoding, four transmit antenna rate 3 schemes with precoding, four transmit antenna rate 4 scheme. In FDD and TDD systems, unitary codebook-based precoding is supported. In this mode, an MS transmits a sounding reference signal in the uplink to assist the scheduling and precoder selection in the BS. The BS signals the resource allocation, MCS, rank, preferred precoder index, and packet size to the MS. The uplink MU-MIMO enables multiple MSs to be spatially multiplexed on the same radio resources. Both open-loop and closed-loop MU-MIMO are supported. The MSs with single transmit antenna can operate in open-loop SU-MIMO/MU-MIMO mode.

25.6 Overview of the IEEE 802.16m MAC Layer

There are various MAC functionalities and features that are specified by IEEE 802.16m standard some of which are extension of the existing features in the mobile WiMAX [8,7]. The following sections briefly describe selected MAC features.

25.6.1 MAC Addressing

IEEE 802.16m standard defines global and logical addresses for an MS that identify the user and its connections during a session. The MS is identified by the globally unique 48-bit IEEE extended unique identifier assigned by the IEEE Registration Authority [10,11]. The MS is further assigned the following logical identifiers: (1) An STID during network entry (or network reentry), which uniquely identifies the MS within the cell, and (2) an FID that uniquely identifies the control connections and transport connections with the MS. A temporary STID is used to protect the mapping between the actual STID during network entry. A deregistration identifier is defined to uniquely identify the MS within the set of paging group identifiers (PGID), paging cycle, and paging offset.

25.6.2 Network Entry

Network entry is the procedure through which an MS detects a cellular network and establishes a connection with that network. The network entry involves the following steps (see Figure 25.14):

- Synchronization with the BS by acquiring the preambles
- Acquiring necessary system information such as BS and NSP identifiers for initial network entry and cell selection
- Initial ranging
- Basic capability negotiation
- Authentication/authorization and key exchange
- Registration and service flow setup

Neighbor search is based on the same downlink signals as initial network search except for some information can be provided by the serving BS (i.e., neighbor advertisement messages). The BS responds to the MS initial ranging code transmission by broadcasting a status indication message in a predefined downlink frame/subframe.

25.6.3 Connection Management

A connection is defined as a mapping between the MAC layers of a BS and one (or several) MS. If there is a one-to-one mapping between one BS and one MS, the connection is called a unicast connection; otherwise, it is called a multicast or broadcast connection. Two types of connections are specified: control connections and transport connections. Control connections are used to carry MAC control messages. Transport connections are used to carry user data including upper-layer signaling messages. A MAC control message is never transferred over transport connection, and user data are never transferred over the control connections. One pair of bidirectional (DL/UL) unicast control connections are automatically established when an MS performs initial network entry. The user data communications are in the context of transport connections. A transport connection is unidirectional and established with a unique FID. Each transport connection is associated with an active service flow to provide various levels of QoS required by the service flow. The transport connection is established when the associated active service flow is admitted or activated, and released when the associated service flow becomes inactive. Transport connections can be preprovisioned or dynamically created. Preprovisioned

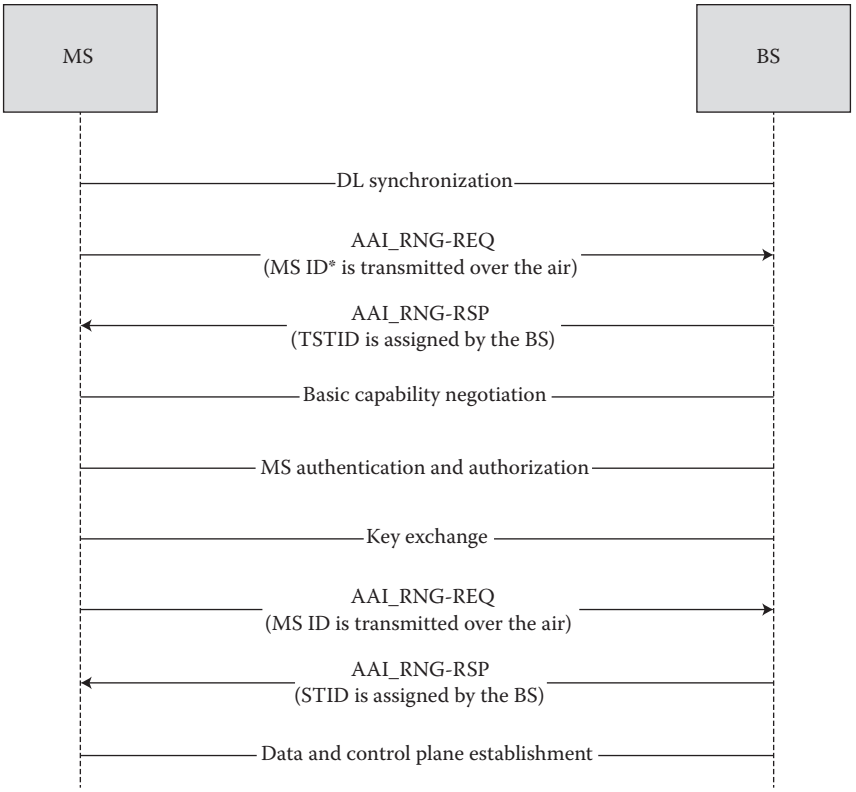

FIGURE 25.14 Network entry procedures. (Adapted from Sassan Ahmadi, *Mobile WiMAX; A Systems Approach to Understanding IEEE 802.16m Radio Access Technology*, 1st Edition, Academic Press, 2010; IEEE Std 802.16m-2011, *IEEE Standard for Local and Metropolitan Area Networks—Part 16: Air Interface for Broadband Wireless Access Systems, Amendment 3: Advanced Air Interface*, May 2011; IEEE 802.16m-08/0034r4, *IEEE 802.16m System Description Document*, (http://ieee802.org/16/tgm/index.html), December 2010.)

connections are those established by system for an MS during the MS network entry. On the other hand, the BS or the MS can create new connections dynamically if required.

25.6.4 Quality of Service

IEEE 802.16m MAC assigns a unidirectional flow of packets with specific QoS requirements with a service flow. A service flow is mapped to a transport connection with an FID. The QoS parameter set is negotiated between the BS and the MS during the service flow setup/change procedure. The QoS parameters can be used to schedule traffic and allocate radio resource. The uplink traffic may be regulated based on the QoS parameters.

IEEE 802.16m supports adaptation of service flow QoS parameters. One or more sets of QoS parameters are defined for each service flow. The MS and BS negotiate the possible QoS parameter sets during service flow setup procedure. When QoS requirement/traffic characteristics for uplink traffic change, the BS may adapt the service flow QoS parameters such as grant/polling interval or grant size based on predefined rules. In addition, the MS may request the BS to switch the service flow QoS parameter set with explicit signaling. The BS then allocates resource according to the new service flow parameter set. In addition to the scheduling services supported by the legacy system, IEEE 802.16m provides a specific

scheduling service and dedicated ranging channel to support real-time nonperiodical applications such as interactive gaming.

25.6.5 MAC Control Messages

To satisfy the latency requirements for network entry, HO, and state transitions, IEEE 802.16m supports fast and reliable transmission of MAC management messages. The transmission of unicast MAC management messages can be made more reliable using HARQ, where retransmissions can be triggered by an unsuccessful outcome from the HARQ entity in the transmitter. If MAC management message is fragmented into multiple MAC service data units, only unsuccessfully transmitted fragments are retransmitted.

25.6.6 MAC Headers

IEEE 802.16m specifies a number of efficient MAC headers for various applications comprising of fewer fields with shorter size compared to legacy standard generic MAC header [6,10,11]. The advanced generic MAC header consists of *Extended Header Indicator, FID*, and *Payload Length* fields. Other MAC header types include two-byte short-packet MAC header, which is defined to support small-payload applications such as VoIP which is characterized by small data packets and non-ARQ connection, Fragmentation extended header, Packing extended header for transport connections, MAC control extended header for control connections, and Multiplexing extended header that is used when data from multiple connections associated with the same security association (SA) are encapsulated in a single MAC protocol data unit. The structures of some MAC headers are shown in Figure 25.15.

25.6.7 ARQ and HARQ Functions

An ARQ block is generated from one or multiple MAC service data units or their fragments. ARQ blocks can be variable in size and are sequentially numbered. When both ARQ and HARQ are applied on a flow, HARQ and ARQ interactions are applied to the corresponding flow. If the HARQ entity in the transmitter determines that the HARQ process was terminated with an unsuccessful outcome, the HARQ entity in the transmitter informs the ARQ entity in the transmitter about the failure of the HARQ burst. The ARQ entity in the transmitter can then initiate retransmission and resegmentation of the appropriate ARQ blocks.

IEEE 802.16m uses adaptive asynchronous and nonadaptive synchronous HARQ schemes in the downlink and uplink, respectively. The HARQ operation is relying on an N-process (multichannel) stop-and-wait protocol. In adaptive asynchronous HARQ, the resource allocation and transmission format for the HARQ retransmissions may be different from the initial transmission. In the case of retransmission, control signaling is required to indicate the resource allocation and transmission format along with other HARQ necessary parameters. A nonadaptive synchronous HARQ scheme is used in the uplink where the parameters and the resource allocation for the retransmission are known in advance.

25.6.8 Mobility Management and HO

IEEE 802.16m supports both network-controlled and MS-assisted HO. The HO procedure may be initiated by either MS or BS; however, the final HO decision and target BS selection are made by the serving BS. The MS executes the HO command as instructed by the BS or cancels the procedure through HO cancellation message. The network reentry procedure with the target BS may be optimized, if the target BS obtains the MS context from the serving BS via core network. The MS may also maintain

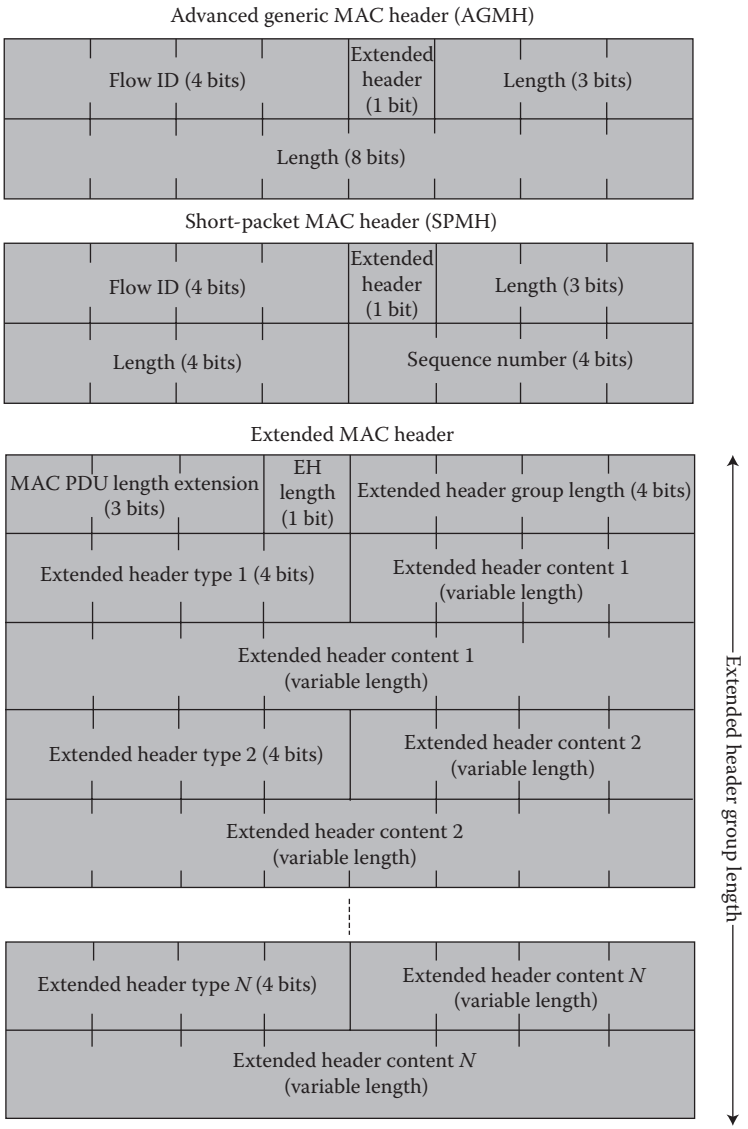

FIGURE 25.15 Structure of the IEEE 802.16m MAC headers. (Adapted from Sassan Ahmadi, *Mobile WiMAX; A Systems Approach to Understanding IEEE 802.16m Radio Access Technology*, 1st Edition, Academic Press, 2010; IEEE Std 802.16m-2011, *IEEE Standard for Local and Metropolitan Area Networks—Part 16: Air Interface for Broadband Wireless Access Systems, Amendment 3: Advanced Air Interface*, May 2011; IEEE 802.16m-08/0034r4, *IEEE 802.16m System Description Document*, (http://ieee802.org/16/tgm/index.html), December 2010.)

communication with serving BS while performing network reentry at target BS as directed by serving BS. Figure 25.16 illustrates the HO procedure.

The HO procedure is divided into three stages (1) HO initialization, (2) HO preparation, and (3) HO execution. Upon completion of HO execution, the MS is ready to perform network reentry with the target BS. In addition, HO cancellation procedure is defined to allow an MS to cancel an HO procedure [6,10].

The HO preparation is completed when the serving BS informs the MS of its HO decision via an HO control command. The signaling may include dedicated ranging resource allocation and resource preallocations for MS at target BS for optimized network reentry. The control signaling includes an action

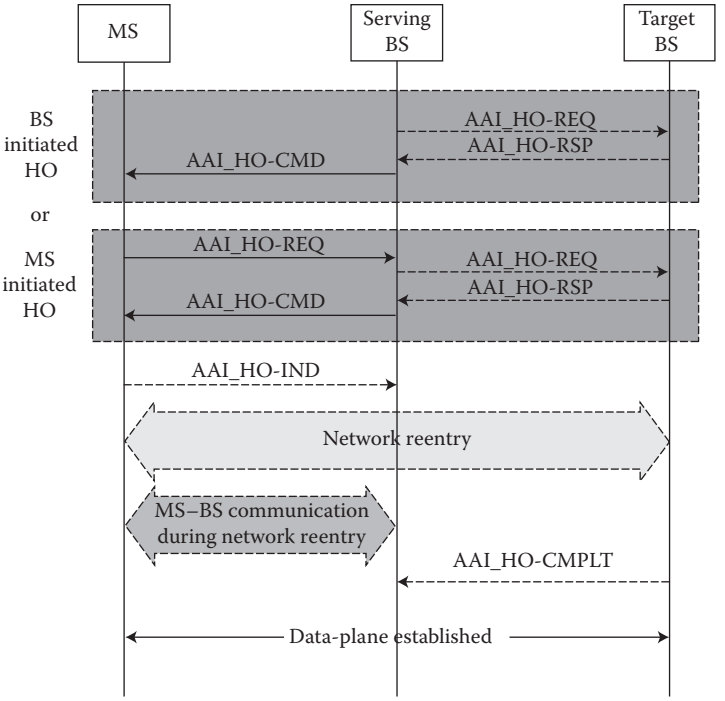

FIGURE 25.16 IEEE 802.16m HO procedure. (Adapted from Sassan Ahmadi, *Mobile WiMAX; A Systems Approach to Understanding IEEE 802.16m Radio Access Technology*, 1st Edition, Academic Press, 2010; IEEE Std 802.16m-2011, *IEEE Standard for Local and Metropolitan Area Networks—Part 16: Air Interface for Broadband Wireless Access Systems, Amendment 3: Advanced Air Interface*, May 2011.)

time for the MS to start network reentry at the target BS and an indication of whether MS should maintain communication with serving BS during network reentry. If the data-plane cannot be maintained between MS and the serving BS during network reentry, the serving BS stops allocating resources to MS for transmission during action time. If the MS is instructed by the serving BS via HO control command, the MS performs network reentry with the target BS during action time while communicating with the serving BS. However, the MS stops communication with the serving BS after completion of the network reentry with target BS. In addition, the MS cannot exchange data with the target BS prior to the completion of network reentry.

25.6.9 Power Management

IEEE 802.16m provides power management functions including sleep mode and idle mode to lower power consumption of the MSs. Sleep mode is a state in which an MS performs prenegotiated periods of absence from the serving BS. The sleep mode may be enacted when an MS is in the connected state. Using the sleep mode, the MS is provided with a series of alternative listening and sleep windows. The listening window is the time interval in which MS is available for transmit/receive of control signaling and data. The IEEE 802.16m has the capability of dynamically adjusting the duration of sleep and listening windows within a sleep cycle based on changing traffic patterns and HARQ operations. When an MS is in the active mode, sleep parameters are negotiated between the MS and BS. The BS instructs the MS to enter sleep mode. MAC control messages can be used for sleep mode request/response [6,10,11]. The period of the sleep cycle is measured in units of frames or superframes and is the sum of sleep and listening windows. During the MS listening window, the BS may transmit the traffic indication message

intended for one or multiple MSs. The listening window can be extended through explicit/implicit signaling. The maximum length of the extension is to the end of the current sleep cycle [6,10].

Idle mode allows the MS to become periodically available for downlink broadcast traffic messaging such as paging message without registration with the network. The network assigns MSs in the idle mode to a paging group during idle mode entry or location update. The MS monitors the paging message during paging-available interval. The start of the paging-available interval is calculated based on paging cycle and paging offset. The paging offset and paging cycle are defined in terms of number of superframes. The serving BS transmits the list of PGID at the predetermined location at the beginning of the paging available interval. An MS may be assigned to one or more paging groups. If an MS is assigned to multiple paging groups, it may also be assigned multiple paging offsets within a paging cycle where each paging offset corresponds to a separate paging group. The MS is not required to perform location update when it moves within its assigned paging groups. The assignment of multiple paging offsets to an MS allows monitoring paging message at different paging offsets when the MS is located in one of these paging groups. When an MS is assigned to >1 paging group, one of the paging groups is called *Primary Paging Group* and others are known as *Secondary Paging Groups*. If an MS is assigned to one paging group, that paging group is considered the *Primary Paging Group*. When different paging offsets are assigned to an MS, the *Primary Paging Offset* is shorter than the *Secondary Paging Offset*s. The distance between two adjacent paging offsets should be long enough so that the MS paged in the first paging offset can inform the network before the next paging offset in the same paging cycle so that the network avoids unnecessary paging of the MS in the next paging offset. An MS, while in paging available interval, wakes up at its primary paging offset and looks for primary PGID information. If the MS does not detect the primary PGID, it will wake up during its secondary paging offset in the same paging cycle. If the MS can find neither primary nor secondary PGIDs, it will perform a location update. The paging message contains identification of the MSs to be notified of pending traffic or location update. The MS determines the start of the paging listening interval based on the paging cycle and paging offset. During paging available interval, the MS monitors the superframe header and if there is an indication of any change in system configuration information, the MS will acquire the latest system information at the next instance of superframe header transmission. To provide location privacy, the paging controller may assign temporary identifiers to uniquely identify the MSs in the idle mode in a particular paging group. The temporary identifiers remain valid as long as the MS stays in the same paging group.

An MS in idle mode performs location update, if either of these conditions is met: paging group location update, timer based location update, or power down location update. The MS performs location update when it detects a change in the paging group. The MS detects the change of paging group by monitoring the PGIDs, which are periodically transmitted by the BS. The MS periodically performs location update procedure prior to the expiration of idle mode timer. At every location update including paging group update, the idle mode timer is reset.

25.6.10 Security

Security functions provide subscribers with privacy, authentication, and confidentiality across IEEE 802.16m network. The MAC packet data units are encrypted over the connections between the MS and BS. Figure 25.17 shows the breakdown of IEEE 802.16m security architecture.

The security architecture is divided into security management, encryption and integrity logical entities. The security management functions include overall security management and control, Extensible Authentication Protocol encapsulation/de-encapsulation, privacy key management (PKM) control, SA management, and identity/location privacy. The encryption and integrity protection functions include user data encryption and authentication, management message authentication, message confidentiality protection [6,10]. Authorization is a process where BS and MS mutually authenticate the identity of each other. Authentication is performed during initial network entry after security capabilities and policies are negotiated. The basic MS capability negotiation is performed prior to authentication and authorization.

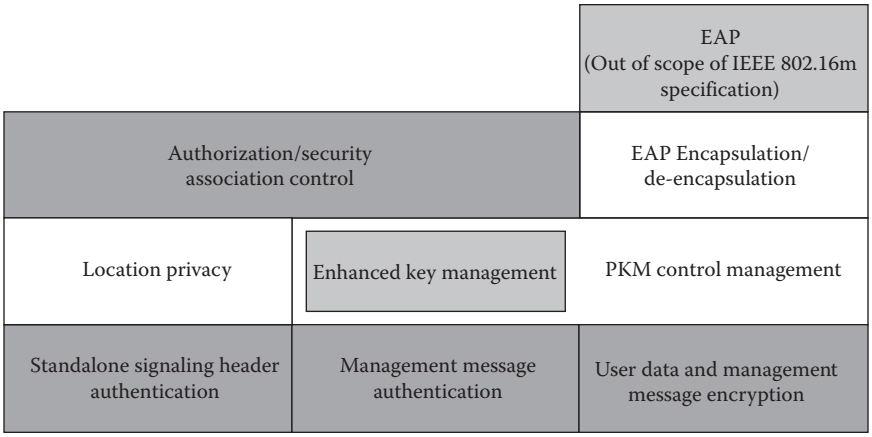

FIGURE 25.17 Functional blocks of IEEE 802.16m security architecture. (Adapted from Sassan Ahmadi, *Mobile WiMAX; A Systems Approach to Understanding IEEE 802.16m Radio Access Technology*, 1st Edition, Academic Press, 2010; IEEE Std 802.16m-2011, *IEEE Standard for Local and Metropolitan Area Networks—Part 16: Air Interface for Broadband Wireless Access Systems, Amendment 3: Advanced Air Interface*, May 2011.)

Reauthentication is performed before the authentication credentials expire. Data transmission may continue during reauthentication process. In the legacy system there is no explicit means by which the identity of a user is protected. During initial ranging and certificate exchange, MS MAC address is transmitted over the air, revealing user identity or user location information that may result in compromising the security aspects of the system. IEEE 802.16m incorporates mechanisms such a pseudo-identity to mitigate this problem. IEEE 802.16m inherits the key hierarchies of the legacy system. The IEEE 802.16m uses the PKMv3 protocol to transparently exchange authentication and authorization messages. The PKM protocol provides mutual and unilateral authentication and establishes confidentiality between the MS and the BS. Some IEEE 802.16m keys are derived and updated by both BS and MS. The key exchange procedure is controlled by the security key state machine, which defines the allowed operations in the specific states. The key exchange state machine is similar to that of the legacy system.

A SA is the set of information required for secure communication between BS and MS. However, the SA is not equally applied to messages within the same flow. According to the value of MAC header fields, the SA is selectively applied to the control connections. When a service flow is established between the BS and the group of MSs, it is considered as multicast and it is serviced by a group SA. The MS and the BS may support encryption methods and algorithms for secure transmission of MAC packet data units. Advanced encryption standard is the only cryptographic method supported in IEEE 802.16m [6,10]. The legacy system does not define confidentiality protection for control-plane signaling. IEEE 802.16m selectively protects the confidentiality of control-plane signaling. The use of MAC message authentication code in legacy systems only proves the originator of messages and ensures integrity of the messages. IEEE 802.16m supports the selective confidentiality protection over MAC control messages. If the selective confidentiality protection is activated, the negotiated keying materials and cipher suites are used to encrypt the management messages. Integrity protection is applied to standalone MAC signaling header.

References

1. Recommendation ITU-R M.1645, Framework and overall objectives of the future development of IMT-2000 and systems beyond IMT-2000, June 2003.
2. Report ITU-R M.2134, Requirements related to technical system performance for IMT-Advanced radio interface(s), November 2008.

3. IEEE 802.16m-07/002r10, *IEEE 802.16m System Requirements*, (http://ieee802.org/16/tgm/index.html), January 2010.
4. Report ITU-R M.2135-1, Guidelines for evaluation of radio interface technologies for IMT-Advanced, December 2009.
5. IEEE 802.16m-08/004r5, *IEEE 802.16m Evaluation Methodology Document*, (http://ieee802.org/16/tgm/index.html), January 2009.
6. Sassan Ahmadi, *Mobile WiMAX; A Systems Approach to Understanding IEEE 802.16m Radio Access Technology*, 1st Edition, Academic Press, 2010.
7. WiMAX Forum Network Architecture Release 1.5 Version 1—Stage 2: Architecture Tenets, Reference Model and Reference Points, http://www.wimaxforum.org/resources/documents/technical/release, September 2009.
8. WiMAX Forum Mobile System Profile, Release 1.5, September 2010 (http://www.wimaxforum.org/resources/documents/technical/release)
9. IEEE 802.16m-08/0034r4, *IEEE 802.16m System Description Document*, (http://ieee802.org/16/tgm/index.html), December 2010.
10. IEEE Std 802.16m-2011, *IEEE Standard for Local and Metropolitan Area Networks—Part 16: Air Interface for Broadband Wireless Access Systems, Amendment 3: Advanced Air Interface*, May 2011.
11. IEEE Std 802.16-2009, *IEEE Standard for Local and Metropolitan Area Networks, PART 16: Air Interface for Broadband Wireless Access Systems*, May 2009.

26

Land Mobile Radio and Professional Mobile Radio: Emergency First Responder Communications

Jerry D. Gibson

26.1 Introduction

While mobile communications have become ubiquitous throughout the World due to the widespread availability of cellular networks, wireless access points, and satellite links, there is another set of wireless communications systems that is critical to our well-being, particularly in the event of natural and man-made disasters. This chapter is about the wireless communications systems used by Emergency First Responders, such as firefighters, police, and other governmental agency personnel. Perhaps surprisingly, these systems are based on much more rudimentary communications technologies than are the commercial systems that we use in our everyday lives. Similar to military communications systems, communications systems for emergency first responders have some very specific special requirements that are not available in most commercial systems and we develop these special requirements here. These emergency communications systems also have a unique evolutionary path that is far from what many consider as the quite revolutionary path blazed by digital cellular and other commercial wireless technologies in the past 25 years [1–3].

It is well known to the public that communications systems relied upon by the public often fail during natural disasters, as in, for example, Hurricane Katrina, the Haiti earthquake, and wildfires near urban areas, wherein switches are flooded, cell sites are toppled, or cellular traffic outstrips cell site capacities. What may be disconcerting is that emergency first responder communication systems have exhibited their own failure modes, such as lack of interoperability, loss of relay stations, and poor voice quality due to background impairments, and that these systems have very limited capabilities for data, video, and other multimedia traffic. The various agencies of the World are attempting to correct these very serious

shortcomings, but research and development, planning, training, equipment options, and budgets are all sorely lacking.

We begin our treatment with an overview of the unique requirements of first responder communications systems and the different scenarios that are envisioned when designing such systems. We then provide discussions on land mobile radio (LMR) Systems in the U.S. and professional mobile radio (PMR) Systems in Europe and elsewhere. We next turn our attention to the planned expansions of emergency responder networks in the United States, particularly with respect to the broadband nationwide connectivity via digital cellular LTE. We also discuss how some standards bodies are attempting to address the needed capabilities. Finally, we outline the shortcomings and the ongoing challenges in first responder communications.

26.2 Unique Requirements of Emergency First Responder Communications

An important point to realize at the outset is that all public safety communication problems are not equal and can greatly differ. In recent years, public safety personnel have responded to terrorist acts, hurricanes, prairie fires, mountain wildfires, tsunamis, earthquakes, and infrastructure failures, such as the Minneapolis bridge collapse [4,5].

The MESA Project recognized the variety of public safety responses that can occur and created the Scenario Class Diagram in Figure 26.1 to help in their classification [6]. As examples of using this diagram, one can classify the Minneapolis bridge failure as Urban/Disaster/Single Spot, whereas a wildfire in mountainous terrain would be classified as Rural/Emergency/Wide Area. Another classification that is useful is time span. The Minneapolis bridge collapse had intense communications for a relatively short period of time (a few hours), whereas a mountainous wildfire can go on for days or weeks and require sustained, coordinated communications of all kinds.

During these events, literally hundreds of responders may be connected, and so large talk groups must be supported, plus there must be a quick-response push-to-talk (PTT) capability so that anyone on the call can comment. Another requirement is for quick response radio-to-radio communications, that is, direct communications between any pair of first responders. For voice communications, these

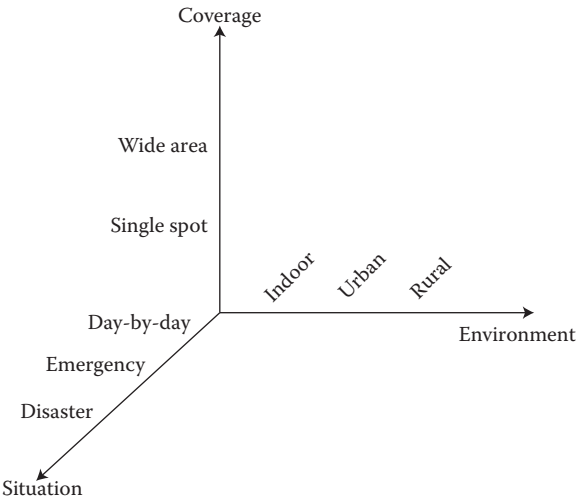

FIGURE 26.1 Characterization of emergency scenarios. (Adapted from Project Mesa; service specification group-services and applications; statement of requirements executive summary. MESA Organizational Partners (ETSI, TIA), 2005. [Online]. Available: www.projectmesa.org.)

requirements are not generally available in commercial digital cellular or WiMAX systems, without what is called "trunking." Trunking means that the channels are shared and usually that communications must be handled by a switch, an example of which would be the base station/mobile switching center in digital cellular systems.

Also important in these events is the support of low speed, but very responsive, data communications. The key term in characterizing first responder communications, whether voice or data, is "mission critical."

A different type of requirement that equipment vendors emphasize is "hardening" of the handsets and other first responder communications equipment. That is, the equipment must withstand substantial amounts of physical abuse due to the environments encountered by first responders. This hardening requirement spills over to the systems themselves, in that a certain level of coverage needs to be maintained even in a catastrophic event. In addition to the required level of geographical coverage that may be needed anywhere an emergency occurs, the coverage must also include the capability to support unexpected spikes of traffic. Of course, these requirements are very different that digital cellular, which can easily suffer from lack of coverage in some areas and which can also experience dropped or blocked calls when cell sites are saturated with traffic. While these latter capabilities of coverage wherever needed and the ability to handle sudden spikes of traffic are often touted for public safety communication systems, mission critical communications by first responders has suffered substantial loss of coverage and blockage of calls in many recent emergencies.

The overall view is that public safety communication networks need to support worst-case situations, while commercial systems often operate on the best effort premise.

26.3 Conventional Land Mobile Radio in the United States

The largest-scale approach to improving first responder communications in the United States is Project 25 (P25), begun in 1988, and designed around the then existing analog FM communications systems. P25 was established to develop and standardize digital radio methods for LMR emergency response applications with the cooperation of the Association of Public Safety Communications Officials (APCO) and the Telecommunications Industry Association (TIA) [7,8], although the driving force is APCO, which is a group of vendors without a government or organized user group providing independent oversight and guidance.

Land mobile radio in the United States has evolved from a system based on narrowband analog channels to systems based on digital modulation and voice compression in the last 20 years. However, the channelization and basic problem has not changed dramatically, and in fact, it is very important to emergency personnel and government agencies that certain functionalities remain intact. We provide an overview of the operation of an LMR analog system from which today's systems are evolving. We use Figure 26.2, adapted from Reference 3, as the focal point for discussion.

The transmissions shown in Figure 26.2 represent voice conversations transmitted using analog frequency modulation (FM) of carrier signals at the frequencies indicated. The consoles shown represent dispatchers for the two frequency groups. Direct mode operation (DMO) is also indicated at the top of the figure at a different carrier frequency to avoid interference. DMO does not go through the base station or switching and therefore delays are minimal, plus the individuals communicating using these units only need to have a good transmission path between them, and do not have to have a good communication link with the base stations. In many first responder communications scenarios, such as in tunnels or buildings or in remote locations, communications with a base station cannot be maintained but communications between units is critically important.

In contrast to the multiple access schemes used in digital cellular or wireless access points for the Internet, the basic channel access scheme for conventional LMR is called "radio discipline"; that is, communications should be limited to short voice calls of 6 s duration, and only information that is essential for personnel safety and emergency response coordination is supposed to be communicated. This type of

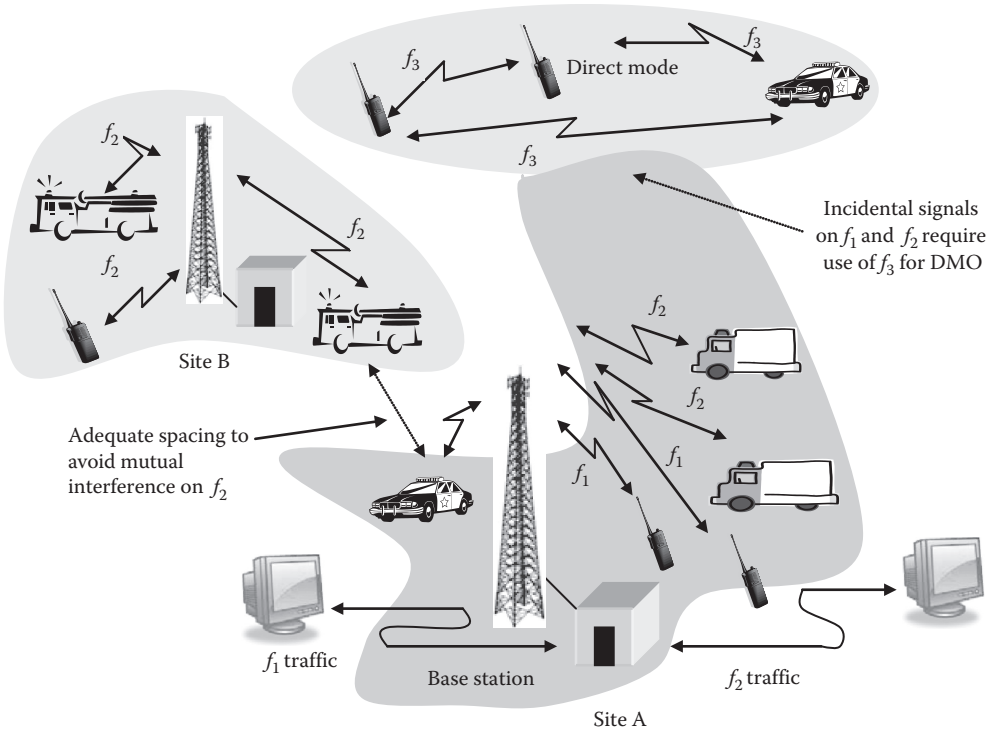

FIGURE 26.2 Conventional analog first responder communications. (Adapted from R. I. Desourdis et al., *Emerging Public Safety Wireless Communication Systems*, Artech House, Inc., Norwood, Massachusetts, 2002.)

communications using large talk groups allows everyone using that carrier frequency to "be on the same page" but congestion can occur as well. Users gain access to the channel by push to talk (PTT) [9], and PTT response times are desired to be on the order of less than a second, but in emergency situations with large talk groups, it may be difficult for a user to gain access to the channel. It is thus clear that latency should be minimal, and the analog modulation method does not add significant latency in the processing of the voice communications since the voice signal directly frequency modulates the carrier.

Analog LMR systems can have inefficient use of allocated spectrum and so the concept of trunking can also be employed. Trunking is where access to a channel using PTT is no longer direct, but the request is submitted through a control channel to a controller for the allocation of a frequency for the communications. If all goes well, the delays are not prohibitive, although the call initialization has additional latency compared to direct PTT access.

To address more demand for communications channels and to incorporate expanded data services as well, efforts were undertaken to move toward digital communication technologies. There are a number of approaches used for digital communications in public safety communications, but two have come to dominate the first responder communications space, usually called "mission critical" applications. These technologies are associated with two standards, Project 25 and TETRA [10,11]. We develop both of these systems in the following sections.

26.4 Project 25 Land Mobile Radio in the United States

Conventional analog LMR systems do not necessarily require much of a standard since they consist of simply FM transmission of voice on a known collection of frequencies. However, the move to digital communications implies a host of possibilities for modulation in a given band, for ways to represent the

voice signal digitally, for data transmission, and for system access. Project 25 is a standard established in the United States to specify the needed requirements. Among the goals of Project 25 are to maintain the same radio channels and allocated bandwidth and also to retain the user experience as much as possible. To make more efficient use of the spectrum, Project 25 also intends to double the number of channels in 25 kHz for Phase I, that is, 12.5 kHz per channel, and then implement 6.25 kHz bandwidth channels in Phase II. Different modulation methods are used as these channel allocations evolve.

The overall block diagram of P25 radios is shown in Figure 26.3 [12]. Following the diagram, we see that the input speech undergoes analog-to-digital conversion and is then passed to a speech coder. This codec has to operate at a bit rate that takes into account the overall allocated bandwidth per channel, the additional bits due to error control coding, and the modulation methods used over the channel. The speech encoder is discussed in detail in a subsequent section. Error control coding (channel coding) bits are then appended and all of the resulting bits are sent to the modulator for transmission. The demodulator has the usual components needed to recover the speech signal.

For Phase I, the allocated channel bandwidths are 12.5 kHz, so the final modulated signal must fit in this bandwidth. There are other desirable attributes as well, such as ease of demodulation, constant envelope transmitted signal, and backward compatibility with analog FM radios. The modulation method for Phase I is C4FM (Compatible 4-Level Frequency Modulation) [2], wherein each pair of bits at the input to the modulator have an assigned frequency deviation from the carrier, with 01 and 11 having +1.8 and −1.8 kHz deviation, respectively, and 00 and 10 having +0.6 kHz and −0.6 kHz deviation, respectively. C4FM has a constant envelope and therefore does not require linear amplifiers, which is a saving in cost and complexity. A block diagram of a C4FM modulator is shown in Figure 26.4. Not illustrated in Figures 26.3 or 26.4 is the multiple access method used for the 12.5 kHz channels within the 25 kHz band. For P25 Phase I, FDMA (frequency division multiple access) is used, thus splitting the frequency band in half. The voice codec used in P25 Phase I is IMBE at 4.4 kbits/s. The voice codecs are discussed in detail in a later section.

For P25 Phase II, the modulation methods are HCPM (hybrid continuous phase modulation) for the uplink (mobile to base) and HDQPSK (harmonized differential quadrature phase shift keying) for the

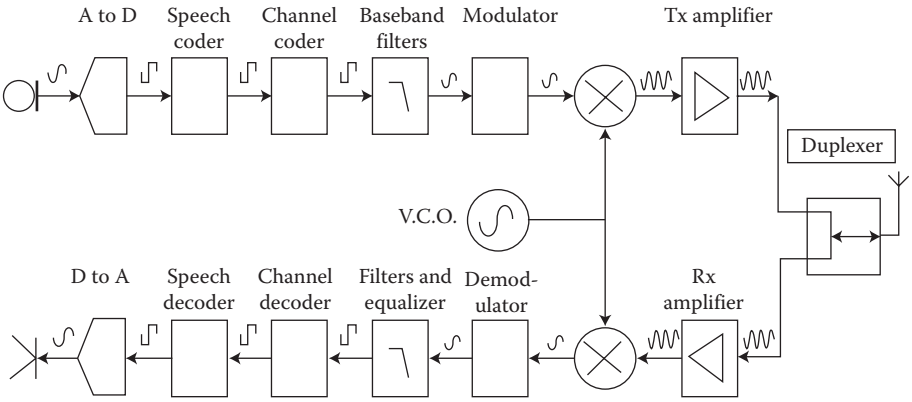

FIGURE 26.3 Block diagram of P25 land mobile radio units. (Adapted from P25 Radio Systems, *Training Guide*, Daniels Electronics Ltd., 2004.)

FIGURE 26.4 The C4FM modulator. (Adapted from P25 Radio Systems, *Training Guide*, Daniels Electronics Ltd., 2004.)

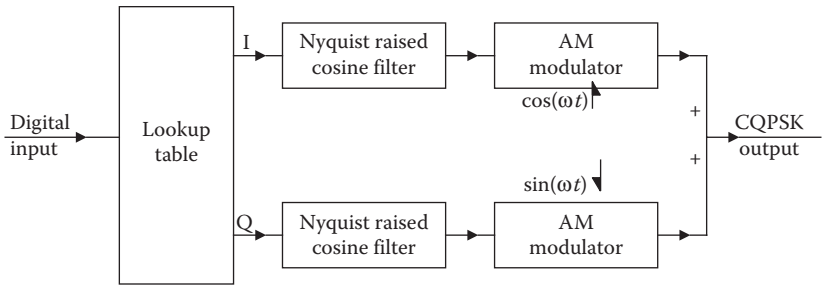

FIGURE 26.5 Modulation method for P25 Phase II. (Adapted from P25 Radio Systems, *Training Guide*, Daniels Electronics Ltd., 2004.)

downlink (base to mobile). There is another modulation method that can be used in the downlink for simulcast systems, and it is not developed here. A block diagram representing the modulator for these two methods is shown in Figure 26.5 [12], where CQPSK is used to denote Compatible Quadrature Phase Shift Keying. The differences between HCPM and HDQPSK are that HCPM has a constant envelope and HDQPSK is not constant envelope (thus requiring linear amplifiers) but it is also easier to demodulate. HCPM is vulnerable to intersymbol interference in addition to requiring a more complex demodulator.

The multiple access method used for Phase II is a combination of FDMA to obtain the 12.5 kHz channels and then 2 slot TDMA on each of these bands to obtain the 6.25 kHz channelization. The voice codec used in Phase II can be AMBE or AMBE+2, both of which can operate at dual rates to be compatible with the lower bandwidth systems.

26.4.1 Voice Codec

The primary need for first responders on Land Mobile Radio is voice communications, and that was the driver for conventional LMR systems. Given the narrow frequency band allocated to each channel in LMR for digital operation, the incoming speech must be sampled and compressed or coded at a low bit rate. For P25 in the United States, the codecs used are the IMBE, AMBE, and AMBE+2 codecs, all of which are based upon the Multiband Excitation (MBE) coding method [12,13]. In P25 Phase I, the Improved MBE, or IMBE, codec at 4.4 kbits/s is used for speech coding and then an additional 2.8 kbits/s is added for error control (channel) coding. This 7.2 kbits/s total then has other synchronization and low-speed data bits incorporated to obtain the final 9.6 kbits/s presented to the modulator. For P25 Phase II, the total rate available for speech and channel coding is half of 7.2 kbits/s or 3.6 kbits/s, which is split as 2.45 kbits/s for voice and 1.15 kbits/s for channel coding.

Block diagrams of the IMBE encoder and decoder are shown in Figures 26.6a and b, and a flow chart showing all the steps in the calculations is shown in Figure 26.7. We describe the basic IMBE codec in the following.

The IMBE vocoder models each segment of speech as a frequency-dependent combination of voiced (more periodic) and unvoiced (more noise-like) speech. This ability to mix voiced and unvoiced energy is a major advantage over traditional speech models that require each segment of speech to be entirely voiced or unvoiced. This flexibility gives the IMBE vocoder higher voice quality and more robustness to background noise.

The IMBE encoder estimates a set of model parameters for each segment of the incoming speech signal, which consists of the speaker pitch or fundamental frequency, a set of Voiced/Unvoiced (V/UV) decisions, which are used to generate the mixture of voiced and unvoiced excitation energy, and a set of spectral magnitudes, to represent the frequency response of the vocal tract. The encoder computes a discrete Fourier transform (DFT) for each segment of speech and then analyzes the frequency content to extract the model parameters for that segment. These model parameters are then quantized into 88 bits, and the

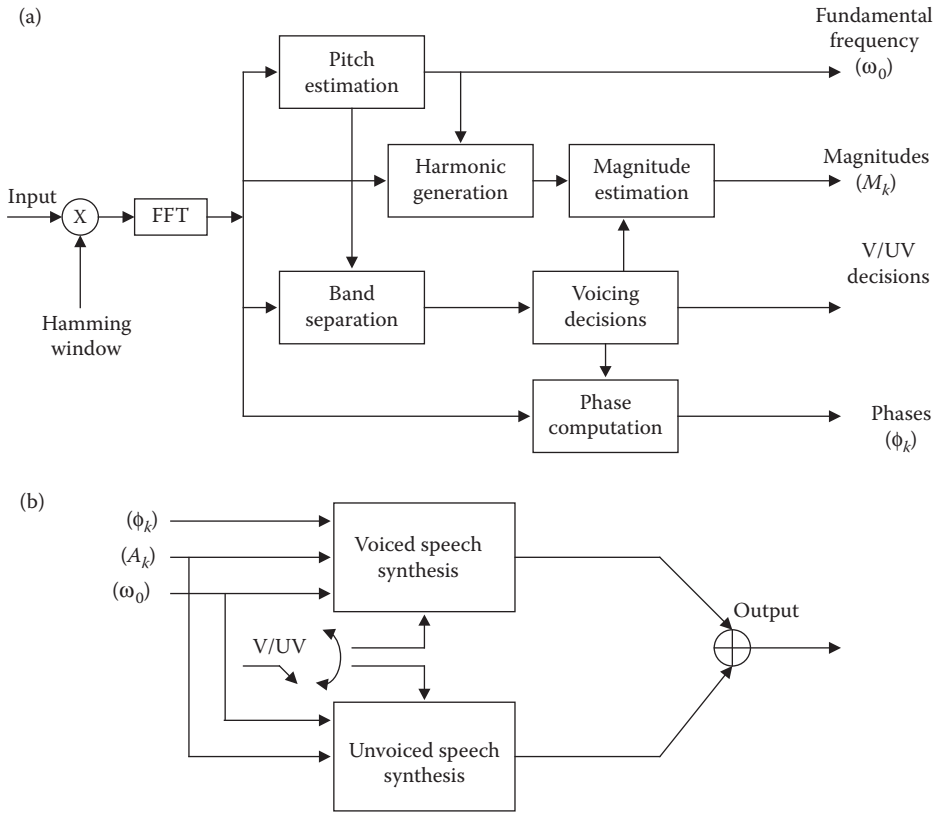

FIGURE 26.6 Block diagrams of IMBE voice codec (a) encoder and (b) decoder.

resulting voice bits are then output as part of the 4.4 kbps of voice information produced by the IMBE encoder.

After error control decoding to try and correct any bit errors that were introduced during the wireless transmission, the IMBE decoder reproduces analog speech from the decoded 4.4 kbps digital bit stream that is remaining. In particular, the model parameters for each segment are decoded and these parameters are used to synthesize both a voiced signal and an unvoiced signal. The voiced signal represents the periodic portions of the speech and is synthesized using a bank of harmonic oscillators. The unvoiced signal represents the noise-like portions of the speech and is produced by filtering white noise. The decoder then combines these two signals and passes the result through a digital-to-analog converter to produce the analog speech output.

DVSI has developed a Half-Rate (3.6 kbps) vocoder that has been proposed for use in P25 Phase 2. Designed as an extension of the current 7.2 kbps IMBE vocoder used in P25, DVSI's new Half-Rate vocoder operates at a net bit rate of 2.45 kbps for voice information and a gross bit rate of 3.6 kbps after error control coding. This represents a 50% reduction in bit rate as compared with the current 7.2 kbps IMBE vocoder used in P25 Phase 1.

DVSI has also introduced new Enhanced Vocoders for P25 based on DVSI's latest AMBE+2 Vocoder technology. These Enhanced Vocoders are backward compatible with both the standard P25 Full-Rate and proposed Half-Rate vocoders, while providing improved voice quality, better noise immunity, tone capability, and other new features. The Enhanced Vocoders significantly improve the voice performance of the P25 system, while facilitating the migration and interoperability between new and existing P25 equipment.

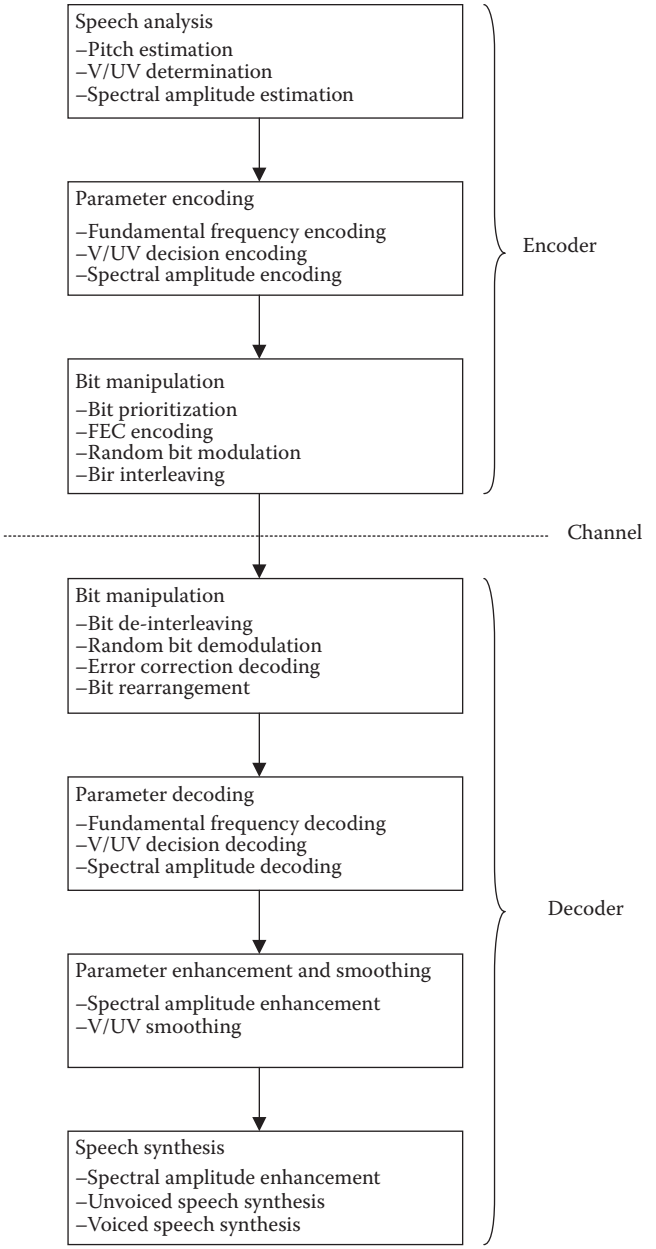

FIGURE 26.7 Flow chart of the IMBE coder and decoder.

For the particular application of interest, four characteristics of the voice codec must be considered carefully: (1) Coded speech quality and intelligibility at the codec operating rate, (2) Codec performance when the input speech is contaminated by noise or the codec is operating in a very noisy environment, (3) codec interoperability with other networks, which directly involves how the voice codec performs for tandem coding with the codecs in the other networks, and (4) complexity of the voice codec, since a lower complexity translates into reduced power consumption for the mobile device and also reduced cost of the mobile device.

First, there is the issue of coded speech quality and intelligibility at the chosen bit rate. For a bit rate in the range of 4–4.8 kbit/s, the IMBE/AMBE set of codecs achieve an MOS of 3.5–3.8 for clean speech input [14]. Since the IMBE/AMBE codecs are proprietary to Digital Voice Systems, Inc. (DVSI), these codecs are much less studied than other voice codecs, and so firmly establishing the MOS values achieved by these codecs is somewhat difficult. DVSI only tests these codecs infrequently and the results are not widely nor clearly documented and disseminated. The scores for the IMBE/AMBE codec as quoted by the vendor are quite good for the operating bit rate; however, the MOS values shown for other voice coding methods in comparison with the IMBE codecs appear low compared to the values obtained in many other independent tests.

Codec performance in a noisy environment is quite different than for clean speech, and this is where the IMBE/AMBE codec shave been shown to be very poor performers by tests done by the Institute for Telecommunications Sciences under the auspices of the U.S. Department of Commerce and by the experience of firefighters in the field [14]. The IMBE/AMBE vocoder has good clear speech performance for its low bit rate, but it is known to perform extremely poorly for noisy (PASS alarms, chainsaws, etc.) input speech and speech from inside a mask (Self-Contained Breathing Apparatus (SCBA) that is essential in firefighting) [14,15]. No fixes have been put forward to address this issue except to require additional training for users. Further, the IMBE/AMBE vocoder has not been fully tested in tandem voice communications connections that require transcoding at network interfaces, such as will be necessary when voice communications enters the LTE network [16–18].

The LMR codecs are standardized for the LMR application, and INMARSAT, but not for commercial VoIP or digital cellular systems [17,19]. Therefore, when voice communications is set up between an individual on an LMR connection and someone on a digital cellular system such as LTE, the voice must be decoded at the network interface and then recoded with the codec available in the other handset. This is called tandem coding and tandem coding degrades quality substantially, adds latency, and increases system complexity. Since the IMBE/AMBE codecs do not tandem well with other standardized codecs, this is a serious issue for voice communications outside of a public safety LMR network.

Voice codec complexity is important in the LMR environment because of cost, battery power usage, and battery weight. The IMBE/AMBE codecs are somewhat complex, and it would be preferable to employ a voice codec that exhibits minimal complexity both in terms of battery power usage and cost.

26.5 Professional Mobile Radio in Europe

The standard used for first responder communications in Europe and the United Kingdom is TETRA, originally Trans European Trunked Radio but now Terrestrial Trunked Radio, and TETRA includes a comprehensive set of standards for the network and the air interface. TETRA was created as a standard for a range of applications in addition to public safety. TETRA operates on 25 kHz channel spacing and is a fully digital system based on four timeslot TDMA to yield the 6.25 kHz channels. No analog mode of operation is available and there is no backward compatibility with conventional analog systems. The modulation method used is $\pi/4$ shifted Differential Quaternary Phase Shift Keying ($\pi/4$ DQPSK), which does not have a constant envelope. As a result, linearity in the transmitters and receivers is necessary. The symbol phase transitions are shown in Figure 26.8. The symbol shaping at the transmitter is square root raised cosine shaping with a 0.35 roll off factor [10,11].

For TETRA, the voice codec is based on code excited linear prediction (CELP) and the speech is coded at 4.567 kbits/s, or alternatively, if the speech is coded in the network or in a mobile handset, the AMR codec at 4.75 kbits/s is used [20]. Block diagrams of the TETRA encoder and decoder are shown in Figures 26.9a and b, respectively. Although it has been stated in some publications that the TETRA codec is older than the MBE codecs, the CELP structure is much newer and more widely studied and evaluated than the MBE class of codecs. Comparing the block diagrams of the IMBE codec in Figure 26.6 and the TETRA codec in Figure 26.9, it is immediately evident that these are two very different approaches to speech

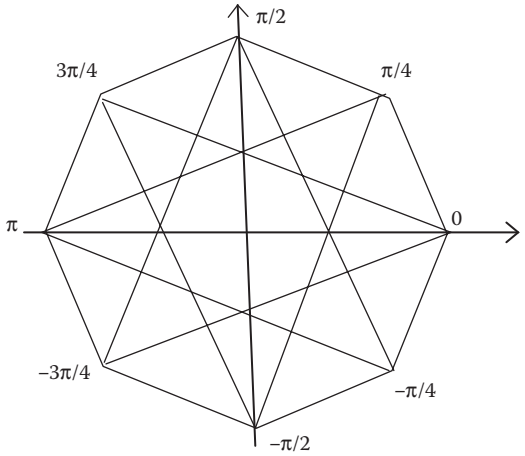

FIGURE 26.8 Symbol transitions in π/4 DQPSK.

coding. The TETRA codecs achieve MOS values in the 3.25–3.5 range for clean speech. The TETRA codecs, although they use a very different coding method than IMBE, are also expected to be vulnerable in high-noise environments, especially at the low rates used in TETRA.

The algorithmic delay of the TETRA voice codec is 30 ms plus an additional 5 ms look ahead. Such a delay is not prohibitive, but a more thorough calculation in the standard estimates an end-to-end delay of 207.2 ms, which is at the edge of what may be acceptable for high-quality voice communications. A round trip delay near 500 ms is known to cause talkers to talk over the user at the other end, thus causing difficulty in communications, especially in emergency environments [10,11].

The complexity of the TETRA codecs has been carefully studied, with the encoder complexity, including operations, ROM, and RAM factors, calculated as 11.923 MOPS and with the decode complexity calculated as 5.383 MOPS.

26.5.1 Broadband Backbone in the United States: LTE

To address the perceived need for high-speed data and video services, a National Broadband Plan (NBP) was released by the FCC to provide for the creation and establishment of a nation-wide interoperable public safety network. The NBP utilizes the 3 GPP Long-Term Evolution (LTE) technology [16].

By adopting LTE for the nationwide interoperable broadband emergency network, the FCC hopes to leverage a widely deployed standard and to save network installation costs by exploiting the efforts of commercial entities. By giving high priority to emergency communications on commercial LTE networks, connectivity can theoretically be provided during critical emergencies. Thus, LTE provides the broadband data while LMR/PMR continues to provide voice communications for first responders. However, this dual LTE/P25 approach ignores several subtle but potentially crippling future problems. One subtle limitation is that current LTE networks are data only in that voice over IP will not be available for sometime [16]. Until VoIP is available, voice will be carried separately over 2 and 3 G digital cellular. Additionally, future LTE VoIP will require transcoding at network interfaces with any LMR connection [16], since LTE does not support the LMR specified IMBE/AMBE vocoder. Further, transcoding experiments of IMBE/AMBE with the projected (but not standardized) LTE AMR codec [16], have not been performed. Transcoding of the IMBE/AMBE vocoder with 2 and 3 G codecs has similarly not been tested. Such transcoding can yield a substantial drop in voice quality and clarity, even under ideal conditions.

LTE and LMR are also poorly matched in that LMR has been a voice centric service emphasizing low latency push-to-talk (PTT) and group talk services where the group size may be 100 or more [9]. These

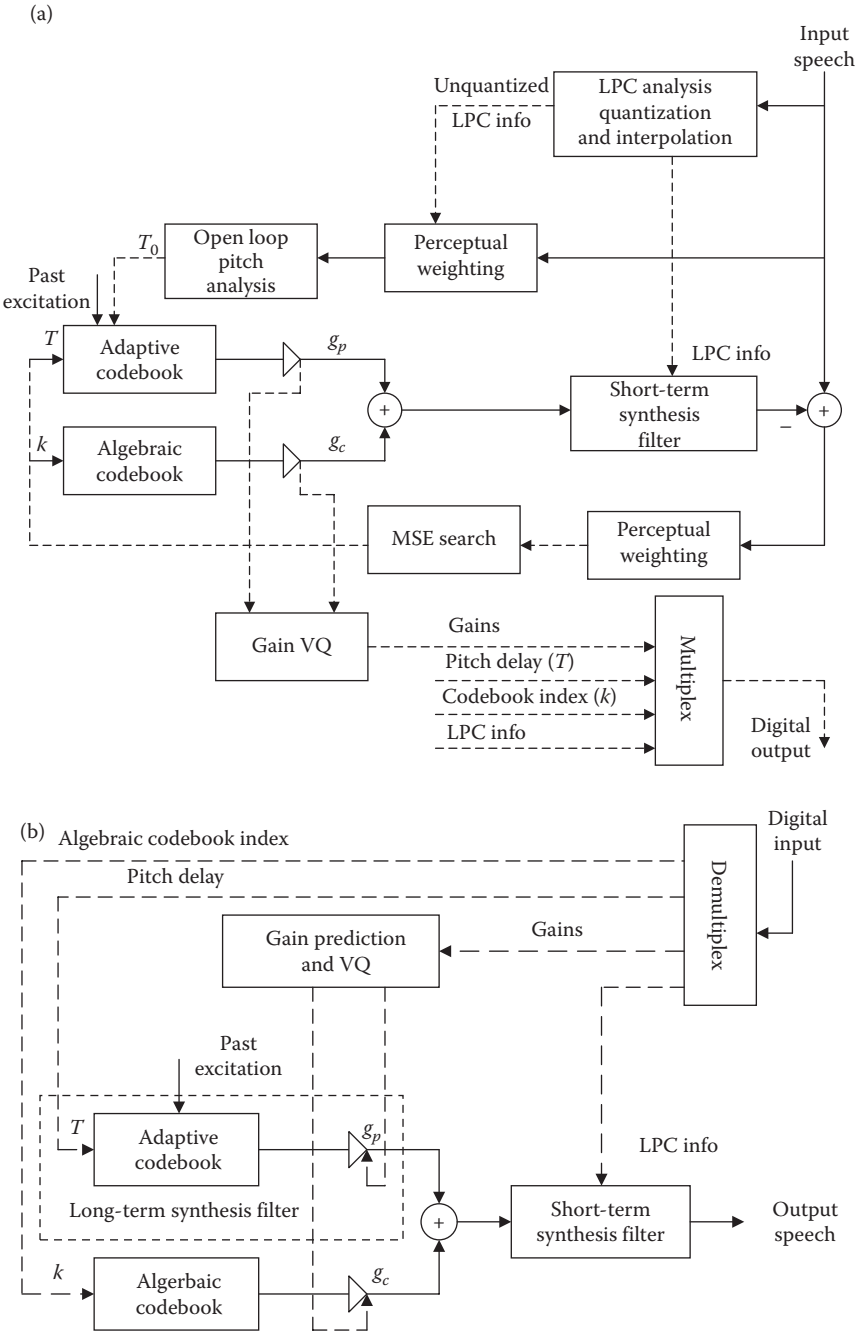

FIGURE 26.9 Block diagrams of the TETRA voice. (a) Encoder and (b) Decoder. (Adapted from ETSI, Terrestrial trunked radio (TETRA); speech codec for full-rate traffic channel; part 2: TETRA codec, *ETSI EN 300-395-2 V1.3.1*, 2005.)

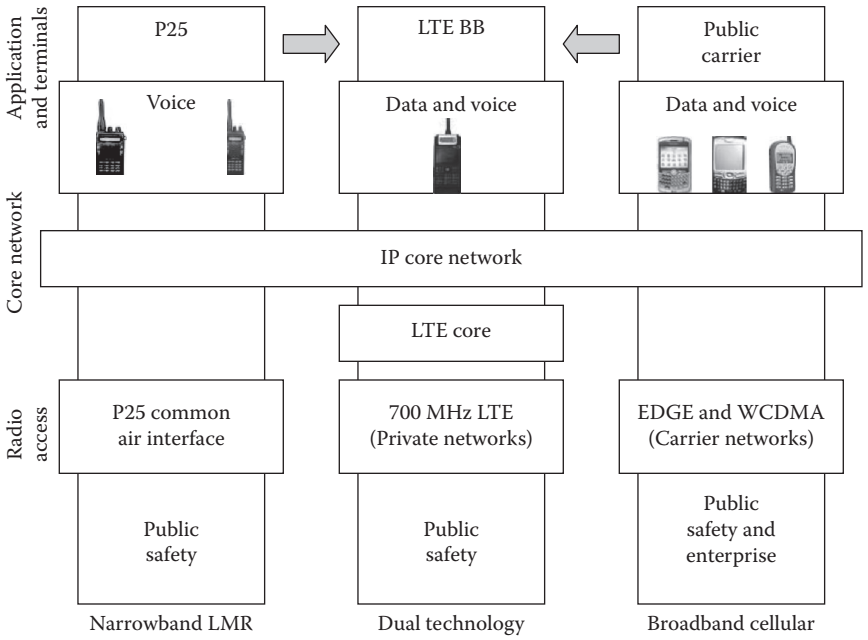

FIGURE 26.10 One approach to combining commercial cellular and LMR. (Adapted from J. Facella, Current state of 700 MHz Broadband for Public Safety, Powerpoint Presentation, Harris Corporation, Nov. 19, 2010.)

offerings are not easily supported by LTE today. The support of peer-to-peer voice communications, called Direct Mode Operation (DMO), without the use of a base station or other trunking infrastructure is particularly important and this has not been addressed by the LTE broadband network proposal [9].

These LTE-based systems only provide broadband backbone services, not voice, and do not address the serious shortcomings of current LMR/PMR systems, including limited interoperability, poor voice quality in disaster scenarios, and restrictive coverage in remote locations and/or where infrastructure has been damaged [21,22]. In addition, the proposed national broadband network based on LTE is not designed to the high-reliability performance standards and rapid response requirements of mission critical applications, is not hardened to natural disasters, is not available in remote locations and is not easily portable and reconfigurable[16].

Therefore, the evolving public safety communications network consists of two silo communications networks, LMR for first responders and commercial LTE for the national broad network. The plan is to "duct tape" these two silos together at the IP network layer. One concept for combining LMR and LTE broadband is shown in Figure 26.10 [23]. The combination of these two silos is not seamless, and each silo has significant limitations for the planned tasks. First, LMR has well-known serious drawbacks, including poor voice quality in high-noise environments and with breathing masks, the number of direct mode calls (peer-to-peer) on one channel using TDMA is limited to one, the LMR codecs are not interoperable with other wireless networks or with other public utility communications such as an electrical utility, and no broadband coverage. The commercial LTE networks are designed for an entirely different set of applications and do not support the standard direct mode voice, talk group voice fast call set up using push to talk (PTT), high reliability, and rural coverage that is needed for emergency first responders.

26.5.2 Evolution

There have been plans for some time to continue to develop the LMR standards in the United States, perhaps combining them in some way with TETRA. There is also a Project 34 effort that has been in

planning for a number of years. The hope is to eventually extend broadband data services and video to LMR, while still maintaining the key voice communications features of LMR such as DMO and PTT with large talk groups.

The market for LMR and PMR is no more than 10% of that for digital cellular and other commercial wireless services, so the competition of the marketplace has not worked well here. The several long time system vendors and one voice codec vendor continue to dominate the market without significant competition in the United States. The TETRA system in Europe is more extensively investigated and standardized, plus there are compatibilities with GSM digital cellular systems that make TETRA at least a "more vetted" system than LMR in the United States.

There are efforts in some countries without LMR or PMR to develop such systems based on WiMAX technologies. Indeed, highly mobile WiMAX systems are being proposed in the United States in order to address catastrophic failures in emergencies or to extend broadband coverage to remote areas.

References

1. L. Miller and Z. Hass, Public safety, *IEEE Communications Magazine*, 44(1), 28–29, 2006.
2. Technologies and standards for mobile radio communications networks, *TAIT Radio Communications*, Tech. Rep., February 2010.
3. R. I. Desourdis, D. R. Smith, W. D. Speights, R. J. Dewey, and J. R. DiSalvo, *Emerging Public Safety Wireless Communication Systems*, Artech House, Inc., Norwood, Massachusetts, 2002.
4. M. Metcalf, Project MESA: Advanced mobile broadband communications for public safety applications, in *The 14th IEEE Proceedings on Personal, Indoor and Mobile Radio Communications*, Beijing, China, Vol. 2, pp. 1159–1161, September 2003.
5. Emergency Communications during the Minneapolis Bridge Disaster: A Technical Case Study by the Federal Communications Commission's Public Safety and Homeland Security Bureau's Communications Systems Analysis Division, pp. 1–61, November 2008.
6. Project Mesa; service specification group-services and applications; statement of requirements executive summary. MESA Organizational Partners (ETSI, TIA), 2005. [Online]. Available: www.projectmesa.org.
7. APCO project 25 statement of requirements P25SoR, P25, 2010.
8. Project 25 Technology Interest Group, http:www.project25.org.
9. L. DaSilva, G. Morgan, C. Bostian, D. Sweeney, S. Midkiff, J. Reed, C. Thompson, W. Newhall, and B. Woerner, There surgence of push-to-talk technologies, *IEEE Communications Magazine*, 44(1), 48–55, 2006.
10. ETSI. Terrestrial Trunked Radio (TETRA); Voice plus Data (V + D); Designers' guide; Part 1: Overview, technical description and radio aspects, *ETR 300-1*, 1997.
11. ETSI, Terrestrial Trunked Radio (TETRA); Voice plus Data (V + D); Part 2: Air Interface (AI), *ETS 300 392-2*, 1999.
12. P25 Radio Systems, *Training Guide*, Daniels Electronics Ltd., Canada, 2004.
13. R. Rudolph and E. Yu, IMBE and AMBE speech compression, *International IC99*, 232–234, 1999.
14. D. Atkinson and A. Catellier, *Intelligibility of Selected Radio Systems in the Presence of Fireground Noise: Test Plan and Results*. NTIA Technical Report, 2008.
15. W. Kushner, S. Harton, R. Novorita, and M. McLaughlin, The acoustic properties of SCBA equipment and its effects on speech communication, *IEEE Communications Magazine*, 44(1), 66–72, 2006.
16. H. Holma and A. Toskala, Eds., *LTE for UMTS OFDMA and SC-FDMA Based Radio Access*, John Wiley & Sons Ltd, Great Britain, 2009.
17. C. Redding, N. DeMinco, and J. Linder, *Voice Quality Assessment of Vocoders in Tandem Configuration*, NTIA Report, pp.1–21, April 2001.

18. S. F. Campos Neto, F. Corcoran, and A. Karahisar, Performance assessment of tandem connection of cellular and satellite-mobile coders, in *1997 IEEE International Conference on Acoustics, Speech, and Signal Processing*, Munich, Bavaria, Germany, Vol. 2, pp. 1379–1382, April 1997.
19. S. F. Campos Neto and F. Corcoran, Performance assessment of tandem connection of cellular and satellite-mobile coders, in *IEEE International Conference on ICASSP*, Phoenix, Arizona, Vol. 1, pp. 177–180, March 1999.
20. ETSI, Terrestrial trunked radio (TETRA); speech codec for full-rate traffic channel; part 2: TETRA codec, *ETSI EN 300-395-2 V1.3.1*, 2005.
21. Background noise and radio performance: Best practices help firefighters and other first responders maximize the intelligibility of two-way radio communications in high-noise environments, Motorola, Tech. Rep., 2008.
22. EADS, White paper: Interoperable mission critical broadband/narrowband solution for public safety communications, Alcatel-Lucent, Tech. Rep., 2010.
23. J. Facella, Current state of 700 MHz Broadband for Public Safety, PowerPoint Presentation, Harris Corporation, Nov. 19, 2010.

27

Digital Audio Broadcasting

Carl-Erik W. Sundberg

27.1 Introduction

With the advent of the CD (compact disc) and higher-quality distribution channels for music, the need for radio broadcasting of digital audio with CD or CD-like quality arose. One immediate problem for enabling such radio broadcasting services was limited radio bandwidth. The CD format uses PCM, which requires a bit rate of about 1.3 Mb/s for stereo. Thus, for successful digital audio broadcasting, efficient high-quality audio compression was required. Since people listen to radio predominantly in cars and not so much at home, another requirement was reliable delivery to moving receivers in cars and on high-speed trains.

Digital Audio Broadcasting (DAB) is more spectrally efficient than analog FM. In addition to the improved quality requirements, this spectral-efficiency advantage of digital over analog was one of the driving forces behind the development of DAB. The increased spectral efficiency of digital transmission (with respect to analog FM) effectively means that a larger number of radio programs can be broadcasted over a given bandwidth. Another key advantage was the flexibility in transmission offered by the digital technology. Thus, auxiliary services (data services) can be obtained in addition to high-quality audio. Examples of such services are traffic information, weather information, stock quotations, image and even video services, and so on.

The first system that was developed was the European Eureka-147 or DAB system. The term DAB is used as a general term for digital audio broadcasting and it is also used as a synonym for Eureka-147. It was an all digital system and required new spectrum. The European Broadcasting Union (EBU) played a leading role in the development of Eureka-147. The system was launched in many European countries, with mixed success, and was also adopted by some countries outside Europe. A key disadvantage with DAB is "old" audio coding (audio compression) technology, which leads to poor spectral efficiency and far from optimum audio quality. A new more efficient version, DAB+ has recently been developed. This system utilizes more efficient audio coding technology at lower bit rates. Unfortunately, it is not backward compatible with DAB.

In the United States, digital audio broadcasting developed along a different path. Since no new spectrum was allocated for this service, it was difficult if not impossible to adopt the all-digital Eureka-147 system. Instead, new "in-band" systems were developed for both the FM and AM bands. The broadcasters wanted an evolutionary path with initially hybrid systems with a digital service added to the existing analog FM and AM broadcasting services. In the future, the analog transmission would be abandoned, freeing bandwidth for additional digital services, including not only extra music and talk show channels, but also multichannel audio and data broadcasting services. The technical name for these systems was hybrid IBOC (in band on channel) and all digital IBOC, both for the FM and AM bands. There is now digital audio broadcasting services in all states in the US, referred to as HD Radio (high definition radio). Companies like Lucent Digital Radio, and USA Digital Radio, later merging into iBiquity Digital Corp., played a major role in the development of digital audio broadcasting in the United States. HD Radio is currently available throughout the US and, although the technology was solely developed for the US market, it is now being considered and tested in many other countries all over the world. IBOC yields increased spectral efficiency and the flexibility in terms of providing a backward compatible way to augment existing systems with data services.

In a separate development, the Digital Radio Mondiale (DRM) consortium, has developed systems for digital shortwave broadcasting as well as systems for the AM and FM band transmission of digital audio including hybrid schemes.

In parallel, there has also been a convergence with digital cellular. Systems like MBMS (Multimedia broadcasting multicast services) have been developed both for 3G CDMA and for OFDM LTE 4G as well as MediaFLO and DVB-H. Finally, other systems worth mentioning include DMB in Korea and China, and audio as part of digital video broadcasting systems like ISDB in Japan and DVB-H.

MBMS is a digital audio broadcasting system integrated into a cellular system. Thus, low-power transmitters are used with small cells. In contrast, all the other terrestrial systems mentioned above, including HD Radio and Eureka-147, as well as traditional analog FM and AM, use high-power transmitters and tall towers with large cells. The MBMS system uses only one radio receiver for cellular and broadcasting while the other systems use two separate receivers for cellular and broadcasting.

In a different development, digital satellite audio broadcasting systems were developed for the United States. CD Radio, later Sirius, and XM Satellite Radio were licensed and they developed similar but somewhat different technologies. Sirius uses geosynchronous satellites and fewer terrestrial gap filters while XM uses geostationary satellites and a large number of gap filters. Later the two companies merged into one company, Sirius XM. The business model is pay radio services with coverage throughout the 48 contiguous US states. The service is also available in countries south of the United States and in Canada.

What does the future hold? There is obviously the option of using (existing) high-quality audio coding schemes yielding superior quality to CD quality. However, it is not clear as to whether or not this is a viable option, since it requires an increase in source bit rates and thus its bandwidth requirements. Multichannel stereo (spatial audio, surround sound) could be of interest for broadcasting in the future. In the further convergence with cellular and wireless broadband, internet radio with a very large number of programs is gaining increasing support, especially with the increasing use of smart phones. This case represents an example where unicasting services are instead providing services traditionally provided by broadcasting.

In the remainder of this chapter we give a brief technical description of many of the systems mentioned in the introduction.

27.2 Eureka-147, DAB, and DAB+

Eureka-147 was an EU (European Union) research project that produced a digital audio broadcasting standard in the 1980s with a start in 1981. The first commercial broadcasts took place in 1995 in the United Kingdom. This system is often referred to as DAB, [F02]. ETSI produced the original specification for DAB, [ETSI_1]. DAB later evolved into DMB (Digital Multimedia Broadcasting), [wDAB] and DAB+, [ETSI_2]. DAB, DAB+, and DMB are currently in operation in many countries in Europe,

Canada, China, Korea, and Australia, [wikiDAB]. DAB, DMB, and DAB+, are all-digital systems for audio broadcasting in new frequency bands. Here we focus on audio services, although, in the case of DMB and DAB+, there is also video broadcasting.

The DAB system uses a wideband transmission technology format in Band III (174–240 MHz) and the L Band (1452–1492 MHz) although in principle the scheme allows operation almost on any band above 30 MHz. DAB offers a number of modes, allowing different countries to use different modes and various frequency bands.

The original DAB format uses the MPEG-1 Audio Layer 2 audio coder. This is also referred to as MP2, [F02]. At 192 kb/s it provides less than adequate audio quality at this high bit rate due to the fact that this audio coder represents "old" technology today. In contrast, the new DAB+ system uses the HE-AAC version 2 Audio Codec (AAC+), [wikiHEAAC,wikiAAC]. This audio coder yields very good stereo audio quality at 64 kb/s.

The DAB system uses punctured convolutional codes with unequal error protection (UEP), [LC04,C91]. Parts of the bit stream are provided with higher levels of error protection than others, to account for the fact that audio quality is much more sensitive to errors on those bits, [ETSI_1]. Interleaving is used to spread out the effect of burst errors and thereby improve the performance of the decoder. In the new DAB+, an additional layer of Reed Solomon outer nonbinary block coding is also used for improved error protection, [ETSI_2].

The modulation system used in DAB is orthogonal frequency division multiplexing (OFDM) with differential quaternary phase shift keying (DQPSK), [ETSI_1]. The OFDM format is used today in many mobile applications (like cellular 4G advanced LTE), [D08]. DAB was actually pioneering the use of this technique. No equalization is used to compensate for multipath propagation effects. As an example, in Transmission Mode I, 1536 sub-carriers (tones) are transmitted in parallel. The overall OFDM symbol duration is 1.246 ms and the cyclic prefix is 246 μs.

With OFDM, DAB can use the concept of a Single Frequency Network (SFN), [ETSI_1]. This is equivalent to a frequency reuse factor of 1. (In contrast analog FM has a frequency reuse factor of 15!). With SFN, the spectral efficiency is dramatically improved. Provided that the transmission delays for signals from different transmission antenna towers are within the cyclic prefix length, OFDM can resolve this multipath, [D08], and actually readily exploit it to provide macro diversity.

The services provided by DAB and DAB+ include primary services, such as audio for main radio stations, but also secondary services, including sports commentaries, data services, video, etc., [ETSI_1, ETSI_2]. The older DAB standard is not forward compatible with the new DAB+, [ETSI_1, ETSI_2].

The minimum bandwidth of Eureka-147 in Mode 1 is 1.536 MHz with 1586 tones. The typical system uses a multiple of such 1.536 MHz bands. Each such band carries a multitude of audio channels in a TDM format, [wikiDAB]. The typical single-frequency network Eureka-147 system has a signal delay of about 2 seconds [wikiDAB].

Countries where DAB, DAB+, and DMB are in use (in 2011) include Canada, Singapore, Australia, China, South Korea, Taiwan, Sweden, Denmark, Norway, United Kingdom, Germany, Switzerland, Netherlands, Belgium, Spain, Portugal, Monaco, Greece, and Croatia, [wikifDAB]. It is interesting to note that a number of countries are in a category labeled "DAB no longer in use," among them Finland. It is also worth noting that in Sweden DAB had nationwide coverage just a few years ago. Today (2011), however, DAB is only available in four large cities while the transmitters in the rest of the country have been switched off, due to low listener rates. The future is indeed uncertain.

27.3 HD-Radio, IBOC-FM, HIBOC-FM, IBOC-AM, and HIBOC-AM

The development of the digital audio broadcasting in the United States took a distinctly different path from the one in Europe. In contrast to Europe where new frequency bands were provided for digital

audio broadcasting, no new frequency spectrum was allocated for this service in the United States. Therefore, adopting a standard like Eureka-147 would have been difficult, if not impossible, in the United States. Furthermore, broadcasters also requested a digital audio broadcasting system for replacing/upgrading analog AM radio. The services provided by AM radio have a significantly large market in the United States, in contrast to Europe, and Eureka-147 offered no solutions for the AM band.

A standardization effort started in the 1990s to develop systems in the existing FM and AM bands. These were labeled In Band on Channel, or, IBOC systems. The idea was to first keep the analog signal and add a digital audio signal in a hybrid in band on channel system both for FM and AM. In the future a migration to an all-digital system in both the FM and AM bands would take place by closing down the analog transmission and utilizing the freed-up spectrum for providing additional digital programming. Other systems like IBAC (in band adjacent channel) schemes were also explored, involving a hybrid system with a digital signal in the channel adjacent to the host analog FM. The IBOC schemes were however preferred.

The commercial label for these systems is High-Definition Radio (HD Radio). Currently (in 2011) both services in the FM and AM bands are offered throughout the United States and a multitude of radios are available. Several car manufacturers have been offering HD radio as an option.

The requirements for digital audio broadcasting were stereo CD-like quality in the FM band and stereo analog FM quality in the AM band with coverage for the digital systems comparable to that of the analog transmission. Thus far (in 2011), only hybrid systems are in use, but both the FM and AM band systems have transmission modes that include all-digital IBOC modes, [wIBQ,wIBQ_P,wIBQ_J], that is, both IBOC-FM and IBOC-AM systems.

Early contributors to the standardization efforts were AT&T and later Lucent Digital Radio, as well as CBS/Westinghouse and USA Digital Radio. Lucent Digital Radio and USA Digital Radio later merged to form iBiquity Digital Corporation, [wIBQ].

Federal Communications Commission (FCC) emission masks for FM and AM regulate the emission levels allowed from an analog FM and AM station [wFCC]. This combined with allowed interference levels for co-channel and adjacent channels form the bases for the IBOC designs. In North America, carrier separations of multiples of 200 kHz are used in the FM band and multiples of 10 kHz are used in the AM band (these numbers are different in, e.g., Europe). The digital signal is added to the analog FM signal in a frequency multiplexing fashion at a lower level (25 dB below the host analog FM signal) on both sides of the analog FM spectrum. In particular, letting f_c denote the carrier frequency of the host analog FM signal, the digital signal is added over bands spanning, for example, the spectrum from $f_c - 200$ kHz to $f_c - 130$ kHz, and from $f_c + 130$ kHz to $f_c + 200$ kHz, [wIBQ_P].

A similar arrangement is being made for AM over the $f_c - 15$ kHz to $f_c + 15$ kHz band, with the analog AM occupying the middle of the spectrum. There is, however, one conceptual difference between the AM and FM systems. In particular, unlike the FM case where the digital signal is added at the edges of the spectrum, in the AM case the analog AM signal is transmitted simultaneously with the digital signal in the center of the $f_c - 15$ to $f_c + 15$ kHz band, since, in the AM case, the digital signal also occupies the center of the band together with the host analog AM signal. This is straightforward to do in the case of analog AM, since AM amounts to linear modulation. In principle it can also be done with nonlinear analog FM, but it requires more complex receiver structures, [PS08,PS98,CS00a], and is thus not included in the current standard.

The HD Radio FM system is described in some detail in [F02,wIBQ_P]. A number of hybrid and all-digital transmission formats or modes have been developed. A control channel is used to inform the radio receiver about which mode is being used.

The audio coding used for HD Radio FM is AAC+ with spectral band replication (SBR) typically at 64 kb/s, [wikiHEAAC,wikiAAC]. The channel codes are complementary punctured pair convolutional (CPPC) codes, which constitute a special class of punctured convolutional codes of a type especially

designed for hybrid IBOC FM, [F02,CS00b]. The signal is transmitted in two separate frequency bands on both sides of the carrier and host analog FM signal. The interference situation is such that a first adjacent signal can sometimes wipe out all or most of one of the two digital-signal sidebands. In this case the receiver is to reconstruct the digital signal based on only the surviving sideband. Sometime both sidebands are received and in this case the receiver softly combines them for more reliable reception, [LS01]. Sometimes a sideband partially damaged by interference can be useful in the context of soft combining.

For the described transmission scenarios so-called classic code combining is a possibility, [CS00b]. However, CPPC codes offer a superior option, [F02,CS00b]. Punctured memory 4, 16-state, rate 2/5 codes are used based on combining two different rate 4/5 codes on the upper and lower sidebands. The pair of rate 4/5 codes is obtained by an optimized complementary puncturing procedure on the rate 2/5 code. In contrast, classical code combining would employ identical rate 4/5 codes on both sidebands. As an example, with memory 4 codes, the optimum rate 4/5 codes would in all cases have a free distance of 4, while for the full rate 2/5 case the CPPC code has a free distance of 11, while the code combining code only have a free distance of 8 (i.e., twice the component-code free distance of 4). This constitutes a rare case of gaining in performance without increasing complexity. The modulation system used in HD Radio FM is OFDM with QPSK. Interleaving, both in time and frequency (tones), is also used, [wIBQ_P].

Initially only one digital program was envisioned, with content identical to the one carried by the host analog FM signal. However, the system evolved into a number of possible digital programs, HD1,HD2, and HD3, depending on the transmission mode employed. HD1 is the original format, with only one program in digital form, while HD2 and HD3, carry two and three programs, respectively. This is achieved by dividing the digital bit stream into separate streams. Different audio coder rates can be used for different programs. This also enables some trade-offs between the number of multiplexed programs and audio quality. Data services are also provided, [F02,wIBQ_P]. In the case that the content carried by the digital program is identical to the content of the host analog FM signal, blending from digital to analog can be used, [F02,wIBQ_P].

Among future possible improvements, the use of a list Viterbi algorithm (LVA) for decoding presents an attractive option for increasing robustness [SS94] at the expense of a small increase in receiver complexity. Audio systems often use error mitigation techniques to reduce the perceptual impact of transmission errors. This is achieved by using an error detecting code on the most important bits. When an error is detected, the audio segment is replaced by predictions from already received segments. By using the LVA, the prediction errors in this operation can be significantly reduced, resulting in improved audio quality. The use of the LVA only modifies the receiver. Another noteworthy option that would allow increasing the digital data rates that can be provided involves simultaneous analog and digital transmission by exploiting "writing-on-dirty-paper coding" schemes [C83]. These rely on inserting a weak digital signal on top of the dominant host analog FM transmission in such a way that the weak digital transmission can be reliably decoded even in the presence of the dominant analog FM interferer [PS08]. Since analog FM has an interference suppression capability, the added weak digital signal does not noticeably distort the demodulated host analog FM signal.

HD Radio AM actually presents a larger design challenge than FM, because of its stringent spectrum limitations, [F02]. A detailed description of the modes is given in [F02,wIBQ_J]. The audio coding used in HD Radio AM is AAC+ with SBR, typically at 24–32 kb/s, [wikiHEAAC,wikiAAC]. Trellis-coded modulation (TCM) and Reed Solomon coding are employed, and multi-stream transmission [S99,L02] (over multiple frequency bands with OFDM and various modems, ranging from BPSK to 64QAM) are used on different carriers. Unlike the FM case where the fading channel can be adequately modeled as a Rayleigh channel, the channel in the AM case behaves more like an additive Gaussian channel with added interference, [F02]. The HD Radio AM system represents a substantial improvement in audio quality over analog AM. Furthermore, stereo is achieved with HD Radio AM. Finally, we remark that,

although the HD Radio schemes were developed in the United States for domestic use, these schemes are being used in and tested for use in several other countries, [wIBQ].

There are currently (in 2011) nearly 2000 FM and AM radio stations throughout the US broadcasting in HD, plus more than 1100 new local FM HD2/HD3 stations, [wHDR]. The Website www.hdradio.com provides a complete list of all radio stations transmitting in HD in the United States.

Portable radios with HD as well as home stand-alone radios with HD are now (in 2011) available at reasonable prices, [wHDR]. Car radio with HD for upgrades in existing vehicles and options in new vehicles for a large number of models are also now available, see [wHDR].

There is an increased adoption and testing/advanced interest for HD radio in many countries outside the United States, [wIBQ_I]. There are now (in 2011) adoption and nationwide operation in the US, Philippines and Puerto Rico. There are adoption and regional use in Mexico, Brazil and Panama. There is limited operation in the Dominican Republic, Jamaica, Switzerland, Ukraine, Thailand, and Indonesia. There is testing and advanced interest in many other countries including Canada.

27.4 Digital Radio Mondiale, DRM, and DRM+

Digital Radio Mondiale (DRM) is an international nonprofit consortium for digitization of broadcast (shortwave mediumwave and longwave) up to 30 MHz, DRM30. The DRM consortium is composed of broadcasters, network providers, transmitter and receiver equipment manufacturers, universities and research institutes. DRM+ extends operation to VHF bands up to 174 MHz, [wDRM]. DRM30, includes digital shortwave radio. The consortium was formed in 1998 and the first broadcast took place in 2003. Data Services are also included [wDRM]. Transmission is organized in a number of different modes, including hybrid adjacent modes, [wDRM].

DRM has ITU support, and the main standard has been published by ETSI. Among the audio coders used by DRM and DRM+ is MPEG-4 HE-AAC with SBR, [wikiHEAAC,wikiAAC]. The modulation used is coded OFDM (COFDM) with QPSK/16-QAM/64-QAM, [wDRM]. The channel codes used by DRM can be chosen to provide UEP with up to 4 different protection classes, [wDRM]. Layered modulation with multilevel coding is also used [RS08].

DRM (DRM 30) is the only international standard for HF (3–30 MHz) use, [wikiDRM]. DRM uses COFDM and it is designed to fit inside existing AM broadcast channels, with 10 kHz bandwidth in the US, and 9 kHz in Europe. For the European version, DRM has modes, which require as little as 45 kHz, [wikiDRM]. For DRM30 Systems with bandwidths of 9, 10, 18, and 20 kHz, see [wikiDRM]. DRM+ Systems use a bandwidth of 100 kHz, [wikiDRM]. For details of the OFDM schemes for DRM30 systems with 88–460 tones depending on mode and bandwidth, see [wikiDRM]. Current broadcasters (in 2011) include ALL India Radio, BBC World Service, Radio Canada International, Deutsche Welle and Voice of Russia, [wikiDRM]. Until recently, a DRM receiver has typically been a personal computer. However, stand-alone DRM receivers are now available, [wikiDRM].

27.5 ISDB, DVB-H, DMB, and Other Systems

ISDB is an ARIB Japanese standard for digital TV and audio. The 1seg part of ISDB is used for digital audio broadcasting to mobiles, [wikiISDB]. The technology is very similar to that used in Eureka-147 and DVB-H. DVB-T (Digital Video Broadcasting, Terrestrial) and DVB-H (Digital Video Broadcasting, Handheld) are digital TV standards developed under ETSI, [wikiDVBH] and as part of these standards there are also a digital audio broadcasting component, [wikiDVBH]. OFDM technology is used in these systems. As mentioned in the introduction, DMB [wDAB] is in use in Korea and China. It includes both digital video and digital audio broadcasting, and employs technology that is very similar to that of DAB and DAB+. All these systems in this section use high-power transmitters for transmission in large cells.

27.6 MediaFLO

This is a proprietary technology developed (and operated) by Qualcomm, [wikiFLO]. FLO stands for Forward Link Only. It is designed for digital video and audio broadcasting in the 716–722 MHz band. MediaFLO is a competitor to Eureka-147/DAB, DAB+, DMB [wDAB] and DVB-H, [wikiDVBH]. The technology is encrypted COFDM with QAM (QPSK and 16QAM) and Layered modulation with multi-level coding [RS08,C07]. High-power transmitters with tall antennas and large coverage areas are used for broadcasting, just like in conventional analog FM broadcasting. A detailed technical description of the physical layer in MediaFLO is given in [C07], [wQC].

27.7 MBMS and Convergence with Cellular

Multimedia Broadcast Multicast Services, or MBMS, is a multimedia broadcasting service standard [w3GPP] that has emerged under the umbrella of cellular and contains digital video and audio broadcasting over the cellular network. It has been developed for 3G UMTS (CDMA) [w3GPP] and there are also proposed versions for 4G LTE [D08]. Systems such as MBMS point to a convergence between digital audio broadcasting and cellular. Since MBMS is part of the cellular system, a single radio is used by the receiver, and only low-power transmitters are used. Additional details about the MBMS system are given in [BH05] and [I08].

MediaFLO and DVB-H are also offered as broadcasting services on mobiles. They however constitute a different (lower) level of convergence, as separate radios are used for cellular and broadcasting radio, and broadcasting has larger coverage areas (large cells) than cellular transmission. In contrast, a single radio is assumed with MBMS, serving both broadcasting and cellular transmission modes. MBMS is flexible enough so that it can be used for broadcasting, as well as for multicasting (transmission only to a selected group of users) and even unicasting [BH05,I08].

27.8 Sirius XM Satellite Radio

Sirius XM is the result of a merger between Sirius and XM in 2008. Sirius (originally Satellite CD Radio) was formed in 1990 and XM in 1992. The joint company provides satellite radio broadcasting in the United States (actually in North America), [wSXM]. The business model is based on the subscription pay radio principle. Nine Satellites are in orbit, 5 from XM, and 4 from Sirius. The frequency band for the satellite segments is the S band, 2.320–2.3325–2.345 GHz and the terrestrial gap filler segments use the same band, [wSXM]. Originally, the two companies Sirius and XM were licensed each in half of the allocated band.

The technologies used by the two companies Sirius and XM are slight variations of each other. Sirius uses geosynchronous satellites, which requires fewer terrestrial gap fillers. The audio coding is a multi-program PAC audio coding [N05] which has some statistical multiplexing benefits. The satellite segment has single carrier QPSK modulation and the terrestrial segment uses OFDM. XM uses geostationary satellites and HE-AAC audio coding, [wikiHEAAC,wikiAAC]. The satellite segment has single carrier QPSK modulation and the terrestrial gap fillers use OFDM. A great advantage with satellite radio in the United States is coverage. Indeed the same set of programs can be received throughout the 48 states in the continental United States.

27.9 Future of Digital Audio Radio

A very simple and inexpensive way to supply digital audio broadcasting is to replace the analog FM transmitter with a GSM type radio [wikiGSM]. This means that the analog FM modulator is replaced by a constant-amplitude GMSK modulator, [AAS86,MH81], yielding an all-digital in-band system using the same high-power transmitter. A significant advantage with such a system is that it uses a lot of the

existing analog FM infrastructure. A new receiver is of course required and no obvious hybrid scheme is available. This is the reason why such schemes have not yet been adopted. A gross bit rate of up to about 150 kb/s before channel coding would be available for one transmitter. Different modes are possible, including multiple audio programs (e.g., one music and one talk program), or a single high-quality music program, and/or data channels. With more advanced Continuous Phase Modulation (CPM) constant-amplitude modulation schemes even higher data rate would be available at the expense of complexity, [AAS86]. For countries where the FM band is only sparingly used, digital transmission can be added on new frequencies. A system along these lines based on CPM has actually been built and field-tested, [BKB03,KAB08].

In Section 27.3, we described two potential future upgrades of the HIBOC-FM system. We described an improved receiver based on the concept of the List Viterbi Algorithm, [SS94]. (In Principle, this would also work for HIBOC-AM, IBOC-AM, and IBOC-FM). The second potential system improvement is related to simultaneous transmission of the host analog FM and digital, [PS08]. The net result of this is an increased data rate for the digital system.

What does the future hold for digital radio broadcasting? Audio coding schemes with higher quality than CD-quality [wikiDVBH,wikiDD] have been developed. They are based on higher audio source bandwidth and higher sampling frequency. As a result, higher audio quality than CD can be achieved. Radio broadcasting schemes with such audio coders would be much bandwidth demanding, since the source bit rate would be higher than in current systems. Multichannel (surround sound) schemes with spatial audio have also already been proposed for inclusion in the current standards. Perhaps unicasting may prove a preferred mode in the future for delivering audio. Indeed digital audio radio is already distributed as internet radio over wireless broadband on smart-phones and other terminals. In this case, it is no longer broadcasting but unicasting, that is, individual delivery instead of transmission to many. Finally, Digital Audio Radio is perhaps a good application area for Software Defined Radio (SDR), [B10].

Acknowledgment

The author wishes to thank Haralabos Papadopoulos for technical discussions and for reviewing the manuscript.

References

[F02] C. Faller et al, Technical advances in digital audio radio broadcasting, *Proc. of the IEEE*, 90(8), 2002, pp. 1303–1333.

[ETSI_1] ETSI EN300400 v1.4.1 Original DAB specification, www.etsi.org

[wDAB] www.eworlddab.org/technology/dab

[ETSI_2] ETSI TS102563 v1.1.1 DAB+ enhancement specification, webapp.etsi.org

[wikiDAB] en.wikipedia.org/wiki/Digital_Audio_Broadcasting

[wikiHEAAC] en.wikipedia.org/wiki/High_Efficiency_Advanced_Audio_Coding

[wikiAAC] en.wikipedia.org/wiki/Advanced_Audio_Coding

[LC04] S. Lin and D. J. Costello, *Error Control Coding*, 2nd Ed, Prentice-Hall, New York, 2004.

[C91] R. V. Cox et al., Sub-band speech coding and matched convolutional channel coding for mobile radio channels, *IEEE Transactions on Acoustics, Speech & Signal Processing*, 39(8), 1717–1731, 1991.

[D08] E. Dahlman et al., *3G Evolution*, 2nd Ed, Academic Press, New York, 2008.

[wikifDAB] en.wikipedia.org/wiki/File:Digital_Audio_Broadcasting.svg

[wIBQ] www.iBiquity.com

[wIBQ_P] P. J. Peyla, The structure and generation of robust waveforms for FM. In *Band on Channel Digital Broadcasting*, www.iBiquity.com

[wIBQ_J] S. A. Johnson, The structure and generation of robust waveforms for AM. In *Band on Channel Digital Broadcasting*, www.iBiquity.coms

[wFCC] www.fcc.gov

[PS08] H. C. Papadopoulos and C.-E. W. Sundberg, Precoded modulo-precancelling systems for simulcasting analog FM and digital data, *IEEE Transactions on Communications*, 56(8), 1279–1288, 2008.

[PS98] H. C. Papadopoulos and C.-E. W. Sundberg, Simultaneous broadcasting of analog FM and digital audio signals by means of adaptive precanceling strategies, *IEEE Transactions on Communications*, 46(9), 1233–1242, 1998.

[CS00a] B. Chen and C.-E. W. Sundberg, Digital audio broadcasting in the FM band by means of contiguous band Insertion and precancelling techniques, *IEEE Transactions on Communications*, 48(10), 1634–1637, 2000.

[CS00b] B. Chen and C.-E. W. Sundberg, Complementary punctured pair convolutional codes for digital audio broadcasting, *IEEE Transactions on Communications*, 48(11), 1829–1839, 2000.

[SS94] N. Seshadri and C.-E. W. Sundberg, List Viterbi decoding algorithms with applications, *IEEE Transactions on Communications*, 42(2/3/4), 313–323, 1994.

[LS01] J. N. Laneman and C.-E. W. Sundberg, Soft selection combining for terrestrial digital audio broadcasting in the FM band, *IEEE Transactions on Broadcasting*, 47(2), 103–114, 2001.

[S99] C.-E. W. Sundberg et al, Multistream Hybrid On Channel Systems for digital audio broadcasting in the FM band, *IEEE Transactions on Broadcasting*, 45(3), 410–417, 1999.

[L02] H.-L. Lou et al, Multi-stream transmission for Hybrid IBOC AM with embedded multidescriptive audio coding, *IEEE Transactions on Broadcasting*, 48(3), 179–192, 2002.

[wHDR] www.hdradio.com

[wIBQ_I] www.ibiquity.com/international

[wDRM] www.drm.org

[RS08] S. A. Ramprashad and C. E. W. Sundberg, Hierarchical QAM BICM MIMO systems with iterative decoding and applications to media broadcast, IEEE WOWMOM 2008, Newport Beach, CA, June 2008.

[wikiDRM] en.wikipedia/wiki/Digital_Radio_Mondiale

[wSXM] www.siriusxm.com

[N05] N. Naik et al, Joint encoding and decoding methods for digital audio broadcasting of multiple programs, *IEEE Transactions on Broadcasting*, 51(4), 439–448, 2005.

[wikiISDB] en.wikipedia.org/wiki/ISDB

[wikiDVBH] en.wikipedia.org/wiki/DVB-H

[wikiFLO] en.wikipedia.org/wiki/MediaFLO

[wQC] www.qualcomm.com

[C07] M. R. Chari et al., FLO Physical Layer: an overview, *IEEE Transactions on Broadcasting*, 53(1), 145–160, 2007.

[w3GPP] www.3gpp.org

[BH05] M. Bakhuizen and U. Horn, Mobile broadcast/multicast in mobile networks, *Ericsson Review*, 82(1), 6–13, 2005.

[I08] J.-A. Ibanez et al., Mobile TV over 3G networks—Service and enablers evolution, *Ericsson Review*, 85(1), 38–42, 2008.

[wikiDD] en.wikipedia.org/wiki/Dolby_Digital

[B10] D. Bodson, Digital audio around the world, *IEEE Vehicular Technology Magazine*, 5(4), 24–30, 2010.

[C83] M. Costa, Writing on dirty paper, *IEEE Transactions on Information Theory*, 29(3), 439–441, 1983.

[wikiGSM] en.wikipedia.org/wiki/GSM

[AAS86] J. B. Anderson, T. M. Aulin, and C.-E. W. Sundberg, *Digital Phase Modulation*, Plenum, New York, 1986.

[MH81] K. Murota and K. Hirade, GMSK modulation for digital mobile telephony, *IEEE Transactions on Communications*, 29(7), 1044–1050, 1981.

[BKB03] G. de Boer, C. Kupfenschmidt, D. Bederov, and H.-P. Kuchenbecker, Digital audio broadcasting in the FM band based on continuous phase modulation, *IEEE Transactions on Broadcasting*, 49(3), 293–303, 2003.

[KAB08] C. Kupfenschmidt, A. Ayadi-Miessen, G. de Boer, R. Patino, and H.-P. Kuchenbecker, Field tests of digital radio broadcasting in the FM band based on continuous phase modulation, *IEEE Transactions on Broadcasting*, 54(2), 236–248, 2008.

III

Source Compression and Quality Assessment

28

Speech Coding for Wireless Communications

Jerry D. Gibson

28.1 Introduction

The goal of speech coding is to represent speech in digital form with as few bits as possible while maintaining the intelligibility and quality required for the particular application. Interest in speech coding is motivated by the evolution to digital communications and the requirement to minimize bit rate, and hence, conserve bandwidth. There is always a trade-off between lowering the bit rate and maintaining the delivered voice quality and intelligibility; however, depending on the application, many other constraints must also be considered, such as complexity, delay, and performance with bit errors or packet losses [1].

Speech coding is fundamental to the operation of the public switched telephone network (PSTN), videoconferencing systems, digital cellular communications, and voice over Internet protocol (VoIP) applications. In particular, efficient, high-quality speech codecs were (and are) essential to the evolution of cellular voice communications from analog to digital systems and for the development and widespread use of VoIP for voice communications.

In this chapter, we discuss the technologies and issues involved in speech coding, with particular applications to digital cellular and VoIP for wireless access points. Interestingly, some quite different issues are involved in these two systems, and in fact, for the most part, the speech codecs are different.

There was almost an exponential growth of speech coding standards in the 1990s for a wide range of networks and applications, including the wired PSTN, digital cellular systems, and multimedia streaming over the Internet. We develop the speech codecs used in digital cellular and wireless VoIP applications,

and we also discuss the ITU-T standardized speech codecs because of the influence some of the ITU-T codec designs have had on the codecs in wireless systems and because some of these codecs appear in wireless applications. We provide comparisons of the performance, complexity, and coding delay of the several most prominent standards, and we examine key challenges for effective voice communications when the various codecs are employed in communications networks.

We also present the requirements and current capabilities, some projected, of new speech coding standards under development at the time of this writing. We begin the chapter by outlining the basic issues in speech coding, followed by some details on the basic speech coding structures that are widely used.

We use the terms speech coding and voice coding interchangeably in this chapter. Generally, it is desired to reproduce the voice signal, since we are interested in not only knowing what was said but also in being able to identify the speaker.

28.2 Basic Issues in Speech Coding

Speech and audio coding can be classified according to the bandwidth occupied by the input and the reproduced source. Narrowband or telephone bandwidth speech occupies the band from 200 to 3400 Hz, and is the band classically associated with telephone quality speech. In the mid- to late 1980s, a new bandwidth of 50 Hz–7 kHz, called wideband speech, became of interest for videoconferencing applications. High-quality audio is generally taken to cover the range of 20 Hz–20 kHz, and this bandwidth is designated today as fullband. In recent years, quite a few other bandwidths have attracted attention, primarily for audio over the Internet applications, and the bandwidth of 50 Hz–14 kHz, designated as superwideband, has gotten considerable recent attention in standardization activities. The discussions in this chapter address all of these bandwidths of interest, although most of the discussions and standardized codecs for wireless applications have emphasized narrowband and wideband speech.

Given a particular source, the classic trade-off in lossy source compression is rate versus distortion—the higher the rate, the smaller the average distortion in the reproduced signal. Of course, since a higher bit rate implies a greater channel or network bandwidth requirement, the goal is always to minimize the rate required to satisfy the distortion constraint. For speech coding, we are interested in achieving a quality as close to the original speech as possible within the rate, complexity, latency, and any other constraints that might be imposed by the application of interest. Encompassed in the term "quality" are intelligibility, speaker identification, and naturalness. Absolute category rating tests are subjective tests of speech quality and involve listeners assigning a category and rating for each speech utterance according to the classifications, such as, excellent (5), good (4), fair (3), poor (2), and bad (1). The average for each utterance over all listeners is the mean opinion score (MOS) [2]. More details on MOS are given in the Appendix.

Although important, the MOS values obtained by listening to isolated utterances do not capture the dynamics of conversational voice communications in the various network environments. It is intuitive that speech codecs should be tested within the environment and while executing the tasks for which they are designed. Thus, since we are interested in conversational (two-way) voice communications, a more realistic test would be conducted in this scenario. The perceptual evaluation of speech quality (PESQ) method was developed to provide an assessment of speech codec performance in conversational voice communications. The PESQ has been standardized by the ITU-T as P.862 and can be used to generate MOS values for both narrowband and wideband speech [3]. The narrowband PESQ performs fairly well for the situations for which it has been qualified, and the wideband PESQ MOS, while initially not very accurate, has become more reliable in recent years.

Throughout this chapter, we quote available MOS values taken from many different sources for all of the codecs. Since MOS values can vary from test to test and across languages, these values should not be interpreted as an exact indicator of performance. Care has been taken only to present MOS values that are consistent with widely known performance results for each codec. For more details on subjective

and objective measures for speech quality assessment, the reader is referred to the Appendix and the references.

Across codecs that achieve roughly the same quality at a specified bit rate, codec complexity can be a distinguishing feature. In standards and in the literature, the number of MIPs (million instructions per second) is often quoted as a broad indicator of implementation complexity, where MIPs numbers generally relate to implementations on digital signal processing (DSP) chips rather than CPUs. Another quantity, called weighted millions of instructions per second (WMOPS), where each operation is assigned a weight based on the number of DSP cycles required to execute the operation is also used. The relationship between MIPS and WMOPS is determined based on the particular DSP. We quote both complexity indicators in this chapter as available in the literature and from other comparisons.

An issue of considerable importance for voice codecs to be employed in conversational applications is the delay associated with the processing at the encoder and the decoder. This is because excessive delay can cause "talk over" and an interruption of the natural flow of the conversation. ITU-T Recommendation G.114 provides specifications for delay when echo is properly controlled [4]. In particular, one-way transmission time (including processing and propagation delay) is categorized as (a) 0–150 ms: acceptable for most user applications; (b) 150–400 ms: acceptable depending upon the transmission time impact; and (c) above 400 ms: unacceptable for general network planning purposes. Figure 28.1 provides a broader view of the estimated impact of delay on user preferences as stated in the ITU-T G.114 standard. From this figure, it is seen that up to 150 ms represents the flat part of the curve, and acceptable delay is sometimes quoted as 200 ms, since delays up to 200 ms fall into the "Users Very Satisfied" category. In spite of the implications of this diagram and the above categorizations, it is generally felt that once the round trip delay is about 300 ms, two-way voice communications is difficult.

When different codecs are used in different but interconnected networks, or when the speech signal must be decoded at network interfaces or switches, the problem of tandem connections of speech codecs can arise. The term "asynchronous tandeming" originally referred to a series connection of speech coders that requires digital to analog conversion followed by resampling and reencoding. Today, and within the context of this chapter, tandeming refers to where the speech samples must be reconstructed and then reencoded by the next codec. Tandem connections of speech codecs can lead to a significant loss in quality, and of course, incur additional delays due to decoding and reencoding. Another possible

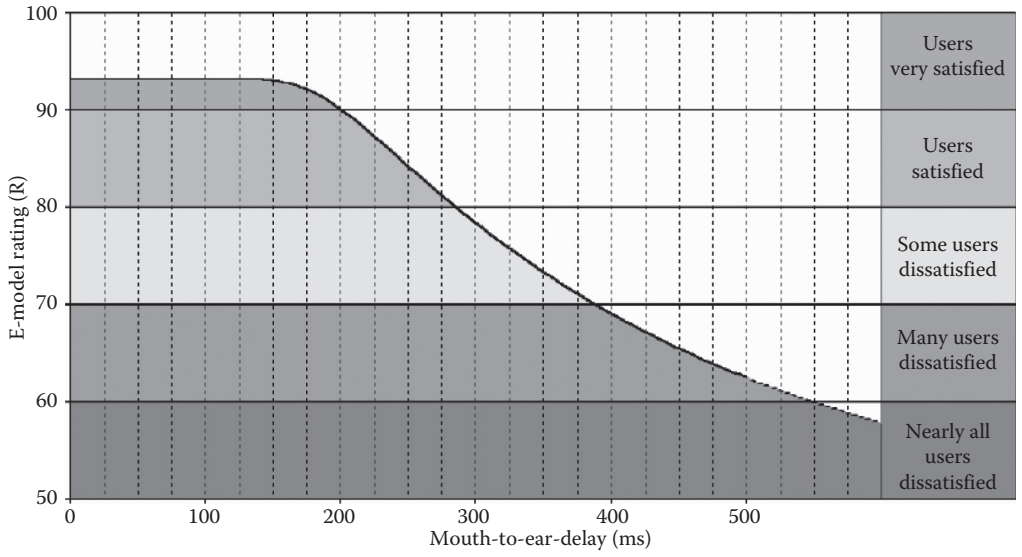

FIGURE 28.1 Effect of one-way delay on speech quality (G.114).

approach to tandem connections of different speech codecs is to map the parameters of one codec into the parameters of the following codec without reconstructing the speech samples themselves. This is usually referred to as transcoding. Transcoding produces some quality loss and delay as well. Tandem connections of speech codecs are often tested as part of the overall codec performance evaluation process.

In many applications, errors can occur during transmission across networks and through wireless links. Errors can show up as individual bit errors or bursts of bit errors, or with the widespread movement toward IP-based protocols, errors can show up as packet losses. In error-prone environments or during error events, it is imperative that the decoded speech be as little affected as possible. Some speech codecs are designed to be robust to bit errors, but it is more common today that packet loss concealment methods are designed and associated with each speech codec. Depending upon the application, robustness to errors, and/or a good packet loss concealment scheme may be a dominating requirement.

It is by now well known that speech codecs should be tested across a wide variety of speakers, but it is also important to note that speech codecs are tested across many different languages as well. It is difficult to incorporate multiple languages into a design philosophy, but suffice it to say, since the characteristics of spoken languages around the world can be so different, codec designs must be evaluated across a representative set of languages to reveal any shortcomings.

28.3 Speech Coding Methods

The most common approaches to narrowband speech coding today center around two paradigms, namely, waveform-following coders and analysis-by-synthesis methods. Waveform-following coders attempt to reproduce the time domain speech waveform as accurately as possible, while analysis-by-synthesis methods utilize the linear prediction model and a perceptual distortion measure to reproduce only those characteristics of the input speech determined to be most important. Another approach to speech coding breaks the speech into separate frequency bands, called subbands, and then codes these subbands separately, perhaps using a waveform coder or analysis-by-synthesis coding, for reconstruction and recombination at the receiver. Extending the resolution of the frequency domain decomposition leads to transform coding, wherein a transform is performed on a frame of input speech and the resulting transform coefficients are quantized and transmitted to reconstruct the speech from the inverse transform. In this section, we provide some background details for each of these approaches to lay the groundwork for the later developments of speech coding standards based upon these principles. A discussion of the class of speech coders called vocoders or purely parametric coders is not included due to space limitations and their more limited range of applications today.

28.3.1 Waveform Coding

Familiar waveform-following methods are logarithmic pulse code modulation (log-PCM) and adaptive differential pulse code modulation (ADPCM), and both have found widespread applications. Log PCM at 64 kilobits/second (kbps) is the speech codec used in the long-distance PSTN at a rate of 64 kbps and it is the most widely employed codec for VoIP applications. It is a simple coder and it achieves what is called toll quality, which is the standard level of performance against which all other narrowband speech coders are judged. Log PCM uses a nonlinear quantizer to reproduce low-amplitude signals, which are important to speech perception, well. There are two closely related types of log-PCM quantizer used in the world—μ-law, which is used in North America and Japan, and A-law, which is used in Europe, Africa, Australia, and South America. Both achieve toll-quality speech, and in terms of the MOS value, it is usually between 4.0 and 4.5 for log-PCM.

ADPCM operates at 32 kbps or lower, and it achieves performance comparable to log-PCM by using an adaptive linear predictor to remove short-term redundancy in the speech signal before quantization. The most common form of ADPCM uses what is called backward adaptation of the predictors and

quantizers to follow the waveform closely. Backward adaptation means that the predictor and quantizer are adapted based upon past reproduced values of the signal that are available at the encoder and decoder. No predictor or quantizer parameters are sent along with the quantized waveform values. By subtracting a predicted value from each input sample, the dynamic range of the signal to be quantized is reduced, and hence, good reproduction of the signal is possible with fewer bits.

28.3.2 Subband and Transform Methods

The process of breaking the input speech into subbands via bandpass filters and coding each band separately is called subband coding. To keep the number of samples to be coded at a minimum, the sampling rate for the signals in each band is reduced by decimation. Of course, since the bandpass filters are not ideal, there is some overlap between adjacent bands and aliasing occurs during decimation. Ignoring the distortion or noise due to compression, quadrature mirror filter (QMF) banks allow the aliasing that occurs during filtering and subsampling at the encoder to be cancelled at the decoder. The codecs used in each band can be PCM, ADPCM, or even an analysis-by-synthesis method. The advantage of subband coding is that each band can be coded differently and that the coding error in each band can be controlled in relation to human perceptual characteristics.

Transform coding methods were first applied to still images but later investigated for speech. The basic principle is that a block of speech samples is operated on by a discrete unitary transform and the resulting transform coefficients are quantized and coded for transmission to the receiver. Low bit rates and good performance can be obtained because more bits can be allocated to the perceptually important coefficients, and for well-designed transforms, many coefficients need not be coded at all, but are simply discarded, and acceptable performance is still achieved.

Although classical transform coding has not had a major impact on narrowband speech coding and subband coding has fallen out of favor in recent years, filter bank and transform methods play a critical role in high-quality audio coding, and several important standards for wideband, superwideband, and fullband speech/audio coding are based upon filter bank and transform methods. Although it is intuitive that subband filtering and discrete transforms are closely related, by the early 1990s, the relationships between filter bank methods and transforms were well understood [5]. Today, the distinction between transforms and filter bank methods is somewhat blurred, and the choice between a filter bank implementation and a transform method may simply be a design choice.

28.3.3 Analysis-by-Synthesis Methods

Analysis-by-synthesis (AbS) methods are a considerable departure from waveform-following techniques and from frequency domain methods as well. The most common and most successful analysis-by-synthesis method is code-excited linear prediction (CELP). In CELP speech coders, a segment of speech (say, 5–10 ms) is synthesized using the linear prediction model along with a long-term redundancy predictor for all possible excitations in what is called a codebook. For each excitation, an error signal is calculated and passed through a perceptual weighting filter. This operation is represented in Figure 28.2a. The excitation that produces the minimum perceptually weighted coding error is selected for use at the decoder as shown in Figure 28.2b. Therefore, the best excitation out of all possible excitations for a given segment of speech is selected by synthesizing all possible representations at the encoder, hence, the name analysis-by-synthesis. The predictor parameters and the excitation codeword are sent to the receiver to decode the speech. It is instructive to contrast the AbS method with waveform coders such as ADPCM where each sample is coded as it arrives at the coder input.

The perceptual weighting is key to obtaining good speech coding performance, and the basic idea is that the coding error is spectrally shaped to fall below the envelope of the input speech across the frequency band of interest. Figure 28.3 illustrates the concept wherein the spectral envelope of a speech segment is shown, along with the coding error spectrum without perceptual weighting (unweighted

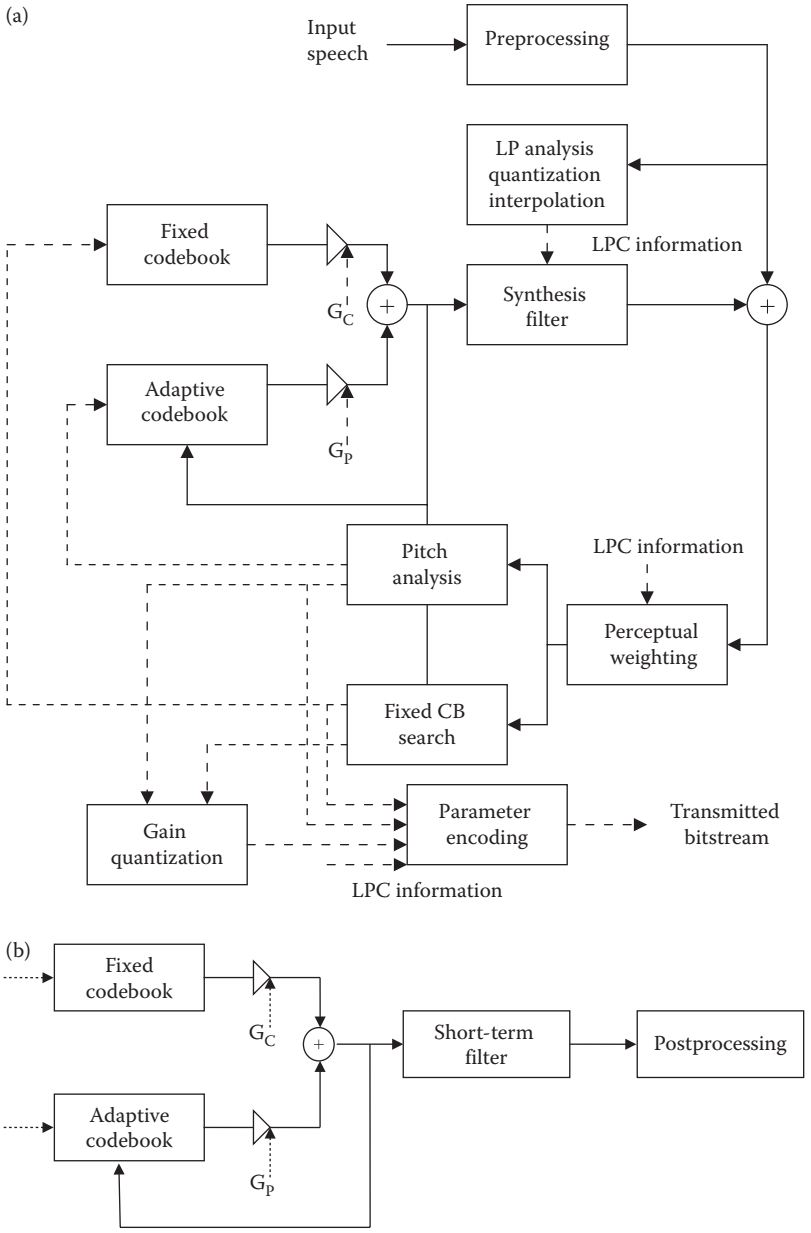

FIGURE 28.2 (a) Encoder for code-excited linear predictive (CELP) coding with an adaptive codebook. (b) CELP decoder with an adaptive codebook and postfiltering.

denoted by short dashes) and the coding error spectrum with perceptual weighting (denoted by long dashes). The perceptually weighted coding error falls below the spectral envelope of the speech across most of the frequency band of interest, just crossing over around 3100 Hz. The coding error is thus masked by the speech signal itself. In contrast, the unweighted error spectrum is above the speech spectral envelope starting at around 1.6 kHz, which produces audible coding distortion for the same bit rate.

In recent years, it has become common to use an adaptive codebook structure to model the long-term memory rather than a cascaded long-term predictor. A decoder using the adaptive codebook approach

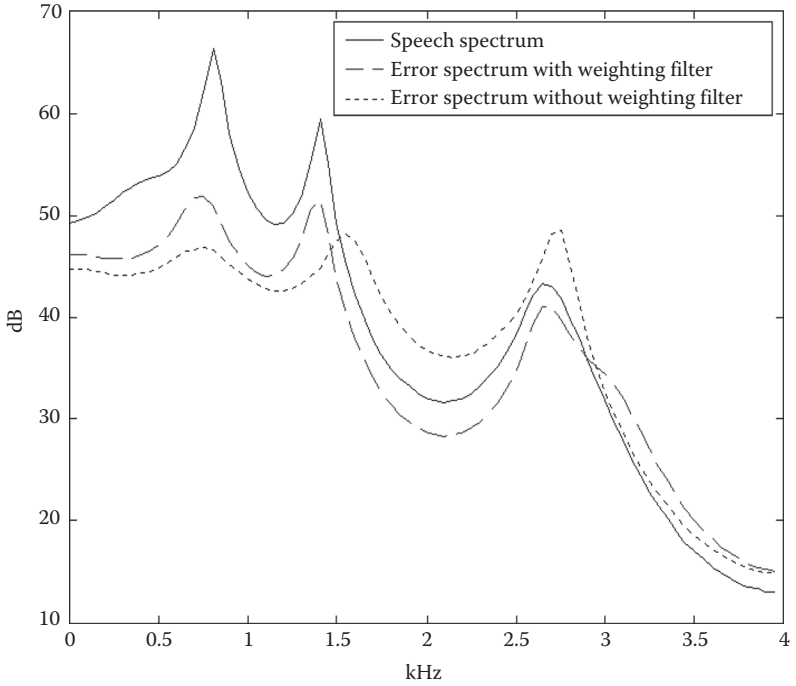

FIGURE 28.3 Perceptual weighting of the coding error as a function of frequency.

is shown in Figure 28.2b. The analysis-by-synthesis procedure is computationally intensive, and it is fortunate that algebraic codebooks, which have mostly zero values and only a few nonzero pulses, have been discovered and work well for the fixed codebook [6].

28.3.4 Postfiltering

Although a perceptual weighting filter is used inside the search loop for the best excitation in the codebook for analysis-by-synthesis methods, there is often still some distortion in the reconstructed speech that is sometimes characterized as "roughness." This distortion is attributed to reconstruction or coding error as a function of frequency that is too high at regions between formants and between pitch harmonics. Several codecs thus employ a postfilter that operates on the reconstructed speech to deemphasize the coding error between formants and between pitch harmonics. This is shown as "postprocessing" in Figure 28.2b. The general frequency response of the postfilter has the form similar to the perceptual weighting filter with a pitch or long-term postfilter added. There is also a spectral tilt correction since the formant-based postfilter results in an increased low-pass filter effect, and a gain correction term [5,6]. The postfilter is usually optimized for a single-stage encoding (however, not always), so if multiple tandem connections of speech codecs occur, the postfilter can cause a degradation in speech quality.

28.3.5 Variable Rate Coding

For more than 30 years, researchers have been interested in assigning network capacity only when a speaker is "active," as in TASI, or removing silent periods in speech to reduce the average bit rate. This was successfully accomplished for some digital cellular coders where silence is removed and coded with a short length code and then replaced at the decoder with "comfort noise." Comfort noise is needed because the background sounds for speech coders are seldom pure silence and inserting pure silence

generates unwelcome artifacts at the decoder and can cause the impression that the call is lost. The result, of course, is a variable rate speech coder. Many codecs use voice activity detection to excise nonspeech signals so that nonspeech regions do not need to be coded explicitly. More sophisticated segmentation can also be performed so that different regions can be coded differently. For example, more bits may be allocated to coding strongly voiced segments and fewer allocated to unvoiced speech. Also, speech onset might be coded differently as well.

When used over fixed rate communications links, variable rate coders require the use of jitter buffers and can be sensitive to bit errors. However, packet switched networks reduce these problems and make variable rate coding attractive for packet networks.

28.3.6 SNR and Bandwidth Scalable Methods

SNR or bit rate scalability refers to the idea of coding the speech in stages such that the quality can be increased simply by appending an additional bit stream. For example, speech may be coded using a minimum bit rate stream that provides acceptable quality, often called a core layer, along with one or more incremental enhancement bit streams. When the first enhancement bit stream is combined with the core layer to reconstruct the speech, improved performance is obtained. SNR or bit rate scalable coding is inherently no better than single-stage encoding at the combined rate, so the challenge is to design good SNR scalable codecs that are as close to single-stage encoding as possible. One attraction of SNR scalable coding is that the enhancement bit stream may be added or dropped, depending upon available transmission bit rate. Another option facilitated by SNR scalable coding is that the core bit stream may be subject to error control coding whereas the enhancement bit stream may be left unprotected.

Bandwidth scalable coding is a method wherein speech with a narrower bandwidth is coded as a base layer bit stream, and an enhancement bit stream is produced that encodes frequencies above the base layer bandwidth. Particular applications of interest might be having a base layer bit stream that codes telephone bandwidth speech from 200 to 3400 Hz and enhancement layer bit streams that codes speech in the additional bands, thus incorporating wideband, superwideband, and fullband audio. The goal is to allow flexibility in bit rate and still have a high-quality representation of the speech at the low band and at additional bands when enhancement layers are combined with the base layer.

28.4 Speech Coding Standards

In this section, we describe the relevant details of current and some past standardized speech codecs for digital cellular and packet switched VoIP for wireless access points. We begin the discussion with ITU-T standardized codecs since some of those codecs have served as the basis for cellular codecs, and further since some of these codecs are used for VoIP applications.

28.4.1 ITU-T Standards

Tables 28.1 and 28.2 list some of the narrowband and wideband/fullband voice codecs that have been standardized by the ITU-T over the years, including details concerning the codec technology, transmitted bit rate, performance, complexity, and algorithmic delay. Those shown include G.711, G.726, G.728, G.729, and G.729A for narrowband (telephone bandwidth) speech (200 to 3400 Hz), G.722, G.722.1 [7], G.722.2 [8], and G.718 for wideband speech (50 Hz–7 kHz) [9], and G.719 for fullband audio [10].

G.711 at 64 kbps is the voice codec most often used in the PSTN and in VoIP today. This codec is based on a nonlinear quantization method called log-PCM, which allows low-amplitude speech signal samples to be quantized with the same accuracy as larger amplitude samples. This codec is the benchmark for narrowband toll-quality voice transmission. G.711 is designed with several asynchronous tandems in mind, since it was possible to encounter several analog switches during a long-distance

TABLE 28.1 Comparison of ITU-T Narrowband Speech Codecs

Standards Body	ITU	ITU	ITU	ITU	ITU
Recommendation	G.711	G.726	G.728	G.729	G.729A
Coder type	Companded PCM	ADPCM	LD-CELP	CS-ACELP	CS-ACELP
Bite rate (kbps)	64	16–40	16	8	8
Complexity (MIPS)	<<1	~1	~30	≤20	≤11
Frame size (ms)	0.125	0.125	0.625	10	10
Lookahead (ms)	0	0	0	5	5
Codec delay (ms)	0.25	0.25	1.25	25	25

TABLE 28.2 ITU-T Wideband and Fullband Speech Coding Standards

Recommendation	ITU-T G.722	ITU-T G.722.1	ITU-T G.722.2 3GPP AMR-WB	ITU-T G.718	ITU-T G.719
Coder type	Subband ADPCM	MLT	ACELP	ACELP, MDCT	Adaptive resolution MDCT, FLVQ
Audio bandwidth (Hz)	50–7000	50–7000	50–7000	50–7000	20–20,000
Bit rate(s) (kbps)	48, 56, 64	24, 32	6.6, 8.85, 12.65, 14.25, 15.85, 18.25, 19.85, 23.05, 23.85	8, 12, 16, 24, 32, and 12.65 (G.722.2, AMR-WB, VMR-WB Interop Mode)	32…128 steps of 4 kbps up to 96 kbps, steps of 8 kbps up to 128 kbps
Frame length (ms)	0.125	20	20	20	20
Algorithmic delay (ms)	1.625	40	25	32.875–43.875	40
Computational complexity	10 MIPS	<5.5 WMOPS	27.2–39.0 WMOPS	57 WMOPS	15.39–21 WMOPS

telephone call prior to the mid-1980s. Even eight asynchronous tandems of G.711 with itself has been shown to still maintain a MOS greater than 4.0 when a single encoding is 4.4–4.5.

The G.726 and G.728 standards not only were required to perform well for single and multiple encodings, but they were also required to be able to pass voiceband modem signals and to have a low coding delay of less than 5 ms. To achieve the desired bit rate of 8 kbps, the low delay and voiceband modem requirements were removed for G.729. The G.729 codec is an analysis-by-synthesis codec based on algebraic code excited linear prediction (ACELP), and it uses an adaptive codebook to incorporate the long-term pitch periodicity. In addition to a lower complexity version of G.729, called G.729A, there is a higher-rate codec based on G.729, designated G.729E. The G.729 codec structure has been very influential on subsequent voice coding standards for VoIP and digital cellular networks.

Even though we are quite comfortable communicating using telephone bandwidth speech (200–3400 Hz), there is considerable interest in compression methods for wideband speech covering the range of 50 Hz–7 kHz. The primary reasons for the interest in this band are that wideband speech improves intelligibility, naturalness, and speaker identifiability. The first application of wideband speech coding was to videoconferencing, and the first standard, G.722, separated the speech into two subbands and used ADPCM to code each band. The G.722 codec is relatively simple and produces good-quality speech at 64 kbps, and lower-quality speech at the two other possible codec rates of 56 and 48 kbps [6]. The G.722 speech codec is still widely available in the H.324 videoconferencing standard, and it is often provided as an option in VoIP systems. G.722 at 64 kbps is often employed as a benchmark for the performance of other wideband codecs.

Two recently developed wideband speech coding standards, designated as G.722.1 and G.722.2, utilize coding methods that are quite different from G.722, as well as completely different from each other.

The G.722.1 standard employs a filter bank/transform decomposition called the modulated lapped transform (MLT) and operates at the rates of 24 and 32 kbps. The coder has an algorithmic delay of 40 ms, which does not include any computational delay. Since G.722.1 employs filter bank methods, it performs well for music and less well for speech.

G.722.2 is actually an ITU-T designation for the adaptive multirate wideband (AMR-WB) speech coder standardized by the 3GPP [11]. This coder operates at rates of 6.6, 8.85, 12.65, 14.25, 15.85, 18.25, 19.85, 23.05, and 23.85 kbps and is based upon an ACELP analysis-by-synthesis codec. Since ACELP utilizes the linear prediction model, the coder works well for speech but less well for music, which does not fit the linear prediction model. G.722.2 achieves good speech quality at rates greater than 12.65 kbps and performance equivalent to G.722 at 64 kbps with a rate of 23.05 kbps and higher.

G.718 is a newer wideband speech codec that has an embedded codec structure and that operates at 8, 12, 16, 24, and 32 kbps, plus a special alternate coding mode that is bit stream compatible with AMR-WB. G.719 is a fullband audio codec that has relatively low complexity and low delay for a fullband audio codec, and the complexity is approximately evenly split between the encoder and decoder. This codec is targeted toward real-time communications such as in videoconferencing systems and the high-definition telepresence applications.

28.4.2 Digital Cellular Standards

The rapid deployment of digital cellular communications was facilitated by the development of efficient, high-quality voice codecs. Digital cellular applications impose a stringent set of requirements on voice codecs in addition to rate and quality, such as complexity, robustness to background impairments, and the ability to perform well over wireless channels. Over the years, standards have been set by different bodies for different segmentations of the market, particularly according to geographic regions and wireless access technologies. More specifically, digital cellular standards were produced in the late 1980s and early 1990s in Europe, Japan, and North America. The competing North American standards then led to standards efforts more pointed toward each of the competing technologies.

Table 28.3 lists some of the codecs standardized for the North American digital cellular systems in the 1990s. All of the voice codecs shown are analysis-by-synthesis linear prediction-based codecs. The excitation codebooks differ somewhat across the standards, although there is considerable similarity between IS-641 and IS-127, both being based on ACELP, and there is also commonality between IS-96 and IS-133 in their variable rate structure. There are two prominent access technologies in Table 28.3, namely time division multiple access (TDMA) and code division multiple access (CDMA). These two access technologies interact with voice coding in different ways. CDMA is an interference limited-access technology and so a variable rate voice codec, as represented by IS-96, IS-133, and IS-127, increases capacity by adjusting

TABLE 28.3 North American Digital Cellular Standardized Voice Codecs

Standard Body	TIA	TIA	TIA	TIA	TIA
Recommendation	IS-54	IS-641	IS-96	IS-127	IS-133
System	TDMA	TDMA	CDMA	CDMA	CDMA
Coder type	VSELP	ACELP	QCELP	ACELP	CELP
Dates	1990	1995	1993	1997	1997
Bit rate (kbps)	7.95	7.4	0.8–8.5	0.8–8	0.8–13
Complexity (MIPS)	20	20	20	20	20
Frame size (ms)	20	20	20	20	20
Lookahead (ms)	5	5	5	5	5
Codec delay (ms)	45	45	45	45	45

the transmission rate according to the needs indicated by the input source. TDMA can also benefit from a variable rate codec, but by reallocating transmission time slots in the physical layer. Thus, the IS-54 and IS-641 codecs operate at a single fixed rate. However, variable rate codecs were soon incorporated into non-CDMA access systems.

The GSM standards developed in Europe were the basis of perhaps the first widely implemented digital cellular systems. Table 28.4 lists voice codecs standardized for GSM systems, wherein FR stands for "full rate" and HR stands for "half rate." The terms "FR" and "HR" refer to the total transmitted bit rate for combined voice coding and error correction (or channel) coding, and FR is always 22.8 kbps and HR is always 11.4 kbps. By subtracting the rate of the voice codec from either 22.8 or 11.4, one obtains the bit rate allocated to error control coding.

The first GSM FR voice codec standardized in 1989 was not an analysis-by-synthesis codec but used a simpler regular pulse excited linear predictive structure with a long-term predictor. As a result, the codec had to be operated at 13 kbps to achieve the needed voice quality, but it had very low complexity. The first GSM HR codec used the same vector sum excited linear prediction analysis-by-synthesis structure that originated with the North American IS-54 TDMA voice codec. The enhanced full rate GSM voice codec moved over to the ACELP structure and that has persisted in later codecs. An important and somewhat dominant voice codec today is the Adaptive Multirate Codec, both narrowband and wideband versions. Note that AMR-NB has multiple rates and can be operated as a FR or HR codec, depending upon the rates. For GSM, the AMR-NB codec rates are not source-controlled as the IS-96 and IS-133 codecs were, but the rates are switchable and usually adjusted by the network. The AMR codec maintains compatibility with other systems by incorporating the GSM EFR codec at 12.2 kbps and IS-641 at 7.4 kbps as two of its selectable rates. The AMR wideband codec, AMR-WB, also based upon ACELP is also a very important codec today; however, note how the complexity has grown.

A few other standardized codecs are not shown in any of the tables. One is the TIA-EIA/IS-893 cdma2000 standard Selectable Mode Vocoder (SMV), which has six different modes that produce different average data rates and voice quality. The highest-quality mode, Mode 0, can achieve a higher MOS than the IS-127 EVRC at an average data rate of 3.744 kbps, and Mode 1 is theoretically equivalent to IS-127. Another codec not shown is the cdma2000® Variable-Rate Multimode Wideband (VMR-WB) speech coding standard that shares the same core algorithm as AMR-WB, and was standardized by the 3GPP2 in March 2003 [12]. The codec has five modes, and the rate can be varied by the speech signal

TABLE 28.4 Selected GSM Voice Codecs

Codec	Year of Standard	Speech Coding Bit Rate (in kbps)	System/Traffic Channel	Speech Coding Algorithm	Complexity WMOPS
FR codec	1989	13.0	GSM FR	Regular pulse excitation– long-term prediction (RPE-LTP)	3.0
HR codec	1995	5.6	GSM HR	Vector-sum excited linear prediction (VSELP)	18.5
EFR codec	1996	12.2	GSM FR	ACELP	15.2
AMR codec	1999	12.2, 10.2, 7.95, 7.4, 6.7, 5.9, 5.15, 4.75	GSM FR (all eight modes), GSM HR (six lowest modes), 3G WCDMA (all modes)	ACELP	16.8
AMR-WB codec	2001	23.85, 23.05, 19.85, 18.25, 15.85, 14.25, 12.65, 8.85, 6.60	GSM FR (seven lowest modes), EDGE (all modes), 3G WCDMA (all modes)	ACELP	35.4

TABLE 28.5 Representative Asynchronous Tandem Performance of Selected Digital Cellular Codecs

Voice Codec	Mean Opinion Score (MOS)
IS-641 × 2	3.62
GSM-EFR × 2	4.13
IS-641 + G.729	3.48
GSM-FR + G.729	3.05
GSM-EFR + G.729	3.53
GSM-EFR + G.729 + G.729	3.21
IS-641 + G.729 + G.729	3.10

characteristics, called source-controlled, or by the traffic conditions on the network, called network-controlled. One mode is fully interoperable with AMR-WB at 12.65, 8.85, and 6.6 kbps and since AMR-WB is standardized for GSM/WCDMA, this could support some cross-system applications. In addition to cdma2000®, the VMR-WB codec was targeted for a wide range of applications, including VoIP, packet-switched mobile-to-mobile calls, multimedia messaging, multimedia streaming, and instant messaging. If appropriate signaling is available, there is also the goal of end-to-end tandem-free operation (TFO) or transcoder-free operation (TrFO) for some mobile-to-mobile calls. The VMR-WB codec has a narrowband signal processing capability in all modes that is implemented by converting the narrowband input sampling rate of 8 kHz to the internal sampling frequency of 12.8 kHz for processing, and then after decoding, converting the sampling rate back to 8 kHz.

Table 28.5 shows available results for multiple tandem encodings for a few of the codecs discussed, including results from tandem connections of these codecs with G.729 used in VoIP. It is clear that tandem encodings result in a drop in performance as seen in the lower MOS values. Furthermore, tandem encodings add to the end-to-end delay because of the algorithmic delays in decoding and reencoding. Tandem encodings often occur today on mobile-to-mobile calls. Tandem connections with PSTN/VoIP codecs are not discussed often within digital cellular applications since the codec for the backbone wireline network is often assumed to be G.711. However, it is recognized that calls connecting through the wired backbone may require tandem encodings with codecs other than G.711, which can lead to a loss in performance, and that tandem encodings constitute a significant problem for end-to-end voice quality. In particular, transcoding at network interfaces and source coding distortion accumulation due to repeated coding has been investigated with the goal of obtaining a transparent transition between certain speech codecs. Some system-wide approaches have also been developed for specific networks. The general tandeming/transcoding problem remains open.

28.4.3 VoIP Standards

VoIP for wireless access points involves many of the same issues as for wireline VoIP, such as voice quality, latency, jitter, packet loss performance, and packetization. One new challenge that arises is that since the physical link in Wi-Fi is wireless, bit errors commonly occur and this, in turn, affects link protocol design and packet loss concealment. A second challenge is that congestion can play a role, thus impacting real-time voice communications. The way these two issues relate to voice codecs are that packet loss concealment methods are more critical and that codec delay should be more carefully managed for such wireless access points.

We do not discuss protocols for these access points here, but in recent years, considerable effort has been expended to try and adjust prior data-centric approaches to accommodate VoIP applications. There have been quite a few studies concerning the number of calls that can be supported by the various wireless access points, including both physical layer and access protocol issues. One of the points that comes out of these studies is that a reduction in transmitted bit rate for the voice codecs may not result

in an equivalent increase in capacity because of the access protocols and packetization issues. Therefore, anyone selecting voice codecs for these applications should familiarize themselves with the trade-offs involved.

Turning our attention to the voice codecs normally implemented in VoIP solutions, we find that at this point in time, almost all codecs are borrowed from other standards bodies. Specifically, G.711, G.729, and G.722 are commonly offered in VoIP products. Additionally, AMR-NB and perhaps AMR-WB are optional voice codecs. All of these codecs have well-developed packet loss concealment methods, which make them quite compatible with wireless applications. One thing to notice is that the AMR codecs are the only ones that are common with any digital cellular standards, and this can lead to tandem coding penalties when digital cellular and wireless VoIP are used for portions of the same connection for a voice call. The need to support multiple codecs can also be an issue as cell phones morph into handheld devices that support both digital cellular and wireless access point connectivity.

28.5 Next-Generation Standards

Standardization efforts for new voice codecs are continuing in several bodies, with some codecs being developed specifically for digital cellular and others being standardized that will be ported to wireless applications. We discuss a few of these here.

The ITU-T standardization efforts have already resulted in G.711.1 and G.729.1, both of which are extensions of existing standards to wider bands and different, higher rates. A superwideband version of G.722 is also expected soon [13]. These codecs could easily appear in future offerings of VoIP for wireless applications.

The dominant standard in going forward apparently worldwide in digital cellular is 3GPP Long Term Evolution (LTE), which is based on Orthogonal Frequency Division Multiple Access (OFDMA) in the downlink and Single Carrier Frequency Division Multiple Access (SC-FDMA) in the uplink. The initial releases of LTE relied upon the AMR voice codecs for voice coding, but now there is a new effort to develop a voice codec for Enhanced Voice Services (EVS). The objectives of the EVS voice codec for LTE are summarized in Table 28.6 [14]. Here, we see that there is a desire to maintain interoperability with the AMR codecs while adding a superwideband capability and giving more attention to in-call music. High-quality audio codecs for nonconversational services such as streaming, broadcasting, and multicasting have been standardized by 3GPP. These codecs are AMR-WB+ and aacPlus, but their high algorithmic delay restrict their importance for two-way conversational voice.

One way to achieve the desired interoperability with AMR codecs would be to use the AMR codecs as a core layer in an embedded structure as suggested in Reference 14. The codec structure then might take the form shown in Figure 28.4. This codec structure reflects many of the characteristics of the integrated codecs developed to code both voice and audio as well or better than existing standards in each area. Examples of such integrated codecs include G.718 which combines ACELP and MDCT technologies, but only covers 50 Hz–7 kHz, and the recently standardized USAC (Unified Speech and Audio Coding)

TABLE 28.6 Summary of the Main Objectives for the EVC Codec

EVS Codec Development Objectives
Enhanced quality and coding efficiency for narrowband (NB: 200–3400 Hz) and wideband (WB: 50–7000 Hz) speech
Enhanced quality by the introduction of super wideband (SWB: 50–14,000 Hz) speech
Enhanced quality for mixed content and music in conversational applications (e.g., in-call music)
Robustness to packet loss and delay jitter leading to optimized behavior in IP environments
Backward interoperability to AMR-WB by EVS modes supporting the AMR-WB codec format
The AMR-WB interoperable operation modes of the EVS codec may be either identical to those in the AMR-WB codec or different but bit-stream interoperable with them. They may become an alternative implementation of the AMR-WB codec, provided that the enhancements are consistently significant

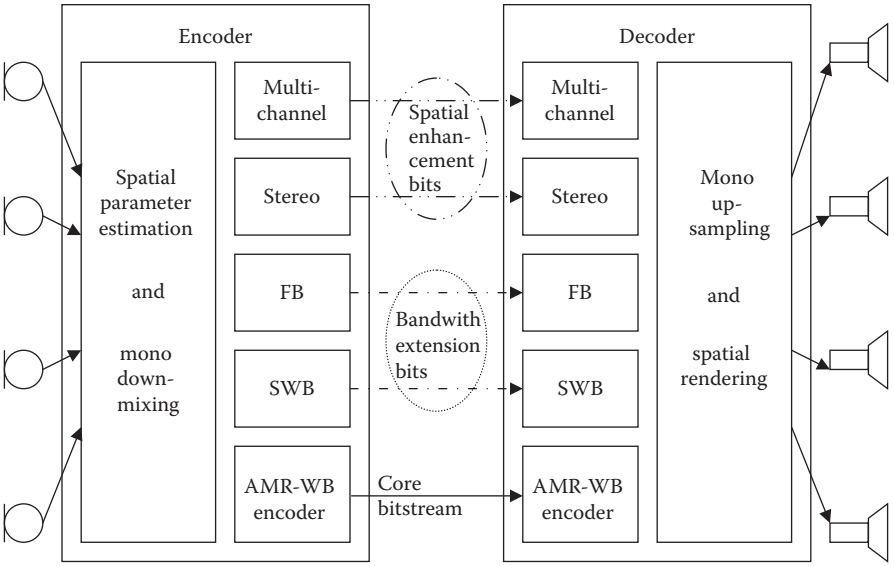

FIGURE 28.4 Embedded codec for EVS (Adapted from K. Jarvinen et al., *Computer Communication*, 1916–1927, 2010).

architecture shown in Figure 28.5, which covers the entire range from 20 Hz to 20 kHz, with the goal of coding voice and fullband audio well [15]. These structures can be viewed as merely bolting together successful codecs for different bands, but the USAC effort notes that it is the handling of the transitions between different coding paradigms that requires innovation beyond a simple combination of known schemes.

A key difference between the USAC effort and the ongoing LTE work is the emphasis of the latter on conversational services, which require low encoding delay. This target application was apparently not specified for the USAC codec standardization. However, there is another codec standardization effort that has the goal of coding narrowband voice all the way up to fullband audio and with the constraint of low delay. The Opus Audio Codec is being designed for interactive voice and audio and has three modes: (a) a linear prediction-based mode for low bit rate coding up to 8 kHz bandwidth, (b) a hybrid linear prediction and MDCT mode for fullband speech/audio at medium bit rates, and (c) an MDCT-only mode for very low latency coding of speech and audio. Details of this codec can be found in Reference 16.

The combination of linear prediction for voice-only coding and the discrete transform/filter bank approaches for music is evident in each of these codecs. There are differences in the applications of interest, and so latency, complexity, and how the complexity is distributed between the encoder and decoder should be an important consideration in wireless applications.

28.6 Outstanding Issues and Future Challenges

It is indeed extraordinary to recognize the large number of voice/audio codecs standardized for a host of applications covering an exhaustive range of desired audio bandwidths and a long list of possible transmitted bit rates. For the most part, these codecs produce the quality and intelligibility needed for the targeted applications. However, there are significant issues remaining. For wireless applications, the codecs are being used in public and perhaps very noisy environments. While great strides have been attained in the robustness of the codecs and in the noise preprocessing algorithms, there is much work left to be done here.

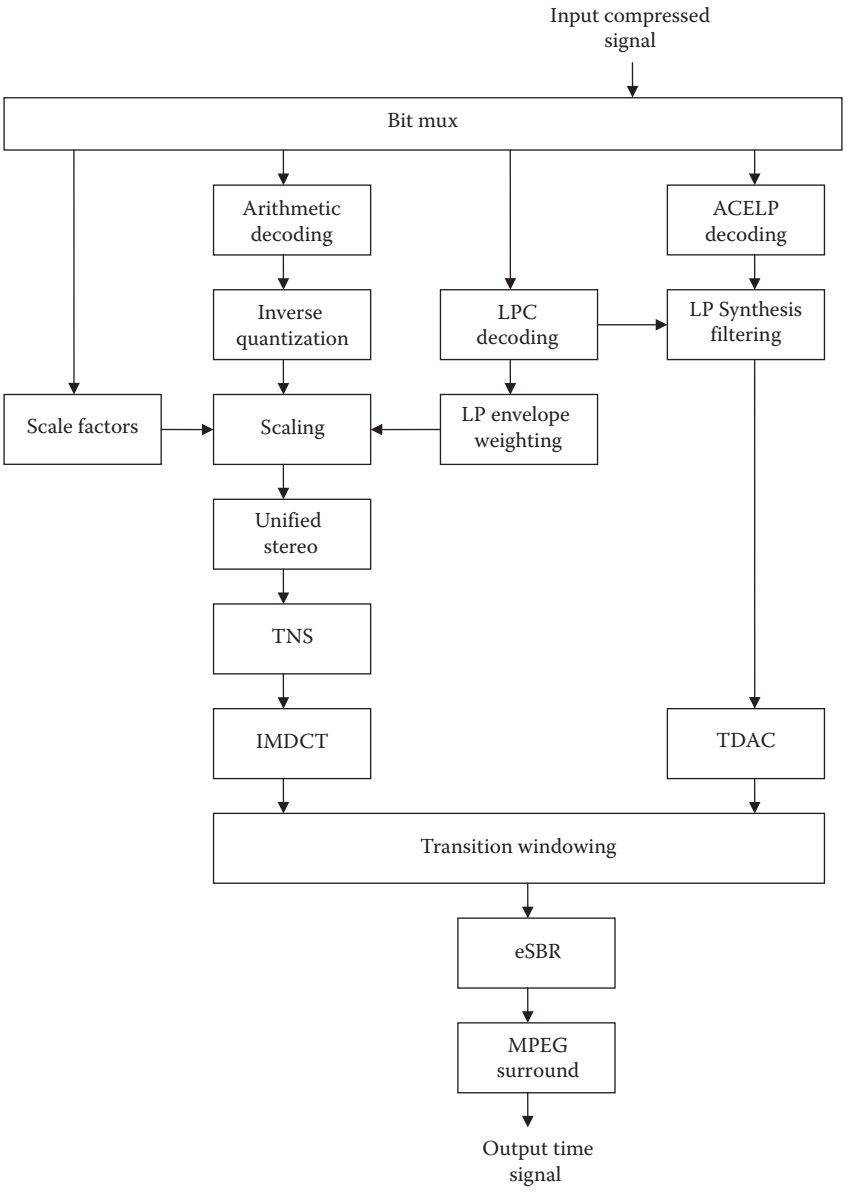

FIGURE 28.5 USAC decoder structure.

Another very significant remaining challenge is that tandem connections of codecs are not being extensively tested prior to standardization and that tandeming is not given a high priority during the standardization processes. However, one way this is being addressed within the setting of particular standards is to maintain interoperable modes. This is seen in the new EVS for LTE effort wherein some AMR mode interoperability is being retained. The issue is primarily the tandeming of codecs in different networks or with different input bandwidths and codec designs. A second way this is being addressed within homogeneous networks, say within a GSM network, is to implement a codec negotiation process.

This is not an option for heterogeneous connections, however. A third way is to have each handset contain implementations of a wide variety of codecs. If the transmitted packets are then appropriately marked, the handset can make the appropriate decoder selection. This approach appears to be prohibitively complicated, and expensive.

One might be tempted to dismiss this problem out of hand since networks are evolving toward all packet transmissions, but the issue is not the transmission technology, the issue is what decoder is available at the other end of the call. When a digital cellular user makes a call to another mobile or to a VoIP user, the codecs at the far end are not known in general. Plus, the usual approach today in digital cellular is to decode at the base station or mobile switching center and reencode using a backbone codec. At the other end, it may be necessary to decode and reencode using a codec supported in the handset at the far end. These tandem encoding/decoding steps incur additional latency and a loss in voice quality and intelligibility. A critical issue is the tandem connections of commercial voice codecs with military/DoD codecs and/or with the codecs used by emergency first responders. These tandem connections are not well tested or analyzed.

As one reads this chapter, two trends are evident in the new standards receiving attention today. There is a desire for the capability to code narrowband speech to fullband music inputs, and the end result is more complexity and increasing latency. The LTE and the Opus Codec attempt to satisfy the former while avoiding the increased complexity and latency. It will be interesting to track their success.

28.7 Summary and Conclusions

Speech coding is an integral part of all wireless communications networks today, and much is being done to extend the capabilities in terms of quality and types of signals supported. This chapter has touched on a host of standardized voice and audio codecs, highlighting their strengths and limitations. Future standards have also been discussed and their proposed roles outlined. Given the increasing demands for wireless communications and the apparent dominance of the wireless paradigm in future communications systems, voice and audio coding are sure to continue to be of critical importance.

Appendix: Speech Quality and Intelligibility

To compare the performance of two speech coders, it is necessary to have some indicator of the intelligibility and quality of the speech produced by each coder. The term "intelligibility" usually refers to whether the output speech is easily understandable, while the term "quality" is an indicator of how natural the speech sounds. It is possible for a coder to produce highly intelligible speech that is low quality in that the speech may sound very machine-like and the speaker is not identifiable. On the other hand, it is unlikely that unintelligible speech would be called high quality, but there are situations in which perceptually pleasing speech does not have high intelligibility. We briefly discuss here the most common measures of intelligibility and quality used in formal tests of speech coders. We also highlight some newer performance indicators that attempt to incorporate the effects of the network on speech coder performance in particular applications.

MOS

The mean opinion score (MOS) is an often-used performance measure [2, Chapter 13]. To establish a MOS for a coder, listeners are asked to classify the quality of the encoded speech in one of five categories: excellent (5), good (4), fair (3), poor (2), or bad (1). The numbers in parentheses are used

to assign a numerical value to the subjective evaluations, and the numerical ratings of all listeners are averaged to produce a MOS for the coder. A MOS between 4.0 and 4.5 usually indicates high quality.

It is important to compute the variance of MOS values. A large variance, which indicates an unreliable test, can occur because participants do not know what categories such as good and bad imply. It is sometimes useful to present examples of good and bad speech to the listeners before the test to calibrate the 5-point scale. Sometimes the percentage of poor and bad votes may be used to predict the number of user complaints. MOS values can and will vary from test to test and so it is important not to put too much emphasis on particular numbers when comparing MOS values across different tests.

DRT

The diagnostic rhyme test (DRT) was devised to test the intelligibility of coders known to produce speech of lower quality. Rhyme tests are so named because the listener must determine which consonant was spoken when presented with a pair of rhyming words; that is, the listener is asked to distinguish between word pairs such as meat–beat, pool–tool, saw–thaw, and caught–taught. Each pair of words differs on only one of six phonemic attributes: voicing, nasality, sustention, sibilation, graveness, and compactness. Specifically, the listener is presented with one spoken word from a pair and asked to decide which word was spoken. The final DRT score is the percent responses computed according to $P = (R - W) \times 100/T$, where R is the number correctly chosen, W is the number of incorrect choices, and T is the total of word pairs tested. Usually, $75 \leq \text{DRT} \leq 95$, with a good being about 90.

DAM

The diagnostic acceptability measure (DAM) developed by Dynastat is an attempt to make the measurement of speech quality more systematic. For the DAM, it is critical that the listener crews be highly trained and repeatedly calibrated in order to get meaningful results. The listeners are each presented with encoded sentences taken from the Harvard 1965 list of phonetically balanced sentences, such as "Cats and dogs each hate the other" and "The pipe began to rust while new." The listener is asked to assign a number between 0 and 100 to characteristics in three classifications—signal qualities, background qualities, and total effect. The ratings of each characteristic are weighted and used in a multiple nonlinear regression. Finally, adjustments are made to compensate for listener performance. A typical DAM score is 45–55%, with 50% corresponding to a good system.

PESQ

An important objective measure is the perceptual evaluation of speech quality (PESQ) method in ITU Recommendation P.862, which attempts to incorporate more than just speech codecs but also end-to-end network measurements [3]. The PESQ has been shown to have good accuracy for the factors listed in Table 28.7. There are parameters for which the PESQ is known to provide inaccurate predictions or is not intended to be used with, such as listening levels, loudness loss, effect of delay in conversational tests, talker echo, and two-way communications. The PESQ also has not been validated to test for packet loss and packet loss concealment with PCM codecs, temporal and amplitude clipping of speech, talker dependencies, music as input to a codec, CELP, and hybrid codecs <4 kbps. There is also a wideband PESQ standard, and it has been improved from an earlier version and is used for evaluating quality for inputs in the 50 Hz to 7 kHz range.

TABLE 28.7 Factors for Which the PESQ Has Demonstrated Acceptable Accuracy

Test Factors
Speech input levels to a codec
Transmission channel errors
Packet loss and packet loss concealment with CELP codecs
Bit rates for multiple bit rate codecs
Transcodings
Environmental noise at the sending side
Effect of varying delay in listening only tests
Short-term time warping of the audio signal
Long-term time warping of the audio signal
Coding Technologies
Waveform codecs such as G.711, G.726, G.727
CELP and hybrid codecs at rates ≥ 4 kbps, such as G.728, G.729, G.723.1
Other codecs: GSM-FR, GSM-HR, GSM-EFR, GSM-AMR, CDMA-EVRC, TDMA-ACELP, TDMA-VSELP, TETRA
Applications
Codec evaluation
Codec selection
Live network testing using a digital or analog connection to the network
Testing of emulated and prototype networks

Acknowledgment

This work has been supported, in part, by NSF Grant No. CCF-0728646.

References

1. J. D. Gibson, Speech coding methods, standards, and applications, *IEEE Circuits and Systems Magazine*, 5, 30–49, 2005.
2. W. B. Kleijn and K. K. Paliwal, eds., *Speech Coding and Synthesis*, Amsterdam, Holland: Elsevier, 1995.
3. ITU-T Recommendation P.862, Perceptual Evaluation of Speech Quality (PESQ), an Objective Method for End-to-End Speech Quality Assessment of Narrowband Telephone Networks and Speech Codecs, February 2001.
4. ITU-T Recommendation G.114, One-Way Transmission Time, May 2000.
5. H. S. Malvar, *Signal Processing with Lapped Transforms*, Norwood, MA: Artech House, 1992.
6. A. M. Kondoz, *Digital Speech: Coding for Low Bit Rate Communication Systems*, West Sussex, England: John Wiley & Sons, 2004.
7. ITU-T Recommendation G.722.1, Coding at 24 and 32 kbit/s for Hands-Free Operation in Systems with Low Frame Loss, September 1999.
8. ITU-T Recommendation G.722.2, Wideband Coding of Speech at around 16 kbit/s Using Adaptive Multi-Rate Wideband (AMR-WB), 2002.
9. ITU-T Recommendation G. 718, Series G: Transmission Systems and Media, Digital Systems and Networks, Digital Terminal Equipments—Coding of Voice and Audio Signals, June 2008.
10. ITU-T Recommendation G. 719, Series G: Transmission Systems and Media, Digital Systems and Networks, Digital Terminal Equipments—Coding of Analogue Signals by Pulse Code Modulation, June 2008.

11. B. Bessette et al., The adaptive multirate wideband speech codec (AMR-WB), *IEEE Transactions on Speech and Audio Processing*, 10, 620–636, 2002.
12. M. Jelinek et al., On the architecture of the cdma2000® variable-rate multimode wideband (VMR -WB) speech coding standard, *Proceedings of ICASSP*, 2004, pp. I-281–I-284.
13. R. Cox, S. F. de Campos Neto, C. Lamblin, and M. H. Sherif, ITU-T coders for wideband, superwideband, and fullband speech communication, *IEEE Communications Magazine*, 106–109, 2009.
14. K. Jarvinen, I. Bouazizi, L. Laaksonen, P. Ojala, and A. Ramo, Media coding for the next generation mobile system LTE, *Computer Communication*, 1916–1927, 2010.
15. M. Neuendorf, P. Gournay, M. Multrus, J. Lecomte, B. Bessette, R. Geiger, S. Bayer et al., A novel scheme for low bitrate unified speech and audio coding-MPEG RM0, *Audio Engineering Society*, Convention Paper 7713, May 2009.
16. IETF Opus Interactive Audio Codec, http://opus-codec.org/, 2011.

29

Video Compression

Do-Kyoung Kwon
Madhukar Budagavi
Vivienne Sze
Woo-Shik Kim

29.1 Introduction

Video compression has been a key enabling technology for a variety of consumer electronics devices and applications such as camera phones, DVD players, personal media players, digital camcorders, streaming video, video conferencing, and etc. This chapter provides an overview of video compression basics and video coding standards developed by ITU-T and ISO/IEC MPEG.

Video sequences contain a lot of redundancies and removing these redundancies is the fundamental objective of video compression. There are several different types of redundancies that exist in video sequences and techniques for removing them are presented first in this section. Early video coding standards including H.261, MPEG-1/2, H.263, and MPEG-4 are briefly introduced as well. Sections 29.2, 29.3, and 29.4 provide an overview of H.264/AVC (advanced video coding), the scalable extensions of H.264/AVC, and the multiview extension of H.264/AVC, respectively. Finally, high-efficiency video coding (HEVC), which is the next-generation video coding standard currently being developed, is briefly introduced in Section 29.5.

29.1.1 Digital Video and Need for Compression

Digital video data consist of a series of images captured using a camera or artificially generated (e.g., computer-generated movies). Figure 29.1a shows four images of a color video sequence captured at 30 frames per second (fps). Each image of color video consists of a luminance (also referred to as luma and denoted by Y) component and two chrominance components (also referred to as chroma and denoted by

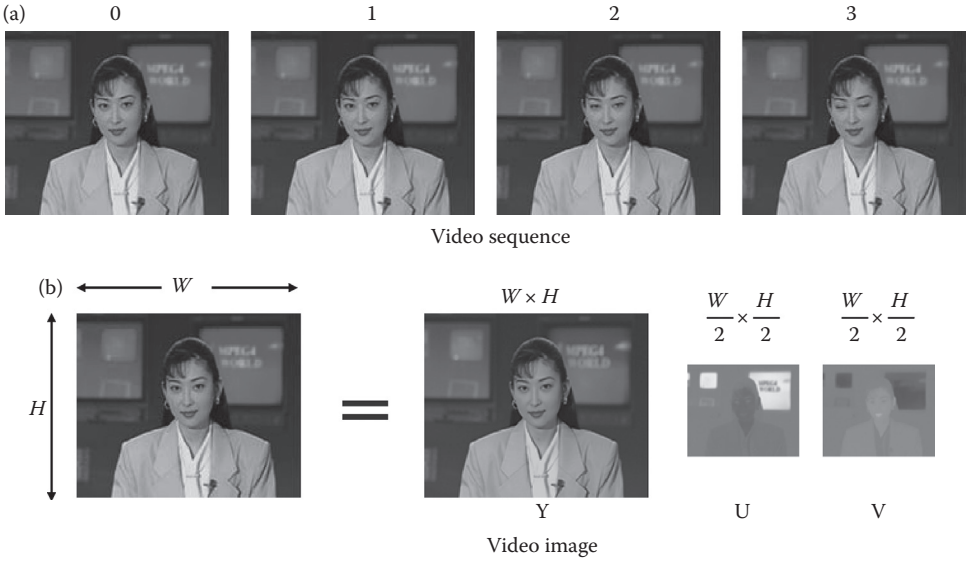

FIGURE 29.1 Digital video data. (a) Video sequence and (b) video image with luma and chroma components.

U and V). Since the human eye is more sensitive to luma than chroma, the chroma components are typically subsampled to lower the data rate. Figure 29.1b shows YUV 4:2:0 format image where the U and V chroma components are quarter the size of luma component. Consumer video is predominantly in the 4:2:0 format with 8 bits per pixel. Higher chroma resolution (no chroma subsampling) and higher bit depth (10-bits or more) are typically used in production quality video generated in studios. Video can be captured in one of two formats—progressive or interlaced. In progressive format all lines in the image are scanned from top to bottom, whereas in interlaced format odd lines in the image are scanned first followed by even lines. The odd lines are called the top field and the even lines are called the bottom field.

Raw digital video requires a lot of data to be stored or transmitted. For example, a 1920 × 1080 (1080p) high-definition (HD) YUV 4:2:0 video sequence with 8 bits per pixel at 60 fps generates around 1.5 Gbps data which are an order of magnitude more than the bandwidth currently supported on broadband networks (~1–10 Mbs). A movie of 90 min would generate around 1 Tbyte of data which are again an order of magnitude more than the capacity available on common storage discs such as Blu-ray (50 GB capacity). Hence, video compression is essential for transmitting or storing digital video.

29.1.2 Video Compression Basics

The goal of video compression is to encode digitized video using as few bits as possible while maintaining acceptable visual quality. Video compression is achieved by removing redundancies in the video signal. Several types of redundancies exist in video signals; spatial, perceptual, statistical, and temporal redundancies.

29.1.2.1 Spatial Redundancy Removal

Most of the time, video data within an image vary smoothly and there is high correlation between spatially adjacent pixels. Spatial redundancy can be removed by spatial prediction and/or by using decorrelating transforms. Figure 29.2 shows an example of spatial prediction where current block is horizontally predicted from the left block. The difference block in this case has less energy than the original block and requires fewer bits to encode than the original block. Figure 29.3 shows the effect of

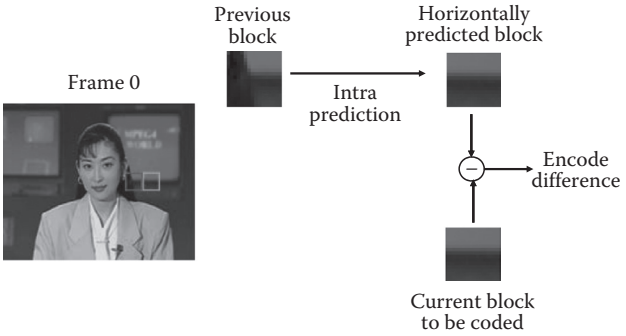

FIGURE 29.2 Example of spatial prediction.

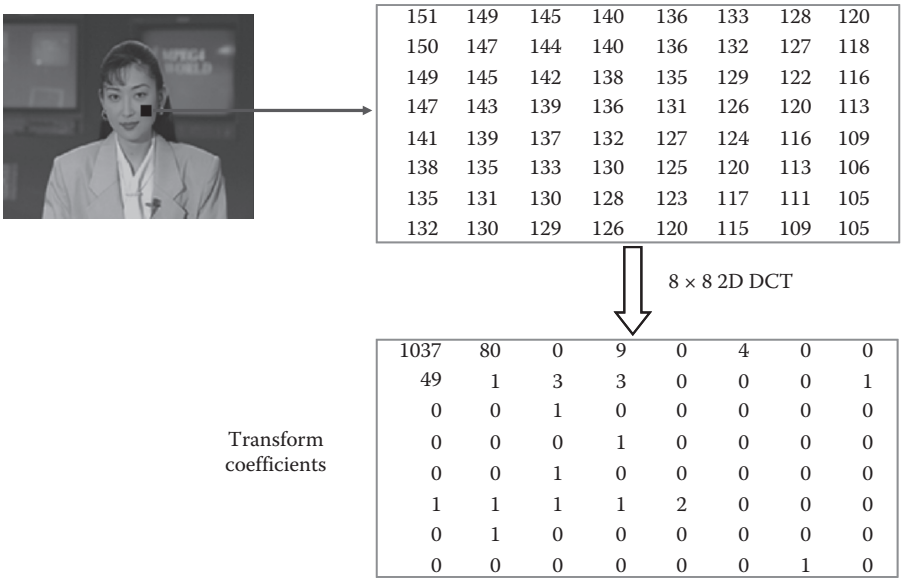

FIGURE 29.3 Spatial redundancy removal by 2D DCT.

using a 2D discrete cosine transform (DCT) on an 8 × 8 region in the cheek area of the person in image. The 2D DCT compacts energy in the input block and renders a lot of transform coefficient values to become zero. These zeros can be efficiently coded using techniques such as run length coding.

29.1.2.2 Perceptual Redundancy Removal

Not all video data are equally significant from a perceptual point of view. For example, in the transform domain, the low-frequency components are perceptually more important than high-frequency components. By sending only the perceptually significant information, data compression can be achieved. Figure 29.4 shows an example where only 36 low frequency DCT coefficients (out of a total of 64 DCT coefficients) for each 8 × 8 block of data are retained. Also, the most significant bits (MSB) of transform coefficients are perceptually more important than the least significant bits (LSB). Quantization which reduces the number of bits used to represent a value also helps in perceptual redundancy removal since it leads to discarding of LSB information.

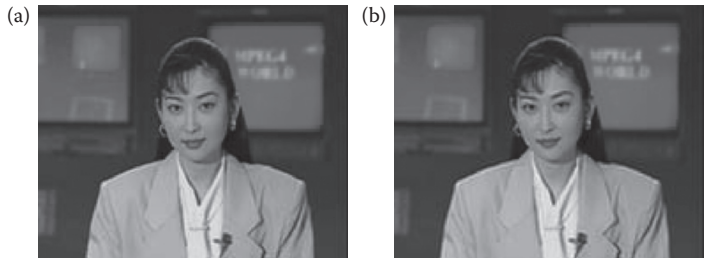

FIGURE 29.4 Perceptual redundancy removal. (a) Original frame and (b) image obtained by retaining 36 low frequency DCT coefficients for each 8 × 8 block.

29.1.2.3 Statistical Redundancy Removal

Not all video data in an image occurs with equal probability. Entropy coding can be used to reduce this statistical redundancy. For example, by using variable length coding (VLC), one can use shorter code words to represent frequent values and longer code words to present less frequent values. On the average this will require less number of bits to code video data than using fixed length coding to code the values. Table 29.1 shows an example of VLC. Assume that there are four types of symbols that need to be transmitted—A, B, C, and D—with probability of occurrence shown in Table 29.1. If one were to use fixed length coding to transmit these symbols, 2 bits per symbol would be required. So to transmit a sequence of A, A, B, D, A, A, A, A, one would require 16 bits. If a variable length code as shown in Table 29.1 were to be used, the number of bits required for transmission would be 1 + 1 + 2 + 3 + 1 + 1 + 1 + 1 = 11 bits.

Figure 29.5a shows the effect of using entropy coding on an example image. The original image uses 8 bits/pixel. If the image were directly coded using variable length code consisting of 256 alphabets, only 7.14 bits will be required to represent a pixel. Alternatively, when VLC is applied on transformed and quantized image (Figure 29.5b), only 1.82 bits will be required to code a pixel.

29.1.2.4 Temporal Redundancy Removal

Significant amount of temporal redundancy exists in video sequences as can be seen from Figure 29.1a where most of the background remains static from one image to the next. There are several ways in which temporal redundancy can be exploited to reduce data rate.

29.1.2.4.1 Conditional Replenishment

This technique encodes only the blocks that have changed from previous picture as shown in Figure 29.6a. The advantage of conditional replenishment is that it requires no additional frame buffers. The received blocks can be directly written into the display frame buffer.

29.1.2.4.2 Frame Difference Coding

This technique encodes frame differences as shown in Figure 29.6b. Difference blocks typically consume fewer bits than original blocks leading to frame difference coding providing better

TABLE 29.1 Example of Variable Length Coding

Symbol	Probability of Occurrence	Fixed Length Coding	Variable Length Coding
A	0.5	00	0
B	0.25	01	10
C	0.125	10	110
D	0.125	11	111

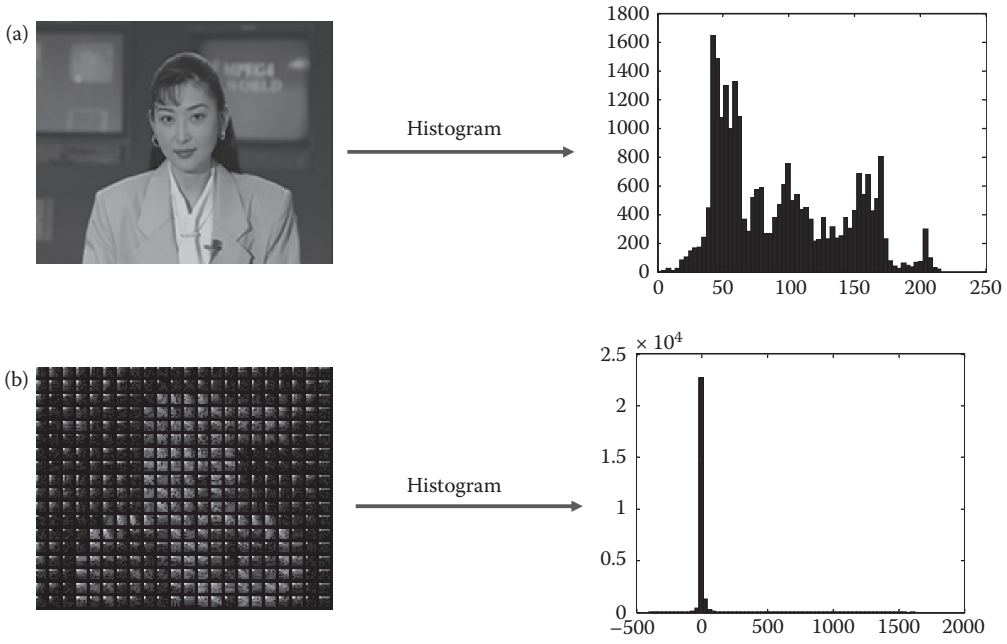

FIGURE 29.5 Effects of statistical redundancy removal on (a) original image: 8 bpp, entropy coding of original image: 7.14 bpp and (b) transformed and quantized image: 1.82 bpp.

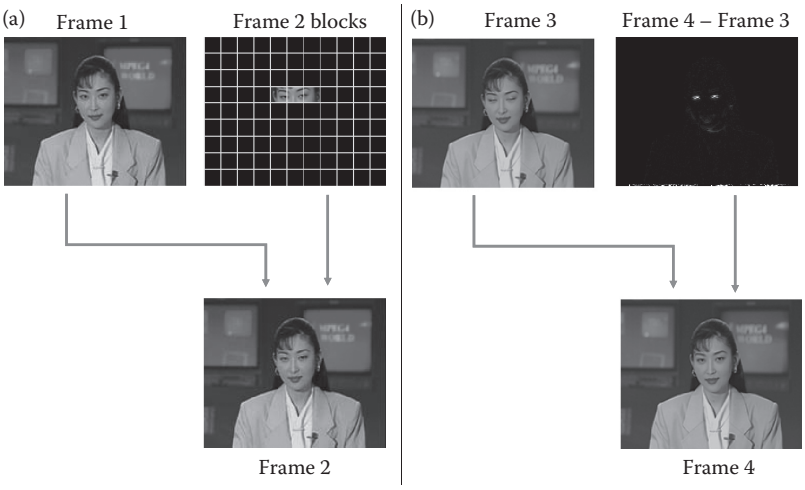

FIGURE 29.6 Temporal redundancy removal by (a) conditional replenishment and (b) frame difference coding.

compression performance than conditional replenishment. However, unlike conditional replenishment, frame difference coding requires a previous frame buffer to be stored in decoder to reconstruct current frame.

29.1.2.4.3 Motion-Compensated Prediction (MCP)

Frame difference coding works well when there is no significant motion between pictures. When there is motion as shown in example of Figure 29.7, frame difference coding will lead to large differences. The

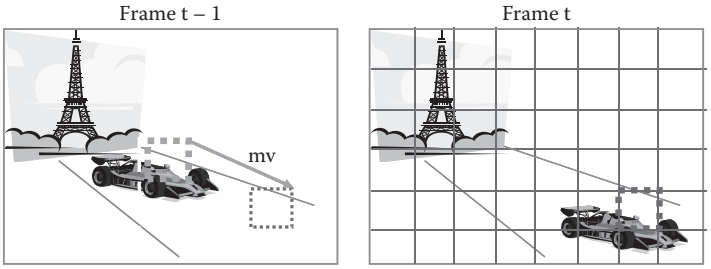

FIGURE 29.7 Example of MCP.

motion between the frames needs to be compensated for before differencing. A popular way of doing this is to use block motion estimation (ME)/compensation. The frame is divided into blocks and, for each block in current picture, the relative motion between the current block and a matching block of the same size in the previous frame is determined through ME. A motion vector (mvx, mvy) is transmitted for each block to indicate the relative motion.

29.1.3 Basic Video Coding Architecture

A common approach in video coding is to combine motion estimation/compensation, spatial prediction, transform, quantization, and entropy coding into a hybrid scheme to exploit all forms of redundancies in video sequences. A video coding architecture that forms a basis of most of the existing video coding standards is shown in Figure 29.8.

Pictures are coded in either of the two modes—INTER or INTRA. In INTRA-coding, the current picture is encoded without any relation to the previous picture. Spatial prediction can be used to predict blocks of pixels from neighboring pixel values. In INTER coding, the current image is predicted from neighboring pictures using block motion compensation and the difference between the current image and the predicted image is encoded. Note that INTER coding requires that a copy of the neighboring pictures be stored in the frame buffer. The first picture in the video sequence is coded in the INTRA-

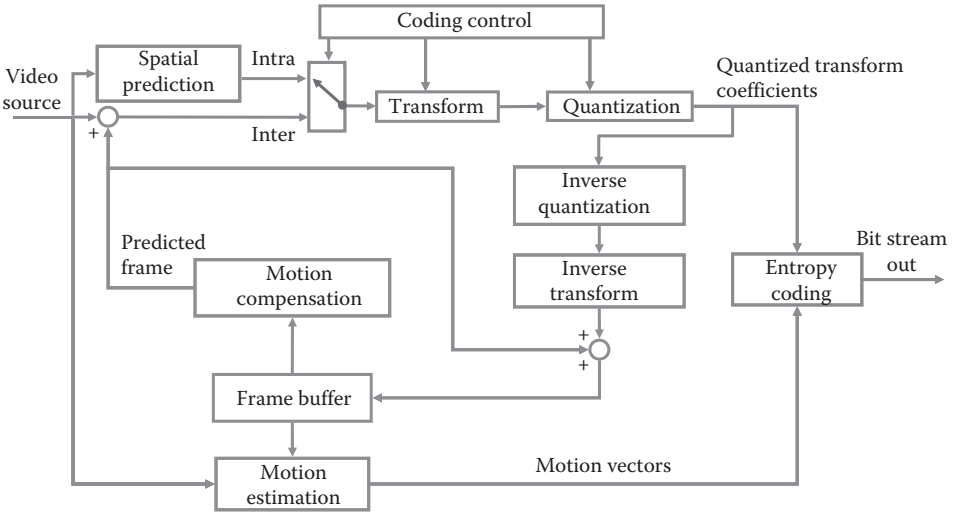

FIGURE 29.8 Basic video coding architecture.

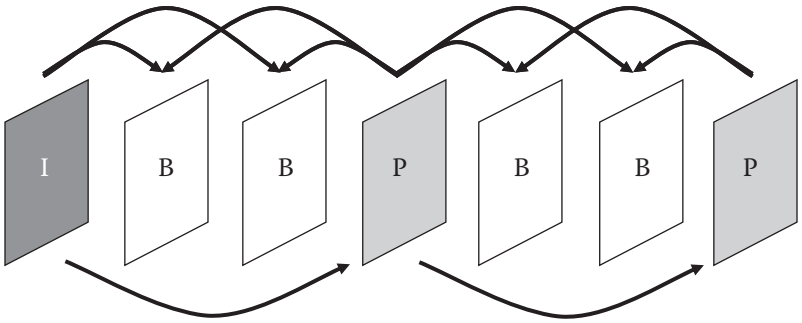

FIGURE 29.9 P and B pictures in IBBP GOP structure.

mode to initialize the frame buffer. There are two types of INTER pictures—P picture and B picture as shown in Figure 29.9. P pictures are coded with respect past pictures where as B pictures are coded with respect to both past and future pictures.

The basic unit of data operated on is called a macroblock (MB) and are the data (both luma and chroma components) corresponding to a block of 16×16 pixels. The input image is split into disjoint MBs and the processing is done on an MB basis. In INTER MBs, ME is performed on the MB to be encoded and motion vector (MV) is estimated between the current picture and neighboring picture for the MB to be encoded. ME is typically done using only the luma component of the video images. For chroma components, the luma MV is appropriately scaled to take care of the different spatial resolutions of the luma and chroma components before it is used. The motion compensation prediction error is calculated by subtracting each pixel in the MB with its motion-shifted counterpart in the neighboring picture. In INTRA-MBs, when spatial prediction is used, the prediction error is calculated by subtracting each pixel in MB from its spatial prediction from neighboring pixel values.

2D DCT is applied on prediction error (if spatial prediction or ME is used) or on original MB (if no prediction is used). The resulting DCT coefficients are then quantized. Depending on the quantization step size, this will result in a significant number of zero-valued coefficients. To efficiently encode the DCT coefficients which remain nonzero after quantization, the DCT coefficients are typically zig-zag scanned and run-length encoded. The run-length-encoded DCT coefficients and the MVs are variable length encoded before transmission. Arithmetic coding can also be used instead of VLC.

The decoder uses a reverse process to reproduce the MB at the receiver. After entropy decoding the received video bitstream, the pixel values of the prediction error are reconstructed by inverse quantization and inverse DCT. The spatially predicted pixels or the motion-compensated pixels from the neighboring picture contained in the frame buffer are added to the prediction error to reconstruct the particular MB transmitted. All MBs of a given picture are decoded and the whole picture is reconstructed.

29.1.4 Early Video Coding Standards

29.1.4.1 H.261

H.261 was standardized by ITU for videoconferencing over ISDN. H.261 supports two standard picture formats—the Common Intermediate Format (CIF–352×288) or the Quarter-CIF (QCIF, 176×144). The luma and chroma resolutions of the CIF and QCIF formats are summarized in Table 29.2. Pictures in H.261 are coded either in INTRA-mode or in INTER modes. Only P pictures are supported and a single MV at integer-pixel resolution is used for each MB. The MBs of either the image or the residual image are split into blocks of size 8×8 which are then transformed using DCT. The resulting DCT coefficient levels are quantized and run-length coded. The run-level pairs are variable length encoded. H.261 is typically operated at a bit rate of $p \times 64$ kbps, where p is an integer from 1 to 30 [1].

TABLE 29.2 QCIF and CIF Resolutions

	Luma	Chroma
QCIF	176 × 144	88 × 72
CIF	352 × 288	176 × 144

29.1.4.2 MPEG-1

MPEG-1 video standard was developed by ISO/IEC. It was designed to provide a digital equivalent of the popular VHS video tape. It is used in Video CD (VCD) with data rates of around 1.5 Mbps. Its supports YUV 4:2:0 video of SIF format (352 × 240 at 30 fps or 352 × 288 at 25 fps). Compared to H.261, MPEG-1 uses MVs at half-pixel resolution and supports both P and B pictures. It also introduced adaptive perceptual quantization where the step size used during quantization of various DCT coefficients can be adapted based on human visual perception considerations [2].

29.1.4.3 MPEG-2

MPEG-2 was developed for digital TV applications. It was built on top of MPEG-1 and introduced support for interlaced video which is used in TVs. MPEG-2 has become a very widely used standard and is used in DVDs, cable and satellite television, HDTVs, and Blu-ray discs. It supports higher resolution than MPEG-1, for example, standard definition TV (SDTV) resolution of 720 × 480 for NTSC and 720 × 576 for PAL, 1080i resolution of 1920 × 1080 interlaced etc. MPEG-2 is used at around 4–8 Mbps for SDTV applications and 10–20 Mbps for HDTV applications. Interlaced video coding tools introduced in MPEG-2 include: field pictures, field/frame motion compensation, MVs for 16 × 8 blocks, frame/field DCT. MPEG-2 also introduced tools for scalable video coding but these are not widely used [3].

29.1.4.4 H.263

H.263 was developed for videoconferencing over plain old telephone system (POTS) at data rates of 28.8 kbps. The video resolution targeted was sub-QCIF (128 × 96) and QCIF. Video conferencing at 28.8 Kbps ended up being very difficult and H.263 started getting used for video conferencing over ISDN and Internet since it provides better quality than H.261. Most of the improvements in H.263 come from using MVs with half-pixel resolution and from using improved VLC to encode DCT coefficients. DCT coefficients are coded using a 3D variable length code table that jointly codes DCT level, runs of zeros, and signaling of the last coefficient in the block. The core of H.263 specification is called the baseline profile. Several other optional modes were introduced in subsequent versions of H.263. These end up being called H.263+ and H.263++. Several of these options get used in the subsequent MPEG-4 simple profile and AVC/H.264 standard. Some of the options are [4]:

- Unrestricted MV mode: In this mode, MVs are allowed to point to pixels outside the picture. The values used for the nonexistent "outside" pixels are simply the values of the corresponding pixels on the nearest edge of the picture. This mode is found to improve the picture quality when there is significant motion at the edges of the image.
- MVs for 8 × 8 blocks.
- Syntax-based arithmetic coding.
- Multiple reference frames for motion compensation.

29.1.4.5 MPEG-4

MPEG-4 was designed to be a broad standard to cover various traditional and emerging applications areas: TV, film, wireless communications, 3D models, and so on. It has several parts: object-based coding, synthetic video coding, wavelet-based still texture coding, and natural video coding. Of all these,

only the parts that cover coding of traditional video get used mainly in digital cameras, camcorder, and streaming video. The parts that get used are: MPEG-4 simple profile tools and advanced simple profile tools [5].

MPEG-4 Simple Profile is a superset of H.263 baseline profile. Additional tools include:

- DCT coefficient prediction from neighboring block for intra coded MBs.
- Unrestricted MV mode and MVs for 8×8 blocks.
- Tools for improving error resilience of bitstreams.
  - *Resync markers*: Resync markers help in resynchronization of the bitstream in case of bitstream errors. Video data between resync markers is called a video packet and contains enough information to carry out decoding independent of neighboring video packet information. Because of the use of variable length encoding, bitstream errors can cause a loss of synchronization in entropy decoding and thereby lead to incorrect reconstruction of video pictures. Resync markers are unique and do not occur in the bitstream other than in the video packet header so a decoder that encounters bitstream errors can search for the next resync marker to achieve synchronization.
  - *Data partitioning*: In data partitioning, video data are split into two partitions with their own headers. The first partition consists of perceptually more significant information such as mode information and MVs. The second partition consists of coefficient data. In case the second partition is lost, the information in the first partition can be used to perform error concealment. Also channel coding techniques such as unequal error protection (UEP) can be used with data partitioning. UEP protects the more significant information at a higher level than the less significant information. So using UEP techniques, the first partition can be error protected more than the second partition.
  - *Reversible VLC*: These can be decoded in both the forward direction and the reverse direction. In the case of bitstream errors one could go to the end of the video packet and start decoding in reverse direction to try to salvage more information from the bitstream.

MPEG-4 advanced simple profile includes support for B pictures and interlaced tools. It also introduces MVs at quarter-pixel resolution and global motion compensation, which allows for signaling of motion parameters for the whole frame.

29.2 H.264/AVC

H.264/AVC (MPEG-4 Part 10) is the video coding standard developed by the joint efforts from ITU-T VCEG and ISO/IEC MPEG [6,7]. There was a call for proposal for H.26L in 1998, on which the start of H.264/AVC was based, and the joint video team (JVT) was formed in 2001 to start the standardization work jointly between VCEG and MPEG. Since the issuance of final draft international standard (FDIS) in 2003, H.264/AVC has been the state-of-the-art video coding standard that has been successfully deployed in various fields of industry including HDTV broadcasting, mobile and internet video services, digital cameras and camcorders, security systems, video conferencing systems, Blu-ray Disc, and so on [8].

Design of H.264/AVC codec inherits that of the previous standards such as MPEG-2 and H.263++. It uses block-based processing with motion prediction and transform coding. However, each traditional coding tool is optimized and new coding tools are introduced to achieve coding efficiency improvement. It has been reported that H.264/AVC can reduce bit rate by half at the same quality compared to its previous international standards [9].

The overview of H.264/AVC coding algorithm is given in Section 29.2.1. Section 29.2.2 discusses how optimal performance can be achieved at the encoder side in terms of coding efficiency. Usage of supplemental enhancement information (SEI) is also described. Finally, in Section 29.2.3, profile and level information is given along with visual quality analysis.

29.2.1 Coding Tools in H.264/AVC

The structure of H.264/AVC codec is similar to one shown in Figure 29.8. However, every coding block in H.264/AVC is improved by adopting new coding tools. This subsection highlights some of those tools.

29.2.1.1 High-Level Syntax and Data Structure

High-level syntax defines bitstream format and network abstraction layer (NAL) unit types. NAL unit types defined in H.264/AVC are shown in Table 29.3. Sequence parameter set (SPS) and picture parameter set (PPS) NAL units contain common information needed at the sequence level and picture level, respectively. SEI NAL unit is an optional NAL unit and can be included to provide additional information that will be useful for decoding or display processing. Coded slice NAL unit contains compressed video information. As shown in Figure 29.10, these form access units (i.e., decoded picture) and each access unit consists of single or multiple slices.

29.2.1.2 Intra Prediction

One of important tools introduced in H.264/AVC is the intra and inter prediction at MB level in variable block size partitions. The partitioned block sizes available for intra and inter predictions are different. When an MB is intra-coded, the MB is divided into the block sizes from 4×4 to 16×16 and the original pixels in each block are predicted from the reconstructed pixels in neighboring blocks to remove spatial correlation. Available prediction modes depend on color component and block size. For 4×4 and 8×8 luma block, 9 modes (1 DC + 8 directional) are defined as illustrated in Figure 29.11. For 16×16 luma, only 4 modes (1 DC + 3 directional) are defined. For chroma sample, only 8×8 intra prediction with the same modes as 16×16 luma prediction is allowed. However, the mode indices used for signaling 16×16 luma and 8×8 chroma prediction directions are slightly different as shown in Tables 29.4 and 29.5.

29.2.1.3 Inter Prediction (MCP)

An MB has more flexibility in its partition size when it is inter-coded. Figure 29.12 shows the partitions available for inter-coded MBs. The luma component can be partitioned into the smaller blocks of 16×16, 16×8, 8×16, or 8×8, and each 8×8 partition (i.e., sub-MB) can be partitioned again into the blocks of 8×8, 8×4, 4×8, or 4×4. The chroma component follows the luma partition after scaling according to the chroma format. Every partition in an inter-coded MB is predicted using its own reference picture and MV to remove temporal correlation as much as possible.

TABLE 29.3 H.264/AVC NAL Units (Nonshaded Rows) and Additional NAL Units for H.264/SVC (Shaded Rows)

nal_unit_type	Content	Symbol
1, 5	Coded slice of non-IDR or IDR pictures	SLICE
6	Supplemental enhancement information (SEI)	SEI
7	SPS	SPS
8	PPS	PPS
14	Prefix NAL unit	PRE
15	Subset SPS	subSPS
20	Coded slice extension	svcSLICE

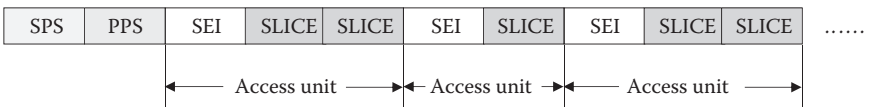

FIGURE 29.10 H.264/AVC NAL units and syntax structure.

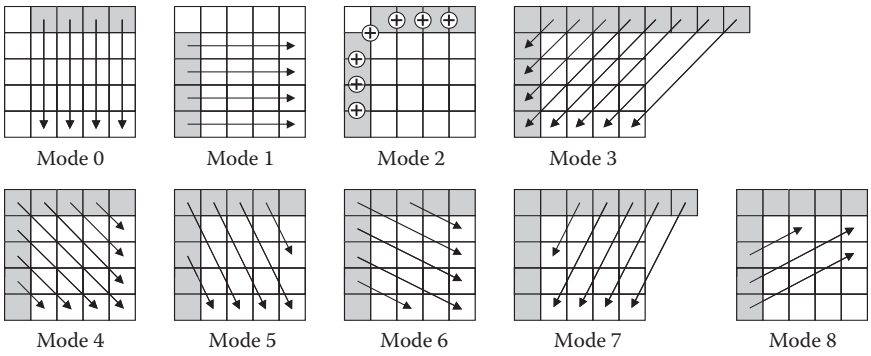

FIGURE 29.11 Intra prediction modes for luma 4 × 4 and 8 × 8 blocks.

TABLE 29.4 Available Intra 16 × 16 Prediction Modes

Intra 16 × 16 PredMode	Name of Intra 16 × 16 PredMode
0	Intra_16 × 16_Vertical
1	Intra_16 × 16_Horizontal
2	Intra_16 × 16_DC
3	Intra_16 × 16_Plane

TABLE 29.5 Available IntraChroma Prediction Modes

Intrachroma_pred_mode	Name of intra_chroma_pred_mode
0	Intra_Chroma_DC
1	Intra_Chroma_Horizontal
2	Intra_Chroma_Vertical
3	Intra_Chroma_Plane

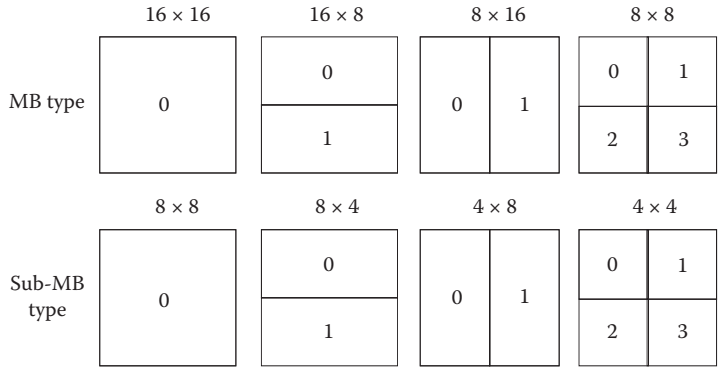

FIGURE 29.12 Available MB partitions and sub-MB partition for inter coded MB.

More than one previously coded picture can be employed for MCP in H.264/AVC. The maximum number of reference pictures that one picture can use is 16. However, since all the blocks in an 8 × 8 partition have the same reference picture, it is possible for one MB to have up to 4 reference pictures. To realize MCP with multiple reference pictures, the decoded picture buffer (DPB) is introduced, in which

previously decoded pictures are stored. DPB provides ways to store and remove decoded pictures flexibly at any time. For example, decoded pictures can stay for a long time in DPB so that they can be used as a reference for successive pictures. By doing so, an H.264/AVC encoder can exploit both short-term and long-term dependencies between pictures.

MCP is performed using MVs at quarter-pixel resolution in H.264/AVC. Temporal prediction samples at finer fractional positions improve the performance of MCP significantly. For luma, the prediction samples at half-pixel positions are derived by filtering integer samples in horizontal and vertical direction separately using a 1-D 6-tap filter. The prediction samples at quarter-pixel positions are obtained by averaging adjacent integer sample and half-pixel sample. Fractional prediction samples for chroma are derived using bilinear interpolation. Because chroma resolution is half of luma resolution in the 4:2:0 format, a MV at quarter-pixel position in luma points to one-eighth sample in chroma.

When there are brightness changes between two pictures, that is, current and reference pictures, the residual signal after MCP will still have high energy even though there is no motion between pictures. Weighted prediction is introduced to improve coding efficiency in such cases, for example, fade-in and fade-out. By the weighted prediction technique, the prediction signal is modulated using scaling factor and offset, which is signaled in the bitstream, so that the brightness change between two pictures can be compensated [10,11].

The spatial direct mode in B picture in addition to temporal direct mode, which is already supported in the previous coding standards, is another source of coding efficiency improvement. With spatial direct mode, the forward and backward MVs of an MB are inferred from those of adjacent blocks, which is more efficient than temporal direct mode in many cases. The improvement of coding efficiency in H.264/AVC is also achieved by allowing B picture to be used as a reference for other pictures [12]. This change results in the use of hierarchical group of picture (GOP) structure. By applying finer quantization (i.e., higher quality) to lower layers that are used as references for higher layer, the coding efficiency can be improved when compared to the conventional IBBP structure of Figure 29.9. Since in H.264/AVC bi-predicted picture can be further used as a reference picture, a different notation is used to indicate bi-prediction picture—small letter b is used to indicate a bi-prediction picture that is not a reference picture and capital letter B is used to indicate a bi-prediction picture that is a reference picture. The conventionally used notation of IBBP coding of Figure 29.9 becomes IbbP coding in the new notation. It is worth noting that, as will be presented in detail in the next section, temporal scalability is supported without any changes by the hierarchical GOP structure.

29.2.1.4 Transform Coding and Quantization

H.264/AVC defines 4×4 and 8×8 block transforms. Both transforms are approximation of 2-D DCT [13] and can be applied by the use of adaptive block size transform (ABT) [14]. Note that only the inverse transform is the normative part defined by the standard. These transforms are integer transforms by means of shifting and multiplication operations, and the quantization is combined with transforms to avoid division operation. Therefore, they have very low computational complexity. Hadamard transform is also adopted into H.264/AVC for DC components in intra 16×16 mode and chroma coding.

29.2.1.5 Context-Adaptive Entropy Coding

Two context-adaptive entropy coding methods are supported: context-adaptive variable length coding (CAVLC) and context-adaptive binary arithmetic coding (CABAC) [15]. CAVLC is applied only to the coding of transform coefficients while normal VLC is used for the coding of other syntax elements. CAVLC encodes transform coefficients using VLC tables that adapt based on the number of nonzero coefficients of neighboring blocks. CABAC is applied to the coding of all the MB-level syntax elements, including MB header and transform coefficients. CABAC is the combination of binary arithmetic coding technique with context modeling, which consists of three operations of binarization, context modeling, and binary arithmetic coding. A syntax element is first converted to binary symbols called bin string and each bin is arithmetic coded with an updated context model. The context modeling is the key

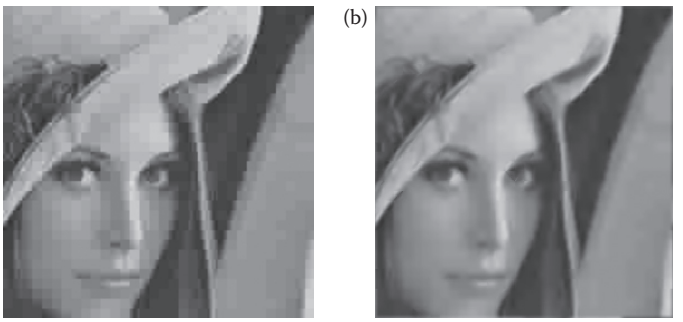

FIGURE 29.13 Visual quality comparison between decoded frames (a) without and (b) with deblocking filter.

to high coding efficiency of CABAC. Based on the statistics of previously coded syntax elements, the probability model of binary symbols is updated and used to encode them. CABAC improves coding efficiency by around 9–14% over CAVLC at the cost of increased complexity.

29.2.1.6 In-Loop Deblocking Filter

Deblocking filter has been widely used as a postprocessing tool to remove blocking artifacts due to block-based processing used in video codecs. In H.264/AVC, deblocking filter is included inside the coding loop. A benefit of doing this is that coding efficiency improvement can be achieved by using the filtered reconstructed frame as reference frame. Both MB boundary and 4×4 block boundary are filtered with different filter strength according to properties such as prediction type, quantization parameter (QP) and so on. Figure 29.13 shows an example of output of H.264/AVC deblocking filter, which provides improved visual quality.

Various other coding tools are supported including interlaced coding, picture adaptive frame/field coding (PICAFF), MB adaptive frame/field coding (MBAFF), lossless coding, RGB coding, switching pictures, and so on.

29.2.2 Encoder Optimization and SEI

The H.264/AVC standard defines only the decoding process as normative part. However, it also provides a guideline and reference software for the encoder [16], which describes optimized mode selection scheme, adaptive rounding control, and so on. In addition, SEI can be used to improve the performance, especially for error resilience coding.

H.264/AVC provides various coding modes. For example, each MB can have intra or inter prediction type. Each prediction type consists of several modes as described in Section 29.2.1. Therefore, it is important to choose the optimal coding mode to improve coding efficiency, that is, to achieve less distortion at lower bitrate. The optimal solution can be found by using the Lagrangian optimization [17,18]. In general, an H.264/AVC encoder tries to calculate the actual bitrate and distortion incurred by each prediction mode, and calculates the rate-distortion (RD) cost as

$$L = D + \lambda R,$$

where L and λ are Lagrange cost and Lagrange multiplier, respectively, D denotes sum of squared error (SSE), and R represents bitrate. The optimal Lagrange multiplier can be selected by taking derivative of distortion and bitrate of the compressed video as a function of quantization step size [19,20]. By exactly measuring bitrate and distortion for each prediction mode, the optimal coding mode can be selected.

Adaptive rounding control [21] is another encoding tool that improves coding efficiency by selecting a rounding offset value during the quantization process. The rounding offset value can be selected to adjust a deadzone size, and the adaptive rounding control accumulates statistics to find optimal offset value. This provides additional compression when the operating bitrate is very high. Various fast ME and fast mode decision algorithms are supported as well in the reference software.

SEI can also be used to improve the performance of H.264/AVC in different environments. SEI is a nonnormative part, which means that it is not mandatory for a decoder to support. However, an encoder can transmit information in the SEI, so that a decoder can support additional features. For example, spare picture SEI defines alternative reference frame to increase error resilience. Subsequence SEI enables UEP by defining hierarchical picture structure. Film grain SEI provides information to emulate film grain noise in an input sequence, so that similar noise can be reproduced at the decoder after coding the sequence without noise.

29.2.3 Profile Information and Performance Analysis

Profiles are defined to specify sets of coding tools used in different applications. A decoder can then conform to a particular profile without supporting all tools in H.264/AVC. In the first version of the standard, three profiles were defined; baseline, main, and extended profiles. Figure 29.14 shows the tools included in these profiles. Baseline profile includes less complex tools, for applications with limited resources, such as mobile applications.

Later, Fidelity Range Extension work [22,23] was added, which results in High, High 10, High 4:2:2, High 4:4:4 profiles. High profile, which includes ABT and quantization matrix in addition to the tools in main profile, is provided for the applications with less restriction in computation, memory, and power, such as HD broadcasting and storage like Blu-ray Disc. The other profiles are for applications requiring very high quality by supporting, for example, 10 bit per pixel, 4:2:2 and 4:4:4 or RGB color formats, lossless coding.

Similarly, levels are also specified for different application by defining maximum bitrate, buffer size, frame size, memory bandwidth, maximum MV range, and so on. For example, level 1 can only support resolutions up to 128×96 at 30.9 fps with 8 stored reference frames, and level 5.1 can support up to 4096×2048 at 30 fps with 5 stored reference frames.

Various studies have also been conducted to assess the performance of H.264/AVC compared to previous standards such as MPEG-2 and MPEG-4 in terms of bitrate reduction and visual quality. The verification test performed inside MPEG [9] reveals that H.264/AVC can achieve more than 50% of bitrate savings with better subjective quality. Figure 29.15 shows an example, where the Crew sequence is compressed using MPEG-2 at 10 Mbps, and H.264/AVC at 6 Mbps. H.264/AVC provides significantly better

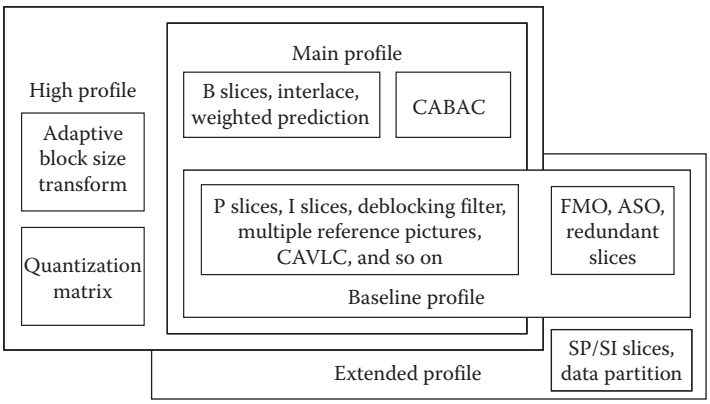

FIGURE 29.14 H.264/AVC profiles and coding tools.

FIGURE 29.15 Visual quality comparisons between coded frames by MPEG-2 and H.264/AVC encoders. (a) is a coded frame using MPEG-2 at 10 Mbps and (b) is a coded frame using H.264/AVC at 6 Mbps.

subjective quality compared to MPEG-2 with reduced blocking artifact and preservation of details in the scene. Another evaluation of H.264/AVC visual quality is also available in [24].

29.3 Scalable Video Coding

Scalable video coding is regarded as an attractive technique because of its potential advantages in providing a variety of transmission solutions over heterogeneous network environment to end-users with different sizes of display devices. By encoding an input video with scalable video coding techniques, a single scalable bitstream can be partially decoded at different levels of temporal and spatial resolution and fidelity depending on transmission channel bandwidth, display size, end-users' preference, and so on. For this reason, scalable coding has drawn attentions in the applications such as personal media display, video streaming, and surveillance.

Simulcast is an alternative approach to scalable video. Multiple streams at various bitrates and resolutions are generated to accommodate different bandwidths and display sizes, and end-users select one of them depending on their conditions. However, this approach is inefficient in several aspects including poor coding efficiency. The size of multiple streams required to satisfy various network conditions may be large. Furthermore, it may not provide enough flexibility to switch among streams adaptively based on end-users' conditions. Once one stream is selected, switching to others on the fly might be restricted or there could be significant drift errors due to switching.

The standardization effort for scalable video began from ISO/IEC MPEG-2 [3] and continued in MPEG-4 [5]. Scalable video coding has not been deployed successfully on a large scale in practical video coding systems mainly due to insufficient coding gain, flexibility and complexity issues. However, with availability of more powerful computing devices and improved coding efficiency by new coding techniques introduced in H.264/AVC [6], there has been an emerging interest again in scalable video coding. Recently, H.264/SVC has been standardized as a scalable extension of H.264/AVC. H.264/SVC aims to offer efficient scalable video coding at low complexity when compared with single-layer coding and simulcast while providing flexible formats of temporal, spatial, and SNR scalability. In this section, H.264/SVC is covered in detail with focus on its features and techniques adopted.

29.3.1 H.264/SVC Overview

H.264/SVC inherits all the features of H.264/AVC, which enable the production of a highly efficient video bitstream. Moreover, it is equipped with added features that support scalability by taking advantage of lower-layer signals in the higher layer encoding to minimize the redundant signal included in a compressed stream. There are mainly three types of scalability supported in the H.264/SVC standard: Temporal, spatial, and SNR scalability. In addition, they can be combined flexibly to provide multiple forms of scalability in a single stream. The coding efficiency of each scalable coding can be found in [25] and [26].

29.3.1.1 Temporal Scalability

Temporal scalability enables decoders to decode and display coded streams at variable frame rates without any drift error. It can be achieved by conventional IbbP GOP structure shown in Figure 29.16, where b picture is not used as a reference for other pictures. In this case, a decoder can display at reduced frame rates by decoding only I, or I and P pictures. In H.264/SVC, the temporal scalability is usually implemented by hierarchical GOP structure, in which pictures cannot use higher temporal-layer pictures as reference MC. Depending on the delay constraint, a GOP can be structured with hierarchical B or P pictures as shown in Figure 29.17, where the pictures at the lowest temporal layer, that is, $T = 0$, are called key pictures. It should be noted that the picture at temporal layer $T = k$ use only reference picture whose T is smaller than or equal to k. Hierarchical B structure is realized by generalized B picture [12] that is used as reference as well for other pictures. While hierarchical B structure introduces a coding delay equal to the distance between two key pictures, there is no coding delay with hierarchical P structure. Suppose that the maximum frame rate is 60 fps when all pictures are decoded and displayed. With the GOP structures shown in Figure 29.17, a decoder can display at four different frame rates, for example, 7.5, 15, 30, and 60 fps by decoding $T = 0$, $T = 0$, 1, $T = 0$, 1, 2, and $T = 0$, 1, 2, 3, respectively. As stated in Section 29.2, the hierarchical GOP structure also improves coding efficiency, and temporal scalability can be realized as well in a H.264/AVC single-layer stream.

29.3.1.2 Spatial Scalability

The spatial scalability of H.264/SVC is based on the conventional layered coding approach with several inter-layer prediction techniques. Figure 29.18 demonstrates a two-layered spatial scalable video encoding process. Each picture of original input video in higher resolution is spatially decimated into a smaller resolution. Then the decimated picture is encoded by a base-layer (BL) encoder, which produces a bitstream fully compatible with the H.264/AVC standard. The original picture is encoded by an enhancement-layer (EL) encoder. The spatial scalable layer is identified by a dependency ID, D. Each EL picture can exploit the coded information of the previously coded BL picture at the same time instant by means of the following inter-layer prediction techniques. Note that the layer employed for inter-layer predictions is called a reference layer of the layer that exploits inter-layer predictions.

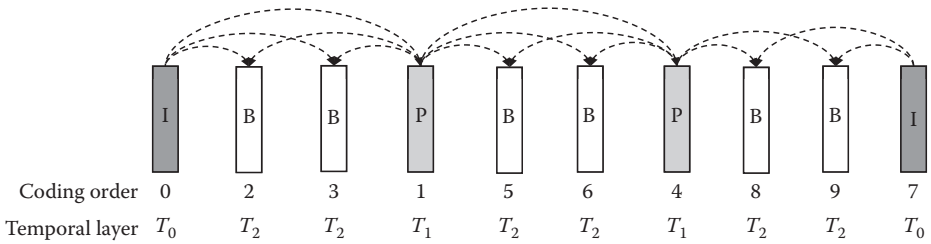

FIGURE 29.16 Temporal scalable coding by the conventional IbbP coding structure. Numbers and arrows represent the coding order and reference frames, respectively.

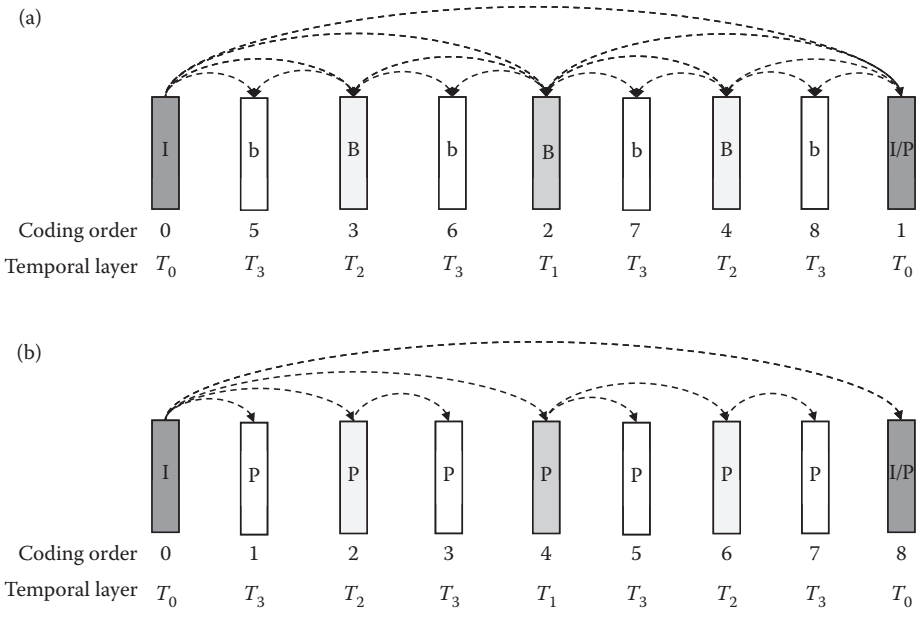

FIGURE 29.17 Temporal scalable coding by (a) hierarchical B picture and (b) hierarchical P pictures.

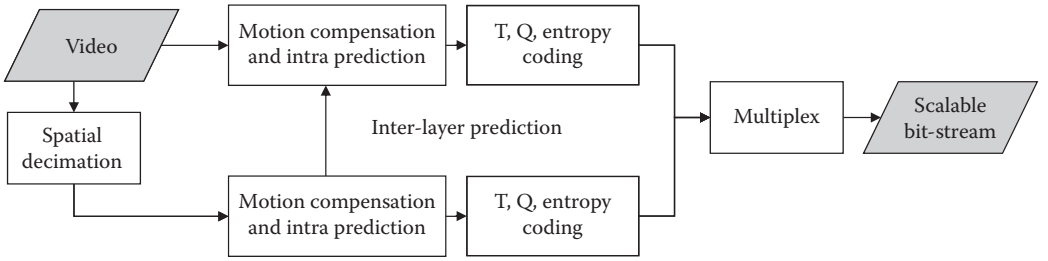

FIGURE 29.18 Two-layer spatial scalable video encoding process. (Adapted from H. Schwarz, D. Marpe, and T. Wiegand, *IEEE Trans. Circuits and Syst. Video Technol.,* 17(9), 2007.)

29.3.1.2.1 Inter-Layer Intra Prediction

This method is used for intra-MB coding. When collocated blocks in a reference layer are intra coded, the reconstructed samples of collocated blocks can be up-sampled and used as the prediction signal for intra coding of the corresponding EL MB. This technique reduces bits of EL intra picture significantly.

29.3.1.2.2 Inter-Layer Motion Prediction

In the AVC base layer, MVs are predicted from neighboring blocks' MVs (e.g., median of neighboring MVs) and their differences are coded. In H.264/SVC, when collocated blocks in a reference layer are inter coded, the corresponding EL MB can reuse their reference indices and scaled MVs for inter coding to reduce bits required to signal them.

29.3.1.2.3 Inter-Layer Residual Prediction

Residual signal still accounts for a significant portion of the bits at high bit rates and reference-layer residual signal can be utilized effectively to reduce bits to encode EL residual signal. The inter-layer residual prediction makes use of the up-sampled inverse-transformed residual signal as the prediction signal for the

corresponding EL MB and encodes only the difference signal. The inter-layer residual prediction is employed only for EL inter MB coding when the collocated blocks in a reference layer are also inter coded.

29.3.1.2.4 Base Mode

Base mode is introduced to fully reuse MB mode information, MB partitions, MVs, and intra-information from the collocated blocks in a reference layer. If the collocated blocks are inter coded, base mode results in EL inter MB and its partitions, as well as MVs including reference indices, to be inferred from those of the collocated blocks. It means that the inter-layer motion prediction is switched on automatically with base mode flag. Inter-layer residual prediction can be switched on or off independently of base mode flag. In general, the residual signals in reference and enhancement layers are highly correlated to each other when base mode is enabled since MVs point to the same area in both layers. As a result, base mode works effectively along with inter-layer residual prediction. If the collocated blocks are intra coded, the base mode MB becomes intra-MB, which is called I_BL mode, and its samples are coded through the inter-layer intra prediction. Base mode is also quite effective in reducing intra coded MB bits.

29.3.1.3 SNR Scalability

H.264/SVC defines two types of SNR scalability, coarse-grain SNR (CGS) and medium-grain SNR (MGS) scalability. Fine-grain scalable coding was initially proposed, but it was not included finally in the standard.

In general, the CGS scalability is achieved by using different QP values across layers. The CGS design follows the same layered coding approach with the spatial scalability and the CGS layer is also identified by a dependency ID, D. CGS scalability is regarded as a special type of spatial scalability that does not involve any spatial resolution change between BL and EL. To be more specific, the input picture does not need to be decimated and all the inter-layer predictions are used without up-sampling of reference layer's reconstructed samples and residual signal and up-scaling of reference-layer's MVs. The only difference with spatial scalability is that the residual prediction in SNR scalability (i.e., both CGS and MGS) is performed in the transform domain before inverse transform.

The MGS layer is distinguished from CGS layers by its quality ID, Q. Multiple MGS layers can be added on top of the spatial or CGS layers, in which MGS layers should have different Q values. MGS scalability provides more flexible and dynamic ways for quality scalable coding. First of all, it supports DCT coefficient partitioning as well as all the scalable coding methods in CGS. All DCT coefficients are allowed to be divided into up to 16 partitions and each partition is sent in different layers. Second, it provides an improved method to trade-off coding efficiency and drift error, which is caused when the MCP processes at encoder and decoder are not synchronized. Unlike spatial and CGS enhancement layers, bitstream switching between MGS layers is allowed at any picture. Under such a scenario, the trade-off between coding efficiency and drift error is an important design issue and several control concepts have been proposed [25].

29.3.1.4 Combined Scalability

In common applications of scalable video, it is expected that a scalable global bitstream will contain all types of scalability. The H.264/SVC standard is designed to support any combination of temporal, spatial, and SNR scalability [27]. Accordingly, an H.264/SVC bitstream can provide great adaptation to the display resolution, channel bandwidth, quality level, and frame rate in various applications. Figure 29.19 shows an example of combined scalability in the T-D-Q space (the values of D, Q, and T represent spatial, quality, and temporal resolution of a slice), where each block in the space specifies an extractable layer representation. The desired layer is extracted and decoded with DQ ID. In H.264/SVC streams, all pictures are identified by distinct DQ ID, which is computed as $(D << 4 + Q)$, and all pictures also have reference-layer DQ ID when any inter-layer prediction method is employed. It should be noted again that T is not necessary to identify a layer, since the temporal scalability is achieved within a layer. In general, a decoder needs to decode only one target layer, which is specified by the target values of T, D,

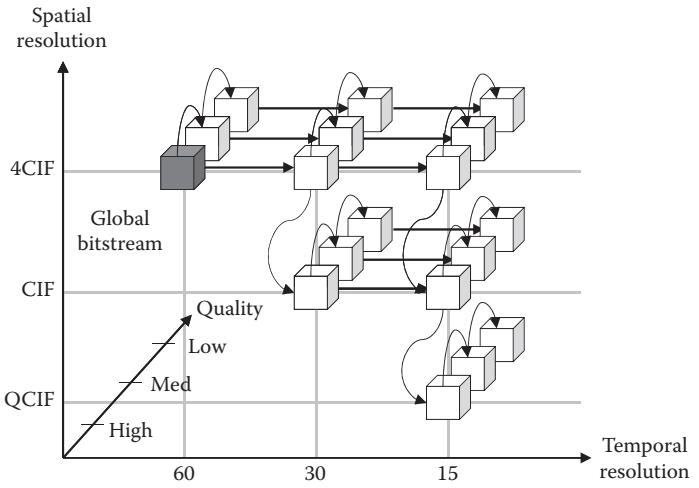

FIGURE 29.19 Combined scalability in T-D-Q space. (Adapted from H. Schwarz et al., In *Proc. ICME*, 2005.)

and Q. Target T, D, and Q determine not only the target layer but also all reference layers required to decode the target layer.

29.3.2 Other H.264/SVC Features

There are other improvements for EL encoding in H.264/SVC besides inter-layer prediction methods. Some of them are briefly covered in this subsection.

29.3.2.1 Inter-Layer Deblocking Filter

In H.264/SVC, the inter-layer deblocking filter is proposed to improve inter-layer intra prediction for spatial scalable coding in addition to the existing deblocking filter. The new filter is intended to remove blocking artifacts in intra-MBs that are used as references for inter-layer intra prediction in spatial EL.

29.3.2.2 Skipped Slice

It is allowed to skip a whole slice in EL, for which only the number of MBs in the slice is signaled. When a slice is skipped, base mode and inter-layer residual prediction are used for all MBs inside it.

29.3.2.3 Intra–Inter Prediction Combination

In spatial scalable coding with the scaling factor other than 2, when base mode is enabled for an EL MB, the collocated blocks in a reference layer can contain both intra- and interblocks. When this occurs, the area mapped to the inter blocks in a reference layer is inter coded while other area is intra coded with inter-layer intra prediction.

29.3.3 H.264/SVC Bitstream Structure

Table 29.3 shows the important NAL units in H.264/SVC with their NAL unit types. In addition to the NAL units (1, 5, 7, and 8) in H.264/AVC, the H.264/SVC standard defines new NAL units to distinguish EL and BL and provides necessary information for scalable video decoding. They include prefix NAL unit, subset SPS, and coded slice extension. The coded slice extension has all MB parameters and data in the EL slice and the subset SPS has sequence-level parameters specific to EL. The prefix NAL unit is appended to the coded slices of BL, so that the information necessary for scalable video decoding can be assigned even to BL slices. Figure 29.20 illustrates the structures of NAL units. The NAL units of H.264/AVC consist of

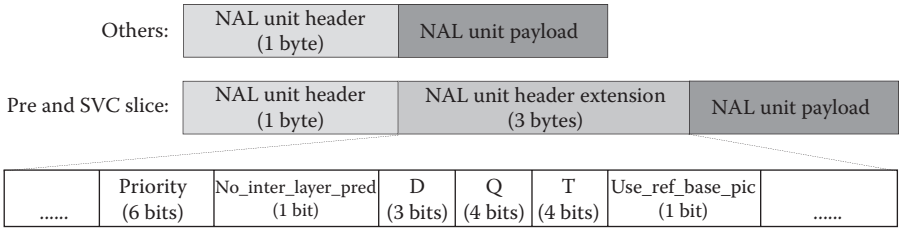

FIGURE 29.20 H.264/SVC NAL unit structures.

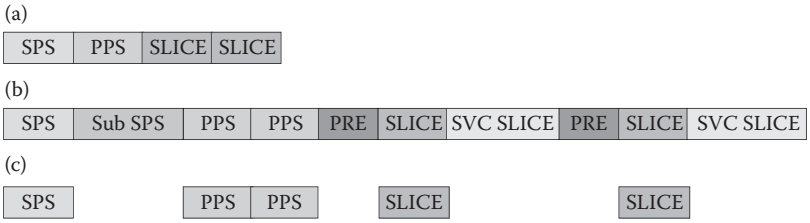

FIGURE 29.21 AVC bitstream extraction from SVC, (a) AVC bitstream, (b) SVC bitstream, and (c) extracted AVC bitstream from (b).

1-byte header, which signals the NAL unit type and NAL unit payload. However, the prefix NAL unit and the coded slice extension have 3-byte NAL unit header extension between NAL unit header and payload, in which D, Q, and T IDs of a slice are signaled. The values of D, Q, and T represent spatial, quality, and temporal resolution of a slice and make it easy for a decoder to detect and extract the target layer that the decoder wants to display. It should be noted that the coded slice extension includes the payload of prefix NAL unit inside its payload.

With the NAL units introduced in H.264/SVC, the generation of a SVC stream from multiple AVC streams and an AVC stream from one SVC stream can be completed simply by adding and removing new NAL units. For example, Figure 29.21 shows AVC, SVC, and extracted AVC stream formats. Suppose that a SVC stream is generated from two simulcast AVC streams. It can be done by adding the Prefix NAL units to coded slices of one AVC stream, converting SPS and coded slice of the other AVC stream to the subset SPS and coded slice extension, respectively and finally arranging them in the correct order. The AVC stream can be recovered again by identifying and removing SVC NAL units.

29.3.4 H.264/SVC Profiles

Three profiles are defined for H.264/SVC; Scalable Baseline, Scalable High, and Scalable High Intra profile. Scalable Baseline profile is defined on top of AVC Baseline profile. AVC base layers in the bitstreams conforming to this profile should be compliant to AVC baseline profile. For ELs, several coding tools allowed in AVC High profile, such as B picture, CABAC and 8×8 transform, are supported. However, interlaced, picture-adaptive field/frame (PICAFF) and MB adaptive field/frame (MBAFF) coding are not allowed. The biggest constraint for ELs is the scaling factor in spatial scalable coding. The scaling factor in SVC Baseline profile is limited to 2 and 1.5. However, there is no restriction to SNR and temporal scalable coding.

Scalable High profile is defined on top of AVC High profile. AVC base layers in the bitstreams conforming to this profile are compliant to AVC High profile. Most of the coding tools in AVC High profile are supported for ELs. Most importantly, arbitrary scaling factors other than 2 and 1.5 are supported for spatial scalable coding in SVC High profile. Scalable High Intra profile is defined for professional

applications such as high-quality movies. The difference with Scalable High profile is that it uses only IDR coding for all layers.

29.4 Multiview Video Coding

The recent advances in camera and display technologies to capture and display multiple view signals, along with the desire for enhanced visual experiences, have brought about new video applications, namely, free viewpoint video (FVV) and stereo 3D video. FVV allows viewers to select any view point interactively, by which viewers can have sense of presence as if they are in the displayed scene. Stereo 3D video bring a new dimension of visual experience by showing left and right views to left and right eyes, respectively. The depth perceived in stereo 3D not only improves sense of presence but also makes the displayed scene look more natural. Stereo 3D video is now penetrating into daily life with the rapid development of consumer electronics such as TV, mobile phone, and tablet with stereo 3D support.

Due to huge raw bit rates of multiple views, the efficient coding of multiview video is key to the success of FVV and stereo 3D video. Accordingly, there have been several studies on compression techniques of multiview video. The simplest way is Simulcast that encodes all the views independently using any existing single-view encoder. However, this results in poor coding efficiency as expected. Recent standardization efforts for multiview video coding have extended the H.264/AVC standard. H.264/AVC has introduced stereo video information and frame packing arrangement SEI messages to support stereo 3D video. And the multiview extension of H.264/AVC, H.264/MVC, has been standardized for highly efficient multiview coding. There is also another activity toward a new 3D video standard under the ISO/IEC MPEG organization. This section introduces these multiview and 3D video coding techniques.

29.4.1 H.264/MVC Overview

H.264/MVC, which is extended from the H.264/AVC standards, has been designed to support efficient coding of multiple views into a single bitstream. Figure 29.22 shows the overall structure of a H.264/MVC system. The temporally synchronized videos from multiple cameras are fed into the H.264/MVC encoder to be coded into a single bitstream. Based on the fact that spatially neighboring pictures are correlated, the encoder saves bits required to encode additional views using so-called interview prediction. The coded stream is decoded and displayed by the H.264/MVC decoder in several ways depending on application. For FVV applications, the decoder decodes the desired view only, that is, target view, among multiple views and can switch the target view whenever necessary. For 3D video application, it is also possible to decode stereo views.

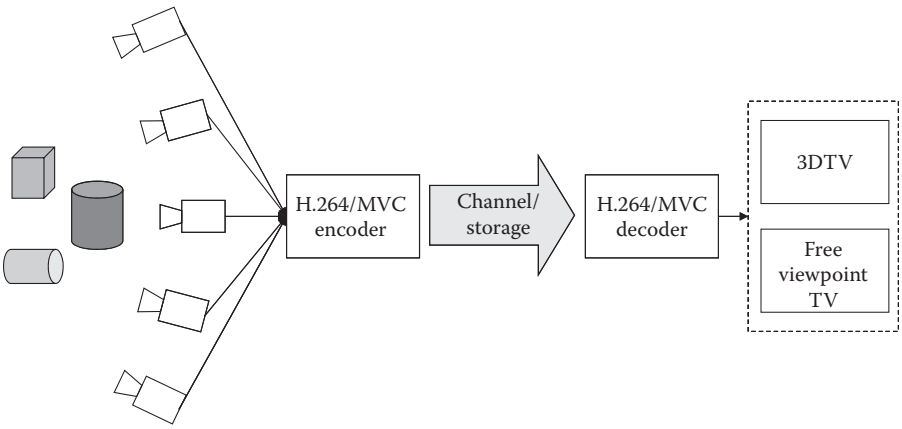

FIGURE 29.22 Multiview video system using H.264/MVC encoder/decoder.

Multiple camera sources can be encoded using various prediction structures, which might depend on camera array size and structures, for example, parallel or circular. Figure 29.23 depicts an exemplary prediction structure in the case of stereo-view encoding, where left view is an AVC base view that is always encoded independently. Figure 29.23a is the simplest way that encodes all views independently without interview prediction. However, as shown in Figure 29.23b and (c), the coding efficiency is improved by allowing nonbase views to be predicted from neighboring views for anchor (I or P) pictures, or both anchor and nonanchor pictures (B), respectively. In general, the interview prediction is more effective for anchor pictures than for nonanchor picture. The performance of interview prediction is well studied in [28].

The same NAL units in Table 29.3 are used for H.264/MVC as well, although their contents are quite different from those for H.264/SVC. For example, the prefix NAL unit and coded slice extension stream have NAL unit header extension between NAL unit header and payload. However, the NAL unit header extension in MVC has different syntax elements such as view ID and interview flag as shown in Figure 29.24. The coded slice extension in MVC is the same to the coded slice (nal_unit_type = 1 or 5) except for the reference picture list generation process due to interview prediction. It means that there is no MB-level change like inter-layer prediction in SVC for enhancement view encoding. The interview prediction is simply realized by adding reconstructed neighboring view pictures in the reference list of the current view. Therefore, the H.264/AVC encoder can be easily extended to support multiview coding.

There are two profiles defined for in H.264/MVC, namely, Multiview High profile and Stereo High profile. The main difference between two profiles is the number of views in a stream. Multiview High profile, which allows more than two views, is defined on top of the AVC High profile with some restrictions. For example, the interlaced picture coding tools including PICAFF and MBAFF are not supported in this profile. The AVC base view in the Stereo High profile is compliant to the AVC High profile as well.

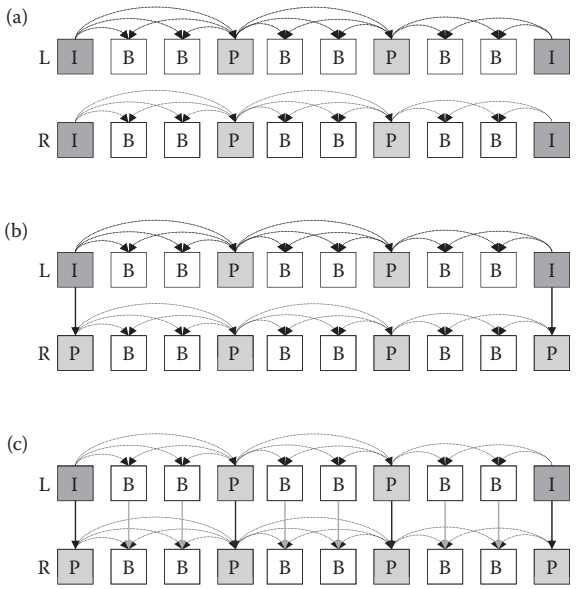

FIGURE 29.23 Prediction structure in H.264/MVC encoder for stereo-view coding, (a) simulcast, (b) interview prediction for anchor frames, and (c) interview prediction for all frames.

non_idr_flag (1 bit)	priority_id (6 bits)	view_id (10 bits)	temporal_id (3 bits)	anchor_pic_flag (1 bit)	inter_view_flag (1 bit)	reserved (1 bit)

FIGURE 29.24 MVC NAL Unit header extension format.

However, the interlaced picture coding tools can be supported in the Stereo High profile, which allows only up to two views.

29.4.2 Stereo 3D Video Coding via H.264/AVC SEI Messages

There are two H.264/AVC SEI messages for stereo 3D video, stereo video information SEI and frame packing arrangement SEI. They are used to support stereo 3D video in H.264/AVC without any change of actual encoding and decoding process. Specifically, they inform a decoder how the decoded picture is generated from two pictures, and the decoder rearranges the decoded picture based on this information for display purpose.

Figure 29.25 describes the overall structure of a 3D video system of H.264/AVC with SEI messages. In the encoder side, temporally synchronized left and right view sequences go through the down converter, by which each picture of left and right view sequences is down-sized by 2 based on the SEI message. The down-sized left and right views are composed into a single picture and coded by an H.264/AVC encoder. In the decoder side, the decoded picture by an H.264/AVC decoder is decomposed into left and right views and both views are up-converted into the original size based on the SEI message. The stereo information and frame packing arrangement SEI messages are similar as both follow the structure in Figure 29.25; however, they define different down- and up-conversion formats. One of formats in the stereo information SEI message is illustrated in Figure 29.26, for which the interview prediction can be realized. As shown in Figure 29.27, by encoding each field separately and allowing bottom field to refer top field, we can have the same effect as the interview prediction in H.264/MVC, with the reduced resolution.

The disadvantage of 3D video by the SEI messages is that it reduces the resolutions of both views by half. However, it is very attractive because it is compatible to existing H.264/AVC codecs and infrastructures. Using the SEI messages, stereo 3D video can be brought to home via existing devices like DVD and Blu-ray

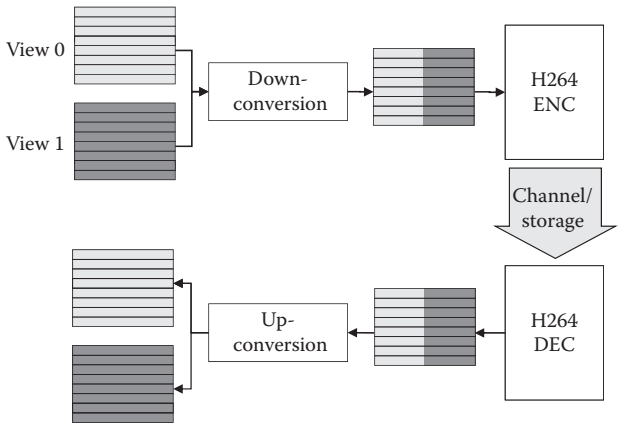

FIGURE 29.25 3D video system using H/264/AVC with side-by-side frame packing SEI messages.

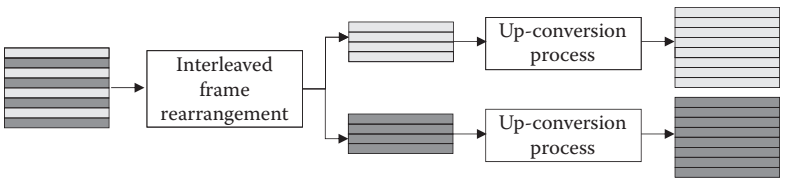

FIGURE 29.26 Rearrangement and up-conversion of interleaved picture using stereo information SEI message.

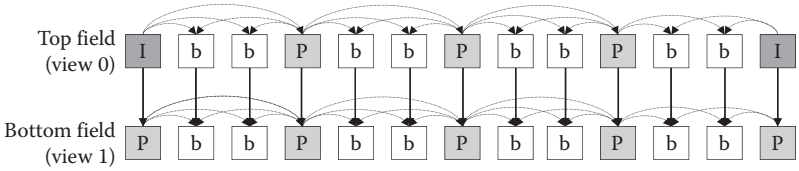

FIGURE 29.27 Stereo video coding of interleaved picture using stereo information SEI message.

players and 3D display with minimal efforts. There is also standardization activity to support full resolution stereo 3D video with the similar approach [29].

29.4.3 MPEG 3D Video

Although the H.264/MVC standard reduces the redundancy by using interview prediction, the amount of data to be stored or transmitted is still very large especially when many views are captured and coded. Improvements to the interview prediction in H.264/MVC are currently being studied. For instance, the illumination and focus mismatch compensation method was proposed in [30], by which the different illumination conditions and focal lengths between a target view and a reference view are compensated for improved interview prediction. In [31] and [32], the interview prediction methods using view interpolation were proposed. In these methods, a target view is synthesized first based on neighboring views and this estimated target view is used as a reference for interview prediction while encoding the target view. The differential signal between the target view and the estimated target view is coded in a stream.

The idea of view interpolation is also applied to a new 3D video format of view plus depth [33]. Figure 29.28 illustrates the overall structure of a 3D system with a view-plus-depth format. The encoder encodes two views and depths into the view-plus-depth format. The decoder not only decodes coded views and depths but also synthesizes any intermediate view using depth image-based rendering (DIBR) technique [34]. Additional data could also be sent in a stream so that the decoder can have better quality of synthesized intermediate view. This 3D video representation is expected to be the most efficient way for multiview video application. However, there are several issues to be addressed for this system.

First, in the case that a ground-truth depth map is not available, the generation of high-quality depth map is the most fundamental issue. While there exist many depth map estimation methods in the literatures [35,36], these methods need to be evaluated in terms of synthesized views' quality to develop the best depth map estimation method for this system. Regardless of whether depth map is ground truth or not, an efficient coding method for depth map should be developed. Since depth map has different characteristic from view picture, conventional video compression techniques may not be efficient. Exploiting the specific characteristics of depth map can enable higher coding efficiency. Second, it should be guaranteed that a view synthesis method employed always generates acceptable intermediate

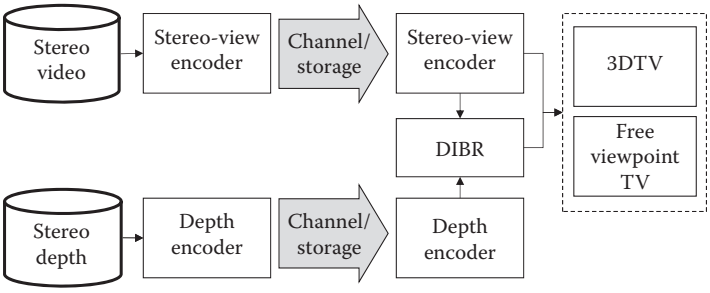

FIGURE 29.28 3D video system with a view plus depth format.

views. The quality of synthesized views will depend on the quality of coded views and depth maps, and the quality of coded and synthesized views should have similar quality. However, when there are large occluded areas between two coded views, it is not easy to synthesize intermediate views as good as coded views. To resolve this issue, the study on the additional data and its transmission method to improve synthesized views' quality at minimum overhead is also essential [37].

The standardization effort for the 3D video coding with view-plus-depth format is being led by the ISO/IEC MPEG organization. They recently issued call for proposal [38] with common test sequences and environment. The primary goal is to define the data format and coding technology to enable high-quality reconstruction of coded and synthesized views for both stereoscopic 3D display and auto-stereoscopic multiview displays. All the issues mentioned in the above are expected to be addressed in the standard.

29.5 High-Efficiency Video Coding

High-efficiency video coding is the next-generation video coding standard currently being developed by the Joint Collaborative Team on Video Coding (JCT-VC) of ITU-T WP3/16 and ISO/IEC JTC 1/SC 29/WG 11 [39]. It is expected to provide around 50% improvement in coding efficiency compared with its predecessor H.264/AVC. The call for proposals occurred in January 2011 and the final draft international standard (FDIS) is expected to be completed in January 2013. In this section, the various new tools that have been adopted into the working draft (WD) of HEVC, based on the outcome of the sixth JCT-VC meeting held in July 2011, are discussed and the differences from H.264/AVC are highlighted.

29.5.1 Coding Block Structure

HEVC is intended for larger resolutions and higher frame rates. Accordingly, HEVC uses larger "macroblocks (MB)" compared to H.264/AVC. In HEVC, the largest coding unit (LCU) is 64×64 pixels, which is 16 times larger than the 16×16 pixel MB used in H.264/AVC. Using a large coding unit helps to improve coding efficiency, particularly for high resolutions where many pixels may share the same characteristics. The largest coding unit can be divided into smaller coding units (CU) using a quadtree structure as shown in Figure 29.29. A split flag is transmitted to indicate whether a CU should be divided into four smaller CUs. The smallest coding unit (SCU) allowed in HEVC is 8×8 pixels. An additional feature in HEVC is that within an LCU, there can be a mixture of inter and intra coding units. The CU can be further divided into prediction units (PU). The PU within a coding unit will undergo the same form of prediction (either all inter or all intra). The allowed PU sizes within a CU depend on whether the CU is inter- or intra predicted. Asymmetric motion partitions (AMP) are allowed for inter predicted PU.

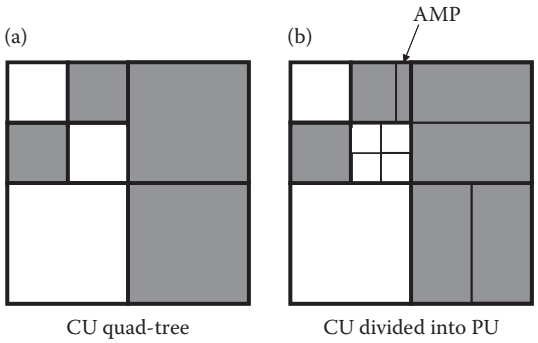

FIGURE 29.29 Coding block structure in HEVC, (a) shows how an LCU is partitioned into CU with a quadtree structure and a mixture of inter predicted (gray) and intra predicted (white) CUs are allowed and (b) shows how CU are further divided into PUs.

29.5.2 Inter Prediction

Similar to H.264/AVC, quarter-pixel resolution MVs are supported in HEVC. HEVC uses a larger 8-tap DCT interpolation filter (DCTIF) that operates directly on the integer pixels rather than the two step 6-tap approach used in H.264/AVC. In addition, advanced motion vector prediction (AMVP) is used to signal the MV data. Compared to H.264/AVC, more neighbors are used for MV prediction. To signal skip or direct mode, merge mode is used, where multiple neighbors are used to predict the MVs and reference index.

29.5.3 Intra Prediction

Depending on the PU size, up to 34 directional modes are used for intra prediction of luma pixels. In addition, there are separate planar and DC modes. Depending on the prediction mode, intrasmoothing is applied to the reference pixels. For chroma pixels, four directional modes can be used, one of which can be the same as the luma mode. In addition, luma-based chroma prediction (LM chroma) can be used where chroma intra prediction is performed using the reconstructed luma pixels.

29.5.4 Transform

To support the larger resolutions, HEVC uses transforms from 4×4 up to 32×32. For a given coding unit, the transform sizes are signaled using a residual quadtree (RQT). For example, a CU of size 16×16 can be split into 16 4x4 transforms using a quadtree of depth 2.

For 4×4, based on intramode, a discrete sine transform (DST) is used for certain prediction modes. Nonsquare transforms (NSQT) with sizes $4 \times 16/16 \times 4$, $8 \times 32/32 \times 8$ are allowed for residual of inter prediction. An adaptive scan order is used for intrapredicted coefficients to map them from the 2-D transform to the 1-D set of coefficients to be coded by the entropy coder.

29.5.5 Loop Filters

A deblocking filter is applied to the 8×8 edges. Similar to H.264/AVC there is both a strong filter, which is applied to 3 pixels on either side of the edge, and a weak filter, which is applied to 2 pixels on either side of the edge. The chroma filter affects 1 pixel on either side of the edge.

Two additional loop filters shown in Figure 29.30 are used in HEVC: sample adaptive offset (SAO) and adaptive loop filter (ALF). After the deblocking filter, SAO is applied on a pixel basis based on the neighboring information. There are two methods of determining the offset with SAO: band offset and edge offset. In band offset, the size of the offset is determined based on the magnitude of the pixel. In edge offset, a two-point gradient is taken around the pixel and the difference dictates the offset that is to be added to the pixel. SAO can be enabled and disabled on an LCU basis, and is signaled using a quadtree.

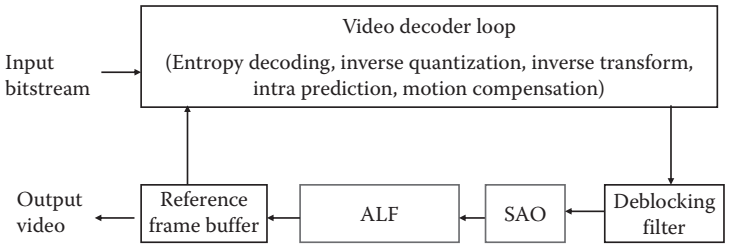

FIGURE 29.30 In-loop filters in HEVC. Adaptive loop filter (ALF) and sample adaptive offset (SAO) are two additional filters highlighted in red.

ALF is an adaptive FIR Wiener filter, which is applied after SAO. The number of filters taps in ALF can change for each slice; within each slice, there are sixteen sets of coefficients. There are two methods of selecting the coefficients: region-based and block-based. Region-based ALF involves breaking a frame into sixteen regions (i.e., dividing the frame into four in both vertical and horizontal directions). A coefficient set can be assigned to each region and all pixels within each region will use the same coefficient set. In block-based ALF, the coefficient set is selected based on the local characteristics of a given block of pixels. A separate filter is used for the chroma components. ALF can be enabled and disabled using the existing CU quadtree of the coding block structure.

29.5.6 Entropy Coding

Similar to H.264/AVC, HEVC uses context adaptive binary arithmetic coding (CABAC). However, improvements have been made to CABAC to enable higher throughput. This includes changes to the binarization and context selection of various syntax elements such as coefficient level, to reduce the number of context coded bins as well as overall number of bins. Bins are also reordered such that context coded bins with similar contexts are grouped together to enable parallel context processing, and bypass bins are grouped together to enable higher throughput.

References

1. Video codec for audiovisual services at $p \times 64$ Kbits/s, ITU-T, Rec. H.261, ITU-T, March 1993.
2. Coding of moving pictures and associated audio for digital storage medic at up to about 1.5 Mbits/s, Part 2: Video, ISO/IEC 11172-2, March 1993.
3. Generic coding of moving pictures and associated audio information, Part 2: Video, ITU-T Rec. H.262 and ISO/IEC 13818-2, November 1994.
4. Video codec for low bit rate communication, ITU-T, Rec. H.263, ITU-T, January 1998.
5. Coding of audiovisual objects, Part 2: Visual, ISO/IEC 14496-2, ISO/IEC JTC 1, May 2004.
6. Advanced video coding for generic audiovisual services, ITU-T Rec. H.264 and ISO/IEC 14496-10, ITU-T and ISO/IEC JTC1, April 2007.
7. T. Wiegand, G. J. Sullivan, G. Bjøntegaard, and A. Luthra, Overview of the H.264/AVC video coding standard. *IEEE Trans. Circuits Syst. Video Technol.*, 13(7), 560–576, 2003.
8. G. Sullivan, Overview of known H.264/MPEG-4 pt. 10/AVC deployment plans and status, Joint Video Team (JVT) of ISO/IEC MPEG & ITU-T VCEG, Document JVT-L009, Jul. 2004.
9. JVT and Test and Video Group, Report of the formal verification tests on AVC/H.264, ISO/IEC JTC1/SC29/WG11, Document N6231, Dec. 2003.
10. J. M. Boyce, Weighted prediction in the H.264/MPEG AVC video coding standard, in *Proc. ISCAS*, 2004.
11. D.-K. Kwon and H. J. Kim, Region-based weighted prediction for real-time H.264 encoder, in *Proc. ICCE*, 2011.
12. M. Flierl and B. Girod, Generalized B pictures and the draft H.264/AVC video compression standard. *IEEE Trans. Circuits and Syst. Video Technol.*, 13(7), 2003.
13. H. Malvar, A. Hallapuro, M. Karczewicz, and L. Kerofsky, Low-complexity transform and quantization in H.264/AVC. *IEEE Trans. Circuits Syst. Video Technol.*, 13(7), 598–603, 2003.
14. M.Wien, Variable block-size transforms for H.264/AVC, *IEEE Trans. Circuits Syst. Video Technol.* 13(7), 604–613, 2003.
15. D. Marpe, H. Schwarz, and T. Wiegand, Context-based adaptive binary arithmetic coding in the H.264/AVC video compression standard. *IEEE Trans. Circuits and Syst. Video Technol.*, 13(7), 2003.
16. A. M. Tourapis, A. Leontaris, K. Sühring, and G. Sullivan, H.264/14496-10 AVC Reference Software Manual (revised for JM 17.1), Joint Video Team (JVT) of ISO/IEC MPEG & ITU-T VCEG, Document JVT-AE010, June 2009.

17. A. Ortega and K. Ramchandran. Rate-distortion techniques in image and video compression. *IEEE Signal Proc. Magazine*, 15(6), 23–50, 1998.
18. G. J. Sullivan and T. Wiegand. Rate-distortion optimization for video compression. *IEEE Signal Proc. Magazine*, 15(6), 74–90, 1998.
19. T. Wiegand and B. Girod. Lagrange multiplier selection in hybrid video coder control. In *Proc. of IEEE Int. Conf. Image Proc., ICIP* 2009, pp. 542–545, Cairo, Egypt, Oct. 2001.
20. T. Wiegand, H. Schwarz, A. Joch, F. Kossentini, and G. J. Sullivan. Rate constrained coder control and comparison of video coding standards. *IEEE Trans. Circuits Syst. Video Technol*., 13(7), 688–703, 2003.
21. G. Sullivan, Adaptive quantization encoding technique using an equal expected-value rule, Joint Video Team (JVT) of ISO/IEC MPEG & ITU-T VCEG, Document JVT-N011, Jan. 2005.
22. G. J. Sullivan, P. Topiwala, and A. Luthra, The H.264/AVC Advanced video coding standard: Overview and introduction to the Fidelity Range Extensions. *SPIE Conference on Applications of Digital Image Processing* XXVII, Aug., 2004.
23. D. Marpe, T. Wiegand, S. Gordon, H.264/MPEG4-AVC Fidelity Range Extensions: Tools, profiles, performance, and application areas. In *Proc. of IEEE Int. Conf. Image Proc.*, ICIP 2005, Sep. 2005.
24. T. Oelbaum, V. Baroncini, T. K. Tan, and C. Fenimore, Subjective quality assessment of the emerging AVC/H.264 video coding standard. International Broadcasting Conference (IBC), Sep., 2004.
25. H. Schwarz, D. Marpe, and T. Wiegand, Overview of the scalable video coding extension of the H.264/AVC standard. *IEEE Trans. Circuits and Syst. Video Technol*., 17(9), 2007.
26. M. Wien, H. Schwarz, and T. Oelbaum, Performance analysis of SVC. *IEEE Trans. Circuits and Syst. Video Technol*., 17(9), 2007.
27. H. Schwarz, D. Marpe, T. Schierl, and T. Wiegand, Combined scalability support for the scalable extension of H.264/AVC. In *Proc. ICME*, 2005.
28. P. Merkle, A. Smolic, K. Muller, and T. Wiegand, Efficient prediction structure for multiview video coding. *IEEE Trans. Circuits and Syst. Video Technol*., 17(9), 2007.
29. A. M. Tourapis, P. Pahalawatta, A. Leontaris, Y. He, Y. Ye, K. Stec, and W. Husak, A frame compatible system for 3D delivery, ISO/IEC JCT1/SC29/WG11, Doc. M17925, July 2010.
30. J. H. Kim, P. Lai, and A. Ortega, New coding tools for illumination and focus mismatch compensation in multiview video coding. *IEEE Trans. Circuits and Syst. Video Technol*., 17(11), 2007.
31. K. Yamamoto, M. Kitahara, H. Kimata, T. Yendo, T. Fujii, M. Tanimoto, S. Shimizu, K. Kamikura, and Y. Yashima, Multiview video coding using view interpolation and color correction. *IEEE Trans. Circuits and Syst. Video Technol*., 17(11), 2007.
32. K. N. Iyer, K. Maiti, B. Navathe, H. Kannan, and A. Sharma, Multiview video coding using depth based 3D warping. In *Proc. ICME*, 2008.
33. P. Merkle, A. Smolic, K. Muller, and T. Wiegand, Multi-view video plus depth representation and coding. In *Proc. ICIP*, 2007.
34. C. Fehn, Depth-image-based rendering (DIBR), compression and transmission for a new approach on 3D-TV. In *Proc. SPIE*, 2004.
35. S. Ince, E. Martinian, S. Yea, and A. Vetro, Depth estimation for view synthesis in multiview video coding. In 3DTV conference, 2007.
36. Q. Zhang, P. An, Y. Zhang, L. Shen, and Z. Zhang, Improved multi-view depth estimation for view synthesis in 3D video coding. In 3DTV conference, 2011.
37. W. S. Kim, A. Ortega, J. Lee, and H. Wey, 3-D video coding using depth transition data. In *Proc. Picture Coding Symposium*, December 2010.
38. Call for Proposals on 3D video coding technology, ISO/IEC JCT1/SC29/WG11, Doc. N12036, March 2011.
39. B. Bross, W.-J. Han, J.-R. Ohm, G. J. Sullivan, T. Wiegand, WD4: Working Draft 4 of High-Efficiency Video Coding, JCTVC-F803, JCT-VC, 6th Meeting: Torino, IT, July14-22, 2011.

30

Machine Assessment of Speech Communication Quality

Wai-Yip Chan

Tiago H. Falk

Internet access has been declared a human right in some countries, ahead of reaching a consensus on this issue at the United Nations. Prior to the Internet, speech telephony provided the most widely available form of instant worldwide connected interactivity. Speech communication does not require the user to be literate, that is, having the ability to read and write. Speech naturally conveys human touch in numerous ways: conveying identity and emotions, enabling interactivity, and so on. With relatively low bandwidth requirement, speech communication can have greater geographical reach and can be supported even when resources are scarce. Thus, speech communication will always remain an essential component of the global communication network. The burgeoning growth of the global network is accomplished by many rapid trials and deployments of new networks and network technology. In such activities, the ability to rapidly and accurately assess end-to-end speech communication quality is needed to ensure that new network connections perform to customer expectations. "Rapid" can only be obtained with machines. Speech-processing algorithms that can run on machines have matured to the point of being able to accurately assess subjective listening quality. This chapter provides a study of up-to-date speech quality assessment algorithms and methods, aiming to enable communication engineers to use them effectively.

30.1 Telephone Speech Communication

The ideal telephone service enables distantly located participants to communicate with one another as if they were collocated. While evolving teleconferencing technologies are moving closer to that ideal, conventional telephone services still provide only voice communication. Telephony speech communication typically involves two persons conversing with each other using terminals ("telephones") connected

to a (tele)communication network. Normal speaking produces speech sounds, which are acoustic signals. Telephones serve to convert between speech as an acoustic signal and speech as an electrical signal. The latter can be manipulated by and transmitted through the network. Telephone users are accustomed to the loss of visual contacts; however, they would prefer their conversations to be unimpeded by the telephone equipment and network, as if they were conversing with one another through an opaque but acoustically transparent wall. This imagined ideal scenario can serve as a reference for gauging the effectiveness of telephone network-mediated conversations. When conversing over the network, if the acoustic signals that arrive at the two ears of each talker are identical to those arriving in the ideal scenario, the network is "transparent" to the signals exchanged in the conversation. The acoustic signals could be a mixture of signals from different sources: the talker, the third-party talker, and sounds from the surrounding background.

Realistic telephone communication deviates from the above ideal scenario in a number of ways. First, for economy, the talker's acoustic speech signal is captured monaurally by a single microphone. In natural settings, humans listen binaurally, with their left and right ears. A faithful binaural capture of speech sounds would require using two microphones, either set inside the ear canals of a head-and-torso (dummy) model of the listener, or with the duo-microphone captured free-field signals postprocessed to replicate the effect of immersing the listener's (upper) body in the sound field. Second, telephones and network equipment cannot preserve the fidelity of the electrical speech signal captured by the microphone. Processing of the electrical signal for transmission and the physical act of transmission degrade the speech signal. The degradations may appear to the ear as speech distortions, dropouts, extraneous signals, noise, and so on. Third, the speech signal takes longer to reach the receiving end through a network than the acoustic speech signal propagating through the ambience to the third-party talker. Fourth, the talker may hear his/her own voice differently from when speaking free of the presence of the telephone and transmission network. A telephone handset may block or otherwise modify the talker's mouth-to-ear propagation path. Moreover, the network may reflect the talker's speech back to his/her telephone earpiece or loudspeaker. The reflected signal is heard as an annoying "echo" when the reflected signal is delayed by more than about 50 ms relative to the talker's own speech signal. A properly engineered transmission network would attenuate echoes to a nonperceptible level before the echoes reach the talker.

30.2 E-Model

Telecommunication engineers have developed models to quantify the severity of the above impediments to carrying out a conversation. These models may serve one or more of the following functions: planning, research and development, benchmarking, monitoring, and maintaining speech telephony equipment and services. Among existing models, the ITU-T G.107 standard (ITU-T Rec. G.107, 2005), often called the "E-model," was originally developed for provisioning (planning) network equipment. Here, we introduce the E-model as it captures the major conversation impairment factors and has wider usage than planning, as we shall show later. Moreover, E-model updates that track emerging technology trends are being developed, and the model has even served as a paradigm for quantifying the quality of other communication modalities such as audio-visual conferencing.

The E-model specifies the computation of a quality measure called "transmission rating" for a conversational connection between two talkers. The quality rating R is expressed as a function of "impairment factors" as follows:

$$R = R_0 - I_s - I_d - I_{e,eff} + A \tag{30.1}$$

where R_0 is a basic rating determined by the signal-to-noise-ratio of the connection. The three I-factors quantify impairments, with subscript "s" denoting "simultaneous" (with the speech signal), "d" denoting

"delayed," and "e,eff" denoting "equipment, effective." Factor I_s encapsulates the effect of impairments occurring at the same time as the speech signal, such as an inappropriate sidetone level, quantization noise produced by mu-law and A-law quantizers used on 64/56 kilobits per second (kbps) digital connections. Sidetone is the talker's speech signal picked up by the telephone mouthpiece and fed back attenuated to the earpiece, in order to give the talker the sensation of hearing his own voice. Quantizers provide the key function of converting the analog amplitudes of signal samples to discrete amplitudes, which are then encoded into bits to form a digital representation. Factor I_d captures rating reduction caused by echoes and other impairments that arise later (greater than 50 ms) than the time point in the speech signal that triggered the impairment. Echoes may occur inside the network, commonly across four-wire-two-wire interfaces called "hybrids" (Gibson 2002), or outside the network, such as due to acoustic coupling between loudspeakers and microphones that terminate the telephone connection. Factor $I_{e,eff}$ accounts for degradations related to nonlinear and/or time-varying phenomena such as distortions caused by low-bit-rate (LBR) speech codecs, packet loss concealment (PLC), and dejitter buffers. LBR speech codecs and PLC are deployed in mobile wireless links and some voice-over-Internet-protocol (VoIP) connections. An essential component of VoIP connections, dejitter buffers serve to reduce dropouts and distortions in the decoded speech signal caused by randomly varying intervoice-packet arrival times at the receiving end. Factor "*A*," denoting "advantage factor," is used to adjust the baseline connection quality rating to reflect variation of user utility expectation with the service setting. "*A*" measures the amount of rating loss users are willing to sacrifice in order to acquire the additional convenience offered by the service. For instance, LBR speech codes used in mobile phones deliver lower speech quality than 64/56 kbps wireline connections. Mobile phone users gain the convenience of mobility and are willing to accept somewhat lower speech quality than a wired connection. "*A*" can be set to the amount of quality rating mobile phone users are willing to give up to exchange for mobility.

Equation 30.1 embodies the idea that transmission impairments can be quantified on the same perceptual scale, and can be combined additively on the scale to form an overall quality measure. Numerically, "*R*" ranges from 0 to 100. A "toll quality" wireline connection would have an *R* value of around 93. Note that the quality of an $R = 100$ connection falls far short of our imagined ideal conversational setting. The E-model is for conventional telephone connections, which convey monaural speech, cut out speech signal frequencies above 3300 Hz ("narrowband speech"), and provide a smaller loudness range than possible with spoken speech and normal hearing. With rapidly expanding new technologies and increasing quality expectations, new rating scales are being considered. They can extend the upper limit to above 100, or redefine the scale so that 100 corresponds to a more enriched quality of experience than conventional telephone conversation.

The E-model offers a methodology for rating the quality of conversations held over telephone connections. The model covers quality factors related to listening, speaking, and interaction. For instance, long transmission delay increases I_d through two phenomena. First, for a given intensity of heard echoes, its annoyance level increases with the delay. Second, large delay inhibits interaction. Talkers may become more hesitant and confused as they find it harder to promptly exchange turn to speak and to interrupt one another.

From the E-model, we see that in order to estimate the conversational quality of a telephone connection, a number of connection parameters have to be measured, such as delay, noise level, echo attenuation, and so on. This can be done using in-service nonintrusive measurement devices (INMDs). The ITU-T P.561 standard specifies requirements that INMDs on the telephone network have to satisfy but does not specify any measurement algorithm (ITU-T Rec. P.561, 2002).

30.3 Listening Quality and Tests

A critical component of conversational quality is listening quality, which refers to how telephone users rate the quality of the speech signals they hear. A common practice to assess listening quality is by

conducting listening tests. These are done by assembling a panel of human subjects to listen to samples of speech signals that have been either recorded in the network or processed to simulate speech signals received under specific transmission conditions. Each listener is asked to assess the quality of each sample heard using an absolute category rating (ACR), that is, by selecting one descriptor out of five: excellent, good, fair, poor, and bad. For analysis of the test results, each rating is assigned an integer value from 5 to 1, with 5 for excellent and 1 for bad. The numerical scores can then be averaged to obtain statistics, such as averaging over all the listener ratings for the speech samples in each transmission condition, to obtain a mean opinion score (MOS) for each condition. MOS values are real numbers between 1 and 5 and are treated as estimates of the opinion of a "typical user" from the user population on the listening quality of the speech signals provided by a particular (set of) transmission condition(s). To facilitate interpreting MOSs, the ITU-T P.800 standard provides guidelines on conducting MOS listening tests (ITU-T Rec. P.800, 1996). The MOSs obtained from such tests are sometimes written as MOS–LQS, where "LQS" stands for "listening quality subjective." (Note: "MOS" is often used synonymously with "ACR" even though ACR is a discrete scale and MOS is obtained from averaging ACR scores obtained from tests performed according to P.800. The ACR scale may in other occasions be used in other kinds of subjective tests.)

A prominent application of MOS listening tests is assessment of speech codec algorithms. By averaging the listener ratings obtained for each codec algorithm under a judiciously selected set of transmission conditions, one obtains a figure of merit for the speech quality provided by each codec. Subjective listening tests have played a pivotal role in the development and selection of speech codecs used in successive generations of mobile phone networks. These tests are nevertheless labor intensive, time consuming, and costly (e.g., $100K+ per test). These drawbacks mean that subjective tests were done sparingly, at critical junctures during codec development and selection competition. With rapid introduction of new mobile and VoIP networks and services, there is a great need to assess the voice quality of newly deployed connections, some of which may comprise a tandem of links, with some links using legacy and others new technologies, that is, combination of wireless, digital wireline, analog wireline, and VoIP links.

MOS is just one of a variety of quality measures that have been proposed and/or used; interested readers can refer to (Deller et al. 1999) and (Quackenbush et al. 1988) for other measures. However, rightly or wrongly, MOSs have been commonly treated as a currency of telephone speech quality, and MOSs have often been used to discriminate between different speech transmission equipment and services. The MOS measure is popular enough that a mapping from the E-model R-rating to MOS is provided (ITU-T Rec. G.107, 2005). The popularity of MOS has led to the ACR scale being used in other contexts. For instance, ITU standard P.835 recommends using the ACR scale to rate three different quality aspects (background only, speech only, and overall) of noise corrupted and noise-reduction processed speech signals (ITU-T Rec. P.835, 2003). P.835 embodies a multidimensional quality measure. The diagnostic acceptability measure (DAM) (Deller et al. 1999) is a well-known multidimensional measure (though the assessment scale of DAM is distinct from ACR). DAM provides altogether 16 perceptual quality attributes, covering the speech signal, background, and overall quality. Each attribute is assessed on a sliding scale to indicate how severe is a specific perceptual element (e.g., "thin" or "nasal" sounding). As a result, multidimensional measures can more precisely "diagnose" quality degradations and pinpoint system problems. MOS-like measures have also been used to rate image (Wang et al. 2004) and video quality (Winkler and Mohandas 2008).

Quality measurement may need to be done when connections are in-service, out-of-service, during installation, or undergoing development in the lab. For such needs as line monitoring, the measurement must be done in real time. Subjective listening tests, however, cannot provide real-time and low-cost assessments. Thus, there has been great interest in developing machine algorithms for estimating subjective listening quality. This can be viewed as a MOS estimation problem, and the MOSs estimated by machines are denoted MOS–LQO, where the suffix "O" stands for "objective."

30.4 Machine-Based Quality Measurement

Today, sophisticated and standardized algorithms are available for measuring listening quality. These algorithms are implemented in software to compute MOS–LQO values from input speech signals. With such capability, MOS–LQO values can be made available instantly if the speech signals were recorded beforehand, or in the case of real-time monitoring, immediately after a sufficient amount of speech signals (and other information that may be required by the algorithm) has transpired. After decades of development, recent algorithms can provide accurate estimates of MOS–LQS, when the algorithms are applied to transmission conditions that have been validated. "Accurate" can be taken to mean that the statistical error of the computed MOS–LQO is roughly of the same extent as the statistical uncertainty of the MOS–LQS obtained from P.800-guided MOS listening tests. Recent standards often provide a computer source code realization of the algorithm, though running and/or commercializing the code might require licensing from intellectual property rights holders.

Quality measurement algorithms can be classified by the type of their inputs: signal-based, parametric, and hybrid. Signal-based algorithms require the input of one or more speech signals. Parametric algorithms input only parameter values and no signals. Hybrid algorithms need both signal and parameter inputs. Signal-based algorithms can be further divided into reference-free, reference-based, and partial-reference. A reference-free algorithm needs only input the ("target") speech signal whose listening quality is to be determined. A reference-based algorithm needs to input two signals: the target itself and the original nondegraded ("clean") version of the target. A partial reference algorithm inputs the target signal as well as parameters that characterize the clean signal. Reference-free algorithms are also characterized as "no-reference," "single-ended," or "nonintrusive"; reference-based algorithms are characterized as "full-reference," "double-ended" or "intrusive"; and partial reference as "reduced-reference." A nonintrusive algorithm can listen in on the target speech signal in order to determine its quality, whereas an intrusive algorithm relies on injecting a clean reference speech signal into a connection to produce the target speech signal. Taking a connection out of service in order to inject a clean signal disrupts (intrudes on) network service. Note that it is possible for the computation of one or more parameters of a parametric algorithm to require reference signal knowledge.

To illustrate, suppose an application based on the E-model is to be developed to monitor speech quality at the receiving end of a VoIP connection. Each of the parameters in Equation 30.1 is computed using formulas or algorithms which require their own input parameters ("subparameters") or signals. The application may be able to obtain parameter values from devices it can communicate with and information carriers it can assess, such as the speech decoder, dejitter buffer, packet headers, INMDs, and so on. In such cases, the application is purely parametric. If in addition to acquiring parameters, the application has to process the received speech signal (e.g., the encoded speech in the packet payloads), then the application embodies a hybrid of signal-based and parametric measurement. If the application needs to input the clean speech signal or parameters that rely on it, the application is reference based or partial-reference based, respectively. The application may be developed to measure listening or conversational quality. For the latter, the application needs to be able to calculate the delay-related impairment factor I_d using parameters measured by INMDs and other network devices. For listening-quality-only measurement, the E-model is operated by nulling unused impairment (sub) parameters such as I_d in Equation 30.1.

In MOS listening tests, human subjects rate the quality of degraded speech signals without listening to their clean versions. The listener compares the heard speech signal with his/her listening-quality expectation established over years of telephone use. A signal-based algorithm can mimic human judgment by comparing the target signal with an expectation model. While reference-free algorithms do provide such a function, building an algorithm that closely mimics human perceptual and cognitive processes is beyond the state of current knowledge about these processes. Instead, state-of-the-art reference-free algorithms are designed to detect abnormal signal behaviors, gauge their severity, and

map the severities of the abnormalities to a quality estimate. These algorithms thus rely on knowledge of perceptually relevant abnormalities, and signal and statistical models to represent such knowledge. Though there are numerous ways of transforming a speech signal that can change its perceived quality, the types of degradation that telephony transmission can impart on speech signals are known to a great extent and can be modeled. Moreover, apart from telephony, a multitude of signal models exists emulating the production and auditory perception of speech signals. These can be deployed to build models of normative behaviors, complementing models of abnormal behaviors. As we shall see below, a variety of models have been employed to build the existing algorithms. Besides such modeling, double-ended algorithms are provided with a clean version of the target speech signal. The clean signal provides a precise description of normative behavior for the target speech signal. Double-ended algorithms that exploit this well can offer more accurate estimates of subjective quality than single-ended algorithms. Thus, much effort has been invested in developing standard double-ended algorithms, the most widely deployed being ITU P.862 (PESQ) (ITU-T Rec. P.862, 2001). The recently standardized successor of PESQ, ITU-T P.863 (ITU-T Rec. P.863, 2011), also known as POLQA for "Perceptual Objective Listening Quality Assessment," caters to a wider range of application conditions, and has been reported to provide more accurate quality estimates.

30.5 Reference-Based Algorithms

Reference-based algorithms (RBAs) rely on having the clean original speech signal $x(t)$ on hand. Usually, we think of this signal as being processed and/or transmitted to produce the target speech signal $y(t)$ whose listening quality is to be estimated. However, as we describe below, the ITU-T P.563 reference-free algorithm estimates a pseudoreference signal, in lieu of a "clean" signal, from the distorted target speech signal. The idea underlying RBAs is simple: the more dissimilar is $y(t)$ from $x(t)$, the greater is the distortion and hence greater quality degradation relative to the quality of $x(t)$. If one takes care to ensure that the $x(t)$ used is chosen to have high quality, for example, Q = 4.4 (MOS–LQS), an RBA can estimate the degradation d($x(t)$, $y(t)$) and the estimated MOS–LQO of $y(t)$ can be taken as Q − d. The notation d($x(t)$, $y(t)$) denotes a mapping of two signals to a nonnegative real value. A common measure of distortion is signal-to-noise-ratio (SNR) which can be written as $||x(t)||^2/||e(t)||^2$, where the notation $||s(t)||^2$ denotes calculating the energy of signal $s(t)$. The "noise" signal $e(t)$ is in fact the "error" signal $e(n) = x(t) - y(t)$. Thus, SNR measures how much $y(t)$ differs from $x(t)$ in terms of the power of the error signal relative to the power of the reference signal. Depending on how $x(t)$ is distorted to produce $y(t)$, SNR can be a very poor measure of degradation. For instance, the two signals $y\_1(t) = 2\,x(t)$ and $y\_2(t) = x(t - 0.2)$ would have (nearly) identical listening quality to $x(t)$ but the SNR is 0 dB for $y\_1(t)$ and below 0 dB for $y\_2(t)$. Thus, the RBA mapping $d(x(t), y(t))$ should only be sensitive to differences between $x(t)$ and $y(t)$ that contribute to the subjective listening quality judgment process. As such, many existing algorithms map the signals $x(t)$ and $y(t)$ into a perceptual domain which mimics the processing done by the human auditory system. A psychoacoustically motivated degradation measure is then used to characterize perceptually relevant distortions and mapped to a final quality rating. It is interesting to observe that in MOS tests, the listeners do not hear $x(t)$, so that no precise differencing between $x(t)$ and y(t) is available to form the subjective rating. Despite this, the recent standard RBAs demonstrate that there exist strong correlations between the measured differences and MOS degradation.

To get an idea of RBA processing, we now examine the ITU-T P.862 PESQ algorithm. At the time of writing (2011), PESQ has been the most widely employed double-ended algorithm for narrowband (up to 4 kHz speech content) speech codecs and networks. PESQ's algorithm structure is similar to that of the newly standardized ITU-T P.863 POLQA algorithm, whose new features are also highlighted below.

PESQ was standardized in 2001 and developed by a consortium of British, Dutch, and German companies (ITU-T Rec. P.862, 2001). PESQ developed around the time packet-based transmission was

increasing in popularity and its predecessor standard quality measurement algorithm, PSQM (for perceptual speech quality measure) (ITU-T Rec. P.861, 1996) failed at predicting the quality of such variable delay communication systems. A key advancement of PESQ over PSQM was the introduction of constant and variable delay estimation techniques between the clean (original) input $x(t)$ and the degraded output $y(t)$ (Rix et al. 2002). Since RBAs depend on distortion parameters extracted by comparing the two signals frame-by-frame, even the smallest frame misalignment (in the order of 1 ms) can result in erroneous quality estimates (Rix et al. 2002). It is thus critical that the delays in $y(t)$ relative to $x(t)$ be detected and accounted for before the degradation measure $d(x(t),y(t))$ is computed. The PESQ algorithm assumes that the delay of the system is piecewise constant, a reasonable assumption for a wide range of systems, including VoIP, and introduces a two-stage constant delay estimation procedure. First, a crude delay estimation step is used based on the location of the maximum cross correlation between the original and processed signal envelopes. It is argued that if the speech signals contain at least 500 ms of speech content, the crude delay estimate could be accurate to within ±8 ms (Rix et al. 2002). Once a crude delay estimate is found, it is further refined via a weighted histogram method of the estimated frame-by-frame delays.

To estimate varying delay, a similar two-stage process is performed on speech utterances, which correspond to 300+ millisecond speech bursts containing no silent period longer than 200 ms. Crude delay estimates are obtained for each utterance and further refined using the weighted histogram approach. To compensate for continuous varying delays during speech, an utterance splitting method is also used. Each utterance is divided in two and the crude/fine delay estimation procedures are applied. If there is evidence supporting a delay change (e.g., an absolute change in delay of 4 ms or greater), subutterance splitting proceeds in a recursive manner to each new "half" until no further delay changes are seen. A last time alignment step incorporated in PESQ consists of a bad frame identification procedure in the perceptual domain (more on this topic to follow). More specifically, it assumes that bad frame alignment will result in abnormally high perceptual disturbances. In such instances, realignment is performed.

Once the original and degraded speech signals are time-aligned, a perceptual auditory mapping (Beerends et al. 2002) is performed to map the signals into an internal representation of perceived loudness both in time and in frequency. This step has been borrowed from PSQM and consists of Bark-scale frequency bin grouping and loudness mapping using frequency-dependent thresholds and exponents. The difference in internal representations of the degraded and reference speech signals is then calculated, representing the audible difference between the two signals. A positive difference indicates that (power-)additive components are present such as background noise; a negative difference indicates that (power-)components were lost, such as in VoIP networks with packet losses. The last processing stage consists of the so-called cognitive modeling step where disturbances are evaluated and aggregated using cognitive "insights" to form a final PESQ quality estimate. For example, positive disturbances and those occurring during active speech periods are thought to be more objectionable than negative disturbances and those occurring during silent intervals, respectively, thus receive higher weights. Additionally, disturbance integration is performed in three steps, first over frequency, then over short-time utterance intervals, and finally over the whole speech signal. Different p values are used in the L_p norm integrations of the three steps to maximize the correlation with subjective quality ratings. It was later observed that an additional mapping was needed in order to fit the PESQ raw scores onto the five-point MOS–LQO scale; this mapping is described in ITU standard P.862.1 (ITU-T Rec. P.862.1, 2003).

In its original form, PESQ can only be used with narrowband speech content. Given the advances in wideband (up to 8 kHz bandwidth) technologies, a wideband extension of PESQ was later standardized in 2005 (ITU-T Rec. P.862.2, 2005). Despite these extensions, the PESQ application guide published at the end of 2007 suggested that the scope of PESQ was inadequate for burgeoning speech networks and technologies. PESQ did not cover electroacoustic transducers, voice quality enhancement algorithms (e.g., noise reduction, bandwidth extension, and automatic gain control), and time-warping/scaling algorithms (ITU-T Rec. P.862.3, 2007). PESQ performance was also compromised for

CDMA codecs (e.g., EVRC), strong linear distortions (e.g., phone's frequency shaping), gain variations, and VoIP-transmitted speech with variable delays around 1 s. In 2011, the new ITU-T P.863 POLQA algorithm was standardized to overcome these limitations and allow for the majority of existing fixed, mobile, IP-based, and hybrid telephone network scenarios to be covered, either in narrow-, wide-, or superwide-band (up to 24 kHz speech bandwidth) modes.

The POLQA RBA is a joint development between three companies from Germany, Switzerland, and the Netherlands, two of which were involved in the development of PESQ. While the core of the POLQA algorithm is similar to that of PESQ, two key modifications have been introduced to tackle the PESQ weaknesses described above. First, a new time alignment algorithm has been proposed. In superwide-band mode, the original reference signal needs to be sampled at 48 kHz. The degraded signal, however, may have been downsampled due to bandwidth constraints and this band limitation is considered a degradation that has to be scored accordingly. POLQA is able to handle this sampling rate discrepancy in conjunction with the delay estimation procedure by analyzing the histogram of estimated delay variations. Similar to PESQ, the delay estimation algorithm operates in multiple steps. First, an overall delay is estimated based on using the cross correlation between (i) the $x(t)$ and $y(t)$ signals in their entirety, and (ii) the first and second half of the signals, respectively. So-called "reparse points," which correspond to transition points between silence and active speech (and vice-versa), are then found using a complex procedure involving the use of a voice activity detector (VAD) on both the reference and degraded speech signals. Once reparse points are found in both signals, their time difference is computed as a coarse estimate of the delay for a particular reparse section. This procedure is conceptually similar to that of PESQ in the sense that it provides delay estimates for each "utterance." Unlike PESQ, however, the refinement of this coarse estimate involves a multidimensional search in the per-frame signal energy and fractal dimension (used as a measure of signal complexity which is assumed to be indirectly related to noise) domains using two different frame sizes. A backtracking algorithm similar to Viterbi's algorithm is used to estimate a finer delay estimate for each speech frame. An additional refinement step is used based on the cross correlation to estimate the exact delay expressed in samples. As can be expected, this time alignment procedure is fairly complex and time consuming. For applications in which fixed or piecewise fixed delays are present, POLQA uses a simpler alternative prealignment method. It is similar to that in PESQ in the sense that it finds a coarse estimate based on the cross correlation of signal envelopes and then refines this estimate by matching segmentwise parts of the original signal with that of the degraded signal. This segmentwise matching procedure is also used to find missing segments in the degraded signal due to, for example, packet losses. This fast alternative may result in very bad delay estimates if time-varying delay is present. As such, an exclusion criterion is run to verify the applicability of the fast prealignment method. If the criterion is not met, the more complex method described above is used.

The second major difference between POLQA and PESQ is in the perceptual model (see Figure 30.1, where shaded blocks represent the different modules available with POLQA) and in the processing of the reference and degraded speech signals. More specifically, POLQA introduces the concept of idealization. Since listeners in a MOS test are not presented with a reference signal, participants likely use an "ideal" reference signal during their quality judgment process. This idealization process is modeled based on subjective experiments that measured human sensitivity to nonoptimal presentation levels and timbre, and low levels of noise when listening to the reference speech signal. As such, POLQA modifies the reference signal in three different stages (see shaded blocks in Figure 30.1) to model this idealization process. Modifications to the degraded signal and its internal representation are also performed but motivated by higher-level cognitive processes. For example, humans are relatively insensitive to linear frequency response distortions and to steady-state wideband noises, thus such disturbances are partially compensated for by the POLQA RBA. Additional processing steps available exclusively with POLQA are frequency dewarping (e.g., in the case of speech processed by bandwidth extension methods), spectral and temporal masking, and playback-level calibration. The latter is performed as the impact of playback level on perceived quality is important, particularly in superwide-band mode, and needs to be accounted for. In essence, these modifications are performed to preserve only relevant speech information and discard

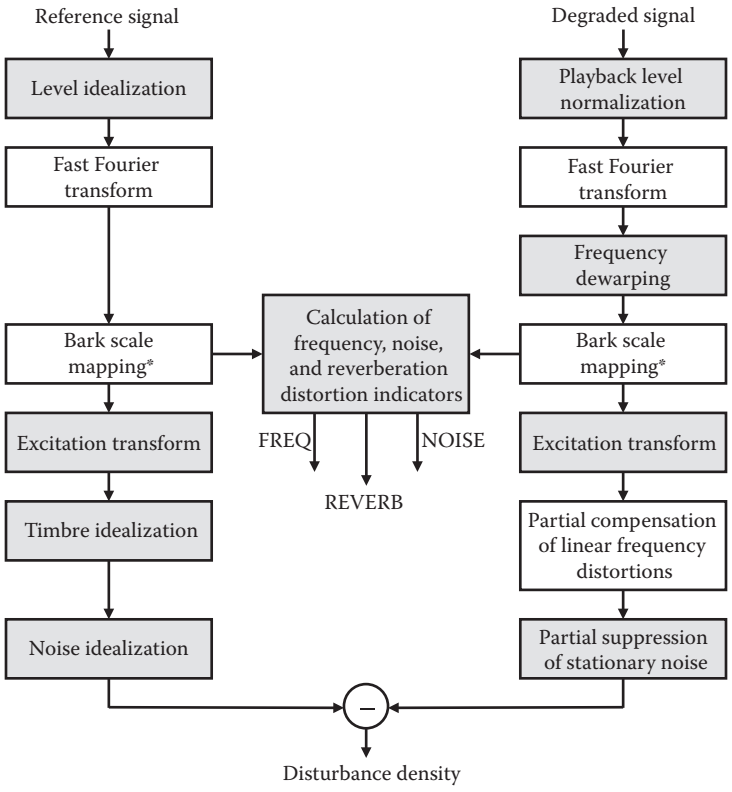

FIGURE 30.1 Block diagram of perceptual model used by PESQ and POLQA. Shaded blocks are exclusive to POLQA and are not available with the PESQ RBA. (*In PESQ, the bark scale mapping is followed by a loudness scale mapping, which is omitted in the block diagram due to space constraints.)

unwanted signal components. The goal is to focus only on speech-related distortions and have additional modules or indicators characterize disturbances related to frequency response, noise, and reverberation, as shown in Figure 30.1. The signal processing steps shown in Figure 30.1 are performed four different times using different internal parameters such that four variants of the time–frequency "disturbance densities" are computed. These variants focus on general distortions, large general distortions, additive distortions only, and large additive distortions. Disturbance densities are aggregated over pitch, short-time utterance intervals, and time using different L_p norm integrations. Aggregate disturbance densities are then combined with level and spectral flatness indicators into a final POLQA raw score. Finally, the raw score is mapped to the MOS–LQO scale using a third-order polynomial mapping that was optimized for the databases used in the P.863 standardization process. In narrow-band mode, the maximum score is 4.5 while in superwide-band mode, this value is 4.75 which corresponds to the extended MOS-scale used with high-definition (HD) voice technologies.

The combined advancements available with ITU-T P.863 POLQA allow for a new range of applications that could not previously be assessed using PESQ, such as voice quality enhancement algorithms and terminals using head-and-torso simulators (HATS). At the time of writing, third-party (i.e., outside the standardization process) POLQA performance results under these special conditions are not available. ITU-T standardization tests did suggest, however, that POLQA provided inaccurate predictions when used with acoustical recordings using free-field microphones without HATS or ear-canal simulators and with some enhanced variable rate codec (EVRC) speech codecs. Moreover, POLQA has not been validated for use with very LBR coding technologies (<4 kilobits/s).

30.6 Reference-Free Algorithms

Unlike RBAs, Reference-free algorithms (RFAs) do not depend on a clean reference signal. RFAs have gained much attention recently as they can be used while the network is in service and obviate the need to take the network "offline" to inject controlled reference signals for quality measurement. RFAs function like participants in MOS listening tests who are only presented with the degraded speech signal and then rate its quality. Humans, through extensive usage of telephony services, have acquired knowledge of normal and abnormal phenomena in speech sounds and use this prior knowledge to judge signal quality. Unlike the POLQA RBA which uses an idealization process to modify the reference signal to take into account this prior knowledge, existing RFAs employ models of normative speech production (Gray et al. 2000), speech perception (ANSI Rec. ANIQUE+ 2006), speech signal feature likelihood (Falk and Chan 2006), or a combination thereof for single-ended quality assessment. The latter scenario is applicable to the ITU-T P.563 algorithm, which was standardized in 2004 after a two-year competition (ITU-T Rec. P.563, 2004). In this competition, two systems stood out: the standardized P.563 algorithm and the runner-up ANIQUE+ algorithm, which later became an American National Standard Institute standard (ANSI Rec. ANIQUE+ 2006). Focus will be placed here on the P.563 algorithm due to its popularity within the quality assessment community.

Since RFAs do not have access to the clean reference speech signal, assumptions have to be made about the received signal. The P.563 algorithm combines three basic principles, such that different distortion types can be covered (ITU-T Rec. P.563, 2004; Malfait et al. 2006). The first principle focuses on the human voice production system, modeling the vocal tract as a series of acoustic tubes of different time-varying cross-sectional areas. From the speech signal, cross-sectional areas are evaluated for unnatural behavior, thus indicating the presence of unnatural distorted speech. More specifically, pitch marks and voiced/unvoiced classification is first performed using a normalized cross-correlation function. Pitch synchronous vocal tract modeling is then applied where tube section areas of eight concatenated lossless acoustic tube sections are obtained via linear predictive (LP) analysis of voiced speech segments. The resulting eight tube sections are then averaged to model three cavity articulators per pitch cycle, namely the rear, middle, and front cavities. Due to human articulatory limitations, temporal changes in vocal tract cavities are smooth. Unnaturally fast variations in the acoustic tube model or excessively large tube sections suggest that the speech signal being analyzed is distorted. In addition to vocal tract analysis, LP and cepstral analyses are performed on voiced speech segments. The skewness and kurtosis of the coefficients are then computed and investigated to see if they lie within the restricted range expected for natural speech. Deviations from this normative range provide further evidence of introduced distortions in the speech signal. The second principle used by P.563 is to reconstruct a pseudoreference signal from the degraded signal by modifying the computed LP coefficients to fit the vocal tract model of a typical human speaker. This is achieved by converting the LP coefficients to line spectral frequencies (LSFs) which are then quantized using two previously trained codebooks. The better of the two LSF approximations is used to reconstruct the pseudoreference signal. A "basic voice quality" measure is then computed using a RBA with the pseudoreference and degraded signals as input. The RBA used is a simplified version of PESQ without the temporal alignment module and with a modified "cognitive" mapping function. The third principle used by P.563 is to identify specific distortions encountered in voice channels, such as noise (additive and multiplicative), temporal clippings, and robotization effects (voice with metallic sounds). Additive noise is characterized by an estimated SNR level which is obtained using VAD decisions computed in the preprocessing stage; both global and local (i.e., between phonemes) levels are estimated. Other parameters such as high-frequency spectral flatness and spectral clarity are also computed to characterize the noise source. Similarly, a segmental SNR measure is used to characterize the multiplicative noise (speech-correlated noise) introduced by cascaded logarithmic pulse-code modulation (PCM) and adaptive differential PCM systems or by waveform speech codecs (Malfait et al. 2006). The analysis of multiplicative noise is based on the evaluation of spectral statistics (i.e., range and deviation) where it is assumed that the noise will have a flat spectral

characteristic which forms a noise floor during active speech periods. Temporal clippings, in turn, are commonly encountered in packet-based networks. P.563 assumes two types of clippings: mutes/interruptions and front/back clippings. Mutes or speech interruptions can occur when silence or comfort noise is inserted as a simple PLC strategy during active speech periods. Front and back clippings may occur in systems that use VADs, such as digital circuit multiplication equipment (Malfait et al. 2006). These abrupt variations in signal energy are detected and estimated by analyzing abrupt variations in the signal envelope and are defined as signal level drops of more than 30 dB within 8 ms or rises by more than 30 dB within 16 ms (Malfait et al. 2006). Lastly, robotization effects often result from transmission errors in mobile radio networks (e.g., GSM) or with LBR codecs, where voiced speech segments sound highly periodic or "robotic." To detect such events, P.563 monitors signal periodicity in the 2.2–3.3 kHz range by means of cross-correlation analysis; similar periodicity measurements are used to detect frame-repeat and unnatural beep impairments. The last step in the P.563 signal processing chain consists of distortion classification and distortion-dependent perceptual weighting. Using a subset of the extracted (internal) parameters, the P.563 algorithm detects one of the following six major distortion classes, listed in decreasing order of "annoyance": high level of background noise, signal interruptions, signal-correlated noise, speech robotization, and unnatural male and female speech. The assumption is that human listeners will focus only on the dominant distortion when different types of degradations occur simultaneously (Malfait et al. 2006). For each dominant distortion class, a subset of the extracted parameters is used to compute an intermediate quality rating. Once a major distortion class is detected, the intermediate score is linearly combined with eleven other parameters to derive a final P.563 raw score. During the standardization process, P.563 attained acceptable performance for a wide range of test factors, coding technologies, and applications. It was not suitable, however, for LBR codecs or applications involving suboptimal listening levels, talker echoes, or sidetones.

30.7 Parametric Methods

Machine "intelligence" can play a critical enabling role in assuring that customers serviced by machines are provided with satisfying quality of experience (QoE). An important component of QoE assurance is quality monitoring. Network-wide automated connection quality monitoring enables not only QoE assurance, but also diagnosis and amelioration of faults. Implementation cost, however, is a critical factor in assessing the viability of network-wide deployment. If a monitoring function is located on portable devices, power consumption also becomes an issue. A distinct advantage of parametric methods is that they can offer very low computational complexity, a key determinant of implementation cost and power consumption. Parametric algorithms can derive their computation economy from having access to or being able to compute one or a few statistics that sufficiently capture the degree of speech degradation. As an example, let us consider monitoring a set of VoIP connections which use a specific speech codec. At the transmit end, the encoder bit stream is loaded onto voice packets in a specific manner, for example, every two 10 ms speech frame onto one voice packet. Under perfect transmission conditions, the voice packets will arrive at the speech decoder with no errors and in exactly the order they were generated, and the difference between the times of arrival of consecutive packets at the decoder will be exactly equal to the difference of the time instances the consecutive packets were dispatched. The decoded speech signal would suffer no transmission-related degradation and would be identical, except for a constant time delay due to transit through the network, to the best speech signal the speech encoder could synthesize from the encoded bits. However, due to network transmission faults such as bit errors, packet discards, and variable transmission delay, some speech packets will not be available error-free by the deadlines the decoder needs to start decoding the packet contents in order to maintain the integrity (e.g., time-continuity) of the speech signal. In such cases, the cause of speech degradation after speech encoding is solely due to packet losses. Without any packet loss, the listening quality of the decoded speech signal is identical to the quality that can be synthesized by the encoder before transmission. Thus, akin to the E-model wherein the overall impairment due to different degradation sources are

combined by summing negative quality ratings corresponding to the sources, the listening quality of the VoIP speech at the receiving end can be estimated by measuring the quality degradation due to packet losses and then using the measurement to adjust the speech quality estimated at the encoder.

Packet loss events can be observed at the decoder and can be modeled as a binary-valued discrete-time random process. A simple approach to estimate quality degradation is to compute statistics of the process and map them to a degradation estimate. For instance, it is easy to see that the severity of speech degradation increases with the average rate of packet loss, and for a given loss rate, the average length of loss bursts. Thus, it is reasonable to expect the severity of degradation to be a monotonically increasing function of each of these two statistics. A mapping from these to a degradation estimate can be obtained by applying regression or machine-learning methods on training data. The data comprises "examples" where each example is a triplet of three values: the two loss statistics and their corresponding amount of quality degradation. The last item can be obtained either from subjective listening tests or from an RBA such as PESQ or POLQA. Through experimenting with different choices of regression function analysis or machine-learning methods, one would obtain a suitable function or mapping from the loss statistics to a degradation estimate. The goal is to find mappings that perform well on novel data, that is, data not in the training set. This goal can be better met by selecting from mappings that have very few parameters that need to be adjusted by the training or regression algorithm, and by validating the trained mapping using novel data. Readers interested in exploring machine-learning techniques can refer to (Bishop 2007). The degradation estimate provided by the mapping can be combined with the speech quality estimated at the encoder end, if the estimate is made available to the decoder end, for example, when piggybacked onto VoIP packets. If unavailable, the degradation estimate can be treated as an amount of reduction of the average speech quality provided at the encoder end.

An embodiment of the above parametric method that has been deployed on VoIP links is VQmon (Clark 2001), which uses a Markov chain to model the packet loss process observed at the receiving end. The empirically observed chain parameters are mapped to an estimate of degradation severity. The parametric method can also be applied to map analog link parameters. For instance, (Karlsson et al. 1999) reported mapping radio link quality parameters measured at GSM radio receivers to a "speech quality index" and obtained more accurate speech quality estimates than using PSQM, the best available RBA at the time. The parametric approach can work well when the unknown amount of (additional) degradation can be attributed to one phenomenon that can be readily measured. When the scenario is complicated by having a greater number and variety of degradation sources and interactions among them, hybrid parametric-cum-signal-based methods can be used. An embodiment of this approach is described in (Falk and Chan 2008), which proposes using a mapping that combines a "base quality" with measurements made on the received speech signal to obtain a quality estimate. The base quality can be obtained from a lookup table. Discrete attributes (e.g., codec type, number of speech frames in a packet) and discretized values (e.g., packet loss rate, average packet-loss-burst length) are used to index the table entries. The signal measurements are then used to cover degradations that are not included in the table, for example, level of background noise and severity of artifacts due to noise reduction processing.

The above parametric measurement examples are not based on standard algorithms. Existing signal-based standard algorithms consume considerably more computational resources than the above parametric algorithms. Network and device design engineers will have to decide whether it is necessary to conform to standards, when nonconformance may garner significant cost savings. Conformance may not be necessary for measurements done within "closed" proprietary (sub)systems. On the other hand, standard algorithms may be required to ensure interoperability between equipment built by different manufacturers. Also, conformance to standards is usually demanded by customers of link and network test equipment.

30.8 Usage Considerations

Speech quality measurement algorithms are designed and tested for a variety of degradation conditions. For ITU standard algorithms, the conditions in which the algorithms have been tested and the outcomes

of the tests are documented. Such information provides important clues to users of the algorithms about the reliability of the quality estimates provided by the algorithms. For each of the conditions listed in the documentation, the algorithm may be characterized as being known to provide reliable or unreliable estimates, or to have undetermined or unresolved reliability. If one desires to apply a standard algorithm to conditions for which the algorithm is not known to provide reliable estimates, additional tests need to be done to validate the estimates, or additional evidence gathered to calibrate them. For instance, suppose one seeks to determine whether a standard algorithm can be "customized" to assess quality under conditions for which the reliability of the algorithm's estimates are uncertain. Suppose a set of speech signals covering the conditions of interest can be listed in decreasing order of preference by listening quality but their MOS–LQS values are unknown. The standard RBA or RFA can be applied to the signals to obtain a corresponding set of MOS–LQO values. These values provide an objective ranking of the signals. The matching between the subjective and objective ranks can be assessed using Spearman's rank correlation coefficient. If this coefficient turns out to be statistically significant and has a value close to 1, the standard algorithm is deemed to be able to discriminate well between the different quality levels represented by the speech signals. This capability could satisfy applications which need only discrimination by quality category as opposed to absolute MOS values. If in addition, MOS–LQS values are available for the set of speech signals, a mapping similar to the one described in Recommendation ITU-T P.862.1 (ITU-T Rec. P.862.1 2003) or the one used in P.863 to map raw scores to MOS–LQO can be designed to maximize the Pearson correlation (or minimize the mean square error) between the MOS–LQS values and the mapping outputs.

Technology for automating measurement of user-perceived quality is rapidly evolving. Proliferation of mobile electronic devices and networking makes human machine interactions a fact of live and provides unprecedented opportunities for machines to amass human-generated data and responses. Mining such information will accelerate the development of automated quality assessment technology and standards.

References

ATIS Recommendation PP-0100005.2006. 2006. Auditory non-intrusive quality estimation plus (ANIQUE+): Perceptual model for non-intrusive estimation of narrow-band speech quality. American National Standards Institute (ANSI).

Beerends, J., Hekstra, A., Rix, A., and Hollier, M. 2002. Perceptual evaluation of speech quality (PESQ) the new ITU standard for end-to-end speech quality assessment. Part II: Psychoacoustic model. *Journal of the Audio Engineering Society* 50(10): 765–778.

Bishop, C. M. 2007. *Pattern Recognition and Machine Learning*, 2nd edition. New York, NY: Springer.

Deller, Jr., J. R., Hansen, J. H. L., and Proakis, J. G. 1999. *Discrete-Time Processing of Speech Signals*. Piscataway, NJ: Wiley-IEEE Press.

Clark, A. D. 2001. Modeling the effects of burst packet loss and recency on subjective voice quality. *Proceedings of the IP-Telephony Workshop* 123–127.

Falk, T. and Chan, W.-Y. 2006. Nonintrusive speech quality estimation using Gaussian mixture models. *IEEE Signal Processing Letters* 13(2): 108–111.

Falk, T. and Chan, W.-Y. 2008. Hybrid signal-and-link-parametric speech quality measurement for VoIP communications. *IEEE Transactions on Audio, Speech & Language Processing* 16(8): 1579–1589.

Gibson, J.D., Ed. 2002. *The Communications Handbook*, 2nd edition. Boca Raton, FL: CRC Press.

Gray, P., Hollier, M., and Massara, R. 2000. Non-intrusive speech quality assessment using vocal tract models. *IEE Proceedings—Vision, Image, and Signal Processing* 147(6): 493–501.

ITU-T Recommendation G.107. 2005. The E-model, a computational model for use in transmission planning. International Telecommunication Union.

ITU-T Recommendation P.561. 2002. In-service non-intrusive measurement device—Voice service measurements. International Telecommunication Union.

ITU-T Recommendation P.563. 2004. Single ended method for objective speech quality assessment in narrow-band telephony applications. International Telecommunication Union.

ITU-T Recommendation P.800. 1996. Methods for subjective determination of transmission quality. International Telecommunication Union.

ITU-T Recommendation P.835. 2003. Subjective test methodology for evaluating speech communication systems that include noise suppression algorithms. International Telecommunication Union.

ITU-T Recommendation P.861. 1996. Perceptual speech quality measure: Objective quality measurement of telephone-band speech codecs. International Telecommunication Union.

ITU-T Recommendation P.862. 2001. Perceptual evaluation of speech quality: An objective method for end-to-end speech quality assessment of narrow-band telephone networks and speech codecs. International Telecommunication Union.

ITU-T Recommendation P.862.1. 2003. Mapping function for transforming P.862 raw result scores to MOS-LQO. International Telecommunication Union.

ITU-T Recommendation P.862.2. 2005. Wideband extension to Recommendation P.862 for the assessment of wideband telephone networks and speech codecs. International Telecommunication Union.

ITU-T Recommendation P.862.3. 2007. Application guide for objective quality measurement based on Recommendations P.862, P.862.1 and P.862.2. International Telecommunication Union.

ITU-T Recommendation P.863. 2011. Perceptual objective listening quality assessment. International Telecommunication Union.

Karlsson, A., Heikkila, G., Minde, T. B., Nordlund, M., Timus, B., and Wiren, N. 1999. Radio link parameter based speech quality index—SQI. *Proc. 1999 IEEE Workshop on Speech Coding* 147–149.

Malfait, L., Berger, J., and Kastner, M. 2006. P.563: The ITU-T standard for single-ended speech quality assessment. *IEEE Transactions Audio, Speech, and Language Processing* 14(6): 1924–1934.

Quackenbush, S., Barnwell, T., and Clements, M. 1988. *Objective Measures of Speech Quality*. Englewood Cliffs, New Jersey: Prentice-Hall.

Rix, A., Hollier, M., Hekstra, A., and Beerends, J. 2002. Perceptual evaluation of speech quality (PESQ) the new ITU standard for end-to-end speech quality assessment. Part I: Time-delay compensation. *Journal of the Audio Engineering Society* 50(10): 755–764.

Wang, Z., Bovik, A.C., Skeikh, H.R., and Simoncelli, E.P. 2004. Image quality assessment: From error visibility to structural similarity. *IEEE Transactions on Image Processing* 13(4): 600–612.

Winkler, S. and Mohandas, P. 2008. The evolution of video quality measurement: From PSNR to hybrid metrics. *IEEE Transactions on Broadcasting* 54(3): 660–668.

IV

Wireless Networks

31

Wireless Network Protocols

Renato Mariz de Moraes

Hamid R. Sadjadpour

31.1 Introduction

Wireless networks are characterized by nodes (or stations, or users) that are connected to each other by wireless links. Accordingly, one main feature of such networks is mobility which results in dynamic topology when the position of nodes changes in time. Network setup in mobile wireless *ad-hoc* network is a tedious task because of rapid dynamic nature of these networks while communication in wired networks (Internet) or even stationary wireless networks is much easier to manage. In wireless networks, the communication channel is a broadcast medium since the transmitted signal by a node can be received by any other node that is in the transmission range of the transmitter. In some cases, a node transmits to a receiver while another node is also trying to send packet to the same receiver. If these two transmitters are outside of each other's transmission range and unaware of the other node existence, it is possible that both nodes try to transmit packets to the same receiver and cause collision. This situation is known as the *hidden terminal problem* and it does not allow the receiver to decode the received signals. Figure 31.1 demonstrates the hidden terminal problem.

Another issue is related to the fact that in some applications, source and destination are not within each other transmission range. Therefore, the source relies on other nodes to relay the message to destination using multihop communications. Since the medium is a broadcast channel, nodes require to coordinate with each other to access the channel in a distributed fashion in order to avoid interference and collision in the network. Consequently, different methods are proposed in the literature to coordinate among nodes to access the channel. Such methods are called medium-access control (MAC) protocols. Further, once a node can access the communication channel to transmit to its neighbors, it needs to find out the path to destination when there is no base station to route the message to destination. Such networks are called *ad-hoc* networks and MAC and routing protocols are two important ingredients of

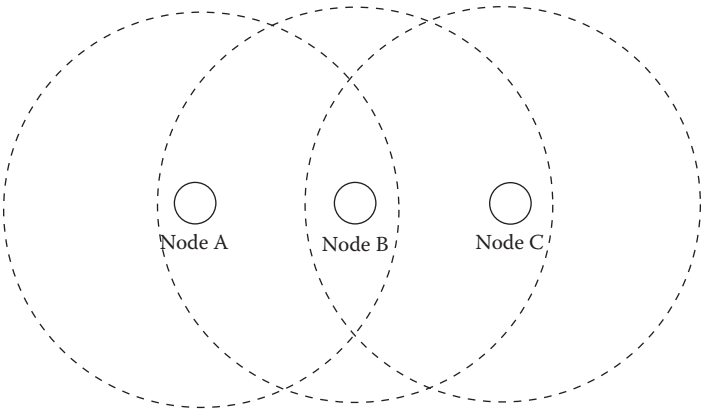

FIGURE 31.1 Hidden terminal problem. Nodes A and C are within transmission range of node B; however, nodes A and C cannot hear each other. If they both try to simultaneously transmit to node B, a collision will occur at node B.

these networks in order to transport information. This chapter provides a short overview of the main MAC and routing strategies proposed for wireless *ad-hoc* networks.

With respect to the MAC protocols, the random access approaches have gained significant attention due to their simplicity and relative efficiency to attain the objective of providing channel access in a distributed fashion. In this regard, Aloha and carrier sense multiple access (CSMA) are by far the most common protocols that are investigated and deployed in wireless *ad-hoc* networks. Section 31.2 presents the Aloha and CSMA protocols with their variants.

With respect to routing strategy, routing protocols can be classified in two types: table-driven (or proactive) and on-demand (or reactive) protocols. In table-driven protocols, the routing algorithm proactively maintains a database called routing table which includes information about path to each destination node in the network and the next hop in a path from source or relay to destination. In on-demand protocols, the routing algorithm reacts to changes in the network topology to obtain updated routes along multiple hops and as link failures occur on an active route, the algorithm can search to obtain a new valid path to destination. Once the communication among source and destination is completed and the route is no longer in use, the relay nodes utilized along the path remove the route information from their database. When a source wants to send data packets to a destination, it initiates the route request. Section 31.3 presents the main features of four important routing protocols for *ad-hoc* networks.

31.2 Medium Access Control Protocols

This section covers the classical Aloha and CSMA protocols proposed in multihop wireless networks. The dynamic aspect of these protocols is due to the random nature of channel access. The stations (or nodes) will compete for the communication medium in a distributed fashion with no coordination in principle. The Aloha protocol was *de facto* the first wireless network protocol implemented in practice and used for transmission of data packets in a wireless network for computer interconnection; however, its low performance prompted other more efficient protocols like the CSMA proposal.

31.2.1 The Aloha Protocol

The Aloha protocol was proposed by Abramson [1] to interconnect the terminals of the University of Hawaii spread on the Hawaiian Islands. The proposal was to use shared broadcast wireless medium employing radio waves to interconnect the host computer in main campus to the other terminals in different islands. One of the key characteristics of this protocol is simplicity and even despite its slow

performance, as it will be shown, today the Aloha idea is the fundamental building block for performance analysis of wireless network protocols.

31.2.2 Pure Aloha

The protocol was designed to be distributed such that any node can randomly access the shared medium. Consequently, a major advantage of this protocol was simplicity since no coordination is required among nodes.

Whenever a station has data, it transmits immediately without any scheduling with other stations. The receiver acknowledges (ACK) if the packet is received successfully. If no ACK is received after two propagation time periods, the transmitter realizes that a collision has occurred. It then waits a random time and retransmits the packet. The station continues this procedure until it receives an ACK for the transmitted packet.

Figure 31.2 shows the basic behavior of the pure Aloha protocol. During the transmission of the reference packet i, if no other packet from another station is transmitted within the indicated vulnerable period, then the transmission is successful, that is, no collision takes place. If the packet length is constant and equals L (in bits) and the channel transmission rate is R (in bits per second), then the vulnerable period commences $T = L/R$ seconds before the start of the transmission of the reference packet i until the end of its transmission, that is, a total of $2T = 2L/R$ seconds. Therefore, if other packets from other stations are transmitted during this period, as illustrated in Figure 31.2, then a collision will take place.

In [1], Abramson assumed that the resulting arrival process of new and retransmitted packets followed a Poisson* distribution with mean of G packets per T seconds, in which T is the packet duration in seconds. G is also known as the *offered load* to the network and equals λT, in which λ is the arrival rate of the Poisson process. Thus, the vulnerable period of a packet transmission is $2T$. On the other hand, the throughput X of the system equals the fraction of the arrival flux that is transmitted without collision. The fraction of time that packets are transmitted successfully equals the probability of no collision. No collision takes place if no packet arrives during the vulnerable period of a packet that is to be transmitted. Accordingly, the throughput of Aloha is given by [1]

$$\begin{aligned} X &= G \times P\{\text{no collision}\} = G \times P\{\text{zero arrivals (i.e., transmissions) in } 2T \text{ seconds}\}, \\ &= G\frac{(2G)^0 e^{-2G}}{0!}, \\ &= Ge^{-2G}. \end{aligned} \tag{31.1}$$

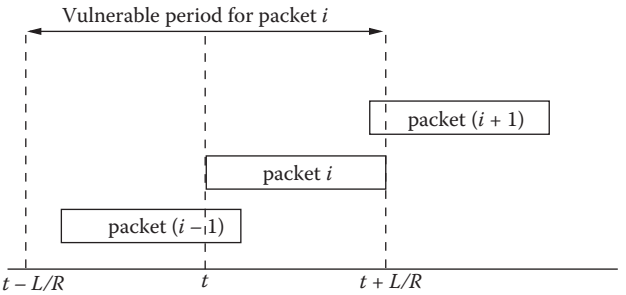

FIGURE 31.2 Vulnerable period in pure Aloha protocol. For successful transmission of packet i, no other packet can be transmitted within the period starting $T = L/R$ seconds before packet i and during its transmission.

* According to a Poisson distribution, the probability of i arrivals in T seconds is given by $((\lambda T)^i e^{-\lambda T})/i!$, in which λ is the arrival rate of the process [2].

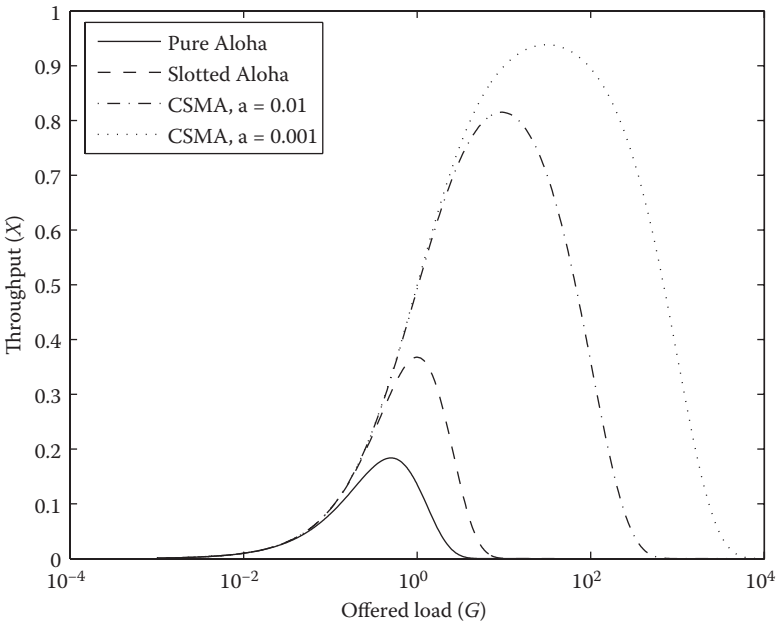

FIGURE 31.3 Throughput as a function of the offered load (G).

Figure 31.3 shows the behavior of X as a function of the offered load. Taking the derivative of X with respect to G and making it equal to zero, one will find that the maximum throughput value is approximately 0.18 attained for $G = 0.5$, which means that the maximum throughput can be attained if on average at every 2T seconds one packet is transmitted. If $G < 0.5$ then the throughput of the system is decreased due to dominance of the idle periods, while if $G > 0.5$ the throughput is reduced due to the large number of collisions. As Figure 31.3 demonstrates, ALOHA only achieves 18% of the maximum throughput which is a very-low-performance result. A modification proposed to the pure Aloha protocol was called slotted Aloha which double the maximum throughput attained as explained in the next section.

31.2.3 Slotted Aloha

In this approach to multiple access, time is divided into slots of fixed size. The duration of slots equals the packet duration which is $T = L/R$ in which L is the length of the packet and R is the transmission rate. The objective of the slotted Aloha protocol [3] was to reduce the probability of collisions by forcing all stations to transmit only at the beginning of time slots. Accordingly, the vulnerable period of slotted Aloha is reduced to T.

Stations are synchronized. If a station has a packet to transmit, it does so at the beginning of the next slot. If a collision takes place,* the source node retransmits the packet at the next slot with probability p. It repeats this procedure until a successful transmission occurs.

The throughput analysis of slotted Aloha is obtained by observing that the vulnerable period is now reduced to a slot duration time T. All packets are assumed to be synchronized and only allowed to transmit at the beginning of a slot. Analogous to the pure Aloha analysis, the throughput of slotted Aloha is derived as [3]

* It is assumed that a feedback from receiver notifies the nodes involved in a collision.

$$
\begin{aligned}
X &= G \times P\{\text{no collision}\} = G \times P\{\text{zero arrivals (i.e., transmissions) in } T \text{ seconds}\},\\
&= G\frac{(G)^0 e^{-G}}{0!},\\
&= Ge^{-G}.
\end{aligned} \tag{31.2}
$$

Figure 31.3 presents the behavior of the throughput of the slotted aloha the maximum value of which is approximately 0.36 at load $G = 1$. By comparing the behavior, it is clear that the slotted Aloha attains twice the maximum throughput value of the pure Aloha. The increase in performance was obtained by reducing the vulnerable period at the cost of synchronization.

31.2.4 Aloha with Random Backoff

Some wireless communication environments like underwater has different characteristics in which the electromagnetic waves are rapidly attenuated due to energy consumption along the propagation path. In such scenarios, the transmission of acoustic waves is more appropriate. Although the acoustic channel has low-speed propagation, it can reach up to 5 km employing frequencies around 50 KHz resulting in transmission rate of the order of 5 kbps [4]. In such cases, a modified Aloha protocol was proposed which can readily be incorporated into the off-the-shelf commercial modems [5].

In Aloha protocol with random backoff [6], each node employs a parameter CW representing a contention window size. The backoff time is divided into slotted time of size τ which should be long enough to obtain channel state information. If a node has a packet for transmission, for example, from application running in upper layers, the node randomly selects a slot in the range [0,CW-1] and decrements its timer if there is no activity on the channel. Accordingly, nodes infer the channel use, if busy or idle, every slot boundary and pause their timers if a packet is being transmitted on the channel, that is, if the channel is determined busy. When the time reaches zero, the node transmits its packet.

In [6], it was shown that Aloha with random backoff is a suitable MAC protocol for underwater communication channel.

31.2.5 The CSMA Protocol

The low performance of ALOHA protocol is due to the large vulnerability period of a packet. In CSMA [7], the stations listen to the channel before transmissions in order to reduce the vulnerability period from the order of a packet length to the maximum channel propagation duration delay (τ). Consequently, the improvement obtained from this approach is based on the fact that τ is assumed much smaller than a packet duration length. By listening before transmission, stations try to reduce the vulnerability period to one propagation delay period. The time required to detect the carrier is negligible. In such an approach, if no other node transmits during τ, the sensing station realizes that the medium is free and captures the channel avoiding collision as no other station will transmit thereafter. Depending on the behavior of the stations when it senses that the medium is busy, there are three possibilities (variants) of the CSMA protocol: nonpersistent, 1-persistent, and p-persistent. Another variation is further obtained if slotted time is used by synchronizing all stations in the network resulting in the slotted CSMA. When a packet is received successfully, the receiver sends and acknowledges (ACK) the packet to the transmitter in order to confirm the delivery of the information.

31.2.6 1-Persistent CSMA

The 1-persistent CSMA protocol is the simplest approach to carrier sensing. In such a protocol, the station keeps listening and transmits as long as the channel is sensed free. If a collision takes place the stations involved in the collision run a backoff algorithm and postpones the next attempt to access the

channel. Accordingly, if there is more than one node listening to the channel with packets to transmit, a collision will certainly take place because these stations will transmit simultaneously into the channel as long as the medium is idle. Indeed, this variant of the CSMA protocol presents high collision rate due to its greedy nature to capture the channel.

31.2.7 Nonpersistent CSMA

In nonpersistent CSMA protocol, if the medium is sensed busy, the station waits a random time (running a backoff algorithm) and try again. In Figure 31.4, a flowchart of the protocol is presented.

In [7], it is shown that the throughput performance of the nonpersistent CSMA is given by

$$X = \frac{Ge^{-aG}}{(1 + 2a)G + e^{-aG}}, \tag{31.3}$$

where $G = \lambda T$, $a = \tau/T$ and λ is the average arrival rate of packets according to a Poisson process as explained in Section 31.2.2.

Figure 31.4 presents the behavior of the nonpersistent CSMA, which shows the improvement in performance of the wireless medium access protocol due to carrier sensing when compared with Aloha cases. It is clear that carrier sensing improves significantly the throughput behavior of random wireless medium access networks. Furthermore, the lower is the ratio between maximum propagation delay and packet length, that is, $a = \tau/L$, the better is the maximum throughput performance of the CSMA protocol.

31.2.8 *p*-Persistent CSMA

In the *p*-persistent CSMA protocol, if the medium is sensed free, the station transmits with probability p and waits with probability $1 - p$ for a backoff time to try again later. Such an approach tries to attain a balance between the 1-persistent and the nonpersistent cases.

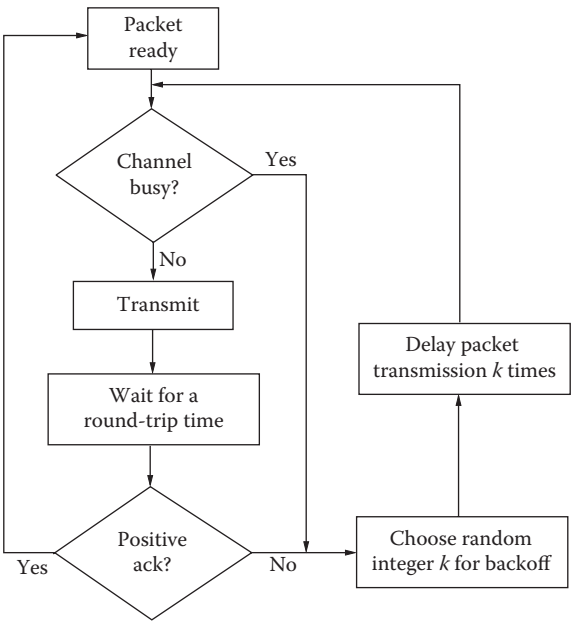

FIGURE 31.4 Flowchart for nonpersistent CSMA protocol.

31.2.8.1 Slotted CSMA

Another variation of the CSMA protocol is to consider the nodes synchronized where sensing is performed at the beginning of a slot which has the maximum propagation delay τ.

31.2.9 CSMA/CA Protocol

Another very important wireless network protocol implemented in the IEEE 802.11 standard [8] is the carrier sense multiple access with collision avoidance (CSMA/CA). This protocol has two modes of operation.

In the first mode, if a station has a packet to transmit, it first senses the channel. If the channel is idle, it transmits its packet. Otherwise, the station will back off by choosing a random integer to decrement every time it senses the channel is free. If the node perceives the channel busy, the counter value stays frozen. When the counter reaches zero, the station transmits the data packet and waits for the acknowledgment. If the ACK is not received, the sender runs the backoff algorithm again.

In the second mode of operation, the CSMA/CA tries to reserve the channel before transmission. The reservation is accomplished by an exchange of short control packets before data packet transmission with CSMA. Figure 31.5 illustrates packet exchange between nodes A and B. If a source node A has a data packet to transmit, it tries first to negotiate with the intended receiver (node B) to reserve the channel by sending a request-to-send (RTS) control packet. This packet carries the information (duration field) of how long the other stations (nodes C and D) have to be silent until the end of communication between nodes A and B. This packet has two objectives: first, it warns the nearby nodes of the transmitter that the source node wants to send a data packet; second, it informs the intended receiver to do the same with its neighbors. Accordingly, if the RTS is successfully received at the destination station, it replies by sending a clear-to-send (CTS) control packet informing the duration field in order to warn nearby stations who did not hear the RTS packet* that destination is going to receive a data packet such that the destination's neighbors keep silent during the entire communication period. Once the CTS is received by the sender, it transmits the data packet which has length much higher than the RTS/CTS control packets. After the destination successfully receives the data packets, it replies to the sender by transmitting an ACK packet and the communication procedure for this packet is completed. The other

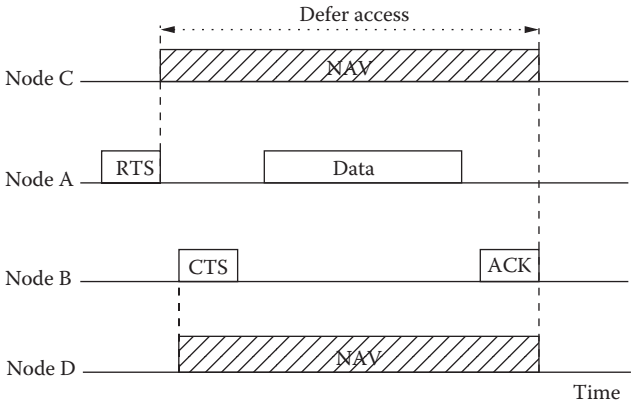

FIGURE 31.5 Virtual channel detection in CSMA/CA protocol. Node C is close to node A, but does not hear node B, while node D is near node B but does not hear node A. RTS/CTS exchange reserves the channel before transmission of a data packet.

* The stations that are within the communication range of the destination node but are outside the transmission range of the sender are called the hidden nodes to the transmitter (see Section 1.1).

stations detecting the duration field adjust their network allocation vector (NAV) to indicate the amount of time the current communication will take place characterizing a virtual channel occupation.

31.3 Routing Protocols

To send information from a source node to a destination node through multihop links by implementing one of the above MAC protocols, routing algorithms were proposed which take into consideration the dynamic nature of wireless networks. This section described four important multihop routing protocols: dynamic source routing (DSR), *ad-hoc* on-demand distance vector (AODV), optimized link state routing (OLSR), and destination-sequenced distance vector (DSDV). DSR and AODV are on-demand (or proactive) routing protocols whereas OLSR and DSDV are classified as table-driven protocols.

31.3.1 *Ad-Hoc* On-Demand Distance Vector Routing

The *ad-hoc* on-demand distance vector (AODV) routing protocol enables dynamic, self-starting, multihop routing between participating mobile nodes wishing to establish and maintain an *ad-hoc* network [9]. The AODV algorithm allows mobile nodes to quickly obtain routes for new destinations, and it does not require nodes to maintain routes to destinations that are not in active communication. Also, AODV routing permits mobile nodes to respond to link breakages and changes in network topology in a timely manner. The main objective of this protocol is to rapidly and dynamically adapt itself to changes of conditions in the network links, for example, due to mobility of nodes.

The AODV protocol works as a pure on-demand route acquisition system. When a source node desires to send a message to some destination node and does not already have a valid route to that destination, it initiates a path discovery process to locate the other node. It broadcasts a route request (RREQ) control packet to its neighbors, which then the first neighbors forward the request to their neighbors, and the RREQ broadcast will continue until either the destination or an intermediate node with a "fresh enough" route to the destination is located.

The AODV protocol utilizes destination sequence numbers to ensure that all routes contain the most recent route information. Each node maintains its own sequence number. During the process of forwarding the RREQ, intermediate nodes record in their routing tables the address of the neighbor from which the first copy of the broadcast packet is received, thereby establishing a reverse path. Once the RREQ reaches the destination or an intermediate node with a fresh-enough route to destination, the destination or the intermediate node responds by unicasting a route reply (RREP) control packet back to the neighbor from which it first received the RREQ which establishes the route path.

31.3.1.1 Route Recovery

The AODV protocol employs a neighbor detection mechanism responsible for checking periodically the connectivity between neighbors that keeps a link on an active route. The connectivity is obtained by a node sending local broadcast messages to its one-hop neighbors, called HELLO messages or beacons. When receiving a request HELLO message, the neighbor on a route replies to the sender with information about that route. If a node does not receive a HELLO message from a neighbor on a route during a certain time, it infers that a link breakage occurred.

An active route is defined as a route which has recently been used to transmit data packets. If a link break occurs while the route is active, the node upstream of the break propagates a route error (RERR) message to the source node to inform it of the now unreachable destination. After receiving the RERR, if the source node still desires the route, it can reinitiate route discovery.

Alternatively, the algorithm may initiate a local repair mechanism when a link failure takes place on an active route and the first node upstream of that break (the predecessor) chooses to repair the link locally if the destination is not too far away. In such cases, the node increments the sequence numbers for the destination and then broadcasts an RREQ for that destination. Thus, local repair attempts will

often be invisible to the source node. The node that initiates the repair waits the discovery period to receive RREP in response to the RREQ. During local repair, data packets should be buffered. If, at the end of the discovery period, the repairing node has not received an RREP (or other control message creating or updating the route) for that destination, the node propagates an RERR. When it happens, long delays and huge losses of packets due to exhaustion of the queues will occur. However, if the repairing node receives an RREP, it ensures lower overhead and delay.

In the approach currently implemented on the AODV protocol, it chooses to do either source repair or local repair depending on the number of hops involved on the path. Note that the choice holds following the condition depicted in Algorithm 1, where *packetForward* is the number of hops from the source node until the upstream node (i.e., the predecessor) before the failure and *predecessorHopCount* is the number of hops from the predecessor node to destination which information is stored in the routing table of the predecessor node. If *packetForward* has more hops than *predecessorHopCount*, the algorithm chooses to make local repair, otherwise the upstream node sends an RERR to the source.

Algorithm 1:

```
1. if (packetForward ≥ predecessorHopCount) then
2. | localRepair();
3. end
4. else
5. | sourceRepair();
6. end
```

Summarizing, the main disadvantage of this protocol is the necessity of periodically sending beacon control packets, whereas the main advantage is the protocol adaptability to changes and being able to locally recover from link failure which makes it particularly appropriate for mobile *ad-hoc* networks.

31.3.2 Dynamic Source Routing Protocol

Dynamic source routing (DSR) is an on-demand routing protocol [10] designed for mobile *ad-hoc* networks with a simple and efficient approach composed of two main mechanisms: *route discovery* and *route maintenance*, which together allow nodes to, respectively, ascertain and preserve routes to arbitrary destinations in the network. The protocol works well of up to approximately 200 nodes even with very high rates of mobility. Another important characteristic of DSR is that it does not require periodic messages (like HELLO messages or beacons as in AODV or table-driven protocols). DSR is loop-free, admits multiple routes to destinations, and allows each sender to select and control the routes used in routing its packets, for example, for use in load balancing or for increased robustness.

DSR employs the source routing feature in which the entire route is part of the header of the packet and utilizes caches to store routes on nodes. Consequently, if a node A needs to send a packet to another node B, but it does not have a route to B, then node A initiates a route discovery and broadcasts (floods) an RREQ message. The RREQ packet contains the sender's address, the destinations address, and a unique request identification (ID) determined by sender A. Each node that receives the RREQ message, appends its own identifier (ID), and forwards the updated RREQ. Eventually, an RREQ will reach the destination node with complete reverse path to source which allows the destination to unicast an RREP back to the source establishing the route. After that, the source can unicast the data packet to destination in which the packet header contains the entire path to destination being forwarded by each node along the route.

The main disadvantages of this protocol are that it cannot repair a broken link locally as the AODV protocol does and that overhead of control packets increases with average number of hops in the network.

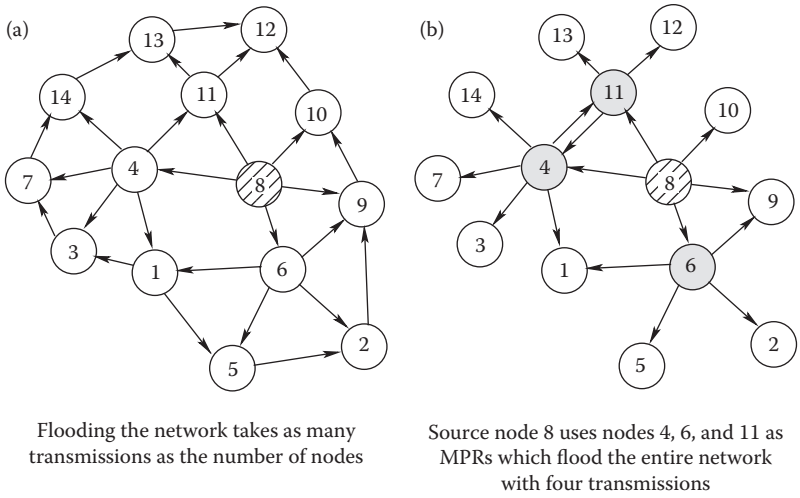

FIGURE 31.6 (a) Classical flooding. (b) OLSR routing protocol employs multipoint relays to reduce the amount of transmissions to flood the entire network.

31.3.3 Optimized Link State Routing Protocol

The optimized link state routing (OLSR) protocol [11] is an optimization of the classical link state algorithm [12] suited to mobile wireless applications. It is a proactive routing using the multipoint relaying mechanism which is an efficient link state packet forwarding scheme. Optimization is attained by reducing the overhead control information by shortening the length of the control packets and by reduction of the amount of links employed to forwarding the link state control packets through the entire network. Accordingly, multipoint relays (MPRs) are the nodes responsible to forward the broadcast control messages due to the flooding process necessary to disseminate the link state information. Differently from the classical link state routing algorithm in which the state information is flooded through all nodes of the network, in OLSR scheme only partial link state information is distributed in the network seeking to attain a minimum number of transmissions of control messages but still reaching all nodes in the network. Figure 31.6 illustrates such behavior for a network with 14 nodes in which node 8 is the source node sending its link state information. In part (a), in classical flooding, all nodes participate in forwarding the message from the source, that is, the number of control messages are of the order of the number of nodes in the network. However, in part (b), with OLSR, only three nodes are selected as MPRs to forward the control messages reducing the amount of broadcast transmissions needed to flood the entire network. This information is then used for route calculation. OLSR provides optimal routes (in terms of number of hops). The protocol is particularly suitable for large and dense networks as the technique of MPRs works well in this context.

The main advantage of the OLSR protocol is the reduction of routing overhead compared to other table-driven protocols; however, it is still a table-driven protocol which needs to periodically send control messages through the network to maintain link state update.

31.3.4 Destination Sequenced Distance-Vector Protocol

The destination sequenced distance-vector (DSDV) protocol was one of the first routing mechanisms proposed for *ad-hoc* networks [13]. It is proactive and based on the distributed Bellman–Ford algorithm proposed to wired networks [14] which considers the shortest path routing to destination. In DSDV,

each node maintains a hop count for each destination and periodically sends their routing tables to neighbors which recalculate shortest path upon the receipt of a routing table update. Accordingly, routes to all destinations are promptly available at each node at all times. When a broken link is detected by a node, it propagates this information to its neighbors such that this information is updated throughout the whole network. Hence, a small change like a single break results in the table update information to be disseminated to the entire network. There are two types of updates: incremental updates and full dumps. The former is used when a node does not observe significant changes in the local topology and the update carries only information changed since last full dump. The latter, full dump, is employed if significant changes in topology is observed and the message conveys all routing table information.

Each entry in the routing table and routing updates is tagged with a sequence number generated by the destination. The destination sequenced number allows identification of stale routes and ensures loop-free operation. In such an approach, routing table entries are updated if a new sequence number is observed. If two or more updates contain the same sequenced number, the node chooses the other with better route metric. In order to reduce the dissemination information convergence, a weighted settling time is used to control the frequency of new advertisements for a route. Consequently, routing availability to all destinations at all times ensures that small delay is obtained in the route establishment process.

Summarizing the DSDV advantages and disadvantages, it is a protocol with lower route request latency, but higher overhead. It performs best in networks with low-to-moderate mobility, few nodes and many data sessions. The main problem is poor efficiency for large *ad-hoc* networks in which nodes need to maintain a complete list of destination routes.

31.4 Summary and Conclusion

Wireless networks are characterized by a broadcast access medium that should be appropriately shared among nodes trying to communicate. Furthermore, in infrastructureless scenarios, the channel access and information forwarding tasks must be distributed among the nodes themselves to make communication feasible among nodes separated by multiple hops. Such networks are classified as *ad-hoc* networks.

Aloha and CSMA with their variants were presented for medium access in which it was shown that CSMA has better performance than Aloha, due to fact that in CSMA carrier sense before transmission is essential in order to reduce the occurrence of collision.

This chapter also presents four important routing schemes proposed for wireless *ad-hoc* networks that try to make the relaying of messages from source to destination an efficient procedure even under the situation of mobility which can cause constant topology changes. Two table-driven routing protocols, DSDV and OLSR, were described which provided nodes with routes to their destinations in the network. These two protocols have high overhead in terms of exchange of control messages in order to keep table entries updated. On the other hand, two reactive routing protocols, AODV and DSR, were reviewed where it was reported that routes are obtained on demand, that is, paths to destinations are obtained upon sources requests causing a smaller control message overhead while requiring longer setup time to establish the route when compared with proactive protocols.

References

1. N. Abramson, The ALOHA system: Another alternative for computer communications. *Proceedings of Fall Joint Computer Conference*, Houston, TX, USA, November 1970.
2. A. Papoulis and S. U. Pillai, *Probability, Random Variables and Stochastic Processes*, McGraw-Hill, Inc., Boston, 2002.
3. L. G. Roberts, ALOHA packet system with and without slots and capture. *Computer Communications Review*, 5(2), 28–42, 1975.
4. M. Stojanovic, On the relationship between capacity and distance in an underwater acoustic communication channel. *Proceedings of ACM WUWNet*, September 2006.

5. L. Freitag, M. Johnson, M. Grund, S. Singh, and J. Priesig, Integrated acoustic communication and navigation for multiple uuvs, *Proceedings of IEEE OCEANS*, November 2001.
6. N. Parrish, L. Tracy, S. Roy, P. Arabshahi, and W. L. J. Fox, System design considerations for undersea networks: Link and multiple access protocols. *IEEE Journal on Selected Areas in Communications*, 26(9), 1720–1730, 2009.
7. L. Kleinrock and F. Tobagi, Packet switch in radio channels: Part I–carrier sense multiple access modes and their throughput-delay characteristics. *IEEE Transactions on Communications*, 23(12), 1400–1416, 1975.
8. IEEE Standard for wireless LAN medium access control (MAC) and physical layer (PHY) specifications, 1999.
9. C. E. Perkins, E. M. Belding-Royer, and S. R. Das, Ad hoc on-demand distance vector routing. *Request for Comments*, 3561, July 2003.
10. D. Johnson, Y. Hu, and D. Maltz, The dynamic source routing protocol (DSR) for mobile ad hoc networks for IPv4. *Request for Comments*, 4728, February, 2007.
11. T. Clausen and P. Jacquet, Optimized link state routing protocol (OLSR), *Request for Comments*, 3626, October 2003.
12. J. M. McQuillan, I. Richer, and E. C. Rosen, The new routing algorithm for the ARPANet. *IEEE Transactions on Communications*, 28(5), 711–719, 1980.
13. C. E. Perkins and P. Bhagwat, Highly dynamic destination-sequenced distance-vector routing (DSDV) for mobile computers. *Proceedings of ACM SIGCOMM*, August 1994.
14. C. Hedrick, Routing information protocol. *Request for Comments*, 1058, June 1988.

Further Reading

Readers interested in wireless *ad hoc* network protocols are recommended the following overview books:

C. S. R. Murthy and B. S. Manoj, *Ad Hoc Wireless Networks Architectures and Protocols*. Prentice-Hall, 2004.

P. Mohapatra and S. Krishnamurthy, *Ad Hoc Networks: Technologies and Protocols*. Springer, 2010.

More information on this topic can be found in *IEEE Transactions on Communications, IEEE Transactions on Wireless Communications, IEEE Transactions on Vehicular Technology, Elsevier Ad Hoc Networks*, and issues of *IEEE Journal on Selected Areas in Communications* covering wireless ad hoc networks.

32

Cross-Layer Design in Wireless Communications

Sayantan Choudhury

Jerry D. Gibson

32.1 Introduction

Wireless communication has become ubiquitous in the last two decades and has challenged modern communication system designers to innovate rapidly to meet the challenges of transmitting signal efficiently in a wireless medium. There has been outstanding progress in technology in all layers of the communication protocol stack from robust coding and physical layer transmission, more efficient medium access control (MAC) protocol design both from a throughput and from an energy standpoint, rethinking of the transport layer and routing in mobile ad hoc networks and also development of new application layer concepts that exploit the knowledge of the lower layers. This has caused wireless system engineers to rethink the traditional protocol stack designed for wire line communications and instead investigate cross-layer design approaches that can exploit the information across various layers. Cross-layer design relies on advances in signal processing, information theory and wireless networking. In this chapter, we try to highlight the use of cross-layer design for a few selected scenarios including wireless local area networks (WLAN) and cellular transmissions. We also provide some insight into the challenges faced by a cross-layer design approach.

32.2 Fundamentals of Cross-Layer Design/Architecture

The increased demand for real-time traffic such as voice, video, and data-traffic has challenged wireless engineers to design more efficient wireless networks. The goal from a system engineering point of view has been to build a wireless network where the user has a perceived quality close to a wireline network [1]. There has been tremendous development in standardization efforts including WLANs and cellular standards including the completion of Long-Term Evolution (LTE) Release 8–10. Apart from the signification developments in the individual layers of the protocol stack including physical and MAC layer transmission, a significant amount of research has been done investigating new wireless transmission architectures using cross-layer design.

Traditional communication networks were based on the layered Open Systems Interconnection (OSI) reference model (reference) shown in Figure 32.1a. A simplification of the modern internet architecture employing the TCP/IP model is shown in Figure 32.1b. The importance of well-designed network architecture cannot be overemphasized [2]. Layered architecture simplifies the network design and it is easier to develop and manage each of the individual elements of the protocol stack independently. In the layered architecture, there is typically communication only across the layers adjacent to a given layer. The physical layer provides an interface for transmission of information over a transmission medium (wired or wireless), the data link layer provides reliability to the transmission by handling acknowledgments and retransmissions, the network layer implements the routing of the packets including the most optimum paths a packet should take from source to destination and also handles congestion, the transport layer provides a higher-layer reliability mechanism ensuring the delivery of error-free data that are in sequence to the upper layers. The application, presentation, and session layers have various functions including data formatting, compression, encryption, initiating logical channels and various management functions required by different applications. An overview of the OSI reference model can be found in [3]. As mentioned earlier, having a clear distinction

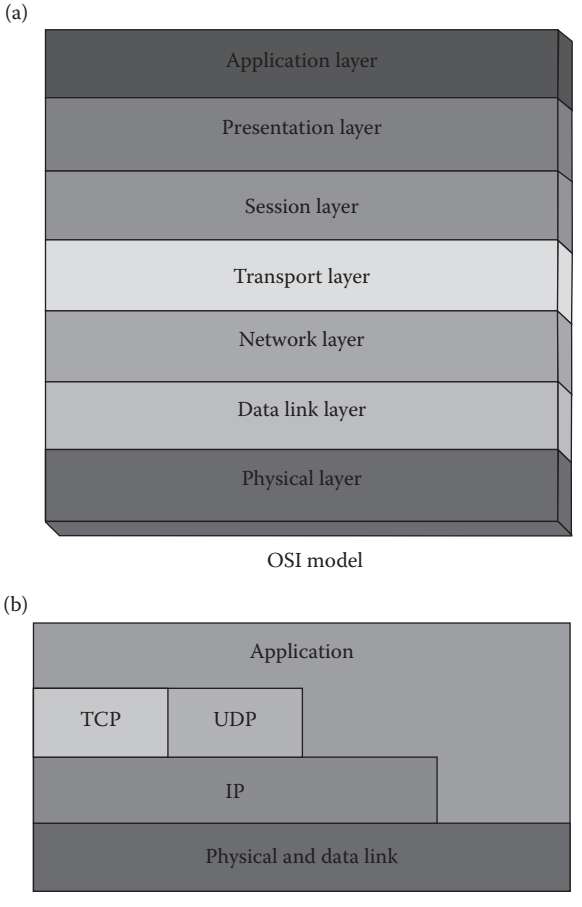

FIGURE 32.1 (a) Layered OSI architecture and (b) TCP/IP model.

between the layers enables a system designer to concentrate on individual layers and optimize them individually.

Wireless networks bring some unique challenges typically not encountered in a wireline network [4]. For instance, wireless channels vary over time and space due to multipath effects resulting in fading signals. Furthermore, propagation losses (including shadow fading caused by obstacles) and mobility cause the wireless signals to vary depending on the location of the users. Moreover, wireless channels being a broadcast medium are also susceptible to interference caused by neighboring transmissions. Finally, wireless networks have a scarcity of spectrum resource making the problems even more challenging. These challenges caused by wireless transmissions have caused researchers and system designers to rethink the traditional OSI architecture with the aim of developing newer architectures capable of optimizing across the protocol stacks.

An excellent survey on the different architectural designs is provided in Reference 5. Here, we summarize some of the essential concepts.

Figure 32.2 shows some of the different kinds of cross-layer design proposals. Traditional network architectures usually allow for interaction across adjacent layers only. In order to overcome this limitation, there have been proposals to create new interfaces that allow communication across nonadjacent layers as shown in Figures 32.2a–c. There have also been proposals to merge adjacent layers (Figure 32.2d), introducing coupling across layers (Figure 32.2e) and also for vertical calibration across layers (Figure 32.2f). Based on the various design proposals, some new architectural proposals that can be implemented in future wireless networks are shown in Figure 32.3, including direct communication between different layers, a shared database concept that allows different layers to share information and finally, developing completely new abstractions that allow rich interactions across the layers. In the next section, we show possible benefits of some of the proposed architecture with examples from WLAN,

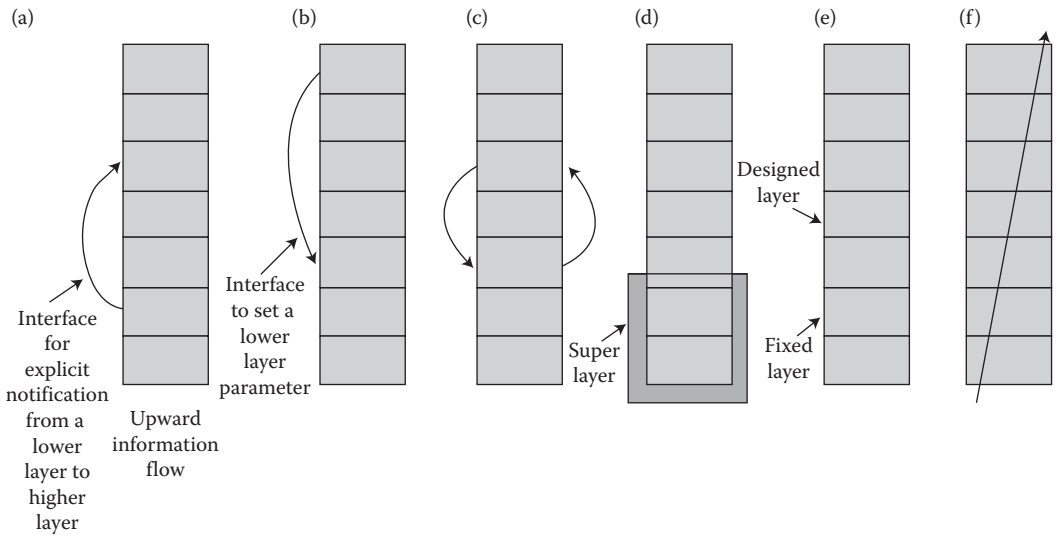

FIGURE 32.2 Different kinds of cross-layer design proposals: (a) Upward information flow, (b) downward information flow, (c) back-and-forth information flow, (d) merging of adjacent layers, (e) design coupling without new interfaces. The designed layer's design is done keeping in mind the processing at the fixed layer, but no new interface is created, and (f) vertical calibration. (Adapted from V. Srivastava, and M. Motani, *IEEE Communications Magazine*, 43(12), 112–119, 2005.)

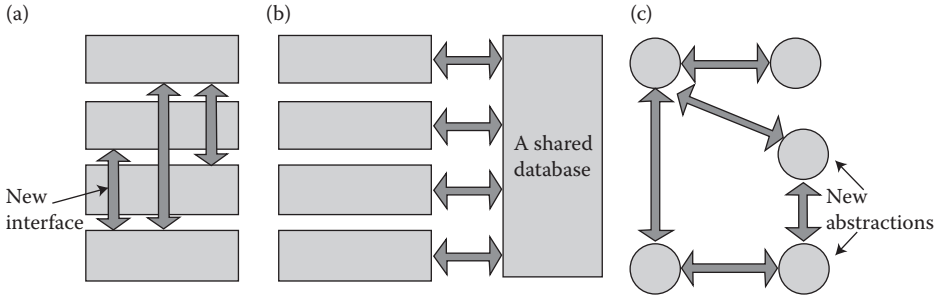

FIGURE 32.3 Some possible wireless communication architectures: (a) Direct communication between the different layers, (b) a shared database, and (c) completely new abstractions (no more protocol layers). (Adapted from V. Srivastava, and M. Motani, *IEEE Communications Magazine*, 43(12), 112–119, 2005.)

cellular and also future wireless networks including cognitive radios. In Section 32.4, we also highlight some of the challenges faced by these new cross-layer approaches.

32.3 Applications of Cross-Layer Design to Wireless Networks

In this section, we review some case studies showing the benefits of cross-layer design principles in wireless networks including WLAN, cellular, and cognitive networks. We also try to show how the different cross-layer techniques can be implemented based on the architectural design principles mentioned in the previous section.

32.3.1 Multimedia Transmission over WLANs

Multimedia transmission over WLANs is quite challenging due to the different quality-of-service (QoS) requirements of different applications. For instance, voice and video traffic have tighter delay constraints while being somewhat more error tolerant compared to data traffic. Hence, depending on the application and usage scenario, there are different optimization metrics that can be used, for example, minimizing delay, maximizing throughput, minimizing energy, and so on. This compounded by the fact that wireless channel undergoes large- and small-scale fading and observed interference at the receiver makes multimedia transmission over WLAN quite challenging. Here, we sample some of the cross-layer approaches mentioned in the research literature that relies on the interactions between the physical, medium access control (MAC) and application layers.

Various design parameters can be optimized depending on the application and usage scenario. For instance, for voice and video traffic, the modulation and coding schemes could be adapted in the physical layer, the number of retransmissions and payload length in the MAC layer, the codec parameters and the application frame sizes in the application layer. We demonstrate the parameter interplay with an example of multimedia transmission over 802.11a network [6–9].

Table 32.1 shows the different modulation and coding rates that can be used for 802.11a transmissions. Depending on the channel condition, the transmitter can dynamically vary the transmission rates by using a different modulation and coding scheme. For instance, at lower signal-to-noise (SNR) ratio, the transmitter uses more robust modulation and coding scheme for example, use a low transmission rate 6Mbps (BPSK with rate 1/2code) while at higher SNRs, it can use a more aggressive transmission rate, for example, 54 Mbps (64 QAM with rate 3/4). Figures 32.4 and 32.5 show the payload headers and protocol overhead encountered during a packet transmission that result in additional overhead during data transmission.

TABLE 32.1 Different Modulation and Coding Rates in IEEE 802.11a Transmission

Data Rate (Mbits/s)	Modulation	Coding Rate (R)	Coded bits/ Subcarrier	Coded Bits/ OFDM Symbol	Data Bits/OFDM Symbol
6	BPSK	1/2	1	48	24
9	BPSK	3/4	1	48	36
12	QPSK	1/2	2	96	48
18	QPSK	3/4	2	96	72
24	16-QAM	1/2	4	192	96
36	16-QAM	3/4	4	192	144
48	64-QAM	2/3	6	288	192
54	64-QAM	3/4	6	288	216

In Reference 6, a cross-layer design approach was proposed that dynamically adapts the PHY transmission rate and payload length depending on the channel conditions in order to maximize the effective throughput. The challenge involving rate and payload selection is that lower rates and smaller payloads are more robust while being inefficient since the MAC and protocol headers become quite large while larger payloads and more aggressive PHY rates reduce the header overhead but can lead to retransmissions in case they cannot be decoded correctly in the first transmission attempt. Hence, in Reference 6, a theoretical model was developed in order to maximize throughput by appropriate payload and rate selection. In Reference 7, the model was extended to incorporate a packet error rate constraint since employing larger payloads might lead to higher error rate in poor channel conditions. In Reference 8, the effect of retransmissions was considered and it was observed that by changing the

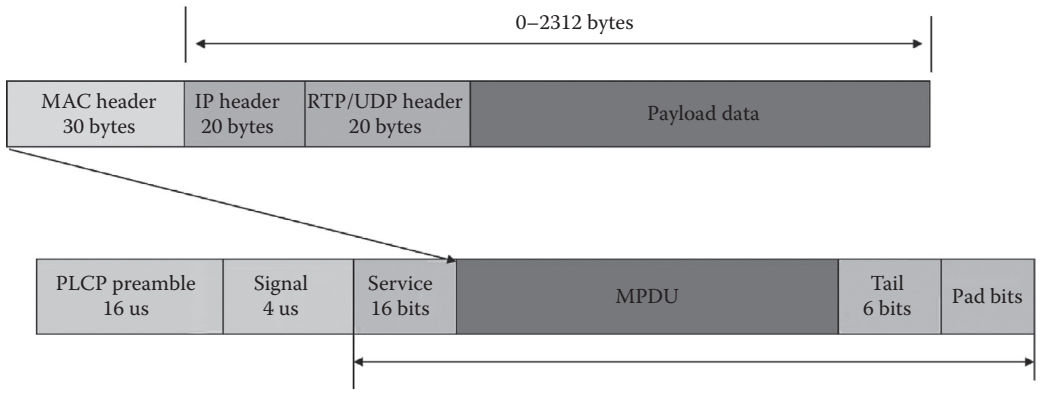

FIGURE 32.4 Payload headers in OFDM based 802.11a/g transmission.

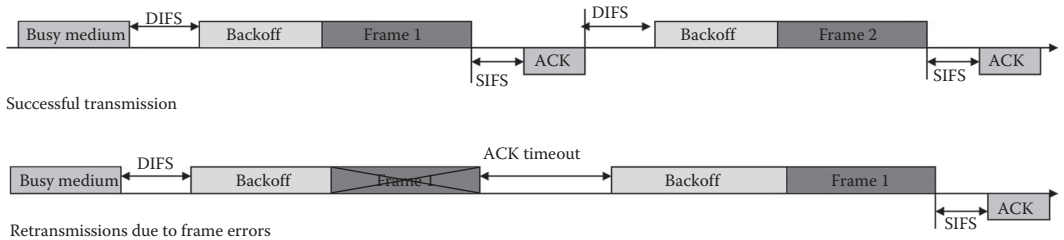

FIGURE 32.5 Protocol overhead in 802.11.

maximum retransmission threshold value, different mix of data and multimedia traffic could be adapted.

There has also been a lot of work on cross-layer design approaches that exploit the application characteristics. In Reference 9, the authors investigated the video user capacity of wireless networks subject to a multiuser perceptual quality constraint. Different parameters were studied including application layer parameters such as quantization parameter, group of picture size along with the PHY/MAC parameters, for example, payload size and data rate in order to optimize the delivered video quality based on a perceptual quality metric. Similar studies were also conducted for voice traffic in Reference 10. For the voice traffic studies, different codecs were also evaluated namely, G.729 and G.722 voice codec that have varying payload sizes and different concealment properties in order to evaluate the voice quality constrained capacity under different fading scenarios. Additional references on multimedia transmission over wireless networks can be obtained in Reference 11.

In the previous discussions, we have provided a few examples of the possible benefits of a cross-layer design approach for multimedia transmission over wireless LANs. Furthermore, the architectural framework that needs to be developed to allow such cross-layer interactions is consistent with the ones shown in Figure 32.3. In particular, either the shared database approach or the direct communication across the physical, MAC, and application layers could be employed.

32.3.2 Cross-Layer Design in OFDMA Networks

The Third Generation Partnership Project (3GPP) Long-Term Evolution (LTE) standardization efforts aim at high-speed broadband cellular data access transmission schemes. In this section, we show how some of the cross-layer interactions are an integral part of LTE design philosophy mainly focusing on the MAC and PHY layers.

Figure 32.6 shows the physical and MAC layer functional blocks and its interactions with the MAC scheduler [12]. Multiple Input Multiple Output (MIMO) transmission is an integral part of LTE design and can be used for transmit diversity, spatial multiplexing, beamforming, multiuser MIMO depending on the usage scenario. Additionally, there are 16 different modulation and coding schemes that are adapted based on the channel conditions. Furthermore, there is a Hybrid Automatic Repeat Request (HARQ) transmission mechanism that can provide fast retransmissions. In Reference 13, the authors investigated the optimal MIMO mode selection (spatial multiplexing or diversity) in order to maximize proportional fairness among users. The work was extended for multiuser MIMO transmission in Reference 14.

Cross-layer optimization for OFDM wireless networks has been extensively studied in References 15 and 16. In Reference 17, the authors present a cross-layer framework for efficient resource allocation in 802.16e OFDMA system. The proposed MAC architecture separates users into two groups: diversity subchannels group for high-mobility users and band adaptive modulation and coding (AMC) group for fairly static and/or high SNR users. Furthermore, the payload length and the number of HARQ retransmissions are also adapted based on the channel conditions. It is observed that by employing a cross-layer framework, the average cell throughput can be increased by 25–65%. The cross-layer framework and MAC simulator architecture is shown in Figure 32.7.

32.3.3 Cross-Layer Design for Future Wireless Devices

In the previous sections, we have shown the benefits of cross-layer design approach in increasing the throughput and multimedia quality. In this section, we provide a brief survey on the use of cross-layer design for future wireless devices focusing on two applications: (a) energy-efficient communication and (b) cognitive devices.

The improvement of battery technology has been slow in keeping up with the increased power consumption required by newer processors [18–20]. This compounded with the fact that newer wireless devices, especially cellular devices, are increasingly supporting multiple radios causing higher

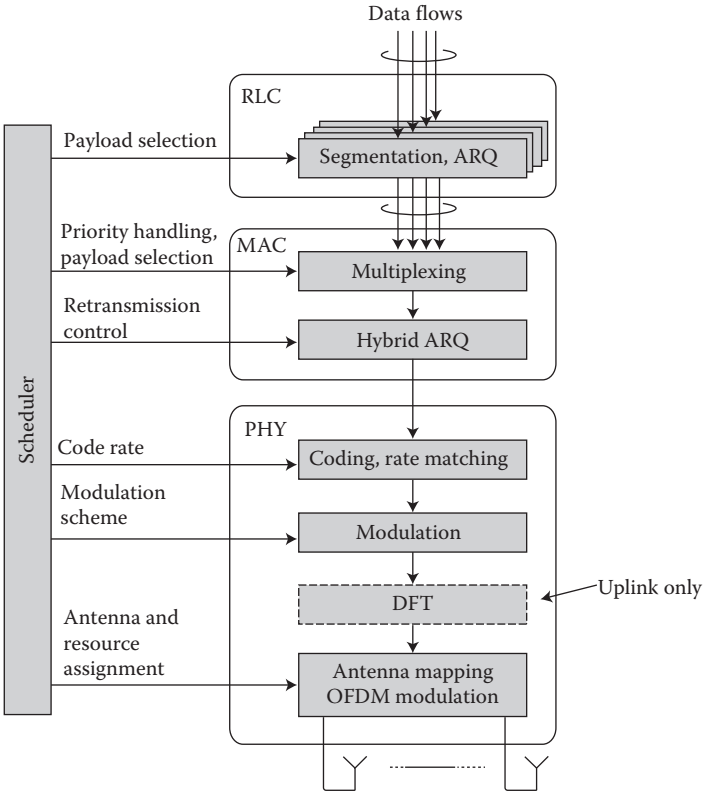

FIGURE 32.6 LTE protocol structure. (Adapted from D. Astely et al. *IEEE Communications Magazine*, 47(4), 44–51, 2009.)

energy consumption, makes cross-layer optimization for energy-efficient communication quite important. The cross-layer framework for optimizing energy is similar to what was mentioned previously for throughput optimization, that is, at the PHY-MAC layers, the modulation and coding scheme, transmit power can be adapted to minimize the energy. However, the optimal solution for energy efficient communication is very different from that obtained for throughput maximization [21]. While throughput maximization aims at selecting the most spectrally efficient modulation schemes, traditional energy-efficient transmission schemes aim at transmitting packets over a long period of time [22]. In Reference 23, it was shown that when the transmitter circuitry energy dissipation is taken into account, it might be better to use higher-order modulation especially for short-range communication. In Reference 24, it was shown that it is more energy efficient to transmit a packet over multiple shorter routes compared to one long route. This suggests that the use of relays might lead to more energy-efficient communication. However, in Reference 24, it was shown that in some situations, it might be better to use longer hops. A detailed survey on cross-layer optimization for energy-efficient communication is found in [20].

The energy efficiency based on modulation order and distance from the base station is shown in Figure 32.8 [19]. It is observed that for users near to the base station, it is better to use higher-order modulation rate while for users further from the base station, lower-order modulation is preferred. While the conclusion is quite similar in the case of traditional link adaptation algorithms, the actual data rates used for the energy-efficient algorithm are quite different as can be observed from the energy consumption for the different algorithms in Figure 32.8. The adaptive algorithms in Figure 32.8 refer to traditional adaptive modulation and coding algorithms with different fixed transmit power levels of 15,

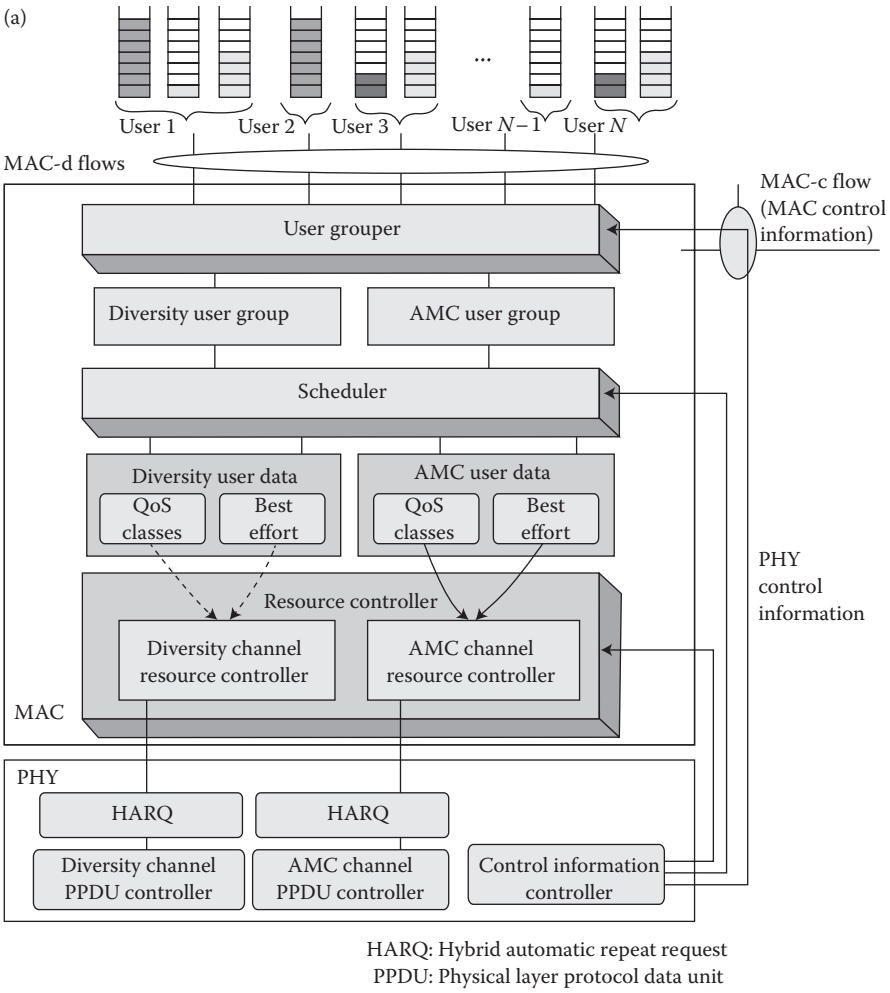

FIGURE 32.7 Cross-layer scheme and MAC architecture for OFDMA networks: (a) Cross-layer adaptation scheme and (b) MAC simulator architecture. (Adapted from T. Kwon et al. *IEEE Communications Magazine*, 43(12), 136–146, 2005.)

20, 25, or 30 dB. It is quite evident from the figure that link adaptation algorithms based on minimizing energy consumption results in much lower energy consumption than throughput maximization-based algorithms. Hence, there is a trade-off between minimizing energy efficiency and maximizing throughput and an optimal scheduler needs to take into account the battery status and the QoS requirements.

As mentioned earlier, MIMO techniques add another dimension to the cross-layer framework. It is well known that MIMO techniques can be used to increase the data rate by using spatial multiplexing of the streams or to increase robustness by employing space-time coding. However, MIMO techniques require multiple transmit and receive antennas and power amplifiers that can increase the energy consumption. A comparison of energy consumption of MIMO techniques vs. single-antenna transmission was done in [25] where it was shown that using fixed modulation, single-antenna techniques are more energy efficient compared to MIMO, especially over small distances. However, by employing adaptive modulation, MIMO transmission can be made more energy efficient over all distances. The authors also showed that by using cooperative MIMO transmission, the energy transmission and delay could be reduced over certain distances.

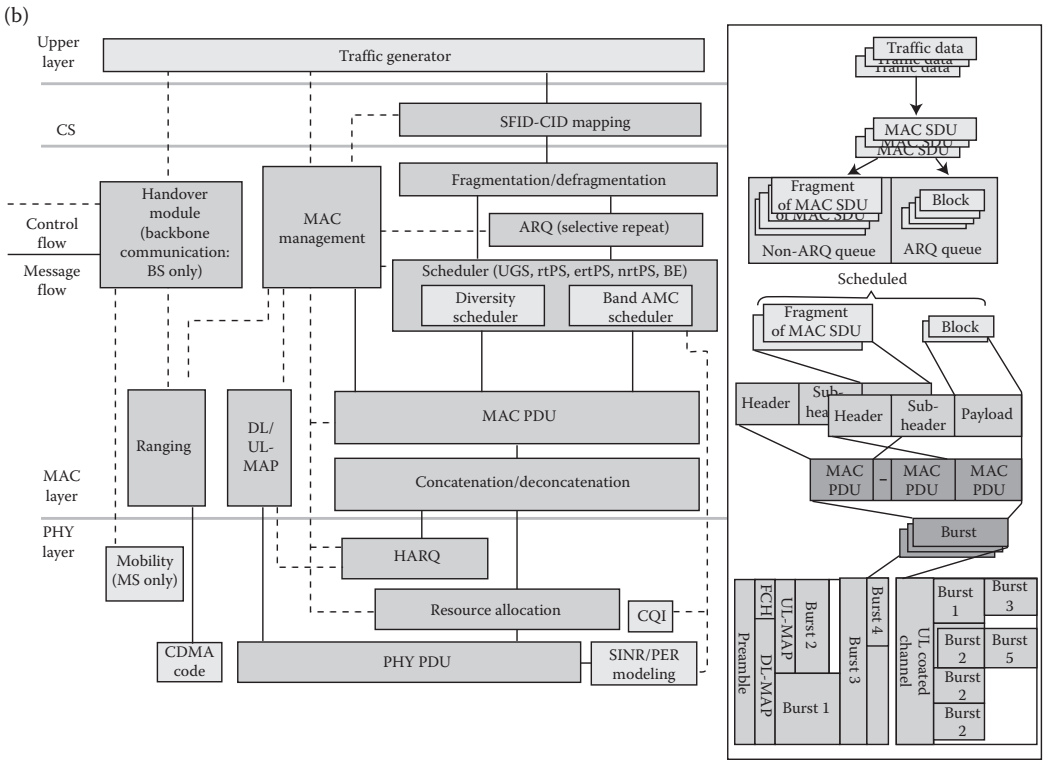

FIGURE 32.7 (Continued) Cross-layer scheme and MAC architecture for OFDMA networks: (a) Cross-layer adaptation scheme and (b) MAC simulator architecture. (Adapted from T. Kwon et al. *IEEE Communications Magazine*, 43(12), 136–146, 2005.)

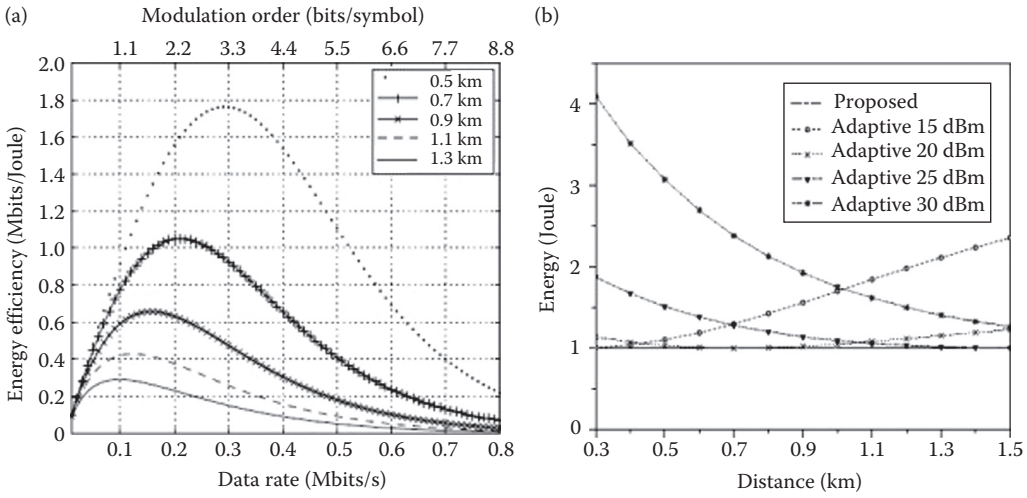

FIGURE 32.8 Link-level energy efficient transmissions: (a) relationship of energy efficiency and (b) normalized energy consumption distance, modulation, and transmission on transmitting one million bits rate. (Adapted from G. Miao et al., *IEEE International Conference on Communications*, May 2008.)

We have illustrated the importance of cross-layer design for improving throughput, robustness and energy efficiency. Another area of increasing importance for cross-layer design is in the area of cognitive radios. In cognitive networks, secondary users use the channel only when it is not occupied by a primary user and if a primary user is detected, the secondary users need to vacate the channel. The primary user can be detected using spectrum sensing or by checking with a database where the primary users are required to register before accessing the channel. Hence, there are quite significant challenges for cross-layer design in cognitive networks. Firstly, channel selection whereby secondary users decide to use an available channel is an important research area. The channel to be used is based on the channel availability, QoS requirement, transport, and routing mechanisms and thus needs an integrated cross-layer framework. Secondly, spectrum handoff is another important problem since the handoff mechanisms need to be aware of the application requirements especially latency [26].

32.4 Challenges with Cross-Layer Design

In the previous sections, we have highlighted some of the benefits of cross-layer design in wireless communications. Cross-layer design can provide throughput enhancements, improved robustness, better multimedia transmission quality and also reduce energy consumption. However, in spite of all these benefits, there are quite a few challenges when it comes to implementing cross-layer protocols. In this section, we highlight a few challenges faced by a cross-layer approach.

As discussed in References 2 and 5, the OSI architecture has made the wireless system design problem scalable since each layer could be independently designed and optimized. However, using a cross-layer approach, there are no more clear boundaries across the protocol layers. Furthermore, there is a need to define a new architecture that allows interaction across the layers. Some of the open issues raised are whether such a cross-layer approach allows coexistence across devices with possible different architecture, whether the different interactions across layers consider thoroughly the interactions across the different layers and possible negative consequences that might not have been accounted for, whether it is possible to standardize the mechanisms/interfaces to share information and also more fundamentally, whether cross-layer design stifles innovation since there might not be a unifying framework for protocol development. It has also been argued that the cross-layer approach might lead to a spaghetti-like design and stifle innovation and proliferation due to the increasing number of new interactions across layers that might lead to every update having a complete redesign and replacement of the existing designs. It was shown in Reference 2 that the interaction of a rate-adaptive MAC protocol with a minimum hop routing protocol might perform worse than a plain 802.11 MAC due to the interaction of the MAC and routing protocols. Hence, from an engineering design perspective, one should be careful to thoroughly analyze the interactions across the layers ensuring that there are no unintended side effects.

32.5 Conclusion

In this chapter, we provide a brief tutorial of the applications of cross-layer design for wireless applications. After explaining the basic concept of cross-layer framework we showed using some applications of the benefits of cross-layer approaches in current and future wireless networks. First, we discussed the benefits of the cross-layer approach for multimedia transmission over WLANs. We then explained some of the integrated cross-layer frameworks in the 3GPP LTE standard and also applications of cross-layer design in future wireless networks focusing on energy enhancements and cognitive radio. Finally, we discussed some of the challenges faced by a cross-layer approach focusing on the some of the system design aspects.

Acknowledgments

Many thanks to Dr. Klaus Doppler, Dr. Chittabrata Ghosh, and Dr. Suchandrima Banerjee for their careful review and comments.

References

1. R. Laroia, S. Uppala, and J. Li, Designing a mobile broadband wireless access network, *IEEE Signal Processing Magazine*, 21(5), 20–28, 2004.
2. V. Kawadia, and P. R. Kumar, A cautionary perspective on cross-layer design, *IEEE Wireless Communications*, 12(1), 3–11, 2005.
3. Larry L. Peterson, and Bruce S. Davie, *Computer Networks: A Systems Approach*, Morgan Kaufmann, 2007.
4. S. Shakkottai, T. S. Rappaport, and P. C. Karlsson, Cross-layer design for wireless networks, *IEEE Communications Magazine*, 41(10), 74–80, 2003.
5. V. Srivastava, and M. Motani, Cross-layer design: A survey and the road ahead, *IEEE Communications Magazine*, 43(12), 112–119, 2005.
6. S. Choudhury and J. D Gibson, Payload length and rate adaptation for multimedia communications in wireless LANs, *IEEE Journal on Selected Areas in Communications*, 25(4), 796–807, May 2007.
7. S. Choudhury and J. D. Gibson, Throughput optimization for wireless LANs in the presence of packet error rate constraints, *IEEE Communications Letters*, 12(1), 11–13, January 2008, doi: 10.1109/LCOMM.2008.071434.
8. S. Choudhury, I. Sheriff, J. D. Gibson, and E. Belding-Royer, Effect of payload length variation and retransmissions on multimedia in WLANs, *ACM International Wireless Communication and Mobile Computing Conference (IWCMC)*, Vancouver, Canada, July 3–6, 2006.
9. J. Hu, S. Choudhury, and J. D. Gibson, Video capacity of WLANs with a multiuser perceptual quality constraint, *IEEE Trans. on Multimedia*, 10(8), 1465–1478, 2008.
10. N. Shetty, S. Choudhury, and J. D. Gibson, Voice capacity under quality constraints for IEEE 802.11a based WLANs, *ACM International Wireless Communication and Mobile Computing Conference (IWCMC)*, Vancouver, Canada, July 3–6, 2006.
11. M. Van der Schaar, and D. S. Turaga, Cross-layer packetization and retransmission strategies for delay-sensitive wireless multimedia transmission, *IEEE Transactions on Multimedia*, 9(1), 185–197, 2007.
12. D. Astely, E. Dahlman, A. Furuskar, Y. Jading, M. Lindstrom, and S. Parkvall, LTE: The evolution of mobile broadband, *IEEE Communications Magazine*, 47(4), 44–51, 2009.
13. S. Lee, S. Choudhury, A. Khoshnevis, S. Xu, and S. Lu, Downlink MIMO with frequency-domain packet scheduling for 3GPP LTE, *IEEE INFOCOM*, Rio de Janeiro, pp. 1269–1277, 19–25 April 2009, doi: 10.1109/INFCOM.2009.5062041.
14. S. Lee, I. Pefkianakis, S. Choudhury, S. Xu, and S. Lu, Exploiting spatial, frequency, and multiuser diversity in 3GPP LTE cellular networks, *IEEE Transactions on Mobile Computing*, vol. PP(99), pp.1, 2011, doi: 10.1109/TMC.2011.206.
15. G. Song, and Ye Li, Cross-layer optimization for OFDM wireless networks-part I: Theoretical framework, *IEEE Transactions on Wireless Communications*, 4(2), 614–624, 2005.
16. G. Song, and Ye Li, Cross-layer optimization for OFDM wireless networks-part II: Algorithm development, *IEEE Transactions on Wireless Communications*, 4(2), 625–634, 2005.
17. T. Kwon, H. Lee, S. Choi, J. Kim, D. Cho, S. Cho, S. Yun, W. Park, and K. Kim, Design and implementation of a simulator based on a cross-layer protocol between MAC and PHY layers in a WiBro Compatible IEEE 802.16e OFDMA system, *IEEE Communications Magazine*, 43(12), 136–146, 2005.
18. K. Lahiri, A. Raghunathan, S. Dey, and D. Panigrahi, Battery-driven system design: A new frontier in lower power design, in *Proc. Intl. Conf. on VLSI Design*, Bangalore, India, Jan. 2002, pp. 261–267
19. G. Miao, N. Himayat, Y. Li, and D. Bormann, Energy efficient design in wireless OFDMA, *IEEE International Conference on Communications, 2008 (ICC '08)*, Beijing, pp. 3307–3312, 19–23 May 2008, doi: 10.1109/ICC.2008.622.
20. G.-W. Miao, N. Himayat, G. Y. Li, and A. Swami, Cross-layer optimization for energy-efficient wireless communications: A survey, *Wiley Journal on Wireless Communications and Mobile Computing*, 9(4), 529–542, 2009.

21. S. Cui, A. J. Goldsmith, and A. Bahai, Energy-constrained modulation optimization, *IEEE Transactions on Wireless Communications*, 4(5), 2349–2360, 2005.
22. A. El Gamal, C. Nair, B. Prabhakar, E. Uysal-Biyikoglu, and S. Zahedi, Energy-efficient scheduling of packet transmissions over wireless networks, *IEEE Proceedings INFOCOM 2002, Twenty-First Annual Joint Conference of the IEEE Computer and Communications Societies*, 3, 1773–1782, 2002.
23. J. Rabaey, J. Ammer, J. L. da Silva, Jr., and D. Patel, PicoRadio: Ad-hoc wireless networking of ubiquitous low-energy sensor/monitor nodes, *Proceedings of IEEE Computer Society Workshop on VLSI*, Orlando, FL, pp. 9–12, 2000, doi: 10.1109/IWV.2000.844522.
24. M. Haenggi, and D. Puccinelli, Routing in ad hoc networks: A case for long hops, *IEEE Communications Magazine*, 43(10), 93–101, 2005.
25. S. Cui, A. J. Goldsmith, and A. Bahai, Energy-efficiency of MIMO and cooperative MIMO techniques in sensor networks, *IEEE Journal on Selected Areas in Communications*, 22(6), 1089–1098, 2004.
26. I. F. Akyildiz, W.-Y. Lee, C. Mehmet, V. S. Mohanty, Next generation/dynamic spectrum access/ cognitive radio wireless networks: A survey, *Computer Networks*, 50(13), 2127–2159, 2006.

33

Cooperative Communication Technologies

Jong-Soo Seo

Zhi Ding

33.1 Introduction

The spectacular development of information technologies over the last two decades has ushered in a new era that increasingly relies on ubiquitous wireless connectivity enabled by advances in wireless communications. Despite numerous progresses in recent years, challenges to high-speed wireless communications remain. Unlike wireline communication systems, wireless channels are prone to physical impairments such as interferences, path loss, channel fading, shadowing, and multipath distortions. These obstacles can severely limit the future enhancement of wireless system capacity for communications and often hamper the practical dependability of wireless links.

Diversity is one of the most effective tools to combat wireless channel uncertainty against loss, distortions, and interferences. Diversity comes in various forms such as temporal, spectral, and spatial diversities. In particular, spatial diversity exploits the difference in channel characteristics exhibited by multiple transmit–receive antenna pairs via MIMO (multiple-input–multiple-output) technologies to provide more reliable wireless connections for communications. Spatial diversity is the key driver and enabler behind recent advances in cooperative communications. Broadly speaking, cooperative communication systems constitute a particular form of spatial diversity through multinode cooperation.

Cooperative communication systems generate and utilize spatially diverse channels by actively coordinating multiple transmit nodes to effectively form virtual MIMO systems. Multinode cooperation allows wireless communication systems and networks to improve reliability of wireless links against channel distortions, fading, and interferences. Cooperative communications can improve wireless coverage, quality of service (QoS), coverage flexibility, and network lifetime. Moreover, multinode cooperation presents additional practical advantages, such as reduced power requirement at each node and limited interfering range when compared against a single node of large transmit power. The advantages of cooperative communications are generally accompanied by a number of difficult challenges, including coordination, synchronization, scheduling, and resource allocation.

33.1.1 Why Cooperative Wireless Communications

The ability of traditional MIMO point-to-point communications to achieve spatial diversity gains and high data throughput is predicated on the condition that wireless terminals have multiple antennas which are sufficiently diverse to generate multiple independently fading channels. Unfortunately, the limited size of mobile terminals can severely undermine channel diversity in a typical wireless scattering environment, thereby leading to correlated multiple channels with weaker diversity. Moreover, typical mobile terminals transmit at low-power levels because of battery capacity and interference control, which limits their coverage range. By coordinating multiple spatially separated nodes, cooperative communications can achieve highly diverse channels and also harness transmission powers from multiple terminals for better coverage. Figure 33.1 presents two examples of cooperative communication systems. Figure 33.1a illustrates the use of relays to achieve path diversity and to expand coverage. Figure 33.1b illustrates how to improve user signal quality at cell-edge by coordinating multiple transmit stations.

33.1.1.1 Diversity-Multiplexity Gain through Cooperation

To overcome the size, cost, and hardware limitations on wireless terminals, spatial diversity via multinode cooperation introduces a practical alternative to multiantenna terminals [1–6]. The basic idea behind cooperative diversity stems from the observation that, in a wireless environment, signals transmitted by the source node are overheard by other nodes, which can be recruited as "relays." The source and other cooperative nodes can jointly process and transmit their information, creating a virtual antenna array even if these nodes are equipped with only one antenna, as shown in the example of Figure 33.1a. Similar to physical antenna arrays, these virtual antenna arrays combat wireless channel fading by letting receivers receive signals transmitted over independent diversity channels.

In a distributed cooperative radio system, multiple virtual channels can carry multiple data signals over all links between the source and the destination. This increased capacity to transmit independent messages is characterized as the multiplexing gain. Users may choose to utilize the multiple channels

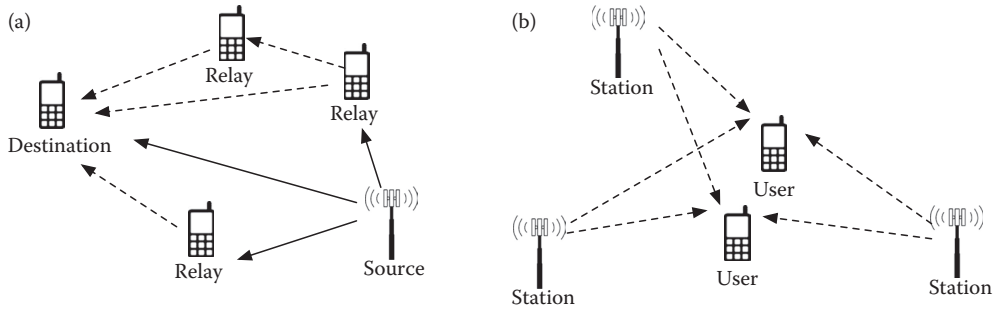

FIGURE 33.1 Concept of cooperative transmit diversity. (a) Multiple relays forming a virtual MIMO for the destination and (b) coordinated multi-point coverage for users near cell-edge.

either for improved diversity of fewer signal streams or for increased multiplexity of more data streams. This issue of diversity and multiplexity trade-off of multichannel systems has been carefully articulated and investigated in Reference 7.

33.1.1.2 Improved Wireless Coverage

Service coverage is mostly dependent on signal strength and signal-to-noise ratio (SNR) at the receiver. Cooperative communications allow multiple users or stations in a wireless network to coordinate their packet transmissions and to mutually share their resources. Without relying on stronger transmitters, such multinode cooperation extends the coverage range and reduces interferences to other users. Moreover, multiple access-point (AP) coordination allows service load to be dynamically shared by several APs. Figure 33.1b illustrates the concept of coordinated multipoint (CoMP) coverage to improve the link quality of users near cell-edge. As a result, users can experience better QoS. Power efficiency, spectrum efficiency, and service coverage can also be considerably improved [8].

33.1.2 Cooperative Diversity Techniques

A key advantage offered by cooperative communication systems is the improved channel diversity. The concept of *diversity* refers to the mechanism of transmitting data symbols over a diverse group of independently fading channels. In mobile communications, because of typical wireless channel fading, relying on a single channel or a single network path would run the risk of poor performance during deep channel or link fades. Channel diversity effectively provides independent multiple paths for data symbols to reach the destination reliably. In general, channel diversity can take forms of time diversity, frequency diversity, spatial diversity, and their different combinations. Cooperative communication systems provide unique opportunities to achieve the important "spatial diversity." To quantify the diversity effect, a standard definition is to consider the symbol error rate or outage probability of an optimized receiver at asymptotically high signal-to-noise ratio (SNR).

Let γ be the average receive SNR. Then the symbol error rate (SER) or the outage probability at high SNR is approximately of the form

$$P_{\text{asymp}} \approx C_0 \gamma^{-d} \tag{33.1}$$

where C_0 is a constant independent of γ. The constant d is the diversity order of this transmission system. Hence, diversity order d is simply the exponential rate at which the probability of error decreases by asymptotically increasing SNR.

33.1.2.1 Time Diversity and Frequency Diversity

Time diversity can be achieved if information on a data packet is transmitted in L multiple time slots whose separation exceeds the channel coherence time. Practical means for achieving time diversity typically rely on coding, interleaving, and automatic retransmission request (ARQ). Similarly, frequency diversity can be achieved by transmitting information of a data packet over multiple frequency bands separated by more than the channel coherence bandwidth. OFDM in fact presents a very simple platform to utilize frequency diversity. In both time diversity and frequency diversity, we can apply maximum ratio combining (MRC) to collect the data information over L multiple time slots or frequency bands. It is well known [9] that the optimum receive diversity can be as high as L in both cases.

33.1.2.2 Spatial Diversity

Spatial diversity relies on multiple antennas at the transmitter and/or the receiver. This MIMO concept is the foundation of cooperative wireless communications. Instead of consuming extra bandwidth and time resources, MIMO systems exploit the multiple channels between each pair of transmit–receive

antennas for diversity gain. Naturally, effective MIMO configuration requires antenna separation to exceed channel *coherence distance*, which typically depends on the local scattering environment at these multiantenna nodes. Thus, to ensure good spatial diversity, antenna configuration needs to have large-enough separation. For example, stations near many scattering objects and near ground tend to have smaller coherence distance of subwavelength, whereas stations in open spaces have large coherence distance of multiple wavelengths. Large-size transceivers are less attractive and less practical especially as mobile devices. In addition, multiple antennas can multiply RF circuit complexity and cost. For these reasons, cooperation of distributed multiple terminals offers a very effective, low cost, and low complexity approach to achieving spatial diversity.

33.1.2.3 Space–Time–Frequency Diversity

In practice, it is very common to integrate space, time, and frequency diversities jointly. Space–time coding-based MIMO systems have effectively integrated space and time diversities. Space-frequency coding in general and MIMO OFDM systems in particular combine space and frequency diversities. Interleaved code words, in conjunction with MIMO–OFDM, have found applications in IEEE 802.11n, IEEE 802.16, and LTE wireless communications exploiting joint space–time–frequency diversity gains in all three dimensions.

33.1.3 Performance Metrices of Cooperative Communications

A number of performance metrices have been proposed and adopted to assess the performance of MIMO communications. Most notably, the performances of cooperative communication system proposals have been measured with respect to metrics such as diversity gains, throughput, and symbol error rate (bound). Specifically, the following metrices are often used to characterize the cooperative system performance.

- *Capacity and ergodic capacity*: Let γ denote the SNR at each receive antenna and let I denote an identity matrix of appropriate size. A typical flat fading MIMO channel with channel response matrix H and bandwidth B achieves

$$\begin{aligned} &\text{System capacity:} \quad C(H) = B \cdot \log_2 \det(I + \gamma HH^H), \\ &\text{Ergodic capacity:} \quad \overline{C} = E_H\{C(H)\}. \end{aligned} \tag{33.2}$$

- *Outage probability*: The probability that the system capacity falls below a threshold transmit rate R

$$P_{\text{out}}(R,\gamma) = \Pr(C(H) < R). \tag{33.3}$$

- *Outage capacity*: The capacity C_{out} that the system can reliably achieve with probability $1 - P_{\text{out}}$

$$\Pr[C(H) \geq C_{\text{out}}] = 1 - P_{\text{out}}. \tag{33.4}$$

- *Diversity gain*: The asymptotic rate d at which outage probability decreases with increasing SNR γ

$$d = -\lim_{\gamma \to \infty} \frac{\log_2 P_{\text{out}}}{\log_2 \gamma}. \tag{33.5}$$

- *Multiplexity gain*: The asymptotic rate m at which the system rate R increases with increasing $\log_2 \gamma$

$$R = m \log_2 \gamma + \text{constant}. \tag{33.6}$$

- *Diversity–multiplexity trade-off*: The manner with which the two gains d and m are coupled:

$$d = -\lim_{\gamma \to \infty} \frac{\log_2 P_{\text{out}}(m \log_2 \gamma)}{\log \gamma} \tag{33.7}$$

Two additional physical layer considerations with respect to cooperative communications system are SNR and spectral efficiency. SNR gain through cooperation is directly related to the diversity gain d whereas spectral efficiency is directly related to the multiplexity gain m. Clearly, high spectral efficiency means more data symbols transmitted within limited bandwidth. Conversely, high SNR requirement of each data symbol sacrifices the spectral efficiency. Thus, for a given cooperation strategy, SNR and spectral efficiency are coupled in a manner similar to the diversity–multiplexity trade-off.

33.1.4 Organizations

Cooperative communications and networking have undoubtedly attracted substantial research attentions in the last decade. Unlike the more traditional point-to-point communication systems, cooperative communications involve additional complex issues such as access scheduling of cooperating nodes, synchronization of multinode transmissions, multinode information sharing, and resource allocations. The breadth of these issues and the associated challenges have stimulated a large number of intensive research activities. As a result, newcomers to this field may be easily overwhelmed by the vast number of relevant publications. The purpose of this chapter is to present an abbreviated introduction to the rich and vast literature of cooperative wireless communications. For reader calibration, we assume that our readers are familiar with fundamentals of wireless communications including point-to-point MIMO technologies.

In terms of organization, we first describe a number of well-known cooperative network configurations and cooperative strategies in Section 33.2. Our discussion spans the simple 3-node relay network and more general multihop multinode relay networks. We consider both one-way relay and two-way relay protocols. We also cover deterministic and dynamic cooperative strategies. In Section 33.3, we summarize several analytical results on the performance of the simple 3-node relay network. This summary provides a general idea about typical analytical issues of interest. Section 33.4 discusses issues of resource allocation in cooperative communication networks with respect to node scheduling and power allocation. Finally, we conclude the chapter by highlighting key remaining challenges in cooperative communications and presenting examples of cooperative communications in practical applications.

33.2 Networks and Strategies for Cooperative Communications

A cooperative wireless network consists of more than two nodes. In addition to a source node where the message originates and a destination node where the message terminates, there should also be one or more wireless nodes to assist the delivery of message signals from source to destination. The first and the most important attribute of a cooperative communication system is the underlying network configuration (topology). As shown in the literature, there exist a number of network configurations for cooperative wireless communications. Most commonly seen configurations include single-node relay, multinode relay, and cooperative multinode networks connected by links in either unidirectional or bidirectional manner. Here we focus our discussions only on several well-known network topologies that are fully wireless.

33.2.1 Simple 3-Node Relay Networks

Figure 33.2 illustrates the simplest configuration of a cooperative wireless network, consisting of 3 nodes: a source sending signal s_0, a relay receiving signal y_1 and transmitting signal x_1 which is a function of y_1

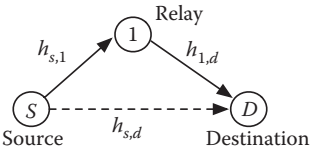

FIGURE 33.2 Simple relay network model with and without direct path.

(as an estimate of s_0), and a destination receiving signal $y_d^{(1)}$ from the relay. In other words, the relay maps its receive data y_1 into its transmit data x_1 through $x_1 = q(y_1)$ according to the relay type in use. The link channel gains $h_{s,d}$, $h_{s,1}$, and $h_{1,d}$ are labeled in Figure 33.2. This single relay network configuration (without direct path) was investigated rigorously by Cover and El-Gamal in Reference 1. In the literature, most single relay networks under investigation are unidirectional, that is, they admit a simple Markov relationship of $s_0 \rightarrow y_1 \rightarrow x_1 \rightarrow y_d^{(1)}$. In a slightly more general case, the direct source–destination path can also be included with relationship $s_0 \rightarrow y_d^{(2)}$.

In hardware implementation, it is generally difficult for a transceiver to transmit and receive simultaneously in the same channel because the receiver will be subject to a very strong interference from its own transmission. Without complex hardware to mitigate this strong self-interference, 3-node relay network cooperation requires two orthogonal channels for half-duplex relay reception and transmission. In Reference 3, the authors imposed the half-duplex constraint on the cooperating nodes and proposed several cooperative transmission protocols. The relay strategies in Reference 3 were classified as either amplify-and-forward (AF), where the relay node retransmits a scaled version of its reception, or decode-and-forward (DF), where the relay decodes the source data before retransmitting. We can use the easiest example of two time-division cooperative protocols [10] which are summarized in Table 33.1. Because of the half-duplex constraint, the two phases for relay to receive and to transmit must take place over 2 orthogonal channels, effectively through time-division, code division, or frequency division. There can be two cooperative protocols, depending on whether the source stays active or idle during the second (relaying) phase. Table 33.1 outlines the two basic protocols of cooperation for the 3-node relay network.

In Protocol I, the signals received at the relay and destination in stage k, respectively, are

$$\text{Relay:} \quad y_1(k) = \sqrt{P_0} h_{s,1} \cdot s_0(k) + n_{s,1}(k), \tag{33.8}$$

$$\text{Destination:} \quad y_d^{(1)}(k) = \sqrt{P_0} h_{s,d} \cdot s_0(k) + n_{s,d}(k), \tag{33.9}$$

$$y_d^{(2)}(k) = \sqrt{P_1} h_{1,d} \cdot x_1(k) + n_{1,d}(k). \tag{33.10}$$

Since each data $s_0(k)$ can reach the destination in 2 diversified paths, this protocol should offer substantial diversity gain at the expense of 50% spectral efficiency loss. In terms of notations, we denote channel noises as $n_{s,d}$, $n_{s,1}$, and $n_{1,d}$ which are complex (and circularly symmetric) Gaussian with zero mean and

TABLE 33.1 Two Cooperation Protocols for the 3-Node Relay Network

		Phase 2	
Node	Phase 1	Protocol I	Protocol II
Source	Transmit $s_0(k)$	Inactive	Transmit $s_0(k+1)$
Relay	Receive $y_1(k)$ from source	Transmit $x_1(k)$ to destination	
Destination	Receive from source	Receive from relay	Receive from relay and source

variance N_0. The transmitted signals s_0 and x_1 both have zero mean and unit power. $h_{s,1}$, $h_{s,d}$, and $h_{1,d}$ are channel responses that degenerate into scalar coefficients for single-antenna flat-fading channels.

It is important to note that Protocol I does not necessarily require the existence of a direct source-to-destination link. It therefore can reduce to a simpler 2 hop relay system. In Protocol II, however, $s_0(k+1)$ only has one path $S \rightarrow D$ which provides no diversity but better multiplexity for a higher spectral efficiency. Notice that in phase 2 of Protocol II, the destination experiences an artificial interference between the source transmission and the relay transmission. Such an interfering network can improve system throughput through multiplexity as long as receivers can separately recover both relay and source transmissions [11].

33.2.1.1 Deterministic Relay Strategies

Cooperative relay strategy, that is, relay functionality, is one of the key characteristics of relay cooperative networks. There are three well-studied types of relays: Amplify-and-Forward (AF), Decode-and-Forward (DF), and Compress-and-Forward (CF). In an AF relay, received signal is simply scaled before retransmission or forwarding. AF relay is the simplest in terms of processing complexity. However, AF relay includes its received noise $n_{s,1}(k)$ in its own transmissions.

The relay transmit signal x_1 as a function of its received signal y_1 can be expressed depending on different relay functionalities as

$$\text{AF:} \quad x_1 = (P_0 \, |h_{s,1}|^2 + N_0)^{-1/2} \sqrt{P_1}\, y_1 \tag{33.11}$$

$$\text{DF:} \quad x_1 = \hat{s}_0 = \arg\max p(s_0 \mid y_1) \tag{33.12}$$

$$\text{CF:} \quad x_1 = q(y_1), \tag{33.13}$$

where $\hat{s}_0$ is the decoded message at the relay of the source signal s_0. For CF, $x_1 = q(y_1)$ is a quantized and a compressed version of y_1 that the relay receives. In any case, the destination benefits from the relay cooperation by estimating the source signal s_0 based on maximum likelihood (ML) detection

$$\arg\max \, p(y_d^{(1)}, y_d^{(2)} \mid s_0) = \arg\max \, p(y_d^{(1)} \mid s_0) p(y_d^{(2)} \mid s_0).$$

In AF, DF, or CF protocols, we often consider a total transmitted power P such that the sum power is limited

$$P_0 + P_1 = P. \tag{33.14}$$

This constraint is for practical purpose of interference limitation and resource conservation. It also provides a measure of fairness when comparing different protocols.

Regardless of the cooperative strategies, in exchange of additional bandwidth taken by the use of two orthogonal channels, this 3-node relay network generally provides several advantages including diversity gain, improved coverage, and interference reduction against co-channel users. There exists a rich literature of studies on deterministic cooperative protocols for both AF and DF relay networks. In [10], the authors analyzed both TDMA-based cooperative protocols for simple fading channels. They confirm the observation that, in terms of bandwidth utilization, cooperation network based on Protocol I of Table 33.1 provides higher cooperative diversity gain whereas Protocol II offers better multiplexity gain, provided that appropriate power control is employed. A comprehensive study on the upper and lower bounds of outage capacity and ergodic capacity of this 3-node relay network can be found in Reference 12, which also presented proposals for optimized power allocation.

33.2.1.2 Dynamic Cooperation Strategies

Deterministic relays would suffer from a loss in bandwidth efficiency. For example, there is a bandwidth efficiency loss of 50% by Protocol I. Unlike deterministic cooperation strategies with which relays always perform the same functionality, dynamic cooperation resorts to more efficient cooperation strategies that flexibly determine different relay activities depending on channel conditions. Representative strategies for dynamic and adaptive relay cooperation include: (1) Selective forwarding (SF); (2) Incremental relaying (IR); (3) Regenerative redundancy (RR). Dynamic relay cooperation typically operates on a packet-by-packet basis instead of a symbol-by-symbol basis.

33.2.1.2.1 Selective Forwarding

In selective forwarding (SF), the relay may assess its channel conditions and only relay its message when its channel condition $h_{s,1}$ is reliable enough to generate sufficiently high SNR during its reception. Particularly with decode-and-forward, selective DF (S-DF) makes it possible to forward only if the relay decoding is deemed accurate, thereby providing highly dependable diversity for joint detection at the destination node.

In phase 1 of SF, the source broadcasts its information to both the destination and the relay which receive y_1 and $y_d^{(1)}$ of (8) and (9), respectively. In phase 2, for a DF cooperation protocol, if the relay is able to decode the transmitted packet correctly, then the relay resends the decoded packet symbols with power P_1 to the destination. The received signal at the destination in phase 2 of selective DF relaying thus becomes

$$y_d^{(2)} = \sqrt{q(P_1)}h_{1,d}x_1 + n_{1,d}. \tag{33.15}$$

where the selection function $q(P_1) = P_1$ if the relay decodes the transmitted symbols correctly; Otherwise $q(P_1) = 0$. Similarly, selective AF can also be designed by defining its selection function $q(P_1)$ based on whether or not its relay SNR exceeds a set threshold.

33.2.1.2.2 Incremental Relaying

In incremental relaying (IR), the destination node may send request to the relay node for partial signal retransmission based on its decoding success and needs. IR strategy can reduce the amount of bandwidth required by the relay node which only sends incrementally redundant signals to the destination to assist the recovery of the full packet. The incremental redundancy depends on the need of the destination node. If the source transmission in the first phase was successful, then there is no second phase, and the source would transmit a new packet in the next time slot without loss of spectral efficiency. On the other hand, if the source transmission was not successful in the first phase, the relay may retransmit part of its received signal. Thus, incremental retransmission may occur multiple times for each packet. In the worst-case scenario, IR must retransmit the entirety of its received packet as in deterministic relaying.

The improvement of spectral efficiency by the IR protocol is clear because the relay does not always need to occupy the entire channel during phase 2. In fact, relay transmission in phase 2 becomes opportunistic depending on the condition of the direct channel between source and destination. Depending on the direct link channel condition, the IR spectral efficiency loss may be anywhere between 0%–50%. Nevertheless, IR still delivers the same diversity order as deterministic relaying. The implementation of IR, however, does require frequent feedback signaling from the destination to the relay. The cost and latency of such IR feedbacks are the cost paid for better spectral efficiency.

33.2.1.2.3 Regenerative Redundancy

Regenerative redundancy (RR) cooperation allows the relay to be more creative. In essence, RR lets the relay generate additional error correcting redundancies for the destination. Instead of viewing data

signals only as pure information packet, s_0 can denote an FEC code packet that consists of sufficient redundancy for a certain level of error correction. In RR cooperation, s_0 is transmitted to both the relay node and the destination node. If $y_d^{(1)}$ has a sufficient quality for an error-free decoding of s_0 at the destination as confirmed by an error detection code such as CRC, then no relay transmission is necessary. If errors remain at the destination, then the relay is requested to assist. The relay node may generate and transmit new parity bits as additional redundancy if it correctly recovers s_0 from y_i by using its own FEC decoder. Alternatively, relay redundancy may be generated when the soft information during decoding such as the log-likelihood ratio (LLR) of a large number of coded bits is sufficiently large to signify good reliability.

33.2.2 Multinode Relay Networks

A natural extension of the simple 3-node cooperative relay network is the configuration of multinode relay networks. Without direct link, the simple 3-node relay network is a single-path dual-hop network. When multiple relays are available, there are three well-studied network configurations: single-path multihop, multipath dual-hop, and multipath multihop.

33.2.2.1 Multipath Dual-Hop Relay Networks

Instead of relying on a single relay node, an immediate generalization of the 3-node network is to place L relays between the source and the destination as in Figure 33.3. The L relays form parallel paths that can substantially enhance the source-to-destination channel diversity. To avoid interference among relays, all relay nodes in this network should operate synchronously in two phases. During the broadcast phase, the source transmits data s_0 to the relays, each of which receives over its channel $h_{s,i}$ a signal

$$y_i = \sqrt{P_0} \cdot h_{s,i} s_0 + n_i, \quad i = 1, \ldots, L. \tag{33.16}$$

During the relay phase, some or all of the relays send their signals to the destination. More specifically, if the ith relay channel is denoted as $h_{i,\mathrm{d}}$, then the destination receives a combined signal

$$y_d = \sum_{i=1}^{L} \sqrt{Pi} \cdot h_{i,d} x_i + n_{i,d}, \tag{33.17}$$

where P_i denotes the ith relay transmit power and $n_{i,\mathrm{d}}$ is the channel noise on the wireless link between the relay and the destination, modeled as Gaussian with zero mean and variance N_0. The relay signal can be written as $x_i = q_i(y_i)$, depending on the relay protocols of DF, AF, or CF.

With the AF scheme, for example, the capacity of such parallel relay system per unit bandwidth can be written as [2,13]

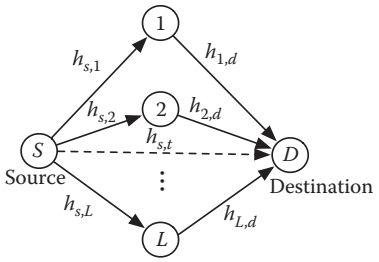

FIGURE 33.3 Multipath dual-hop relay networks.

$$C_{\mathrm{AF}} = \frac{1}{2}\log_2\left[1 + \sum_{i=1}^{L} \frac{\left|h_{s,i}h_{i,d}\right|^2 P_0 P_i}{\left|h_{s,i}\right|^2 P_0 + \left|h_{i,d}\right|^2 P_0 P_i + N_0}\right],$$

which can be achieved via optimum power allocation of P_i using a water-filling algorithm [13]. In a more flexible protocol, we may only designate a subset among L relays to participate in cooperation. For example, optimum AF node selection allows the destination to pick the "best" nodes for AF relaying by selecting a subset of nodes that can provide the highest source-to-destination capacity. As described in [14], the node selection AF cooperation can achieve higher throughput and consumes less control signaling bandwidth than the conventional "all-participation" L-node relay networks.

33.2.2.2 Linear Multihop Relay Networks

When the source and destination nodes are spaced far apart, multiple relays can often bridge their link via a single-path multihop relay network. As shown in Figure 33.4, the linear multihop topology is a straightforward concatenation of single-hop links, whose transport capacity has been investigated in Reference 15. This linear relay network is a classic configuration of long-distance relay communications used throughout human history. Even in the field of wireless communications, microwave relay links are well-known practical examples of linear relay networks.

In the absence of direct-link, CF and adaptive relay strategies tend to be unreliable in linear multihop relay networks. As a result, AF and DF are the two commonly studied relay strategies for multihop linear relay networks. In order to simplify hardware requirements, we only consider half-duplex relay nodes that can only transmit and receive simultaneously on orthogonal channels. The simplest form of channel orthogonality takes the form of time-division. Different relays may implement DF or AF strategies uniformly or heterogeneously.

33.2.2.2.1 Hop-by-Hop DF Relays

In Figure 33.4, each DF relay ℓ decodes the signal transmitted from its preceding node $\ell - 1$. Such a hop-by-hop relay network is viewed as a concatenation of DF links without diversity combining. Therefore, transmission of a message from source to destination is successful only if every relay node successfully decodes the message before passing it forward.

Let $h_{\ell,k}$ be the channel gain between nodes ℓ and k. Here we have $l, k \in \{S, 1, \ldots, L, D\}$. Let P_ℓ be the transmit power at node ℓ. Then the hop-by-hop (HBH) SNR at each relay node is simply

$$\gamma_\ell^{(\mathbf{HBH})} = P_{\ell-1} \mid h_{\ell-1,\ell} \mid^2 / N_0.$$

Generally, the decoding at node ℓ is successful only if γ_ℓ exceeds the SNR threshold γ_{th}. Therefore, the HBH outage probability at node D is

$$P_{\mathrm{out}} = 1 - \Pr(\gamma_D > \gamma_{\mathrm{th}}) \cdot \prod_{\ell=1}^{L} \Pr(\gamma_\ell > \gamma_{\mathrm{th}}). \tag{33.18}$$

Clearly, the outage probability increases as the number of hops increases.

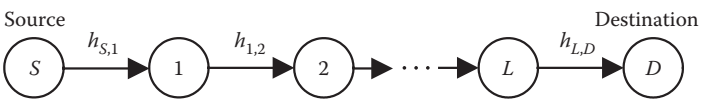

FIGURE 33.4 A multihop linear relay network.

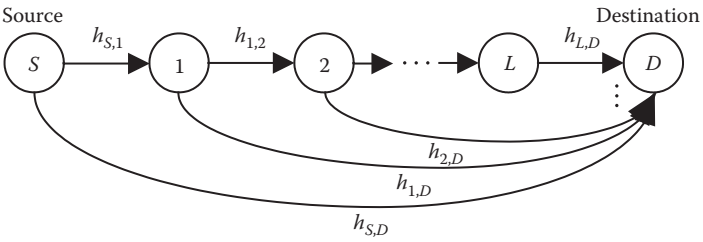

FIGURE 33.5 A multihop cooperative network for a diversity combining at the destination.

33.2.2.2.2 Maximum Ratio Combining for DF Relays

In practice, relays in multihop networks may have the ability to buffer earlier signal receptions that can be coherently combined with subsequent transmissions. For example, the work of [16] presented multihop diversity channel analysis of AF and DF linear relay networks, where each relay node combines signals received from all preceding nodes before decoding and relaying. Furthermore, [17] developed a class of more general cooperative protocols. Figure 33.5 illustrates an exemplary maximum ratio combining (MRC) stage for joint decoding at the destination node.

In terms of performance gains, MRC at relay node ℓ leads to a higher SNR as

$$\gamma_{\ell}^{(\mathbf{MRC})} = N_0^{-1} \cdot \left(P_0 \mid h_{s,\ell} \mid^2 + \sum_{k=1}^{\ell-1} P_k \mid h_{k,\ell} \mid^2 \right).$$

Assuming that all the relays successfully decode the source message, the outage probability at the destination can be approximated as

$$P_{\text{out,MRC}} \approx \Pr\left[N_0^{-1} \cdot \left(P_0 \mid h_{s,\ell} \mid^2 + \sum_{k=1}^{\ell-1} P_k \mid h_{k,\ell} \mid^2 \right) < \gamma_{\text{th}} \right]. \tag{33.19}$$

Particularly at higher SNR, the MRC for DF relays can substantially improve the successful packet transmission rate over HBH relays. Such a multihop diversity combining allows the relays and the network to effectively battle the negative effects of path loss. The authors of Reference 18 presented the performance bounds with respect to outage probability and average bit error rate for multihop diversity combining and transmissions over Nakagami fading channels.

33.2.2.3 Multihop AF Relays

Though most of conventional multihop relay systems adopt a DF relaying, multihop transmission can be achieved similarly by using an AF relaying. In hop-by-hop relaying, each AF relay node receives signal transmitted by its immediate upstream node. In Reference 19, similar to DF relays, MRC receiver can be also applied at AF nodes to provide better diversity and reliability. However, compared to DF relays, AF relays amplify both signal and noise in each hop. The accumulated noises over increasing hops may lead to substantial performance loss. Naturally, as the number of hops increases, the outage probability of AF multihop networks will grow much faster than DF relays, as pointed in Reference 20.

33.2.2.4 Multihop Ad Hoc Relay Networks

An extension of the multipath dual-hop relay network involves an ad hoc network of multiple nodes between sources and destinations. As shown in Figure 33.6, such a generic ad hoc relay network may

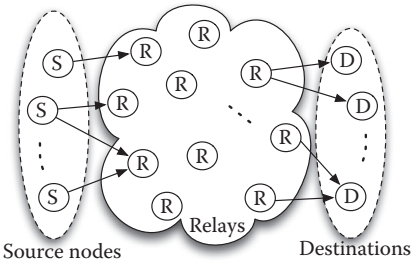

FIGURE 33.6 A multihop ad hoc relay network.

have a single source node or multiple source nodes. There may also be one or multiple destination nodes.

Multihop ad hoc relay networks facilitate a number of flexible cooperation strategies and protocols. In addition to the consideration of power allocation and channel access, such networks also require network control protocols including traffic routing, relay selection, scheduling, and node coordinations for data-throughput improvement, reduced delay, and interference mitigation. Because of the large variety of multihop ad hoc networks in terms of configurations, protocols, and practical constraints, there exist many interesting research directions and results on such networks.

In terms of relay strategies, the comprehensive work of Kramer et al. [21] presented DF and CF relay strategies for generic multinode relay networks that consist of multiple relays, sources, and destination nodes, each of which is equipped with multiple antennas. The results show that DF strategies are better for relays closer to sources nodes, whereas CF strategies are better for relays closer to destinations. Another major practical concern is the selection of relays for participating in cooperation. The work of Bletsas et al. [22] focused on "network path selection" between a source and a destination. This "opportunistic relaying strategy" chooses relays to form the strongest transmitter-relay-receiver path among multiple candidates in a distributed fashion using instantaneous channel strength information. Beres and Adve [23] analyzed the high-SNR outage probability for a source–destination pair by selecting a single cooperative relay based on the best instantaneous channel quality. For multiple signal flow transmissions, they further proposed several relay selection schemes based on various centralization and complexity requirements.

The work of Ribeiro et al. [24] analyzed the symbol error rate of multibranch multihop AF relay networks between a pair of source and destination nodes. Ng and Yu [25] proposed a general optimization framework for joint optimization of the best relay node, the best relay strategy, and the best resource allocations in terms of power, bandwidth, and throughput rate in a cellular network. Zhao and Valenti [26] presented an integrated protocol for multihop relay by incorporating practical hybrid-ARQ.

With respect to total capacity that a network can carry, the work of Xie and Kumar [15] investigated the transport capacity of a large multinode relay network with multiple source–destination pairs. The scaling law result answers the asymptotic performance question of how much information of an asymptotically large multinode relay wireless network can be transported as a scaling function of the number of nodes. The work of Bolcskei et al. [27] presented further analysis on the behavior of MIMO wireless relay network in terms of the capacity scaling law with multihop relays.

33.2.3 Distributed Space–Time Signaling for Cooperative MIMO

We note that even in a simple 3-node relay network, signal transmissions from the relay and the source in Protocol II can be viewed as signaling cooperation or a form of space–time coding [6,10]. Typically,

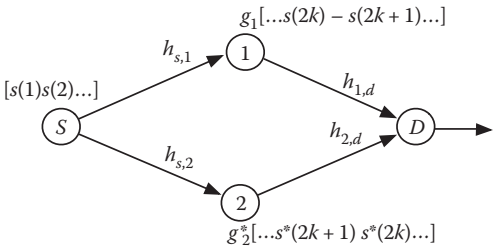

FIGURE 33.7 Distributed space–time (or space–frequency) coding configuration.

each relay can send signals based on its own reception without coordinated signaling. Such relay strategies are easy to implement and require only timing synchronization of all participating relays. Better relay cooperation achieved by optimized precoding requires destinations to determine the precoder according to the relay channel information and to feedback the precoder parameters needed by each relay node. Such feedback information takes up valuable resources, if feedback precision and timeliness are needed. In systems involving fast-fading channels, such feedbacks would require too much bandwidth and may be too slow. For this reason, the cooperative MIMO strategy of distributed space–time coding (DSTC) or distributed space–frequency coding (DSFC) becomes highly attractive because of their ability to achieve full diversity without a receiver feedback.

A simple network of Figure 33.7 illustrates how multiple relays can effectively cooperate to form a distributed space–time code or a distributed space–frequency code. DSTC and DSFC essentially are the traditional MIMO signaling techniques that are made possible by treating multiple relay nodes as virtual source antennas in a virtual multiple-input-multiple-output (Virtual MIMO or V-MIMO) system. This means that signals transmitted at different relay nodes must be synchronized. DSTC utilizes multiple virtual antennas across multiple time slots, whereas DSFC encodes signals across multiple subcarrier frequencies. They differ only in terms of the time vs. frequency orthogonal channels in use. Because there is no conceptual difference between DSTC and DSFC, we focus on the more familiar DSTC in this section by using the simpler Alamouti space–time-block-code (STBC) example. Various DSTC/DSFC strategies can be found in References 29 through 33.

33.2.3.1 DSTC with S-DF Relays

Let us consider the relay network of Figure 33.7. The concept of distributed DSTC can be implemented with 2 relay nodes corresponding to 2 phases. During the broadcasting phase 1, the source sends a packet of data symbols $[s(0)\ s(1)\ \ldots\ s(K)]$ to the two relays. The ith relay receives

$$y_i(k) = \sqrt{P_0}h_{s,i}s(k) + n_{s,i}(k), \quad i = 1,2. \tag{33.20}$$

In phase 2, the selective DF (S-DF) relay transmits its decoded data to the destination if and only if its packet passes the CRC error detection check. This decision variable at each relay is denoted by a scalar

$$g_i = \begin{cases} 1, \text{relay } i \text{ decodes correctly}, \\ 0, \text{relay } i \text{ decodes incorrectly}, \end{cases}$$

In the case of 2 relay nodes as shown in Figure 33.7, relay 1 transmits $g_1\ [\ldots\ s(2k) - s(2k+1);\ \ldots]$, whereas relay 2 can transmit $g_2^*[s^*(2k+1)\ s^*(2k);]$.

We can now form a 2×2 STBC matrix X_k. The well-known Alamouti code matrix requires 2 relay nodes and it is given by

$$\boldsymbol{X}_k \begin{bmatrix} s(2k) & s^*(2k+1) \\ -s(2k+1) & s^*(2k) \end{bmatrix}.$$

The first column of $\boldsymbol{X}_k$ is the 1st relay transmission in 2 successive time slots, whereas the second column corresponds to the 2nd relay signal transmitted in the same two time slots. If each relay transmits with equal power P_1, the signals received at the destination over the two time slots become

$$y_d(k) = \sqrt{P_1}\boldsymbol{X}_k \underbrace{\begin{bmatrix} g_1 h_{1,d} \\ g_2^* h_{2,d} \end{bmatrix}}_{\boldsymbol{H}_{rd}} + n_d(k). \tag{33.21}$$

We note that the composite channel matrix $\boldsymbol{H}_{rd}$ consists of the physical link channel response $h_{i,d}$ and the associated binary relay gain g_i. In fact, from the diagram of Figure 33.7, it is very clear that $g_i h_{1,d}$ and $g_2^* h_{2,d}$ become the equivalent channel responses on the two links during the second hop.

Given the composite form of the effective channel matrix $\boldsymbol{H}_{rd}$, the DSTC through S-DF relays is identical to the well-known Alamouti STBC. Therefore, existing analysis on the coding gain and the diversity order of Alamouti STBC can be directly applied to the DSTC system. Unlike in the traditional STBC formulation, there is no assurance that both relay nodes will recover $s(k)$ without error. Thus, the binary gains g_1 and g_2 essentially change the effective channel responses between the relays and the destination, thereby affecting the DSTC coding gain and diversity order. Using S-DF relays, each data symbol achieves the maximum possible coding gain of $(|g_1 h_{1,d}|^2 + |g_2 h_{2,d}|^2)$. The achieved diversity order equals $g_1 + g_2$, which may vary from packet-to-packet.

More generally, given L such relays, there are L relay switch gains $[g_1, g_2, \ldots, g_L]$. Any traditional $K \times L$ STBC code block $\boldsymbol{X}_k$ can be constructed by the L S-DF relays. In general, the received signal vector at the destination can be written as

$$y_d(k) = \sqrt{P_1}\boldsymbol{X}_k \cdot \boldsymbol{H}_{rd} + n_d(k), \quad \text{where } \boldsymbol{H}_{rd} = \left[g_1 h_{1,d}^T \, g_2 h_{2,d}^T \cdots g_L h_{L,d}^T \right]^T. \tag{33.22}$$

The relay-to-destination channel responses $\{h_{i,d}\}$ can be a scalar, a vector, or a submatrix corresponding to single-input-single-output, single-input-multiple-output, and multiple-input-multiple-output links, respectively. More detailed analysis of different DSTC with DF relays can be found in References 28 through 31 and 34.

33.2.3.2 DSTC with AF Relays

Similarly with AF relays, DSTC can also be developed [32]. In particular, the orthogonal Alamouti STBC codeword can be constructed by using the scaled signals received at the relays as estimates of the source data. In particular, the AF relays estimate the source data through power normalization as

$$\begin{aligned} \hat{s}(k) &= \sqrt{(P_0 \mid h_{s,i} \mid^2 + N_0)^{-1}}\, y_1(k) \\ &= g_i s(k) + v_i(k) \end{aligned} \tag{33.23}$$

where

$$g_i = \sqrt{P_0 (P_0 \mid h_{s,i} \mid^2 + N_0)^{-1}}\, h_{s,i}, \tag{33.24}$$

and

$$v_i(k) = \sqrt{(P_0 \mid h_{s,i} \mid^2 + N_0)^{-1}}\, n_{s,i}(k).$$

The amplified noises $v_i(k)$ have variance $\sigma^2_{v_i} = N_0(P_0 \mid h_{s,i} \mid^2 + N_0)^{-1}$.

The AF code block of STBC can be expressed as

$$\begin{aligned}\hat{X}_k &= \begin{bmatrix} \hat{s}(2k) & \hat{s}^*(2k+1) \\ -\hat{s}(2k+1) & \hat{s}^*(2k) \end{bmatrix} \\ &= \begin{bmatrix} g_1 s(2k) & g_2^* s^*(2k+1) \\ -g_1 s(2k+1) & g_2^* s^*(2k) \end{bmatrix} + \underbrace{\begin{bmatrix} v_1(2k) & v_2^*(2k+1) \\ -v_1(2k+1) & v_2^*(2k) \end{bmatrix}}_{V_k}. \end{aligned} \tag{33.25}$$

The destination node then receives an orthogonal space–time code as follows

$$y_d(k) = \sqrt{P_1}\boldsymbol{X}_k \cdot \boldsymbol{H}_{rd} + \sqrt{P_1}\boldsymbol{V}_k \begin{bmatrix} h_{1,d} \\ h_{2,d} \end{bmatrix} + n_d(k), \tag{33.26}$$

where the effective channel responses are scaled by the AF gains as

$$\boldsymbol{H}_{rd} = [g_1 h_{1,d} \quad g_2^* h_{2,d}]^T.$$

Compared with DF relays, there are two major differences in the space–time code matrix formed by AF relays. First, there is an extra noise transmission $\boldsymbol{V}_k$ which will degrade the SNR at the destination. In addition, the effective channel matrix $\boldsymbol{H}_{rd}$ consists of nonbinary AF gains g_1 and g_2 as defined in Equation 33.24. As a result, we can see that the diversity order of DSTC with AF relays will always be equal to the traditional STBC $\boldsymbol{X}_k$, since g_1 and g_2 are non-zero scalars. In particular, each coded symbol will achieve full diversity coding gain as

$$(\mid g_1 \mid^2 \mid h_{1,d} \mid^2 + \mid g_2 \mid^2 \mid h_{2,d} \mid^2).$$

Similarly to the case of DSTC with S-DF relays, AF relays can also construct general STBC code blocks of size $K \times L$ involving L relays. The only differences lie in the extra additive noise matrix V_k and the composite channel matrix

$$\boldsymbol{H}_{rd} = [g_1 h_{1,d}\ g_2 h_{2,d} \cdots g_L h_{L,d}]^T.$$

Therefore, both S-DF and AF relays can improve the diversity order and provide a coding gain to the relayed data receptions. As shown in Reference 34 (Chapter 7), AF relays also make it possible to extend a general class of linear transformation on the received data vector before forming its own STBC codewords for transmission.

33.2.4 Bidirectional AF Relay Networks: A Network Coding Perspective

So far, we have focused on unidirectional relay networks in which signals flow in the direction from source to destination. In these networks, the source nodes transmit while the destination nodes receive. A more general cooperative relay model involves bi-directional relays to bridge two or more transceivers, each of which acts as a signal source and a signal destination. In bidirectional relay networks, the role of

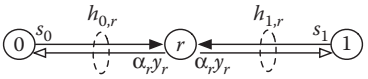

FIGURE 33.8 Bidirectional relay in a dual-hop network.

relay nodes can be expanded to facilitate better spectrum efficiency if the concept of "network coding" is incorporated.

The concept of network coding was first popularized by the works of References 35 through 37. Although the original network coding was presented in the binary field of information bits at the transport level, physical layer network coding has also gained substantial popularity that often involves intermediate network nodes that concurrently receive baseband signals from multiple transmitters [38,40].

Let us consider the simple 3-node dual hop relay network of Figure 33.8. Relay node r lies in between node 0 and node 1. It is assumed that the bidirectional channel gains are reciprocal. Node 0 and node 1 transmit signals $s_0(k)$ and $s_1(k)$ with powers P_0 and P_1, respectively. The relay operation is divided into two phases. In phase 1, both node 0 and node 1 transmit their own packets concurrently to the relay, like a multiple access channel. Briefly, the relay r receives the superimposed signal

$$y_{r1}(k) = \sqrt{P_0}h_{0,r}s_0(k) + \sqrt{P_1}h_{1,r}s_1(k) + n_r(k), \tag{33.27}$$

where $n_r(k)$ is the multiple access channel noise. The two source signals are superimposed into $y_r(k)$ by the shared wireless physical channel. In phase 2, the relay node broadcasts its received signal $y_r(k)$ in phase 1 to both node 0 and node 1, like a broadcast channel. The combined signal is normalized by α_r for power control. The two nodes will receive, respectively,

$$y_0(k) = \alpha_r h_{0,r}\left[\sqrt{P_0}h_{0,r}s_0(k) + \sqrt{P_1}h_{1,r}s_1(k) + n_r(k)\right] + n_0(k) \tag{33.28}$$

$$y_1(k) = \alpha_r h_{1,r}\left[\sqrt{P_0}h_{0,r}s_0(k) + \sqrt{P_1}h_{1,r}s_1(k) + n_r(k)\right] + n_1(k) \tag{33.29}$$

Because both node 0 and node 1 have a prior knowledge of their own data $s_0(k)$ and $s_1(k)$, they are capable of recovering their individual signal of $s_1(k)$ or $s_0(k)$ from $y_0(k)$ and $y_1(k)$.

This AF strategy by the relay node can improve the bandwidth efficiency by a factor of 2 over the traditional uni-directional relay strategy that separately receives and relays the two transmissions. The AF relay strategy for superimposing multiple signal receptions is often known as "physical layer network-coding." To investigate further, the readers are referred to the works of References 38 and 39 that extended the network coding concept to the simple bidirectional physical-layer relay networking. Further discussions on joint source coding and network coding can be found in References 40 and 41.

We note that DF is more reliable but less efficient bi-directional protocol that would require three phases instead of two phases. In phase 1 and phase 2, node 0 and node 1 take turns transmitting s_0 and s_1 to the relay r, respectively. In phase 3, the relay can broadcast the "network"-coded packet $(s_0 \oplus s_1)$ after decoding both packets s_0 and s_1. It is therefore evident that AF relays are spectrally more efficient in physical layer network coding.

33.3 Performance Comparison of Cooperative Relays

Given a large number of different cooperative network topologies and cooperative strategies, it is difficult to present even a moderately detailed discussion on their performances in the limited space here. In

this section, let us focus on the simple 3-node cooperative network configuration by explaining some basic analytical results that compare different cooperative strategies and relaying protocols. In particular, we characterize the performance of AF and DF relays in terms of outage probability and symbol error rate (SER). Analysis at asymptotic high SNR can be found in the results of References 3 and 42. These results are summarized here to highlight the typical approaches and metrices used to analyze AF and DF relay networks. Similar analysis has been applied to more advanced and complex cooperative network configurations in the literature. More detailed treatment on the performance of cooperative communication systems can be found in a comprehensive textbook by Liu et al. [34].

33.3.1 Diversity Gain in Outage Probability

To establish a baseline for performance comparison, we first visit the simple scenario of a direct source–destination link. We denote $\gamma_0 = P_0/N_0$ as the base SNR. It is well-known that the mutual information per unit bandwidth achieved by independent and identically distributed (i.i.d.) zero-mean, circularly symmetric complex Gaussian source equals to

$$I_D = \log_2(1 + \gamma_0 \mid h_{s,d} \mid^2). \tag{33.30}$$

This mutual information rate is a function of random channel response $h_{s,d}$. We generally assume that $h_{s,d}$ is a Rayleigh fading channel, with zero mean and variance of $\sigma_{s,d}^2$. The outage probability for transmission rate R is therefore given by

$$\Pr[I_D < R] = 1 - \exp\left(-\frac{2^R - 1}{\sigma_{s,d}^2 \gamma_0}\right) \simeq \sigma_{s,d}^{-2} \frac{2^R - 1}{\gamma_0}. \tag{33.31}$$

33.3.1.1 Deterministic AF Relaying

In Section 33.2.1.1, we have described the deterministic AF relay model and the associated signals and notations. Focusing on the simpler Protocol I, the AF relay retransmits the received signal after normalizing the transmit power to P_1 such that the destination receives signal expressed as

$$y_d^{(2)} = h_{1,d} \cdot \beta \cdot y_1 + n_{1,d} \tag{33.32}$$

where

$$\beta = (P_0 \mid h_{s,1} \mid^2 + N_0)^{-1/2} \sqrt{P_1}. \tag{33.33}$$

At the destination node, we assume to use a maximal ratio combining (MRC) receiver to maximize the overall SNR. Equipped with a knowledge of the link channel coefficients, the output of the MRC detector at the destination can be written as

$$y = \alpha_1 y_d^{(1)} + \alpha_2 y_d^{(2)}. \tag{33.34}$$

The combining factors α_1 and α_2 in MRC receiver are chosen to maximize the combined SNR of y. Notice that α_1 and α_2 are not unique as there can be a scalar ambiguity. Nevertheless, finding the optimal combining coefficients is a straightforward Lagrangian problem. One pair of optimum MRC coefficients [3,43] are

$$\alpha_1 = h_{s,d}^*, \quad \alpha_2 = \frac{\beta}{1+\beta^2 \mid h_{1,d} \mid^2} h_{s,1}^* h_{1,d}^*. \tag{33.35}$$

The maximum SNR at the output of the MRC receiver is therefore given by

$$\mathrm{SNR}_{\max} = \underbrace{\frac{P_0}{N_0} \mid h_{s,d} \mid^2}_{\gamma_1} + \underbrace{\frac{P_0}{N_0} \cdot \frac{\mid h_{s,1} h_{1,d} \mid^2}{1 + \frac{P_0}{N_0} \mid h_{s,1} \mid^2 + \frac{P_1}{N_0} \mid h_{1,d} \mid^2}}_{\gamma_2}. \tag{33.36}$$

In essence, the total SNR at the MRC receiver is the sum of the direct link SNR γ_1 and an equivalent relay link SNR γ_2. Thus, the achievable information rate per unit bandwidth is given by

$$I_{\mathrm{AF}} = \frac{1}{2}\log(1 + \mathrm{SNR}_{\max}), \tag{33.37}$$

where the factor of 1/2 characterizes the loss of spectral efficiency resulting from the use of two time phases per data packet transmission.

Outage probability analysis of the Protocol *I* with AF relaying requires the probability distribution of I_{AF} in Equation 33.37. First, we often assume random complex Gaussian fading channels $h_{s,1}$, $h_{1,d}$, and $h_{s,d}$ that are all of zero mean. Let us denote their variances as $\sigma_{s,1}^2, \sigma_{1,d}^2$, and $\sigma_{s,d}^2$, respectively. We recognize that the exact probability density function of I_{AF} is difficult to characterize. This complexity may be circumvented by considering high-SNR scenarios and by limiting our focus on the special case of equal transmit power $P_0 = P_1$. Then, the outage probability at high SNR can be approximated by

$$\Pr[I_{\mathrm{AF}} < R] \simeq \frac{1}{2}\sigma_{s,d}^{-2}(\sigma_{s,1}^{-2} + \sigma_{1,d}^{-2})\left(\frac{2^{2R}-1}{\gamma_0}\right)^2. \tag{33.38}$$

Note that the outage probability decreases at the rate of γ_0^{-2}, which means that the AF protocol achieves diversity order of 2.

33.3.1.1.1 Deterministic DF Relaying

Although deterministic DF relaying is advantageous over AF relaying in its ability to mitigate phase 1 channel noise at the relay, DF relaying may forward incorrectly detected signals to the destination. When considering mutual information, if the relay forwards incorrectly detected symbols, then the forwarded signal confuses the destination, which results in a detection failure. For this reason, the mutual information of DF relaying is dominated by the minimum of the source-relay information rate and the composite source-plus-relay-to-destination information rate:

$$I_{\mathrm{DF}} = \frac{1}{2}\min\{\log(1 + P_0 N_0^{-1} \mid h_{s,1} \mid^2), \log(1 + P_0 N_0^{-1} \mid h_{s,d} \mid^2 + P_1 N_0^{-1} \mid h_{1,d} \mid^2)\}. \tag{33.39}$$

If we consider equal power allocation of $P_0 = P_1$, then the outage probability at high SNR is given by

$$\Pr[I_{\mathrm{DF}} < R] \simeq \sigma_{s,1}^{-2}\frac{2^{2R}-1}{\gamma_0}. \tag{33.40}$$

Thus, from the perspective of asymptotic outage probability, the DF outage probability has diversity order of 1. Compared with the outage probability of direct link in Equation 33.30, this result implies that the deterministic DF offers no diversity gain for large SNR. This somewhat surprising result is a direct consequence of requiring the relay to correctly decode the source information. In essence, the performance of the deterministic DF relay network relies on the quality of the single link between source and relay, which exhibits no channel diversity gain over the direct link channel without cooperation.

33.3.1.2 Selective DF Relaying

In a selective DF relaying, if the receive SNR at the relay exceeds a certain threshold, the relay decodes the received signal and forwards the decoded information to the destination. If the SNR is below the threshold, the relay stays idle. Such an S-DF relay strategy should outperform a deterministic DF relaying, provided that the SNR threshold is selected to allow the relay to correctly decode the source signals with very high probability. One such SNR threshold is $(2^{2R} - 1)$ which is the expected SNR needed to achieve the point-to-point Shannon rate of R. Given this threshold, the SNR of the MRC receiver at destination is the sum of the receive SNR from the source and the relay. Thus, the mutual information for the S-DF relaying is given by

$$I_{\text{S-DF}} = \begin{cases} \frac{1}{2}\log(1 + \gamma_0 \mid h_{s,d} \mid^2), & \gamma_0 \mid h_{s,1} \mid^2 < (2^{2R} - 1) \\ \frac{1}{2}\log(1 + \gamma_0 \mid h_{s,d} \mid^2 + P_1 N_0^{-1} \mid h_{1,d} \mid^2), & \gamma_0 \mid h_{s,1} \mid^2 \geq (2^{2R} - 1). \end{cases} \tag{33.41}$$

Considering the special case of $P_0 = P_1$, that is, an equal power allocation, the outage probability at high SNR equals

$$\Pr[I_{\text{S-DF}} < R] \simeq \frac{1}{2}\sigma_{s,d}^{-2}(\sigma_{s,1}^{-2} + \sigma_{1,d}^{-2})\left(\frac{2^{2R} - 1}{\gamma_0}\right)^2. \tag{33.42}$$

It is hence clear that this selective relaying strategy can now achieve diversity order of 2. For an outage to occur, either the source–destination and source–relay channels must be in outage, or the combined source–destination and relay–destination channel must be in outage. Therefore, both AF relaying and selective DF relaying can achieve the same diversity order of 2 and the same asymptotic outage performance.

33.3.2 Cooperation Gain in Symbol Error Rate

To evaluate the symbol error rate (SER) of a cooperative communication system, the underlying modulation (signaling) scheme plays an important role. Because of the prevalent popularity of QAM and PSK modulations in practice, SER analysis typically focuses on the more popular cases of rectangular M-ary QAM (or M-QAM) and M-ary PSK (or M-PSK) modulations.

33.3.2.1 Asymptotic Symbol Error Rate

We first define several useful coefficients that are functions of M to be used later:

$$\delta_1 = \left(\frac{3(M-1)}{2M} + \frac{\sin(2\pi/M)}{\pi} - \frac{\sin(4\pi/M)}{8\pi}\right)\frac{\sin^{-4}(\pi/M)}{4} \tag{33.43}$$

$$\delta_2 = \frac{(M-1)^2}{3}\left[\frac{1-M^{-1}}{2} + \frac{4(1-M^{-1/2})^2}{3\pi}\right] \tag{33.44}$$

$$\mu_1 = \frac{(2\pi + \sin(2\pi/M))^2}{16\pi^2 \sin^4(\pi/M)\cdot \delta_1} \tag{33.45}$$

$$\mu_2 = \frac{4(M-1)^2 M^{-3}}{9\delta_2}\cdot\left[\frac{M-1}{2} + \frac{(M^{1/2}-1)^2}{\pi}\right]^2. \tag{33.46}$$

33.3.2.1.1 Deterministic AF Relaying

For deterministic AF relays, the SER of M-ary QAM and PSK source signals can be derived by following the process of [34, Ch. 5]. If all channel links in the 3-node network are nonzero, as SNRs P_0/N_0 and P_1/N_0 grow asymptotically large, the SER of AF cooperation with M-PSK and M-QAM signals can be closely approximated by

$$M\text{-PSK:}\quad P_{\text{PSK}}^{\text{AF}}(M) \approx \delta_1 \frac{N_0^2}{P_0\sigma_{s,d}^2}\left(\frac{1}{P_0\sigma_{s,1}^2} + \frac{1}{P_0\sigma_{1,d}^2}\right), \tag{33.47}$$

$$M\text{-QAM:}\quad P_{\text{QAM}}^{\text{AF}}(M) \approx \delta_2 \cdot \frac{N_0^2}{P_0\sigma_{s,d}^2}\left(\frac{1}{P_0\sigma_{s,1}^2} + \frac{1}{P_1\sigma_{1,d}^2}\right). \tag{33.48}$$

We can see that, for both modulations, the SER drops as a function of $(P_0/N_0)^{-2}$. Thus, from the perspective of SER, the AF cooperation also provides a diversity order of 2, which is similar to the AF outage probability analysis.

33.3.2.1.2 Deterministic DF Relaying

For sufficiently high SNR, the SER of DF cooperation systems can be similarly approximated [34, Ch. 5] as

$$M\text{-PSK:}\quad P_{\text{PSK}}^{\text{DF}}(M) \approx \delta_1 \frac{N_0^2}{P_0\sigma_{s,d}^2}\left(\frac{\mu_1}{P_0\sigma_{s,1}^2} + \frac{1}{P_1\sigma_{1,d}^2}\right) \tag{33.49}$$

$$M\text{-QAM:}\quad P_{\text{QAM}}^{\text{DF}}(M) \approx \delta_2 \cdot \frac{N_0^2}{P_0\sigma_{s,d}^2}\left(\frac{\mu_2}{P_0\sigma_{s,1}^2} + \frac{1}{P_1\sigma_{1,d}^2}\right). \tag{33.50}$$

It is clear from the comparison of symbol error rates between AF and DF cooperations that their difference in SER lies in an extra scalar of μ_1 for M-PSK and μ_2 for M-QAM, respectively. As shown in Equations 33.49 and 33.50, the SER of both modulations in DF relay would also decrease asymptotically as a function of $(P_0/N_0)^{-2}$. Thus, from the SER point of view, both DF and AF offer cooperation diversity order of 2 at high SNR. This conclusion differs from the outage probability analysis. Such discrepancy is due to the fact that for DF relays, it is much harder for the entire packet to be correctly decoded whereas it is much more likely for most individual symbols to be correctly decoded.

33.3.2.2 DF versus AF Cooperation Gains

To quantify the cooperation gain in terms of SER reduction, we can assume that all channel statistical informations $\sigma_{s,d}$, $\sigma_{s,1}$, and $\sigma_{1,d}$ are known to all 3-nodes. By imposing a sum power constraint $P_0 + P_1 \le P$, the

asymptotic SER of Equations 33.49 and 33.50 can be optimized directly via constrained minimization. As discussed in Reference 34, Chapter 5, the optimized asymptotic symbol error rate can be found to be

$$P_{\mathrm{DF}}^{\circ} \approx \left(\Delta_{\mathrm{DF}} \frac{P}{N_0}\right)^{-2}, \tag{33.51}$$

where we find the *DF cooperation gains* of M-PSK and M-QAM signals, respectively, as

$$M\text{-PSK:} \quad \Delta_{\mathrm{DF}} = \sqrt{\frac{8}{\delta_1}} \frac{\sigma_{s,d}\sigma_{s,1}\sigma_{1,d}\left(\sigma_{s,1} + \sqrt{\sigma_{s,1}^2 + 8_{\mu_1}\sigma_{1,d}^2}\right)^{1/2}}{\left(3\sigma_{s,1} + \sqrt{\sigma_{s,1}^2 + 8_{\mu_1}\sigma_{1,d}^2}\right)^{3/2}} \tag{33.52}$$

$$M\text{-QAM:} \quad \Delta_{\mathrm{DF}} = \sqrt{\frac{8}{\delta_2}} \frac{\sigma_{s,d}\sigma_{s,1}\sigma_{1,d}\left(\sigma_{s,1} + \sqrt{\sigma_{s,1}^2 + 8_{\mu_2}\sigma_{1,d}^2}\right)^{1/2}}{\left(3\sigma_{s,1} + \sqrt{\sigma_{s,1}^2 + 8_{\mu_2}\sigma_{1,d}^2}\right)^{3/2}}. \tag{33.53}$$

The cooperation gains depend on the random channel variances that characterize the statistical strength of different channel links. Following the approach used in determining the optimum power allocation for DF, the AF power allocation can be similarly optimized by minimizing the AF symbol error rate of Equations 33.47 and 33.48. Because of their similarities with the DF symbol error rate, the resulting minimum SER is asymptotically equal to

$$P_{\mathrm{AF}}^{\circ} \approx \Delta_{\mathrm{AF}}^{-2}\left(\frac{P}{N_0}\right)^{-2}. \tag{33.54}$$

Note that, by setting $\mu_1 = 1$ and $\mu_2 = 1$ in the DF cooperation gain, we have

$$M\text{-PSK:} \quad \Delta_{\mathrm{AF}} = \sqrt{\frac{8}{\delta_1}} \frac{\sigma_{s,d}\sigma_{s,1}\sigma_{1,d}\left(\sigma_{s,1} + \sqrt{\sigma_{s,1}^2 + 8\sigma_{1,d}^2}\right)^{1/2}}{\left(3\sigma_{s,1} + \sqrt{\sigma_{s,1}^2 + 8\sigma_{1,d}^2}\right)^{3/2}} \tag{33.55}$$

$$M\text{-QAM:} \quad \Delta_{\mathrm{AF}} = \sqrt{\frac{8}{\delta_2}} \frac{\sigma_{s,d}\sigma_{s,1}\sigma_{1,d}\left(\sigma_{s,1} + \sqrt{\sigma_{s,1}^2 + 8\sigma_{1,d}^2}\right)^{1/2}}{\left(3\sigma_{s,1} + \sqrt{\sigma_{s,1}^2 + 8\sigma_{1,d}^2}\right)^{3/2}}. \tag{33.56}$$

Δ_{AF} is the *cooperation* gain of the deterministic AF cooperation systems, and indicates the best asymptotic performance gain of the AF cooperation protocol with the optimum power allocation.

Clearly, the difference between the AF and the DF gains depends on the coefficients μ_1 and μ_2 which are both functions of the constellation size M. We can use the *cooperation gain ratio* $\Delta_{\mathrm{DF}}/\Delta_{\mathrm{AF}}$ to illustrate the difference of performance gains by using the two deterministic relaying strategies. We provide the cooperation gain ratio in Table 33.2 for various statistical channel relationship and different constellations. The comparison shows that, in terms of SER reduction, DF cooperation gain is always larger than AF cooperation gain for both M-PSK and M-QAM modulations. It is important to note, however, that the performance advantage of DF cooperation is based on the following conditions: (i) statistical channel information is available to allow optimized power allocation; (ii) the channel link quality between the relay and the destination is much stronger than that between the source and the

TABLE 33.2 DF-to-AF Cooperation Gain Ratio according to Modulation Schemes

Modulation	$\sigma_{s,1}^2 \ll \sigma_{1,d}^2$	$\sigma_{s,1}^2 = \sigma_{1,d}^2$	$\sigma_{s,1}^2 \gg \sigma_{1,d}^2$
BPSK	$\sqrt{3}$	1.1514	1
QPSK	1.3214	1.0851	1
8PSK	1.2393	1.0670	1
M—PSK (*M* large)	1.2247	1.0635	1
16QAM	1.1245	1.0378	1
M—QAM (*M* large)	1.0175	1.0058	1

relay, and (iii) the signal constellation size is not large such that the relay makes fewer errors. Because of the higher complexity required by the DF relay, there is a performance versus complexity trade-off. For high-rate cooperative communications utilizing large constellations, AF cooperation may be more preferable since AF relaying requires lower complexity and delivers comparable performance in terms of SER.

33.4 Cooperative Scheduling and Resource Allocation

33.4.1 Resource Allocation Issues

Unlike point-to-point transmission systems, cooperative communications require the resources such as the bandwidth and the power to be properly allocated among the source and relay nodes. For example, in OFDM-based cooperative systems, the power needs to be allocated, not only between the source and the relays, but also among their subcarriers (subchannels). Furthermore, the subchannels also need to be carefully allocated between the source and the relays.

Such issues of resource allocation are of critical importance to cooperative systems for two reasons. First, for cooperation, choosing the right nodes to cooperatively transmit at the right time and in the right subchannel is vital. If the channel between a source and a relay or the channel between a relay and a destination is in deep fading, relay transmission wastes precious system resources. Second, subchannels may experience time-varying SNR. Because the benefit of cooperation is more significant to low-SNR subchannels, optimizing subchannel allocation among different nodes can lead to substantial performance improvement. Given the strict bandwidth and power resources in practice, medium access scheduling and power allocation are two of the most important considerations in cooperative networks.

33.4.2 Medium Access Scheduling

Transmission scheduling of different nodes in a cooperative wireless network is essential to optimum traffic routing and throughput maximization. It must also take into account other key issues such as interference control and fairness. Even for a moderately complex network configuration with a plurality of source and intermediate nodes, medium access control can be a challenging issue. Indeed, transmission scheduling of various nodes is essential to effective cooperation and efficient bandwidth usage.

Node scheduling must overcome a number of practical constraints: half-duplexity of the relay nodes, finite relay power or lifetime, and interference tolerance. As discussed earlier, half-duplex relays force each node to operate in at least two phases. Additionally, mutual interference among cooperate nodes must be controlled such that source signals can be fully recovered by destination nodes, possibly through joint detection or interference cancellation.

For these aforementioned reasons, scheduling depends to a large extent on the network topology. We use the linear multihop relay network as a concrete example to illustrate several possible ways of relay scheduling and cooperation.

33.4.2.1 Hop-by-Hop Linear Multihop Scheduling

The simplest linear relay scheduling is to use the hop-by-hop (HBH) protocol as shown in Figure 33.9. In HBH, each node transmits directly to its next node in a simple handoff manner. This naive protocol requires $L + 1$ stages in an L-relay network. It accommodates half-duplex relay nodes, requires only one pair of active transceiving nodes, and requires no special interference management. Its major disadvantage is the $L + 1$ packet slots required to transmit a single packet, leading to a low throughput of $1/(L + 1)$. The second shortcoming is that this network performance is dominated by the weakest link among the $L + 1$ hops.

33.4.2.2 Time-Division-Node Access

A slight modification of HBH is to divide the $L + 1$ links into odd and even node groups. In short, the entire access time is split into 2 alternating time slots. In the odd time slot, the odd relays are scheduled for transmission whereas during the even time slot, the even relays are scheduled. Table 33.3 clearly illustrates how the odd and even relays are scheduled for transmission of their own packets. This time-division-node access (TDNA) protocol can achieve a much higher throughput of 1/2.

In comparison with HBH, one major drawback of TDNA is the need for interference management. Notice that relay $2i + 1$ during reception will hear both transmissions from nodes $2i$ and $2i + 2$. At time k, relay $2i + 1$ will hear a new packet $k - i$ from node $2i - 1$ and also an old packet $k - i - 1$ from node $2i + 2$. This interference effect can be overcome by relay $2i + 1$ via interference cancellation. More specifically, node $2i + 1$ should buffer the last packet $k - i - 1$ in advance. When receiving packet $k - i$, node $2i + 1$ can recover the new packet $k - i$ by cancelling the known interference from packet $k - i - 1$ in its received signals.

Naturally, the concept of TDNA can be easily generalized by splitting the relay nodes into K groups. The members in each access group are separated by $K - 1$ other groups. Allocating K time slots for relay node access, this more general TDNA protocol would achieve a lower throughput of $1/K$. In exchange for the reduced throughput, its interference from downstream nodes becomes much weaker and easier to manage.

33.4.3 Virtual MIMO Relay Cooperation

It is clear that because of the linear relay network topology, both HBH and TDNA suffer from the weakest link problem. In fact, to mitigate the weakest link problem, relay functions need to be strengthened. One concept for improving the reliability of relay reception in HBH is to form a virtual

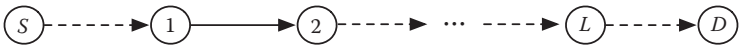

FIGURE 33.9 Hop-by-hop scheduling in a multihop network showing an active second hop.

TABLE 33.3 Alternating Time-Division Node Scheduling in Linear Multihop Networks

Node	Phase 1	Phase 2
Source	Transmit packet k	Receive packet $k + 1$
Relay number $2i + 1$	Receive packet k ☒ i	Transmit packet k ☒ i
Relay number $2i + 2$	Transmit packet k ☒ $i - 1$	Receive packet k ☒ i
Destination	Receive packet $k - [L/2]$	

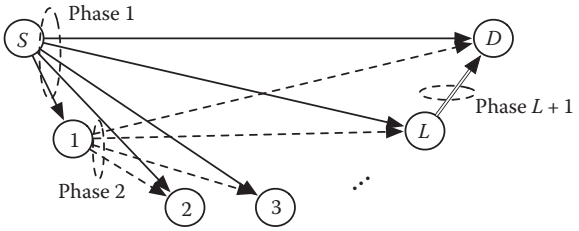

FIGURE 33.10 Virtual MIMO relay network.

MIMO (or V-MIMO). The basic idea of V-MIMO is illustrated in Figure 33.10. V-MIMO can be realized by letting each downstream relay listen to and buffer packets transmitted by *all or a subset of* its upstream relay nodes. During its own packet decoding, node ℓ in effect can rely on the multiple transmissions received from ℓ previous transmissions of the same packet from node $\ell - F$ to node $\ell - 1$.

As shown in Reference 17, we can allow node ℓ to collect the last F signal transmissions of the same data packet s_k from the F preceding nodes,

$$y_\ell^{(i)}(k) = \sqrt{P} h_{\ell-i,\ell} s_0(k) + n_\ell^{(i)}(k), \quad i = 1,2,\ldots,F. \tag{33.57}$$

Node ℓ can jointly utilize $y_\ell^{(i)}(k)$ to detect the common packet of interest $s_0(k)$. Applying DF at each relay, the virtual ℓ-channel MIMO system can substantially improve the diversity gain of the transmission. Each link's channel gain is improved by a factor of

$$| h_{\ell-1,\ell} |^{-2} \sum_{i=1}^{F} | h_{\ell-i,\ell} |^2.$$

Effectively given F multiple channels in V-MIMO, node ℓ can better overcome the performance loss if the channel condition worsens between node $\ell - 1$ and node ℓ. Thus, V-MIMO no longer suffers from the weakest link problem. Such relay nodes are also known as "cumulative" relays [44]. Although this V-MIMO relay strategy has the same throughput rate as HBH, the much improved diversity at each relay node decoding makes V-MIMO far more reliable, thereby reducing substantially the need for additional bandwidth required for retransmission.

33.4.4 Turbo Relaying

An even more sophisticated retransmission strategy, known as turbo-relay, can also apply the V-MIMO principle by utilizing the concept of FEC and incremental redundancy. Developed in Reference 45, turbo-relay allows the source node, along with several *critical nodes* in the relay chain, to broadcast the entire packet downstream. From there, each relay downstream from the critical node will simply store and attempt to decode the packet. If the CRC of a relay's packet decoding ends in error, the relay will simply wait for its upstream relays to decode the packet before receiving additional FEC parity bits or symbols sent by these (noncritical) relays. Note that the noncritical relays do not broadcast the full packet and transmit only a fraction of their FEC parity bits, which allows lower bandwidth usage by noncritical relays. Thus, turbo-relay can improve the overall network throughput of HBH substantially. Let a linear multihop link consist of L_0 noncritical relays and $L - L_0$ critical relays. By shortening the turbo-relay fraction time to $1/F$ of the entire data packet, turbo relay can shorten the time required for

a packet delivery from L to $(L - L_0) + L_0/F$. The throughput improvement factor can be substantial when $L_0 \gg L - L_0$.

33.4.5 Dynamic Relay Scheduling for Multiple Source–Destination Pairs

When a network of relays serves multiple source–destination pairs, the challenges of relay scheduling for different source–destination pairs lie in the variety of competing performance considerations, including high throughput, user fairness, low power consumption, and channel state information (CSI) sharing. Dynamic relay scheduling should rely on certain amount of CSI access. For example, Hammerström et al. [4] proposed a channel-adaptive relay scheduling, in which, focusing on AF relays, the multiple destinations cooperate by selecting relay scheduling for different destinations based on their cumulative SNR comparison. In the dual-destination case, relays can be scheduled to serve two destination nodes according to their time-varying channel gains. Additionally, random phase offsets can be applied to relay outputs [4] to achieve better diversity and average relay throughput.

33.4.6 Power Allocation

Optimum power allocation among sources and relay nodes is a key process to realize the full potentials of cooperative communications. Three fundamental issues in cooperative networks are often at the center of investigation [34,42,46]:

- Transmit power allocation in the broadcasting and relaying phases
- Power allocation to the source and relay nodes in the relaying phase
- Power allocation to each hop in the multihop communications

Clearly, CSI information is essential to power allocation optimization. Without CSI, equal power allocation is a simple and effective approach, though in general not optimum. But with full or partial knowledge of the CSI, significant improvement in terms of BER, outage probability, or capacity can be attained by applying optimal power allocation among cooperating nodes [47].

Let us take the simple 3-node relay network as an example. The relay node may be closer to the source, or closer to the destination. In the first scenario, equal power allocation between the two nodes is near optimal. But when the relay is closer to the destination, more power should be allocated to the source node as the link between the source and the relay becomes less reliable. Specifically, if the link quality of source–relay is much worse than that of relay-destination, then we should allocate all power to the source and ignore the relay. On the other hand, if the link quality of source–relay is much better than that of relay–destination, then equal power allocation to source and relay tends to be optimum.

It is clear that solutions to the fundamental issues of power allocation would differ for various network topologies, multiple access scheduling, cooperation strategies, and CSI access. In this section, we specifically focus on the simple 3-node relay network that cooperates using Protocol I. We consider both AF relaying and DF relaying strategies. We further assume that statistical CSI is available to all three nodes when deriving optimized power allocations for AF and DF relays.

33.4.6.1 Asymptotic Optimum Power Allocation in 3-Node DF Cooperation

From the SER analysis of 3-node relay systems, the asymptotic SER at high SNR equals

$$P^{\mathrm{DF}}(M) \approx \delta_i \frac{N_0^2}{P_0 \sigma_{s,d}^2} \left(\frac{\mu_i}{P_0 \sigma_{s,1}^2} + \frac{1}{P_1 \sigma_{1,d}^2} \right), \tag{33.58}$$

where $i = 1$ denotes the case of M-PSK and $i = 2$ denotes the case of M-QAM.

Given the total sum power constraint of $P_0 + P_1 = P$, we can formulate the optimum power allocation problem by minimizing the symbol error rate $P^{\text{DF}}(M)$. Using a Lagrangian [34, Ch. 5], the optimum power allocation can be formulated as

$$\max_{P_0,P_1} \frac{1}{P_0\sigma_{s,d}^2}\left(\frac{\mu_i}{P_0\sigma_{s,1}^2} + \frac{1}{P_1\sigma_{1,d}^2}\right) \quad \text{subject to} \quad P_0 + P_1 = P. \tag{33.59}$$

Thus, at high SNR, the respective optimum power allocations for M-PSK and M-QAM are [34],

$$M\text{-PSK:} \quad \overline{P}_0 = \frac{\sigma_{s,1} + \sqrt{\sigma_{s,1}^2 + 8\mu_1\sigma_{1,d}^2}}{3\sigma_{s,1} + \sqrt{\sigma_{s,1}^2 + 8\mu_1\sigma_{1,d}^2}} P, \tag{33.60}$$

$$M\text{-QAM:} \quad \overline{P}_0 = \frac{\sigma_{s,1} + \sqrt{\sigma_{s,1}^2 + 8\mu_2\sigma_{1,d}^2}}{3\sigma_{s,1} + \sqrt{\sigma_{s,1}^2 + 8\mu_2\sigma_{1,d}^2}} P. \tag{33.61}$$

We see that the asymptotic optimum power allocation does not depend on the channel link between source and destination. Instead, it depends on the channel link of source-to-relay and the link of relay-to-destination. Moreover, we can see that the optimum source power allocation $\overline{P}_0$ is between $P/2$ and P. Thus, we should always allocate more power to the source and less to the relay.

33.4.6.2 Asymptotic Optimum Power Allocation for AF Cooperation

The optimum power allocation for AF is a special case of the DF optimization. By simply letting $\mu_i = 1$, we immediately find the optimum source power allocation for M-PSK and M-QAM to be identically,

$$M\text{-PSK and } M\text{-QAM:} \quad \overline{P}_0 = \frac{\sigma_{s,1} + \sqrt{\sigma_{s,1}^2 + 8\sigma_{1,d}^2}}{3\sigma_{s,1} + \sqrt{\sigma_{s,1}^2 + 8\sigma_{1,d}^2}} P. \tag{33.62}$$

Hence, unlike in DF cooperation, the optimum power allocation for AF cooperation systems does not change with the modulation format. The difference arises from the fact that in DF cooperation, the relay must decode the modulated source signal before forwarding. The accuracy of relay decoder therefore would be different for different modulations.

Similar to the case of DF relaying, we can see from Equation 33.62 that the optimum source power $\overline{P}_0$ is between $P/2$ and P. Thus, more power is given to the source and less power to the relay in general. Another interesting note is that, similar to the case of DF relay, optimum power allocation for AF relay is also insensitive to the statistical strength of the channel $h_{s,d}$ between source and destination.

33.5 Theory and Practice

This chapter presents a rather abbreviated introduction to the highly active research field of cooperative communications. For comprehensive discussions on various aspects of this subject, interested readers should consult several tutorial papers such as [48–50] and books specially dedicated to this subject field [34,51,52]. As shown in preceding sections, much of the literature on cooperative communications remains theoretical. Typically, such theoretical works are constrained by their often idealized assumptions. Most works on cooperative communications tend to assume that the receivers have full or partial knowledge of channel state information (CSI). Although in practice, channel estimates may be available

TABLE 33.4 Comparison of Cooperative Protocols in IEEE WiMAX, 3GPP LTE-A, and IEEE802.11s

	IEEE 802.16j	3GPP LTE-Advanced	IEEE 802.11s
Scheduling	Centralized/distributed	Centralized	Distributed
Cooperation type	DF	DF	DF
Topology	Relay	Relay, cooperative MIMO	Relay
Backward compatibility	Yes	Yes	Yes
Cell-edge enhancement	No	Yes	No
Coverage expansion	Yes	No	Yes
Throughput enhancement	Yes	Yes	Yes
Number of cooperative nodes	≥2	≥2	≥2

when the channel changes are slow with respect to packet rate, they are not easy to acquire in fast-fading environments. Cooperative diversity can save the required transmit power owing to the diversity gains of cooperation. However, one must take into account the extra processing and power consumption at the relay and destination nodes required for the cooperation. Future studies on cooperative communications must carefully address these trade-off issues and further relax the reliance on assumptions of accurate CSI knowledge.

Despite the predominantly theoretical nature of the literature on cooperative communications, practical applications of cooperative communication systems and networking are beginning to emerge. Wireless cooperative communication technologies have been brought into the standardization process of next-generation broadband communication systems such as LTE-Advanced Release 10 (LTE-A R10) [53,54], IEEE 802.16j (WiMAX) [55], and IEEE 802.11s. Basically, relay technologies in the LTE-A R10 and WiMAX are very similar. In both cases, a relay is essentially an orthogonal frequency division multiple access (OFDMA) subbase station with a wireless backhaul link. However, some open issues, such as mobility, power saving, multihop architecture, transparent relaying, multicarrier transmission, and cooperative transmission, are still left as challenges. In IEEE 802.11s, the concept and operation of Mesh Access Point (MAP) has been defined. MAPs are wireless access points serving as two-way relays between the root node and the mobile stations. MAP deployment can be found in IEEE 802.11s products [56] which are facilitated by the proposed cooperative MAC [57]. More recently, 3GPP has initiated the standardization discussion of coordinated multipoint (CoMP) transmission by coordinating multiple neighboring base stations in LTE-Advanced (Release 11) [58]. Table 33.4 summarizes the current status of wireless cooperation networks in practical applications. Without a doubt, practical applications of cooperative communications are expected to grow rapidly as both theories and technologies continue to develop.

References

1. T. Cover and A. El Gamal, Capacity theorems for the relay channel, *IEEE Trans. on Information Theory*, IT-25(5): 572–584, 1979.
2. G. Kramer, I. Maric, and R. D. Yates, Cooperative communications, *Foundations and Trends in Networking*, 1(3–4): 271–425, 2006.
3. J. N. Laneman, D. N. C. Tse, and G. W. Wornell, Cooperative diversity in wireless networks: Efficient protocols and outage behavior, *IEEE Trans. Inf. Theory*, 50(12): 3062–3080, 2004.
4. I. Hammerström, M. Kuhn, and A. Wittneben, Channel adaptive scheduling for cooperative relay networks, *IEEE Vehicular Technology Conference*, VTC Fall 2004, Los Angeles, September 2004.
5. A. Sendonaris, E. Erkip, and B. Aazhang, User cooperation diversity—part I: System description, *IEEE Trans. Comm.*, 51: 1927–1938, 2003.

6. J. N. Laneman and G. W. Wornell, Distributed space–time-coded protocols for exploiting cooperative diversity in wireless networks, *IEEE Trans. Inf. Theory*, 49(10): 2415–2425, 2003.
7. L. Zheng and D. N. C. Tse, Diversity and multiplexing: A fundamental tradeoff in multiple-antenna channels, *IEEE Trans. Inf. Theory*, 49(5): 1073–1096, 2003.
8. S. Huixia, Evolution and interference analysis of cooperative communication systems., *ZTE Commun.*, 8(1): 17–20, 2010.
9. A. Goldsmith, *Wireless Communications*, Cambridge University Press, New York, NY, 2005.
10. R. U. Nabar, H. Bolcskei, and F. W. Kneubuhler, Fading relay channels: Performance limits and space–time signal design, *IEEE J. Selected Areas Commun.*, 22: 1099–1109, 2004.
11. A. S. Avestimehr, S. Diggavi, and D. N. C. Tse, A deterministic approach to wireless relay networks, *Proc. Allerton Conference on Communications, Control and Computing*, Monticello, IL, USA, October 2007.
12. A. Host-Madsen and J. Zhang, Capacity bounds and power allocation in wireless relay channel, *IEEE Trans. on Information Theory*, 51: 2020–2040, 2005.
13. I. Maric and R. D. Yates, Bandwidth and power allocation for cooperative strategies in Gaussian relay networks, *Proc. 38th Asilomar Conf. Signal, System Computers*, pp. 1907–1911, November 2004.
14. Y. Zhao, R. Adve, and T.-J. Lim, Improving amplify-and-forward relay networks: Optimal power allocation versus selection, *IEEE Trans. Wireless Communications,* 6(8):1234–1238, 2006.
15. L-L. Xie and P. R. Kumar, A network information theory for wireless communication: Scaling laws and optimal operation, *IEEE Trans. Inf. Theory*, 50(5): 748–767, 2004.
16. J. Boyer, D. D. Falconer, and H. Yanikomeroglu, Multihop diversity in wireless relaying channels, *IEEE Trans. on Commun.*, 52(10): 1820–1830, 2004.
17. A. K. Sadek, W. Su, and K. J. R. Liu, Multinode cooperative communications in wireless networks, *IEEE Trans. Signal Processing*, 55(1): 341–355, 2007.
18. G. K. Karagiannidis, T. Tsiftsis, and R. K. Mallik, Bounds for multihop relayed communications in Nakagami fading, *IEEE Trans. Communications*, 54(1): 18–22, 2006.
19. M. O. Hasna and M. S. Alouini, Outage probability of multihop transmission over Nakagami fading channels, *IEEE Comm. Letters*, 7(5): 216–218, 2003.
20. M. S. P. Kumar, P. Herhold, R. Bhattacharjee, and G. Fettweis, Cooperative multi-hop relaying over fading channels using cascaded 2-hop technique, Proceedings of the IEEE INDICON 2004, pp. 139–142, December 20–22, 2004.
21. G. Kramer, M. Gastpar, and P. Gupta, Cooperative strategies and capacity theorems for relay networks, *IEEE Trans. Inf. Theory*, 51(9): 3037–3063, 2005.
22. A. Bletsas, A. Khisti, D. P. Reed, and A. Lippman, A simple cooperative diversity method based on network path selection, *IEEE J. Select. Areas Commun.*, 24(3): 659–672, 2006.
23. E. Beres and R. Adve, Selection cooperation in multi-source cooperative networks, *IEEE Trans. Wireless Communications*, 7(1): 118–127, 2008.
24. A. Ribeiro, X. Cai, and G. B. Giannakis, Symbol error probabilities for general cooperative links, *IEEE Trans. Wireless Communications*, 4(3): 1264–1273, 2005.
25. T. C.-Y. Ng and W. Yu, Joint optimization of relay strategies and resource allocations in cooperative cellular networks, *IEEE J. Select. Areas Commun.*, 25(2): 328–339, 2007.
26. B. Zhao and M. C. Valenti, Practical relay networks: A generalization of hybrid-ARQ, *IEEE J. Select. Areas Commun.*, 23(1): 7–18, 2005.
27. H. Bolcskei, R. U. Nabar, O. Oyman, and A. J. Paulraj, Capacity scaling laws in MIMO relay networks, *IEEE Trans. Wireless Commun.*, 5(6): 1433–1444, 2006.
28. G. Scutari and S. Barbarossa, Distributed space–time coding for regenerative relay networks, *IEEE Trans. Wireless Commun.*, 4(5): 2387–2399, 2005.
29. S. Yiu, R. Schober, and L. Lampe, Distributed space–time block coding, *IEEE Trans. Communications*, 55(7): 1195–1206, 2006.
30. P. A. Anghel, G. Leus, and M. Kaveh, Distributed space–time cooperative systems with regenerative relays, *IEEE Trans. Wireless Commun.*, 5(11): 3130–3141, 2006.

31. Y. Jing and B. Hassibi, Distributed space–time coding in wireless relay networks, *IEEE Trans. Wireless Commun.*, 5(12): 3524–3536, 2006.
32. S. Yang and J-C. Belfiore, Optimal space–time codes for the MIMO amplify-and-forward cooperative channel, *IEEE Trans. Inf. Theory*, 53(2): 647–663, 2007.
33. B. Sirkeci-Mergen and A. Scaglione, Randomized space–time coding for distributed cooperative communication, *IEEE Trans. Signal Process.*, 55(10): 5003–5017, 2007.
34. K. J. R. Liu, A. K. Sadek, W. Su, and A. Kwasinski, *Cooperative Communications and Networking*, Cambridge University Press, New York, NY, USA, 2009.
35. R. Ahlswede, N. Cai, S-Y. R. Li, and R. W-H. Yeung, Network information flow, *IEEE Trans. on Information Theory*, 46: 1204–1216, 2000.
36. S. Li, R. Yeung, and N. Cai, Linear network coding, *IEEE Trans. on Information Theory*, 49(2): 371–381, 2003.
37. R. Koetter and M. Medard, An algebraic approach to network coding, *IEEE Trans. on Networking*, 11(5):782–796, October 2003.
38. S. Zhang, S. C. Liew, and P. P. Lam, *Physical-Layer Network Coding*, ACM MobiCom, Los Angeles, USA, September 2006.
39. B. Rankov and A. Wittneben, Spectral efficient protocols for half-duplex fading relay channels, *IEEE J. Select. Areas Commun.*, 25(2): 379–389, 2007.
40. K. Narayanan, M. P. Wilson, and A. Sprintson, Joint physical layer coding and network coding for bi-directional relaying, *Proc. Allerton Conference on Communication, Control and Computing*, Monticello, IL, USA, 2007.
41. F. Xue and S. Sandhu, PHY-Layer Network Coding for Broadcast Channel with Side Information, ITW 2007, Lake Tahoe, California, September 2–6, 2007.
42. E. G. Larsson and Y. Cao, Collaborative transmit diversity with adaptive radio resource and power allocation, *IEEE Comm. Lett.*, 9(6): 511–513, 2005.
43. M. Yuksel and E. Erkip, Diversity in relaying protocols with amplify and forward, *IEEE Global Telecommunications Conference, 2003*, vol. 4, pp. 2025–2029, December 1–5, 2003.
44. I. Maric and R. D. Yates, Cooperative multihop broadcast for wireless networks, *IEEE J. Selected Areas in Communications*, 22(6): 1080–1088, 2004.
45. O. Gurewitz, A. de Baynast, and E. W. Knightly, Cooperative strategies and achievable rate for tree networks with optimal spatial reuse, *IEEE Trans. Inf. Theory*, 53(10): 3596–3614, 2007.
46. X. Deng and A. M. Haimovich, Power allocation for cooperative relaying in wireless networks, *IEEE Comm. Letters*, 9(11): 994–996, 2005.
47. Y-W. Hong, W-J. Huang, F-H. Chiu, and C.-C. J. Kuo, Cooperative communications in resource-constrained wireless networks, *IEEE Signal Processing Mag.*, 24(3): 47–57, 2007.
48. A. Nosratinia, T. E. Hunter, and A. Hedayat, Cooperative communication in wireless networks, *IEEE Comm. Magazine*, 42(10): 74–80, 2004.
49. R. Pabst et al. Relay-based deployment concepts for wireless and mobile broadband radio, *IEEE Comm. Magazine*, 42(9): 80–89, 2004.
50. A. Scaglione, D. L. Goeckel, and J. N. Laneman, Cooperative communications in mobile Ad Hoc networks, *IEEE Signal Processing Magazine*, 23(5): 18–29, 2006.
51. M. Dohler and Y. Li, *Cooperative Communications: Hardware, Channel & PHY*, Wiley, Hoboken, NJ, 2010.
52. P. Y.-W. Hong, W.-J. Huang, and C.-C. J. Kuo, *Cooperative Communications and Networking: Technologies and System Design*, Springer, New York, 2010.
53. K. Loa, C-C. Wu, S-T. Sheu, Y. Yuan, M. Chion, D. Huo, and X. Ling, IMT-advanced relay standards, *IEEE Comm. Magazine*, 48(8): 40–48, 2010.
54. Y. Yang, H. Hu, J. Xu, and G. Mao, Relay technologies for WiMAX and LTE-advanced mobile systems, *IEEE Comm. Magazine*, 47(10): 1–7, 2009.
55. S. W. Peters and R. W. Heath, Jr., The future of WiMAX: Multihop relaying with IEEE 802.16j, *IEEE Comm. Magazine*, 47(1): 104–111, 2009.

56. J. Camp and E. Knightly, The IEEE 802.11s extended service set mesh networking standard, *IEEE Comm. Magazine*, 46(8): 120–126, 2008.
57. P. Liu, Z. Tao, S. Narayanan, T. Korakis, and S. S. Panwar, CoopMAC: A cooperative MAC for wireless LANs, *IEEE J. on Selected Areas in Communications*, 25(2): 340–354, 2007.
58. A. Ghosh, R. Ratasuk, B. Mondal, N. Mangalvedhe, and T. Thomas, LTE-advanced: Next-generation wireless broadband technology, *IEEE Wireless Communications*, 17(3): 10–22, 2010.

34

Cross-Layer Cooperative Communication in Wireless Networks

Matthew Nokleby
Gareth Middleton
Behnaam Aazhang

34.1 Introduction

Research in cooperative communications was inaugurated by the advent of the relay channel [1,2]. In this simple three-node model, a relay aids the communication a source–destination pair by overhearing the source's signal and forwarding some function of it to the destination. The Shannon capacity of the relay channel is unknown, but Reference 2 describes simple schemes that allow the relay to greatly improve throughput. Cooperative communications has been studied more recently for wireless networks in References 3 through 5. While specifics of topology, relay schemes, and so on differ between works, they share a common thread: users assist each other by forwarding each other's messages, leading to an improvement in rate and/or reliability.

Despite its promise of improved performance, cooperative communication is yet to see widespread adoption in practical wireless networks.* Increased overhead is an obvious culprit; introducing relays typically requires additional channel state information and at least minimal synchronization among nodes. Beyond the obvious difficulties of overhead, we identify two additional issues, which are addressed in this chapter. First, cooperative communications by definition involves energy expenditure on behalf of other users. Especially in cellular systems, where mobile users face severe energy limitations, cooperation may entail energy demands that are undesirable from the perspective of individual users. Thus, a means for efficient, fair energy sharing is required. Second, the coordinated-terminal,

* A preliminary deployment, known as a "Mobile Multihop Relay," is proposed in the specification of IEEE 802.16j, it but has yet to see implementation [6].

constructive-interference aspect of cooperation significantly complicates medium-access issues, particularly in larger *ad hoc* networks. Efficient, practical algorithms are required that simultaneously manage relay selection, interference management, and routing in order to exploit the potential of cooperative communications.

To address these issues, we must look at several layers of the network stack. Cooperation is intrinsically a signal-level, physical-layer phenomenon, but both the link and medium access layers must be modified in order to appropriately incorporate cooperation. Accordingly, we describe techniques that operate at multiple layers in order to facilitate and manage cooperation between users.

In Section 34.2, we introduce the relay channel, which forms the atomic unit of the techniques described. We review the information-theoretic techniques described in Reference 2, focusing specifically on the decode-and-forward rates that are achievable via block Markov encoding.

In Section 34.3, we describe an approach to fair, efficient energy sharing between users in a small cellular scenario. In order to facilitate cooperation between energy-selfish users, we cast the problem as an infinite-stage game in which users choose relay power allocations in order to maximize the bits-per-energy efficiency. We detail a method for efficiently finding the power allocations that satisfy the Nash bargaining solution [7], which is well known to give a fair, efficient solution on the boundary of the achievable region. Numerical results show that cooperation can simultaneously improve each user's bits-per-energy efficiency for a wide variety of channel conditions, and that the Nash bargain results in a "fair" distribution of resources, allowing weaker users to benefit the most from cooperation.

In Section 34.4, we describe a cross-layer model for network resource allocation, within which we study the scheduling and routing problem while permitting information-theoretic rate control on wireless links. Rate control enables cooperative communications to be integrated into the broader resource-allocation paradigm of large *ad hoc* networks. This model results in a polynomial-time algorithm for efficient relay selection, scheduling, routing, and power control. Numerical results show that cooperation significantly impacts on routing and scheduling decisions and permits a substantial improvement in network throughput with only minor increases in computational complexity and information overhead.

34.2 Relay Channel

The relay channel, depicted in Figure 34.1, is the fundamental unit of cooperative communications. Three terminals comprise the relay channel: a source with a message to transmit, a destination intending to receive the source's message, and a relay willing to facilitate communication with the destination. In the AWGN relay channel, the source and relay transmit signals X_s and X_r, and the relay and destination receive signals Y_r and Y_d, as follows:

$$Y_r = X_s + Z_r$$
$$Y_d = X_s + X_r + Z_d,$$

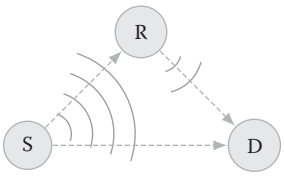

FIGURE 34.1 The classical three-terminal relay network. The source's transmission is received at both the relay and the destination. The relay coordinates its transmission with the source to help the destination decode the intended message.

where $Z_r \sim \mathcal{N}(0, N_r)$ and $Z_d \sim \mathcal{N}(0, N_d)$. We impose transmit power constraints $E[X_s^2] \leq P_s$ and $E[X_r^2] \leq P_r$ on the source and relay. We consider the case of a *full-duplex* relay, which can simultaneously transmit and receive, and a *half-duplex* relay, which can only transmit or receive at any given time. By causality, the relay's signal X_r can depend only on previously received signals Y_r.

In general, the Shannon capacity of the relay channel is unknown. In Reference 2, Cover and El Gamal derive upper and lower bounds on the capacity of the full-duplex relay channel which remain the tightest known. The upper bound follows from a cut-set argument:

$$C_f^+ = \max_{0\le\alpha\le1} \min\left\{\frac{1}{2}\log_2\left(1+(1-\alpha)P_s\left(\frac{1}{N_r}+\frac{1}{N_d}\right)\right), \frac{1}{2}\log_2\left(1+\frac{P_s+P_r+2\sqrt{\alpha P_s P_r}}{N_d}\right)\right\}. \tag{34.1}$$

The capacity of the relay channel is bounded below by the achievable rate of one of several proposed schemes. The two most popular achievable schemes are the *decode-and-forward* and *compress-and-forward* schemes, both presented in Reference 2. The material presented in this chapter makes use of decode-and-forward, in which the relay decodes the source's message entirely and retransmits (perhaps a portion of) it to the destination. In the full-duplex case, decode-and-forward achieves rates satisfying

$$R < \max_{0\le\alpha\le1} \min\left\{\frac{1}{2}\log_2\left(1+\frac{\bar{\alpha}P_s}{N_r}\right), \frac{1}{2}\log_2\left(1+\frac{P_s+P_r+2\sqrt{\alpha P_s P_r}}{N_d}\right)\right\}, \tag{34.2}$$

where α denotes the split of the source's power between sending fresh information and resolution information to the destination, and $\bar{\alpha} = 1 - \alpha$. In the half-duplex case, decode-and-forward achieves rates satisfying [8]

$$R < \max_{0\le t,\alpha,\gamma\le1} \min\left\{\frac{t}{2}\log_2\left(1+\frac{\gamma P_s}{tN_r}\right)+\frac{\bar{t}}{2}\log_2\left(1+\frac{\bar{\alpha}\bar{\gamma}P_s}{\bar{t}N_d}\right), \frac{t}{2}\log_2\left(1+\frac{\gamma P_s}{tN_d}\right)+\frac{\bar{t}}{2}\log_2\left(1+\frac{\bar{\gamma}P_s+P_r+2\sqrt{\alpha\bar{\gamma}P_s P_r}}{\bar{t}N_d}\right)\right\}, \tag{34.3}$$

where t specifies the fraction of time in which the relay acts as receiver, γ specifies the division of source power between stages, and α specifies the division of source power between sending fresh information and sending resolution information.

For both full-duplex and half-duplex relays, decode-and-forward achieves capacity asymptotically as the link between source and relay becomes strong, but in general its rates are suboptimal. The decode-and-forward rates are achieved using block Markov encoding, in which the source sends a message during one block and in the next block collaborates with the relay to send resolution information to the destination. We briefly review the list decoding method proposed for full-duplex relaying in Reference 2, which is depicted in Table 34.1.

In block Markov encoding, we need two codebooks: a primary codebook C_s with 2^{nR} codewords and a resolution codebook C_r with 2^{nR0} codewords. Each codeword is generated from a Gaussian distribution having unit average power. The source transmits fresh codewords from C_s, and the source and relay

TABLE 34.1 Block Markov Encoding

	$b = 1$	$b = 2$	...	$b = B + 1$
Source	$c_s(1)$	$c_s(2) + c_r(1)$	...	$c_r(B)$
Relay	–	$c_r(1)$	...	$c_r(B)$

cooperatively send resolution codewords from C_r to help the destination decode the desired message. The source and relay transmit B messages over $B + 1$ blocks of n channel uses each.

During the first block, the source transmits

$$X_s^{(1)} = \sqrt{P_s\bar{\alpha}}c_s(1)$$

where $c_s(1) \in C_s$ is the codeword associated with the message for block 1. The relay decodes $c_s(1)$ from $Y_r^{(1)}$ using typical sequence decoding, which is possible if n is large and

$$R < \frac{1}{2}\log_2\left(1 + \frac{\bar{\alpha}P_s}{N_r}\right). \tag{34.4}$$

The destination cannot yet decode $c_s(1)$, but instead creates a list $L(Y_d^{(1)})$ of codewords that are jointly typical with $Y_d^{(1)}$. During the next time block, in addition to sending $c_s(2)$, the source collaborates with the relay to send resolution information to the destination. This is accomplished via random binning. Let $B(i)$ be a function mapping the 2^{nR} indices of C_s to the first 2^{nR0} integers. This binning function is chosen randomly: each of the 2^{nR} indices is randomly and uniformly assigned an integer. The source and relay encode the bin index into $c_r(1)$, which they collaboratively transmit to the destination:

$$X_s^{(2)} = \sqrt{P_s\bar{\alpha}}c_s(2) + \sqrt{P_s\alpha}c_r(1)$$
$$X_r^{(2)} = \sqrt{P_r}c_r(1).$$

The destination decodes the bin index, treating $\bar{\alpha}P_s c_s(2)$ as noise. This is successful with low probability of error as long as

$$R_0 < \frac{1}{2}\log_2\left(1 + \frac{\alpha P_s + P_r + 2\sqrt{\alpha P_s P_r}}{N_d + \bar{\alpha}P_s}\right). \tag{34.5}$$

Now in possession of the bin index, the destination looks for codewords in $L(Y_d^{(1)})$ that also correspond to the bin index just decoded. Averaging over the possible binning functions, there is a unique such codeword as long as

$$R - R_0 < \frac{1}{2}\log_2\left(1 + \frac{\bar{\alpha}P_s}{N_r}\right). \tag{34.6}$$

The encoding and decoding proceeds in this fashion: at block t, the source transmits $c_s(t)$, while source and relay cooperatively send $c_r(t - 1)$. This continues until block $B + 1$, in which only the resolution information $c_r(B)$ is sent. The destination successfully decodes nRB bits in $n(B + 1)$

channel uses. For large B, the overall rate is arbitrarily close to R. Combining Equations 34.4, 34.5, and 34.6, we get the rates promised in Equation 34.2.

For half-duplex relaying, we adjust the encoding procedure slightly. Since the relay cannot transmit and receive simultaneously, it cannot decode the fresh codeword $c_s(t)$ while transmitting $c_r(t-1)$. So, while the source and relay cooperatively send $c_r(t-1)$, the source transmits a fresh codeword, never decoded by the relay, to the destination. We omit the details for brevity, but this scheme achieves the rates promised in Equation 34.3.

34.3 Physical-Layer Cooperation: Energy Efficiency

As we saw in the previous section, relaying can substantially improve the throughput of a wireless link. However, the simple relay channel tacitly assumes the existence of a relay terminal whose *raison d'être* is to assist the source terminal. While it is possible to deploy dedicated relays in a wireless network, in practice, terminals serve users who have their own data to send and their own resources to conserve. This is particularly evident in cellular systems, in which devices are battery-powered and face severe energy limitations. Each user has an incentive to conserve energy as much as possible, precluding the possibility of cooperation.

We examine the issue of user cooperation from a game-theoretic perspective. We consider a simple two-user cellular network in which each user wants to maximize its energy efficiency as measured in bits per joule. Casting the scenario as an infinite-stage game, it is possible for selfish users to negotiate a compromise that mutually improves performance.

34.3.1 System Model

Consider a simple cellular uplink scenario in which two mobile users communicate with a common base station (BS). In a typical cellular scenario, users' transmissions are orthogonalized; for simplicity, suppose they are time-division multiplexed. User 1 transmits its data to the BS during odd time blocks, while user 2 transmits its data during even time blocks. The idle user can choose to act as a relay for the active user in order to help increase the active user's rate. In other words, during odd time blocks (when user 1 transmits its data), user 2 can act as a relay node, and vice versa during even time blocks. The two users and the BS thus form a three-terminal relay channel in which the roles of source and relay are exchanged at each time block, as depicted in Figure 34.2.

We assume a complex baseband, Rayleigh-distributed, block-fading channel model. During each time block $t \in \{1,2,\ldots\}$, the channel coefficients h_{ij} between node i and j remain constant, and coefficients at different time blocks are statistically independent. The channel distributions are specified by the expected gains $E[|h_{ij}|^2]$, which remain constant for all t. We assume that the mobile users are capable of full-duplex transmission and that channel state information is available globally. During odd (respectively,

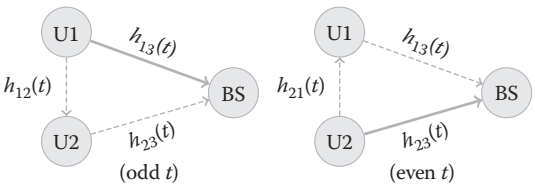

FIGURE 34.2 Transmission schedule. During odd time blocks, user 1 acts as source and user 2 acts as relay, and vice versa for even time blocks.

even) time blocks, the source user transmits symbols $X_1(t)$ ($X_2(t)$) to the relay and base station, and the relay user transmits symbols $X_2(t)$ ($X_1(t)$) to the base station to facilitate the source user's transmission. The received signals at the relay and destination are then

$$\begin{aligned} Y_1(t) &= h_{21}(t)X_2(t) + N_1(t) \quad \text{(even } t\text{)} \\ Y_2(t) &= h_{12}(t)X_1(t) + N_2(t) \quad \text{(odd } t\text{)} \\ Y_3(t) &= h_{13}(t)X_1(t) + h_{23}(t)X_2(t) + N_3(t), \end{aligned}$$

where each $N_i(t)$ is additive white Gaussian noise with unit variance. To model the mobile users' power constraints, we limit the average source and relay powers during each block:

$$\begin{aligned} p_{s1}(t) = E\left[|X_1(t)|^2\right] \le 1, \quad p_{r2}(t) = E\left[|X_2(t)|^2\right] \le 1 \quad \text{(odd } t\text{)} \\ p_{r1}(t) = E\left[|X_1(t)|^2\right] \le 1, \quad p_{s2}(t) = E\left[|X_2(t)|^2\right] \le 1 \quad \text{(even } t\text{)}, \end{aligned}$$

where $p_{si}(t)$ is the power allocated by user i while acting as the source node, and $p_{ri}(t)$ is the power allocated by user i while acting as the relay. In other words, $p_{si}(t)$ represents power user i spends on its own transmissions; $p_{ri}(t)$ represents power spent relaying for user i.

Assuming that each time block is sufficiently long, we can use codebooks that achieve the information-theoretic rates for the relay channel presented in Section 34.2. Although we could choose a different relay scheme, we use decode-and-forward, since it is a simple, well-studied approach that leads to a tractable expression for the achievable rate. It also achieves rates near capacity when the interuser channels are much stronger than the channels between users and the BS. Since we may reasonably assume that geographically close users will be paired up for cooperation, decode-and-forward is a logical choice. Applying Equation 34.2 to the present scenario, the achievable rates are

$$r_i(t) = \max_{\alpha} \min\left\{\max\left\{\log\left(1 + |h_{ij}|^2\right), \log_2\left(1 + \bar{\alpha}\,|h_{i3}|^2\right)\right\} \log_2(1 + |h_{13}|^2 + |h_{23}|^2 + 2\sqrt{\alpha}\,|h_{13}h_{23}|)\right\},$$

for $i \neq j$. The terms inside the min function correspond to the two possible bottlenecks of the decode-and-forward relay channel: the point-to-point channel between either the source and relay or the source and destination (whichever is greater), and the broadcast channel formed by the source, relay, and destination. Note that the achievable rate is always lower-bounded by the capacity of the source–destination channel.

34.3.2 Bits-per-Energy Efficiency

Bits-per-energy efficiency has been studied previously, most notably in Reference 9, where an elegant information-theoretic characterization for the single-user, multiple-access, and interference channels is given. In Reference 10, the energy efficiency of the relay channel is studied. However, maximizing energy efficiency almost invariably drives users to the low-SNR regime, where rates are arbitrarily small. Strict maximization of energy efficiency, then, is not typically useful in practice when users have target rates to meet or delay constraints to satisfy.

To sidestep this obstacle, we impose limitations on the bits-per-energy maximization. First, we define the bits-per-energy efficiency. Since each time block has the same duration, the amount of data having reached the base station is proportional to the sum of rates over all previous time blocks. Similarly, the total energy expenditure is proportional to the sum of the power allocations in previous time blocks. So, the total bits-per-energy efficiency for each user is proportional to

$$e_1 = \frac{\sum_{t\ \text{odd}} r_1(t)}{\sum_{t\,\text{odd}} p_{s1}(t) + \sum_{t\,\text{even}} p_{r1}(t)} = \frac{E_h[r_1]}{E_h[p_{s1}(\mathbf{h}) + p_{r1}(\mathbf{h})]}$$
$$e_2 = \frac{\sum_{t\ \text{even}} r_2(t)}{\sum_{t\,\text{even}} p_{s1}(t) + \sum_{t\,\text{odd}} p_{r1}(t)} = \frac{E_h[r_2]}{E_h[p_{s2}(\mathbf{h}) + p_{r2}(\mathbf{h})]},$$

where the sums converge to expectations because the channels are ergodic, allowing us to write the power allocations as functions of the channel coefficients, denoted by the vector $\mathbf{h}$. The units of e_1 and e_2 are *normalized* bits per joule: if each user's transmitter power were 1 W and each channel were 1 Hz wide, the units of e_1 and e_2 would be bits per joule; we simply refer to the units as "bits per energy."

Now, to sidestep the obstacle of users' rates becoming small, we constrain each user to employ full power for its own transmission. That is, we always have $p_{si}(t) = 1$, meaning that each user's rate is at least as high as the capacity of its link with the BS. In addition to bounding users' rates away from zero, this restriction approximates a cellular environment, where users simply use the available power to achieve the highest possible quality of service (neglecting, perhaps, the need for power control). Thus, in our framework, user cooperation is an appendage to the existing cellular system, which can be used to improve both data rates and bits-per-energy efficiency. Now, we can write the energy efficiencies as

$$e_i(p_{r1}, p_{r2}) = \frac{E_h[r_i(p_{rj}(\mathbf{h}))]}{1 + E_h[p_{ri}(\mathbf{h})]} \tag{34.7}$$

With the energy efficiencies defined, we define the achievable bits-per-energy region for our system:

$$\mathcal{E} = \{(e_1(p_{r1}, p_{r2}), e_2(p_{r1}, p_{r2})) : 0 \le p_{r1}(\mathbf{h}), p_{r2}(\mathbf{h}) \le 1\}.$$

The bits-per-energy region is entirely characterized by the channel statistics $E[|h_{ij}|^2]$. $\mathcal{E}$ is necessarily compact, but it need not be convex, since time-sharing between power allocations does not result in convex combinations of bits-per-energy efficiencies. Each point in $\mathcal{E}$ is achieved by using a different relay power allocation pair $(p_{r1}(\mathbf{h}), p_{r2}(\mathbf{h}))$. While the set of feasible power allocations is infinite-dimensional, we can characterize the power allocations associated with the outer boundary of $\mathcal{E}$.

Definition 34.1

A point $(e_1, e_2) \in \mathcal{E}$ *is a* (Pareto) boundary point *if, for any other point* $(f_1, f_2) \in \mathcal{E}$, $f_1 > e_1$ *implies* $f_2 < e_2$, *and* $f_2 > e_2$ *implies* $f_1 < e_1$. *In other words, there is no point that gives increased energy efficiency to one user without decreasing the efficiency of the other user.*

Theorem 34.1

Let p_{r1}^* *and* p_{r2}^* *be relay power allocations with average power* $E_h[p_{r1}^*] = \alpha_1$ *and* $E_h[p_{r2}^*] = \alpha_2$, *respectively. Then, the point* $(e_1(p_{r1}^*, p_2^*), e_2(p_{r1}^*, p_{r2}^*)) \in \mathcal{E}$ *is a Pareto boundary point only if, for* $i \neq j$,

$$\begin{aligned} p_{ri}^* = \arg \max_{0 \le p_{ri}(\mathbf{h}) \le 1} \quad & E_h[r_j(p_{ri})] \\ \text{subject to} \quad & E_h[p_{ri}] = \alpha_i. \end{aligned} \tag{34.8}$$

Proof.
We argue by contradiction. Let $(e_1(p_{r1}^*, p_2^*), e_2(p_{r1}^*, p_{r2}^*)) \in \mathcal{E}$ be a Pareto boundary point, and choose $i \neq j$. Supposing that p_{ri}^* is not a solution to Equation 34.8, there must exist some p_{ri} such that $E_h[r_j(p_{ri})] > E_h[r_j(p_{ri}^*)]$ and $E_h[p_{ri}] = E_h[p_{ri}^*] = \alpha_i$. Thus, $(e_j(p_{ri}, p_{rj}^*) > e_j(p_{ri}^*, p_{rj}^*)$, but $e_i(p_{ri}, p_{ri}^*) = e_i(p_{ri}^*, p_{ri}^*)$ by definition. So, $(e_1(p_{r1}^*, p_{r2}^*), e_2(p_{r1}^*, p_{r2}^*))$ cannot be a boundary point, which is a contradiction. ■

The content of Theorem 34.1 is that, in order to achieve a boundary point, power must be allocated *efficiently*. That is, if a user commits a certain average power for relaying, then that power should be allocated to increase the other user's rate as much as possible. Theorem 34.1 is useful because the maximization of the expected rate is a convex problem. Therefore, to achieve boundary points, we can transform the high-dimensional problem of finding relay power allocations into a series of (relatively) simple convex programs. Conceptually, instead of searching over the entire set of permissible power allocations, we need only to search over the (α_1, α_2) pairs to find the desired boundary point.

Even with this characterization of the Pareto boundary, however, it remains to be seen to what extent user cooperation can improve users' bits-per-energy efficiency. Each user's rate increases only logarithmically with the other user's relay power, so it is still possible that refusing to relay is ideal in terms of bits-per-energy. To answer this question definitively, we turn to a game-theoretic approach.

34.3.3 Game-Theoretic Formulation

User cooperation has recently received game-theoretic attention in the literature. In Reference 11, the effectiveness of transmitter and receiver cooperation is studied from the perspective of coalitional game theory, and user cooperation is examined under a repeated-game framework in Reference 12. However, neither of these works considers energy efficiency. In a work more similar to ours [13], Nash bargaining is used to facilitate user cooperation in a throughput-per-energy setting, although the work considers a simple bandwidth sharing rather than information-theoretic cooperation.

A game is formally defined by three objects: a set of players, a set of strategies that those players can enact, and a set of utility functions denoting the payoff each player derives from the strategies enacted. We cast our scenario as a game in which each mobile user is a player whose strategies are the relay power allocations p_{ri} and whose utility functions are the bits-per-energy efficiencies $e_i(p_{r1}, p_{r2})$.

34.3.3.1 Noncooperative Games

The solution to a game depends on the particular game-theoretic framework employed. The simplest possible framework is a single-stage noncooperative game, where selfish players select strategies that maximize individual utility without regard for the utility of other players. Players simply select their strategies, collect their payoff, and never interact again. The classic solution concept for a noncooperative game is the Nash equilibrium (NE) [14], which is a strategy selection such that no player can improve its utility by unilaterally changing its strategy. An NE is therefore stable with respect to selfish players, as they have no incentive to deviate from the equilibrium point. However, while the NE is optimal from the perspective of each player individually, it is notoriously inefficient. Players who are willing to cooperate frequently can achieve higher utilities than the NE. For example, under a single-stage game, user cooperation is never an NE, regardless of the benefits of relaying. Each user can improve its payoff by lowering its relay power, so the unique NE is $p_{ri}(\mathbf{h}) = 0$, resulting in payoffs

$$e_i^{NE} = e_i(0,0) = E_h[\log_2(1+ |h_{i3}|^2)].$$

34.3.3.2 Nash Bargaining Solution

To improve upon the single-stage NE, we turn to the Nash bargaining solution (NBS) from cooperative game theory [7]. Formally, a two-player bargaining game is defined by a set of feasible utilities $\mathcal{U}$

and a disagreement point $\delta \in \mathcal{U}$. The set $\mathcal{U}$ contains utility vectors $\mathbf{u} = (u_1, u_2)$, denoting the payoff to both players, for all possible strategies the players may implement. The disagreement point δ represents the "status quo" prior to bargaining or utility guaranteed to each player should bargaining fail. In bargaining games, players cooperatively choose a compromise point. That is, rather than individually focusing on payoff maximization, players jointly choose a mutually agreeable utility vector and agree to enact the strategies associated therewith. The Nash bargain is an axiomatic solution, meaning that the solution point is defined by a set of (ostensibly) reasonable axioms rather than a concrete bargaining process. Rather than give a full description of the axioms, we briefly note that the NBS is characterized as the point on the Pareto boundary that satisfies affine invariance, symmetry between players, and independence to irrelevant alternatives. Nash showed that the unique* point satisfying the specified axioms is

$$\mathbf{u}^{NBS} = \arg\max_{\mathbf{u}\in\mathcal{U}} [u_1 - \delta_1]^+ [u_2 - \delta_2]^+, \tag{34.9}$$

where $[\cdot]^+ = \max(\cdot, 0)$. In other words, the NBS is the point that maximizes the product in Equation 34.9, called the *Nash product*. For our problem, the set of feasible utilities is $\mathcal{E}$, and we take the disagreement point to be $\delta = (e_1^{NE}, e_2^{NE})$, the single-stage NE utilities. So, finding the NBS results in the following optimization problem:

$$\max_{0\le p_{r1}, p_{r2}\le 1} [e_1(p_{r1}, p_{r2}) - e_1^{NE}]^+ [e_2(p_{r1}, p_{r2}) - e_2^{NE}]^+. \tag{34.10}$$

The Nash bargain offers several advantages. First, the NBS point is on the Pareto boundary, guaranteeing an efficient solution. Second, the NBS is well known for providing a fair compromise between players, as we will empirically verify in Section 34.3.4. Finally, since we maximize the product of players utilities in Equation 34.10, we are guaranteed that, when possible, the NBS gives improved energy efficiency to both users. Otherwise, the NBS simply results in the noncooperative solution in which both users refuse to relay. By finding the Nash bargaining solution, we can say definitively whether it is possible to improve both users' energy efficiency via user cooperation.

The optimization problem in Equation 34.10 is nonconvex, making it difficult to find the NBS power allocations directly. Fortunately, since the NBS point is on the Pareto boundary, we can appeal to Theorem 34.1. Then, we need only to search over (α_1, α_2) pairs in order to find the NBS power allocations, suggesting a straightforward optimization scheme. By deriving a simple upper bound on the Nash product, we can efficiently search over the set of (α_1, α_2) pairs using branch-and-bound techniques [16]. For each (α_1, α_2) pair, we find the bits-per-energy efficiencies according to Equation 34.8 and evaluate the Nash product. We continue the process until the Nash product is maximized. Note that we can modify this approach to find any point on the Pareto boundary: we can find the max–min point, maximize the sum efficiency, or find other bargaining solutions with this approach.

34.3.3.3 Infinite-Stage Games

As a final note, we point out that by casting our scenario as an infinite-stage game, we can make the NBS power allocations a Nash equilibrium, meaning that even purely selfish players can be enticed to cooperate. Rather than simply making a single decision and never interacting again, players in an infinite-stage game repeatedly interact, making decisions again and again that affect their long-term payoff. Players in infinite-stage games therefore must consider the future consequences of their decisions, which introduces notions of reputation and reciprocity: players may reward or punish players for "good" and "bad"

* Strictly speaking, the NBS is defined only when the set of utilities is convex. The NBS can be generalized to nonconvex sets [15], but for brevity's sake we omit the technicalities.

behaviors. In our case, one user may agree to relay for a user provided the other user agrees to do the same in the future. With the additional incentives, cooperative behavior can often be sustained as an NE of an infinite-stage game.

In an infinite-stage game, players' strategies are expressed as functions of the strategies played in previous stages. So, for each stage, players specify what strategies they will play for every possible history of plays up to that stage. In other words, players specify their strategies for all possible "contingencies." For our scenario, the players are the two users, and each stage is a time block t. At each time block, only the relay user has a decision to make, which is how much relay power $p_{ri}(t)$ to use; this decision is a function of all previous decisions made by both players. The utilities are the bits-per-energy utilities (34.7). A Nash equilibrium of an infinite-stage game is a set of strategies (including all possible contingencies) such that no single player can improve its payoff by deviating.

Theorem 34.2

There exists a (subgame perfect) Nash equilibrium in the infinite-stage game such that the users select the NBS power allocations defined in Equation 34.10.

Proof.
We omit the proof for brevity; it closely mirrors the proof of the so-called folk theorem for repeated games [17]. ■

34.3.4 Numerical Results

To see to what extent user cooperation can benefit users—and to demonstrate the performance of the NBS—we show the results of numerical experiments. First, we plot the achievable bits-per-energy region

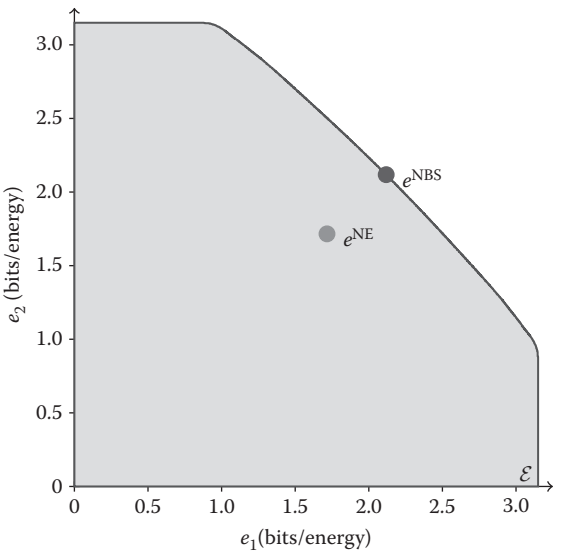

FIGURE 34.3 Bits-per-energy region when $E[|h_{12}|^2] = E[|h_{21}|^2] = 20$ dB and $E[|h_{13}|^2] = E[|h_{23}|^2] = 5$ dB. The single-stage Nash equilibrium and Nash bargaining points are shown. (Adapted from M. Nokleby and B. Aazhang, User cooperation for energy-efficient cellular communications, *IEEE International Conference on Communications*, Cape Town, South Africa, May 2010.)

for a given set of channel conditions. Let $E[|h_{12}|^2] = E[|h_{21}|^2] = 20$ dB and $E[|h_{13}|^2] = E[|h_{23}|^2] = 5$ dB, so that the interuser channels are stronger on average than the channels with the BS. We numerically sweep over the (α_1,α_2) pairs, allowing us to find the Pareto boundary and compute ε. In Figure 34.3, we plot ε as well as the NE and NBS points. In this case, since the NE point is not on the Pareto boundary, both users see significant improvement in energy efficiency through cooperation.

Since we cannot show the NBS for all possible channel statistics, we focus on a family of meaningful cases. For Figure 34.4, we set the expected interuser gains to $E[|h_{12}|^2] = E[|h_{21}|^2] = 20$ dB, set user 2's expected gain at $E[|h_{23}|^2] = 10$ dB, and let $E[|h_{13}|^2]$ vary between −5 dB and 20 dB. This range allows us to see the NBS performance when users' channel conditions are asymmetric, thus giving us insight as to the fairness of the results. Figure 34.4 shows each user's bits-per-energy efficiencies, both without cooperation and under the NBS. In Figure 34.5, we show the results in terms of percent gain to each user. First, we note that regardless of the channel statistics, the NBS is nontrivial, and both users obtain improved energy efficiency through cooperation. The gains are significant—in excess of 100% for user 1

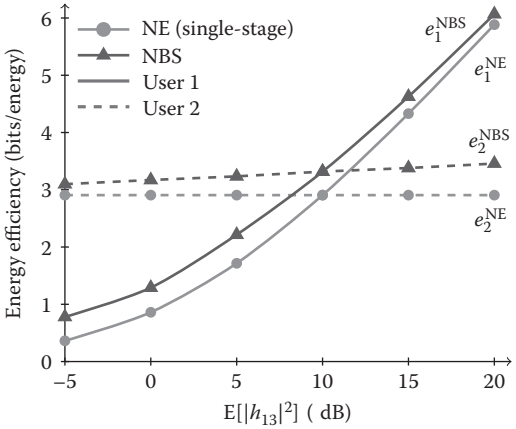

FIGURE 34.4 Bits-per-energy efficiency under the single-stage NE (where users do not cooperate) and the NBS as a function of $E[|h_{13}|^2]$. (Adapted from M. Nokleby and B. Aazhang, User cooperation for energy-efficient cellular communications, *IEEE International Conference on Communications*, Cape Town, South Africa, May 2010.)

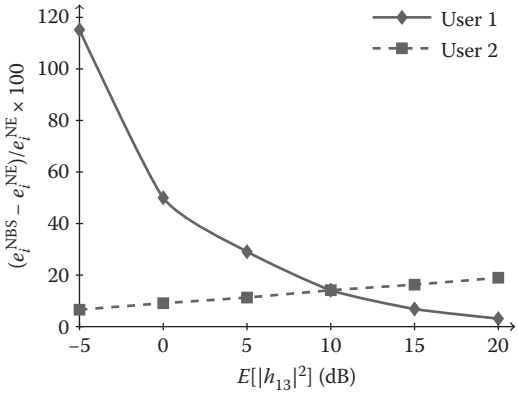

FIGURE 34.5 Percent gain to each user, also as a function of $E[|h_{13}|^2]$. (Adapted from M. Nokleby and B. Aazhang, User cooperation for energy-efficient cellular communications, *IEEE International Conference on Communications*, Cape Town, South Africa, May 2010.)

when its link with the BS is weak, and approximately 15% for each user when their links are identical. We also see a notion of "fairness" in the bargaining: when $E[|h_{13}|^2]$ is small, user 1 is at a relative disadvantage but experiences the greater increase in efficiency; conversely, when $E[|h_{13}|^2]$ is large, user 1 is at a relative advantage and experiences the lesser increase.

Of course, we have not explored the entire space of channel statistics, but we can make commonsense extrapolations from the data. Obviously, the effectiveness of cooperation increases with the relative strength of the interuser links; as $E[|h_{12}|^2]$ and $E[|h_{21}|^2]$ increase and decrease, so do the benefits of cooperation. But, while there exist circumstances in which user cooperation can provide only limited improvement, we have seen nontrivial improvement in a variety of reasonable channel conditions, suggesting that user cooperation is a widely applicable means for improving energy efficiency.

34.4 Cooperation at the Medium-Access Layer: Network Resource Allocation

Section 34.3 has discussed the energy-expenditure fairness issues associated with cooperation, and in particular, has identified regimes of operation within which cooperation among several users is desirable. Until now, we have considered the network to be operating in an isolated environment, such that there is no penalty to cooperation beyond power use at the relay terminal. Indeed, we have seen that cooperation is a clear choice for improving the throughput of a source–destination link.

In a broader network with many simultaneously active terminals, the isolation assumption can no longer be considered as true. When forwarding information in a cooperative mode, relay terminals contribute interference in the network which may disrupt ongoing transmission elsewhere. Large networks are inherently interference-limited [18], leading to a variety of interference-management schemes.

In general, these schemes are the domain of the medium-access layer,* and are typically classified into *scheduling* and *routing* techniques. The scheduling problem has been effectively solved in an asymptotic throughput-maximization sense [20], and similarly for the routing problem [21,22].

As was described in the previous section, user cooperation is fundamentally the coordinated action of two nearby terminals over two timeslots: there is coupling in both space and time. In essence, when used in the cooperative sense, the "interference" from the source and relay can be beneficial. This presents challenges to existing scheduling and routing protocols, which have used the atomic link—one source communicating to one destination—as the basis for their design, and have optimized the maximum number of atomic links which can be simultaneously active, often leveraging spatial and temporal reuse. These algorithms must be redesigned to now recognize that *some* simultaneous transmissions *should* be coscheduled, and that *some* data should be routed through a relay terminal.

In this section, we will describe a technique for resource allocation across a network, allowing for cooperation communications but not explicitly requiring it. Instead, this technique utilizes relay terminals when they can constructively aid transmission without excessively interfering with nearby network traffic.

34.4.1 System Model and Constraints

We focus on a time-slotted network of N half-duplex terminals in a square region of size A^2. The terminals are distributed according to a two-dimensional Poisson process of intensity λ, and form the set $\mathcal{N}$. Each terminal is accorded a maximum transmission power P_{Tx}, and there is Gaussian thermal noise N_o at each terminal. To model the channel, we assume a pathloss-dominant environment with propagation loss parameter α.

* While this has been true generally, recent work on interference alignment [19] brings this issue squarely to the signal-level physical layer.

Most network-layer studies consider data to be composed of packets, which are of a predetermined size. Success of transmission is then binary: a sufficient signal-to-interference-and-noise (SINR) ratio or good proximity to the receiver guarantees that the entire packet is received. To incorporate cooperative communication, this assumption is removed and replaced by the notion of the *rate control* element of the model, describing the size of a packet using Shannon's capacity equation [23], here specifying the size of packet k traveling from terminal x to terminal y in timeslot t:

$$R_t^k = \log_2\left(1 + \frac{P_t(x) \cdot D_{x,y}^{-\alpha}}{N_o + \gamma_t(y)}\right), \tag{34.11}$$

where $P_t(x)$ is the transmission power of terminal x at time t, $\gamma_t(y)$ denotes the interference at the receiving terminal, and $D_{x,y}$ is the distance between the terminals. For clarity of exposition but without loss of generality, timeslots are normalized to 1 s and bandwith to 1 Hz, allowing one to view Shannon's rate as the size in bits of a packet transmitted on a point-to-point link.

We arbitrarily choose $F = \frac{N}{2}$ pairs of terminals to act as sources and destinations for F information flows. These will be labeled $s(k)$ and $d(k)$ for each packet k. We assume that all other terminals are capable of helping to transmit information, both by forwarding packets and by storing them.

Within this configuration, the problem is to determine the throughput-optimal schedule, route, and power allocation for packets traveling between their sources and destinations. Where necessary and useful, cooperation should be there to assist in the transmission. However, a number of constraints must be met to ensure a realistic solution. Only packet source terminals are backlogged, and are infinitely so. All other terminals are free of traffic and possess large buffers to store data. Mathematically, we represent transmission between terminals with a binary variable $I_t^k(x,y)$, which is 1 if terminal x is transmitting packet k to terminal y at time t. The optimization constraints are formalized as such:

$$\sum_{x,y \in \mathcal{N}} I_t^k(x,y) > 0 \quad \forall\ t,k \tag{34.12}$$

$$\sum_k \left(\sum_{x \in \mathcal{N} \setminus y} I_t^k(x,y) + \sum_{x \in \mathcal{N} \setminus y} I_t^k(y,z) \right) \le 1 \quad \forall\ t,k \tag{34.13}$$

$$\sum_{y \in \mathcal{N}} I_1^k(s(k),y) = 1 \quad \forall\ k \tag{34.14}$$

$$\sum_{x \in \mathcal{N}} I_T^k(x,d(k)) = 1 \quad \forall\ k \tag{34.15}$$

$$\sum_{x \in \mathcal{N}} I_t^k(x,y) = \sum_{z \in \mathcal{N}} I_{t+1}^k(y,z) \quad \forall\ t,k \tag{34.16}$$

The first constraint requires that information is accounted for in each times-lot, either in transmission or data storage. The second constraint ensures that all terminals operate in a half-duplex mode, while the third and fourth guarantee that flows start at their sources and terminate at their destinations. The last constraint guarantees route continuity. Lastly, the power at transmitting nodes $P_t(x)$ is required to be in $[0, P_{Tx}]$ and to be identically zero when the node is not transmitting:

$$0 \le P_t(x) \le P_{\text{Tx}} \quad \forall\ t \ge T \tag{34.17}$$

$$P_t(x) \le P_{\text{Tx}} \cdot \sum_k \sum_{y \in \mathcal{N} \setminus x} I_t^k(x, y) \quad \forall\ x \in \mathcal{N} \tag{34.18}$$

For each link in packet k's route, we denote its data rate as R_t^k. This value is determined using Equation 34.11, and a packet is naturally limited by its bottleneck rate. Since there is no constraint on schedule length, a nonempty set of feasible schedules S and power allocations $\mathcal{P}$ exists which satisfies these constraints. We wish to choose the schedule and routes $S \in S$ and power allocation $P \in \mathcal{P}$ for all nodes in the network so as to maximize the throughput for each flow. Specifically we wish to solve

$$\max_{P,S} \min_k \min_t \frac{R_t^k}{L(p^k)}, \tag{34.19}$$

where $L(p^k)$ is the length of packet k's route. This problem reduces to mixed-integer programming, and as posed is known to be NP-hard [24], requiring exhaustive searches in both the continuous and integer domains to guarantee an optimal solution. Although branch-and-cut methods exist to attack this problem, they have no guarantee on their running time, leading us to search for a computationally efficient approach.

34.4.2 Approach and Example

We will now describe a general approach for allocating resources in multiflow networks with rate control. Following that, it will be shown that this approach is amenable to the incorporation of cooperative technologies.

34.4.2.1 Network-Flow Interaction Chart

A framework for performing resource allocation in large networks has been developed in References 25 and 26, and will be summarized here. It allocates resources for large networks with multiple flows, and does so in $O(N^3)$ time.

Fundamentally, the approach hinges on a data structure called the *network-flow interaction chart*, which specifies the detailed interactions of data and terminals at all time instances in the network. The terminals are represented as nodes in the chart, replicated in the x direction to represent the time-slotted communication. Edges $e_t^{x,y}$ are drawn between nodes to represent transmission between two terminals at a specific timeslot. This data structure is well suited to dynamic programming techniques, which enable the scheduling and routing of data for maximum throughput on a per-packet basis while guaranteeing that constraints (34.12) through (34.16) are met.

34.4.2.2 Dynamic Programming

Edges are assigned weights corresponding to the rate achievable (34.11) between the anchoring terminals at time t. When allocating resources for packet k, the node corresponding to terminal $s(k)$ is assigned weight ∞. Edges are then updated with the minimum of either their initial weight or the weight of their source node: this is the notation that a link cannot sustain more traffic than is either at its source or than its channel can bear. Nodes are then updated with the maximum of their incoming edge weights, such that as much data propagate through the network as fast as possible. This procedure is repeated across timeslots until all node weights have stabilized, indicating that all data-maximizing paths have been established. The path from node representing $d(k)$ with highest value, taken across timeslots, is the then data-maximizing route for packet k. This specifies its route and schedule simultaneously. Power is selected for each link on the route such that all links operate at the same rate.

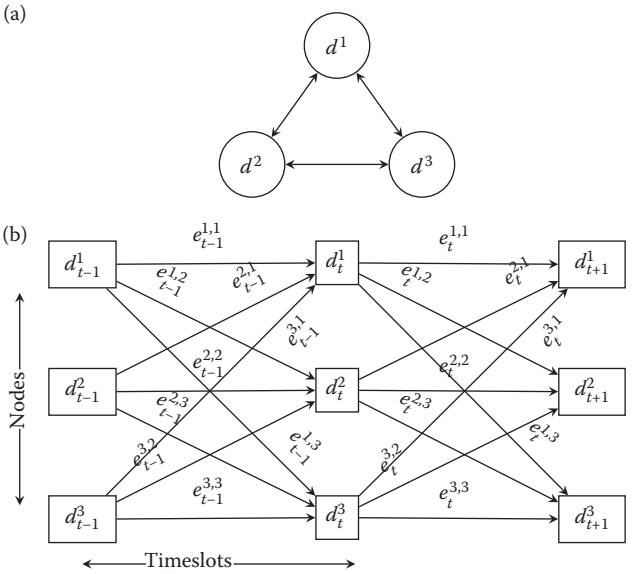

FIGURE 34.6 An example topology (a) and the NFIC (b). Note that all nodes interfere with all others, and so the NFIC is fully connected. (Adapted from G. B. Middleton, B. Aazhang, and J. Lilleberg, A flexible framework for polynomial-time resource allocation in multiflow wireless networks, *Proceedings of the 47th Allerton Conference on Communication, Control and Computing*, September 2009.)

After packet k has been allocated, edges handling packet k and incident on terminals handling packet k are then "zeroed out" to make them unavailable, thereby enforcing duplexing constraints. Similarly, terminals not transmitting or receiving an allocated packet have their edge values scaled down to prevent interference from affecting the existing packets. A network and corresponding NFIC is shown in Figure 34.6.

34.4.2.3 Metanodes

In order to incorporate cooperative links into the framework, a new type of node is developed for the NFIC framework, termed as the *metanode*. It represents the notion of data flowing to *two destinations* in one timeslot (the cooperative BC phase), and *constructively combining* in a subsequent timeslot (the cooperative MA phase) [3].

Nodes in the NFIC traditionally represent exactly one terminal in the network. As a distinct class of nodes, the metanodes represent the coordinated combination of terminals, in this case the cooperative unit of a particular source, relay, and destination. An edge *entering* a metanode corresponds in the schedule to data being transmitted from the source terminal to the intended destination and also the associated relay. An edge *exiting* a metanode corresponds in the schedule to the coordinated transmission of both the relay and source, where signals constructively combine at the destination. The weight on *both* the entering and departing metanode edges is set as the overall rate the cooperative unit can achieve, which (although not known explicitly) can be bounded in the time-shared relay case as [8,27,28]

$$R_t^K = \min \begin{cases} \log_2\left(1 + P_s^{(1)} h_{sr}^{(1)}\right) + \log_2\left(1 + P_s^{(2)} h_{sd}^{(2)}\right) \\ \log_2\left(1 + P_s^{(1)} h_{sd}^{(1)}\right) + \log_2\left(1 + P_s^{(2)} h_{sd}^{(2)} + P_r^{(2)} h_{rd}^{(2)}\right), \end{cases} \tag{34.20}$$

where P_s and P_r are transmission powers at the source and relay, respectively, with channels h between all terminals being similarly labeled. Cooperation must explicitly aid the transmission, that is, that the channel is degraded: $\min\{|h_{sr}|^2, |h_{rd}|^2\} \geq |h_{sd}|^2$. Note that there is zero correlation between the relay and source transmissions, and that the relay channel is in the BC and MA phases for equal amounts of time.

Example 34.1: Metanodes in the NFIC

To illuminate the concept of a metanode in the NFIC, consider the small network of five nodes, shown in the upper pane of Figure 34.7. The channels are dominated by pathloss.

Here, two sources *S*1 and *S*2 are attempting to communicate with two matching destinations *D*1 and *D*2. The NFIC corresponding to this network is shown in the lower pane of Figure 34.7, where we have added the metanode M to capture the notion of cooperation occurring between S2, R, and D2. In particular, the edge between S21 and M2 corresponds to the second source transmitting, but with that transmission being received by both the relay node and the intended destination. The edge from M2 to D23 then corresponds to both the relay and source transmitting in the second timeslot.

The NFIC solution and corresponding network activity is shown in Figure 34.7. Here, we preserve clarity by not drawing all edges in the NFIC, rather including only those that are relevant as data emanate from the sources. Note that in the second timeslot, although only one edge in the NFIC is active, two transmissions are occurring in the network!

In this way, the same polynomial-time routing and scheduling technologies described in References 25 and 26 can be employed in networks where cooperation is used.

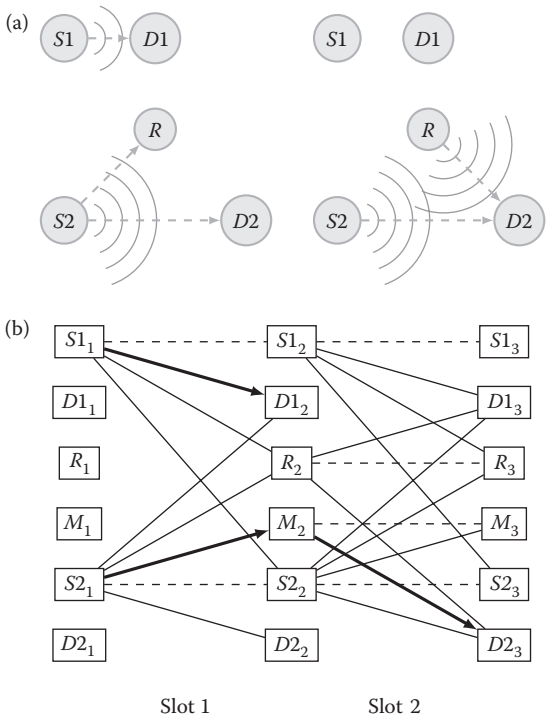

FIGURE 34.7 (a) Network activity in timeslots 1 and 2. Both sources transmit in the first slot, their intended destinations shown by the broken lines. In timeslot 2, *S*2 and *R* transmit together in the MA stage of cooperation. (b) The NFIC corresponding to this network and its activity. Note how the metanode *M* describes the cooperative behavior shown above.

TABLE 34.2 Percentage Increase in Memory Requirements over Multihop NFIC and Sparsity of NFIC Representation

Metanodes per Terminal	Raw Storage Increase (%)	Sparsity (%)
1	300	75
3	1500	93.75
5	3500	97.22
7	6300	98.44

34.4.2.4 Adding Metanodes: Memory Complexity

The choice of best relay terminal for a given packet route is known to be NP-hard in the general fading environment [24], which when considered jointly with the NP-hard routing and scheduling problem, results in a doubly complex selection problem. In this framework, choosing the metanode—the source–relay–destination triple—can be simplified with the use of geographical information. The pathloss-dominant fading environment allows consideration of only nearby terminals as potential relays. Thus, for each terminal which may act as a source, relays are locally selected along with corresponding destinations. These form the metanodes, which may be incorporated into the NFIC resource allocation decisions.

The algorithms are $O(N^3)$ in the number of nodes in the NFIC, which means that adding metanodes to each terminal does not increase the order of the complexity. However, it does increase memory requirements, as new edges and terminals are introduced to the NFIC with weights which must be stored. Table 34.2 shows memory data for the NFIC with a varying number of metanodes defined per terminal. Memory requirements increase considerably over the multihop NFIC, although since all but two edges into and out of metanodes are zero, the sparsity of the resulting NFIC is considerable. This means that even for large numbers of defined metanodes, memory complexity does not overwhelm the algorithm.

34.4.3 Broader Network Allocation

The use of metanodes in the resource allocation algorithm as illustrated above can be applied to much larger networks, where the polynomial-time nature of our solutions permits allocations in networks of near-arbitrary size.

Example 34.2

We choose to illustrate these concepts with networks in which pathloss is the dominant channel effect, but this assumption is not required for these techniques to apply. We make this choice since it helps to illustrate where cooperative gains exist in the network. An example of resource allocation with cooperation is shown in Figure 34.8. Here, two flows compete for network resources, and both are able to leverage cooperative links. Since the network is dominated by pathloss, cooperation will assist the overall throughput of the flows only on the longest hop in the route, which is the throughput bottleneck.

This is clearly illustrated in the example network, where the routing decision for the lightly-shaded flow *changed* as a result of the cooperative metanode being available in the NFIC. Had cooperation not been available, the red flow would have followed the sequence of terminals indicated by the broken line.

34.4.4 Metanode Selection

In the previous example, the network was constructed to highlight the use of a metanode in the NFIC to contribute rate improvement. However, because Equation 34.20 determines cooperative rates with terminals in the specific roles of (source, relay, destination), the triple ($S2$, R, $D2$) supports a rate which

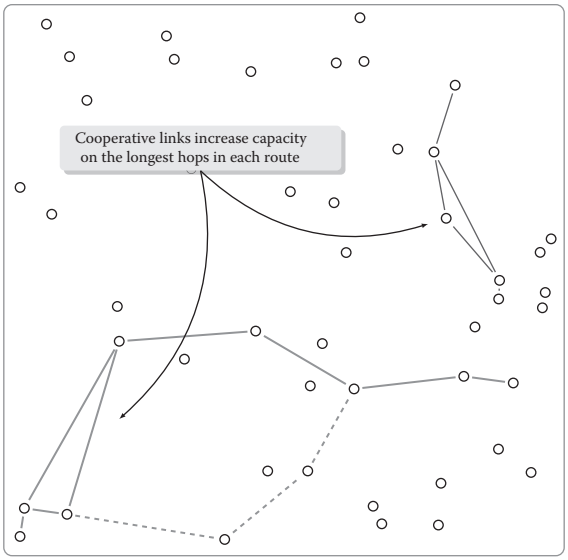

FIGURE 34.8 Two-flow network in which NFIC resource allocation was used with metanodes available. In the allocation, metanodes corresponding to the cooperative terminals shown above were found optimal by the dynamic programming routines, and in the case of the lightly-shaded flow, use of the cooperative metanode completely changed the routing decision for the flow.

may be different from ($S2$, $D2$, R), requiring those triples to be represented as *separate* metanodes in the NFIC, even though the terminals involved are the same.

For the resource allocation algorithms to have access to all possible cooperative resources, a metanode must be created for each combination of source, relay, and destination. This requires considering all possible permutations of three terminals from the set of N, given by

$$ {}_N P_3 = \frac{N!}{(N-3)!} \tag{34.21}$$

In the case of $N = 40$, the number of possible metanodes is 59,280. This clearly introduces combinatorial complexity and memory demands to the NFIC algorithms, completely overshadowing the efficiency gains they offer for noncooperative resource allocation. As such, an efficient method of defining metanodes is needed such that the allocation algorithms have a useful selection of cooperative links without enumerating all triples.

The channel structure in the pathloss environment can be exploited, to narrow the domain of potential metanodes available for enumeration in the NFIC. Specifically, because pathloss dominates the channel conditions, we can require that cooperation (use of the metanode) explicitly aid in transmission, that is, the channel is *degraded*: $\min\{|h_{sr}|^2, |h_{rd}|^2\} \geq |h_{sd}|^2$. As such, a metanode will never be defined for which the both h_{sr} and h_{rd} are small. Since the channel coefficient h is dictated primarily by distance, it should be ensured that enough metanodes are defined such that the scheduling and routing algorithms can exploit them to pass data through the network. In other words, sufficient geographical coverage must be offered to justify the increase in algorithmic complexity.

Algorithm 1: Distance-Based Metanodes

The first approach is to define, for each terminal, a specific number N_R of cooperative triples. These triples are selected based solely on distance: for terminal x, the nearest N_R terminals (which will

become relays) are identified and for each one, choose the nearest terminal *not* nearer to x to act as the destination in the triple. Thus, here and in the following algorithms, the number of metanodes is $N{\cdot}N_R$, so the total number of nodes in the NFIC is $N(1 + N_R)$. This algorithm is formalized as Algorithm 1.

Algorithm 2: Geographical Metanodes

The previous algorithm is geographically insensitive, in that it defines metanodes for each terminal based only on the nearest terminals, but without consideration for their relative positions. As illustrated in Figure 34.9, topological condition may result in all metanodes for a particular terminal being defined in the same general direction, which is not necessarily helpful to the routing algorithms. As such, we describe another approach, in which metanodes are defined in as uniform a spatial manner as possible. In this approach, the area around each terminal is partitioned into N_R sectors, and the nearest terminal in the sector is chosen to act as the relay. Given the source and relay, the destination is chosen as in Algorithm 1.

Algorithm 1: Distance-Based Metanode Selection Algorithm

Data: Set of N network terminals $\mathcal{T}$
Result: Set of $N(1 + N_R)$ nodes $\mathcal{N}$ for the NFIC
Create an empty set of metanodes:
$\mathcal{M} \leftarrow \emptyset$
foreach $t \in \mathcal{T}$ **do**
  Create an ordered list of other terminals, starting with the nearest to t: $\{t_1, t_2, \ldots, t_{N-1}\}$
  foreach $i \in \{1, 2, \ldots, N_R\}$ **do**
    Assign terminal t_i as relay r_i
    Assign terminal nearest to r_i but not closer to t as destination d_i
    Add the metanode: $\mathcal{M} \leftarrow (t, r_i, d_i)$
    Calculate edge for $\mathcal{E}$ using (2)
Set of nodes is union of terminals and metanodes:
$\mathcal{N} \leftarrow \mathcal{T} \cup \mathcal{M}$

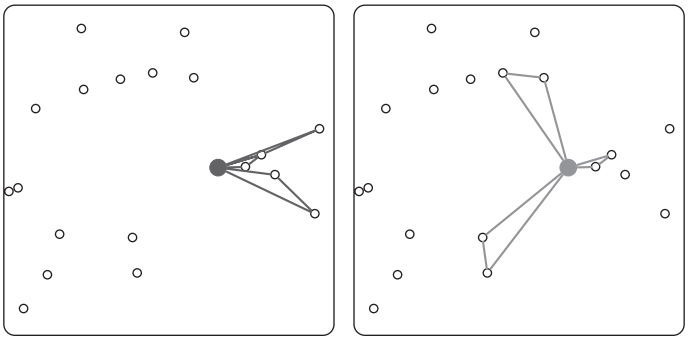

FIGURE 34.9 Comparison of metanode definition algorithms with $N_R = 3$ for the same terminal in the same network. On the left, distance-based Algorithm 1 chooses metanodes in the same general direction. On the right, geographically equalized Algorithm 2 selects metanodes with coverage to all parts of the region.

Algorithm 2: Spatially-Aware Metanode Selection Algorithm

Data: Set of N network terminals $\mathcal{T}$
Result: Set of $N(1 + N_R)$ nodes $\mathcal{N}$ for the NFIC
Create an empty set of metanodes:
$\mathcal{M} \leftarrow \emptyset$
foreach $t \in \mathcal{T}$ **do**
  Create an equi-angular partition of the area A around t with N_R sectors υ_i such that $\bigcup_{i=1}^{N_r} \upsilon_i = A$
  foreach $i \in \{1, 2, \ldots, N_R\}$ **do**
    Assign terminal nearest to t in υ_i as relay r_i
    Assign terminal nearest to r_i as destination d_i
    Add the metanode: $\mathcal{M} \leftarrow (t, r_i, d_i)$
    Add edge to $\mathcal{E}$ using (2)
Set of nodes is union of terminals and metanodes:
$\mathcal{N} \leftarrow \mathcal{T} \cup \mathcal{M}$

Algorithm 3: Range-Extension Metanodes

The third mechanism we describe is a hybrid of the previous two, designed to exploit cooperative benefit to allow larger packets to cross the network in fewer hops. Relays are used to aid in the transmission of large packets from the source well beyond nearby intermediate terminals, thereby increasing throughput by reducing a packet's time in transit. For each terminal in the network, the geographic partitioning approach of Algorithm 2 is synthesized with the distance-based approach of Algorithm 1. A key distinction is that instead of choosing the nearest terminal in the sector as the relay, the terminal in the γth distance percentile to the destination is selected, and the terminal near the halfway-point to the source is chosen as the relay. The effect of the percentile parameter γ on throughput is shown in Figure 34.10. In this manner, metanodes are defined to exploit the cooperative advantage to move larger packets further, in all directions of the network.

34.4.5 Simulation Results

34.4.5.1 Cooperative Benefits in Large Networks

To compare the benefits of NFIC-metanode resource allocation to multihop routing, we simulate networks and allocate resources under the two different paradigms, using the general network model

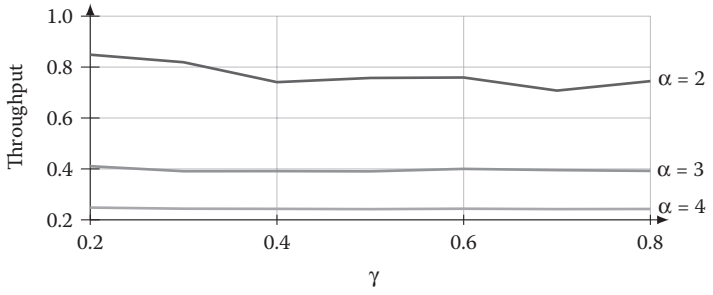

FIGURE 34.10 Study of how the percentile parameter γ in Algorithm 3 affects throughput for a variety of path-loss environments. As illustrated especially for $\alpha = 2$, NFIC allocation algorithms do not make use of range extension, instead deriving higher throughput by forming routes of nearby, higher-rate cooperative units.

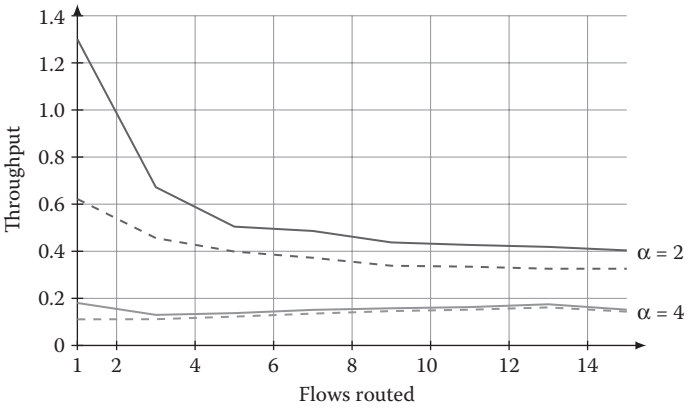

FIGURE 34.11 Mean throughput for networks with cooperative links (solid) and multihop-only routes (broken). Cooperative links, represented by metanodes in the NFIC, considerably increase throughputs for low-pathloss environments, especially when only few flows are competing for resources.

described above. We study the mean throughput for a varying number of flows in the region, where the schedules and routes have been calculated using NFIC techniques. Shown in Figure 34.11 is a comparison of throughputs for two pathloss environments, free space ($\alpha = 2$) and urban ($\alpha = 4$) as a function of the number of flows demanding resources. The solid lines are mean flow throughputs when three metanodes per terminal are included in the NFIC, allowing the algorithm to exploit cooperative technologies where needed. The broken line indicates throughputs for multihop-only allocation.

We observe improvements over multihop in both environments and for all levels of congestion, although the improvements are most pronounced with low pathloss and few flows, where data rates can increase by a factor of 2. Gains diminish for higher pathloss and as congestion increases, since cooperative gains are affected by the overall higher interference temperature in the network.

34.4.5.2 Number of Metanodes

As discussed above, the number of metanodes chosen for the NFIC affects not only memory complexity but also the resource allocation selected. If a relatively small number of metanodes are defined, they may not be useful in the routes required by the flows. Increasing the number of metanodes defined per terminal does increase memory requirements, but also makes cooperative links available to more parts of the network. It is interesting to study network performance as a function of how many metanodes are defined for each terminal in the network.

Figure 34.12 show this relationship. For each terminal, we define a number of metanodes using local relays as described above, and calculate a resource allocation for that topology with two information flows. We then redefine more metanodes and recalculate the allocation, plotting the mean throughput for the flows as a function of number of metanodes we have defined. This is repeated for a thousand topologies, and average results are reported. Throughput increases considerably if more metanodes are defined in the case of low pathloss, less so if pathloss is high. This is because the throughput on a route is determined by the "bottleneck link" which, once aided with cooperation, may remain the cooperative link. This is the case in high-pathloss environments, where the cooperative advantage is smaller. Cooperative units are much more effective in lower-pathloss environments, where all three channels are stronger.

34.4.5.3 Comparison of Metanode Selection Algorithms

Using simulations, we now compare the three algorithms presented above. Our simulations are conducted in a 20-m square region, with $P_{Tx} = 1$ and $N_o = 0.1$. The intensity of the Poisson process distributing the terminals is 0.1, resulting in an average of 40 terminals per network realization, distributed

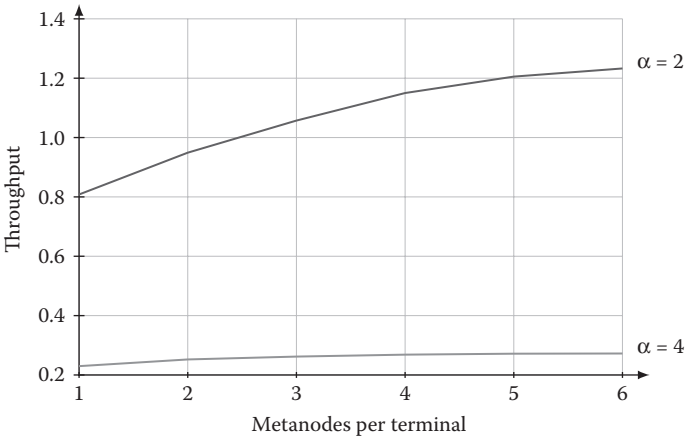

FIGURE 34.12 Mean throughput of two flows as a function of the number of metanodes defined for each terminal in the network. More metanodes are helpful in low-pathloss regimes, though they do increase memory requirements.

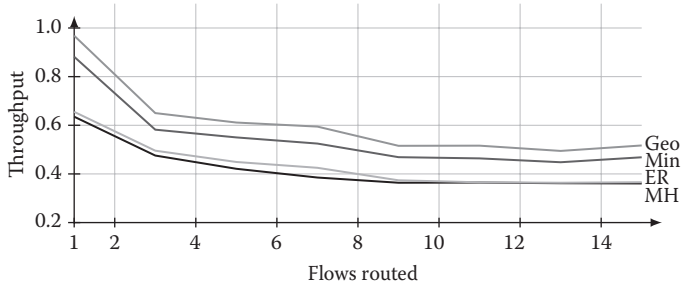

FIGURE 34.13 Comparison of metanode definition schemes under a variety of network loads. Consistently, the geographic definition algorithm outperforms the other two, and all three outperform the non-cooperative multihop (MH) case.

uniformly over the region. Sources and destinations are randomly chosen, and the pathloss exponent is varied.

We first compare the throughput of NFIC-allocated schedules for a variety of flow demands under the three metanode-definition paradigms. For each randomly selected topology, we allocate $N_R = 4$ metanodes for each terminal according to the algorithms described above. This is repeated 1000 times for different numbers of flows requiring service; mean throughputs are reported in Figure 34.13. In this simulation, $\alpha = 2$ and $\gamma = 0.65$.

Here, we note that regardless of the competition for resources, geographically aware metanode definition (Algorithm 2) outperforms the others. In particular, the range-extension definition performs only half as well, particularly when competition among flows for resources is heavy. This suggests that although range-extension cooperative units may be helpful in theory, they do not benefit actual topologies nearly as much as cooperative units offering routing advantages in all directions. This is further borne out by the fact that distance-based definition (Algorithm 1) is also completely dominated by geographically aware definition, suggesting that *routing must be considered with cooperation*.

The range-extension algorithm is parameterized by γ, a fractional measure of the range extension expected in each sector. For three flows, we compare mean throughputs for several values of γ. Note that for all α and especially for free-range propagation, range extension offers no clear benefit to overall

resource allocation. This suggests that, while relays can be helpful for transmitting isolated packets across long distances, they are more useful in increasing data rates over short hops.

34.5 Summary and Perspectives

34.5.1 Summary

Multiuser cooperation holds great promise as a technology to increase both data rates and reliability in next-generation networks, but there are significant challenges to its deployment. From a technical perspective, the challenges span several layers: from the question of signal design at the physical layer to the question of mitigating network-wide interference at the medium-access layer, there are a variety of problems which must be addressed before cooperation can be deployed in large networks.

However, barriers to introducing user cooperation go beyond the purely technical. In this chapter, we have examined cooperation from an energy-efficiency perspective, in which we considered the energy cost to individual users for employing cooperative techniques. Cooperative technology exists to improve users' performance, but only if users are willing to sacrifice energy on behalf of others. This problem naturally lent itself to a game-theoretic analysis. We saw that even if users are purely selfish, they have incentive to cooperate if they look at payoffs in the long term. Particularly, the energy-efficiency pair corresponding to the Nash bargaining solution, which benefits both users, is a Nash equilibrium of the infinite-stage game. Selfish users can "negotiate" with each other to cooperate in a mutually beneficial way.

By deriving a characterization of the Nash bargaining solution based on convex optimization, we constructed an algorithm that efficiently finds the power allocations associated with the Nash bargain. Simulation results showed that cooperation permits significant gains in energy efficiency, up to 100% for users with weak links to the base station.

In a larger network, the primary adverse effect of cooperation is the additional interference it causes. A cooperative link requires two extra transmissions, spread both temporally and spatially: the source transmits twice and a geographically separate relay transmits once. Nearby transmissions will be affected negatively by this interference, requiring medium-access control mechanisms to carefully manage where and when cooperation is deployed.

Here, we have described a methodology to simultaneously study the gains offered by large-scale cooperation and also control its deployment at the MAC layer, ensuring that it is used only where it benefits the network at large. Doing so required solving a mixed-integer NP-hard program, for which we presented an approximate solution via a decomposition approach. Since scheduling and routing algorithms act on the level of an atomic link, we described a low-complexity method of representing the cooperative structure as such to these algorithms. The results from the framework showed that not only does cooperation benefit the broader network, but the gains can be substantial under the favorable conditions of high pathloss.

34.5.2 Perspectives

This chapter reviews but a small piece of field concerning cooperative communication.

For fair, energy-efficient cooperation at the physical layer, several practical issues remain. We have assumed that users are already paired up for cooperation and have the necessary information to compute the bargained power allocations. In practice, a means for identifying cellular users that are both close by and have sufficient battery life to consider cooperation is necessary. There also is required a means for distributing channel state information among cooperating users.

In terms of cooperation at the medium-access layer, several key issues remain open. One is the question of whether to use cooperation to increase reliability or throughput; in our study here, throughput maximization was the goal. However, in large networks, a cooperative link could bolster an otherwise tenuous link across a large distance, for example. The optimization program here takes a different form,

and will result in a different solution from what we have seen in this work, since under this objective cooperation may be used to overcome interference from *other users*.

Another issue at this layer is that of delay. The throughput-delay trade-off in resource allocation decisions has been characterized for certain types of cellular and mobile networks, but never when cooperation has been available. Synthesizing the throughput-centric work presented in this chapter with a delay-optimal solution will reveal how cooperation best aids the broader networks: whether by increasing short-distance throughput or through longer yet lower rate hops.

This area promises to remain active for several years to come, and we expect to see deployments of cooperative schemes in consumer technology in the near future.

References

1. E. C. van der Meulen, Three-terminal communication channels, *Advanced Applied Probability*, 3, 120–154, 1971.
2. T. Cover and A. E. Gamal, Capacity theorems for the relay channel, *IEEE Transactions on Information Theory*, 25, 572–584, 1979.
3. A. Sendonaris, E. Erkip, and B. Aazhang, User cooperation diversity. Part I. System description, *IEEE Transactions on Communications*, 51, 1927–1938, 2003.
4. J. N. Laneman and G. W. Wornell, Distributed space-time coded protocols for exploiting cooperative diversity in wireless networks, *IEEE Transactions on Information Theory*, 49(10), 2415–2525, 2003.
5. J. N. Laneman, D. N. C. Tse, and G. W. Wornell, Cooperative diversity in wireless networks: Efficient protocols and outage behavior, *IEEE Transactions on Information Theory*, 50(12), 3062–3080, 2005.
6. IEEE standard for local and metropolitan area networks, part 16: Air interface for broadband wireless access systems, amendment 1: Multihop relay specification, IEEE LAN/MAN Standards Committee, 2009.
7. J. F. Nash, The bargaining problem, *Econometrica*, 18, 155–162, 1950.
8. M. A. Khojastepour, Distributed cooperative communications in wireless networks, Ph.D. dissertation, Rice University, Houston, TX, 2005.
9. S. Verdú, On channel capacity per unit cost, *IEEE Transactions on Information Theory*, 36, 1019–1030, 1990.
10. A. E. Gamal, M. Mohseni, and S. Zahedi, Bounds on capacity and minimum energy-per-bit for AWGN relay channels, *IEEE Transactions on Information Theory*, 52, 1545–1561, 2006.
11. S. Mathur, L. Sankar, and N. B. Mandayam, Coalitions in cooperative wireless networks, *IEEE Journal on Selected Areas in Communications*, 26, 1104–1115, 2008.
12. Y. Chen and S. Kishnore, A game-theoretic analysis of decode-and-forward user cooperation, *IEEE Transactions on Wireless Communications*, 7, 1941–1951, 2008.
13. Z. Zhang, J. Shi, H.-H. Chen, M. Guizani, and P. Qiu, A cooperation strategy based on Nash bargaining solution in cooperative relay networks, *IEEE Transactions on Vehicular Technology*, 57, 2570–2577, 2008.
14. J. F. Nash, Non-cooperative games, *Annals of Mathematics*, 54, 286–295, 1951.
15. M. Kaneko, An extension of the Nash bargaining problem and the Nash social welfare function, *Theory and Decision*, 12, 135–148, 1980.
16. R. Horst and N. V. Thoai, DC programming: Overview, *Journal of Optimization Theory and Applications*, 103, 1–43, 1999.
17. J. W. Friedman, A non-cooperative equilibrium for supergames, *The Review of Economic Studies*, 38, 1–12, 1971.
18. P. Gupta and P. R. Kumar, The capacity of wireless networks, *IEEE Transactions on Information Theory*, 46, 388–404, 2000.

19. V. R. Cadambe and S. A. Jafar, On calculating power-aware connected dominating sets for efficient routing in ad hoc wireless networks, *IEEE International Conference on Communications*, pp. 971–975, May 2008.
20. L. Tassiulas and S. Sarkar, Maxmin fair scheduling in wireless networks, *Proceedings of the 21st Annual IEEE INFOCOM*, New York, NY, vol. 1, pp. 763–772, 2002.
21. E. Dijkstra, A note on two problems in connexion with graphs, *Numerische Mathematik*, 1, 269–271, 1959.
22. R. Bellman, On a routing problem, *Quartely Applied Mathematics*, 16(1), 87–90, 1959.
23. C. E. Shannon, A mathematical theory of communication, *Bell Systems Technical Journal*, 27, 369–423, 1948.
24. T. H. Corman, C. E. Leiserson, and R. L. Rivest, *Introduction to Algorithms*. McGraw-Hill, Cambridge, MA, 1996.
25. G. B. Middleton, B. Aazhang, and J. Lilleberg, A flexible framework for polynomial-time resource allocation in multiflow wireless networks, *Proceedings of the 47th Allerton Conference on Communication, Control and Computing*, Monticello, IL, September 2009.
26. G. B. Middleton, B. Aazhang, and J. Lilleberg, Efficient resource allocation and interference management for streaming multiflow wireless networks, *International Conference on Communications*, Cape Town, South Africa, May 2010.
27. T. M. Cover and A. E. Gamal, Capacity theorems for the relay channel, *IEEE Transactions on Information Theory*, 25, 572–584, 1979.
28. A. Host-Madsen and J. Zhang, Capacity bounds and power allocation for wireless relay channels, *IEEE Transactions on Information Theory*, 51(6), 2020–2040, 2005.
29. M. Nokleby and B. Aazhang, User cooperation for energy-efficient cellular communications, *IEEE International Conference on Communications*, Cape Town, South Africa, May 2010.

35

Wireless Mesh Networks

Hyunok Lee

35.1 Introduction

Multihop wireless communication networks have been of increasing interest over the last decade. Two main types of such networks have emerged: mobile ad-hoc networks (MANETs) and wireless mesh networks (WMNs). MANETs are infrastructure-less, nonhierarchical wireless networks where all network entities can move and function as routers and discover and maintain routes to other entities in the network. On the other hand, WMNs typically have a hierarchical structure and are supported by an infrastructure. Furthermore, the functionalities of the network entities may vary significantly across the layers of the hierarchical network structure. While MANETs have been historically envisioned to serve very specialized applications, such as battlefields and emergency situations, WMNs have inspired numerous general applications ranging from broadband home networking to community networks to high-speed metropolitan area networks (MANs) [1–3]. Particularly, large-scale WMNs with infrastructure support have been considered as an affordable and scalable solution to provide broadband packet data communications across wide geographic areas, thanks to their inherent advantages such as robustness to node failures, ease of deployment and maintenance, and low initial deployment cost [1–3].

In this chapter, we consider large-scale WMNs that serve as wireless access networks over large geographic areas. Such an application scenario of WMNs has often been proposed to have a layered network structure [4,5], which typically contains end-users (EUs) at the lowest layer, wireless mesh routers (MRs) in the middle layer, and other aggregation nodes at the top layer. The aggregation nodes of the highest layer may include another set of wireless entities that communicate wirelessly with the wireless MRs of the middle layer, or may be entirely wired through, for example, optical or DSL networks. In this chapter, we focus on the two lowest layers that consist of EUs and wireless MRs. A set of wireless MRs is assumed to be colocated with wired network entities called gateway routers (GRs).

Substantial research on WMNs has been conducted and several protocols have been proposed by various standardization bodies [3]. Particularly, routing for multihop wireless communication networks has been extensively studied in the context of MANETs [6–9] and more recently for WMNs [10–12]. Compared to routing, research on medium access control (MAC) for WMNs has been relatively sparse. The majority of the studies on MAC for WMNs consider contention-based schemes such as the

IEEE 802.11 MAC protocol that is based on the carrier sense multiple access (CSMA) with collision avoidance (CA) principle. CSMA/CA-based schemes initiate the assessment of the availability of the medium or resources for transferring data packets mainly by sensing or measuring the power level of the medium directly. On the other hand, another type of MAC schemes [13–15] has been proposed. These schemes allocate separate resources for control and data packets, and the availability of resources for transferring data packets is assessed through exchanging control packets using control resources. Data resources are then reserved through these control packets.

The former type of MAC schemes based on the CSMA/CA principle inherently has less control overhead compared to the latter type of MAC schemes and thus may lead to higher network throughput when the traffic load is light. However, as the traffic load increases and more nodes need to acquire the medium simultaneously, it may become possible to coordinate data packet transmissions among nodes more efficiently when resources are divided for control and data packets and the availability or usage of data resources can be known and controlled by exchanging control packets. In this chapter, we focus on the latter type of MAC schemes.

In this chapter, we present the performance of large-scale WMNs that serve as access networks over large geographic areas. The WMNs employ a set of MAC protocols created in [16–18] that belongs to the latter type of MAC schemes described above, and their performance is evaluated through a large simulator developed in [16–19] that includes measurements-based models for radio propagation and interference calculation for a large built-in urban area. The simulator also captures the stochastic network behavior resulting from random traffic arrivals, admission control, and queuing. Through extensive simulations incorporating such details, we determine the performance of the WMNs. Primary factors are identified across the physical (PHY), MAC, and routing layers of network functions that affect the performance and their intricate interactions are examined to explain the behavior of fundamental performance metrics including the network throughput, per-session throughput, and blocking and dropping rates.

35.2 MAC Framework and Protocols

35.2.1 MAC Framework

We consider a MAC framework that supports explicit cooperation among MRs for resource reservation for data transmission. We consider a time division multiple access (TDMA) and time division duplex (TDD)-based framework with a single-frequency channel. MRs and EUs share the same frequency channel. Time is divided into time slots and there are two types of time slots: one for control and the other for data. In our TDMA, an MR uses different data time slots for serving different EUs. However, each data time slot is reused across the network. In TDD, an MR or an EU cannot transmit and receive simultaneously.

Within this framework, the overall operation of the network is as follows. When the network is deployed, it enters the preoperation phase during which the network runs a control time slot assignment protocol. Once control time slots are assigned to MRs, the network starts to run a routing protocol to construct routing tables at MRs. Once the network is set up, it enters the normal operation phase during which it executes a data time slot access control protocol to serve EUs. The network needs to rerun the control time slot assignment protocol if a new MR is added to the network. In addition, routing tables need to be reconstructed if an MR fails or a new MR is added to the network. The network could perform such reconfiguration of control time slots or routing tables proactively by entering the preoperation phase periodically.

35.2.2 Control Time Slot Assignment Protocol

Control time slots provide a random access channel for EUs so that EUs can discover the network and request admission to the network. Control time slots also provide a means for MRs to exchange control

messages among themselves for such operations as network discovery, routing table construction, and resource negotiation. Each MR is associated with one control time slot.

Assigning broadcast time slots to network entities in a multihop wireless network has been studied in TDMA/FDMA-based multihop wireless networks [13,14,20–23]. In these studies, the underlying physical-layer behavior and the interactions among network entities have been often oversimplified by not representing the vagaries of radio propagation and interference encountered in actual networks. For example, it is assumed that two nodes either perfectly communicate with each other or do not interact with each other at all. In reality, however, even when two nodes cannot communicate with each other, a node may still interfere with another node depending on the propagation condition between the two nodes. Due to different assumptions on models for radio propagation and interference calculation, these protocols are not directly applicable to the network considered in this chapter.

In this chapter, we consider the protocol created in [16], a protocol through which every MR in the WMN acquires one broadcast time slot that supports a minimum average received signal-to-interference-plus-noise ratio (SINR) from the MR to its entire neighbor MRs. The protocol is based on contention-based reservation mechanisms in a topology-dependent manner similar to those in [13,14], yet incorporating more realistic, measurement-based models for the underlying physical-layer characteristics and behavior exemplified above.

35.2.3 Data Time Slot Access Control Protocol

Data time slots are used to transmit user data. We consider the protocol created in [17,18] for controlling access over data time slots. Through the protocol, network entities (MRs and EUs) exchange resource negotiation requests over control time slots to transfer user data over data time slots. The protocol supports two types of negotiation among network entities. One is between an EU and its associated MR, and the other is among one-hop neighbor MRs. In the former, a new EU's admission request is controlled, and in the latter, a resource request by a neighbor MR is controlled.

The data time slot access control protocol is fully cooperative and distributed: network entities negotiate among themselves for resource allocation, and the messages are exchanged only among one-hop neighbor MRs or between an EU and its associated MR. Furthermore, the protocol supports adaptive resource allocation through dynamic allocation of data time slots and PHY transmission modes over the slots as well as through user/queue prioritization.

35.2.3.1 Admission and Congestion Control

A crucial component of the data time slot access control protocol is admission and congestion control (ACC). When admitting new users, it is critical to consider the current resource usage of existing users. If the network admits more users than it can support, the quality-of-service (QoS) as measured by delay or throughput of existing users may degrade to an unacceptable level. For multihop networks, it is more challenging to assess the resource usage of existing users because one has to examine resources beyond the first hop, that is, beyond the admitting router.

Various forms of admission control have been considered for multihop wireless networks. In [13–15,17,24], schemes have been considered that examine the medium availability only for the first hop but not beyond it. Although these schemes based on the resource availability for the first hop may be simple and even work well under light traffic loads, they fail to serve the admitted users under heavy traffic loads. Another approach [25,26] explicitly probes the resource availability at each router along the way to the destination node before admitting a new traffic request. The network admits a new traffic request only if a resource is available at the time of probe. Although this approach enables the network to detect congestion sooner, it increases the setup delay before a new user is admitted. Another drawback is that exchanging probe messages incurs excessive control overhead.

In [18], a different ACC scheme is proposed. Under the scheme, an MR admits an admission request if and only if each of the queues at the MR has been assigned "sufficient" resources, and the MR has

additional resources for receiving data for the request. The ACC policy incorporates the resource availability at the routers along the path to the destination router, and yet utilizes only local information available at the admitting router and has a minimal increase in control overhead. In [18], the scheme is shown to stabilize the network even under heavy traffic loads.

Later in this chapter, network performance is presented under the ACC scheme created in [18], and compared with that under the scheme considered in [17]. The latter scheme in [17] does not consider the resource availability beyond the admitting MR and tends to admit more sessions than the network can support.

35.2.4 Routing Protocol

The WMN simulator considered in this chapter implements a proactive routing protocol that is based on minimum-cost spanning trees, similar to the hybrid wireless mesh protocol with mesh portals of the IEEE 802.11s standards [27,28]. Routing tables are constructed at the beginning of each simulation run and remain the same throughout the run.

Two link metrics are considered in this chapter for best-effort web traffic: one link metric is a constant, and the other link metric is the PHY transmission time (or air-time) per unit data size under a certain idealized scenario (see [19] for more detailed description of the routing metrics). The path or routing metric is defined as the sum of the link metrics along the path. Under the former link metric, the path or routing metric becomes the number of hops along the path, and an MR selects the shortest path toward the destination node. Under the latter metric, the path or routing metric becomes the sum of air-time along the path under the aforementioned idealized scenario. Either of the metrics does not include the processing delay and the medium access acquisition delay at intermediate MRs.

35.3 Performance Evaluation

In this section, we present the performance of the WMN that employs the control time slot assignment protocol, data time slot access control protocol, and routing protocol described in the previous section. Various performance metrics are determined including mean network throughput, per-session throughput, blocking rate, and dropping rate. The mean network throughput is calculated as the aggregate size of successfully completed sessions across the network per unit time, and the per-session throughput is calculated as the session data size divided by the session delay for a successfully completed session. The blocking rate is the ratio of the number of blocked sessions to the number of arrived sessions, and the dropping rate is the ratio of the number of dropped sessions to the number of admitted sessions. An EU is blocked if its admission request is not accepted after a maximum number of retires. On the other hand, an admitted EU is dropped if it runs out of data time slots before it completes transmitting its data to the network.

35.3.1 Performance under Two Different ACC Schemes

In this section, we present the network performance under two different ACC schemes created in [17,18]. The scheme created in [17] is denoted as AC_RO, and the one considered in [18] as AC_RF.

35.3.1.1 Network Throughput

As seen in Figure 35.1, when the traffic arrival rate is small, the network throughput behaves quite similarly under both AC_RO and AC_RF: the mean network throughput increases almost linearly as a function of the session arrival rate, successfully serving most of the EUs arriving to the network. However, as the arrival rate increases, the network throughput shows a remarkable difference: the network throughput starts to decrease under AC_RO while it continues to increase under AC_RF.

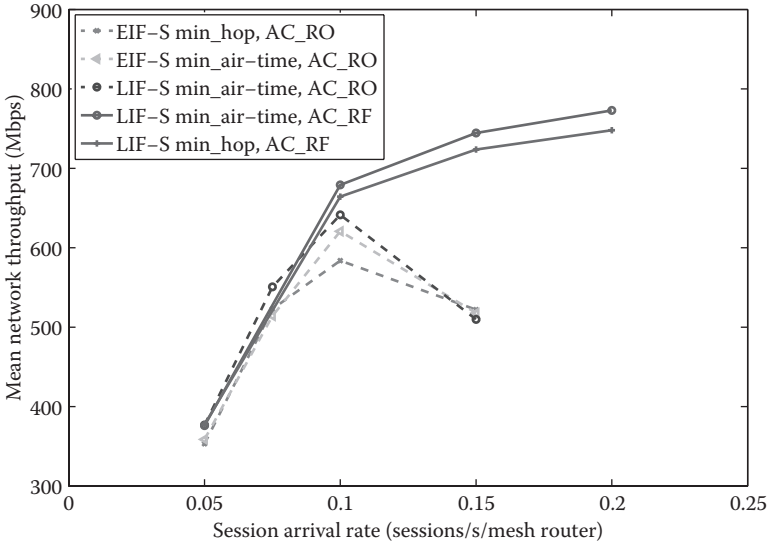

FIGURE 35.1 Mean network throughput for successfully completed sessions versus session arrival rate for two different admission and congestion control schemes under (#MRs):(#GRs) = 40:1. (From H. Lee and D. Cox, *Proceedings of IEEE Wireless Communications and Networking Conference (WCNC)*, (Figure 2a), Apr. 2010; H. Lee, Wireless mesh networks: Protocol design and performance evaluation (Figure 4.7a). PhD dissertation, Stanford University, Stanford, CA, USA, Mar. 2010. With permission.)

The decrease in the network throughput under AC_RO can be explained as follows. If the arrival rate keeps increasing, at some point, all the data time slots become exhausted. At this point, the network must start blocking new EUs. However, many of the MRs may still find resources available for reception at themselves under AC_RO, and those MRs continue to admit new EUs. These admitted EUs incur additional interference to the network, leading to lower PHY rates. The resultant aggregate data size transported by the network thus decreases, leading to the decrease in the network throughput. On the other hand, under AC_RF, the network begins to block new EUs as the network starts to saturate. When the MRs near GRs start to become congested such that some of their existing queues do not receive sufficient resources, the MRs stop accepting admission requests. Then, their children MRs successively stop accepting admission requests until their existing queues receive sufficient resources from these parents MRs, and so on. As a result, the network reaches a balance in which the network admits only as many EUs as it can support without *destabilizing* itself. The diminishing increment with the increasing arrival rate results from the fact that the network becomes increasingly utilized and the idling fraction of the network diminishes as the network becomes increasingly loaded.

We note that the difference resulting from the two different routing metrics described in a previous section is insignificant compared to the difference from the two different ACC policies. This somewhat small difference follows from the fact that the simulated WMN has rather shallow spanning trees for routing.

35.3.1.2 Per-Session Throughput

As seen in Figure 35.2, under both AC_RO and AC_RF, the mean per-session throughput decreases as the traffic arrival rate increases. However, under AC_RO, under a heavy traffic load, the number of active EUs in the network keeps increasing and the session delay also keeps increasing as the system evolves over time. The network employing AC_RO thus cannot guarantee a stable per-session throughput under modest or heavy traffic loads. On the other hand, under AC_RF, the network remains stable under heavy traffic loads. The number of active EUs in the network and the session delay remain

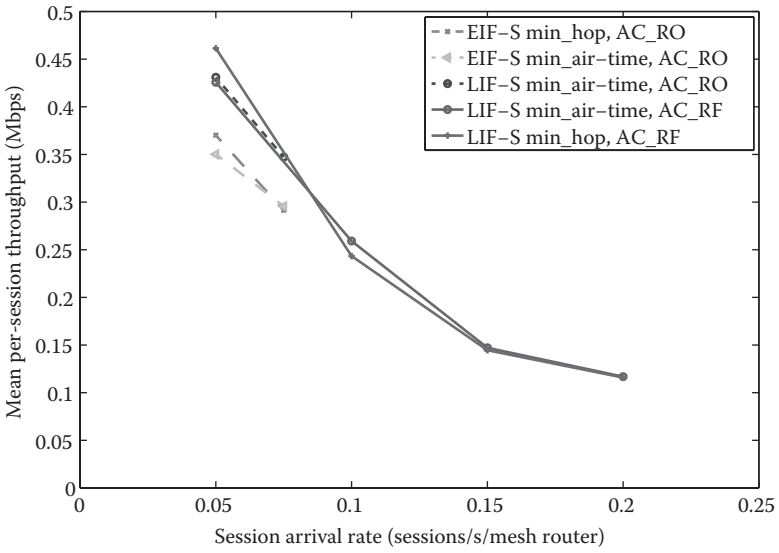

FIGURE 35.2 Mean per-session throughput for successfully completed sessions versus session arrival rate for two different admission and congestion control schemes under (#MRs):(#GRs) = 40:1. (Adapted from H. Lee and D. Cox, *Proceedings of IEEE Wireless Communications and Networking Conference (WCNC)*, (Figure 2b), Apr. 2010; H. Lee, Wireless mesh networks: Protocol design and performance evaluation (Figure 4.7b). PhD dissertation, Stanford University, Stanford, CA, USA, Mar. 2010.)

stationary over time and consequently, the network can guarantee a stable mean per-session throughput even under heavy traffic loads. The decrement in the per-session throughput diminishes with the increasing traffic arrival rate. We expect that the mean per-session throughput would converge as the network resources are increasingly utilized with the increasing traffic arrival rate.

35.3.2 Performance under Different Mesh Sizes

In this section, we present the scalability behavior of several fundamental performance metrics as we vary the network topology by deploying different numbers of GRs while keeping the number and locations of MRs the same. Recall that GRs are colocated with MRs. The number of MRs served by one GR is varied over 1, 2, 5, 10, 20, 40, and 80. We consider the "min_air-time" routing metric and the AC_RF ACC scheme in this section.

35.3.2.1 Network Throughput

As seen in Figure 35.3, the mean network throughput generally increases as the session arrival rate increases given the network topology and the routing metric. However, as the arrival rate keeps increasing, the network becomes overloaded and starts to saturate, and the increment in the mean network throughput decreases and eventually diminishes.

The network throughput behavior can be explained with two related quantities: the mean PHY transmission rate of successfully received data packets, and the mean aggregate number of active data time slots used across the network. As more EUs arrive and are admitted to the network under a higher session arrival rate, the interference level on data time slots becomes higher and thus, the supportable PHY transmission rate becomes lower and more data time slots are used. As the session arrival rate keeps increasing, all the usable data time slots eventually become exhausted, and both of the aggregate number of used data time slots across the network and the mean supportable PHY transmission rate saturate.

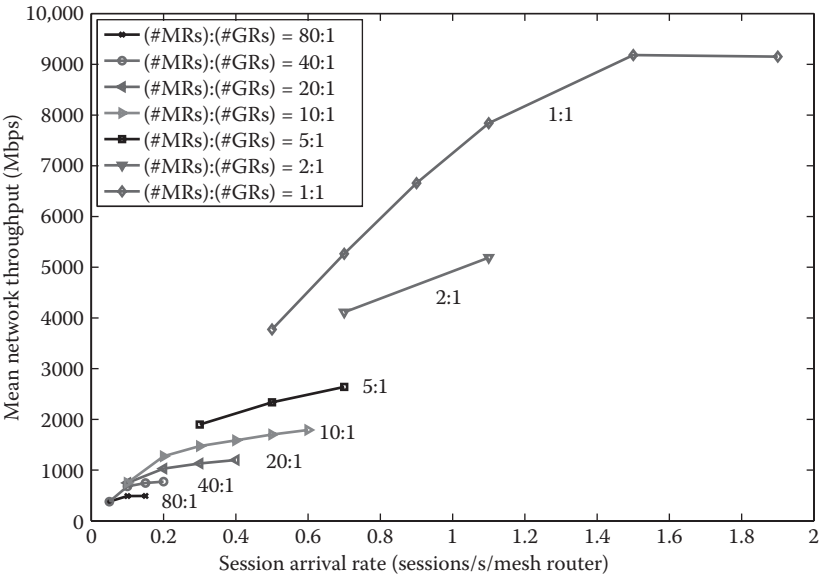

FIGURE 35.3 Mean network throughput versus session arrival rate under different gateway router topologies. In all cases, the routing metric "min_air-time" and the ACC scheme AC_RF is employed. (Adapted from H. Lee, Wireless mesh networks: Protocol design and performance evaluation, (Figure 5.3). PhD dissertation, Stanford University, Stanford, CA, USA, Mar. 2010.)

Figure 35.3 shows that the network throughput improves significantly as more GRs are deployed. There are two major factors that lead to such improvement. One is the shorter average path length, that is, fewer MRs, which each EU data go through to reach the backbone network. Another key factor is the fact that each GR serves fewer MRs on average, and thus each MR interacts with fewer other MRs. This leads to fewer constraints on the usage of a data time slot at an MR and in turn to increased reuse of each data time slot. With more deployed GRs, significantly more data time slots can be used simultaneously and each data time slot can be reused considerably more.

35.3.2.2 Per-Session Throughput

As seen in Figure 35.4, the mean per-session throughput generally decreases with the increasing session arrival rate given the network topology and the routing metric. The lower per-session throughput under a higher arrival rate results from a longer session delay, which is in turn attributed to two main factors: the lower mean PHY transmission rate on data time slots due to increased interference, and the longer delay in acquiring resources at MRs due to more EUs competing for the same resources. Figure 35.4 also demonstrates that for an admitted EU, a stable mean per-session throughput is provided under each session arrival rate and that the mean per-session throughput does not diminish even under heavy traffic loads. It also indicates that the mean per-session throughput considerably improves with more deployed GRs.

Due to the tree structure of the routing tables, the mean per-session throughput provided at an MR greatly varies depending on the path length from the MR to its best GR and the number of MRs served by the same GR. Generally, a significantly larger mean per-session throughput is provided at an MR that is fewer hops away from its best GR. As more GRs are deployed, the per-session throughput increases while the overall trend with the increasing session arrival rate remains the same under each GR topology scenario.

35.3.2.3 Blocking Rate

As seen in Figure 35.5, the blocking rate increases with the increasing session arrival rate given the network topology and the routing metric. This monotonicity follows from the fact that under a higher

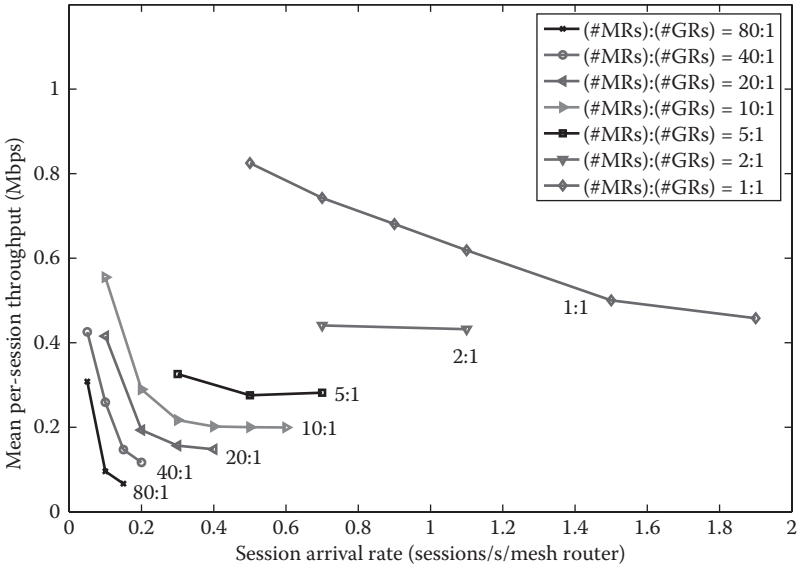

FIGURE 35.4 Mean per-session throughput for successfully completed sessions versus session arrival rate under different gateway router topologies. In all cases, the routing metric "min_air-time" and the ACC scheme AC_RF is employed. (Adapted from H. Lee, Wireless mesh networks: Protocol design and performance evaluation (Figure 5.6). PhD dissertation, Stanford University, Stanford, CA, USA, Mar. 2010.)

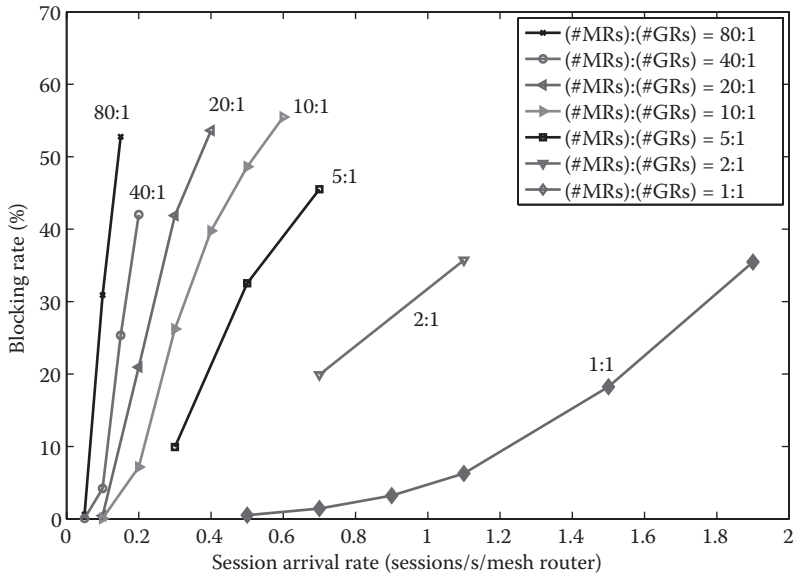

FIGURE 35.5 Blocking rate versus session arrival rate under different gateway router topologies. In all cases, the routing metric "min_air-time" and the ACC scheme AC_RF is employed. (Adapted from H. Lee, Wireless mesh networks: Protocol design and performance evaluation (Figure 5.8). PhD dissertation, Stanford University, Stanford, CA, USA, Mar. 2010.)

arrival rate, a new EU arriving to the network sees more EUs on average that are being served at the MR to associate with, and thus has a higher probability of being blocked. As the network starts to saturate with the increasing session arrival rate, the blocking rate increases very sharply as seen in Figure 35.5. This sharp increase results from the fact that the number of EUs supportable by the network saturates with the increasing arrival rate.

We also calculate the blocking rate for each MR_n, where MR_n denotes an MR that is n hops away from its best GR. The blocking rate at MR_0 is significantly smaller than those at MR_n, $n > 0$ in all cases. This is due to the fact that blocking at MR_0 occurs only when there is no resource left for receiving data for a new EU. It turns out that MR_0 still tends to have a few data time slots available for reception for a new EU even when the overall blocking rate becomes as high as 50%.

On the other hand, one has to consider two main factors to understand the blocking rates at MR_n, $n > 0$. One factor is the amount of opportunity that MR_n acquires for forwarding data, and the other factor is the amount of radio resources, that is, data time slots and the supportable PHY transmission rates over them, which are available at MR_n. The chance or opportunity that MR_{n2} acquires for forwarding data is smaller than that of MR_{n1}, $n1 < n2$. On the other hand, due to the tree structure of the routing tables, MR_{n2} serves fewer EUs on average and thus tends to have more available data time slots and higher supportable PHY rates than MR_{n1}. Depending on the mesh size and the traffic load in the network, the blocking rate at MR_{n1} can be smaller or larger than MR_{n2}. Please refer to [19] for more detailed discussions.

35.3.2.4 Dropping Rate

Recall that an EU releases a data time slot after a maximum number of unsuccessful retransmissions on the slot, and becomes dropped if it runs out of data time slots. The successive retransmission failures are primarily due to new interfering transmissions on the same data slot that were not seen when the data slot was assigned to this new EU. As seen in Figure 35.6, when the network is lightly loaded, the

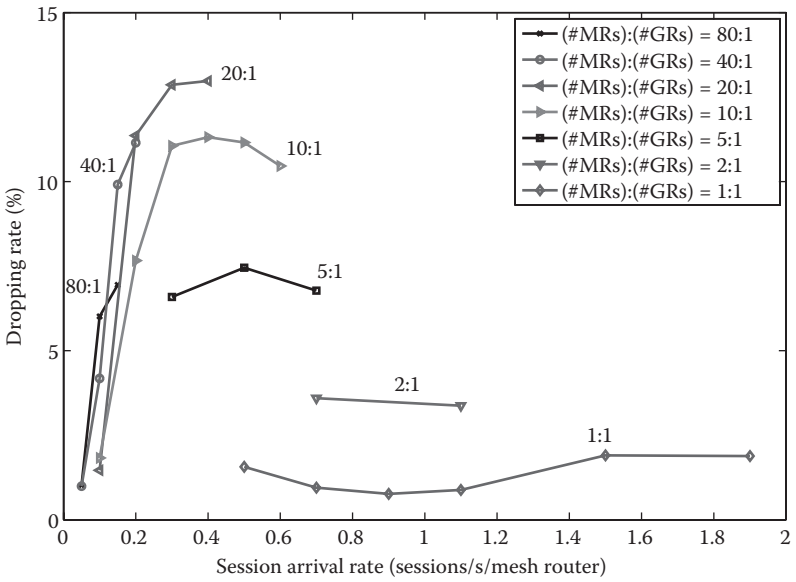

FIGURE 35.6 Dropping rate versus session arrival rate under different gateway router topologies. In all cases, the routing metric "min_air-time" and the ACC scheme AC_RF is employed. (Adapted from H. Lee, Wireless mesh networks: Protocol design and performance evaluation (Figure 5.10). PhD dissertation, Stanford University, Stanford, CA, USA, Mar. 2010.)

dropping rate generally increases with the increasing session arrival rate. This monotonic increase under light traffic loads follows from two factors: one is that there are more new transmissions on each data time slot when more new EUs are admitted across the network under a higher arrival rate. The other factor is that when the network is lightly loaded, the interference level on a data time slot is low enough so that multiple MRs across the network may see the same data time slot available and assign the slot to new transmissions.

As the arrival rate keeps increasing and the network becomes increasingly saturated, the number of new EUs that are admitted at once across the network tends to saturate as well. Consequently, the probability of a new EU getting dropped due to additional new transmissions also tends to saturate. Furthermore, as seen in Figure 35.6, the dropping rate may even start to decrease with the increasing arrival rate in some cases. This decrease can be explained as follows. If the mesh size is small enough and the traffic load in the network is high enough so that the interference level on data time slots is too high for the same data time slot to be assigned to multiple new transmissions simultaneously, then, each data time slot assigned to a new EU or new transmission may not suffer from as much increase in the cochannel interference as it did under a lower arrival rate, leading to a decrease in the dropping rate.

We also calculate the dropping rate for each MR_n. The dropping rate at MR_{n2} tends to be smaller than that at MR_{n1}, $n1 < n2$. This is because MR_{n2} tends to have more available data time slots on average than MR_{n1}, and thus a data time slot chosen for a new EU at MR_{n2} tends to have a lower interference level under the employed data time slot selection algorithm. The reason why the dropping rate at MR_0 is noticeably higher than those at MR_n, $n > 0$ is that the blocking rate at MR_0 is significantly smaller than those at MR_n, $n > 0$, and thus an admitted EU tends to get assigned data time slots with far stronger interference.

35.4 Conclusion

In this chapter, we focused on WMNs that serve as access networks over large geographic areas, and presented protocols and performance behavior that are based on more realistic models for physical and networking layers of network functions that have been often oversimplified in the literature. We first presented a set of MAC protocols that incorporate such models for the WMNs. We then presented the performance of the WMNs obtained through a large simulator that incorporates measurement-based models for radio propagation and interference calculation for a large built-in urban area. We first compared the impact of two ACC schemes on the network performance, and demonstrated that the ACC scheme AC_RF was able to stabilize the network even under heavy traffic loads. We then investigated the impact of different mesh sizes on the performance, and demonstrated that with more deployed GRs, that is, more backbone support to the network, the network throughput and per-session throughput improved significantly. Under each simulated scenario, we identified major factors that affect the performance behavior and showed that the PHY, MAC, and routing layers of network functions interact with one another in a complicated manner to determine the network performance.

References

1. I. Akyildiz and X. Wang, A survey on wireless mesh networks. *IEEE Communications Magazine*, 43(9), S23–S30, 2005.
2. R. Bruno, M. Conti, and E. Gregori, Mesh networks: Commodity multihop ad hoc networks. *IEEE Communications Magazine*, 43(3), 123–131, 2005.
3. M.J. Lee, J. Zheng, Y.-B. Ko, and D.M. Shrestha, Emerging standards for wireless mesh technology, *IEEE Wireless Communications Magazine*, 13(2), 56–63, 2006.
4. Google, Inc. [Online]. Available: http://www.google.com/corporate/.

5. Tropos, Inc. [Online]. Available: http://www.tropos.com.
6. E. Perkins, E. Belding-Royer, and S. Das. (2003, Jul.) Ad hoc on demand distance vector (AODV) routing. [Online]. Available: http://www.ietf.org/rfc/rfc3561.txt.
7. C. Perkins and P. Bhagwat, Highly dynamic destination-sequenced distance-vector (DSDV) routing for mobile computers. *ACM SIGCOMM Computer Communication Review*, 24(4), 234–244, 1994.
8. D. Johnson and D. Maltz, Dynamic source routing in ad hoc wireless networks. *Mobile Computing*, 353, 153–181, 1996.
9. T. Clausen and P. Jaquet. (2003, Oct.) Optimized link state routing protocol (OLSR). [Online]. Available: http://www.ietf.org/rfc/rfc3626.txt.
10. R. Draves, J. Padhye, and B. Zill, Comparisons of routing metrics for static multi-hop wireless networks. *Prof. of ACM Special Interest Group on Data Communications Conference (SIGCOMM)*, pp. 133–144, Aug. 2004.
11. R. Draves, J. Padhye, and B. Zill, Routing in multi-radio, multi-hop wireless mesh networks. *Proceedings of ACM Mobile Computing and Networking Conference (MOBICOM)*, Philadelphia, PA, pp. 114–128, Sep. 2004.
12. D. Couto et al., A high-throughput path metric for multi-hop wireless routing. *Wireless Networks*, 11(4), 419–434, 2005.
13. Z. Tang and J. Garcia-Luna-Aceves, A protocol for topology-dependent transmission scheduling in wireless networks. *Proceedings of IEEE Wireless Communications and Networking Conference (WCNC)*, New Orleans, LA, pp. 1333–1337, Sep. 1999.
14. C. Zhu and M. Corson, A five-phase reservation protocol (FPRP) for mobile ad hoc networks. *Wireless Networks*, 7(4), 371–384, 2001.
15. C. Zhu and M. Corson, An evolutionary-TDMA scheduling protocol (E-TDMA) for mobile ad hoc networks, *Proceedings of Advanced Telecommunications/Information Distribution Research Program (ATIRP)*, College Park, MD, Mar. 2000.
16. H. Lee and D. Cox, A fully-distributed control time slot assignment protocol for large wireless mesh networks. *Proceedings of IEEE Military Communications Conference (MILCOM)*, San Diego, CA, Nov. 2008.
17. H. Lee and D. Cox, A fully cooperative and distributed medium access control protocol for large TDMA/TDD-based wireless mesh networks. *Proceedings of IEEE Vehicular Technology Conference (VTC)-Spring*, Barcelona, Spain, Apr. 2009.
18. H. Lee and D. Cox, Admission and congestion control for large-scale wireless mesh access networks. *Proceedings of IEEE Wireless Communications and Networking Conference (WCNC)*, Sydney, Australia, Apr. 2010.
19. H. Lee, Wireless mesh networks: Protocol design and performance evaluation. PhD dissertation, Stanford University, Stanford, CA, USA, Mar. 2010.
20. I. Chlamtac and S. Kutten, A spatial-reuse of TDMA/FDMA for mobile multi- hop radio networks. *Proceedings of IEEE Conference on Computer Communications (INFOCOM)*, Washington, DC, 1985.
21. I. Cidon and M. Sidi, Distributed assignment algorithms for multihop packet radio networks. *IEEE Transactions on Computers*, 38(10), 1353–1361, 1989.
22. A. Ephremedis and T. Truong, Scheduling broadcasts in multihop radio net works. *IEEE Transactions on Communications*, 38(4), 456–460, 1990.
23. S. Ramanathan, A unified framework and algorithm for channel assignment in wireless networks. *Wireless Networks*, 5(2), 81–94, 1999.
24. IEEE Std. 802.11, 1999 Edition (R2003), Information technology Telecommunications and information exchange between systems—Local and metropolitan area networks—Specific requirements—Part 11: Wireless LAN Medium Access Control (MAC) and Physical Layer (PHY) Specifications.
25. D. Zhao, J. Zou, and T. Todd, Admission control with load balancing in IEEE 802.11-based ESS mesh networks. *Wireless Networks*, 13(3), 351–359, 2007.

26. C. Zhu and M. Corson, Qos routing for mobile ad hoc networks, *Proceedings of IEEE Conference on Computer Communications (INFOCOM)*, New York, NY, pp. 958–967, Jun. 2002.
27. I. P802.11s/D0.01, *Draft Amendment to Standard IEEE 802.11: ESS Mesh Networking. IEEE*, Mar. 2006, work in progress.
28. M. Bahr, Proposed routing for IEEE 802.11s WLAN mesh network. *Proceedings of Wireless Internet Conference (WICON)*, Boston, MA, Aug. 2006.

36

IP Multimedia Subsystem: Analysis of Scalability and Integration*

Lava N. Al-Doski

Rabindra Ghimire

Seshadri Mohan

36.1 Introduction

IP multimedia subsystem (IMS) is an architectural framework for delivering multimedia services standardized by the Third-Generation Partnership (3GPP/3GPP2) in late 1999. IMS enables multimedia and voice services to be delivered in a well-structured manner. It facilitates services integration over disparate networks, including the Internet and cellular networks. IMS enables advanced services such as email, video conference, presence, chat, push to talk (PTT), and IPTV to become widely available to the users.

The services infrastructure has traditionally evolved in a "stove-piped" manner as shown in Figure 36.1a, where services are established, maintained, and terminated independently of each other. A number of functions common to many services such as billing, quality of service (QoS), and user profile are developed and maintained specifically for each service, thereby increasing the cost of development and maintenance as well as decreasing the utilization of resources. The stove piped arrangement is unsuitable because of its inability to share common functions and in view of the tremendous demand for new types of services together with the exponential increase in the number of users.

The IMS system is organized as a layered architecture where functions are built on top of each other in a horizontal manner as illustrated in Figure 36.1b. When structured in this manner, the system allows multiple services to share a common set of functions without the need to redevelop each function separately for each service. This concept of reuse of functions and/or capabilities will pave the way for rapid service development and eliminate redundant development efforts associated with every new service development.

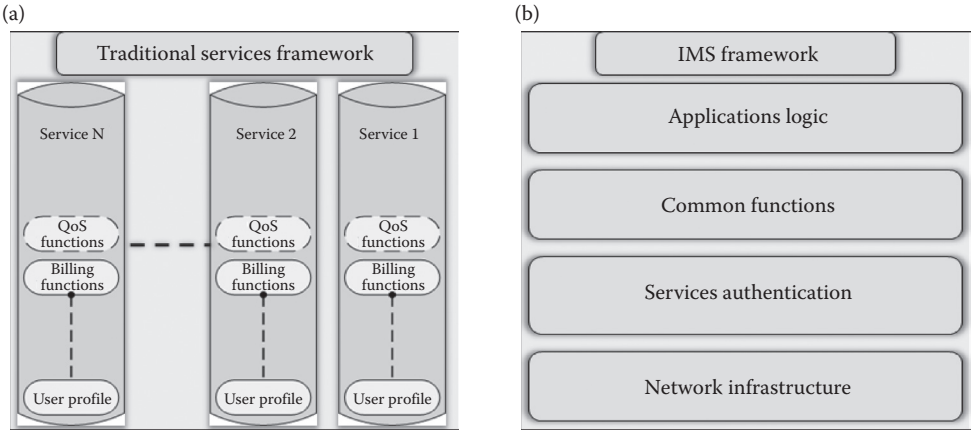

FIGURE 36.1 (a) Traditional service framework and (b) IMS framework.

IMS is access and device independent. It can be integrated with 3G and 4G networks regardless of the network technology (WLAN, LTE, WiMax, etc.). The user can use IMS services regardless of the device used. IMS is capable of delivering services with QoS to the user. It facilitates rapid service development, and has the potential to offer a rich suite of applications to the users. This approach encourages service providers to establish a service creation platform open to third-party vendors. In addition to 3GPP, other standardization bodies have embraced IMS protocol developments which are based on the IETF-defined session control [1]. A complementary effort by Open Mobile Alliance (OMA) [2] is aimed at stimulating the creation and adoption of new enhanced mobile services such as video, entertainment, and information services. The alliance works toward standardization and interoperability of all application-related issues.

After an introduction to IMS in Section 36.2 with an overview of the architecture, the protocol suite, and the control structures, Sections 36.3 provides an analysis of the impact of introducing services and integrating IMS with CDMA/WLAN hybrid networks. Section 36.4 provides a summary of the insights from the analysis of Section 36.3.

36.2 IP Multimedia Subsystem

Service providers anticipate that IMS will benefit the end users by

- Facilitating delivery of services with QoS to the end user
- Enabling an environment for the development of new and advanced blended services
- Ensuring secure transactions of user information
- Facilitating the collection of all services utilized by a user that can be supplied to the billing systems to create an integrated bill
- Facilitating the delivery of services over disparate networks
- Facilitating ease of use of services by allowing users to create a single profile and register once for all the services

Figure 36.2 illustrates the relationship between the IMS layer, different types of wireless and wireline networks such as WiFi, universal mobile telecommunications system (UMTS), long-term evolution (LTE), and the public switched telephone network (PSTN), and the application layer.

The IMS layer provides many common services, including registration, authentication, user data provisioning, session negotiations, and data collection for billing and charging purposes. This layer includes IMS entities such as call session control functions (CSCFs) and home subscriber server (HSS).

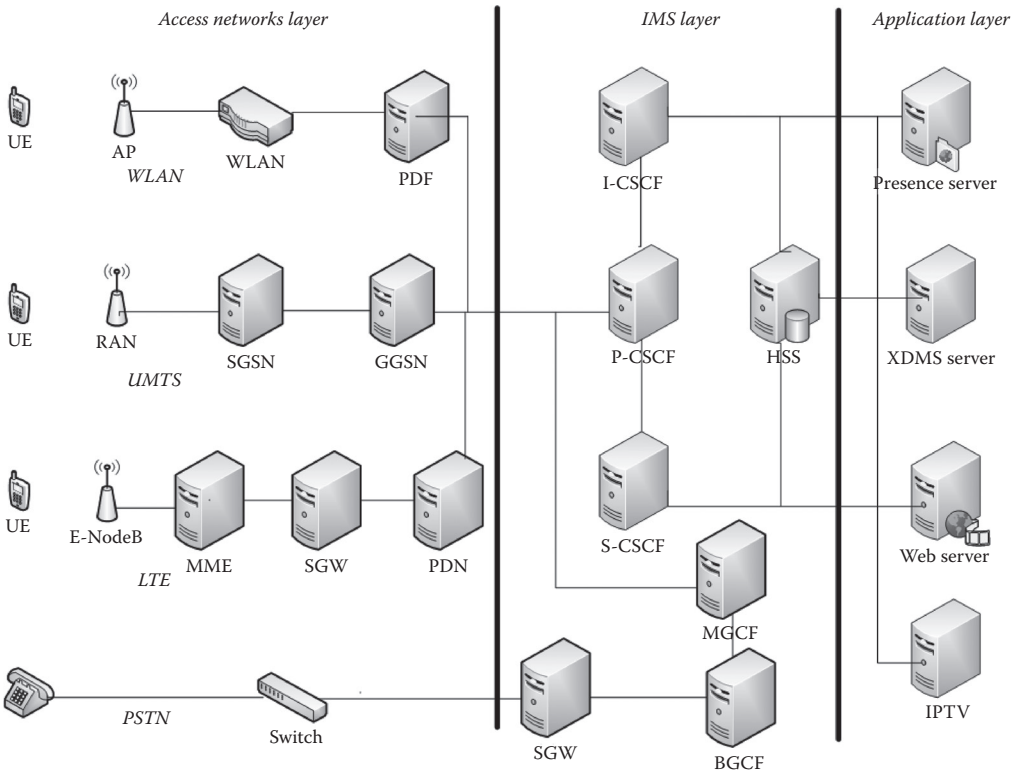

FIGURE 36.2 IMS architecture.

The application layer includes all the application servers that offer a variety of services and applications to the end user. Most of these application servers utilize the session initiation protocol (SIP) as the signaling protocol for services negotiation.

In a typical service scenario, a user requests a service via an access network. The request is subsequently transferred from the access network to the IMS subsystem, where the request is processed and then forwarded to the application layer. Figure 36.1 shows some example applications such as presence, Parlay X, and IPTV.

IMS's core network server is a CSCF server. This function takes on four different variations, which are proxy, serving, interrogating, and emergency call session control functions, abbreviated as P-CSCF, S-CSCF, I-CSCF, and E-CSCF, respectively. The serving CSCF is considered to be the brain of IMS. Each server performs different tasks to ensure service delivery to the user.

36.2.1 IMS Control Functions

The P-CSCF, being located in the visitor's network, serves as the first point of contact for the user. Subsequently, the user's requests are processed by I-CSCF and then P-CSCF. In order to access the IMS system, users need to have at least one address of the IMS system. In the 3GPP design, users need to perform P-CSCF discovery mechanism. P-CSCF carries out several tasks as highlighted below [3]:

- During a registration request, P-CSCF will review the request and then reroute it to the appropriate I-CSCF based on the user's home location.
- After acquiring the address of S-CSCF during the registration process, P-CSCF is responsible for rerouting SIP packets to S-CSCF.

- P-CSCF is responsible for maintaining a secure connection with the user.
- It composes and decomposes SIP messages.
- It manages emergency calls and forward them to the E-CSCF server [1].
- It generates charging information and forward it to the charging entity.
- It updates the SIP packets with the network information.
- In some cases, it hides the network topology.

The I-CSCF, which is located in the home network, can access the IMS system data base HSS. The following list highlights the tasks performed by I-CSCF:

- It is responsible for retrieving the S-CSCF address from HSS and rerouting SIP packets to S-CSCF
- It is responsible for rerouting packets to a different IMS network.
- It is responsible for receiving and rerouting SIP messages arriving from a different IMS system.

The S-CSC is considered the most important server that is located in the home network and that maintains access to HSS. S-CSCF carries out major tasks within the IMS system as highlighted below:

- Authorizing and authenticating users during registration
- Serving as an SIP registrar, accessing HSS using the diameter protocol, and providing HSS with the user information to ensure secure sessions
- Checking SIP messages to determine if an application server is needed and filtering the messages using trigger points, and forwarding the message to the correct application server
- Managing and terminating sessions as necessary [4] and handling user requests for registration and downloading user profile from HSS
- Collecting charging information for services utilized by the users and proving the information to the charging unit
- Deregistering users when required
- Routing SIP messages to IMS systems in different domains

The E-CSCF server has been added recently by 3GPP standardization and Federal Communications Commission (FCC) to provide emergency access to users. The server's task is to overview emergency calls. On receiving an emergency call, it retrieves user location and information through dedicated location servers and then forward the location of the user to the appropriate emergency dispatcher service. E-CSCF provides an essential delay-sensitive service to the user [1].

The HSS serves as the main database of the IMS system by maintaining profiles of users with information to identify, register, authenticate, and authorize users so as to enable the users to avail the rich multimedia services enabled by IMS. There might be more than one HSS so that the system can scale with increasing subscribers. HSS keeps the subscription information of the user by applying a criterion known as *initial filter criteria* (iFC), which are logical filters that contain trigger points that get downloaded to S-CSCF when the user registers.

Application servers represent the end point that process requests for services initiated by the user. IMS has multiple servers assigned to perform various services. Most of these servers have built-in SIP proxies [5]. To ensure that every user is served by the requested services, the HSS will choose the right application server based on the user-requested services and the applicable policies. Application servers are considered as some of the most essential entities as they facilitate the use of a rich set of services by the user. Service providers are deploying what is referred to as *service-oriented architectures* (SOA) to provide integrated services to end users. SOA is capable of supporting third-party applications [3].

Media resource function (MRF) is a node responsible for media control in the home network. It is divided into two functions, *media resource function controller* (MFRC) and *media resource function processor* (MRFP). MRFC performs media control such as sending announcements and transcoding of media whereas MRFP processes MRFC instructions, media streaming by multiple parties, and codec media information. An H.248 interface [6] facilitates media capability negotiation between the nodes requesting the establishment of a session.

Breakout gateway control function (BGCF) is responsible for routing SIP messages to a circuit switching network; it uses telephone numbers to route calls to the PSTN.

36.2.2 IMS Protocol Suite

Within the IMS system, a number of protocols play an important role in facilitating the IMS system to successfully deliver services to the end user. Some significant ones are briefly described below.

1. *Session initiation protocol (SIP)* SIP is an application layer protocol created by IETF (Internet Engineering Task Force). SIP is one of the most essential protocols for multimedia session management that is used to create, maintain, and terminate sessions. SIP is responsible for the session management of services such as video conference, voice over IP (VoIP), chat, and multimedia streaming. For this reason, SIP was adopted by 3GPP as the signaling protocol for session management. Media stream is transported using the real-time transport protocol (RTP) [7].
2. *Session description protocol (SDP)* The SDP created by IETF defines the format of the SIP messages. SIP defines the type of information being sent, while SDP represents the format of these messages.
3. *Real-time transport protocol (RTP)* The RTP protocol introduced by IETF defines the formats of the media packets to be delivered. It is used to deliver multimedia steams in services such as VoIP, video conference, and other IMS applications.
4. *Diameter protocol* The diameter protocol designed by IETF is an authorization, authentication, and accounting (AAA) protocol, and is a successor to the RADUIS protocol. The diameter protocol is chosen to manage the delivery of IMS client information between I-CSCF, S-CSCF, and HSS.

SIP being the most important of the protocols within the IMS suite of protocols, a brief description of the protocol is provided below.

36.2.3 SIP Architecture

To keep track of the users and the session, SIP requires all the users to register before establishing a session. SIP entities include the following:

User agent client (UAC) is the entity that requests a session or service. Prior to requesting service, the SIP client needs to register (see Figure 36.3).

User agent server (UAS) is the entity that receives and responds to the service request initiated by UAC. A SIP server can be another user's agent.

*SIP proxy i*s the entity that reroutes SIP messages. This capability facilitates SIP messages to be routed to the final destination by multiple SIP proxies. Unlike the "best-effort" IP routing, SIP message requests and responses should follow the same routing hops to keep track of the session state. However, that is not the situation with RTP packets that carry media stream. The media stream in either direction follows the best-effort IP routing scheme.

SIP registrar: Each UAC needs to register with the service. The registration request is processed by the SIP registrar server, which keeps track of user registrations. The SIP registrar is usually integrated with the SIP proxy.

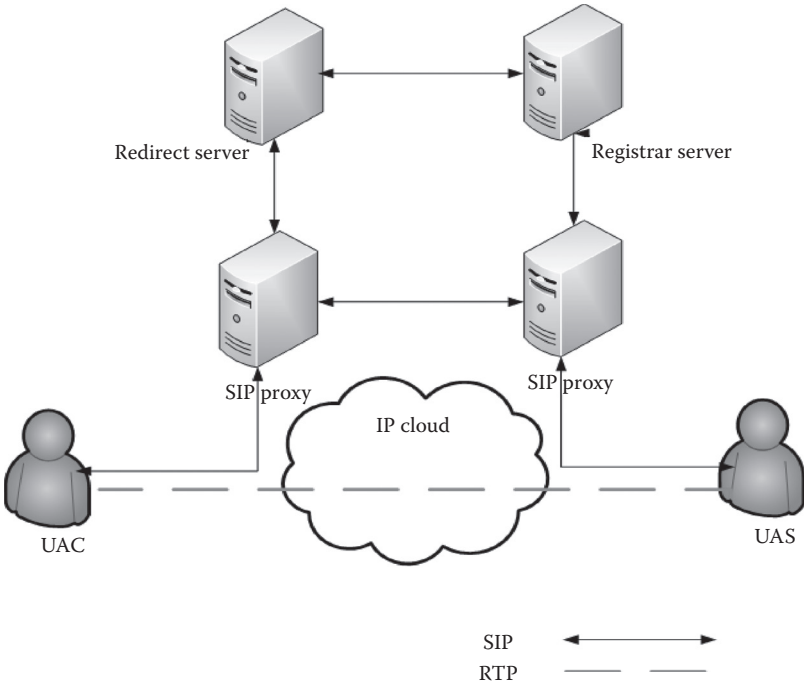

FIGURE 36.3 SIP architecture.

36.2.4 SIP Methods

As shown in Figure 36.4 [7], SIP messages are described using SDP. The first part of the message is the message header which represents the purpose of the message indicated by the SIP method type, the initiating and receiving address information, and the sequence of the message. The second part of the message (separated by space) represents information about the media such as encoding and decoding

```
INVITE sip:name1@operator.com SIP/2.0
V=SIP/2.0/UDP
193.215.131.000;maddr=239.128.16.254;ttl=16
V:SIP/2.0/UDP 128.16.64.19
F:sip:name2@operator.com
I:62729-27@128.16.64.19
C:application/sdp
CSeq:4711 INVITE
1:187
V=0

O=user153655765235687637 in IP4 128.3.4.5
S=Mbone Audio
I=Discussion of Engineering Issues
E=company@operator.com
C= In IP4 224.2.0.1/127
T=0
M=Audio3456/RTP/AVP0
```

FIGURE 36.4 SIP INVITE.

TABLE 36.1 SIP Methods

SIP Method	Meaning
INVITE	A UAC invokes the INVITE method to request session establishment
REGISTER	Register the address listed in the To header of the SIP message
CANCEL	Cancel pending requests
OPTIONS	Queries the server for its capabilities
SUBSCRIBE	Subscribe the user for event
PUBLISH	Publish an event to the server
NOTIFY	Notify the user of a new event
INFO	Send midsession information, no modification applied to the states
MESSAGE	Transport instant messages by SIP
ACK	Acknowledge the invite request
UPDATE	Modify the session state
PRACK	Provisional acknowledgment

information (codec specifications), device information, a line indicating the SIP method, together with the main purpose of the SIP message and the address which initiated the request.

Besides the INVITE method, SIP deploys various other methods while communicating with nodes. SIP messages or methods [1] are sent and received within the SIP packets. Table 36.1 lists the SIP methods.

36.2.5 User Identification in IMS

The IMS system uses different kinds of identities to identify the user within the system; each has its own purpose. The users' IDs may be public or private.

IMS users' public user identities are used as a contact address or a business card and it is used by IMS to route SIP messages to other users. Public user identity comes in the format of SIP URL (name@operator.com or 000-00-0000@operator.com) or as a TEL URL (+000-00-0000). Users may have multiple public user identities.

Each IMS user may be assigned one or more private user identities. This identity is used internally by IMS to identify user information while registering or authenticating. Users are normally not aware of this address, which is in the format of network access identifier (name@operator.com). Both private and public identities are stored in HSS.

36.2.6 IMS Services

IMS provides powerful session and service management. The following list highlights the most common services:

Presence service provides information concerning the status and availability of the users. This service, which updates users' presence information dynamically in real time, makes communications among users more convenient. User information may include [3]

- Availability
- User device capabilities
- User location
- Current activity
- Communication preferences

Presence servers are part of the IMS application layer. IMS users subscribe with their presence information "*presentities*" to resources list (user contact list). Users who request the resources list are called

"*Watchers*." The IMS user updates "*publish*" their "*presentities*" to the resources list to be watched by others.

Conferencing facilitates session establishment between two or more users due to powerful session management mechanism.

Push to talk enhances a user's experience with a Walki Talki-like service by allowing users to push a terminal button and speak with another user without the need to dial. PTT server is also associated with XDMS server.

Instant message enables users to send IM messages through the IMS system. IMS has two modes for sending IM. The first mode is session based, and the second is pager based.

36.2.7 Quality of Service

Service providers are required to provide a certain level of service performance for the users depending on the service level subscription. Service providers reserve resource to ensure service delivery with QoS. In IMS, different priorities may be assigned to different services, as some services are less delay tolerant than others. QoS is impacted upon by the following factors [8,9]:

- Delay and jitter
- Cost
- Bit error rate
- Likelihood of failure
- Throughput

QoS is a key metric that may be related to the user experience. QoS may be enforced using the differentiated services or *Diffserv* technique defined by IETF [10] and adopted by 3GPP for use by IMS. Diffserv follows the idea of differentiating packet flows into 3GPP QoS classes shown in Table 36.2.

36.2.8 IMS Procedures

36.2.8.1 P-CSCF Discovery

Before using IMS services, users need a starting point to reach and interact with the IMS system to perform registration and authentication. Since P-CSCF is the first and only contact with users, UACs obtain the address of P-CSCF by a discovery process. Two standards are used for proxy discovery; the first one is by using the dynamic host configuration protocol (DHCP), and the second by the discovery process used in GPRS. In the DHCP procedure, the user sends a query to the DHCP server, the server queries the domain name system (DNS) server and forward the proxy address to the user [3]. In the GPRS discovery process, users request P-CSCF address in the PDP context activation request. The gateway GPRS support node (GGSN) processes the request and sends the proxy address to the user.

36.2.8.2 IMS Registration

IMS users need to perform the registration procedure with the system before establishing any service. The registration procedure in general establishes a connection with the user, loads the user's profile, authenticates the user and allocates resources, and establishes security agreements. During registration,

TABLE 36.2 3GPP QoS Classes

Class Type	Service Example
Conversational class	Voice
Streaming class	Video conference
Interactive class	Web browsing
Background class	Email

IMS terminals register their public user identities with the home network. Usually, the P-CSCF, which is located in the visitor network, ensures that capabilities and roaming agreements are available to contact the home network. The user starts the registration by sending an SIP registration request [4]. The registration process is illustrated in Figure 36.5.

1. The user initiates the SIP method REGISTER; P-CSCF, being located in the visitor's network, will perform DNS query for the URI of I-CSCF. When forwarding the REGISTER method, the proxy inserts its address to make sure it receives back SIP methods to its own address.
2. The I-CSCF serves as a router and a load balancer. The I-CSCF will look into the REGISTER message and extract the user public and private identities and network ID and then send diameter protocol user-authentication request (UAR) to the HSS [11].
3. The HSS examines the received information, and verifies that roaming agreements are in place in case a visitor network ID is received.
4. The HSS authenticates the user and assigns the appropriate S-CSCF to the user, then forward them in its response diameter user-authentication answer (UAA).
5. The I-CSCF receives the UAA and extracts the S-CSCF address and then forward the SIP REGISTER to the S-CSCF.
6. The S-CSCF receives the REGISTER request and sends the multimedia authorization answer (MAA).
7. Upon receiving the MAA message, the HSS saves the S-CSCF URI. The HSS sends MAA back to the S-CSCF which contains authentication information of the user.
8. As part of the security system, IMS users are required to accept a challenge. Basically, the IMS proposes a challenge for the user as a form of protecting the system from flooding with fake users' request.
9. The user will send a registration request again with the challenge reply which gets processed as before.

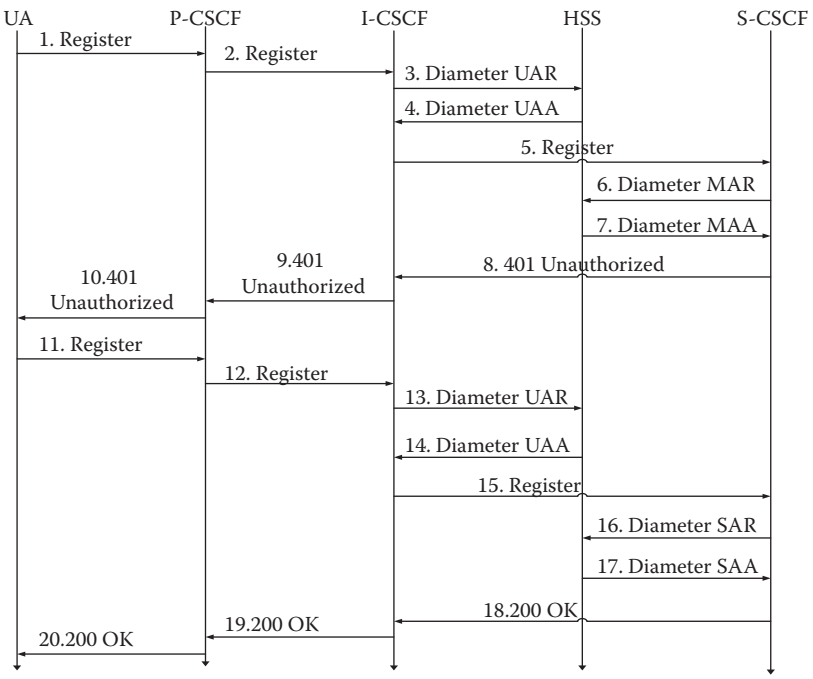

FIGURE 36.5 IMS user registration procedure.

10. In the second attempt, the I-CSCF will send the registration information to the HSS in the form of UAR.
11. The HSS sends back UAA which includes the address of the S-CSCF allocated to the user.
12. The I-CSCF sends the REGISTER to the S-CSCF with the user information.
13. The S-CSCF receives the user information and sends the SAR diameter message to notify the HSS that the user is registered and authenticated.
14. The HSS receives SAR diameter message and sends the user profile, user public identity, and the iFC to indicate the application server with which the user will be connected.
15. The S-CSCF sends 200 OK to indicate the registration procedure was successful.

36.3 Scalability Analysis of IMS

36.3.1 Impact of Service Usage

The goal of IMS is to bring forth the flexibility and power of the Internet to 3G cellular systems and to evolve cellular networks along their path toward and beyond 3G. Among the services facilitated by IMS are video conferencing, chat, instant messaging, PTT. The SIP, whose purpose is to handle sessions, forms a major protocol of the IMS standard. SIP facilitates the establishment, modification, and termination of sessions in IMS. The IMS system is designed to have registration areas. Registration areas constitute a number of cells. Whenever a user arrives at a registration area, the user terminal initiates a registration request. The analysis shows the rate of queries/updates to IMS servers, which are triggered as a result of a user's request for a service or due to users moving into a new registration area. The analysis assumes several parameters of a 3G system such as the density of the 3G terminals, total number of cells per registration area, average speed of a terminal, and the average rate at which each service is initiated by a terminal. The analysis incorporates mobility models to ensure realistic performance analysis. The analysis utilizes the fluid flow model which has been applied to ANSI-41 and GSM systems [12,13]. The analysis utilizes gamma and uniform distributions for the residence time of a user in a registration area to determine the registration rate. The analysis examines the effects of the gamma distribution for the residence time by varying gamma's parameters (shape parameter and the scale parameters). In order to conduct the analysis, the following assumptions are made, some of which are taken from earlier papers (see Reference 13). According to the fluid flow mobility model, the rate of registration, R, is given by

$$R = \frac{\rho v L}{\pi}$$

where ρ is the terminal density per unit area, v the velocity of the terminal km/h, and L the length of the perimeter length of the region (km).

Assumptions:

- Total number of registration areas = 226
- Registration area size = 60 km^2
- L = 30. 984 km
- Speed v = 6 km/h
- Mean density = 48 IMS terminals/km^2
- Average IM rate = 2/h/terminal
- Average chat rate = 1.5/hr/terminal
- Average PTT rate = 3/h/terminal
- Average number of video conferences = 1/h/terminal

As an example of sizing calculations, the above equation can be applied to calculate registration rate initiated by users following the fluid flow model. Each registration request then initiates a signaling flow

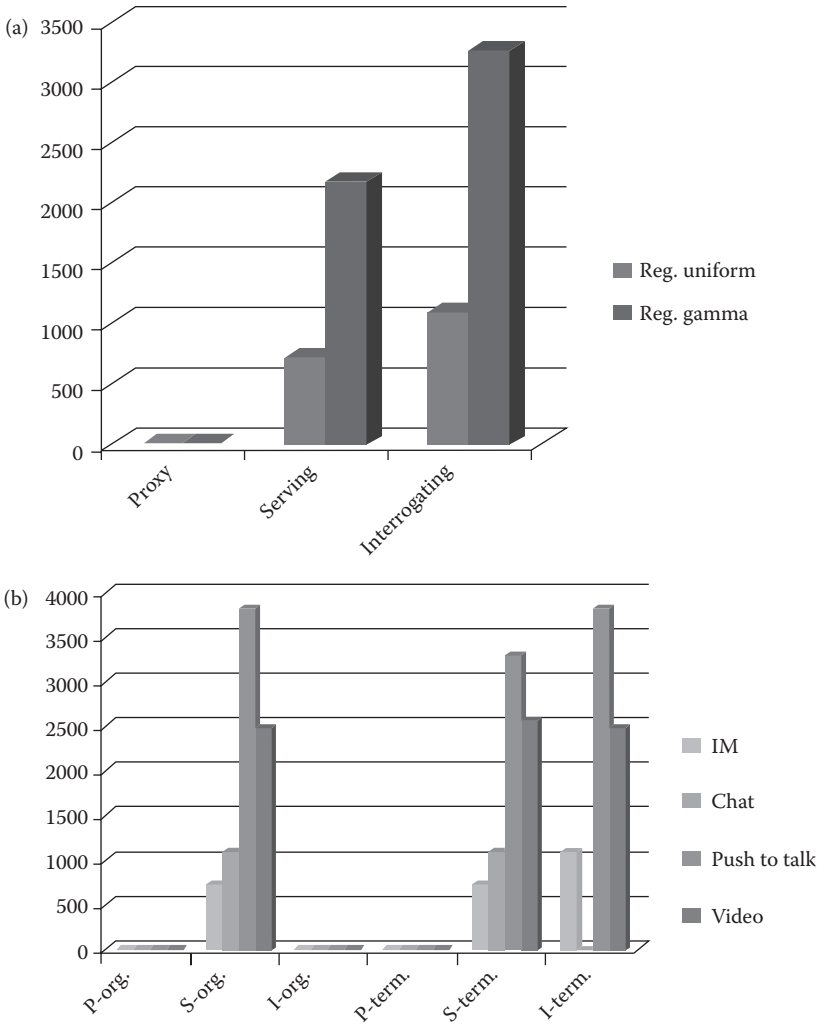

FIGURE 36.6 (a) The registration rate on the IMS servers when using two kinds of distributions for the residence time of the users. (b) Queries to originating and terminating IMS servers while using various services.

using which one can calculate the rate of queries/updates to each IMS server due to user mobility leading to registration requests. Using the service mix assumptions stated above, and the signaling flow for each service, rate of queries/updates to each server can be calculated. The signaling flows due to registration as well as other services are not shown here due to space limitations (see Reference 3 for further details). Figure 36.6a shows the number of hits while requesting registration. Figure 36.6b shows the number of queries to the IMS servers while using services mix consisting of instant messaging, PTT, chat, and video conferencing for both the originating and the terminating ends.

36.3.2 Impact of CDMA2000–WLAN Integration

This analysis shows the impact of delivering 3G services to user terminals over hybrid WLAN/CDMA2000 networks. Such hybrid networks have multifaceted objectives: offer improved 3G multimedia services to users, increase the reliability of the system, and enhance in-building coverage thereby

facilitating service providers to extend wireless services to enterprises. The hybrid network will also facilitate terminals to access different networks to obtain the needed services without being obligated to have different billing information or different accounts. The IMS service infrastructure will facilitate service delivery transparently over the hybrid CDMA2000 and WLAN network to different types of terminals, thereby providing transparency of service delivery to networks and terminal types. Besides its applicability to 3G networks, IMS is also being considered by researchers as part of the 4G family due to its advanced features and the number of disparate services that can be provided such as PTT, video conferencing, presence, and web services to the user. In designing a service infrastructure for either 3G or 4G networks, IMS components are distributed according to their functions into the integrated design as part of the service and application layer. To mimic user movement, the analysis considers mobility models. The analysis carried out is intended to help network designers and architects of 3G and 4G networks with insights into the signaling load generated by IMS due to user mobility and the frequency of invocation of services as well as into ways to distribute the load and scale network design.

36.3.2.1 CDMA2000 and WLAN Interworking

We analyze the deployment of IMS within the CDMA2000/WLAN hybrid network. The integration between different networks will facilitate the development of new services that can be attractive to the users. The users will also have different networks to connect to depending on their location. Expanding this idea can serve well for the 3G and beyond services development [14]. The hybrid network structure provides WLAN users with IMS services, which will require the integration of WLAN with a service provider's CDMA2000 network. The interworking of WLAN within CDMA2000 will provide a view of the user benefits of having hybrid networks. The scheme is adapted from Reference 15. In this scheme, WLANs serve as the access provider network and CDMA2000 network serves as the backbone network, where the IMS main core belongs. The authors in Reference 16 proposed two interworking schemes, tightly coupled interworking and loosely coupled interworking. Loosely coupled integration is a more flexible scheme in comparison with the tightly coupled integration. The tightly coupled integration requires that either or both networks belong to the same service provider or, in the case of multiple service providers, it requires having certain physical interfaces between the networks. In loosely coupled integration, the WLAN gateway is connected to the packet control function (PCF) through the Internet. The PCF views the WLAN network as another 3G network and reroutes the packets to the packet data serving node (PDSN), which, in turn, routes the packets to the home network. Here, PDSN acts as the connection point between the radio access and IP network.

36.3.2.2 IMS Integration

Figure 36.7 shows the overall design of the system. Since P-CSCF is the first contact with the user, the P-CSCF is integrated with PCF. The HSS is integrated with home-AAA (H-AAA) to provide access to the user profile for updates and authentication purposes. The entities S,I-CSCF are integrated with home agent (HA) to facilitate access to the HSS and to ensure accessibility by I-CSCF to other 3G networks. CDMA2000 supports mobile IP [17], which requires that all visitor networks contain the foreign agent (FA) and the foreign-authentication authorization accounting (F-AAA) servers while the home networks contain the HA and the H-AAA server.

36.3.2.3 Scenarios

The CDMA2000 network consists of registration areas (shown hexagonal in shape). It is assumed that these areas have a uniform size and they contain WLAN networks (hot spots) such as airport, university, libraries, and so on, as shown in Figure 36.7. It is preferable for the mobile terminal to switch to the WLAN network in order to utilize the increased bandwidth available within the WLAN. Two scenarios are considered: in the first one, the mobile terminal moves from CDMA2000 to WLAN network. The second complementary scenario assumes that a mobile terminal also roams in the WLAN network while using IMS services.

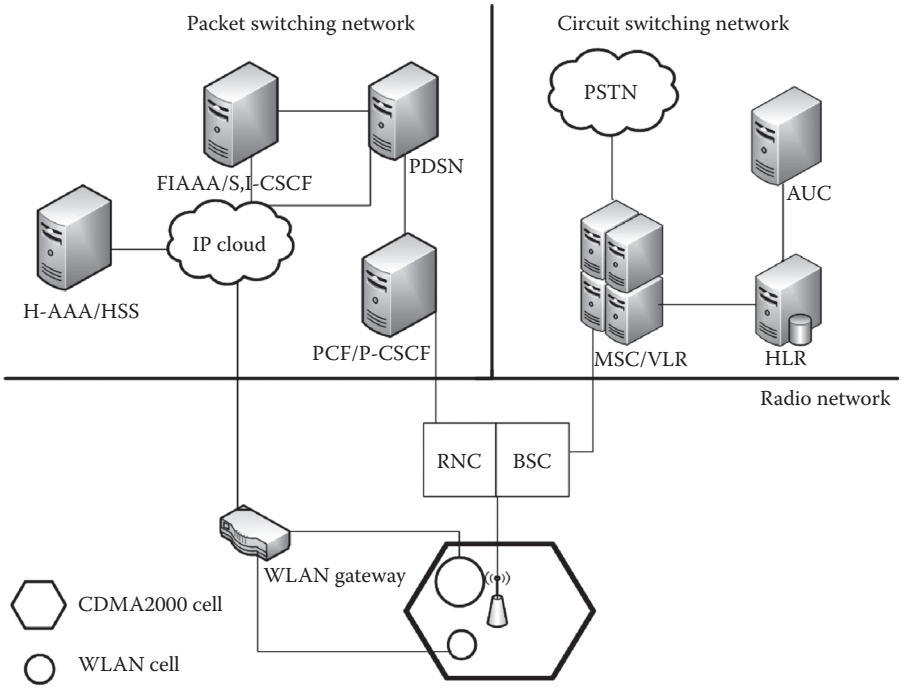

FIGURE 36.7 Hybrid network architecture.

The mobile terminal may roam from the WLAN network back to the CDMA2000 network. In order to capture the services offered by the system, it is assumed that, in both scenarios, the mobile terminal utilizes IMS services while moving from one network to the other. It is also suggested in both scenarios that a user will automatically switch to the WLAN network as soon as that user enters the WLAN network. In order to ensure service continuity, a mobile terminal needs to register while moving to a new network. The registration should take place within the access network and the IMS service plane itself. To examine the design complexity of such a system, user mobility should be modeled appropriately. The CDMA2000 network users' movement is considered to be of faster pace compared to the WLAN users, the movement of which is modeled by fluid flow mobility model. Users within WLAN network tend to move slower and exercise more random movements in comparison with CDMA2000 network users, for which the random walk mobility model is suitable. The following section further explains the two mobility models. The analysis is illustrated via an example, which requires that further assumptions be made as follows:

- Total number of registration areas within the CDMA2000 service provider domain = 50
- Registration area size = 30 km^2
- L = 15.5 km
- Speed v = 6 km/h in the CDMA area
- Mean density ρ = 210 IMS terminals/km^2
- Number of WLAN areas = 10
- WLAN radius = 20, 40, 60, 80, 100 m
- WLAN density = 0.1 terminals/m^2
- Total number users within the hybrid system of networks = 3,15,000

The analysis is carried out by assuming a CDMA2000 network model with 50 cells. This network model includes 10 WLANs. User density is different in both networks. User density within WLAN is

assumed to be greater than that in CDMA2000 due to the nature of these networks. The WLAN networks will generally be of different sizes. It is assumed that a small fraction of the users in the CDMA2000 will join the WLANs as they move into hot spots covered by the WLANs such as airports, shopping malls, restaurants, universities, or others, stay within the WLANs for a period of time, and then move back into the CDMA2000 network. The design assumes loosely coupled interworking between WLANs and the CDMA2000 network. Calculations are carried out for the five different WLAN radii ranging from 20 to 100 m. Registration needs to take a place each time a user moves from CDMA2000 network to a WLAN and vice versa. Figure 36.8 shows the registration flow diagram when users move from CDMA2000 network to a WLAN. Figure 36.9 depicts the registration flow diagram for the scenario of a user moving from a WLAN into CDMA2000 network. When WLANs are integrated with the

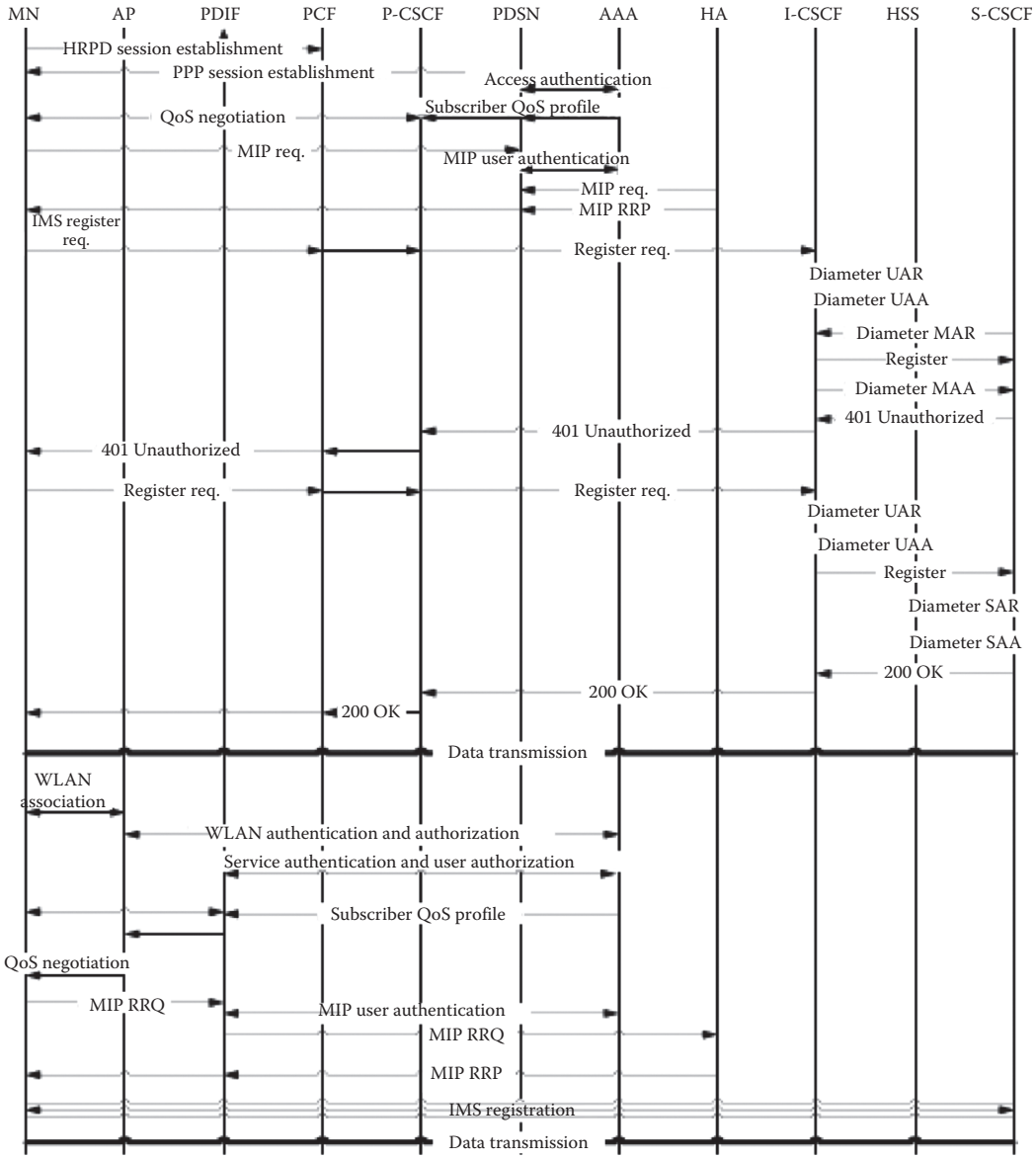

FIGURE 36.8 Flow diagram of user moving from CDMA2000 to WLAN while using IMS.

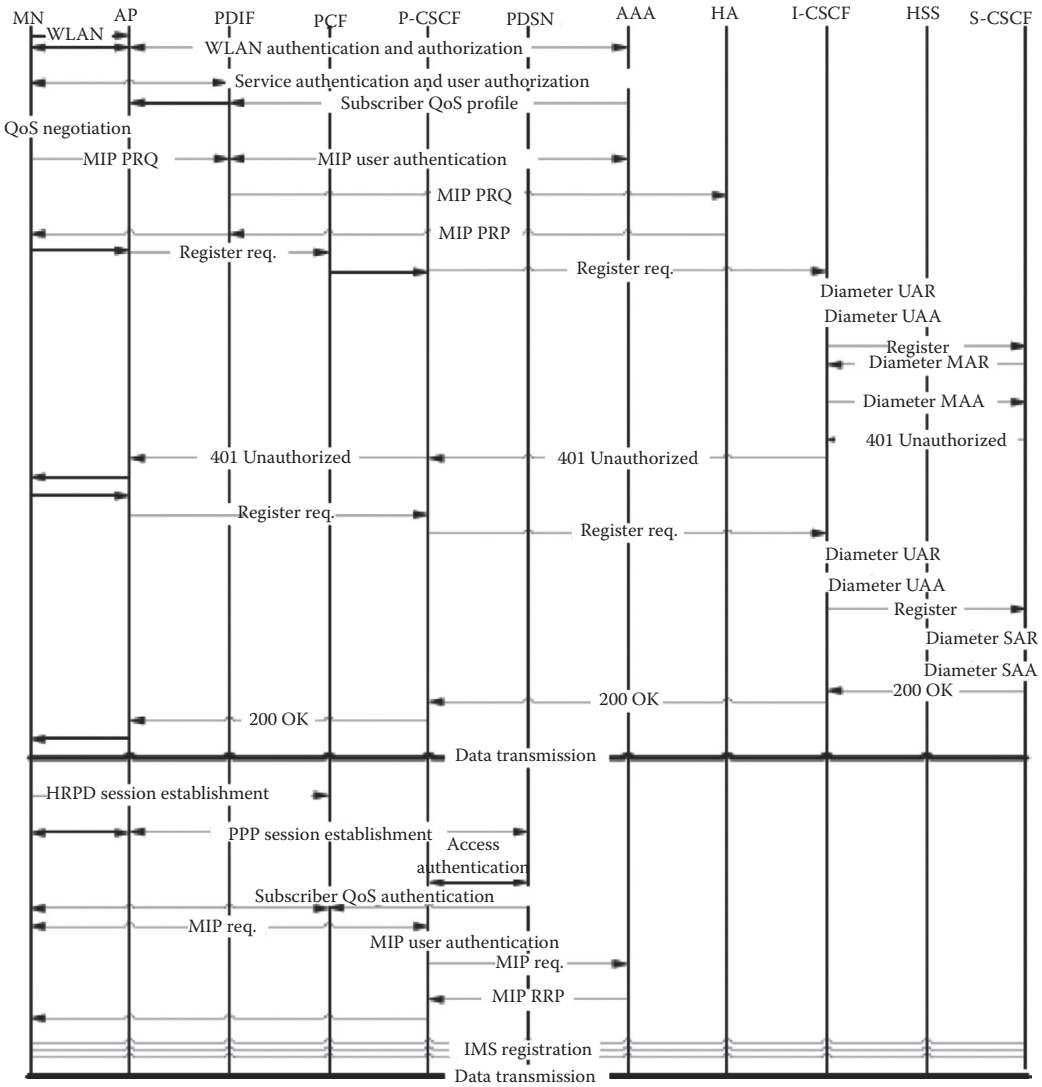

FIGURE 36.9 Flow diagram of user moving from WLAN to CDMA2000 while using IMS.

CDMA2000 network to form a hybrid network, the rate of access to the IMS servers increases. Based on the assumptions, the load can be determined by knowing the total number of users moving into WLANs per unit time and multiplying by the accesses to each server per activity. The flow diagrams show the number of accesses to each IMS server while performing registration. As an example, in Figure 36.8, the number of access to the AAA server due to registration of a terminal is 5. Note that, in both scenarios, the rate of accesses to each server is found by multiplying the average user crossing times the number of access to each server taken from the flow diagrams. Fluid flow represents the user movement pattern within the CDMA2000 network from which the rate of boundary crossings from CDMA2000 to a WLAN is determined. The total number of accesses is then given by

$$\text{Total number of accesses} = R.\ A,$$

where R is the fluid flow rate of registration and A is the number of access to each of the IMS entities. For the random walk model, a MATLAB® simulation model is used, cell residence time is assumed to be

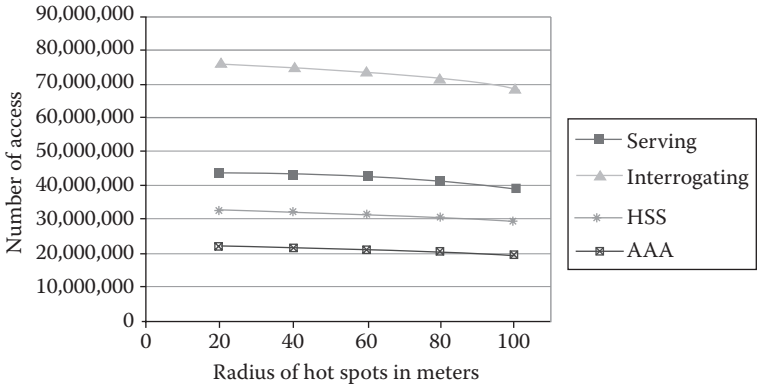

FIGURE 36.10 Rate of access to the IMS servers prior to the deployment of WLANs.

exponentially distributed. The duration of calls is exponential with mean equal to $1/\mu$ and new call arrival to the mobile terminal is a Poisson process with rate λ. The call-to-mobility ratio represents the average number of calls the user receives divided by the average number of registration areas visited by the user. The CMR is assumed to be equal to 5. Figure 36.10 shows the number of accesses to IMS servers (P-CSCF, I-CSCF, and S-CSCF) per second with pure CDMA2000 network taking into consideration the existence of hot spots. We assume that the user mobility within the hotspots follows fluid flow model. The figure shows that the rate of accesses to the IMS servers actually decreases with increasing hot spot radius. The reason for the decrease in rate is due to the fact that the users move slowly within a hot spot than within the CDMA2000 network. WLAN deployment in these areas will be based on customer demands and needs. We assume that in order to enhance the service offering WLAN is considered integrated with the CDMA2000 network, Figure 36.11 shows the incremental access rate to the IMS servers and CDMA2000 servers per second with the hybrid network case incorporating WLANs. As the area increases the number of users within the WLAN increases which increases the crossing rate. As the figure shows, the P-CSCF and the S-CSCF process the added signaling. However, since the I-CSCF sever reroutes incoming queries to the S-CSCF server or other networks and also accesses the HSS server, it is affected the most, processing maximum number of additional queries among the IMS servers [18].

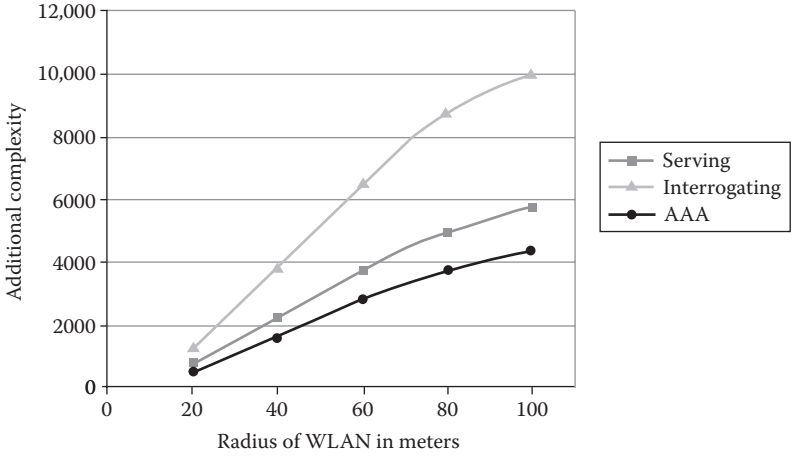

FIGURE 36.11 The increased rate of access to the IMS servers over Figure 36.10 due to WLAN deployment.

36.4 Conclusions

The analysis in Section 36.3 reveals that the rate of queries/updates to services due to service requests initiated by users can be an order of magnitude more than that due to registration activity alone. As the number of services increases, and along with it the associated signaling, it is clear that heavy load will be placed on the IMS servers, which must therefore be designed to handle the load. The analysis also reveals that user mobility patterns influence the signaling load. For example, assuming suitable shape and scale parameters, one can show that Gamma distribution can place three times as much load on IMS servers due to registration signaling as does the fluid flow mobility model. Consequently, network engineers must ensure that they take into account appropriate user mobility patterns. The analysis also reveals that S-CSCF is loaded the most among the IMS servers due to service requests while I-CSCF is loaded the most during registration [19].

The analysis further provides insight into the impact on signaling due to the integration of IMS with a CDMA2000 and WLAN hybrid network. Two types of mobility are considered: the first one represents the movement of the user from CDMA2000 to WLAN and the second one represents the movement from WLAN to CDMA2000. The integration is analyzed using fluid flow for the first scenario and random walk for the second scenario; assumptions are made concerning a service provider's deployment. A MATLAB simulation model is utilized for the random walk model to analyze the rate of accesses to the IMS servers. The results reveal that integrating CDMA2000 with WLAN will increase the signaling to IMS servers. The number of accesses to the servers may vary depending on the assumptions made.

The analysis provides network designers insights into the size of the IMS servers required to support WLAN and 3G users by determining the overall load on the system. It provides designers with the necessary tools to scale the IMS system with growth in the number of users, and usage rate. To reproduce such analysis, the designer should determine the user mobility behavior, and based on the mobility model(s), the number of the boundary crossings. Knowing the rate of boundary crossings by users, the number of registrations initiated by users from one network to another can be estimated and subsequently, by determining the number of queries to each server, the registration load can be determined. The analysis is targeted mainly to help IMS network designers and architects and therefore the flow diagram only takes into consideration the IMS entities.

Acknowledgment

This research was supported in part by the National Science Foundation Grant EPS-0701890.

References

1. 3rd Generation Partnership Project (3GPP), IP Multimedia Subsystem (IMS), TS23.228, Rel10.
2. http://www.openmobilealliance.org/.
3. M. Poikselka, G. Mayer, H. Khartabil, and A. Niemi, *The IMS IP Multimedia Concepts and Services for the Mobile Domain*, Wiley, 2004, ISBN 0-470-87113-X.
4. G. Camarillo and M. Garcia-Martin, *The 3G IP Multimedia Subsystem (IMS)*, John Wiley, 2006, ISBN 0-470-01818-6.
5. M. Koukal and R. Bestak, Architecture of IP multimedia subsystem, *Proceedings of the 48th International Symposium*, Zadar, Croatia, pp. 323–326, 2006.
6. F. Cuervo, N. Greene, A. Rayhan, C. Huitema, B. Rosen, and J. Segers, Megaco protocol version 1.0, IETF RFC Request for Comments: 3015, November 2000.
7. Internet Engineering Task Force (IETF), Session initiation protocol (SIP), RFC 3261, June 2002.
8. M. Wuthnow, M. Stafford, and J Shih, *IMS A New Model for Blending Applications*, Informal Telecoms & Media, 2009.

9. U. Iqbal, S. Sohail, and M. Javed, SIP based QoS management architecture for IP multimedia subsystems over IP access networks, World Academy of Science, Engineering and Technology, 64, 2010.
10. S. Blake, D. Black, M. Carlson, E. Davies, Z. Wang, and W. Weiss, An architecture for differentiated services, *IETF RFC Request for Comments*, December, 2475, 1998.
11. Z. Bei, Analysis of SIP in UMTS IP multimedia subsystem, PhD thesis, North Carolina State University, USA, p. 91, 2003.
12. W. Wang and I. Akyildiz, intersystem location update and paging schemes for multitier wireless networks, *International Conference on Mobile Computing and Networking*, Massachusetts, USA, 2000, pp. 99–109.
13. S. Mohan and R. Jain, Two user location strategies for personal communications services *IEEE Personal Communications*, 1, 42–50, 1994.
14. D. Dunwang, L. Xia, and Z. Hua, Study of multi-connection mechanism in IMS, *Communications and Mobile Computing (CMC) International Conference*, Shenzhen, China, vol. 1, pp. 345–349, 2010.
15. J. Xiao, C. Huang, and J. Yan, A flow-based traffic model for SIP messages in IMS *IEEE GLOBCOM 09*, pp. 1–7, 2009.
16. M. Buddhikot, G. Chandranmenon et al., Design and implementation of a WLAN/CDMA2000 interworking architecture, *IEEE Communications Magazine*, 41, 90–100, 2003.
17. H. Mahmood and B. Gage, An architecture for integrating CDMA2000 and 802.11 WLAN Networks, *IEEE 58th Vehicular Technology Conference*, VTC2003, vol. 3, 2003.
18. L. Saleem, R. Ghimire, and S. Mohan, An analysis of IP multimedia subsystems for a hybrid network, *IEEE 4th International Conference on Internet Multimedia Services Architecture and Applications (IMSAA)*, Bangalore, India, pp. 1–6, 2010.
19. L. Saleem and S. Mohan, A complexity analysis of IP multimedia subsystems (IMS), *First International Symposium on Advanced Networks and Telecommunications Systems (ANT*S), Mumbai, India, December 2007.

37

Cognitive Radio Networks

Kwang-Cheng Chen

37.1 Introduction

Since J. Mitola III proposed the concept of cognitive radio (CR) [1], cognitive radio technology with federal communication commission (FCC) endorsement has been widely considered as an emerging solution of crowded spectrum for future wireless communications. Haykins' classic paper in 2005 [2] summarized important tasks to facilitate CRs. Particularly, the CR-transmitter (CR-Tx) shall identify the spectrum hole or white space in the spectrum for primary system (PS), such that CR-Tx can take this opportunity to transmit its message or packet(s) to the CR-receiver (CR-Rx). We may name such a link-level transportation of packets between CR-Tx and CR-Rx as a sort of opportunistic transmission. However, another major challenge arises to deal with multiuser opportunistic transmissions and to network CRs through opportunistic transmissions into the multihop cognitive radio network (CRN). This chapter therefore summarizes state-of-the-art CRN technology and its research opportunities at the horizon.

37.2 Cooperative Cognitive Radio Networks and Modeling

Once CR-Rx successfully receives the packet (or a message) from CR-Tx; an immediate challenge would be to transport such a packet from source (node) to destination (node). Multihop ad hoc network of CRs obviously serves the general purpose of CRN. Similar concepts were developed independently in earlier days around the birth of CR to demonstrate more networking efficiency [3,4]. However, we can leverage cooperative networking among coexisting multiradio networks that can be heterogeneous PSs and heterogeneous CR ad hoc networks, to form the most general CRN. In other words, as shown in Figure 37.1, cooperative relays among nodes in PSs and heterogeneous CR ad hoc networks can be used to realize a general-sense multihop CRN, say in Reference 5.

As a matter of fact, multihop CRN via cooperative relay forms heterogeneous wireless networks. We still wish to know whether CR can improve network efficiency or not, which is the ultimate purpose of CRN. A simple exploration was conducted in Reference 6, by considering a CR source node to send a

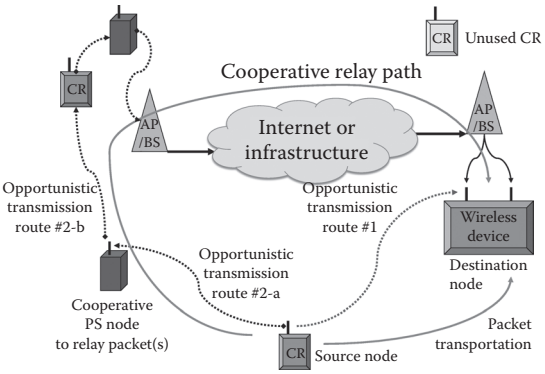

FIGURE 37.1 Cooperative multihop cognitive radio network.

packet to the CR destination node via cooperative and opportunistic relay through a primary system/network, without the interfering PS operating. The networking coding concept is used to develop the principles of routing algorithm. By generating random network topology to simulate such a scenario, without extra bandwidth (i.e., just using transmission opportunities from PS), 130% networking throughput gain is observed in average, with 92% chances to have gain (i.e., no gain due to prohibition to interfere PS in some cases). This experiment supports a critical fact that multihop CRN can indeed greatly enhance networking throughput without increasing frequency spectrum, much more than increasing at the physical layer due to transmission opportunities.

CRN can be categorized into three types to reuse spectrum opportunities: interweave, overlay, and underlay [7]. The *interweave* paradigm is the original idea of cognitive radio to create the opportunistic communications (or transmission opportunities) if the primary system is not transmitting. The overall spectrum utilization is enhanced by opportunistic reuse when spectrum holes (or white spaces) exist. The *overlay* paradigm proceeds under the assumption that cognitive radios know the channel gains, codebooks, and messages from noncognitive radios. CRs can transmit simultaneously with noncognitive radios, and appropriate using of a part of the CR's power to relay the message can offset CR's interference to noncognitive radios. Overlay may be close to information theoretic limit. A more practical paradigm of CRN targeting higher spectrum utilization (than interweave) is *underlay* to allow CRs transmitting simultaneously with non-CRs as long as the invoked interference is below the acceptable limit, and typically through spatial reuse to achieve this goal. In this chapter, we treat interweave paradigm as the link-level CR and underlay as the new paradigm of CRN consisting of multiple CR links.

To realize general-sense multihop CRN, we have to first understand the nature of opportunistic links and appropriate model(s) to develop technologies of CRN. Note that CR can transmit only when PS is not transmitting, for any single link. Assuming that a primary communication system (or pair(s) of transmitter and receiver) is functioning, a cognitive radio that is the secondary user for the spectrum explores channel status and seeks an opportunity to utilize such a spectrum for communication. The channel can be commonly modeled as an Elliot–Gilbert channel with two possible states: existence of primary user's activity (i.e., CR transmission opportunity not available) and nonexistence of primary user's activity (i.e., CR's transmission opportunity available). Stefan Geirhofer, Lang Tong, and Brian M. Sadler have measured WLAN systems to statistically model the "white space" for cognitive radio transmission by the semi-Markov model [8]. Considering the practical operation of CRs, Figure 37.2 summarizes CR opportunistic operation using an embedded continuous-time Markov chain model, which may serve a basis to study more functions of CRN. Of course, there are more detailed studies of CR modeling, such as References 9 and 10. However, Figure 37.2 offers an opportunity to initiate useful explorations on the networking functions of CRN.

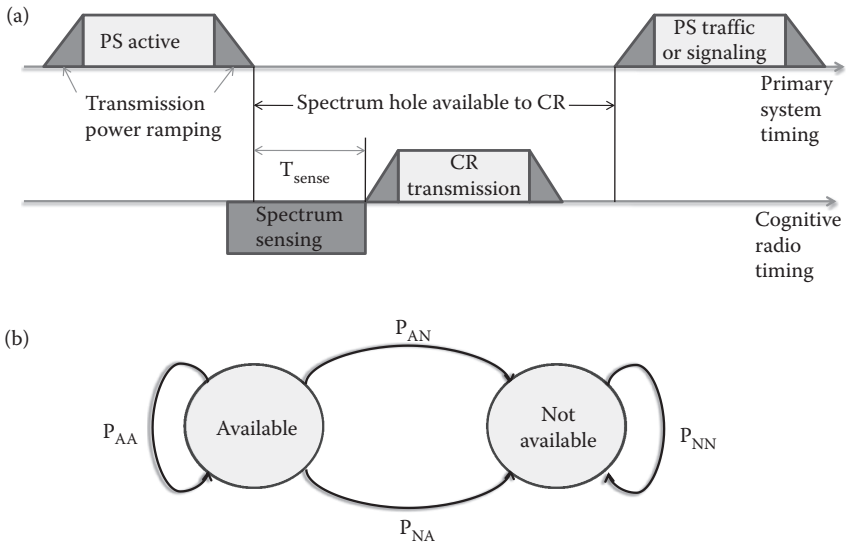

FIGURE 37.2 A model of CR link availability. (a) CR transmission opportunity window and (b) State transition of embedded markov chain for link availability.

37.3 Spectrum Sensing and Tomography for CRN

Conventional spectrum sensing to detect or to sense spectrum hole(s) or white space(s) at the link level (i.e., for an opportunistic transmission between a CR-Tx and CR-Rx pair) targets at a single primary system and is used to decide between the two hypotheses in discrete-time statistical signal processing [11], namely

$$y[n] = \begin{cases} w[n] \\ hs[n] + w[n] \end{cases} n = 1,\ldots,N \begin{matrix} H_0 \\ H_1 \end{matrix}$$

where $y[n]$ represent observation samples, $s[n]$ and $w[n]$ are contributed from PS signal and noise, respectively, and h is the channel gain observed at the CR. Numerous techniques to achieve the goal of spectrum sensing have been proposed, while details can be found in References 11 and 12. Generally speaking, among extensive literatures, the basic principles include

- Energy detection
- Matched filtering
- Cyclostationary detection
- Wavelet detection
- Covariance-based detection
- Multiple antenna

However, local detection at the CR might not be enough. Figure 37.3 delineates the well-known hidden terminal problem to reveal insufficiency of local sensing at CR due to either blocking or fading. A helpful approach is through cooperation, which is known as cooperative sensing [13–15] by placing multiple sensors/detectors in different locations. To implement cooperative spectrum sensing, CRs first send the raw data they collect to a combining user or fusion center. Alternatively, each node may

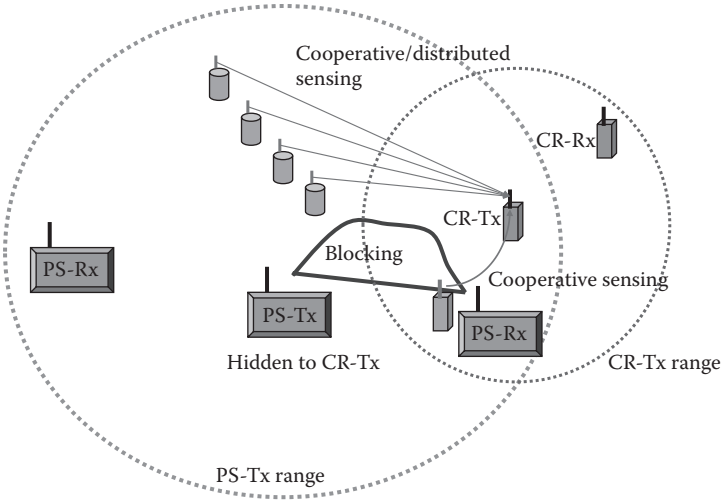

FIGURE 37.3 Hidden terminal problem and cooperative spectrum sensing.

independently perform local spectrum sensing, then reports either binary decision or test statistics to a combining node. Finally, the combining node makes a decision on the presence or absence of the licensed signal based on its received information.

A straightforward form of cooperative spectrum sensing is to transmit and to combine the samples received by all CR nodes/sensors in the local spectrum sensing phase [12]. Using random matrix theory, combining to process all the samples can be developed. Considering total K CRs and each taking N samples, we denote $y_k(n)$ as the sample received by the kth CR/sensor at the nth time instant, to construct the observation matrix

$$Y = \begin{bmatrix} y_1(1) & y_1(2) & \cdots & y_1(N) \\ y_2(1) & y_2(2) & & y_2(N) \\ \vdots & & \ddots & \vdots \\ y_K(1) & y_K(2) & \cdots & y_K(N) \end{bmatrix}$$

Although multiple CRs are involved, opportunistic link establishment is still the only concern in cooperative sensing. CRN must transport packets under multiple opportunistic links, and thus spectrum sensing must be able to support networking function such as medium access control (MAC) and routing for multiple CRs in the CRN, which creates a new scenario of spectrum sensing beyond traditional detection and estimation for a specific radio link. A possible approach is to use statistical inference [16] or even learning to learn radio resource availability of portion or entire radio resource of CRN. A simple, but useful, example to leverage statistical inference into such scenario can be illustrated. Suppose that a CR-Tx can observe link behaviors of a PS transmitter–receiver pair, which can be represented as "1" for active transmission and "0" for inactive in a given time slot. We may model such behavior as a Bernoulli process (i.e., each observation following an i.i.d. Bernoulli random variable). The key question is "can we predict the availability of the next time slot based on an earlier observation of L time slots?" Actually, this can be achieved by the well-known *Laplace* formula [16]. Let n_L be inactive (radio resource available) time slots among these L observations. The probability of the next slot available for CR utilization (radio resource available) is

$$\hat{p} = \frac{n_L + 1}{L + 2}$$

Generalizing this concept with well-known tomography, CRN tomography has been developed [17] to know a lot more information than traditional sensing over a single radio link, in CRN operation. Consequently, spectrum sensing of CRN can be treated into four categories on the following bases: (i) active probing or passive detection and (ii) to acquire link-level information or to acquire network-level information. Passive detection on link availability as traditional CR spectrum sensing falls into one of these four categories. With realizing network-level information such as radio resource, readers can easily tell the difference between sensing for CR's transmission opportunity and sensing for CRN, under this framework. Another statistical technique, information fusion, is useful in spectrum sensing. To obtain the observation matrix, some extra transmissions from cooperative sensors are needed, which wastes a lot of communication bandwidth that is targeted to save in cognitive radio. In [54], heterogeneous information fusion is introduced to observe different types of information at the CR-transmitter. Appropriate fusion can infer spectrum availability as good as cooperative sensing, without cooperative sensors. Currently, significant amount of research efforts are taken toward reliable spectrum sensing as its key role in dynamic spectrum access.

37.4 Spectrum Sharing and Dynamic Spectrum Management

As a matter of fact, multiuser CR communications have been discussed extensively in Haykins' classic paper [2], including coordination of transmissions (widely known as MAC), transmission power control, and the associated game theory treatment.

MAC of cognitive radios when spectrum opportunities are available has been discussed in various ways. A straightforward thinking is to treat MAC of these CRs as the classical multiple access. As CRs are usually distributed and centralized control may not exist unless a common control channel is available in those systems such as IEEE 802.22, distributed random access mechanisms are usually considered, such as ALOHA and CSMA (carrier sense multiple access), while Reference 18 summarizes a review of several interesting explorations.

Another interesting approach is to study the MAC design as a mathematical optimization. Let us consider a set of frequency bands to represent the general case, although more dimensional radio resource can be considered. Suppose the frequency bands that we are interested in (typically PS operating) are a set of numbered bands, $\mathcal{M} = \{1,\ldots,M\}$. At time t_n, the CRN operation allows an update of spectrum utilization. The nth observation (or allocation) time interval is $[t_n, t_{n+1})$. Due to the opportunistic nature of each link (thus frequency band) modeled as a Markov chain, the ith frequency band is available following a Bernoulli process with probability π_i available, and is invariant to time.

We define the following indicator function:

$$1_i[n] = \begin{cases} 1, & \text{channel } i \text{ available in } [t_n, t_{n+1}) \\ 0, & \text{otherwise} \end{cases} \tag{37.1}$$

For perfect spectrum sensing, we can determine (37.1) in a reliable way. However, any spectrum sensing has some vulnerable situations, and thus we need to consider more to decide MAC. Following (37.1), the probability mass function (pmf) of Bernoulli random variable at the ith frequency band is

$$f_{1_i[n]}(x|\pi_i) = \pi_i x + (1 - \pi_i)\delta(x) \tag{37.2}$$

It is reasonable to assume $\{1_i[n]\}_{i=1}^{M}$ independent, $n = 1, \ldots, L$, where L implies the observation interval depth. Denote

$$\pi = [\pi_1, \ldots, \pi_M]$$

For reliable CR operation, spectrum sensing is necessary, so that CR-Tx can have information about the availability of each frequency band. However, for network operations on top of CR links, the strategy would be highly related to π.

Case 1: π is known.
Case 2: π is unknown.
Case 3: π can be detected or estimated via some CRN sensing or tomography methods.

Traditional CR functions as follows: At time t_n, CR learns the availability of a selected frequency band s_n (typically via spectrum sensing). If $1_{s_n}(n) = 1$, information amount B can be successfully transmitted. For L time durations, the overall throughput is

$$W = \sum_{n=1}^{L} 1_{s_n}(n) \tag{37.3}$$

In case π is known, the spectrum sensing strategy for a CR is simply to select channel $\hat{t} = arg\ max_{i \in \mathcal{M}} \pi_i$ to sense. Then, access decision is therefore optimally or suboptimally made based on certain decision criterion and conditions, such as formation as a partially observed Makovian decision process [19]. More in-depth explorations can be found in Reference 20, and some detailed reviews in References 12 and 21. The authors in Reference 22 consequently suggest a framework for CRN functions, one step closer to realistic CRN.

Keen readers may note that effective access and thus throughput really relies on effective sensing. The relationship between throughput and sensing is therefore important. In a CRN, the secondary users are allowed to utilize the frequency bands of primary users when these bands are not currently being used. To support this spectrum reuse functionality achieving spectrum efficiency, the secondary users shall sense the radio frequency environments for transmission opportunities. This can be viewed from two parameters associated with spectrum sensing: probability of detection and probability of false alarm. The higher the probability of detection, the better the primary users are protected. However, from the secondary users' perspective, the lower the probability of false alarm, the more chances the channel can be reused when it is available, thus the higher the achievable throughput for the secondary network. In Reference 23, authors study the problem of designing the sensing duration to maximize the achievable throughput for the secondary network under the constraint that the primary users are sufficiently protected. Sensing-throughput is thus a trade-off mathematically. Using an energy detection sensing scheme, the existence of optimal sensing time is proved, which yields the highest throughput for the secondary network [23]. This optimal sensing time decreases when distributed spectrum sensing is applied. An optimal joint design has been proposed [24]. However, almost all existing research efforts assume synchronous operation of CRs and PS, which is obviously far away from the true situation, as it takes a huge amount of communication overhead to reach this status, or is nearly impossible due to the nature of CRs' operation. An ice-breaking study in Reference 25 considers *asynchronous dynamic channel access* with only *prior* knowledge about the frame length. Under the new operating philosophy facilitated by game theory, asynchronous dynamic spectrum access achieves surprising performance better than that of synchronous operation, which opens a new door toward practical CRN design in a distributed way as the most recent state of the art.

On the other hand, the above optimization of channel utilization leads to a new research subject of spectrum sharing or spectrum management, that is, how to utilize a collection of frequency bands, $\mathcal{M}$, for homogeneous or heterogeneous CRN(s). To fully exploit spectrum management, we have to consider a more general situation related to networking technology and networking economy. What is the reason for PS to allow CR operation? The reasons might be that (i) PS users can gain some incentives from such a way of operation and (ii) the CR concept can indeed enhance entire spectrum utilization so that the regulator would enforce CR as a policy. As the spectrum access or utilization actually involves more than technical concerns and also economic incentives, it brings spectrum management under CRN to a

new wide-open interdisciplinary study. Game theory (auction could be considered as a game) has been introduced to model such behaviors [26,27], which set up the ground for possible commercial operation of CRN. Spectrum sharing has been studied not only in centralized infrastructure wireless networks but also in multihop ad hoc networks [28]. There exist some good follow-up explorations. To be practically feasible, we have to ensure satisfaction from four parties in the CRN operation:

1. Primary system users
2. Cognitive radios (secondary) users
3. Service provider(s)
4. Regulator wishing to optimize total spectrum utilization

A spectrum-management policy framework based on the Vickrey auction has been proposed [29] such that CR mobile stations can compete for utilization of the primary user network spectrum bands available for opportunistic transmissions. It is shown that CRN can indeed satisfy the above four different parties to achieve a win–win situation, as a practical technoeconomic foundation of CRN.

37.5 Routing, Power and Interference Control, and QoS Guarantees

The fundamental task of networking functions might be routing in multihop CRN. As a matter of fact, routing for mobile ad hoc networks has been extensively studied in the literature and we do not repeat it here. Due to the opportunistic and dynamic nature of CRN, routing appears to be a great intellectual challenge in multihop CRN. Reference 11 gives a summary of some initial thinking to completely deal with such challenges, namely, opportunistic links, sensing reliability and overhead, dynamic topology, likely unidirectional links, heterogeneous wireless networks, calerability, and so on which suggests a wide-open research opportunity, particularly for multihop ad hoc CRN.

Since the basic CR operation must not interfere with the transmissions of the licensed or primary users (PUs), this generally incurs a trade-off in the CRN performance. In order to evaluate this trade-off, a distributed CR routing protocol for ad hoc networks (CRP) is proposed [30] to achieve (i) explicit protection for PU receivers that are generally not detected during spectrum sensing, (ii) allowing multiple classes of routes based on service differentiation in CR networks, and (iii) scalable, joint route-spectrum selection. A key novelty of CRP is the mapping of spectrum selection metrics and local PU interference observations to a packet forwarding delay over the control channel. This allows the route formation undertaken over a control channel to capture the environmental and spectrum information for all the intermediate nodes, thereby reducing the computational overhead at the destination. Further underlay ad hoc CRN routing is still subject to innovative breakthroughs.

As a matter of fact, another major challenge of CRN functions is its operating in the interference-limited environments, particular for underlay CRN that brings the benefits of spectrum efficiency as a major attraction of CRN. Consequently, good mathematical modeling of interference in wireless networks is greatly needed. The mathematical model of network interference has been well organized and demonstrated how to model CRs [31]. The interference in large wireless networks has remarkably been explored in Reference 32, which is useful to understand some fundamental behaviors in interference-limited wireless networks. As each link in such wireless link may suffer severe fading and potential outage, random graph model of wireless networks becomes an important analytical tool, while Reference 33 presents an award-winning review, based on stochastic geometry. There are generally three critical factors in such modeling:

1. Spatial distribution of the nodes
2. Wireless propagation characterization
3. Overall impact of interferers including mobility and session lifetime

We can always describe network topology via a graph $\mathcal{G} = (V, E)$, defined by the collection of vertices, V, and the collection of edges, E. A vertex represents a node in a wireless network and an edge represents a link between two nodes. Erdös and Rényi pioneered the random graph theory. Among a number of random graph methodologies, we usually model the spatial distribution of the nodes according to a homogeneous *Poisson* point process in the two-dimensional infinite plane. The probability of n nodes being inside a region $\mathcal{R}$ (not necessarily connected) depends only on the total area A_R of the region and is given by

$$\mathbb{P}\{n \mid \mathcal{R}\} = \frac{(\lambda A_R)^n}{n!} e^{-\lambda A_R}, \quad n \geq 0$$

where λ is the spatial density of (interfering) nodes.

Regarding propagation and fading effect, the received power, P_{Rx}, at a distance r from a transmitter with power P_{Tx} is

$$P_{Rx} = \frac{P_{Tx} \Pi_k Z_k}{r^{2d}}$$

where d is the amplitude loss exponent depending on the environment with typical range from 0.8 (hallways) to 4 (dense urban), and 1 for free-space propagation from point source. $\{Z_k\}$ are independent random variables to account for propagation effects such as fading and shadowing. An earlier model of link availability can also serve the purpose of modeling session lifetime.

Based on such analytical methodology, some important issues can be derived for routing (and other network functions) of CRN. The first wanted might be connectivity for a node in CRN [34], and its resulting delay. Transmission capacity is also desirable to know but it is hard to calculate precisely, with bound being available in [35]. As the connectivity is critical for routing algorithm, connectivity of cooperative multihop ad hoc CRNs can be found [36]. We do expect a lot of fruitful results coming from global researchers. However, there are more network functions for CRN as new challenges, particularly under the random nature of opportunistic links in CRN. MIMO-empowered multihop CRN to optimize throughout was introduced [37]. While dealing with end-to-end control, Figure 37.4 suggests a view to form multiple paths between source and destination for multihop CRN. After reorganization, these paths are just like MIMO by a directed graph between source node and destination node. This concept was first applied to end-to-end error control [38]. With a hybrid ARQ on top of a multipath concept, we can achieve reliable communications, while any single path of multipath may fail, without feedback control that is particularly critical for opportunistic links. When we have to deal with quality of service (QoS) as the fundamental need of networking, we can again apply formation of multipath to reach statistical control of QoS [39], and further consider routing and QoS together [40] with help from the effective bandwidth.

There are more issues of concern in CRN networking, for example, QoS provisioning of heterogeneous services in CRN [41] and delay of real-time traffic over CRN [42]. Furthermore, for multimedia communications, in addition to typical QoS factors such as radio link reliability, maximum tolerable communication delay, and spectral efficiency, CR spectrum sensing frequency and packet-loading scheme have great impacts on multimedia QoS. The optimal spectrum-sensing frequency and packet-loading solutions for a multichannel can be obtained by using the combination of Hughes–Hartogs and discrete particle swarm optimization (DPSO) algorithms with experimental verifications [43]. Associated with QoS, call admission and capacity analysis are considered in Reference 44.

Researchers have started to note spectrum sensing associated with location for different purposes [45]. A different thinking may arise when implementing routing algorithms, to route based on the spectrum map. The spectrum map indicates radio resource versus location information, at a given time and a given frequency band. Such spectrum map was first constructed via synthetic aperture radar [46]. As CRN routing may not require precise information from the spectrum to save communication overhead, a compressed

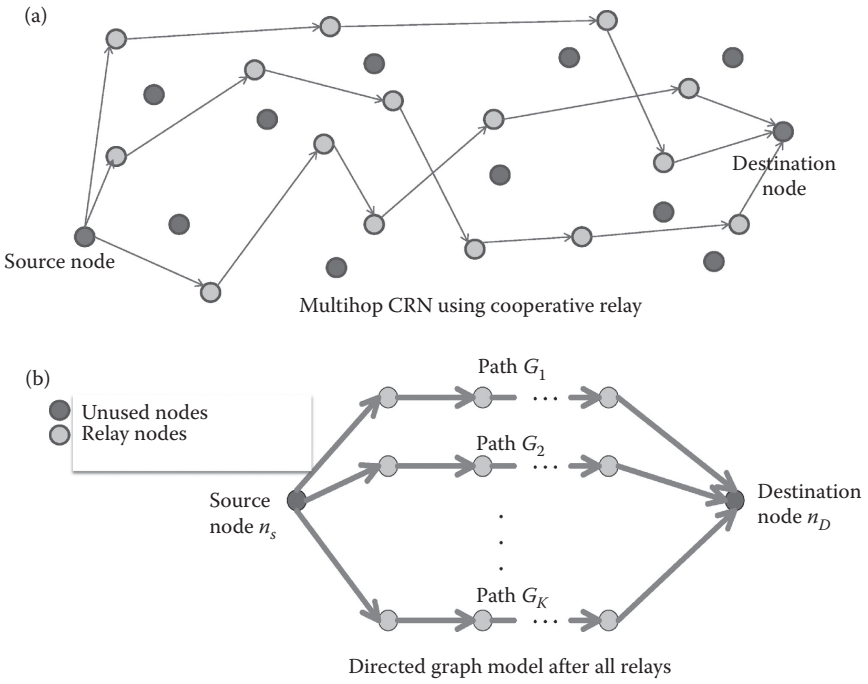

FIGURE 37.4 Multipath formation of multihop CRN. (a) Using cooperative relay. (b) Graph model of multipath relay.

sensing-based approach has been proposed [47]. With the aid from spectrum map, routing for CRN can be facilitated through modifying well-known opportunistic routing over opportunistic links [48].

37.6 Applications to Cellular Systems and Machine-to-Machine Communications and International Standards

Although it might take a while to really facilitate complete CRN technology for wide applications, we can still take advantage of the CRN concept into the immediate system application scenario. A possible application scenario is femto-cell technology in 3GPP so that 3G LTE (long-term evolution) and LTE-A can well extend network coverage and thus better networking throughput. However, femto-cell systems are not arranged in a perfectly controlled way as traditional 3G cellular systems, due to easy installation. This creates a lot of new challenges in system design such as synchronization, interference alignment, or radio resource management. Let us look at radio resource management of OFDMA, that is, to allocate radio block (RB, grid of frequency–time transmission bandwidth).

As a misalignment between femto-cells and Macrocell to greatly degrade system performance, we may propose that the cognitive radio resource management (CRRM) consists of the following steps [49]:

1. The femto-BS periodically senses the channel to identify which RB to be occupied by the Macrocell. The sensing period is T_s frames and each channel sensing persists for one frame, to align with RB on the cell boundary. Thus, for the femto-cell, a frame is referred to the "sensing frame" if the femto-BS performs channel sensing at that frame. On the other hand, a frame is referred to the "data frame" if the femto-BS does not perform channel sensing at that frame. The femto-BS cannot perform data transmission and reception within the sensing frame.

2. The femto-BS senses the *received interference power* on each RB within the sensing frame.
   a. If the *received interference power* on an RB exceeds a certain threshold, the RB is identified as being occupied by the Macrocell.
   b. Otherwise, the RB is unoccupied by the Macrocell.
3. In subsequent data frames, the femto-BS only allocates unoccupied RBs sensed in the sensing frame to its femto-MSs.
4. The femto-BS also extracts the following parameters from channel sensing:
   a. The traffic load of the Macrocell
   b. The RBs allocation correlation probability of the Macro cell
   c. The fraction of correlated RBs allocation of the Macrocell through the effective bandwidth facilitation of radio resource allocation

This approach to leverage CR's sensing to greatly improve RB allocation is adopted in 3GPP and can be generalized into two-tier macro-femto heterogeneous wireless networks. Various ways are summarized to implement such a concept into different types of systems [50], as an immediate realization of CRN.

As a matter of fact, another promising application for CRN is machine-to-machine (M2M) communications, which has to deal with a tremendous number of wireless devices and likely has to transport traffic through spectrum sharing mechanism due to the scare spectrum. Figure 37.5 depicts such an application scenario, similar to Internet of Things (IoT) or cyber-physical systems (CPS). It is challenging to establish effective communication between cloud and data aggregators or even machines. 3GPP LTE-A is therefore considering *machine-type communication* (MTC), and access for such massive devices becomes an immediate challenge [55]. For the "swarm communications" at the edge of the Internet for tremendous amount of sensors and machines to data aggregators as local networks shown in Figure 37.5, spectrum-sharing networks, likely CRN, might be the only solution.

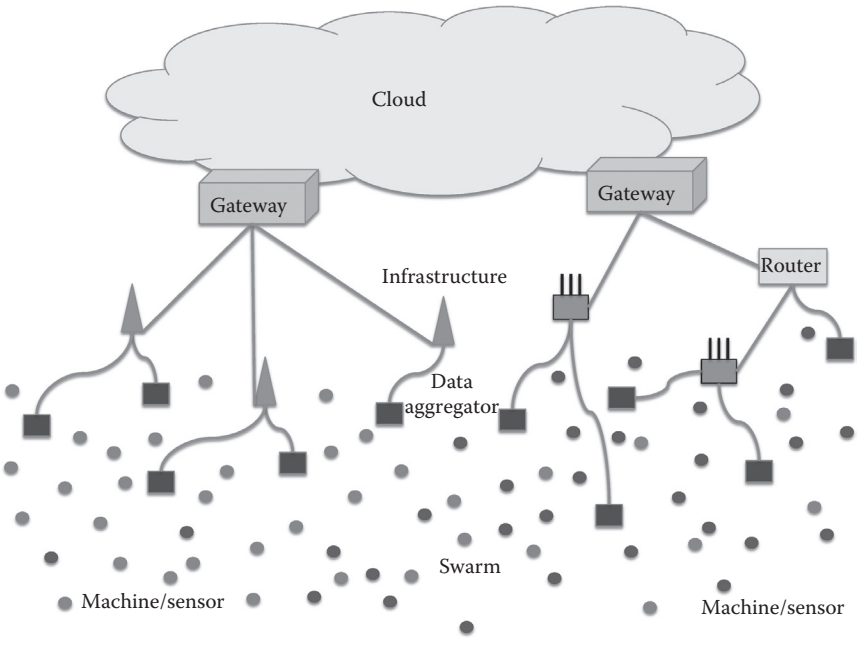

FIGURE 37.5 Scenario of M2M communications.

The concept of cognitive radio has been adopted in international communication standards for years. While dealing with the coexistence in Bluetooth 2.0 and IEEE 802.15.2 in the first couple of years of the twenty-first century (shortly after the birth of cognitive radio in 1999), adaptive frequency hopping (AFH) technology was applied by first conducting spectrum sensing at the 2.4 GHz ISM band, and then real-time adjusting hopping patterns to avoid interference from other systems for successful transmission, particularly for stream traffic. The later examples include sensing to avoid radar signals in 5 GHz wireless LANs, and Detect-And-Avoid (DAA) for ultra-wide-band communications. However, they are just examples of cognitive radio as a core technology in a standard. The very first international standard effort for cognitive radio should be IEEE 802.22 to allow transmission over TV white spaces. Actually, IEEE 802.19 is dealing with technical advisory to multiradio coexisting systems, while cognitive radio technology is definitely within the scope. The IEEE 802.22 Working Group was formed in November 2004 for Wireless Regional Area Networks (WRAN). This working group is dedicated to develop an air interface (i.e., MAC and PHY) based on CRs for unlicensed operations in the TV broadcast bands. This standard plays a key role in the evolution of CRs and goals at defining an international standard that may regulate in any regulatory regime.

The IEEE P1900 Standards Group was established in 2005 jointly by the IEEE Communications Society and the IEEE Electromagnetic Compatibility Society. The objective is to develop supporting standards dealing with new technologies and techniques for next-generation radio and advanced spectrum management. Note that this sponsor group was called SCC41—The Standards Coordination Committee 41. Currently, there is an ever-increasing number of international standards considering CRN technology due to the shortage of radio spectrum. Both ITU and ETSI are seriously considering CR into wireless communications and networks [51].

As a conclusion to this chapter, although facing tremendous technology challenges subject to more imaginative approaches such as biology-inspired thinking [52] or sociological thinking [53], CRNs are definitely the direction for future wireless communications and networks so that a large number of wireless devices can be connected to improve the quality of human life.

References

1. J. Mitola, III, G.Q. Maguire, Cognitive radio: Making software radios more personal, *IEEE Pers. Commun.*, 6(4), 13–18, 1999.
2. S. Haykins, Cognitive radio: Brain-empowered wireless communications, *IEEE J. Selected Areas Commun.*, 23(2), 201–220, 2005.
3. T.J. Shepard, *Decentralized Channel Management in Scalable Multihop Spread-Spectrum Packet Radio Networks*, PhD dissertation, MIT, Cambridge, MA, 1995.
4. P. Gupta and P.R. Kumar, The capacity of wireless networks, *IEEE Trans. Inform. Theory*, 46(2), 388–404, 2000.
5. K.-C. Chen, P.-Y. Chen, N. Prasad, Y.-C. Liang, and S. Sun, Trusted cognitive radio networking, *Wireless Communications and Mobile Computing*, Wiley, 2010.
6. C.-H. Huang, Y.-C. Lai, and K.-C. Chen, Network capacity of cognitive radio relay networks, *Phys. Commun.*, 1(2), 112–120, 2008.
7. A. Goldsmith, S.A. Jafar, I. Maric, and S. Srinivasa, Breaking spectrum gridlock with cognitive radios: An information theoretic perspective, *Proc. IEEE*, 97(5), 894–914, 2009.
8. S. Geirhofer, L. Tong, and B. M. Sadler, Dynamic spectrum access in the time domain: Modeling and exploiting white space, *IEEE Commun. Mag.*, pp. 66–72, May 2007.
9. V. Pla, J.R. Vidal, J. Martinez-Bauset, and L. Guijarro, Modeling and characterization of spectrum white spaces for underlay cognitive radio networks, Cape Town, *IEEE International Conference on Communications*, 2010.

10. B. Canberk, I.F. Akyildiz, and S. Oktug, Primary user activity modeling using first-difference filter clustering and correlation in cognitive radio networks, to appear *IEEE/ACM Transactions on Networking*, 19(1), 170–183, Feb. 2011.
11. K.-C. Chen, B.K. Cetin, Y.-C. Peng, N. Prasad, J. Wang, and S. Lee, Routing for cognitive radio networks consisting of opportunistic links, *Wireless Communications and Mobile Computing*, 10(4), 451–466, 2010.
12. Y.C. Liang, K.C. Chen, Y.J. Li, and P. Mähönen, Cognitive radio networking and communications: An overview, *IEEE Trans. Vehicular Technol.*, 60(7), 3386–3407, 2011.
13. G. Ganesan and J. Li, Cooperative spectrum sensing in cognitive radio, Part I: Two-user networks, *IEEE Trans. Wireless Commun.*, 6(6), 2204–2213, 2007.
14. G. Ganesan and J. Li, Cooperative spectrum sensing in cognitive radio, Part II: Multiuser networks, *IEEE Trans. Wireless Commun.*, 6(6), 2214–2222, 2007.
15. J. Unnikrishnan and V. V. Veeravalli, Cooperative sensing for primary detection in cognitive radio, *IEEE J. Selected Topics Signal Process.*, 2(1), 18–27, 2008.
16. K.C. Chen, S. Y. Tu, and C. K. Yu, Statistical inference in cognitive radio networks, *IEEE ChinaCom*, Xi-An, August 2009.
17. C.K. Yu, S. Cheng, and K. C. Chen, Cognitive radio network tomography, the special issue of achievements and road ahead: The first decade of cognitive radio. *IEEE Trans. Vehicular Technol.*, 59(4), 1980–1997, 2010.
18. C. Cormio and K. R. Chowdhury, A survey on MAC protocols for cognitive radio networks, *Ad Hoc Networks*, 7, 1315–1329, 2009.
19. Q. Zhao, L. Tong, A. Awami, and Y. Chen, Decentralized cognitive MAC for opportunistic spectrum access in ad hoc networks: A POMDP framework, *IEEE J. Selected Areas Commun.*, 25(3), 589–600, 2007.
20. L. Lai, H. El Gamal, H. Jiang, and H.V. Poor, Cognitive medium access: Exploration, exploitation, and competition, *IEEE Trans. Mobile Comput.*, 10(2), 239–253, 2011.
21. K.C. Chen and R. Prasad, *Cognitive Radio Networks*, West Sussex, UK, Wiley, 2009.
22. W.-Y. Lee and I.F. Akyildiz, A spectrum decision framework for cognitive radio networks, *IEEE Trans. Mobile Comput.*, 10(2), 161–174, 2011.
23. Y.-C. Liang, Y. Zeng, E.C.Y. Peh, and A.T. Hoang, Sensing-throughput tradeoff for cognitive radio networks, *IEEE Trans. Wireless Commun.*, 7(4), 1326–1337, 2008.
24. A.A. El-Sherif and K.J.R. Liu, Joint design of spectrum sensing and channel access in cognitive radio networks, *IEEE Trans. Wireless Commun.*, 10(6), 1743–1753, 2011.
25. Y.Y. Lin and K. C. Chen, Asynchronous dynamics spectrum access, *IEEE Trans. Vehicular Technol.*, 61(1), 222–236, January 2012.
26. D. Niyato and E. Hossain, Competitive pricing for spectrum sharing in cognitive radio networks: Dynamic game, inefficiency of Nash equilibrium, and collusion, *IEEE J. Selected Areas Commun.*, 26(1), 192–202, 2008.
27. D. Niyato and E. Hossain, Competitive spectrum sharing in cognitive radio networks: A dynamic game approach, *IEEE Trans. Wireless Commun.*, 7, 2651–2660, 2008.
28. Y. Thomas Hou and Y. Shi, Spectrum sharing for multi-hop networking with cognitive radio, *IEEE J. Selected Areas Commun.*, 26(1), 146–155, 2008.
29. H.B. Chang and K.C. Chen, Auction based spectrum management of cognitive radio networks, the special issue of achievements and road ahead: The first decade of cognitive radio, *IEEE Trans. Vehicular Technol.*, 59(4), 1923–1935, 2010.
30. K.R. Chowdhury and I.F. Akyildiz, CRP: A routing protocol for cognitive radio ad hoc networks, *IEEE J. Selected Areas Commun.*, 29(4), 794–804, 2011.
31. M.Z. Win, P.C. Pinto, and L.A. Sheep, A mathematical theory of network interference and its applications, *Proc. IEEE*, 97(2), 205–230, 2009.

32. M. Haenggi and R.K. Ganti, Interference in large wireless networks, *Foundations Trends Networking*, 3(2), 127–248, 2008.
33. M. Haenggi, J. Andrews, F. Baccelli, O. Dousse, and M. Franceschetti, Stochastic geometry and random graphs for the analysis and design of wireless networks, *IEEE J. Selected Areas Commun.*, 27(7), 1029–1046, 2009.
34. W. Ren, Q. Zhao, and A. Swami, On the connectivity and multihop delay of ad hoc cognitive radio networks, *IEEE J. Selected Areas Commun.*, 29(4), 805–818, 2011.
35. W.C. Ao and K.C. Chen, Upper bound on broadcast transmission capacity of heterogeneous wireless ad hoc networks, *IEEE Commun. Lett.*, 15(11), pp. 1172–1174, 2011.
36. W.C. Ao, S.M. Cheng, and K.C. Chen, Connectivity of multiple cooperative cognitive radio ad hoc networks, *IEEE J. Selected Areas Commun.*, 30(2), 263–270, February 2012.
37. C. Gao, Y. Shi, Y.T. Hou, and S. Kompella, On the throughput of MIMO-empowered multihop cognitive radio networks, *IEEE Trans. Mobile Comput.*, 10(1), 1506–1519, 2011.
38. W.C. Ao and K.C. Chen, End-to-end HARQ in cognitive radio networks, *IEEE Wireless Communications and Networking Conference*, Sydney, 2010.
39. H.B. Chang, S.M. Cheng, S.Y. Lien, and K.C. Chen, Statistical delay control of opportunistic links in cognitive radio networks, *IEEE International Symposium on Personal Indoor Mobile Radio Communications*, Istanbul, 2010.
40. P.Y. Chen, S.M. Cheng, W.C. Ao, and K.C. Chen, Multi-path routing with end-to-end statistical QoS provisioning in underlay cognitive radio networks, *IEEE INFOCOM Workshop*, Shanghai, 2011.
41. A. Alshamrano, X.S. Shen, and L.-L. Xie, QoS provisioning for heterogeneous services in cooperative cognitive radio networks, *IEEE J. Selected Areas Commun.*, 29(4), 819–820, 2011.
42. Z. Liang, S. Feng, D. Zhao, and X. Shen, Delay performance analysis for supporting real-time traffic in a cognitive radio sensor network, *IEEE Trans. Wireless Commun.*, 10(1), 325–335, 2011.
43. X.-L. Huang, G. Wang, F. Hu, and S. Kumar, The impact of spectrum sensing frequency and packet-loading scheme on multimedia transmission over cognitive radio networks, *IEEE Trans. Multimedia*, 13(4), 748–761, 2011.
44. S. Gunawardena and W. Zhuang, Capacity analysis and call admission control in distributed cognitive radio networks, *IEEE Trans. Wireless Commun.*, 10(9), 3110–3120, 2011.
45. T. Do and B.L. Mark, Joint spatial-temporal spectrum sensing for cognitive radio networks, *IEEE Trans. Vehicular Technol.*, 59(7), 3480–3490, 2010.
46. T.W. Chiang and K.C. Chen, Synthetic aperture radar construction of spectrum map for cognitive radio networking, *International Conference on Wireless Communications and Mobile Computing*, Caen, France, 2010.
47. S.Y. Shih and K.C. Chen, Compressed sensing construction of spectrum map for routing in cognitive radio networks, *IEEE Vehicular Technology Conference—Spring*, Budapest, 2011.
48. S.C. Lin and K.C. Chen, Spectrum aware opportunistic routing in cognitive radio networks, *IEEE GLOBECOM*, Miami, 2010.
49. S.Y. Lien, Y.Y. Lin, and K.C. Chen, Cognitive and game-theoretical radio resource management for autonomous femtocells with QoS guarantees, 10(7), 2196–2206, *IEEE Trans. Wireless Commun.*, 2011.
50. S.M. Cheng, S.Y. Lien, F.S. Chu, and K.C. Chen, On exploiting cognitive radio to mitigate interference in macro/femto heterogeneous networks, *IEEE Wireless Commun.*, special issue on Heterogeneous Networks, 18(3), 40–47, 2011.
51. S. Filin, H. Harada, H. Murakami, and K. Ishizu, International standardization of cognitive radio systems, *IEEE Commun. Mag.*, pp. 82–89, March 2011.
52. P. Di Lorenzo and S. Barbarossa, A bio-inspired swarming algorithm for decentralized access in cognitive radio, *IEEE Trans. Signal Process.*, 59(1), 6160–6174, 2011.

53. H. Li and Z. Han, Socially optimal queuing control in cognitive radio networks subject to service interruptions: To queue or not to queue? *IEEE Trans. Wireless Commun.*, 10(5), 1656–1666, 2011.
54. C.H. Huang, and K.C. Chen, Dual-observation time division spectrum sensing for cognitive radios, *IEEE Trans. Vehicular Technol.*, 60(7), 3712–3725, 2011.
55. S.Y. Lien, K.C. Chen, and Y.H. Lin, Toward ubiquitous massive accesses in 3GPP machine-to-machine communications, *IEEE Commun. Mag.*, 49(4), 66–74, 2011.

V

Emerging Applications

38

Vehicular Communications

Antonio Servetti

Paolo Bucciol

Juan Carlos De Martin

38.1 Introduction and Motivations

The "always connected" paradigm is becoming a reality for more and more people. Users, in fact, clearly appreciate being constantly connected with each other and to the Internet. Consequently, companies are supporting such appreciation with a wide offer of mobile devices and applications. As a result, there has been an increasing effort in the design and development of applications and systems able to provide connectivity to people wherever they happen to be.

Among the numerous scenarios, vehicle-based communication has been receiving increasing attention. In rich countries, in fact, individuals spend on average over 100 h a year in commuting time alone (see, e.g., the United States case (US Census Bureau 2011)), with an upward trend (DFT 2011). The same is expected to happen to approximately three billion people living in today's defined "developing countries" by 2050, when they will obtain a purchasing power comparable to today's average US citizen (Goldman Sachs, 2011). Moreover, besides the communications needs of individuals, motor vehicles are ripe to start communicating per se, as objects. Communicating with other vehicles as well as with the roadside infrastructure and with the world at large, for reasons ranging from security to parking, from traffic optimization to energy conservation. The communications technology—from wireless to software—is, in fact, finally mature for breaking the traditional informational autism of vehicles. It is true that at least 10% of the cars will need to be equipped with communication units in order to reach the minimum penetration rate to trigger the wide adoption of inter-vehicle applications and services

(Ergen 2010). But when that tipping point is reached, inter-vehicle communications are expected to spread rapidly.

Initially conceived for the communication of data coming from local sensors, inter-vehicle communications are now being studied in the context of a much larger range of applications, as mentioned above. This chapter intends to describe the main concepts behind inter-vehicle communication technology, and to present some of the most promising standards, applications and projects.

The rest of this section is devoted to familiarizing the reader with some key concepts, while the rest of the chapter is organized as follows. Section 38.2 characterizes the models used in vehicle-to-vehicle data communication. Section 38.3 analyzes current and emerging applications of interests. Section 38.4 presents a survey of existing testbeds and projects, as well as thematic and joint actions and networks. Finally, Section 38.5 draws the conclusions.

38.1.1 Inter-Vehicle Networks

At the time of writing, a global consensus on how to refer to a generic communication involving vehicles has not yet been reached due to the heterogeneity of characteristics involved in this scenario: moving nodes (vehicles), fixed nodes (roadside infrastructure), *ad hoc* networking, mesh networking.

The most common acronym that is now used to refer to inter-vehicle communications, VANET (Vehicular *Ad hoc* NETworks), has been coined only recently by Laberteaux in 2004, with respect to the first studies in this area of research that can be dated back to the 1980s. Although originally adopted to reflect the *ad hoc* nature of inter-vehicle networks (Hartenstein and Laberteaux 2008), VANET is now commonly used to indicate a generic communication system where one or more communicating devices are located on vehicles (Hartenstein and Laberteaux 2010). Other taxonomies include the V2X (Ström et al. 2010) and VC (Sichitiu and Kihl 2008) schools where the term V2X identifies Vehicle-to-X connections, while the term *VC identifies *-vehicle communications. Table 38.1 presents a detailed list of acronyms and their meaning with respect to the type of communication they refer to.

Throughout this chapter, we will use the notation that provides case-by-case the best clarity in the context. A more detailed analysis of the topic is carried out in Section 38.2.

38.1.2 Channel Characterization and Mobility Models

Defining appropriate channel characterization and mobility models in inter-vehicle communications is a challenging task. VANETs represent in fact a particularly challenging class of Mobile *Ad hoc* NETworks (MANETs) (Chlamtac et al. 2003) due to the peculiar features of channel and nodes. On one side, channel conditions are rapidly varying in an unpredictable way, depending for instance on the location (urban or rural surrounding environment) and on the time of the day (rush hours or not). On the other side, the high mobility of the nodes causes extreme difficulty in creating a realistic mobility model. Section 38.2 discusses with more details the aspects concerning channel characterization and node mobility.

TABLE 38.1 V2X and *VC Taxonomies

	Communication Type		
Taxonomy	Between Vehicles	Between Vehicles and Infrastructure	Between Vehicles and Infrastructure through Vehicles
V2X	V2V (Vehicle-to-vehicle)	V2I (Vehicle-to-infrastructure)	V2V2I (Vehicle-to-vehicle-to-infrastructure)
*VC	IVC (Inter-vehicle communication)	RVC (Roadside-vehicle communication)	HVC (Hybrid-vehicle communication)

38.1.3 Standardization Actions

Although in theory several existing communication technologies can be employed to provide connectivity in VANETs (e.g., cellular mobile networks and Wimax), the peculiarities of inter-vehicle communications considerably reduce their effectiveness and, as a consequence, make their adoption for Intelligent Transportation Systems (ITS) applications all but straightforward. Several public and private standardization bodies and consortia are proposing their own standards and protocols suited to inter-vehicle communication. This implies the assignation of specific frequency bands, and the definition of communication protocols, frameworks, and standards for interoperability.

Table 38.2 shows a resume of the frequency bands assigned for ITS. Although almost all regions concentrate the dedicated bands in the frequency interval 5.7–5.9 GHz, it can be observed that a frequency band common for all regions still does not exist. In order to promote the interoperability of inter-vehicle communications, there is an ongoing joint action, supported mainly by the ETSI Technical Committee on ITS (ETSI TC ITS), trying to define a universal frequency band to be dedicated to ITS, most likely in the range of 5.8–5.9 GHz.

For what concerns the communication protocols, three main standardization actions can be identified:

- *WAVE, IEEE 1609 WG*. The IEEE Working Group 1609, constituted in 2006, is developing the Wireless Access in Vehicular Environment (WAVE) family of standards. WAVE, also known as 802.11p, is an extension of the IEEE 802.11 standard aimed at enhancing the behavior of 802.11 in ITS applications. It is based on Dedicated Short-Range Communications (DSRC, ASTM standard E2213-03). Figure 38.1 shows a synthetic view of the WAVE protocol stack. The WAVE standards family is composed by IEEE 1609.0 (WAVE architecture), 1609.1 (Remote Management Services), 1609.2 (Security Services), 1609.3 (Network Services), 1609.4 (Multichannel operations), and 1609.11 (Over-the-air Electronic Funds Collection) (WAVE 2011).
- *CALM, ISO TC 204 WG 16*. The Technical Committee 204, Working Group 16 of the International Organization for Standardization (ISO) started in 2001 the development of the "Basic Set of ITS Communication Standards" under the work title "Communication Access for Land Mobiles" (CALM). CALM intends to define a family of international standards for a common architecture, protocols and interface definitions for wireless communications, in order to provide interoperable access technologies for ITS applications and services (CALM 2011).
- *ETSI TC ITS*. The mission of the European Telecommunications Standards Institute (ETSI) ETSI's Technical Committee on ITS, constituted in 2007, is the creation, harmonization and maintenance of standards and specifications for the use of information and communications technologies in future transport systems. Most of the 'ongoing standardization activities within this TC are focused on wireless communications for vehicle-to-vehicle and vehicle-to-roadside communications (ETSI 2011). On September 2010 the ETSI TC ITS WG published the standard named ETSI EN 302 665 on the ITS communication architecture.

Finally, to promote interoperability, the US Department of Transportation developed the SAE J2735 (version 2, 2009) Message Set Dictionary to support interoperability among DSRC applications through the use of standardized message sets, data frames, and data elements (SAE 2011).

TABLE 38.2 Frequency Bands Allocated for ITS

Region	Frequency Bands (MHz)	Reference
ITU-R (ISM band)	5725–5875	Art. 5 of Radio Regulations
Europe	5795–5915; 5855/5875–5905/5925	ETS 202-663, ETSI EN 302-571, ETSI EN 301-893
North America	902–928, 5850–5925	FCC 47 CFR Parts 90 and 95
Japan	715–725, 5770–5850	MIC EO Article 49

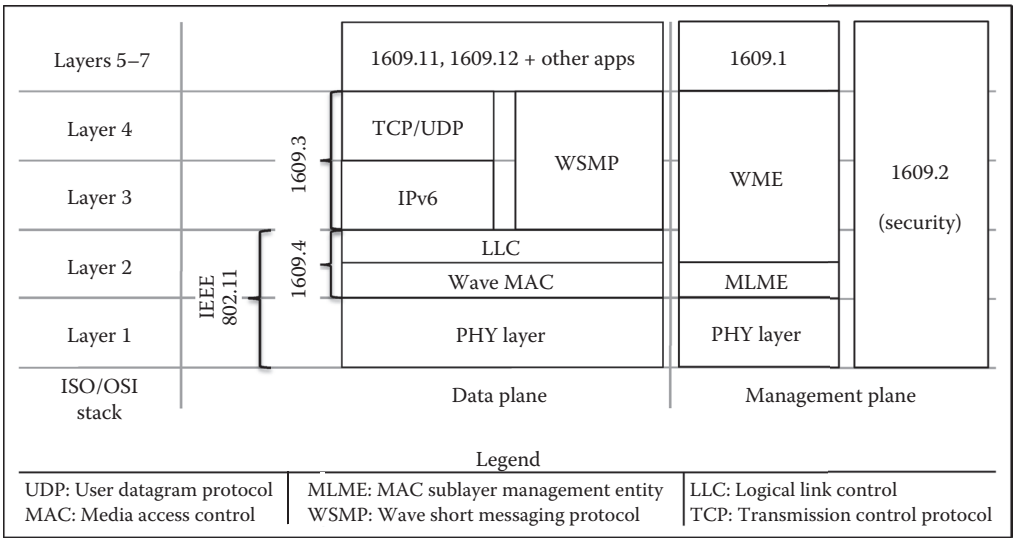

FIGURE 38.1 The IEEE P1609 standards family.

38.1.4 Overview of the Applications of Interest

Future vehicles will be accessorized with a number of electronic controls and devices. Such equipment will pave the way for a variety of possible applications to improve both road safety and traffic efficiency. More and more participants, not only governments and vehicle manufacturers, but also local retailers and consumers, will be attracted to VANETs and will benefit from it. A survey on the three main categories of VANET applications and a characterization of the recurring communication patterns is presented in Section 38.4.

38.2 Data Communication

The increased interest of the scientific and industrial community on VANETs has produced a significant amount of surveys on the various aspects related to this scenario. This section focuses on the definition of the inter-vehicle communication paradigms, mobility models and routing schemes. For readers requiring more details on these topics, an accurate survey on mobility models can be found in Härri et al. (2009), while Sichitiu and Kihl (2008) and Willke et al. (2009) focus more on the requirements and characteristics of intervehicle communication protocols.

38.2.1 Communication Paradigms

We can identify three main systems for vehicular communication: vehicle-to-vehicle (V2V), vehicle-to-infrastructure (V2I), and vehicle-to-vehicle-to-infrastructure (V2V2I) (here we follow the taxonomy of Sichitiu and Kihl 2008).

V2V systems are pure *ad hoc* networks that rely only on the in-vehicle communication equipment and do not connect to any fixed roadside infrastructure. They can be further divided in single-hop and multi-hop V2V systems. The former allow only short-range communications, while the latter are used to extend the communication range at the expenses of an increased complexity of the system. In multi-hop V2V the intermediate vehicles relay the messages to the vehicles that are not in the transmission range of the original sender, thus a network layer capable of multi-hop routing is needed.

In V2I systems vehicles communicate solely with roadside infrastructure when inside the transmission range. Hot spots, like road intersections, parking lots, gas stations, and so on, are relatively easily to cover for providing special services to passing by vehicles. On the contrary, road coverage is extremely expensive using 802.11 wireless technology and 802.16 or 3G is required.

V2V2I systems are frequently suggested to extend the coverage of V2I systems through vehicle-to-vehicle message relay. As in multihop V2V systems, mobile nodes behave as routers and allow other vehicles to connect to the infrastructure even if they are not in the direct transmission range. In urban scenarios, with a high vehicle density, V2V2I systems may allow a considerable reduction in the number of roadside equipment with respect to V2I only systems.

38.2.2 Channel and Mobility Models

Intervehicle communications are hard to model. VANETs can be in fact assimilated to distributed systems made of nodes moving with variable speeds and various degrees in movement patterns (Blum et al. 2004). Due to the very high number of varying parameters involved, an accurate and general model does not exist yet. Each model presents its advantages and disadvantages based on how it addresses the peculiar characteristics of intervehicle communications. An extensive survey of mobility models for VANETs can be found in Härri et al. (2009). In the following we focus on three peculiar characteristics: the place and time of the communication, and the mobility model.

- *Place of the transmission.* Channel conditions vary based on the surrounding environment (e.g., urban or rural). The environment has a dramatic effect on the quality of the received signal. For example, intervehicle communication in urban environments is usually disturbed by the presence of several objects and obstacles that lead to a lower signal quality (Moške et al. 2004).
- *Time of the transmission.* The time in which communication is performed is very important to deduct the actual characteristics of the communication channel. For example, a vehicle-to-vehicle communication has far more probability to experience transmission errors if performed during peak time in the center of a big city than if performed on an extra-urban road segment without traffic (Bucciol et al. 2005).
- *Mobility model.* Movement of cars follows specific patterns. When VANETs were introduced, several papers focused on the random waypoint mobility model (nodes randomly change speed and direction during the simulation). A good model should take into account the geographical positioning of the communicating objects (e.g., road maps), as well as usual car mobility patterns (e.g., cars tend to accelerate after crossing an intersection) (Härri et al. 2009).

38.2.3 Routing Schemes

Great research efforts have been spent in the last decade on routing in MANETs and a number of routing protocols were developed in that context; for example, optimized link state routing (OLSR) (Jacquet et al. 1998), *ad hoc* on-demand distance vector (AODV) (Perkins and Royer 1999) (Perkins et al. 2003), dynamic source routing (DSR) (Johnson and Maltz 1996) (Hu et al. 2007), and so on. The same protocols, often with some modifications to better suit the different scenario, were proposed for VANETs. However, the vehicular scenario is characterized by specific properties, at the routing level, that make them suboptimal for multihop communication in an IVC system. In fact, in a VANET, routing protocols can be optimized assuming that the position of the vehicles is known—hopefully all cars will be equipped with a global positioning system (GPS)—and that their movements can be predicted with a good degree of precision having some knowledge of the road layout. Additionally, vehicle mobility patterns need to be considered in the design of a routing protocol for two main reasons, first, because the high mobility of nodes causes frequent network partitioning and merging, and second, because mobility can be exploited to increase the performance of the network, as shown in Grossglauser and Tse (2002).

TABLE 38.3 Taxonomy of Routing Protocols

	Topology	Position	Geocast	Mobility
General	AODV DSR OLSR	DREAM GSR	GAMER LBM	VTRADE
Sparse		MDDV		MDDV VADD
Dense	HSR	GPCR CPSR	GeoGRID	UMB

We identify five categories, summarized in Table 38.3, to briefly describe the most common approaches presented in the literature: topology-based, cluster-based, geographical, movement-based, and broadcast routing.

38.2.3.1 Topology-Based Routing

VANETs and MANETs share some *ad hoc* routing protocols based on the network topology, that is, how nodes are connected together. However, VANETs present a much more dynamic topology than MANETs and studies have demonstrated that this type of protocols—for example, AODV, OLSR, and DSR—suffer from the high vehicle mobility pattern showing poor route convergence and low communication throughput (Fussler et al. 2003). Several modification have been proposed to reduce the effect of frequent route breakages, for example in Menouar et al. (2005) adding a prediction of the future position as a function of the current position, direction, and speed, or in Namboodiri et al. (2004) trying to predict the link lifetimes.

38.2.3.2 Geographical Routing

In this category we consider both *position-based protocols* (e.g., LAR, DREAM, GPSR (Karp and Kung 2000)) and *geocast protocols* (e.g., GAMER, LBM) where the former are related to one-to-one communications and the latter to one-to-many communications. Vehicle location can be determined by the onboard GPS equipment and routing strategies are based on the geographical position of the destination of a packet, if possible exploiting also the limitations of vehicle movements, that must follow the road layout, and the analytical models of traffic patterns. Studies (Fussler et al. 2003) have proved geographical routing algorithms a promising approach for VANETs compared to topology-based routing.

In the *Greedy Perimeter Stateless Routing (GPSR)* (Karp and Kung 2000) packets are always forwarded to the node that is geographically closest to the destination in order to maximize the progress of the packet toward its destination. If the greedy approach fails reaching a dead end, face routing is used to identify another node from which the greedy algorithm can be resumed. In metropolitan scenarios this technique is heavily limited by the frequent obstacles that prevent direct communication between vehicles. To address this issue Lochert (Lochert et al. 2003) proposed the *Geographic Source Routing* (GSR) protocol that adds knowledge from a digital street map to identify junctions that must be traversed using a shortest path algorithm. Forwarding between junctions is then done in a position-based manner. The same author proposed the *Greedy Perimeter Coordinator Routing (GPCR)* protocol (Lochert et al. 2004) that does not need access to a street map and do not use source routing. Two algorithms are used to detect vehicles in a junction as a function of the position and direct reachability of their neighbors. Such vehicles are then elected as coordinators and take care of the true routing process, in fact, as long as nodes are in a street, a restricted algorithm is used. A more advanced algorithm was proposed in Liu et al. (2004), *Anchor-based Street and Traffic Aware Routing (A-STAR)*, which incorporates traffic awareness by using both static and dynamic rated maps.

Geocast protocols (Maihofer 2004) are a specialization of multicast routing where flooding is restricted to a specific location called *zone of relevance (ZOR).* Most algorithms are based on modifications of broadcast flooding to minimize the network overhead by reducing the number of re-broadcasts.

That is, nodes do not rebroadcast packets immediately, but wait for some time to make a decision about it. For example, a vehicle may choose not to rebroadcast if it overhears a peer farther from the source doing so (Yang et al. 2004). To deal with frequent network partitions Maihöfer (Maihofer and Eberhardt 2004) proposed to add a small cache to the routing layer to hold packets that cannot be forwarded instantly, messages are then forwarded when another vehicle comes in the node transmission range. Maihöfer also proposed the *abiding geocast* (Maihofer et al. 2005), that is, a time stable geocast protocol, where senders can define a lifetime for the permanence of the message in the zone of relevance. The message is then retransmitted whenever a node inside the destination region detects a new neighbor.

38.2.3.3 Mobility-Based Routing

In addition to the information on vehicle position and road layout, mobility-based routing protocols explicitly exploit vehicle mobility for information dissemination (e.g., VADD (Zhao and Cao 2006), VTRADE (Sun et al. 2000), UMB (Korkmaz et al. 2004)). Here the problem of network sparsity and network partitioning is addressed making messages move forward the destination by means of vehicle movements. The *Mobility-Centric Data Dissemination protocol* (MDDV) (Wu et al. 2004) is a combination of opportunistic, geographical, and trajectory-based forwarding where the message is carried by vehicles (called *message head*) moving in the direction of the destination. Only message heads are in charge of the routing, nearby nodes (that cannot help moving the message closer to the destination) contribute exchanging meta-data information that includes "estimated" message head location and transmission time.

38.2.3.4 Cluster-Based Routing

Cluster-based routing is a form of hierarchical routing that defines two or more levels of routing to reduce the amount of routing information overhead. It can be adapted to topological (e.g., HSR (Iwata et al. 1999), geographical (e.g., GeoGRID (Maihofer 2004)) and other kind of protocols. The cluster is a—as much as possible—stable set of connected vehicles. Within the cluster nodes communicate via direct links (or through broadcast (Durresi et al. 2005)), while between clusters messages are forwarded by cluster-heads that act as gateways. The definition of the hierarchical network infrastructure is crucial for the protocol, but the overhead required to create and maintain such information increases with the network dynamics and clusters tend to be too short-lived.

38.2.3.5 Broadcast Routing

Broadcast is frequently useful in VANETs, however, the bandwidth requested for the transmission can increase exponentially with the number of nodes. Thus, broadcast protocols employ different methods to reduce such overhead using probability-based (Alshaer and Horlait 2005), location-based (Benslimane 2004), direction-based (Korkmaz et al. 2004), hierarchical (Little and Agarwal 2005) or message-utility-based (Wischhof and Rohling 2005) algorithms.

38.3 Vehicular Applications

Advances in "on vehicle" electronics, computing, communications, and sensing have significantly increased the interest for innovative applications being able to exploit the unique potential, and relative low operational cost, of vehicular communication networks to increase traffic safety (Sengupta et al. 2007). Although the prime motivation of such applications will always be to reduce the number of accidents and save human lives, this wireless scenario provides also a promising platform for other services ranging from traffic management to commercial or comfort applications.

In contrast with conventional *ad hoc* networks, vehicular *ad hoc* networks (VANETs) offer a rich set of opportunities for embedding intelligent communication-based systems to solve real-life problems such as tourist information and assistance, parking availability notification, and traffic condition warnings. VANETs have fewer constraints on processing power and provide much more storage,

processing, and communication capacity than personal or sensor-based *ad hoc* networks. As a consequence vehicles can form a perfect mobile platform for data gathering, processing, and dissemination (i.e., Vehicular Sensor Networks (Lee et al. 2006, 2009)).

In the challenging vehicular networking scenario where performance of links is highly variable and where a complete path from source to destination does not exist for most of the time, nodes play a threefold role as producers, consumers, and forwarders of information (e.g., road, traffic, weather condition reports). Advanced services may be offered if vehicles actively contribute to the system also as intermediaries taking custody of data during blackouts and forwarding it when connectivity resumes (i.e., store-carry-forward message switching mechanism (Wisitpongphan et al. 2007)).

In the following we identify the three main categories used to classify vehicular applications and analyze four recurrent communication patterns that form the basis for the design of such applications.

38.3.1 Categories

Communication-based applications for vehicular networks are commonly classified into three major categories: vehicle safety, traffic management, and infotainment.

Vehicle safety. Surrounding vehicles, traffic signals, and road conditions are actively monitored in order to warn drivers against potential dangers such as collisions with other vehicles and obstacles (collision warning), signal violations (violation warning), or bad road conditions. The major characteristic of these applications is that they have very strict real-time demands, both on communication reliability and latency (less than 100 ms of delay are needed for collision avoidance (Biswas, Tatchikou, and Dion 2006)).

Traffic management. Traffic and road conditions are actively monitored by vehicles on the road that share this information with other nodes in the surrounding area or in a specific location (e.g., an intersection). The main objective is to enable a more efficient traffic flow control reducing both congestion problems and travel times, and, ultimately, improving driver satisfaction (Nadeem et al. 2004). Typical applications (e.g., congested road notification, parking availability location, intersection assistance, emergency vehicle signaling) have less strict requirement on latency and reliability than safety applications. On the other hand, they rely on routing protocols that take advantage of the relatively long communication range provided by DSRC to disseminate the information in a particular direction or area, also called zone-of-relevance (ZOR).

Infotainment. Different information services are provided to drivers to make the travel more efficient, productive, and pleasant. Various traveler information and service announcement applications belong to this category (i.e., gas station, restaurant, hotels advertisement) (Nandan et al. 2006). In this case roadside infrastructure and multi-hop communication is used to propagate messages from a certain location to the surroundings as the drivers pass by. Most work has also been focused on connecting vehicular networks to the Internet for email access, web browsing, and content download in order to extend the car entertainment system, for example, with real-time multimedia streaming (Guo et al. 2005).

38.3.2 Communication-Based Characterization

Looking at the three categories of vehicular services from a communication-based perspective we can identify some networking issues that clearly affect various design aspect of the applications envisioned so far. Accordingly, we can group the communication characteristics and requirements to define a set of common design patterns, often called *communication patterns* (Schoch et al. 2008), which form the basis for building a VANET application.

38.3.2.1 Network-Related Application Requirements

Each application defines some network-related requirements that drive the choice of the communication architecture and protocols to be used. We highlight some of them as follows.

- *Zone-of-relevance (ZOR)* is the geographical region that should be covered by the communication network. Depending on the application can be small, medium, or large. In particular, safety applications (e.g., collision warning, violation warning) propagate their messages only in a small area that usually is no more than a few hundred meters. On the other hand, traffic management and infotainment applications tend to cover larger areas, approximately in the order of kilometers for road or traffic condition information and virtually everywhere for content download.
- *Application trigger condition (ATC)* defines how a message transmission is scheduled and it can be periodic, event driven, or user initiated. Safety applications tend to send periodic messages to constantly inform the surrounding vehicles of the danger. Traffic management applications are usually triggered by some events, such as traffic congestions. While infotainment applications are manually activated by the driver (e.g., music download) or by a software agent in the car (e.g., announcement of a closer and cheap gas station of the preferred brand).
- *Transmission pattern (TP)* specifies how many nodes are involved in the transmission and reception of the messages and it can be one-to-many, one-to-a-zone, one-to-one, and many-to-one. Some safety applications inform all vehicles in every direction (one-to-many) for example to prevent a crash. Other safety applications and most of the traffic management ones address vehicles within a specific zone (one-to-a-zone). Instead, infotainment applications are more prone to the one-to-one transmission pattern.

38.3.2.2 Communication Patterns

The particular set of network characteristics associated to each kind of application lead to a specific design of the communication system. We summarize from Schoch et al. (2008) the most recurring system architectures in three plus one communication pattern: beaconing, geobroadcast, unicast, and information dissemination.

Beaconing is characterized by a periodic single-hop broadcast scheme to continuously inform all the nodes in the reception range. The communication scheme is rather simple, that is, it is periodic, strictly unidirectional, and messages are not forwarded. On the other hand, being this scheme typically used for safety applications, the latency and reliability demands are very high (Rossi, Fracchia, and Meo 2008).

Geobroadcast refers to the immediate transmission to other vehicles in a certain area. Message forwarding is based on node location instead than on their address. Most traffic management applications rely on location-based multicast routing. The transmission is unidirectional and generally triggered by an event (e.g., vehicle collision or traffic congestion). The forwarding scheme must be tailored not to cause congestion problems in high node density conditions: in order to minimize the number of unnecessary transmissions each node needs to use some heuristic to decide whether to forward a message or not. Latency needs are less strict than in safety applications, but certain services like accident warning may require a high delivery success ratio.

Unicast is the most common choice for infotainment applications that are activated by the user interaction and may require a connection-oriented bi-directional one-to-one communication channel (e.g., Internet browsing). Safety and traffic management applications do not usually require bidirectional channels as in unicast, so this pattern is commonly associated to low priority communications that tolerate high delays and exploit packet retransmissions.

Information dissemination is a natural extension of the previous three information forwarding patterns. First, store-carry-forward message switching mechanisms are required to allow node communications if no simultaneous multihop paths are available at any time. In this type of pattern, the mobility of devices becomes an opportunity for communication rather than a challenge, routes are built dynamically and any possible node can opportunistically be used as the next hop, if it is likely to bring the message closer to the final destination(s). Second, exploiting the communication opportunities between mobile vehicles for message forwarding is only the first step, that is, vehicles can collaborate also by sharing resources, information, and processing power. In this scenario data are not only routed to the destination, but also processed and enriched by the intermediate nodes. This enables the possibility to efficiently solve collaborative tasks such as detecting a traffic jam. In context-adaptive data dissemination studies (Kosch et al. 2006) messages are not given an explicit destination, but information is spread according to its contextual relevance that also defines its forwarding priority if bandwidth is scarce. Clearly, this mechanism can be adopted when latency requirements are somewhat relaxed and effective message dissemination is by far the most important QoS parameter together with information quality and its convergence within the network.

38.4 Projects and Actions

The first projects on intervehicle communications were developed in the seventies and focused on group cooperative driving by the Association of Electronic Technology for Automobile Traffic and Driving (JSK) in Japan. Since then, the evolution in the fields of computing and radio communication and the constant increase in the number of cars (together with consequent issues and challenges) have paved the way to the proliferation of several initiatives worldwide aimed at solving some of the ITS challenges through the intelligent adoption of intervehicle communication techniques.

VANET-related activities are particularly active in three regions: the European Union, the United States, and Japan.* The European Commission is the main promoter of this kind of activities in Europe, especially through the *eSafety* (http://ec.europa.eu/information_society/activities/esafety/) and ICT programmes. eSafety is the program of the Europe's Information Society that intends to promote a quicker development and increased use of smart road safety and eco-driving technologies. Since 2002, the program has co-funded several projects in the context of intervehicle communications. In the United States, activities are boosted by the US Department of Transportation (USDOT, http://www.its.dot.gov/), while in Japan the role is covered by ITS Japan (http://www.its-jp.org/).

This section summarizes in a nonexhaustive way some of the main projects, consortia and testbeds created in the three regions as reported in Table 38.4. The list does not include standardization actions

TABLE 38.4 Summary of Existing Projects, Consortia, and Testbeds

	Consortia	Safety	Communication	Other Services	Testbeds
EU	C2C-CC AKTIV	eSafetySupport PReVENT SAFESPOT SEVECOM PRESERVE WATCH-OVER	DIRICOM GeoNet NOW AutoNomos C-VIS	SEISCIENTOS DRIVE-IN	iTetris PRE-DRIVE SIM-TD
USA	VII CAMP PATH		CarTel	CarTorrent	C-VeT
Japan	ITS Japan	ASV			

* We will not mention here initiatives pushed by private companies only.

by governments and public entities, which have already been covered in Section 38.1. The following five categories of actions have been identified:

1. *Consortia*. The lack of globally recognized standards for intervehicle communication, as well as the relative novelty of IVC technologies, has given birth to a significant number of consortia, trying to put together a critical mass and reach a general consensus in specific regions of the world and within specific topics, such as, communication protocols and security.
2. *Safety*. In the context of IVC, safety has the double meaning of road safety (targeted to decreasing the number of accidents) and data safety (targeted to securing the data communications). The two aspects are partially overlapping, since in order to provide a safe system, secure interchange of data to avoid the risk, among others, of cheating and malicious attacks, has to be guaranteed.
3. *Communication*. This category groups the studies on the communication protocols and strategies that fall out of the context of public standardization bodies and entities.
4. *Testbeds*. Before the commercialization and the deployment of IVC solutions and platforms, they have to be carefully tested. This category intends to review real-life experiments on IVC.
5. *Other services*. This category groups projects that, such as the wireless toll collection mechanisms, aim at providing value-added services through IVC.

The rest of the section is dedicated to a short description of the main actions for each category.

38.4.1 Consortia

Adaptive and Cooperative Technologies for the Intelligent Traffic (Aktiv, http://www.aktiv-online.org/english/). Aktiv is a German research initiative that brings together 29 partners focused on three main projects: traffic management, active safety and cooperative cars. Aktiv's goal is to improve both traffic safety and traffic flow in the future.

California Partners for Advanced Transportation Technology (PATH, http://www.path.berkeley.edu/). PATH, established in 1986, is administered by the Institute of Transportation Studies (ITS) of the University of California, Berkeley, in collaboration with the California Department of Transportation (Caltrans). PATH is a multi-disciplinary program with staff, faculty and students from universities statewide, and cooperative projects with private industry, state and local agencies, and nonprofit institutions.

Car2Car Communication Consortium (C2C-CC, http://www.car-to-car.org/). C2C-CC is a nonprofit industrial-driven organization initiated by European vehicle manufacturers supported by equipment suppliers, research organizations, and other partners. C2C-CC is dedicated to the objective of further increasing road traffic safety and efficiency by means intervehicle communication.

Crash Avoidance Metrics Partnership (CAMP). CAMP is an initiative started in 1995 by Ford and General Motors intended to facilitate industry consensus on the objectives of future crash avoidance countermeasure systems and the way of testing them. CAMP has supported several research projects with the US Department of Transport, including the Vehicle Safety Communications (VSC-I, VSC-II, VSC-A) projects and smaller focused consortia, such as the Crash Imminent Braking (CIB) consortium and the Vehicle Safety Communications consortium (VSCC).

ITS Japan (http://www.its-jp.org/english/). ITS Japan is a consortium of Japanese governmental entities whose objective is to reduce the effect of traffic accidents, traffic congestion, environmental pollution, and massive consumption of fossil fuels by means of ITS systems.

Vehicle Infrastructure Integration (VII, http://www.vehicle-infrastructure.org/). The Vehicle Infrastructure Integration (VII) Initiative is a cooperative effort between Federal and State departments of transportation (DOT's) and automobile manufacturers. Together they are

evaluating the technical, economic, and social/political feasibility of deploying a communications system that will be used primarily for improving the safety and efficiency of the nation's road transportation system.

38.4.2 Safety Projects

Advanced Safety Vehicle (ASV). The 20 years-long, four phases ASV project, founded by the Japan's Ministry of Land, Infrastructure, and Transport, employed inter-vehicle communications to achieve the objectives of developing active safety mechanisms to avoid road accidents. ASV-enabled cars are currently being produced in Japan.

eSafetySupport (http://www.esafetysupport.org/). eSafety Support is a joint industry-public sector initiative driven by the European Commission and co-chaired by ERTICO—ITS Europe and ACEA (Association of European Car Manufacturers), with the aim to promote the development, deployment, and use of Intelligent Vehicle Safety Systems to enhance road safety throughout Europe.

Preparing Secure Vehicle-to-X Communication Systems (PRESERVE, http://lib.bioinfo.pl/projects/view/22954). The goal of PRESERVE is to bring secure and privacy-protected V2X communication closer to reality by providing and field testing a security and privacy subsystem for V2X systems. PRESERVE will combine and extend results from the earlier research projects SEVECOM, PRECIOSA, EVITA, and OVERSEE.

PreVENT (http://www.prevent-ip.org/). The goal of PReVENT, co-funded by the European Commission and ended in 2008, was to to contribute to road safety by developing and demonstrating preventive safety applications and technologies.

SafeSpot (http://www.safespot-eu.org/). SAFESPOT creates dynamic cooperative networks where the vehicles and the road infrastructure communicate to share information gathered on board and at the roadside to enhance the drivers' perception of the vehicle surroundings.

SEcure VEhicle COMmunication (SEVECOM, http://www.sevecom.org/). SEVECOM aims to define a consistent and future-proof solution to the problem of security of data exchanged through intervehicle communications.

WATCH-OVER (http://www.watchover-eu.org/). The WATCH-OVER project, ended in 2008, targeted to increasing the road safety, intends to examine the detection of vulnerable road users in the complexity of traffic scenarios in which pedestrians, cyclists, and motorcyclists are walking or moving together with cars and other vehicles.

38.4.3 Communication

AutoNomos (http://www.auto-nomos.de/). AutoNomos is a German national research project aimed at the definition of a distributed and self-regulated approach for the self-organization of a large system of many self-driven, mobile objects.

CarTel (http://cartel.csail.mit.edu/). CarTel is a distributed, mobile sensor network and telematics system. Applications built on top of this system can collect, process, deliver, analyze, and visualize data from sensors located on mobile units such as automobiles and smartphones.

Cooperative Vehicle-Infrastructure Systems (CVIS, http://www.cvisproject.org/). CVIS is a major new European research and development project aiming to design, develop and test the technologies needed to allow cars to communicate with each other and with the nearby roadside infrastructure. Based on such real-time road and traffic information, many novel applications can be produced. The consequence will be increased road safety and efficiency, and reduced environmental impact.

GeoNet (http://www.geonet-project.eu/). GeoNet focuses on geographic addressing and routing, where information is disseminated over multiple hops until every vehicle has received this information within the destination area.

Intelligent Design of Wireless Communication Networks (DIRICOM, http://diricom.lcc.uma.es/). The DIRICOM project, financed by the Spanish government, aims at using metaheuristics in order to solve VANET design problems.

Network On Wheels (NOW, http://www.network-on-wheels.de/). The main objectives of NOW, ended in 2008, were to solve technical key questions on the communication protocols and data security for car-to-car communications.

38.4.4 Testbeds

C-VeT (http://www.vehicularlab.org/). C-VeT is the future Vehicular Testbed of the University of California at Los Angeles (UCLA), built by the Network Research Lab at UCLA.

SimTD (http://www.simtd.de). SimTD is the Daimler's research project on inter-vehicle communication and applications. The project started in 2008 and will last four years. Realistic traffic scenarios will be addressed in a large-scale test field infrastructure around Frankfurt.

iTetris (http://www.ict-itetris.eu/). iTetris is aimed at producing the necessary building blocks and interfaces to conduct large-scale tests in open source integrated wireless and traffic emulation platforms to propose and optimize innovative V2V and V2I communication capabilities to improve road traffic management.

PRE-DRIVE (http://www.pre-drive-c2x.eu/). Based on the European COMeSafety architecture for a V2X communication system, the PRE-DRIVE project, ended in June 2010, developed a detailed specification for such a system and a functionally verified prototype.

38.4.5 Other Services

CarTorrent (http://nrlweb.cs.ucla.edu/). CarTorrent a peer-to-peer file sharing application modeled after BitTorrent that allows users to share their files in the vehicular *ad hoc* networks.

DRIVE-IN (http://drive-in.cmuportugal.org/). The goal of the DRIVE-IN project is to investigate how vehicle-to-vehicle communication can improve the user experience and the overall efficiency of vehicle and road utilization. DRIVE-IN focuses on traffic flow optimization and infotainment applications, which so far have received much less attention both from the scientific community and from major industrial players.

Providing adaptive ubiquitous services in vehicular contexts (SEISCIENTOS, http://www.grc.upv.es/600/). SEISCIENTOS is aimed at creating a framework that meets the needs for communication and for the infrastructure to provide dedicated services to end-user in ubiquitous vehicular environments.

38.5 Summary

Vehicular Area NETworks will play a fundamental role in future Intelligent Transportation Systems with the perspective of being also a relevant research and market direction attracting the attention of both academia and industry. A growing number of project and actions appears every year with the aim of addressing the key questions of mobile communications in such a challenging scenario. However, besides the advances we reported in this chapter, many issues need to be further investigated. With respect to the two main application contexts, that is, road safety and traffic efficiency, we identify two main design objectives for future research.

First, the need to improve link-layer reliability and responsiveness, which is a critical requirement for safety applications. Second, the need of a significant shift in the management of information dis-

semination for traffic-related services. The traditional packet forwarding approach has to be redefined considering the active role of each node in the network that, as a consequence of the highly dynamic nature of VANETs, can combine, alter, or even invalidate the information to be routed as a function of the changes in the network context.

Thus, given the abundance of processing power, storage, energy, and communication capacity in the electronic equipment of modern vehicles, these networks will increasingly exploit the capabilities of each node well beyond *ad hoc* mobile networking and toward cooperative, and intelligent, systems.

Acknowledgments

This work has been supported in part by the S2EuNet European Project (FP7–People/IRSES n. 247083).

References

Alshaer, H. and E. Horlait. 2005. An optimized adaptive broadcast scheme for inter-vehicle communication. In *IEEE Vehicular Technology Conference*, 5: 2840–2844.

Benslimane, A. 2004. Optimized dissemination of alarm messages in vehicular ad-hoc networks (VANET). In *High Speed Networks and Multimedia Communications*, 655–666. Berlin: Springer.

Biswas, S., R. Tatchikou, and F. Dion. 2006. Vehicle-to-vehicle wireless communication protocols for enhancing highway traffic safety. *IEEE Communications Magazine*, 44(1): 74–82.

Blum, J.J., A. Eskandarian, and L.J. Hoffman. 2004. Challenges of intervehicle ad hoc networks. In *IEEE Transactions on Intelligent Transportation Systems*, 5(4): 347–351.

Bucciol, P., E. Masala, N. Kawaguchi, K. Takeda, and J.C. De Martin. 2005. Performance Evaluation of H.264 Video Streaming over Inter-Vehicular 802.11 Ad Hoc Networks. In *Proc. of 16th Annual IEEE Int. Symposium on Personal, Indoor and Mobile Radio Communications.*

CALM. ISO TC 204 WG 16. 2011. Communications access for land mobiles (CALM). http://www.isotc204wg16.org/home (accessed February 25, 2011).

Chlamtac, I., M. Conti, and J. J.-N. Liu. 2003. Mobile Ad Hoc networking: Imperatives and challenges. *Ad Hoc Networks*, 1(1): 13–64.

DFT 2011. UK Department for Transport (DFT). Trends in travel. http://www.dft.gov.uk/pgr/statistics/datatablespublications/trends/current/section2ptbm.pdf (accessed February 25, 2011).

Durresi, M., A. Durresi, and L. Barolli. 2005. Emergency broadcast protocol for inter-vehicle communications. In *11th International Conference on Parallel and Distributed Systems,* 402–406.

Ergen, M. 2010. Critical penetration for vehicular networks. *IEEE Communications Letters*. 14(5): 414–416.

ETSI. 2011. ETSI Technical Committee on Intelligent Transport Systems. http://www.etsi.org/website/Technologies/IntelligentTransportSystems.aspx (accessed February 25, 2011)

Fussler, H., M. Mauve, H. Hartenstein, M. Kasemann, and D. Vollmer. 2003. Location-based routing for vehicular ad-hoc networks. *ACM SIGMOBILE Mobile Computing and Communications Review,* 7(1): 47–49.

Goldman Sachs. 2011. Dreaming with BRICs: The Path to 2050. http://www2.goldmansachs.com/ideas/brics/book/99-dreaming.pdf (accessed February 25, 2011).

Grossglauser, M. and D.N.C. Tse. 2002. Mobility increases the capacity of ad hoc wireless networks. *IEEE/ACM Transactions on Networking*, 10(4): 477–486.

Guo, M., M.H. Ammar, and E.W. Zegura. 2005. V3: A vehicle-to-vehicle live video streaming architecture. In *IEEE International Conference on Pervasive Computing and Communications*. New York: IEEE Press.

Härri, J., F. Filali, and C. Bonnet. 2009. Mobility models for vehicular Ad Hoc networks: A survey and taxonomy. *IEEE Communications Surveys & Tutorials*, 11(4): 19–41.

Hartenstein, H. and K.P. Laberteaux. 2008. A tutorial survey on vehicular ad hoc networks. *IEEE Communications Magazine*, 46(6): 164–171.

Hartenstein, H. and K. Laberteaux. 2010. *VANET Vehicular Applications and Inter-Networking Technologies.* Ed. Hannes Hartenstein and Kenneth P Laberteaux Technology. John Wiley & Sons, Ltd. ISBN: 978-0-470-74056-9.

Hu, Y., D. Johnson, and D. Maltz. 2007. RFC 4728—The Dynamic Source Routing Protocol (DSR) for Mobile Ad Hoc Networks for IPv4. *Internet RFCs*. http://www.rfc-editor.org/rfc/rfc4728.txt (accessed February 25, 2011).

Iwata, A., C. Chiang, G. Pei, M. Gerla, and T. Chen. 1999. Scalable routing strategies for ad hoc wireless networks. *IEEE Journal on Selected Areas in Communications, Special Issue on Ad-Hoc Networks*, 7(8): 1369–1379.

Jacquet, P., P. Muhlethaler, A. Qayyum, A. Laouiti, L. Viennot, and T. Clausen. 1998. Optimized link state routing protocol. RFC 3626 IETF. http://www.ietf.org/rfc/rfc3626.txt.

Johnson, D.B. and D.A. Maltz. 1996. Dynamic source routing in ad hoc wireless networks. In *Mobile Computing,* 353: 153–181. US Springer.

Karp, B. and H.T. Kung. 2000. GPSR: Greedy perimeter stateless routing for wireless networks. In *ACM/IEEE International Conference on Mobile Computing and Networking*, 243–254. New York: ACM Press.

Korkmaz, G., E. Ekici, F. Ozguner, and U. Ozguner. 2004. Urban multi-hop broad-cast protocol for inter-vehicle communication systems. In *First ACM International Workshop on Vehicular Ad Hoc Networks*, 76–85. New York: ACM Press.

Kosch, T., C.J. Adler, S. Eichler, C. Schroth, and M. Strassberger. 2006. The scalability problem of vehicular ad hoc networks and how to solve it. *IEEE Wireless Communications,* 13(5): 22–28.

Lee, U., B. Zhou, M. Gerla, E. Magistretti, P. Bellavista, and A. Corradi, 2006. Mobeyes: Smart mobs for urban monitoring with a vehicular sensor network. *IEEE Wireless Communications,* 13(5): 52–57.

Lee, U., M. Magistretti, M. Gerla, P. Bellavista, and A. Corradi. 2009. Dissemination and harvesting of urban data using vehicular sensing platforms. *IEEE Transactions on Vehicular Technology,* 58(2): 882–901.

Little T. and A. Agarwal. 2005. An information propagation scheme for VANETs. In *8th International IEEE Conference on Intelligent Transportation Systems*, 155–160. New York: IEEE Press.

Liu, G., B.-S. Lee, B.-C. Seet, C.H. Foh, K.J. Wong, and K.-K. Lee. 2004. A routing strategy for metropolis vehicular communications. In *International Conference on Information Networking,* 134–143, US: Springer Press.

Lochert, C., H. Hannes, T. Jing, H. Fussler, H. Dagmar, and M. Mauve. 2003. A routing strategy for vehicular ad hoc networks in city environments. In *IEEE Intelligent Vehicles Symposium*, 1: 156–161. New York: IEEE Press.

Lochert, C., M. Mauve, H. FuBler, and H. Hartenstein. 2004. Geographic routing in city scenarios. In *ACM SIGMOBILE Mobile Computing and Communications Review*, 9(1): 69–72. New York: ACM Press.

Maihofer. C. 2004. A survey of geocast routing protocols. *IEEE Communications Surveys & Tutorials*, 6(2): 32–42.

Maihofer, C. and R. Eberhardt. 2004. Geocast in vehicular environments: caching and transmission range control for improved efficiency. In *IEEE Intelligent Vehicles Symposium*, 951–956. New York: IEEE Press.

Maihofer, C., T. Leinmuller, and E. Schoch. 2005. Abiding geocast: Time–stable geocast for ad hoc networks. In *Second ACM international workshop on Vehicular ad hoc networks*, 20–29. New York: ACM Press.

Menouar, H., M. Lenardi, and F. Filali. 2005. A movement prediction-based routing protocol for vehicle-to-vehicle communications. In *First International Vehicle-to-Vehicle Communications Workshop.*

Moške, M., H. Füβlet, H. Hartenstein, and W. Franz. 2004. Performance measurements of a vehicular ad hoc network. In *Proc. IEEE Vehicular Technology Conference,* 4: 2116–2120.

Nandan, A., S. Tewari, S. Das, M. Gerla, and L. Kleinrock. 2006. Adtorrent: Delivering location cognizant advertisements to car networks. In *Third IEEE/IFIP Annual Conference on Wireless On-demand Network Systems and Services*. New York: IEEE Press.

Nadeem, T., S. Dashtinezhad, C. Liao, and L. Iftode. 2004. Traffic view: Traffic data dissemination using car-to-car communication. *ACM Mobile Computing and Communications Review*, 8(3): 6–19.

Namboodiri, V., M. Agarwal, and L. Gao. 2004. A study on the feasibility of mobile gateways for vehicular ad-hoc networks. In *First International Workshop on Vehicular Ad Hoc Networks*, 66–75.

Perkins, C.E. and E.M. Royer. 1999. Ad-hoc on-demand distance vector routing. In *Second IEEE Workshop on Mobile Computing Systems and Applications*, 90–100. New York: IEEE Press.

Perkins, C., E. Belding-Royer, and S. Das. 2003. RFC3561: Ad hoc On-Demand Distance Vector (AODV) Routing. *Internet RFCs*. http://www.ietf.org/rfc/rfc3561.txt (accessed February 25, 2011).

Rossi, D., R. Fracchia, and M. Meo. 2008. VANETs: Why Use Beaconing at All? *IEEE Int. Conf. on Communications*, 2745–2751.

SAE. 2011. US Department of Transportation. SAE J2735—Dedicated Short Range Communications (DSRC) Message Set Dictionary. http://www.standards.its.dot.gov/fact_sheet.asp?f=71. (accessed February 25, 2011).

Schoch, E., F. Kargl, M. Weber, and T. Leinmuller. 2008. Communication patterns in VANETs. *IEEE Communications Magazine*, 46(1): 119–125.

Sengupta, R., S. Rezaei, S. Shladover, D. Cody, S. Dockey, and H. Krishnan. 2007. Cooperative collision warning systems: Concept definition and experimental implementation. *Journal of Intelligent Transportation Systems,* 11(3): 143–155.

Sichitiu, M.L. and M. Kihl. 2008. Inter-vehicle communication systems: A survey. *IEEE Communications Surveys & Tutorials*, 10(2): 88–105.

Ström, E., H. Hartenstein, P. Santi, and W. Wiesbeck. 2010. Vehicular communications: Ubiquitous networks for sustainable mobility. *Proceedings of the IEEE*, 98(7): 111–112.

Sun, M., W. Feng, T. Lai, K. Yamada, H. Okada, and K. Fujimura. 2000. GPS-based message broadcasting for inter-vehicle communication. In *International Conference on Parallel Processing*, 279–286.

US Census Bureau. 2011. US Census Bureau. Average commute times in the USA. http://factfinder.census.gov/home/saff/main.html (accessed February 25, 2011).

WAVE. 2011. IEEE 1609 WG—Dedicated Short Range Communication Working Group. 2011. Wireless Access in Vehicular Environments (WAVE). http://standards.ieee.org/develop/wg/1609_WG.html (accessed February 25, 2011).

Willke, T.L., P. Tientrakool, and N.F. Maxemchuk. 2009. A Survey of inter-vehicle communication protocols and their applications. *IEEE Communications Surveys & Tutorials*, 11(2): 3–20.

Wischhof, L. and H. Rohling. 2005. Congestion control in vehicular ad hoc networks. In *IEEE International Conference on Vehicular Electronics and Safety*, 58–63. New York: IEEE Press.

Wisitpongphan, N., F. Bai, P. Mudalidge, V. Sadekar, and O. Tonguz. 2007. Routing in sparse vehicular ad hoc wireless networks. In *IEEE Journal on Selected Areas in Communications*, 25(8): 1538–1556.

Wu, H., R.M. Fujimoto, R. Guensler, and M. Hunter. 2004. MDDV: a mobility-centric data dissemination algorithm for vehicular networks. In *First ACM International Workshop on Vehicular Ad Hoc Networks*, 47–56. New York: IEEE Press.

Yang, X., L. Liu, N.H. Vaidya, and F. Zhao. 2004. A vehicle-to-vehicle communication protocol for cooperative collision warning. In *First Annual International Conference on Mobile and Ubiquitous Systems: Networking and Services*, 114–123. New York: IEEE Press.

Zhao, J. and G. Cao. 2006. VADD: Vehicle-assisted data delivery in vehicular ad hoc networks. In *IEEE International Conference on Computer Communications*, 1–12. New York: IEEE Press.

Further Reading

Information on governmental actions can be found on the Europe's Information Society portal (Intelligent Car Initiative, url: http://ec.europa.eu/information_society/activities/intelligentcar/) for European countries; on the US Department of Transport portal (Research and Innovative Technology Administration - ITS, URL: http://www.its.dot.gov/) for the United States; and on the Ministry of Land, Infrastructure, Transport and Tourism of Japan portal (URL: http://www.mlit.go.jp/index_e.html) for Japan.

Information on standardization actions can be found on the IEEE, ISO and ETSI portals (references (WAVE 2011), (CALM 2011), and (ETSI 2011)).

Reference (Hartenstein and Laberteaux 2010) provides more details on the topics discusses within this chapter.

Advances in the state of the art of VANETs are regularly published in the following journals and workshops: *IEEE Transactions on Intelligent Transportation Systems*; *IEEE Transactions on Vehicular Technology*; *IEEE Communications Magazine*; *ACM VANET*.

39

60 GHz Wireless Communication

Upamanyu Madhow

Sumit Singh

In contrast to the scarcity of bandwidth typical at lower frequencies, large swathes of unlicensed spectrum are available worldwide in the 60 GHz band (including 7 GHz of spectrum from 57–64 GHz in the United States). Such "millimeter (mm) wave" frequencies have been used in cost-insensitive applications such as military radar and communication systems for decades, using expensively packaged radio frequency-integrated circuits (RFICs) implemented in low-volume compound semiconductor processes. However, intense commercial interest in the 60 GHz band has developed in recent years, because it is now becoming possible to realize 60 GHz radios using silicon radio frequency-integrated circuits (RFICs) in cost-effective packaging. The goal of this chapter is to provide a glimpse of potential applications and system design considerations for emerging 60 GHz wireless systems that capitalize on these hardware advances. We begin with a brief discussion on such applications, but devote most of the exposition to a discussion on the new design considerations relative to those in the cellular and WiFi networks that wireless designers are most familiar with. These design considerations arise from the order of magnitude smaller carrier wavelength at 60 GHz relative to these existing systems, which has significant implications for transceiver hardware, physical layer modeling and design, signal processing architectures, and network protocol design. For outdoor communication, another important feature of the 60 GHz band is its oxygen absorption, which leads to a propagation loss of about 16 dB/km on top of the loss due to free space propagation. Rain leads to further loss (e.g., about an additional 21 dB/km for heavy rain of 50 mm per hour).

Since the technology of 60 GHz communication, and the associated literature, is evolving rapidly, we restrict attention here to a discussion on broad issues that are expected to be relevant to this evolution, rather than emphasizing specific design approaches. A few references on ongoing research and development are provided.

39.1 Potential Applications

Since walls block mm-wave signals quite effectively, the 60 GHz band is well suited to indoor wireless communication with aggressive spatial reuse, providing multiGigabit networks within a room with link

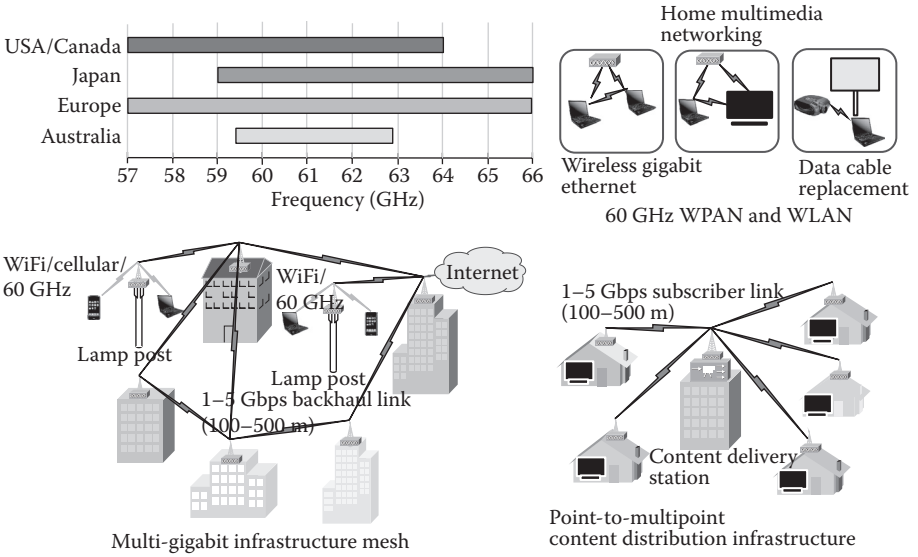

FIGURE 39.1 Millimeter-wave spectral allocation and potential applications.

ranges of the order of 10 m or less: these could result in Wireless Personal Area Networks (WPANs), or be integrated with existing Wireless Local Area Networks (WLANs). WPAN standards for 60 GHz have been issued by ECMA [1] and by the IEEE 802.15.3c group [2]. A draft WLAN standard has been issued by the IEEE 802.11ad group [3,4], with significant involvement of the Wireless Gigabit (WiGig) Alliance [5], a broad-based industry consortium. All these standards include rates exceeding a Gigabit per second (Gbps), with the 802.11ad standard having a maximum rate of 7 Gbps. For example, the use of 60 GHz in IEEE 802.11-based WLANs could potentially increase link rates by an order of magnitude relative to existing WiFi links at lower carrier frequencies (2.4 and 5 GHz), while falling back on these links when a 60 GHz link cannot be realized due to range limitation or blockage.

In addition to these indoor applications, 60 GHz links are attractive for *short-range* outdoor links, despite the large propagation losses due to oxygen absorption and rain. The combined propagation loss due to oxygen absorption and heavy rain (50 mm/h) is about 36 dB/km, which makes it difficult to achieve link ranges of the order of kilometers. However, at 100 m range, this loss can be handled with a modest 3.6 dB addition to the link budget. Mesh networks based on such short-range links [6] could, for example, provide easily deployable wireless backhaul for picocellular networks. Indeed, as demand for wireless data continues scaling up and the cost of 60 GHz transceivers scales down, 60 GHz links directly between picocellular base stations and mobile handsets may become an attractive means of providing Gigabit data rate connectivity with high spatial reuse [7]. Figure 39.1 illustrates some potential indoor and outdoor applications of the 60 GHz spectrum and the spectral allocations.

39.2 The Role of Directionality

The Friis formula for received power under free space propagation at range R can be written as

$$P_{RX} = P_{TX} G_{TX} G_{RX} \frac{\lambda^2}{16\pi^2 R^2}, \tag{39.1}$$

where P_{RX} is the received power, P_{TX} is the transmitted power, G_{TX} and G_{RX} are the transmit and receive antenna gains, and λ is the carrier wavelength. Thus, for fixed antenna gains and transmit power, the

received power scales as λ^2, so that 60 GHz would be 28 dB worse than 2.4 GHz. However, for a fixed antenna aperture, the antenna gain scales as $1/\lambda^2$, so that the use of directional antennas at both ends provides a net directivity gain scaling as $1/\lambda^4$, leading to an overall scaling of propagation gain as $1/\lambda^2$. Thus, if we use directional transmission and reception with constraints on form factor, 60 GHz can actually be 28 dB better than 2.4 GHz. Given the difficulty of providing large amounts of power using low-cost RFICs at 60 GHz, it is almost essential to use directionality at both the transmitter and the receiver for 60 GHz links. Since antenna elements at such small carrier wavelengths can be realized as patterns of metal on the circuit board, it is possible to build electronically steerable antenna arrays with compact form factor that provide directional transmission/reception over a fairly broad angular range.

39.2.1 Link Budgets

Figure 39.2 presents an example link budget for a 60 GHz line-of-sight link of range R. For an indoor link with $R = 10$ m, the required transmit power plus transmit and receive antenna gain required to close the link is 36 dBm. Assuming a transmit power of 10 dBm (achievable with a CMOS power amplifier), the required antenna gain G at the transmitter and the receiver is 13 dBi, corresponding, for example, to horizontal and vertical beamwidths of 45° each. For an outdoor link with $R = 100$ m, the link budget requirement is 58 dBm, which assuming a transmit power of 10 dBm, yields $G = 24$ dBi, requiring far narrower beamwidths. As we discuss soon, these narrow beamwidths imply that the corresponding channels are also drastically different from those for omnidirectional communication at lower frequencies.

Electronically steerable phased arrays are an appealing means of realizing these high antenna gains while providing flexibility of coverage. We can get high directivity from an array of moderately directive antennas, where the overall antenna pattern and hence directivity of a phased array can be calculated by multiplying the element pattern and the array factor. In addition to the directivity gains provided by the transmit and receive arrays, we obtain *power pooling* gains for the transmit array, thus substantially relaxing the requirements for the power amplifier (PA) design for each antenna element. For example, consider again a 100 m outdoor QPSK link with 2 Gbps data rate, under heavy rain which adds about 2 dB to the link budget requirement in our previous outdoor link budget example: the total transmit power plus transmit and receive antenna gain required is now 60 dBm. Assuming an array design with patch elements with about 2.5 dBi element gain, each being driven by its own 10 dBm PA (realizable in CMOS technology), we can meet the required link budget using 32 elements at each end: 10 dBm (transmit power per element) + 2.5 dBi (element gain) + 15 dBi (transmit array again) + 15 dB (array power pooling gain) + 2.5 dBi (receive element gain) + 15 dBi (receive array gain) = 60 dBm. Hence, a 32-element phased array with 10 dBm PAs can sustain a 100 m outdoor link even in heavy rain.

In order to explore range-rate trade-offs in general, key parameters to play with are the per-element transmit power (which can be increased, for example, by going from CMOS to SiGe realizations, while still exploiting the economies of scale provided by silicon semiconductor processes), the number of elements, and the element antenna pattern. The combination of transmit power and antenna directivity is

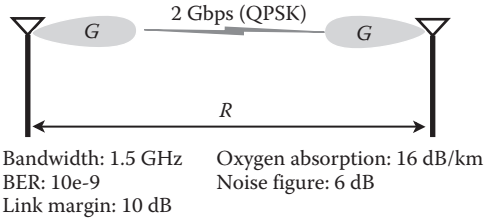

FIGURE 39.2 Example 60 GHz link budget: 2 Gbps QPSK link of range R.

typically limited by regulatory bodies. For example, in the US, current FCC regulations for the power density and radiation exposure in the 60 GHz band constrain the effective isotropic radiated power (EIRP), the sum of the transmit power and the transmit directivity on a dB scale, to 40 dBm average and 43 dBm peak, with peak transmit power not exceeding 500 mW (27 dBm) for an emission bandwidth greater than 100 MHz. For a given directivity, we can trade off the number of elements and the directivity of an individual element in an array. Antenna elements of fairly high directivity can be synthesized at low cost and with compact form factor as patterns of metal on the circuit board. Thus, if we are willing to reduce the angular coverage of the array, each element can be made more directive and fewer elements can be used, thereby lowering signal processing complexity and simplifying array adaptation.

Given the importance of directionality in 60 GHz links, the design of compact antennas has received a great deal of recent attention (e.g., see Reference 8 and references therein). Important constraints in the design of an individual antenna element include ensuring that it operates over the entire band of interest, which is typically quite large (e.g., 57–64 GHz for 60 GHz unlicensed communication in the United States), and that it is small enough to allow for subwavelength placement in an array (in order to avoid grating lobes in the array pattern).

39.2.2 System Design Consequences

The inherent directionality of 60 GHz links has significant design consequences, both for physical channel characteristics and accompanying physical layer choices, and for network protocol design. Many paths, even when not significantly attenuated by reflection, fall outside the typically narrow beamwidths employed at both the transmitter and the receiver, so that we can accurately characterize the 60 GHz channel using ray tracing with a small number of rays corresponding to dominant paths falling within both beams. This, in turn, implies that the geometry of diversity and multiplexing trade-offs is fundamentally different from that of the richer scattering environments typical of lower carrier frequencies. While the preambles which are typically a part of any protocol can be employed for training a receive beamformer, we must now also ensure that transmit beamforming is supported. The IEEE 802.11ad 60 GHz standard, for example, explicitly supports a training phase for transmit beamforming in its medium-access control (MAC) protocol. Directionality also has more fundamental consequences for MAC design. Consider Figure 39.3 where node A has packets to send to node B, but node B is beamformed toward node C for directional transmission or reception. Since node A cannot sense the ongoing communication between nodes B and C, it may attempt a transmission toward node B which would fail given node B is beamformed toward node C. This would lead to node A's transmission attempts to node B to fail repeatedly and may lead to unfairness or deadlock, especially when the protocol requires exponential backoff in the case of failed transmit attempts. This *deafness* caused by directionality implies that it is difficult to employ carrier sense multiple access (CSMA) as used in current WiFi systems, without making clumsy design choices such as switching between omnidirectional and directional modes. On the other hand, directionality also cuts down on mutual interference. Thus, while MAC design for omnidirectional networking at lower carrier frequencies is principally concerned with interference avoidance and management, a key MAC design consideration at 60 GHz is transmitter–receiver coordination in the face of deafness.

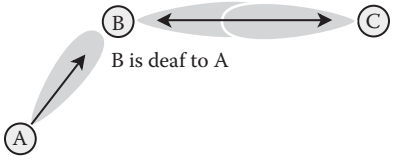

FIGURE 39.3 Deafness in directional networks.

39.3 Diversity and Multiplexing

Propagation measurements and channel modeling for both indoor and outdoor 60 GHz links have been studied for decades (e.g., see References 9 and 10). Here, we seek to provide insight, through two simple examples, of the *design* consequences of 60 GHz propagation.

Spatial Multiplexing: The conventional wisdom from lower carrier frequencies is that spatial multiplexing requires a rich multipath environment. This ensures that transmit antennas spaced a moderate distance apart see different enough spatial responses at the receive antenna array that they can send parallel data streams which the receiver can separate out using spatial processing. More precisely, the channel matrix between the transmit and receive arrays must have rank at least as large as the number of parallel data streams. As we discuss below, however, this rank condition can be satisfied even in line-of-sight (LoS) conditions, provided the antennas in the transmit and/or receive array have "large enough" separation relative to the carrier wavelength. Thus, as the carrier wavelength decreases, so do the required antenna separations, and it becomes possible to achieve spatial multiplexing in LoS settings with nodes of a relatively compact form factor. Let us develop quantitative insight via the scenario depicted in Figure 39.4, where a linear transmit antenna array with N elements spaced by distance D is communicating over a range R with a receive array with identical geometry. It can be shown (e.g., see Reference 11) that, assuming $R \gg D$ (range significantly bigger than antenna spacing), the receive array responses seen by different transmit elements are *orthogonal* if $D = \sqrt{R\lambda/N}$. This is the *Rayleigh criterion* for optical resolution: it tells us the spacing required so that the receive array can "resolve" the transmit arrays. If the receive array responses for different transmit elements are orthogonal (or even just linearly independent), the receiver can separate out the parallel data streams using linear spatial processing, for example. Note that, for a given range, the required interelement distance scales as $\sqrt{\lambda}$, so that spatial multiplexing in LoS or near-LoS environments becomes more feasible as we decrease the carrier wavelength.

As a numerical example, consider an indoor 60 GHz ($\lambda = 5$ mm) link at a range $R = 10$ m. For $N = 4$ we obtain that $D \approx 11$ cm, so that the length of the array is about $(N-1)D \approx 33$ cm. This is consistent with the form factor of electronic devices such as televisions, set-top boxes, laptops, and projectors, and shows that we can get four-fold spatial multiplexing gains even with sparse multipath. The antenna spacing D is a large multiple of the carrier wavelength: $D/\lambda = \sqrt{R/\lambda N} \approx 22$ for our example. Thus, the interelement spacing is big enough that each element in our spatial multiplexing array could be implemented as, say a 4×4 subarray of $\lambda/3$ spaced elements which provides beamsteering. Once the subarrays at each end perform beamforming, we are left with an $N \times N$ MIMO system which provides N-fold spatial multiplexing gains. This basic architecture works even when there is multipath (spatial multiplexing gains typically only improve with multipath). Of course, as the range gets larger, the node size for an LoS MIMO link may become somewhat bulky despite the small carrier wavelength. For example, for an outdoor link at 100 m range, twofold ($N = 2$) LOS spatial multiplexing requires an interelement spacing $D = 0.5$ m (this may still be acceptable in certain applications, for example, for a rooftop-to-rooftop link).

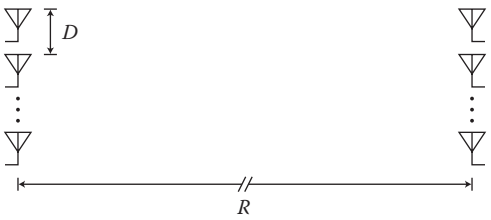

FIGURE 39.4 Line-of-sight spatial multiplexing.

Diversity: To get a sense of the effect of sparse multipath, consider a link with an LoS path and a single reflected path, as shown in Figure 39.5a. If the transmitter and receiver are both using directional beams along the LoS, then the reflected path makes a negligible contribution until it falls within these beams. For a large range R, the angle between the LoS ray and the reflected ray is approximately $\theta \approx (2h/R)$. For example, if we take $h = 5$ m and $\theta = 10°$, then $R \approx 57$ m. These numbers might apply, for example, for a lamppost-based deployment (with lamppost height of about 5 m) in which the transmitter and receiver use narrow beams, with the reflected component starting to make a significant contribution for $\theta = 10°$. In this case, this simple computation predicts that we will begin to see multipath fading for ranges in excess of about 50 m. The phase of the reflected component relative to the LoS component depends on the reflector material and the angle of incidence, but for grazing incidence, reflection produces about a 180° phase shift. The overall phase difference equals the sum of this phase shift and the phase change due to the length difference between the LoS and reflected paths. For $R \gg h$, a simple and standard calculation shows that this path length difference is given by $L \oplus (2h^2/R)$, so that the overall phase difference ϕ can be approximated as

$$\phi \approx \pi + \frac{4\pi h^2}{R\lambda}.$$

For the small carrier wavelengths of interest here, the second term sees large fluctuations due to small changes in h and R, so that the relative phase ϕ can be well modeled as random, uniformly distributed over $[0,2\pi]$. We would therefore expect to see significant amplitude fluctuations due to constructive and destructive interference between the two paths. While this is a particularly simple scenario, qualitatively similar conclusions hold even when we consider more reflections and account more carefully for antenna patterns and reflection coefficients: for narrow beamwidths, multipath fading becomes significant after a critical range, and beyond this range, it can be as severe as in rich scattering environments.

The three major "dimensions" along which we could provide diversity to combat fading are time, frequency, and space. For quasi-stationary nodes, such as an indoor link between a laptop and a television, or an outdoor lamppost-to-lamppost link in a backhaul mesh network, time diversity cannot be relied on. Frequency diversity is useful when the signal bandwidth is large compared to the channel coherence bandwidth, which scales as the inverse of the delay spread. To estimate the delay spread, consider again the 2-ray model depicted in Figure 39.5a. The path length difference between the LoS and reflected path was computed as $L \oplus (2h^2/R)$. For $h = 5$ m and $R = 100$ m, we obtain $L = 0.5$ m. At the speed of light, this corresponds to a delay of 1.67 ns. Such a delay spread corresponds to a coherence bandwidth of about 500 MHz, so that it may be possible to obtain some frequency diversity if using bandwidths of the order of a Gigahertz or more. While frequency diversity depends on available

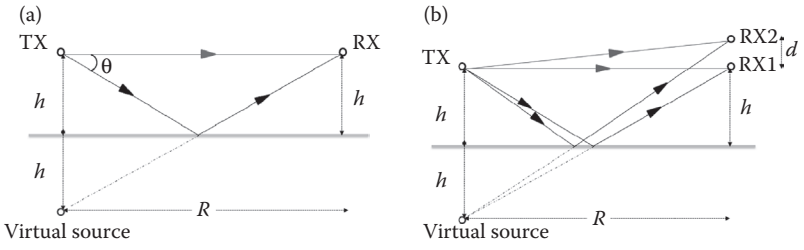

FIGURE 39.5 (a) 2-ray model illustrates the effects of sparse multipath. (The virtual source shown is a standard means of tracing rays.) (b) Dual receive diversity, the difference in path lengths between the two reflected rays provides diversity.

bandwidth, spatial diversity depends on form factor constraints, which determine the feasible antenna spacing. Consider, for example, two receive antennas spaced as shown in Figure 39.5b. The path length difference between the LoS paths from the transmit antenna to these receive antennas can be shown to be negligible for typical parameters, but the path length differences between the reflected paths to the two different receive antenna scales roughly as hd/R, producing phase differences scaling as $2\pi hd/R\lambda$. Thus, for a given range of h and R, it is possible to choose the antenna spacing d such that, if one receive antenna is seeing a destructive fade, then the other sees a constructive fade. For example, for $h = 5$ m and $R = 100$ m, it can be shown that we need d/λ of the order of 5–10 to provide spatial diversity in this manner. While this deterministic reasoning does not extend to a larger number of rays, the qualitative conclusions remain the same [12]: spatial diversity in sparse multipath requires the antenna separation to be a substantial multiple of the carrier wavelength (but still much smaller than what would be needed for near-LoS spatial multiplexing), and for the appropriate antenna spacing, the diversity gains are stronger than for independent and identically distributed Rayleigh fading. As in our discussion on multiplexing, note that the antennas in our discussion are directional, and can themselves be implemented as electronically steerable arrays of subwavelength spaced elements.

The common theme that emerges is that, in contrast to rich scattering environments for which spatial diversity and multiplexing can be achieved with antenna spacings of a wavelength or less, the antenna spacings need to be several multiples of the wavelength for sparse multipath. Fortunately, the small carrier wavelength at 60 GHz implies that these antenna spacings are often compatible with the form factors of interest for both short range indoor applications and moderate range outdoor applications. We also note that diversity and multiplexing can simply be layered on top of beamforming, by replacing each element in a diversity/multiplexing array by a beamforming subarray with subwavelength interelement spacing.

39.4 Signal Processing Challenges

The analog-to-digital converter (ADC) is a core component of the modern digital signal processing (DSP)-based transceiver implementations that have led to low-cost, mass-market cellular and WiFi devices. As we scale up to multiple GHz of bandwidth for 60 GHz communication, the ADC becomes a bottleneck, since high-speed, high-precision ADCs are costly, power-hungry, and difficult to implement. An important topic for further investigation, therefore, is the design of low-cost 60 GHz transceivers capable of efficient signal processing with ADC constraints. While the capacity penalty due to ADC constraints is moderate for idealized channel models [13], low-cost, low-power architectures for receiver functionalities such as MIMO processing, synchronization, and equalization may often require clever co-design of analog and digital signal processing. For example, the mm-wave MIMO prototype in Reference 14 employs digitally controlled analog MIMO processing for spatial demultiplexing, followed by demodulation of the parallel data streams after they have been demultiplexed. Since the separated streams have smaller dynamic range, they are amenable to digital signal processing of the output of low-precision ADCs.

Another key challenge is to devise efficient signal processing and hardware architectures for large adaptive antenna arrays capable of providing flexible coverage as well as narrow beams. Many MIMO signal processing algorithms assume that the complex baseband waveform corresponding to each antenna element is available separately, but this approach does not scale to the large number of antenna elements that can be accommodated with compact form factor in the 60 GHz band. The beamforming ICs that have appeared in recent RFIC literature (e.g., [15]) are for 16–32 elements, and perform phase (and possibly amplitude) combining of signals at RF. Thus, adaptive signal processing architectures for RF beamsteering that scale to a large number of elements are required, and it is an interesting question as to whether mechanisms can be devised for rapidly adapting such arrays to cope with the time variations in, say, a 60 GHz link from a picocellular base station to a mobile device.

39.5 Blockage, Deafness, and Interference

Electromagnetic waves can diffract around obstacles, but the amount of diffracted power decreases with carrier wavelength. In other words, obstacles "look bigger" at smaller carrier wavelengths, so that blockage is an important impairment in 60 GHz communication, especially indoors. In order to develop a quantitative feel for this problem, recall that Huygens' principle tells us that every point on a wavefront originating from a source can be thought of as a virtual source, or "wavelet," with the field at the destination being given by the complex sum of the fields due to these wavelets [16]. The effect of an obstacle between the source and the destination can then be modeled using the wavelets when the wavefront reaches the obstacle, and blocking off the wavelets corresponding to the obstacle. The concept of Fresnel zones (see Figure 39.6) provides quick insight. When we take a cross-section perpendicular to the LoS, the wavelets in a given Fresnel zone produce phases at the destination in a given range. The wavelets in the first Fresnel zone account for most of the received power, and as a rule of thumb, obstruction of more than 40% of the first Fresnel zone leads to blockage. The radius r_n of the nth Fresnel zone at distance d_1 from the transmitter and d_2 from the receiver is given by $r_n = \sqrt{n\lambda d_1 d_2/(d_1 + d_2)}$, where $d_1 + d_2 = R$. This radius is largest midway between the transmitter and the receiver: setting $d_1 = d_2 = (R/2)$, we obtain that $r_1 = (\sqrt{\lambda R}/2)$, which is about 11 cm at the midpoint of a 10 m link at 60 GHz. Thus, the size of an obstacle needed to block the link scales as $\sqrt{R\lambda}$, and for an indoor 60 GHz link, an obstacle of size 10s of cm or bigger (which includes humans and almost any piece of furniture) is too big to diffract around.

A major design issue for indoor 60 GHz networking, therefore, is to devise techniques and protocols that are robust to link blockages, where link blockages can be time-varying (e.g., due to the motion of humans, or doors opening and closing). Techniques that have been considered for maintaining connectivity include using electronic beamforming around obstacles using bounces off walls or ceiling, or by deploying relays (it turns out that a small number of relays suffice for typical scenarios that might be encountered for in-room networks [17]). Given time-varying link blockages and directionality, an important challenge is to devise effective network protocols for discovering new neighbors as well as for tracking local topology changes.

Another key protocol challenge is handling deafness, illustrated earlier in Figure 39.3. One approach is to employ time division multiplexed (TDM) style schemes in which transmitters and receivers can agree on when to communicate, rather than establishing communication via carrier sense. Such TDM schedules could be managed centrally (e.g., an access point controlling a small in-room network), or in a distributed fashion for large networks [6].

Interference is greatly reduced by using directional links, and is further reduced by oxygen absorption for outdoor networks. Since quantification of the effects of interference requires taking a detailed account of the antenna patterns and of node activity, we restrict ourselves to providing quick analytical insight. Consider a simple "flat-top" antenna model, in which the antenna gain is constant over a beam angle $\Delta\phi$, and zero outside. Consider the "desired" receiver in a directional link, and a potentially interfering "undesired" transmitter for another directional link. This undesired transmitter can only

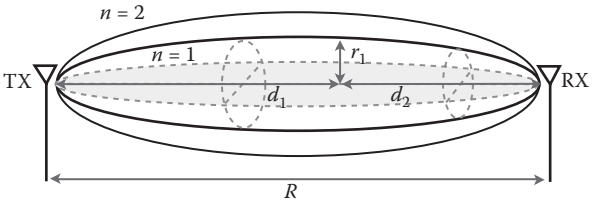

FIGURE 39.6 Fresnel zones provide rules of thumb for link blockage.

interfere with the desired receiver if (a) it is directing its beam toward the desired receiver, (b) the desired receiver is directing its beam toward the undesired receiver, and (c) the undesired transmitter is close enough to the desired receiver. Figure 39.7 shows the geometry of interference in this setting. Assuming that all links are randomly oriented, (a) and (b) are independent events, each occurring with probability $\Delta\phi/2\pi$.For (c), let us assume that the undesired transmitter can only create a collision if it is within an interference radius R_I (determined by the amount of interference the physical layer can tolerate). Suppose that transmitters are distributed on the plane according to a Poisson distribution with density ρ, then the number of undesired transmitters that satisfy criteria (a)–(c) is a Poisson random variable X with mean $\lambda = \rho(\Delta\phi/2\pi)^2\pi R_I^2$. The collision probability is therefore given by $P[X \geq 1] = 1 - e^{-\lambda}$. This simple analysis conveys the basic insight that small beamwidths attenuate the effective number of interferers a transmitter has to contend with. However, the approach is easily extended [18] to account for arbitrary directional antenna patterns and oxygen absorption. Furthermore, while the preceding analysis is for a "protocol model," in which we are interested in the probability of *some* interferer exceeding a threshold, it is possible to provide a more sophisticated analysis [18] for a "physical model," in which we compute the probability of the *sum* of the interference due to all interferers exceeding a threshold. (The terms protocol and physical model have been adapted from Reference 19.) A typical result from Reference 18 regarding an outdoor 60 GHz mesh network with highly directional links and nominal link range of 100 m is that, for a desired SINR of 15 dB, collision probabilities of less than 10% result even with uncoordinated transmission.

Such reduced interference has a significant impact on MAC design. For example, if the links in a network are "directional enough" such that multiple links in close spatial proximity can be active at the same time, then the MAC protocol could ignore interference when scheduling transmissions, and simply react to the occasional collision when it happens [6,18]. However, more investigation is required into spatial reuse and MAC design for 60 GHz networks in a variety of environments, especially for indoor environments with significant scattering, where explicit interference mitigation techniques may be more important [20]. In particular, trade-offs must be made between how to handle different impairments: multihop relay may be required to route around blockage, but it has the effect of creating more interference.

While the literature in this area is evolving rapidly, a representative set of recent papers on indoor 60 GHz networking are [20–22,17], while papers on 60 GHz outdoor networking include [7,6,18].

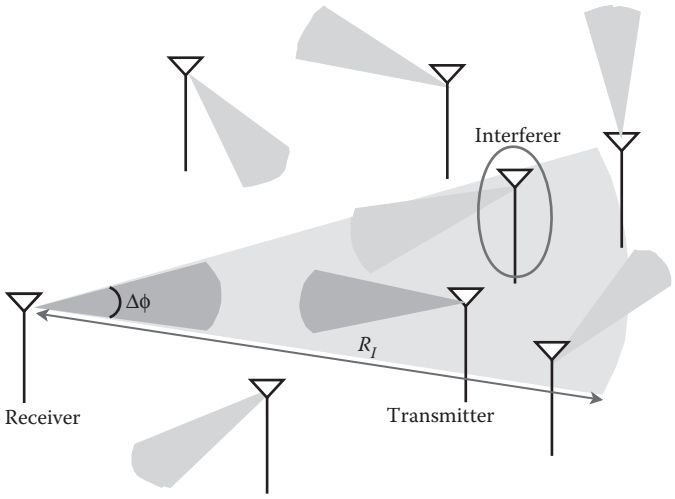

FIGURE 39.7 Interference in 60 GHz outdoor mesh networks.

39.6 Conclusions

Advances in mm-wave hardware have paved the way for the emergence of multiGigabit wireless networks based on the 60 GHz unlicensed band. System design for this band will, of course, draw upon the significant expertise in wireless networking built up over the last two decades for cellular and WiFi systems. However, it is hoped that the material in this chapter makes it clear that existing models and design approaches may require modification because of the unique features of 60 GHz communication (arising from the order of magnitude smaller wavelength compared to existing wireless systems). Since 60 GHz technology and standards are evolving rapidly, we have focused on broad concepts that are relevant for system design, rather than on specific designs. We reiterate some key design considerations:

- 60 GHz links are inherently directional, susceptible to blockage, and are characterized by sparse multipath propagation.
- Signal processing challenges include beamforming with large antenna arrays and handling large bandwidths, and may require closer coupling with hardware than for existing WiFi and cellular systems.
- While classical MIMO techniques apply, the geometry of diversity and multiplexing is different because of the small carrier wavelength and sparse multipath.
- Because of the highly directional nature of 60 GHz links, MAC design should be rethought in order to address coordination in the face of deafness, while taking advantage of the reduced interference. For indoor 60 GHz networks, MAC protocols must in addition deal with time-varying blockage.

It is interesting to note that, while 60 GHz links may often operate in quasi-stationary environments, the growth of 60 GHz networks is intimately linked to that of smart mobile devices with large amounts of memory and rich multimedia capabilities. Indoor 60 GHz networks provide Gigabit connectivity between these devices and other household and enterprise electronic devices (e.g., laptops, televisions/screens, projectors), while outdoor 60 GHz networks may provide multiGigabit backhaul for a picocellular infrastructure deployed to provide the increasing data rates demanded by these devices, or even direct links to such devices.

Acknowledgments

This chapter draws upon perspective acquired from several years of mm-wave communications research at UCSB [23], supported by the National Science Foundation under grants CNS-0520335, ECS-0636621 and CCF-0729222, and by the Institute for Collaborative Biotechnologies through grants DAAD19-03-D-0004 and W911NF-09-0001 from the U.S. Army Research Office. Collaborators on this research include Professor Mark Rodwell, Professor Elizabeth Belding, Professor Raghu Mudumbai, Dr. Munkyo Seo, Dr. Colin Sheldon, Dr. Eric Torkildson, Hong Zhang, and Federico Ziliotto.

References

1. Standard ECMA-387 High Rate 60 GHz PHY, MAC and HDMI PAL. http://www.ecma-international.org/publications/standards/Ecma-387.htm.
2. IEEE 802.15.3c: Wireless Medium Access Control (MAC) and Physical Layer (PHY) Specifications for High Rate Wireless Personal Area Networks (WPANs), Amendment 2: Millimeter-wave based alternative physical layer extension, 2009. http://standards.ieee.org/about/get/802/802.15.html.
3. IEEE 802.11 Task Group AD. http://www.ieee802.org/11/Reports/tgad_update.htm.
4. E. Perahia, C. Cordeiro, M. Park, and L. L. Yang. *IEEE 802.11ad: Defining the Next Generation Multi-Gbps WiFi*, pp. 1–5, January 2010.
5. Wireless Gigabit Alliance. http://wirelessgigabitalliance.org/.

6. S. Singh, R. Mudumbai, and U. Madhow. Distributed coordination with deaf neighbors: Efficient medium access for 60 GHz mesh networks. In *Proc. IEEE Infocom 2010*, San Diego, CA, USA, March 2010.
7. Z. Pi and F. Khan. An introduction to millimeter-wave mobile broadband systems. *IEEE Communications Magazine*, 49(6): 101–107, 2009.
8. Y. P. Zhang and D. Liu. Antenna-on-chip and antenna-in-package solutions to highly integrated millimeter-wave devices for wireless communications. *Antennas and Propagation, IEEE Transactions on*, 57(10): 2830–2841, October 2009.
9. S. Geng, J. Kivinen, X. Zhao, and P. Vainikainen. Millimeter-wave propagation channel characterization for short-range wireless communications. *IEEE Transactions on Vehicular Technology*, 58(1): 3–13, 2009.
10. H. Xu, V. Kukshya, and T. S. Rappaport. Spatial and temporal characteristics of 60-GHz indoor channels. *IEEE Journal on Selected Areas in Communications*, 20(3): 620–630, 2002.
11. E. Torkildson, C. Sheldon, U. Madhow, and M. Rodwell. Nonuniform array design for robust millimeter-wave MIMO links. In *2009 IEEE Global Communications Conference (Globecom 2009)*, November 2009.
12. H. Zhang, S. Venkateswaran, and U. Madhow. Channel modeling and MIMO capacity for outdoor millimeter wave links. In *Proc. IEEE WCNC 2010*, April 2010.
13. J. Singh, O. Dabeer, and U. Madhow. On the limits of communication with low-precision analog-to-digital conversion at the receiver. *IEEE Transactions on Communications*, 57(12): 3629–3639, 2009.
14. C. Sheldon, M. Seo, E. Torkildson, U. Madhow, and M. Rodwell. A 2.4 Gb/s millimeter-wave link using adaptive spatial multiplexing. pages 1–4, July 2010.
15. S. K. Reynolds et al. A 16-element phased-array receiver IC for 60-GHz communications in SiGe BiCMOS. In *Proc. 2010 IEEE Radio Frequency Integrated Circuits Symposium*, Anaheim, CA, USA, May 2010.
16. J. D. Kraus. *Electromagnetics*. McGraw-Hill, Inc., New York, 1991.
17. S. Singh, F. Zilliotto, U. Madhow, E. M. Belding, and M. Rodwell. Blockage and directivity in 60 ghz wireless personal area networks: From cross-layer model to multihop mac design. *IEEE Journal on Selected Areas in Communications, Special Issue on Realizing Gbps Wireless Personal Area Networks*, 27(8): 1400–1413, 2009.
18. S. Singh, R. Mudumbai, and U. Madhow. Interference analysis for highly directional 60-GHz mesh networks: The case for rethinking medium access control. *IEEE/ACM Transactions on Networking*, 19(5):1513–1527, 2011.
19. P. Gupta and P. R. Kumar. The capacity of wireless networks. *Information Theory, IEEE Transactions on*, 46(2): 388–404, 2000.
20. M. Park, P. Gopalakrishnan, and R. Roberts. Interference mitigation techniques in 60 Ghz wireless networks. *IEEE Communications Magazine*, 47(12): 34–40, 2009.
21. A. Maltsev, R. Maslennikov, A. Sevastyanov, A. Khoryaev, and A. Lomayev. Experimental investigations of 60 GHz WLAN systems in office environment. *IEEE Journal on Selected Areas in Communications, special issue on Realizing Gbps Wireless Personal Area Networks*, 27(8):1488–1499, October 2009.
22. M. Park and P. Gopalakrishnan. Analysis on spatial reuse and interference in 60-GHz wireless networks. *IEEE Journal on Selected Areas in Communications, special issue on Realizing Gbps Wireless Personal Area Networks*, 27(8): 1443–1452, 2009.
23. Millimeter wave communication systems research at UCSB. http://www.ece.ucsb.edu/wcsl/mmwcsresearch/doku.php.

Glossary

Adaptive equalizer: A channel equalizer whose parameters are updated automatically and adaptively during transmission of data.

Additive white Gaussian noise (AWGN) channel: The channel whose model is that of corrupting a transmitted waveform by the addition of white (i.e., spectrally flat) Gaussian noise.

Autocorrelation of a sequence: The complex inner product of the sequence with a shifted version itself.

Bandpass waveform: The spectrum of the waveform is nonzero for frequencies in some band concentrated about a frequency $f_c \gg 0$; f_c is called the carrier frequency.

Bandwidth efficiency: Transmission efficiency of a digital modulation scheme measured in units of bits per second per Hertz of bandwidth.

Baseband signal: A signal with frequency content centered around DC.

Baseband waveform: The spectrum of the waveform is nonzero for frequencies near $f = 0$.

Basis (basis functions): An independent set of vectors in a linear space in terms of which any vector in the space can be represented as a linear combination.

Bessel's inequality: The statement that the norm squared of any vector in a vector space is greater or equal to the sum of the squares of the projections onto a set of orthonormal basis vectors.

Binary source code: A mapping from a set of messages into binary strings.

Bit (symbol) interval: The period of time over which a single symbol is transmitted.

Cauchy sequence: A convergent sequence whose members become progressively closer as the limit is approached.

Channel capacity: The highest rate at which information can be transmitted reliably across a channel.

Channel equalizer: A device that is used to reduce the effects of channel distortion in a received signal.

Communication channel: The medium over which communication signals are transmitted. Examples are fiber optic cables, free space, or telephone lines.

Complete: The idea that a basis set is extensive enough to represent any vector in the space as a Fourier sum.

Complex envelope: The function $g(t)$ of a bandpass waveform $v(t)$ where the bandpass waveform is described by

$$v(t) = \mathrm{Re}\left\{g(t)e^{j\omega_c t}\right\}.$$

Continuous phase modulation: Frequency modulation where the phase varies in a continuous manner.

Convergence: A sequence of elements $\{\mathbf{x}_k\}$ in a metric space converges to a limit $\mathbf{x}$ if $\lim_{k\to\infty} d(\mathbf{x},\mathbf{x}_k) = 0$ where $d(\mathbf{x},\mathbf{x}_k)$ is the metric in the space.

Correlation or matched filter receiver: The optimal receiver structure for digital communications in AWGN.

Countable: A set that can be put in one-to-one correspondence with the positive integers.

Cross-correlation of two sequences: The complex inner product of the first sequence with a shifted version of the second sequence.

Decision boundary: The boundary in signal space between the various regions where the receiver declares H_i. Typically, a hyperplane when dealing with AWGN channels.

Decision-directed mode: Mode for adjustment of the equalizer coefficient adaptively based on the use of the detected symbols at the output of the detector.

Decision-feedback equalizer (DFE): An adaptive equalizer that consists of a feedforward filter and a feedback filter, where the latter is fed with previously detected symbols that are used to eliminate the intersymbol interference due to the tail in the channel impulse response.

Dimension: A vector space is n-dimensional if it possesses a set of n independent vectors, but every set of $n + 1$ vectors is linearly dependent.

Discrete memoryless channel: A channel model characterized by discrete input and output alphabets and a probability mass function on the output conditioned on the input.

Dispersive channel: A channel that elongates and distorts the transmitted signal. Normally modeled as a time-varying linear system.

Entropy: A measure of the average uncertainty of a random variable. For a random variable with distribution $p(x)$, the entropy $H(X)$ is defined as $-\sum_x p(x)\log p(x)$.

Equivalent discrete-time transfer function: A discrete-time transfer function (z transform) that relates the transmitted amplitudes to received samples in the absence of noise.

Excess bandwidth: That percentage of the baseband transmitted spectrum which is not contained within the Nyquist band.

Eye diagram: Superposition of segments of a received PAM signal that indicates the amount of intersymbol interference present.

Fourier sum: An approximation of a function in a Hilbert space as a linear combination of orthonormal basis functions where the coefficient of each basis function is the projection of the function onto the respective basis function.

Fourier transform: If $w(t)$ is a waveform, then the Fourier transform of $w(t)$ is

$$W(f) = F[w(t)] = \int_{-\infty}^{\infty} w(t)\mathrm{e}^{-j2\pi ft}\,\mathrm{d}t$$

where f has units of hertz.

Fractionally spaced equalizer: A tapped-delay line channel equalizer in which the delay between adjacent taps is less than the duration of a transmitted symbol.

Frequency-shift keying: A digital modulation technique in which the transmitted pulse is sinusoidal, where the frequency is determined by the source bits.

Gaussian minimum shift keying: MSK where the data signal is prefiltered with a Gaussian filter prior to FM.

Gram–Schmidt procedure: An algorithm that produces a set of orthonormal vectors from a linearly independent set of vectors.

Hilbert space: A normed linear space complete in its natural metric.

Huffman coding: A procedure that constructs a code of minimum average length for a random variable.

Identity element: An element in a vector space that when multiplied by any vector reproduces that vector.

Independent vectors: A set of vectors is independent if any one of them cannot be expressed as a linear combination of the others.

Inner product: A function of ordered pairs of vectors in a vector space, which is analogous to the dot product in ordinary Euclidean vector space.

Intersymbol interference: The ill-effect of one symbol smearing into adjacent symbols thus interfering with the detection process. This is a consequence of the channel filtering the transmitted signals and therefore elongating their duration, see dispersive channel.

Karhunen–Loève expansion: A representation for second-order random processes that allows one to express a random process in terms of a superposition of deterministic waveforms. The scale values are uncorrelated random variables obtained from the waveform.

Lempel–Ziv coding: A procedure for coding that does not use the probability distribution of the source but nevertheless is asymptotically optimal.

Linear combination: Linear sum of a set of vectors in a vector space with each member in the sum, in general, multiplied by a different constant.

Linear manifold: A subspace of a Hilbert space that contains the origin and is closed under addition of elements.

Linearly dependent (dependent): A set of vectors that is not linearly independent.

Linearly independent (independent): A set of vectors, none of which can be expressed as a linear combination of the others.

LMS algorithm: See stochastic gradient algorithm.

Matched filter: The receiver filter with impulse response equal to the time-reversed, complex conjugate impulse response of the combined transmitter filter-channel impulse response.

Maximum likelihood estimate: An estimate for a parameter that maximizes the likelihood function.

Maximum-likelihood sequence detector: A detector for estimating the most probable sequence of data symbols by maximizing the likelihood function of the received signal.

***m* Sequence:** A periodic binary {0,1} sequence that is generated by a shift register with linear feedback and which has maximal possible period given the number of stages in the shift register.

Mean-square equivalence: Two random vectors or time-limited waveforms are mean-square equivalent if and only if the expected value of their mean-square error is zero.

Mean-square estimation: Estimation of a random variable by a linear combination of n other random variables that minimizes the expectation of the squared difference between the random variable to be estimated and the approximating linear combination.

Metric: A real-valued function of two vectors in a vector space that is analogous to the distance between them in the ordinary Euclidean sense.

Metric space: A vector space in which a metric is defined.

Minimum shift keying: A special form of CPM having linear phase trajectories and a modulation index of 1/2.

Modulated signal: The bandpass signal

$$s(t) = \mathrm{Re}\left\{ g(t)\mathrm{e}^{j\omega_c t} \right\}$$

where fluctuations of $g(t)$ are caused by the information source such as audio, video, or data.

Modulation: The information source, $m(t)$, that causes fluctuations in a bandpass signal.

Mutual information: A measure for the amount of information that a random variable gives about another.

Norm: A function of a single vector in a vector space that is analogous to the length of a vector in ordinary Euclidean vector space.

Normed vector space: A vector space in which a norm has been defined.

Nyquist band: The narrowest frequency band that can support a PAM signal without intersymbol interference (the interval $[-1/(2T), 1/(2T)]$ where $1/T$ is the symbol rate).

Nyquist criterion: A condition on the overall frequency response of a PAM system that ensures the absence of intersymbol interference.

Observation space: The space of all possible received data vectors in a signal detection or estimation problem.

Orthogonal: The property of two vectors expressed by their inner product being zero.

Orthogonal complement: The space of vectors that are orthogonal to a linear manifold or subspace.

Orthogonal frequency division multiple access (OFDMA): Multiple access technique in which a different subset of OFDM subcarriers are assigned to individual users, leading to a multicarrier transmission scheme.

Orthogonal frequency division multiplexing (OFDM): Multicarrier modulation by using a collection of low-bit-rate orthogonal subcarriers.

Orthogonality principle: A theorem stating that the minimum mean-square estimate of a random variable in terms of a linear combination of n other random variables requires the difference between the random variable and linear combination, or error, to be statistically orthogonal to each random variable in the linear combination (i.e., the expectation of the product of the error and each random variable is zero), also called the *projection theorem*.

Orthonormal: The property of two or more vectors or time-limited waveforms being mutually orthogonal and individually having unit length.

Orthonormal basis: A basis set for which the basis vectors are orthonormal.

Outage probability: The probability of failing to achieve adequate reception of the signal due to, for instance, co-channel interference.

Parseval's equality: The statement that the norm squared of a vector in a complete Hilbert space equals the sum of the squares of the vector's projections onto an orthonormal basis set in the space.

Partial-response signaling: A signaling technique in which a controlled amount of intersymbol interference is introduced at the transmitter in order to shape the transmitted spectrum.

Phase shift keying: Modulation where the instantaneous phase of the carrier varies linearly with the data signal.

Power efficiency: Received SINR that is required to achieve reliable communication with specified bandwidth efficiency.

Power spectral density: Relative power in a modulated signal as a function of frequency.

Precoding: A transformation of source symbols at the transmitter that compensates for intersymbol interference introduced by the channel.

Preset equalizer: A channel equalizer whose parameters are fixed (time-invariant) during transmission of data.

Projection theorem: See orthogonality principle.

Pseudonoise sequences: Also referred to as pseudorandom sequences (PN), these are sequences that are deterministically generated and yet possess some properties that one would expect to find in randomly generated sequences.

Pulse amplitude modulation (PAM): A digital modulation technique in which the source bits are mapped to a sequence of amplitudes that modulate a transmitted pulse.

Pulse code modulation: A serial bit stream that consists of binary words which represent quantized sample values of an analog signal.

Quadrature amplitude modulation: Modulation where information is transmitted in the amplitude of the cosine and sine components of the carrier.

Quantizing: Replacing a sample value with the closest allowed value.

Raised cosine pulse: A pulse shape with Fourier transform that decays to zero according to a raised cosine; see Equation 3.18. The amount of excess bandwidth is conveniently determined by a single parameter (α).

Rate distortion function: The minimum rate at which a source can be described to the given average distortion.

Rayleigh channel: A channel that randomly scales the transmitted waveform by a Rayleigh random variable while adding an independent uniform phase to the carrier.

Real envelope: The function $R(t) = |g(t)|$ of a bandpass waveform $v(t)$ where the bandpass waveform is described by

$$v(t) = \mathrm{Re}\left\{ g(t)e^{j\omega_c t} \right\}.$$

Riesz–Fischer theorem: A theorem stating the conditions under which an element of a space of square-integrable functions can be represented in terms of an infinite orthonormal set.

Root-raised cosine pulse: A pulse shape with Fourier transform that is the square root of the raised cosine spectrum shown in Equation 3.18.

Schwarz's inequality: An inequality expressing the fact that the absolute value of the inner product of any pair of vectors in a Hilbert space is less than or equal to the product of their respective norms.

Separable: A Hilbert space in which a countable set of elements exists that can be used to represent any element in the space to any degree of accuracy desired as a linear combination of the members of the set.

Shift-register sequence: A sequence with symbols drawn from a field, which satisfies a linear-recurrence relation and that can be implemented using a shift register.

Signal constellation: The permitted values of the complex envelope for a digital modulating source.

Signal space: An abstraction for representing a time-limited waveform in a low-dimensional vector space. Usually arrived at through the application of the Karhunen–Loève transformation.

Signal vector: A vector representing a received signal in a signal detection or estimation problem.

Single carrier frequency division multiple access (SC-FDMA): Multiple access technique in which non-overlapping subcarriers are assigned to different users, leading to a single carrier transmit signal.

Spanning set: The set of elements of a separable Hilbert space used to represent an arbitrary element with any degree of accuracy desired.

Spectrum efficiency: A measure of how efficiently space, frequency, and time are used. It is expressed in erlang per square meter per hertz.

Spread spectrum: A signaling technique in which the pulse bandwidth is many times wider than the Nyquist bandwidth.

Stochastic gradient algorithm: An algorithm for adaptively adjusting the coefficients of an equalizer based on the use of (noise-corrupted) estimates of the gradients.

Symbol-spaced equalizer: A tapped-delay line channel equalizer in which the delay between adjacent taps is equal to the duration of a transmitted symbol.

Total probability of error: The probability of classifying the received waveform into any of the symbols that were not transmitted over a particular bit interval.

Training mode: Mode for adjustment of the equalizer coefficients based on the transmission of a known sequence of transmitted symbols.

Triangle inequality: An inequality of a normed linear space that is analogous to the fact that the length of the vector sum of any two sides of a triangle is less than or equal to the sum of their respective lengths.

Trunking efficiency: A function relating the number of subscribers per channel and the number of channels per cell for different values of blocking probability.

Vector: An element of a linear, or vector, space.

Vector space: A space of elements, called vectors, which obey certain laws of associativity and commutativity and have identity elements for scalar multiplication and element addition.

Volterra filter: A filter whose output at a given time depends not only linearly of present and past inputs, but on powers and products of present and past inputs.

Wavelet: See wavelet transform.

Wavelet transform: Resolution of a signal into a set of basis functions called wavelets. As a parameter of the wavelet is changed, the behavior of the signal over progressively shorter time intervals is resolved.

Zero-forcing criterion: A design constraint which specifies that intersymbol interference be eliminated.

Zero-forcing equalizer: A channel equalizer whose parameters are adjusted to completely eliminate intersymbol interference in a sequence of transmitted data symbols.

Electrical Engineering

MOBILE COMMUNICATIONS HANDBOOK Third Edition

With 26 entirely new and 5 extensively revised chapters out of the total of 39, the **Mobile Communications Handbook, Third Edition** presents an in-depth and up-to-date overview of the full range of wireless and mobile technologies that we rely on every day. This includes, but is not limited to, everything from digital cellular mobile radio and evolving personal communication systems to wireless data and wireless networks.

Illustrating the extraordinary evolution of wireless communications and networks in the last 15 years, this book is divided into five sections:

- ***Basic Principles*** provides the essential underpinnings for the wide-ranging mobile communication technologies currently in use throughout the world.
- ***Wireless Standards*** contains technical details of the standards we use every day, as well as insights into their development.
- ***Source Compression and Quality Assessment*** covers the compression techniques used to represent voice and video for transmission over mobile communications systems as well as how the delivered voice and video quality are assessed.
- ***Wireless Networks*** examines the wide range of current and developing wireless networks and wireless methodologies.
- ***Emerging Applications*** explores newly developed areas of vehicular communications and 60 GHz wireless communications.

Written by experts from industry and academia, this book provides a succinct overview of each topic, quickly bringing the reader up to date, but with sufficient detail and references to enable deeper investigations. Providing much more than a “just the facts” presentation, contributors use their experience in the field to provide insights into how each topic has emerged and to point toward forthcoming developments in mobile communications.

K10892

CRC Press
Taylor & Francis Group
an **informa** business
www.crcpress.com

6000 Broken Sound Parkway, NW
Suite 300, Boca Raton, FL 33487
711 Third Avenue
New York, NY 10017
2 Park Square, Milton Park
Abingdon, Oxon OX14 4RN, UK

ISBN: 978-1-4398-1723-0
90000
9 781439 817230